Virchows Arch (2008) 453:1–8
DOI 10.1007/s00428-008-0611-z

REVIEW AND PERSPECTIVE

Pathogenesis of lymphangiomas

Susanne Wiegand · Behfar Eivazi · Peter J. Barth · Dirk Berens von Rautenfeld · Benedikt J. Folz · Robert Mandic · Jochen A. Werner

Received: 13 December 2007 / Revised: 27 March 2008 / Accepted: 28 March 2008 / Published online: 24 May 2008

Abstract Based on various hypotheses concerning lymphangiogenesis published in the literature, different putative mechanisms of lymphangioma development are discussed including failure of the lymphatic system to connect with or separate from the venous system, abnormal budding of the lymphatic system from the cardinal vein, or acquired processes such as traumata, infections, chronic inflammations, and obstructions. Increasingly, the possible influence of lymphangiogenic growth factors on the development of lymphangiomas is discussed. The proved expression of different growth factors in the endothelium of lymphangiomas leads to new hypotheses regarding the pathogenesis of lymphangiomas. Thus, further studies on the lymphangiogenesis and the development of lymphangiomas will have to clarify as to whether lymphangiomas are true malformations or neoplastic in nature.

S. Wiegand (✉) · B. Eivazi · R. Mandic · J. A. Werner
Department of Otolaryngology, Head and Neck Surgery,
Philipps-University of Marburg,
Deutschhausstr. 3,
35037 Marburg, Germany
e-mail: swiegand@med.uni-marburg.de

P. J. Barth
Institute of Pathology, Philipps-University of Marburg,
Marburg, Germany

D. B. von Rautenfeld
Department of Functional and Applied Anatomy,
Hannover Medical School,
Hannover, Germany

B. J. Folz
Department of Otolaryngology, Karl-Hansen Medical Center,
Bad Lippspringe, Germany

Keywords Lymphangioma · Lymphangiogenesis · Growth factor

Introduction

Lymphangiomas are benign malformations of the lymphatic system. Morphologically, lymphangiomas are composed of thin-walled, cystically dilated vascular channels lined by inconspicuous endothelial cells and filled with proteinaceous lymph fluid (Fig. 1). Immunhistochemistry confirms the endothelial line of differentiation in lymphangiomas. Lymphangiomas often grow proportional to the patients' body growth. Depending on the location of the lymphangioma, an acute increase in size that is frequently triggered by infectious diseases may lead to life-threatening complications, as well as severe functional and aesthetic impairments for the patients.

Lymphangiomas are equally distributed among genders and races [55]. In the pertinent literature, their incidence in children is estimated to amount to 6% of all benign tumors [2]. In about half of the patients the disease is already obvious at the time of birth. During the first and second year of life, the occurrence of lymphangioma is diagnosed in 80–90% of the cases due to clinical symptoms [50]. About 60% of all lymphangiomas are found in the head and neck region, primarily affecting the tongue and the floor of the mouth [9, 44].

Traditionally, lymphangiomas are classified according to their histological appearance into capillary, cavernous, and cystic lymphangiomas [4]. This classification, however, is being replaced by a classification based on morphologic aspects into macrocystic, microcystic, and combined lymphangiomas [29] (Figs. 2 and 3).

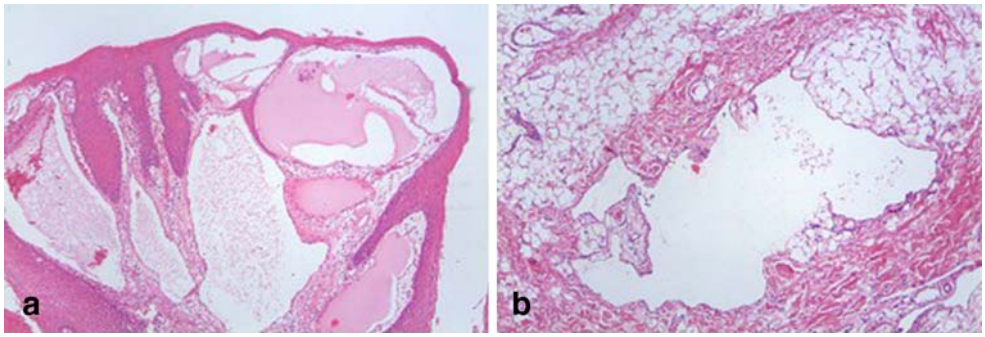

Fig. 1 **a** Microcystic lymphangioma of the tongue composed of dilated thin-walled lymphatic channels that are covered by a partially atrophic squamous epithelium. **b** Macrocystic lymphangioma situated within normal connective tissue. The lumen contains proteinaceous fluid and few lymphocytes

Lymphangiomas have to be distinguished from other lymphatic tumors like acquired progressive lymphangioma, lymphangiosarcoma and lymphangiomatosis. Acquired progressive lymphangioma (lymphangioendothelioma) is a cutaneous vascular neoplasm that typically presents as a solitary, well-demarked patch or plaque on which small erythematous papules may arise. Lesions are typically slowly but progressively enlarging to a considerable size [33]. Histologically, lymphangioendothelioma seems to be similar to a low-grade malignancy. It is characterized by vascular channels infiltrating the dermis in a diffuse and dissecting manner, but in contrast to lymphangiosarcoma, there is an absence of mitotic figures and significant nuclear polymorphism [35]. Disseminated lymphangiomatosis is a rare disease that is represented by a proliferation of lymph vessels involving soft tissue, parenchymal organs, dermis, and the skeletal system. North et al. [34] recently described a further entity, the so-called multifocal lymphangioendotheliomatosis. It describes the presence of multilocular lesions similar to acquired progressive lymphangioma that is typically solitary. Multifocal lymphangioendotheliomatosis was accompanied by a significant thrombocytopenia in all patients resembling the coagulopathy that is found in Kasabach–Merritt syndrome [34]. Lympangiosarcoma is a rare, aggressive, vascular neoplasm typically arising within the chronic lymphedema of the upper limb after mastectomy and radiotherapy for carcinoma of the breast but also in chronic congenital or idiopathic lymphedema. It is characterized by an irregular, diffusely infiltrative growth and abnormal mitotic figures [33]. In addition to these lymphatic tumors, the histological and immunohistochemical features of vascular neoplasms with a hobnail cytomorphology like hobnail hemangioma and retiform hemangioendothelioma suggest that they also represent tumors of the lymphatic vessels [32].

While a large amount of information on the clinical and histological appearance of lymphangiomas is already available and even the appropriate therapeutic strategies are summarized in several review articles [51], up to now,

Fig. 2 Macrocystic lymphangioma of the neck

Fig. 3 Microcystic lymphangioma of the orbit

the pathogenesis of lymphangiomas was less focussed in clinical as well as morphologic studies. The present review summarizes the current knowledge of the physiological development of lymphatic vessels as well as information on the etiology and pathogenesis of lymphangiomas and, based on this, discusses the different theories regarding the mechanisms of lymphangioma formation.

Embryology of the lymphatic system

It is characteristic for the genesis of lymphangiomas that they most commonly occur in locations where the lymphatic system is formed by the six primitive formations of the lymph sacs during embryogenesis. Therefore, it seems to be obvious that the development of lymphangiomas is closely related to the maturation of the lymphatic system.

Lymphatic vessels were first described in the seventeenth century by Gasparo Aselli as "venae lactae" [3], and they have been studied extensively during the beginning of the last century. Since the embryonic development of the lymphatic system is very complex, different theories are discussed regarding its origin.

The first morphologically visible anlage of the lymphatic system can be revealed in the sixth to seventh week of the embryonic development. The primordial lymphatic formations, the lymph sacs, consist of two jugulo-axillary lymph sacs in the area of the confluence of the subclavian vein and the internal jugular vein, from which the lymph vessels of the head, neck, and arms sprout. Furthermore, they consist of two lumbo-iliacal lymph sacs, being the origin of the lymph vessels of the inferior part of the body, the retroperitoneal lymph sac, and the chylocyst [8] (Fig. 4).

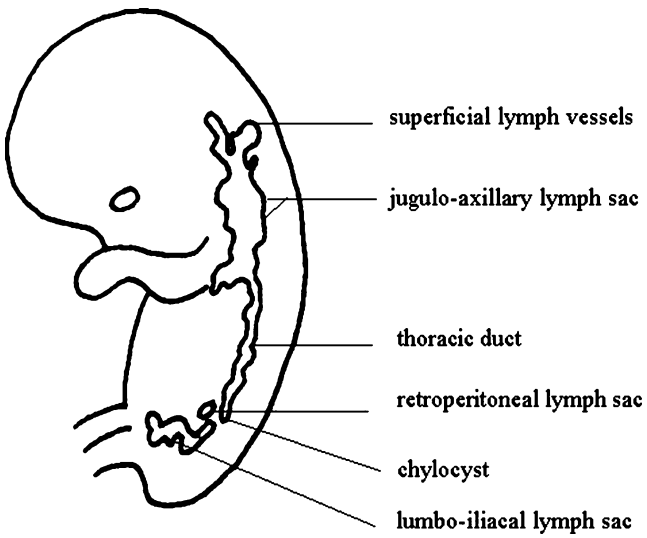

Fig. 4 Description of the primitive lymphatic system of the primary lymphatic sacs of a 42 day-old human embryo (modified according to Sabin [39])

Theory of centrifugal development

Sabin [39] assumed that the lymphatic system develops by budding from embryonic veins of the already existing venous system. According to this theory, endothelial cells of the veins sprout into the surrounding tissues, and through coating of the perivascular intercellular gaps with endothelial tissue, the whole lymphatic system develops (Fig. 5). Thus, lymphatic endothelial cells exclusively derive from the endothelium of the venous system. Studies performed by van der Putte [48], Wigle and coworkers [53], as well as Jain and Padera [15] confirmed this assumption of a venous origin of the lymphatic system. With this background, endothelial cells of the cardinal vein of the early embryo first express Lyve-1 and vascular endothelial growth factor receptor 3 (VEGFR-3) that are also found on normal adult lymphatic vessels. The lymphatic differentiation of the cells is introduced by a signaling mechanism that is not yet clearly identified and that triggers the expression of transcription factor Prox-1. Cells expressing Lyve-1, VEGFR-3, and Prox-1 secrete particular lymphoid chemokines and increase their VEGFR-3 expression, thus initiating the development of the lymphatic system [15]. Therefore, the endothelial cells of the cardinal vein are probably initially bipotent, and the expression of Prox-1 causes the transformation of those cells into cells of lymphatic differentiation.

Theory of centripetal development

This theory is based on the assumption that the peripheral lymphatic vessels develop from putative mesenchymal lymphangioblasts [18, 40]. The confluence of mesenchymal clefts leads to the formation of lymphatic vessels that fuse with the veins due to centripetal growth (Fig. 6). Therefore, according to the centripetal theory, the lymphatic spaces arise independently from the veins, spread from the periphery of the embryo by annexing with other similar spaces, and only secondarily obtain a connection to the venous system. This assumption is supported by examinations performed by Schneider et al. [40] who showed that lymphangioblasts are already present in the peripheral mesenchyme before the occurrence of the jugulo-axillary lymph sacs.

Theory of combined venous–mesenchymal origin of the lymphatic system

This theory combines the two previous theories and supports the venous-mesenchymal origin. It was implemented by van der Jagt [47] and Kutsuna [22] who suggested that the central lymph vessels develop by sprouting from lymph sacs and therefore have a venous

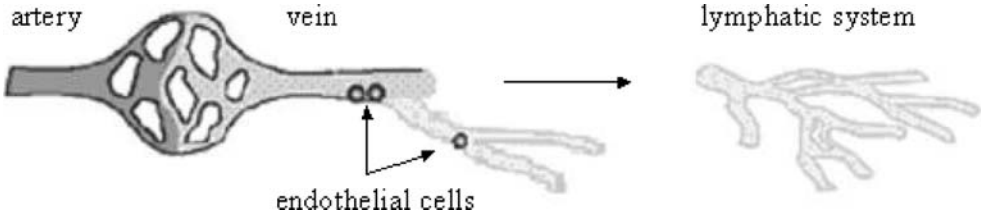

Fig. 5 Theory of centrifugal development (according to Sabin [39])

origin and the peripheral lymph vessels arise by in situ differentiation of mesenchymal precursors and therefore have a mesenchymal origin. To conclude, this model proposes that both abovementioned theories occur simultaneously.

The previous theories show that the origin and the development of the lymphatic system are still controversial issues that have to be clarified definitely. Considering the different theories with regard to the development of the lymphatic system, however, the hypotheses on the genesis of lymphangiomas may be better understood.

Theories regarding the pathogenesis of lymphangiomas

A failure of the lymphatic system to connect with or separate from the venous system or an abnormal budding of lymphatic tissue from the cardinal vein are discussed as reasons for the development of lymphangiomas. Even traumata, infections, chronic inflammations, and obstructions during the embryonic development are suspected to trigger development of lymphangiomas [4].

Sequestration of lymph tissue

Other authors think that lymphangiomas develop as a result of sequestration of portions of the primitive lymphatic anlage [23]. As a consequence of sequestered lymphatic tissue during the embryonic development in regions without regular connection to the normal lymphatic system [37], the missing communication to the lymphatic system could avoid the drainage of lymph fluid from the sequestered parts. Therefore, a lymphatic blockade may arise in a circumscribed area, possibly increasing in size as consequence of infections or traumata. This theory may explain the formation and morphology of peripherally located smaller lymphangiomas.

Abnormal budding of lymph vessels

Some studies assume that the development of lymphangiomas is due to an abnormal budding of lymphatic vessels from the primitive lymphatic anlage. Those structures probably possess further growth potential [5]; however, they loose their connection to the primary lymphatic buds and thus also the possibility of lymphatic drainage so that lymphangiomas may develop [58].

Lack of fusion with the venous system

Assuming a mesenchymal origin of the lymphatic system, other authors postulate that a non-fusion of the lymph sacs with the venous system leads to the development of lymphangiomas [31]. Weingast [49] also supposed that a missing connection of primordial lymphatic sacs to the venous system leads to isolated lymphatic canals that dilate and thus form the lymphangioma. This mechanism is made responsible for the genesis of cystic hygromas of the neck. The study results of Zadvinskis and co-workers [58] seem to reveal that the missing drainage of the jugulo-axillary lymph sac into the internal jugular vein is responsible for the pathogenesis of cystic hygromas. This assumption is supported by the results found by van der Putte who could show that cystic hygromas are associated with a missing connection between lymphatic system and venous system in the jugulo-subclavian area [48].

Obstruction of lymph vessels

Furthermore, the theory is discussed that an obstruction of the efferent lymphatic vessels causes accumulation of lymph and dilatation of the lymph canals proximal to this obstruction. This mechanism could result in the development of lymphangioma [48].

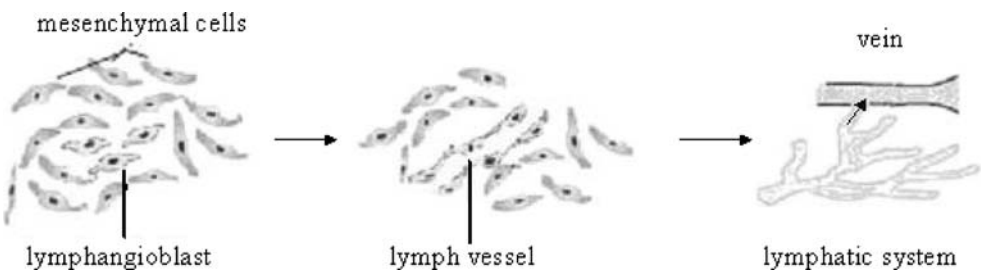

Fig. 6 Theory of centripetal development (according to Huntington and McClure [12] and Kampmeier [18])

Genesis of lymphangiomas in adults

Even if the majority of lymphangiomas is diagnosed in embryos, newborns, or infants, lymphangiomas may be clinically apparent later in adults. In those cases, most of the study groups assume that only a small defect exists in the lymphatic system, which can be compensated under healthy conditions. Pathologic conditions associated with an increased lymphatic volume may then lead to the formation of lymphangioma. Suk et al. [45] consider that the origin of sudden occurrence of lymphangiomas in adults is due to a delayed proliferation of cell rests. Triggering stimuli for this proliferation are suspected to be infections and traumata [52].

Molecular characteristics of lymphatics and lymphangiomas

In contrast to the mentioned established theories on the genesis of lymphangiomas, recent studies assume that in lymphangiomas single lymphatic vessels have a tumorous proliferative behavior and thus show neoplastic growth [25]. This mechanism leads to a network of initial lymphatics that never achieve sufficient anastomosis with larger lymphatic vessels [25]. Enzinger and Weiss [7] suppose that lymphangiomas have their origin in a hyperplasia of transformed lymphatic endothelial or stroma cells, which is caused by a dysregulation of growth factors [11]. In this case, an aberrant regulation of growth factors might modulate the pathogenesis of lymphangiomas.

Recently, the expression of several markers of lymphatic endothelial cells like lymphatic endothelial hyaluron receptor-1 (Lyve-1) and Podoplanin was detectable in lymphangiomas (Fig. 7) and different specific lymphangiogenic growth factors could be identified that are expressed on healthy lymphatic endothelium and that are made responsible for lymphangiogenesis. Some of these growth factors, such as vascular endothelial growth factor C (VEGF-C), VEGFR-3, and Prox-1, are meanwhile correlated with the genesis of lymphangiomas, and their expression in lymphangiomas is examined (Table 1).

One growth factor that is associated with the genesis of lymphangiomas is the transcription factor Prox-1. Although Prox-1 is expressed in a variety of cell types, its expression in endothelial cells of the vascular system, however, is reserved to lymphatic endothelial cells and lymphangioblasts. The expression of Prox-1 could also be detected in the endothelium of human lymphangiomas [38, 57]. Different examinations could show that Prox-1 causes an up-regulation of cell markers of the lymphatic endothelium, such as VEGFR-3 [10, 19]. Moreover, it could be shown that, based on the theory of a venous origin of the lymphatic system, Prox-1 probably mainly influences the molecular mechanism leading to the separation of initial lymphatics from the cardinal vein [15, 36, 57]. Therefore, it could be revealed that in Prox-1-deficient mouse embryos, the budding of lymphatic vessels from the cardinal vein

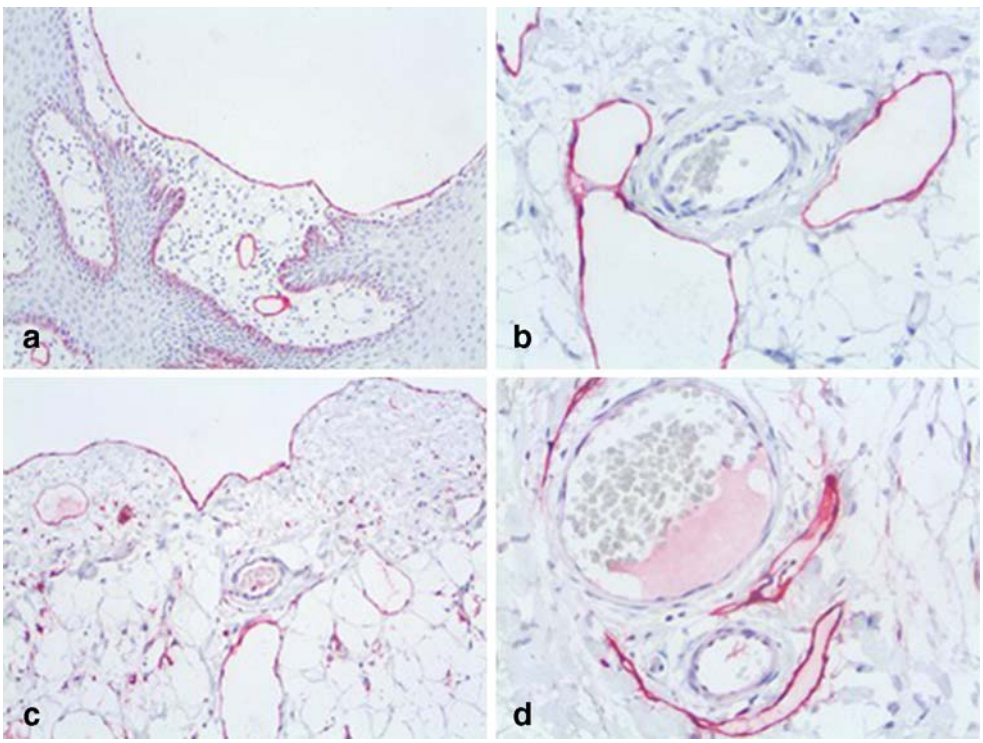

Fig. 7 **a** Positive staining for podoplanin is observed in the endothelial cells lining this microcystic lymphangioma of the tongue. There is also slight podoplanin immunostaining in the basal cells of the covering squamous epithelium. The endothelial cells of adjacent blood vessels reveal no podoplanin immunoreactivity. **b** Podoplanin immunohistochemistry displays positive staining of the endothelial cells lining this macrocystic lymphangioma of the neck, whereas endothelial cells of neighbouring blood vessels show no specific staining for podoplanin. **c**, **d** Lyve-1 immunoreactivity is found in the endothelial cells of this lymphangioma of the neck; by contrast, endothelial cells lining adjacent blood vessels display no immunoreactivity for Lyve-1

Table 1 Factors potentially associated with the pathogenesis of lymphangiomas

Antigen	Function	Reference
VEGF-C	Tyrosinkinase	11
VEGFR-3	Tyrosinkinase receptor	11, 26, 56, 57
Prox-1	Transcription factor	38, 57
bFGF	Growth factor	42
PEDF	Inhibitor of angiogenesis	42
Thrombospondin	Inhibitor of angiogenesis	42
Reelin	Glycoprotein	56
cMAF	Transcription factor	56
Integrin-α1, -α9	Transmembrane proteins	56

does not occur, and lymphatic vessels do not develop while the development of the vascular system is uneventful [54].

Another growth factor that is associated with the genesis of lymphangiomas is VEGF-C. This factor belongs to the PDGF/VEGF family of growth factors and is a ligand for the endothelial-specific receptors VEGF-receptor-3 and VEGF-receptor-2 to which it ligates with high affinity [16]. The mouse model could reveal that, during embryonic development, VEGF-C selectively induces lymphatic but not endothelial cell proliferation and hyperplasia of the vessels [11] and that a normal concentration of VEGF-C is essential for normal development of the lymphatic vessels [19]. Furthermore, the animal model could confirm that the expression of VEGF-C receptor VEGFR-3 is restricted to the lymphatic vessels in later stages of the embryonic development [17]. Studies comparing the expression of VEGFR-3 in lymphatic endothelium of lymphangiomas and healthy lymphatic vessels could show a higher expression of VEGFR-3 in lymphangiomas [26]. This result was confirmed by other study groups, which were able to detect an increased VEGFR-3 expression in lymphangioma [17, 37, 56].

Huang et al. [11] revealed the expression of VEGF-C as well as its receptor VEGFR-3 only in endothelial cells of lymphangiomas; however, they were not found in the adjacent connective tissue or healthy lympho-endothelium. Furthermore, no VEGF-C expression could be revealed in hemangiomas and angiosarcomas [11]. Finally, it could be shown that the occurrence of a genetic mutation in the VEGFR-3 gene is associated with the so-called Nonne–Milroy syndrome, which is accompanied by a lymphatic hypoplasia and leads to the development of hereditary lymphedema [13]. Besides, Karkkainen et al. [19] were able to show that mutations inactivating VEGF-C lead to the development of a primary lymphedema. Based on these results, VEGF-C and its receptor VEGFR-3 are discussed as being possible markers for lymphangiomas. Their occurrence might play a key role in the development of lymphangiomas [11].

Additionally, Wilting and co-workers [56] could prove the expression of different cell markers occurring in the lympho-endothelium of healthy lymphatic vessels, such as the glycoprotein reelin, the transcription factor cMAF as well as the transmembrane proteins integrin-α1 and integrin-α9, even in the endothelial cells of lymphangiomas.

A further factor that was examined in lymphangiomas is Wilms tumor 1 gene (WT1). WT1 was initially identified as one of the key players in the development of Wilms tumor but is also expressed in cancers of other origins. Lawley et al. [24] examined the expression in vascular tumors and found a decreased endothelial staining in vascular malformations including lymphangiomas, while in hemangiomas, strong endothelial staining was demonstrated. Therefore, WT1 seems to be a marker that distinguishes hemangiomas from vascular malformations and the loss of WT1 probably leads to the phenotype of vascular malformation by enhancing the production of platelet-derived growth factor family members. Moreover, the defective investment of WT1-deficient endothelial cells by smooth muscle in vascular malformations might be caused through loss of WT1 [24].

Finally, the significance of factors that mainly influence angiogenesis was examined in lymphangiomas. For example, the influence of PEDF, which inhibits angiogenesis was discussed for the development of lymphangiomas. Sidle et al. [42] could reveal an increased expression of VEGF and a reduced expression of PEDF in lymphangiomas and, thus, a high angiogenous activity. Moreover, a high level of basic fibroblast growth factor (bFGF) could be observed in lymphangioma cells as well as low levels of thrombospondin-1, which is a natural inhibitor of angiogenesis. These observations might indicate that lymphangiomas are influenced by an increased angiogenesis for development and growth. If this hypothesis turns out to be true, the benefit of antiangiogenetic therapies could be tested in the therapy of lymphangiomas [27].

Based on the abovementioned theories, it can be assumed that lymphangiomas at least partially and temporarily depend on an active lymphangiogenesis and possible even on an increased angiogenesis with its biological patterns. This correlation is well examined for tumor diseases. According to the results in tumor diseases, it can be assumed that a series of growth factors can stimulate or inhibit lymphangiogenesis. An increased VEGF-C expression in different tumors, for instance, is associated with a stimulation of lymphangiogenesis and an increased lymphogenic metastatic spread [28, 43]. In this context, it could be shown that tumors themselves are able to induce lymphangiogenesis [1, 6, 46]. VEGF-C secreted by the tumor stimulates the budding of new lymph vessels and thus increases the infiltrative potential of the tumor and lymphogenic metastasis. Furthermore, due to endothelial

proliferation of the vascular wall intraluminal VEGF-C leads to dilatation of the lymph vessels, assuring the lymphatic drainage from the tumor [1]. Different study groups [19, 41] could demonstrate that tumor-associated macrophages are related to peritumoral lymphangiogenesis and lymphovascular invasion by expressing VEGF-C. Moreover, Jackowski et al. [14] could show that radiogenic lymphangiogenesis during the first years after postoperative radiotherapy for breast cancer might be mediated by VEGF-C expression by invading macrophages. As macrophages are able to express VEGF-C and thus induce local sprouting of lymphatic endothelial cells and trigger growth, and hyperplasia of lymphatic vessels [20] and macrophages seem to be able to transdifferentiate into lymphatic endothelial cells as suggested by Maruyama [30], they may have a crucial role in lymphangiogenesis. However, as VEGF-C leads to peritumoral lymphatic vessel expansion, the finding that the peritumoral lymphatic hyperplasia initiated by VEGF-C overexpression can be reduced by application of anti-VEGFR-3 antibodies [21] seems to be of particular importance.

Conclusion

While in tumor diseases the impact of factors such as VEGF-C und VEGFR-3 on the modulation of the lymphatic system and the induction of lymphangiogenesis was examined in many studies, scientific publications revealing a correlation between lymphangiomas and lymph-angiogenous growth factors are still very rare. Further studies on lymphangiogenesis and the detection of markers of lymphangiogenesis will be necessary to further prove this correlation. Based on this background, therapeutic approaches for the treatment of lymphangiomas could then be developed via modulation of the growth factors.

Conflict of interest statement We declare that we have no conflict of interest.

References

1. Alitalo K (2007) Inhibition of VEGF-C/VEGFR-3 mediated angiogenesis, lymphangiogenesis and metastasis. 2nd International Symposium on Cancer and the lymphovascular System: Basis for rational therapy, San Francisco
2. Alqahtani A, Nguyen LT, Flageole H, Shaw K, Laberge JM (1999) 25 years' experience with lymphangiomas in children. J Pediatr Surg 34:1456–1463
3. Asellius G (1627) De lactibus sive lacteis venis. Milan, J.B. Bidellium, Mediolani
4. Bloom DC, Perkins JA, Manning SC (2004) Management of lymphatic malformations. Curr Opin Otolaryngol Head Neck Surg 12:500–504
5. Brandrup F (1976) Lymphangioma circumscriptum of the tongue. Plast Reconstr Surg 153:191
6. Detmar M (2007) Tumor and lymph node lymphangiogenesis: Impact on metastasis. 2nd International Symposium on Cancer and the Lymphovascular System: Basis for Rational Therapy, San Francisco
7. Enzinger FM, Weiss SW (1995) Tumors of lymph vessels. In: Enzinger FM, Weiss SW (eds) Soft tissue tumors. Mosby-Year Book, St. Louis, pp 679–688
8. Faul JL, Berry GJ, Colby TV, Ruoss SJ, Walter MB, Rosen GD, Raffin TA (2000) Thoracic lymphangiomas, lymphangiectasis, lymphangiomatosis, and lymphatic dysplasia syndrome. Am J Respir Crit Care Med 161:1037–1046
9. Heether J, Whalen T, Doolin E (1994) Follow-up of complex unresectable lymphangiomas. Am Surg 60:840–841
10. Hong YK, Harvey N, Noh YH, Schacht V, Hirakawa S, Detmar M, Oliver G (2002) Prox1 is a master control gene in the program specifying lymphatic endothelial cell fate. Dev Dyn 225:351–357
11. Huang HY, Ho CC, Huang PH, Hsu SM (2001) Co-expression of VEGF and its receptors, VEGFR-2 and VEGFR-3, in endothelial cells of lymphangioma. Implication in autocrine or paracrine regulation of lymphangioma. Lab Invest 81:1729–1734
12. Huntington GS, McClure CFW (1908) The anatomy and development of the jugular lymph sac in the domestic cat. Anat Rec 2:1–19
13. Irrthum A, Karkkainen MJ, Devriendt K, Alitalo K, Vikkula M (2000) Congenital hereditary lymphedema caused by a mutation that inactivates VEGFR-3 tyrosine kinase. Am J Hum Genet 67:295–301
14. Jackowski S, Janusch M, Fiedler E, Marsch WC, Ulbrich EJ, Gaisbauer G, Dunst J, Kerjaschki D, Helmbold P (2007) Radiogenic lymphangiogenesis in the skin. Am J Pathol 171:338–348
15. Jain RK, Padera TP (2003) Lymphatics make the break. Science 299:209–210
16. Joukov V, Pajusola K, Kaipainen A, Chilov D, Lahtinen I, Kukk E, Saksela O, Kalkkinen N, Alitalo K (1996) A novel vascular endothelial growth factor, VEGF-C, is a ligand for the Flt4 (VEGFR-3) and KDR (VEGFR-2) receptor tyrosine kinases. EMBO J 15:290–298
17. Kaipainen A, Korhonen J, Mustonen T, Van Hinsberg V, Fang G, Dumont D, Breitman M, Alitalo K (1995) Expression of the fms-like tyrosine kinase 4 gene becomes restricted to lymphatic endothelium during development. Proc Natl Acad Sci U S A 92:3566–3570
18. Kampmeier OF (1912) The value of the injection method in the study of the lymphatic development. Anat Rec 6:223–233
19. Karkkainen MJ, Haiko P, Sainio K, Partanen J, Taipale J, Petrova TV, Jeltsch M, Jackson DG, Talikka M, Rauvala H, Bersholtz C, Alialo K (2004) Vascular endothelial growth factor C is required for sprouting of the first lymphatic vessels from embryonic veins. Nat. Immun 5:74–80
20. Kerjaschki D (2005) The crucial role of macrophages in lymphangiogenesis. J Clin Invest 115:2316–2319
21. Kuo AH, Hoshida T, Isaka N, Hagendoorn J, di Tomaso E, Chen Y, Pytowski B, Fukumura D, Padera TP, Jain RK (2007) Vascular endothelial growth factor receptor-3 signaling via vascular endothelial growth factor-C increases lymphatic metastasis by influencing tumor cell entry into lymphatic vessels. 2nd International Symposium on Cancer and the Lymphovascular System: Basis for Rational Therapy, San Francisco
22. Kutsuna M (1933) Beiträge zur Kenntnis der Entwicklung des Lymphgefäßsystems der Vögel. Acta Sch Med Kyoto 16:16–25
23. Laurence KM (1955) Congenital cystic pulmonary lymphangioectasis. J Pathol Bacteriol 70:325–333

24. Lawley LP, Cerimele F, Weiss W, North P, Cohen C, Kozakewich HPW, Mulliken JB, Arbiser JL (2005) Expression of Wilms tumor 1 gene distinguishes vascular malformations from proliferative endothelial lesions. Arch Dermatol 141:1297–1300
25. Lee KJ, Klein TR (1980) Surgery of cysts and tumors of the neck. In: Paparella MM, Shumrick DA (eds) Otolaryngology. 2nd ed. WB Saunders, Philadelphia, PA, pp 2987–2989
26. Lymboussaki A, Partanen TA, Oloffson B, Thomas-Crusells J, Fletcher CDM, de Waal RMW, Kaipainen A, Alitalo K (1998) Expression of vascular endothelial growth factor receptor VEGFR-3 in lymphatic endothelium of the skin and in vascular tumors. Am J Pathol 153:395–493
27. Maddalozzo J, Hughes CA, Huang L, Mu Y, Ludemann J, Crawfort S (1999) High angiogenic activity in cells isolated from cystic hygroma: role of bFGF. Arch Otolaryngol Head Neck Surg 125:45–48
28. Madriota SJ, Jussila L, Jeltsch M, Compagni A, Baetens D, Prevo R, Banerji S, Quarte J, Montesano R, Jackson DG, Orci L, Alitalo K, Christofori G, Pepper MS (2001) Vascular endothelial growth factor-C-mediated lymphangiogenesis promotes tumour metastasis. EMBO J 20:672–682
29. Marler J, Mulliken J (2005) Current management of hemangiomas and vascular malformations. Clin Plastic Surg 32:99–116
30. Maruyama K, Ii M, Cursiefen C, Jackson DG, Keino H, Tomita M, Van Rooijen N, Takenaka H, Dámore PA, Stein-Streilein J, Losordo DW, Streilein JW (2005) Inflammation-induced lymphangiogenesis in the cornea arises from CD11b-positive macrophages. J Clin Invest 115:2363–2372
31. McClure CFW, Silvester CF (1909) A comparative study of the lymphatic-venous communication in adult mammals. Anat Rec 3:534–553
32. Mentzel T, Kutzner H (2002) Tumors of the lymphatic vessels of the skin and soft tissue. Pathologe 23:118–127
33. Mentzel T, Kutzner H (2003) Benign and malign lymphatic tumours of skin and soft tissue. In: Browse N, Burnand KG, Mortimer PS (eds) Diseases of the lymphatics. Arnold, London, pp 85–101
34. North PE, Kahn T, Cordisco MR, Dadras SS, Detmar M, Frieden IJ (2004) Multifocal lymphangioendotheliomatosis with thrombocytopenia. Arch Dermatol 140:599–606
35. Paik AS, Lee PHA, O'Grady TC (2007) Acquired progressive lymphangioma in an HIV-positive patient. J Cutan Pathol 34:882–885
36. Petrova TV, Mäkinen T, Mäkela TP, Saarela J, Virtanen I, Ferrell RE, Finegold DN, Kerjaschki D, Ylä-Herttuala S, Alitalo K (2002) Lymphatic endothelial reprogramming of vascular endothelial cells by the Prox-1 homeobox transcription factor. EMBO J 21:4593–4599
37. Phillips HE, McGahan JP (1981) Intrauterine fetal cystic hygroma: sonographic detection. Am J Roentgenol 136:799–802
38. Reis RM, Reis-Filho JS, Longatto Filho A, Tomarev S, Silva P, Lopes JM (2005) Differential Prox-1 and CD 31 expression in mucousae, cutaneous and soft tissue vascular lesions and tumors. Pathol Res Pract 201:771–776
39. Sabin FR (1909) The lymphatic system in human embryos with a consideration of the system as a whole. Am J Anat 9:43–91
40. Schneider M, Othman-Hassan K, Christ B, Wilting J (1999) Lymphangioblasts in the avian wing bud. Dev Dyn 216:311–319
41. Schoppmann SF, Birner P, Stockl J, Kalt R, Ullrich R, Caucig C, Kriehuber E, Nagy K, Alital K, Kerjaschki D (2002) Tumor-associated macrophages express lymphatic endothelial growth factors and are related to peritumoral lymphangiogenesis. Am J Pathol 161:947–956
42. Sidle DM, Maddalozzo J, Meier JD, Cornwell M, Stellmach V, Crawfort SE (2005) Altered pigment epithelium-derived factor and vascular endothelial growth factor levels in lymphangioma pathogenesis and clinical recurrence. Arch Otolaryngol Head Neck Surg 131:990–995
43. Skobe M, Hawighorst T, Jackson DG, Prevo R, Janes L, Velasco P, Riccardi L, Alialo K, Claffey K, Detmar M (2001) Induction of tumor lymphangiogenesis by VEGF-C promotes breast cancer metastasis. Nat Med 7:192–198
44. Song TB, Kim CH, Kim SM, Kim YH, Byun JS, Kim EK (2002) Fetal axillary cystic hygroma detected by prenatal ultrasonography: a case report. J Korean Med Sci 17:400–402
45. Suk S, Sheridan M, Saenger JS (1997) Adult lymphangioma: a case report. Ear Nose Throat J 76:881–883
46. Teymoortash A, Schrader C, Shimoda H, Kato S, Werner JA (2007) Evidence of lymphangiogenesis in Warthin`s tumor of the parotid gland. Oral Oncol 43:614–618
47. Van der Jagt ER (1932) The origin and development of the anterior lymph sacs in the sea turtle. Q J Microbiol Sci 75:151–165
48. Van der Putte SCJ (1977) Lymphatic malformation in human fetuses. Virchows Arch 376:233–246
49. Weingast GR (1988) Congenital lymphangiectasia with fetal cystic hygroma: report of two cases with co-existent Down's syndrome. JCU 16:553–668
50. Werner JA, Dünne AA, Folz BJ, Rochels R, Bien S, Ramaswamy A, Lippert BM (2001) Current concepts in the classification, diagnosis and treatment of hemangiomas and vascular malformations of the head and neck. Eur Arch Otorhinolaryngol 258:141–149
51. Werner JA, Eivazi B, Folz BJ, Dünne AA (2006) State of the art of classification, diagnostics and therapy for cervicofacial hemangiomas and vascular malformations. Laryngorhinootologie 85:883–889
52. Wiggs WJ Jr, Sismanis A (1994) Cystic hygroma in the adult: two case reports. Otolaryngol Head Neck Surg 110:239–241
53. Wigle JT, Harvey N, Detmar M, Lagutina I, Grosveld G, Gunn MD, Jackson DG, Oliver G (2002) An essential role for Prox1 in induction of the lymphatic endothelial cell phenotype. EMBO J 21:1505–1513
54. Wigle JT, Oliver G (1999) Prox1 function is required for the development of the murine lymphatic system. Cell 98:769–778
55. Williams HB (1982) Hemangiomas and lymphangiomas. Adv Surg 15:317–349
56. Wilting J, Kasten P, Schöning G, Bergmann A, Papoutsi M, Weich HA (2007) Model system to study lymphangiogenesis and angiogenesis: lessons for tumor biology. 2nd International Symposium on Cancer and the Lymphovascular System: Basis for Rational Therapy, San Francisco
57. Wilting J, Papoutsi M, Christ B, Nicolaides KH, von Kaisenberg CS, Borges J, Stark GB, Alitalo K, Tomarev SI, Niemeyer C, Rossler J (2002) The transcription factor Prox1 is a marker for lymphatic endothelial cells in normal and diseased human tissues. FASEB J 16:1271–1273
58. Zadvinskis DP, Benson MT, Kerr HH, Mancuso AA, Cacciarelli AA, Madrazo BL, Mafee MF, Dalen K (1992) Congenital malformations of the cervicothoracic lymphatic system: embryology and pathogenesis. Radiographics 12:1175–1189

Virchows Arch (2008) 453:9–16
DOI 10.1007/s00428-008-0637-2

ORIGINAL ARTICLE

Reduced mRNA expression in paraffin-embedded tissue identifies MLH1- and MSH2-deficient colorectal tumours and potential mutation carriers

Annegret Müller · Dirk Zielinski · Nicolaus Friedrichs · Barbara Oberschmid · Sabine Merkelbach-Bruse · Hans K. Schackert · Markus Linnebacher · Magnus von Knebel Doeberitz · Reinhard Büttner · Josef Rüschoff · The German HNPCC Consortium, German Cancer Aid (Deutsche Krebshilfe)

Received: 13 March 2008 / Revised: 2 May 2008 / Accepted: 30 May 2008 / Published online: 26 June 2008

Abstract Based on the principle of nonsense-mediated mRNA decay, we sought to identify MLH1 or MSH2-deficient colorectal tumours through relative quantification of mRNA expression with real-time PCR (RT-PCR) analysis. *MLH1* and *MSH2* mRNAs were almost equally expressed as defined by *MLH1* to *MSH2* transcript ratio (mean 1.41) in microsatellite stable, mismatch repair (MMR) proficient tumours (n=16). A close correlation between loss of protein expression and MMR–mRNA levels was found in highly microsatellite instable (MSI-H) tumours deficient of MLH1 or MSH2. MLH1/MSH2 ratio was low in 11 sporadic and nine hereditary MLH1-deficient carcinomas (mean 0.51), whereas the ratio was high in 17 MSH2-deficient hereditary non-polyposis colorectal cancer (HNPCC) associated carcinomas (mean 6.8). Notably, in the normal tissues of HNPCC patients with *MSH2* mutations, the MLH1/MSH2 transcript ratios were significantly elevated (ratio>2.0) as compared to the ratios of normal mucosa in patients with MMR-proficient tumours (27 of 32 ratio<2.0; p=0.00113). Analysis of B-lymphocytes of HNPCC patients with proven MMR gene mutation confirmed these findings. In conclusion, RT-PCR allows relative quantification of MMR gene mRNA expression in formalin-fixed and paraffin-embedded tissue. Furthermore, this approach enables quantification of haploinsufficiency due to nonsense-mediated mRNA decay in normal tissue and B-lymphocytes from patients carrying MSH2 germline mutations and may be useful for identification of asymptomatic carriers of pathogenic germline mutations.

Keywords Diagnostic tool · MMR-deficient tumours · Nonsense-mediated decay · qRT-PCR

Hereditary non-polyposis colorectal cancer (HNPCC) is an autosomal dominantly inherited syndrome that accounts for approximately 1–3% of all colorectal carcinomas [1, 8, 20, 21].

Members of the German HNPCC Consortium are listed in the Appendix.

A. Müller
Department of General Surgery, University of Göttingen, Göttingen, Germany

A. Müller · D. Zielinski · B. Oberschmid · J. Rüschoff
Institute of Pathology Nordhessen and Targos Molecular Pathology GmbH,
Kassel, Germany

N. Friedrichs · S. Merkelbach-Bruse · R. Büttner (✉)
Institute of Pathology, University Hospital Bonn,
Sigmund Freud Strasse 25,
53125 Bonn, Germany
e-mail: Reinhard.Buettner@ukb.uni-bonn.de

H. K. Schackert
Department of Surgical Research,
Technische Universität Dresden,
Dresden, Germany

M. Linnebacher
Institute of Molecular Diagnostics, University of Rostock,
Rostock, Germany

M. von Knebel Doeberitz
Institute of Molecular Pathology, University of Heidelberg,
Heidelberg, Germany

HNPCC is caused by mutations in DNA mismatch repair (MMR) genes *MSH2*, *MLH1*, *MSH6* and *PMS2* [2, 8, 20, 21, 29]. The vast majority of HNPCC cases are carriers of mutations in *MSH2* and *MLH1*, most of which result in protein truncation [19]. Germline mutations in *MSH6* or *PMS2* seem to be rare [2, 11, 19, 25, 26]. It has been estimated that the lifetime risk for cancer approaches 80% for carriers of MMR germline mutations [2, 11, 9, 14, 19, 25, 26].

Consequently, detection of mutation carriers before tumour development is crucial since early and intensive screening measures can reduce morbidity and mortality in individuals at risk. Screening methods are microsatellite instable (MSI) testing as a functional analysis of the MMR system [15, 18, 28, 12] and immunohistochemical analysis of MMR gene expression in tumours [9, 22, 30] which identifies the mutated gene and allows focused mutation analysis [6, 27].

Expression of one wildtype allele seems to be sufficient to sustain mismatch repair capacity in normal tissue in carriers of one mutated MMR gene allele. Somatic inactivation of the wildtype allele is necessary for tumour development. Therefore, analysis of protein expression of MMR genes and MSI testing are meaningful if applied to tumours but not if applied to normal tissue. Consequently, carcinoma tissue of an index patient must be available to identify the deficient MMR gene and, based on these results, testing for germline mutation can be initiated.

It has to be assumed that protein expression of MMR genes in normal and tumour tissue correlates with the amount of corresponding mRNA. Nonsense-mediated mRNA decay (for review see Hentze and Kulozik [10]) results in decreased expression of the mutated MMR allele in normal tissue of carriers of pathogenic germline mutations. Almost complete loss of mRNA expression may be found in tumours, which have lost the wildtype allele in addition [3, 13, 17]. Based on these assumptions, we developed a real-time qRT-PCR approach for mRNA quantification of the mismatch repair genes *MSH2* and *MLH1* and compared mRNA levels with protein levels in paraffin-embedded tumours. Normal tissue and B-lymphocytes from carriers of pathogenic MMR gene mutations served as controls.

Materials and methods

Patient and tissue specimens

Our study included 54 pairs of paraffin-embedded tissue samples representing matched normal mucosa and tumour from 53 patients who had undergone surgery for colorectal cancer (Table 1).

Tissue blocks were selected from the archives of the Institutes of Pathology, Klinikum Kassel and University of Bonn (Germany). All specimens were supplied by the German HNPCC Consortium.

Three different study groups were created:

1. Sixteen cases had microsatellite stable (MSS) carcinomas with regular immunohistochemical expression of MLH1 and MSH2. Patients' age ranged from 33 to 82 years (mean 65).
2. The second group consisted of 11 patients with highly microsatellite instable (MSI-H) tumours which exhibited immunohistochemical loss of MLH1 protein expression. Patients' age ranged from 64 to 92 years (mean 79) and they had a negative family history. In these cases, the MLH1 gene was most likely inactivated by promoter hypermethylation.
3. The third group comprised 27 tumours from 26 patients. All carcinomas were MSI-H and immunohistochemistry revealed complete loss of either MLH1 or MSH2 protein expression except for one patient with

Table 1 Summary of tissue samples used for this study

	MMR status			
	Proficient	Deficient		
		MLH1-sporadic	MLH1-hereditary	MSH2-hereditary
Tissue				
Tumour	16	11	9	17
Normal	16	11	10	17
	Non-pathogenic mutation		Pathogenic mutation	
Cell lines	3	–	5	9

Tissue samples and B-lymphocyte cultures are given according to their mismatch repair status (MMR). The MMR-deficient cases were separated into a *MLH1* sporadic, a *MLH1* and a *MSH2* HNPCC-associated group. In one MLH1-deficient HNPCC-associated case, RT-PCR data of tumour tissue did not meet the quality inclusion criteria; only the normal tissue was included

two synchronous right-sided carcinomas. One tumour expressed MSH2 and the other was MSH2 negative. Patients' age ranged from 33 to 66 years (mean 58 years). These cases met the Amsterdam criteria for HNPCC and genetic testing revealed pathogenic *MSH2* or *MLH1* mutations in 19 of 27 cases. All mutations lead to a stop codon, reflecting the loss of protein expression. We did not find a pathogenic mutation in all cases probably due to mutations in the promotor region or large genomic deletions. The percentage of pathogenic mutations in these patients is in the range of the HNPCC international study group.

Lymphocyte cell cultures

B-lymphocytes were obtained from 14 HNPCC patients with proven pathogenic mutation of MLH1 (n=5) and MSH2 (n=9) genes. Three cell lines of healthy individuals served as controls. The generation of B-lymphocyte cell cultures was performed as described previously [16].

MSI analysis and immunohistochemical analyses

All tumour tissues were subjected to MSI analysis as described in detail previously [20].

In accordance with the recommendation of the NCI and the ICG–HNPCC [24], five microsatellite loci were used in all tumour lesions for MSI analysis, two loci with mononucleotide repeats (BAT25 and BAT26) and three loci with CA dinucleotide repeats (D2S123, D5S346 and D17S250). If all microsatellites were identical in tumour and normal tissues, the case was reported as MSS; if two or more microsatellites differed between tumour and normal tissues, the case was reported as MSI-H. Losses of heterozygosity were not regarded as microsatellite instable. If only one microsatellite differed between tumour and normal tissues, the five additional microsatellites recommended by the IHC–HNPCC were analysed. Cases with a minimum of two unstable loci were reported as MSI-H. The primer sequences of these microsatellite loci were reported previously [6].

Loss of MMR protein expression was determined by immunohistochemical analysis in carcinomas using monoclonal antibodies against MSH2 and MLH1 as described in detail earlier [28]. Only slides with distinct positive nuclear staining in the basal crypt cells of normal mucosa, stromal as well as inflammatory cells were evaluated. Loss of MMR protein expression within the neoplastic lesions was defined as complete when less than 10% of tumour cells were stained. Incomplete loss (10–50% stained cells) or only focal staining (cohesive nests of stained tumour cells) was recorded as positive.

RNA extraction and cDNA synthesis

Total RNA of tumour tissue and corresponding normal tissue were prepared from formalin-fixed deparaffinised sections with HighPure RNA Paraffin Kit (Roche) according to the manufacturer's instructions. To avoid sampling errors, only parts of the tissue sections that contained either at least 80% malignant cells in the carcinomas or only normal mucosa in the matched controls were used.

Total RNA of cells cultured in vitro was extracted using the HighPure RNA Extraction Kit (Roche) according to the manufacturer's instructions.

Extracted RNA from tissues and cell cultures were reverse transcribed to cDNA using the AMV-RT Kit (Roche) with MLH1rev and MSH2rev as specific primers (Table 2) and G6PDH as the reference transcript (Roche).

Relative quantification of mRNA expression by real-time PCR (RT-PCR) analysis

To analyse the expression status of the genes of interest, the relative amount of the synthesised cDNA molecules was determined by quantitative real-time PCR (LightCycler System, Roche) using the RelQuant Software (Roche). As control, mRNA from cultured cell lines with defined levels

Table 2 Primers used for real-time PCR

Primer	Sequence 5′→3′	Length	5′ position
MLH1 for	GATTACCCCTTCTGATTGACA	21	1,934
MLH1 rev	ACTGAGGCTTTCAAAACA	19	2,052
MLH1 anchor	GGAGGGACTGCCTATCTTCAT–fluorescein	21	1,971
MLH1 red	LightCycler Red 640-TTCGACTAGCACTGAGGTGAA	22	1,994
MSH2 for	CAGTATATTGGAGAATCGCA	20	2,631
MSH2 rev	AGGGCATTTGTTTCACC	17	2,754
MSH2 anchor	CATGGAACCAGCAGCAAAGA–fluorescein	20	2,663
MSH2 red	LightCycler Red 640-TGCTATCTGGAAAGAGAGCAAGG	23	2,685
G6PDH	LightCycler ref. detection mixes from DPD mRNA Quantif. KitPlus (Roche)		

of MLH1 and MSH2 mRNA was used (DPD mRNA Quantif. KitPlus, Roche) and after reverse transcription taken as calibrator cDNA.

The PCR results were controlled using polyacrylamide gel electrophoresis and the PCR products were sequenced using the ABI PRISM 310® Genetic Analyzer (Applied Biosystems) to verify the nucleotide sequence.

For standardisation and exclusion of low quality specimens, expression analysis of glucose-6-phosphatase-dehydrogenase (G6PDH) was run as an internal quality control. Through dilution series a cut-off of 10^2 G6PDH copies was determined as the lower level of detection. In order to compensate for further potential inter-individual or inter-specimen variations, a quotient from MLH1 (numerator) to MSH2 (denominator) was formed by calculating their crossing point as follows: The RelQuant software (Roche) uses crossing point (CP) as basis for the calculation of different mRNA (cDNA) levels. In a first step, the software determined the ratio concentration, which is defined by the ratio of the median CP value of the numerator replicates divided by the median CP value of the denominator replicates. For normalisation, the following algorithm was used: normalised ratio=[ratio concentration sample/(ratio conc. calibrator)×correction factor]×multiplication factor. Calibrator RNA derived from a cell line as well as correction and multiplication factor were provided by the manufacturer (DPD mRNA Quantif. KitPlus, Roche). Overexpression or a loss of expression was defined in relation to the calibrator. In case of identical ratio values from sample to calibrator, both mRNA species must be expressed equally. In addition, values of MLH1 or MSH2 mRNA copy number were only accepted for further calculation if the deviation of the CP value from the sample duplicates in LightCycler runs was <1.0. All measurements were done in triplicate. From a biological point of view, this reflects recent observations that in quantitative RT-PCR analyses housekeeping genes such as G6PDH vary between different tissues and thus must be defined according to the sample studies [7]. In addition, there is strong evidence that MLH1 and MSH2 are co-regulated, e.g. by hypoxia leading to the coordinated repression of MLH1 and MSH2 [5]. Thus, putting MLH1 and MSH2 in a quotient compensates for such superimposed alterations in expression and activation patterns affecting both DNA repair genes.

Data analysis

Statistical data analysis was performed using the JMP software Version 4 (SAS Institute Inc., Cary, USA). Wilcoxon test was used to assess the significance of intergroup differences. The cut-off point for significance was set to $p<0.05$.

Results

Feasibility of relative quantification of MMR gene expression by qRT-PCR

Quantification of mRNA of MLH1 and MSH2 in paraffin-embedded tissues and in B-lymphocytes cultured in vitro turned out to be a reliable and reproducible technique if adequate controls were used.

After exclusion of 16% of initially analysed samples due to low copy number (data not shown), all cases included in this study had G6PDH mRNA copy numbers over 10^2. The mean MLH1/MSH2 ratio value of MSS normal and tumour tissue was used as cut-off value in paraffin-embedded tissue being 1.2 in normal and 1.4 in tumour samples and of about 1.0 in B-lymphocytes cultured in vitro from patients with MMR-proficient tumours.

qRT-PCR in tumour tissue

In tumour tissue, there was a close correlation between mRNA and immunohistochemical expression levels (Fig. 1). The mean ratio of MLH1 and MSH2 mRNA expression measured by LightCycler qRT-PCR was 1.41 (range 0.47 to 5.13) in MMR-proficient colorectal cancer samples. Only in one case the tumour tissue (MLH1 deficient) was excluded from analysis due to the abovementioned quality control measures (Table 1).

In the MLH1-deficient tumours, the ratio values were below 1 with mean values of 0.51 in hereditary and 0.42 in sporadic tumours indicative of a reduced MLH1 mRNA copy number.

In the MSH2-deficient tumour group, the mean MLH1/MSH2 ratio value was 6.02 in hereditary tumours indicating a severely reduced MSH2 mRNA copy number. One patient carried two synchronous MSI-H colon cancers with loss of MSH2 expression in one tumour and preserved MSH2 protein expression in the second tumour. As shown in Fig. 1, the MLH1/MSH2 ratio depicts this difference by a high value in the MSH2-negative (ratio 8.94) and a low value (ratio 0.46) in the MSH2-positive carcinoma.

The difference in MLH1 and MSH2 ratios between MLH1- or MSH2-deficient and proficient tumours was statistically highly significant ($p<0.001$).

qRT-PCR in normal tissue

The mean value ratio of MLH1 and MSH2 mRNA measured by LightCycler PCRs was 1.22 (range 0.25 to 1.93) in normal MSS tissue samples (Fig. 2a). Consistently, very similar ratios were measured in normal mucosa

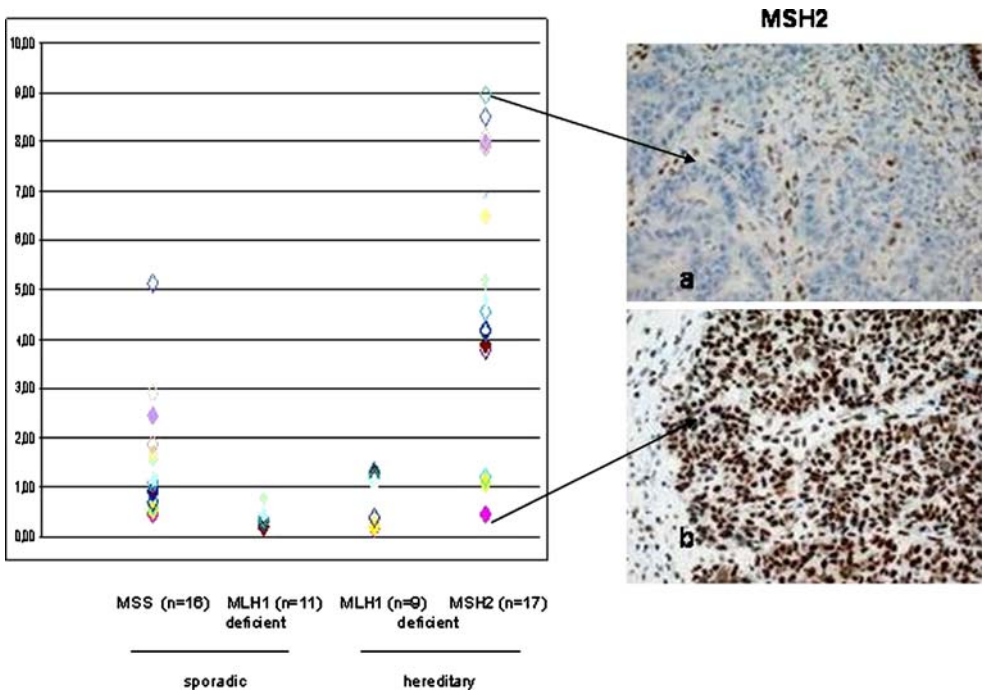

Fig. 1 Results of the real-time PCR LightCycler (RT-PCR) analysis in tumour tissue calculated as the ratio of quantitative expression of MLH1 through MSH2. Each symbol represents the analysis of one tissue as a mean of three runs. The correlation of protein expression level as evidenced by immunohistochemistry and mRNA levels is shown by representative pictures in a HNPCC patient with two synchronous tumours. The tumour with loss of protein expression (**a**) revealed the highest MLH1/MSH2 mRNA ratio, whereas the tumour with retained expression (**b**) showed the lowest corresponding ratio value. The mean value of MSS tumour tissue without loss of repair gene expression is given as *dotted line*

samples from patients with sporadic MLH1-deficient tumours (mean 1.27; range 0.25 to 2.12).

In patients with hereditary MSH2-deficient carcinomas, the ratios were equal or higher than 2.0, which is a statistically highly significant elevation compared to the ratios in the normal mucosa of cases with MSS or sporadic MLH1-deficient carcinomas ($p=0.00113$). These data indicate haploinsufficiency of *MSH2* in normal cells of HNPCC patients. Apparently, this difference is below the level of detection by immunohistochemistry as the staining intensi-

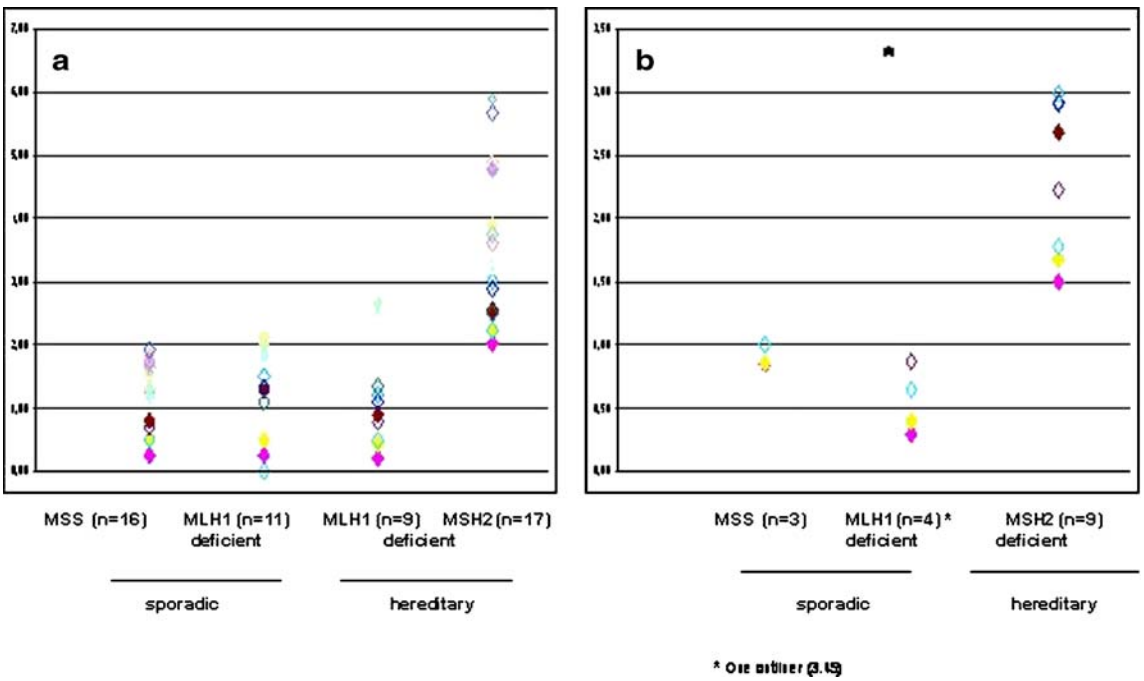

Fig. 2 Results of the RT-PCR analysis of corresponding normal mucosa tissue calculated as the ratio of quantitative expression of MLH1 through MSH2 in normal mucosa (**a**) and in B-lymphocyte cell lines (**b**). The mean value of the three normal control B-lymphocyte cell lines without loss of repair gene expression is given as *dotted line*

ties in MSS, MLH1 and MSH2 deficient tissue samples were identical (data not shown).

The ratios in normal tissue of hereditary MLH1-deficient patients were not significantly different from the MSS- and sporadic MLH1-deficient mucosa samples. It is known that MLH1 deficiency in these tumours results from promotor methylation and possibly variable mRNA expression occurs in the respective normal tissue.

qRT-PCR in B-lymphocytes

The mean value ratio of MLH1/MSH2 mRNA in B-lymphocytes of normal controls (n=3) was 0.9 (range 0.85–1.00). All MSH2-deficient cell lines (n=9) had ratio values above this value (Fig. 2b), whereas in four of five MLH1-deficient cell lines, ratio values were below this value (ranging from 0.30 to 0.87 with one outlier with 3.45). These data again are in favour of significant haploinsufficiency in MSH2 gene expression in B-lymphocytes of patients with MSH2 germline mutations (p<0.001).

Discussion

The present study demonstrates for the first time that quantification of mRNA expression of the mismatch repair genes *MLH1* and *MSH2* in routinely formalin-fixed and paraffin-embedded tissue is a valid and reliable method using quantitative real-time PCR (qRT-PCR). Determination of the ratio between *MLH1* and *MSH2* mRNA copy numbers showed a close correlation with immunohistochemical loss of MMR gene expression. Furthermore, we demonstrate that reduced mRNA expression of *MSH2* in normal tissue of HNPCC patients carrying pathogenic mutations, which is most likely due to haploinsufficiency, can be quantified by our approach.

For quality control and standardisation, calibrator RNA served as a reference for the samples against a stable system and controlled for variation of reverse transcription and PCR performance. Low copy numbers of the calibrator point to an error during analysis, whereas low copy numbers of the patient samples are a sign of flaws during the process of tissue sampling via fixation to RNA isolation. Special attention was paid to the quality of samples. Accordingly, we used the reference gene G6PDH as a further internal control for RNA integrity. Only reactions that showed a copy number of at least 10^2 mRNA molecules were evaluated. In addition, values of MLH1 or MSH2 gene copy numbers were only accepted for further calculation if the difference of the double-checked CP values was <1.0. Using these safety precautions, we could clearly identify and exclude from evaluation four samples that were sent in for consultation without information on type of fixation and age of sample (data not shown).

We calculated the transcript ratio of *MLH1* to *MSH2*, which further compensates for potential inter-individual and inter-specimen variations. Indeed, this ratio turned out to be a valid parameter for detection of differences in MMR gene mRNA expression and correlated very well with immunohistochemical results. This reflects recent observations that in quantitative RT-PCR analyses housekeeping genes such as G6PDH vary between different tissues and thus must be defined according to the sample studies [7]. In addition, there is strong evidence that MLH1 and MSH2 are co-regulated, e.g. by hypoxia leading to the coordinated repression of MLH1 and MSH2 [5].

Accordingly, carcinomas with complete loss of MLH1 protein had ratios at the lower range level (most <0.5). In contrast, tumours showing complete loss of MSH2 protein expression were in the upper range level (>3.0). In one HNPCC patient with synchronous MSI-H colonic carcinomas, one tumour showed complete loss of MSH2 and thus the ratio was high with 8.94. Remarkably, the second tumour stained strongly MSH2 positive, and consistently the ratio was very low (0.46). A possible explanation for this observation might be that the two tumours differ in their second hit mutation leading to a still expressed, albeit not functional, protein in one and to a truncated non-detectable protein in the other tumour.

Another interesting observation is related to the expression levels within the normal mucosa. Regarding specimens of patients with sporadic MSS carcinomas, ratios between MLH1 and MSH2 were similar to ratios in normal tissue of MLH1-deficient tumours, while ratios of normal tissue of patients carrying MSH2-deficient tumours were significantly higher. This observation was clearly confirmed by our data with B-lymphocytes obtained and cultured in vitro from patients with proven germline mutations in the MMR genes and indicate a haploinsufficiency of *MSH2* in non-tumorigenic cells of HNPCC patients.

The ratios of MLH1-associated HNPCC cases were not statistically significantly different from the sporadic cases. We should have expected that MLH1 to MSH2 ratios were very low compared to the sporadic cases. This was demonstrated by Tournier et al. showing a reduced MLH1 mRNA level of HNPCC patients versus normal blood donors on a denaturing high-performance liquid chromatography-based method [31]. In our study, we analysed colonic mucosa, where the phenomenon of increasing methylation of the colonic mucosa with age is one factor leading to similar results in both groups.

To our knowledge, this study shows for the first time the possibility to evaluate the expression of mismatch repair protein mRNA by means of quantitative RT-PCR in paraffin-embedded archival tissue. We expect an even more distinctive separation of MMR-proficient and MMR-deficient tumours on one hand and between MLH1- and MSH2-deficient

normal tissues if more refined sampling procedures such as laser microdissection and methylation-specific analysis will be used [4, 23, 25].

Thus, we regard this technique as a real step forward in MMR gene expression analysis particularly in normal tissue where immunohistochemistry alone does not allow any differentiation between cases with or without germline mutation in one of the MMR genes.

Our approach, if confirmed within the ongoing studies of the German HNPCC Consortium, which currently serves for more than 3,000 families being at risk for HNPCC, may be a potential screening tool for identification of asymptomatic carriers of a pathogenic germline mutation.

Acknowledgements The work of the Consortium is supported by a multi-center grant from the Deutsche Krebshilfe (German Cancer Aid), Bonn, Germany. This study is in part the diploma thesis of D.Z. We thank Katja Bräutigam and Katja Goldacker for excellent technical assistance.

This work is also supported by the DFG-Grand 1304 (Klinische Forschergruppe 179)

Conflict of interest statement We declare that we have no conflict of interest

Appendix

The German HNPCC Consortium consists of the following centers (in alphabetic order): Bochum (K Schulmann, FE Brasch, JT Epplen, KM Müller, C Pox, S Stemmler, J Willert), Bonn (in addition to authors: W Friedl, J Girmscheid, A Hirner, C Lamberti, M Mathiak, P Propping, T Sauerbruch, K Siberg), Düsseldorf (G Moeslein, T Goecke, A Hansmann, S Höwer, C Poremba, A Unger, C Wieland), Dresden (in addition to authors: D Aust, F Balck, R Höhl, S Krüger, E Schröck, S Pistorius), Heidelberg (in addition to authors: F Cremer, J Gebert, M Keller, P Kienle, M Kloor, U Mazitschek, M Tariverdian), München/Regensburg (in addition to authors: I Becker, E Holinski-Feder, G Keller, R Kopp, Y Müller-Koch, K Ott, P Rümmele), center for reference pathology Kassel and center for documentation and biometry in Leipzig (in addition to authors: J Forberg, M Herold, M Loeffler, J Schaefer, R Speer).

References

1. Aaltonen LA, Salovaara R, Kristo P, Canzian F, Hemminki A, Peltomäki P, Chadwick RB, Kääriäinen H, Eskelinen M, Järvinen H, Mecklin JP, Chapelle de la (1998) Incidence of hereditary nonpolyposis colorectal cancer and the feasibility of molecular screening for the disease. N Engl J Med 338(21):1481–1487
2. Aarnio M, Sankila R, Pukkala E, Aaltonen LA, de la Chapelle A, Peltomäki P, Mecklin JP, Jarvin HJ (1998) Cancer risk in mutation carriers of DNA-mismatch-repair genes. Int J Cancer 81(2):214–218
3. Abu-Safieh L, Vithana EN, Mantel I, Holder GE, Pelosini L, Bird AC, Bhattacharya SS (2006) A large deletion in the adRP gene PRPF31: evidence that haploinsufficiency is the cause of disease. Mol Vis 18:384–388
4. Bai AH, To KF, Chan WF, Man EP, Lo KW, Lee JF, Sung JJ, Leung WK (2004) Promotor hypermethylation of tumor-related genes in the progression of colorectal neoplasia. Int J Cancer 10:846–853
5. Brinda RS, Glazer PM (2007) Co-repression of mismatch repair gene expression by hypoxia in cancer cells: role of the Myc/Max network. Cancer Lett 252:93–103
6. Dietmaier W, Wallinger S, Bocker T, Kullmann F, Fishel R, Rüschoff J (1997) Diagnostic microsatellite instability: definition and correlation with mismatch repair protein expression. Cancer Res 57:4749–4756
7. Durand-Faucher K, Rabinovitch-Chable H, Dzugan H, Charret S, Aubry K, Genet D, Léobon S, Tubiana-Mathieu N, Cook-Moreau J, Rigaud M, Sturtz FG (2005) A quantitative RT-PCR method to determine topoisomerase I mRNA levels in human tissue samples. Clin Chem Lab 43:707–714
8. Evans DG, Walsh S, Jeacock J (1997) Incidence of hereditary non-polyposis colorectal cancer in a population-based study of 1137 consecutive cases of colorectal cancer. Br J Surg 84 (9):1281–1285
9. Gryfe R, Gallinger S (2001) Microsatellite instability, mismatch repair deficiency, and colorectal cancer. Surgery 130:17–20
10. Hentze MW, Kulozik AE (1999) A perfect message: RNA surveillance and nonsense-mediated decay. Cell 5:3007–3010
11. Holmberg M, Kristo P, Chadwicks RB, Mecklin JP, Jarvinen H, de la Chapelle A, Nystrom-Lahti M, Peltomaki P (1998) Mutation sharing, predominant involvement of the MLH1 gene and description of four novel mutations in hereditary nonpolyposis colorectal cancer. Mutations in brief no. 144. Online.. Hum Mutat 11(6):482–486
12. Jass JR (2000) hMLH1 and hMSH2 immunostaining in colorectal cancer. Gut 47:315–316
13. Laimer M, Klausegger A, Aberer W et al (2006) Haploinsufficiency due to deletion within the 3′-UTR of C1-IHN-gene associated with hereditary angioedema. Gent Med 8:249–254
14. Lamberti C, Kruse R, Ruelfs C, Caspari R, Wang Y, Jungck M, Mathiak M, Malayeri HR, Friedl W, Sauerbruch T, Propping P (1999) Microsatellite instability—a useful diagnostic tool to select patients at high risk for hereditary non-polyposis colorectal cancer: a study in different groups of patients with colorectal cancer. Gut 44:839–843
15. Lanza G, Gafà R, Maestri I, Santini A, Matteuzzi M, Cavazzini L (2002) Immunohistochemical pattern of MLH1/MSH2 expression is related to clinical and pathological features in colorectal adenocarcinomas with microsatellite instability. Mod Pathol 15:741–749
16. Linnebacher M, Gebert J, Woerner S, Yuan YP, Bork P, von Knebel Doeberitz M (2004) Frameshift peptode-derived T-cell epitopes: a source of novel tumor-specific antigens. Int J Cancer 2001; 93:6–11
17. Liu Q, Jiang L, Liu WL, Kang XJ, Ao Y, Sun M, Luo Y, Song Y, Lo WH, Zhang X (2006) Two novel mutations and evidence for haploinsufficiency of the ADAR gene in dyschromatosis symmetrica hereditaria. Br J Dermatol 154:636–642
18. Loukola A, Eklin K, Laiho P, Salovaara R, Kristo P, Jarvinen H, Mecklin JP, Launonen V, Aaltonen LA (2001) Microsatellite marker analysis in screening for hereditary nonpolyposis colorectal cancer (HNPCC). Cancer Res 61:4545–4549
19. Lynch HT, de la Chapelle A (1999) Genetic susceptibility to non-polyposis colorectal cancer. J Med Genet 36:801–818
20. Lynch HT, Chapelle de la A (2003) Hereditary colorectal cancer. N Engl J Med 2 348:919–932

21. Mangold E, Pagenstecher C, Friedl W, The German HNPCC Consortium (2005) Spectrum and frequencies of mutations in MSH2 and MLH1 identified in 1721 German families suspected of hereditary nonpolyposis colorectal cancer. Int J Cancer 2005:692–702
22. Müller W, Burgart LJ, Krause-Paulus R, Thibodeau SN, Almeida M, Bocker Edmonston T, Boland CR, Sutter C, Jass JR, Lindblom A, Lubinski J, MacDermot K, Sanders DSA, Morreau H, Müller A, Oliani C, Orntoft T, Ponz De Leon M, Rosty C, Rodriguez-Bigas M, Rüschoff J, Ruszkiewicz A, Sabourin J, Salovaara R, Möslein G, the ICG-HNPCC (2001) The reliability of immunohistochemistry as a prescreening method for the diagnosis of hereditary nonpolyposis colorectal cancer (HNPCC)—results of an international collaborative study. Familial Cancer 1:87–92
23. Müller A, Guiffre G, Bocker Edmonston T, Mathiak M, Roggendorf B, Heinmöller E, Brodegger T, Tuccari G, Mangold E, Buettner R, Rüschoff J (2004) Challenges and pitfalls in HNPCC screening by microsatellite analysis and immunohistochemistry. J Mol Diag 6:308–315
24. Nuovo GJ, Nakagawa H, Sotamaa K et al (2006) Hypermethylation of the MLH1 promotor with concomitant absence of transcript and protein occurs in small patches of crypt cells in unaffected mucosa from sporadic colorectal carcinoma. Diag Mol Path 15:17–23
25. Plaschke J, Krüger ST, Pistorius ST, Theissig F, Saeger HD, Schackert HK (2002) Involvement of hMSH6 in the development of hereditary and sporadic colorectal cancer revealed by immunostaining is based on germline mutations, but rarely on somatic inactivation. Int J Cancer 97:643–648
26. Peltomäki P (2001) Deficient DNA mismatch repair: a common etiologic factor for colon cancer. Hum Mol Genet 10:735–740
27. Rigau V, Sebbagh N, Olschwang S, Paraf F, Mourra N, Parc Y, Flejou JF (2003) Microsatellite instability in colorectal carcinoma. The comparison of immunohistochemistry and molecular biology suggests a role for hMSH6 immunostaining. Arch Pathol Lab Med 127:694–700
28. Rüschoff J, Bocker T, Schlegel J, Stamm G, Hofstaedter F (1995) Microsatellite instability: new aspects in the carcinogenesis of colorectal carcinoma. Virchow Arch 426:215–222
29. Salovaara R, Loukola A, Kristo P, Kääriäinen H, Ahtola H, Eskelinen M, Härkönen N, Julkunen R, Kangas E, Ojala S, Tulikoura J, Valkamo E, Järvinen H, Mecjklin JP, Aaltonen LA, Chapelle de la A (2000) Population-based molecular detection of hereditary nonpolyposis colorectal cancer. J Clin Oncol 11:2193–2200
30. Thibodeau SN, French AJ, Roche PC, Roche PC, Cunningham JM, Tester DJ, Lindor NM, Moslein G, Baker SM, Liskay RM, Burgart LJ, Honchel R, Halling KC (1996) Altered expression of hMSH2 and hMLH1 in tumors with microsatellite instability and genetic alterations in mismatch repair genes. Cancer Res 56:4836–4840
31. Tournier I, Raux G, Di Fiore F, Marechal I, Leclerc C, Martin C, Wang Q, Buisine MP, Stoppa-Lyonnet D, Olschwang S, Frebourg T, Tosi M (2004) Analysis of the allele-specific expression of the mismatch repair gene MLH1 using a simple DHPLC-based method. Hum Mutat 23(4):379–384

Virchows Arch (2008) 453:17–24
DOI 10.1007/s00428-008-0601-1

ORIGINAL ARTICLE

Strategies for optimizing pathologic staging of sentinel lymph nodes in breast cancer patients

Eva V. E. Madsen · Jan van Dalen · Joost van Gorp · Inne H. M. Borel Rinkes · Thijs van Dalen

Received: 24 November 2007 / Revised: 17 February 2008 / Accepted: 19 February 2008 / Published online: 18 June 2008

Abstract Due to the extensive pathologic evaluation of the sentinel lymph node (SLN), micrometastases are frequently observed. If micrometastases are clinically relevant, the histopathologic examination of SLNs should be sensitive enough to detect them. The probability of detecting micrometastases was calculated when examining the SLN according to the current Dutch pathology protocol and strategies evaluated to optimize the chance of detection. The dimensions of 20 consecutive axillary SLNs in patients with cT1-2N0 breast cancer were measured. In a mathematical model, the probability of detecting micrometastases in a SLN was calculated. Similarly, strategies to optimize the probability of detecting micrometastases were explored. When applying the pathology guidelines, the calculated probability to detect a micrometastasis was 18% for a 200-μm micrometastasis and 69% for a 2.0-mm metastasis in a median sized SLN. To detect the smallest micrometastasis in a median-sized SLN with a 95% probability, the interval between the sections must be decreased to 200 μm, and 20 levels from both halves must be examined. Given a prognostic significance of micrometastases, our current pathology guidelines are not sensitive enough. The number of sections should be increased, while the interval between cuts should be no more than 200 μm.

Keywords Breast cancer · Micrometastases · Pathology · Sentinel lymph node · Staging

E. V. E. Madsen · T. van Dalen (✉)
Department of Surgery, Diakonessenhuis,
Bosboomstraat 1,
3582 KE Utrecht, The Netherlands
e-mail: TvDalen@diakhuis.nl

J. van Gorp
Department of Pathology, Diakonessenhuis,
Utrecht, The Netherlands

J. van Dalen
Department of Information and Decision Sciences,
RSM Erasmus University Rotterdam,
Rotterdam, The Netherlands

I. H. M. Borel Rinkes
Department of Surgery, University Medical Center Utrecht,
Utrecht, The Netherlands

Introduction

Sentinel lymph node (SLN) biopsy has proven to be an accurate staging procedure in breast cancer patients and has replaced axillary lymph node dissection (ALND) in clinically "node negative" axillas [20].

The extensive pathology workup of SLNs has resulted in a frequent observation of micrometastases [2, 6]. The clinical relevance of small lymph node metastasis (TNM-stage N1mi) is still under debate. Some argue that the prognosis of patients with N1mi is similar to the outcome of patients with no lymph node (N0) involvement. Others, however, believe that N1mi is of prognostic significance and hence consider TNM-stage N1mi as an indication for adjuvant systemic therapy [15, 16, 18, 22].

When micrometastases are clinically relevant, it is important that the histopathologic examination is sensitive enough to detect them. The current Dutch pathology guideline advocates to bisect a SLN, submit both slices, and examine three levels at 250-μm intervals. Yet, various other protocols are in use by different laboratories [7]. The pathology protocol may well have an effect on the probability to detect micrometastases and consequently influence treatment [2, 13].

Using a mathematical model, the probability of finding micrometastases within a SLN, examined according to the

national guidelines, was calculated. Subsequently, the model was used to optimize histopathologic workup of SLNs.

Materials and methods

A mathematical model was designed to calculate the probabilities of detecting micrometastases within a SLN. To address these probabilities for an average SLN, the size of a SLN in breast cancer patients was assessed first. Subsequently, the model was used to assess the chances of detecting micrometastases when a SLN was examined following the national pathology guideline. Lastly, alternative strategies to optimize histopathologic workup were tested.

The Dutch national pathology guideline for the examination of SLNs and definition of micrometastases

The guideline for evaluating SLNs advocates to bisect SLNs and to take three cuts from both halves starting from the center with 250-μm distance between two cuts. SLNs thicker than 10 mm are sectioned into 2-mm slices. It is advised that samples are stained both with hematoxylin and immunohistochemically with antibodies to cytokeratin [3].

A micrometastasis was defined as a tumor deposit in the SLN ≥200 μm and ≤2 mm corresponding with N-stage N1mi in the latest TNM classification [24].

The size of a SLN

Twenty consecutive SLNs were retrieved during the operations of 12 women with cT1-2N0 breast cancer. After surgical extirpation and clearance of the surrounding fat of the SLN and before fixation in the pathology department, the SLN was measured by the pathologist. Length, height, width, and volume of the SLN were assessed. Volume was measured by placing the SLN in a cylinder with water, determining the volume of the SLN by the volume shift of the water.

The probability of detecting metastases in a SLN

A mathematical model was designed to calculate the probability that a single lymph node micrometastasis would be detected by the nationally advocated histopathologic examination protocol for SLN in breast cancer patients.

Figure 1 sketches the various assumptions and quantities involved in modeling the detection of metastasis in a SLN. A SLN is assumed to be aptly represented by a triaxial ellipsoid shape with parameters (half lengths) a_x, a_y, and b corresponding with the Euclidian dimensions x, y and z, where x and y are the dimensions of a coupe (with zero thickness) and z is the dimension from which the cuts are taken. In line with current Dutch guidelines, it holds that $a_x \geq a_y \geq b > 0$. The metastasis is represented as a ball shape with diameter m. A circular shape of a micrometastasis and random location of the micrometastasis within the SLN were assumed.

When applying the Dutch pathology guideline, detection of micrometastases is based on six cuts (three cuts for both halves) of the ellipsoid starting from the center. Each cut has a vertical size equal to c (5 μm) and a horizontal dimension equal to the size of the ellipsoid (therefore depending on the location of the cut). In between cuts, there is a vertical distance equal d (250 μm).

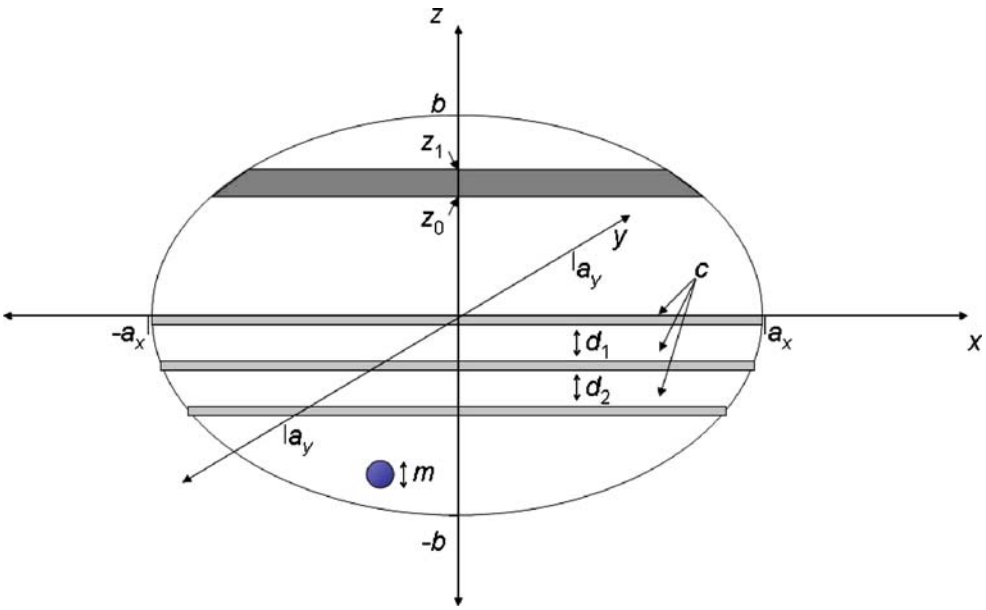

Fig. 1 a_x half length of SLN; a_y half width of SLN; b half height of SLN; c vertical size of a cut (5 μm); d vertical size in between cuts (250 μm); x and y; dimensions of a coupe of a SLN; z dimension from which a cut is taken; m metastasis

Determination of volumes

Based on the model assumptions, mathematical expressions can be determined for the content of several relevant parts of the tissue. We made expressions for:

1. the volume of the entire lymph node,
2. an arbitrary slice from the lymph node, and
3. the volume of the metastasis.

Volume of a lymph node

The contour of lymph nodes is modeled with a triaxial ellipsoid whose Euclidian coordinates are defined as:

$$\frac{x^2}{a_x^2}+\frac{y^2}{a_y^2}+\frac{z^2}{b^2}=1 \tag{1}$$

The parameters a_x, a_y, and b are half the size of the ellipsoid in each of the corresponding dimensions, $a_x \geq a_y \geq b>0$. Based on 1, an arbitrary cut from this ellipsoid at a given z position ($-b \leq z \leq b$) is described in terms of its x, y coordinates as:

$$\frac{x^2}{a_x^2\left(1-\frac{z^2}{b^2}\right)}+\frac{y^2}{a_y^2\left(1-\frac{z^2}{b^2}\right)}=1 \tag{2}$$

Which has surface S_z defined as:

$$\begin{aligned} S_z &= \pi\sqrt{a_x^2\left(1-\frac{z^2}{b^2}\right)}\sqrt{a_y^2\left(1-\frac{z^2}{b^2}\right)} \\ &= \pi a_x a_y\left(1-\frac{z^2}{b^2}\right) \end{aligned} \tag{3}$$

Integrating the cut surfaces S_z over the relevant range of z values, the vertical dimension of the ellipsoid, gives the desired volume of the ellipsoid $I(-b, b)$:

$$I(-b,b)=\int_{-b}^{b}\pi a_x a_y\left(1-\frac{z^2}{b^2}\right)dz=\frac{4\pi}{3}a_x a_y b \tag{4}$$

Volume of a histopathologic cut

A similar expression for the volume of an arbitrary section $I(z_0,z_1)$ taken from the ellipsoid between z_0 and z_1 in vertical direction, $-b \leq z_0 < z_1 \leq b$, is derived using 4 as:

$$\begin{aligned} I(z_0,z_1) &= \int_{z_0}^{z_1}\pi a_x a_y\left(1-\frac{z^2}{b^2}\right)dz \\ &= \pi a_x a_y\left((z_1-z_0)-\frac{1}{3b^2}\left(z_1^3-z_0^3\right)\right) \end{aligned} \tag{5}$$

Determining the volumes within the SLN where a metastasis will or may be detected

Large metastases with a diameter ≥250 μm will always be detected in the area between the outer cuts of the upper and lower halves of the ellipsoid. The area within the SLN, i.e., the vertical distance from the center line of the ellipsoid where a metastasis will be detected, if present, is equal to: three cuts plus two inter-cut spaces plus one diameter of the metastasis (representing metastases just on the outer cut): $3c + 2d + m$. Using 5, the volume of the remaining top and bottom part of the SLN, or detection area $D_{m \geq d}$ is obtained as:

$$D_{m\geq d}=I(-(3c+2d+m),\quad (3c+2d+m)) \tag{6}$$

Small micrometastases with a diameter between 200 and 250 μm may be located between the cuts without leaving traces in one of the neighboring cuts. The previously determined "detection area" for larger metastases needs to be corrected for this. If the metastasis is just next to the first cut, then the unseen area is $(c + m, c + d)$. If it is between the second and third cut, then the unseen area is $(c, c + d - m)$. This way two corrections are obtained:

- between cuts 1 and 2: $(I(c,\quad c+d-m)+I(c+m,\quad c+d))/2$
- between cuts 2 and 3: $(I(2c+d,\quad 2c+2d-m)+I(2c+d+m,\quad 2c+2d))/2$

Combining the volume of the area between the outer cuts with these corrections and considering that corrections apply to both the upper and lower halve of the ellipsoid gives the volume of the detection area $D_{m<d}$

$$\begin{aligned} D_{m<d} = {} & I(-(3c+2d+m),\quad (3c+2d+m)) \\ & -(I(c,\quad c+d-m)+I(c+m,\quad c+d)) \\ & -(I(2c+d,\quad 2c+2d-m)+I(2c+d+m,\quad 2c+2d)) \end{aligned} \tag{7}$$

Determining the probability of detection

The probability of detection is obtained as the volume of the detectable part of the ellipsoid divided by the total volume of the detectable part of the ellipsoid. In case of the "largest micrometastasis" (2 mm), this probability is:

$$P(\text{detection}|m \geq d)=\frac{D_{m\geq d}}{I(-b,b)} \tag{8}$$

In case of the "smallest micrometastasis" (200 μm), the probability of detection is

$$P(\text{detection}|m < d)=\frac{D_{m<d}}{I(-b,b)} \tag{9}$$

The probability of not detecting a metastasis is equal to 1 minus the probability of detection. Note that these

probabilities depend on the vertical size of the lymph node, but not on the horizontal dimensions of the coupe, as the parameters a_x and a_y as multiplication factors in 5 and 4 cancel from the ratios in 8 and 9.

Optimizing the detection of micrometastases

We subsequently used the model to develop a histopathologic examination strategy with a 95% detection probability of finding N1mi by:

1. varying the number of cuts and
2. decreasing the interval between the cuts (200 μm instead of 250 μm).

Results

The median volume of a SLN was 0.8 cm^3 (range 0.3–3.45). The dimensions of the median sized SLN were: length 15 mm, width 10 mm, and height 10 mm. The dimensions of the smallest SLN were 10, 7, and 5 mm, respectively, and of the largest SLN 25, 20, and 12 mm, respectively.

The probabilities of detecting micrometastases in a SLN using the mathematical model and applying the Dutch pathology guideline are summarized in Table 1. The chance of missing a 200-μm micrometastasis was 82% in a median sized SLN, the probability of missing a 2-mm micrometastasis 31%. When examining SLNs according to the guideline, only the chance to find the largest micrometastases in the smallest SLN would exceed the 95% probability.

Table 1 Probability of detecting micrometastases (TNM-stage N1mi) using the current Dutch pathology guidelines

	P_{detect}[b] micrometastasis	
	Smallest micrometastasis 200 μm	Largest micrometastasis 2 mm
Volume and measures of the SLN[a]		
Median SLN		
0.8 cm^3; 15×10×10 mm	0.18	0.69
Smallest SLN		
0.3 cm^3; 10×7×5 mm	0.36	1.0
Largest SLN		
3.45 cm^3; 25×20×12 mm	0.15	0.59
	0.11[c]	1.0[c]

[a] *SLN* sentinel lymph node, [b] P_{detect} probability of detection
[c] When examined according to the examination protocol for SLNs thicker than 10 mm

Sectioning and examining SLNs at 2-mm intervals, as proposed for SLNs thicker than 10 mm, would result in a 100% probability of finding 2-mm micrometastases in the largest SLN, but at the expense of a lower chance of detecting 200-μm micrometastases (11% instead of 15%).

The effect of augmenting the number of cuts (taken at 250-μm intervals) on the probability of detecting micrometastases is plotted for the median SLN in Fig. 2. By adding seven additional cuts from both halves, a 95% probability of detecting 2-mm metastases is reached. Yet, even when the number of cuts is maximized, the probability to detect 200-μm micrometastases does not exceed 81%.

In Fig. 3, the effects of consecutive cuts at 200-μm intervals is plotted. To detect a 200-μm metastasis in a median SLN with a 95% probability, a total number of 20 cuts from both halves of the SLN must be examined (Table 2). When a 5% risk of missing the smallest micrometastasis is considered acceptable, examination of the outer one sixth of the height of both halves of the SLN may be omitted.

Discussion

We demonstrated that the risk of missing micrometastases in the SLN in breast cancer patients is substantial when a SLN is examined according to the current Dutch pathology guideline. If discrimination between TNM-stage N0 and N1mi is clinically relevant, histopathologic examination of the SLN should be adjusted. The interval between the cuts should be decreased, and the size of the SLN should be taken into account. Starting from the center of the node, cuts from both halves at 200-μm intervals should be examined comprehending at least 90% of the height of the SLN.

The SLN concept has gained wide acceptance as a staging procedure for breast cancer patients, yet the method of examining SLNs varies considerably. A recent international survey among 240 pathology laboratories reported 123 different protocols for the workup of SLNs. Pathology protocols ranged between two and five section levels per lymph node to step sectioning SLNs at 40-μm intervals [7, 28]. While the accepted risk of a false-negative procedure (i.e., a SLN with no metastasis and a non-SLN with metastasis) is estimated to range between 2% and 10% [5, 12, 17, 25, 27], less is published about the sensitivity of the pathologic examination of the SLN itself (i.e., not detecting a metastasis that is present in a SLN). Cserni [8] calculated, also based on a model, that to detect macrometastases sections at steps of 1 mm are sufficient and for the detection of micrometastases sections at steps of 200–250 μm should suffice. Our study demonstrates that intervals between the cuts should be 200 μm at most.

More slices at smaller intervals are likely to lead to a more frequent detection of micrometastases [9, 11, 26, 29].

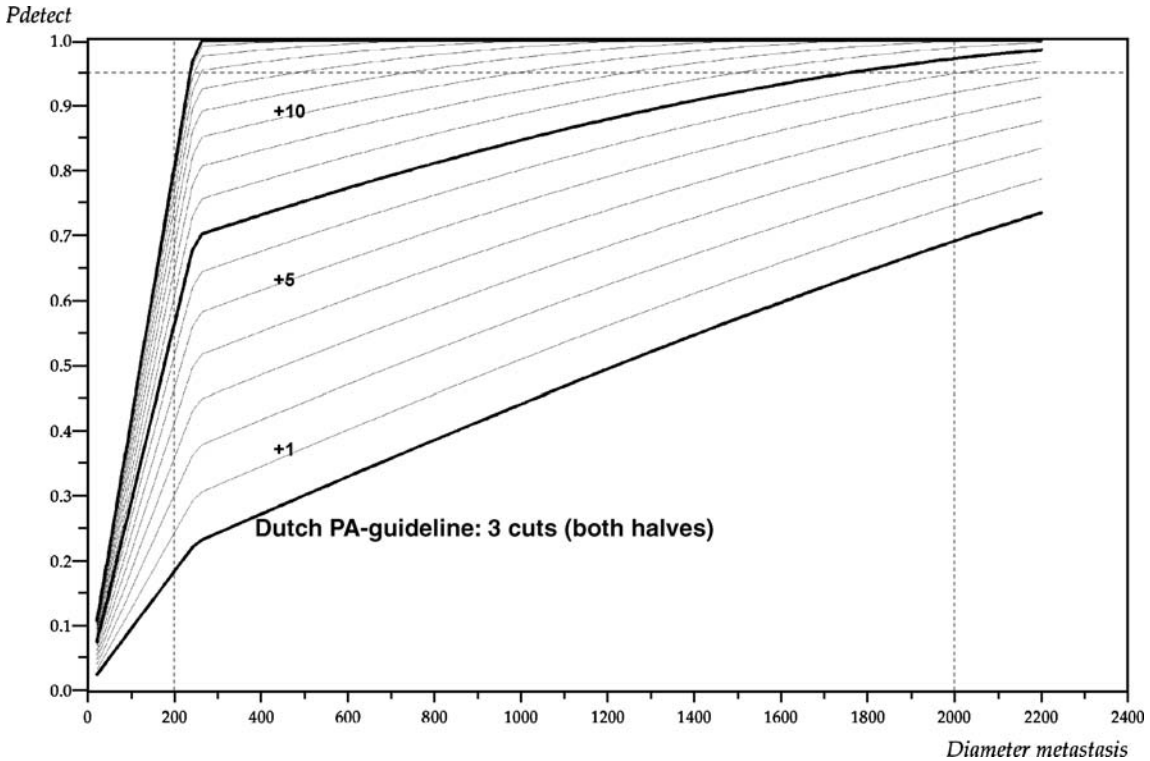

Fig. 2 P_{detect}, detection chance; $+n$, number of extra cuts taken from each half of the SLN

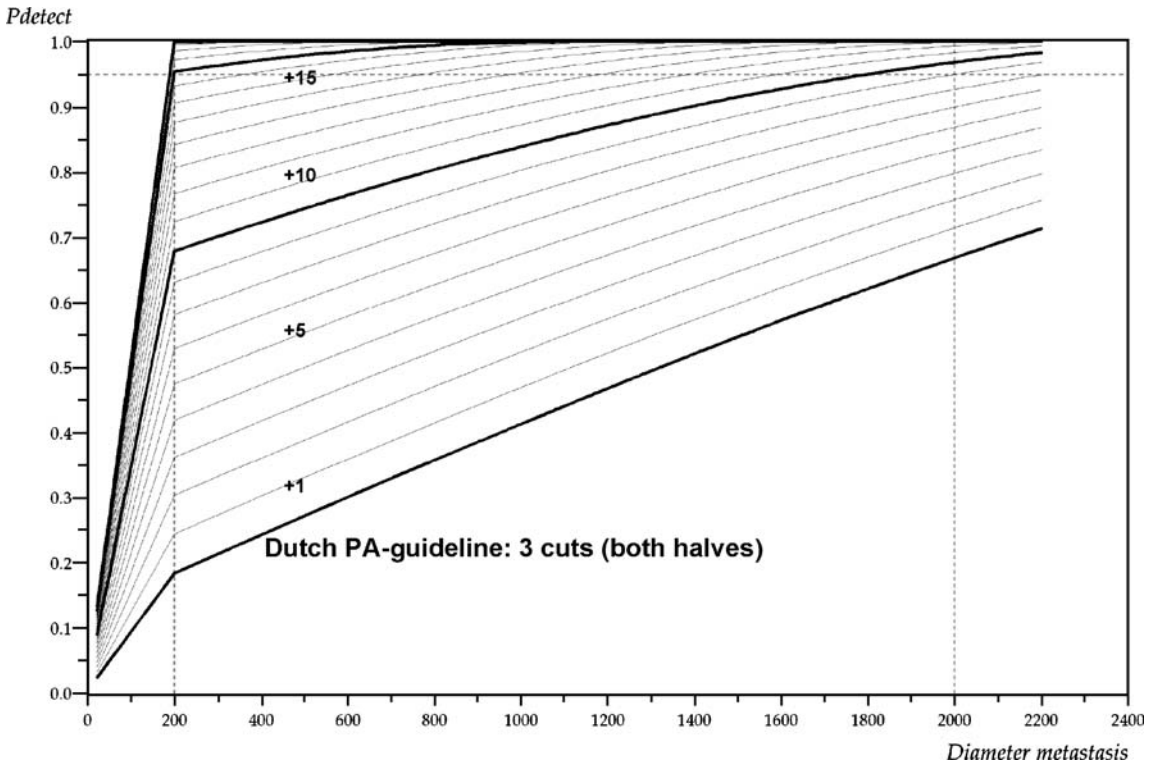

Fig. 3 P_{detect}, detection chance; $+n$, number of extra cuts taken from each half of the SLN

Table 2 Number of pathology cuts necessary to detect the smallest micrometastasis (200 μm) with a 95% probability

	No. of cuts needed[a] for 95% detection probability	Maximum No. of cuts[a]
Interval between cuts 250 μm		
Median SLN		
0.8 cm^3; 15×10×10 mm	nr[b]	19
Smallest SLN		
0.3 cm^3; 10×7×5 mm	nr[b]	9
Largest SLN		
3.45 cm^3; 25×20×12 mm	nr[b]	23
Interval between cuts 200 μm		
Median SLN		
0.8 cm^3; 15×10×10 mm	20	24
Smallest SLN		
0.3 cm^3; 10×7×5 mm	10	12
Largest SLN		
3.45 cm^3; 25×20×12 mm	24	29

[a] Number of cuts taken from each half starting from the center of the SLN

[b] *nr* 95% detection probability not reached

Before the introduction of the SLN procedure, lymph nodes were halved, and one cut from the center was stained with hematoxylin and examined. The current practice, involving more cuts and additional coloring with immunohistochemical techniques, is time-consuming for the pathologist and more expensive [11]. While the Dutch guideline states that the guideline already is "a balance between the practical feasibility and the sensitivity of the procedure"[21], optimizing the pathology workup to reach a 95% sensitivity would imply a sevenfold increase of the number of cuts to be examined.

Worldwide, many pathology protocols are used for the pathology workup of SLNs [7]. In Fig. 4, the yield of the Dutch protocol is compared to the yield of a "commonly used" pathology protocol (bisecting the SLN and examining six cuts of both halves at 150-μm intervals) [7] and the yield of the "Milan" protocol (bisecting a SLN, 15 levels of each side at 40-μm intervals and the remainder at 100-μm intervals) [27]. Only the latter protocol resulted in a truly substantial improvement of the probability of detection. At the same time, the number of examined slices per lymph node was 112 instead of six.

However, if breast cancer patients with TNM-stage N1mi have a worse prognosis in comparison to patients staged as N0, extra work for the pathologist is not an acceptable reason to perform a suboptimal examination.

To date, it is unclear whether "missing" lymphogenic micrometastases is a clinical problem. It all comes down to the question whether TNM-stage N1mi is of prognostic importance. Older studies gave conflicting results, some suggesting a prognosis similar to patients with N0 breast cancer [1, 14, 30] while others reported prognosis compa-

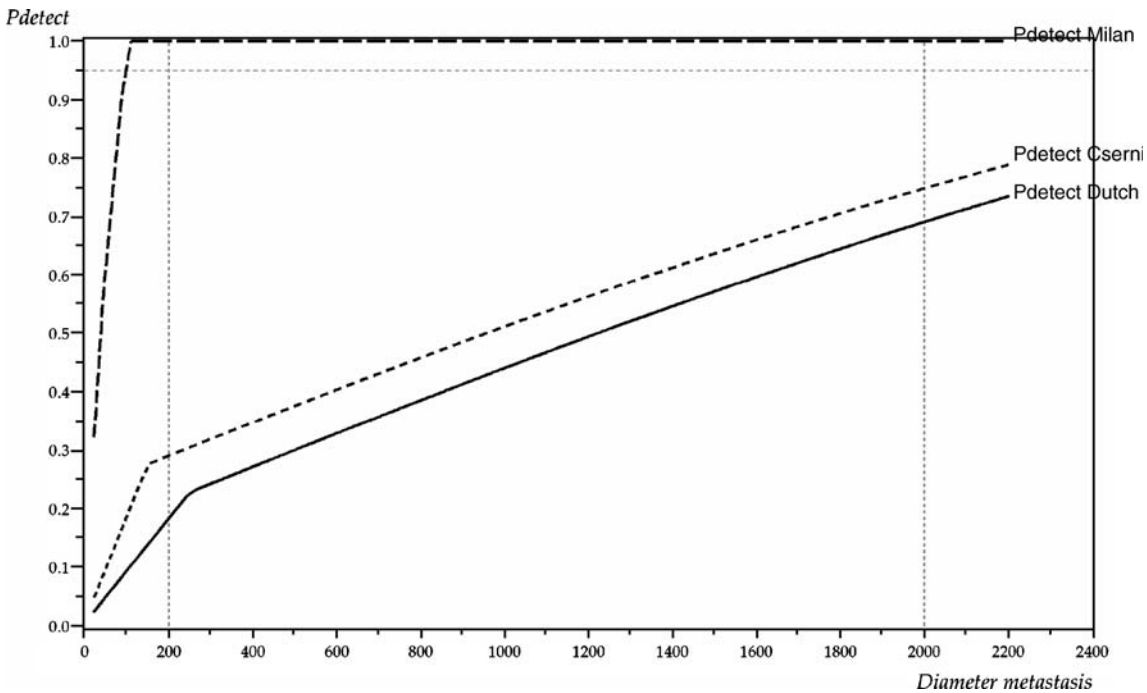

Fig. 4 P_{detect}, detection chance; P_{detect} Dutch, detection chance in the Dutch pathology protocol; P_{detect} Cserni, detection chance in most common European protocol; P_{detect} Milan, detection chance in protocol used in Milan

rable to patients with N1 disease [23]. Studies based on examination of the SLN have a very limited follow-up and have not shown any difference in overall survival. Then again, a difference between N0 and N1mi for disease-free and metastasis-free survival was observed by Colleoni et al. [4] in a large series of patients. Long-term data should be awaited, but there appears to be some clinical relevance of TNM-stage N1mi.

In the meantime, many medical oncologists tend to advise systemic treatment for patients with lymphogenic micrometastasis, considering micrometastasis in the regional lymph nodes of similar importance as macrometastasis. In that respect, it is important to note that the current guideline carries a risk of "missing" macrometastases too. We showed that the chance of missing the largest micrometastasis (2 mm), i.e., the smallest macrometastasis is 31% in a SLN of median size.

On the other hand, if TNM-stage N1mi is not clinically relevant, examination of the SLN by sectioning at 2-mm intervals, as advised for SLNs thicker than 10 mm, instead of 250-μm intervals would be a more sensible approach than the current guideline. This would result in fewer sections, but nonetheless a 100% yield of detecting the smallest macrometastases.

An important limitation of our study is that the mathematical model does not take several biological aspects into account. Firstly, the location of a micrometastasis within a lymph node. We have assumed a random distribution of the metastases within the node, while the periphery of the lymph node seems to be the preferred localization of micrometastases [10, 19]. Secondly, formalin fixation leads to shrinking of tissue; this affects both the volume of the "detection area" as well as the volume of the metastasis to be detected. Furthermore, the model assumes that every micrometastasis that appears in a cut is observed too. Lastly, a micrometastasis that is seen in one cut may well be larger than appears under the microscope when studying that cut only. We do not know what the overall effect of these biological factors is. Yet, despite these limitations, it is unlikely that our mathematical model substantially under- or overestimates the risk of missing micrometastases.

In conclusion, the current Dutch pathology guideline is insufficient to detect small lymph node metastases. If we wish to detect micrometastases with a 95% probability rate, more extensive histopathologic workup is required. Finally, not doing so would also imply that we will never know the exact prognostic significance of these small metastases.

Acknowledgment No financial support was received for this study.

Conflict of interest statement We declare that we have no conflict of interest.

References

1. Attiyeh FF, Jensen M, Huvos AG, Fracchia A (1977) Axillary micrometastasis and macrometastasis in carcinoma of the breast. Surg Gynecol Obstet 144:839–842
2. Bolster MJ, Bult P, Schapers RF, Meijer JW, Strobbe LJ, van Berlo CL, Klinkenbijl JH, Peer PG, Wobbes T, Tjan-Heijnen VC (2006) Differences in sentinel lymph node pathology protocols lead to differences in surgical strategy in breast cancer patients. Ann Surg Oncol 13:1466–1473
3. CBO-richtlijn mammacarcinoom (2004) Nederlandse Vereniging voor Pathologie. http://www.pathology.nl. Cited Apr 2004
4. Colleoni M, Rotmensz N, Peruzzotti G, Maisonneuve P, Mazzarol G, Pruneri G, Luini A, Intra M, Veronesi P, Galimberti V, Torrisi R, Cardillo A, Goldhirsch A, Viale G (2005) Size of breast cancer metastases in axillary lymph nodes: clinical relevance of minimal lymph node involvement. J Clin Oncol 23(7):1379–1389
5. Cox CE, Pendas S, Cox JM, Joseph E, Shons AR, Yeatman T, Ku NN, Lyman GH, Berman C, Haddad F, Reintgen DS (1998) Guidelines for sentinel node biopsy and lymphatic mapping of patients with breast cancer. Ann Surg 227:645–651
6. Cserni G, Gregori D, Merletti F, Sapino A, Mano MP, Ponti A, Sandrucci S, Baltas B, Bussolati G (2004) Meta-analysis of non-sentinel node metastases associated with micrometastatic sentinel nodes in breast cancer. Br J Surg 91:1245–1252
7. Cserni G, Amendoeira I, Apostolikas N, Bellocq JP, Bianchi S, Boecker W, Borisch B, Connolly CE, Decker T, Dervan P, Drijkoningen M, Ellis IO, Elston CW, Eusebi V, Faverly D, Heikkila P, Holland R, Kerner H, Kulka J, Jacquemier J, Lacerda M, Martinez-Penuela J, De Miguel C, Peterse JL, Rank F, Regitnig P, Reiner A, Sapino A, Sigal-Zafrani B, Tanous AM, Thorstenson S, Zozaya E, Fejes G, Wells CA (2004) Discrepancies in current practice of pathological evaluation of sentinel lymph nodes in breast cancer. Results of a questionnaire based survey by the European Working Group for Breast Screening Pathology. J Clin Pathol 57:695–701
8. Cserni G (2004) A model for determining the optimum histology of sentinel lymph nodes in breast cancer. J Clin Pathol 57:467–471
9. Cserni G (2002) Complete sectioning of axillary sentinel nodes in patients with breast cancer. Analysis of two different step sectioning and immunohistochemistry protocols in 246 patients. J Clin Pathol 55:926–931
10. Cserni G (2000) Mapping metastases in sentinel lymph nodes of breast cancer. Am J Clin Pathol 113:351–354
11. Farshid G, Pradhan M, Kollias J, Gill PG (2000) Computer simulations of lymph node metastasis for optimizing the pathologic examination of sentinel lymph nodes in patients with breast carcinoma. Cancer 89:2527–2537
12. Giuliano AE, Jones RC, Brennan M, Statman R (1997) Sentinel lymphadenectomy in breast cancer. J Clin Oncol 15:2345–2350
13. Groen RS, Oosterhuis AWJ, Boers JE (2007) Pathologic examination of sentinel lymph nodes in breast cancer by a single haematoxylin–eosin slide versus serial sectioning and immunocytokeratin staining: clinical implications. Breast Cancer Res Treat 105:1–5
14. Huvos AG, Hutter RV, Berg JW (1971) Significance of axillary macrometastases and micrometastases in mammary cancer. Ann Surg 173:44–46
15. International (Ludwig) Breast Cancer Study Group (1990) Prognostic importance of occult axillary lymph node micrometastases from breast cancers. Lancet 335:1565–1568
16. Krauth JS, Charitansky H, Isaac S, Bobin JY (2006) Clinical implications of axillary sentinel lymph node 'micrometastases' in breast cancer. Eur J Surg Oncol 32:400–404

17. Lyman GH, Giuliano AE, Somerfield MR, Benson AB III, Bodurka DC, Burstein HJ, Cochran AJ, Cody HS III, Edge SB, Galper S, Hayman JA, Kim TY, Perkins CL, Podoloff DA, Sivasubramaniam VH, Turner RR, Wahl R, Weaver DL, Wolff AC, Winer EP (2005) American Society of Clinical Oncology guideline recommendations for sentinel lymph node biopsy in early-stage breast cancer. J Clin Oncol 23:7703–7720
18. Maibenco DC, Dombi GW, Kau TY, Severson RK (2006) Significance of micrometastases on the survival of women with T1 breast cancer. Cancer 107:1234–1239
19. Meyer JS (1998) Sentinel lymph node biopsy: strategies for pathologic examination of the specimen. J Surg Oncol 69:212–218
20. Miltenburg DM, Miller C, Karamlou TB, Brunicardi FC (1999) Meta-analysis of sentinel lymph node biopsy in breast cancer. J Surg Res 84:138–142
21. Richtlijn Behandeling van het mammacarcinoom (2004) Kwaliteitsinstituut voor de Gezondheidszorg CBO
22. van Rijk MC, Peterse JL, Nieweg OE, Oldenburg HS, Rutgers EJ, Kroon BB (2006) Additional axillary metastases and stage migration in breast cancer patients with micrometastases or submicrometastases in sentinel lymph nodes. Cancer 107:467–471
23. Rosen PP, Saigo PE, Braun DW, Weathers E, Fracchia AA, Kinne DW (1981) Axillary micro- and macrometastases in breast cancer. Ann Surg 194:585–591
24. Sobin LH, Wittekind Ch (2002) TNM classification of malignant tumours, 6th edn. Wiley, Hoboken, New Jersey
25. Turner RR, Ollila DW, Krasne DL, Giuliano AE (1997) Histopathologic validation of the sentinel lymph node hypothesis for breast carcinoma. Ann Surg 226:271–276
26. Turner RR, Giuliano AE, Hoon DS, Glass EC, Krasne DL (2001) Pathologic examination of sentinel lymph node for breast carcinoma. World J Surg 25:798–805
27. Veronesi U, Paganelli G, Viale G, Luini A, Zurrida S, Galimberti V, Intra M, Veronesi P, Maisonneuve P, Gatti G, Mazzarol G, De Cicco C, Manfredi G, Fernandez JR (2006) Sentinel-lymph-node biopsy as a staging procedure in breast cancer: update of a randomised controlled study. Lancet Oncol 7:983–990
28. Viale G, Mastropasqua MG, Maiorano E, Mazzarol G (2006) Pathologic examination of the axillary sentinel lymph nodes in patients with early-stage breast carcinoma: current and resolving controversies on the basis of the European Institute of Oncology experience. Virchows Arch 448:241–247
29. Viale G, Maiorano E, Mazzarol G, Zurrida S, Galimberti V, Luini A, Renne G, Pruneri G, Maisonneuve P, Veronesi U (2001) Histologic detection and clinical implications of micrometastases in axillary sentinel lymph nodes for patients with breast carcinoma. Cancer 92:1378–1384
30. Wilkinson EJ, Hause LL, Hoffman RG, Kuzma JF, Rothwell DJ, Donegan WL, Clowry LJ, Almagro UA, Choi H, Rimm AA (1982) Occult axillary lymph node metastases in invasive breast carcinoma: characteristics of the primary tumor and significance of the metastases. Pathol Annu 17(Pt 2):67–91

Virchows Arch (2008) 453:25–31
DOI 10.1007/s00428-008-0619-4

ORIGINAL ARTICLE

Three German fibrinogen Aα-chain amyloidosis patients with the p.Glu526Val mutation

Magdalena Eriksson · Stefan Schönland · Raoul Bergner · Ute Hegenbart · Peter Lohse · Hartmut Schmidt · Christoph Röcken

Received: 24 January 2008 / Revised: 17 March 2008 / Accepted: 12 April 2008 / Published online: 24 May 2008

Abstract Plasma protein fibrinogen variants cause fibrinogen Aα-chain (AFib) amyloidosis, which presents with hypertension, proteinuria, and azotemia. Six AFib mutations have been reported thus far. We identified three patients who presented with marked proteinuria and serum creatinine elevations. Their kidney biopsies revealed destruction of the glomerular architecture by amyloid deposits with typical, apple-green birefringence in polarized light after Congo red staining. We found immunoreactivity against fibrinogen, which is typical for this type of amyloidosis. We sequenced the *FGA* exon 5 and demonstrated heterozygosity for the p.Glu526Val mutation in all three cases. This amino acid substitution is the most common fibrinogen Aα-chain variant causing AFib amyloidosis. The mutation has been reported in individuals of European and American descent but not yet in German patients. AFib amyloidosis should therefore be considered an important differential diagnosis in German patients with renal amyloidosis. In the cases described here, the use of antibodies directed against fibrinogen, followed by direct gene sequencing, revealed the underlying cause.

Keywords Kidney · Amyloid · Fibrinogen · FGA · E526V

Abbreviations

FGA	fibrinogen Aα-chain gene
HRA	hereditary renal amyloidosis
TTR	transthyretin
Fib	fibrinogen Aα-chain
Lys	lysozyme
ApoAI	apolipoprotein AI
ApoAII	apolipoprotein AII

Introduction

Hereditary amyloidosis is an autosomal-dominant disease characterized by insoluble protein deposits in various organs. Hereditary amyloidosis has been associated with variant apolipoprotein AI, apolipoprotein AII, gelsolin, lysozyme, fibrinogen Aα-chain, or transthyretin proteins. The most frequent form is the transthyretin-derived ATTR amyloidosis, which clinically presents with polyneuropathy and/or cardiomyopathy [3]. These symptoms clearly differ from hereditary renal amyloidosis (HRA), where nephropathy is the main manifestation. Several HRA kindred have been reported since Ostertag [18] first described a German family in 1932. Common HRA proteins are fibrinogen (AFib amyloidosis), lysozyme (ALys amyloidosis), apolipoprotein

M. Eriksson · C. Röcken (✉)
Department of Pathology, Charité University Hospital,
Charitéplatz 1,
10117 Berlin, Germany
e-mail: christoph.roecken@charite.de

S. Schönland · U. Hegenbart
Department of Hematology and Oncology,
University of Heidelberg, Heidelberg, Germany

R. Bergner
Medical Clinic A, Klinikum der Stadt Ludwigshafen,
Ludwigshafen, Germany

P. Lohse
Department of Clincal Chemistry—Grosshadern,
University of Munich, Munich, Germany

H. Schmidt
Transplant Hepatology, University of Münster,
Münster, Germany

AI (AApoAI amyloidosis), and apolipoprotein AII (AApoAII amyloidosis). One ApoAI variant was reported to also cause neuropathy [17, 18]. Six mutations in the fibrinogen Aα-chain (FGA) cause AFib amyloidosis. The most common variant is p.Glu526Val, which was first described in 1994 in two Irish families [20]. The sole clinical manifestation in those patients was a nephropathy appearing at age 40–60 years without any sign of neuropathy [21]. Five additional mutations causing AFib amyloidosis were since reported. One was a single base deletion at nucleotide 4897 resulting in p.Thr522fs first described in a French family [10]. A G-to-T transversion leading to the amino acid exchange p.Arg554Leu was observed in a kindred of Peruvian descent [4]. A single base deletion at nucleotide 4904 resulting in p.Ser524fs was found in the US [22]. A p.Glu540Val replacement was described in a German patient [6], and the p.Asp517_Thr522delinsGlnSer mutation was recently found in a 7-year-old Korean girl [13] (Table 1).

Clinically, AFib amyloidosis presents with hypertension, proteinuria, and azotemia. Amyloid is typically found in the renal glomeruli, while the liver and spleen are only involved in more advanced cases [2]. With the exception of one reported case from Portugal, no neuropathy has been observed in AFib amyloidosis. Fibrinogen is involved in the coagulation process; however, the aforementioned variants do not seem to affect the normal function of fibrinogen [19]. Although hereditary amyloidosis is relatively uncommon, 5% of patients referred to the UK National Amyloidosis Center with an apparent diagnosis of acquired AL amyloidosis carried the p.Glu526Val variant of the fibrinogen Aα-chain [14].

Treatment options for this disease are limited. Renal transplantation is associated with rapid recurrence of amyloid deposits in the graft, resulting in subsequent renal failure. Combined renal and hepatic transplantation was reportedly successful in two amyloidogenic variants and could be effective in all AFib amyloid cases. In the presence of a normal liver, the variant fibrinogen is eliminated from the serum, and the amyloid deposits can be mobilized from the affected organs [15, 24]. We describe three German patients with fibrinogen Aα-chain amyloidosis due to the p.Glu526Val mutation. Since pathologists will ultimately make the diagnosis of such patients, their thorough knowledge of the genetic basis is highly important for subsequent therapeutic plans.

Clinical history

Patient no. 1

A 62-year-old woman developed myalgia and low-grade fever over a 20-year period. Hypertension developed after 10 years. Proteinuria of >1 g/day and a creatinine concentration of 2.3 mg/dl were observed 18 years after symptom onset. A renal biopsy was then performed. Amyloidosis of unknown cause and subtype was diagnosed. Rheumatological examination ruled out a periodic fever syndrome. The patient was then referred to the Amyloidosis Clinic, University of Heidelberg. She had no macroglossia and no cutaneous bleeding. The heart, liver, and gastrointestinal tract were not affected. However, the patient showed early signs of a sensory polyneuropathy in fingers and feet, which was confirmed by electrophysiological examination. Laboratory tests showed no monoclonal gammopathy. The free light chain test and a bone marrow biopsy were also normal. The family history provided no evidence of a hereditary amyloidosis or hereditary kidney disease.

Patient no. 2

A 49-year-old man without known kidney disease but with hypertension, hyperlipidemia, and coronary artery

Table 1 FGA mutations in AFib amyloidosis

Mutation	Clinical features	Geographic origin	Age of onset (years)
p.Glu526Val	Nephropathy	Americans of Irish descent [20]	40–60
	Nephropathy–neuropathy	Portugal [7]	55
	Nephropathy	Canadians of Polish descent [1, 21]	~50
	Nephropathy	UK [14]	
	Nephropathy	Germany (current report)	40–65
p.Arg554Leu	Nephropathy	Mexicans of Peruvian descent [4]	~30
	Nephropathy	France [11]	~50
	Nephropathy	African–American [23]	~60
p.Ser524fs	Nephropathy	US [22]	~40
p.Thr522fs	Nephropathy	France [10]	~30 and 12
p.Glu540Val	Nephropathy	Germany [6]	40–50
p.Asp517_Thr522delinsGlnSer	Nephropathy	Korea [13]	7

disease was admitted to hospital with rising serum creatinine levels and severe nephrotic syndrome. On admission, the proteinuria was 15 g/day and the creatinine clearance was 11 ml/min. A kidney biopsy revealed renal amyloidosis (Fig. 1). No other organs were involved. The patient's mother had an unknown renal disease and died of a myocardial infarction at the age of 61 years.

Patient no. 3

A 64-year-old man was admitted to the Amyloidosis Clinic, University of Heidelberg, after a kidney biopsy disclosed amyloidosis. He had developed hypertension 20 years earlier and noted progressive dyspnea for 4 years. His physician observed progressive proteinuria and renal failure

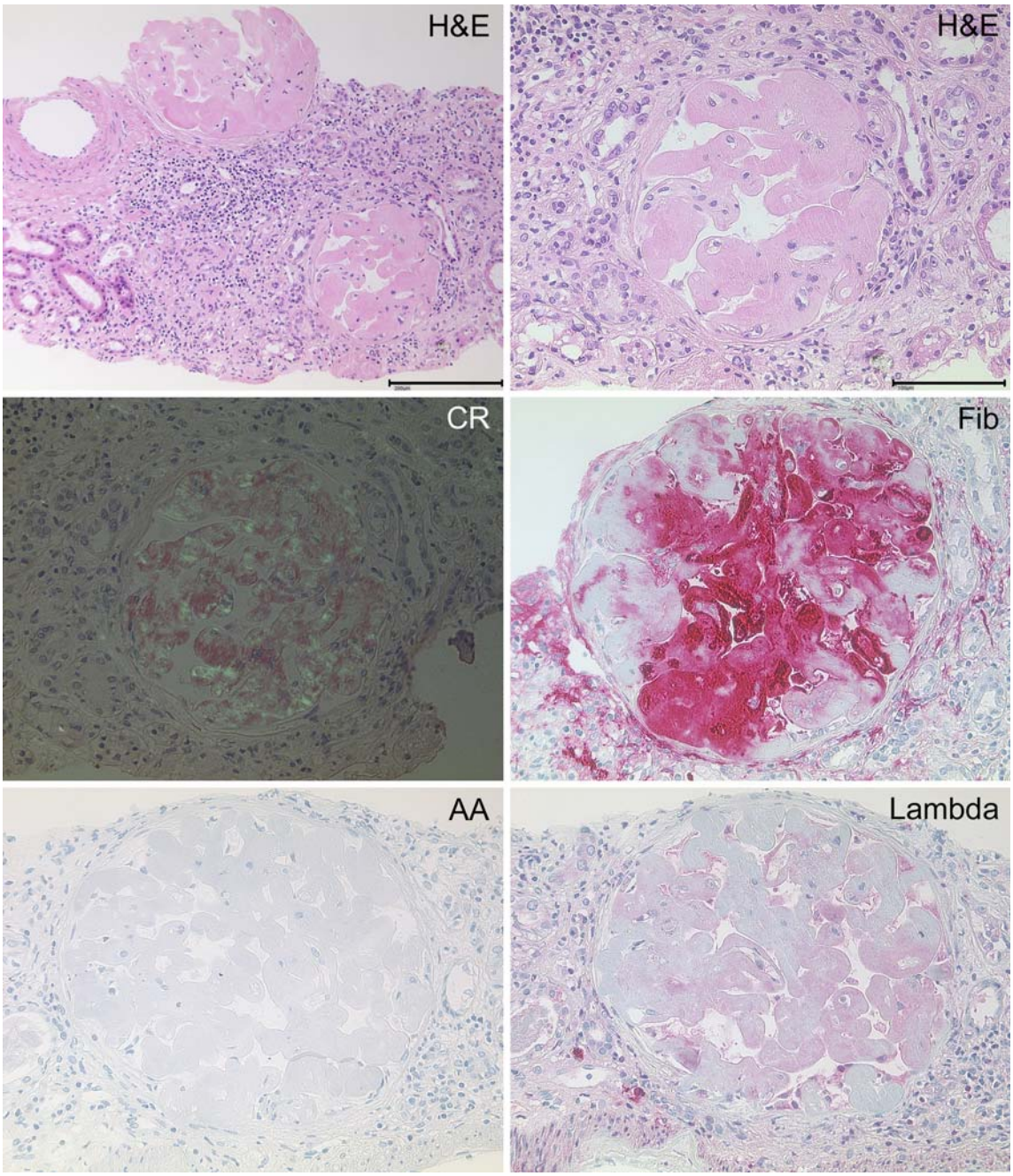

Fig. 1 Kidney biopsy obtained from patient no. 2. Hematoxylin-and-eosin-stained (H&E) sections showed extensive destruction of the glomerular architecture by amorphous eosinophilic material. Congo red staining (*CR*) and polarization microscopy demonstrated the typical apple-green birefringence of amyloid. The amyloid deposits were immunostained with an antibody directed against fibrinogen (Fib), while no immunostaining was found with antibodies directed against AA amyloid (AA) or λ-light chain (Lambda). Original magnifications 100- (*left upper panel*) and 200-fold (*all other panels*). Hematoxylin counterstain

that culminated in dialysis. No monoclonal gammopathy, free light chains, or increased plasma cells were found. Amyloidosis elsewhere could not be established in this patient.

Materials and methods

Histology and immunohistochemistry

The kidney biopsies were fixed in formalin and embedded in paraffin. Serial sections were stained with hematoxylin and eosin. Amyloid was detected in Congo-red-stained sections viewed under cross-polarized light. Immunohistochemistry was performed with commercially available monoclonal antibodies directed against AA amyloid (1:600) and polyclonal antibodies against amyloid P-component (1:5,000), fibrinogen (1:2,000), lysozyme (1:3,000), transthyretin (1:4,000), λ-light chain (1:160,000), κ-light chain (1:160,000), and β2-microglobulin (β2 M; 1:2,000; all DAKO, Hamburg, Germany), as well as with noncommercially available polyclonal antibodies directed against apolipoprotein AI (anti-apo-AI; dilution 1:1,000) [9], λ-light chain-derived amyloid proteins (anti-AL1 antibody; dilution 1:3,000) [5], and anti-λ-light chain-peptide antibodies (AL3, dilution 1:250; AL7, 1:500). Immunostaining was done with the BenchMark® XT immunostainer using the ultraView™ Universal Alkaline Phosphatase Red Detection Kit (both Ventana Medical Systems, Inc., Tucson, AZ, USA). Prior to incubation with anti-amyloid P component, -apoAI, -λ and -κ light chain, -transthyretin antibodies, and AL7, sections were pretreated with cell conditioning 1 according to the manufacturer's instructions (CC1; Ventana). The specificity of immunostaining was verified using specimens containing known classes of amyloid (AA amyloid, apolipoprotein AI, β2 microglobulin, transthyretin, λ-light chain) or by using positive controls recommended by the manufacturers (remaining antibodies). Omission of the primary antibodies served as a negative control.

DNA isolation, PCR amplification, and sequence analysis

The participating subjects gave their written, informed consent prior to the genetic analysis and the ethical committee approved the study. Ethylene diamine tetraacetic acid blood was drawn, and the genomic DNA was isolated from peripheral blood leukocytes using the DNA blood mini kit from Qiagen (Hilden, Germany). Amplification of the 3′ end of *FGA* exon 5, encoding amino acids 508-611, was performed in a 50-μl volume containing 1× reaction buffer (Qiagen), 1.5 mM $MgCl_2$, 125 μM dNTPs, 400 nM each of the forward and reverse primer, approximately 200 ng genomic DNA, and 2.5 U of HotStartTaq DNA polymerase (Qiagen). The following thermocycling conditions were used: an initial denaturation step of 15 min at 95°C to activate the Taq polymerase, followed by 40 cycles of 95°C for 20 s, 62°C for 20 s, and 72°C for 20 s, and a final extension step of 72°C for 10 min. The polymerase chain reaction (PCR) product size and quantity was analyzed by agarose gel electrophoresis. Fragments were purified with the ExoSAP-IT® kit for PCR product cleanup (USB Corp., Cleveland, OH, USA) and sequenced with the ABI PRISM® BigDye Terminator v3.1 Ready Reaction Cycle Sequencing kit (Applied Biosystems, Foster City, CA, USA). Sequences were analyzed on an ABI PRISM® 3130 Genetic Analyzer.

Results

Histology and immunohistochemistry

The kidney biopsies of all three patients showed extensive effacement of the glomerular architecture by amorphous amyloid deposits with typical apple-green birefringence in polarized light after Congo red staining (Fig. 1). The amyloid deposits were purely glomerular in all three patients. The amyloid deposits were immunoreactive for amyloid P component but not for any of the other antibodies directed against AA amyloid, ApoAI, lysozyme, β2-microglobulin, λ- and κ-light chain, or transthyretin. An antibody directed against fibrinogen stained some of the deposits intensely and raised the suspicion of a hereditary AFib amyloidosis in all patients (Fig. 1).

Sequence analysis

All three patients were shown to be heterozygous for a c.1577A>T substitution in exon 5 of the *FGA* gene, leading to the replacement of glutamic acid (GAG), by valine (GTG) at residue 526. No mutations were found in the genes coding for transthyretin, apolipoprotein AI, apolipoprotein AII, or lysozyme. Furthermore, we established that the patients were not related.

Examination of family members

The daughter and son of patient no. 1 are clinically well. Only the daughter underwent mutation screening and harbored the p.Glu526Val mutation (Fig. 2a). The mother of patient no. 2 had an undefined kidney disease and died of myocardial infarction at the age of 61; her DNA was never analyzed. The mother's sister carries the mutation but is asymptomatic thus far. Her daughter and grandchildren have not undergone genetic testing. Two other siblings died

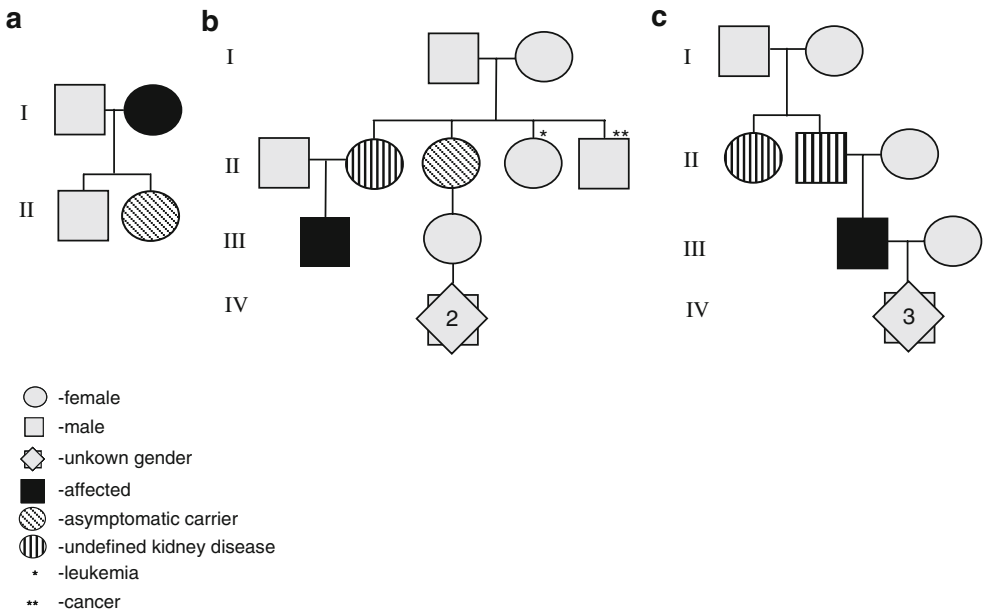

Fig. 2 Pedigree analysis. **a** Patient no. 1 is represented by the *filled circle* in generation I. Her daughter is carrying the p.Glu526Val mutation without any symptoms and her son is healthy and not genetically examined. **b** Patient no. 2 is represented by the *filled square* in generation III. The mother suffered from an undefined kidney disease and died of myocardial infarction at the age 61. The mother's sister carries the p.Glu526Val mutation asymptomatically. It is unknown whether her daughter (generation II) and granddaughters (generation IV) carry the mutation. The other two siblings of the mother (generation II) were not genetically examined and died of leukemia and cancer at the age of 50 and 59 years, respectively. **c** Patient no. 3 is represented by the *filled square* in generation III. The patient's father and aunt suffered from chronic kidney disease but were not genetically examined. Individuals that are not genetically examined are represented by *gray squares* or *circles*

of leukemia and cancer at the age of 50 and 59 years, respectively (Fig. 2b). No information about the death of the patient's grandparents (generation I) was available. The patient himself has no siblings or children. The father and aunt of patient no. 3 developed chronic kidney disease (Fig. 2c). The patient's three children are healthy. None of the family members has undergone genetic testing thus far.

Discussion

The pathologist serves as consultant to the clinician. Modern genetic analysis now enables the pathologist not only to make highly specific, mechanistic diagnoses, but also to provide clinically relevant information for the entire family. Furthermore, steady progress is being made in the development of novel amyloidosis therapies. These treatments may also be gene specific in terms of efficacy. The mutations we describe have hitherto fore not been described in Germany.

Fibrinogen is a coagulation plasma protein synthesized mainly in the liver [16]. The fibrinogen molecule is a 45-nm structure consisting of two sets of disulfide-bridged Aα-, Bβ-, and γ-chains. The Aα chain is the largest of the three with 610 amino acids and a molecular weight of 66 kDa [8]. The *FGA* gene spans over 7 kb and contains six exons. Alternative splicing results in two isoforms, which vary in the carboxyterminus [16]. Although *FGA* mutations are rare, their effects are profound, namely dysfibrinogenemia, hypofibrinogenemia, afibrinogenemia, or AFib amyloidosis [16]. All six AFib amyloidosis mutations observed thus far are located in exon 5 and affect one ore more residues at amino acid positions 517–554. In patients carrying the p.Arg554Leu variant, the amyloid fibril subunit protein contains the fibrinogen α-chain residues 500–580. A similar deposited peptide is found in p.Glu526Val carriers. The two frame shifts, p.Ser524fs and p.Thr522fs, both result in a premature stop codon in amino acid residue 548 [10, 22]. These four peptides found in amyloid deposits all share the unchanged amino acid sequence 500–521. Serpell et al. [19] believed that this 21-residue fragment is responsible for the formation of amyloid fibrils, although that could not be the case with the indel mutation, affecting amino acids 517–522.

Similar to other forms of hereditary amyloidosis, the mechanisms underlying fibril formation in Aα-chain amyloidosis are principally unknown. In contrast to ATTR amyloidosis, where both the variant *and* the wild-type protein are able to form amyloid, only the variants of the fibrinogen Aα-chain are amyloidogenic. In some cases of AFib amyloidosis, only the variant protein was found in the blood [4, 10], while in others, the normal peptide was also

found [7, 20, 22, 23]. Furthermore, no clear pattern regarding the same type of mutation has been described.

The phenotypic penetrance of AFib amyloidosis is low and most patients do not have a family history [12]. In our cases, for example, the aunt of patient no. 2 is a carrier of the same mutation but does not have any nephropathy. Her daughter and granddaughters were not examined. Although the patient's mother could not be genetically examined, she probably carried the mutation since she had an undiagnosed renal disease. Similarly, no family history of renal amyloidosis was present for patient no. 1; however, genetic examination of the daughter revealed that she also carried the p.Glu526Val mutation. Probably one of the patient's parents harbored the mutation, although clinical manifestations were not present or diagnosed.

Our results emphasize the importance of immunohistochemical classification, combined with genetic analysis, in the diagnostic workup of renal amyloidosis. Immunohistochemistry excluded other causes of renal amyloidosis, particularly the AA and AL types, and raised suspicion of AFib amyloidosis. AFib was indeed confirmed by genetic testing in all our patients. The correct classification of the responsible protein is crucial in the clinical decision to perform organ transplantation. Conceivably, combined kidney and liver transplantation provides the solely effective clinical approach to this disease. Diagnosis of HRA can readily be made, for example, by direct DNA sequencing or single-strand conformation polymorphism analysis. The nucleotide substitution resulting in the p.Glu526Val exchange also creates a Mae III restriction endonuclease recognition site and can therefore also be analyzed by restriction enzyme digestion [2]. In our three cases, the use of polyclonal antibodies raised against fibrinogen was suggestive for this type of amyloidosis. Direct sequencing of *FGA* exon 5 then revealed the responsible p.Glu526Val mutation. The onset of Aα-chain amyloidosis occurs mostly at the age of 30–50 [4, 20, 24]. One African–American kindred showed a later onset (60 years) [22]. Two affected children aged 7 and 12 years also have been reported (Table 1) [13, 10]. One of the patients described here was 63 years old at the time of diagnosis, a slightly later onset than observed in the other patients carrying the p.Glu526Val mutation.

The p.Glu526Val substitution is the most common fibrinogen Aα-chain defect connected with amyloidosis and has been reported in kindred and individuals of European and American descent; however, this mutation has not been previously observed in German patients. HRA was first described in a German family in an abstract in 1932 and as a full paper in 1950. At that time, the molecular cause could not be established [18]. Since then, the only reported amyloidogenic mutation in the fibrinogen Aα-chain gene found in a single German kindred was the p.Glu540Val variant reported in abstract form by Bybee et al. in 2004 [6]. We here describe three additional German patients with the p.Glu526Val variant also leading to AFib amyloidosis, which may be more prevalent in the German population than previously suspected. AFib amyloidosis should therefore be included in the differential diagnosis of every German patient presenting with renal amyloidosis. The diagnostic workup described here, including immunohistochemical classification of the amyloid protein followed by direct DNA sequencing, is reliable and excludes other causes of amyloidosis.

Acknowledgements This project was supported by grants of the European Union (EU FP6 EURAMY). We wish to thank Dr. August (Münster), Prof. Krenn (Trier) and Prof. Waldherr (Heidelberg) for kindly providing the kidney biopsies for immunohistochemical analyses, Dr. Thomas Ackermann (Mechernich) and Dr. Kerstin Traser (Halle/Saale) for admission of the patients and Prof. Luft (Berlin) for his critical revision of the manuscript.

Conflict of interest statement We declare that we have no conflict of interest.

References

1. Alexander F, Atkins EL (1975) Familial renal amyloidosis. Case reports, literature review and classification. Am J Med 59:121–128
2. Benson MD (2005) Ostertag revisited: the inherited systemic amyloidoses without neuropathy. Amyloid 12:75–87
3. Benson MD, Kincaid JC (2007) The molecular biology and clinical features of amyloid neuropathy. Muscle Nerve 36:411–423
4. Benson MD, Liepnieks J, Uemichi T, Wheeler G, Correa R (1993) Hereditary renal amyloidosis associated with a mutant fibrinogen alpha-chain. Nat Genet 3:252–255
5. Bohne S, Sletten K, Menard R, Buhling F, Vockler S, Wrenger E, Roessner A, Rocken C (2004) Cleavage of AL amyloid proteins and AL amyloid deposits by cathepsins B, K, and L. J Pathol 203:528–537
6. Bybee, A., Hollenbeck, M., Debusman, E., Gopaul, D., Gilbertson, J., and Lachmann, H. J. (2004) Hereditary renal amyloidosis in a German family associated with fibrinogen Aalhpa chain Glu540Val. In: Xth International Symposium on Amyloid and Amyloidosis, Tours, Loire Valley, France,71.
7. de Carvalho M, Linke RP, Domingos F, Evangelista T, Ducla-Soares JL, Nathrath WB, zevedo-Coutinho C, Lima R, Saraiva MJ (2004) Mutant fibrinogen A-alpha-chain associated with hereditary renal amyloidosis and peripheral neuropathy. Amyloid 11:200–207
8. Doolittle RF, Watt KW, Cottrell BA, Strong DD, Riley M (1979) The amino acid sequence of the alpha-chain of human fibrinogen. Nature 280:464–468
9. Gregorini G, Izzi C, Obici L, Tardanico R, Rocken C, Viola BF, Capistrano M, Donadei S, Biasi L, Scalvini T, Merlini G, Scolari F (2005) Renal apolipoprotein A-I amyloidosis: a rare and usually ignored cause of hereditary tubulointerstitial nephritis. J Am Soc Nephrol 16:3680–3686
10. Hamidi AL, Liepnieks JJ, Uemichi T, Rebibou JM, Justrabo E, Droz D, Mousson C, Chalopin JM, Benson MD, Delpech M, Grateau G (1997) Renal amyloidosis with a frame shift mutation

in fibrinogen a alpha-chain gene producing a novel amyloid protein. Blood 90:4799–4805
11. Hamidi AL, Fournier V, Billerey C, Justrabo E, Chevet D, Droz D, Pecheux C, Delpech M, Grateau G (1998) Fibrinogen A alpha chain mutation (Arg554 Leu) associated with hereditary renal amyloidosis in a French family. Amyloid 5:279–284
12. Hawkins PN (2003) Hereditary systemic amyloidosis with renal involvement. J Nephrol 16:443–448
13. Kang HG, Bybee A, Ha IS, Park MS, Gilbertson JA, Cheong HI, Choi Y, Hawkins PN (2005) Hereditary amyloidosis in early childhood associated with a novel insertion–deletion (indel) in the fibrinogen A alpha chain gene. Kidney Int 68:1994–1998
14. Lachmann HJ, Booth DR, Booth SE, Bybee A, Gilbertson JA, Gillmore JD, Pepys MB, Hawkins PN (2002) Misdiagnosis of hereditary amyloidosis as AL (primary) amyloidosis. N Engl J Med 346:1786–1791
15. Mousson C, Heyd B, Justrabo E, Rebibou JM, Tanter Y, Miguet JP, Rifle G (2006) Successful hepatorenal transplantation in hereditary amyloidosis caused by a frame-shift mutation in fibrinogen A alpha-chain gene. Am J Transplant 6:632–635
16. Neerman-Arbez M (2006) Molecular basis of fibrinogen deficiency. Pathophysiol Haemost Thromb 35:187–198
17. Nichols WC, Dwulet FE, Liepnieks J, Benson MD (1988) Variant apolipoprotein AI as a major constituent of a human hereditary amyloid. Biochem Biophys Res Commun 156:762–768
18. Ostertag B (1950) Familiere amyloid-erkrankung. Zeitschrift für Menschliches Vererbungs und Konstitutionslehre 30:105–115
19. Serpell LC, Benson M, Liepnieks JJ, Fraser PE (2007) Structural analyses of fibrinogen amyloid fibrils. Amyloid 14:199–203
20. Uemichi T, Liepnieks JJ, Benson MD (1994) Hereditary renal amyloidosis with a novel variant fibrinogen. J Clin Invest 93:731–736
21. Uemichi T, Liepnieks JJ, Alexander F, Benson MD (1996) The molecular basis of renal amyloidosis in Irish–American and Polish–Canadian kindreds. QJM 89:745–750
22. Uemichi T, Liepnieks JJ, Yamada T, Gertz MA, Bang N, Benson MD (1996) A frame shift mutation in the fibrinogen A alpha chain gene in a kindred with renal amyloidosis. Blood 87:4197–4203
23. Uemichi T, Liepnieks JJ, Gertz MA, Benson MD (1998) Fibrinogen A alpha chain Leu 554: an African–American kindred with late onset renal amyloidosis. Amyloid 5:188–192
24. Zeldenrust S, Gertz M, Uemichi T, Bjornsson J, Wiesner R, Schwab T, Benson M (2003) Orthotopic liver transplantation for hereditary fibrinogen amyloidosis. Transplantation 75:560–561

Virchows Arch (2008) 453:33–41
DOI 10.1007/s00428-008-0631-8

ORIGINAL ARTICLE

Re-expression of nestin in the myocardium of postinfarcted patients

J. Mokry · R. Pudil · J. Ehrmann · D. Cizkova · J. Osterreicher · S. Filip · Z. Kolar

Received: 4 January 2008 / Revised: 30 April 2008 / Accepted: 14 May 2008 / Published online: 11 June 2008

Abstract Intact cardiac muscle cells in the adult heart do not express intermediate filament nestin. In this study, we report on widespread expression of intermediate filament nestin in human myocardium of patients who died from the myocardial infarction. Nestin was detected in cardiomyocytes, endothelial cells, and few interstitial cells. Elevated levels of nestin were observed in cardiac muscle cells in all specimens, although the intensity of immunoreactivity and distribution of the signal differed. The strongest immunoreactivity was observed from 4 days after myocardial infarction in the infarction border zone where nestin was distributed homogeneously in the entire sarcoplasm of cardiac muscle cells. Within the following week, nestin in immunoreactive cardiomyocytes was redistributed and restricted to small subsarcolemmal foci and to intercalated discs. Angiogenic capillaries that grew between vital nestin-positive cardiomyocytes and entered the necrotic area expressed also high levels of nestin. Nestin-positive endothelial cells were often observed in mutual interactions with nestin-positive cardiac muscle cells. These findings document a crucial role of nestin in remodeling cytoskeleton of cells in the human postinfarcted myocardium.

Keywords Human heart · Nestin · Cardiac muscle cells · Myocardium infarction · Myocardium regeneration

Abbreviation
PCNA proliferating cell nuclear antigen

J. Mokry · D. Cizkova · S. Filip
Department of Histology and Embryology,
Medical Faculty in Hradec Kralove, Charles University in Prague,
Hradec Kralove, Czech Republic

R. Pudil
Department of Internal Medicine, Faculty Hospital,
Hradec Kralove, Czech Republic

J. Ehrmann · Z. Kolar
Department of Pathology, Palacky University,
Medical Faculty in Olomouc,
Olomouc, Czech Republic

J. Osterreicher
Department of Radiobiology, Faculty of Military Health Sciences,
University of Defence,
Hradec Kralove, Czech Republic

J. Mokry (✉)
Department of Histology and Embryology,
Charles University Medical Faculty,
Simkova 870,
500 38 Hradec Kralove, Czech Republic
e-mail: mokry@lfhk.cuni.cz

Introduction

Intermediate filament protein nestin received its name according to its high expression in neuroepithelial cells (NEuroepithelial STem cell proteIN) [9]. However, nestin expression is not limited to neural stem cells, but it can be detected in other immature neural cells, undifferentiated muscular tissue, newly formed endothelial cells [12, 14] and few other cell types (reviewed in [13]). Nestin is expressed temporarily in immature cells and in the course of cell differentiation it is gradually replaced with another intermediate filament; as a result terminally differentiated cells do not express nestin. For example in nervous cells, nestin is replaced with neurofilaments, in astrocytes with GFAP (glial fibrillary acidic protein), in muscular elements with desmin and in endothelial cells with vimentin. This means that nestin expression is restricted to early develop-

mental stages of few cell types and as the cells differentiate, nestin levels are downregulated. For this property nestin can be considered as a unique marker of undifferentiated cells of a given lineage from differentiated elements. Although nestin is absent in terminally differentiated cells, it may be re-expressed in adult tissues under conditions associated with production of new cells, e.g. during physiological turnover, tumorigenesis or after repair of tissues after injury or transplantation [14].

In the course of myogenesis, nestin is expressed in immature muscle elements and as these differentiate it is gradually replaced for vimentin and subsequently for desmin [20]. In smooth muscle, for example in the wall of fetal intestines, nestin is expressed in low levels. In the course of neovascularization, nestin can be detected in myocytes of arteries and veins. In the skeletal muscle, high levels of nestin can be detected in the course of embryonic and fetal development; nestin is expressed in myoblasts and myotubes. In adulthood, skeletal muscle fibres almost do not contain nestin with the exception of tiny sarcoplasmic areas associated with motor plate and myotendinous junctions [28].

Nestin expression in the course of cardiac muscle development was reported by Kachinsky et al. [7]. The authors gave evidence of transient nestin expression in developing murine cardiomyocytes that lasted less than 2 days. After embryonic day 11, the signal disappeared from the myocardium and was completely absent in the foetal and adult mouse heart. In the adult rat heart, re-expression of nestin was detected in the scar tissue that formed after myocardial infarction induced by coronary artery ligation [3]. The authors concluded that nestin was expressed by neural stem cells that contributed to innervation of the scar. Analysis performed recently in mice revealed nestin mRNA levels up-regulated shortly after experimentally induced myocardial infarction [19]. Nestin mRNA levels were also increased in tissue samples from 14 human patients with chronically failing hearts and in three samples from acutely infarcted hearts [19].

Although the cardiac muscle had been long time considered as incapable of regeneration due to high specialisation of its cells, identification of cardiac muscle stem cells [2, 11] confirmed that the adult myocardium may be still capable of regeneration. Because undifferentiated muscular progeny expresses nestin, we performed immunohistochemical analysis of this intermediate filament protein in samples of the myocardium taken from patients who died at different intervals postinfarction. Using antibody specific for human nestin, we studied nestin expression in the myocardium of patients suffering from ischemic heart disease and described morphological characteristics and temporal changes in nestin distribution in cardiac cells in time from the heart attack.

Materials and methods

The tissue was obtained during necropsy in 25 patients who died at different time periods after acute myocardial infarction (age varied from 29 to 85 years, arithmetic mean 70.8 years). All these patients were diagnosed with atherosclerotic disease II or III. For the other clinical data see Table 1. Control tissue was obtained from seven patients (aged from 27 to 41 years, mean 34.3 years) with accidental death. The myocardial tissue was fixed in 10% formalin for 7 days and then embedded in paraffin. One slice in a series of parallel sections was stained with haematoxylin and eosin; the neighbouring slices were processed for immunohistochemistry.

Pseudoperoxidase activity in deparaffinized sections was suppressed in solution of 3% H_2O_2 in methanol. Revitalisation of epitopes was performed by pretreatment in the microwave oven [13]. After a thorough washing in phosphate-buffered solution (PBS) containing 5% Triton X-100 (Sigma), sections were incubated with a primary antibody at 4°C overnight. Nestin in the human tissue was identified with monoclonal antibody 10C2 (Chemicon, UK). After washing with PBS, sites where primary antibody bound to nestin epitopes were visualized with a goat anti-mouse biotinylated antibody, streptavidin conjugated to horseradish peroxidase and diaminobenzidine (Sigma).

Sections were counterstained with the methyl green or haematoxylin. To receive intense signal, some detections were twice amplified with biotinylated tyramine and visualized with streptavidin conjugated to fluorochrome Cy3 (Jackson ImmunoResearch Laboratories). Detection of proliferating cell nuclear antigen (PCNA) was performed is serial sections using monoclonal antibody 5A10 (Immunotech, France). Co-expression of nestin with intermediate filament desmin in cardiomyocytes was detected with rabbit polyclonal anti-desmin antibody (Chemicon, UK), which was recognized with goat anti-rabbit immunoglobulin conjugated to fluorochrome Cy2 (Jackson Immunoresearch Laboratories). Sections processed with omission of the primary antibody were used as controls. Nuclei were then counterstained with DAPI and sections were mounted in polyvinylalcohol/glycerol with DABCO; for light microscopy the sections were mounted in DPX. Sections were examined in Olympus BX51 microscope equipped with epifluorescence and DP-70 camera.

Results

The intact differentiated myocardium of adult people was devoid of nestin immunoreactivity. However, in the infarcted myocardium, nestin was re-expressed by many cardiomyocytes as well as by endothelial cells (Table 1).

Table 1 Patients' characteristics

No.	Gender	Age	Survival	Localization	Previous MI	Hypertrophy	Therapy, other diseases	Nestin immunoreactivity
1	M	80	18 h	TM	2 weeks	LV, RV	C, AC, ACVB 6 days, AAD, HTN	EC ++, CMC + (homogenous; subsarcolemmal)
2	M	80	10 h	SE	−	LV (mild)	C, AAD	EC-, faint signal in few CMC only
3	M	59	36 h	SE	+	LV, RV	AC, D	EC ++, CMC + (subsarcolemmal)
4	M	81	3 days	TM:AS	2 weeks		DIG, BB, AC, DM	EC +, CMC ++ (mostly homogenous)
5	F	61	8 days	TM:AS	−	LV, RV	C, SMα1	EC ++, homogenous in small CMC ++
6	M	70	28 days	SE	−	LV, RV	ACEI, BB, ACVB 3 days,	EC ++, CMC + (faint, subsarcolemmal)
7	F	80	36 h	TM:AL	−	LV	AAD, SMα1, PTCA 3 days, HTN	EC +, CMC faint signal in few cells
8	M	80	7 days	TM	8 years	LV	D, BB, AC, DM, HTN	EC-, CMC ++ (homog; subsarcolemmal), IC+
9	M	77	2 days	TM:AS	3 years	LV, RV	C, AC, N, DM, HTN	EC ++, CMC + (subsarcolemmal)
10	M	59	3 days	TM	−	LV	C, DM, CA	sporadic small CMC + (homogenous)
11	F	76	10 days	TM:IL	37 days	LV, R	C, AC, ACEI, BB	EC ±, CMC ++ (subsarcolemmal)
12	M	79	3 h	SE	−	LV	C, D, HTN, DM, CA	CMC + (homogenous, small groups)
13	F	70	10 h	TM:AL	+	LV	C, AC, atropine, HTN	sporadic CMC ±
14	M	63	8 days	TM,S	−		C, DM, haemodialysis	EC +, CMC ++ (subsarcolemmal; homogenous)
15	M	56	5 days	TM:AS	−	LV, RV	C, AAD, AC, PTCA (5 days)	EC ++, few CMC + (subsarcolemmal; homogenous)
16	F	75	24 h	SE	−	LV, RV	C, ACVB (1 day), HTN	EC-, CMC-
17	F	85	6 days	TM:AL	+		C, N, BB	EC +, CMC + (homogenous)
18	F	29	5 days	TM:AS	−	RV (mild)	AC, AOE, DM, PTCA (5 days)	EC +, few small CMC ++ (homogenous)
19	M	81	24 h	SE	+	LV, RV	C, AC, BB	EC ++, CMC (subsarcolemmal ++, homogenous+)
20	M	68	8 days	SE	7 years		ACVB (7 years), DM, HTN	EC +, CMC ++ (subsarcolemmal), IC+
21	M	75	3 h	TM	−	LV, RV	C, atropine, DM, HTN	no immunoreactivity
22	F	66	24 h	SE	10 days	LV, RV	C, ACVB (1 day)	EC +, CMC ++ (homogenous)
23	F	84	3 days	TM	+	LV (mild)	TED, FNF	few CMC + (subsarcolemmal; homogenous)
24	F	71	11 days	TM: AS	−	LV, RV	D, BB, ACEI, AC	EC +, CMC + (subsarcolemmal; homogenous)
25	M	66	3 days	SE	2 years	LV, RV	C, AC, AAD, D,	CMC + (subsarcolemmal; few CMC homogenous)

Explanation and abbreviations: Survival: time from symptoms/diagnosis to death; Localization (of the infarction): *TM* transmural, *SE* subendocardial, *AS* anteroseptal, *AL* anterolateral, *IL* inferolateral, *S* septal; Previous MI (previous myocardial infarction in patient's history): + indicates histopathological findings of previous MI (scar) without knowledge of time of previous MI in patient's history; Hypertrophy (of the heart): *LV* left ventricle, *RV* right ventricle; Therapy, other diseases: *AAD* antiarrhythmic drugs, *AC* anticoagulants, *ACEI* ACE inhibitor, *ACVB* aortocoronary venous bypass, *AOE* antioedematic drugs, *BB* beta blocker, *C* catecholamine, *CA* carcinoma, *D* digitalis, *DM* diabetes mellitus, *FNF* fractured neck of femur, *HTN* hypertension, *N* nitrate, *PTCA* percutaneous coronary angioplasty, *SMα1* sympatomimetic α1 drugs, *TED* thromboembolic disease; Nestin immunoreactivity: *EC* endothelial cells, *CMC* cardiac muscle cells, *IC* interstitial cells.

Nestin$^+$ cardiomyocytes were found in frequent clusters in vicinity to necrotic areas or in a small distance from them. Each sample contained a different ratio of nestin$^-$ and nestin$^+$ cardiomyocytes. In early infarctions (approximately 10 h after heart attack), there were only few nestin$^+$ cardiomyocytes, whereas by 4 to 5 days after infarction there was an increase in the number of immunoreactive cardiac cells and in lesions more than 1 week postinfarction almost all cardiomyocytes neighbouring the scar areas were nestin-positive. The largest amount of nestin$^+$ cardiomyocytes was detected in the tissue obtained from patients suffering from chronic ischemic disease.

Nestin levels as well as sarcoplasmic distribution of this protein also differed between samples. The changes likely corresponded to the time period from the onset of acute infarction. Histological sections, taken from patients who died after four to 5 days, contained small and intensively stained cells with nestin homogenously distributed in their

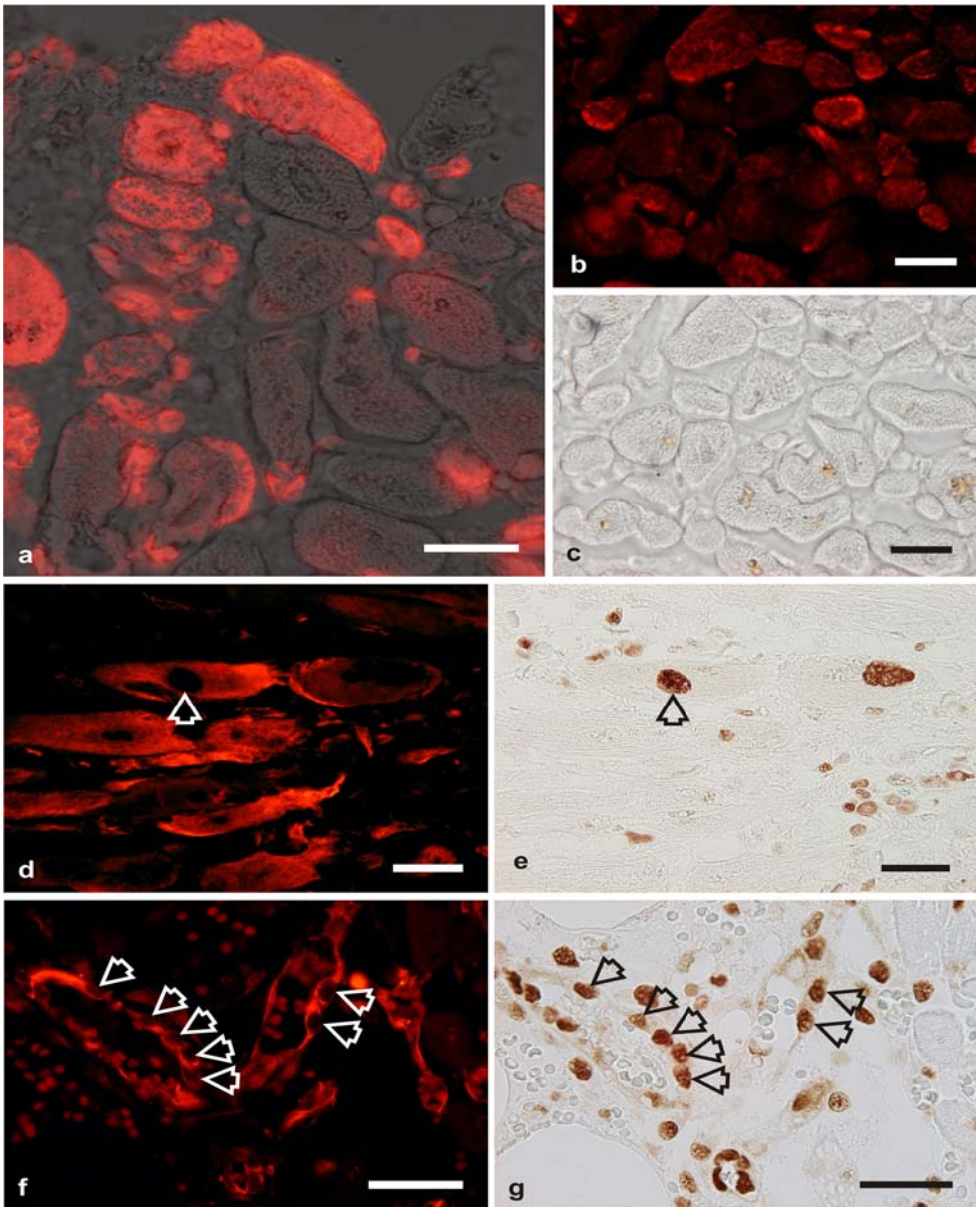

Fig. 1 Nestin-immunoreactive cells in the infarcted human myocardium. The largest nestin-positive cells are represented by cardiomyocytes (**a**–**d**). Few days after infarction, nestin is homogeneously distributed in their cell sarcoplasm. Nestin is expressed in many but not in all cardiac muscle cells (e.g. in **b**); phase contrast (**c**) allows visualization of all cells in the microscopic field. Some of the nestin^{+} cardiomyocytes express proliferating marker PCNA (*arrow* in **d** and **e**) while the others not. On the contrary, all nestin^{+} endothelial cells (*arrows* in **f**) in angiogenic capillaries in this tissue express PCNA (corresponding PCNA^{+} cell nuclei indicated with arrows in **g**). *Scale bars* indicate 40 μm

sarcoplasm (Figs. 1a,b,d, and Fig.3a–b). After 10 days, in most immunoreactive cells, signal was concentrated in one to two subsarcolemmal foci and in the remaining sarcoplasmic areas, nestin was downregulated (Figs. 2a–c) and replaced with desmin (Figs. 2b, f). Quite frequently we also observed cardiomyocytes containing nestin just in the vicinity to the intercalated discs. Such nestin distribution intensively visualized areas of intercalated discs between coupled cardiomyocytes especially if nestin^{+} cardiac muscle cell was connected with nestin cell (Figs. 2d,f).

Localization of the myocardial infarction had no effect on intensity or distribution of immunoreactivity. In intramural infarctions, nestin-immunoreactivity was often identified in a tissue adjacent to the endocardium or pericardium. We observed nestin expression in all samples including the tissues of elderly people (including eight patients who died from myocardial infarction at the age from 80 to 85 years).

Cardiac muscle cells were not the only cells that expressed nestin. Nestin was heavily expressed in blood vessels, especially in capillaries (Figs. 3d–e). High levels of nestin were observed in capillaries growing in the necrotic tissue. The irregular endothelial cells at tips of such capillaries had bizarre shapes sending tiny cytoplasmic protrusions. Nestin^{+} elements present in the infarcted myocardium occupied distinct zones (Figs. 2e and 3c). In the centre of the necrotic area (zone I), no nestin^{+} cells were observed. In the border area (zone II), numerous nestin^{+} capillaries grew into the necrotic tissue. In the next adjacent

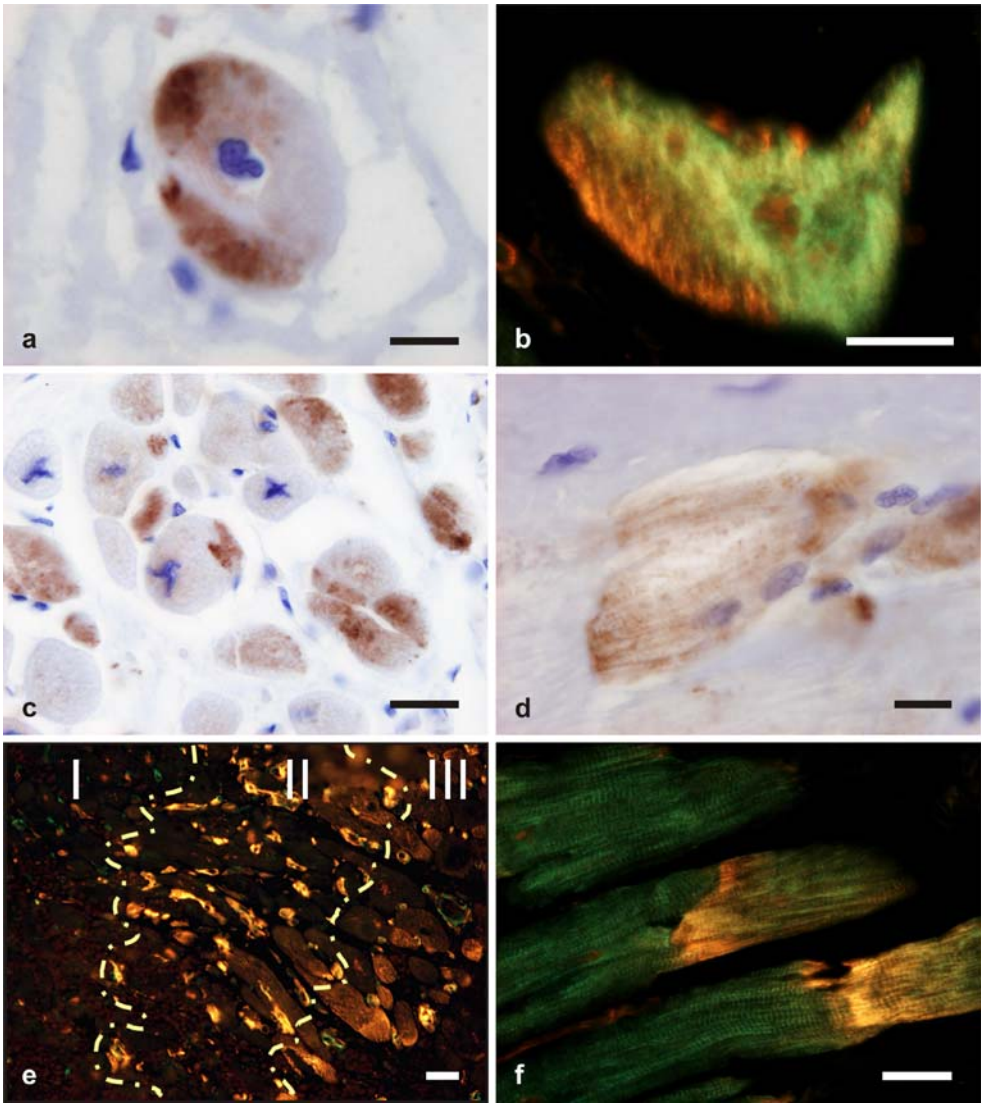

Fig. 2 Changes in nestin sarcoplasmic distribution (**a**–**d**, **f**). After 10 days from the onset of the myocardial infarction, nestin still remains in cardiac muscle cells, but it does not occupy the entire sarcoplasm but becomes confined to some foci in the peripheral sarcoplasm. Nestin-negative areas contain intermediate filament desmin (green signal in **b** and **f**, nestin is visualized in *red*). In longitudinal sections, nestin becomes confined to areas of intercalated discs (**d**, **f**). In **d** and **f**, nestin$^+$ cardiomyocyte is coupled with nestin-cardiomyocytes. In the infarcted myocardium, nestin$^+$ elements show characteristic zonal arrangement (**e**). Necrotic tissue in zone I is nestin$^-$. The adjacent border zone (II) contains nestin$^+$ capillaries that are followed by the zone III, which contains additionally nestin$^+$ cardiomyocytes. *Scale bars* indicate 20 μm in a, b, d and 50 μm in c, e, f

zone (zone III), nestin$^+$ capillaries were found between nestin$^+$ cardiac muscle cells. Often nestin$^+$ endothelial cells were in a close and intimate contact with nestin$^+$ cardiac muscle cells, which indicated that active interaction between these distinct nestin$^+$ elements occurred in the zone III.

Rarely, few nestin$^+$ cells were encountered in the interstitial tissue. Morphology of these cells differed from cardiomyocytes and endothelial cells; they were usually spindle-shaped with elongated cellular processes (Fig. 3f).

To identify whether appearance of nestin in the cell cytoplasm is associated with cell proliferation a double immunostaining was performed to recognize which nestin$^+$ cells co-expressed PCNA. Anti-PCNA immunohistochemistry stained most cells in the granulation tissue including infiltrating elements. Immunostaining of capillaries was distinct in areas of the regenerating myocardium where the connective tissue was reduced. In blood capillaries, nestin$^+$ endothelial cells co-expressed a proliferating marker PCNA in their nuclei (Figs. 1f–g). As opposed to endothelial cells, only a low portion of cardiomyocytes expressed PCNA; nevertheless, most PCNA$^+$ cardiomyocytes expressed nestin (Figs. 1d–e).

Discussion

We provide evidence on nestin expression in cardiac muscle in patients who died from myocardial infarction. The cells that expressed nestin positivity included cardiomyocytes, endothelial cells and few other cell types. Cardiac muscle cells of patients after heart attack expressed high levels of nestin, whereas in the intact adult myocardium nestin was not expressed.

During development, nestin is transiently expressed in the embryonic cardiac muscle cells. In the course of cardiac

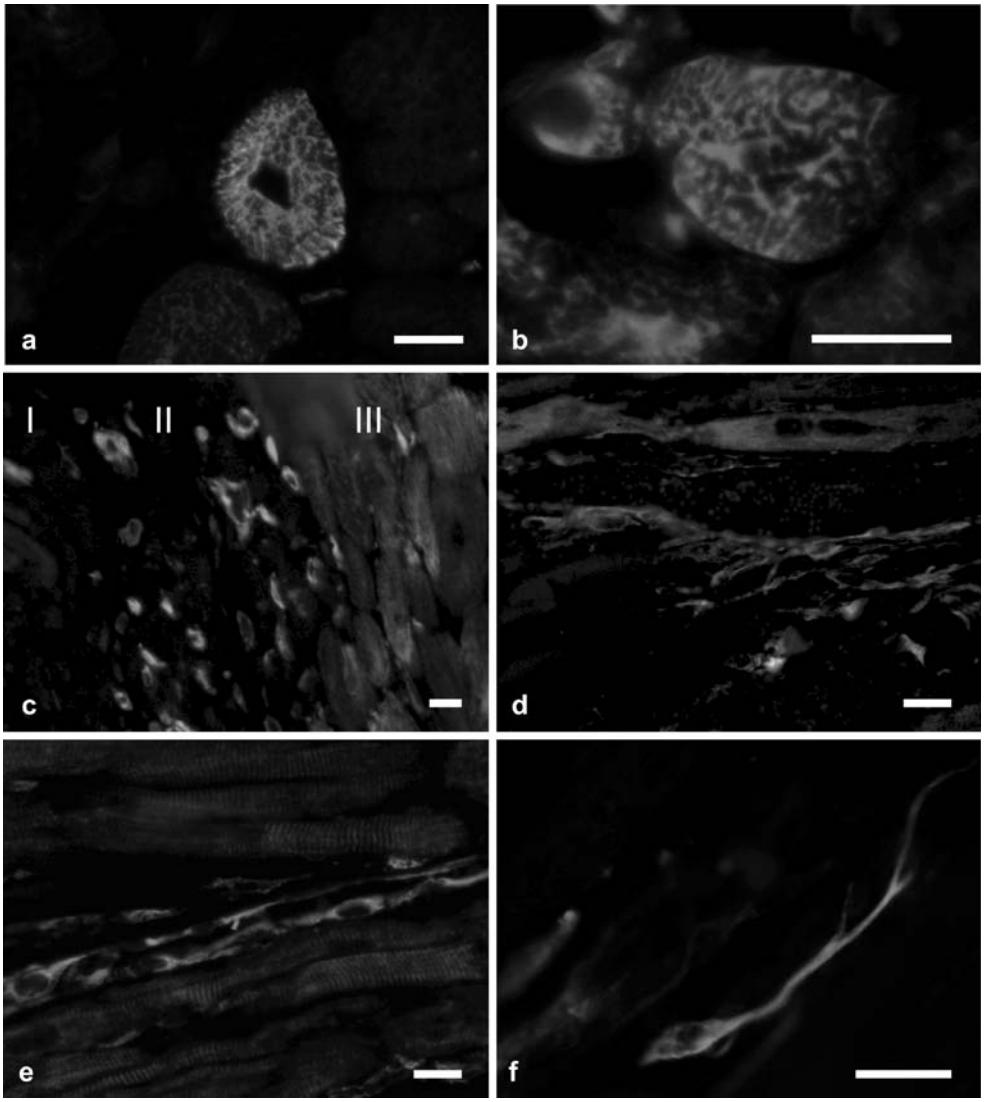

Fig. 3 Nestin expression in distinct cell types of the infarcted myocardium. Few days after myocardial infarction, nestin is re-expressed in cardiac muscle cells; the specific signal is homogenously distributed throughout the sarcoplasm (**a**, **b**). Nestin^{+} cardiomyocytes and endothelial cells are distributed in three characteristic zones (**c**). In the infarction border zone, nestin is also expressed in endothelial cells of angiogenic capillaries (**d**, **e**). On occasions, nestin appears also in interstitial cells that differ from endothelia and cardiomyocytes in their morphology and location (**f**). *Scale bars* indicate 40 μm

myogenesis in mice, nestin was detected in atrial and ventricular cells throughout the heart from embryonic day 9 (ED9) and its expression lasted until ED10.5 [7]. From ED11 to adulthood, nestin was absent from cardiac myocytes. These data are in concordance with our unpublished results of nestin expression in the rat and human embryonic myocardium.

Despite the dogma that the myocardium is incapable of reparation, it has been recently evidenced that the heart is also capable of regeneration. In the intact adult cardiac muscle, proliferation of cardiomyocytes occurs at low frequency, which increases more than 50 times in response to acute ischemic injury [1]. Recent identification of multipotent cardiac stem cells [2, 11] confirms that the myocardium has its own reservoir of endogenous tissue-specific stem cells, which are able to produce the major structural components of the heart tissue including cardiac muscle, endothelial and smooth muscle cells (the latter participate in the formation of blood vessels). The stem cells are activated after ischemic injury [27]. Thus, new cardiomyocytes can be generated directly by cardiac tissue-specific stem cells.

Another source for production of cardiac myocytes can be also represented by neural crest stem cells because their derivates during development contribute to generation of the myocardium and cardiomyocytes [26]. Usually cardiomyocytes are considered to be derived from the mesenchymal stem cells. In adulthood, mesenchymal stem cells can be isolated from the bone marrow as bone marrow stromal stem cells or as multipotent adult progenitor cells [16, 18]. It may be hypothesized that similar stem cells could be also identified in other tissues derived from the mesenchyma. Bone marrow stem cells have enormous plasticity and after transplantation of bone marrow cells in chick embryonic heart, the grafted cells can be converted in cardiomyocytes [4]. Even after intracoronary or intramyocardial transplanta-

tion these stem cells participate in regeneration of the infarcted myocardium in mice and human patients [15, 24, 29] although results of some other authors do not confirm effective participation of the transplanted bone marrow cells in the repair of the infarcted heart tissue [8, 19].

Nevertheless, even cultured bone marrow mesenchymal stem cells, according to our unpublished data and those of others, can express nestin. Some authors consider nestin as a marker of stem cells. Although nestin is expressed in neural stem cells [5] and few other types of stem cells, it is not found in all stem cell types, e.g. it is absent in embryonic and haemopoietic stem cells. Nevertheless, our finding of nestin immunoreactivity in slim [17] elements with tiny elongated cytoplasmic processes (Fig. 3f) could indicate recruitment of at least few mesenchymal (stem) cells in reparative heart processes in response to ischemic damage.

The findings of widespread nestin expression in the human infarcted myocardium described in this study might indicate that nestin reappearance in the adult myocardium subjected to ischemia is likely associated with regenerative processes and possibly with generation of new cells. This hypothesis is supported with the following findings:

1. First, the formation of new blood vessels is a prerequisite for nutrition of the healing tissue. Expression of nestin was regularly observed in angiogenic capillaries found most abundantly at the border zone. Some capillaries were observed at the edges of the necrotic tissue, while the others grew among surviving cardiac muscle cells. Endothelial cells in these capillaries expressed high levels of nestin and co-expressed PCNA in their nuclei, which confirmed that these cells were newly formed. Nestin upregulation was well documented, e.g. in dividing neuroepithelial and endothelial cells [5]. Nestin$^+$ endothelial cells at tips of growing capillaries had bizarre shapes with irregular tiny processes. Nestin$^+$ endothelial cells found between living cardiac muscle cells were often observed in a close interaction with cardiac muscle cells, which might indicate that cell-to-cell interactions help to promote cardiomyocyte survival. Similar interactions accompanied by secretion of trophic factors released by endothelial cells have been documented to play an important role in hepatogenesis and neurogenesis [10, 21].
2. Second, it is absence of nestin in the intact myocardium of healthy adult people and its upregulation in few days following ischemic heart failure.
3. Third, it is the intensity of nestin immunoreactivity and characteristic pattern of its temporal and spatial distribution in the sarcoplasm of cardiomyocytes. In early time points after heart attack, there appear only few nestin$^+$ cardiac muscle cells and nestin is homogeneously distributed over their sarcoplasm. After 4 to 7 days, more nestin$^+$ cardiomyocytes appear and subsequently nestin is distributed to certain compartments of their sarcoplasm. After approximately 10 days from myocardial infarction, nestin is confined to small foci of subsarcolemmal cytoplasm and to intercalated discs. This pattern of changes in sarcoplasmic distribution corresponds to pattern observed in developing and regenerating skeletal muscle fibres [28] where first the entire sarcoplasm is filled with nestin intermediate filaments and finally after nestin levels are downregulated; it is confined to the areas of myotendinous junctions and motor end plate, while in the remaining sarcoplasm nestin was lost.
4. Finally, we observed nestin immunoreactivity in cardiac muscle cells that co-expressed PCNA in their nuclei. Most (but not all) nestin$^+$ cardiac muscle cells were PCNA$^-$ because in the infarcted myocardium PCNA was expressed only in a low portion of cardiomyocytes. However, PCNA$^+$ cardiomyocytes co-expressed nestin, which may be consistent with findings on rare mitotic divisions observed in cardiomyocytes described earlier by Beltrami [1].

Scobioala et al. [19] who observed upregulation of nestin mRNA levels in the infarcted hearts performed a proteomic analysis of tissue samples obtained from mouse model of myocardial infarction. They found that nestin was co-expressed with the stem cell markers c-kit, Sca-1, Mdr-1, and ABCG2 in small interstitial cells and concluded that enhanced nestin expression might reflect regenerative processes in the injured heart. Our observation of nestin-immunoreactivity in newly formed (i.e. PCNA$^+$) endothelial cells is in agreement with the conclusion of Scobioala et al. that nestin expression reflects regenerative processes in the heart. Therefore nestin can be considered as a useful marker of regenerative processes in the myocardium. On the contrary, only a small number of nestin$^+$ cardiomyocytes in our study was found to co-express proliferative marker PCNA, which indicated that most nestin$^+$ cardiomyocytes were not newly generated.

We hypothesize that nestin expression in such cells is associated with the reorganization of the cytoskeleton in the cardiomyocytes subjected to ischemic injury and/or dynamic changes after myocardial infarction. Ventricular cardiomyocytes that are preserved and remain functional after myocardial infarction must compensate the loss in myocardial necrotic tissue to maintain vital circulation. The permanent loss of the necrotic heart tissue results in haemodynamic overload of the functional cardiomyocytes, which is followed by morphological changes. Cytoskeletal alterations that occur in cardiomyocytes in coronary artery

disease, dilated cardiomyopathy or pressure-overload hypertrophy include an increase in content, density and distribution of desmin, vimentin and other cytoskeleton components [6, 22, 25]. It is likely that after increased functional demands in the postinfarcted heart, nestin participates in rebuilding cardiomyocyte cytoskeleton in proportion to new dynamic changes, but it forms heterodimers and heterotetramers with other intermediate filaments that makes the intermediate filament network less stable [23].

This leads to the fragmentation and disassembly of the original filamentous cytoskeleton components allowing cardiomyocyte remodelling proportionate to changed haemodynamic loads. Thus in addition to being a marker of regenerative events, nestin may be considered as a morphological correlate for the dynamical changes that occur in the structure of affected cardiomyocytes.

Myocardial biopsies have proved useful in exploring cytoskeletal alterations in cardiac diseases. Future studies focused on nestin participation in cytoskeleton remodelling of cardiomyocytes might greatly benefit by this approach and bring new data on nestin temporal and topographical localization in the infarcted heart.

Taken together, our data on widespread expression of nestin that occurs in the human myocardium after the myocardial infarction support the idea that this intermediate filament is one of the key structural proteins involved in the cellular processes associated with the repair of the myocardium. Nestin is re-expressed in cardiomyocytes, endothelium of angiogenic capillaries and few other cell types. In cardiac muscle cells subjected to ischemic injury, nestin transient re-expression shows characteristic spatial and temporal distribution. Similar pattern of nestin expression in cardiomyocytes was observed in specimens obtained both from young and elderly patients, which confirms the uniform adaptation of cells to the myocardial injury throughout the entire lifespan. According to our results, nestin can be considered as a useful marker for analysis of changes that occur in the infarcted heart.

Acknowledgement The authors thank Mrs. Helena Rückerová and Mrs. Hana Hollerová for their skillful technical assistance. The study was supported by the project MSM0021620817.

Conflict of interest statement We declare that we have no conflict of interest.

References

1. Beltrami AP, Urbanek K, Kajstura J, Yan S, Finto N, Bussani R, Nadal-Ginard B, Silvestri F, Leri A, Beltrami A, Anversa P (2001) Evidence that human cardiac myocytes divide after myocardial infarction. N Engl J Med 344:1750–1757
2. Beltrami AP, Barlucchi L, Torella D, Baker M, Limana F, Chimenti J, Kasahara H, Rota M, Musso E, Urbanek K, Leri A, Kajstura J, Nada L, Ginard B, Anversa P (2003) Adult cardiac stem cells are multipotent and support myocardium regeneration. Cell 114:763–776
3. Drapeau J, El-Helou V, Clement R, Bel-Hadj S, Gosselin H, Trudeau L-E, Villeneuve L, Calderone A (2005) Nestin-expressing neural stem cells identified in the scar following myocardial infarction. J Cell Physiol 204:51–62
4. Eisenberg CA, Burch JBE, Eisenberg LM (2006) Bone marrow cells transdifferentiate to cardiomyocytes when introduced into the embryonic heart. Stem Cells 24:1263–1245
5. Frederiksen K, McKay RDG (1988) Proliferation and differentiation of rat neuroepithelial precursor cells in vivo. J Neurosci 8:1144–1151
6. Ganote C, Armstrong S (1993) Ischaemia and the myocyte cytoskeleton: review and speculation. Cardiovasc Res 27:1387–1403
7. Kachinsky AM, Dominov JA, Miller JB (1995) Intermediate filaments in cardiac myogenesis: nestin in the developing mouse heart. J Histochem Cytochem 43:843–847
8. Kuethe F, Richartz BM, Sayer HG, Kasper C, Werner GS, Hoffken K, Figulla HR (2004) Lack of regeneration of myocardium by autologous intracoronary mononuclear bone marrow cell transplantation in humans with large anterior myocardial infarctions. Int J Cardiol 97:123–127
9. Lendahl U, Zimmermann LB, McKay RD (1990) CNS stem cells express a new class of intermediate filament protein. Cell 60:585–595
10. Matsumoto K, Yoshitomi H, Rossant J, Zaret KS (2001) Liver organogenesis promoted by endothelial cells prior to vascular function. Science 294:530–531
11. Messina E, Angelis L, Frati G, Morrone S, Chimenti S, Fiordaliso F, Salio M, Battaglia M, Latronico MVG, Coletta EV, Frati L, Cossu G, Giacomello A (2004) Isolation and expansion of adult cardiac stem cells from human and murine heart. Circ Res 95:911–921
12. Mokry J, Nemecek S (1998) Angiogenesis of extra- and intra-embryonic blood vessels is associated with expression of nestin in endothelial cells. Folia Biol (Prague) 44:155–161
13. Mokry J, Nemecek S (1998) Immunohistochemical detection of intermediate filament nestin. Acta Med (Hradec Kralove) 41:73–80
14. Mokry J, Cizkova D, Filip S, Hermann J, Österreicher J, Kolar Z, English D (2004) Nestin expression by newly formed human blood vessels. Stem Cells Dev 13:658–664
15. Orlic D, Kajstura J, Chimenti S, Jakoniuk I, Anderson SM, Li B, Pickem J, McKay R, Nadal-Ginard B, Bodine DM, Leri A, Anversa P (2001) Bone marrow cells regenerate infarcted myocardium. Nature 410:701–705
16. Prockop DJ (1997) Marrow stromal cells as stem cells for nonhematopoietic tissues. Science 276:71–74
17. Ramalho-Santos M, Yoon S, Matsuzaki Y, Mulligan RC, Melton DA (2002) Transcriptional profiling of embryonic and adult stem cells. Science 298:597–600
18. Reyes M, Verfaillie CM (2001) Characterization of multipotent adult progenitor cells, a subpopulation of mesenchymal stem cells. Ann N Y Acad Sci 938:231–233
19. Scobioala S, Klocke R, Kuhlmann M, Tian W, Hasib L, Milting H, Koenig S, Stelljes M, El-Banayosy A, Tenderich G, Michel G, Breithardt G, Nikol S (2008) Up-regulation of nestin in the infarcted myocardium potentially indicates differentiation of resident cardiac stem cells into various lineages including cardiomyocytes. FASEB J 22:1021–1031
20. Sejersen T, Lendahl U (1993) Transient expression of the intermediate filament nestin during skeletal muscle development. J Cell Sci 106:1291–1300
21. Shen Q, Goderie SK, Jin L, Karanth N, Sun Y, Aramova N, Vincent P, Pumiglia K, Temple S (2004) Endothelial cells

stimulate self-renewal and expand neurogenesis of neural stem cells. Science 304:1338–1340
22. Somma S, Marotta M, Salvatore G, Cudemo G, Cuda G, Vivo F, Benedetto MP, Ciaramella F, Caputo G, Divitiis O (2000) Changes in myocardial cytoskeletal intermediate filaments and myocyte contractile dysfunction in dilated cardiomyopathy: an in vivo study in humans. Heart 84:659–667
23. Steinert PM, Chou YM, Prahland V, Parry DA, Marekov LN, Wu K, Jang SI, Goldman RD (1999) A high molecular weight intermediate filament-associated protein in BHK-21 cells is nestin, a type VI intermediate filament protein. Limited co-assembly in vitro to form heteropolymers with type III vimentin and type IV α-internexin. J Biol Chem 274:9881–9890
24. Strauer BE, Brehm M, Zeus T, Köstering M, Hernandez A, Sorg RV, Kögler G, Wernet P (2002) Repair of infarcted myocardium by autologous intracoronary mononuclear bone marrow cell transplantation in humans. Circulation 106:1913–1925
25. Tagawa H, Wang N, NArishige T, Ingber DE, Zile MR, Cooper G (1997) Cytoskeletal mechanics in pressure-overload cardiac hypertrophy. Circ Res 80:295–296
26. Tomita Y, Matsumura K, Wakamatsu Y, Matsuzaki Y, Shibuya I, Kawaguchi H, Ieda M, Kanakubo S, Shimazaki T, Ogawa S, Osumi N, Okano H, Fukuda K (2005) Cardiac neural crest cells contribute to the dormant multipotent stem cell in the mammalian heart. J Cell Biol 170:1135–1146
27. Urbanek K, Torella D, Sheikh F, Angelis A, Nurzynska D, Silvestri F, Beltrami CA, Bussani R, Beltrami AP, Quaini F, Bolli R, Leri A, Kajstura J, Anversa P (2005) Myocardial regeneration by activation of multipotent cardiac stem cells in ischemic heart failure. Proc Natl Acad Sci U S A 102:8692–8697
28. Vaaittinen S, Lukka R, Sahlgren C, Rantanen J, Hurme T, Lendahl U, Eriksson JE, Kalimo H (1999) Specific and innervation-regulated expression of the intermediate filament protein nestin at neuromuscular and myotendinous junctions in skeletal muscle. Am J Pathol 154:591–600
29. Yoon Y, Wecker A, Heyd L, Park JS, Tkebuchava T, Kusano K, Hanley A, Scadova H, Qin G, Cha DH, Johnson KL, Aikawa R, Sahara T, Losordo DW (2005) Clonally expanded novel multipotent stem cells from human bone marrow regenerate myocardium after myocardial infarction. J Clin Invest 115:326–338

Virchows Arch (2008) 453:43–46
DOI 10.1007/s00428-008-0622-9

ORIGINAL ARTICLE

The construction of high-density paraffin tissue microarrays with 0.43-mm-diameter paraffin tissue core biopsies is technically feasible

Ulrich F. Vogel

Received: 15 March 2007 / Revised: 7 April 2008 / Accepted: 21 April 2008 / Published online: 13 June 2008

Abstract Paraffin tissue microarrays (PTMAs) are blocks of paraffin containing up to 1,000 paraffin tissue core biopsies (PTCBs). The growing number of publications in recent years bears eloquent witness to the advantages of these PTMAs in high-throughput molecular profiling of tumor specimens. In order to conserve the often minute quantities of available tumor tissue with precisely recorded follow-up data and to store the greatest possible number of PTCBs in one block, researchers often try to reduce PTCBs to the smallest possible diameter. Until now, the smallest feasible diameter for PTCBs was 0.6 mm. Experiments with diameters below 0.6 mm have failed due to the instability of the paraffin tissue punch. The process described allows the construction of PTMAs with PTCBs only 0.43 mm in diameter utilizing simple, inexpensive, self-made paraffin tissue punches and predrilled recipient blocks.

Keywords Pathology · Methods · Histologic techniques · Tissue microarrays · Paraffin tissue core biopsies

Introduction

Paraffin tissue microarrays (PTMAs) are blocks of paraffin containing up to 1,000 paraffin tissue core biopsies (PTCBs) [1]. The growing number of publications in recent years and the large array of commercially available PTMAs bear eloquent witness to the advantages of these PTMAs in high-throughput molecular profiling of tumor specimens and on-slide controls for immunohistochemistry [1, 3]. In order to conserve the often minute quantities of available tumor tissue with precisely recorded follow-up data and to store the greatest possible number of PTCBs in one block, researchers often try to reduce PTCBs to the smallest possible diameter. Until now, the smallest feasible diameter for PTCBs was 0.6 mm. Experiments with diameters below 0.6 mm have failed due to the instability of the paraffin tissue punch ("broken needles 0.4 mm in diameter", personal communication Prof. Sauter, Hamburg). To increase the density of PTCBs in a single PTMA and as a result increase the efficiency of PTMAs, paraffin tissue punches with 0.43 mm in diameter were tested.

Material and methods

To construct a PTMA one basically requires a paraffin tissue punch and a recipient paraffin block with holes to accommodate the PTCBs. As described by Wan et al. [8], we manufactured the paraffin tissue punches using ordinary hypodermic needles of different diameters. Briefly, hypodermic needles (black needle: 22G, 0.70 mm outer diameter×30 mm length; inner diameter, approximately 0.43 mm; Sterican, B. Braun Melsungen AG, Melsungen, Germany) were shortened to a length of 2 cm and sharpened using a drill grinder (Micromot 50/E, Proxxon, Niersbach, Germany; cost, $50) fitted with a cutting disc (Fig. 1a). In order to push the punched PTCBs out of the needles, stylets were constructed out of hypodermic needles with an outer diameter corresponding to the inner diameter of the needle punches described above (white needle: 27G; 0.40 mm outer diameter×20 mm length, Sterican, B. Braun Melsungen AG, Melsungen, Germany) (Fig. 1a). The holes

U. F. Vogel (✉)
Institute of Pathology, University Hospital,
Eberhard-Karls-University,
Liebermeisterstrasse 8,
72076 Tuebingen, Germany
e-mail: ulrich.vogel@med.uni-tuebingen.de

in the paraffin receptor block were drilled using an ordinary microcompound table and a drill grinder or a computer numerical control (CNC) drilling machine as described in earlier papers [6, 7]. Briefly, an ordinary paraffin block with a plastic cassette was fixed in a small water bath milled out of a block of polyvinyl chloride. This water bath was placed on a microcompound table (K70, Proxxon, Niersbach, Germany; cost, $85) in a drill stand (MB140/S, Proxxon, Niersbach, Germany; cost, $50) (Fig. 1b). A drill grinder was fitted with a 0.43-mm-diameter drill bit to bore the holes (HSS, DIN 338, RW, Gühring oHG, Albstadt, Germany). By turning the wheels of the microcompound table in 0.7-mm steps, a regular pattern was produced with 0.27 mm between each 0.43-mm-diameter hole. The temperature of the water bath was maintained at 15–20°C. Alternatively, the water bath with the paraffin block was put on the x–y stage of a CNC drilling machine (Maho MH400E, Deckel-Maho-Gildemeister, Bielefeld, Germany) to create the holes in the recipient block. To obtain the PTCBs the operator punched PTCBs out of the donor blocks holding the stylet withdrawn a few millimeters. These PTCBs were then manually transferred to the predrilled recipient block by plunging the stylet down (Fig. 1c). This procedure was facilitated by the use of a magnifying glass and lamp for proper illumination of the recipient block. A cold light source was used so the paraffin of the recipient block would not be softened by the heat of the lamp. Once all of the holes were filled, the recipient block was pressed against a flat surface such as a glass slide to push the PTCBs deeper into the holes and to even out the surface of the PTMA, since individual PTCBs may look out above the surface of the paraffin block. As an optional,

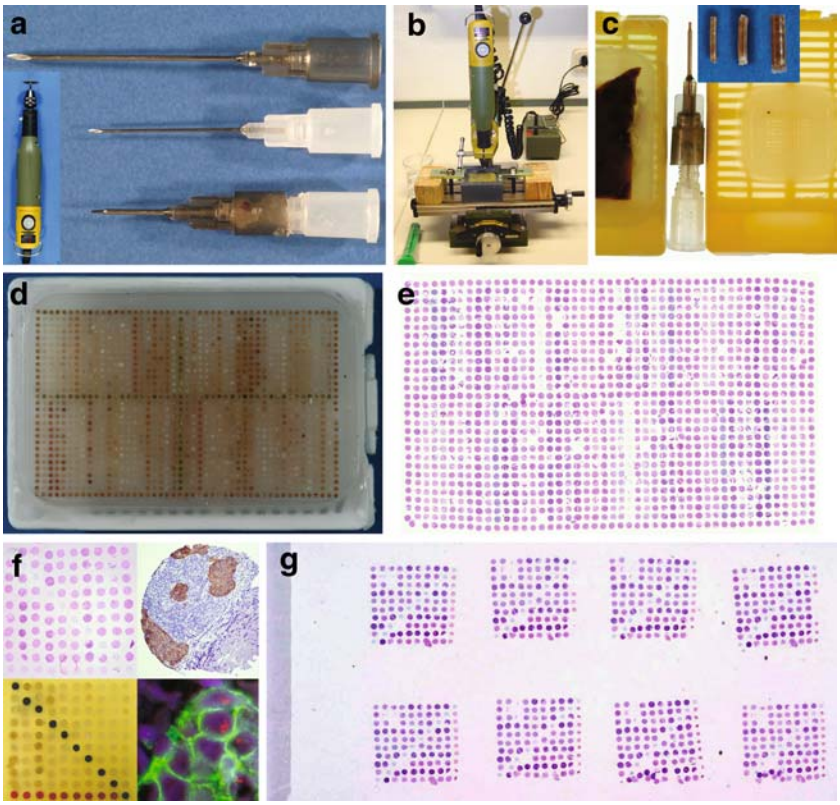

Fig. 1 **a-g** Construction of paraffin tissue microarrays (PTMAs) with paraffin tissue core biopsies (PTCBs) 0.43 mm in diameter. **a** Construction of paraffin tissue punches out of conventional hypodermic needles with a drill grinder fitted with a cutting disc (*inset*). Paraffin tissue punch (*black*; 22 G; outer diameter, 0.7 mm; inner diameter, 0.43 mm) and stylet (*white*; 27G; outer diameter, 0.4 mm) after shortening and sharpening. **b** Drilling of the holes of the PTMA with a drill grinder in a drill stand on an ordinary microcompound table. The plastic cassette is fixed in a water bath to cool the drill (distilled water, 15–20°C). **c** Manual transfer of the PTCBs from the donor blocks to the predrilled recipient block with a self-made paraffin tissue punch. Recipient block: 100 holes; 0.43 mm in diameter; distance between holes, 0.27 mm. Caution: Stylet must be withdrawn several millimeters before punching the tissue. The length of the PTCBs did not depend on the diameter of the tissue punch but on the thickness of the tissue in the donor block (*inset*: PTCBs 0.43 mm, 0.6 mm and 1.0 mm in diameter; from left to right). **d** PTMA with 1363 PTCBs of 0.43 mm in diameter. **e** Correspondent H- and E-stained section of the PTMA comprising 1,363 PTCBs (d). PTCBs displaying a weak staining consist of lung tissue and cell block material. **f** PTMA with 100 PTCBs 0.43 mm in diameter. PTMA with 100 PTCBs 0.43 mm in diameter after cutting (*lower left*). Section stained with H and E (*upper left*). Section stained with anti-HER2 (DAB, breast carcinoma, 100×) (*upper right*). Double staining of the PTMA section: Immunofluorescence (membranous green staining, FITC-anti-HER2) and fluorescence in situ hybridization (red nuclear signals, amplification of the HER2 gene; DAPI: nuclear counterstain, 1,000×) (*bottom right*). **g** Eight sections of a PTMA with 100 PTCBs on a single slide with a total of 800 PTCBs

additional step the PTMA was placed into an oven for 15 min or longer at a temperature of 50°C in order to make the paraffins of the recipient block and the PTCBs sticky. The purpose of this extra step was to improve the contact between the paraffins in order to prevent the PTCBs from curling up after sectioning. The PTMA was then slowly cooled to prevent the formation of cracks in the paraffin. Subsequent cutting and staining followed routine protocols for paraffin blocks. To validate the technique PTMAs were constructed utilizing 1.0-mm, 0.6-mm, and 0.43-mm-diameter PTCBs of synovial sarcomas, endocrine tumors, and renal cell carcinomas. Furthermore, some PTMAs contained PTCBs of different tissues like breast carcinomas. The PTMAs held up to 1,363 PTCBs each. Sections of these PTMAs were stained immunohistochemically and by immunofluorescence (e.g., anti-calretinin, anti-CD10, anti-chromogranin (all with heat-induced antigen retrieval)) and by fluorescence in situ hybridization (e.g., HER2 (PathVysion, Abbott-Vysis)).

Results

As shown in Fig. 1d and e, it is possible to construct PTMAs with up to 1,363 PTCBs 0.43 mm in diameter using a standard paraffin block (3,7×2,3 cm; distance of the PTCBs, 0.27 mm). With the method described I did not encounter any of the problems with breaking paraffin tissue punches that were reported in earlier trials. If the donor tissue was well fixed and paraffinized there was also no problem with the stability of the PTCBs. The length of the PTCBs did not depend on the diameter of the tissue punch, but on the thickness of the tissue in the donor block (Fig. 1c, inset). Until now, about 3,000 PTCBs could be punched with the home-made tissue punch from the donor blocks without breakage of the punch. No stitch injuries occurred at punching and transferring the PTCBs to the holes of the recipient block. The use of a magnifying glass and good illumination facilitated the filling of the holes of the recipient block so that no holes were skipped. The PTMA with 1,363 PTCBs of 0.43 mm in diameter was constructed within about 6 h. The smaller PTMAs with about 100 PTCBs did not show any difference in the construction time between the PTCBs 1.0, 0.6, and 0.43 mm in diameter. I did find that when the room temperature exceeded 20–22°C in my nonairconditioned laboratory during the summer months, the paraffin of the recipient block and the PTCBs became soft, making it difficult to fill the PTMAs. The curling of sectioned PTCBs could be largely prevented by cutting thin sections (2–5 μm). Although the individual PTCBs had a small diameter, a sufficient number of cells (>60 cells) were present to be evaluated after staining (Fig. 1f). Routine staining, immunohistochemistry, and fluorescence in situ hybridization could be performed using standard procedures (Fig. 1f). The number of noninformative cores differed only minimally (0–4 cores per immunohistochemically stained section) between the PTMAs made of PTCBs 0.43 mm in diameter and those constructed with PTCBs 0.6 mm and 1.0 mm in diameter.

Discussion

In 1998 Kononen et al. demanded smaller PTCBs to provide a much higher density of specimens per PTMA [1]. Rimm et al. reported on new needles, which were under development that may allow as many as 2,000 or more spots per slide [4]. Until now, however, it was not possible to produce PTCBs with diameters smaller than 0.6 mm. Paraffin punches with smaller diameters were not stable enough to punch PTCBs without breaking ("broken needles 0.4 mm in diameter", personal communication, Prof. Sauter, Hamburg). These unsuccessful experiments were performed using punches provided with the manual tissue puncher/arrayer from Beecher Instruments (Beecher Instruments, Sun Prairie, WI, USA). My punches were made of ordinary hypodermic needles, as described by Wan et al. [8] and Rodrigues Cordovil Pires et al. [5]. I suspect that they had slightly thicker walls than the Beecher punches, providing the decisive plus in stability especially for tissues with a high consistency such as myometrium or densely packed fibrous tissue. By reducing the diameter of the PTCBs, I was able to achieve a higher density of specimens in a PTMA, packing up to 1,363 PTCBs in a standard paraffin block (3,7×2,3 cm) (Fig. 1d, e) or 100 PTCBs within an area less than 1 cm^2 (Fig. 1f). This density might even be increased by reducing the distance between the PTCBs when using a machine (e.g., Beecher tissue arrayer, Alphelys tissue arrayer) to construct the PTMA. This higher density made it possible to construct small PTMAs of approximately 100 PTCBs and arrange six to eight small PTMAs (e.g., with different subsets of tumors) for a particular stain on a single slide thereby enhancing the flexibility of the PTMA technique (Fig. 1g). Moreover, smaller PTMAs can reduce sectioning artifacts such as the splitting of sections on the hot water bath. There should be no difference in the number of sections which can be cut from a PTMA filled with PTCBs 0.43 mm, 0.6 mm, or 1.0 mm in diameter because the length of the PTCBs depends on the thickness of the tissue in the donor block and not on the diameter of the tissue punch (Fig. 1c, inset). Despite their small diameter, these PTCBs generally still contained a sufficient number of cells (>60 cells) for proper evaluation (Fig. 1f). Furthermore, by taking up to three PTCBs per case, I very rarely found that I had insufficient

tissue for interpretation after staining. According to some guidelines for the evaluation of stainings approved by the Food and Drug Administration (FDA) of the United States of America, 60 cells seem to be sufficient (e.g., PathVysion kit, Abbott-Vysis). Moreover, LeBaron stated that about 200 cells are adequate for some cell evaluations [2]. Concerning the representativity of the 0.43 mm diameter PTCBs for the whole tumor, as is the case for all PTMAs, this technique is only suited for the evaluation of antigens or genome sequences which will be found in the majority of the cells evaluated (e.g., E-cadherin, synaptophysin). Moreover, the greatest benefit of this technique will be achieved with densely packed cells of interest such as endocrine tumors or renal cell carcinomas.

In summary, it is possible to construct PTMAs with PTCBs as small as 0.43 mm in diameter. Up to 1,363 PTCBs can be installed in a standard size paraffin block (3,7×2,3 cm).

Densely packed, small PTMAs provide increased flexibility by making it possible to position multiple PTMAs with different subsets of tumors (about 800 PTCBs in all) on a single slide.

Conflict of interest statement I declare that I have no conflict of interest.

References

1. Kononen J, Bubendorf L, Kallioniemi A, Bärlund M, Schraml P, Leighton S, Torhorst J, Mihatsch MJ, Sauter G, Kallioniemi O-P (1998) Tissue microarrays for high-throughput molecular profiling of tumor specimens. Nat Med 4:844–847
2. LeBaron MJ, Crismon HR, Utama FE, Neilson LM, Sultan AS, Johnson KJ, Andersson EC, Rui H (2005) Ultrahigh density microarrays of solid samples. Nat Methods 2:511–513
3. Mengel M, Kreipe H, von Wasielewski R (2003) Rapid and large-scale transition of new tumor biomarkers to clinical biopsy material by innovative tissue microarray systems. Appl Immunohistochem Mol Morph 11:261–268
4. Rimm DL, Camp RL, Charette LA, Olsen DA, Provost E (2001) Amplification of tissue by construction of tissue microarrays. Exp Mol Pathol 70:255–264
5. Rodrigues Cordovil Pires A, da Matta Andreiuolo F, Rabello de Souza S (2006) TMA for all: a new method for the construction of tissue microarrays without recipient paraffin block using custom-built needles. Diagn Pathol 1:14
6. Vogel UF, Bueltmann BD (2006) Simple, inexpensive, and precise paraffin tissue microarrays constructed with a conventional micro-compound table and a drill grinder. Am J Clin Pathol 126:342–348
7. Vogel UF (2007) Inexpensive and precise paraffin tissue micro-arrays constructed with a Computer Numerical Control (CNC) drilling machine. Histopathology 51:136–137
8. Wan WH, Fortuna MB, Furmanski P (1987) A rapid and efficient method for testing immunohistochemical reactivity of monoclonal antibodies against multiple tissue samples simultaneously. J Immunol Methods 103:121–129

Virchows Arch (2008) 453:47–55
DOI 10.1007/s00428-008-0633-6

ORIGINAL ARTICLE

Comparison of different techniques for the detection of genetic risk-identifying chromosomal gains and losses in neuroblastoma

Eva Villamón · Marta Piqueras · Carlos Mackintosh · Javier Alonso · Enrique de Álava · Samuel Navarro · Rosa Noguera

Received: 4 February 2008 / Revised: 6 May 2008 / Accepted: 13 May 2008 / Published online: 24 June 2008

Abstract Neuroblastoma (NB) is a pediatric neoplasia that shows complex combinations of acquired genetic aberrations. The specific genes and the molecular mechanisms responsible for development and progression of NB remain poorly understood. Our main objective is to compare the results obtained with different techniques for the detection of genomic data in 20 patients with NB using the information obtained to select the appropriate technique in routine analysis for the therapeutic stratification. The genetic methods used in this study are multiprobe fluorescence in situ hybridization (FISH) assay, metaphasic comparative genomic hybridization (mCGH), array comparative genomic hybridization (aCGH), and the multiplex ligation-dependent probe amplification (MLPA). Genomic copy number abnormalities were used to group the cases in four categories: *MYCN* amplification cases; 11q deletion tumors; cases with partial chromosome gains or losses and samples with entire chromosome alterations. The data obtained from the multigenomic techniques showed a high degree of concordance and our findings support the hypothesis that NB consists of biologically distinct subgroups that differ by genetic characteristics of prognostic relevance. FISH will be essential for the mandatory study of *MYCN* status. The use of MLPA as routine technique is an advantage procedure for detecting the implication of the common genetic alterations in NB.

Keywords Neuroblastoma · FISH · mCGH · aCGH · MLPA

E. Villamón · M. Piqueras · S. Navarro · R. Noguera (✉)
Department of Pathology, Medical School, University of Valencia,
Avda/Blasco Ibáñez, 17,
46010 Valencia, Spain
e-mail: rosa.noguera@uv.es

C. Mackintosh · E. de Álava
Centre of Cancer Investigation-IBMCC,
University of Salamanca-CSIC,
Salamanca, Spain

J. Alonso
Institute of Biomedical Investigations CSIC-UAM,
Madrid, Spain

Introduction

Neuroblastoma (NB) is an embryonal solid tumor of childhood believed to originate from immature neural crest cells committed to the adrenal medulla and sympathetic nervous system [23, 39]. NB is the most frequent extracranial pediatric solid tumor [10]. The neoplastic disease has a variable clinical course, ranging from spontaneous regression to malignant progression [3, 17]. The prediction of prognosis is one of the most urgent demands before initiating the treatment of NB. The International Neuroblastoma Staging System currently stratifies patients into low-, intermediate-, or high-risk categories based upon well-defined prognostic factors [11]. These included age, stage, histopathology, and status of *MYCN* oncogene [7, 12, 29, 48]. A new and uniform International Neuroblastoma Risk Group classification system and strategies for risk-based therapies are now being developed [33].

One of the biological hallmarks of NB is its complex genetic heterogeneity; several recurrent genetic alterations have been identified. Indicators of poor prognosis include diploidy or tetraploidy [30, 31], *MYCN* amplification [21, 46], deletion of 1p [21, 22], and gain of 17q [9, 13]. In addition, different losses of heterozygosity have been

reported for other chromosomal regions in NB as 2q, 3p, 4p, 9p, 11q, 14q, and 18q [4, 8, 14, 53–57]. Some of these abnormalities such as 11q deletion are powerful prognostic markers independent of the clinical features [4, 50]. Despite the evident clinical relevance of these genomic aberrations, no definitive NB suppressor gene has been identified.

To date, many different methods have been used for the detection of deletions and gains including chromosome analysis [5, 19, 36, 52], Southern blot [41], fluorescence in situ hybridization (FISH) [49, 59], metaphasic comparative genomic hybridization (mCGH) [29, 38, 43], and real-time quantitative polymerase chain reaction (PCR) [6]. However, these methods have some limitations. Conventional cytogenetic analysis is only sporadically successful; PCR-based methodologies for the detection of loss of heterozygosity are extremely sensitive to the amount of normal DNA contaminating the tumor sample, a problem inherent in any human cancer molecular diagnostic setting; Southern blot suffers from the disadvantages of a 1–2-week turnaround time and a requirement for relatively large quantities of DNA (5–10 μg); FISH is expensive, time-consuming, and difficult to implement as multiplex assays; mGCH does not recognize a situation in which loss of one allele is followed by duplication of another. More recently, array CGH (aCGH) has been applied in order to detect genomic alterations in NB [16, 20, 42, 47]. This method improves the resolution and sensitivity of mCGH; it is a very robust technique for the detection of cryptic chromosome rearrangements but it is labor intensive and requires expensive equipment. Multiplex ligation-dependent probe amplification (MLPA) is a new and fast method. The technique was first described in 2002 [45] and different studies have been published, the majority using commercial MLPA assays to detect gene deletions and duplications in different disorders [1, 25, 27, 28, 35]. This method identifies the target sequence by hybridization of two adjacent probes that are joined by ligation reaction. After denaturation, the target sequences are amplified by PCR using a unique primer pair that matches the linkers attached to each probe. Only probes that hybridize to the target sequence have been ligated and can be amplified by the PCR reaction. After size separation by capillary gel electrophoresis, the amplification products can be analyzed. The peak area of each amplification product reflects the relative copy number of that target sequence, enabling the detection of chromosome alterations. The introduction of the MLPA technique in the study of genomic copy number abnormalities in 54 primary NB tumors was presented by Elliott et al. [24]. The advantage of the mCGH and aCGH techniques is to obtain a pangenomic profile; using FISH and MLPA techniques is only possible to study just semigenomic profiles; FISH needs to choose the adequate probes in order to detect if the concrete alterations and MLPA with these specific kits covers the ten chromosomal regions of highest interest in NB.

The main objective is to use different genomic techniques (FISH, mCGH, aCGH, and MLPA) to detect chromosomal and gene alterations in 20 patients with NB, the information obtained allows us to select the appropriate technique in routine analysis for the therapeutic stratification. In this study, the genetic results obtained by aCGH or MLPA have allowed us to group the tumors in four different categories. The genetic data obtained confirmed the importance of use of these techniques to elucidate the heterogeneous genetic profile of NB for the therapeutic stratification.

Materials and methods

Patient samples and tissue processing

Samples and DNA were referred to the Spanish Reference Center for NB biological and Pathological Studies and to the Spanish Institute of Biomedical Investigations Higher Council for Scientific Research-Autonomous University of Madrid. Table 1 gives an overview of clinical data on all cases. Tumour samples were obtained at the time of diagnosis by needle core or surgical biopsy. Touch preparations and paraffin slides were stained with hematoxylin and eosin and examined by the pathologist to evaluate the amount of neuroblastic cells and histopathologic categorized following International Neuroblastoma Pathology Classification. Touch preparations were used for FISH. Tumors included for subsequent DNA extraction had a minimum of 50% of neuroblastic cells. DNA was extracted using a phenol–chloroform–isoamyl alcohol extraction after proteinase K treatment.

FISH and Southern blot analysis

MYCN copy number and 1p deletion were investigated with commercial probes (*MYCN* (2p24)/*LAF* (2q11) and 1p36 (*D1Z2*)/SE 1 cocktail probes dual color direct labeled—Kreatech, Biotechnology, Amsterdam, The Netherlands). Both probes were applied and hybridized according to the manufacturer's instructions. The results were captured using a Zeiss Axioplan 2 fluorescence microscope (Carl Zeiss AG, Oberkochen, Germany). Initially, the status of *MYCN* was analyzed by FISH in all cases except for three tumors (NB-6, NB-7, and NB-17) where Southern blot was used as the diagnostic technique. Detection of *MYCN* status by Southern blot analysis was done according to standard procedures.

mCGH

Fourteen cases were analyzed by mCGH. The technique was applied using a nick translation labeling kit, Spectrum

Table 1 Clinical data of the 20 neuroblastoma samples used in the study

Tumour	Age at diagnosis[a]	Histology	Stage[b]	Metastasis at diagnosis	Alive–died
NB-1	23	NB PD	4	Yes	0
NB-2	78	NB PD	4	Yes	0
NB-3	40	NB	4	Yes	1
NB-4	37	NB	4	Yes	0
NB-5	107	NB PD	4	Yes	1
NB-6	18	NB	3	No	0
NB-7	4	NB	4	Yes	1
NB-8	32	NB NOS	4	Yes	1
NB-9	62	NB PD	4	Yes	n/a
NB-10	42	NB PD	4	Yes	0
NB-11	44	NB	4	Yes	0
NB-12	10	NB PD	4	Yes	0
NB-13	1	NB NOS	4s	Yes	0
NB-14	13	NB NOS	1	No	0
NB-15	3	NB PD	1	No	0
NB-16	51	NB NOS	1	No	0
NB-17	25	GNB	2	No	0
NB-18	0.25	NB NOS	4s	Yes	0
NB-19	66	NB PD	2	No	0
NB-20	4	NB PD	1	No	0

NB Neuroblastoma, *GNB* ganglioneuroblastoma, *PD* poorly differentiated, *NOS* not otherwise, *0* alive, *1* died, *n/a* not available
[a] Months
[b] According to the International Neuroblastoma Staging System

Green deoxyuridine triphosphate, CGH control slides, Cot-1 DNA, and Spectrum Red DNA control (Vysis Inc., Downers Grove, IL, USA) and following the manufacturer's instructions. Hybridized metaphases were captured using a Zeiss Axioplan 2 fluorescent microscope and analyzed with Isis software (MetaSystem, Belmont, MA, USA). Regions with a ratio profile that exceeded the limits of 1.20 to 0.8 were defined as those with copy number gains and losses, respectively.

aCGH

All samples were studied using the pangenomic aCGH technique. A bacterial artificial chromosome (BAC) arrays platform was used corresponding to a genomic library 1 Mb Sanger, on Codelink (Amersham, Piscataway, NJ, USA) glasses. The BACs were extracted and amplified by degenerate oligonucleotide and amino-linking PCR. The deposition on the glass was made in triplicate with a Microgrid II robot (Genomic Solutions, Cambridgeshire, UK). The DNA was marked with a homemade kit of Random Priming: Cy5 for the DNA tumor and Cy3 for the control DNA (pool of 40 healthy individuals; Amersham, Piscataway, NJ, USA). The hybridization was made during 48 h at 42°C. The samples were captured with an Axon 4000b scanner and analyzed with GenePrix software (Axon, Union City USA). The bioconductor package (R, CRAN) snapCGH was used with algorithms for the analysis and segmentation of the data (Circular Binary Segmentation algorithm).

MLPA

For this multigenomic technique, a specifically designed set of probes was used to test for chromosomal abnormalities in NB, SALSA MLPA Kit P251/P252/P253 (MRC-Holland, Amsterdam, The Netherlands) and was performed in all 20 patients. The P251 probe mix contains 38 probes for chromosomes 1, 3, and 11; P252 probe mix contains 36 probes for chromosomes 2 and 17; P253 probe mix contains 32 probes for chromosomes 4, 7, 9, 12, and 14. Each of these three probe mixes contains five control fragments in chromosomal regions rarely altered in NB. MLPA was performed as described by the manufacturer with minor modifications. The ligation products were amplified by PCR using the common primer set with the 6-FAM label distributed by the supplier. NB in which the *MYCN* gene has been amplified can result in MLPA sample pictures displaying enormous *MYCN* peaks, while other probe signals are barely visible. To prevent missing any additional mutations, it is important to analyze the other probe signals as well. For this reason, *MYCN* silencer solution is used. This solution binds to the complete hybridizing sequence and part of the primer sequence of

the *MYCN* probes, thereby preventing the probes amplification during the PCR reaction. The other probes can now be easily detected and analyzed. Fragments were separated and quantified by electrophoresis on an ABI Prism 310 capillary sequencer and Genemapper analysis (Applied Biosystems). In each set of MLPA experiments, we included at least three normal control DNA samples for data processing. Reference DNAs were isolated from blood of healthy volunteers. Data analysis was performed with Coffalyser MLPA-DAT software (MRC-Holland, Amsterdam, The Netherlands) generating the normalized peak value or the so-called probe ratio. The threshold to detect losses and gains in tumor samples was set at 0.75 and 1.25, respectively.

Results

The results obtained with the different genetic techniques are summarized in Fig. 1. The genetic alterations allowed us to group the cases into four categories. In the first group, we included the cases with *MYCN* amplification (8/20; NB-1 to NB-8); the second group was formed with tumors that presented deletion of 11q (4/20; NB-9 to NB-12); the third group was formed with tumors with partial chromosome gains or losses (4/20; NB-13 to NB-16); samples with entire chromosome gains or losses were included in the fourth group (4/20; NB-17 to NB-20).

In the first group of tumors, eight cases, the amplification of *MYCN* was associated with the following alterations: (a) other gains of 2p were present in five samples detected by aCGH; (b) loss of 1p was observed in the eight tumors with at least one technique. In the case of NB-4, there was a discordance between the results obtained with MLPA and the other techniques; (c) 17q gain was present in 87.5% of the cases; (d) other segmental imbalances, such as deletion of 11q (two cases), deletion of 3p (two cases), and deletion of 14q (three cases). NB-5 also presented loss of 11q and 3p. Figure 2 shows the results obtained by the different techniques in the sample NB-2.

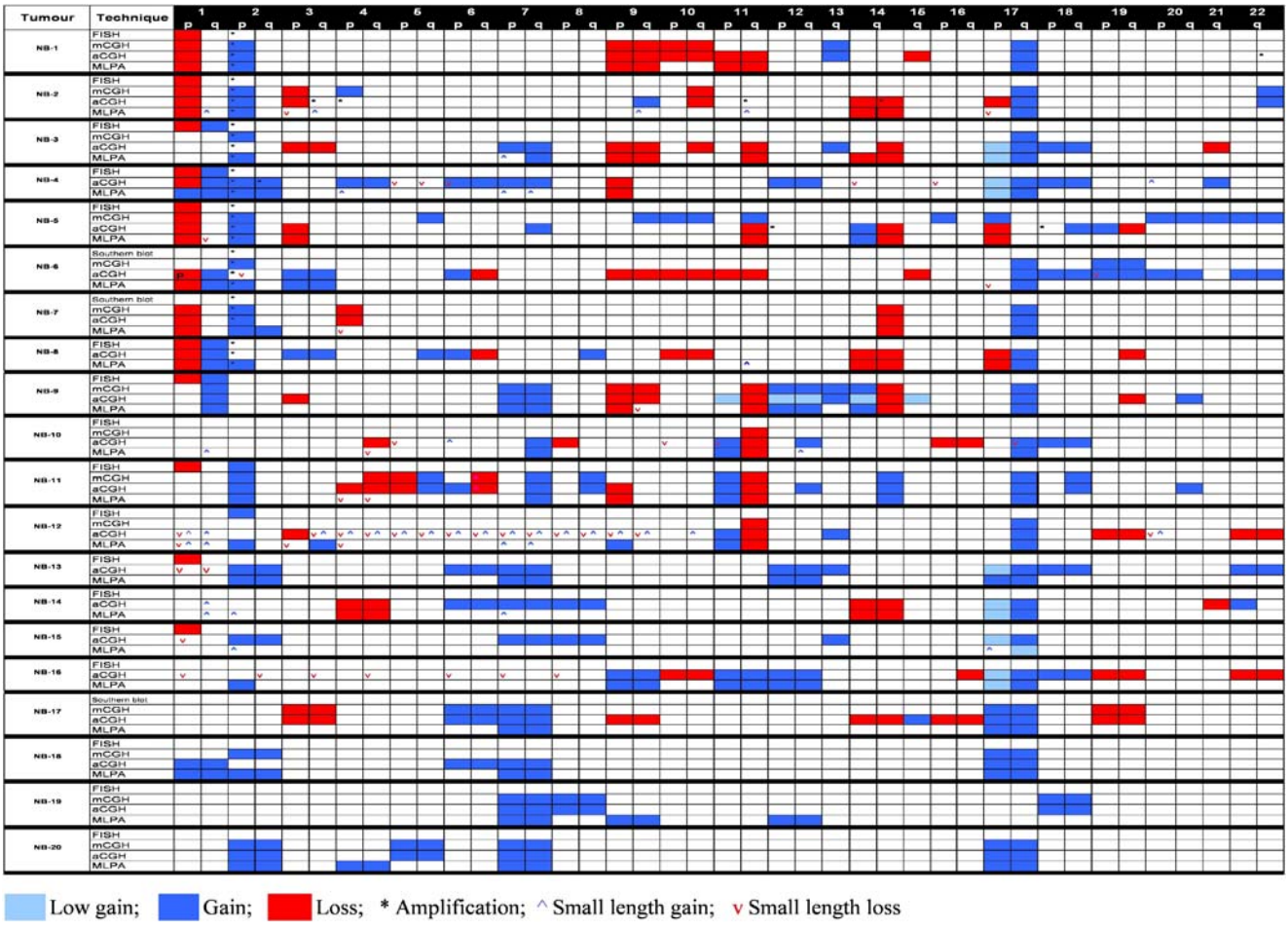

Fig. 1 Genetic alterations detected with the different genetic techniques. *FISH* fluorescence in situ hybridization; *mCGH* metaphasic comparative genomic hybridization; *aCGH* array comparative genomic hybridization; *MLPA* multiplex ligation-dependent probe amplification

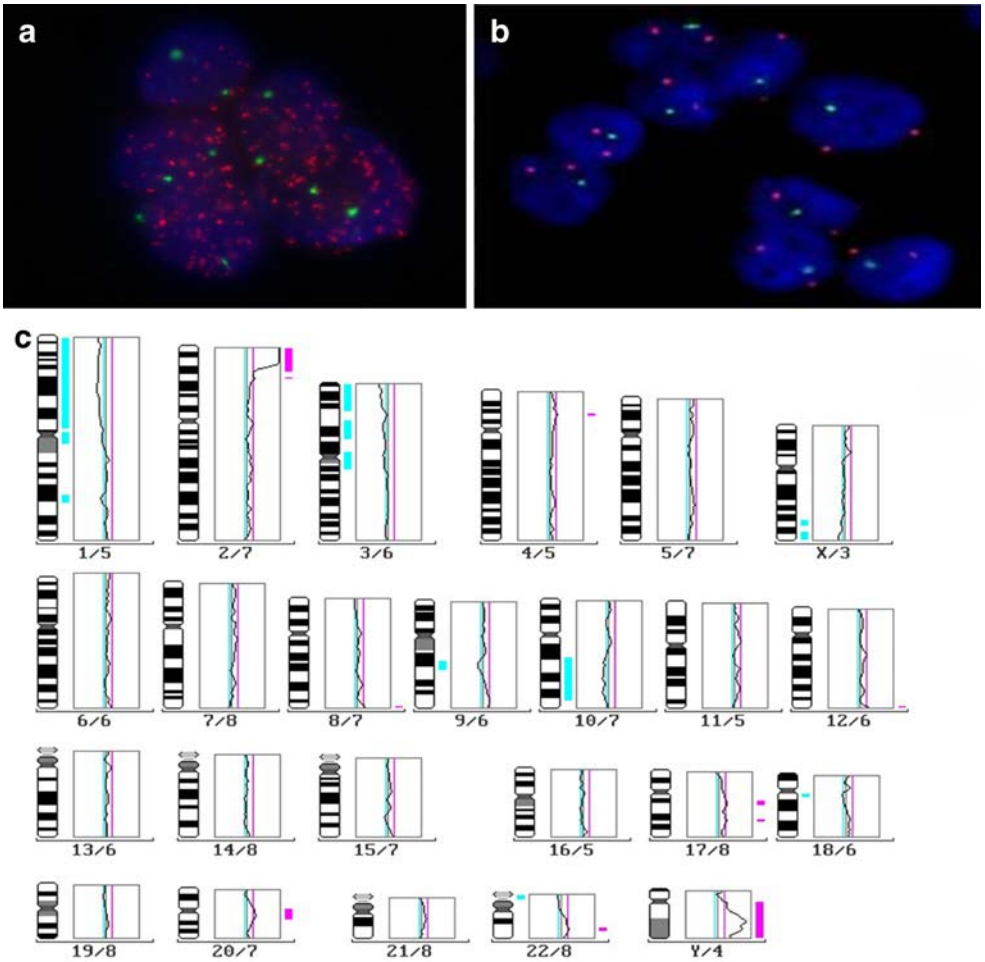

Fig. 2 Results obtained by the different techniques in NB-2. **a**, **b** FISH analysis: **a** *MYCN* (2p24) red/*LAF* (2q11) green. *MYCN* amplification: over fourfold increase of the *MYCN* signal number in relation to the number of control *LAF* signal. **b** 1p36 (D1Z2) red/SE 1 green. 1p36 deletion: only one signal for 1p36 present. **c** mCGH results: losses are indicated by a *bar in red* and gains by a *bar in green*. **d**, **e** MLPA results: **d** *MYCN* gene has been amplified displaying enormous peaks while other probe signals are not visible. **e** Using silencer solution preventing the *MYCN* probes amplification during PCR reaction, the other alterations can be analyzed. **f** aCGH copy number profile. The X-axis represents the chromosomes and the Y-axis the normalized $\log_2$ Cy3/Cy5 fluorescence intensity

The second group consisted of four cases that presented 11q loss as the principal alteration. These tumors did not show *MYCN* amplification, but in two cases (NB-11 and NB-12) a 2p gain was detected. Using FISH, a deletion of 1p was observed in two cases (NB-9 and NB-11). When aCGH and MLPA were used, NB-12 presented a 1p loss localized in a small area. The 11q loss was associated with 17q gain in all cases. Two cases presented loss of 3p detected by aCGH; one of these showed imbalances in chromosome 14. Chromosome 14 gain was found in NB-11.

The third group was formed of samples with partial chromosome gains or losses. All cases presented different genetic alterations in chromosome 2 and segmental chromosome 1 imbalances. These tumors had as principal alteration a polysomy of chromosome 17 plus a gain of 17q.

The last group consisted of four cases with entire chromosome gains or losses. Two tumors (NB-18 and NB-20) showed gain of chromosome 2. The four tumors included in this group presented entire gain of chromosome 7, and in three cases a gain of chromosome 17 was found. Case NB-17 presented loss of chromosome 3 that was not detected by MLPA and loss of chromosome 14 that was only detected by aCGH. Chromosome 18 gain was found in case NB-19.

Discussion

The primary aim of this study was to combine the use of different genetic techniques (FISH, mCGH, aCGH, and MLPA) for the screening of chromosomal rearrangements in NB.

NB has served as a paradigm for the clinical importance of tumor genomic data [4, 32, 58]. A large number of genomic aberrations have been defined in NB, and the pattern of these somatically acquired changes correlate with tumor behavior [10]. Our results, as previously known, showed that molecular biology of human NB is complex. Maximal prognostic information can be obtained when the entire genomic profile is analyzed. Amplification of the *MYCN* oncogene at 2p24 remains a powerful biomarker of aggressive phenotype and poor survival [18, 44]. *MYCN* is the only tumor genetic marker used as a basis for treatment stratification in NB clinical trials [34, 44]. *MYCN* amplification has been found in approximately 20% of newly diagnosed tumors and in up to 50% of high-stage cases of NB [46]. We have previously studied the status of *MYCN* by FISH because this determination is routinely used in order to establish the prognosis and treatment of NB [2].

Fig. 2 (continued)

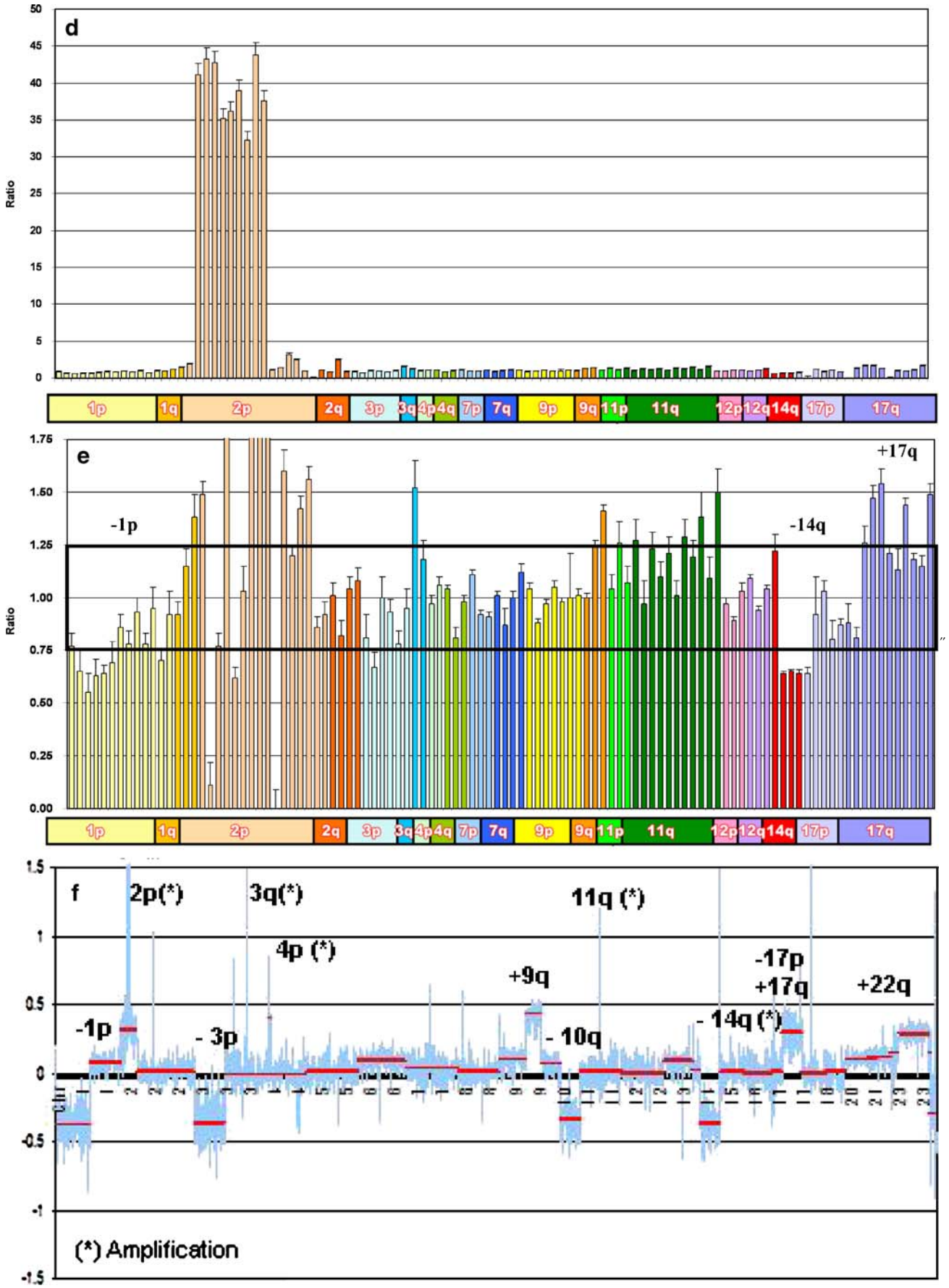

The molecular analysis of tumor DNA by Southern blot was used to analyze *MYCN* amplification in three cases. Tumor biopsies sufficient to provide enough material for molecular genetic analysis are therefore highly encouraged at the time of diagnosis. It is remarkable that, among our first group of *MYCN* amplified cases, 50% of patients (4/8) died of disease, reinforcing the adverse prognosis of this group of patients.

It has been shown that 1p deletion is associated with adverse clinical and genetic indicators such as *MYCN* amplification [26]. There has been ongoing controversy about the precise prognostic power of 1p deletion in relation to other variables, particularly *MYCN* [15, 40]. Some studies showed that an inverse relationship exists between 11q loss and amplification of *MYCN*, indicating that these abnormalities represent distinct genetic subtypes of advanced-stage NB [38]; multiple studies found a significant association between 11q, 3p, and 14q loss [49–51]. In our study, an interesting observation was found in two tumors with *MYCN* amplification which showed 11q loss associated to 3p and/or 14p loss. Unbalanced gain of 17q material is the most common genomic abnormality seen in primary NB. It has been published that this alteration is associated with other known prognostic factors but is in itself a powerful, although controversial, independent predictor of adverse outcome [13]. Several analyses have described that gains or deletions of whole chromosomes (entire chromosomal imbalance) confer better prognosis and are associated with low stage of disease [29]. A segmental chromosomal imbalance profile was recently associated with NB of infants with poor prognosis [60].

High-resolution methods are necessary for a more accurate tumor classification, including the atypical genetic profiles, and turn these discoveries into effective treatment strategies. Conventional mCGH profiling of NB has identified many genomic aberrations, but the resolution of mCGH is approximately only 10 Mb and does not allow the detailed analysis of chromosome breakpoints [29, 37, 38, 43]. This could be the cause of the majority of discrepancies observed in our results. Further studies using other techniques such as aCGH or MLPA are necessary to map the breakpoints precisely.

The use of aCGH enables new chromosomal alterations to be detected in patients with NB [16, 20, 42, 47]. With this technique, thousands of sites can be simultaneously investigated in one patient, allowing partial or total coverage of the genome. However, aCGH is unlikely to be introduced into diagnostics due to the cost of the arrays. With this technique, it is easier to detect the partial gains and/or losses of small lengths.

MLPA is an alternative multigenetic technique because it is rather robust and easy to perform, and is a fast technique for the screening of large number of samples. In this study, the MLPA technique was used to detect the genetic alterations in NB, and the results presented a high concordance with those obtained by aCGH. The number of targets that can be screened by MLPA is limited; however, multiple samples can be simultaneously tested at a lower cost than for one aCGH hybridization. In this study, we combined genomic data from aCGH and MLPA studies to classify the NB into four groups: *MYCN* amplification, 11q loss, segmental chromosomal imbalance, and entire chromosomal imbalance.

To increase our understanding of the genetic basis for NB heterogeneity and to prioritize regional candidate genes for further analyses, we propose: (a) use of FISH technique to visualize isolated cells and detect alterations present in a low percentage of tumor cells. For example, gene amplification present in only a minority of cells may well lead to bad interpretation by molecular analysis but will be readily apparent by FISH. This technique will be essential for the mandatory study of *MYCN* status; (b) use of MLPA as routine technique will be a very interesting procedure for detecting the implication of the common genetic alterations in NB. It will provide important information for the estimation of prognosis and therapy available for patients to be obtained and provide important information regarding delineation of critical regions of gain and loss in NB, which should facilitate further selection of candidate oncogenes or tumor suppressor genes; (c) further investigations to extend and validate whether the genes and signaling pathways involved can represent an essential step towards the development of more efficient molecular targeted therapies.

In conclusion, this study shows that the genomic data obtained in NB diagnostic biopsies can be used to subcategorize the disease into molecular subsets. Ongoing studies will test whether DNA or RNA alterations are more useful in a clinical setting or whether the two will provide complementary information.

Acknowledgement Supported by the grants FIS RD06/0020/0102 (Instituto de Salud Carlos III; Ministerio de Sanidad y Consumo, Spain), RD06/0020/0059, and PI06/1576; PI4/07-36 (Fundación Sociedad Española de Oncología Pediátrica). We are grateful to Dr. Schuit (MRC-Holland) and Dr. Ambros for the probe mix MLPA developed, to Dra. Dolores Sánchez for the mCGH analysis, and to Elisa Alonso and Estela Pons for their technical support.

Conflict of interest statement We declare that we have no conflict of interest.

References

1. Alibakhshi R, Kianishirazi R, Cassiman JJ, Zamani M, Cuppens H (2008) Analysis of the CFTR gene in Iranian cystic fibrosis patients: identification of eight novel mutations. J Cyst Fibros 7:102–109

2. Ambros IM, Benard J, Boavida M, Bown N, Caron H, Combaret V, Couturier J, Darnfors C, Delattre O, Freeman-Edward J, Gambini C, Gross N, Hattinger CM, Luegmayr A, Lunec J, Martinsson T, Mazzocco K, Navarro S, Noguera R, O'Neill S, Potschger U, Rumpler S, Speleman F, Tonini GP, Valent A, Van Roy N, Amann G, De Bernardi B, Kogner P, Ladenstein R, Michon J, Pearson AD, Ambros PF (2003) Quality assessment of genetic markers used for therapy stratification. J Clin Oncol 21:2077–2084
3. Ara T, DeClerck YA (2006) Mechanisms of invasion and metastasis in human neuroblastoma. Cancer Metastasis Rev 25:645–657
4. Attiyeh EF, London WB, Mosse YP, Wang Q, Winter C, Khazi D, McGrady PW, Seeger RC, Look AT, Shimada H, Brodeur GM, Cohn SL, Matthay KK, Maris JM (2005) Chromosome 1p and 11q deletions and outcome in neuroblastoma. N Engl J Med 353:2243–2253
5. Betts DR, Cohen N, Leibundgut KE, Kuhne T, Caflisch U, Greiner J, Traktenbrot L, Niggli FK (2005) Characterization of karyotypic events and evolution in neuroblastoma. Pediatr Blood Cancer 44:147–157
6. Boensch M, Oberthuer A, Fischer M, Skowron M, Oestreich J, Berthold F, Spitz R (2005) Quantitative real-time PCR for quick simultaneous determination of therapy-stratifying markers MYCN amplification, deletion 1p and 11q. Diagn Mol Pathol 14:177–182
7. Bown N (2001) Neuroblastoma tumour genetics: clinical and biological aspects. J Clin Pathol 54:897–910
8. Breen CJ, O'Meara A, McDermott M, Mullarkey M, Stallings RL (2000) Coordinate deletion of chromosome 3p and 11q in neuroblastoma detected by comparative genomic hybridization. Cancer Genet Cytogenet 120:44–49
9. Brinkschmidt C, Poremba C, Christiansen H, Simon R, Schafer KL, Terpe HJ, Lampert F, Boecker W, Dockhorn-Dworniczak B (1998) Comparative genomic hybridization and telomerase activity analysis identify two biologically different groups of 4s neuroblastomas. Br J Cancer 77:2223–2229
10. Brodeur GM (2003) Neuroblastoma: biological insights into a clinical enigma. Nat Rev Cancer 3:203–216
11. Brodeur GM, Pritchard J, Berthold F, Carlsen NL, Castel V, Castelberry RP, De Bernardi B, Evans AE, Favrot M, Hedborg F et al (1993) Revisions of the international criteria for neuroblastoma diagnosis, staging, and response to treatment. J Clin Oncol 11:1466–1477
12. Burgues O, Navarro S, Noguera R, Pellin A, Ruiz A, Castel V, Llombart-Bosch A (2006) Prognostic value of the international neuroblastoma pathology classification in neuroblastoma (Schwannian stroma-poor) and comparison with other prognostic factors: a study of 182 cases from the Spanish Neuroblastoma Registry. Virchows Arch 449:410–420
13. Caron H (1995) Allelic loss of chromosome 1 and additional chromosome 17 material are both unfavourable prognostic markers in neuroblastoma. Med Pediatr Oncol 24:215–221
14. Caron H, van Sluis P, Buschman R, Pereira do Tanque R, Maes P, Beks L, de Kraker J, Voute PA, Vergnaud G, Westerveld A, Slater R, Versteeg R (1996) Allelic loss of the short arm of chromosome 4 in neuroblastoma suggests a novel tumour suppressor gene locus. Hum Genet 97:834–837
15. Caron H, van Sluis P, de Kraker J, Bokkerink J, Egeler M, Laureys G, Slater R, Westerveld A, Voute PA, Versteeg R (1996) Allelic loss of chromosome 1p as a predictor of unfavorable outcome in patients with neuroblastoma. N Engl J Med 334:225–230
16. Carr J, Bown NP, Case MC, Hall AG, Lunec J, Tweddle DA (2007) High-resolution analysis of allelic imbalance in neuroblastoma cell lines by single nucleotide polymorphism arrays. Cancer Genet Cytogenet 172:127–138
17. Castel V, Grau E, Noguera R, Martinez F (2007) Molecular biology of neuroblastoma. Clin Transl Oncol 9:478–483
18. Cohn SL, Tweddle DA (2004) MYCN amplification remains prognostically strong 20 years after its "clinical debut". Eur J Cancer 40:2639–2642
19. Combaret V, Turc-Carel C, Thiesse P, Rebillard AC, Frappaz D, Haus O, Philip T, Favrot MC (1995) Sensitive detection of numerical and structural aberrations of chromosome 1 in neuroblastoma by interphase fluorescence in situ hybridization. Comparison with restriction fragment length polymorphism and conventional cytogenetic analyses. Int J Cancer 61:185–191
20. Chen QR, Bilke S, Wei JS, Whiteford CC, Cenacchi N, Krasnoselsky AL, Greer BT, Son CG, Westermann F, Berthold F, Schwab M, Catchpoole D, Khan J (2004) cDNA array-CGH profiling identifies genomic alterations specific to stage and MYCN-amplification in neuroblastoma. BMC Genomics 5:70
21. Christiansen H, Sahin K, Berthold F, Hero B, Terpe HJ, Lampert F (1995) Comparison of DNA aneuploidy, chromosome 1 abnormalities, MYCN amplification and CD44 expression as prognostic factors in neuroblastoma. Eur J Cancer 31A:541–544
22. Christiansen H, Schestag J, Christiansen NM, Grzeschik KH, Lampert F (1992) Clinical impact of chromosome 1 aberrations in neuroblastoma: a metaphase and interphase cytogenetic study. Genes Chromosomes Cancer 5:141–149
23. De Preter K, Vandesompele J, Heimann P, Yigit N, Beckman S, Schramm A, Eggert A, Stallings RL, Benoit Y, Renard M, De Paepe A, Laureys G, Pahlman S, Speleman F (2006) Human fetal neuroblast and neuroblastoma transcriptome analysis confirms neuroblast origin and highlights neuroblastoma candidate genes. Genome Biol 7:R84
24. Elliott A, Baker A, Board J, Tweddle D, Curtis A, Bown N (2007) MLPA analysis of neuroblastoma tumours. Chromosome Res 15:164–165
25. Erlandson A, Samuelsson L, Hagberg B, Kyllerman M, Vujic M, Wahlstrom J (2003) Multiplex ligation-dependent probe amplification (MLPA) detects large deletions in the MECP2 gene of Swedish Rett syndrome patients. Genet Test 7:329–332
26. Fong CT, Dracopoli NC, White PS, Merrill PT, Griffith RC, Housman DE, Brodeur GM (1989) Loss of heterozygosity for the short arm of chromosome 1 in human neuroblastomas: correlation with N-myc amplification. Proc Natl Acad Sci U S A 86:3753–3757
27. Hogervorst FB, Nederlof PM, Gille JJ, McElgunn CJ, Grippeling M, Pruntel R, Regnerus R, van Welsem T, van Spaendonk R, Menko FH, Kluijt I, Dommering C, Verhoef S, Schouten JP, van't Veer LJ, Pals G (2003) Large genomic deletions and duplications in the BRCA1 gene identified by a novel quantitative method. Cancer Res 63:1449–1453
28. Jeuken J, Cornelissen S, Boots-Sprenger S, Gijsen S, Wesseling P (2006) Multiplex ligation-dependent probe amplification: a diagnostic tool for simultaneous identification of different genetic markers in glial tumors. J Mol Diagn 8:433–443
29. Lastowska M, Cullinane C, Variend S, Cotterill S, Bown N, O'Neill S, Mazzocco K, Roberts P, Nicholson J, Ellershaw C, Pearson AD, Jackson MS (2001) Comprehensive genetic and histopathologic study reveals three types of neuroblastoma tumors. J Clin Oncol 19:3080–3090
30. Look AT, Hayes FA, Nitschke R, McWilliams NB, Green AA (1984) Cellular DNA content as a predictor of response to chemotherapy in infants with unresectable neuroblastoma. N Engl J Med 311:231–235
31. Look AT, Hayes FA, Shuster JJ, Douglass EC, Castleberry RP, Bowman LC, Smith EI, Brodeur GM (1991) Clinical relevance of tumor cell ploidy and N-myc gene amplification in childhood neuroblastoma: a Pediatric Oncology Group study. J Clin Oncol 9:581–591
32. Maris JM (2005) The biologic basis for neuroblastoma heterogeneity and risk stratification. Curr Opin Pediatr 17:7–13

33. Maris JM, Hogarty MD, Bagatell R, Cohn SL (2007) Neuroblastoma. Lancet 369:2106–2120
34. Matthay KK, Perez C, Seeger RC, Brodeur GM, Shimada H, Atkinson JB, Black CT, Gerbing R, Haase GM, Stram DO, Swift P, Lukens JN (1998) Successful treatment of stage III neuroblastoma based on prospective biologic staging: a Children's Cancer Group study. J Clin Oncol 16:1256–1264
35. Nakagawa H, Hampel H, de la Chapelle A (2003) Identification and characterization of genomic rearrangements of MSH2 and MLH1 in Lynch syndrome (HNPCC) by novel techniques. Hum Mutat 22:258
36. Noguera R, Canete A, Pellin A, Ruiz A, Tasso M, Navarro S, Castel V, Llombart-Bosch A (2003) MYCN gain and MYCN amplification in a stage 4S neuroblastoma. Cancer Genet Cytogenet 140:157–161
37. Noguera Salva R, Piqueras Franco M, Ruiz Sauri A, Llombart-Bosch A, Castel Sanchez V, Navarro Fos S (2006) Genomic profile in high risk neuroblastoma by comparative genomic hybridization. An Pediatr (Barc) 64:449–456
38. Plantaz D, Vandesompele J, Van Roy N, Lastowska M, Bown N, Combaret V, Favrot MC, Delattre O, Michon J, Benard J, Hartmann O, Nicholson JC, Ross FM, Brinkschmidt C, Laureys G, Caron H, Matthay KK, Feuerstein BG, Speleman F (2001) Comparative genomic hybridization (CGH) analysis of stage 4 neuroblastoma reveals high frequency of 11q deletion in tumors lacking MYCN amplification. Int J Cancer 91:680–686
39. Ross RA, Spengler BA, Domenech C, Porubcin M, Rettig WJ, Biedler JL (1995) Human neuroblastoma I-type cells are malignant neural crest stem cells. Cell Growth Differ 6:449–456
40. Rubie H, Delattre O, Hartmann O, Combaret V, Michon J, Benard J, Peyroulet MC, Plantaz D, Coze C, Chastagner P, Baranzelli MC, Frappaz D, Lemerle J, Sommelet D (1997) Loss of chromosome 1p may have a prognostic value in localised neuroblastoma: results of the French NBL 90 Study Neuroblastoma Study Group of the Societe Francaise d'Oncologie Pediatrique (SFOP). Eur J Cancer 33:1917–1922
41. Sartelet H, Grossi L, Pasquier D, Combaret V, Bouvier R, Ranchere D, Plantaz D, Munzer M, Philip T, Birembaut P, Zahm JM, Bergeron C, Gaillard D, Pasquier B (2002) Detection of N-myc amplification by FISH in immature areas of fixed neuroblastomas: more efficient than Southern blot/PCR. J Pathol 198:83–91
42. Scaruffi P, Coco S, Cifuentes F, Albino D, Nair M, Defferrari R, Mazzocco K, Tonini GP (2007) Identification and characterization of DNA imbalances in neuroblastoma by high-resolution oligonucleotide array comparative genomic hybridization. Cancer Genet Cytogenet 177:20–29
43. Schleiermacher G, Michon J, Huon I, d'Enghien CD, Klijanienko J, Brisse H, Ribeiro A, Mosseri V, Rubie H, Munzer C, Thomas C, Valteau-Couanet D, Auvrignon A, Plantaz D, Delattre O, Couturier J (2007) Chromosomal CGH identifies patients with a higher risk of relapse in neuroblastoma without MYCN amplification. Br J Cancer 97:238–246
44. Schmidt ML, Lukens JN, Seeger RC, Brodeur GM, Shimada H, Gerbing RB, Stram DO, Perez C, Haase GM, Matthay KK (2000) Biologic factors determine prognosis in infants with stage IV neuroblastoma: a prospective Children's Cancer Group study. J Clin Oncol 18:1260–1268
45. Schouten JP, McElgunn CJ, Waaijer R, Zwijnenburg D, Diepvens F, Pals G (2002) Relative quantification of 40 nucleic acid sequences by multiplex ligation-dependent probe amplification. Nucleic Acids Res 30:e57
46. Seeger RC, Brodeur GM, Sather H, Dalton A, Siegel SE, Wong KY, Hammond D (1985) Association of multiple copies of the N-myc oncogene with rapid progression of neuroblastomas. N Engl J Med 313:1111–1116
47. Selzer RR, Richmond TA, Pofahl NJ, Green RD, Eis PS, Nair P, Brothman AR, Stallings RL (2005) Analysis of chromosome breakpoints in neuroblastoma at sub-kilobase resolution using fine-tiling oligonucleotide array CGH. Genes Chromosomes Cancer 44:305–319
48. Shimada H, Aotama C, Newton WA Jr (1987) Neuroblastoma; biology and prognostic factors. Gan To Kagaku Ryoho 14:44–49
49. Spitz R, Hero B, Ernestus K, Berthold F (2003) Deletions in chromosome arms 3p and 11q are new prognostic markers in localized and 4s neuroblastoma. Clin Cancer Res 9:52–58
50. Spitz R, Hero B, Simon T, Berthold F (2006) Loss in chromosome 11q identifies tumors with increased risk for metastatic relapses in localized and 4S neuroblastoma. Clin Cancer Res 12:3368–3373
51. Srivatsan ES, Ying KL, Seeger RC (1993) Deletion of chromosome 11 and of 14q sequences in neuroblastoma. Genes Chromosomes Cancer 7:32–37
52. Stark B, Jeison M, Bar-Am I, Glaser-Gabay L, Mardoukh J, Luria D, Feinmesser M, Goshen Y, Stein J, Abramov A, Zaizov R, Yaniv I (2002) Distinct cytogenetic pathways of advanced-stage neuroblastoma tumors, detected by spectral karyotyping. Genes Chromosomes Cancer 34:313–324
53. Suzuki T, Yokota J, Mugishima H, Okabe I, Ookuni M, Sugimura T, Terada M (1989) Frequent loss of heterozygosity on chromosome 14q in neuroblastoma. Cancer Res 49:1095–1098
54. Takita J, Hayashi Y, Kohno T, Yamaguchi N, Hanada R, Yamamoto K, Yokota J (1997) Deletion map of chromosome 9 and p16 (CDKN2A) gene alterations in neuroblastoma. Cancer Res 57:907–912
55. Takita J, Hayashi Y, Takei K, Yamaguchi N, Hanada R, Yamamoto K, Yokota J (2000) Allelic imbalance on chromosome 18 in neuroblastoma. Eur J Cancer 36:508–513
56. Takita J, Yang HW, Chen YY, Hanada R, Yamamoto K, Teitz T, Kidd V, Hayashi Y (2001) Allelic imbalance on chromosome 2q and alterations of the caspase 8 gene in neuroblastoma. Oncogene 20:4424–4432
57. Thompson PM, Seifried BA, Kyemba SK, Jensen SJ, Guo C, Maris JM, Brodeur GM, Stram DO, Seeger RC, Gerbing R, Matthay KK, Matise TC, White PS (2001) Loss of heterozygosity for chromosome 14q in neuroblastoma. Med Pediatr Oncol 36:28–31
58. Vandesompele J, Baudis M, De Preter K, Van Roy N, Ambros P, Bown N, Brinkschmidt C, Christiansen H, Combaret V, Lastowska M, Nicholson J, O'Meara A, Plantaz D, Stallings R, Brichard B, Van den Broecke C, De Bie S, De Paepe A, Laureys G, Speleman F (2005) Unequivocal delineation of clinicogenetic subgroups and development of a new model for improved outcome prediction in neuroblastoma. J Clin Oncol 23:2280–2299
59. Wan TS, Ma ES, Chan GC, Chan LC (2004) Investigation of MYCN status in neuroblastoma by fluorescence in situ hybridization. Int J Mol Med 14:981–987
60. Wang Q, Diskin S, Rappaport E, Attiyeh E, Mosse Y, Shue D, Seiser E, Jagannathan J, Shusterman S, Bansal M, Khazi D, Winter C, Okawa E, Grant G, Cnaan A, Zhao H, Cheung NK, Gerald W, London W, Matthay KK, Brodeur GM, Maris JM (2006) Integrative genomics identifies distinct molecular classes of neuroblastoma and shows that multiple genes are targeted by regional alterations in DNA copy number. Cancer Res 66: 6050–6062

Virchows Arch (2008) 453:57–67
DOI 10.1007/s00428-008-0626-5

ORIGINAL ARTICLE

Differential expression of fatty acid synthase (FAS) and ErbB2 in nonmalignant and malignant oral keratinocytes

Sabrina D. Silva · Isabela W. Cunha · Ana Lúcia C. A. Rangel · Jacks Jorge · Karina G. Zecchin · Michelle Agostini · Luiz P. Kowalski · Ricardo D. Coletta · Edgard Graner

Received: 23 November 2007 / Accepted: 5 May 2008 / Published online: 6 June 2008

Abstract The aim of this study was to investigate fatty acid synthase (FAS) and ErbB2 expression in nonmalignant oral epithelium and oral or head and neck squamous cell carcinomas (OSCC/HNSCC). Morphologically normal, hyperkeratotic, and dysplastic oral epithelium as well as well-differentiated and poorly differentiated OSCC were immunohistochemically evaluated for FAS, ErbB2, and Ki-67. These proteins were also analyzed in a tissue microarray with 55 HNSCC. SCC-9 cells were used to study FAS and ErbB2 during differentiation. FAS expression was higher in hyperkeratosis, dysplasias, and OSCC than in normal epithelium. Well-differentiated OSCC/HNSCC were more positive for FAS than the poorly differentiated tumors. ErbB2 was observed at the surface of nonmalignant and well-differentiated OSCC/HNSCC keratinocytes and in the cytoplasm of poorly differentiated cells. Ki-67 index was progressively higher from normal oral epithelium to OSCC, inversely correlated with cell surface ErbB2, and positively correlated with intracytoplasmic ErbB2. Finally, SCC-9 cell cultures were enriched in membrane ErbB2-positive cells after differentiation by anchorage deprivation. In conclusion, FAS is overexpressed in OSCC/HNSCC and hyperkeratotic oral epithelium and ErbB2 is found at the cell surface of differentiating keratinocytes and in the cytoplasm of poorly differentiated tumor cells. Ki-67 index is higher in epithelial dysplasias and OSCC than in morphologically normal oral epithelium.

Keywords ErbB2 · Fatty acid synthase · Ki-67 · SCC-9 · Oral squamous cell carcinoma · Keratinization

This work was supported by a grant from Fundação de Amparo à Pesquisa do Estado de São Paulo (FAPESP grant 02/08030-1 and CEPID/FAPESP grant 9814335). S.D. Silva, A.L.C.A. Rangel, and M. Agostini are supported by FAPESP fellowships (grants 04/06398-7, 04/13904-6, and 04/06397-0).

S. D. Silva · A. L. C. A. Rangel · J. Jorge · M. Agostini · R. D. Coletta · E. Graner (✉)
Departament of Oral Diagnosis, School of Dentistry of Piracicaba, State University of Campinas (UNICAMP), Av. Limeira 901, CP 52, Areão, Piracicaba CEP 13414-018 SP, Brazil
e-mail: egraner@fop.unicamp.br

I. W. Cunha
Departament of Anatomical Pathology, A.C. Camargo Cancer Hospital, São Paulo, SP, Brazil

K. G. Zecchin
Department of Clinical Pathology, School of Medical Sciences, State University of Campinas (UNICAMP), Campinas, SP, Brazil

L. P. Kowalski
Department of Head and Neck Surgery and Otorhinolaryngology, A.C. Camargo Cancer Hospital, São Paulo, SP, Brazil

Introduction

Fatty acid synthase (FAS, EC2.3.1.85) is the cytosolic multifunctional enzyme responsible for the endogenous production of saturated long-chain fatty acids from acetyl-CoA and malonyl-CoA [6, 22]. FAS is arranged as a homodimer and each ~250 kDa polypeptide chain contains seven distinct catalytic sites that sequentially act to generate

the 16-carbon saturated fatty acid palmitate [8]. Normal cells (with exception of liver, lactating breast, fetal lung, and adipose tissue) have low FAS activity because most of the fatty acids are supplied by the diet [22, 51]. However, despite its apparently marginal role in adult tissues, FAS is essential during embryogenesis, since FAS *n*−/− and FAS *n*+/− mice die in utero even in the presence of a diet rich in saturated fatty acids [9]. It has been recently demonstrated that FAS expression is upregulated in a variety of human epithelial cancers, including prostate, breast, ovarian, lung, stomach, colon, and melanoma [3, 10, 17, 23, 32, 35, 38, 45, 49], as well as in soft tissue sarcomas [39, 46], and often associated with a poor prognosis [2, 3, 12, 17, 46]. FAS expression and activity are elevated in oral squamous cell carcinoma (OSCC) [1, 15, 21, 41]; however, in contrast with several FAS-overexpressing malignancies, well-differentiated OSCC produces more FAS than their poorly differentiated counterparts [21, 41]. FAS specific inhibitors block cell cycle progression and cause apoptosis in prostate, breast, colon, and promyelocytic leukemia cancer cell lines [11, 25, 33]. Similarly, OSCC cell lines exposed to the FAS inhibitor cerulenin show reduced proliferation and enhanced apoptotic cell death [1, 55]. Moreover, inhibition of FAS activity decreases the size of prostate and ovarian cancer xenographs [20, 34, 35].

The regulation of FAS production is complex. Progesterone stimulates FAS expression in breast cancer cell lines [24] and androgens or epidermal growth factor upregulate FAS production and activity in the androgen-dependent prostate cancer cell line LNCaP [16, 43, 44, 48]. However, FAS is also overexpressed in androgen-independent prostate cancers [29, 34]. Recent experimental evidences demonstrate a direct connection between the cell surface receptor ErbB2 and FAS expression in cancer cells [26, 27]. Previous work from our laboratory showed that OSCC cell lines have very low androgen receptor protein but high ErbB2 protein levels [1] and that the expression of the latter one is positively correlated with the FAS protein amount in OSCC tissue samples [41]. Besides its transcriptional control, it was recently shown that FAS protein can be ubiquitinated and degraded by proteasomes in LNCaP prostate cancer cells, which can be reversed by the interaction with the isopeptidase ubiquitin-specific protease 2a [13].

In order to better understand the high expression of FAS in well-differentiated OSCC and verify its correlation with ErbB2, we performed immunohistochemical reactions in tissue sections obtained from morphologically normal, dysplastic, and hyperkeratotic oral epithelium, as well as well-differentiated and poorly differentiated tumors. Additionally, we describe the expression of these molecules during the keratinization process using a cell culture model.

Materials and methods

Study population

The tissue samples included in this study were obtained from the archives of the Orocentro (Center for Diagnosis and Treatment of Oral Diseases, UNICAMP, Piracicaba, Brazil) and comprised of nine fibrous hyperplasias, nine hyperkeratoses, 20 epithelial dysplasias, and 28 OSCCs. A tissue microarray (TMA) was constructed with head and neck squamous cell carcinoma (HNSCC) samples obtained from the primary tumors of 55 patients who had metastasis to the lungs and were treated at the Department of Head and Neck Surgery and Otorhinolaryngology, A.C. Camargo Cancer Hospital, São Paulo, Brazil (Tables 1 and 2). These cases were reviewed to confirm diagnosis and the degree of epithelial dysplasia as well as tumor differentiation were classified according to WHO classification by four of the authors (SDS, IWC, JJ, and EG). All samples were collected after explicit informed consent and with local ethical committee approval.

TMA construction

From the previous defined areas, core biopsies were taken using a Tissue Microarrayer (Beecher Instruments, Silver Springs, USA). Tissue cores with a dimension of 1.0 mm from each specimen were punched and arrayed in duplicate on a recipient paraffin block. Each core was spaced 0.2 mm apart. Sections of the recipient block were transferred with an adhesive tape to coated slides for subsequent ultraviolet cross-linkage (Instrumedics, Hackensack, NJ, USA); the slides dipped in a layer of paraffin to prevent oxidation and kept at −20°C.

Immunostaining

The paraffin-embedded samples were cut (3 μm) and mounted on silane-coated glass slides for hematoxylin and eosin staining and immunohistochemistry. FAS, ErbB2, and Ki-67 immunodetection was performed as previously described [5, 38]. Briefly, the sections were deparaffinized, rehydrated in graded ethanol solutions, and immersed in 3% H_2O_2 for 25 min at room temperature. Microwave (1380 W; Panasonic, Brazil) antigen retrieval consisted of two periods of 12 min in 10 mM citric acid solution (pH 6.0) followed by a washing step with phosphate-buffered saline (PBS). The incubations with the primary antibodies diluted in PBS were made overnight at 4°C: anti-FAS (1:3,000—Transduction Laboratories, Lexington, KY, USA), anti-ErbB2 (1:200—Dako, Carpinteria, CA, USA), and anti-Ki-67 MIB 1 (1:200—Dako). Sections were washed again and incubated with biotinylated secondary

Table 1 Relationship among FAS, membrane, and cytoplasmic ErbB2 expression with lifestyle and clinical variables in the invasive OSCC tumors

Variables	Category	FAS *n* (%)		Membrane ErbB2 n(%)		Cytoplasmic ErbB2 *n* (%)	
		Negative	Positive	Negative	Positive	Negative	Positive
Gender	Male	30 (91.18)	21 (95.55)	48 (96)	3 (60) *	30 (96.77)	21 (87.5)
	Female	3 (8.82)	1 (4.45)	2 (4)	2 (40)	1 (3.23)	3 (12.5)
Race	Caucasian	29 (87.88)	12 (81.82)	40 (81.63)	5 (100)	24 (80)	21 (87.5)
	Non-Caucasian	4 (12.12)	4 (18.18)	9 (18.37)	0	6 (20)	3 (12.5)
Smoking habit	Yes	3 (9.68)	1 (4.45)	2 (4.26)	2 (40)*	1 (3.57)	3 (12.5)
	No	28 (90.32)	21 (95.55)	45 (95.74)	3 (60)	27 (96.43)	21 (87.5)
Alcohol consumption	Yes	7 (22.58)	1 (4.55)	6 (12.77)	2 (40)	3 (10.71)	5 (20.83)
	No	24 (77.42)	21 (95.55)	41 (87.23)	3 (60)	25 (89.29)	19 (79.17)
Clinical stage	T1+T2	7 (31.82)	3 (23.08)	10 (32.26)	0	6 (30)	4 (30.77)
	T3+T4	15 (68.18)	10 (76.92)	21 (67.74)	2 (100)	14 (70)	9 (69.23)
Lymph nodes	N0	1 (3.23)	0	1 (2.13)	0	1 (3.23)	0
	N+	30 (96.77)	19 (100)	46 (97.87)	2 (100)	30 (96.77)	18 (100)

Percentages considering cases with complete information
*$p \leq 0.05$

antibodies for 30 min followed by the streptavidin–biotin–peroxidase (Strept ABC complex/HRP Duet kit, Dako) for 30 min at room temperature. Reactions were developed with a solution containing 0.6 mg/ml of 3,3′-diaminobenzidine tetrahydrochloride (DAB, Sigma, St. Louis, MO, USA) and 0.01% H_2O_2 and counter stained with Carazzi's hematoxylin. Positive and negative controls were included in all reactions. The intensity of the immunostaining was classified as negative, weak, or strong for FAS or ErbB2 in a blinded analysis performed by two of the authors (SDS and EG). The percentage of Ki-67 positive nuclei was calculated with the aid of an image computer analyzer (Kontron 400, Carl Zeiss, Germany).

SCC-9 cells (ATCC, Manassas, VA, USA) were plated in eight-well chamber slides (Lab Tek, Nunc, Naperville, IL, USA) and fixed in 3.7% paraformaldehyde. Primary antibodies anti-FAS (1:3,000) and anti-cytokeratin (1:500—PAN, AE1/AE3, Dako) were incubated overnight at 4°C

Table 2 Relationship among FAS, membrane, and cytoplasmic ErbB2 expression with pathological variables and recurrence information in the invasive OSCC tumors

Variables	Category	FAS *n* (%)		Membrane ErbB2 *n* (%)		Cytoplasmic ErbB2 *n* (%)	
		Negative	Positive	Negative	Positive	Negative	Positive
Histological grade	I	10 (31.25)	13 (59.09)*	21 (43.75)	2 (40)	13 (43.33)	10 (43.48)
	II	16 (50)	9 (40.91)	21 (43.75)	3 (60)	14 (46.67)	10 (43.48)
	III	6 (18.75)	0	6 (12.5)	0	3 (10)	3 (13.04)
Involved margins	No	26 (86.67)	15 (71.43)	36 (80)	3 (60)	21 (75)	18 (81.82)
	Yes	4 (13.33)	6 (28.57)	9 (20)	2 (40)	7 (25)	4 (18.18)
Lymphatic permeation	No	13 (46.43)	10 (50)	20 (46.51)	4 (80)	11 (39.29)	13 (65)
	Yes	15 (53.57)	10 (50)	23 (53.49)	1 (20)	17 (60.71)	7 (35)
Rupture	No	13 (40.62)	9 (40.91)	20 (41.67)	1 (20)	11 (36.67)	10 (43.48)
	Yes	19 (59.38)	13 (59.09)	28 (58.33)	4 (80)	19 (63.33)	13 (56.52)
Vascular embolization	No	24 (85.71)	19 (95)	38 (88.37)	5 (100)	24 (85.71)	19 (95)
	Yes	4 (14.29)	1 (5)	5 (11.63)	0	4 (14.29)	1 (5)
Perineural infiltration	No	10 (35.71)	7 (35)	17 (39.53)	0*	11 (39.29)	6 (30)
	Yes	18 (64.29)	13 (65)	26 (60.47)	5 (100)	17 (60.71)	14 (70)
Local recurrence	No	14 (41.18)	10 (45.45)	22 (44)	2 (40)	16 (51.61)	8 (33.33)
	Yes	20 (58.82)	12 (54.55)	28 (56)	3 (60)	15 (48.39)	16 (66.67)
Cervical recurrence	No	22 (64.71)	13 (59.09)	32 (64)	2 (40)	22 (70.97)	12 (50)
	Yes	12 (35.29)	9 (40.91)	18 (36)	3 (60)	9 (29.03)	12 (50)

Percentages considering cases with complete information
*$p \leq 0.05$

and washed in PBS. After incubation with secondary antibodies and the streptavidin–biotin complex, the reactions were developed as described above. Immunofluorescence reactions using 3.7% paraformaldehyde-fixed SCC-9 cells were performed with anti-ErbB2 antibodies (1:50–1:100—BD PharMingen, clone 9G6, San Diego, CA, USA) diluted in PBS 0.1% bovine serum albumin (BSA) for 1 h at room temperature. After incubation with fluorescein isothiocyanate (FITC)-conjugated anti-rabbit immunoglobulin G (1:500–1:1,000—Vector Laboratories, Burlingame, CA, USA) for 1 h, the reactions were mounted in Vectashield with DAPI (Vector Laboratories) and documented in a Leica DMR microscope equipped with epifluorescence (Leica Microsystems, Germany). The staining of living cells was made by incubating the primary antibodies (1:50–1:200) for 1 h at 4°C in Dulbecco's modified eagle's medium (DMEM)/F12 medium containing 0.1% BSA, followed by fixation and immersion in secondary antibody solution as described above.

Suspension-induced differentiation of SCC cells

The cell line SCC-9 was maintained in DMEM/F12 medium (Invitrogen, Carlsbad, CA, USA) supplemented with 10% fetal bovine serum (FBS; Cultilab, Brazil), 400-ng/ml hydrocortisone, and 100-μg/ml gentamicin and kanamycin at 37°C in a humidified atmosphere of 5% CO_2. In order to differentiate the SCC-9 cells [36], suspension cultures were performed according to Monk et al. [28]. Briefly, serum-free methylcellulose-containing DMEM-F12 was used to keep the SCC-9 cells in suspension ($1–2\times10^6$ cells/ml of methylcellulose-DMEM-F12 medium in a 25-cm^2 culture flask) at 37°C in a humidified atmosphere of 5% CO_2. After different periods of time (5–10 h), cells were harvested by diluting the methylcellulose medium ten-fold with prewarmed PBS followed by centrifugation at 1,000×*g* for 4 min. Differentiated SCC-9 cells were then plated (5×10^4) in each well of eight-well chamber slides (Lab Tek, Nunc). Similarly, cells grown in DMEM-F12

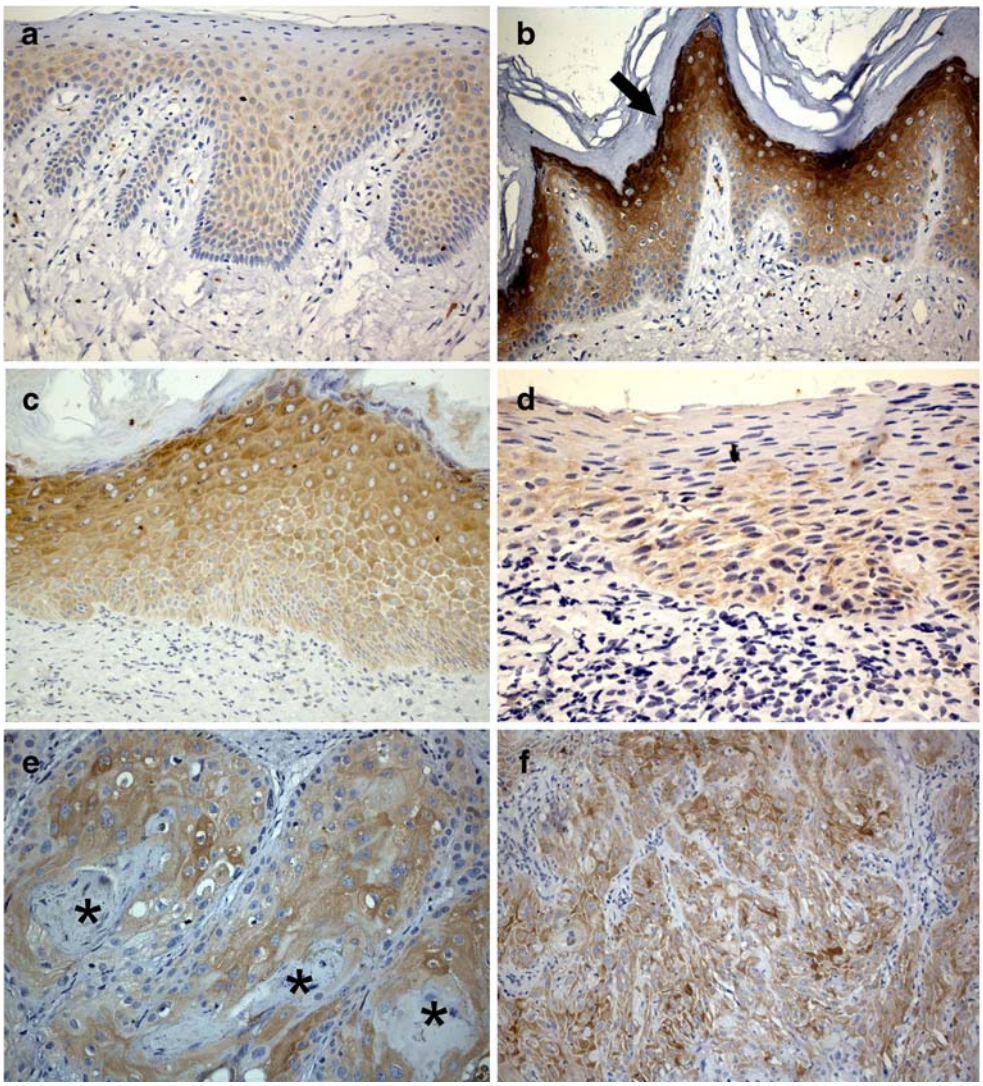

Fig. 1 Immunohistochemical detection of FAS in morphologically normal oral epithelium (**a**), hyperkeratosis (**b**), mild dysplasia (**c**), severe dysplasia (**d**), well-differentiated OSCC (**e**), and poorly differentiated OSCC (**f**). *Arrow* = stratum granulosum; * = keratin pearls; **a**, **b**, **c**, **e,** and **f** = original magnification, ×200; **d** = original magnification, ×400

containing 10% FBS were plated (2×10^4 in each well) as controls. After 12–16 h, the cells were fixed in 3.7% paraformaldehyde for immunocytochemistry or 90% ethanol for Papanicolaou staining. The positivity for ErbB2 at the cell membrane of differentiated and undifferentiated SCC-9 cells was analyzed by immunofluorescence and flow cytometry. For the flow cytometry experiments, cells were incubated for 1 h at room temperature with anti-ErbB2 antibodies (BD PharMingen) 1:50, washed three times with PBS and incubated with anti-mouse FITC conjugated at 1:250 for 1 h. After a new washing step, samples were analyzed in a Becton Dickinson FACSCalibur flow cytometer (San Jose, CA, USA) equipped with an argon laser and CellQuest software. Five thousand events were collected for each sample. Cell populations were identified by their light-scattering characteristics, enclosed in electronic gates, and analyzed for the intensity of the fluorescent probe signal.

Statistical analysis

For frequency analysis in contingency tables, statistical analysis of associations between variables was performed by the Fisher's exact test and for continuous variables, the nonparametric Mann–Whitney *U* test. Pearson correlation analyses were used to evaluate associations between FAS, ErbB2, and Ki-67 expression. Kruskal–Wallis test was used in order to compare Ki-67 expression levels in the studied samples. Significance was set for $p<0.05$.

Results

The cytoplasmic immunohistochemical labeling for the FAS protein was weak and restricted to the lower layers of the stratum spinosum in the morphologically normal oral epithelium (Figs. 1a and 2a). In most of the dysplastic samples (Fig. 1c, d), FAS positivity was more intense than in normal tissues and widely spread to the upper epithelial cell layers. OSCC tissue samples showed strong reactions for FAS (Fig. 1e,f), which were more prominent in well-differentiated OSCC than in the poorly undifferentiated tumors (Fig. 2a). Intense FAS staining was also observed in the hyperkeratotic oral mucosa samples (Figs. 1b and 2a), in which all cell layers, especially the stratum granulosum, were labeled. In the TMA with HNSCC samples, a significant correlation between the histological grade and FAS expression was observed. Twenty-two cases (40%) were positive for FAS and this positivity was more intense in well-differentiated (grade I; 59.1%) than in moderately differentiated (grade II) or poorly differentiated (grade III) tumors ($p<0.05$; Table 2).

Two distinct patterns of ErbB2 positivity were found. The canonical cell membrane staining for ErbB2 was clearly

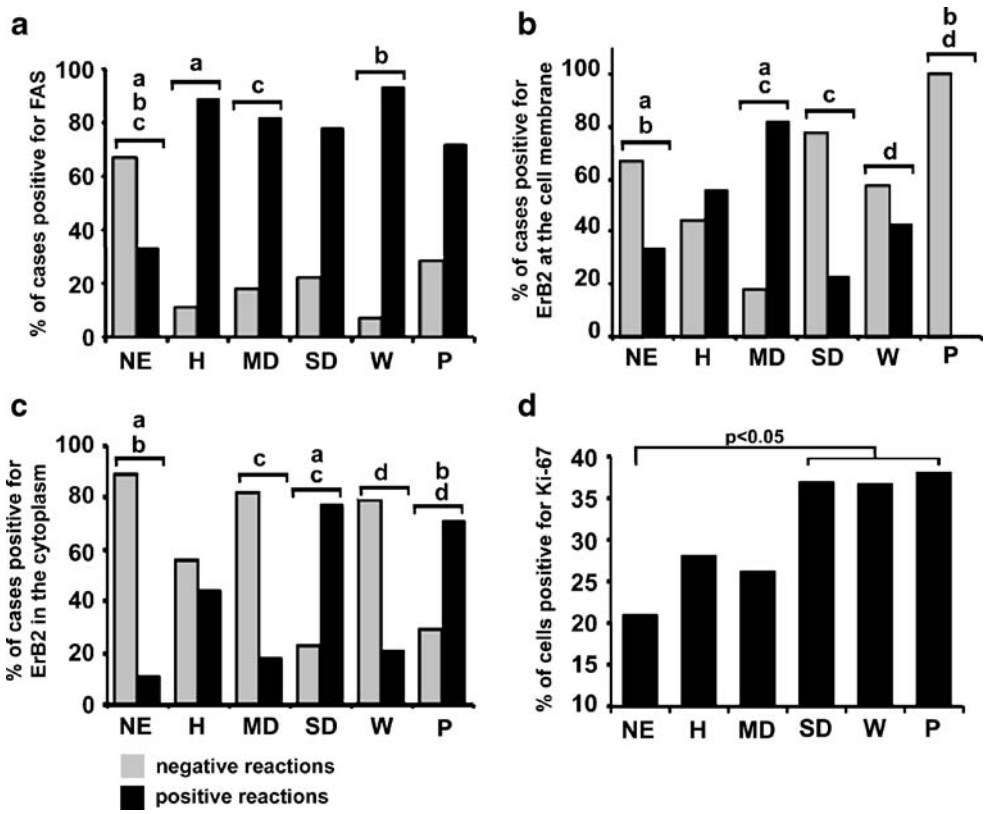

Fig. 2 Analysis of FAS, ErbB2, and Ki-67 expression in normal epithelium (*NE*), hyperkeratosis (*H*), mild dysplasia (*MD*), severe dysplasia (*SD*), well-differentiated OSCC (*W*) and poorly differentiated OSCC (*P*). Graphical representation of FAS positivity (**a**) (Fisher exact test, *a*: $p=0.05$, *b*: $p=0.005$, *c*: $p=0.065$), ErbB2 at the cell membrane (**b**) (Fisher exact test, *a*: $p=0.065$, *b*: $p=0.047$, *c*: $p=0.022$, *d*: $p=0.008$), and ErbB2 in the cytoplasm (**c**) (Fisher exact test, *a*: $p=0.015$, *b*: $p=0.009$, *c*: $p=0.022$, *d*: $p=0.023$). The Ki-67 index was progressively higher from normal oral epithelium to OSCC (**d**) (Kruskal–Wallis test)

evident in the stratum spinosum of the normal epithelium, hyperkeratosis, mild epithelial dysplasias, well-differentiated OSCC, and hyperkeratosis (Fig. 3a–c,e). A diffuse cytoplasmic staining for this receptor was found at the basal cell layer of the normal epithelium, in most of the severe dysplasias and poorly differentiated OSCC as well as in some areas of well-differentiated OSCC (Figs. 2b,c and 3a,d–f).

Taking in consideration the OSCC samples only, an inverse correlation was found between the ErbB2 positivity at the cell membrane and its cytoplasmic staining ($p=0.02$, $r=-0.3$) as well as between the former and the cell proliferation index, as measured by the Ki-67 nuclear positivity ($p=0.04$, $r=-0.24$). A positive correlation was found between the Ki-67 index and the cytoplasmic ErbB2 staining ($p=0.06$, $r=0.23$). By comparing the normal oral epithelium and well-differentiated OSCC, the intensity of the FAS staining was positively correlated with the Ki-67 index ($p=0.002$, $r=0.61$) and with the cytoplasmic ErbB2 ($p=0.06$, $r=0.4$). Although not statistically significant, FAS positivity in normal epithelium and poorly differentiated OSCC was also positively associated with the Ki-67 index ($p=0.09$, $r=0.36$). Inverse correlations between the Ki-67 index and ErbB2 at the cell surface ($p=0.003$, $r=-0.59$) and between the latter and the ErbB2 cytoplasmic staining ($p=0.04$, $r=-0.43$) were observed in the same samples. When well- and poorly differentiated OSCC were compared, ErbB2 at the cell membrane was positively associated with FAS staining ($p=0.03$, $r=0.41$) and inversely correlated with the ErbB2 in the cytoplasm ($p=0.04$, $r=-0.38$). The immunohistochemical reactions performed in the TMA with aggressive HNSCC samples that metastasized to the lungs confirmed these results since ErbB2 at the cell membrane was correlated with FAS ($p=0.014$) and both inversely associated with the ErbB2 in the cytoplasm ($p=0.032$). ErbB2 positivity at the cell membrane was also associated with perineural infiltration in the same samples

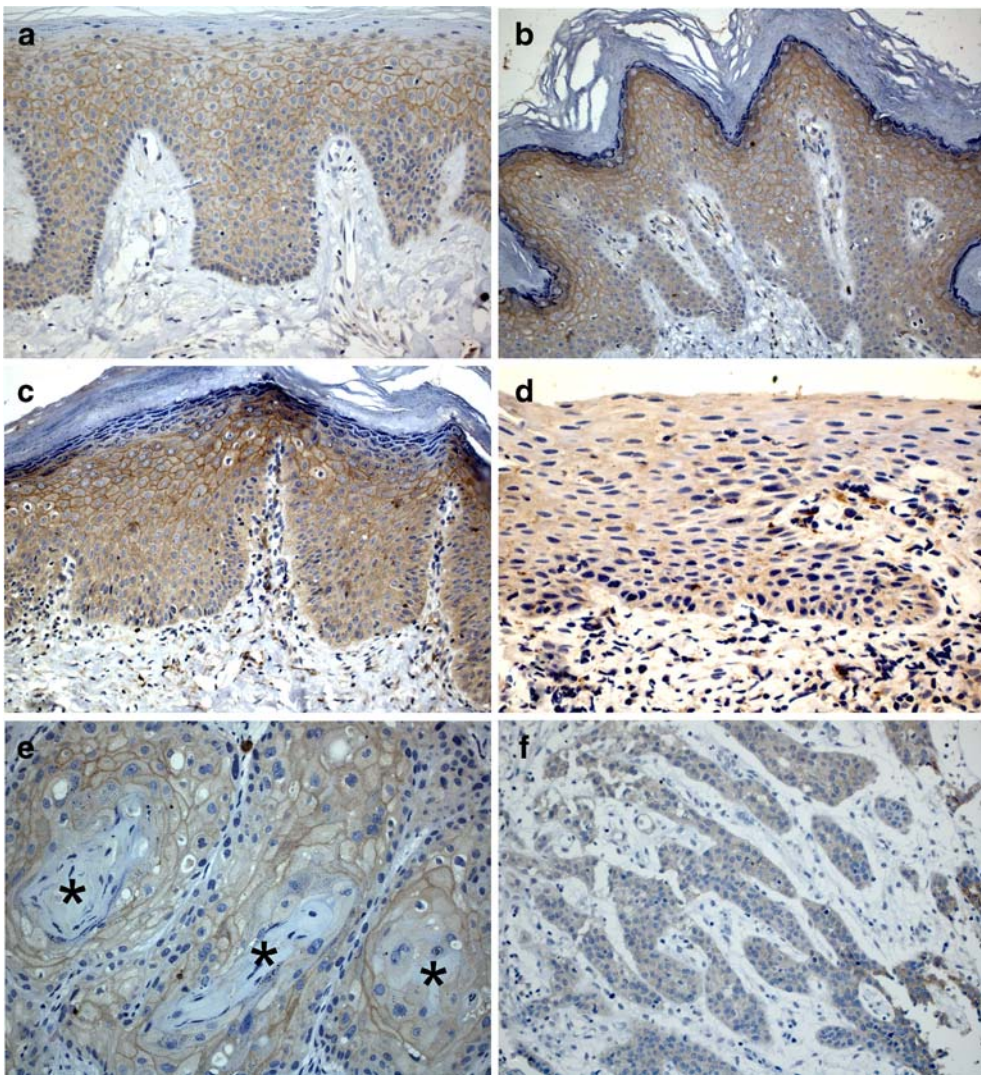

Fig. 3 Immunohistochemical detection of ErbB2 in morphologically normal oral epithelium (**a**), hyperkeratosis (**b**), mild dysplasia (**c**), severe dysplasia (**d**), well-differentiated OSCC (**e**), and poorly differentiated OSCC (**f**). * = keratin pearls; **a**, **b**, **c**, **e**, and **f** = original magnification, ×200; **d** = original magnification, ×400

(Table 2). A comparative analysis of the proliferative status of the oral epithelial cells showed that the Ki-67 index is progressively higher from normal oral epithelium to OSCC (Fig. 2d). Interestingly, the samples with hyperkeratosis also had a higher Ki-67 score than the normal epithelium (Fig. 2d).

In order to better understand the expression of FAS in well-differentiated OSCC and HNSCC, we induced the differentiation of an OSCC cell line as described by Rheinwald and Beckett [36] and Monk et al. [28]. Figure 4a and b show that following anchorage and serum deprivation, SCC-9 cells lost their typical morphology with abundant cytoplasm and irregular shape and became small, round, and eosinophilic. Keratinization was clearly evident by both Papanicolaou staining (Fig. 4c,d) and immunocytochemistry (Fig. 4e,f). A finely granular FAS cytoplasmic staining was observed in undifferentiated SCC-9 cells, whereas differentiated cells showed strong positivity for FAS within large and heterogeneous granules (Fig. 4g,h). Finally, regularly growing SCC-9 cells were positive for ErbB2 both in the cytoplasm and cell membrane (Fig. 5a,b), and after the incubation in semisolid cell culture medium, the expression of this receptor was found at the surface of most differentiated cells (Fig. 5c). In order to better

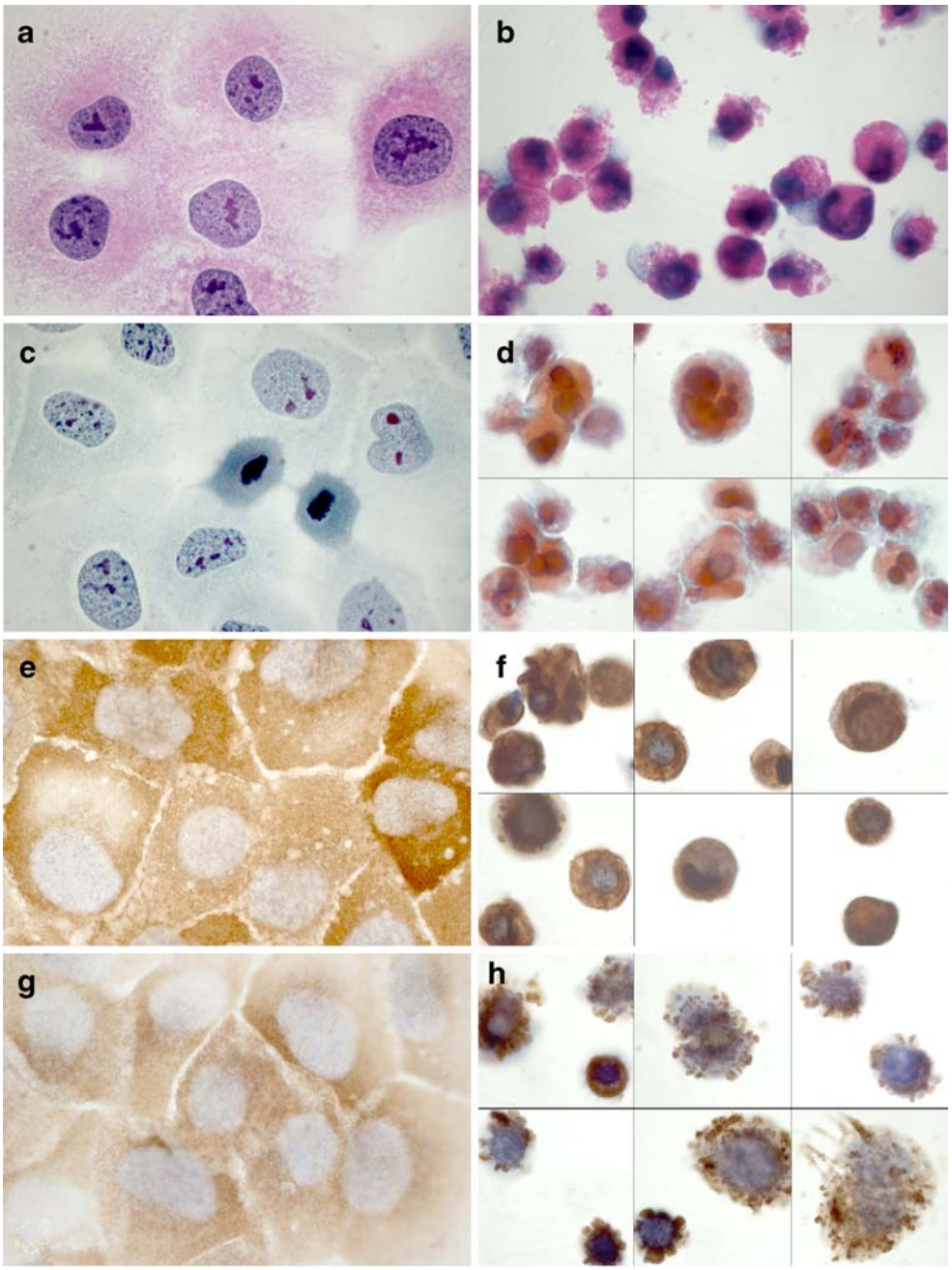

Fig. 4 Anchorage deprivation of SCC-9 cells promotes keratinocyte differentiation. The *left column* shows undifferentiated and the *right column* differentiated SCC-9 cells. Hematoxylin and eosin staining (**a**, **b**), Papanicolaou staining showing undifferentiated cells labeled in *green* (**c**) and differentiated cells in *orange* (**d**), and immunocytochemical reaction using antibodies against cytokeratins (AE1/AE3) (**e**, **f**) or FAS (**g**, **h**). Original magnification, ×400

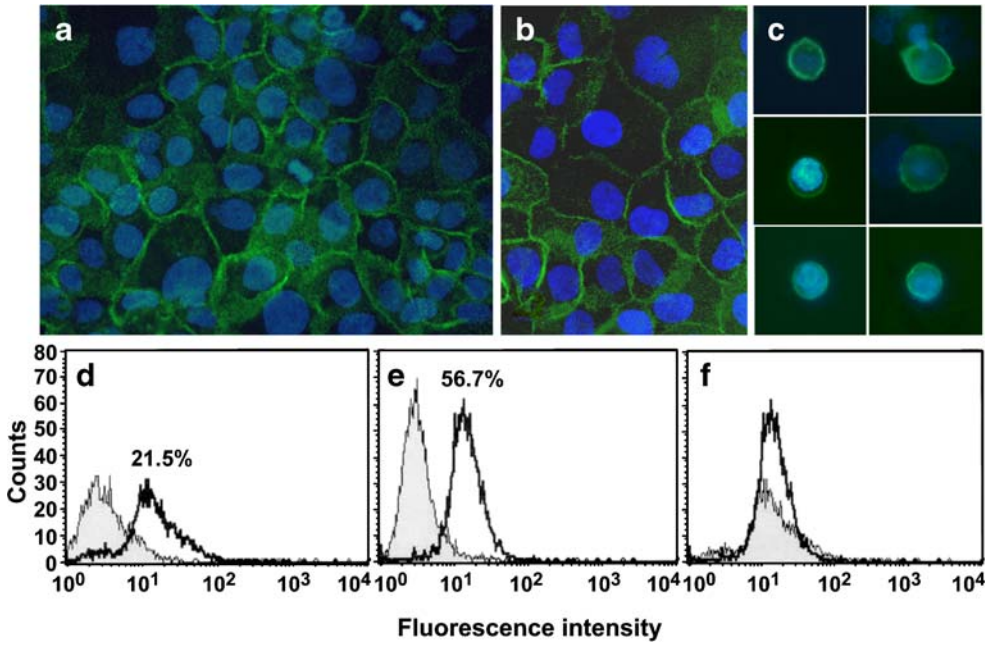

Fig. 5 Detection of ErbB2 protein in the cytoplasm and at the cell membrane of paraformaldehyde-fixed SCC-9 cells by immunofluorescence (**a**). ErbB2 was observed at the cell surface of undifferentiated (**b**) and differentiated (**c**) living SCC-9 cells. Original magnification, ×400; nuclei were stained with DAPI. Flow cytometry analysis of ErbB2 expression at the cell surface of undifferentiated and differentiated SCC-9 cells (**d**, **e**). Note the increase from 21.5% to 56.7% of ErbB2 positive cells after serum and anchorage deprivation (*filled* = negative control; *unfilled* = anti-ErbB2). The superimposition of the peaks representing both undifferentiated (*filled*) and differentiated (*unfilled*) ErbB2-positive cells is shown in **f**

understand the pattern of ErbB2 positivity during keratinization, we performed flow cytometry analysis, which showed an increase from 21% to 56% in the number of ErbB2 positive cells following anchorage deprivation (Fig. 5d–f).

Discussion

In the last few years, FAS expression and activity have shown to be abnormally high in several human cancers [3, 6, 10, 17, 23, 31, 32, 35, 38–40, 45, 46, 49] and associated with a poor prognosis in some tumors [2, 3, 12, 17, 40, 46]. Although the enhanced FAS expression and activity found in OSCC, well-differentiated tumors have been described as more positive for FAS than the poorly differentiated lesions [21, 41]. Indeed, in the present work, we confirm that the production of FAS is higher in OSCC and HNSCC in comparison with the morphologically normal epithelium and that its immunohistochemical expression in well-differentiated tumors is stronger than in poorly differentiated lesions. FAS expression in keratinized human oral epithelium has been detected in the stratum granulosum and uppermost layer of the stratum spinosum and coincides with the expression of the cutaneous fatty acid-binding protein, which is involved in the transport of long-chain fatty acids to the lamellar bodies [47, 50]. We included in the present work tissue sections of hyperkeratotic oral mucosa which showed, as expected, intense FAS immunostaining. Based on these observations, it is conceivable that in well-differentiated OSCC, both neoplastic- and keratinization-associated FAS production are superimposed, making these samples even more positive than the poorly differentiated tumors. This fact might explain why FAS expression is not more prominent in poorly differentiated and aggressive OSCC or HNSCC, as it occurs in several cancers.

ErbB2 overexpression or gene amplification have been described in OSCC and HNSCC by several authors [7, 18, 19, 30, 52–54]. We have previously shown that ErbB2 is preferentially expressed at the cell membrane in well-differentiated lesions [41] and, here, we extend these results by demonstrating that ErbB2 expression at the cell surface occurs in the morphologically normal and hyperkeratotic oral epithelium, epithelial dysplasias, and well-differentiated OSCC and HNSCC. A direct connection between the expression of this receptor and FAS was recently evidenced by Menendez et al. [26, 27]. According to these authors, the inhibition of FAS expression by means of RNAi or its natural specific inhibitor cerulenin downregulates ErbB2 mRNA in breast and ovarian cancer cell lines. Moreover, the association of cerulenin with Trastuzumab (Herceptin) synergistically enhances apoptotic cell death in a breast cancer cell line. Conversely, ErbB2 overexpressing NIH-3T3

cells show high FAS protein levels and cerulenin is able to inhibit their growth in soft agar as well as to induce enhanced apoptotic cell death, in comparison with the wild type cells. In our well-differentiated OSCC and HNSCC cases, ErbB2 was present at the cell membrane mainly in the regions close to the keratin pearls, while poorly differentiated tumors expressed ErbB2 in the cytoplasm only. The positivity for ErbB2 at the cell membrane was inversely correlated to its cytoplasmic staining, which was in turn correlated with cell proliferation, as measured by the Ki-67 index. The biological significance of these distinct patterns of ErbB2 distribution is not known; however, our results suggest that when at the cell surface, this receptor has a role in squamous cell differentiation (fact that was clearly evident in hyperkeratosis; Fig. 3b). Indeed, a statistically significant correlation was found between ErbB2 at the cell surface and FAS positivity when well-differentiated and poorly differentiated tumors were compared. Furthermore, simultaneous positivity for FAS and ErbB2 at the cell surface may be a predictor of good prognosis and a larger clinical study will be necessary to confirm these findings.

OSCC-derived cell lines, such as SCC-4, SCC-9, SCC-15, and SCC-25, homogeneously express FAS in the cytoplasm and their growth can be efficiently inhibited by cerulenin [1]. Interestingly, in our previous work with antibodies directed against an intracytoplasmic domain of the ErbB2 protein (anti-c-erbB-2 oncoprotein; A0485, Dako), we observed expression of ErbB2 in the cytoplasm of these cells, whereas epidermal growth factor receptor, the prototype member of the ErbB family of receptors, was found at the cell membranes [1]. Here, we show ErbB2 positivity in both the cytoplasm and cell surface by using antibodies directed against an extracellular domain of this receptor. Anchorage deprivation by culture in methylcellulose-containing medium terminally differentiates and keratinizes SCC cells [36]. In the present work, we used similar culture conditions in order to promote the differentiation of SCC-9 cells and analyze the expression of FAS and ErbB2 during keratinization. Differentiated SCC-9 cells expressed FAS in cytoplasmic granular structures and had a higher frequency of ErbB2 at the cell membrane than the undifferentiated controls, corroborating the immunohistochemical results of this and previous study [41]. The gross granular pattern of FAS expression in differentiated SCC-9 cells may represent the lipid-accumulating lamellar granules found in the stratum spinosum and granulosum of the stratified epithelium [37, 42]. Accordingly, the fatty acid synthesis seems to have increased during squamous cell differentiation, when short-chain fatty acids are replaced by long-chain saturated fatty acids [4, 14].

In summary, the results presented here show that FAS expression is higher in oral hyperkeratosis, epithelial dysplasias, OSCC, and HNSCC than in the normal oral epithelium. ErbB2 expression was observed at the cell surface of nontumoral and well-differentiated OSCC and HNSCC, whereas its cytoplasmic localization was found in poorly differentiated tumors. The Ki-67 index was progressively higher from the normal oral epithelium to OSCC and positively associated with the ErbB2 cytoplasmic labeling. Finally, the in vitro differentiation increased the number of cell membrane ErbB2 positive cells. Taken together, these findings suggest that FAS is involved in both neoplastic cell proliferation and epithelial differentiation and explain why well-differentiated OSCC express more FAS than their poorly differentiated counterparts. Further studies will be necessary to elucidate the exact role of ErbB2 in the FAS gene expression in oral cancer cells.

Conflict of interest statement We declare that we have no conflict of interest.

References

1. Agostini M, Silva SD, Zecchin KG, Coletta RD, Jorge J, Loda M, Graner E (2004) Fatty acid synthase is required for the proliferation of human oral squamous carcinoma cells. Oral Oncol 40:728–735
2. Alo PL, Visca P, Framarino ML, Botti C, Monaco S, Sebastiani V, Serpieri DE, Di Tondo U (2000) Immunohistochemical study of fatty acid synthase in ovarian neoplasms. Oncol Rep 7:1383–1388
3. Alo PL, Visca P, Marci A, Mangoni A, Botti C, Di Tondo U (1996) Expression of fatty acid synthase (FAS) as a predictor of recurrence in stage I breast carcinoma patients. Cancer 77:474–482
4. Ansari MN, Nicolaides N, Fu HC (1970) Fatty acid composition of the living layer and stratum corneum lipids of human sole skin epidermis. Lipids 5:838–845
5. Araujo CS, Graner E, Almeida OP, Sauk JJ, Coletta RD (2003) Histomorphometric characteristics and expression of epidermal growth factor and its receptor by epithelial cells of normal gingiva and hereditary gingival fibromatosis. J Periodontal Res 38:237–241
6. Baron A, Migita T, Tang D, Loda M (2004) Fatty acid synthase: a metabolic oncogene in prostate cancer? J Cell Biochem 91:47–53
7. Bei R, Pompa G, Vitolo D, Moriconi E, Ciocci L, Quaranta M, Frati L, Kraus MH, Muraro R (2001) Co-localization of multiple ErbB receptors in stratified epithelium of oral squamous cell carcinoma. J Pathol 195:343–348
8. Brink J, Ludtke SJ, Yang CY, Gu ZW, Wakil SJ, Chiu W (2002) Quaternary structure of human fatty acid synthase by electron cryomicroscopy. Proc Natl Acad Sci U S A 99:138–143
9. Chirala SS, Chang H, Matzuk M, Abu-Elheiga L, Mao J, Mahon K, Finegold M, Wakil SJ (2003) Fatty acid synthesis is essential in embryonic development: fatty acid synthase null mutants and most of the heterozygotes die in utero. Proc Natl Acad Sci U S A 100:6358–6363
10. Dhanasekaran SM, Barrette TR, Ghosh D, Shah R, Varambally S, Kurachi K, Pienta KJ, Rubin MA, Chinnaiyan AM (2001) Delineation of prognostic biomarkers in prostate cancer. Nature 412:822–826

11. Furuya Y, Akimoto S, Yasuda K, Ito H (1997) Apoptosis of androgen-independent prostate cell line induced by inhibition of fatty acid synthesis. Anticancer Res 17:4589–4593
12. Gansler TS, Hardman W, 3rd Hunt DA, Schaffel S, Hennigar RA (1997) Increased expression of fatty acid synthase (OA-519) in ovarian neoplasms predicts shorter survival. Human Pathol 28:686–692
13. Graner E, Tang D, Rossi S, Baron A, Migita T, Weinstein LJ, Lechpammer M, Huesken D, Zimmermann J, Signoretti S, Loda M (2004) The isopeptidase USP2a regulates the stability of fatty acid synthase in prostate cancer. Cancer Cell 5:253–261
14. Gray GM, Yardley HJ (1975) Different populations of pig epidermal cells: isolation and lipid composition. J Lipid Res 16:441–447
15. Guo CB, Cui NH, Yu GY, Liu DX, Meng SC, Song Q (2003) Effects of cerulenin on the endogenous fatty acid synthetic activity in squamous cell carcinoma of the oral cavity. J Oral Maxillofac Surg 61:909–912
16. Heemers H, Maes B, Foufelle F, Heyns W, Verhoeven G, Swinnen JV (2001) Androgens stimulate lipogenic gene expression in prostate cancer cells by activation of the sterol regulatory element-binding protein cleavage activating protein/sterol regulatory element-binding protein pathway. Mol Endocrinol 15:1817–1828
17. Innocenzi D, Alo PL, Balzani A, Sebastiani V, Silipo V, La Torre G, Ricciardi G, Bosman C, Calvieri S (2003) Fatty acid synthase expression in melanoma. J Cutan Pathol 30:23–28
18. Khademi B, Shirazi FM, Vasei M, Doroudchi M, Gandomi B, Modjtahedi H, Pezeshki AM, Ghaderi A (2002) The expression of p53, c-erbB-1 and c-erbB-2 molecules and their correlation with prognostic markers in patients with head and neck tumors. Cancer Lett 184:223–230
19. Khan AJ, King BL, Smith BD, Smith GL, DiGiovanna MP, Carter D, Haffty BG (2002) Characterization of the HER-2/neu oncogene by immunohistochemical and fluorescence in situ hybridization analysis in oral and oropharyngeal squamous cell carcinoma. Clin Cancer Res 8:540–548
20. Kridel SJ, Axelrod F, Rozenkrantz N, Smith JW (2004) Orlistat is a novel inhibitor of fatty acid synthase with antitumor activity. Cancer Res 64:2070–2075
21. Krontiras H, Roye GD, Beenken SE, Myers RB, Mayo MS, Peters GE, Grizzle WE (1999) Fatty acid synthase expression is increased in neoplastic lesions of the oral tongue. Head Neck 21:325–329
22. Kuhajda FP (2000) Fatty-acid synthase and human cancer: new perspectives on its role in tumor biology. Nutrition 16:202–208
23. Kusakabe T, Nashimoto A, Honma K, Suzuki T (2002) Fatty acid synthase is highly expressed in carcinoma, adenoma and in regenerative epithelium and intestinal metaplasia of the stomach. Histopathology 40:71–79
24. Lacasa D, Le Liepvre X, Ferre P, Dugail I (2001) Progesterone stimulates adipocyte determination and differentiation 1/sterol regulatory element-binding protein 1c gene expression: potential mechanism for the lipogenic effect of progesterone in adipose tissue. J Biol Chem 276:11512–11516
25. Li JN, Gorospe M, Chrest FJ, Kumaravel TS, Evans MK, Han WF, Pizer ES (2001) Pharmacological inhibition of fatty acid synthase activity produces both cytostatic and cytotoxic effects modulated by p53. Cancer Res 61:1493–1499
26. Menendez JA, Mehmi I, Verma VA, Teng PK, Lupu R (2004) Pharmacological inhibition of fatty acid synthase (FAS): a novel therapeutic approach for breast cancer chemoprevention through its ability to suppress Her-2/neu (erbB-2) oncogene-induced malignant transformation. Mol Carcinog 41:164–178
27. Menendez JA, Vellon L, Mehmi I, Oza BP, Ropero S, Colomer R, Lupu R (2004) Inhibition of fatty acid synthase (FAS) suppresses HER2/neu (erbB-2) oncogene overexpression in cancer cells. Proc Natl Acad Sci U S A 101:10715–10720
28. Monk SA, Denison MS, Rice RH (2001) Transient expression of CYP1A1 in rat epithelial cells cultured in suspension. Arch Biochem Biophys 393:154–162
29. Myers RB, Oelschlager DK, Weiss HL, Frost AR, Grizzle WE (2001) Fatty acid synthase: an early molecular marker of progression of prostatic adenocarcinoma to androgen independence. J Urol 165:1027–1032
30. Nagler RM, Kerner H, Laufer D, Ben-Eliezer S, Minkov I, Ben-Itzhak O (2002) Squamous cell carcinoma of the tongue: the prevalence and prognostic roles of p53, Bcl-2, c-erbB-2 and apoptotic rate as related to clinical and pathological characteristics in a retrospective study. Cancer Lett 186:137–150
31. Oskouian B (2000) Overexpression of fatty acid synthase in SKBR3 breast cancer cell line is mediated via a transcriptional mechanism. Cancer Lett 149:43–51
32. Piyathilake CJ, Frost AR, Manne U, Bell WC, Weiss H, Heimburger DC, Grizzle WE (2000) The expression of fatty acid synthase (FASE) is an early event in the development and progression of squamous cell carcinoma of the lung. Human Pathol 31:1068–1073
33. Pizer ES, Chrest FJ, DiGiuseppe JA, Han WF (1998) Pharmacological inhibitors of mammalian fatty acid synthase suppress DNA replication and induce apoptosis in tumor cell lines. Cancer Res 58:4611–4615
34. Pizer ES, Pflug BR, Bova GS, Han WF, Udan MS, Nelson JB (2001) Increased fatty acid synthase as a therapeutic target in androgen-independent prostate cancer progression. Prostate 47:102–110
35. Pizer ES, Wood FD, Heine HS, Romantsev FE, Pasternack GR, Kuhajda FP (1996) Inhibition of fatty acid synthesis delays disease progression in a xenograft model of ovarian cancer. Cancer Res 56:1189–1193
36. Rheinwald JG, Beckett MA (1980) Defective terminal differentiation in culture as a consistent and selectable character of malignant human keratinocytes. Cell 22:629–632
37. Ricardo Martinez I Jr, Peters A (1971) Membrane-coating granules and membrane modifications in keratinizing epithelia. Am J Anat 130:93–119
38. Rossi S, Graner E, Febbo P, Weinstein L, Bhattacharya N, Onody T, Bubley G, Balk S, Loda M (2003) Fatty acid synthase expression defines distinct molecular signatures in prostate cancer. Mol Cancer Res 1:707–715
39. Rossi S, Ou W, Tang D, Bhattacharya N, Dei Tos A, Fletcher J, Loda M (2006) Gastrointestinal stromal tumours overexpress fatty acid synthase. J Pathol 209:369–375
40. Shurbaji MS, Kalbfleisch JH, Thurmond TS (1996) Immunohistochemical detection of a fatty acid synthase (OA-519) as a predictor of progression of prostate cancer. Human Pathol 27:917–921
41. Silva SD, Agostini M, Nishimoto IN, Coletta RD, Alves FA, Lopes MA, Kowalski LP, Graner E (2004) Expression of fatty acid synthase, ErbB2 and Ki-67 in head and neck squamous cell carcinoma. A clinicopathological study. Oral Oncol 40:688–696
42. Squier CA, Kremer MJ (2001) Biology of oral mucosa and esophagus. J Natl Cancer Inst Monogr 29:7–15
43. Swinnen JV, Esquenet M, Goossens K, Heyns W, Verhoeven G (1997) Androgens stimulate fatty acid synthase in the human prostate cancer cell line LNCaP. Cancer Res 57:1086–1090
44. Swinnen JV, Heemers H, Deboel L, Foufelle F, Heyns W, Verhoeven G (2000) Stimulation of tumor-associated fatty acid synthase expression by growth factor activation of the sterol regulatory element-binding protein pathway. Oncogene 19:5173–5181
45. Swinnen JV, Roskams T, Joniau S, Van Poppel H, Oyen R, Baert L, Heyns W, Verhoeven G (2002) Overexpression of fatty acid synthase is an early and common event in the development of prostate cancer. Int J Cancer 98:19–22

46. Takahiro T, Shinichi K, Toshimitsu S (2003) Expression of fatty acid synthase as a prognostic indicator in soft tissue sarcomas. Clin Cancer Res 9:2204–2212
47. Uchiyama N, Yamamoto A, Kameda K, Yamaguchi H, Ito M (2000) The activity of fatty acid synthase of epidermal keratinocytes is regulated in the lower stratum spinousum and the stratum basale by local inflammation rather than by circulating hormones. J Dermatol Sci 24:134–141
48. Van de Sande T, De Schrijver E, Heyns W, Verhoeven G, Swinnen JV (2002) Role of the phosphatidylinositol 3¢-kinase/PTEN/Akt kinase pathway in the overexpression of fatty acid synthase in LNCaP prostate cancer cells. Cancer Res 62:642–646
49. Visca P, Alo PL, Del Nonno F, Botti C, Trombetta G, Marandino F, Filippi S, Di Tondo U, Donnorso RP (1999) Immunohistochemical expression of fatty acid synthase, apoptotic-regulating genes, proliferating factors, and ras protein product in colorectal adenomas, carcinomas, and adjacent nonneoplastic mucosa. Clin Cancer Res 5:4111–4118
50. Watanabe R, Fujii H, Yamamoto A, Yamaguchi H, Takenouchi T, Kameda K, Ito M, Ono T (1996) Expression of cutaneous fatty acid-binding protein and its mRNA in rat skin. Arch Dermatol Res 288:481–483
51. Weiss L, Hoffmann GE, Schreiber R, Andres H, Fuchs E, Korber E, Kolb HJ (1986) Fatty-acid biosynthesis in man, a pathway of minor importance. Purification, optimal assay conditions, and organ distribution of fatty-acid synthase. Biol Chem Hoppe Seyler 367:905–912
52. Werkmeister R, Brandt B, Joos U (2000) Clinical relevance of erbB-1 and -2 oncogenes in oral carcinomas. Oral Oncol 36:100–105
53. Xia W, Lau YK, Zhang HZ, Liu AR, Li L, Kiyokawa N, Clayman GL, Katz RL, Hung MC (1997) Strong correlation between c-erbB-2 overexpression and overall survival of patients with oral squamous cell carcinoma. Clin Cancer Res 3:3–9
54. Xia W, Lau YK, Zhang HZ, Xiao FY, Johnston DA, Liu AR, Li L, Katz RL, Hung MC (1999) Combination of EGFR, HER-2/neu, and HER-3 is a stronger predictor for the outcome of oral squamous cell carcinoma than any individual family members. Clin Cancer Res 5:4164–4174
55. Zhang Y, Guo C, Yu G (2005) A pilot study of fatty acid metabolism in oral squamous cell carcinoma. Int J Oral Maxillofac Surg 34:78–81

Virchows Arch (2008) 453:69–77
DOI 10.1007/s00428-008-0629-2

ORIGINAL ARTICLE

Amalgamation of *Chlamydia pneumoniae* inclusions with lipid droplets in foam cells in human atherosclerotic plaque

Yuri V. Bobryshev · Murray C. Killingsworth · Dihn Tran · Reginald Lord

Received: 26 November 2007 / Revised: 14 March 2008 / Accepted: 13 May 2008 / Published online: 6 June 2008

Abstract *Chlamydia pneumoniae* (*Chlamydophila pneumoniae*) infect macrophages and accelerates foam cell formation in in vitro experiments, but whether this might occur in human atherosclerosis is unknown. In the present study, we examined 17 carotid artery segments, obtained by endarterectomy, in which the presence of *C. pneumoniae* was confirmed by both polymerase chain reaction and immunohistochemistry. Electron microscopy demonstrated the presence of structures with the appearance of elementary, reticulate and aberrant bodies of *C. pneumoniae* in the cytoplasm of macrophage foam cells. The volume of the cytoplasm that was free from vacuoles and lipid droplets in *C. pneumoniae*-infected foam cells was dramatically reduced, and a phenomenon of the amalgamation of *C. pneumoniae* inclusions with lipid droplets was detected. Double immunohistochemistry showed that *C. pneumoniae*-infected foam cells contained a large number of oxidized low-density lipoproteins. The observations provide support to the hypothesis that *C. pneumoniae* could affect foam cell formation in human atherosclerosis.

Keywords Atherosclerosis · Arteries · Macrophages · *Chlamydia pneumoniae*

Y. V. Bobryshev (✉)
Faculty of Medicine, University of New South Wales,
Kensington, NSW 2052, Australia
e-mail: y.bobryshev@unsw.edu.au

Y. V. Bobryshev · M. C. Killingsworth
Department of Anatomical Pathology,
South Western Area Pathology Service,
Liverpool, NSW 2170, Australia

D. Tran
Division of Anatomical Pathology, St. Vincent's Hospital Sydney,
Sidney, Australia

R. Lord
St Vincent's Hospital Sydney,
Suite 601,
Darlinghurst, NSW 2010, Australia

R. Lord
School of Medicine, University of Western Sydney,
Campbelltown, NSW 2055, Australia

Introduction

In 1988, Saikku et al. [56] described an association of *Chlamydia pneumoniae* with chronic coronary heart disease and acute myocardial infarction. Since then, the role of *C. pneumoniae* in vascular diseases, including atherosclerosis, has become a topic of increasing interest [1, 10, 31, 41, 44, 45].

A possible aetiologic involvement of *C. pneumoniae* in vascular pathology remains controversial [1, 10, 47]. Some studies have failed to detect any *C. pneumoniae* in atherosclerotic lesions [2, 49, 59], while others have evidenced of an association of *C. pneumoniae* with atherosclerosis by means of seroepidemiology analysis, detection of the microorganism in atheromas by culture, polymerase chain reaction (PCR), immunohistochemically and in situ hybridisation [20, 26, 28, 37, 38, 42, 53, 58, 62]. In the arterial wall, *C. pneumoniae* was detected in a variety of cell types including macrophages, smooth muscle cells and endothelial cells [1, 10, 31]. The organism can be detected in circulating monocytes, and this led to the suggestion that *C. pneumoniae*-infected monocytes/macrophages migrating to the arterial wall from the blood stream have the capacity to infect all atheroma cell types [9, 14, 21, 40, 46, 51]. A number of in vitro studies have investigated the molecular mechanisms involved in the

functional alterations of cells infected by *C. pneumoniae* [1, 35, 46, 47, 48, 50]. The infection of arterial cells with *C. pneumoniae* has been shown to lead to the induction of the expression of inflammatory cytokines, pro-coagulants, matrix metalloproteinase and adhesion molecules [19, 25, 48]. However, the question of whether *C. pneumoniae* is just a concomitant phenomenon or a causative in atherosclerosis has not been yet clarified [1, 41, 47].

In a previous work, we used a combination of immunohistochemistry and PCR to search for *C. pneumoniae* in atherosclerotic plaques obtained by endarterectomy, and we particularly focused on a possible infection of dendritic cells with the microorganism [8]. In that study, *C. pneumoniae* was identified by both immunohistochemistry (IH) and PCR in 17 of 60 arterial specimens analysed (28%; PCR^+/IH^+ specimens) [8]. In two specimens (3%), *C. pneumoniae* was identified by immunohistochemistry only (PCR^-/IH^+ specimens), and in 19 specimens (32%), *C. pneumoniae* was detected by PCR only (PCR^+/IH^- specimens). In 22 specimens (37%), no *C. pneumoniae* was detected by either techniques (PCR^-/IH^- specimens). It was found that the presence of *C. pneumoniae* in the arterial specimens did not relate to the age or sex of the patient, the length of clinical history or any clinical data available [8]. During that study, we noted that *C. pneumoniae* immunopositivity was associated with foam cells located around the lipid/necrotic core of atherosclerotic plaques (unpublished observation).

The formation and accumulation of foam cells are key events in atherosclerosis [54]. In vitro studies have established that *C. pneumoniae* induces human and murine macrophage foam cell formation [30]. Despite the obvious interest in elucidating whether this process might occur in atherosclerotic plaque in situ, no previous work has investigated the features of infected foam cells in the arterial wall. The present study focuses on examining the features of arterial foam cells infected with *C. pneumoniae*.

Materials and methods

Archival tissue specimens

The carotid artery specimens were obtained by endarterectomy from 60 patients whose ages ranged from 46 to 75 years (33 men and 27 women), as reported previously [8]. The study was carried out in accordance with the principles outlined in the Helsinki Declaration. The study was approved by the institutional review board of St. Vincent's Hospital, Sydney, and informed consent was obtained from each patient. Atherosclerotic plaques in each specimen were identified macroscopically and were divided into three parts. One tissue part from each plaque was embedded in optimal cutting temperature (OCT) compound, frozen in liquid nitrogen and stored at −70°C until cryostat sectioning. A second tissue part from each specimen was fixed in 10% buffered formalin, processed and embedded in paraffin wax. The remaining tissue parts were used for electron microscopic analysis as detailed below.

The presence or absence of *C. pneumoniae* in the specimens was established by a combination of immunohistochemistry and PCR, carried out according to Campbell et al. [12] as reported previously [8]. In the present study, only specimens ($n=17$), showing double positive results [8] were examined.

Antibodies and immunohistochemical procedures

Anti-*C. pneumoniae* monoclonal antibody (DakoCytomation; clone RR402) was used to detect *C. pneumoniae* in the sections as detailed previously [8]. Avidin–biotin complex (ABC) method [27] was utilised for single immunostaining, and negative controls were carried out according to the recommendations of Dowell et al. [17] as previously described [8].

Sets of parallel sections were immunostained with anti-*C. pneumoniae* monoclonal antibody (DakoCytomation; clone RR402), anti-CD68 (DakoCytomation), anti-oxidised low-density lipoproteins (LDL; a kind gift of Dr Franz Tatzber, Biomedica, Austria) and anti-Toll-like receptor 2 (TLR2, Santa Cruz Biotechnology) antibodies. The sections were stained using ABC technique, and appropriate negative controls were carried out. To prevent lipid peroxidation in the tissue sections in which the distribution of oxidised LDL was studied, the sections were pretreated with 0.3% H_2O_2 in phosphate-buffered saline (PBS) containing 0.5 μM butylated hydroxytoluene (Sigma) for 10 min to block endogenous peroxidase as used previously [7].

Double immunostaining was used to analyse a possible association of *C. pneumoniae* with oxidised LDL according to the procedures described in detail in earlier publications [6, 7].

Laser capture microdissection and electron microscopy of *C. pneumoniae*-immunopositive cells

For laser capture microdissection, tissue segments fixed in a solution containing 4% paraformaldehyde, 0.05% glutaraldehyde in PBS were cut into thin tissue slices (about 1.5 mm in thickness). Immunohistochemical reactions were carried out in the floating tissue slices using ABC technique. After the immunohistochemical procedures were completed, the tissue slices were washed in PBS and re-fixed in 0.5% glutaraldehyde in PBS. After being washed in PBS, the tissue slices were oriented and embedded in OCT compound in liquid nitrogen. After being cut on a cryostat, sections were placed onto slides covered with polyethylene-naphtalate membranes

(PALM Microlaser Technologies; 1440–1000). A PALM Laser-MicroBeam System (PALM Microlaser Technologies), which enabled the contact-free isolation of single cells, was used for microdissection. Microdissected cells were catapulted into lids of 0.5-ml reaction tubes using the laser pressure catapulting technique of the instrument.

Preparation of microdissected cells for electron microscopy was carried out according to a modified technique described by Grant and Jerome [24], as used previously [4]. The entire lids of 0.5-ml reaction tubes with microdissected cells were fixed in 1% glutaraldehyde in PBS, post-fixed in 1% OsO_4 and embedded in Araldite. Serial ultrathin sections of the embedded lids containing microdissected cells were then cut and placed on formvar-coated grids. The ultrathin sections were stained with uranyl acetate and lead citrate and were examined with the aid of an electron microscope. After affirmation that the microdissected cells indeed contained *C. pneumoniae*, a systematic electron microscopic examination of the tissue samples was carried out.

Routine electron microscopy and electron microscopic immunohistochemistry

For routine electron microscopy, tissue samples fixed in 2.5% and 1% OsO_4 were dehydrated and embedded in Araldite resin as previously described [5]. For electron microscopic

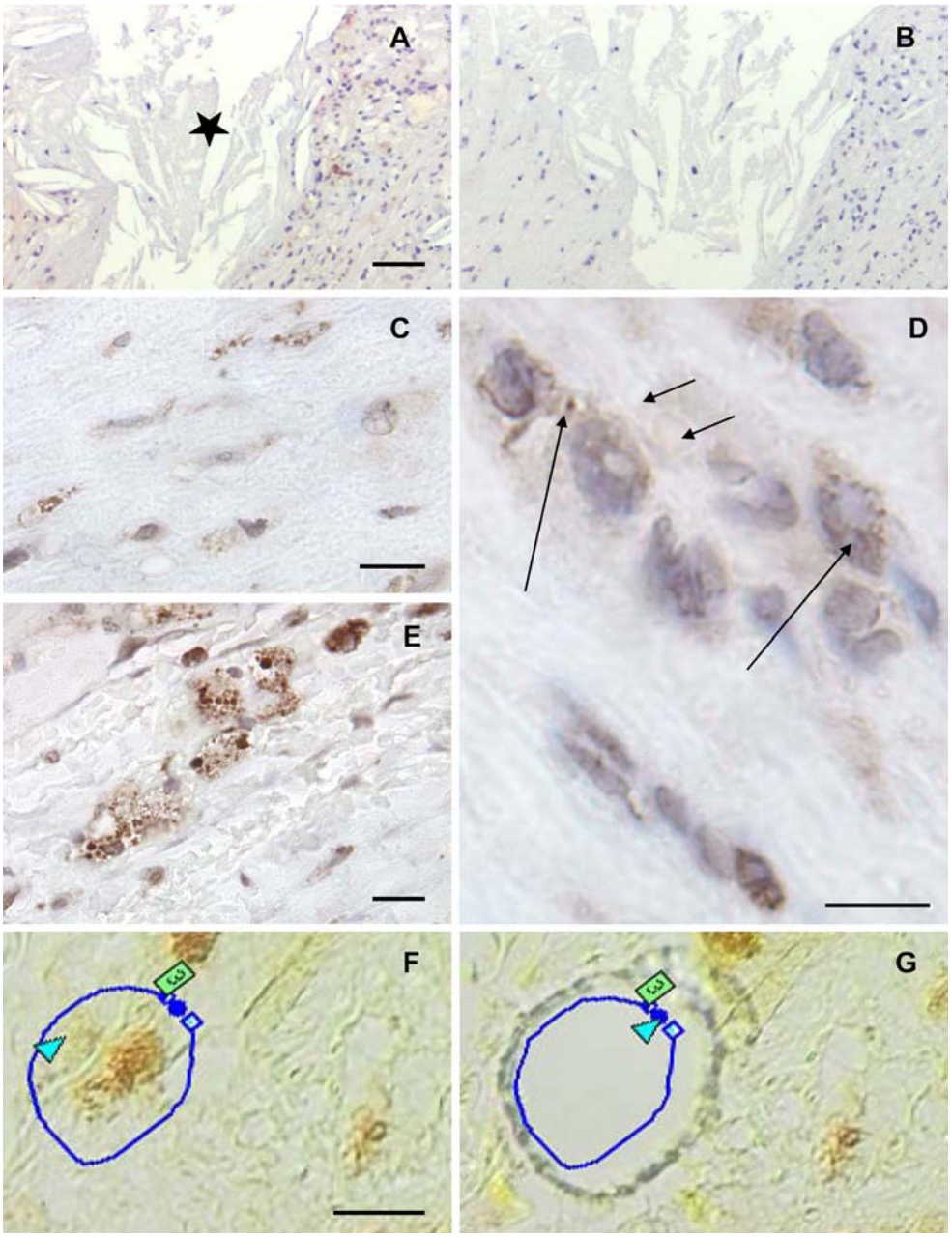

Fig. 1 Patterns of distribution of *C. pneumoniae* immunopositivity in atherosclerotic plaques identified using anti-*C. pneumoniae* (DakoCytomation; clone RR402) antibody (**a**–**g**). **a** Low magnification image showing the distribution of *C. pneumoniae* immunopositivity along the border of an acellular lipid/necrotic core in which the presence of cholesterol crystals is evident. **b** Negative control. **a** and **b** are parallel sections. In **a**, the lipid core is marked by a *star*. In **c**–**e**, note the granular and agranular patterns of immunopositive material in the cytoplasm of plaque cells (shown by *large arrows* in **d**) and agranular immunopositive staining of the surrounding extracellular matrix (shown by *small arrows* in **d**). **f** and **g** Consecutive stages of laser capture microdissection. **a**–**g** ABC immunoperoxidase technique; counterstaining with Mayer's haematoxylin. Bars = 150 μm (**a**) and 20 μm (**c**–**g**)

immunohistochemistry, tissue pieces were fixed in 0.2% glutaraldehyde and 3% paraformaldehyde in PBS (pH 7.4) and embedded in LR White resin according to the protocol described by Keita et al. [34]. Post-embedding immunohistochemistry on ultrathin sections was carried out using anti-*C. pneumoniae* antibody according to the technique of Keita et al. [34] with gold-labelled secondary antibody prepared according to Simmons et al. [57]. Colloidal gold particles were prepared by the reduction of a solution of $HAuCl_4$ by a mixture of sodium citrate and tannic acid [57]. The contrast of ultrathin sections was increased by treatment with uranyl acetate. Electron microscopic identification of cell types in atherosclerotic plaques was carried out as described in detail previously [5].

Results

All of the arterial specimens contained advanced atherosclerotic plaques with well-developed lipid/necrotic cores. In atherosclerotic plaques, *C. pneumoniae* immunopositivity was most often seen around the lipid/necrotic cores (Fig. 1a,b). This pattern of *C. pneumoniae* distribution was typical for all 17 specimens examined. *C. pneumoniae* immunopositivity was presented mostly by granular staining located in the cytoplasm (Fig. 1c,d). A pale non-granular staining was also identifiable in the cytoplasm of *C. pneumoniae*-immunopositive cells and the surrounding extracellular matrix (Fig. 1c,d). The presence of *C. pneumoniae* immunopositivity was observed also in areas of neovascularisation in plaque shoulders adjacent to the lipid/necrotic cores (Fig. 1e).

To examine the ultrastructure of *C. pneumoniae*-immunopositive cells, the cells were microdissected from plaques using laser capture microdissection technique (Fig. 1f,g). Electron microscopic analyses demonstrated that the microdissected cells contained structures, the appearances of which were typical of inclusions, elementary bodies (EBs) and reticulate bodies (RBs) of *C. pneumoniae* (Fig. 2a,b) [11, 36, 60, 61]. The presence of structures resembling EBs and RBs of *C. pneumoniae* were observed in the surrounding extracellular space (Fig. 2c). Electron microscopic immunochemistry confirmed that *C. pneumoniae* antigens were present in atherosclerotic plaques (Fig. 3a).

Routine ultrastructural examination of plaque areas, where, according to immunohistochemistry, *C. pneumoniae* antigens were most frequently present, identified inclusions, EBs and RBs of *C. pneumoniae* in all analysed specimens. In some *C. pneumoniae*-infected cells, the cytoplasm contained a large number of *C. pneumoniae* inclusions (Fig. 3b). In these cells, the surrounding membranes of neighbouring *C. pneumoniae* inclusions were often apposed to each other (Fig. 3b). In these foci,

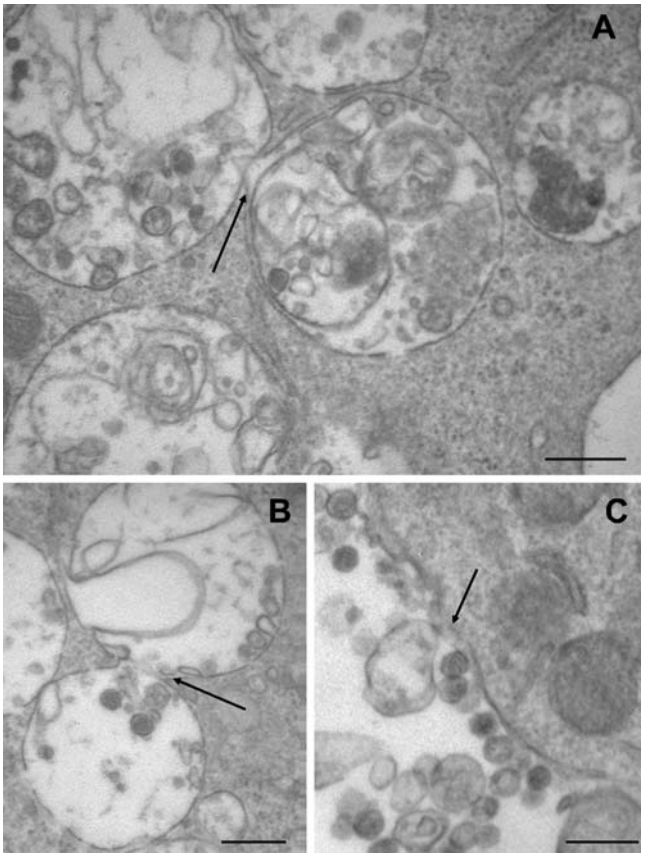

Fig. 2 Electron micrographs demonstrating the presence of *C. pneumoniae* organisms at different stages of development within inclusions in the cytoplasm of laser capture microdissected cells (**a**–**c**). In **a** and **b**, *arrows* show zones of the adhesion and fusion of *C. pneumoniae* inclusions. In **c**, the *arrow* shows an area where the external cellular membrane (plasmalemma) is damaged. Note the large number of *C. pneumoniae* RBs and aberrant bodies in the surrounding extracellular space. Bars=0.5 μm (**a**–**c**)

the apposed membranes of the inclusions were frequently interrupted, and this led to the formation of a direct association between the neighbouring inclusions (Fig. 3c). RBs and EBs as well as intermediate forms of *C. pneumoniae* were observed within the interconnected inclusions (Fig. 3b–e). Extensive consolidation of individual *C. pneumoniae* inclusions (Fig. 3f), resulting in the formation of huge inclusions (Fig. 3g), was especially prominent in cells, containing "lipid droplets", identifiable as foam cells. *C. pneumoniae* inclusions were seen in direct contacts with lipid droplets (Fig. 3c,f and g). In foam cells where the majority of *C. pneumoniae* inclusions were fused, a phenomenon of an amalgamation of *C. pneumoniae* conclusions with lipid droplets was observed (Fig. 4a,b). Electron microscopy also suggested that in some foam cells, the accumulation of lipids occurred within individual *C. pneumoniae* inclusions (Fig. 5a,b).

The ultrastructural examination of *C. pneumoniae*-infected foam cells suggested their macrophage origin. This was in agreement with immunohistochemical staining

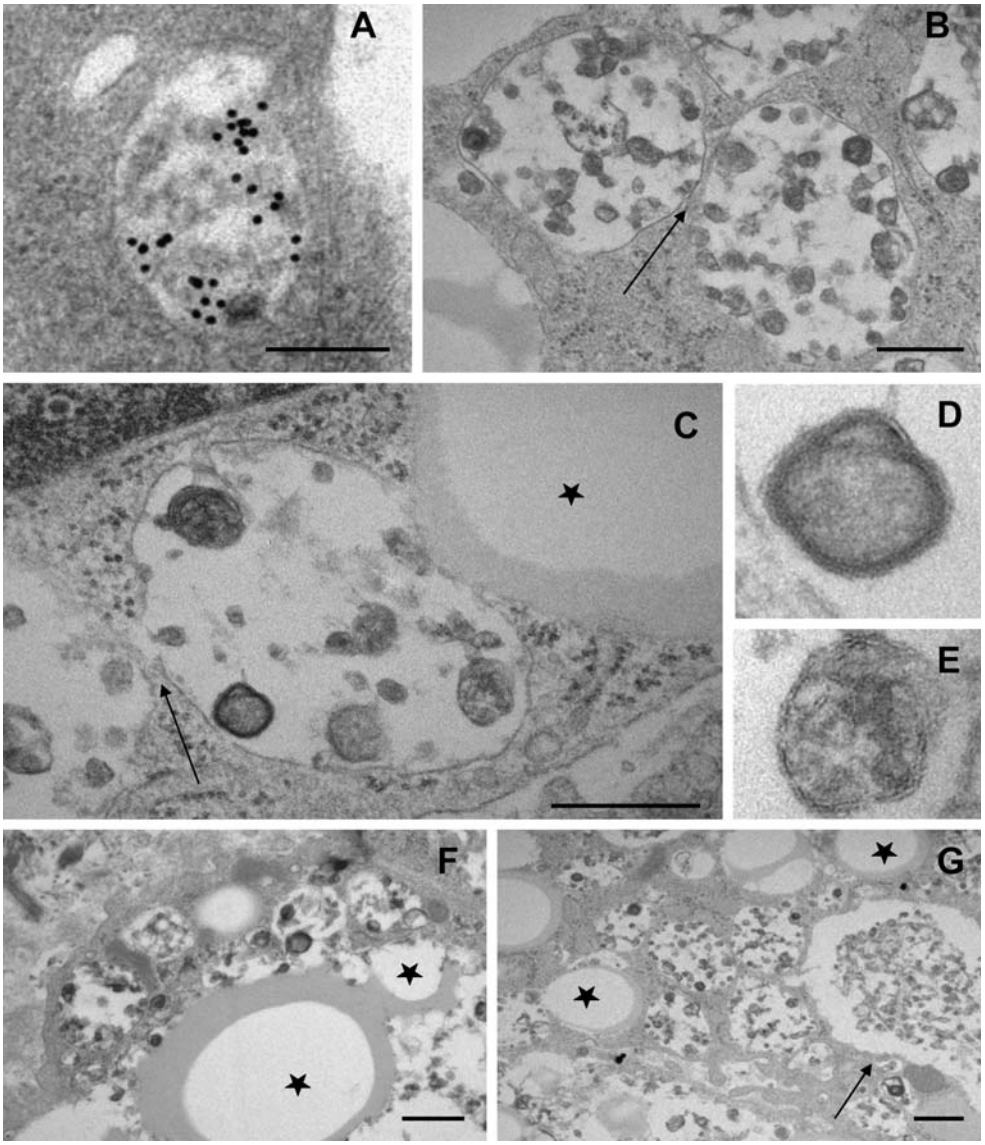

Fig. 3 *C. pneumoniae* inclusions located in cells distributed along the border of the lipid/necrotic cores in atherosclerotic plaques (**a**–**g**). **a** *C. pneumoniae* immunopositivity in inclusions revealed by electron microscopic immunohistochemistry utilising immunogold technique. **b**, **c** Aggregation and fusion of *C. pneumoniae* inclusions between each other (shown by *arrows* in **b** and **c**) and with a "lipid droplet" (marked by a *star* in **c**). **d**, **e** Details of **c**. **f**, **g** Accumulation of large numbers of *C. pneumoniae* inclusions and their fusion in foam cells. Lipid droplets are marked by *stars*. In **g**, the *arrow* shows a huge inclusion, presumably formed by the fusion of several *C. pneumoniae* inclusions. **a**–**g** Electron microscopy. Bars= 0.5 μm (**a**–**c**, **f** and **g**)

of parallel sections with anti-*C. pneumoniae* antibody (DakoCytomation; clone RR402) and anti-CD68 antibody (Fig. 6a,b). Analysis of adjacent parallel sections stained with anti-TLR2 and anti-oxidised LDL antibodies demonstrated overlapping patterns of immunopositivity of *C. pneumoniae*, CD68, TLR2 and oxidised LDL (Fig. 6a–d). Double immunohistochemistry confirmed that *C. pneumoniae* was co-localised with oxidised LDL (Fig. 6e). Some *C. pneumoniae*-infected foam cells displayed signs of extensive edema of the cytoplasm and degeneration, but no fragmentation of chromatin or formation of typical apoptotic bodies was observed.

Discussion

To our knowledge, this is the first study to demonstrate that different stages of the development of *C. pneumoniae* can be identifiable in foam cells in human atherosclerotic plaques. The observations support a view that the microorganism may develop in the cytoplasm of infected cells in the arterial wall in vivo. In all specimens studied in this study, *C. pneumoniae* inclusions, EBs, RBs and aberrant bodies were detected in infected foam cells located predominantly around the lipid cores of atherosclerotic plaques. Foam cells which harboured *C. pneumoniae* were identified as cells of macrophage origin.

Monocyte migration into the arterial wall from the blood stream, followed by their differentiation into macrophages, which eventually become foam cells, are key events in the formation and progression of atherosclerotic lesions [16, 22, 44, 54]. The transformation of macrophages into foam cells depends on the contact of the cells with modified lipoproteins [16, 22, 54]. The major storage form of cholesterol in these macrophages is cholesteryl fatty acid esters which are structurally identifiable as lipid droplets

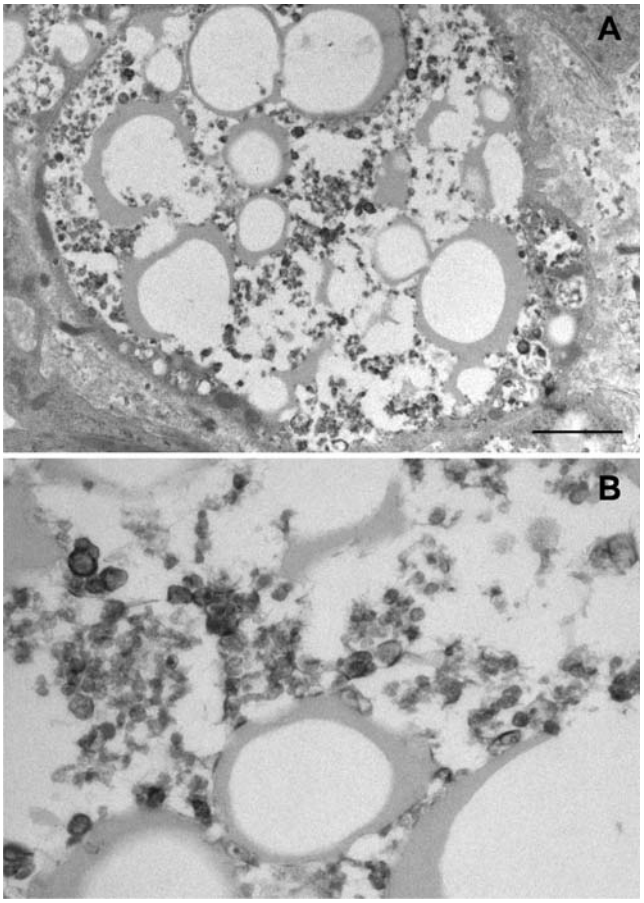

Fig. 4 Amalgamation of *C. pneumoniae* inclusions and lipid droplets in the cytoplasm of a foam cell (**a**, **b**). **b** Detail of **a**. Electron microscopy. Bar=1 μm

[16, 39, 43]. It has been shown that *C. pneumoniae* can induce macrophage foam cell formation in the presence of LDL [30]. Several mechanisms may support the ability of *C. pneumoniae* to induce macrophage foam cell formation. *C. pneumoniae* can cause macrophage activation, resulting in LDL oxidation and scavenger receptor up-regulation, which may be followed by an increase in the uptake of the oxidised LDL by macrophages [32, 33]. Cell activation by *C. pneumoniae* has been reported to be mediated by both TLR2 and TLR4, with TLR2 playing the predominant role [13, 15, 52, 63]. Cao et al. [13] provided in vitro evidence of the ability of *C. pneumoniae* to induce foam cell formation in a TLR2-dependent fashion. The observations of an overlap between patterns of the distribution of *C. pneumoniae*, oxidised LDL and the TLR2 expression in plaque tissue specimens reinforce an opinion that there is a link between *C. pneumoniae*, oxidised LDL and the TLR2 in atherosclerosis [13, 18].

The present study has shown that the accumulation of a large number of *C. pneumoniae* inclusions in foam cells is accompanied by a dramatic reduction in the volume of the cytoplasm which is free from *C. pneumoniae* inclusions and lipid droplets. The close apposition of the external membranes of individual *C. pneumoniae* inclusions in foam cells can lead to the fusion of the inclusions. In some foam cells, this process is expansive, with the most of the cytoplasm being replaced by fused *C. pneumoniae* inclusions and lipid droplets. The present study recognises a phenomenon of the amalgamation of *C. pneumoniae* inclusions and lipid droplets resulting from the incorporation of lipid droplets into fused *C. pneumoniae* inclusions.

In an infection, the infecting organism seeks to utilise the host's resources to multiply, usually to the detriment of the host. Therefore, the association of infecting microorganisms with various organelles and structures in the host's cells occurs at all stages of the development of the microorganisms. In foam cells, the amalgamation of *C. pneumoniae* inclusions with lipid droplets might occur simply as a result of the simultaneous and continuous increase in the numbers of both *C. pneumoniae* inclusions and lipid droplets within a limited space of the cytoplasm of the infected cells. The amalgamation of *C. pneumoniae* inclusions with lipid droplets might affect not only the development of the microorganism but also the intensity of transformation of the infected cells into foam cells. One also cannot exclude that the amalgamation of *C. pneumoniae* inclusions with lipid droplets might represent a

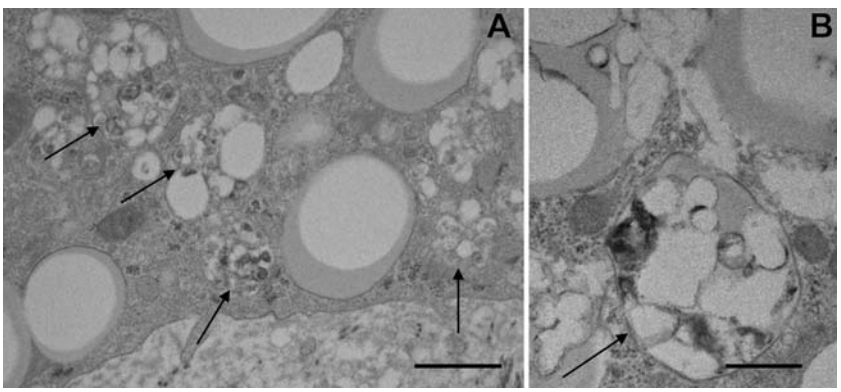

Fig. 5 The appearance of the structures (shown by *arrows*) resulting from the accumulation of lipids within *C. pneumoniae* inclusions (**a**, **b**). Electron microscopy. Bars=1.5 μm (**a**) and 0.5 μm (**b**)

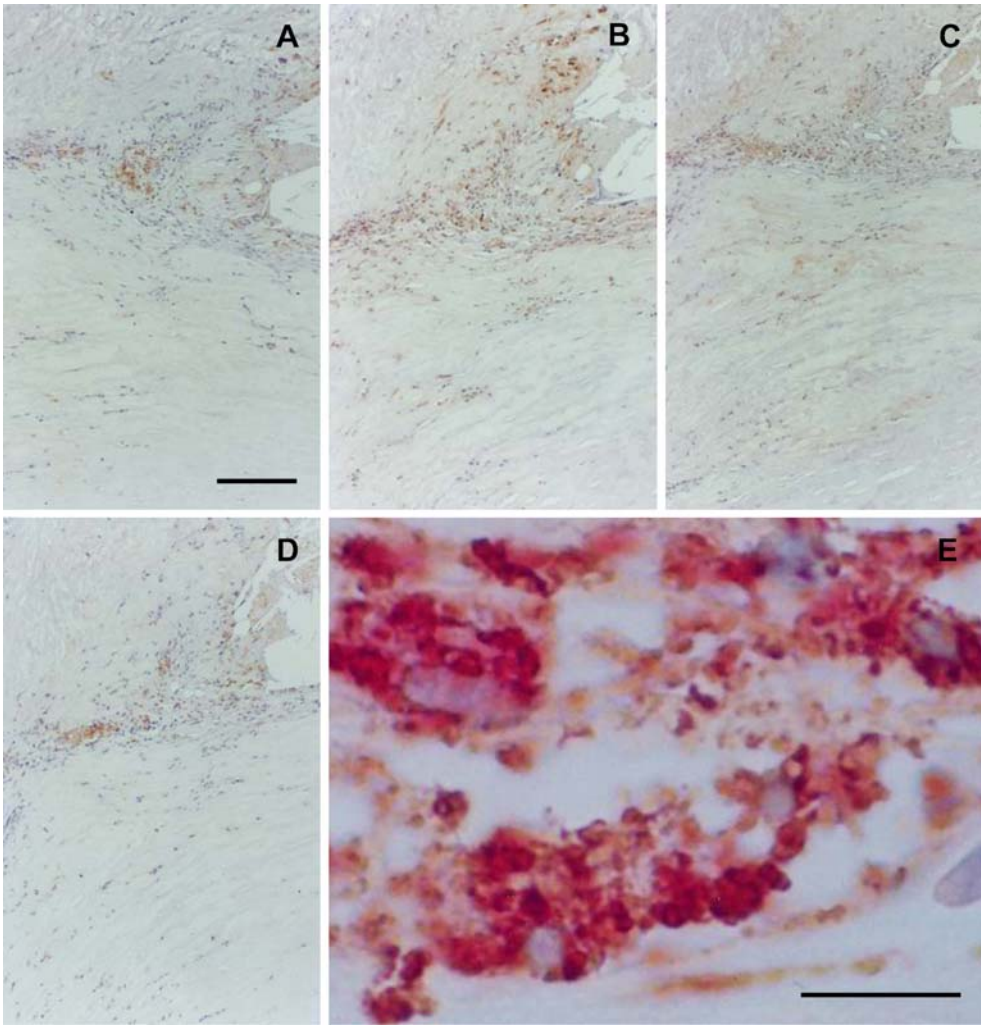

Fig. 6 Co-localisation of *C. pneumoniae* with lipids, oxidised LDL and TLR2 in macrophage foam cells (**a**–**e**). **a**–**d** Low magnification images of consecutive parallel sections stained with anti-*C. pneumoniae* (DakoCytomation; clone RR402) (**a**), anti-CD68 (**b**), anti-oxidised LDL (**c**) and anti-TLR2 (**d**) antibodies showing an overlapping pattern of the distribution of the antigens. **a**–**d** ABC immunoperoxidase technique; counterstaining with Mayer's haematoxylin. **e** Double immunostaining showing the presence of oxidised LDL in the cytoplasm of foam cells infected with *C. pneumoniae*. Oxidised LDL were identified with alkaline phosphatase-anti-alkaline phosphatase (*APAAP*) technique (*rose*), while *C. pneumoniae* was visualised by peroxidase-anti-peroxidase (*PAP*) technique (*brown*). Counterstaining with Mayer's haematoxylin. Bars= 200 μm (**a**) and 20 μm (**e**)

secondary process occurring after the degenerative alteration of *C. pneumoniae* in forming foam cells.

In vitro studies have found that lipid loading of RAW 264.7 cells and mouse peritoneal macrophages with either oxidised or acetylated LDL significantly inhibits the growth of *C. pneumoniae* [3]. Modified forms of LDL are not directly toxic to *C. pneumoniae* and do not inhibit either the initial binding or internalisation of *C. pneumoniae* by macrophages in vitro [3]. A treatment of lipid-loaded macrophages with *C. pneumoniae* stimulates secretion of a variety of cytokines [3]. *C. pneumoniae* has been shown to induce the expression of messenger RNA for tumor necrosis factor-α in foam cells in vitro despite the inhibition of nuclear factor-B binding to DNA by prior treatment with oxidised LDL [3].

In vitro studies have shown that foam cell formation is not conducive to the growth of *C. pneumoniae* but does not inhibit the *C pneumoniae*-induced secretion of pro-inflammatory cytokines [3]. However, it is not yet known whether foam cells have the capacity to support or inhibit the growth of *C. pneumoniae* in the arterial wall in vivo. The presence of a large number of *C. pneumoniae* inclusions in some foam cells, shown by the present work, suggests that *C. pneumoniae* could develop in the cytoplasm containing lipid droplets. Furthermore, the presence of different development stages of the microorganism within fused *C. pneumoniae* inclusions, in which lipid droplets have been incorporated, supports a possibility that foam cells in human atherosclerosis might not critically inhibit the growth of the microorganism. However, the amalgamation of *C. pneumoniae* inclusions with lipid droplets in arterial foam cells likely creates a microenvironment in which the development of the microorganism and its release from host cells might be affected. This phenomenon might explain the observations of relatively few cells that are actually infected in atheromatous lesions [37, 38, 53, 58] and the fact that there are difficulties in culturing *C. pneumoniae* from artery specimens [1, 23, 47].

Blessing et al. [3] have shown that despite the resistance to *C. pneumoniae* infection, foam cells retain their capacity to secret pro-inflammatory cytokines and chemokines in response to the binding of *C. pneumoniae*. Because foam cells are a major cellular component of atherosclerotic lesions

[54], *C. pneumoniae* can contribute to the atherogenesis without requiring a widespread infection. A chronic infection of foam cells with *C. pneumoniae* around the plaque lipid/necrotic cores might augment the focal lipid-induced inflammatory response, accelerate cell death and contribute to the expansion of the necrotic core and the thinning of the fibrous cap and thus affect plaque stability [3].

Acknowledgements The research was supported by the Vascular Fund, St. Vincent's Hospital, Sydney and by School of Medicine, University of Western Sydney.

The experiments comply with the current laws of Australia.

Conflict of interest statement We have no commercial associations (i.e. pharmaceutical stock ownership, consultancy, advisory board membership, or relevant patents) that might pose a conflict of interest. We declare that we have no conflict of interest.

References

1. Belland RJ, Ouellette SP, Gieffers J, Byrne GI (2004) Chlamydia pneumoniae and atherosclerosis. Cell Microbiol 6:117–127
2. Bishara J, Pitlik S, Kazakov A, Sahar G, Haddad M, Vojdani A, Rosenberg S, Samra Z (2003) Failure to detect *Chlamydia pneumoniae* by cell culture and polymerase chain reaction in major arteries of 93 patients with atherosclerosis. Eur J Clin Microbiol Infect Dis 22:300–302
3. Blessing E, Kuo CC, Lin TM, Campbell LA, Bea F, Chesebro B, Rosenfeld ME (2002) Foam cell formation inhibits growth of *Chlamydia pneumoniae* but does not attenuate *Chlamydia pneumoniae*-induced secretion of proinflammatory cytokines. Circulation 105:1976–1982
4. Bobryshev YV (2005) Intracellular localization of oxidized low-density lipoproteins in atherosclerotic plaque cells revealed by electron microscopy combined with laser capture microdissection. J Histochem Cytochem 53:793–797
5. Bobryshev YV, Lord RSA (1996) Langhans cells of human arterial intima: uniform by stellate appearance but different by nature. Tissue Cell 28:177–194
6. Bobryshev YV, Lord RSA (1998) Mapping of vascular dendritic cells in atherosclerotic arteries suggests their involvement in local immune-inflammatory reactions. Cardiovasc Res 37:799–810
7. Bobryshev YV, Lord RSA, Watanabe T, Ikezawa T (1998) The cell adhesion molecule E-cadherin is widely expressed in human atherosclerotic lesions. Cardiovasc Res 40:191–205
8. Bobryshev YV, Cao W, Phoon MC, Tran D, Chow VT, Lord RS, Lu J (2004) Detection of *Chlamydophila pneumoniae* in dendritic cells in atherosclerotic lesions. Atherosclerosis 173:185–195
9. Boman J, Gaydos CA (2000) Polymerase chain reaction detection of *Chlamydia pneumoniae* in circulating white blood cells. J Infect Dis 181:S452–S454
10. Campbell LA, Kuo CC (2004) *Chlamydia pneumoniae*—an infectious risk factor for atherosclerosis? Nat Rev Microbiol 2:23–32
11. Campbell LA, Kuo CC, Grayston JT (1998) *Chlamydia pneumoniae* and cardiovascular disease. Emerg Infect Dis 4:571–579
12. Campbell LA, Perez Melgosa M, Hamilton DJ, Kuo CC, Grayston JT (1992) Detection of *Chlamydia pneumoniae* by polymerase chain reaction. J Clin Microbiol 30:434–439
13. Cao F, Castrillo A, Tontonoz P, Re F, Byrne GI (2007) *Chlamydia pneumoniae*-induced macrophage foam cell formation is mediated by Toll-like receptor 2. Infect Immun 75:753–759
14. Cirino F, Webley WC, West C, Croteau NL, Andrzejewski C Jr, Stuart ES (2006) Detection of Chlamydia in the peripheral blood cells of normal donors using in vitro culture, immunofluorescence microscopy and flow cytometry techniques. BMC Infect Dis 6:23
15. Da Costa CU, Wantia N, Kirschning CJ, Busch DH, Rodriguez N, Wagner H, Miethke T (2004) Heat shock protein 60 from *Chlamydia pneumoniae* elicits an unusual set of inflammatory responses via Toll-like receptor 2 and 4 in vivo. Eur J Immunol 34:2874–2884
16. de Villiers WJ, Smart EJ (1999) Macrophage scavenger receptors and foam cell formation. J Leukoc Biol 66:740–746
17. Dowell SF, Peeling RW, Boman J, Carlone GM, Fields BS, Guarner J, Hammerschlag MR, Jackson LA, Kuo CC, Maass M, Messmer TO, Talkington DF, Tondella ML, Zaki SR (2001) Standardizing *Chlamydia pneumoniae* assays: recommendations from the Centers for Disease Control and Prevention (USA) and the Laboratory Centre for Disease Control (Canada). Clin Infect Dis 33:492–503
18. Edfeldt K, Swedenborg J, Hansson GK, Yan ZQ (2002) Expression of Toll-like receptors in human atherosclerotic lesions: a possible pathway for plaque activation. Circulation 105:1158–1161
19. Fryer RH, Schwobe EP, Woods ML, Rodgers GM (1997) Chlamydia species infect human vascular endothelial cells and induce procoagulant activity. J Investig Med 45:168–174
20. Gaydos CA, Summersgill JT, Sahney NN, Ramirez JA, Quinn TC (1996) Replication of *Chlamydia pneumoniae* in vitro in human macrophages, endothelial cells, and aortic artery smooth muscle cells. Infect Immun 64:1614–1620
21. Gieffers J, Füllgraf H, Jahn J, Klinger M, Dalhoff K, Katus HA, Solbach W, Maass M (2001) *Chlamydia pneumoniae* infection in circulating human monocytes is refractory to antibiotic treatment. Circulation 103:351–356
22. Glass CK, Witztum JL (2001) Atherosclerosis. The road ahead. Cell 104:503–516
23. Godzik KL, O'Brien ER, Wang SK, Kuo CC (1995) In vitro susceptibility of human vascular wall cells to infection with *Chlamydia pneumoniae*. J Clin Microbiol 33:2411–2414
24. Grant K, Jerome WG (2002) Laser capture microdissection as an aid to ultrastructural analysis. Microsc Microanal 8:170–175
25. Heinemann M, Susa M, Simnacher U, Marre R, Essig A (1996) Growth of *Chlamydia pneumoniae* induces cytokine production and expression of CD14 in a human monocytic cell line. Infect Immun 64:4872–4875
26. Hortovanyi E, Illyes G, Glasz T, Kadar A (2002) *Chlamydia pneumoniae* in different coronary artery segments in the young. Pathol Res Pract 198:19–23
27. Hsu SM, Raine L, Fanger H (1981) Use of avidin–biotin–peroxidase complex (ABC) in immunoperoxidase techniques: a comparison between ABC and unlabeled antibody (PAP) procedures. J Histochem Cytochem 29:577–580
28. Jackson LA, Campbell LA, Kuo CC, Rodriguez DI, Lee A, Grayston JT (1997) Isolation of *Chlamydia pneumoniae* from carotid endarterectomy specimen. J Infect Dis 176:292–295
29. Kalayoglu MV, Byrne GI (1998) A *Chlamydia pneumoniae* component that induces macrophage foam cell formation is chlamydial lipopolysaccharide. Infect Immun 66:5067–5072
30. Kalayoglu MV, Byrne GI (1998) Induction of macrophage foam cell formation by *Chlamydia pneumoniae*. J Infect Dis 177:725–729
31. Kalayoglu MV, Libby P, Byrne GI (2002) *Chlamydia pneumoniae* as an emerging risk factor in cardiovascular disease. JAMA 288:2724–2731
32. Kalayoglu MV, Hoerneman B, LaVerda D, Morrison SG, Morrison RP, Byrne GI (1999) Cellular oxidation of low-density lipoprotein by *Chlamydia pneumoniae*. J Infect Dis 180:780–790
33. Kalayoglu MV, Indrawati, Morrison RP, Morrison SG, Yuan Y, Byrne GI (2000) Chlamydial virulence determinants in athero-

genesis: the role of chlamydial lipopolysaccharide and heat shock protein 60 in macrophage-lipoprotein interactions. J Infect Dis 181(Suppl 3):S483–S489
34. Keita M, Magy L, Richard L, Piaser M, Vallat JM (2002) LR white post-embedding colloidal gold method to immunostain MBP, P0, NF and S100 in glutaraldehyde-fixed peripheral nerve tissue. J Peripher Nerv Syst 7:128–133
35. Krüll M, Maass M, Suttorp N, Rupp J (2005) *Chlamydophila pneumoniae*. Mechanisms of target cell infection and activation. Thromb Haemost 94:319–326
36. Kutlin A, Flegg C, Stenzel D, Reznik T, Roblin PM, Mathews S, Timms P, Hammerschlag MR (2001) Ultrastructural study of *Chlamydia pneumoniae* in a continuous-infection model. J Clin Microbiol 39:3721–3723
37. Kuo CC, Gown AM, Benditt EP, Grayston JT (1993) Detection of *Chlamydia pneumoniae* in aortic lesions of atherosclerosis by immunocytochemical stain. Arterioscler Thromb 13:1501–1504
38. Kuo CC, Shor A, Campbell LA, Fukushi H, Patton DL, Grayston JT (1993) Demonstration of *Chlamydia pneumoniae* in atherosclerotic lesions of coronary arteries. J Infect Dis 167:841–849
39. Lang PD, Insull W Jr (1970) Lipid droplets in atherosclerotic fatty streaks of human aorta. J Clin Invest 49:1479–1488
40. Lin TM, Campbell LA, Rosenfeld ME, Kuo CC (2000) Monocyte-endothelial cell coculture enhances infection of endothelial cells with *Chlamydia pneumoniae*. J Infect Dis 181: 1096–1100
41. Liu L, Hu H, Ji H, Murdin AD, Pierce GN, Zhong G (2000) *Chlamydia pneumoniae* infection significantly exacerbates aortic atherosclerosis in an LDLR−/− mouse model within six months. Mol Cell Biochem 215:123–128
42. Loehe F, Bittmann I, Weilbach C, Lauterjung L, Schildberg FW, Heiss MM (2002) *Chlamydia pneumoniae* in atherosclerotic lesions of patients undergoing vascular surgery. Ann Vasc Surg 16:467–73
43. Lundberg B (1985) Chemical composition and physical state of lipid deposits in atherosclerosis. Atherosclerosis 56:93–110
44. Lusis AJ (2000) Atherosclerosis. Nature 407:233–241
45. Moazed TC, Campbell LA, Rosenfeld ME, Grayston JT, Kuo CC (1999) *Chlamydia pneumoniae* infection accelerates the progression of atherosclerosis in apolipoprotein E-deficient mice. J Infect Dis 180:238–241
46. Moazed TC, Kuo CC, Grayston JT, Campbell LA (1998) Evidence of systemic dissemination of *Chlamydia pneumoniae* via macrophages in the mouse. J Infect Dis 177:1322–1325
47. Mussa FF, Chai H, Wang X, Yao Q, Lumsden AB, Chen C (2006) *Chlamydia pneumoniae* and vascular disease: an update. J Vasc Surg 43:1301–1307
48. Netea MG, Selzman CH, Kullberg BJ, Galama JM, Weinberg A, Stalenhoef AF, Van der Meer JW, Dinarello CA (2000) Acellular components of *Chlamydia pneumoniae* stimulate cytokine production in human blood mononuclear cells. Eur J Immunol 30:541–549
49. Ong GM, Coyle PV, Barros D'Sa AA, McCluggage WG, Duprex WP, O'Neill HJ, Wyatt DE, Bamford KB, O'Loughlin B, McCaughey C (2001) Non-detection of Chlamydia species in carotid atheroma using generic primers by nested PCR in a population with a high prevalence of *Chlamydia pneumoniae* antibody. BMC Infect Dis 1:12
50. Peters J, Hess S, Endlich K, Thalmann J, Holzberg D, Kracht M, Schaefer M, Bartling G, Klos A (2005) Silencing or permanent activation: host-cell responses in models of persistent *Chlamydia pneumoniae* infection. Cell Microbiol 7:1099–1108
51. Prager M, Türel Z, Speidl WS, Zorn G, Kaun C, Niessner A, Heinze G, Huk I, Maurer G, Huber K, Wojta J (2002) *Chlamydia pneumoniae* in carotid artery atherosclerosis: a comparison of its presence in atherosclerotic plaque, healthy vessels, and circulating leukocytes from the same individuals. Stroke 33:2756–2761
52. Prebeck S, Kirschning C, Dürr S, da Costa C, Donath B, Brand K, Redecke V, Wagner H, Miethke T (2001) Predominant role of Toll-like receptor 2 versus 4 in *Chlamydia pneumoniae*-induced activation of dendritic cells. J Immunol 167:3316–3323
53. Rassu M, Cazzavillan S, Scagnelli M, Peron A, Bevilacqua PA, Facco M, Bertoloni G, Lauro FM, Zambello R, Bonoldi E (2001) Demonstration of *Chlamydia pneumoniae* in atherosclerotic arteries from various vascular regions. Atherosclerosis 158:73–79
54. Ross R (1999) Atherosclerosis—an inflammatory disease. N Engl J Med 340:115–126
55. Rupp J, Koch M, van Zandbergen G, Solbach W, Brandt E, Maass M (2005) Transmission of *Chlamydia pneumoniae* infection from blood monocytes to vascular cells in a novel transendothelial migration model. FEMS Microbiol Lett 242:203–208
56. Saikku P, Leinonen M, Mattila K, Ekman MR, Nieminen MS, Mäkelä PH, Huttunen JK, Valtonen V (1988) Serological evidence of an association of a novel Chlamydia, TWAR, with chronic coronary heart disease and acute myocardial infarction. Lancet 2:983–986
57. Simmons SR, Sims PA, Albrecht RM (1997) Alpha IIb beta 3 redistribution triggered by receptor cross-linking. Arterioscler Thromb Vasc Biol 17:3311–3320
58. Vink A, Poppen M, Schoneveld AH, Roholl PJ, de Kleijn DP, Borst C, Pasterkamp G (2001) Distribution of *Chlamydia pneumoniae* in the human arterial system and its relation to the local amount of atherosclerosis within the individual. Circulation 103:1613–1617
59. Weiss SM, Roblin PM, Gaydos CA, Cummings P, Patton DL, Schulhoff N, Shani J, Frankel R, Penney K, Quinn TC, Hammerschlag MR, Schachter J (1996) Failure to detect *Chlamydia pneumoniae* in coronary atheromas of patients undergoing atherectomy. J Infect Dis 173:957–962
60. Wolf K, Fischer E, Hackstadt T (2000) Ultrastructural analysis of developmental events in *Chlamydia pneumoniae*-infected cells. Infect Immun 68:2379–12385
61. Wolf K, Fischer E, Hackstadt T (2005) Degradation of *Chlamydia pneumoniae* by peripheral blood monocytic cells. Infect Immun 73:4560–4570
62. Yamashita K, Ouchi K, Shirai M, Gondo T, Nakazawa T, Ito H (1998) Distribution of *Chlamydia pneumoniae* infection in the atherosclerotic carotid artery. Stroke 29:773–778
63. Yaraei K, Campbell LA, Zhu X, Liles WC, Kuo CC, Rosenfeld ME (2005) Effect of *Chlamydia pneumoniae* on cellular ATP content in mouse macrophages: role of Toll-like receptor 2. Infect Immun 73:4323–4326

Virchows Arch (2008) 453:79–87
DOI 10.1007/s00428-008-0617-6

ORIGINAL ARTICLE

Expression and intracellular localization of matrix metalloproteinases in intraductal papillary mucinous neoplasms of the pancreas

Urara Tamahashi · Jiro Kumagai · Touichiro Takizawa · Masaki Sekine · Yoshinobu Eishi

Received: 1 December 2007 / Accepted: 7 April 2008 / Published online: 24 May 2008

Abstract To analyze the expression of matrix metalloproteinases (MMPs) and their relationships with the histological grades of the intraductal papillary mucinous neoplasm (IPMN) of the pancreas, we examined the frequency of expression and intracellular localization of MMP1, MMP2, MMP3, MMP7, and MMP9 in IPMN by immunohistochemistry. A total of 45 IPMN lesions (14 adenomas, 17 borderline lesions, nine noninvasive carcinomas, and five invasive lesions) from 21 patients were examined. MMP1, MMP2, MMP7, and MMP9 were expressed in tumor cells. Frequency of tumor cells expressing MMP7 was low in adenomas (median, 5.0%), higher in borderline lesions (median, 30.0%), in noninvasive carcinomas (median, 50.0%), and in invasive lesions (median, 80.0%), with a significant trend ($P<0.0001$). Such a trend was also observed when the lesions were classified into gastric and intestinal subtypes ($P<0.0001$ and $P=0.011$, respectively). Basolateral expression of MMP7 in tumor cells was more prominent in lesions with higher histological grades ($P<0.0001$). The frequency and the localization of MMP1, MMP2, and MMP9 did not correlate to the histological grades. MMP7 may contribute to the process by which IPMN advances from adenoma to carcinoma and to subsequent invasion of tumor cells in IPMN.

Keywords Intraductal papillary mucinous neoplasm · Matrix metalloproteinase · Immunohistochemistry

U. Tamahashi · J. Kumagai (✉) · Y. Eishi
Department of Human Pathology,
Tokyo Medical and Dental University,
1-5-45, Yushima,
Bunkyo-ku, Tokyo 113-8519, Japan
e-mail: j.kuma.pth1@tmd.ac.jp

T. Takizawa
Department of Molecular Pathophysiology,
School of Health Sciences, Tokyo Medical and Dental University,
Tokyo, Japan

M. Sekine
Laboratory of Pathology,
Tokyo Medical and Dental University Hospital,
Tokyo, Japan

Introduction

Intraductal papillary mucinous neoplasms (IPMNs) are pancreatic neoplasms characterized by mucin production, cystic dilatation of the pancreatic ducts, and intraductal papillary growth [1]. Prognosis is favorable for patients with IPMNs without invasion, but poor for those with invasion, which account for approximately 30% of patients [1]. The progression of IPMN is thought to be stepwise from adenoma to borderline lesion, noninvasive carcinoma, and finally to invasive carcinoma [14]. The factors which contribute to this progression, however, remain unclear.

Among the many factors related to the invasion process of malignant tumors, the matrix metalloproteinases (MMPs) are thought to play a key role, and their functions have been extensively investigated in many kinds of advanced carcinoma including invasive ductal carcinoma of the pancreas (IDC) [2, 7, 16]. MMPs have been shown to be involved in the early stages of tumor progression such as tumor initiation, cell proliferation, and apoptosis in many organs [3, 6, 10, 12]. A recent study has shown that their functions differ according to their intracellular localization pattern in tumor cells [5]. However, whether MMPs are involved in the progression of IPMN is unknown.

To determine whether MMPs play a role in the progression of IPMN, we analyzed the expression of MMPs in each histological grade of IPMN. MMP expression

in IPMN and IDC were evaluated using an immunohistochemical method. We compared the frequency of cells which express MMPs and the intracellular localization of MMPs between the different histological grades of IPMN and between the invasive lesions of IPMN and IDC.

Materials and methods

Patients and specimens

The IPMN specimens used in this study were obtained from 21 consecutive patients with IPMN who underwent pancreatectomy at the Tokyo Medical and Dental University from 1998 to 2007. The IDC specimens were obtained from ten consecutive patients as above from 2003 to 2005. Written informed consent for the use of the surgical material was obtained from all patients.

The clinical and histopathological stages of the tumors were determined according to the TNM classification published in 2002 [15]. The tumors were classified according to the histological grade of WHO classification [9].

Immunohistochemistry

The pancreatectomy specimens were fixed in 3.6% buffered formalin for 48 h. Each specimen was then cut perpendicular to the main pancreatic duct into 5-mm-thick slices. All the slices were embedded in paraffin. Sections 4 μm thick were stained with hematoxylin and eosin and subsequently examined under a microscope to identify the lesions. Then, a section which contained the lesion with the highest histological grade was selected from each patient and immunostained.

These sections were deparaffinized in xylene, rehydrated in graded alcohol, and transferred to phosphate-buffered saline (PBS). The procedures of antigen retrieval, blocking of nonspecific reaction, working dilutions, and tissue used as positive control for each primary antibody are listed in Table 1. All the primary antibodies were incubated overnight with the tissues. After the reaction of primary antibodies, samples were rinsed four times with PBS. The antibodies except E-cadherin were stained by diaminobenzidine using the EnVision Kit (EnVision/HRP, DAKO, Carpinteria, CA, USA) according to the manufacturer's protocol. For E-cadherin, R.T.U. VECTASTAIN Universal Elite ABC Kit (Vector Laboratories, Peterborough, UK) was used for staining according to the manufacturer's protocol. The sections were then washed three times with PBS, counterstained with hematoxylin, and again washed three times with PBS. The slides were mounted in Malinol (Muto Pure Chemicals, Tokyo, Japan).

Evaluation of the results

The immunostaining results were analyzed to determine the frequency of tumor cells expressing MMPs and the intracellular localization of MMPs. When two or more histological grades were identified in a section, we recorded the results of each histological grade separately. The frequencies of tumor cells expressing MMPs were expressed as the percentage of MMP-expressing cells in all the tumor cells, each 5% grade, for each histological grade of IPMN and in IDC. When the expression of MMPs was localized to a specific area of the tumor cells, the percentage of the tumor cells which showed this intracellular localization was recorded for each lesion.

The staining results of tumor-associated antigens MUC1, MUC2, and MUC5AC were considered to be positive when cytoplasmic staining was observed in more than 5% of all tumor cells.

E-cadherin results were considered to be positive when clear membranous staining was observed.

Table 1 Antibodies for immunohistochemistry

Specificity	Clone	Manufacturer	Antigen retrieval	Blocking	Working dilution	Positive control
MMP1	41-1E5	DFC	PK 5 min	NGS	1:100	Colonic cancer (E,S)
MMP2	42-5D11	DFC	AC 20 min	NGS	1:100	Colonic cancer (S)
MMP3	55-2A4	DFC	MW 10 min	NGS	1:100	Esophageal cancer (E)
MMP7	141-7B2	DFC	MW 20 min	–	1:2,500	Pancreatic cancer (E)
MMP9	56-2A4	DFC	MW 20 min	NGS	1:100	Trophoblast
MUC1	Ma695	Novocastra	–	–	1:1,000	Normal pancreatic duct
MUC2	Ccp58	Novocastra	AC 20 min	–	1:100	Colonic mucosa
MUC5AC	CLH2	Novocastra	MW 40 min	–	1:50	Gastric foveolar epithelium
E-cadherin	NCH-38	DAKO	MW 40 min	NHS	1:100	Normal pancreas tissue

All the listed antibodies are mouse monoclonal antibodies.
Antigen: *MMP* matrix metalloproteinase, *MUC* core protein of mucin antigen; Manufacturer: *DFC* Daiichi Fine Chemical Co. Ltd., Takaoka, Japan, *Novocastra* Novocastra Laboratories Ltd., New Castle upon Tyne, UK, *DAKO*, DAKO Cytomation, Carpinteria, CA, USA; Antigen retrieval: *AC* autoclave 121°C, *MW* microwave 96°C, *PK* proteinase K; Blocking: *NGS* normal goat serum, *NHS* normal horse serum; Positive control: *E* epithelial cell, *S* stromal cell

Table 2 Clinicopathological data of IPMNs

Patient no.	Age (years)	Sex	Localization	Subtype	Diagnosis	Type of lesion in an examined section (shown as % in each section)				Mucinous subtype
						AD	BL	NIC	IC	
1	67	M	Ph	MX	Adenoma	100	–	–	–	G
2	72	M	Ph	B	Borderline	90	10	–	–	G
3	79	M	Ph	MX	Borderline	60	40	–	–	I
4	83	M	Ph	B	Borderline	60	40	–	–	G
5	74	M	Ph	MX	Borderline	60	40	–	–	G
6	74	M	Ph	MX	Borderline	50	50	–	–	G
7	62	M	Ph	B	Borderline	50	50	–	–	G
8	78	F	Ph	MX	Borderline	10	90	–	–	I
9	75	F	Pbt	MX	Borderline	10	90	–	–	G
10	67	M	Pbt	MX	Borderline	20	80	–	–	G
11	76	M	Ph	MX	Borderline	30	70	–	–	I
12	74	M	Ph	MX	Borderline	80	20	–	–	G
13	63	M	Ph	MX	Noninvasive ca	30	60	10	–	G
14	58	M	Ph	B	Noninvasive ca	–	40	60	–	I
15	67	M	Pbt	MX	Noninvasive ca	–	20	80	–	I
16	72	M	Pbt	B	Noninvasive ca	–	10	90	–	I
17	59	F	Phbt	MX	Invasive ca	25	25	10	40	G + PB
18	71	M	Ph	B	Invasive ca	–	15	80	5	G
19	66	M	Phbt	B	Invasive ca	–	–	80	20	I
20	60	M	Pbt	B	Invasive ca	–	–	90	10	I
21	83	F	Pbt	MX	Invasive ca	–	–	10	90	G
					Total number of each lesion	14	17	9	5	

Lesions: *AD* adenoma, *BL* borderline lesion, *NIC* noninvasive carcinoma, *IC* invasive lesion of IPMN; Subtype: *MX* mixed, *B* branched; Localization: *Ph* pancreas head, *Pbt* pancreas body and tail; Mucinous subtype: *G* gastric type, *I* intestinal type, *PB* pancreatobiliary type

Statistical analysis

All statistical analyses were performed using SPSS software (SPSS 11.5.1J, SPSS Japan, Tokyo, Japan). The trend in the frequency of MMP expression according to histological grade was analyzed by Spearman's rank correlation analysis. The data on the frequency of lesions for each grade of apical or basolateral pattern were analyzed by the chi-square test. A P value of less than 0.05 was considered to be statistically significant.

Table 3 Clinicopathological data of invasive ductal carcinoma

Patient no.	Age (years)	Sex	Localization	Differentiation	TS	Size	*T*	*N*	*M*
1	71	F	Pb	Mod>wel>por	1	1.5	3	1	0
2	34	M	Ph	Wel	2	2.3	3	3	0
3	64	M	Ph	mod = por	2	2.3	3	1	1
4	71	F	Ph	mod = por	2	2.5	4	0	0
5	80	F	Ph	mod	2	3	3	3	0
6	69	M	Ph	wel	2	3.5	2	1	0
7	74	M	Ph	mod = por	2	3.5	3	1	0
8	86	M	Ph	mod = por	2	3.5	3	1	0
9	51	M	Ph	mod = wel	2	4	3	1	0
10	80	F	Pbt	wel = mod	4	6.5	4	3	1

Localization: *Ph* pancreas head, *Pbt* pancreas body and tail; Differentiation: *wel* well differentiated, *mod* moderately differentiated, *por* poorly differentiated

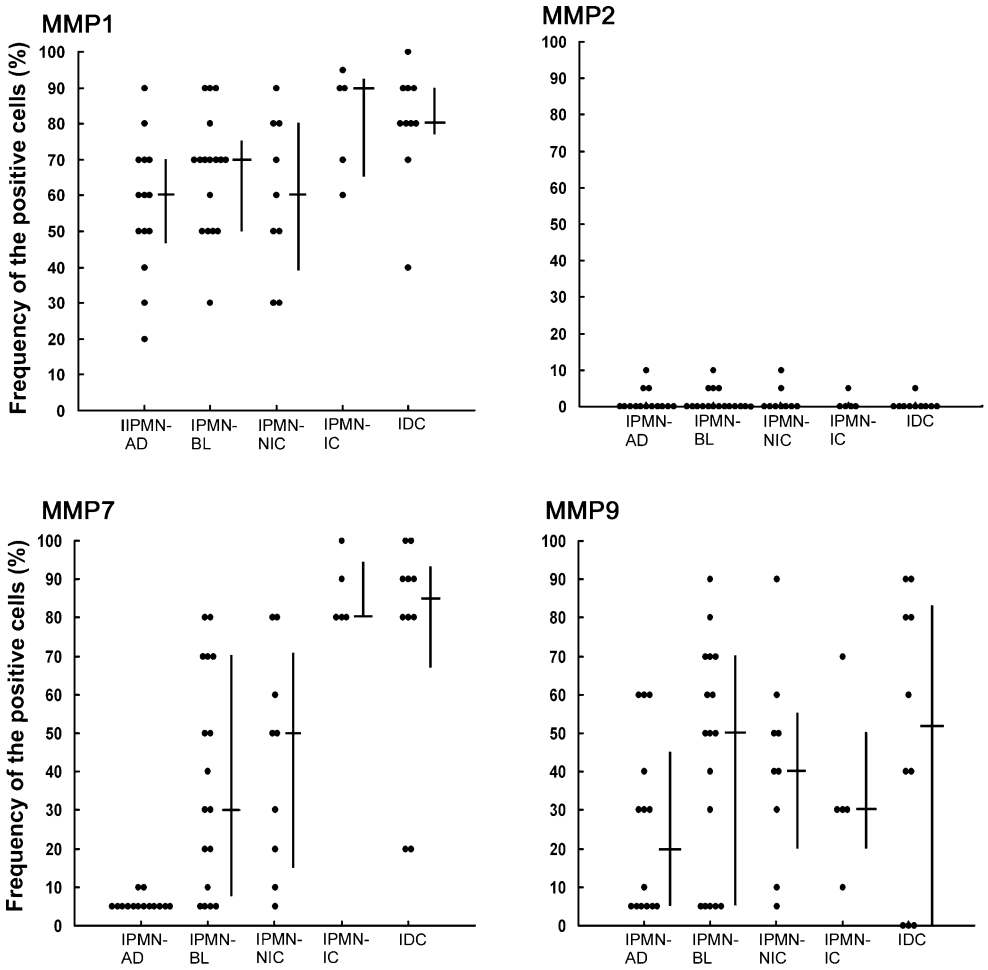

Fig. 1 Frequency of the tumor cells expressing MMP1, MMP2, MMP7, and MMP9. The *horizontal bars* indicate the median and the *vertical bars* indicate interquartile range. Frequency of tumor cells expressing MMP7 showed a significant trend in accordance with the histological grades of IPMN ($P<0.0001$). The results for MMP3 were excluded from this figure because they were negative. *AD* adenoma, *BL* borderline lesion, *NIC* noninvasive carcinoma, *IC* invasive lesion of IPMN

Results

Clinicopathological data

The clinicopathological data of the 21 patients with IPMN and of the ten patients with IDC are shown in Tables 2 and 3, respectively.

The age distribution of patients with IPMN was 59 to 83 (mean, 70.5) years and the male–female ratio was 17:4. Sections from each patient contained lesions of various histological grades: adenoma in 14 patients, borderline lesions in 17 patients, noninvasive carcinoma in nine patients and invasive lesions in five patients. The pathological diagnosis in the table shows the highest grade for each patient. Histologically, all five invasive lesions were tubular carcinoma with scirrhous invasion.

The age distribution of patients with IDC was 34 to 86 (mean, 68.0) years and the male–female ratio was 6:4. Nine patients had lymph node metastasis, and two patients had distant metastasis to the liver.

The IPMN lesions were classified into subtypes according to their MUC expression profile [4]: 12 patients had lesions which were classified as the gastric subtype (MUC1−, MUC2−, and MUC5AC+) and eight had the intestinal subtype (MUC1−, MUC2+, and MUC5AC+/−). A section from one patient showed a mixture of two mucinous subtypes, the gastric and pancreatobiliary (MUC1+, MUC2−, and MUC5AC−). Sections of the gastric subtype contained adenoma in 11 patients, borderline lesions in 11 patients, noninvasive carcinoma in four patients, and invasive lesions in three patients. Sections of the intestinal subtype contained adenoma in three patients, borderline lesions in six patients, noninvasive carcinoma in five cases, and invasive lesions in two patients. The histological grade of the lesion classified as pancreatobiliary subtype was adenoma.

MMP and E-cadherin expression in normal pancreas

In normal pancreas, MMP1 was expressed in ductal metaplasia [13], fibroblasts, and macrophages. MMP2 was expressed in fibroblasts in the stroma. MMP3 was expressed in neither the epithelium nor the stroma. MMP7 was expressed in the small pancreatic duct in the atrophic lobule and ductal metaplasia. MMP9 was expressed in acinar cells, macrophages, neutrophils, and lymphocytes. E-cadherin was expressed in all epithelial cells in a membranous pattern.

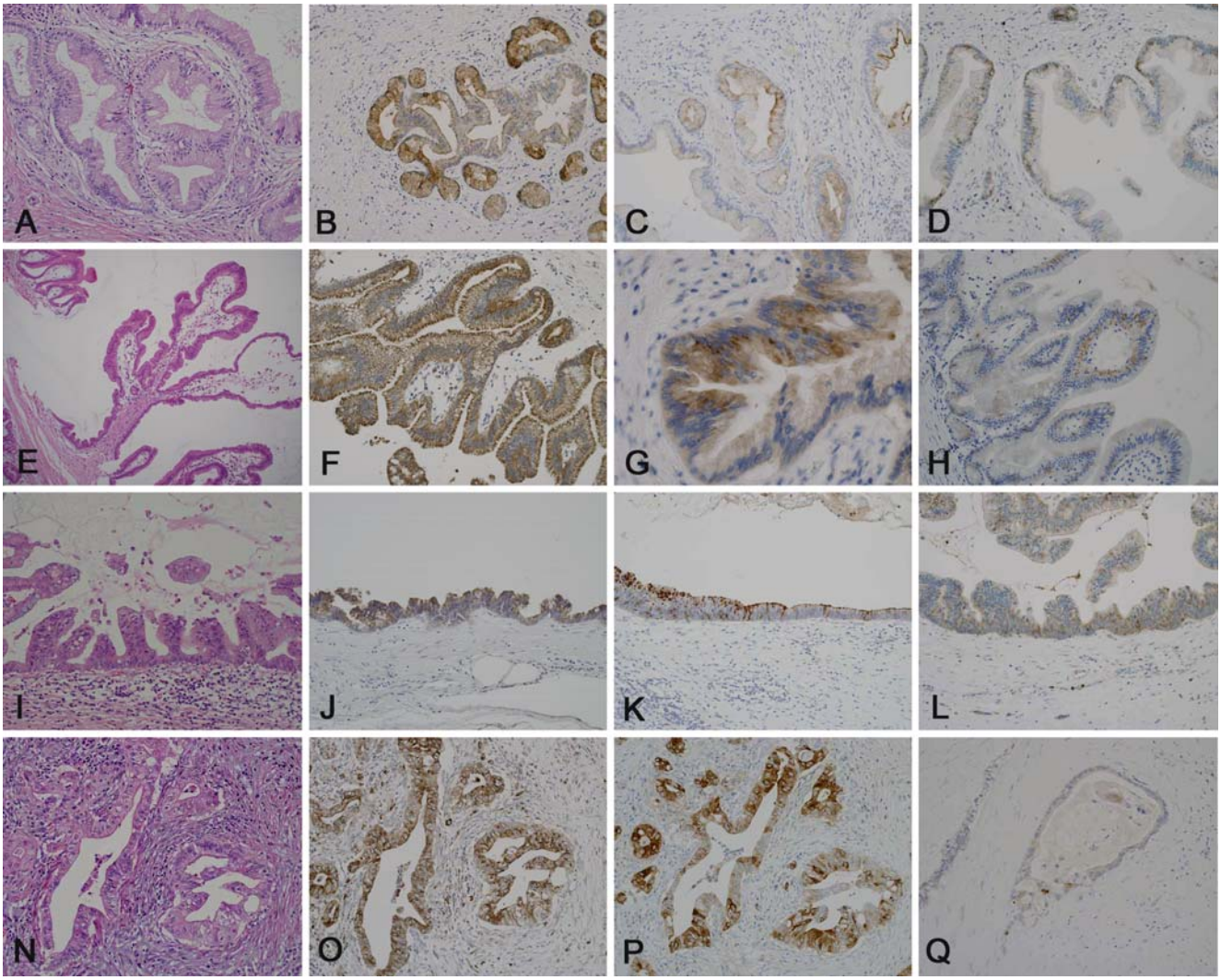

Fig. 2 The representative histological and immunohistochemical findings of the lesions. **a**–**d** adenomas; **e**–**h** borderline lesions; **i**–**l** noninvasive carcinoma; **n**–**q** invasive lesions of IPMN. **a**, **e**, **i**, and **n** HE staining; **b**, **f**, **j**, and **o** MMP1; **c**, **g**, **k**, and **p** MMP7; **d**, **h**, **l**, and **q** MMP9. Frequency of tumor cells expressing MMP7 was low in adenomas, higher in borderline lesions and noninvasive carcinomas, and still higher in invasive lesions. The intracellular expression of MMP1 was generally diffuse in the cytoplasm and that of MMP9 was apical. The findings of MMP2 and MMP3 are not shown in this figure because the frequency of cells expressing these MMPs was nil or very low

Frequency of tumor cells expressing MMPs

MMP1, MMP2, MMP7, and MMP9 were expressed in the lesions of IPMN. MMP1, MMP7, and MMP9 were expressed mainly in tumor cells, whereas MMP2 was expressed mainly in stromal cells. MMP3 was expressed in neither tumor cells nor stromal cells. The frequency of the tumor cells expressing MMP1, MMP2, MMP7, and MMP9 are shown in Fig. 1. The median of the frequency of tumor cells expressing MMP7 were 5.0% in adenomas, 30.0% in borderline lesions, 50.0% in noninvasive carcinomas, and 80.0% in invasive lesions. These values were positively correlated to the histological grade ($P<0.0001$). The frequencies of cells expressing MMP1, MMP2, and MMP9 did not show correlation with the histological grades ($P=0.412$, 0.403, and 0.168, respectively). Figure 2 shows representative histological and immunohistochemical findings.

The correlation between the frequency of MMP7 expression and the histological grades in each subtype was also analyzed (Fig. 3). In the gastric subtype, the median of the frequencies of tumor cells expressing MMP7 were 5.0% in adenomas, 30.0% in borderline lesions, 35.0% in noninvasive carcinomas, and 80.0% in invasive lesions. In the intestinal subtype, the median were 5.0% in adenomas, 55.0% in borderline lesions, 60.0% in noninvasive carcinomas, and 90.0% in invasive lesions. The frequencies were positively correlated to the histological grade in both subtypes ($P<0.0001$ in the gastric type; $P=0.011$ in the intestinal type). The lesion classified as the pancreato-

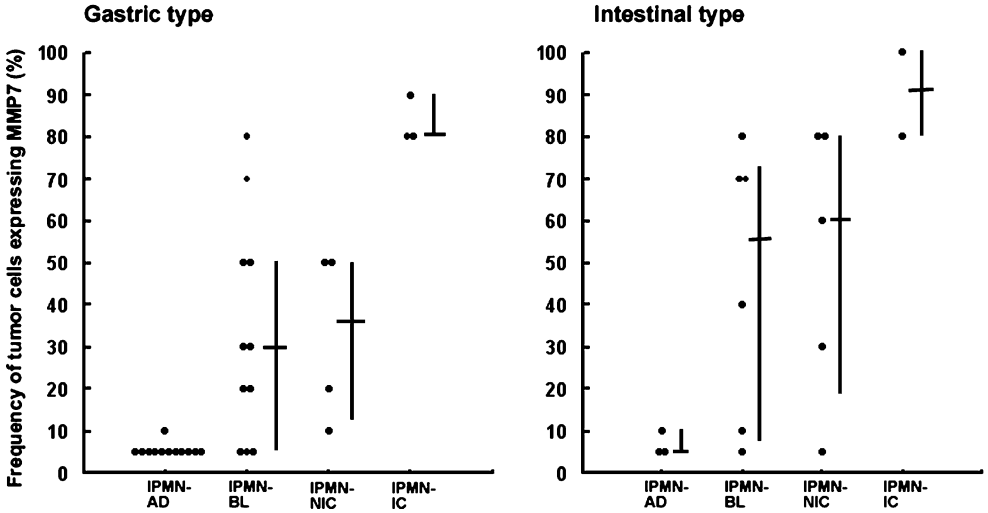

Fig. 3 Frequency of the tumor cells expressing MMP7 in the gastric and intestinal subtype of IPMN. The *horizontal bars* indicate the median and the *vertical bars* indicate the interquartile range. In both subtypes, the frequencies positively correlated with the histological grades of IPMN (gastric subtype, $P<0.0001$; intestinal subtype, $P=0.011$). *AD* adenoma, *BL* borderline lesion, *NIC* noninvasive carcinoma, *IC* invasive lesion of IPMN

biliary subtype was excluded from the analysis because only one lesion of this subtype was included in this study.

In IDC, MMP1, MMP2, MMP7, and MMP9 were expressed in tumor cells. MMP3 was expressed in neither tumor cells nor stromal cells. The frequencies of tumor cells expressing MMPs are also shown in Fig. 1. No significant difference was found in the frequencies between the invasive lesions of IPMN and IDC for any of the MMPs.

Intracellular localization of MMPs

MMP1 was expressed diffusely in the cytoplasm of tumor cells in all histological grades and was not localized to any specific area.

The number of tumor cells expressing MMP2 was so small that the localization could not be evaluated.

Localized expression of MMP7 in the apical portion was consistently observed in the MMP7-expressing tumor cells. Localized expression in the basolateral portion was more frequent in lesions of higher histological grades. Tumor cells expressing MMP7 in the basolateral portion were classified into three groups according to their frequency, and the number and frequency of the lesions for each histological grade were recorded (Table 4). The frequencies of basolateral localization for each of the three groups were significantly different between histological grades ($P<0.0001$). Representative findings are shown in Fig. 4.

In all tumor cells expressing MMP9, the expression was localized to the apical portion of the tumor cells.

In IDC, the expression of MMPs in the cytoplasm of the tumor cells was diffuse and was not localized to any specific area.

Expression of E-cadherin in IPMN

In adenomas, borderline lesions, and noninvasive carcinomas, almost all tumor cells expressed E-cadherin. Although focal attenuation of E-cadherin expression was noted in invasive lesions, the distribution of such attenuated expression did not necessarily coincide with that of basolateral MMP7 expression (Fig. 5).

Discussion

Our immunohistochemical analysis showed that the frequency of cells expressing MMP7 and of their basolateral localization was positively correlated to the histological

Table 4 Frequency of basolateral expression of MMP7 for each histological grade of IPMN

Frequency of tumor cells expressing MMP7 in basolateral portion	Number (%) of the lesions in			
	Adenoma ($n=14$)	Borderline ($n=17$)	Noninvasive ($n=9$)	Invasive ($n=5$)
None	7 (50%)	2 (11.8%)	0	0
<50%	7 (50%)	11 (64.7%)	2 (22.2%)	0
≥50%	0	4 (23.5%)	7 (77.8%)	5 (100%)

Adenoma adenoma of IPMN, *Borderline* borderline lesion of IPMN, *Noninvasive* noninvasive carcinoma of IPMN, *Invasive* invasive lesion of IPMN

$P<0.0001$ by chi-square test

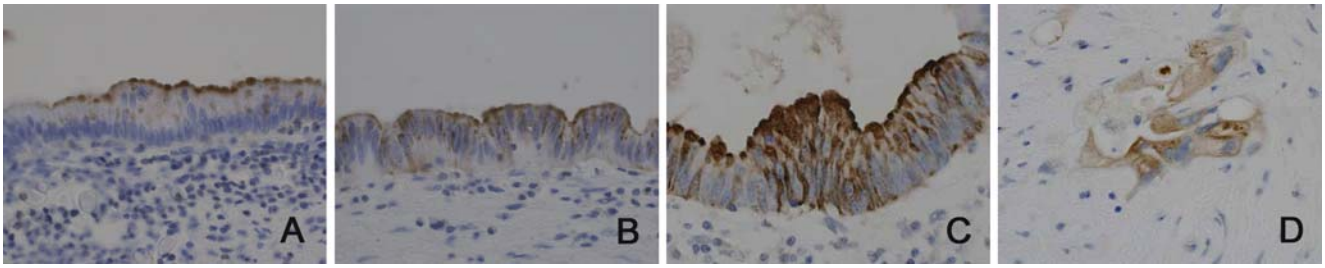

Fig. 4 The intracellular localization of MMP7 in each histological grade. **a** Adenoma; **b** borderline lesion; **c** noninvasive carcinoma; **d** invasive lesion of IPMN. The frequency of the basolateral expression was higher in the lesions of higher histological grades

grades of IPMN. We also found that MMP1, MMP2, and MMP9 are expressed in the tumor cells of IPMN of all histological grades.

The positive correlation between the frequency of MMP7 expression and the histological grades of IPMN suggests that MMP7 may be involved in the tumor progression process by which IPMN advances from adenoma to carcinoma. The precise function of MMP7 in this progression has not yet been clarified. However, previous studies in colorectal and breast carcinogenesis have suggested that the function of MMP7 in the early stages of tumor progression may be related to cell proliferation. A study on the roles of MMPs in colorectal adenoma has shown that MMP7 is induced by and interact with the beta-catenin signaling pathway and consequently promotes cell proliferation [8]. Another study using mammary gland cell lines has shown that MMP7 expression activates ErbB4 receptors to promote cell proliferation and subsequent transformation [11]. These studies suggest that MMP7 is involved in the process of cell proliferation in the early stages of IPMN. In the present study, both the gastric and intestinal subtypes of IPMN showed positive correlation with histological grades, suggesting that those two subtypes of IPMN share the same function of MMP7 in the early stages of tumor progression, as discussed above.

The positive correlation between the basolateral localization of MMP7 and the histological grades of IPMN suggests that this localization pattern is associated with tumor progression by which IPMN advances from adenoma to carcinoma including its invasive stage. A recent study [5] has shown an association between the functions of MMP7 and its intracellular localization. The study showed that apical expression of MMP7 was responsible for cell

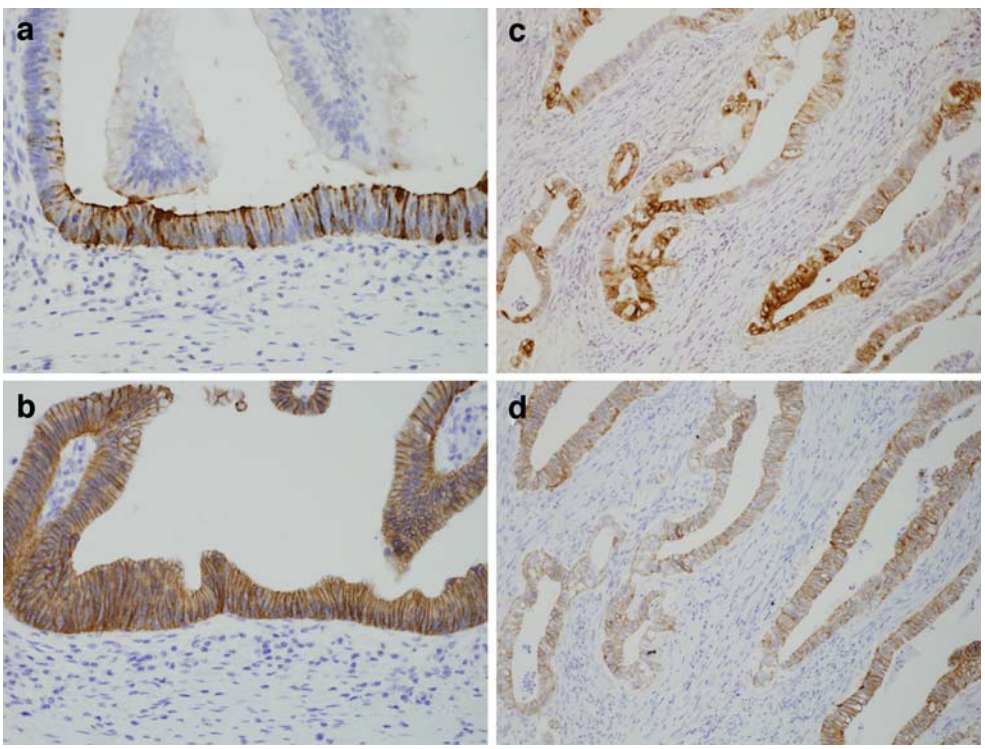

Fig. 5 E-cadherin and MMP7 expression of IPMN noninvasive carcinoma and invasive lesion. **a** and **b** Noninvasive carcinoma; **c** and **d** invasive lesion; **a** and **c** MMP7; **b** and **d** E-cadherin. In noninvasive carcinoma, E-cadherin was expressed in almost all tumor cells with membranous pattern. The tumor cells expressing MMP basolaterally did not show the attenuation of E-cadherin expression. In invasive lesion, focal attenuation of E-cadherin expression was observed. The distribution of the attenuated expression of E-cadherin did not coincide with the basolateral MMP7 expression

proliferation, a result of the MMP acting on an apically located substrate. The findings of the study allow us to hypothesize that basolateral localization of MMP7 is related to the functions of basolaterally located substrates of tumor cells. Considering that cell adhesion molecules and basement membrane components such as E-cadherin, fibronectin, laminin, and type IV collagen are substrates of MMP7, their degradation by MMP7 may initiate invasion. However, in the present study, no significant relationship was found between the basolateral expression of MMP7 and the expression of E-cadherin. One explanation for this lack of correspondence may be that the cleavage of E-cadherin by MMP7 secreted basolaterally may require co-secretion of a MMP7 activator, as basolaterally secreted MMP7 is mainly latent [5]. Another possible explanation is that MMP7 secreted basolaterally targets molecules other than E-cadherin, such as components of tight junctions.

MMP1, MMP2, and MMP9 are expressed in all histological grades of IPMN. This suggests that these MMPs may also be involved in tumor progression. However, their functions may be different from those of MMP7 because both the frequency of expression and the intracellular localization did not correlate with the histological grades. The roles of these MMPs in carcinogenesis or tumor progression have been described in recent studies. Studies on colorectal cancer development have reported complex interactions of these MMPs with the oncogenes and tumor suppressor genes such as APC, k-ras, smad4, and p53 in the early stages of tumor development [8]. Considering that these genes also play a role in the tumor progression of IPMN [14], it is likely that the interactions between these genes and MMPs contribute to tumor progression.

For all MMPs examined, no significant difference was found between IDC and the invasive lesions of IPMN, neither in the frequency of the positive cells nor in intracellular localization. This lack of significant difference is not definitive because the present study included only tubular carcinoma, not mucinous carcinoma, and only five lesions of invasive carcinoma.

In conclusion, our study shows that the frequency of tumor cells expressing MMP7 and of their basolateral localization exhibits positive correlations with the histological grades of IPMN, both gastric and intestinal subtypes. The present study also confirms that MMP1, MMP2, and MMP9 are expressed equally in all histological grades of IPMN, suggesting that MMP1, MMP2, and MMP9 may be involved in the tumor progression process in the early stages of IPMN. Taken together, these results indicate that MMP7 plays a role in the process of tumor progression by which IPMN advances from adenoma to carcinoma. Additionally, the basolateral expression of MMP7 possibly relates to the initiation of invasion. MMP1, MMP2, and MMP9 may be involved in the tumor progression process in the early stage of IPMN.

Conflict of interest statement We declare that we have no conflict of interest.

References

1. Adsay NV, Conlon KC, Zee SY, Brennan MF, Klimstra DS (2002) Intraductal papillary-mucinous neoplasms of the pancreas: an analysis of in situ and invasive carcinomas in 28 patients. Cancer 94:62–77
2. Bloomston M, Zervos EE, Rosemurgy AS (2002) Matrix metalloproteinase and their role in pancreatic cancer: a review of preclinical studies and clinical trials. Ann Surg Oncol 9:668–674
3. Folgueras AR, Pendás AM, Sánchez LM, López-Otín C (2004) Matrix metalloproteinase in cancers: from new functions to improved inhibition strategies. Int J Dev Biol 48:411–424
4. Furukawa T, Kloppel G, Volkan Adsay N, Albores-Saavedra J, Fukushima N, Horii A, Hruban R, Kato Y, Klimstra DS, Longnecker DS, Luttges J, Offerhaus GJA, Shimizu M, Sunamura M, Suriawinata A, Takaori K, Yonezawa S (2005) Classification of types of intraductal papillary-mucinous neoplasm of the pancreas: a consensus study. Virchows Arch 447:794–799
5. Harrel PC, McCawley LJ, Fingleton B, McIntyre O, Matrisian LM (2005) Proliferative effects of apical, but not basal, matrix metalloproteinase-7 activity in polarized MDCK cells. Exp Cell Res 303:308–320
6. Ii M, Yamamoto H, Adachi Y, Maruyama Y, Shinomura Y (2006) Role of matrix metalloproteinase-7 (matrilysin) in human cancer invasion, apoptosis, growth, metalloproteinase and tissue inhibitor expression in pancreatic cancer: Increased expression of matrix metalloproteinase-7 predicts poor survival. Clin Cancer Res 10:2832–2845
7. Jones LE, Humphreys MJ, Campbell F, Neoptolemos JP, Boyd MT (2004) Comprehensive analysis of matrix metalloproteinase and tissue inhibitor expression in pancreatic cancer: increased expression of matrix metalloproteinase-7 predicts poor survival. Clin Cancer Res 10:2832–2845
8. Leeman ML, Curan S, Murray GI (2003) New insights into the roles of matrix metalloproteinases in colorectal cancer development and progression. J Pathol 201:528–534
9. Longnecker DS, Hruban RH, Adler G, Kloppel (2002) Intraductal papillary-mucinous neoplasms of the pancreas. In: Hamilton SR, Aaltonen LA (eds) Pathology and genetics of tumors of the digestive system (World Health Organization classification of tumours). IARC, Lyon, pp 237–240
10. Lynch CC, Matrisian LM (2002) Matrix metalloproteinases in tumor-host cell communication. Differentiation 70:561–573
11. Lynch CC, Vargo-Gogola T, Martin MD, Fingleton B, Crawford HC, Matrisian LM (2007) Matrix metalloproteinase 7 mediates epithelial cell tumorigenesis through the ErbB4 receptor. Cancer Res 67:6760–6767
12. Nelson AR, Fingleton B, Rothenberg ML, Matrisian LM (2000) Matrix metalloproteinases: biological activity and clinical implications. J Clin Oncol 18:1135–1149

13. Parsa I, Longnecker DS, Scarpelli DG, Pour P, Reddy JK, Lefkowitz M (1985) Ductal metaplasia of human exocrine pancreas and its association with carcinoma. Cancer Res 45:1285–1290
14. Sasaki S, Yamamoto H, Kaneto H, Ozeki I, Adachi Y, Takagi H, Matsumoto T, Itoh H, Nagakawa T, Miyakawa H, Muraoka S, Fujinaga A, Suga T, Satoh M, Itoh F, Endo T, Imai K (2003) Differential roles of alterations of p53, p16, and SMAD4 expression in the progression of intraductal papillary-mucinous tumors of the pancreas. Oncol Rep 10:21–25
15. Sobin LH, Wittekind CH (eds) (2002) TNM clinical classification, pancreas. UICC TNM classification of malignant tumours, 6th edn. Wiley-Liss, New York, pp 93–96
16. Yamamoto H, Ito F, Iku S, Adachi Y, Fukushima H, Sasaki S, Mukaiya M, Hirata K, Imai K (2000) Expression of matrix metalloproteinases and tissue inhibitors of metalloproteinases in human pancreatic adenocarcinomas: clinicopathologic and prognostic significance of matrilysin expression. J Clin Oncol 19:1118–1127

Virchows Arch (2008) 453:89–96
DOI 10.1007/s00428-008-0608-7

ORIGINAL ARTICLE

Correlations between reduced expression of the metastasis suppressor gene KAI-1 and accumulation of p53 in uterine carcinomas and sarcomas

Juliane Briese · Heinrich M. Schulte · Maria Sajin · Christoph Bamberger · Katja Redlin · Karin Milde-Langosch · Thomas Löning · Ana-Maria Bamberger

Received: 4 September 2007 / Revised: 4 March 2008 / Accepted: 11 March 2008 / Published online: 16 April 2008

Abstract Kangai (KAI)-1 (CD82) is a metastasis suppressor gene, which belongs to the family of tetraspanin proteins. A loss of KAI-1 expression is associated with the advanced stages of many human malignancies. The present study was designed to investigate the expression pattern of KAI-1 in the normal endometrium and uterine tumors and to correlate it with the expression of tumor suppressor protein p53. KAI-1 could be found in the normal endometrium throughout the menstrual cycle. Thirteen of 42 endometrial carcinomas demonstrated moderate KAI-1 expression, but low expression of p53. Twenty-nine of 42 endometrial carcinomas showed reduced or absent KAI-1 expression, which correlated with strong expression of p53 ($p<0.001$). There were significant correlations between KAI-1 expression and histological type, e.g., 93% of endometrioid carcinomas displayed a low or moderate immunostaining for KAI-1, whereas nearly all of the serous/clear cell carcinomas were KAI-1 negative ($p<0.001$); tumor grading, e.g., 73% of high grade tumors showed no KAI-1 expression ($p<0.001$). Most of the investigated uterine sarcomas were negative for KAI-1, whereas they displayed a strong immunostaining for p53. In conclusion, KAI-1 and p53 show inverse expression. The reduced KAI-1 expression may be the result of dysregulated p53 function and could be an important step in the endometrial carcinogenesis.

Keywords KAI-1 · Metastasis suppressor · p53 · CD82 · Endometrium · Uterine tumor · Sarcoma

J. Briese · C. Bamberger · A.-M. Bamberger
Section on Endocrinology and Metabolism of Ageing,
University Clinic Hamburg-Eppendorf,
Hamburg, Germany

J. Briese (✉) · H. M. Schulte · K. Redlin
Department of Pathology and Tumor Biology,
University of Leeds, St. James's Hospital,
Beckett Street,
LS9 7TF Leeds, UK
e-mail: j.briese@leeds.ac.uk

M. Sajin
Endokrinologikum,
Hamburg, Germany

K. Milde-Langosch
Department of Morphopathology, University of Bucharest,
Bucharest, Romania

T. Löning
Department of Gynecology,
University Clinic Hamburg-Eppendorf,
Hamburg, Germany

J. Briese · H. M. Schulte · M. Sajin · C. Bamberger · K. Redlin · K. Milde-Langosch · T. Löning · A.-M. Bamberger
Department of Pathology,
Centre for Cytology and Gynecopathology,
University Clinic Hamburg-Eppendorf,
Hamburg, Germany

Introduction

Endometrial carcinoma is the most common malignant epithelial tumor of the female genital tract in developed countries. Two different clinicopathological types can be distinguished: the estrogen-related endometrioid type (type I) and the non-estrogen-related non-endometrioid type (serous or clear cell carcinoma) (type II) [17]. Type I carcinomas (approximately 80%) are associated with hyperestrogenicity [25]. At the molecular level, mutations of

DNA mismatch repair genes (MutS protein homolog (MSH)1, MSH2) [9] of ß-catenin [10], k-ras [9], phosphatase and tensin homolog, and the loss of the estrogen receptor (ER) and progesterone receptor (PR) [9] may play a central role for type I tumors and the transformation to more aggressive carcinomas. Only 15% to 20% of the cases are type II carcinomas, which typically develop from the atrophic endometrium of postmenopausal woman and invade the myometrium [28]. Mutation of the p53 gene seems to be important for these tumors [16]. Uterine sarcoma is a rare form of uterine malignancy and occurs in 2% to 5% of all patients with uterine tumors [29]. There are four recognized types of uterine sarcoma: leiomyosarcomas (35%), endometrial stromal sarcomas (10%), mixed mesodermal tumors (7%), and other uterine sarcomas (3%). Malignant mixed mullerian tumors (MMMT), which contain epithelial and stromal elements, are considered as a subset to the endometrial carcinoma (sarcomatoid carcinoma) (45%) [31]. Whereas estrogens tend to play a causal role in the pathogenesis of the most endometrial adenocarcinomas, such a link has not been established for the uterine sarcomas in general, although it may exist for the MMMT variant [35].

Recently, Kangai (KAI)-1 has emerged as a metastasis suppressor. KAI-1 (CD82) is a member of the transmembrane 4 protein superfamily (TM4SF) and is located in the p11.2 region on the human chromosome 11 [7]. TM4SF members are characterized by the four highly conserved transmembrane domains, two relatively divergent extracellular domains, and two short cytoplasmic domains at the NH_2 and COOH termini. The precise biochemical function of the TM4SF is not clear yet; however, the current data suggest a role for this superfamily largely in the regulation of the cell proliferation, activation, and motility [23]. About 20 members of this family have been identified including MRP-1/CD9, TAPA-1/CD81, ME491/CD63, and KAI-1/CD82 [36]. A growing body of evidence suggests that CD9, one member in TM4SF, which has a 54% identity with KAI-1, is involved in the cell motility and metastasis [13]. Expression of CD9 in malignant melanoma cells significantly suppressed the metastatic potential [3]. KAI-1 expression was reduced in the human cell lines derived from metastatic prostate tumors as compared with its expression in normal prostate tissue [7]. Downregulation of the KAI-1 protein was also observed during the progression of human prostate cancer [8]. It was reported that loss of KAI-1 expression correlates with the progression of a variety of human cancers such as non-small cell lung cancer and cancer of the pancreas [6]. In addition, expression of KAI-1 in colon cancer cells and melanoma cells resulted in reduced cell motility and invasiveness in vitro and in the suppressed experimental metastasis in vivo in melanoma cells [34].

It is known that KAI-1 is expressed in a wide range of tissues, but its expression in the uterine stromal and epithelial tumors in correlation with the tumor suppressor p53 and with the clinical and histological parameters has not previously been investigated. The present study was designed to examine for the first time the expression pattern of KAI-1 in the endometrial hyperplasias and uterine tumors such as endometrial carcinomas and sarcomas and thus, its potential role as an additional diagnostic marker for these tumors.

Materials and methods

Tissue collection

For immunohistochemistry, surgical specimens that had been routinely fixed in the 4% formaldehyde and embedded in the paraffin were used. Forty-two endometrial carcinomas (30 endometrioid, eight serous, and four clear cell carcinomas), 15 sarcomas of the uterus (five carcinosarcomas, eight low grade endometrial stromal sarcomas, and two leiomyosarcomas), and 17 endometrial hyperplasias (six cases of simple hyperplasia without atypia, three cases of simple hyperplasia with atypia, four cases of complex hyperplasia without atypia, and four cases of complex hyperplasia with atypia) were analyzed. Of the endometrial carcinomas, eight tumors were International Federation of Obstetricians and Gynecologists (FIGO) stage Ia, 17 tumors FIGO Ib, seven tumors FIGO Ic, and ten tumors FIGO stage II. Twenty samples of normal endometrium (ten of the early and late proliferative phase and ten of the early and late secretory phase) were additionally included. The age of all patients ranged from 33 to 90 years with a mean of 59 years. The median age of the patients with endometrial carcinoma was 65 years. The tissue material was selected following histological review from the files of the Department of Gynecopathology, University Hospital Hamburg-Eppendorf. All lesions were classified according to the most recent WHO criteria.

Immunohistochemistry

Serial sections of 4–6 μm were cut from the paraffin blocks and mounted on 3-aminopropyl-triethoxysilan-coated slides, deparaffinized in xylene and rehydrated in the graded alcohol to Tris-buffered saline (TBS; 50 mmol/L Tris, 150 mmol/L NaCl, pH 7.4). For the detection of KAI-1, the slides were microwaved for 5×2 min in a 10 mmol/L citrate, pH 6.0. After cooling down for 20 min, the slides were washed with a phosphate-buffered saline (PBS), blocked for 10 min at room temperature with avidin–biotin blocking system (DAKO, Denmark), and incubated with an

anti-KAI-1 mouse monoclonal antibody (G2) (Santa Cruz Biotechnology, Santa Cruz, CA, USA) at a dilution of 1:200. The slides were then reacted with biotinylated secondary antibody (DAKO, Glostrup, Denmark) for 10 min. Staining was performed using peroxidase-labeled streptavidin (DAKO) and 3,3′-diaminobenzidine (DAB) (DAB tetrahydrochloride containing 0.03% H_2O_2; Sigma, Chemical Co.). Sections were counterstained with hematoxylin (Hemalaun Meyer; Merck, Germany), dehydrated, and mounted (Eukitt; Labo-Med, Germany). For p53 immunohistochemistry, deparaffinized tissue sections were washed in a phosphate-buffered saline and preincubated in a 0.5% blocking serum for 5 min. The slides were incubated overnight at 4°C using the mouse monoclonal p53 antibody DO7 (DAKO), which recognizes the wild type and mutant p53 at a dilution 1:150. Slides were then rinsed in PBS solution and incubated with the secondary antibody (1:200 dilution, DAKO) for 30 min and again rinsed and incubated with the ancillary antibody (StrepAB complex/HRP Duet) for another 30 min. Revelation was performed with DAB (Sigma) immersion in 37°C for 5 min and hematoxilin counterstaining. Paraffin slides from the human prostate tumor served as a positive control (Santa Cruz Biotechnology, CA, USA) and P19 cells, which served as negative control, were obtained from American Type Culture Collection (Manassas, VA, USA). Positivity was characterized by the dark brown staining of the nucleus.

Microscopic evaluation

Histological and immunohistochemical evaluation was performed independently by two pathologists. Every tumor was given a score in which both the intensity of the staining (no staining=0; low staining=1; medium staining=2; strong staining=3) and the percent of stained epithelial cells (0%=0; under 10%=1; 10% to 50%=2; 51% to 80%=3; over 80%=4) were multiplicated. In normal endometrium, the given score consisted of staining intensity and the percent of stained glands. In addition, the immunohistochemical localization pattern was noted.

Statistical analysis

The SPSS11.0 program was used for calculation of interrelationships between the analyzed KAI-1 protein expression, p53 staining, and the histological or clinical factors by the chi-square test. Probability values less than 0.05 were regarded as statistically significant.

Protein isolation and Western blot analysis

Western blot analysis was performed on normal and tumor samples for which fresh-frozen material could be obtained. Protein concentration was determined following the standard protocols and using the bovine serum albumin standards. Extraction of proteins from endometrial tissue for Western blot analysis was carried out in PBS in the presence of 1% NP40 and protease inhibitors [23]. Proteins were electrophoresed on 10% sodium dodecyl sulfate (SDS)-polyacrylamide gels (NuPAGE Bis-Tris; Invitrogen) and transferred by the tank blotting onto the polyvinylidene difluoride Immmobilon membranes (Millipore Corp.). For electrophoresis, lysates were added to an equal volume of LDS sample Buffer (10 mM Tris, 10% SDS, 20% glycerol, 0.01% bromophenol blue; Invitrogen), and antioxidant was added to the NuPAGE transfer buffer (Invitrogen). For the detection of KAI-1, the monoclonal antibody G2 (Santa Cruz Biotechnology) was used at 1:200. Monoclonal antibody against glyceraldehyde-3-phosphate dehydrogenase (GAPDH) (clone 6C5; HyTest, Turku, Finland) was used at 1:10,000. Immunodetection was performed with the enhanced chemiluminescence system (SuperSignal; Pierce). Cell lysates 95–267 (Santa Cruz) and transiently KAI-1-transfected MDAMB-231 cells [11] were used as the positive control.

Results

Immunohistochemistry

Immunohistochemistry was performed on the paraffin-embedded samples of the endometrial carcinoma, sarcoma, endometrial hyperplasia, and normal endometrium. The results are presented in Fig. 1 and in Table 1, 2, 3.

KAI-1 expression in normal endometrium, endometrial hyperplasia, and endometrial carcinoma

In the normal human endometrium of 20 patients (Table 1), KAI-1 expression could be found throughout the menstrual cycle and was localized to epithelial cells of the endometrial glands and surface epithelium (data not shown) showing the clear plasma membrane localization. Normal endometrial samples did not show immunohistochemical reaction for p53 using the monoclonal antibody DO7 (data not shown). The low level of p53 is usually due to rapid turnover of p53. However, Pohnke et al. [32] demonstrated that the wild-type (wt) p53 (using CM1 antibody, Novocastra, UK) protein increases in the normal endometrium with the progression throughout the menstrual cycle.

Five of the 17 (29%) samples of endometrial hyperplasia displayed a strong cytoplasmic immunostaining for KAI-1 (score 8–12; Table 1) in the endometrial glands. Samples of complex atypical hyperplasia demonstrated a reduced

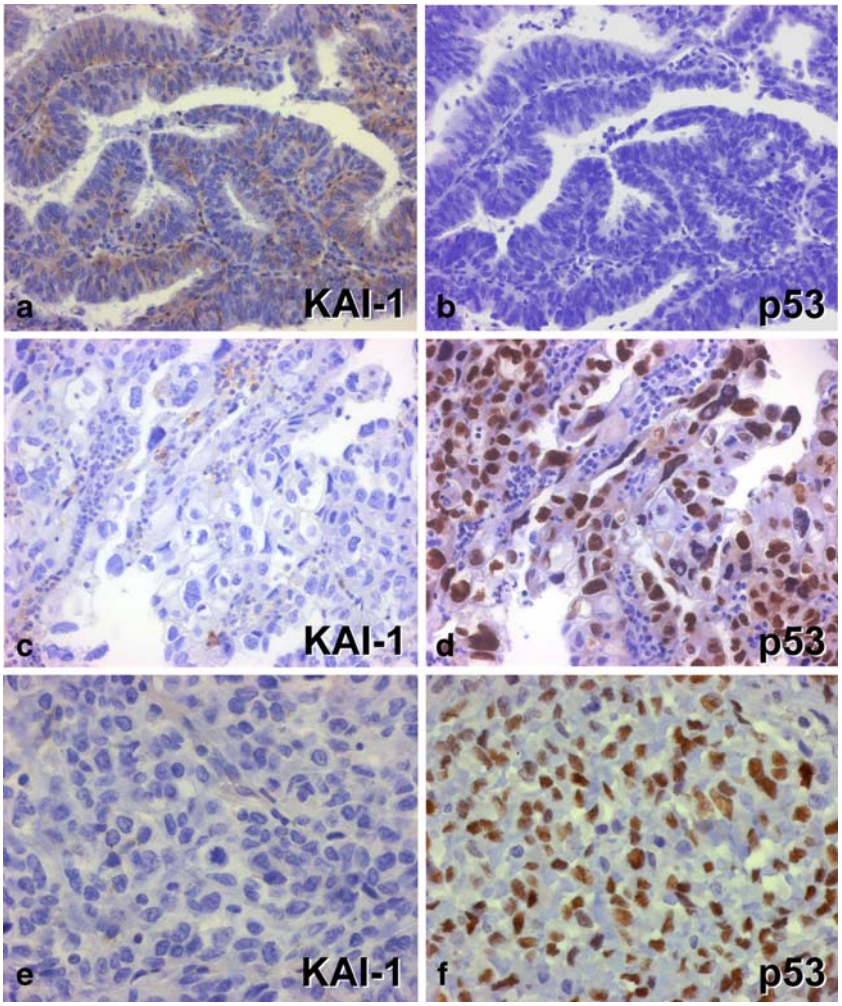

Fig. 1 Immunohistochemical localization of KAI-1 and p53 in the uterine neoplasias of the epithelial and stromal origin. **a** Moderate KAI-1 staining of a well-differentiated endometrioid carcinoma of histopathological grade G1 (×200). **b** Absence of p53 expression pattern in the same sample (×200). **c** Absence of KAI-1 expression in a clear-cell carcinoma (×200). **d** Strong staining for p53 in the same clear cell carcinoma. **e** and **f** Demonstrate an absence of KAI-1 expression (**e**) and a strong staining for p53 in a uterine sarcoma (**f**)

expression pattern of KAI-1 in comparison with the simple non-atypical endometrial hyperplasia. In two of these samples, focal regions of squamous metaplasia were observed, which were positive (not shown). In only two cases of hyperplasia that we observed nuclear expression of p53, which was focal and restricted to the atypical complex hyperplasia next to the carcinoma as demonstrated in a previous study [33].

A series of 42 endometrial carcinomas was analyzed for the KAI-1 expression immunohistochemically. For

Table 1 KAI-1 staining pattern in the normal human endometrium, hyperplasias, and uterine neoplasias of epithelial and stromal origin

	n	Negative KAI-1 (s=0)		Low KAI-1 (s=1–3)		Moderate KAI-1 (s=4–7)		High KAI-1 (s=8–12)	
		n	%	*n*	%	*n*	%	*n*	%
Normal human endometrium (*n*=20)									
Proliferative phase	10	0		0		4	(35.0)	6	(65.0)
Secretory phase	10	0		0		2	(22.0)	8	(88.0)
Endometrial hyperplasia (*n*=17)									
Simple (absence of atypia)	6	0		0		3	(50.0)	3	(50.0)
Simple (presence of atypia)	3	0		0		3	(75.0)	0	
Complex (absence of atypia)	4	0		0		2	(50.0)	2	(50.0)
Complex (presence of atypia)	4	0		2	(50.0)	2	(50.0)	0	
Endometrial carcinomas	42	13	(31.0)	16	(38.0)	13	(31.0)	0	
Sarcomas	15	12	(70.)	5	(30.0)	0		0	

s Score

Table 2 Correlation of KAI-1 staining with FIGO grading in endometrioid carcinomas

	n	Negative KAI-1 (s=0)		Low KAI-1 (s=1–3)		Moderate KAI-1 (s=4–7)		Significance
		n	%	*n*	%	*n*	%	
FIGO grading (*n*=30)								
G1	15	0		5	(32.0)	10	(68.0)	
G2	12	2	(17.0)	7	(58.0)	3	(25.0)	
G3	3	0		3	(100)	0		$p<0.0001$

s Score, *G1–G3* grade

this analysis, the tumors have been divided into three categories, from negative to moderate expression (score 4–7). Ten G1 and three G2 endometrioid tumors of 42 (31%) demonstrated a moderate score (4–7) of cytoplasmic KAI-1 expression. It is interesting that these KAI-1 positive tumors were all well or moderately differentiated endometrioid carcinomas (Fig. 1a, Tables 1 and 2). The comparison with the expression level of p53 in these tumors showed that most of those that had a moderate score (4–7) for KAI-1 had negative/low p53 staining (Fig. 1b—showing negative p53 expression in endometrioid carcinoma). Absent or reduced KAI-1 expression was observed in 29 of 42 (69%) adenocarcinomas, of which five specimens could be graded as G1, nine as G2, and three as G3 endometrioid carcinomas (Tables 1 and 3; Fig. 1c—showing negative KAI-1 expression in a clear cell endometrial carcinoma). This result correlated with the strong expression of p53 ($p<0.001$; Fig. 1d—showing p53 expression in a clear cell endometrial carcinoma). The protein was localized to the nucleus showing a diffuse granular pattern. Table 3 represents the correlation of KAI-1 expression with histological and clinical parameters. The results of endometrial carcinomas demonstrate a strong inverse correlation between KAI-1 and the expression of p53 as detected with the monoclonal DO7 antibody (Table 3). Additionally, there were significant correlations between KAI-1 expression and histological type, tumor grade, and high stage ($p<0.001$). Histological type—28 (93%) of 30 endometrioid carcinomas displayed a low or moderate cytoplasmic immunostaining for KAI-1, whereas 11 (92%) of 12 serous/clear cell carcinomas were KAI-1 negative ($p<0.001$; Table 3); grading—25 (93%) of 27 tumors of malignancy grade G1/G2 were KAI-1 positive; however, 11 (73%) of 15 high grade tumors showed no KAI-1 expression ($p<0.001$; Table 3). We also could observe a significant association between low KAI-1 expression and/or high stage ($p=0.0157$; Table 3).

KAI-1 expression in uterine tumors of stromal origin

In addition to the epithelial uterine tumors, we investigated the KAI-1 expression by the immunohistochemical analysis in the 15 sarcomas, which were mostly of the stromal origin (including five carcinosarcomas, eight low grade endometrial stromal sarcomas, and two leiomyosarcomas; Table 1). Nearly all sarcoma samples demonstrated absent or very low KAI-1 expression (Fig. 1e). Fifty percent of sarcomas

Table 3 Correlation of KAI-1 staining with the histological and clinical parameters in the endometrial carcinomas

	n	Negative KAI-1 (s=0)		Low KAI-1 (s=1–3)		Moderate KAI-1 (s=4–7)		Significance
		n	%	*n*	%	*n*	%	
FIGO grading (*n*=42)								
G1	15	0		5	(32.0%)	10	(68.0%)	
G2	12	2	(17.0%)	7	(58.0%)	3	(25.0%)	
G3	15	11	(73.0%)	4	(27.0%)	0		$p<0.0001$
Histological type (*n*=42)								
Endometrioid	30	2	(7.0%)	15	(50.0%)	13	(43.0%)	
Serous/clear cell	12	11	(92.0%)	1	(8.0%)	0		$p<0.0001$
Clinical stage (*n*=42)								
Ia/Ib	25	4	(16.0%)	10	(40.0%)	11	(44.0%)	
Ic/II	17	9	(53.0%)	6	(35.0%)	2	(12.0%)	$p=0.0157$
p53 status (*n*=42)								
Negative/low	13	0		4	(30.0%)	9	(70.0%)	
Moderate	14	3	(21.0%)	7	(50.0%)	4	(29.0%)	
High	15	10	(67.0%)	5	(33.0%)	0		$p<0.0001$
Total	42		13		16		13	

s score, *G1–G3* grade

demonstrated a strong positivity in the nucleus for p53 whereas 50% showed a lower immunoreactivity (Fig. 1f). The same inverse correlation between KAI-1 and p53 expression could be found. There was no correlation between the histological type and the KAI-1 expression pattern.

Immunoblot analysis of KAI-1 expression

To verify the results of immunohistochemistry, Western blot analysis was performed. Protein lysates were used from the 15 samples including the normal endometrium, endometrial hyperplasia, endometrial carcinomas, and uterine sarcomas (Fig. 2). The KAI-1 protein was exclusively found in the cytoplasmic/microsomal preparation and was absent from the nuclear fraction [11]. Western blot analysis with anti-KAI-1 antibody detected a 43-kDa protein band. Such specific band has been found in the normal endometrium (lanes 1, 3, 5) whereas carcinoma (lanes 2, 4, 6) and sarcoma (lane 7) samples showed reduced or negative protein expression of KAI-1. As a positive control, we used prepared cytosolic extracts from MDA-MB-231 human breast cancer cells (lane 8) which had been transfected with an expression vector for the human KAI-1 [18].

Discussion

It is known that in the oncogenic process, genetic changes result in an imbalance of cellular growth regulation, leading to uncontrolled proliferation. However, unrestrained growth does not, by itself, result in the invasion and metastasis. The ability of tumor cells to metastasize often requires additional genetic changes [20], which result in the activation and inactivation of metastasis stimulating and metastasis suppressor genes [4]. Loss of function of metastasis suppressor genes has been demonstrated to contribute to the metastatic progression of tumor cells [14].

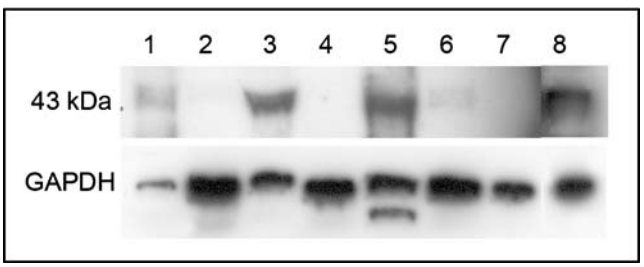

Fig. 2 Western blot analysis of KAI-1 protein expression in normal endometrium and epithelial and stromal uterine neoplasias. *Lanes 1*, *3*, and *5*—KAI-1 expression of normal endometrium (secretory phase); *lanes 2*, *4*, and *6*—uterine carcinoma (serous, clear cell type, endometrioid (G2), respectively); *lane 7*—uterine carcinosarcoma. As a positive control, cytosolic extract was prepared from MDA–MB-231 cells which had been transfected with a KAI-1 expression vector (*lane 8*). Per lane, 20 μg of protein were loaded. The blot was immunodetected with KAI-1 antibody G2, then stripped and reprobed with GAPDH antibody as a loading control. Migration of size markers is indicated in kDa

In this study, we investigated the expression pattern of the metastasis suppressor gene KAI-1 in the uterine tumors of epithelial and stromal origin compared to the normal endometrium and its correlation with the expression of p53 using immunohistochemistry. The normal endometrium displayed a strong expression of KAI-1 localized to epithelial cells throughout the menstrual cycle and also in decidualized endometrial stromal cells, as we have recently shown [11]. Most of the KAI-1 positive tumors were well-differentiated endometrioid carcinomas of malignancy grade G1/G2. Twenty-nine of the 42 analyzed endometrial carcinomas and 12 of the 15 uterine sarcomas showed a very low or absent expression of KAI-1, indicating that loss of KAI-1 expression may play an important part in the pathogenesis of such tumors. The interpretation of these results with respect to tumor progression should consider that most likely endometrioid and serous carcinomas follow the different pathways of tumorigenesis [18]. The endometrioid carcinoma is related to hyperestrogenism by the association with endometrial hyperplasia and frequent expression of estrogen and progesterone receptors, whereas serous carcinoma is unrelated to estrogen and associated with atrophic endometrium [18]. Estrogen, which is expressed throughout the cycle of the human endometrium, seems to play a role for the expression of KAI-1 in the normal endometrium, in endometrial hyperplasias, and also in the low grade endometrioid carcinomas (type I). However, the association between those and the role, these hormones that could play for the metastasis suppressor gene KAI-1 need to be elucidated. The fact that most endometrioid carcinomas show at least a weak ER and/or PR expression and often contain well-differentiated carcinoma foci favors the progression along an estrogen-driven pathway [18]. As we could demonstrate as well, most of these carcinomas showed a low or intermediate staining for KAI-1. Therefore, it could be very important to investigate the mechanism underlying the KAI-1 expression in normal endometrium as well as in endometrioid carcinomas and to answer the question if estrogen triggers or inhibits KAI-1. Type II endometrial carcinomas associated with atrophic endometrium and which are usually ER negative revealed a negative KAI-1 expression for most of the cases in our study.

It is clear that metastasis requires genetic changes to occur [6]. Loss of function of metastasis suppressor gene(s) is an important event during the progression of a tumor cell from a nonmetastatic to a metastatic phenotype [4]. KAI-1 is a recently identified metastasis suppressor gene for prostatic cancer. The expression of KAI-1 was reduced in the human cell lines derived from metastatic prostate

tumors as compared with its expression in the normal prostate tissue [28]. It was noted later that KAI-1 protein expression was downregulated during the progression of human prostate cancers [36]. Liu et al. demonstrated a frequent downregulation of the KAI-1 metastasis suppressor gene in epithelial ovarian carcinoma [21]. Another group could find a downregulation of KAI-1 in cervical and some endometrial carcinomas, but there was no differentiation between histological types and no comparison with the suppressor molecule p53, two important prognostic and diagnostic factors [22]. A loss of KAI-1 expression occurs in the advanced stages of many cancers. It is associated with a poor patient prognosis in the non-small cell lung cancer [1] and recurrence in the breast and bladder tumors [30]. Identification of patients whose tumor cells show reduced KAI-1 expression may allow them to be targeted for tailored therapy to inhibit metastasis. Strategies to restore KAI-1 expression might be explored to limit the spread of tumor cells.

Comparison of the KAI-1 immunostaining with p53 expression levels showed that most of our investigated uterine tumors with low/absent KAI-1 level displayed a strong expression of p53 (using the monoclonal antibody DO-7 which also recognizes the mutated p53). This strong expression might be the result of the accumulated mutated p53 indicating that loss of KAI-1 expression may be implicated in the progression to the development of a more aggressive histology. Normal endometrial samples did not show any immunohistochemical reaction for p53 with this antibody. However, another research group could demonstrate an increased expression of p53 (using an antibody against wild-type p53) in normal endometrium with progression throughout the menstrual cycle [32].

Here we could demonstrate for the first time an inverse correlation between KAI-1 and p53. We suppose that the loss of KAI-1 may be connected with a dysfunction of probably mutated p53—the accumulation of which is detected immunohistochemically using the antibody DO-7. p53 might be implicated in regulating KAI-1 expression [2]. Tumor cells of the human organism have very often the phenomenon of a high level of p53 protein, which is usually dysfunctional. p53 dysfunction, amplification, overexpression of human epidermal growth factor receptor 2, loss of p16 [27], and cell cycle inhibitor p27 [5] expression are considered rare and late events during progression and dedifferentiation of endometrioid carcinoma, since they are predominantly found in the grade 3 tumors, rarely in grade 1 [15]. However, dysfunctional p53 was found in 80% of stromal tumors and of nonendometrioid carcinomas [15]. p53 is the most frequently inactivated tumor suppressor in the human cancer. [12]. A variety of mechanisms can lead to such functional inactivation including genetic alteration and interaction with the oncogenic cellular or viral proteins. A substantial number of candidate p53 target genes, which contain p53-binding sites in their promoter regions and are transcriptionally activated by wild-type p53 have been successively identified [19].

In this context, the recent suggestion of a direct link between p53 and the KAI-1 gene is of particular interest. A sequence exhibiting a significant homology with the p53 consensus binding site was identified at the position −896 to −863 bp of the KAI-1 promoter. An induction of endogenous KAI-1 gene expression was detected by reverse transcriptase-polymerase chain reaction 48 h after cellular transfection of a wt-p53 expression plasmid into a human prostatic carcinoma cell line [26]. Marreiros et al. [24] could confirm that a 76-bp region (residues −922 to −847) of the KAI-1 promoter, with binding motifs for p53, AP1, and AP2, is required for the high level activity of a KAI-1 reporter in the prostate cancer. Western blotting analysis showed that an absence of wt-p53, and a loss of junB or AP2 protein expression, correlated with downregulation of KAI-1 mRNA levels. In our study, we could find a reduced or absent KAI-1 expression in the endometrial carcinomas and uterine sarcomas and a strong expression of p53 which most likely represents accumulation of mutated p53. The molecular basis for downregulation of KAI-1 expression in advanced tumors and identification of the normal functional role of KAI-1 need further investigation.

Since decreased KAI-1 expression is already seen in the early stages of endometrial cancer and in a subset of atypical complex endometrial hyperplasias, we speculate that downregulation of this gene might be an important part in the development of endometrial cancer and sarcomas.

Acknowledgements The authors would like to thank Mr. J. Koppelmeyer for the help with the photographic work and Mrs. B. Kelp and I. Brand for the technical assistance. This work was supported in part by a grant from the Deutsche Krebshilfe foundation to AM.B. (Grant No. 107170).

Conflict of interest statement We declare that we have no conflict of interest.

References

1. Adachi M, Taki T, Leki Y, Huang CL, Higashiyama M, Miyake M (1996) Correlation of KAI-1/CD82 gene expression with good prognosis in patients with non small cell lung cancer. Cancer Res 56:1751–1755
2. Ashcroft M, Vousden KH (1999) Regulation of p53 stability. Oncogene 18:7637–7643

3. Atkinson B, Ernst CS, Ghrist BF, Herlyn M, Blaszczyk M, Ross AH, Herlyn D, Steplewski Z, Koprowski H (1984) Identification of melanoma-associated antigens using fixed tissue screening of antibodies. Cancer Res 44:2577–2581
4. Aznavoorian S, Murphy AN, Stetler-Stevenson WG, Liotta LA (1993) Molecular aspects of tumor cell invasion and metastasis. Cancer 71:1368–1383
5. Bamberger AM, Riethdorf L, Milde-Langosch K, Bamberger CM, Thuneke I, Erdmann I, Schulte HM, Löning T (1999) Strongly reduced expression of the cell cycle inhibitor p27 in endometrial neoplasia. Virchows Arch 434:423–428
6. Chen Z, Mustafa T, Trjanowicz B, Brauckhoff M, Gimm O, Schmutzler C, Köhrle J, Holzhausen HJ, Kehlen A, Klonisch T, Finke R, Henning D, Hoang-Vu C (2004) CD82, and CD63 in thyroid cancer. Int J Mol Med 14:517–527
7. Dong JT, Lamb PW, Rinker-Schaeffer CW, Vukanovic J, Ichikawa T, Isaacs JT, Barrett JC (1995) KAI-1, a metastasis suppressor gene for prostate cancer on human chromosome 11p11.2. Science 268:884–886
8. Dong JT, Suzuki H, Pin SS, Bova GS, Schalken JA, Isaacs WB, Barrett JC, Isaacs JT (1996) Down-regulation of the KAI-1 metastasis suppressor gene during the progression of human prostatic cancer infrequently involves gene mutation or allelic loss. Cancer Res 56:4387–4390
9. Esteller M, Levine R, Baylin SB, Ellenson LH, Herman JG (1998) MLH1 promoter hypermethylation is associated with the microsatellite instability phenotype in sporadic endometrial carcinomas. Oncogene 17:2413–2417
10. Fukuchi T, Sakamoto M, Tsuda H, Maruyama K, Nozawa S, Hiroshashi S (1998) β-catenin mutations in carcinoma of the uterine endometrium. Cancer Res 58:3526–3528
11. Gellersen B, Briese J, Oberndörfer M, Redlin K, Samalecos A, Richter DU, Löning T, Schulte HM, Bamberger AM (2007) Expression of the metastasis suppressor KAI-1 in decidual cells at the human maternal-fetal interface: regulation and functional implications. Am J Pathol 170(1):126–139
12. Hainaut P, Hernandez T, Robinson A, Rodriguez-Tome P, Flores T, Hollstein M, Harris CC, Montesano R (1998) IARC database of p53 gene mutations in human tumors and cell lines: updated compilation, revised formats and new visualization tools. Nucleic Acids Res 26:205–213
13. Higashiyama M, Taki T, Ieki Y, Adachi M, Huang CL, Koh T, Kodama K, Doi O, Miyake M (1995) Reduced motility related protein-1 (MRP-1/CD9) gene expression as a factor of poor prognosis in non-small cell lung cancer. Cancer Res 55:6040–6044
14. Ichikawa T, Ichikawa Y, Isaacs JT (1991) Genetic factors and metastatic potential of prostatic cancer. Cancer Surv 11:35–42
15. Ioffe OB, Papadimitriou JC, Drachenberg CB (1998) Correlation of proliferation indices, apoptosis, and related oncogene expression (bcl-2 and c-erbB-2) and p53 in proliferative, hyperplastic, and, malignant endometrium. Human Pathol 29:1150–1159
16. Kohler MF, Berchuck A, Davidoff AM, Humphrey PA, Dodge RK, Iglehart JD, Soper JT, Clarke- Pearson DL, Bast RC Jr, Marks JR (1992) Overexpression and mutation of p53 in endometrial carcinoma. Cancer Res 52:1622–1627
17. Kurman RJ (1987) Endometrial carcinoma. Springer Verlag, New York
18. Lax SF (2004) Molecular genetic pathways in various types of endometrial carcinoma: from a phenotypical to a molecular-based classification. Virchows Arch 444:213–223
19. Levine AJ (1997) p53, the cellular gatekeeper for growth and division. Cell 88:323–331
20. Liotta LA, Steeg PS, Stetler-Stevenson WG (1991) Cancer metastasis and angiogenesis: an imbalance of positive and negative regulation. Cell 64:327–336
21. Liu FS, Dong JT, Chen JT, Hsieh YT, Ho ES, Hung MJ (2000) Frequent down-regulation and lack of mutation of the KAI-1 metastasis suppressor gene in epithelial ovarian carcinoma. Gynecol Oncol 78:10–15
22. Liu FS, Dong JT, Chen JT, Hsieh YT, Lin AJ, Ho ES, Hung MJ, Lu CH, Chiou LC (2003) KAI-1 metastasis suppressor protein is down-regulated during the progression of human endometrial cancer. Clin Cancer Res 9:1393–1398
23. Maecker HT, Todd SC, Levy S (1997) The tetraspanin superfamily: molecular facilitators. FASEB J 11:428–442
24. Marreiros A, Dudgeon K, Dao V, Grimm MO, Czolij R, Crossley M, Jackson P (2006) KAI-1 promoter activity is dependent on p53, junB and AP2: evidence for a possible mechanism underlying loss of KAI-1 expression in cancer cells. Oncogene 24:637–649
25. Marth C, Daxenbichler G (1996) Prognostic factors in endometrial cancer. In: Pasqualini JR, Katzenellenbogen BS (eds) Hormone-dependent cancer. Marcel Dekker, New York, pp 499–508
26. Mashimo T, Watabe M, Hirota S, Hosobe S, Miura K, Tegtmeyer PJ, Rinker-Schaeffer CW, Watabe K (1998) The expression of the KAI-1 gene, a tumor metastasis suppressor, is directly activated by p53. Proc Natl Acad Sci 95:11307–11311
27. Milde-Langosch K, Riethdorf L, Bamberger AM, Löning T (1999) P16/MTS1 and pRB expression in endometrial carcinomas. Virchows Arch 434:23–28
28. Mueck AO, Seeger H (2004) Hormone therapy after endometrial cancer. Horm Res 62:40–48
29. Murphy GP, Lawrence W Jr, Lenhard RE Jr (eds) (1995) In: American Cancer Society textbook of clinical oncology. 2nd edn. American Cancer Society, Atlanta, GA, pp 573–574
30. Ono M, Handa K, Withers DA, Hakomori SI (1999) Motility inhibition and apoptosis are induced by metastasis-suppressing gene product CD82 and its analogue CD9, with concurrent glycosylation. Cancer Res 59:2335–2339
31. Press MF, Scully RE (1985) Endometrial "sarcomas" complicating ovarian thecoma, polycystic ovarian disease and estrogen therapy. Gynecol Oncol 21:135–154
32. Pohnke Y, Schneider-Merck T, Fahnenstich J, Kempf R, Christian M, Milde-Langosch K, Brosens JJ, Gellersen B (2004) Wild-type p53 protein is up-regulated upon cyclic adenosine monophosphate-induced differentiation of human endometrial stromal cells. J Clin Endocrinol Metab 89:5233–5244
33. Riethdorf L, Begemann C, Riethdorf S, Milde-Langosch K, Löning T (1996) Comparison of benign and malignant endometrial lesions for their p53 state, using immunohistochemistry and temperature-gradient gel electrophoresis. Virchows Arch 428:47–51
34. Takaoka A, Hinoda Y, Sato S, Itoh F, Adachi M, Hareyama M, Imai K (1998) Reduced invasive and metastatic potentials of KAI-1-transfected melanoma cells. Jpn J Cancer Res 89:397–404
35. Wade K, Quinn MA, Hammond I (1990) Uterine sarcoma: steroid receptors and response to hormonal therapy. Gynecol Oncol 39:364–367
36. Wright MD, Tomlinson MG (1994) The ins and outs of the transmembrane 4 superfamily. Immunol Today 15:588–594

Virchows Arch (2008) 453:97–106
DOI 10.1007/s00428-008-0618-5

ORIGINAL ARTICLE

Involvement of bone marrow-derived endothelial progenitor cells in glomerular capillary repair in habu snake venom-induced glomerulonephritis

Yoko Abe-Yoshio · Katsushige Abe · Masanobu Miyazaki · Akira Furusu · Tomoya Nishino · Takashi Harada · Takehiko Koji · Shigeru Kohno

Received: 29 June 2007 / Revised: 7 April 2008 / Accepted: 14 April 2008 / Published online: 13 June 2008

Abstract Neovasculogenesis is essential in tissue remodeling. Endothelial progenitor cells (EPCs) mobilize from bone marrow (BM) and participate in neovasculogenesis. This study examined the role of EPCs in a model of reversible glomerulonephritis induced by habu snake venom (HSV). Lethally irradiated FVB/N wild-type mice were transplanted with BM cells from donor transgenic mice expressing β-galactosidase gene under the control of endothelial-specific *tie-2* promoter. HSV or saline was injected intravenously after BM transplantation (BMT). The kidneys were removed before injection and at days 1, 7, 28, and 56 after injection. β-Galactosidase-expressing cells were identified by X-gal staining. The expressions of CD31 (endothelial cell marker) and vascular endothelial cell growth factor (VEGF) in renal tissues were examined by immunohistochemistry. In BMT mice injected with saline, few X-gal-positive cells were detected in glomeruli. In HSV-injected mice, X-gal-positive EPCs were increased in damaged glomeruli, reaching maximum at day 28. Recovery of glomeruli was observed at day 56 in association with reduction of X-gal-positive EPCs. VEGF overexpression was detected in glomerular epithelial and endothelial cells, mesangial cells, and EPCs. Our results indicated that EPCs were mobilized into the damaged glomeruli, suggesting EPCs participation in glomerular capillary repair of damaged glomeruli in HSV-induced glomerulonephritis.

Keywords Endothelial progenitor cell · Angiogenesis · Vascular endothelial cell growth factor (VEGF)

Y. Abe-Yoshio (✉) · K. Abe (✉) · M. Miyazaki · A. Furusu · T. Nishino · S. Kohno
Division of Nephrology, Second Department of Internal Medicine, Nagasaki University School of Medicine,
1-7-1 Sakamoto,
Nagasaki 852-8501, Japan
e-mail: yyoshiwo@hotmail.com
e-mail: rukonyan@ga2.so-net.ne.jp

T. Harada
Division of Renal Care Unit,
Nagasaki University School of Medicine,
Nagasaki, Japan

T. Koji
Department of Histology and Cell Biology,
Nagasaki University School of Medicine,
Nagasaki, Japan

Introduction

Neovasculogenesis is an important process associated with both physiological and pathological conditions such as organ development, menstrual cycle, wound healing, tumor growth, and ischemic diseases [3, 6, 10–12, 26]. During embryonic development, new blood vessels are formed from primitive endothelial progenitor cells (EPCs), a process referred to as vasculogenesis. On the other hand, postnatal neovascular development is thought to result from proliferation, migration, and remodeling of fully differentiated endothelial cells derived from pre-existing blood vessels, i.e., angiogenesis [33]. Recent studies showed the presence of bone marrow-derived EPCs in systemic circulation. Their number was augmented in response to certain cytokines and/or tissue ischemia, and home to as well as incorporate into the site of neovascularization during hindlimb ischemia, postmyocardial infarction, hormone-induced ovulation, wound healing, corneal neovascularization, and cerebral ischemia [2, 4, 15, 21, 31, 37, 40].

In models of reversible glomerulonephritis such as anti-Thy-1.1 antibody-induced (Thy-1) glomerulonephritis and habu snake venom (HSV)-induced glomerulonephritis, it has been postulated that proliferation of glomerular endothelial cells participates in capillary repair and restoration of glomerular architecture [17, 25, 37]. In addition, other studies demonstrated that the destruction of glomerular capillary network and the subsequent incomplete angiogenic capillary repair lead to glomerular sclerosis in anti-glomerular basement membrane (GBM) glomerulonephritis [36]. These findings suggest the importance of glomerular endothelial cell proliferation during the glomerular capillary regeneration process. On the other hand, the expression of angiogenic growth factor, vascular endothelial cell growth factor (VEGF), is highly up-regulated in the damaged glomeruli [17, 24], and systemic administration of VEGF enhances the capillary repair and prevents the deterioration of glomerular structure from progressing to glomerular sclerosis in experimental glomerulonephritis induced by anti-Thy-1.1 antibody and HSV [29]. These results suggest that VEGF is a key factor in angiogenic glomerular capillary repair and that glomerular endothelial cell regeneration is an important process for glomerular reconstruction after glomerular injury.

In the present study, we investigated whether bone marrow (BM)-derived EPCs are the source of glomerular endothelial cells and if so, determine the association between recruited EPCs and glomerular capillary repair in a model of HSV-induced reversible glomerulonephritis.

Materials and methods

Mice

FVB/N-TgN [TIE2LacZ] 182Sato male mice (TIE2/LZ mice) of 25±3 g body weight (mean ± SD), obtained from The Jackson Laboratory (Bar Harbor, ME, USA), were used as donors for bone marrow transplantation (BMT). This transgenic mouse constitutively expresses β-galactosidase encoded by *lacZ* under the transcriptional regulation of an endothelial cell-specific promoter, Tie-2 [4, 37]. In a preliminary study, we ascertained that β-galactosidase-expressing cells also expressed Tie-2, suggesting that the expression of β-galactosidase was restricted to endothelial cells in the donor mouse (data not shown). FVB/N wild-type male mice (WT mice) were also purchased (The Jackson Laboratory) and served as recipients of BMT. All mice were housed in standard rodent cages, in rooms set at constant ambient temperature (22±1°C) and humidity (85%), with 10 h of lights-on each day. Drinking water and pellet rodent food were provided ad libitum.

Experimental design

The experimental protocol was inspected by the Animal Care and Use Committee of Nagasaki University School and approved by the President of Nagasaki University School. BM cells were obtained by flushing the tibias and femurs of age-matched donor transgenic mice. Recipient mice, 7-week-old, were lethally irradiated (11 Gy) and injected intravenously with 1×10^6 BM cells. Subsequent analysis showed no radiation-induced glomerular injury in this model, suggesting that the effect of irradiation on glomerular capillary recovery is marginal. Preliminary studies demonstrated that the BM of the recipient mice was reconstituted 4 weeks after the transplantation [4, 31, 37].

At that stage, transplanted mice were injected with HSV (*Trimeresurus flavoviridis*; Wako Pure Chemical Industries, Osaka, Japan) dissolved in saline at a dose of 2 mg/kg body weight intravenously (HSV group: n=25). Mice of another group were injected with saline alone (S group: n=25). Mice were sacrificed before injections and at days 1, 7, 28, or 56 after injections (n=5, each), and renal tissues were dissected out carefully. Tissues were fixed with 4% paraformaldehyde (PFA) immediately after sampling for 24 h and embedded in paraffin and cut into 4-μm-thick sections for histological assessment of renal injury. Frozen tissues were also prepared by mounting in optimal cutting temperature compound (Miles, Inc., Elkhart, IN, USA) and rapidly frozen in dry ice and stored at −80°C until use. Fresh frozen tissues were cut into 4-μm-thick sections using a microtome and placed onto aminopropyltriethoxysilane-coated slide glasses.

Histological and immunohistochemical examination

To assess the morphological changes in the kidney, paraffin-embedded tissue sections were stained with periodic acid-Schiff reaction. We identified β-galactosidase-expressing cells using the X-gal Staining Assay Kit (A10300K, Gene Therapy Systems, San Diego, CA, USA) and immunohistochemically by using rabbit anti-β-galactosidase antibody. Immunohistochemical staining was performed using the following antibodies: (1) rat anti-mouse CD31 antibody diluted 1/50 (1625-01, Southern Biotechnology, Birmingham, AL, USA), which was used as a marker of endothelial cells; (2) rabbit anti-Tie-2 antibody diluted 1/200 (sc-324, Santa Cruz Biotechnology, Santa Cruz, CA, USA), which is the receptor for angiopoietin-1 and angiopoietin-2; (3) rabbit anti-VEGF antibody diluted 1/100 (sc-507, Santa Cruz Biotechnology); (4) rabbit anti-β-galactosidase antibody diluted 1/100 (ab616, Abcam, Cambridge, UK); and (5) horseradish peroxidase (HRP)-labeled dextran polymer-conjugated mouse anti-proliferating cell nuclear antigen (PCNA) antibody (U7032, DAKO, Glostrup, Denmark) as a marker of proliferating cells. To block endogenous peroxidase, renal

sections were reacted with methanol containing 0.3% H_2O_2 for 15 min at room temperature. Indirect immunohistochemical technique was used for the detection of CD31, Tie-2, and β-galactosidase. For CD31 and β-galactosidase antibodies, frozen sections were fixed with acetone for 15 min at room temperature and incubated for 30 min with a blocking buffer containing 5% normal goat serum, 5% fetal calf serum, 5% bovine serum albumin, and 20% normal swine serum in phosphate-buffered saline (PBS). The sections were then reacted with the primary antibodies diluted in the same blocking buffer. For a better identification of CD31-positive capillaries, we performed the three-layer method, as described previously [1]. After reacting with anti-CD31 antibody at room temperature for 1 h, the sections were reacted with HRP conjugated rabbit anti-rat immunoglobulins (DAKO P0450), as the secondary antibody diluted 1/100 for 30 min at room temperature and then, reacted with HRP-conjugated swine anti-rabbit immunoglobulins (DAKO P0399) as the third antibody diluted 1/50 for 30 min at room temperature. For β-galactosidase antibody, sections were reacted with HRP-conjugated swine anti-rabbit immunoglobulins diluted 1/50 for 30 min at room temperature and a complex of rabbit anti-HRP antibody and HRP (DAKO Z0113) diluted 1/100 for 30 min at room temperature. For Tie-2 staining, frozen sections were fixed with 4% PFA for 15 min at room temperature and then incubated for 30 min with the aforementioned blocking buffer. Subsequently, the sections were reacted with anti-Tie-2 antibody for 1 h at room temperature and HRP-conjugated swine anti-rabbit immunoglobulins diluted 1/50 for 30 min at room temperature and a complex of rabbit anti-HRP antibody and HRP diluted 1/100 for 30 min at room temperature. For VEGF staining, we applied the peroxidase and avidin–biotin complex technique using Vectastatin *Elite* ABC kit (Vector Laboratories, Burlingame, CA, USA), which yielded the strongest signal for VEGF. For blocking of endogenous biotin, deparaffinized tissue sections were incubated with avidin D blocking solution (SP-2001, Vector Laboratories) for 15 min, rinsed with buffer, and incubated with the biotin blocking solution (SP-2001, Vector Laboratories) before reacting with the first antibody. Subsequently, the tissue sections were reacted with the primary antibody for 16 h at 4°C. We used direct immunohistochemical technique for PCNA staining. After deparaffinization, the sections were incubated for 30 min with a blocking buffer similar to that described above and then reacted with anti-PCNA antibody for 1 h at room temperature. Reaction products were visualized by treating sections with H_2O_2 and 3′,3-diaminobenzidine tetrahydrochloride. Finally, the sections were counterstained with methyl green and mounted.

Tissue sections were also double-stained for X-gal and Tie-2 or X-gal and VEGF. After X-gal staining using the X-gal staining assay kit, sections were incubated with each antibody and stained as described above. Indirect immunohistochemistry was performed using β-galactosidase antibody for CD31/β-galactosidase double staining. After CD31 staining as described above, sections were washed in PBS to stop the color reaction and incubated with double staining enhancer (50-056, Zymed Laboratories Inc., San Francisco, CA, USA). Thereafter, the sections were reacted with anti-β-galactosidase antibody followed by incubation with HRP-conjugated antibody as mentioned above. A second chromogen, True blue (71-00-64, KPL, Gaithersburg, MD, USA), was then applied, which stained positive cells in blue. The tissue sections were not counterstained with methyl green, since this counterstaining could interfere with the color from the chromogen.

Immunostaining with irrelevant rat IgG2a (0117-01, Southern Biotechnology) or normal rabbit immunoglobulin (DAKO X0903), as negative controls, yielded no positive signal in erythrocytes or any other cells.

Fifteen glomeruli from each animal, each with an equatorial plane cross-section, were analyzed. We counted the number of CD31-positive glomerular capillary loops, X-gal-positive cells, and VEGF-positive cells in each glomerular cross-section in 15 glomeruli per kidney of five mice at each time point. In this study, CD31-positive glomerular capillary loops represented glomerular capillary loops with CD31-positive area occupying more than 30% of the entire capillary loop. Based on preliminary studies, the 30% cutoff value was selected arbitrarily in order to avoid overestimating the count by the inclusion of structures that could not be identified with certainty as capillary loops. Thus, we used sections with well-preserved tissue morphology to identify the CD31-positive capillary loops.

Statistical analysis

Data were expressed as mean ± SD. Differences among groups were examined for statistical significance using repeated measures ANOVA (Bonferroni/Dunn test). A P value less than 0.05 denoted the presence of statistically significant difference.

Results

Histopathological changes and alteration of glomerular endothelial cells in HSV-induced glomerulonephritis

In the S group, no mesangiolysis or mesangial matrix expansion was observed, and the number of CD31-positive glomerular capillary loops did not change throughout the experimental period (Fig. 1a and b). On the other hand,

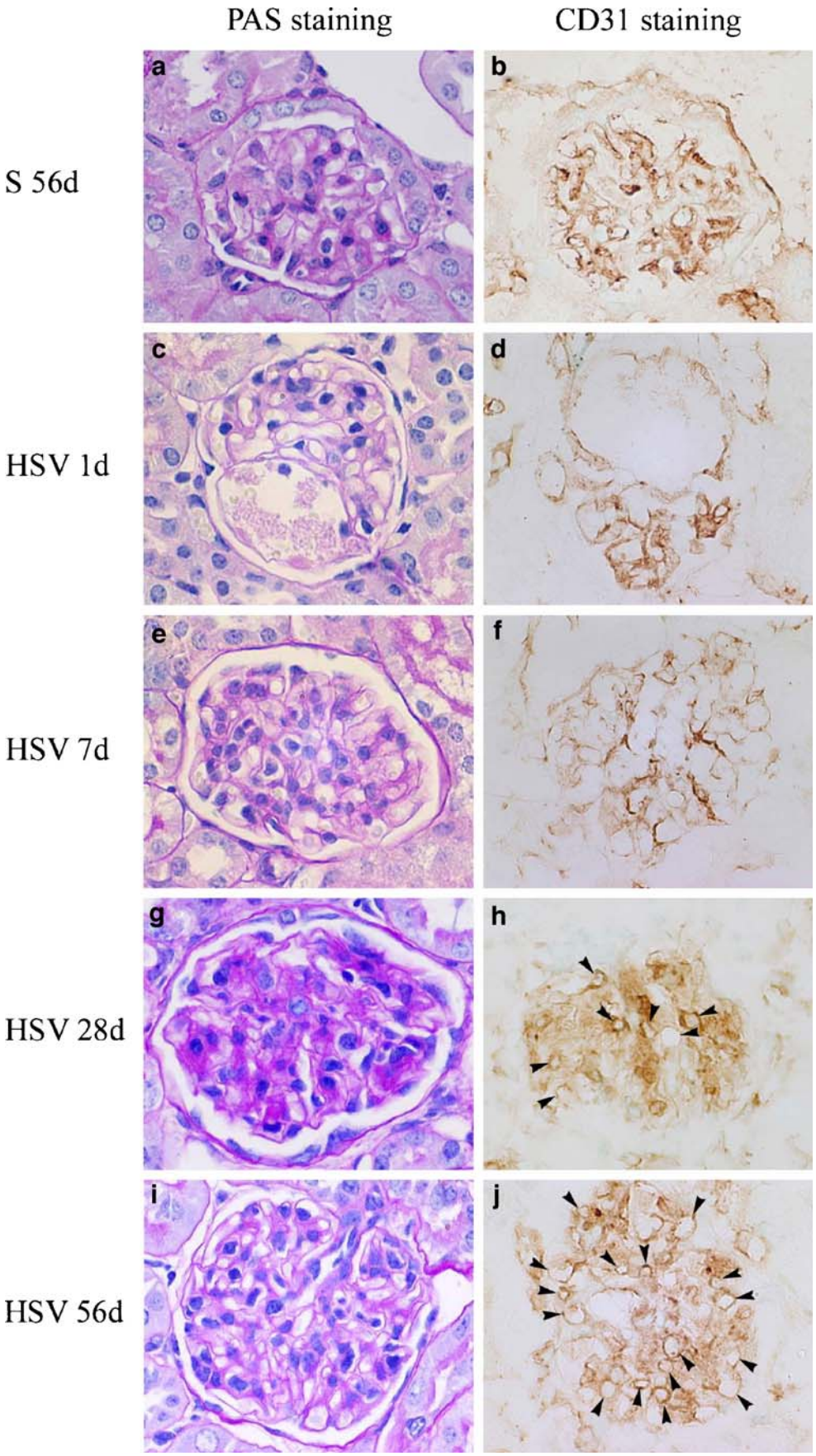

Fig. 1 Histological examination and CD31 expression. In saline-injected mice (S group), no morphological changes such as mesangiolysis and mesangial matrix expansion were observed in glomeruli (**a** and **b**: S 56d). On the other hand, note the ballooning of glomerular capillary and reduction of CD31-positive endothelial cells in habu snake venom (HSV)-injected mice (HSV group) at day 1 (**c** and **d**: HSV 1d). At day 7, reduction of cystic lesions accompanied the increased number of CD31-positive capillary loops (**e** and **f**: HSV 7d). At day 28, mesangial matrix expanded and the number of CD31-positive capillary number was decreased (**g** and **h**: HSV 28d). At day 56, mesangial expansion was reduced and CD31-positive capillary number returned to almost baseline levels, following glomerular structure repair (**i** and **j**: HSV 56d). **a**, **b**, **e**, **g**, and **i**: PAS staining. **b**, **d**, **f**, **h**, and **j**: immunohistochemistry for CD31. Magnification: ×400. *Arrowheads*: CD31-positive capillary loops

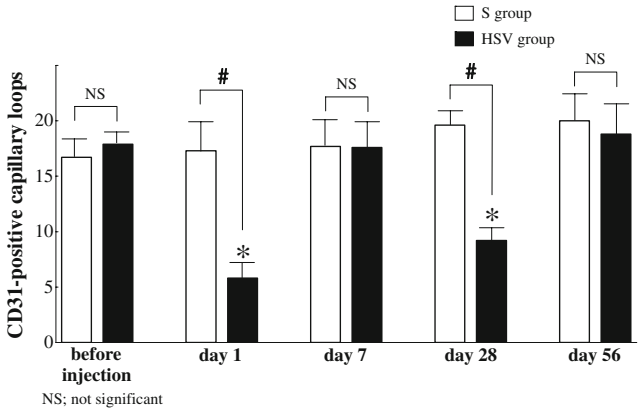

Fig. 2 Quantitative analysis of the number of CD31 in glomeruli. We counted the number of CD31-positive glomerular capillary loops per cross-section of the glomerulus in 15 glomeruli per kidney of five mice at each time point. Data are mean ± SD. *$P<0.01$ versus before injection, days 7 and 56 in HSV group. #$P<0.01$ versus the S group

injection of HSV induced mesangiolysis at day 1, as reported previously [30]. Loss of the mesangial cells led to ballooning of glomerular capillary loops and induced cystic lesions, accompanied by a significant reduction in the number of CD31-positive capillary loops (Figs. 1c,d and 2). At day 7, after acute mesangial injury, the cystic lesions were diminished (Fig. 1e), and the number of glomerular capillary loops increased to reach the levels noted at baseline before HSV injection (Figs. 1f and 2). Subsequently, the mesangial matrix expanded and the number of CD31-positive capillary loops diminished. These changes were most extensive and significant at day 28 (Figs. 1g,h and 2). At day 56, mesangial matrix expansion was further diminished, together with further increase in the number of CD31-positive capillary loops (Fig. 2). This resulted in reconstitution of the glomerular structure and the final appearance resembled normal glomeruli (Fig. 1i and j).

Involvement of BM-derived EPCs in glomeruli

To identify BM-derived EPCs, we used the X-gal staining technique. Before HSV injection, few cells were positive for X-gal staining in glomeruli (Fig. 3a; $n=0.9\pm0.8$). In HSV group, a small number of X-gal-positive cells was detected in damaged glomeruli at days 1 ($n=1.8\pm1.1$) and 7 ($n=2.1\pm1.3$; Fig. 3b). At day 28, the number of X-gal-positive EPCs was significantly higher ($n=2.9\pm1.7$) in parallel with mesangial matrix expansion (Fig. 3c and Table 1). Then, the number of X-gal-positive cells decreased gradually, but they were still found in the glomeruli at day 56 ($n=2.3\pm1.0$; Fig. 3d). In mice of the S group, a few cells positive for X-gal were observed from day 1 to day 56 in this experiment (Fig. 3e and Table 1).

In the HSV group, some cells double-stained for CD31 and β-galactosidase were identified from day 1 to day 56 (Fig. 4 and Table 1). The number of such cells was significantly higher at day 28 but was decreased at day 56 in HSV group (Table 2).

VEGF and PCNA expression during HSV-induced glomerulonephritis

Before HSV injection, few cells were positive for VEGF in glomeruli (Fig. 5a and Table 1). In HSV-injected mice, the number of VEGF-positive cells was very small at days 1 and 7 (Fig. 5b and c, respectively and Table 1), and their number was the same as that in non-HSV-injected mice (Table 1). At day 28, when mesangial matrix expansion and reduction of CD31-positive capillary loops were noted, the number of VEGF-positive cells was significantly increased in the damaged glomeruli (Fig. 5d and Table 1). VEGF was expressed mainly in glomerular epithelial cells and in some mesangial cells and glomerular endothelial cells. Reconstruction of glomerular capillaries was associated with a decrease in the number of VEGF-positive cells at day 56 (Fig. 5e and Table 1). In the tubulointerstitial area, a few tubular epithelial cells were also positive for VEGF at days 1, 7, 28, and 56. In mice of the S group, a weak expression of VEGF in glomeruli was observed throughout the experimental period (1.2 ± 1.2, 1.8 ± 1.2, 1.3 ± 0.2, and 0.9 ± 0.8 cells/glomerulus, at days 1, 7, 28, and 56, respectively). We also performed double staining for VEGF and X-gal in the same sections to examine the expression of VEGF on BM-derived endothelial cells. In glomeruli obtained from HSV-injected mice, some X-gal-positive BM-derived EPCs were also positive for VEGF in this model at days 1, 7, 28 (Fig. 5d), and 56. We also examined the expression of PCNA, a marker of cell proliferation. PCNA-positive cells were identified in damaged glomeruli from day 1 to day 56. The number of cells positive for PCNA was very small; however, a statistically significant increase in the number of PCNA-positive cells was only observed at day 28 in HSV-injected mice (day 7: Fig. 6a; day 28: Fig. 6b and Table 1).

Discussion

The present study demonstrated that the BM-derived endothelial cells were mobilized into glomeruli and the number of BM-derived cells was increased in injured glomeruli in HSV-induced glomerulonephritis. We also showed that BM-derived endothelial cells were the potential source of glomerular endothelial cells, and that these cells are involved in the reconstruction of glomerular structure through VEGF expression in HSV-induced glomerulonephritis.

Transplantation of TIE2/LZ BM cells into syngeneic WT mice is a well-established method for examining the influence of EPCs in BM cells on neovasculogenesis

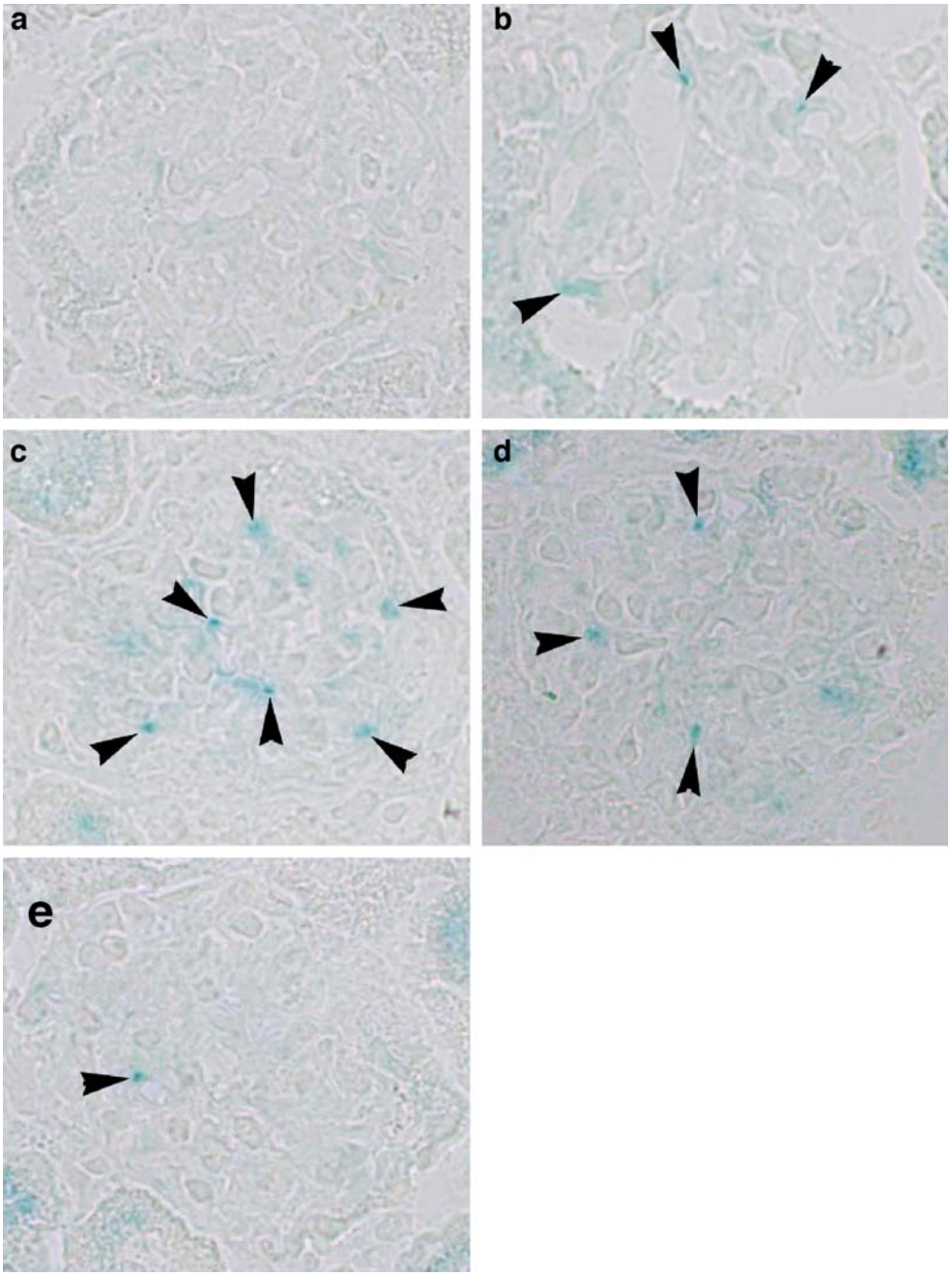

Fig. 3 X-gal staining of the glomeruli. In saline-injected mice, few cells were positive for X-gal staining at day 1 (**a**). In comparison, a larger number of X-gal-positive cells was detected in glomeruli showing cystic lesions in HSV-injected mice at day 1 (**b**). At day 28, note the large number of X-gal-positive cells (**c**) and X-gal-positive cells were still observed at day 56 (**d**). In mice of the S group at day 56, few X-gal-positive cells were observed (**e**). Magnification: ×400. *Arrowheads*: X-gal-positive cells

because the expression of β-galactosidase is restricted to Tie-2-expressing endothelial cells in TIE2/LZ mouse [4, 31, 40]. In fact, accumulated evidence suggests the contribution of BM-derived endothelial cells to neovascularization in BMT animal models, such as hindlimb ischemia, myocardial infarction, retinal ischemia, cutaneous wounds, and tumor growth [4, 8, 22, 23, 27, 39]. In the present study, we used the HSV-induced glomerulonephritis model; a single injection of HSV caused mesangial matrix lysis and exhibited toxic effects on the endothelium, leading to ballooning of glomerular capillaries, formation of microaneurysms, and loss of endothelial cells, followed by a repair phase characterized by mesangial and endothelial cell proliferation [7, 25, 30]. In our TIE2/LZ BM cell-transplanted mice, we demonstrated that HSV-induced glomerular changes were associated with immigration of BM-derived Tie-2 expressing endothelial cells. At day 28, we observed an increase in the number of BM-derived endothelial cells compared with the control, followed by a slight decrease over the next 4 weeks. Following the increased migration of BM-derived endothelial cells, CD31-positive glomerular capillaries were also increased in the damaged glomeruli. These results indicate that glomerular capillary repair cannot only be attributed to

Table 1 Number of cells positive for X-gal, VEGF and PCNA

	Number of positive cells/glomerulus									
	Day 0		Day 1		Day 7		Day 28		Day 56	
	S	HSV	S	HSV	S	HSV	S	HSV	S	HSV
X-gal	0.8±0.7	0.9±0.8	0.9±0.8	1.8±1.1	1.0±0.8	2.1±1.3	1.1±0.6	2.9±1.7*,**	1.1±1.0	2.3±1.0
VEGF	0.8±0.7	0.9±0.8	1.2±1.2	1.6±1.2	1.8±1.2	0.9±0.8	1.3±0.2	8.3±2.4*,**	0.9±0.8	1.7±1.2
PCNA	N.D.	0	N.D.	1.3±1.3	N.D.	1.5±1.0	N.D.	4.6±1.2***	N.D.	1.8±1.3

Data are mean ± SD, $n=5$ for each day
S Saline group, *HSV* habu snake venom group, *N.D.* not determined
*$P<0.01$ versus day 0 in HSV group; **$P<0.01$ versus S group; ***$P<0.01$ versus day 0

proliferation of resident endothelial cells but also bone marrow-derived endothelial cells.

In the present study, we could not determine the relative contribution of BM-derived endothelial cells to glomerular capillary repair compared to residential endothelial regeneration. Extensive endothelial cell loss and proliferation of these cells have been reported in HSV-induced glomerulonephritis [25]. Since the number of migrating BM-derived endothelial cells in glomeruli was clearly less than that of resident endothelial cells, we presume that the number of endothelial cells of BM origin is limited. Previous studies showed the differentiation of BM-derived cells to renal cells in humans and animals [9, 14, 16, 18, 28, 32, 34]. For example, Poulsom et al. [32] identified frequent Y chromosomes containing tubular and glomerular epithelial cells within the kidneys of female mice that had received BM transplantation from male mice. Other studies also demonstrated that BM cells could give rise to mesangial and glomerular endothelial cells [9, 14, 16, 18, 34] and that the ratio of BM-derived cells to glomerular cells was only 11–12% [18]. More recently, Lin et al. [28] demonstrated that in BM cell-transplanted mice, the kidneys contained 8% BM-derived cells at 28 days after ischemia–reperfusion injury. Among them, 10.6% were glomerular cells, of which 3.8% were glomerular endothelial cells. We showed that β-galactosidase expressing cells were also positive for CD31 staining, suggesting that BM-derived endothelial cells have the capacity to home to injured glomeruli and differentiate into glomerular endothelial cells. Interestingly, we also showed that the number of β-galactosidase-positive CD31-positive cells was increased at day 28, but decreased at day 56. While the exact reason for this decrease is not clear, recent studies demonstrated apoptosis of glomerular endothelial cells in anti-GBM-GN [35, 36]. Since apoptosis is widely recognized as a controlled mode of cell death, endothelial cell apoptosis might explain the disappearance of endothelial cells during capillary regression. Further studies are warranted to examine the contribution of BM-derived cells to glomerular capillary repair by using perfusion fixation of the kidneys or ultrastructural examination using electron microscopy.

We also demonstrated that BM-derived endothelial cells did not only migrate into the damaged glomeruli but also secreted a potent angiogenic ligand, VEGF, in this model. VEGF is a strong chemoattractant factor for EPCs from BM, and VEGF administration promotes mobilization of EPCs to peripheral blood [5, 13, 20]. Previous studies demonstrated that EPCs express and secrete a variety of

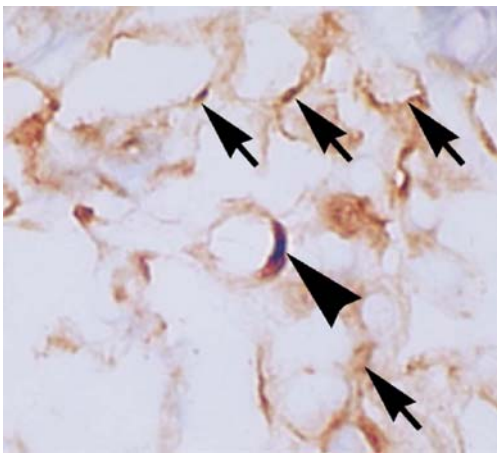

Fig. 4 Double immunostaining for CD31 (*brown*) and β-galactosidase (*blue*). Note that some of CD31-positive cells also expressed β-galactosidase (*arrowhead*), while others were not (*arrow*). Magnification: ×800

Table 2 Number of CD31- and β-galactosidase-double positive cells in HSV-injected mice

	Number of double-positive cells/glomerulus				
	Day 0	Day 1	Day 7	Day 28	Day 56
CD31/β-galactosidase	0.8±0.8	1.6±0.8	1.5±1.2	3.0±1.3*	2.3±1.3

Data are mean ± SD, $n=5$ for each day
*$P<0.01$ versus day 0

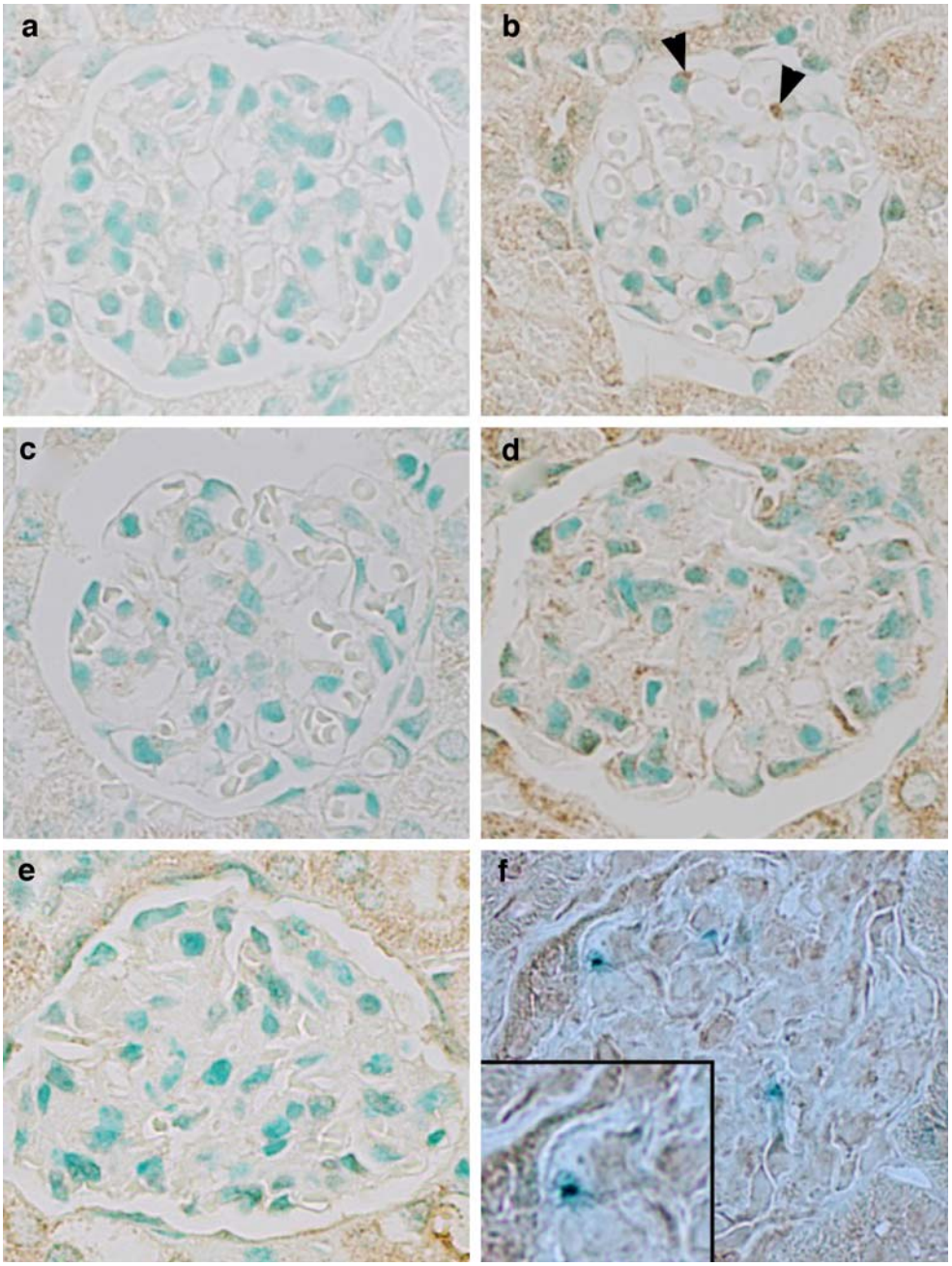

Fig. 5 Immunohistochemistry for VEGF in HSV-induced glomerulonephritis. In mice of the S group, VEGF expression was not observed in glomeruli at day 56 (**a**). In HSV group, some cells were positive for VEGF in the damaged glomeruli at day 1 (***b***; *arrowheads*). At day 7, the increased number of glomerular capillaries was associated with diminished VEGF expression (**c**). Subsequently, reduction of glomerular capillaries was associated with increased number of VEGF-expressing cells at day 28 (**d**). This was followed by reduced expression of VEGF with recovery of glomerular architecture at day 56 (**e**). Double staining for VEGF (*brown*) and X-gal (*blue*) in the same section of HSV-group showed that some VEGF-positive cells were also positive for X-gal (**f**, day 28). **a**–**f** Magnification: ×400. *Inset* in (**f**), magnification: ×800. *Arrowheads*: VEGF-positive cells

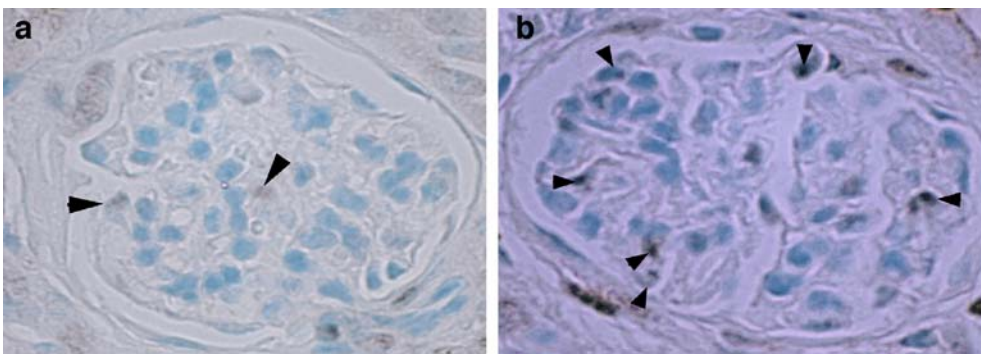

Fig. 6 Immunohistochemistry for PCNA. In glomeruli of HSV-injected mice, a few PCNA-positive cells were observed at day 7 (**a**), but their number increased at day 28 (**b**). Magnification: ×400. *Arrowheads*: PCNA-positive cells

growth factors, including VEGF [19, 38]. Furthermore, it has been suggested that EPC-induced neovascularization is not only due to the incorporation of EPC into the newly formed vessels but also influenced by the release of pro-angiogenic factors in a paracrine manner [19, 38]. In our study, we showed that the increase in the number of VEGF-positive cells paralleled the influx of BM-derived endothelial cells at day 28. In addition, PCNA-positive cells were also increased in damaged glomeruli, accompanied by migration of EPC in glomeruli at day 28. We presume that the contribution of BM-derived EPC to the reconstruction of glomeruli is smaller than resident glomerular endothelial cells. However, taken together with the above results, we speculate that BM-derived EPCs lead the proliferation of endothelial cells and participate, at least in part, in the glomerular capillary repair through VEGF expression in our model.

In summary, our findings indicated that BM-derived endothelial cells contribute not only to the glomerular endothelial cell turnover but also to the regeneration of glomerular microvasculature in pathologic conditions. In other organs, EPCs augment tissue neovascularization after ischemia and contribute to reendothelialization after endothelial injury [21, 8, 22, 23], highlighting the potential therapeutic usefulness of targeting such cells. Our findings, therefore, may provide the basis for the development of new therapeutic strategies for renal diseases, by targeting mobilization, differentiation, and proliferation of BM-derived endothelial progenitor cells.

Acknowledgment The authors thank Ms. Tomomi Kurashige for the excellent technical assistance.

Conflict of interest statement The authors declare that they have no conflict of interest.

References

1. Abe K, Miyazaki M, Koji T, Furusu A, Ozono Y, Harada T, Sakai H, Nakane PK, Kohno S (1998) Expression of decay accelerating factor mRNA and complement C3 mRNA in human diseased kidney. Kidney Int 54:120–130
2. Aicher A, Zeiher AM, Dimmeler S (2005) Mobilizing endothelial progenitor cells. Hypertension 45:321–325
3. Arnold F, West DC (1991) Angiogenesis in wound healing. Pharmacol Ther 52:407–422
4. Asahara T, Masuda H, Takahashi T, Kalka C, Pastore C, Silver M, Kearne M, Magner M, Isner JM (1999) Bone marrow origin of endothelial progenitor cells responsible for postnatal vasculogenesis in physiological and pathological neovascularization. Circ Res 85:221–228
5. Asahara T, Takahashi T, Masuda H, Kalka C, Chen D, Iwaguro H, Inai Y, Silver M, Isner JM (1999) VEGF contributes to postnatal neovascularization by mobilizing bone marrow-derived endothelial progenitor cells. EMBO J 18:3964–3972
6. Breier G, Damert A, Plate KH, Risau W (1997) Angiogenesis in embryos and ischemic diseases. Thromb Haemost 78:678–683
7. Cattell V, Bradfield JW (1977) Focal mesangial proliferative glomerulonephritis in the rat caused by habu snake venom. A morphologic study. Am J Pathol 87:511–524
8. Choi JH, Hur J, Yoon CH, Kim JH, Lee CS, Youn SW, Oh IY, Skurk C, Murohara T, Park YB, Walsh K, Kim HS (2004) Augmentation of therapeutic angiogenesis using genetically modified human endothelial progenitor cells with altered glycogen synthase kinase-3beta activity. J Biol Chem 279:49430–49438
9. Cornacchia F, Fornoni A, Plati AR, Thomas A, Wang Y, Inverardi L, Striker LJ, Striker GE (2001) Glomerulosclerosis is transmitted by bone marrow-derived mesangial cell progenitors. J Clin Invest 108:1649–1656
10. D'Amore PA (1986) Growth factors, angiogenesis and metastasis. Prog Clin Biol Res 212:269–285
11. Folkman J (1985) Tumor angiogenesis. Adv Cancer Res 43:175–203
12. Folkman J, Shing Y (1992) Angiogenesis. J Biol Chem 267:10931–10934
13. Hicklin DJ, Ellis LM (2005) Role of the vascular endothelial growth factor pathway in tumor growth and angiogenesis. J Clin Oncol 23:1011–1027
14. Ikarashi K, Li B, Suwa M, Kawamura K, Morioka T, Yao J, Khan F, Uchiyama M, Oite T (2005) Bone marrow cells contribute to regeneration of damaged glomerular endothelial cells. Kidney Int 67:1925–1933
15. Ikenaga S, Hamano K, Nishida M, Kobayashi T, Li TS, Kobayashi S, Matsuzaki M, Zempo N, Esato K (2001) Autologous bone marrow implantation induced angiogenesis and improved deteriorated exercise capacity in a rat ischemic hindlimb model. J Surg Res 96:277–283
16. Imasawa T, Utsunomiya Y, Kawamura T, Zhong Y, Nagasawa R, Okabe M, Maruyama N, Hosoya T, Ohno T (2001) The potential of bone marrow-derived cells to differentiate to glomerular mesangial cells. J Am Soc Nephrol 12:1401–1409
17. Iruela-Arispe L, Gordon K, Hugo C, Duijvestijn AM, Claffey KP, Reilly M, Couser WG, Alpers CE, Johnson RJ (1995) Participation of glomerular endothelial cells in the capillary repair of glomerulonephritis. Am J Pathol 147:1715–1727
18. Ito T, Suzuki A, Imai E, Okabe M, Hori M (2001) Bone marrow is a reservoir of repopulating mesangial cells during glomerular remodeling. J Am Soc Nephrol 12:2625–2635
19. Jiang M, Wang B, Wang C, He B, Fan H, Guo TB, Shao Q, Gao L, Liu Y (2006) Inhibition of hypoxia-inducible factor-1 alpha and endothelial progenitor cell differentiation by adenoviral transfer of small interfering RNA in vitro. J Vasc Res 43:511–521
20. Kalka C, Tehrani H, Laudenberg B, Vale PR, Isner JM, Asahara T, Symes JF (2000) VEGF gene transfer mobilizes endothelial progenitor cells in patients with inoperable coronary disease. Ann Thorac Surg 70:829–834
21. Kawamoto A, Asahara T, Losordo DW (2002) Transplantation of endothelial progenitor cells for therapeutic neovascularization. Cardiovasc Radiat Med 3:221–225
22. Kawamoto A, Gwon HC, Iwaguro H, Yamaguchi JI, Uchida S, Masuda H, Silver M, Ma H, Kearney M, Isner JM, Asahara T (2001) Therapeutic potential of ex vivo expanded endothelial progenitor cells for myocardial ischemia. Circulation 103:634–637
23. Kawamoto A, Tkebuchava T, Yamaguchi J, Nishimura H, Yoon YS, Milliken C, Uchida S, Masuo O, Iwaguro H, Ma H, Hanley A, Silver M, Kearney M, Losordo DW, Isner JM, Asahara T (2003) Intramyocardial transplantation of autologous endothelial progenitor cells for therapeutic neovascularization of myocardial ischemia. Circulation 107:461–468
24. Kelly DJ, Hepper C, Wu LL, Cox AJ, Gilbert RE (2003) Vascular endothelial growth factor expression and glomerular endothelial

cell loss in the remnant kidney model. Nephrol Dial Transplant 18:1286–1292
25. Kitamura H, Sugisaki Y, Yamanaka N (1995) Endothelial regeneration during the repair process following Habu snake venom-induced glomerular injury. Virchows Arch 427:195–204
26. Klagsbrun M, D'Amore PA (1991) Regulators of angiogenesis. Annu Rev Physiol 53:217–239
27. Kong D, Melo LG, Gnecchi M, Zhang L, Mostoslavsky G, Liew CC, Pratt RE, Dzau VJ (2004) Cytokine-induced mobilization of circulating endothelial progenitor cells enhances repair of injured arteries. Circulation 110:2039–2046
28. Lin F, Mora A, Igarashi P (2005) Intrarenal cells, not bone marrow-derived cells, are the major source for regeneration in postischemic kidney. J Clin Invest 115:1756–1764
29. Masuda Y, Shimizu A, Mori T, Ishiwata T, Kitamura H, Ohashi R, Ishizaki M, Asano G, Sugisaki Y, Yamanaka N (2001) Vascular endothelial growth factor enhances glomerular capillary repair and accelerates resolution of experimentally induced glomerulonephritis. Am J Pathol 159:599–608
30. Morita T, Yamamoto T, Churg J (1998) Mesangiolysis: an update. Am J Kidney Dis 31:559–573
31. Murayama T, Tepper OM, Silver M, Ma H, Losordo DW, Isner JM, Asahara T, Kalka C (2002) Determination of bone marrow-derived endothelial progenitor cell significance in angiogenic growth factor-induced neovascularization in vivo. Exp Hematol 30:967–972
32. Poulsom R, Forbes SJ, Hodivala-Dilke K, Ryan E, Wyles S, Navaratnarasah S, Jeffery R, Hunt T, Alison M, Cook T, Pusey C, Wright NA (2001) Bone marrow contributes to renal parenchymal turnover and regeneration. J Pathol 195:229–235
33. Risau W (1997) Mechanisms of angiogenesis. Nature 386:671–674
34. Rookmaaker MB, Smits AM, Tolboom H, Van 't Wout K, Martens AC, Goldschmeding R, Joles JA, Van Zonneveld AJ, Grone HJ, Rabelink TJ, Verhaar MC (2003) Bone-marrow-derived cells contribute to glomerular endothelial repair in experimental glomerulonephritis. Am J Pathol 163:553–562
35. Shimizu A, Kitamura H, Masuda Y, Ishizaki M, Sugisaki Y, Yamanaka N (1997) Rare glomerular capillary regeneration and subsequent capillary regression with endothelial cell apoptosis in progressive glomerulonephritis. Am J Pathol 151:1231–1239
36. Shimizu A, Masuda Y, Kitamura H, Ishizaki M, Sugisaki Y, Yamanaka N (1998) Recovery of damaged glomerular capillary network with endothelial cell apoptosis in experimental proliferative glomerulonephritis. Nephron 79:206–214
37. Takahashi T, Kalka C, Masuda H, Chen D, Silver M, Kearney M, Magner M, Isner JM, Asahara T (1999) Ischemia- and cytokine-induced mobilization of bone marrow-derived endothelial progenitor cells for neovascularization. Nat Med 5:434–438
38. Urbich C, Aicher A, Heeschen C, Dernbach E, Hormann WK, Zeiher AM Dimmeler S (2005) Soluble factors released by endothelial progenitor cells promote migration of endothelial cells and cardiac resident progenitor cells. J Mol Cell Cardiol 39:733–742
39. Walter DH, Dimmeler S (2002) Endothelial progenitor cells: regulation and contribution to adult neovascularization. Herz 27:579–588
40. Zhang ZG, Zhang L, Jiang Q, Chopp M (2002) Bone marrow-derived endothelial progenitor cells participate in cerebral neovascularization after focal cerebral ischemia in the adult mouse. Circ Res 90:284–288

Virchows Arch (2008) 453:107–115
DOI 10.1007/s00428-008-0620-y

CASE REPORT

Genetics of a combined lung small cell carcinoma and large cell neuroendocrine carcinoma with adenocarcinoma

Giovanni Fellegara · Tiziana D'Adda · Francesco P. Pilato · Elisabetta Froio · Luca Ampollini · Michele Rusca · Guido Rindi

Received: 29 February 2008 / Revised: 15 April 2008 / Accepted: 16 April 2008 / Published online: 13 June 2008

Abstract Combined nonneuroendocrine–neuroendocrine lung tumors are relatively infrequent and little is known as for their genetic basis. Here, we report the case of a 69-year-old male with a solitary neoplasm in the upper lobe of the right lung. At histological examination, the tumor showed two components. The main part was an adenocarcinoma of the acinar type. The second part showed morphological and immunohistochemical phenotype of a neuroendocrine carcinoma composed of a small cell lung carcinoma and a large cell neuroendocrine carcinoma. The aim of our study was to investigate the genetic relationship between neuroendocrine and nonneuroendocrine tumor components. To this purpose, we performed a loss of heterozygosity (LOH) analysis with 40 chromosomal microsatellite markers. Microallelotyping revealed a common genetic profile in the different tumor areas. In 9 of 30 informative regions analyzed, LOH involved the same allele in all components, regardless of their histological type and grade. These findings support the true combined nature of this exocrine–neuroendocrine carcinoma of the lung and suggest a common monoclonal origin from a pluripotent epithelial (alveolar or bronchial) precursor cell for the two different tumor components.

G. Fellegara · T. D'Adda · F. P. Pilato · E. Froio · G. Rindi (✉)
Department of Pathology and Laboratory Medicine,
Section of Anatomic Pathology, University of Parma,
Via Gramsci, 14,
43100 Parma, Italy
e-mail: guido.rindi@unipr.it

L. Ampollini · M. Rusca
Department of Surgery, Thoracic Unit, University of Parma,
Parma, Italy

Keywords Combined lung cancer · Adenocarcinoma · Large cell neuroendocrine carcinoma · Small cell lung carcinoma · Pluripotent epithelial precursor

Introduction

The World Health Organization (WHO) classifies lung tumors with neuroendocrine phenotype in four diagnostic categories: typical carcinoid (TC), atypical carcinoid (AC), large cell neuroendocrine carcinoma (LCNEC), and small cell carcinoma (SCLC) [21]. Such entities represent a spectrum of increasingly aggressive tumor lesions, ranging from the less aggressive TC and AC (low- and intermediate-grade malignant) to the highly aggressive LCNEC and SCLC (high-grade malignant) [15]. Published data suggest that low–intermediate-grade (TC and AC) and high-grade (LCNEC and SCLC) neuroendocrine tumors represent two biologically separate entities, potentially void of any cross-evolutivity [21].

Both pulmonary high-grade neuroendocrine carcinomas may be associated with other major histologic types. WHO classification defines as combined SCLC the association of SCLC with an additional non-small-cell component represented by squamous cell, adenocarcinoma (ADC) or large cell carcinoma (LCC) and, less commonly, giant cell and/or spindle cell carcinoma [21]. When the additional component is represented by LCC, a 10% cutoff was established [21]. Similar criteria define combined LCNEC; however, when even a minor SCLC component is present, these tumors are classified as combined SCLC [21]. Rare cases with TC or AC components are also reported, many of which are colliding lesions rather than true mixed tumors [2, 17, 18].

Relatively few data are available regarding the genetic background of nonneuroendocrine–neuroendocrine combined cancers of the lung. Here, we report the case of a lung cancer made of an ADC associated with a neuroendocrine carcinoma displaying different growth patterns spanning from LCNEC to SCLC. The analysis of the tumor components was performed by conventional histology and immunohistochemistry for specific markers. In addition, loss of heterozygosity (LOH) investigation was conducted for 40 microsatellite markers mapping at chromosomal loci, harboring known or putative tumor suppressor genes and involved in lung carcinogenesis. Microallelotyping analysis proved effective in discriminating the polyclonal or monoclonal origin of combined, mixed, collision, and multiple cancers of several organs including lung [6, 9, 11, 12, 24]. The aim of this work was to analyze the genetic relationship between the neuroendocrine and exocrine components, to confirm the true combined nature of this neoplasm, and to gain information on its histogenesis.

Clinical history

A 69-year-old man, with 40-pack-per-year smoking history and no occupational risk factors, was admitted for the incidental finding of a single right lung opacity at direct chest X-ray performed for cardiac disease. His past medical history showed mild hypertension and chronic atrophic gastritis. Four years before, he underwent myocardial revascularization by coronary artery bypass grafting for acute myocardial infarction. At admission, his physical examination was unremarkable. Routine laboratory tests were normal. A chest computed tomography (CT) scan revealed a solitary pulmonary nodule in the right upper lobe. Fiber optic bronchoscopy and transthoracic fine-needle aspiration biopsy did not allow a diagnosis. Abdomen and brain CT scans were negative for metastatic deposits.

At surgery, a single white–gray nodule at cut surface, measuring 2.0×2.5×2.5 cm in size, was removed. One third of the nodule was processed for intraoperative diagnosis on frozen section. After a positive cancer diagnosis was made, a formal right upper lobectomy with mediastinal lymphadenectomy was performed through a right posterolateral thoracotomy. The entire lung lobe specimen measured 6.0×3.0×3.5 cm; 20 lymph nodes were isolated. No intraoperative complications occurred. The postoperative course was uneventful and the patient was discharged at day 9 after surgery. The disease stage was T1N0M0. The patient did not receive any adjuvant chemotherapy, did not experience any complication or recurrence at 31 months of follow-up, and gave informed consent to realize this investigation.

Materials and methods

Histology and immunohistochemistry

After fixation in 10% buffered formalin, the surgical specimen including the entire tumor was sampled according to standard procedures and processed into paraffin. Serial 4-μm-thick sections were stained with hematoxylin–eosin for conventional histology, periodic acid–Schiff (PAS),and PAS–diastase for mucin detection. The diagnosis was made according to the most recent WHO classification criteria for lung tumors. [21] Mitoses were counted on a minimum of 50 high-power fields (HPF, 10 HPF=2 mm^2). Ki67 proliferative index was assessed by nuclear count (Table 1) on the same areas using a digital image elaboration software (Image ProPlus, Media Cybernetics, Silver Spring, USA).

Immunoperoxidase tests were performed with a polymer detection system (UltraVision LP Large Volume Detection System, LabVision, Fremont, CA, USA). The primary antibodies included chromogranin A (mouse clones LK2H10+PHE5, dilution 1:1,000, Neomarkers, Fremont, CA, USA); neuron-specific enolase (NSE; BBS/NC/VI-H14 dilution 1:1,000, Dako, Glostrup, Denmark); synaptophysin (rabbit polyclonal, dilution 1:800, Cell Marque, Hot

Table 1 Mitotic index and immunohistochemical data of the histologic components of a combined tumor of the lung

Tumor component	Mitosis (*n*/2 mm^2)	Ki67 (%)	TTF-1	CDX-2	CgA	Syn	CD56	NSE
ADC	54	39	+	−	−	−	−	−
Transition	na	na	+[a]	−	+[b]	+[b]	+[b]	+[b]
LCNEC "A"	19	30	−/+	−	+	+	+	+
LCNEC "B"	63	51	−	−	+	+	+	+
SCLC	66	72	+	−	+/−	+	+	+

TTF-1 Thyroid transcription factor 1, *CDX-2* caudal type homeobox transcription factor 2, *CgA* chromogranin A, *Syn* synaptophysin, *CD56/N-CAM* neural cell adhesion molecule, *NSE* neuron-specific enolase, *ADC* adenocarcinoma, *LCNEC* large cell neuroendocrine carcinoma, *SCLC* small cell lung carcinoma, *na* not available

[a] ADC component only

[b] LCNEC "A" component only

Springs, AR, USA); CD56/N-CAM (rabbit polyclonal, dilution 1:1,000, Neomarker, Fremont, CA, USA); thyroid transcription factor (TTF-1; clone 8G7G3/1 Dako, Glostrup, Denmark, dilution 1:50); CDX2 (mouse monoclonal CDX2-88, dilution 1:300, Novocastra, New Castle, UK); Ki67 (mouse monoclonal clone MIB-1, dilution 1:100, Dakocytomation, Glostrup, Denmark). Antigen retrieval by protease or microwave pretreatment was performed for synaptophysin, CD56/N-CAM, TTF-1, CDX-2, and Ki67 before applying the primary antibody. Controls consisted of omission of the first layer and use of tissue with or without the pertinent antigen. Double immunostaining tests were performed on the same section using diaminobenzidine and Fast Red as chromogens for TTF-1 and for chromogranin A or synaptophysin, respectively.

Genetic analysis

For DNA extraction, serial 4-μm-thick sections were stained with hematoxylin and examined under a stereo microscope. Normal areas and each of the different tumor components were separately microdissected using sterile scalpels. At least 80% neoplastic cell enrichment was obtained for each tumor sample. Microdissected tissues were suspended in an optimized buffer for tissue lysis and incubated overnight with Proteinase K, and DNA was extracted and purified with a commercial kit according to the manufacturer protocol (DNeasy Tissue kit, QIAgen Inc., Valencia, CA, USA). DNA quality was assessed by polymerase chain reaction (PCR) amplification of human beta-globin gene.

LOH was investigated by PCR amplification of 40 highly polymorphic microsatellite markers on 13 chromosomes (Table 2), on tumor and control DNA samples with primers labeled with Beckman Coulter WellRED fluorescent dyes D2, D3, D4 (Beckman Coulter, Fullerton, CA, USA). Microsatellites markers were chosen according to different criteria: some located in chromosomal regions commonly lost in lung carcinomas (3p, 5q, 9p, 17p), others in regions reported to be possibly discriminating between small cell and large cell neuroendocrine carcinoma (10q, 16q, X) [5, 23]. Additionally, microsatellite instability (MSI) was tested with a panel of markers including the specific mononucleotide repeat markers BAT40 and BAT26 [1].

For PCR amplification, 2 μl of diluted DNA were combined in 25-μl reaction mix containing 10 mM Tris–HCl (pH 9.0), 50 mM KCl, 0.1% Triton X-100, 200 μM of each deoxyribonucleotide triphosphate (Promega, Madison, WI, USA), 0.4 μM of each primer, 1.5–2.0 mM $MgCl_2$, and 1.25 U Taq polymerase (Promega). PCR amplifications of 35 cycles were performed in an AB 2700 thermal cycler (Applied Biosystems, Foster City, CA, USA). The presence and correct size of PCR amplimers was checked by electrophoresis on 2% agarose gel (Qbiogene Inc., Carlsbad, CA, USA).

PCR products were run on a CEQ™ 8000 capillary DNA sequencer and CEQ™ 8000 Fragment Analysis software was used for electrophoretic profile analysis (Beckman Coulter Inc., Fullerton, CA, USA). Area and height of peaks were proportional to the concentration of the PCR fragments in the sample. Peak height data produced by the CEQ™ 8000 Fragment Analysis software were used to calculate the following ratio: $(\text{lower allele/higher allele})_{\text{tum}}/(\text{lower allele/higher allele})_{\text{norm}}$. Values below 0.6 or above 1.67, reflecting an allelic imbalance of 40% or more, indicated LOH.

The fractional allelic loss index (FAL, i.e., number of markers with LOH divided by the total number of informative markers) was calculated. High FAL values are considered as a positive marker of genetic instability.

Statistical analysis

Frequencies of allelic losses in the different tumor components were compared with Fisher's exact test. All P values were based on two-sided tests. P values less than 0.05 were considered statistically significant.

Results

Histology and immunohistochemistry

The tumor was composed of two distinct, though intermingled, growth patterns (see Figs. 1, 2 and Table 1).

The major tumor part (~70% of the lesion) was made by neoplastic glands, irregular in shape and lined by atypical cells with abundant PAS–diastase-positive cytoplasm, large nuclei with a single, evident nucleolus, consistent with the diagnosis of ADC of the acinar type (Fig. 1a,b). At immunohistochemistry, the ADC cells were positive for TTF-1 and negative for CDX-2, consistent with a pulmonary origin of the tumor. All neuroendocrine markers were negative. The proliferative index for Ki67 was 39%.

The remaining part of the tumor showed an overall organoid structure consistent with a neuroendocrine phenotype (Fig. 1a,c) at its periphery intimately intermingled with the ADC component and often budding off from gland structures (Fig. 1d). In transition areas, ADC cells were positive for TTF-1 and negative for all neuroendocrine markers while, vice versa, the neuroendocrine tumor cells were negative for TTF-1 and positive for chromogranin A, synaptophysin, CD56/N-CAM, and NSE (Fig. 1e,f).

In the remaining neuroendocrine part, three different growth patterns were distinguished (Fig. 2a–c). The first pattern was structured in small, solid islets with evident

Table 2 Results of the microallelotype analysis on the different histologic components of a combined tumor of the lung

Micro-satellite Marker[a]	Cytogenetic Site[a]	Gene of interest	ADC	LCNEC "A"	LCNEC "B"	SCLC
MYC-L1	1p34-35		★	★	★	★
BAT4	1p13.1		❍ no MSI	❍ no MSI	● no MSI	● no MSI
D2S123	2p16		★	★	★	★
BAT26	2p16	hMSH2	no MSI	no MSI	no MSI	no MSI
D3S1100	3p22-21.3		★	★	★	★
D3S1478	3p21.3-21.2	RASSF1	★	★	★	★
D3S1621	3p21.2-14.2		●	●	●	●
D3S1481	3p14.2	FHIT	●	●	●	●
D4S2397	4p15.2		❍	❍	❍	❍
D5S346	5q21-22	APC	❍	❍	●	❍
D5S422	5q32-33		❍	❍	●	❍
D8S254	8p22		★	★	★	★
D9S157	9p23-22	p15-p16	❍	❍	●	●
D9S171	9p21		❍	❍	●	●
D10S1765	10q23-24	PTEN	●	●	●	●
D10S1671	10q24		★	★	★	★
D10S209	10q25.3-26.1		●	●	●	●
PYGM	11q13.1		❍	❍	❍	❍
D11S4945	11q13		★	★	★	★
D11S4946	11q13	MEN-1	❍	❍	❍	●
D11S913	11q13		❍	❍	❍	●
D11S916	11q13-q23		❍	❍	❍	❍
D11S1365	11q13-q14		❍	❍	●	●
D11S29	11q23.3		❍	❍	❍	●
D11S387	11q25		❍	❍	❍	●
D16S301	16q22.1	P/E -	★	★	★	★
D16S421	16q22.1	Cadherin	●	●	●	●
D16S496	16q22.1		●	●	●	●
D16S507	16q23.2	H -	●	●	●	●
D16S422	16q24.2	Cadherin	●	●	●	●
TP53	17p13.1	p53	●	●	●	●
D17S250	17q11.2-q12		●	❍	❍	●
D18S1147	18q21-23		❍	❍	❍	❍
D18S483	18q21.3-22		❍	●	❍	❍
D18S477	18q21-23		❍	●	❍	❍
D18S61	18q22.3		❍	●	❍	❍
D18S58	18q22.3-q23		★	★	★	★
DXYS233	Xp22.32/Yp11.3		❍	❍	❍	❍
SHOX	Xp22.32/Yp11.3	SHOX	❍	❍	❍	❍
DXYS154	Xqter/Yqter		❍	❍	●	❍
FAL			0.33	0.40	0.53	0.60

ADC Adenocarcinoma, *LCNEC* large cell neuroendocrine carcinoma, *SCLC* small cell lung carcinoma, ● loss of heterozygosity (loss of allele #1), ● loss of heterozygosity (loss of allele #2), ❍ retention of heterozygosity, ★ not informative,*MSI* microsatellite instability,*FAL* fractional allelic loss index

[a] Primer sequences and microsatellite marker localizations are available at Genome Database (www.gdb.org) and PubMed UniSTS (http://www.ncbi.nlm.nih.gov) web sites

peripheral palisading and pseudoglandular pattern, in the absence of necrosis, with relatively regular, monomorphic tumor cells, abundant eosinophilic cytoplasm, and low cytological atypia (Fig. 2a and inset). The mitotic count was of 19 mitoses per 2 mm^2 and the proliferation index for Ki67 accounted for 30% of tumor cells (Fig. 2d, left). At immunohistochemistry, tumor cells stained intensely and uniformly for chromogranin A, synaptophysin, CD56/N-CAM, and NSE, while TTF-1 was occasionally positive (Fig. 2d center, right). The high mitotic index allocated this cancer component in the category of high-grade neuroendocrine neoplasia, large cell neuroendocrine carcinoma (LCNEC component "A").

The second neuroendocrine pattern showed a solid structure with cohesive large tumor sheets and evident central, comedo-type necrosis (Fig. 2b and inset). Tumor cells were similar in shape to those of the first neuroendocrine component, though relatively larger in size, with abundant cytoplasm, higher cytological atypia, and evident nucleoli. The mitotic count was of 63 mitosis per 2 mm^2 and the Ki67 proliferation index accounted for 51% of tumor cells (Fig. 2e, left). At immunohistochemistry, tumor cells stained intensely and uniformly for chromogranin A, synaptophysin, CD56/N-CAM, and NSE, with negative TTF-1 (Fig. 2e, center, right). These features were consistent with a diagnosis of poorly differentiated, high-grade neuroendocrine neoplasia, large cell neuroendocrine carcinoma (LCNEC component "B").

The third neuroendocrine pattern showed solid sheets made of densely packed, severely atypical cells, often spindle in shape, with high nucleus-to-cytoplasm ratio and scant cytoplasm. Cell borders were not clearly detectable.

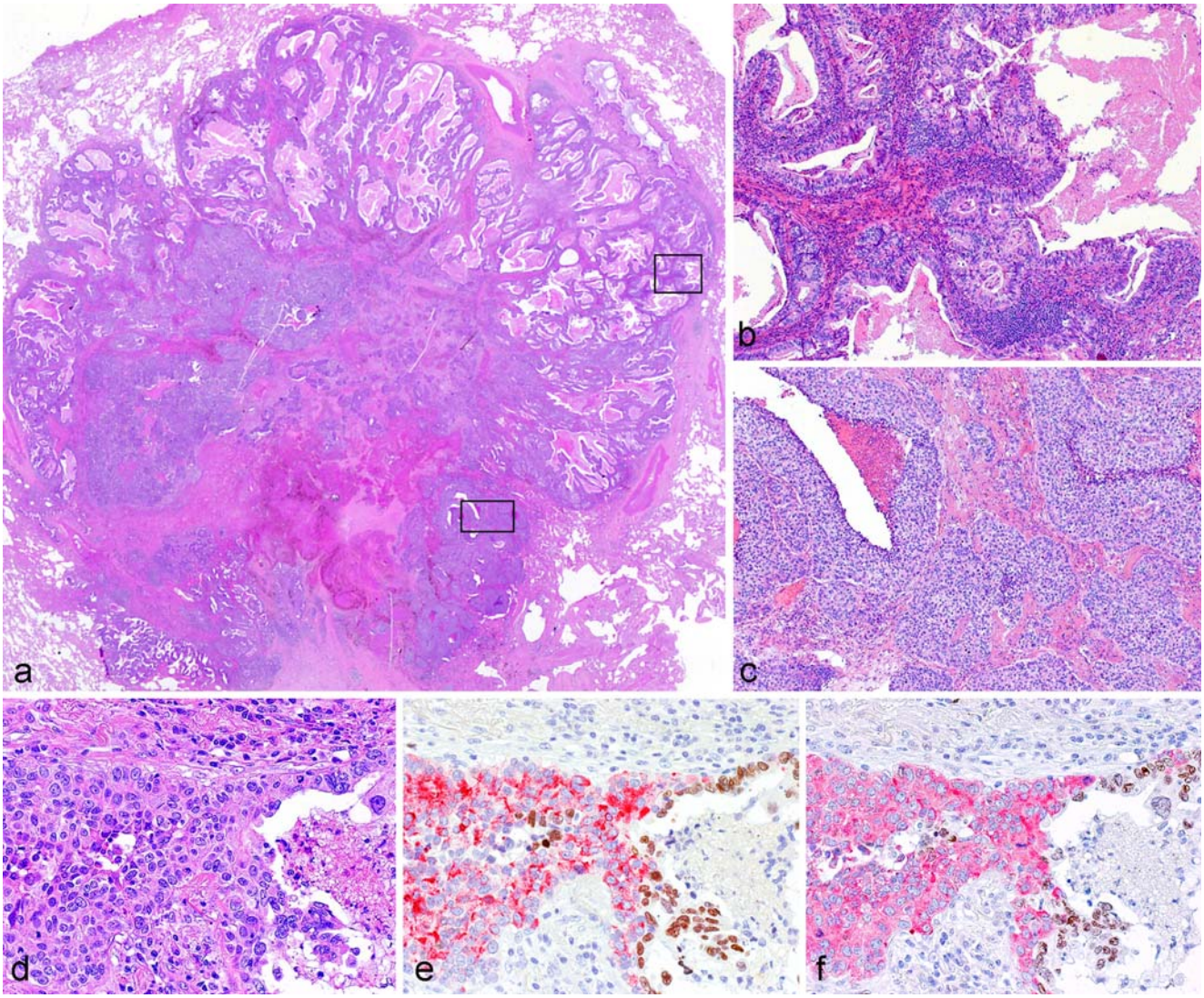

Fig. 1 Whole section (**a**): ADC component, periphery of the nodule (**b**, enlargement of the *upper square* in **a**) and neuroendocrine component, central area (**c**, enlargement of the *lower square* in **a**). Transition area (**d**–**f**): neuroendocrine cancer cells bud off ADC glands, and are positive for CgA (**e**, red stain) and synaptophysin (**f**, red stain), while TTF-1 is restricted to ADC cells (**e**, **f**, brown stain). H & E, original magnification ×5 (**a**), ×40 (**b**, **c**), ×200 (**d**); double immunoperoxidase, ×200 (**e**,**f**)

The nuclei were ovoid with finely granular chromatin and inconspicuous nucleoli. Nuclear molding was sometimes present (Fig. 2c, and inset). The mitotic count was of 66 mitosis per 2 mm^2 and the Ki67 proliferation index was 72% (Fig. 2f, left). At immunohistochemistry, tumor cells stained intensely and uniformly for synaptophysin, CD56/N-CAM, NSE, and TTF-1, with almost absent chromogranin A positivity (Fig. 2f, center, right). These features were consistent with a diagnosis of poorly differentiated, high-grade neuroendocrine neoplasia, SCLC.

All lymph nodes, as well as the visceral pleura and the bronchial resection margin, resulted void of any metastatic deposit.

Genetic analysis

Of the microsatellite markers investigated in the present study, 30 out of 40 were informative for LOH analysis (75%). No MSI was observed in any tumor component, either with the two specific mononucleotide repeats BAT26 and BAT40 and any other microsatellite investigated (see Table 2).

LOH was observed for 24 of 30 informative microsatellite markers (80%), 14 of 24 (58%) involving at least two tumor components and nine (38%) involving all four components. In 13 out of 14 markers with LOH, alterations involved the very same allele (Fig. 3), the only exception being D11S1365 for which different alleles were lost in the

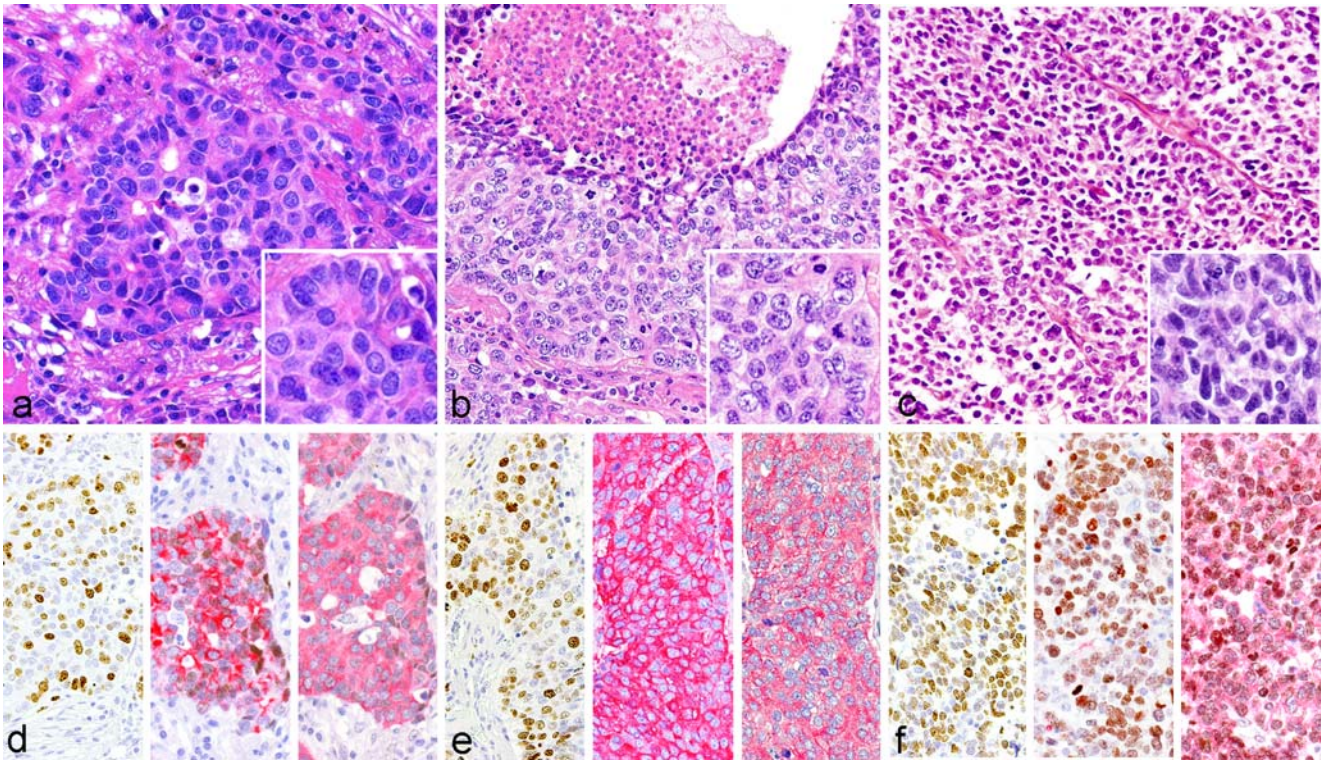

Fig. 2 **a** LCNEC component "A": cancer cells display disperse chromatin without prominent nucleoli, mitoses are not evident (**a**, *inset*) and Ki67 labels about 1/3 of cells (**d**, *left*). At double immunohistochemistry, cancer cells are strongly positive for chromogranin A (**d**, *center*, red stain) and synaptophysin (**d**, *right*, red stain), and occasionally for TTF-1 (**d**, *center* and *right*, brown stain). **b** LCNEC component "B": classic solid areas with comedo-type necrosis; cancer cells display abundant cytoplasm, evident nucleoli (**b**, *inset*), frequent mitoses and Ki67 labels about 1/2 of cells (**e**, *left*). At double immunohistochemistry, cancer cells are strongly positive for chromogranin A (**e**, *center*, red stain) and synaptophysin (**e**, *right*, red stain), with negative TTF-1 (**e**, *center* and *right*, brown stain). **c** SCLC: solid structure with severe atypia and noncohesive cells void of nucleoli (**c**, *inset*), with Ki67 labeling in 2/3 of cells (**f**, *left*). At double immunohistochemistry, cancer cells are negative for chromogranin A (**f**, *center*, red stain), while strongly positive for synaptophysin (**f**, *right*, red stain) and TTF-1 (**f**, *center* and *right*, brown stain). H & E, original magnification ×200 (**a**–**c**), ×400 (**a**–**c** inset); immunoperoxidase, original magnification ×200 (**d**–**f**)

LCNEC component "B" and SCLC (higher vs lower molecular weight allele loss, respectively). The same allele was lost in all tumor components for nine markers on chromosomes 3p, 10q, 16q, and 17p (TP53), while four further markers (BAT40, D9S157 and D9S171, D17S250) involved only two tumor components.

Comparison between tumor components showed lower FAL index for ADC (0.33), increasing from LCNEC component "A" (0.40) to LCNEC component "B" (0.53) and SCLC (0.60; Fig. 3, top). Only the comparison ADC vs SCLC approached the statistical significance (P=0.069).

In the ADC, allelic losses involving all informative markers investigated were found at chromosomes 3p, 10q, 16q, and 17 (including LOH at TP53). Overall, the FAL index in the ADC component was 0.33.

In the LCNEC component "A", allelic losses involving all the informative markers investigated were found at chromosomes 3p, 10q, and 16q. A single loss at chromosome 17p (TP53) was observed, with retention of the 17q marker (D17S250). All microsatellite markers at 18q were lost, with the only exception of the most centromeric one (D18S1147). Overall, the FAL index in the LCNEC component "A" was 0.40.

The LCNEC component "B" displayed allelic losses involving all the informative markers investigated at chromosomes 3p, 5q, 9p, 10q, and 16q. Single losses were observed at chromosomes 1p (BAT40), 11q (D11S1365), 17p (TP53) and at the pseudoautosomal region (DXYS154). Overall, the FAL index in the LCNEC component "B" was 0.53.

In the SCLC component, allelic losses involving all the informative markers investigated were found at chromosomes 3p, 9p, 10q, 16q, and 17 (including TP53). Loss of the single informative marker investigated was found at chromosome 1p (BAT40). Most informative microsatellite markers at 11q were lost, with the exception of the most centromeric one (PYGM) and of D11S916. Overall, the FAL index in the SCLC component was 0.60.

Losses at 9p were found in both LCNEC component "B" and SCLC, while losses at both markers on 17 chromosomes were common to ADC and SCLC. LOH at

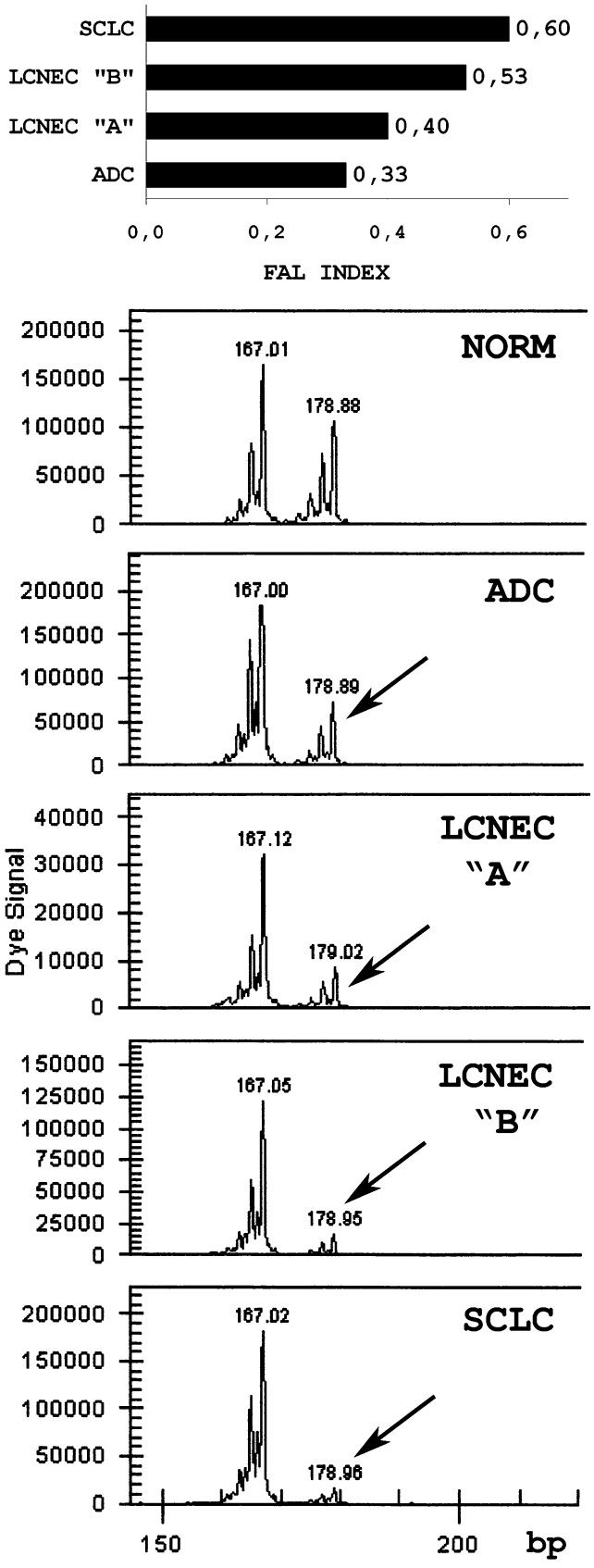

Fig. 3 From *top* to *bottom*; fractional allelic loss index of the different components of the combined lung cancer (*top panel*). Electrophoretic profiles for the microsatellite D10S1765, showing loss of the same allele (*arrow*) in all components, with reduction of peak height progressively more extensive from ADC to SCLC. X axis, size of the PCR fragments in base pairs (bp); Y axis, intensity of fluorescence (peak heights). *NORM*: normal tissue, *ADC*: adenocarcinoma, *LCNEC*: large cell neuroendocrine carcinoma, *SCLC*: small cell lung carcinoma

chromosome 18q was distinctive for LCNEC component "A". Similarly, losses at 5q (APC) were solely found in the LCNEC component "B" while multiple losses at chromosome 11q were an exclusive hallmark of SCLC.

Discussion

Cellular heterogeneity is a well-known phenomenon in lung cancer [7, 16], almost 50% of primary tumors showing more than one of the major histologic types [21]. Combined SCLC is the only subtype of SCLC recognized in WHO classification [21]. It is a relatively rare neoplasm, and in older studies based on small biopsies, accounted for 1–3.2% of all SCLC [8, 14]. In a recent large surgical series of 1,158 cases, the prevalence of combined neuroendocrine–nonneuroendocrine tumors was 1.8% (21/1,158) [17]. However, the real prevalence of combined neuroendocrine–nonneuroendocrine lung tumors may well be underestimated. In fact, in a series of 100 resected SCLC, the combined subtype was as high as 28% of cases [14]. Patients with diagnosis of SCLC made on needle biopsy in fact receive surgical treatment in selected cases only [3]. Moreover, needle biopsy may miss a minor nonneuroendocrine component [18].

In the case presented here, the neoplasm was characterized by two distinct components, the main one consisting of an ADC, the minor one belonging to the spectrum of aggressive neuroendocrine neoplasms. This lesion may represent a collision between two independent neoplasms or a true combined tumor of the lung. Both morphological and immunohistochemical data favor the latter hypothesis. The pulmonary origin of both components is confirmed by the total negativity for CDX-2 and by the TTF-1 nuclear staining. Interestingly, TTF1 expression was restricted to transition areas and the SCLC component, while negative in the LCNEC component. This latter finding fits the expected 50% frequency reported for LCNEC [19–21]. Moreover, the neoplasm consisted of a single well-demarked nodular lesion, showing a transition zone between the ADC and the neuroendocrine carcinoma, apparently taking origin from malignant glandular structures.

The above features suggest a common origin for both the neuroendocrine and exocrine components, as already

proposed for combined neoplasms of the lung [7, 10, 16] and in others sites [11, 12]. This hypothesis is supported by the close genetic relationship we observed between tumor components. LOH was found for 24 out of 30 informative microsatellite markers, 13 involving the same allele in at least two tumor components and nine involving all four components regardless of their histological type and grade. The latter losses involved 3p21–3p14, 10q23–10q26, 16q22–16q24, and 17p13; chromosomal regions known to harbor tumor suppressor genes such as FHIT, PTEN, P/E-cadherin, H-cadherin, and P53 play a critical role in lung cancerogenesis [4, 13, 22]. Since shared, these losses may represent an early event during tumorigenesis, likely occurring in a pluripotent epithelial precursor (bronchial or alveolar) cell differentiating toward two divergent neoplastic phenotypes. Huang et al. [12] proposed that this differentiation could be driven through the influence of different host–environmental factors affecting progeny cells derived from this common precursor. Conversely, this common precursor could retain the ability to differentiate into cells with either exocrine or endocrine phenotype [12]. Given the large number of common genetic alterations observed here in both the endocrine and the exocrine component, we favor the latter hypothesis. The incremental FAL index trend from ADC to LCNEC and SCLC, although statistically not significant, may suggest that additional genetic damages account for the increased histological grade in the neuroendocrine component.

The LCNEC part displayed heterogeneity, with the LCNEC component "A" being characterized by absence of necrosis, small islets, and pseudoglandular pattern. 18q LOH was specifically observed in this component only, suggesting some difference from the more classic LCNEC component "B". We speculate that LCNEC component "A" may represents a more differentiated stage of the high-grade neuroendocrine carcinomas.

The absence of a low–intermediate-grade lesion (TC and AC) in the present case is in line with the exceedingly rare occurrence of TC or AC lesions in combined lung carcinomas reported in the literature [2, 18, 22]. This finding supports the hypothesis that TC, AC, and high-grade neuroendocrine neoplasms (LCNEC and SCLC) may follow different tumorigenic pathways [21]. Moreover, this may suggest that, at least in combined SCLC–ADC lung cancers, ADC shares histogenetic and pathogenetic mechanisms with high-grade neuroendocrine neoplasms, similar to what was suggested for mixed endocrine–exocrine tumors in the gut [24].

In conclusion, our data suggest a monoclonal origin from a pluripotential epithelial stem cell for the combined neuroendocrine–exocrine carcinoma of the lung presented here. We speculate that the same genetic background may determine both the neuroendocrine and nonneuroendocrine carcinoma of the lung, the histological type depending on yet unknown host or environmental factors. Further studies on larger number of cases are necessary to confirm this hypothesis.

Acknowledgements The authors thank Doctor Nicoletta Campanini, Mrs. Gabriella Becchi, and Mrs. Emilia Corradini, University of Parma, for their excellent technical assistance. This work has been supported by grants from MURST (COFIN 05) and the University of Parma (FIL 05).

Conflict of interest statement The Authors declare the absence of any conflict of interest.

References

1. Boland CR, Thibodeau SN, Hamilton SR, Sidransky D, Eshleman JR, Burt RW, Meltzer SJ, Rodriguez-Bigas MA, Fodde R, Ranzani GN, Srivastava S (1998) A National Cancer Institute workshop on microsatellite instability for cancer detection and familial predisposition: development of international criteria for the determination of microsatellite instability in colorectal cancer. Cancer Res 58:5248–5257
2. Cavazza A, Toffanetti R, Ferrari G, Piana S, Putrino I, Gardini G (2001) Combined neoplasia of the lung: description of a case of adenocarcinoma mixed with typical carcinoid. Pathologica 93:216–220
3. Cooper WA, Thourani VH, Gal AA, Lee RB, Mansour KA, Miller JI (2001) The surgical spectrum of pulmonary neuroendocrine neoplasms. Chest 119:14–18
4. Dacic S (2007) Molecular profiling of lung carcinoma: identifying clinically useful tumor markers for diagnosis and prognosis. Expert Rev Mol Diagn 7:77–86
5. D'Adda T, Bottarelli L, Azzoni C, Pizzi S, Bongiovanni M, Papotti M, Pelosi G, Maisonneuve P, Antonetti T, Rindi G, Bordi C (2005) Malignancy-associated X chromosome allelic losses in foregut endocrine neoplasms: further evidence from lung tumors. Mod Pathol 18:795–805
6. D'Adda T, Pelosi G, Lagrasta C, Azzoni C, Bottarelli L, Pizzi S, Troisi I, Rindi G, Bordi C (2008) Genetic alterations in combined neuroendocrine neoplasms of the lung. Mod Pathol 21:414–422
7. Dunnill MS, Gatter KC (1986) Cellular heterogeneity in lung cancer. Histopathology 10:461–475
8. Fraire AE, Johnson EH, Yesner R, Zhang XB, Spjut HJ, Greenberg SD (1992) Prognostic significance of histopathologic subtype and stage in small cell lung cancer. Hum Pathol 23:520–528
9. Froio E, D'Adda T, Fellegara G, Ampollini L, Carbognani P, Rindi G (2008) Three different synchronous primary lung tumours: a case report with extensive genetic analysis and review of the literature. Lung Cancer 59:395–402
10. Fukui T, Tsuta K, Furuta K, Watanabe SI, Asamura H, Ohe Y, Maeshima AM, Shibata T, Masuda N, Matsuno Y (2007) Epidermal growth factor receptor mutation status and clinicopathological features of combined small cell carcinoma with adenocarcinoma of the lung. Cancer Sci 98:1714–1719
11. Furlan D, Cerutti R, Genasetti A, Pelosi G, Uccella S, La Rosa S, Capella C (2003) Microallelotyping defines the monoclonal or the polyclonal origin of mixed and collision endocrine–exocrine tumors of the gut. Lab Invest 83:963–971
12. Huang J, Behrens C, Wistuba II, Gazdar AF, Jagirdar J (2002) Clonality of combined tumors. Arch Pathol Lab Med 126:437–441
13. Hung J, Kishimoto Y, Sugio K, Virmani A, McIntire DD, Minna JD, Gazdar AF (1995) Allele-specific chromosome 3p deletions occur at

an early stage in the pathogenesis of lung carcinoma. JAMA 273:558–563
14. Nicholson SA, Beasley MB, Brambilla E, Hasleton PS, Colby TV, Sheppard MN, Falk R, Travis WD (2002) Small cell lung carcinoma (SCLC): a clinicopathologic study of 100 cases with surgical specimens. Am J Surg Pathol 26:1184–1197
15. Onuki N, Wistuba II, Travis WD, Virmani AK, Yashima K, Brambilla E, Hasleton P, Gazdar AF (1999) Genetic changes in the spectrum of neuroendocrine lung tumors. Cancer 85:600–607
16. Roggli VL, Vollmer RT, Greenberg SD, McGavran MH, Spjut HJ, Yesner R (1985) Lung cancer heterogeneity: a blinded and randomized study of 100 consecutive cases. Hum Pathol 16:569–579
17. Ruffini E, Rena O, Oliaro A, Filosso PL, Bongiovanni M, Arslanian A, Papalia E, Maggi G (2002) Lung tumors with mixed histologic pattern. Clinico-pathologic characteristics and prognostic significance. Eur J Cardiothorac Surg 22:701–707
18. Sen F, Borczuk AC (1998) Combined carcinoid tumor of the lung: a combination of carcinoid and adenocarcinoma. Lung Cancer 21:53–58
19. Sturm N, Lantuejoul S, Laverriere MH, Papotti M, Brichon PY, Brambilla C, Brambilla E (2001) Thyroid transcription factor 1 and cytokeratins 1, 5, 10, 14 (34betaE12) expression in basaloid and large-cell neuroendocrine carcinomas of the lung. Hum Pathol 32:918–925
20. Sturm N, Rossi G, Lantuejoul S, Papotti M, Frachon S, Claraz C, Brichon PY, Brambilla C, Brambilla E (2002) Expression of thyroid transcription factor-1 in the spectrum of neuroendocrine cell lung proliferations with special interest in carcinoids. Hum Pathol 33:175–182
21. Travis WD, Brambilla E, Müller-Hermelink HK, Harris CC (eds) (2004) In: World Health Organization classification of tumours. Pathology and genetics of tumours of the lung, pleura, thymus and heart. IARC Press, Lyon
22. Ullmann R, Schwendel A, Klemen H, Wolf G, Petersen I, Popper HH (1998) Unbalanced chromosomal aberrations in neuroendocrine lung tumors as detected by comparative genomic hybridization. Hum Pathol 29:1145–1149
23. Ullmann R, Petzmann S, Sharma A, Cagle PT, Popper HH (2001) Chromosomal aberrations in a series of large-cell neuroendocrine carcinomas: unexpected divergence from small-cell carcinoma of the lung. Hum Pathol 32:1059–1063
24. Vortmeyer AO, Lubensky IA, Merino MJ, Wang CY, Pham T, Furth EE, Zhuang Z (1997) Concordance of genetic alterations in poorly differentiated colorectal neuroendocrine carcinomas and associated adenocarcinomas. J Natl Cancer Inst 89:1448–1453

Virchows Arch (2008) 453:117–119
DOI 10.1007/s00428-008-0635-4

LETTER TO THE EDITOR

Bioethics considerations for medical research in human archive tissues: the point of view of the researcher

Giorgio Stanta · Alberto Cescato · Serena Bonin · Renzo Barbazza

Received: 27 March 2008 / Revised: 15 May 2008 / Accepted: 16 May 2008 / Published online: 13 June 2008

Keywords Bioethics · Human tissues · Informed consent · Archive tissues · Prospective and retrospective studies

Dear Sir,

One of the central points of molecular medicine research is the need to check the results of basic research in human clinical case studies. For this reason, human tissues like blood and tissues from surgical specimens are often used. These studies are usually performed before direct clinical trials to give more information for future clinical research. The goal performed in human tissue research is usually a preclinical or clinical validation of specific molecular biomarkers. Bioethics rules can directly modify the possibility and the time period in which this type of studies can be conducted.

Globally, the vast majority of medical research does not involve very sensitive ethical issues. Within this research area, we would like to point out the difference between research investigating genetic aspects, which could seriously harm privacy, and more strictly pathological research, the kind of medical research that is most commonly carried out. In this case, delicate genetic aspects are often completely marginal or absent. The first kind of research could be defined as "molecular genetics" and the second one as "molecular pathology". The difference between those two kinds of research is that in molecular genetics research is carried out mostly by studying DNA in normal cells of our body (such as blood circulating cells), which could give information not only about the patients themselves, but also about their relatives. Research in molecular pathology focuses rather on cells, which are altered with respect to normal cells and which, in many cases (such as in tumor cells), are not really suitable to provide correct information of genetic nature, because their DNA is altered compared to the DNA in the same patient's normal cells. In this research, other biological macromolecules, like RNA and proteins, are mostly analyzed and such molecules are little suitable for recognition of genetic information.

In clinical research, there are colliding interests, which should be correctly estimated and weighed with care: from a general point of view, research toward more effective and safer medicine is in the interest of our health, but on the other hand, we should respect the right to personal information confidentiality and grant a "right of property" to our tissues. The ethical arguing involving a good balance of interests doesn't always lead to a satisfying conclusion. Anyway, the researcher has to point out that too restrictive bioethics norms could slow down research in an unjustified way and cause many yearlong delays with evident damage for a very large number of future patients. The matter is a rational and not an emotional mediation between those important interests.

Objectives of the research. As already mentioned, nowadays the central goal is to find a kind of medicine based on the knowledge of molecular mechanisms lying at the origin of diseases and on the understanding of an

G. Stanta · A. Cescato · S. Bonin
Department of Clinical, Morphological and Technological Sciences, University of Trieste and International Centre for Genetic Engineering and Biotechnology, Trieste, Italy

R. Barbazza
Pathology Department ULSS 2, Feltre, Italy

G. Stanta (✉)
Surgical Pathology Unit, Cattinara Hospital, Strada di Fiume 447, 34149 Trieste, Italy
e-mail: stanta@icgeb.org

effective and safe therapy, maybe even personalized for each patient. The reductionism imposed by the knowledge gained in traditional medicine so far, with systematic classification of diseases in large groups, should be overcome by a more personalized approach. That does not mean that diseases are different from what we used to know, but to treat them in an effective way they should be divided into increasingly homogeneous subgroups. For this reason, the need is to study "molecular biomarkers", which will be possible only with access to human tissues. Everyone could agree with the goals of this kind of research, as their ethical value is high (therefore they are not subject to a cautionary bioethical evaluation). Anyway, we are guaranteed that the goals of a research involving humans are well oriented and ethical because in Europe the research projects are first presented for evaluation to ethical committees, by which they have to be examined and approved.

Methods used in research. The methods which should be used in research at this level are well defined and refer in particular to those used by "molecular biology" and "proteomics". These are powerful and sophisticated methods, which are freely utilized by thousands of medical-biological research laboratories in the world and, if they are employed for lawful purposes, they do not need to be subject to ethical concerns.

Biological material. The biological material on which this research is developed is human tissues, the use of which is crucial to achieve the goals. Therefore, this kind of research needs huge case studies of human tissues. The origin and the kind of collection of those tissues could largely vary. Tissues could be collected specifically for research (from blood, for example, to perform genetic research), in this case the patients or the volunteers providing their blood samples are directly informed to obtain their consent. However, in most cases tissues are collected for other purposes: for example, for biopsies of small tissue fragments or for ablation of tissues during a surgical treatment and then used for a histological diagnosis. In such cases, the patients give their informed consent to diagnostic or therapeutic procedure. The remaining tissues can be stored in archives for different periods of time, according to the country's law, and then they are discarded. From large surgical specimens, small pieces of tissue are collected for histological examination, while most tissues are discarded immediately. In this way, we dispose of a huge amount of tissues with a very relative value for the patients. Such tissues can be used for medical research instead of being wasted.

Type of research. Concerning the typology of studies, we need to differentiate retrospective research, in which the examined clinical cases are old closed cases recovered from hospital archives, from prospective research, in which cases are selected from patients who are currently being treated. In the study on biomarkers, retrospective research on archive human tissues is the first to be performed. The retrospective phase of the research is important because it allows shifting to a prospective clinical phase with more chances of success. This retrospective phase is the one that is most able to reduce the research time, giving important information to orient the following prospective studies. On the other hand, prospective research has well codified times and ways, which are difficult to be modified. In those two different research typologies, ethical evaluation could raise different considerations.

As for research on patients *in prospective clinical trials*, consent is needed and the ethical approach to be followed and the tools to be used are clearly defined. In such cases, prospective research is planned, with a selection of subjects carrying a certain disease at the moment the examination is performed. Before starting the study of experimental diagnosis/therapy, the patient has to be informed about what is going to be done and cannot take part to this study before having obtained an "informed consent". In these trials, a still experimental therapy, for example, is suggested. However, this therapy is perfectly oriented to gain the cure or the control of the disease, and all the already performed preliminary studies should point it as probably more effective than the treatments used so far. Also in this case, a high level of well-defined information is given; in this way the patients can provide their consent because they have been well informed and are in a position to make a decision.

For many reasons, *the retrospective research* in human tissues is often quite different from prospective clinical research also from a bioethical point of view [3, 5]. These types of studies are performed on tissues related to closed clinical cases stored in hospital archives. Tissues derived from diagnostic procedures or from surgical left-over are in any case to be wasted. Depending on the local country rules, they can be eliminated directly or stored for 10–20 years. It should also be considered that many patients could be deceased in the meantime. Tracing old patients is a very long and demanding job that can delay the research for a very long time, even years.

In this retrospective phase of medical research, the expected results are mostly hypothetical and ill defined because the research is oriented to reach or to confirm new knowledge. For this reason, scientists are not able to give detailed information to the patients. The hypotheses are not confirmed, and any explanation needs to take into consideration very complex molecular pathway considerations. It is easy to imagine that patients are not able to understand and evaluate correctly a complex molecular hypothesis and that the scientists themselves are not completely aware of the possible results of the research. Moreover, there is very little or no information deriving from previous experiences at the moment these studies are conducted. In such a way, any informed consent should not be valid and could be persecuted in any court of any European country. The

reason is that no really detailed information was delivered to the patients, so they are unable to give an informed consent. In this situation, a better solution could be a generic "presumed consent" to any possible research performed on the stored tissues [2]. If the patients do not deny the possible use of their stored archive tissues in a clear way, these can be included in any research program with ethically approved finalities and important opportunities for the welfare of mankind. In this way, patients would be always free to express their personal choice to deny their permission to tissues utilization.

The UNESCO Universal Declaration on Bioethics and Human Rights mentions the consent in article 6 and states the possibility to avoid the informed consent, in relationship with country standards about bioethical rules [6]. As a matter of fact, these tissues are not related to an actual patient's direct interest because in any way they are discarded. Even more as a further guarantee, according to European directories, no economical interests are allowed in the use of these tissues [1].

Likewise, the possibility of privacy breach in this kind of study is very low because of the professional secret the hospital personnel has to keep. The Helsinki Declaration of the World Medical Association (WMA) correlates the human tissue research in identifiable patients to the same directories used in prospective clinical trials [7]. To avoid this, it is mandatory to codify or anonymize the cases [4]. One of the chances is to give the responsibility of "guarantor" for that specific research to a suitable person. This guarantor could be the coordinator of the research, who will respond for any breach to data confidentiality. A doctor who is already bound by the professional secret could be the guarantor of anonymization and of coding of personal data. In this case, further important data (such as data concerning complications or relapses that will take place later in time, or the survival of patients), which are not available in the early stage of the research, could be added because the guarantor can repeatedly take such extremely important information into consideration and anonymously complete it.

Conclusions

In retrospective research, if the goals are lawful or even highly desirable, the problem to be faced involves the biological material used in the study. For human tissues, if the above-mentioned precautions are taken, we should be able to guarantee the rights of the single patient and extremely fast medical progress at the same time. We should consider indeed that the clinical advantages from recognition and validation of clinical molecular biomarkers for a more personalized therapy cannot be reached without such studies. The benefits we gain are clearly higher than the risks for an unlikely privacy breach or very small damage to the right of property of the individual (all the tissues are sooner or later wasted anyway), but at the same time the personal choices to deny the use of these tissues can be completely guaranteed. In this way, shorter research times could allow these new discoveries to reach a higher number of patients who are closer to us in time and who would probably be excluded from the benefits.

Pathologists should discuss these or similar considerations with public representatives and with bioethics experts of any country to try to harmonize the ethical concern with the research needs, to obtain the expected advantages for patients as a very high ethical goal of medicine.

Aknowledgments This report was written thanks to the support and the discussion developed in two European projects: IMPACTS and ACUME2.

The authors thank Dr. Valentina Melita for the English revision of the manuscript.

Conflict of interest statement The authors declare that they have no conflict of interest.

References

1. Article 21 of the European Convention on Human Rights and Biomedicine- http://conventions.coe.int/Treaty/EN/CadreListeTraites.htm
2. Charo RA (2006) Body of research—ownership and use of human tissue. N Engl J Med 355(15):1517–1519
3. Knoppers BM, Laberge CM (1995) Research and stored tissues. Persons as sources, samples as persons? JAMA 274(22):1806–1807
4. Oosterhuis JW, Coebergh JW, van Veen EB (2003) Tumour banks: well-guarded treasures in the interest of patients. Nat Rev 3(1):73–77
5. Wendler D (2002) What research with stored samples teaches us about research with human subjects. Bioethics 16(1):33–54
6. Wolinsky H (2006) Bioethics for the world. EMBO Rep 7(4):354–358
7. World Medical Association, Helsinki Do (revised in Edinburgh, October 2000)- http://www.wma.net

Virchows Arch (2008) 453:121
DOI 10.1007/s00428-008-0625-6

ERRATUM

Correlations between reduced expression of the metastasis suppressor gene KAI-1 and accumulation of p53 in uterine carcinomas and sarcomas

Juliane Briese · Heinrich M. Schulte · Maria Sajin · Christoph Bamberger · Katja Redlin · Karin Milde-Langosch · Thomas Löning · Ana-Maria Bamberger

Published online: 5 July 2008

The author's affiliations were given incorrectly. The correct affiliations are given here.

The online version of the original article can be found at http://dx.doi.org/10.1007/s00428-008-0608-7

J. Briese · C. Bamberger · A.-M. Bamberger
Section on Endocrinology and Metabolism of Ageing,
University Clinic Hamburg-Eppendorf,
Hamburg, Germany

J. Briese (✉)
Department of Pathology and Tumor Biology,
University of Leeds, St. James's Hospital,
Beckett Street,
LS9 7TF Leeds, UK
e-mail: j.briese@leeds.ac.uk

H. M. Schulte · K. Redlin
Endokrinologikum,
Hamburg, Germany

M. Sajin
Department of Morphopathology,
University of Bucharest,
Bucharest, Romania

K. Milde-Langosch
Department of Gynecology,
University Clinic Hamburg-Eppendorf,
Hamburg, Germany

T. Löning
Department of Pathology, Albertinen-Hospital,
Hamburg, Germany

Virchows Arch (2008) 453:123–132
DOI 10.1007/s00428-008-0644-3

ORIGINAL ARTICLE

Identification of molecular phenotypes in canine mammary carcinomas with clinical implications: application of the human classification

A. Gama · A. Alves · F. Schmitt

Received: 24 April 2008 / Accepted: 7 July 2008 / Published online: 2 August 2008

Abstract Similarly to humans, canine mammary cancer represents a heterogeneous group in terms of morphology and biological behaviour. In the present study, we evaluated a series of canine mammary carcinomas based on a new human classification, initially based on gene expression profiling analysis. Similarly to human breast cancer, by using an immunohistochemistry surrogate panel based on five molecular markers [estrogen receptor, human epidermal growth factor receptor 2 (HER2), cytokeratin 5, p63 and P-cadherin], we were able to classify canine mammary carcinomas into four different subtypes: luminal A [estrogen receptor (ER)+/HER2−; 44.8%], luminal B (ER+/HER2+; 13.5%), basal (ER−/HER2− and a basal marker positive; 29.2%) and HER2 overexpressing tumours (ER−/HER2+; 8.3%). Luminal A-type tumours were characterised by lower grade and proliferation rate, whereas basal-type tumours were mostly high grade, high proliferative and positive for cytokeratin 5, p63 and P-cadherin. In addition, as in humans, basal subtype was significantly associated with shorter disease-free and overall survival rates, and we propose canine mammary carcinomas as a suitable natural model for the study of this particular subset of human carcinomas.

A. Gama · A. Alves
Department of Veterinary Sciences, CECAV,
University of Trás-os-Montes and Alto Douro (UTAD),
5001-811 Vila Real, Portugal

F. Schmitt (✉)
Institute of Molecular Pathology and Immunology of the
University of Porto (IPATIMUP),
4200-465 Porto, Portugal
e-mail: fernando.schmitt@ipatimup.pt

F. Schmitt
Medical Faculty, University of Porto,
Porto, Portugal

Keywords Canine · Mammary carcinoma · Immunohistochemistry · Classification

Introduction

Mammary gland tumours are the most commonly occurring neoplasm in the female dog and represent a remarkably heterogeneous group in terms of morphology and biological behaviour [32, 43]. About half of canine mammary tumours are considered malignant, and the identification of reliable prognostic factors is essential in order to estimate the individual risk of unfavourable clinical outcome [29, 54].

Several studies have recognised some reliable prognostic factors such as tumour size, histologic type, histologic grade and lymph node status [19, 30, 31]. Moreover, in recent literature, we found an increasing number of investigations searching for suitable prognostic markers for canine mammary cancer [54], including proliferation markers [25], hormone receptors [23], p53 and human epidermal growth factor receptor 2 (HER2) [21, 24] and adhesion molecules [14, 26], among others. The clinical experience is still limited, however, and reliable results of prospective studies are not always available.

Human and canine mammary cancer studies based on single molecular markers probably cannot accurately account for the heterogeneity of this disease [39]. Given the large number of cellular events involved in cell growth, differentiation, proliferation, invasion and metastases [4], the investigation of multiple molecular alterations in concert has been assuming great importance due to the introduction of high-throughput technologies [39]. In fact, recent gene expression profiling studies on human breast tumours have identified distinct molecular subtypes of breast carcinomas, which differ in their pathobiology and

clinical outcomes [36, 47, 48]. Sorlie et al. [48] analysed the expression profiles of 115 sporadic breast tumour samples and categorised them into five main groups: luminal A, luminal B, HER2-overexpressing, basal like and normal breast tissue like. Luminal A and B subtypes are based on the expression of estrogen receptor (ER), usually with luminal cytokeratin (CK) expression, whereas the basal-like subtype is characterised by the absence of hormonal receptors and expression of basal cell markers [5, 33].

Given that gene expression profiling is impractical as a routine diagnostic tool, there are immunohistochemistry surrogate panels proposed that can potentially distinguish breast cancer subtypes [27, 33]. In the present study, we sought to identify phenotypical subtypes in canine mammary cancer with possible clinical implications. To accomplish this goal, we have characterised by immunohistochemical analysis 102 canine mammary carcinomas based on the immunohistochemical panel proposed by Matos et al. [27], which involved the evaluation of five molecular markers (ER, HER2, CK5, p63 and P-cadherin).

Materials and methods

Tumour specimens

The present study is based on a series of 102 cases of canine malignant mammary tumours (n=102) selected from the histopathological files of the University of Trás-os-Montes and Alto Douro, Vila Real and from the Institute of Biomedical Science at the University of Porto, Portugal. The material was fixed in 10% neutral formalin and embedded in paraffin wax. Sections (3 μm) were cut and stained with haematoxylin and eosin for histological examination or used to perform immunohistochemistry.

Follow-up data

Sixty-nine cases (n=69) had available follow-up data, with a median overall survival time of 15 months (range 5–74 months). Overall survival (OS) was defined as the period between surgery and animal natural death or euthanasia due to cancer. Disease-free survival (DFS) was defined as the period of time between surgery and recurrent or metastatic disease. During the follow-up period, according to the referring surgeons, 35 animals died or were euthanized due to metastatic disease and/or local recurrence.

Histological examination

Tumours were diagnosed according to the WHO criteria for canine mammary neoplasms [30]. Clinicopathological variables included in the present study were age, ovariohysterectomy status, contraceptive administration, tumour size, tumour location, tumour histological type and grade, presence of intra-tumoral necrosis, presence of vascular invasion and presence of lymph node metastasis.

Tumours were evaluated for grade in accordance with the Nottingham method for human breast tumours [11] based on the assessment of three morphological features: tubule formation, nuclear pleomorphism and mitotic counts. Each of these features was scored on a scale of 1 to 3 to indicate whether it was present in slight, moderate or marked degree, giving a putative total of three to nine points. Grade was allocated by an arbitrary division of the total points as follows: grade I (well differentiated), 3, 4 or 5 points; grade II (moderately differentiated), 6 or 7 points; and grade III (poorly differentiated), 8 or 9 points.

Immunohistochemistry

Tissue sections were incubated with primary monoclonal antibodies against ER, HER2, CK5, p63, P-cadherin and Ki67. Table 1 summarises the antibodies used and the staining procedures adopted for each antibody. Antigen retrieval was carried out by microwave treatment in a 10 mM citrate buffer, pH 6.0, with the exception of P-cadherin, which was performed with an EDTA buffer, pH 8.0 (Lab Vision, USA) in a boiling bath, during 20 min. For Ki-67, slides were previously incubated with 0.2 mg/mL trypsin (Merck) in phosphate-buffered saline (PBS) for 10 min at 37°C. After cooling (20 min at room temperature), the sections were immersed in 3% hydrogen peroxide

Table 1 Primary monoclonal antibodies and immunostaining protocols used

Antibody	Origin	Clone	Dilution	Pretreatment	Incubation
ER	Novocastra, UK	NCL-LH2	1:40	Microwave	2 h
HER2	Novocastra, UK	NCL-CB11	1:40	Microwave	Overnight
CK5	Neomarkers, USA	XM26	1:25	Microwave	Overnight
P63	Neomarkers, USA	4A4	1:150	Microwave	Overnight
PCAD	BD Transduction, USA	56	1:50	Water bath, 98°C	Overnight
Ki67	Dako, Denmark	Mib1	1:50	Trypsin+microwave	Overnight

(H_2O_2) and distillated water during 30 min to block endogenous peroxidase activity. All slides were then incubated with a blocking serum (Lab Vision) for 10 min and then incubated with the specific antibody. After incubation, slides sections were incubated with biotinylated secondary antibody, followed by streptavidin-conjugated peroxidase (Lab Vision), except for ER and HER2. For these antibodies, a polymeric labelling methodology was used as a detection system (Novolink Polymer Detection System, Novocastra, Newcastle, United Kingdom), following the manufacturer's instructions. Subsequently, the colour was developed with 3,3-diaminobenzidine tetrahydrochloride, and slides were counterstained with Gill's haematoxylin, dehydrated and mounted for evaluation by light microscopy.

Adjacent normal mammary tissues were used as internal positive controls for CK5, p63, P-cadherin (basal and myoepithelial cells) and Ki67. As positive controls, we also used canine uterus sections for ER and a human breast carcinoma with proved amplification (by FISH) and overexpression for HER2. Negative controls were carried out by replacing the primary antibody with PBS.

Evaluation of the immunohistochemical data

Nuclear ER immunoreactivity was considered positive when more than 10% of the neoplastic cells expressed this marker. To evaluate HER2 expression, Herceptest scoring system was applied (0=no membrane staining or <10% of cells stained; 1+=incomplete membrane staining in >10% of cells; 2+=>10% of cells with weak to moderate complete membrane staining; and 3+=strong and complete membrane staining in >10% of cells), with 2+ and 3+ cases considered positive. As for CK5 and p63, a semi-quantitative analysis was performed as follows: 0, <10% positive cells; 1, 10–50% positive cells; and 2, >50% positive cells, with a cytoplasmic (CK5) or nuclear (p63) pattern of cellular distribution. Ki-67 and P-cadherin immunostainings were evaluated as previously described in canine tissues [13, 14]. CK5, p63 and P-cadherin were considered positive when more than 50% of the neoplastic cells expressed each marker.

Statistical analysis

For statistical analysis, association between subtype tumour groups and continuous variables (mitotic and Ki-67 indices) was assessed with non-parametric Kruskal–Wallis test. Associations between groups and categorical variables such as tumour size, histological type, histological grade and invasion were performed using the chi-square test. Survival curves were generated by the Kaplan–Meier method, and the survival rates were compared using the log-rank test. All statistical analysis was performed using SPSS 11.5 statistical software. A P value <0.05 was considered statistically significant.

Results

Patients and tumour characteristics

The mean age of dogs at the time of surgical removal of tumours was 9.7±2.5 years (range 4–16 years of age). The mean maximum tumour diameter was 4.21±3.4 cm (range 0.5–18 cm), with tumours more frequently located in caudal mammary glands (n=36; 59%). In ten (15.2%) out of the 66 female dogs with available clinical information, ovariohysterectomy was performed prior to the removal of mammary tumours. Contraceptive administration was confirmed in eight (13.8%) cases. Histological evaluation yielded 39 (42.4%) simple carcinoma, 41 (44.6%) complex carcinoma and 12 (13%) carcinosarcoma subtypes. According to the Nottingham method, tumours were classified as grade I (n=14, 15.2%), grade II (n=33, 35.9%) and grade III (n=45, 48.9%). Necrosis was present in 87 (94.6%) cases, and vascular invasion was present in 51 (55.4%) cases. Lymph nodes were available in 49 cases, with confirmed metastasis in 26 cases (53.1%).

Immunohistochemistry profiles in canine tumours

The results of the immunohistochemical analysis performed for ER, HER2, CK5, p63 and P-cadherin are shown in Table 2 and Fig. 1. The immunohistochemical detection of ER was reliable in 96 cases: The remaining tumours have lost ER antigenicity (adjacent mammary gland was negative) and were excluded. Immunohistochemical evaluation of HER2 and P-cadherin was available in 100 and 96 cases, respectively.

ER and p63 positive cases showed the characteristic nuclear staining, whereas CK5-positive ones showed a cytoplasmic pattern of expression. HER2 positive tumours showed a membranous staining, and P-cadherin positive tumours showed a cytoplasmic and/or membranous immu-

Table 2 Immunohistochemical results in the present study

Molecular marker	Positive staining [n (%)]	Negative staining [n (%)]
ER[a]	56 (58.3)	40 (41.7)
HER2[a]	21 (21)	79 (79)
CK5	33 (32.4)	69 (67.6)
P63	33 (32.4)	69 (67.6)
PCAD[a]	42 (42.8)	54 (56.3)

[a] Immunohistochemical evaluation of ER and P-cadherin was available in 96 cases, and HER2 was available in 100 cases.

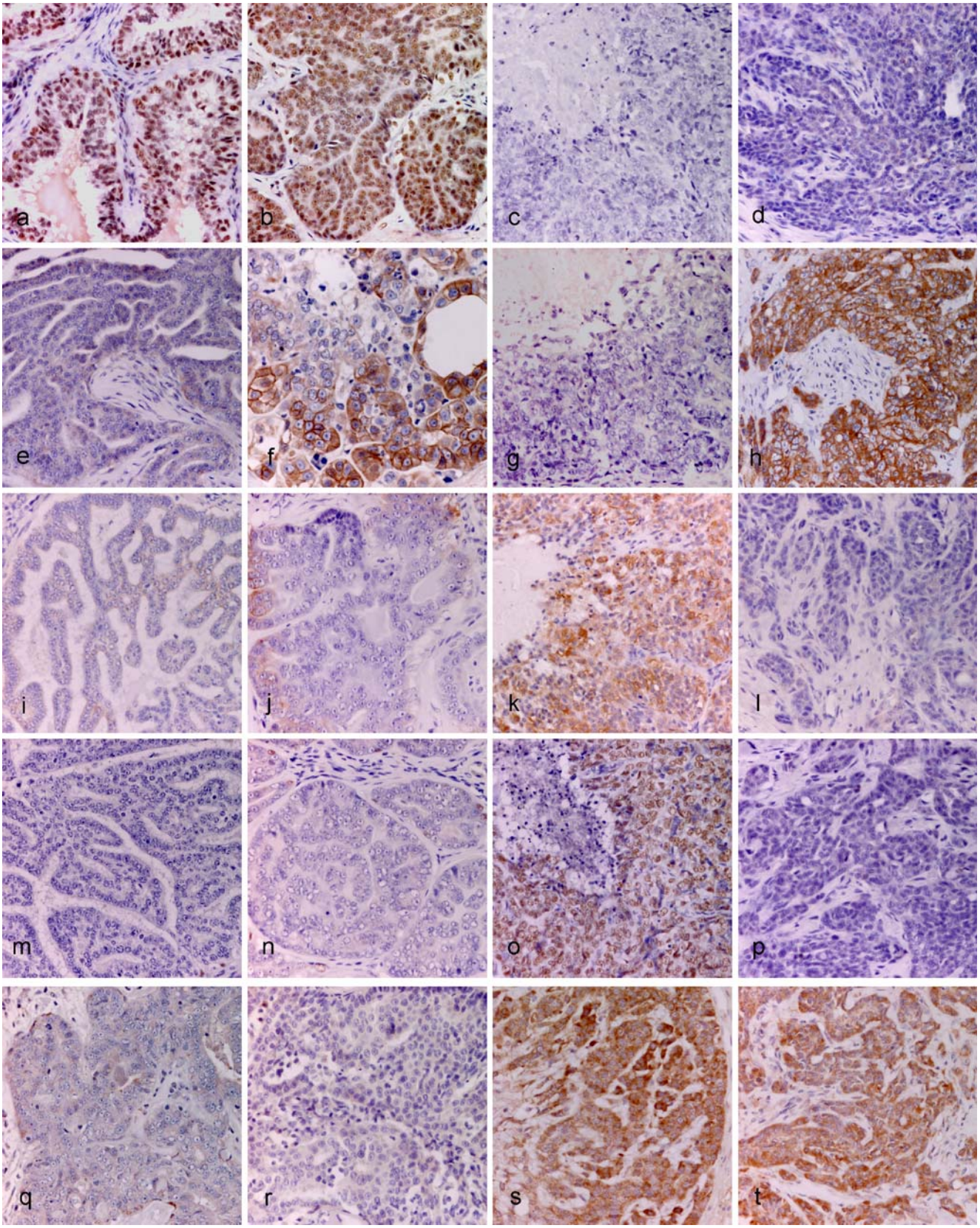

Fig. 1 Immunohistochemical expression of the different proteins studied by IHC in canine mammary carcinomas. **a**–**d** ER staining, **e**–**h** HER2 staining, **i**–**l** CK5 staining, **m**–**p** p63 staining, **q**–**t** P-cadherin staining. Each column represents a distinct molecular subtype. From *left* to *right*, each column represents luminal A, luminal B, basal and HER2 overexpressing subtypes. (Original magnification ×400)

Table 3 Frequencies of immunohistochemically defined subtypes of canine mammary carcinomas (n=96)

Subtype	ER	HER2	P-CD and/or p63 and/or CK5	Frequency [n (%)]
Luminal A	Positive	Negative	Positive/negative	43 (44.8%)
Luminal B	Positive	Positive	Positive/negative	13 (13.5%)
Basal	Negative	Negative	Positive	28 (29.2%)
HER2-overexpressing	Negative	Positive	Positive/negative	8 (8.3%)
Negative/null phenotype	Negative	Negative	Negative	4 (4.2%)

nostaining. We observed that 58.3% of canine mammary carcinomas in our series were ER positive, whereas 21% were HER2 positive (2+ and 3+). A positive basal cell marker expression was present in 32.4% tumours for both CK5 and p63 and in 42.8% tumours for P-cadherin.

According to Nielsen et al. [33], we classified each tumour based on its ER and HER2 expression. A total of 96 cases were immunohistochemically interpretable to allow sample characterisation into one of five categories (Table 3). If a tumour was ER positive, it was classified as

Table 4 Association between tumour subtypes and clinicopathological characteristics

	Luminal A [n (%)]	Luminal B [n (%)]	Basal [n (%)]	HER2 overexpressing [n (%)]	P
Age					
≤9 years old	18 (43.9%)	6 (14.6%)	13 (31.7%)	4 (9.8%)	0.90
>9 years old	24 (51.1%)	6 (12.8%)	14 (29.8%)	3 (6.4%)	
Tumour size					
<3 cm	17 (53.1%)	6 (18.8%)	8 (25%)	1 (3.1%)	0.37
3–5 cm	14 (46.7%)	4 (13.3%)	8 (26.7%)	4 (13.3%)	
>5 cm	9 (39.1%)	1 (4.3%)	10 (43.5%)	3 (13%)	
Tumour location					
Cranial glands	2 (50%)	0 (0%)	1 (25%)	1 (25%)	0.09
Medial gland	6 (60%)	2 (20%)	1 (10%)	1 (10%)	
Caudal glands	12 (33.3%)	4 (11.1%)	10 (50%)	2 (5.6%)	
Multiple	8 (72.7%)	2 (18.2%)	0 (0%)	1 (20%)	
Ovariohysterectomy					
No	18 (39.1%)	7 (15.2%)	17 (37%)	4 (8.7%)	0.057
Yes, prior to tumour development	9 (90%)	0 (0%)	0 (0%)	1 (10%)	
Yes, performed with mastectomy	6 (60%)	0 (0%)	4 (40%)	0 (0%)	
Contraception					
No	22 (44%)	6 (12%)	17 (34%)	5 (10%)	0.36
Yes	6 (75%)	0 (0%)	2 (25%)	0 (0%)	
Histological type					
Simple carcinoma	9 (23.1%)	8 (20.5%)	17 (43.6%)	5 (12.8%)	<0.0001
Complex carcinoma	32 (78%)	5 (12.2%)	3 (7.3%)	1 (2.4%)	
Carcinosarcoma	2 (16.7%)	0 (0%)	8 (66.7%)	2 (16.7%)	
Histological grade					
Grade I	14 (100%)	0 (0%)	0 (0%)	0 (0%)	<0.0001
Grade II	23 (69.7%)	5 (15.2%)	3 (9.1%)	2 (6.1%)	
Grade III	6 (13.3%)	8 (17.8%)	25 (55.6%)	6 (13.3%)	
Necrosis					
Absent	4 (80%)	1 (20%)	0 (0%)	0 (0%)	0.29
Present	39 (44.8%)	12 (13.8%)	28 (32.3%)	8 (9.2%)	
Lymphovascular invasion					
Absent	29 (70.7%)	6 (14.6%)	4 (9.8%)	2 (4.9%)	<0.0001
Present	14 (27.5%)	7 (13.7%)	24 (47.1%)	6 (11.8%)	
Lymph node metastasis[a]					
Absent	13 (56.5%)	6 (26.1%)	3 (13%)	1 (4.3%)	0.1
Present	8 (30.8%)	5 (19.2%)	11 (42.3%)	2 (7.7%)	

[a] Lymph nodes were available in 49 cases.

luminal; moreover, we distinguish luminal A and B on the basis of HER2 overexpression. If a tumour was ER positive and HER2 negative (0 or 1+), it would be classified as luminal A (ER+/HER2−); however, if it was ER and HER2 positive, it would be classified as luminal B (ER+/HER2+). If a tumour was ER negative and HER2 positive (ER−/HER2+), it would be classified as HER2-overexpressing, and if it was both ER− and HER2− negative but positive for at least one basal marker (CK5 and/or p63 and/or P-cadherin), it would be classified as basal (ER−/HER2−). If a tumour did not show expression for any of these markers, it would be classified as negative (null phenotype) and would not be considered in the remaining analyses.

Using this definition, we observed that luminal A and B subtypes comprised 44.8% and 13.5% of all tumours, respectively; basal subtype comprised 29.2%; HER2 overexpressing subtype represented 8.3%, and negative/null phenotype accounted for 4.2% in this tumour series (Table 3).

Statistically strong significant differences between the four groups were observed in this study when related with some relevant clinicopathological parameters (Table 4). Basal and HER2 overexpressing subtypes were associated with simple or carcinosarcoma histological types, whereas complex carcinomas were mostly of luminal A subtype ($P<0.0001$). In addition, basal subtype tumours presented higher histological grade, representing 55.6% of grade III tumours ($P<0.0001$) and were also significantly associated with the presence of vascular invasion ($P<0.0001$).

Basal marker expression clearly differed across distinct molecular subtypes (Table 5). Basal and HER2-overexpressing tumours demonstrated a higher frequency of the basal cell markers p63 and P-cadherin ($P<0.0001$ and $P=0.001$), and CK5-positive tumours were frequently basal subtype tumours ($P=0.001$). In contrast, luminal pattern was associated with a lower expression of basal markers. In fact, when analysing basal marker expression simultaneously, we found that the majority of luminal tumours were simultaneously negative to CK5, p63 and P-cadherin. All HER2-overexpressing tumours expressed at least one basal marker, and the basal subtype tumours showed frequently the expression of two or all basal markers ($P<0.0001$).

With regard to proliferation indices, luminal A tumours showed lower median mitotic and Ki67 labelling indices ($P=0.001$ and $P<0.0001$, respectively), whereas all other groups were characterised by higher proliferation rates, with basal subtype showing the highest Ki67 index.

Follow-up data revealed that basal subtype was significantly associated with lower overall ($P=0.002$, Fig. 2a) and disease-free ($P=0.01$, Fig. 2b) survival rates, whereas the other groups showed higher survival rates, including the HER2-overexpressing group.

Discussion

Recently, gene expression profiling has redefined breast cancer taxonomy and identified five distinct subtypes of carcinomas: luminal A, luminal B, normal breast like, HER2 overexpressing and basal like [36, 47, 48, 53]. These molecular subtypes not only reflect the heterogeneity of breast carcinomas and the possible different cell lineage pathways in breast carcinogenesis but also demonstrate the difference in clinical outcome, with basal-like subtype associated with a more aggressive behaviour [1, 47, 48, 52, 53].

Table 5 Association between different subtypes versus basal marker expression and proliferation indices

	Luminal A [*n* (%)]	Luminal B [*n* (%)]	Basal [*n* (%)]	HER2 overexpressing [*n* (%)]	*P*
CK5					
Negative	36 (60%)	8 (13.3%)	11 (18.3%)	5 (8.3%)	0.001
Positive	7 (21.9%)	5 (15.6%)	17 (53.1%)	3 (9.4%)	
P63					
Negative	32 (53.3%)	13 (21.7%)	11 (18.3%)	4 (6.7%)	<0.0001
Positive	11 (34.4%)	0 (0%)	17 (53.1%)	4 (12.5%)	
P-cadherin					
Negative	26 (56.5%)	10 (21.7%)	9 (19.6%)	1 (2.2%)	0.001
Positive	13 (31.7%)	3 (7.3%)	18 (43.9%)	7 (17.1%)	
Basal markers					
All negative	21 (77.8%)	6 (22.2%)	0 (0%)	0 (0%)	<0.0001
One positive	11 (39.3%)	6 (21.4%)	8 (28.6%)	3 (10.7%)	
Two positive	5 (20%)	1 (4%)	15 (60%)	4 (16%)	
All positive	2 (25%)	0 (0%)	5 (62.5%)	1 (12.5%)	
Median mitotic index[a] (Min–Max)	0.44 (0–1.59)	1.0 (0.1–2.99)	0.94 (0.1–2.09)	0.7 (0.3–1.9)	0.001
Median Ki67 index[a] (Min–Max)	17.89 (5.39–56.36)	26.7 (15–44.8)	28.14 (12.10–49.2)	26.4 (22.5–35.86)	<0.0001

[a] Proliferative indices were available in 86 cases.

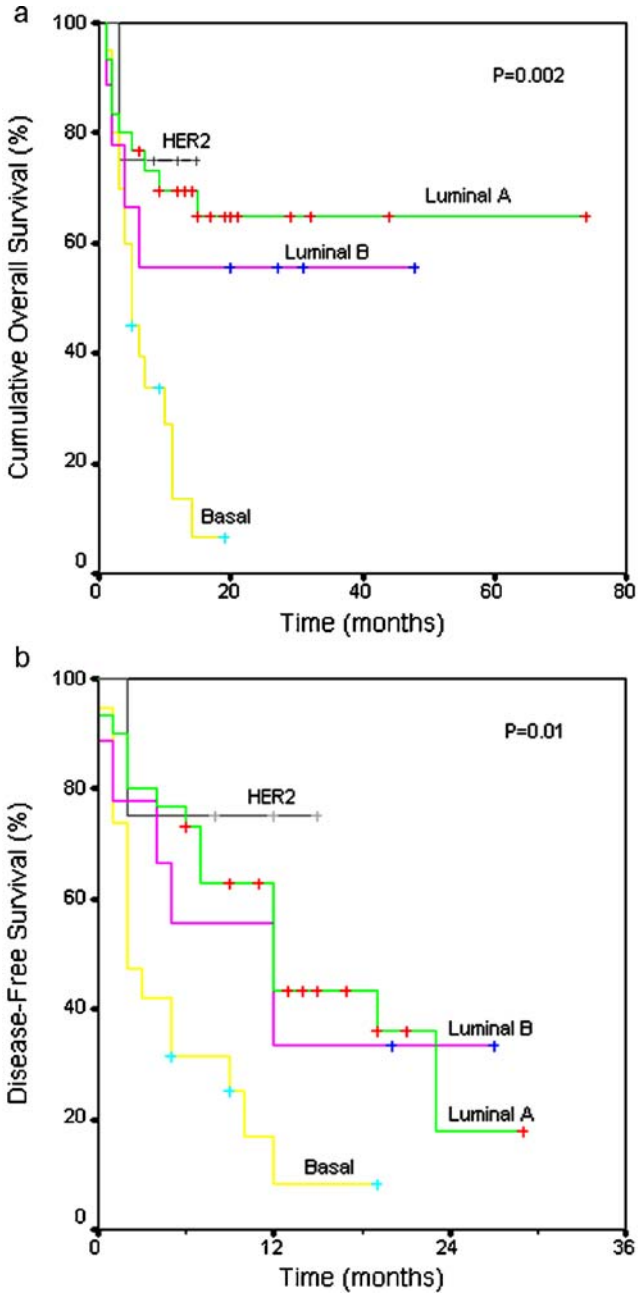

Fig. 2 Kaplan–Meier overall survival (**a**) and disease-free survival (**b**) curves of the different subtype groups

Although gene expression profiling is still considered the "gold standard" for the identification of breast carcinoma subtypes, this technology requires highly sophisticated technical equipment and is not readily available for clinical application or for retrospective studies using formalin-fixed, paraffin-embedded samples [39]. For this reason, immunohistochemistry has been used in several studies, and the evaluation of a limited panel of immunohistochemical cell markers have shown that breast carcinomas can be subdivided into subgroups remarkably similar to the ones defined by gene expression profiling [1, 3, 22, 27, 33, 38, 52].

In the present study, we found in a series of canine mammary tumours similar findings observed in human breast cancer. We have also identified distinct phenotypical subtypes in a series of canine mammary carcinomas by using an immunohistochemical panel, which included five molecular markers (ER, HER2, CK5, p63 and P-cadherin). Based on ER/HER2 molecular classification, we defined four main subgroups: luminal A (ER+/HER2−, 44.8%), luminal B (ER+/HER2+, 13.5%), basal-like (ER−/HER2−, 29.2%) and HER2 overexpressing (ER−/HER2+, 8.3%). In contrast, Sarli et al. [44] have only identified luminal A and B subtypes when studying a series of 39 canine mammary carcinomas. Although using a similar terminology, they used a distinct panel of molecular markers, and the adopted classification was not identical, with luminal subtype defined as CK19 positive tumours, regardless of hormonal status (luminal A, HER2− and luminal B, HER2+), and HER2 overexpressing and basal-like subtypes defined as CK19 negative tumours, HER2+ and HER2−, respectively.

In the current study, we found statistically strong significant differences between the four groups, with ER positive luminal A tumours more frequently associated with complex tumour type, low histological grade, less invasive and low proliferative tumours, whereas basal-like and HER2 overexpressing subtypes were associated with simple and carcinosarcoma tumour types, high histological grade, lymphovascular invasion and high proliferation, features that are in accordance to the ones described in recent human literature for basal-like cancers [20, 22, 27, 40].

CK5, p63 and P-cadherin are proteins that are expressed early in epithelial differentiation and may contribute to a committed stem cell and/or progenitor phenotype [6, 7, 9, 35]. In this study, we demonstrate that these markers are upregulated in the basal subtype, similarly to the previous results of Matos et al. [27]. In fact, the basal subtype rarely expressed just one basal marker but frequently expressed them simultaneously, which suggests a more undifferentiated profile. HER2-overexpressing subtype was also characterised by an up-regulation of basal markers, confirming some human breast studies, which suggested that HER2-overexpressing tumours should be included in a bona fide basal-like subclass [5, 27]. In contrast, the majority of luminal tumours in our series were simultaneously negative for basal cell markers, with some cases showing basal marker expression, which was also described by some authors who reported tumours co-expressing basal CK and hormone receptors or HER2 [40, 50].

Similarly to human breast cancers, in this study, we further demonstrate the molecular heterogeneity of canine mammary cancer. A "hierarchy or stem cell" model of breast cancer oncogenesis has been proposed to elucidate the observed functional heterogeneity of tumours. In this model, transformation occurs in a stem cell or in a

progenitor "highly proliferating" cell, and expansion proceeds until various maturation stages, depending on the genomic alterations. Specific genetic alterations would lead to distinct cellular transcriptomic programmes, including the change of hormonal receptors and CK expression pattern, characterising distinct subgroups of breast carcinomas [5, 8, 39].

Survival analysis revealed that distinct subtypes were associated with different clinical outcomes, with basal subtype associated with lower survival rates, similarly to human breast cancer studies [36, 47, 48]. These results also corroborate a previous study in canine mammary cancer performed by Griffey et al. [16], which firstly described basal carcinomas as having poor prognostic features. Despite many different studies associating basal-like tumours with a more aggressive clinical history and shorter survival [3, 33, 37, 47–49, 52], others did not find such a prognostic significance [12, 18]. These variations are probably related to differences between studies in patient cohorts, analytic methods and, most importantly, the immunohistochemical definitions of basal-like breast cancer [39]. Recently, Tang et al. [51], comparing several classifications with similar terminology but different definitions (such as ER/HER and triple negative classification), concluded that these classifications are related but not interchangeable.

In contrast to basal subgroup, luminal and HER2 overexpressing subtypes showed increased survival rates. The fact that luminal tumours were associated with a better prognosis is not surprising since ER positive human breast carcinomas are usually associated with a more favourable clinical outcome. In veterinary pathology, however, the prognostic value of ER in canine mammary cancer is still a matter of debate. Previous studies using biochemical [45] and immunohistochemical [34] methodologies have demonstrated the prognostic value of ER, but others have failed this confirmation [23, 28]. The observed discrepancies between different studies are probably related with sample selection, differences in antibodies, staining procedure and evaluation or sensitivity of the detection system. In our series, luminal tumours were mostly of complex type, which comes in accordance to previous canine studies reporting complex carcinomas as being more likely ER positive [15, 23, 28]. Given that this tumour type is generally associated with a better clinical outcome, its high proportion in luminal subtype groups is probably in part responsible for their favourable prognosis.

Despite HER2 recognition as a prognostic factor in human breast cancer [41, 46], the significance of HER2 overexpression in dogs with mammary carcinoma is still unclear. Some studies have shown that either HER2 amplification or protein overexpression are present in canine mammary carcinomas [2, 42], while others found no gene amplification [24]. Similarly to previous studies [10, 24], HER-2 overexpressing tumours were found usually associated with established indicators of poor prognosis such as large tumour size, high histologic grade, invasion, simple histologic type and high proliferative indices. However, Kaplan–Meier analysis revealed that this subtype was related with a more favourable clinical outcome, findings that are in contrast with human studies, which describe similar survival rates for HER2 overexpressing and basal-like subtypes [36, 47, 48] and are probably related to the small number of cases that comprise the HER2 overexpressing subtype. However, a recent study performed by Hsu et al. [17] revealed that HER2 overexpression in canine malignant mammary tumours is associated with higher survival rates. Additional large-scale studies are warranted to further explore the value of HER2 in canine mammary carcinomas.

In conclusion, as in humans, our study defined distinct molecular phenotypes in canine mammary carcinomas based on immunohistochemical analysis. Moreover, we have identified a basal-like subtype representing almost 30% of our series, which was associated with a more aggressive clinical behaviour. We believe that canine mammary carcinomas would be suitable natural models for the study of this particular subset of carcinomas. However, more studies are needed regarding the prognostic value of these immunohistochemically determined subtypes in canine mammary cancer.

Acknowledgements The authors thank Prof. Fátima Gärtner (Institute of Biomedical Science at the University of Porto, Portugal) for the contribution of some cases included in this study. We also thank Mrs Lígia Bento for expert technical assistance. This work was supported by the Centro de Ciência Animal e Veterinária (CECAV)—University of Trás-os-Montes e Alto Douro (UTAD), Vila Real, Portugal and by Portuguese Science and Technology Foundation, project POCTI/CVT/57795/2004.

Conflict of interest statement We declare that we have no conflict of interest.

References

1. Abd El-Rehim DM, Pinder SE, Paish CE, Bell J, Blamey RW, Robertson JF, Nicholson RI, Ellis IO (2004) Expression of luminal and basal cytokeratins in human breast carcinoma. J Pathol 203:661–671
2. Ahern TE, Bird RC, Church Bird AE, Wolfe LG (1996) Expression of the oncogene c-*erb*B-2 in canine mammary cancers and tumor-derived cell lines. Am J Vet Res 57:693–696
3. Banerjee S, Reis-Filho JS, Ashley S, Steele D, Ashworth A, Lakhani SR, Smith IE (2006) Basal-like breast carcinomas: clinical outcome and response to chemotherapy. J Clin Pathol 59:729–735
4. Beckmann MW, Niederacher D, Schnürch HG, Gusterson BA, Bender HG (1997) Multistep carcinogenesis of breast cancer and tumour heterogeneity. J Mol Med 75:429–439

5. Birnbaum D, Bertucci F, Ginestier C, Tagett R, Jacquemier J, Charafe-Jauffret E (2004) Basal and luminal breast cancers: basic or luminous? Int J Oncol 25:249–258
6. Boecker W, Buerger H (2003) Evidence of progenitor cells of glandular and myoepithelial cell lineages in the human adult female breast epithelium: a new progenitor (adult stem) cell concept. Cell Prolif 36(Suppl 1):73–84
7. Boecker W, Moll R, Poremba C, Holland R, Van Diest PJ, Dervan P, Burger H, Wai D, Ina Diallo R, Brandt B, Herbst H, Schmidt A, Lerch MM, Buchwallow IB (2002) Common adult stem cells in the human breast give rise to glandular and myoepithelial cell lineages: a new cell biological concept. Lab Invest 82:737–746
8. Dick JE (2003) Breast cancer stem cells revealed. Proc Natl Acad Sci U S A 100:3547–3549
9. DiRenzo J, Signoretti S, Nakamura N, Rivera-Gonzalez R, Sellers W, Loda M, Brown M (2002) Growth factor requirements and basal phenotype of an immortalized mammary epithelial cell line. Cancer Res 62:89–98
10. Dutra AP, Granja NVM, Schmitt FC, Cassali GD (2004) c-erbB-2 expression and nuclear pleomorphism in canine mammary tumors. Braz J Med Biol Res 37:1673–1681
11. Elston CW, Ellis IO (1998) Assessment of histological grade. In: Elston CW, Ellis IO (eds) Systemic pathology. The breast. 3rd edn. Churchill Livingstone, London, pp 365–384
12. Fulford LG, Reis-Filho JS, Ryder K, Jones C, Gillett CE, Hanby A, Easton D, Lakhani SR (2007) Basal-like grade III invasive ductal carcinoma of the breast: patterns of metastasis and long-term survival. Breast Cancer Res 9:R4
13. Gama A, Paredes J, Albergaria A, Gartner F, Schmitt FC (2004) P-cadherin expression in canine mammary tissues. J Comp Pathol 130:13–20
14. Gama A, Paredes J, Gartner F, Alves A, Schmitt FC (2008) Expression of E-cadherin, P-cadherin and b-catenin in canine malignant mammary tumours in relation to clinicopathological parameters, proliferation and survival. Vet J. 177:45–53 doi:10.1016/j.tvjl.2007.05.024
15. Geraldes M, Gärtner F, Schmitt F (2000) Immunohistochemical study of hormonal receptors and cell proliferation in normal canine mammary glands and spontaneous mammary tumours. Vet Rec 146:403–406
16. Griffey SM, Madewell BR, Dairkee SH, Hunt JE, Naydan DK, Higgins RJ (1993) Immunohistochemical reactivity of basal and luminal epithelium-specific cytokeratin antibodies within normal and neoplastic canine mammary glands. Vet Pathol 30:155–161
17. Hsu W-L, Huang H-M, Liao J-W, Wong M-L, Chang S-C (2007) Increased survival in dogs with malignant mammary tumours overexpressing HER-2 protein and detection of a silent single nucleotide polymorphism in the canine HER-2 gene. Vet J. doi:10.1016/j.tvjl.2007.10.013
18. Jumppanen M, Gruvberger-Saal S, Kauraniemi P, Tanner M, Bendahl PO, Lundin M, Krogh M, Kataja P, Borg A, Fernö M, Isola J (2007) Basal-like phenotype is not associated with patient survival in estrogen receptor negative breast cancers. Breast Cancer Res 9:R16
19. Karayannopoulou M, Kaldrymidou E, Constantinidis TC, Dessiris A (2005) Histological grading and prognosis in dogs with mammary carcinomas: application of a human grading method. J Comp Pathol 133:246–252
20. Kim MJ, Ro JY, Ahn SH, Kim HH, Kim SB, Gong G (2006) Clinicopathologic significance of the basal-like subtype of breast cancer: a comparison with hormone receptor and Her2/neu-overexpressing phenotypes. Human Pathol 37:1217–1226
21. Lee CH, Kim WH, Lim JH, Kang MS, Kim DY, Kweon OK (2004) Mutation and overexpression of p53 as a prognostic factor in canine mammary tumors. J Vet Sci 5:63–69
22. Livasy CA, Karaca G, Nanda R, Tretiakova MS, Olopade OI, Moore DT, Perou CM (2006) Phenotypic evaluation of the basal-like subtype of invasive breast carcinoma. Mod Path 19:264–271
23. Martin de las Mulas J, Millán Y, Dios R (2005) A prospective analysis of immunohistochemically determined estrogen receptor a and progesterone receptor expression and host and tumor factors as predictors of disease-free period in mammary tumors of the dog. Vet Pathol 42:200–212
24. Martin de las Mulas J, Ordás J, Millán Y, Fernández-Soria V, Ramón y Cajal S (2003) Oncogene HER-2 in canine mammary gland carcinomas: an immunohistochemical and chromogenic in situ hybridization study. Breast Cancer Res Treat 80:363–367
25. Matos AJ, Lopes CC, Faustino AM, Carvalheira JG, dos Santos MS, Rutteman GR, Gartner F (2006) MIB-1 labelling indices according to clinico-pathological variables in canine mammary tumours: a multivariate study. Anticancer Res 26:1821–1826
26. Matos AJ, Lopes CC, Faustino AM, Carvalheira JG, Rutteman GR, Gärtner MF (2007) E-cadherin, beta-catenin, invasion and lymph node metastases in canine malignant mammary tumours. APMIS 115:327–334
27. Matos I, Dufloth R, Alvarenga M, Zeferino LC, Schmitt F (2005) p63, cytokeratin 5, and P-cadherin: three molecular markers to distinguish basal phenotype in breast carcinomas. Virchows Arch 447:688–694
28. Millanta F, Calandrella M, Bari G, Niccolini M, Vannozzi I, Poli A (2005) Comparison of steroid receptor expression in normal, dysplastic, and neoplastic canine and feline mammary tissues. Res Vet Sci 79:225–232
29. Misdorp W (2002) Tumours of the mammary gland. In: Meuten DJ (ed) Tumors in domestic animals. 4th edn. Iowa State Press, Iowa, pp 575–606
30. Misdorp W, Else RW, Hellmén E, Lipscomb TP (1999) Histological classification of mammary tumors of the dog and the cat, Vol VII, 2nd series. Armed Forces Institute of Pathology, American Registry of Pathology, Washington D.C., and the World Health Organization Collaborating Center for Worldwide Reference on Comparative Oncology, pp 1–59
31. Misdorp W, Hart AA (1976) Prognostic factors in canine mammary cancer. J Natl Cancer Inst 56:779–786
32. Nerurkar VR, Chitale AR, Jalnakurpar BV, Naik SN, Lalitha VS (1989) Comparative pathology of canine mammary tumours. J Comp Pathol 101:389–397
33. Nielsen TO, Hsu FD, Jensen K, Cheang M, Karaca G, Hu Z, Hernandez-Boussard T, Livasy C, Cowan D, Dressler L, Akslen LA, Ragaz J, Gown AM, Gilks CB, van de Rijn M, Perou CM (2004) Immunohistochemical and clinical characterization of the basal-like subtype of invasive breast carcinoma. Clin Cancer Res 10:5367–5374
34. Nieto A, Peña L, Perez-Alenza MD, Sanchez MA, Flores JM, Castaño M (2000) Immunohistologic detection of estrogen receptor alpha in canine mammary tumors: clinical and pathologic associations and prognostic significance. Vet Pathol 37:239–247
35. Peralta Soler A, Knudsen KA, Salazar H, Han AC, Keshgegian AA (1999) P-cadherin expression in breast carcinoma indicates poor survival. Cancer 86:1263–1272
36. Perou CM, Sorlie T, Eisen MB, van de Rijn M, Jeffrey SS, Rees CA, Pollack JR, Ross DT, Johnsen H, Akslen LA, Fluge O, Pergamenschikov A, Williams C, Zhu SX, Lonning PE, Borresen-Dale AL, Brown PO, Botstein D (2000) Molecular portraits of human breast tumours. Nature 406:747–752
37. Rakha EA, El-Rehim DA, Paish C, Green AR, Lee AH, Robertson JF, Blamey RW, Macmillan D, Ellis IO (2006a) Basal phenotype identifies a poor prognostic subgroup of breast cancer of clinical importance. Eur J Cancer 42:3149–3156
38. Rakha EA, El-Sayed ME, Green AR, Paish EC, Lee AH, Ellis IO (2007) Breast carcinoma with basal differentiation: a proposal for

pathology definition based on basal cytokeratin expression. Histopathology 50:434–438
39. Rakha EA, El-Sayed ME, Reis-Filho J, Ellis IO (2008) Pathobiological aspects of basal-like breast cancer. Breast Cancer Res Treat. doi:10.1007/s10549-008-9952-1
40. Rakha EA, Putti TC, Abd El-Rehim DM, Paish C, Green AR, Powe DG, Lee AH, Robertson JF, Ellis IO (2006b) Morphological and immunophenotypic analysis of breast carcinomas with basal and myoepithelial differentiation. J Pathol 208:495–506
41. Revillion F, Bonnetarre J, Peyrat JP (1998) ErbB-2 oncogene in human breast cancer and its clinical significance. Eur J Cancer 34:791–808
42. Rungsipipat A, Tateyama S, Yamaguchi R, Uchida K, Miyoshi N, Hayashi T (1999) Immunohistochemical analysis of c-yes and c-erbB-2 oncogene products and p53 tumor suppressor protein in canine mammary tumors. J Vet Med Sci 61:27–32
43. Rutteman GR, Withrow SJ, MacEwen EG (2001) Tumors of the mammary gland. In: Withrow SJ, MacEwen BR (eds) Small animal clinical oncology. Saunders, Philadelphia, pp 455–477
44. Sarli G, Sassi F, Brunetti B, Benazzi C (2007) Luminal-like A and B types in canine mammary carcinomas. 25th Annual Meeting ESVP, Munich (Germany), pp. 187
45. Sartin EA, Barnes S, Kwapien RP, Wolfe LG (1992) Estrogen and progesterone receptor status of mammary carcinomas and correlation with clinical outcome in dogs. Am J Vet Res 53: 2196–2200
46. Slamon DJ, Clark GM, Wong SG, Levin WJ, Ullrich A, McGuire WL (1987) Human breast cancer: correlation of relapse and survival with amplification of the HER-2/neu oncogene. Science 235:177–182
47. Sorlie T, Perou CM, Tibshirani R, Aas T, Geisler S, Johnsen H, Hastie T, Eisen MB, Rijn MV, Jeffrey SS, Thorsen T, Quist H, Matese JC, Brown PO, Botstein D, Lonning PE, Borresen-Dale AL (2001) Gene expression patterns of breast carcinomas distinguish tumor subclasses with clinical implications. Proc Natl Acad Sci U S A 98:10869–10874
48. Sorlie T, Tibshirani R, Parker J, Hastie T, Marron JS, Nobel A, Deng S, Johnsen H, Pesich R, Geisler S, Demeter J, Perou CM, Lonning PE, Brown PO, Borresen-Dale AL, Botstein D (2003) Repeated observation of breast tumor subtypes in independent gene expression data sets. Proc Natl Acad Sci U S A 100:8418–8423
49. Sotiriou C, Neo SY, McShane LM, Korn EL, Long PM, Jazaeri A, Martiat P, Fox SB, Harris AL, Liu ET (2003) Breast cancer classification and prognosis based on gene expression profiles from a population-based study. Proc Natl Acad Sci U S A 100:10393–10398
50. Tan DS, Marchió C, Jones RL, Savage K, Smith IE, Dowsett M, Reis-Filho JS (2008) Triple negative breast cancer: molecular profiling and prognostic impact in adjuvant anthracycline-treated patients. Breast Cancer Res Treat. 111:27–44 doi:10.1007/s10549-007-9756-8
51. Tang P, Wang J, Bourne P (2008) Molecular classifications of breast carcinoma with similar terminology and different definitions: are they the same? Human Pathol 39:506–513
52. van de Rijn M, Perou CM, Tibshirani R, Haas P, Kallioniemi O, Kononen J, Torhorst J, Sauter G, Zuber M, Kochli OR, Mross F, Dieterich H, Seitz R, Ross D, Botstein D, Brown P (2002) Expression of cytokeratins 17 and 5 identifies a group of breast carcinomas with poor clinical outcome. Am J Pathol 161:1991–1996
53. van't Veer LJ, Dai H, van de Vijver MJ, He YD, Hart AA, Mao M, Peterse HL, van der Kooy K, Marton MJ, Witteveen AT, Schreiber GJ, Kerkhoven RM, Roberts C, Linsley PS, Bernards R, Friend SH (2002) Gene expression profiling predicts clinical outcome of breast cancer. Nature 415:530–536
54. Zaidan Dagli ML (2008) The search for suitable prognostic markers for canine mammary tumors: a promising outlook. Vet J 177:3–5

Virchows Arch (2008) 453:133–139
DOI 10.1007/s00428-008-0643-4

ORIGINAL ARTICLE

Exon 20 PIK3CA mutations decreases survival in aggressive (HER-2 positive) breast carcinomas

Enrique Lerma · Lluis Catasus · Alberto Gallardo · Gloria Peiro · Carmen Alonso · Ignacio Aranda · Agusti Barnadas · Jaime Prat

Received: 28 March 2008 / Accepted: 7 July 2008 / Published online: 5 August 2008

Abstract PIK3CA mutations at 9 and 20 exons were studied in a series of 56 selected aggressive breast carcinomas (BC): 27 with Her-2 over-expression and negativity for estrogen receptors (ER) and progesterone receptors (PR), and 29 "triple negative" BC (negative for ER, PR and Her-2). Also, immunohistochemical studies of p53, ki-67, Her-1 (EGFR), pIGF-1R, PTEN, p110α, and pAkt were performed. Six mutations in exon 20 PIK3CA were identified among the 27 Her-2 positive BC, whereas only one exon 9 PIK3CA mutation was detected in a triple negative tumor (p=0.035). Furthermore, PIK3CA mutations were associated with p110α over-expression (p=0.001). Overall survival was shorter in cases with PIK3CA mutations (p=0.015 in all series; and p=0.041 for Her-2+ tumors), although multivariate analyses did not show statistical differences. No statistical significance was related with disease-free survival. Exon 20 PIK3CA mutations are relatively frequent in Her-2+ tumors and shorten survival, whereas neither exons 9 and 20 mutations seem related with "triple negative" breast carcinomas.

Keywords Breast carcinoma · Her2-neu · p110 · PIK3CA mutations

E. Lerma · L. Catasus · A. Gallardo · J. Prat
Department of Pathology, Hospital de la Santa Creu i Sant Pau, Autonomous University of Barcelona, Barcelona, Spain

C. Alonso · A. Barnadas
Department of Oncology, Hospital de la Santa Creu i Sant Pau, Barcelona, Spain

G. Peiro · I. Aranda
Department of Pathology, Hospital General Universitario, Alicante, Spain

E. Lerma (✉)
Department of Pathology, Hospital de la Santa Creu i Sant Pau, Avda. Sant Antoni Ma Claret 167, 08025 Barcelona, Spain
e-mail: elerma@santpau.es

Introduction

Although breast cancer (BC) survival is improving due to more effective treatment and early detection, the incidence of the disease has steadily increased throughout the world over the past few decades [6]. Approximately two thirds of BCs are hormone-dependent and a good response to endocrine therapy is achieved in a large proportion of tumors. Hormone-independent tumors are usually more aggressive and grow by activation of membrane growth factor receptors or by unknown mechanisms. Nevertheless, membrane growth factor receptors could interfere with estrogen-signaling pathways and thus play a role in endocrine therapy resistance in hormone-dependent tumors [28].

The phosphatidylinositol 3′-kinase (PIK3)/AKT signaling pathway is frequently activated in multiple human epithelial cancers, including breast carcinomas [5, 8, 12, 14, 15]. PIK3 (p110α) phosphorylates PIP2 (phosphatidylinositol 4,5-biphosphate) to generate the second messenger PIP3 (phosphatidylinositol 3,4,5-triphosphate), in response to diverse stimuli. These PtdIns(3,4,5)P3 signals are localized in the inner leaflet of the plasma membrane, and activate AKT counteracting PTEN activity. After AKT activation, various downstream target genes inhibit apoptosis and promote cell proliferation [8, 27]. Besides PTEN, there are several tumor suppresser genes in the PIK3 signaling pathway, such as TSC1, TSC2, LKB 1, Foxo1a,

Foxo3a and possibly PHLPP. Most of these genes could render cancers insensitive to PIK3 inhibitors [25].

PIK3CA (phosphoinositide-3-kinase, catalytic, alpha polypeptide) mutations may be an important event in progression to the aggressive phenotype in low-grade colorectal and lung tumors [18] while in gastric and liver cancers they have a key role in earlier stage [12]. They may also be seen in glioblastomas, medulloblastomas, ovarian neoplasms, and acute leukemia [8].

Several works have studied PIK3CA mutations in BC [1, 4, 5, 14, 15, 17, 19, 21, 22, 27, 30] and in cell lines from BC [1, 10, 29, 30]. According to one recent review [8], these mutations may be present in ≈26% of BC, ≈85% of which are located in the helical domain mutants E542K and E545K and in the catalytic domain mutant H1047R. Their significance however, is controversial. In the present paper, we studied the mutations in these two exons to determine their possible role in aggressive hormone-independent BC with Her-2 over-expression or "Triple negative" tumors.

Material and methods

Material and histopathological analysis

A total of 56 breast carcinoma with negativity for estrogen receptors (ER) and progesterone receptors (PR) were collected retrospectively from two hospitals, 45 from the Department of Pathology at Hospital de la Santa Creu i Sant Pau, Autonomous University, Barcelona, Spain, and 11 from the Department of Pathology at the General Hospital, Alicante, Spain. Tumors were fixed in 4% formalin for 18–24 h. Most patients underwent a tumorectomy or a modified radical mastectomy, with dissection of axillary lymph nodes. Patients were staged according to the WHO system and tumors were histologically graded. After pathological diagnosis, adjuvant chemo or radiotherapy was done according to standard protocols. Five patients with Her-2+ tumors were also treated with Trastuzumab®. Mean follow-up was 75 months (range, 9–180). Clinicopathological data were revised for the present study and the patients were subclassified into two groups: one of 27 tumors with marked Her-2/neu over-expression (+++), and another of 29 tumors with Her-2/neu negative (triple negative, TN). None of these 29 tumors showed myoepithelial differentiation as actin and S-100 were negative [13].

This work was approved by the ethical committees of both institutions

Immunohistochemistry

Tissue micro-arrays (TMA) were prepared from paraffin-embedded tissue taken from three representative areas of each tumor. Serial, 5-μm thick sections were stained using the Envision method (DAKO). Antibodies, dilutions, antigen retrieval methods, and suppliers are listed in Table 1. ER, PR and Her-2 (Ab A-0485, Herceptest®) were repeated to confirm initial results, other membrane receptors such as Her-1 (EGFR) and pIGF-IR were studied, as well as p53 and Ki-67. Investigation of the PIK3/PTEN/Akt pathway included analysis of PTEN, pAkt, and PIK3CA (p110α). Previous BC with positivity for the Ab were used as positive controls, and consecutive tissue section from the TMA's incubated without primary Ab were the negative controls.

Distinct membrane staining in >10% of tumor cells for EGFR, pIGF-IR was counted as positive for expression. The percentage of stained nuclei was evaluated, independently of intensity, for ki67 and p53. Immunostaining cytoplasmic scores for PTEN, pAkt, and p110α were calculated by multiplying the percentage of labeled cells by the intensity of the staining (range 0–300). Loss of PTEN were considered for Scores <150, whereas p110α and pAkt over-expression for Scores >150. Three pathologists (EL, GP, and AG) separately evaluated the immunohistochemical staining, and discordant results were reviewed to achieve agreement. These evaluations were done before the statistical and survival analyses.

Mutational analysis of PIK3CA

Genomic DNA was extracted by proteinase K digestion and QUIAamp DNA Mini Kit (Quiagen, GmbH, Hilden, Germany), following the manufacturer's instructions, from frozen tumor tissue. PIK3CA mutations were assessed on

Table 1 List of primary Ab for the immunohistochemical study

Antibody	Clone	Dilution	Ag retrieval	Supplier
ER	6F11	1:40	1	Novocastra
PR	16	1:200	1	Novocastra
Her-2	A-0485	1:1		Dako
S-100	Polyclonal	1:3000	4	Dako
Alpha-actin	1A4	1:100	1	Dako
EGFR	2–18C9	1:1	5	Dako
pIGF-IR	Polyclonal	1:50	3	Cell Signaling
Ki-67	MIB-1	1:1	1	Dako
p53	BP53-12-1	1:150	1	Biogenex
PTEN	6H2.1	1:50	2	Cascade Biosciences
p110α	Polyclonal	1:50	3	Cell Signaling
pAKT	Polyclonal	1:100	3	Cell Signaling

1 Citrate buffer pH 6, autoclave 8 min, *2* citrate buffer pH 6, waterbath 95°C 30 min, *3* EDTA buffer pH 8, autoclave 8 min, *4* pepsin 0.1% 30 min, *5* proteinase K 0.1% 5 min

tumor DNA by PCR amplification and subsequent sequencing analysis, using previously reported PCR conditions and primers for exons 9 and 20 of PIK3CA [23]. The thermal cycling conditions included an initial cycle of 12 min at 94°C, followed by 40 cycles of 45 s at 94°C, 45 s at specific annealing primer temperature of 52–62°C, 1 min at 72°C, and a final extension of 10 min at 72°C. The PCR conditions for exon 9 of PIK3CA were optimized to avoid mispriming with the PIK3CA pseudogene spanning exons 9 to 13 on chromosome 22. The PCR products were purified using the exoSAP-IT (USB, Cleveland, OH) and subjected to direct sequencing using ABI PRISMTM Big Dye terminator v1.1 cycle sequencing Kit (Applied Biosystems, Foster City, CA). Sequencing fragments were detected by capillary electrophoresis using an automated ABI Prism 310 Genetic Analyzer (Applied Biosystems). Mutational analyses were done before knowing follow-up and statistics.

Follow-up and statistical analyses

Statistical analyses were performed with the SPSS/win 15.0 statistical software package (SPSS, Chicago, IL, USA). Continuous and ordinal variables between the two groups were compared using the Student's *T* test. Dichotomous variables were compared with the Fisher exact test. The overall survival analysis was estimated using the Kaplan–Meier method and compared using the log-rank test. The univariate and multivariate Cox regression analyses were used to identify the independent predictive factors that significantly influenced the overall survival. A *p*-value of 0.05 was considered significant.

Results

Both groups of tumors will be described separately and the main clinico-pathological features are comparatively presented in Table 2.

Clinico-pathological characteristics of Her-2 positive carcinomas

Twenty-seven patients were included in this group. The mean age was 60 years and 9 months (range, 42–101 years). Axillary lymph node dissection at levels I and II was

Table 2 Pathological, immunohistochemical and genetic characteristics of both subtypes of aggressive breast carcinomas

		Her-2 (n=27)	TNC (n=29)	Statistics (comparison)
Size	<2 cm	5 (18.5%)	0	Ns
	2–5 cm	19 (70.4%)	22 (75.9%)	
	>5 cm	3 (11.1%)	7 (24.1%)	
Stage	I	2 (7.5%)	4 (13.8%)	Ns
	II	17 (63%)	15 (51.7%)	
	III	6 (22.2%)	6 (20.7%)	
	IV	2 (7.5%)	4 (13.8%)	
Histol. grade	II	8 (29.6%)	4 (13.8%)	Ns
	III	19 (70.3%)	25 (86.2%)	
Ductal in situ carc.	>10%	16 (59.3%)	10 (34.5%)	Ns
	>25%	8 (29.6%)	2 (6.9%)	
Necrosis	>10%	7 (25.9%)	19 (65.6%)	0.08
Vascular invasion	Present	9 (33.3%)	8 (27.6%)	Ns
EGFR overexpr	>10%	4 (14.8%)	11 (38%)	Ns
pIGF-IR	>10%	6 (22.2%)	8 (27.6%)	
Ki 67	Median	12	50	0.007
Ki 67	<20%	15 (55.5%)	4 (13.8%)	
	20–50%	9 (33.3%)	10 (34.5%)	
	>50%	3 (11.1%)	15 (51.7%)	
P53	>10% nuclei	12 (44.4%)	16 (55.2%)	Ns
PTEN loss	<150	4 (14.8%)	3 (10.3%)	0.16
p110α	Overexpres.	4 (14.8%)	0	0.23
pAKT	>150	4 (14.8%)	1 (3.4%)	0.14
PIK3CA mutations	Exon 9 G1633A 4 E545K	0	1 (3.4%)	Ns
	Exon 20 A3140G H1047R	6 (22.2%)	0	0.008

performed in 15 patients with a mean of 14 nodes examined per patient (median, 15; range 8–27)

Mean tumor size was 3 cm (range from 1.5 to 6 cm). Five tumors (18.5%) measured less than 2 cm, 19 (70.4%) between 2–5 cm and three (11.1%) were >5 cm. The pathological stage at diagnosis was determined in all patients: two patients were stage I (7.5%), ten were stage IIA (37%), seven were IIB (25.9%), six were III (22.2%), and two were IV (7.5%).

Most carcinomas were of the ductal type (NOS), although two had mixed ductal–lobular differentiation. Histological grading was II in eight (29.6%) tumors and III in 19 (70.3%). A ductal "in situ" (DCIS) component >10% was present in 16 (59.3%) tumors, and >25% in eight (29.6%). Tumor necrosis was evident in seven (25.9%) and vascular invasion was detected in nine (33.3%).

Exon 20 PIK3CA mutations in Her-2 positive carcinomas are associated with poor prognosis and p110 over-expression

Considering the total series, seven out of 56 aggressive BC had PIK3CA mutations (12.5%), but most of them were related with Her-2+ carcinomas. Effectively, six PIK3CA somatic missense mutations were identified among the 27 Her-2 BC (22.2%). All occurred in the kinase domain (exon 20, nucleotide A3140G, aminoacid H1047R; Fig. 1), and none in the helical domain (exon 9). These mutations were more frequent in Her-2 than in TN-BC (p=0.035).

Among the Her-2+ tumors, other immunohistochemical studies showed over-expression of EGFR in four (14.8%) cases and of pIGF-IR in six (22.2%). The mean percentage of Ki67 positive nuclei was 19.3% (range 10–80%) and the median was 12; 15 cases had less than 20%, nine between 20–50% and only three tumors had a Ki67>50%. Aberrant p53 expression (>10% of nuclei) was present in 12 (44.4%) cases. Loss of PTEN expression was found in four cases. p110α over-expression (Fig. 2) was found only in four (14.8%) and pAKT in four (14.8%).

Kaplan Meyer's survival analysis for all cases (Fig. 3), as for patients with Her-2+ tumors (Fig. 4) showed shorter mean survival in cases with PIK3CA mutations (mean survival of 46 vs. 65 months in all cases, p=0.015; mean survival of Her-2+ patients 42 vs. 87 months p=0.03, p= 0.041). Disease-free survival was unrelated with mutations, because a significant number of patients were in advanced stage at diagnosis. Response to transtuzumab was not analyzed due to the scanty number of cases with this treatment and these patients were excluded from survival analyses. Furthermore, PIK3CA mutations were associated with p110α over-expression (p=0.001), and some correlation was also detected with p53 over-expression (0.068), and EGFR over-expression (p=0.14).

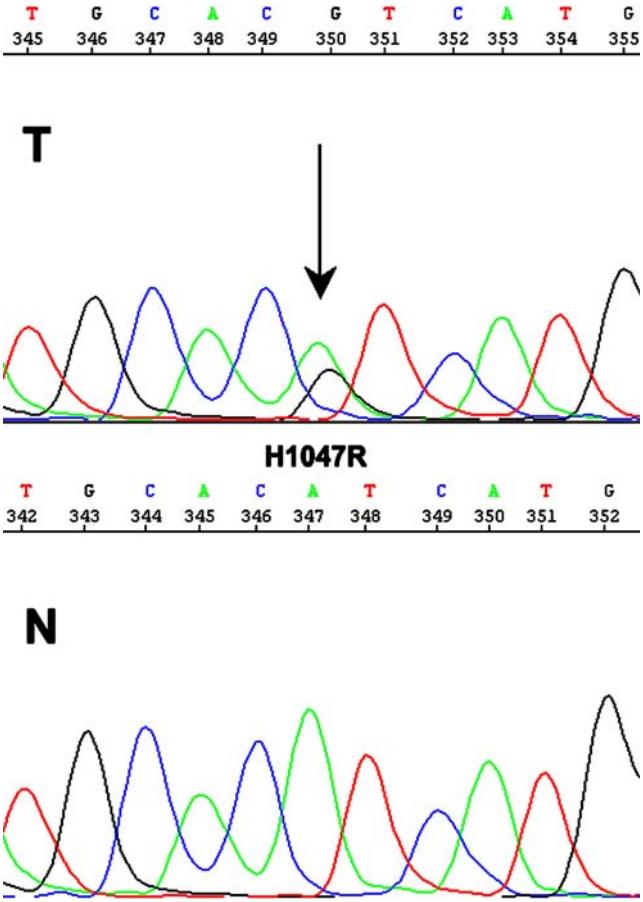

Fig. 1 Exon 20 PIK3CA mutation (nucleotide A3140G, aminoacid *H1047R*). Partial representative nucleotide sequence of sense strand around codon 1047. Sequence analysis of PCR products of tumor DNA (*T*) compared with normal DNA (*N*) revealed a missense mutation (*arrow*)

Conventional clinico-pathological features or other immunohistochemical studied molecules were statistically unrelated with PIK3CA mutations.

Clinico-pathological characteristics of triple negative carcinomas

This group included 29 patients. Mean age was 53 years, (range, 25–86 years). Tumorectomy or mastectomy was done in all cases and axillary lymph node dissection at levels I and II was performed in 27 patients, with a mean of 18 nodes per patient (median: 15; range 5–33). Mean tumor size was 6 cm (range from 2.3 to 20 cm). No tumors measured less than 2 cm, 22 (75.9%) were between 2–5 cm and seven (24.1%) were >5 cm. The pathological stage at diagnosis was determined in all patients: four were stage I (13.8% %), nine were IIA (31%), six were IIB (20.7%), six were III (20.7%), and four were IV (13.8%).

Most carcinomas were of the ductal type (NOS), although four were of the medullar histological type.

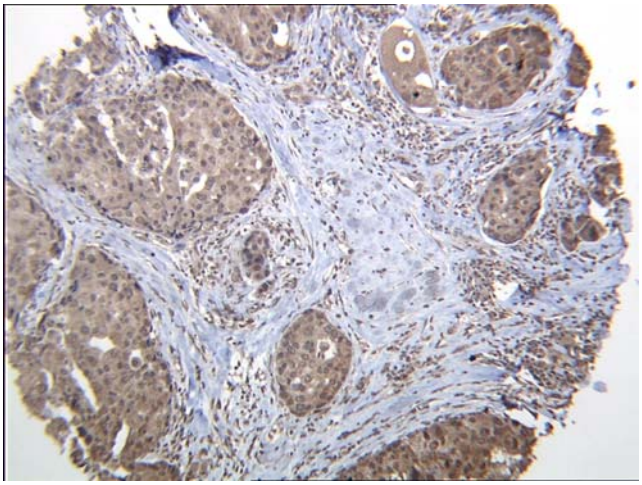

Fig. 2 Her-2+ tumor with intense p110α cytoplasmic over-expression (×40)

Histological grading was II in four (13.8%) tumors and III in 25 (86.2%). A ductal "in situ" (DCIS) component >10% was present in ten (34.5%) tumors, and >25% in two (6.9%) of them. Necrosis >10% was detected in 19 (65.6%) tumors and vascular invasion was detected in eight (27.6%).

PIK3CA mutations are very uncommon in TN carcinomas, and unrelated with other immunohistochemical or clinico-pathological features

Only one PIK3CA somatic missense mutation was identified among the 29 triple negative breast neoplasms. This occurred in the helical domain (exon 9, nucleotide G1633A, aminoacid E545K). Over-expression of EGFR was detected in 11 (38%) cases and pIGF-IR in eight (27.6%). The mean percentage of Ki67 positive nuclei was 41.3% (range 13–90%) and the median was of 50; four (13.8%) cases had less than 20%, ten (34.5%) between 20–50% and 15 (51.7%) tumors had a Ki67 >50%. Figure 5 shows that triple negative tumors had a much higher Ki67 index than Her-2 tumors (p=0.007). Aberrant p53 expression (>10% of nuclei) was present in 16 (55.2%) cases. Loss of PTEN expression was found in three (10.3%) cases. p110α over-expression was not observed and pAKT was detected in one case (3.4%). Conventional clinical varia-

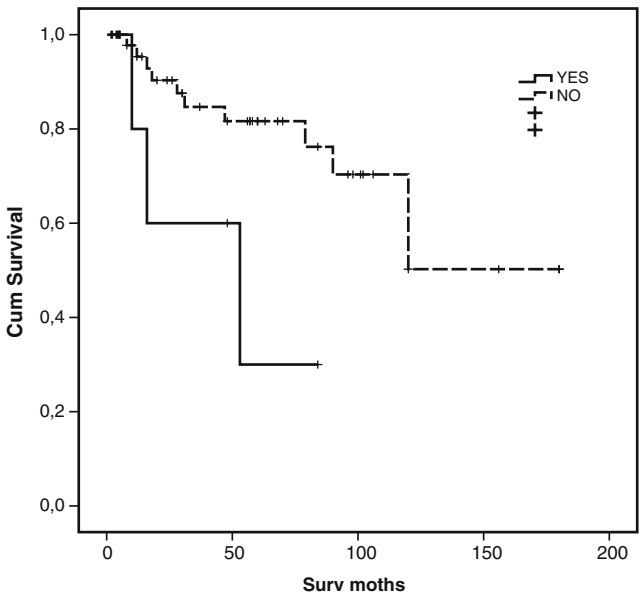

Fig. 3 Kaplan Meyer's survival analysis for all patients. Shorter survival is related with the presence of PIK3CA mutations (*continuous* versus *discontinuous lines*; p=0.03)

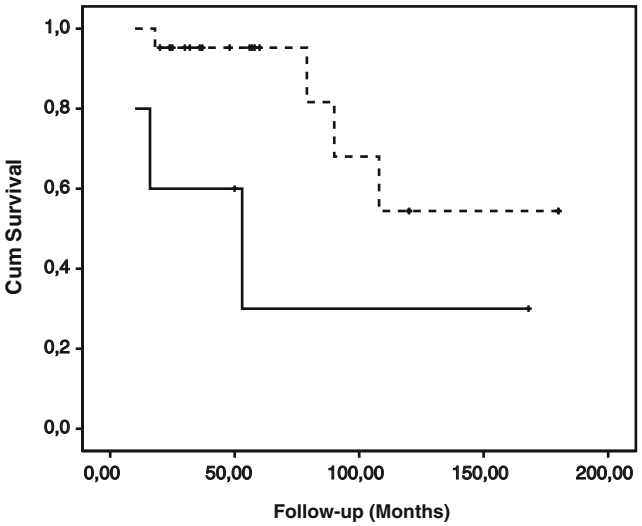

Fig. 4 Kaplan Meyer's survival analysis for patients with Her-2+ tumors, related with/without the presence of PIK3CA mutations (*continuous* versus *discontinuous lines*; p=0.03)

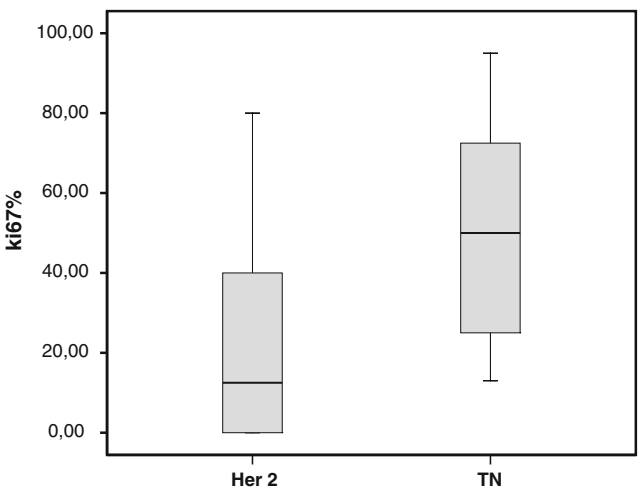

Fig. 5 Plot-box graph representing percentage of positive cells for Ki 67proliferation index; Her-2+ breast carcinomas showed lower Ki67 index (median 12.5% of positive cells) than triple negative tumors (median 50%positive cells; p=0.007 Mann Whitney test)

bles, pathological and immunohistochemical data did not show relationship with PIK3CA mutations in these tumors.

Discussion

The c-DNA microchip analysis allow the identification of three major subgroups of BC: a luminal one, equivalent to the hormone-dependent tumors that is the most common variety, and two more aggressive subgroups characterized either by Her-2/neu over-expression or the denominated basal-like or triple negative (TN) carcinomas (ER, PR, and Her-2 negatives) with less defined growth stimulus [20, 24, 26]. In the present work, we studied the significance of PIK3CA mutations in these two subgroups of aggressive BC.

PIK3CA mutations were described in 20%–40% of BC [1, 4, 5, 14, 15, 17, 19, 21, 22, 27, 30], and a recent review [8] estimated that a mean of 26% breast cancers harbor missense mutations. Approximately, 85% of these appear in three hot spots: H1047R, located in the kinase domain and coded by exon 20; E542K and E545K located in the helical domain and coded by the exon 9. Mutations are distributed in both exons with the same frequency (≈12%) [3, 4, 8, 17], and the protein resulting from these mutations (p110α) has capacity to induce oncogenic transformation in chicken embryo fibroblasts [7]. Relationship between PIK3CA mutations with other BC prognostic features was not found in initial studies [1, 5, 12]. Nevertheless, others associated these mutations with nodal metastases, Her2 receptor over-expression /amplification [22], and good prognosis [4, 17, 19].

In our series, PIK3CA mutations were present in only ≈12% of cases. However, a significant (22.2%) proportion of BC with Her-2 over-expression had exon 20 mutations. This was higher than expected and in concordance with a previous study by Saal et al. [22]. Furthermore, exon 20 mutations were associated with higher carcinogenic potential, aggressiveness [2] and, recently, with poor survival in multivariate analyses of 152 patients with BC [11] as also suggests the present study. Nevertheless, PIK3CA mutations were exceptionally uncommon in TN-BC. The aggressiveness of these tumors as well as the Ki67 index higher than in Her-2 BC could be related with alteration of other pathologic pathways, i.e., RAS mutations [10]. Indeed, TN-BC are not equivalent to "basal-like", because there are some differences in the histopathological pattern and in the immunohistochemical expression of basal cytokeratins or EGFR. These tumors do not constitute a homogeneous group [13].

Exon 9 mutations have been associated with lobular carcinomas [3, 4, 17], although most of these tumors are ERα positive, with good prognosis. Nevertheless, these mutations were recently related with aggressiveness [3] and we found one mutation in a TN-BC.

p110α overproduction was clearly associated with PIK3CA mutations in our series (p=0.001). Nevertheless, the relationship between PIK3CA mutations or p110 over-expression and loss of PTEN or Akt activation [9, 17, 22] could not be demonstrated in our cases, as in other series [4, 15, 19, 21]. It has recently been found that PIK3CA mutations and PTEN loss are not mutually exclusive [19] as was initially suggested [22]. Indeed, PIK3CA mutations and PTEN loss should be associated with similar pathologic factors [19] and both could have a relationship with Akt activation, ER-α positivity [9, 17, 19, 22], low histologic grades [17], and lobular histologic type [29].

Activation of the PIK3/PTEN/Akt pathway may also play an important role to therapy resistance in BC [9]. PIK3CA mutations has been related with radiosensitivity [19] and chemosensitivity [16], and a variety of molecules that inhibit PIK3 [25] or Akt [29] are new potential tools for the BC treatment.

In summary, TN breast carcinomas were very rarely related with exon 9 and 20 PIK3CA mutations. Exon 20 mutations, however, are more frequent than previously suspected and shorten survival of patients with Her-2 BC. It could potentially open new ways for their treatment, but further investigations with larger number of patients and prospective studies are needed.

Acknowledgments Thanks to Ms. Carolyn Newey for your help with English text and to Mr. Daniel Martinez for your technical help. This work is supported by grants from Fondo de Investigaciones Sanitarias (FIS PI06-0709), Instituto Carlos III RTICCCFIS RD06/0020/0015. (Department of Health), Madrid, and Pfizer Grant for breast cancer research

Disclosure/conflict of interest statement We declare that we have no conflict of interest.

References

1. Bachman KE, Argani P, Samuels Y, Silliman N, Ptak J, Szabo S, Konishi H, Karakas B, Blair BG, Lin C, Peters BA, Velculescu VE, Park BH (2004) The PIK3CA gene is mutated with high frequency in human breast cancers. Cancer Biol Ther 3:772–775
2. Bader AG, Kang S, Zhao L, Vogt PK (2005) Oncogenic PIK3 deregulates transcription and translation. Nat Rev Cancer 5:921–929
3. Barbareschi M, Buttitta F, Felicioni L, Cotrupi S, Barassi F, Del Grammastro M, Ferro A, Dalla Palma P, Galligioni E, Marchetti A (2007) Different prognostic roles of mutations in the helical and kinase domains of the PIK3CA gene in breast carcinoma. Clin Cancer Res 13:6064–6069
4. Buttitta F, Felicioni L, Barassi F, Martella C, Paolizzi D, Fresu G, Salvatore S, Cuccurullo F, Mezzetti A, Campani D, Marchetti A (2006) PIK3CA mutation and histological type in breast carcinoma: high frequency of mutations in lobular carcinoma. J Pathol 208:350–355
5. Campbell IG, Russell SE, Choong DY, Montgomery KG, Ciavarella ML, Hooi CS, Cristiano BE, Pearson RB, Phillips

WA (2004) Mutation of the PIK3CA gene in ovarian and breast cancer. Cancer Res 64:7678–7681
6. Ferlay P, Autier P, Boniol M, Heanue M, Colombet M, Boyle P (2007) Estimates of the cancer incidence and mortality in Europe in 2006. Ann Oncol 18:581–592
7. Kang S, Bader AG, Vogt PK (2005) Phosphatidylinositol 3-kinase mutations identified in human cancer are oncogenic. Proc Natl Acad Sci USA 102:802–807
8. Karakas B, Bachman KE, Park BH (2006) Mutation of the PIK3CA oncogene in human cancers. Br J Cancer 94:455–459
9. Kirkegaard T, Witton CJ, McGlynn LM, Tovey SM, Dunne B, Lyon A, Barlett JM (2005) AKT activation predicts outcome in breast cancer patients treated with tamoxifen. J Pathol 207:139–146
10. Hollestelle A, Elstrodt F, Nagel JH, Kallemeijn WW, Schutte M (2007) Phosphatidylinositol-3-OH kinase or RAS pathway mutations in human breast cancer cell lines. Mol Cancer Res 5:195–201
11. Lai YL, Mau BL, Cheng WH, Chen HM, Chiu HH, Tzen CY (2008) PIK3CA exon 20 mutation is independently associated with poor prognosis in breast cancer patients. Ann Surg Oncol Jan 9 PMID:18183466
12. Lee JW, Soung YH, Kim SY, Lee HW, Park WS, Nam SW, Kim SH, Lee JY, Yoo NJ, Lee SH (2005) PIK3CA gene is frequently mutated in breast carcinomas and hepatocellular carcinomas. Oncogene 24:1477–1480
13. Lerma E, Peiro G, Ramon y Cajal T, Fernandez S, Martinez D, Pons C, Muñoz F, Sabate JM, Alonso C, Ojeda B, Prat J, Barnadas A (2007) Immunohistochemical heterogeneity of breast carcinomas negative for estrogen receptors, progesterone receptors and Her2/neu (basal like breast carcinomas). Modern Pathology 20:1200–1207
14. Levine DA, Bogomolniy F, Yee CJ, Lash A, Barakat RR, Borgen PI, Boyd J (2005) Frequent mutation of the PIK3CA gene in ovarian and breast cancers. Clin Cancer Res 11:2875–2878
15. Li SY, Rong M, Grieu F, Iacopetta B (2006) PIK3CA mutations in breast cancer are associated with poor outcome. Breast Cancer ResTreat 96:91–95
16. Liang K, Lu Y, Li X, Glazer RI, Mills GB, Fan Z (2006) Differential roles of phosphoinositide-dependent protein kinase-1 and Akt1 expression and phosphorylation in breast cancer cell resistance to paclitaxel, doxorubicin, and gemcitabine. Mol Pharmacol 70:1045–1052
17. Maruyama N, Miyoshi Y, Taguchi T, Tamaki Y, Monden M, Noguchi S (2007) Clinicopathologic analysis of breast cancers with PIK3CA mutations in Japanese women. Clin Cancer Res 3:408–414
18. Massion PP, Taflan PM, Shyr Y, Rahman SM, Yildiz P, Shakthour B, Edgerton ME, Ninan M, Andersen JJ, Gonzalez AL (2004) Early involvement of the phosphatidylinositol 3-kinase/Akt pathway in lung cancer progression. Am J Respir Crit Care Med 170:1088–1094
19. Pérez-Tenorio G, Alkhori L, Olsson B, Waltersson MA, Nordenskjöld B, Rutqvist LE, Skoog L, Stål O (2007) PIK3CA mutations and PTEN loss correlate with similar prognostic factors and are not mutually exclusive in breast cancer. Clin Cancer Res 13:3577–3584
20. Perou CM, Sørlie T, Eisen MB, van de Rijn M, Jeffrey SS, Rees CA, Pollack JR, Ross DT, Johnsen H, Akslen LA, Fluge O, Pergamenschikov A, Williams C, Zhu SX, Lønning PE, Børresen-Dale AL, Brown PO, Botstein D (2000) Molecular portraits of human breast tumors. Nature 406:747–752
21. Saal LH, Johansson P, Holm K, Gruvberger-Saal SK, She QB, Maurer M, Koujak S, Ferrando AA, Malmström P, Memeo L, Isola J, Bendahl PO, Rosen N, Hibshoosh H, Ringnér M, Borg A, Parsons R (2007) Poor prognosis in carcinoma is associated with a gene expression signature of aberrant PTEN tumor suppressor pathway activity. Proc Natl Acad Sci U S A 104:7564–7569
22. Saal LH, Holm K, Maurer M, Memeo L, Su T, Wang X, Yu JS, Malmström PO, Mansukhani M, Enoksson J, Hibshoosh H, Borg A, Parsons R (2005) PIK3CA mutations correlate with hormone receptors, node metastasis, and ERBB2, and are mutually exclusive with PTEN loss in human breast carcinoma. Cancer Res 65:2554–2559
23. Samuels Y, Wang Z, Bardelli A, Silliman N, Ptak J, Szabo S, Yan H, Gazdar A, Powell SM, Riggins GJ, Willson JK, Markowitz S, Kinzler KW, Vogelstein B, Velculescu VE (2004) High frequency of mutations of the PIK3CA gene in human cancers. Science 304:554
24. Sorlie T, Tibshirani R, Parker J, Hastie T, Marron JS, Nobel A, Deng S, Johnsen H, Pesich R, Geisler S, Demeter J, Perou CM, Lønning PE, Brown PO, Børresen-Dale AL, Botstein D (2003) Repeated observation of breast tumor subtypes in independent gene expression data sets. Proc Natl Acad Sci USA 100: 8418–8423
25. Stephens L, Williams R, Hawkins P (2003) Phosphoinositide 3-kinases as drug targets in cancer. Curr Opinion in Pharmacology 5:357–365
26. van de Vijver MJ, He YD, van't Veer LJ, Dai H, Hart AA, Voskuil DW, Schreiber GJ, Peterse JL, Roberts C, Marton MJ, Parrish M, Atsma D, Witteveen A, Glas A, Delahaye L, van der Velde T, Bartelink H, Rodenhuis S, Rutgers ET, Friend SH, Bernards R (2002) A gene expression signature as a predictor of survival in breast cancer. N Eng J Med 347:1999–2009
27. Vivanco I, Sawyers CL (2002) The phosphatidylinositol 3-kinase AKT pathway in human cancer. Nat Rev Cancer 2:489–501
28. Weinberg OK, Marquez-Garban DC, Pietras RJ (2005) New approaches to reverse resistance to hormonal therapy in human breast cancer. Drug Resist Updates 8:219–233
29. Whyte DB, Holbeck SL (2006) Correlation of PIK3Ca mutations with gene expression and drug sensitivity in NCI-60 cell lines. Biochem Biophys Res Comunn 340:469–475
30. Wu G, Xing M, Mambo E, Huang X, Liu J, Guo Z, Chatterjee A, Goldenberg D, Gollin SM, Sukumar S, Trink B, Sidransky D (2005) Somatic mutation and gain of copy number of PIK3CA in human breast cancer. Breast Cancer Res 7:R609–R616

Virchows Arch (2008) 453:141–153
DOI 10.1007/s00428-008-0639-0

ORIGINAL ARTICLE

Clinicopathological features with outcomes of a series of conventional and proximal-type epithelioid sarcomas, diagnosed over a period of 10 years at a tertiary cancer hospital in India

Bharat Rekhi · Biru D. Gorad · R. F. Chinoy

Received: 18 March 2008 / Revised: 29 May 2008 / Accepted: 18 June 2008 / Published online: 8 July 2008

Abstract Epithelioid sarcoma (ES) is an uncommon sarcoma. Lately, its variants, including proximal-type ES, have been recognized. The present study highlights clinicopathological features of 26 (65%) conventional and 14 (35%) cases of proximal-type ES. Thirty-eight percent of cases were seen in 21–30-year age group, including 77.5% cases in men. Extremities were the commonest sites in both the subtypes. Histologically, conventional-type ES displayed nodular tumor aggregates with necrosis, while proximal-type showed solid arrangement of large, "rhabdoid-like" cells. More cases (64.2%) of the proximal type were of grade 3. A range of differential diagnoses was considered. Most important immunohistochemical markers were vimentin, epithelial membrane antigen, cytokeratin, CD34, and desmin. Maximum (72.5%) cases were treated surgically. Recurrences and metastasis were observed more in the proximal type. The 7-year disease-free survival was 19.4% in the conventional and nil in the proximal subtype (p=0.06). The overall survival rate was also lower in the proximal (31.3%) than conventional type (90.2%; p<0.001). Other unfavorable parameters were deeper location, larger size, and higher tumor stage. This unusual sarcoma, with characteristic growth patterns, merits a proper histological evaluation, as it has many mimics. Proximal-type ES is rather a morphological subtype, associated with an aggressive course.

B. Rekhi (✉) · B. D. Gorad · R. F. Chinoy
Deparment of Pathology, Tata Memorial Hospital,
Dr E.B. Road, Parel,
Mumbai, India, 400012
e-mail: rekhi.bharat@gmail.com

Keywords Epithelioid sarcoma · Proximal-type epithelioid sarcoma · Uncommon sarcomas

Introduction

Epithelioid sarcoma (ES), first described by Franz Enzinger [7], is an uncommon malignant soft tissue neoplasm, with an uncertain histogenesis, and is predominantly seen in the distal extremities. It is a slow-growing tumor and mainly occurs in young adult men, predominantly affecting the subcutaneous tissues, fascia, or tendon sheaths of the extremities, with a predilection for the hands and forearms [4, 8, 21]. Unusual primary sites include the vulva, penis, and perineum [12, 14, 27]. It involves the viscera only secondarily [4].

Histologically, a conventional ES shows an admixture of epithelioid cells and spindle cells that are often arranged in nodular aggregates around central necrosis, creating a superficial resemblance to a necrobiotic granuloma [2, 4, 8, 21]. Lately, variants of an ES have been identified namely, a "fibroma-like" variant that shows a collagen-rich storiform pattern, reminiscent of a fibroma or a fibrous histiocytoma, an angiomatoid variant, revealing a pseudovascular growth pattern due abundant intralesional hemorrhage, and a proximal-type ES [10, 17, 18, 26]. A proximal-type ES, first described by Guillou et al. [10], with a distinct clinical profile, is characterized by a solid growth pattern of large, "rhabdoid-like" tumor cells. Immunohistochemically, an ES shows epithelial and mesenchymal differentiation.

The present study was carried out to study the clinico-pathological spectrum, including prognostic parameters,

immunophenotypic profile, and outcomes of 40 cases of conventional and proximal-type ESs identified over a 10-year duration.

Materials and methods

A retrospective study of 40 cases of ESs, diagnosed in the surgical pathology department of a tertiary cancer referral hospital, from July 1996 to June 2006, was undertaken.

Clinical charts of the patients and the hospital data information system were assessed for various clinicopathological parameters, including chief complaints. Documentation of treatment details, tumor recurrence, and metastasis was made. Radiological findings were accessed from the picture-archiving and communication system at Centricity.

The diagnostic material included "in-house" operative specimens, as well as from peripheral hospitals, in the form of paraffin blocks and slides or specimens.

All the widely excised, amputated, or disarticulated specimens were processed routinely.

Details regarding tumor location, gross examination, tumor size in the largest dimension, circumscription, degree of hemorrhage, and necrosis were noted.

Conventional hematoxylin and eosin (H&E)-stained sections were available in all cases.

On microscopic examination, various histomorphological parameters were analyzed including tumor circumscription, cellularity, growth pattern, in terms of morphological types, number of mitoses per ten high-power fields (hpf), areas of hemorrhage, necrosis, presence of lymphovascular emboli, perineural invasion, and calcification. In addition, marginal status, wherever possible, was documented.

Surgical excisions were categorized as Rx R0, R1, and R2. While Rx was an excision lacking a marginal status, R0 was a resection with gross and microscopically free margins, R1 was with grossly free and microscopically positive margins, and R2 was an excision with gross and microscopic positive margins.

Diagnostic criteria for ES, including the proximal type, were as documented earlier [4, 10]. Even though, according to the World Health Organization guidelines, tumor grading has not been recommended for an ES, we, like Casanova et al. [3], attempted grading in our cases by using French Federation of Cancer Centers (FNCLCC) three-tier grading system [9]. This included parameters like differentiation score, mitotic counts, and percentage tumor necrosis. Staging was done using the American Joint Committee on Cancer/ International Union Against Cancer staging system [6, 22].

Immunohistochemistry (IHC) staining was carried out on formalin-fixed, paraffin-embedded tissue, using a avidin–biotin peroxidase complex system. A wide panel of antibody markers was performed to substantiate the diagnosis (Table 1). Appropriate positive and negative controls were used.

Statistical analysis

Statistical analysis was carried out using SPSS (version 14) software. In order to compare the differences between proximal- and conventional-type ES for variables like age, location, gender, and tumor size, grade, and stage, Chi-square test was employed. A p value less than 0.05 was considered as statistically significant (S).

Table 1 List of various primary antibodies used in cases of ESs

Antigen	Type	Dilution	Antigen retrieval	Source
Vimentin	Monoclonal	1:50	Microwave	Dako, Produkionsveg, Glostrup, Denmark
CK	Monoclonal	1:100	Pronase (enzymatic)	Dako
CK 7	Monoclonal	1:50	Microwave	Dako
EMA	Monoclonal	1:100	Pepsin (enzymatic)	Dako
Desmin	Monoclonal	1:50	Microwave	Dako
CD34	Monoclonal	1:100	Microwave	Dako
SMA	Monoclonal	1:200	Pepsin (Enzymatic)	Dako
CK20	Monoclonal	1:100	Microwave	Dako
CEA	Polyclonal	1:400	Pepsin (enzymatic)	Dako
S-100	Polyclonal	1:300	Pepsin (enzymatic)	Dako
Myo D-1	Monoclonal	1:20	Pressure cooker and EDTA	Dako
HMB-45	Monoclonal	1:50	Microwave	Dako
LCA	Monoclonal	1:100	Microwave	Dako
C-KIT	Polyclonal	1:100	Microwave	Dako
CD31	Monoclonal	1:40	Microwave	Dako

CK Cytokeratin, *EMA* epithelial membrane antigen, *SMA* smooth muscle actin, *CEA* carcinoembryogenic antigen, *LCA* leukocyte common antigen

Survival proportions were estimated using the Kaplan–Meir method. For each subject, the starting date of follow-up was defined as the date of first presentation. The end of follow-up was set to 30th March 2008 or date of death if this event occurred earlier. The log rank test was used to test the equality of survival functions across the groups. Patients were followed up for a maximum of 7 years, with an average follow up of 71 months.

Progression of the disease was defined in terms of local recurrence and distant metastasis. Disease-free survival (DFS) and overall survival (OAS) were obtained from the follow-up data. Follow-up details with outcomes were available in 33 cases, while details pertaining to recurrences and metastatic status in individual cases were available in 37 cases. Analysis were done separately, considering recurrence or metastasis as the event of interest (DFS) and death due to any cause (most likely ES) as the event of interest (OAS).

Cox proportion hazard model was used to estimate hazard ratios (HR) and its 95% confidence interval (CI) for the DFS from ES, according to age, location, size, grade, stage, and the two morphological subtypes.

Results

A total of 40 cases were identified as ESs and substantiated with IHC results.

Clinical parameters

A wide age range was noted, with the youngest patient being 6 years old and oldest of 70 years age. Maximum cases were seen in the age group of 21–30 years, i.e., 15 (37.5%) cases, with men outnumbering women (M/F ratio= 3.44:1). Mean age was 32 years, and median age was 27 years.

Clinically, 30 (75%) patients presented with a painless swelling/mass, eight cases had skin ulceration, followed by swelling, and the remaining two cases complained of painful swellings. The duration of symptoms ranged from 3 months to 10 years, with a mean of 17 months.

In maximum cases, i.e., 33 (82.5%), the tumor was found to be superficially located, while in seven (17.5%) cases, it was deep seated within the muscles. The most common site of involvement was the upper extremity, i.e., in 18 (45%) cases, followed by the lower extremity in 12 (30%) cases, gluteal region in two (5%) cases, and groin region in five (12.5%) cases. Out of 18 cases in the upper extremity, ten were seen involving the wrist and forearm and four, each, in the hand and the arm, respectively. Out of the 12 cases in the lower extremities, eight were located in the thigh, three in the foot, and one in the calf region. The remaining one case, each, was seen in the chest wall, perineum, and the scalp, respectively.

Gross features

The primary tumor size varied from 2 to 15 cm in the largest dimension (mean=6 cm). It was less than or equal to 3 cm in 12 (30%) cases and greater than 3 cm in 28 (70%) cases. Twelve (85.4%) out of 14 cases of proximal-type ES had tumor size greater than 3 cm, and 16 (61.5%) of 26 cases of conventional ES had tumor size greater than 3 cm. Overall, 12 (30%) cases had a tumor size less than or equal to 3 cm, and 20 (50%) cases had a tumor size less than or equal to 5 cm. Grossly, most of the cases showed presence of a lobulated mass, which, on the cut surface, was fleshy with areas of hemorrhage and necrosis. Eight (20%) cases were associated with overlying skin ulceration. In three cases, the tumor was seen involving the underlying bones (Table 2).

Microscopic features

In 26 (65%) cases, the tumor displayed the classic "granuloma-like" appearance. The predominant cells were oval to polygonal shaped with large vesicular nuclei, prominent nucleoli, and abundant eosinophilic cytoplasm. Admixed were spindle cells, predominantly in the periphery of the nodules. These cases were labeled as conventional-type ES. Two such cases showed focal dystrophic calcification. In few cases, tumor infiltration was seen along the muscle fibers, as an isolated nodule or as single cell infiltration.

Fourteen cases (35%) showed a diffuse, sheet-like arrangement of large polygonal cells with vesicular, pleomorphic nuclei, prominent nucleoli, and moderate to abundant eosinophilic cytoplasm. Out of these, two cases displayed focal tumor cell disintegration like a pseudo-angiosarcomatous pattern. Noteworthy, all these cases showed varying number of cells with distinct intracytoplasmic eosinophilic inclusions, reminiscent of "rhabdoid" morphology. Four such cases showed tumor giant cells. These cases were labeled as proximal-type ES (Fig. 1).

Mitotic activity was assessed in all cases. Maximum cases (25; 62.5%) had mitoses less than nine per ten hpf. Thirteen cases (32.5%) had mitoses ranging from 10 to 19 per ten hpf, and the remaining two cases had mitoses greater than 20 per ten hpf.

As per FNCLCC grading system, all cases revealed a differentiation score of 3. Further, 26 (65%) cases were of grade 2, and 14 (35%) cases were of grade 3.

Table 2 Clinicopathological features of 40 cases conventional and proximal-type of ES

Sr. no.	Age	Sex	Site	Tumor size (cm)	Morphological subtype	Treatment given		Local recurrence (number)	Metastasis (site)	Outcomes
						Type (Resection)	Adjuvant CT/RT			
1	18	M	Elbow	15.0	Proximal	Above elbow amputation (R0)	CT+RT	1	B/L Multiple Lung	DOD
2	52	F	Thigh	10.0	Proximal	WE (R1)	CT+RT	2	Nil	Lost to FU
3	26	M	Thigh	13.0	Proximal	Palliative CT RT	–	Nil	B/L Lung, Pleural effusion, Ascitis.	DOD
4	29	M	Hand	3.0	Proximal	Below elbow Amputation (R0)	CT+RT	Nil	Nil	FOD
5	43	F	Gluteal region	11.0	Proximal	WE (R2)	–	1	Nil	AWD
6	35	M	Gluteal region	13.5	Proximal	WE+GND (R0)	RT	1	Nil	DOD
7	30	M	Scalp	5.5	Proximal	WE (R0)	–	1	NK	Lost to FU
8	28	F	Thigh	4.0	Proximal	WE (RX)	–	NK	NK	Lost to FU
9	60	M	Thigh	6.5	Proximal	WE+GND (R0)	CT+RT	1	Lymph nodes Groin	DOD
10	46	M	Thigh	8.5	Proximal	WE (Rx)	NK	NK	NK	Lost to FU
11	15	M	Forearm	6.0	Proximal	Above elbow amputation (R1)	CT+RT	1	B/L lung	DOD
12	26	M	Calf	6.2	Proximal	WE (R0)	CT+RT	1	Lymph nodes Groin	AWD
13	70	M	Groin	2.5	Proximal	WE (R0)	–	1	Nil	AWD
14	47	M	Perineum	4.6	Proximal	WE (R0)	–	1	Nil	AWD
15	45	M	Groin	3.5	Conventional	WE (R0)	CT+RT	Nil	Nil	FOD
16	16	M	Foot	12.0	Conventional	Below knee amputation (R0)	–	Nil	Finger	FOD
17	27	M	Forearm	10.0	Conventional	Forequarter amputation (R0)	CT+RT	Nil	Nil	FOD
18	21	M	Forearm	8.0	Conventional	Above elbow Amputation (R0)	CT+RT	2	Nil	FOD
19	36	M	Foot	4.5	Conventional	WE+GND (R0)	CT+RT	Nil	Lung, Lymph nodes Groin	DOD
20	39	M	Groin	7.0	Conventional	WE (R0)	CT+RT	1	Lymph nodes Groin	AWD
21	32	M	Groin	9.0	Conventional	WE+ND (R0)	CT+RT	Nil	Lymph nodes Infrapancreatic	DOD
22	16	M	Forearm	3.0	Conventional	WE (R0)	CT+RT	1	Nil	FOD
23	19	F	Arm	4.7	Conventional	WE (R0)	–	1	Nil	FOD
24	18	M	Thigh	3.0	Conventional	WE (R0)	CT+RT	Nil	Nil	FOD
25	48	F	Hand	2.0	Conventional	Middle finger amputation (R0)	–	Nil	Nil	FOD
26	24	M	Thigh	10.0	Conventional	WE (R0)	CT+RT	Nil	Nil	FOD
27	35	M	Arm	2.2	Conventional	WE (RX)	CT+RT	NK	Lymph nodes Axilla	Lost to FU
28	58	M	Chest wall	4.0	Conventional	WE (R0)	CT+RT	NK	NK	Lost to FU
29	48	F	Groin	6.5	Conventional	WE(R0)	RT	1	Nil	FOD
30	25	M	Foot	5.5	Conventional	WE (R0)	–	1	NK	Lost to FU
31	17	F	Hand	3.0	Conventional	WE (R0)	CT+RT	3	Nil	FOD
32	25	M	Elbow	2.8	Conventional	WE (R0)	CT+RT	1	Nil	FOD
33	27	F	Arm	2.7	Conventional	WE (R0)	–	1	Nil	FOD
34	21	M	Forearm	5.4	Conventional	WE (R0)	–	Nil	Lymph nodes Axilla	FOD
35	37	M	Forearm	3.0	Conventional	WE (R0)	CT+RT	1	Nil	FOD
36	21	M	Forearm	7.0	Conventional	Above elbow amputation (R0)	CT+RT	2	Nil	FOD
37	6	F	Hand	2.0	Conventional	WE (R0)	–	1	Nil	FOD
38	47	M	Thigh	2.5	Conventional	WE (R0)	–	1	Nil	FOD
39	21	M	Hand	3.8	Conventional	WE (R0)	CT+RT	Nil	Nil	FOD
40	29	M	Forearm	4.5	Conventional	Above elbow amputation (R0)	CT+RT	2	Finger	FOD

M Male, *F* female, mean age=32 years, median age=27 years, *WE* wide excision, *ND* node dissection, *GND* groin node dissection, *AND* axillary node dissection, *R* resection, *CT* chemotherapy, *RT* radiotherapy, *B/L* bilateral, *AWD* alive with residual disease, *FOD* free of disease, *DOD* died of disease, *FU* follow-up, *NK* not known

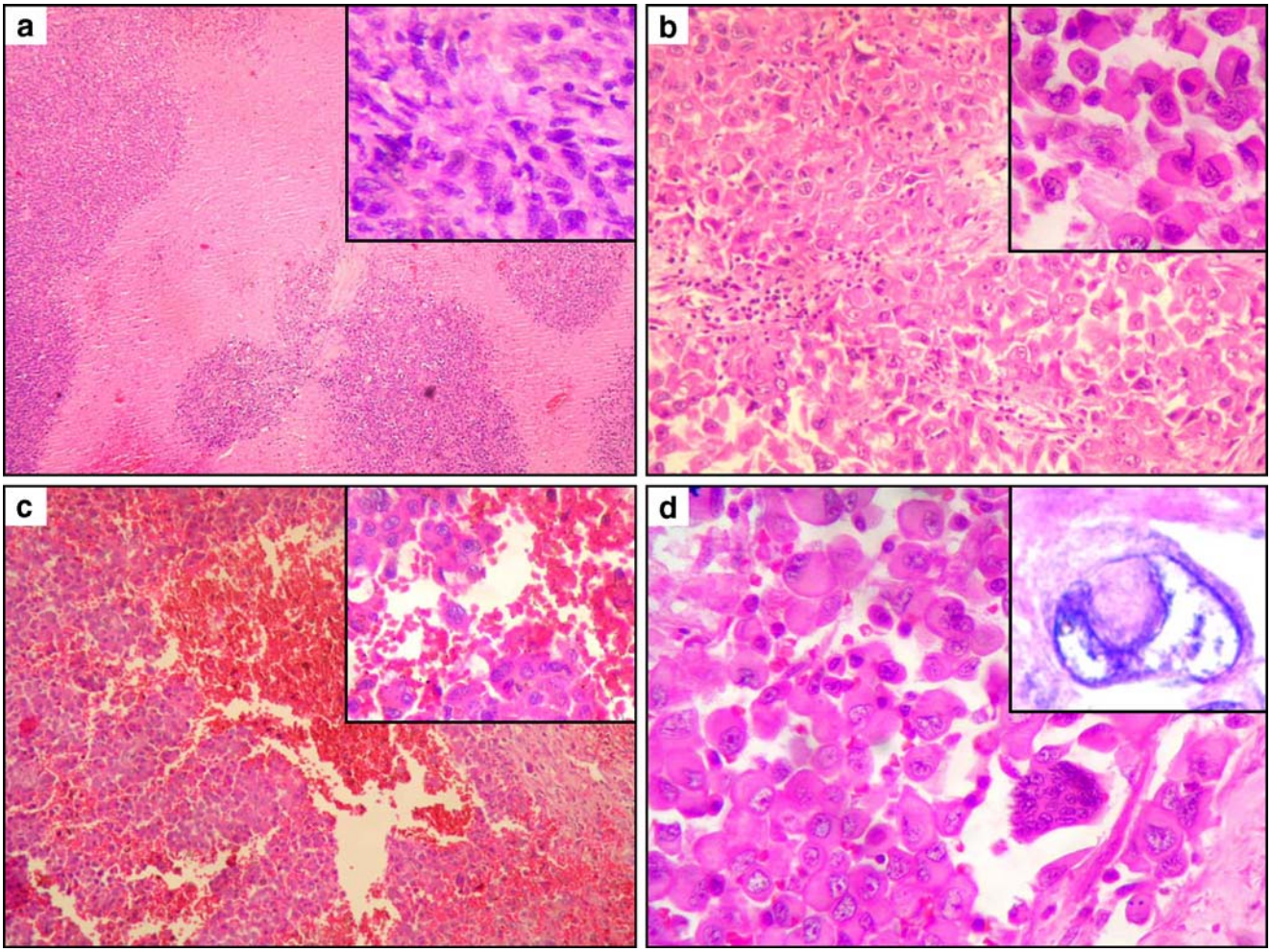

Fig. 1 **a** Conventional-type epithelioid sarcoma. Nodular aggregates of tumor cells around areas of necrosis. H&E ×100. *Inset*, showing polygonal and spindly cells forming tumor aggregates. H&E ×400. **b** Proximal-type epithelioid sarcoma. Solid sheet-like pattern of large, eosinophilic cells. H&E ×200. *Inset*, showing large, polygonal cells with abundant, eosinophilic cytoplasm. H&E ×400. **c** Areas of hemorrhage reminiscent of pseudoangiosarcomatous pattern. H&E ×100. *Inset*, showing large cells in juxtaposition with areas of hemorrhage. H&E ×100. **d** Higher magnification showing large, rhabdoid cells with intracytoplasmic inclusions indenting nucleus, showing prominent nucleoli. H&E ×400. *Inset*, showing a binucleate cell with a conspicuous intracytoplasmic inclusion. H&E ×1,000

Among the various IHC markers performed, diffuse, strong, cytoplasmic vimentin positivity was seen in all the cases, followed by cytoplasmic or membranous epithelial membrane antigen (EMA) positivity in 37 (92.5%) cases. Cytoplasmic cytokeratin (CK) positivity was seen in 30 (75%) cases. Most of the cases showed its widespread expression. It was focal but discrete in the remaining. CK7, employed in case, was diffusely positive. CD34 positivity was cytoplasmic membranous, in 25 (62.5%) cases, within most of the tumor cells. CD31 was not found positive in any of the cases it was used. Focal desmin positivity was seen in eight (20%) cases of proximal-type ES. S-100 showed focal intranuclear and cytoplasmic positivity in four cases. While focal S-100 expression was identified in more cases of the proximal-type ES, CD34 was seen in more cases of conventional ES. (Fig. 2; Table 3).

Further comparisons between the two subtypes with other clinical parameters showed a similar age and gender distribution, with no statistically significant difference. However, in terms of location, more cases of conventional ES were seen in upper extremities, while the lower extremity formed the commonest site of occurrence in the proximal type. Moreover, the cases of proximal-type were significantly more commonly associated with a deeper location (p=0.000). In terms of tumor size, maximum cases of conventional ES were less than or equal to 5 cm in size, in contrast to the proximal type, wherein maximum cases (71.4%) had tumor size greater than 5 cm (p=0.04, S). Seventeen (65.3%) cases of conventional ES were of stage III, and nine (34.6%) cases were of stage IV. Eight (57.4%) cases of the proximal type were in stage III, and six (42.6%) were in stage IV. The statistical correlation was not

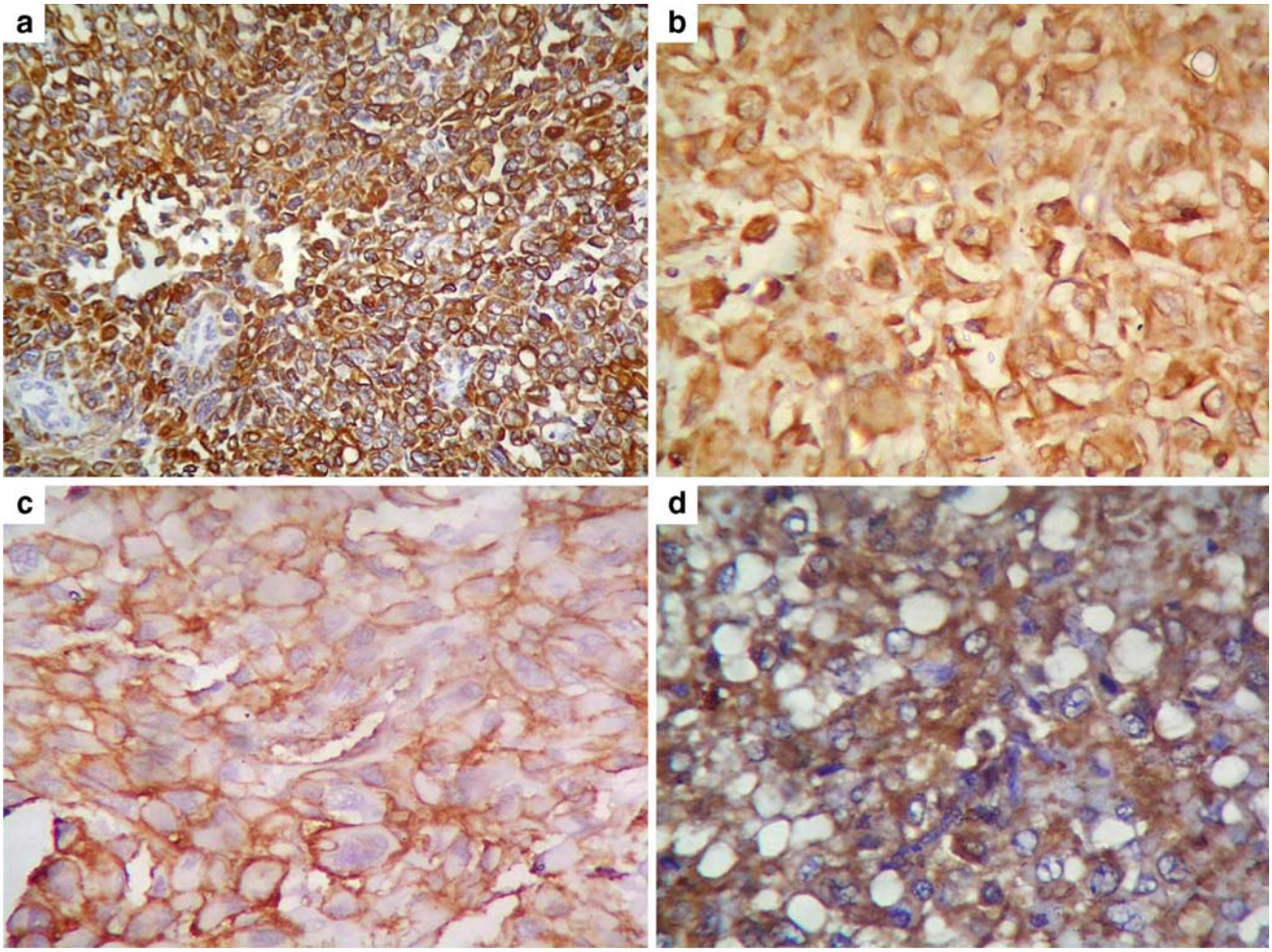

Fig. 2 Immunohistochemical p Immunohistochemical profile of epithelioid sarcoma. **a** Tumor cells showing diffuse cytokeratin positivity. DAB ×100. **b** Strong, diffuse vimentin positivity. DAB ×400. **c** Membranous positivity with CD34. DAB ×400. **d** Tumor cells showing desmin expression in one of the few cases. DAB ×400

significant (p=0.61). Although more cases of proximal ES were associated with recurrences and metastasis, as compared to the conventional type, the differences were statistically insignificant (Table 4).

Management

Maximum patients (30; 75%) were treated with a wide excision. Nine (22.5%) patients underwent amputation. One patient had metastasis at the time of presentation and was offered palliative treatment. Marginal evaluation was possible in 37 cases. Of these, 35 cases underwent R0 resections with free margins, while one case, each, of the proximal subtype had either miscroscopically positive (R1) or both grossly and microscopically positive (R2) margins. Four cases underwent nodal dissection. Based on oncologists' preference, adjuvant radiotherapy (RT) was offered in two (5%) cases, while, both RT and chemotherapy (CT) were offered in 23 (57.5%) cases. One case was offered palliative CT at the upfront, in view of bilateral lung

Table 3 Immunohistochemical marker expression in various cases of ES

IHC marker	Conventional-type ES (N=26)	Proximal-type ES (N=14)	Total (N)	Percentage
Vimentin	26 (100%)	14 (100%)	40	100
EMA	23 (88.5%)	14 (100%)	37	92.5
CK	19 (73%)	11 (78%)	30	75
CD34	17 (65%)	8 (57%)	25	62.5
Desmin	0	8 (57%)	8	20
S-100	1 (3.8%)	3 (21.4%)	4	10

N Total number of cases

Table 4 Various clinicopathological variables in cases of conventional and proximal-type ES

Variable	Conventional-type: number of cases (%)	Proximal-type: number of cases (%)	*p* value[a]
Age (years)			*p*=0.67 (NS)
≤35	18 (69.2%)	8 (57.1%)	
>35	8 (30.8%)	6 (42.9%)	
Mean=29.1(C) 37.5 (P)			
Median=26 (C) 32 (P)			
Location			*p*=0.000 (HS)
Superficial	26 (100%)	7 (50%)	
Deep	0	7 (50%)	
Gender			*p*=1.0 (NS)
Male	20 (76.9%)	11 (78.5%)	
Female	6 (23.0%)	3 (21.4%)	
T size (cm)			
≤3	10 (38.5%)	2 (14.2%)	*p*=0.22 (NS)
>3	16 (61.5%)	12 (85.8%)	
≤5	16 (61.5%)	4 (28.5%)	*p*=0.04 (S)
>5	10 (38.5%)	10 (71. 4%)	
Largest=12 (C) 15 (P)			
Mean=5 (C) 7.8 (P)			
Grade			
1	0	0	
2	21 (80.7%)	5 (35.8%)	*p*=0.012 (S)
3	5 (19.3%)	9 (64.2%)	
Stage			*p*=0.61 (NS)
I	0	0	
II	0	0	
III	17 (65.5%)	8 (57.0%)	
V	9 (35.0%)	6 (64.2%)	
Resections			NE
Rx	1 (3.8%)	2 (14.3%)	
Ro	25 (96.2%)	10 (71.4%)	
R1	0	1 (7.1%)	
R2	0	1 (7.1%)	
Adjuvant CT/RT			NE
CT+RT	17 (65.4%)	6 (42.9%)	
RT	1 (3.8%)	1 (7.1%)	
Not offered	8 (30.8%)	5 (35.7%)	
Not known	0	1 (7.1%)	
Palliative	0	1 (7.1%)	
Recurrences[b]	14/24 (58.3%)	10/12 (83.3%)	*p*=0.13 (NS)
Metastasis[b]	7/24 (29.1%)	5/12 (41.6%)	*p*=0.45 (NS)
Alive with disease[c]	1/23 (4.3%)	4/10 (40%)	*p*=0.008 (HS)
Free of disease[c]	20/23 (86.9%)	1/10(10%)	*p*=0.0001 (HS)
Died of disease[c]	2/23 (8.6%)	5/10 (50%)	*p*=0.007 (HS)

T Tumor, *(C)* conventional, *(P)* proximal, *S* significant, *HS* highly significant, *NS* not significant

[a] *p* values obtained by chi square test. *NE p* value could not be estimated

[b] =Status known in 36 cases

[c] =Status known in 33 cases

deposits with pleural and peritonel effusion along with large tumor size. The drug regimes for adjuvant CT included three cycles of ifosamide (intravenous [i.v.] infusion, 1,500 mg/m^2, days 1–4) and adriamycin (i.v. continuous infusion, 20 mg/m^2 per day, days 1–3) with growth factor support, in cases of large-sized, high-grade tumors with or without incomplete resection and/or in cases of metastasis. Similarly, adjuvant RT was also offered in large-sized tumors and/or in cases showing recurrences or metastasis. The dosages were 30 fractions of 60 Gy in cases or Ro (complete) resection, 66 Gy in R1 (incomplete), and 70 Gy in cases of residual disease.

Local recurrences were noted in 24 (60%) cases. Out of these, 19 (47.5%) cases had a single local recurrence, four had two recurrences, and one case had three local recurrences. Fourteen (30%) cases had no evidence of disease at the last follow-up. Twelve (30%) cases developed distant metastasis, including nodal metastases in seven (17.5%) cases, lung metastases in four cases, and multifocal spread in three cases.

Outcomes

Out of 33 cases with available outcomes, 21 (52.5%) cases were free of disease, while seven (12.5%) died of disease, including one case where palliative CT was offered. Five patients were alive with residual disease. Seven patients were lost to follow-up (Table 3).

DFS at the end of 3, 5, and 7 years was 29.2%, 20.8%, and 13.9%, respectively.

Seven patients succumbed to the disease within 16–80 months (mean=36 months). Seven patients were alive with residual disease, and the remaining 21 patients were free of disease at the last follow-up.

A statistically insignificant decrease in the 7-year DFS was found in cases of grade 3 tumors (16.7%), as compared to grade 2 tumors (17.2%; p=0. 11). Deep-seated tumors showed a significantly lower DFS of median 6 months vs. superficially located tumors that showed a median DFS of 15 months (p=0.02). A decrease in DFS was also observed with proximal-type ES (0), in contrast to conventional-type ES (19.4%), with median DFS values of 9 months in the former and 16 months in the latter type. Adjuvant treatment reduced the DFS but was statistically insignificant (p=0.74).

The OAS at the end of 3, 5, and 7 years was 83.6%, 79.6%, and 74.6%, respectively. Over 7 years, it was reduced in men (65.7%), as compared to that in women (100%; p= 0.09). The significant difference in OAS was observed with initial tumor size. It was 93.3% in cases with tumor size less than or equal to 5 cm, compared to 52.7% in patients with tumor size greater than 5 cm (p=0.020). It was significantly more for the patients in stage III, i.e., 100%, as compared to the 24.8% for the patients in stage IV (p< 0.001). It was significantly lesser in cases of the proximal type (31.3%), compared to those of the conventional type (90.2%; p<0.001; Table 5). (Figs. 3 and 4). More percentage cases of proximal-type ES showed recurrences and metastasis, i.e., 83.3% and 41.6%, respectively, in contrast to the conventional type. The percentage of patients who died of disease was more in the proximal type (50%), whereas increased percentage of patients, free of disease, were of conventional-type ES (86.9%). Adjuvant treatments did not improve OAS (Tables 4 and 5)

On univariate analysis of DFS, according to selected variables, increased risk of recurrences, or metastasis was noted in cases of proximal-type ES vs. the conventional type (HR=1.98, 95% CI=0.91–4.31). Tumor location was identified as a significant prognostic factor, both for DFS and OAS. Tumor stage could not be included for multivariate analysis due to high colinearity with grade (Table 6). The OAS was significantly reduced in the proximal vs. conventional type on univariate (HR=10.8, CI=2.08–56.34) and multivariate (HR=22.9, CI=0.95–553.79) analysis.

Discussion

The present study attempts to describe the various clinicomorphologic features, including outcomes of 26 cases of conventional-type and 14 cases of proximal-type ES.

Age range and symptomatology in the present study was comparable to earlier studies [2–4, 8, 21, 24].

In cases of conventional-type ES, upper extremity was the commonest site of involvement, whereas thigh was the commonest site in cases of proximal-type ES. Similar gender predisposition was noted in both the subtypes. Even though a differing clinical profile, especially in terms of a specific site of location, has been noted for a proximal-type ES vs. the conventional type, we did not find this as a significant difference [10, 13]. Nonetheless, a single case, each in the perineum and scalp region, was of the proximal type, whereas one case in the chest wall was of the conventional type. A significant percentage (45.5. %) of cases of proximal-type ES have been noted at nonproximal sites by Casanova et al. [3].

Maximum cases in our series were superficially located, as noted earlier [2–4, 21]. However, Bose et al. [2] identified most of these tumors in deep location. While all cases of conventional-type ES, in our study, were superficially located, all the deep-seated tumors were of proximal-type, as noted by Guillou et al. [10].

A wide size range was observed. The tumors that were more proximally located had a larger tumor size than the tumors located more distally. In their premier study, Chase and Enzinger [4] observed tumor sizes ranging from 1.5 to 15 cm, with a mean of 3.6 cm. We noted a similar variation in our series. However, the mean tumor size was 6 cm as most of our cases presented at a locally advanced stage. Moreover, a higher percentage (85.5%) of our cases of the proximal-type ES had a size greater than 3 cm, in contrast to the conventional type where 61.5% cases had a tumor size greater than 3 cm. Tumors in the thigh and groin region were larger than those seen in the upper extremity. Similar findings were observed in all other studies [2, 8, 13].

As sarcomas exhibit a wide range of clinical behavior, in order to determine accurate prognosis and guidance for therapeutic decisions, their grading becomes vital. However, tumors like ES, alveolar soft part sarcoma, and clear cell sarcomas of tendon sheath have, lately, been included in the category of "ungradable" sarcomas [5]. This might be due to the rarity of substantial studies on these sarcomas and possibility of interplay of other clinical factors influencing their biological outcome. Nevertheless, we, like Casanova et al. [3], graded our cases and observed a similarity with results that included 65% cases with grade 2 and 35% cases of grade 3. In addition, they observed a higher number of cases of grade 3 of the proximal-type ES (66.6%), a feature similar to our study, wherein 64.2% cases of grade 3 were of

Table 5 Seven years survival for ES according to selected prognostic factors

Variable	Number of cases	Disease-free survival					Overall survival				
		Number of events	Mean (M)	Median (M)	Percent	*p* value	Number of events	Mean (M)	Median (M)	Percent	*p* value
Age											
≤35 years	26	21	33.82	12	15.6	0.69	5	NE	187.85	73.3	0.98
>35 years	14	9	28.4 7	18	13.9		2	NE	144.97	77.1	
Gender											
Male	31	24	34.05	12	19.4	0.39	7	132.22	NE	65.7	0.09
Female	09	6	40.90	48	12.5		0	-	NE	100	
Morphology											
Conventional	26	19	42.60	16	19.4	*0.06*	2	220.36	NE	90.2	*<0.001*
Proximal	14	11	15.25	9	0		5	55.12	36	31.3	
T size (cm)											
≤3	12	10	25.25	9	0	0.79	0	NE	NE	100	*0.017*
>3	28	20	35.61	12	15.8		7	113	NE	56.6	
≤5	20	14	27.14	12	0	0..90	1	226.13	NE	93.3	*0.020*
>5	20	16	35.68	13	15.8		6	107.94	NE	52.7	
Location											
Superficial	33	24	39.60	15	17.5	*0.02*	4	205.64	NE	82	*0.002*
Deep	07	6	13	6	0		3	43	20	25	
Grade											
2	26	20	40.77	16	17.2	0.11	5	195.78	NE	79.2	0.54
3	14	10	11.50	8	16.7		2	75.20	80	40	
Stage											
3	25	16	31.87	18	13.7	0.26	0	NE	NE	100	*<0.001*
4	15	14	23.26	12	10.8		7	77.01	48	24.8	
Resection											
Rx	3	1	NE	NE	NE	NE	0	NE	NE	NE	NE
Ro	35	27	36.18	12	15.9		6	192.16	NE	77.2	
R1	1	1	13	NE	NE		1	80	NE	0	
R2	1	1	48	NE	NE		0	NE	NE	NE	
Adjuvant CT/RT											
(CT+RT)/RT	25	18	26.34	12	18.5	0.74	6	135.40	NE	67.5	0.09
Not offered	13	11	35.39	15	12.8		0	NE	NE	100	
Not known	1	0	NE	NE	NE		0	NE	NE	NE	
Palliative	1	1	NE	NE	NE		1	20.10	20	0	
Recurrence											
Yes	–	27	NA	NA	NA	NE	7	179.37	NE	69.8	0.21
No		06	NA	NA	NA		0	NE	NE	100	
Metastasis											
Yes	–	12	NA	NA	NA	NE	5	94.20	80	38.8	*<0.016*
No		21	NA	NA	NA		2	217.90	NE	84.6	

p values were obtained by log rank test. Significant values have been written in italics.
T Tumor, *M* months, *NA* not applicable, *NE* values could not be estimated

the proximal type, further supporting a significant association of proximal-type ES with a higher tumor grade ($p=0.003$). However, grade was not found to be significant in terms of survival in these cases.

As we are a tertiary cancer referral center, a substantial number of cases in our study were in high tumor stage, in contrast to findings of Spillane et al. [24].

Histomorphologically, we identified 26 (65%) cases of conventional subtype and 14 of proximal-type ES. Hasegawa et al. [13] described 20 cases of proximal-type ES. Miettinen et al. [17] and Laskin et al. [16] identified 9 of 112 (8%) cases and 7 of 95 (7.3%) cases, respectively, of the proximal subtype. A relatively higher number of such cases in our study, compared to the latter two, were due to the fact that even though some of our cases displayed focal "pseudoangiosarcoma-like" pattern, these were labeled as proximal type, rather than a distinct angiomatoid variant or other variants that were identified

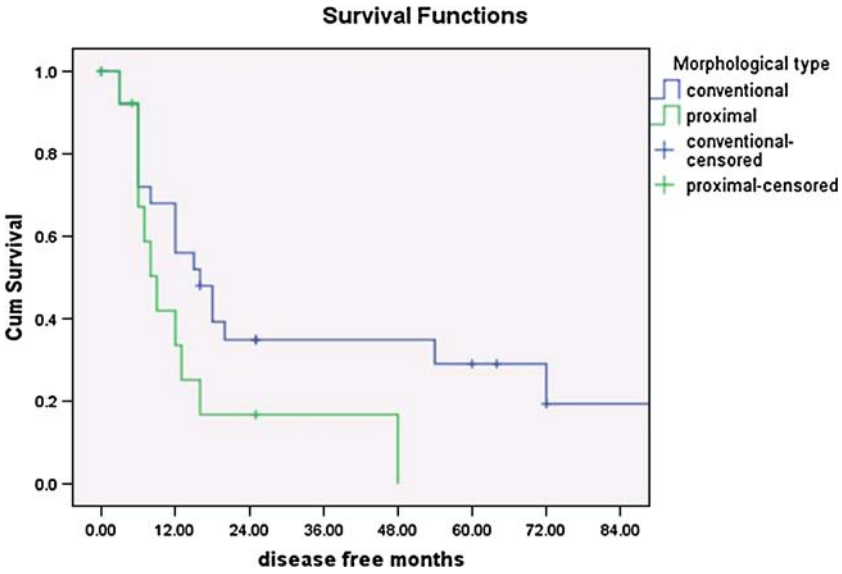

Fig. 3 Comparison between disease-free survival and morphological pattern. Difference in disease free survival in conventional (19.4%) vs. proximal-type ES (0) over a period of 7 years (p=0.06)

in these studies. Moreover, in view of ours being a tertiary cancer center, more numbers of our cases are of higher grades with unfavorable histological patterns. A "pseudoangiosarcomatous" morphological feature in proximal-type ES was also noted by Guillou et al. [10]. In our series, the cases displaying a pseudoangiosarcomatous pattern invariably showed presence of rhabdoid cells, which correlated with an unfavorable outcome, thereby suggesting that the angiomatoid variant might actually represent a form of a proximal subtype of ES. In two cases, an increase in the population of rhabdoid cells was noted in the recurrent lesions, further suggesting the associated aggressiveness of the tumor with "rhabdoid" cells. Prat et al. [21] noticed an increase in the pleomorphic cells in recurrent lesions and in metastatic deposits. Similar findings were noted in one of our cases that showed metastatic lymph nodes. The presence of multinucleated giant cells, without significant nuclear pleomorphism, was seen in four cases. Chase and Enzinger [4] also noted multinucleate giant cells in 5% cases. As described in the literature [2, 4, 8, 21], variable amounts of necrosis ranging from scanty foci to large areas of geographic necrosis were noted in 80% of our cases. Mitotic rates were variable. The cases of the proximal subtype revealed an increased mitotic rate, as also noted by others [2–4, 12, 20]. Tumors greater than 5 cm in size and deeply seated had a high mitotic activity.

Microscopically, a wide range of differential diagnoses were entertained, including a melanoma/clear cell sarcoma of tendon sheath, an alveolar rhabdomyosarcoma, an epithelioid monophasic synovial sarcoma (SS), along with other sarcomas revealing epithelioid traits, and a poorly

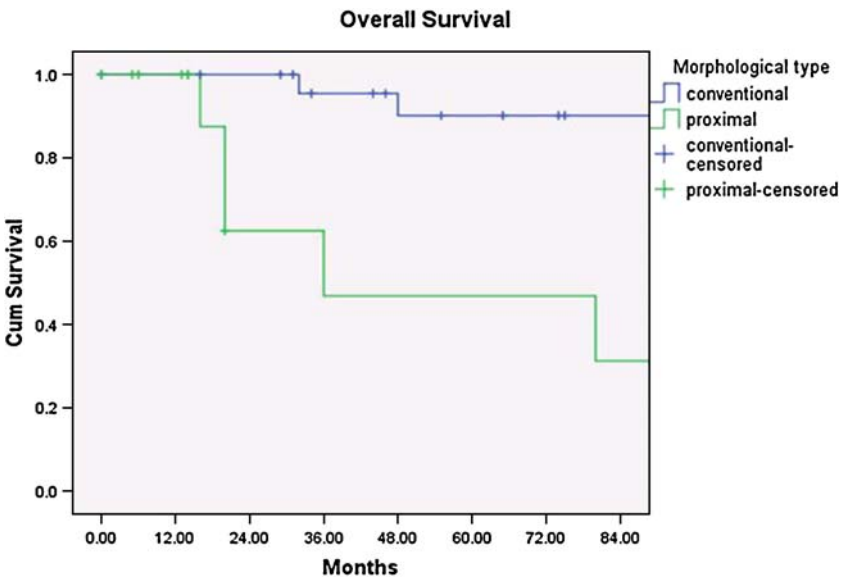

Fig. 4 Comparison between overall survival and morphological types. The significant decrease in disease-free survival was observed with proximal-type ES (31.3%), in contrast to its conventional type (90.2%) over an average period of 7 years (p<0.001)

Table 6 Hazard ratio (HR) of DFS according to selected risk factors in cases of ES

Variable	Number of events	HR[a]	95% CI	HR[b]	95% CI
Age[c]					
≤35 years	21	1.0		1.0	–
>35 years	9	0.85	038–1.92	0.72	0.30–1.71
Location[c]					
Superficial	24	1.0	–	1.0	–
Deep	6	2.56	1.01–6.48	3.01	0.80–11.34
T size[c]					
≤5 cm	14	1.0	–	1.0	–
>5 cm	16	0.96	0.46–1.99	0.59	0.25–1.39
Grade[c]					
2	20	1.0	–	1.0	–
3	10	1.6	0.32–8.69	1.74	0.64–4.75
Stage					
3	16	1.0	–		
4	14	1.49	0.70–3.18	NE	NE
Morphological type[c]					
Conventional	19	1.0	–	1.0	–
Proximal	11	1.98	0.91–4.31	1.26	0.37–4.31

CI Confidence interval, *NE* not estimated due to high colinearity with grade
[a] HR by univariate analysis
[b] HR by multivariate analysis
[c] Reference category

differentiated carcinoma [9, 13, 17]. In few cases of the conventional subtype, exhibiting superficial ulceration, the cells had bland morphology and showed nodular arrangements with areas of necrosis, raising a possibility of a necrotizing granuloma [4, 7, 17]. A long-standing history of a nonhealing ulcer was noted in some of our referral cases.

Melanoma was the commonest differential diagnosis, especially in cases of the proximal subtype. CD34 and EMA positivity helped in ruling out this diagnosis. Epithelioid monophasic SS was another differential diagnosis in view of its similar clinical profile and dual immunoreactivity for epithelial and mesenchymal markers [13]. However, the presence of the superficial location, lack of nodular pattern, and CD34 immunoreactivity were helpful in substantiating an ES over a SS. An epithelioid hemangioendothelioma and an epithelioid angiosarcoma were ruled out with CD31 negativity [1]. A rhabdomyosarcoma was excluded in view of negative MyoD1 and myogenin expression. A metastatic carcinoma was ruled out based upon clinicoradiological findings and CD34 reactivity. This was also helpful in excluding an epithelioid malignant peripheral nerve sheath tumor. CD30 negativity ruled out an anaplastic large cell lymphoma.

In this way, the morphological diagnosis was substantiated with IHC in all cases. All our cases showed vimentin positivity (100%). EMA positivity was noted in 92.5% cases, as noted by others [10, 13, 17]. This confirmed a dual immunoexpession of this tumor for epithelial and mesenchymal markers. Similar to the findings of Chase and Enzinger [4], CK immunoreactivity was observed in 75% cases. However, it was seen in a lesser number of cases, in contrast to other studies [10, 13, 17]. Lately, specific cytokeratins viz. CK8 and CK18, although not performed in our study, have also been found to show varying immunoreactivity in cases of ES [20]. CD34 immunoreactivity in 62.5% of our cases indicates its value in differentiating an ES from other differential diagnoses [25]. It was seen in a higher proportion of our cases than described earlier [10, 13, 17]. This reinforces its value in ascertaining a diagnosis of an ES. Eight (57.1%) out of 14 of our cases of proximal-type ES showed focal desmin expression. Gulliuo et al. [10] identified desmin positivity in 62.5% cases of their cases of proximal-type ES. This was in contrast to the study of Miettinen et al. [17], who did not find this expression. Focal S-100 positivity was seen in four (10%) cases, as observed by others, suggesting possibility of perineural differentiation in some cases [13, 16, 23]. Other markers were performed to rule out various other differential diagnoses. Based on our findings, an optimal panel of immunomarkers for an objective confirmation of an ES is constituted by Vimentin, EMA, CK, CD34, and desmin, the latter reinforcing a possibility of myogenic differentiation in certain cases.

Ultrastructural analysis of a proximal-type ES has unraveled the presence of well-defined filamentous aggregates, indenting the nucleus eccentrically to form intracytoplasmic inclusions, reminiscent of rhabdoid cells, seen with this tumor [10]. However, we did not perform ultrastructural analysis. Further, mutations simulating an extrarenal rhabdoid tumor (ETRT), characterized by inactivation/deletion of both the alleles of tumor suppressor gene *hsNF5/INI11* on chromosome 22q11.2 have been noted, raising a possibility that a proximal-type ES could possibly represent a complex rhabdoid tumor [19]. The aggressive course of the disease has been attributed to the presence of "rhabdoid-like" cells. In fact, the presence of rhabdoid features in malignant tumors have been noted to be correlating with aggressive behavior, multimodal resistance, and a rapidly "down-hill" course, as noted in some of our cases [11, 15, 20].

Therapeutically, maximum cases in our series were treated with a wide excision with clear resection margins (R0 resection). Adjuvant CT/RT were offered in individual cases, mostly related to larger tumor size. Certain cases, despite large size, were spared in view of poor general condition of those patients. Local recurrence following initial treatment was noted in 60% cases, a feature commonly seen with this sarcoma [3, 4, 8, 21, 24]. Distant metastasis was seen in 30% cases, most commonly in the

lymph nodes. The recurrences were noted proximal to initial sites in some of our cases as noted earlier [4]. Prat et al. [21] observed 63% cases with local recurrences after initial treatment and 58% cases with metastasis on a longer follow-up. Spillane et al. [24] observed a low recurrence rate. In our study, maximum cases with recurrences and metastasis were of the proximal type.

The DFS in our study was slightly higher than that observed by Spillane et al. [24]. The most important variables associated with a lower DFS were deeper location and proximal type. The DFS was significantly lower in deep-seated tumors. There was an almost statistically significant difference in DFS between conventional and proximal subtypes with a median of 19.4 months in the former and nil in the latter type ($p=0.06$). An increased risk of recurrences and metastasis was noted with proximal-type ES on univariate analysis (HR=1.98, CI=091–4.31). Deep-seated tumors also showed a significantly higher risk for recurrences and metastasis.

OAS over a period of 7 years was 75%, falling within the range of established literature [18]. The important prognostic factors affecting the OAS were location, morphological subtype, tumor size, metastasis, and tumor stage. In terms of gender, we observed a higher but statistically insignificant OAS in women (100%) than in men (67.5%). Chase and Enzinger [4] observed an OAS of 78% in female and 64% in male patients. However, Spillane et al. [24] observed a lower OAS in the women (55%), as compared to men (75%). Noteworthy among morphological subtypes was a higher OAS in cases of conventional-type vs. proximal-type ES ($p<0.001$). A lower OAS was noted with proximal-type vs. conventional-type ES, on univariate (HR=10.98, CI=2.08–56.34) and multivariate (HR=22.9, CI=0.95–553.79) analysis. However, the CI was wide due to a lesser number of cases in our study. Casanova et al. [3] did not observe a statistical significance between the two subtypes.

Regarding tumor size, the tumors sized greater than 5 cm behaved badly, in contrast to the tumors sized less than or equal to 5 cm ($p=0.02$). Evans and Baer [8] made similar observations. When we classified tumors as less than or equal to and greater than 3 cm, we found that cases with less than or equal to 3 cm size showed a significant survival vs. tumors sized greater than 3 cm ($p=0.017$). However, on adjustment with other variables, size could not retain its statistical significance. This might be due to limited number of cases in our study. Casanova et al. [3] described tumor size as less important in predicting outcome when the cutoff value was 5 cm, in contrast to the same becoming significant if the 3-cm value was considered. Similar to the findings of Bos et al. [2], we observed that deep-seated tumors had significantly shorter survivals than those in superficial locations ($p=0.003$). In terms of tumor stage, stage III cases had higher survival rate than of stage IV cases ($p<0.001$). Tumor stage could not be included in multivariate analysis due to colinearity with grade since most of our cases are referred ones and present with high grade and stage. Spillane et al. [24] found that there was no significance of stage in predicting the survival of the patients. This again might be due to the fact that most of our patients presented with an advanced disease, while maximum patients in their study were in stage II. Histological grade was found to be insignificant in terms of DFS ($p=0.11$) and OAS ($p=0.54$). Metastasis was a detrimental factor in our series as noted by Prat et al. [21]. The survival was significantly lower in patients with metastasis than those without ($p=0.001$). The most common site of metastasis in the patients who died of the disease was lung (57.1%).

Unlike Bos et al. [2], we did not observe an association of tumor necrosis with poor survival rate. Adjuvant CT/RT increased the DFS in our series, though statistically insignificant. However, OAS was not increased, rather seemingly reduced, since most of the cases for adjuvant treatments were of high grade, large size, and at a higher tumor stage. Other reason included an influence on follow-up.

In conclusion, an ES is an unusual sarcoma with a very characteristic growth pattern and merits a proper histological evaluation as it has many mimics. The proximal-type ES is rather a morphological subtype, characterized by large, rhabdoid-like cells and is associated with an aggressive course, with its lower OAS and possibility for increased risk of recurrence and metastasis. These tumors are best treated with a wide excision with optional adjuvant CT/RT in individual cases. Further, substantial studies, including those with molecular analysis, would contribute to the existing literature, especially in terms of outcomes and would be helpful in providing newer insights for management of this tumor and its aggressive subtype.

Acknowledgments We are highly grateful to Dr. Rajesh Dikshit, Ph. D., Epidemiologist, and Mr. Sanjay Talole, Scientific Officer, Biostatistics and Epidemiology division, for the statistical analysis. We would like to thank Dr. Siddharth Laskar, M.D., Associate Professor, Radiation Oncology, for his valuable inputs in the treatment details. We thank Mr. Nilesh Ganthade, Officer In-charge, Medical Graphics Department for his inputs in formatting the images. We have no financial relationship with any organization in terms of this study.

Conflict of interest statement We declare that we have no conflict of interest.

References

1. Billings SD, Folpe AL, Weiss SW (2003) Epithelioid sarcoma-like hemangioendothelioma. Am J Surg Pathol 27:48–57

2. Bos GD, Pritchard DJ, Reiman HM, Dobyns JH, Ilstrup DM, Landon GC (1988) Epithelioid sarcoma. An analysis of fifty-one cases. J Bone Jt Surg Am 70:862–870
3. Casanova M, Ferrari A, Collini P, Bisogno G, Alaggio R, Cecchetto G, Gronchi A, Meazza C, Garaventa A, Di Cataldo A, Carli M, Italian Soft Tissue Sarcoma Committee (2006) Epithelioid sarcoma in children and adolescents: a report from the Italian Soft Tissue Sarcoma Committee. Cancer 106:708–717
4. Chase DR, Enzinger FM (1985) Epithelioid sarcoma. Diagnosis, prognostic indicators, and treatment. Am J Surg Pathol 9:241–263
5. Deyrup AT, Weiss SW (2006) Grading of soft tissue sarcomas: the challenge of providing precise information in an imprecise world. Histopathology 48:42–50
6. Enneking WF, Spanier SS, Goodman MD (1990) A system for the surgical staging of musculoskeletal sarcoma. Clin Orthop Relat Res 153:106–120
7. Enzinger FM (1970) Epithelioid sarcoma: a sarcoma simulating a granuloma or a carcinoma. Cancer 26:1029–1041
8. Evans HL, Baer SC (1993) Epithelioid sarcoma: a clinicopathologic and prognostic study of 26 cases. Semin Diagn Pathol 10:286–291
9. Fletcher CDM, Unni KK, Mertens F (2002) In: Fletcher CDM, Unni KK, Mertens F (eds) World Health Organization (WHO) classification of tumors of soft tissues and bones. Pathology and genetics. IARC, Lyon, France
10. Guillou L, Wadden C, Coindre JM, Krausz T, Fletcher CD (1997) "Proximal-type" epithelioid sarcoma, a distinctive aggressive neoplasm showing rhabdoid features. Clinicopathologic, immunohistochemical, and ultrastructural study of a series. Am J Surg Pathol 21:130–146
11. Gururangan S, Bowman LC, Parham DM, Wilimas JA, Rao B, Pratt CB, Douglass EC (1993) Primary extracranial rhabdoid tumors. Clinicopathologic features and response to ifosfamide. Cancer 71:2653–2659
12. Hall DJ Grimes MM, Goplerud DR (1980) Epithelioid sarcoma of vulva. Gynecol Oncol 9:237–246
13. Hasegawa T, Matsuno Y, Shimoda T, Umeda T, Yokoyama R, Hirohashi S (2001) Proximal-type epithelioid sarcoma: a clinicopathologic study of 20 cases. Mod Pathol 14:655–663
14. Iossifides I, Ayala AG, Johnson DE (1979) Epithelioid sarcoma of penis. Urology 14:190–191
15. Kodet R, Newton WA Jr, Sachs N, Hamoudi AB, Raney RB, Asmar L, Gehan EA (1991) Rhabdoid tumors of soft tissues: a clinicopathologic study of 26 cases enrolled on the Intergroup Rhabdomyosarcoma Study. Human Pathol 22:674–684
16. Laskin WB, Miettinen M (2003) Epithelioid sarcoma: new insights based on an extended immunohistochemical analysis. Arch Pathol Lab Med 127:1161–1168
17. Miettinen M, Fanburg-Smith JC, Virolainen M, Shmookler BM, Fetsch JF (1999) Epithelioid sarcoma: an immunohistochemical analysis of 11 classical and variant cases and a discussion of the differential diagnosis. Human Pathol 30:934–942
18. Mirra JM, Kessler S, Bhuta S, Eckardt J (1992) The fibroma-like variant of epithelioid sarcoma. A fibrohistiocytic/myoid cell lesion often confused with benign and malignant spindle cell tumors. Cancer 69:1382–1395
19. Modena P, Lualdi E, Facchinetti F, Galli L, Teixeira MR, Pilotti S, Sozzi G (2005) SMARCB1/INI1 tumor suppressor gene is frequently inactivated in epithelioid sarcomas. Cancer Res 15:4012–4019
20. Molenaar WM, DeJong B, Dam-Meiring A, Postma A, DeVries J, Hoekstra HJ (1989) Epithelioid sarcoma or malignant rhabdoid tumor of soft tissue? Epithelioid immunophenotype and rhabdoid karyotype. Human Pathol 4:347–351
21. Prat J, Woodruff JM, Marcove RC (1978) Epithelioid sarcoma: an analysis of 22 cases indicating the prognostic significance of vascular invasion and regional lymph node metastasis. Cancer 41:1472–1487
22. Ramanathan RC, A'Hern R, Fisher C, Thomas JM (1999) Modified staging system for extremity soft tissue sarcomas. Ann Surg Oncol 6:57–69
23. Smith MEF, Awasthi R, O'Shaugnessy S et al (2005) Evaluation of perineurial differentiation in epithelioid sarcoma. Histopathology 47:575–581
24. Spillane AJ, Thomas JM, Fisher C (2000) Epithelioid sarcoma: the clinicopathological complexities of this rare soft tissue sarcoma. Ann Surg Oncol 7:218–225
25. van de Rijn M, Rouse RV (1994) CD34: A review. Appl Immunohistochem 2:71–80
26. von Hochstetter AR, Grant JW, Meyer VE, Honegger HP, Schreiber A (1990) Angiomatoid variant of epithelioid sarcoma. The value of immunohistochemistry in the differential diagnosis. Chir Organi Mov 75:158–162
27. Zevallos-Giampietri EA, Barrionuevo C (2005) Proximal-type epithelioid sarcoma: report of two cases in the perineum: differential diagnosis and review of soft tissue tumors with epithelioid and/or rhabdoid features. Appl Immunohistochem Mol Morphol 13:221–230

Virchows Arch (2008) 453:155–163
DOI 10.1007/s00428-008-0640-7

ORIGINAL ARTICLE

Systemic EBV+ T-cell lymphoma in elderly patients: comparison with children and young adult patients

Sanghui Park · Kihyun Kim · Won Seog Kim · Keon Hee Yoo · Hong-Hoe Koo · Young-Hyeh Ko

Received: 7 April 2008 / Revised: 27 May 2008 / Accepted: 18 June 2008 / Published online: 18 July 2008

Abstract Fulminant Epstein–Barr virus (EBV+) T-cell lymphoma in immunocompetent elderly patients is rare and its character has not been well defined. This study analyzed the clinicopathological features of five elderly patients (group A: 50–84 years) and compared them with those of eight children and young adult patients with systemic T-cell lymphomas (group B: 10–34 years). Group A more commonly presented with generalized lymphadenopathy (n=3) than did group B (n=1). Chronic active EBV infection (n=3) and hydroa vacciniforme-like eruptions (n=1) were seen in group B, while group A showed no evidence of chronic EBV infection, but did show chronic hepatitis B or C virus infections (n=3). The histological and immunophenotypical findings were similar. All patients died within 1 to 14 months of diagnosis. These findings suggest that EBV+ T-cell lymphoma in elderly patients is a unique disease with an underlying derangement of T-cell immunity and failure to eradicate infected virus. Additional factors related to senility may play a role in the disruption of homeostasis between the virus and the host's immune system.

Keywords Epstein–Barr virus · Lymphoma · T-cell

S. Park
Department of Pathology, Gil Medical Center,
Gachon University of Medicine and Science,
Namdonggu, Guwoldong,
1198 Incheon, South Korea

K. Kim · W. S. Kim
Division of Hematology and Oncology, Internal Medicine,
Samsung Medical Center,
Sungkyunkwan University School of Medicine,
Kangnamgu, Ilwondong 50,
Seoul, South Korea

K. H. Yoo · H.-H. Koo
Department of Pediatrics, Samsung Medical Center,
Sungkyunkwan University School of Medicine,
Kangnamgu, Ilwondong 50,
Seoul, South Korea

Y.-H. Ko (✉)
Department of Pathology, Samsung Medical Center,
Sungkyunkwan University School of Medicine,
Kangnamgu, Ilwondong 50,
Seoul, South Korea
e-mail: yhko310@skku.edu

Introduction

Primary infection with Epstein–Barr virus (EBV) is usually asymptomatic, and EBV has been shown to be latent in B cells for life in normal hosts after primary infection; however, some children and more often, adolescents and young adults, develop infectious mononucleosis (IM) [26]. IM is characterized by fever, hepatosplenomegaly, lymphadenopathy, and an increase in activated CD8+ T lymphocytes in the peripheral blood [1, 26]. Although IM usually follows a self-limited course without severe complications, uncommonly, acute EBV infections with fulminant manifestations such as persistent fever, severe hepatosplenomegaly, severe cytopenia, coagulopathy, central nervous system abnormalities, and vascular dysfunction have been demonstrated, and histiocytic erythrophagocytosis has been found in the bone marrow and secondary lymphoid organs of most of these patients [15, 28]. Those fulminant cases have been reported mainly in Asian countries, including Taiwan and Japan, and have been described under a variety of terms including fulminant EBV+ T-cell lymphoproliferative disease(LPD) of childhood, and sporadic fatal infectious mononucleosis. These diseases occur shortly after primary EBV infection

or are associated with a long prodromal syndrome referred to as chronic active EBV (CAEBV) infection.

CAEBV infection is characterized by chronic or recurrent infectious mononucleosis-like symptoms persisting for at least 6 months and by an unusual pattern of anti-EBV antibodies [24]. Severe CAEBV infection is a more severe form of the disease, with a high mortality and high morbidity and life-threatening complications such as virus-associated hemophagocytic syndrome, interstitial pneumonia, lymphoma, coronary aneurysms, and central nervous system involvement [10, 16, 21, 22, 25]. Many studies have reported that clonal expansion of EBV-infected T or natural killer (NK) cells might be associated with CAEBV infection [7, 8, 10, 11, 14, 16, 17, 23, 31].

A new World Health Organization classification for fulminant EBV+ T-cell lymphoproliferative disorders, which will appear in 2008, establishes a new disease category of systemic EBV+ T-cell lymphoma. The disease is defined as a life-threatening illness of children and young adults characterized by a clonal proliferation of EBV-infected T cells with an activated cytotoxic phenotype.

Whereas systemic EBV+ T-cell lymphomas most commonly occur in children and young adults, the similar entity of fulminant EBV+ T-cell lymphoma can occur in immunocompetent adult patients. In our institution, we have noted several cases of fulminant EBV+ systemic T-cell lymphomas in elderly patients with no known immunodeficiency. Those cases have clinicopathological features similar to those of the systemic T-cell lymphoma of children and young adults, but some differences were also observed. Herein, we describe the clinicopathological features and molecular and immunohistochemical findings of 14 cases of fulminant EBV+ T-cell lymphoma to define the characteristics of systemic EBV+ T-cell lymphoma in elderly patients and to elucidate the relationship of these tumors to those in children and young adult patients.

Materials and methods

Patients

The criteria for the inclusion of case were as follows: (1) an aggressive clinical presentation with or without hemophagocytic syndrome; (2) EBER positivity in a majority of infiltrated lymphocytes; (3) clonal T-cell proliferation, as supported by either T-cell receptor gene rearrangement studies, or marked cytological atypia of CD3-positive cells; and (4) available paraffin block(s) for additional studies. This study was approved by the Institutional Review Board in accordance with the Declaration of Helsinki.

The surgical pathology files of the Department of Pathology, Samsung Medical Center from 1995 to 2007 were searched. Of the 20 cases that showed EBV+ T-cell lymphoproliferation, 13 cases were selected. Of the seven cases excluded, the clinical history was unavailable for two, one case had a history of rheumatoid arthritis, two cases were of indolent cutaneous lymphoproliferative disorders, one case was a typical hemophagocytic lymphohistiocytosis (HLH) according to the definition of Henter et al. [6], and one case showed polyclonal T-cell receptor gene rearrangements.

All patients were previously healthy, with no opportunistic infections or other indications of congenital immunodeficiency, nor had they received immunosuppressive medications. We segregated our 13 cases into two groups: elderly patients more than 50 years old, and children and young adults.

Formalin-fixed, paraffin-embedded tissue blocks of liver, bone marrow, lymph node, pharynx, tonsil, larynx, stomach, duodenum, colon, retroperitoneum, and skin biopsies were used for evaluation. All slides were reviewed by two pathologists.

Immunophenotype studies

Immunohistochemical analysis was performed on paraffin sections using monoclonal and polyclonal antibodies for the detection of lineage-specific or lineage characteristic antigens including CD3 (Dakopatts, Copenhagen, Denmark), CD20 (Dakopatts), CD56 (Monosan, Uden, The Netherlands), CD4 (Novocastra, Newcastle upon Tyne, UK), CD8 (Novocastra), βF1 (Endogen, Rockford, IL, USA), and granzyme B (Zymed, South San Francisco, CA, USA).

EBV studies

Serological studies of EBV infection were performed, including the detection of antiviral capsid antigen IgG and IgM (EBV-VCA IgG and IgM) and antiearly antigen IgG (EBV-EA IgG) using indirect immunofluorescence methods, and antinuclear antigen (EBNA) using an anticomplement immunofluorescence method.

EBV RNA was detected by an in situ hybridization technique. Paraffin-embedded sections (5 μm) were dewaxed with xylene, followed by treatment with proteinase K, and hybridized with FITC-conjugated EBER-1 and EBER-2 oligonucleotide probes (Novocastra). Following incubation with anti-FITC antibody tagged with alkaline phosphatase, slides were covered with nitrobluetetrazolium, 5-bromo-4-chloro-3-indolyl phosphate, and 1 M levamisole. We used EBV-negative lymphoid tissues and the hybridization mixture without EBV oligonucleotides as negative controls.

Real-time quantitative polymerase chain reaction (PCR) assays for EBV DNA were performed using instruments from Roche Molecular Diagnostics (Mannheim, Germany) and the LightCycler EBV quantification kit as described

[5]. The amount of EBV DNA was calculated as the number of virus copies per 5 μl whole blood. The EBV detection limit of this assay is approximately ten copies per reaction for whole blood and the linear measuring range of the assay is 10^2 to 10^6 per reaction.

Molecular studies

For PCR amplification of the TCR-γ locus, DNA was prepared by standard proteinase K digestion and phenol/chloroform extraction. PCR followed by single-stranded conformational polymorphism analysis was performed as previously described [18].

Detection of chromosomal abnormalities

Unstimulated isolated bone marrow cells were cultured for 24 h and G-banded according to standard procedures. Metaphases were analyzed and karyotyped according to the nomenclature system proposed by the International System for Human Cytogenetic Nomenclature, 1995.

Results

Clinical findings

The clinical characteristics of the patients are summarized in Tables 1 and 2. All patients were Korean, with eight male and five female patients, ranging in age from 10 to 84 years (mean 35.4 years). The elderly group consisted of five patients (four males and one female), ranging from 50 to 84 years (mean 62 years), and the children and young adult group consisted of eight patients (four males and four females), ranging in age from 10 to 34 years (mean 16.7 years).

The clinical presentations of the children and young adult group and the elderly group were similar, but with some differences. In the elderly patients, three of the five patients presented with generalized lymphadenopathy as well as fever, cytopenia, and liver dysfunction (cases 1, 2, and 5). One patient had fever, liver dysfunction, pancytopenia, and gastrointestinal symptoms (case 3). Biopsies from the duodenum and colon revealed atypical cells. One patient presented with abdominal pain and a retroperitoneal mass (case 4). Anemia and thrombocytopenia were observed in all patients. Bone marrow biopsy revealed hemophagocytosis in one patient (case 3). A history of hypersensitivity to mosquito bite or CAEBV infection was not observed.

Among the children and young adults, four of eight patients presented with acute onset of fever, general malaise, and hepatosplenomegaly (cases 7–9 and 11). Laboratory testing showed pancytopenia and liver function abnormalities. Among the other four patients, three had a history compatible with chronic EBV infection. One of them had a history of liver dysfunction and enlarged cervical lymph nodes for 2 years (case 6). Other two patients had intermittent fever of unknown origin for 6 months and 1 year respectively (cases 12 and 13). One patient presented with hydroa vacciniforme-like skin lesions on the light-exposed areas such as the face and arms occurring over several years, along with IgA nephropathy (case 10). At admission, the larynx was involved by EBV+ T-cell lymphoma. Generalized lymphadenopathy was identified in only one case (case 6). Bone marrow was initially infiltrated by hemophagocytic histiocytes or atypical tumor cells in the majority of cases.

All patients were treated with steroids or chemotherapy, with various regimens depending on the patient's general condition; however, the clinical course was fulminant or aggressive, with all patients dying within 10 days to 14 months of diagnosis. Causes of death for the elderly patients were septic shock (four patients) and systemic mucormycosis (one patient). The children and young adults died of sepsis with disseminated intravascular coagulation (two patients), pneumocystis pneumonia with disseminated intravascular coagulation (one patient), multi-organ failure (one patients), liver failure and tumor lysis syndrome (one patient), and renal failure(one patient). Cause of death was not known in one children.

Histological findings

Four out of five patients with lymphadenopathy had lymph node biopsies. The lymph nodes in three patients (cases 1, 2, and 5) showed diffuse effacement of the normal nodal architecture by infiltration of relatively monotonous small, medium, or large lymphocytes with hyperchromatic nuclei and irregular nuclear contours. Inflammatory cells such as eosinophils and plasma cells were frequently found. The lymph nodes from case 6 showed preserved but partially effaced lymph node architecture and intact capsules and sinuses. The interfollicular T zone was widened and infiltrated by small lymphocytes lacking significant cytological atypia. Some of the lymphocytes were large. Epithelioid histiocytes or small granulomas were scattered.

The bone marrow was involved in three patients. Tumor cells massively infiltrated the bone marrow in case 11, whereas case 7 and case 9 showed scattered pleomorphic atypical cells with or without hemophagocytosis. Five patients showed an infiltration of hemophagocytic histiocytes and increased small T lymphocytes without cytological atypia.

Skin biopsies were performed in three cases (cases 1, 3, and 10). Erythematous papules with or without ulceration

Table 1 Characteristics of five elderly patients and eight children and young adult patients

No.	Sex	Age (years)	Onset (months)	Associated disease	Treatment	Follow-up (months)	Outcome	EBV serology	EBV DNA in PB[a]	Histologic grade (necrosis)	Cell type	TCR gene rearrangement
Elderly patients (n=5)												
1	M	50	1[b]	HBV carrier[c]	CHOP	7	Dead	Anti-VCA IgG+, IgM−, EA−, EBNA+	~30,530	3	αβ-T CD8>CD4, CD56−	Monoclonal
2	M	51	1	HBV carrier[c]	CHOP, A-DHAP, autoPBSCT	14	Dead	Anti-VCA IgG+, IgM−, EA−, EBNA+	~187	3	αβ-T CD8>CD4 CD56−	Monoclonal
3	M	60	<1	None	CHOP	5	Dead	Anti-VCA IgG+, IgM−, EA±, EBNA+	~14,770	1(+)	γδ-T[d], CD4−, CD8-CD56−	Monoclonal
4	F	64	<1	Hepatitis C[c]	Cytoxan, VCR	1	Dead	NA	NA	2	NA CD56−	NA
5	M	84	<1	Prostate ca	Cytoxan, VCR	3	Dead	NA	NA	2	αβ-T CD8+, CD56−	Monoclonal
Children and young adults (n=8)												
6	M	10	24	CAEBV	106B, VCR, TMX	10	Dead	Anti-VCA IgG+, IgM−, EA+, EBNA−	~14,680	1	αβ-T CD4>CD8 CD56−	Monoclonal
7	M	11	<1	None	106B	1	Dead	Anti-VCA IgG+, IgM−, EA−, EBNA+	NA	2	αβ-T[e] CD8+ CD56−	Monoclonal
8	M	11	<1	None	Steroid	0.3	Dead	NA	19,220	2(+)	αβ-T CD8+	Monoclonal
9	F	14	<1	None		1	Dead	Anti-VCA IgG+, IgM−, EBNA−	NA	3	NA CD56−	NA
10	F	15	12	Hydroa[f] vacciniforme	CHOP, ESHAP	6	Dead	NA	NA	2	αβ-T CD8+, CD56−	NA
11	M	16	<1	None	CHOP, DHAP, IMVP-16/PD, EPHOCH	6	Dead	NA	NA	3	αβ-T CD8+, CD56−	NA
12	F	20	6	CAEBV	CHOP, IMVP-16/PD, DHAP, ICE	12	Dead	Anti-VCA IgG+, IgM−, EA+ EBNA±	NA	1	αβ-T CD8>CD4 CD56−	Monoclonal
13	F	34	12	CAEBV	CHOP	3	Dead	Anti-VCA IgG+, IgM−, EA± EBNA−	NA	2(+)	NA	Monoclonal

106B Prednisolone+cyclophosphamide+daunorubicin+vincristine+L-asparaginase, *VCR* vincristine, *TMX* trimethoprim-sulfamethoxazol, *CHOP* cyclophosphamide+adriamycin+vincristine +prednisolone, *DHAP* dexametasone+cytarabine+cisplatin, *IMVP-16/PD* ifosfamide+methotrexate+VP-16 (etoposide)+prednisolone, *EPHOCH* etoposide+cytoxan+doxorubicin+vincristine +prednisolone, *ESHAP*, etoposide+methylprednisolone+cytarabine+cisplatin, *ICE*, ifosfamide+carboplatin+etoposide, *NA* not available

[a] Copies/reaction (5 μl) using whole blood

[b] Enlarged lymph node at infraauricular area at 45 years old, followed by decreased size

[c] The patients had no treatment for hepatitis.

[d] This case was regarded of γ/δ phenotype due to the lack of staining with the βF1 antibody in the proper reactivity with internal control.

[e] Determined by flow cytometry

[f] Hydroa vacciniform-like skin lesion with photosensitivity on face and arm for many years

Table 2 Comparison of clinical features between five elderly patients and eight children and young adult patients at presentation

Symptoms and signs	Elderly patient	Percent	Children and young adults	Percent
Fever	3/5	60	8/8	100
Anemia	5/5	100	7/8	87.5
Thrombocytopenia	5/5	100	7/8	87.5
Pancytopenia	4/5	80	6/8	75
Liver dysfunction	4/5	80	5/8	62.5
Hepatosplenomegaly	2/5	40	7/8	87.5
Lymphadenopathy	3/5	60	2/8	25
Skin rash	0/5	0	1/8	12.5
G-I symptoms	2/5	40	2/8	25
Pleural effusion/ascites	4/5	80	3/8	37.5
Bone marrow involvement	0/5	0	3/8	37.5
Hemophagocytosis in bone marrow	1/5	20	4/8	50
Associated disease				
Hepatitis B or C virus infection	3/5	60	0/8	0
Hydroa vacciniforme	0/5	0	1/8	12.5
Chronic active EBV infection	0/5	0	4/8	50

were documented clinically and showed perivascular and periappendageal lymphocytic infiltration in the upper dermis, with or without necrosis. One case showed a subcutaneous infiltration of lymphocytes (case 3). The patient with the hydroa vacciniforme-like eruption (case 10) showed characteristic skin lesions. A biopsy of necrotic vesicles demonstrated necrosis of the epidermis and subjacent dermis. Perivascular and periappendageal lymphocytic infiltration of small lymphocytes with angioinvasion and mild atypia was observed.

Endoscopic biopsies from the stomach, duodenum, and colon were performed for suspicious lesions from elderly patients (cases 2 and 3). One patient showed mucosal erosion with many T cells showing mild atypia and villous atrophy (case 3) and no obvious atypical infiltrates were observed in the other patient.

To compare the degree of histological change between the elderly group and the children and young adult group, we classified the 13 cases into three grades according to histology (Figs. 1, 2 and 3). We defined grade 1 as cases with polymorphic infiltrates including plasma cells, histiocytes, and small lymphocytes without significant atypia; grade 2 as cases with monomorphic infiltrates with predominantly small to medium lymphocytes showing mild atypia; grade 3 as cases with overt lymphoma showing monomorphic infiltrates with medium to large lymphocytes showing marked atypia. The cytological atypia of grade 1 cases was minimal or equivocal, so if EBER in situ hybridization is not performed, the lesion can be easily overlooked as chronic inflammation. The elderly group and the children and young adult group showed no significant difference in the histological changes. The elderly group showed one grade 1, two grade 2, and two grade 3 cases, and the children and young adult group showed two grade 1, four grade 2, and two grade 3 cases.

Immunophenotypic findings

Immunophenotypic features are summarized in Table 1. The infiltrate in all cases was composed of CD3+ T cells. The CD4/8 phenotype was evaluated in four cases from the elderly group and six cases from the children and young

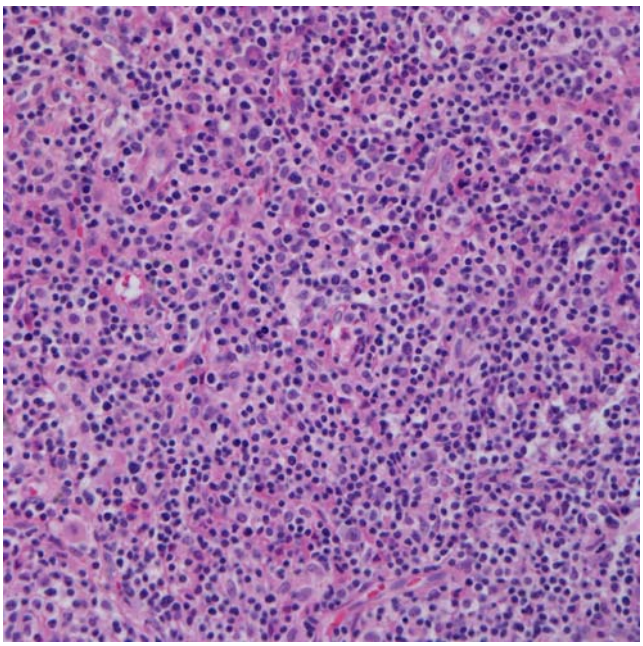

Fig. 1 Microscopic finding of grade 1. There are polymorphic infiltrates of plasma cells, histiocytes, and small lymphocytes without significant atypia (case 6)

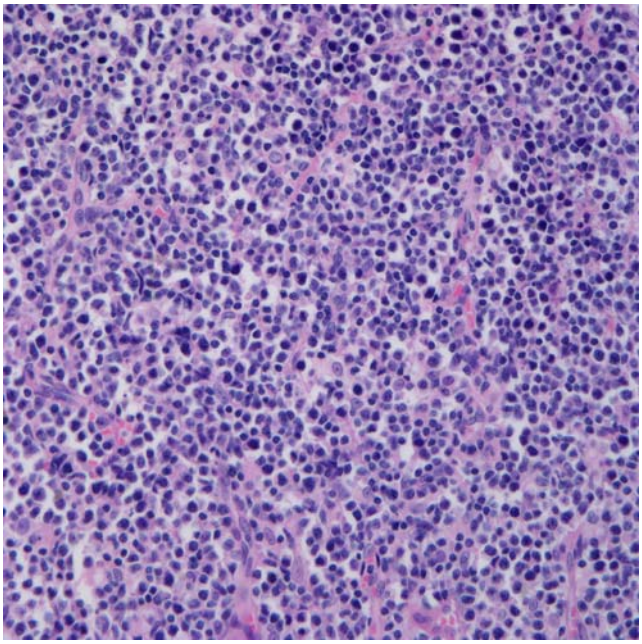

Fig. 2 Microscopic finding of grade 2. Monotonous infiltrates with predominantly small to medium lymphocytes showing mild atypia (case 4)

adults group. Nine cases were evaluated by immunohistochemistry and one case by flow cytometry. The infiltrate was predominantly cytotoxic CD8+ αβ T cells in eight cases (3/4 in the elderly group and 5/6 in the children and young adults group). CD4+ and CD8+ T cells were admixed with slight CD4 predominance in one case (1/6 in the children and young adult group). One elderly patient was regarded of γ/δ phenotype due to the lack of staining with the βF1 antibody in the proper reactivity with internal control. Three cases did not have specimens available for CD4 and CD8 study. All cases were negative for CD56 and positive for granzyme B.

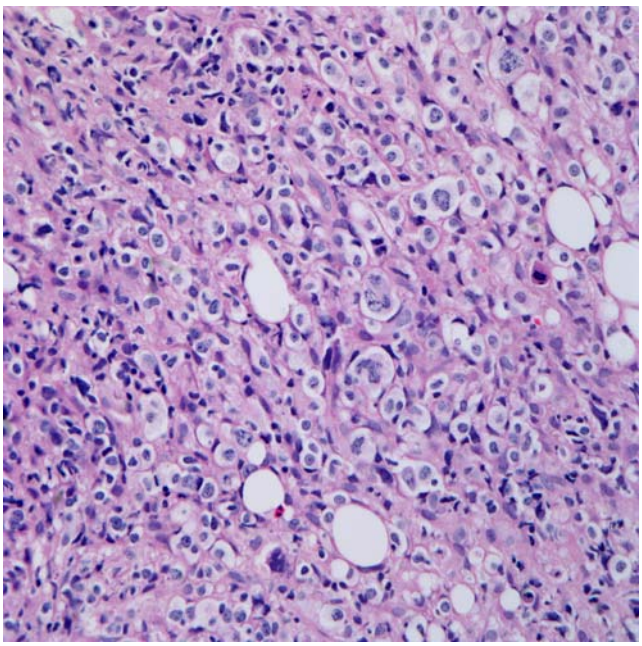

Fig. 3 Microscopic finding of grade 3. Overt lymphoma showing monomorphic infiltrates of large lymphocytes with marked atypia (case 11)

EBV analysis

EBV serology was available in eight patients. The EBV-related antibody of each patient was detected, as shown in Table 1. In all the cases examined, EBV-VCA IgG was positive in the absence of EBV-VCA IgM. EBV-EA was positive in two of five cases in the children and young adult patients, but was consistently negative in the elderly patients.

In situ hybridization (EBER-1) showed the presence of EBV-infected cells in the tissues. All cases showed numerous EBER-1 positive cells (Fig. 4).

Peripheral blood was obtained from five patients and the viral load was determined by quantitative real-time PCR. In four patients, the viral loads were measured serially over observation periods ranging from 5 to 9 months (mean, 6.5 months). The highest results were shown in Table 1.

Gene rearrangement study

Analysis by PCR of paraffin-embedded tissue was performed in nine cases—four from the elderly patient group and five from the children and young adult patient group—and showed clonal rearrangements of TCR-γ genes in all cases.

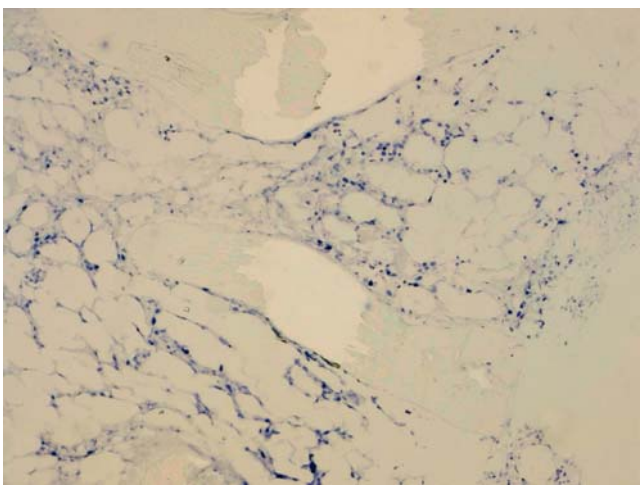

Fig. 4 EBER in situ hybridization showing numerous positive cells (case 7)

Chromosomal study

Cytogenetic studies were successfully performed using isolated bone marrow cells from six patients (five children and young adult cases and one elderly patient case). Only two patients from the children and young adults group showed chromosomal abnormalities. The karyotypes of those cases were 46XY, inv(14)(q11.2q32)[7]/46,XY[13] (case 7) and 47,Y,-X,+19,+mar[1]/47,idem,add(12)(p12)[2] (case 9).

Discussion

EBV-positive systemic T-cell lymphoma has been clinically recognized as EBV-associated hemophagocytic lymphohistiocytosis or EBV-associated hemophagocytic syndrome, severe CAEBV infection, and fatal IM. Even though this disease entity is rare, there have been many sporadic reports describing fulminant T-cell LPD following acute EBV infection and CAEBV infection in Asian countries especially Japan and Taiwan [15, 28]. The patients were mainly children or young adults, with cases occurring in elderly patients hard to find in the literature.

In this study, we compared the clinicopathological features and immunohistochemical and molecular findings of five elderly patients and eight children or young adult patients. Although the study has limitations because of the small number of elderly patients, the data suggested some differences in the clinicopathological features. The cases in the children and young adult group usually presented with chronic intermittent or acute onset of fever, general malaise, and hepatosplenomegaly. The bone marrow or liver was the initial site of involvement and generalized lymphadenopathy was unusual. Laboratory tests showed pancytopenia and liver function abnormalities. The elderly patients more commonly presented with generalized lymphadenopathy. Hemophagocytosis or the involvement of bone marrow by tumor cells was not common at initial presentation.

Regarding the underlying disease, a hydroa vacciniforme-like skin lesion was seen in one patient and chronic active EBV infection in three patients in the children and young adults group. Therefore, about 50% of the systemic T-cell lymphomas in the children and young adult group seem to develop through a prodromal period of chronic EBV infection. This incidence of preceding chronic EBV infection is higher than those reported previously by Quintanilla-Martinez et al. [23]. Our five elderly patients had no history of either CAEBV infection or hydroa vacciniforme-like eruptions. Instead, three of five patients were hepatitis B virus carriers or had chronic hepatitis C virus infection. Although the patients had no proven immune defects, the common association with hepatitis virus in these patients suggests an apparently ineffective antiviral T-cell response.

It is intriguing that IgA nephropathy was present in the girl with the hydroa vacciniforme-like skin lesions and subsequent development of T-cell lymphoma. A previous study demonstrated the EBV genome in seven of 12 patients with IgA nephropathy (58%) and suggested that EBV contributes to glomerular mesangial injury [9].

The histological features of 13 cases showed broad cytological appearances ranging from a reactive appearance to overt lymphoma, and there were no significant differences between the children and the elderly patients. Grade 1 histology was identified in two cases that revealed monoclonality according to TCR gene rearrangement and numerous EBV-positive cells by in situ hybridization. The differential diagnosis between reactive change and lymphoma was difficult on morphologic grounds alone. EBER in situ hybridization is essential to avoid misdiagnosis.

We analyzed EBV-related antibodies in eight patients. In primary EBV infection in healthy hosts, IgM antibodies to VCA rise first, followed by VCA IgG and EBV-EA. EBV IgM and EBV-EA will eventually disappear, and lastly, an antibody to EBNA arises at least 1 month after the onset of symptoms [30]. EBV IgG and EBNA will remain for life. In many people, detection of antibody to the early antigen is a sign of active infection. In the absence of EBNA, EBV-EA indicates primary infection. Considering this principle, the serologic profiles of the members of the children and young adult group were more compatible with primary and active EBV infection while those of the elderly patients were compatible with past infection. However, high viral loads and acute onset of disease in cases 1 and 3 in the elderly group indicate active EBV infection. A recent study demonstrated low frequencies of EBV-specific CD8+ T cells in patients with chronic active EBV infection [29]. Failure to produce an antibody against EBV in elderly patients seems to be associated with underlying antiviral T-cell dysfunction.

The immunophenotype of the proliferating cells in the children and young adults group in our study were predominantly CD8-positive cytotoxic αβ T cells. Only one case developed from a CAEBV infection and consisted of mixed CD4+ and CD8+ cells with a predominance of CD4+ cells. The elderly group showed similar results, with a case with a γδ T-cell phenotype. Sporadic reports of fulminant EBV+ T-cell LPD showed a predominantly CD8+ phenotype with a few mixed CD4 and CD8 phenotype cells [2–4, 13, 19, 20, 27, 32]. However, other studies could not find any subset predominance in EBV-infected cells. Quintanilla-Martinez et al. [23] reported six cases of fulminant EBV-positive clonal T-cell LPD after acute or chronic EBV infection. The cells in two cases were CD4+, two CD8+, and two had admixed CD4+ and CD8+

cells. All were CD56-negative. In a recent retrospective study of 43 children and young adult patients with EBV-associated T/NK-cell lymphoproliferative disorders (severe chronic active EBV infection), eight cases were compatible with fulminant or subacute EBV+ T-cell LPD following CAEBV infection, one case with a CD8+ phenotype, two with a CD4+ phenotype, three with an admixture of CD8+ and CD4+ cells, and two showed a CD4−/CD8− phenotype. Six cases had αβ T cells and two γδ T cells [16]. Kasahara et al. analyzed the frequency of EBV-infected cells in circulating lymphocyte subpopulations from four patients with acute EBV-HLH and four with CAEBV infection [12], and they showed that EBV-infected cells in the acute phase of EBV-HLH were mainly an activated CD8+ T-cell population, whereas the EBV-infected populations in CAEBV infection were heterogeneous, including CD4, CD8, B, and NK cells.

In conclusion, fulminant EBV+ systemic T-cell lymphoma of elderly patients is a rare disease that shares similar clinical and pathologic findings with those seen in children and young adults, but which has some differences in clinical features. Although those elderly patients showed no obvious immune defect, a common association with chronic hepatitis virus infection suggests an underlying derangement of T-cell immunity and failure to eradicate infected virus. In these patients, additional factors related to senility may play a role in the disruption of homeostasis between the virus and the host's immune system, eventually leading to neoplastic transformation of EBV-infected T lymphocytes.

Conflict of interest statement We declare that we have no conflict of interest.

References

1. Callan MF, Steven N, Krausa P et al (1996) Large clonal expansions of CD8+ T cells in acute infectious mononucleosis. Nat Med 2:906–911
2. Chan LC, Srivastava G, Pittaluga S, Kwong YL, Liu HW, Yuen HL (1992) Detection of clonal Epstein–Barr virus in malignant proliferation of peripheral blood CD3+ CD8+ T cells. Leukemia 6:952–956
3. Craig FE, Clare CN, Sklar JL, Banks PM (1992) T-cell lymphoma and the virus-associated hemophagocytic syndrome. Am J Clin Pathol 97:189–194
4. Gaillard F, Mechinaud-Lacroix F, Papin S et al (1992) Primary Epstein–Barr virus infection with clonal T-cell lymphoproliferation. Am J Clin Pathol 98:324–333
5. Gulley ML, Fan H, Elmore SH (2006) Validation of Roche LightCycler Epstein–Barr virus quantification reagents in a clinical laboratory setting. J Mol Diagn 8:589–597
6. Henter JI, Horne A, Arico M et al (2007) HLH-2004: diagnostic and therapeutic guidelines for hemophagocytic lymphohistiocytosis. Pediatr Blood Cancer 48:124–131
7. Imai S, Sugiura M, Oikawa O et al (1996) Epstein–Barr virus (EBV)-carrying and -expressing T-cell lines established from severe chronic active EBV infection. Blood 87:1446–1457
8. Ishihara S, Okada S, Wakiguchi H, Kurashige T, Hirai K, Kawa-Ha K (1997) Clonal lymphoproliferation following chronic active Epstein–Barr virus infection and hypersensitivity to mosquito bites. Am J Hematol 54:276–281
9. Iwama H, Horikoshi S, Shirato I, Tomino Y (1998) Epstein–Barr virus detection in kidney biopsy specimens correlates with glomerular mesangial injury. Am J Kidney Dis 32:785–793
10. Jones JF, Shurin S, Abramowsky C et al (1988) T-cell lymphomas containing Epstein–Barr viral DNA in patients with chronic Epstein–Barr virus infections. N Engl J Med 318:733–741
11. Kanegane H, Bhatia K, Gutierrez M et al (1998) A syndrome of peripheral blood T-cell infection with Epstein–Barr virus (EBV) followed by EBV-positive T-cell lymphoma. Blood 91:2085–2091
12. Kasahara Y, Yachie A, Takei K et al (2001) Differential cellular targets of Epstein–Barr virus (EBV) infection between acute EBV-associated hemophagocytic lymphohistiocytosis and chronic active EBV infection. Blood 98:1882–1888
13. Kawaguchi H, Miyashita T, Herbst H et al (1993) Epstein–Barr virus-infected T lymphocytes in Epstein–Barr virus-associated hemophagocytic syndrome. J Clin Invest 92:1444–1450
14. Kawa-Ha K, Ishihara S, Ninomiya T et al (1989) CD3-negative lymphoproliferative disease of granular lymphocytes containing Epstein–Barr viral DNA. J Clin Invest 84:51–55
15. Kikuta H, Sakiyama Y, Matsumoto S et al (1993) Fatal Epstein–Barr virus-associated hemophagocytic syndrome. Blood 82: 3259–64
16. Kikuta H, Taguchi Y, Tomizawa K et al (1988) Epstein–Barr virus genome-positive T lymphocytes in a boy with chronic active EBV infection associated with Kawasaki-like disease. Nature 333: 455–457
17. Kimura H, Hoshino Y, Kanegane H et al (2001) Clinical and virologic characteristics of chronic active Epstein–Barr virus infection. Blood 98:280–286
18. Ko YH, Ree HJ, Kim WS, Choi WH, Moon WS, Kim SW (2000) Clinicopathologic and genotypic study of extranodal nasal-type natural killer/T-cell lymphoma and natural killer precursor lymphoma among Koreans. Cancer 89:2106–2116
19. Mori M, Kurozumi H, Akagi K, Tanaka Y, Imai S, Osato T (1992) Monoclonal proliferation of T cells containing Epstein–Barr virus in fatal mononucleosis. N Engl J Med 327:58
20. Noma T, Kou K, Yoshizawa I et al (1994) Monoclonal proliferation of Epstein–Barr virus-infected T-cells in a patient with virus-associated haemophagocytic syndrome. Eur J Pediatr 153:734–738
21. Ohga S, Takada H, Honda K et al (1999) Central nervous system T-cell lymphoproliferative disorder in a patient with chronic active Epstein–Barr virus infection. J Pediatr Hematol Oncol 21:42–46
22. Okano M, Matsumoto S, Osato T, Sakiyama Y, Thiele GM, Purtilo DT (1991) Severe chronic active Epstein–Barr virus infection syndrome. Clin Microbiol Rev 4:129–135
23. Quintanilla-Martinez L, Kumar S, Fend F et al (2000) Fulminant EBV(+) T-cell lymphoproliferative disorder following acute/chronic EBV infection: a distinct clinicopathologic syndrome. Blood 96:443–451

24. Rickinson AB (1986) Chronic, symptomatic Epstein–Barr virus infections. Immunol Today 7:13–14
25. Schooley RT, Carey RW, Miller G et al (1986) Chronic Epstein–Barr virus infection associated with fever and interstitial pneumonitis. Clinical and serologic features and response to antiviral chemotherapy. Ann Intern Med 104:636–643
26. Straus SE, Cohen JI, Tosato G, Meier J (1993) NIH conference. Epstein–Barr virus infections: biology, pathogenesis, and management. Ann Intern Med 118:45–58
27. Su IJ, Lin KH, Chen CJ et al (1990) Epstein–Barr virus-associated peripheral T-cell lymphoma of activated CD8 phenotype. Cancer 66:2557–2562
28. Su IJ, Wang CH, Cheng AL, Chen RL (1995) Hemophagocytic syndrome in Epstein–Barr virus-associated T-lymphoproliferative disorders: disease spectrum, pathogenesis, and management. Leuk Lymphoma 19:401–406
29. Sugaya N, Kimura H, Hara S et al (2004) Quantitative analysis of Epstein–Barr virus (EBV)-specific CD8+ T cells in patients with chronic active EBV infection. J Infect Dis 190:985–988
30. Sumaya CV, Ench Y (1985) Epstein–Barr virus infectious mononucleosis in children. I. Clinical and general laboratory findings. Pediatrics 75:1003–1010
31. Suzuki K, Ohshima K, Karube K et al (2004) Clinicopathological states of Epstein–Barr virus-associated T/NK-cell lymphoproliferative disorders (severe chronic active EBV infection) of children and young adults. Int J Oncol 24: 1165–1174
32. Tazawa Y, Nishinomiya F, Noguchi H et al (1993) A case of fatal infectious mononucleosis presenting with fulminant hepatic failure associated with an extensive CD8-positive lymphocyte infiltration in the liver. Hum Pathol 24: 1135–1139

Virchows Arch (2008) 453:165–170
DOI 10.1007/s00428-008-0638-1

ORIGINAL ARTICLE

Expression of alpha-methylacyl-CoA racemase correlates with histopathologic grading in noninvasive bladder cancer

Sven Gunia · Matthias May · Katharina Scholmann · Stephan Störkel · Bernd Hoschke · Stefan Koch · Manfred Dietel · Glen Kristiansen

Received: 29 February 2008 / Revised: 5 May 2008 / Accepted: 12 June 2008 / Published online: 22 July 2008

Abstract Alpha-methylacyl-CoA racemase (AMACR, p504S), an enzyme involved in cellular energy metabolism by the oxidation of branched-chain fatty acids, is a biomarker that is known to be overexpressed in prostatic and colorectal carcinoma as well as in papillary renal cell carcinoma. We aimed to correlate its immunohistochemically detected expression with histopathological grading in noninvasive bladder cancer in order to hint at a so far unknown role of AMACR in the pathobiology of this tumor entity. Therefore, a cohort of 163 patients (mean age 65.3 years) diagnosed with noninvasive bladder cancer was immunohistochemically investigated in terms of AMACR expression. There was variable positive AMACR staining in 52 (31.9%) of the cases investigated. All tumors were graded by three independent clinical histopathologists according to the 1973 World Health Organization (WHO) and the 1998 WHO/International Society of Urological Pathology (ISUP) system. We found a significant positive correlation between AMACR expression and higher tumor grades using both histopathologic grading schemes. These novel findings clearly allow including high-grade noninvasive bladder carcinomas in the group of AMACR-positive neoplasms and might reflect a so far unknown role of AMACR racemase in the pathobiology and tumor cell energy metabolism of the latter tumor entity.

Keywords Pathobiology of noninvasive bladder cancer · Histopathologic grading schemes · Alpha-methylacyl-CoA racemase

S. Gunia (✉) · S. Koch
Department of Pathology, HELIOS Klinikum Bad Saarow,
Charité-University Medicine Teaching Hospital,
Pieskower Straße 33,
15526 Bad Saarow, Germany
e-mail: sven.gunia@helios-kliniken.de

M. May · B. Hoschke
Department of Urology, Carl-Thiem Klinikum Cottbus,
Charité-University Medicine Teaching Hospital,
Cottbus, Germany

K. Scholmann · M. Dietel
Department of Pathology, Campus Charité Mitte,
Charité-University Medicine,
Berlin, Germany

S. Störkel
Department of Pathology, HELIOS Klinikum Wuppertal,
University Witten/Herdecke,
Wuppertal, Germany

G. Kristiansen
Department of Surgical Pathology, University Hospital Zürich,
Zürich, Switzerland

Introduction

Noninvasive bladder cancer is a common neoplasm with a male preponderance frequently encountered in histopathological practice. For 2008, 68,810 new cases of bladder cancer (noninvasive and invasive) are expected in the USA alone [4]. Typically, noninvasive bladder cancer is frequently seen to recur after surgical resection [17] and can progress to invasive neoplasms, which have a comparatively worse prognosis. Since it is difficult at present to reliably predict the individual course of the disease, several studies have recently addressed the issue of identifying new prognostic biomarkers.

Alpha-methyl-CoA racemase (AMACR, p504s), a biomarker with diagnostic potential in various solid tumors, is a peroxisomal and mitochondrial enzyme involved in the oxidation of branched-chain fatty acids and cholesterol

metabolites [1]. AMACR is widely used as a positive marker of prostate cancer and has additionally been shown to bear prognostic significance in prostatic and in colorectal cancer [7, 10]. Lately, AMACR immunostaining has also been proposed as a diagnostically useful marker in terms of discriminating dysplastic from reactive epithelium in Barrett's esophagus [2, 8].

So far, little is known about AMACR expression in noninvasive bladder cancer. This is the first comprehensive study aiming to correlate the immunohistochemically detected AMACR expression with both histopathologic grading schemes established in noninvasive bladder cancer (1973 World Health Organization and the 1998 WHO/International Society of Urological Pathology (ISUP) system) in order to shed light on the so far neglected role of AMACR in the pathobiology of noninvasive bladder cancer.

In order to compare AMACR staining results with other classic but not entirely validated markers, serial sections from all samples were additionally stained with monoclonal antibodies directed against p53 and Ki67. No attempt was made to correlate marker expression with the risk of tumor progression and/or recurrence during postsurgical follow-up.

Materials and methods

Selection of tumor samples

Retrospective computerized database analysis was performed in order to identify all patients with newly diagnosed noninvasive bladder cancer who underwent transurethral surgical resection (TUR) at the Carl-Thiem Klinikum Cottbus, Germany, between 1997 and 2004. This analysis yielded a total of 147 individuals with the following distribution: 102 tumors were graded as G1, 42 tumors were graded as G2, and only three tumors were graded as G3, respectively. In order to expand the latter "critical" group, a thorough retrospective medical chart review was performed at the archives of the HELIOS Klinikum Bad Saarow (the former HUMAINE Klinikum), Germany. Surveying the period of time between 1977 and 2007, another 27 archived wax-embedded noninvasive tumors graded as G3 were subsequently retrieved from the Department of Pathology, HELIOS Klinikum Bad Saarow to be also investigated in this study. Therefore, wax-embedded archived tissues sampled from a total of 174 patients diagnosed with noninvasive bladder cancer (102 G1, 42 G2, and 30 G3 tumors; 144 low-grade and 30 high-grade tumors according to WHO/ISUP 1998) were retrieved for this study. Notably, papillary urothelial neoplasms of low malignant potential (PUNLMP) and invasive bladder cancer were not assessed.

Central review of histology

Hematoxylin and eosin (H&E)-stained tissue sections were reviewed for histopathologic stage and grade by three independent clinical histopathologists (S.G., G.K., and S.S.). The tumors, all pTa according to the latest TNM classification [11], were graded by the 1973 World Health Organization (WHO) and by the 1998 WHO/International Society of Urological Pathology (ISUP) systems. In equivocal cases, final judgement of grading to be used for statistical analyses was consistently performed by the reference histopathologist of this study (S.S.).

Tissue microarray construction

Formalin-fixed wax-embedded surgically resected tissues were retrieved from the surgical pathology archives at Carl-Thiem Klinikum Cottbus, Germany and from the HELIOS Klinikum Bad Saarow, Germany. Suitable areas for tissue retrieval were marked on H&E-stained sections, punched out of the paraffin block (1.5 mm punch diameter), and one punch from each tumor investigated was subsequently inserted into a recipient block as described elsewhere [6]. The tissue arrayer was purchased from Beecher Instruments (Woodland, USA). The tissue array was cut into 4 μm sections without any sectioning aids like tapes or additionally coated slides. Eleven samples (6.3%) were lost during tissue arraying and sectioning. Therefore, this study was finally conducted upon a total of 163 individuals (Table 1).

Immunohistochemistry

Immunohistochemical staining for AMACR was performed on the tissue microarray (TMA) slides using the standard streptavidin–biotin–peroxidase procedure. Freshly cut (4 μm) sections were mounted on superfrost slides (Menzel-Gläser, Germany), dewaxed with xylene, and gradually hydrated. The primary antibody was a rabbit monoclonal AMACR antibody (Biologo, Kronshagen, Germany; clone 13H4), which was diluted 1:200 using a background reducing dilution buffer from Zytomed Systems (Berlin, Germany). No other blocking agents were employed. The primary antibody was incubated at room temperature for 1 h, following IVIEW detection on the Ventana Benchmark XT (pretreatment "CC1 mild").

In order to investigate the distribution pattern of AMACR expression within the tumor tissue (diffuse versus patchy/focal cytoplasmic expression), a total of 60 randomly selected tumor samples were stained prior to TMA generation. These selected samples also contained adjacent nonneoplastic urothelial mucosa for comparative assessment of AMACR expression.

Table 1 AMACR expression in the tumor samples investigated

	AMACR staining intensity				Tissue loss during tissue arraying	Total number of cases
	0	1	2	3		
Grading by WHO 1973						
G1	85	8	4	–	5	102
G2	24	6	2	4	6	42
G3	2	9	10	9	–	30
Grading by WHO/ISUP 1998						
Low grade	86	9	4	2	6	107
High grade	25	14	12	11	5	67

Semiquantification of AMACR immunostaining was performed at high power (×40 objective) according to the approach recently published by Lin et al. [7] with minor modifications. Briefly, positive staining was defined as to having more than 5% of tumor cells showing diffuse cytoplasmic staining. This cut-off was chosen in order to exclude possible nonspecific and/or artificial staining. The staining intensity was graded as negative (0), weak (1+), moderate (2+), or strong (3+). Examples are illustrated in Fig. 1. Since the distribution of AMACR immunoreactivity in the tumors was fairly homogeneous, evaluation of the staining intensity was straightforward, allowing for omittance to incorporate the percentage of positive tumor cells.

Using serial sections, all samples were additionally stained with monoclonal antibodies directed against p53 (DAKO; clone DO-7; dilution 1:50) and against Ki67 (DAKO; clone MiB-1; dilution 1:100), respectively. The latter two markers were semiquantified by recording the percentage of positively stained tumor cell nuclei considering all tumor cells depicted by means of each punch investigated.

In each experiment, a negative control was included in which the primary antibody was replaced by nonhuman reactive rabbit IgG (DAKO). Positive controls used in this study were sections from a prostate that contained both adenocarcinoma and benign prostatic glands. The slides were independently read by three clinical histopathologists (S.G., G.K., and K.S.) blinded with respect to the specimens. In order to assess reproducibility of the data, the slides were reassessed some weeks later.

Statistical analysis

The Spearman correlation was used to determine the magnitude and direction of the association between marker expression and histopathological tumor grade according to

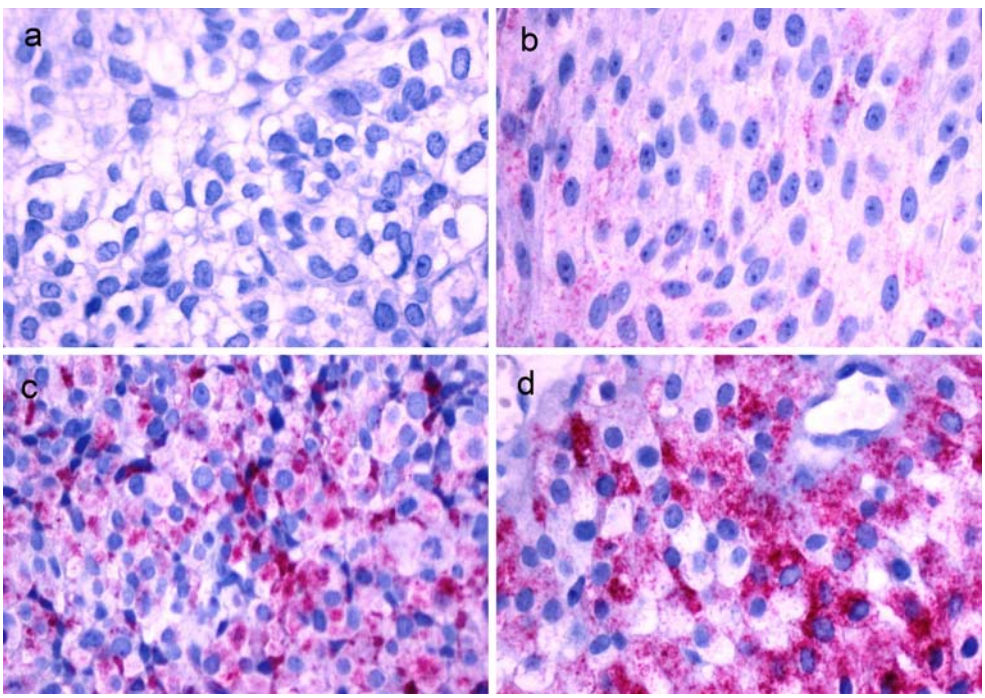

Fig. 1 Noninvasive bladder cancer with lacking (**a**), weak (**b**), moderate (**c**), and strong (**d**) cytoplasmic AMACR expression. Anti-AMACR (×40 objective)

the 1973 World Health Organization (WHO) and the 1998 WHO/International Society of Urological Pathology (ISUP) systems. All differences were considered statistically significant if $p<0.05$; p values are two-tailed. All calculations were performed using the statistical software package SPSS version 13.0.

Results

Reproducibility of staining evaluation

Intraobserver and interobserver variability of staining evaluation was found to be less than 2%. The rare equivocal cases were critically discussed among the clinical histopathologists involved in this study in order to establish consensus.

AMACR expression in tumor samples and in nonneoplastic urothelium

In all 60 randomly selected tumor samples immunohistochemically investigated prior to TMA construction, cytoplasmic expression of AMACR was found to be evenly distributed throughout the entire tumor tissue in a fairly homogeneous pattern. There was no focal and/or patchy staining pattern. The adjacent nonneoplastic urothelium either failed to show any AMACR expression at all or showed only patchy weak expression (Table 2). AMACR expression did not appear to be related to foci of mucosal inflammation.

Correlation between AMACR expression and histopathologic grading

Among the 163 tumor samples included in the final analysis, positive staining was detected in 52 (31.9%) carcinomas. Twenty-three cases (14.1%) showed weak, 16 cases (9.8%) showed moderate, and 13 cases (7.9%) showed strong immunostaining. The remaining 111 samples (68.1%) showed no immunoreactivity at all (Table 1).

There was a significant positive correlation between AMACR expression and grading by WHO 1973 (correlation coefficient $\rho=0.62$; $p<0.01$) and also between AMACR expression and grading by the WHO/ISUP system (correlation coefficient $\rho=0.48$; $p<0.01$).

Correlation of p53 and Ki67 with histopathologic grading

There was no significant correlation between p53 expression and grading by WHO 1973 (correlation coefficient $\rho=0.19$; $p=0.35$) or between p53 expression and grading by the WHO/ISUP system (correlation coefficient $\rho=0.13$; $p=0.16$).

Ki67 expression showed a significant positive correlation with tumor grading by WHO 1973 (correlation coefficient $\rho=0.25$; $p=0.02$) but failed to show any significant correlation with tumor grading by the WHO/ISUP system (correlation coefficient $\rho=0.06$; $p=0.54$), respectively.

Discussion

Among the limited number of studies reporting on AMACR expression in bladder cancer [12, 13], this is the first comprehensive study that correlates the immunohistochemically detected AMACR (racemase) expression with both established histopathologic grading schemes in a larger cohort of noninvasive urothelial carcinomas. So far, the rates of AMACR expression and its role in the pathobiology of noninvasive bladder cancer are essentially unknown.

Alpha-methylacyl-CoA racemase (AMACR, p504s), a peroxisomal and mitochondrial enzyme involved in the oxidation of branched-chain fatty acids and cholesterol metabolites, has recently emerged as a novel tumor biomarker [1]. Since AMACR is not tissue-specific, its diagnostic utility is restricted to specific clearly defined

Table 2 AMACR expression in nonneoplastic urothelium adjacent to noninvasive bladder cancer ($n=60$)

	Cytoplasmic AMACR staining intensity in nonneoplastic urothelium adjacent to noninvasive bladder cancer				Total number of cases ($n=60$)
	0	1	2	3	
Grading of the adjacent tumor by WHO 1973					
G1	17	3	0	0	20
G2	19	1	0	0	20
G3	18	2	0	0	20
Grading of the adjacent tumor by WHO/ISUP 1998					
Low grade	37	3	0	0	40
High grade	18	2	0	0	20

areas [14]. AMACR expression proved to be a sensitive and specific biomarker for the diagnosis of prostate cancer except for a few uncommon variants (e.g., atrophic, foamy gland, and pseudohyperplastic variants) [3] and was also suggested to bear clinical significance in colorectal carcinoma [7]. Our findings are in keeping with previous studies reporting on the insignificant association between p53 expression and both grading schemes [15, 16].

Evaluating a total of 20 specimens, Krüger et al. found Ki67 to be correlated with tumor grade in noninvasive bladder cancer [17]. Surveying a much larger cohort, our data support this notion in terms of tumor grading by WHO 1973 but failed to establish a significant correlation between Ki67 and tumor grading by the WHO/ISUP system. This discrepancy might be explained by the strikingly different total number of specimens assessed.

Compared with the latter classic but not entirely validated markers, our immunostaining data suggest AMACR to be implicated in the pathobiology of noninvasive bladder cancer. One reasonable interpretation of this novel observation is based on the notion that endogenous fatty acids represent an exploitable storage of energy for human bladder cancer [18]. Fatty acid synthase (FAS), a key lipogenic enzyme, is involved in the biological activities of bladder cancer in which it has been reported to be overexpressed [19]. Since both established histopathological grading systems of noninvasive bladder cancer conventionally reflect cellular differentiation, one might suggest cellular dedifferentiation occurring in the latter tumor entity to be accompanied by a possible change in tumor cell energy metabolism characterized by increased oxidation of branched-chain fatty acids which might be brought about by AMACR [20]. The observation that AMACR expression appears to be evenly distributed throughout the entire tumor tissue while being absent or only weakly expressed in the adjacent urothelium strongly supports the concept of intrinsic genetic alterations rather than aberrant epiphenomenon. The lacking association between AMACR expression and foci of mucosal inflammation also supports this hypothesis. However, it should be kept in mind that immunohistochemically detected AMACR expression at the cellular protein level does not necessarily reflect enzymatic activity. Therefore, further in vitro studies are clearly needed. The elucidation of a so far unknown possible implication of AMACR racemase in the pathobiology of invasive bladder cancer might also be an interesting focus to be targeted in the future.

Our observations contrast with the inverse correlation which has been reported between AMACR expression and histopathologic grading in colorectal cancer [5]. This discrepancy might be attributable to a completely different pivotal biological role of AMACR which might be involved in the tumorigenesis of colon cancer by bringing about the oxidation of branched-chain fatty acids from red meat and certain dairy products, the consumption of which increases the risk of colorectal cancer [5, 9]. With respect to noninvasive bladder cancer, there is currently no scientific data that might suggest any link between AMACR and the carcinogenesis behind the development of the latter tumor entity. However, our findings might hint at a so far neglected role of AMACR in the pathobiology of noninvasive bladder cancer, and—according to our immunostaining data—might suggest a possible implication in tumor cellular energy metabolism. Thus, further studies are clearly needed to back this up and to clarify whether this observation might provide the basis for novel targeted therapy strategies applicable in a subset of noninvasive bladder cancer.

However, given the relatively low rate of its expression in low-grade tumors observed in our study, it appears unlikely that AMACR might become a diagnostic biomarker in low-grade bladder cancer contrasting with its possible role as a diagnostic marker in high-grade noninvasive tumors. Further studies including detailed follow-up data in terms of tumor progression and recurrence are needed to address the issue of a possible prognostic value of AMACR in bladder cancer which might be suggested by its positive correlation to higher tumor grades.

Acknowledgements The authors gratefully thank Inna Spivak, Ph.D., Department of applied Mathematics, Faculty of Mathematics, Natural Sciences and Computer Science, Brandenburg University of Technology Cottbus (B T U), Germany, for her excellent assistance in the statistical evaluation of the data. We also gratefully thank Olaf Kaufmann, M.D., for allowing us to investigate the archived specimens assessed in this study. We are also greatly indebted to the Sonnenfeld Stiftung (Berlin, Germany) for sponsoring the tissue micro arrayer to the uropathological working group of G.K. We declare that the experiments comply with the current laws of the country in which they were performed.

Disclosure of Conflict of Interest We declare that we have no conflict of interest.

References

1. Daugherty SE, Platz EA, Shugart YY, Fallin MD, Isaacs WB, Chatterjee N, Welch R, Huang WY, Hayes RB (2007) Variants in the alpha-methylacyl-CoA racemase gene and the association with advanced distal colorectal adenoma. Cancer Epidemiol Biomark Prev 16:1536–1542
2. Dorer R, Odze RD (2006) AMACR immunostaining is useful in detecting dysplastic epithelium in Barrett's esophagus. Am J Surg Pathol 30:871–877
3. Hameed O, Humphrey PA (2005) Immunohistochemistry in diagnostic surgical pathology of the prostate. Semin Diagn Pathol 22:88–104
4. Jemal A, Siegel R, Ward E, Hao Y, Xu J, Murray T, Thun MJ (2008) Cancer statistics, 2008. CA Cancer J Clin 58(2):71–96
5. Jiang Z, Fanger GR, Banner BF, Woda BA, Algate P, Dresser K, Xu J, Reed SG, Rock KL, Chu PG (2003) A dietary enzyme:

alpha-methylacyl-CoA racemase/P504S is overexpressed in colon carcinoma. Cancer Detect Prev 27:422–426
6. Kononen J, Bubendorf L, Kallioniemi A, Bärlund M, Schraml P, Leighton S, Torhorst J, Mihatsch MJ, Sauter G, Kallioniemi OP (1998) Tissue microarrays for high-throughput molecular profiling of tumor specimens. Nat Med 4:844–847
7. Lin A, Weiser MR, Klimstra DS, Paty PB, Tang LH, Al-Ahmadie H, Hoo Park S, Guillem JG, Temple L, Wong WD, Gerald WL, Shia J (2007) Differential expression of alpha-methylacyl-coencyme A racemase in colorectal carcinoma bears clinical and pathologic significance. Hum Pathol 38:850–856
8. Lisovsky M, Falkowski O, Bhuiya T (2006) Expression of alpha-methylacyl-coencyme A racemase in dysplastic Barrett's epithelium. Hum Pathol 37:1601–1606
9. Sesink AL, Termont DS, Kleibeuker JH, Van der Meer R (2000) Red meat and colon cancer: dietary haem, but not fat, has cytotoxic and hyperproliferative effects on rat colonic epithelium. Carcinogenesis 21:1909–1915
10. Skinnider BF, Oliva E, Young RH, Amin MB (2004) Expression of alpha-methylacyl-CoA racemase (P504S) in nephrogenic adenoma: a significant immunohistochemical pitfall compounding the differential diagnosis with prostatic adenocarcinoma. Am J Surg Pathol 28:701–705
11. Sobin LH, Wittekind CH (1997) TNM classification of malignant tumors, 5th edn. Wiley-Liss, New York, pp 187–190
12. Suh N, Yang XJ, Tretiakova MS, Humphrey PA, Wang HL (2005) Value of CDX2, villin, and alpha-methylacyl coencyme A racemase immunostains in the distinction between primary adenocarcinoma of the bladder and secondary colorectal adenocarcinoma. Mod Pathol 18:1217–1222
13. Jiang Z, Fanger GR, Woda BA, Banner BF, Algate P, Dresser K, Xu J, Chu PG (2003) Expression of alpha-methylacyl-CoA racemase (P504s) in various malignant neoplasms and normal tissues: a study of 761 cases. Hum Pathol 34:792–796
14. Went PT, Sauter G, Oberholzer M, Bubendorf L (2006) Abundant expression of AMACR in many distinct tumour types. Pathology 38:426–432
15. Karakök M, Aydin A, Bakir K, Ucak R, Korkmaz C (2001) AgNOR/P53 expression compared with different grades in bladder carcinomas. Int Urol Nephrol 33:353–355
16. Vatne V, Maartmann-Moe H, Hoestmark J (1995) The prognostic value of p53 in superficially infiltrating transitional cell carcinoma. Scand J Urol Nephrol 29:491–495
17. Krüger S, Müller H (1995) Correlation of morphometry, nucleolar organizerregions, proliferating cell nuclear antigen and Ki67 antigen expression with grading and staging in urinary bladder carcinomas. Br J Urol 75:480–484
18. Visca P, Sebastiani V, Pizer ES, Botti C, De Carli P, Filippi S, Monaco S, Alo PL (2003) Immunohistochemical expression and prognostic significance of FAS and GLUT1 in bladder carcinoma. Anticancer Res 23:335–339
19. Turyn J, Schlichtholz B, Dettlaff-Pokora A, Presler M, Goyke E, Matuszewski M, Kmiec Z, Krajka K, Swierczynski J (2003) Increased activity of glycerol 3-phosphate dehydrogenase and other lipogenic enzymes in human bladder cancer. Horm Metab Res 35:565–569
20. Zha S, Ferdinadusse S, Hicks JL, Denis S, Dunn TA, Wanders RJ, Luo J, De Marzo AM, Isaacs WB (2005) Peroxisomal branched chain fatty acid beta-oxidation pathway is upregulated in prostate cancer. Prostate 63:316–323

Virchows Arch (2008) 453:171–176
DOI 10.1007/s00428-008-0636-3

ORIGINAL ARTICLE

Lymph node pathology in pulmonary veno-occlusive disease and pulmonary capillary heamangiomatosis

Vincent Thomas de Montpréville · Élisabeth Dulmet · Élie Fadel · Philippe Dartevelle

Received: 19 March 2008 / Accepted: 20 May 2008 / Published online: 13 June 2008

Abstract To assess the histological bases of lymphadenomegaly, which has been reported as a frequent radiological finding in pulmonary veno-occlusive disease (PVOD), we have reviewed pulmonary and mediastinal lymph nodes resected during lung transplantations in 19 patients suffering from PVOD and related pulmonary capillary haemangiomatosis (PCH). Lymphatic congestion was common and was often obvious in subsegmental and segmental lymph nodes. Vascular transformation of the sinuses, intra-sinusal haemorrhage with erythrophagocytosis and lymphoid follicular hyperplasia were frequent especially in lobar, hilar and mediastinal lymph nodes. These lesions were very significantly less frequent in 33 cases of pulmonary hypertension unrelated to PVOD. Due to their thoracic location, these non-specific lesions could simulate other diagnoses such as Castleman disease or lymphangioleiomyomatosis. However, in the setting of pulmonary hypertension, they should suggest PVOD and PCH. They are probably secondary to venous congestion, veno-lymphatic shunts and angiogenetic factors associated with these diseases.

V. Thomas de Montpréville · É. Dulmet
Department of Pathology, Marie Lannelongue Surgical Centre, Le Plessis Robinson, France

É. Fadel · P. Dartevelle
Department of Thoracic and Vascular Surgery and Heart-Lung Transplantation, Marie Lannelongue Surgical Centre, Le Plessis Robinson, France

V. Thomas de Montpréville (✉)
Service d'anatomie pathologique,
Centre chirurgical Marie Lannelongue,
133 Avenue de la Résistance,
92350 Le Plessis Robinson, France
e-mail: v.thomasdemontprevil@ccml.fr

Keywords Pulmonary veno-occlusive disease · Pulmonary capillary haemangiomatosis · Lymph nodes · Vascular transformation of sinuses · Erythrophagocytosis

Introduction

Pulmonary veno-occlusive disease (PVOD) is a rare and generally idiopathic cause of pulmonary arterial hypertension [10]. This disease is characterised by obstruction of small intrapulmonary veins. Pulmonary capillary haemangiomatosis (PCH) has been sometimes considered a separate entity, but is more likely a secondary process of the same disease occurring in smaller veins [5, 8]. The prognosis is poor and pulmonary transplantation is usually the only effective treatment. PVOD and PCH may be suspected in patients with clinically primary pulmonary hypertension showing radiographic evidence of pulmonary venous congestion [5]. Mediastinal and hilar lymphadenomegaly has also been recognised as frequent (three in nine cases) [6] and even as a very suggestive radiological feature (12/15 cases) of PVOD [13]. Oedema and sinus histiocytosis [14], congestion and capillary-sized blood vessels [7], capillary proliferation [3] and vascular transformation of sinuses [4] have only been reported in single cases, but no study has specifically dealt with lymph nodes pathology in PVOD and PCH. Therefore, we undertook a review of a series of pulmonary and mediastinal lymph nodes resected with native lungs during transplantation for PVOD and PCH in our institution.

Materials and methods

Between October 2000 and September 2006, 113 patients underwent pulmonary transplantation in our institution. The

Table 1 Frequency of main lymph nodes lesions in PVOD and PCH compared with other forms of pulmonary hypertension

	PVOD and PCH (n=19)	Control cases (n=33)	p value (Fisher's exact test)
Increased size and number (see text for criteria)	7 (37%)	1 (3%)	0.00231
Lymphatic congestion (score 2–3)	15 (79%)	5 (15%)	0.0001217
Vascular transformation of sinuses (score 2–3)	8 (42%)	2 (6%)	0.002721
Sinusal haemorrhage and haemophagocytosis (score 1–3)	14 (74%)	8 (24%)	0.00105

main clinicopathologic diagnosis was pulmonary hypertension in 52 cases. The 33 cases with plexogenic primary hypertension (n=29), chronic thromboembolic disease (n=3) and hypertension secondary to interventricular communication (n=1) were used as control cases. The 19 cases with PVOD or PCH, which form the basis of the study, occurred in nine female and ten male patients aged 14 to 60 years (mean=37±14). One patient suffered from dyspnea for 12 years, and others had symptoms for 3 to 48 months (mean=22±11) before transplantation. Mean pulmonary artery pressure ranged from 34 to 90 mmHg (mean=68±11, 10<N<20), and cardiac index ranged from 1.60 to 4.08 l min^{-1} m^{-2} (mean=2.46±0.76, N=3.5±0.7). One patient suffered from CREST syndrome. One patient had had a mediastinoscopy for suspicion of sarcoidosis 2 years before transplantation. There were seven bipulmonary and 12 cardiopulmonary transplantations.

Slides stained with haematein and eosin were reviewed. Sampled lymph nodes sections were counted and their short-axis diameter measured. Lymph nodes with a long-axis diameter under 2 mm were not considered. When the exact location had not been specified, peribronchial lymph nodes were classified as hilar/lobar when sampled with no other structure or with bronchial or vascular sections, or as segmental/subsegmental when sampled with lung parenchyma. Each lesion was scored on a semi-quantitative scale: (0) absent, (1) discreet or focal, (2) moderate or multifocal and (3) prominent or diffuse.

Sections of lymph nodes were stained with Perls' iron stain and Gomori silver stain for reticulin fibres. Immunohis-

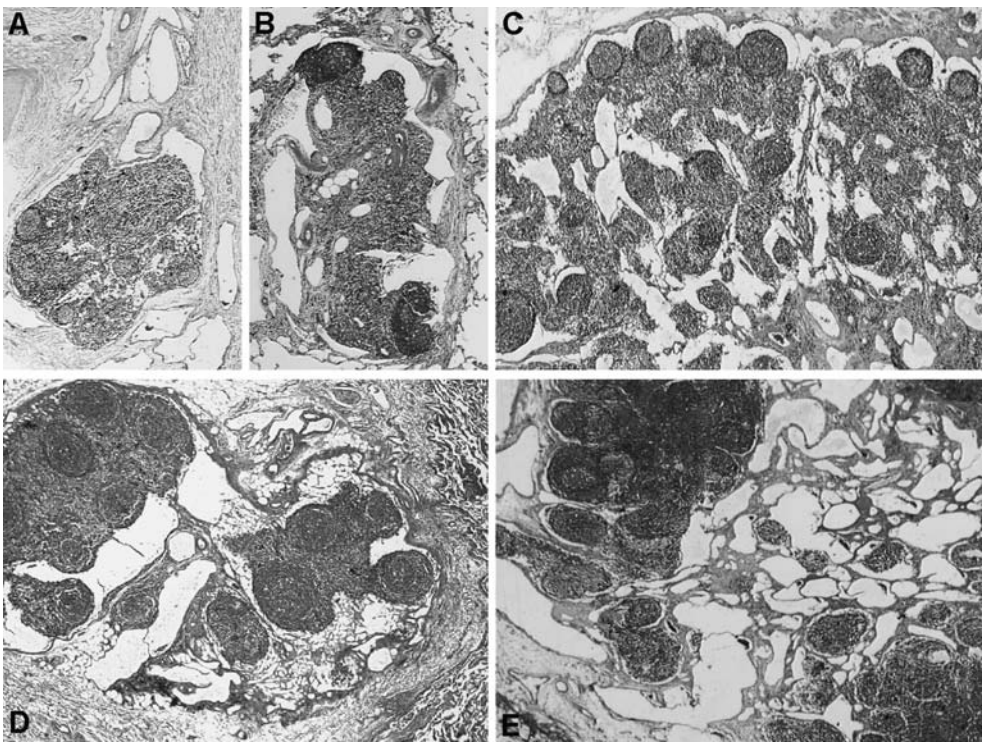

Fig. 1 Congestive lymph nodes in PVOD and PCH: association with ectasic peribronchial lymphatic vessels (**A**), congestion in a small intra-pulmonary lymph node (**B**), ectasic empty-looking sinuses in a large lymph node (**C**), association with lymphoid follicular hyperplasia and vascular transformation of sinuses (**D**) and ectasic sinuses with lymphangiomatous appearance (**E**)

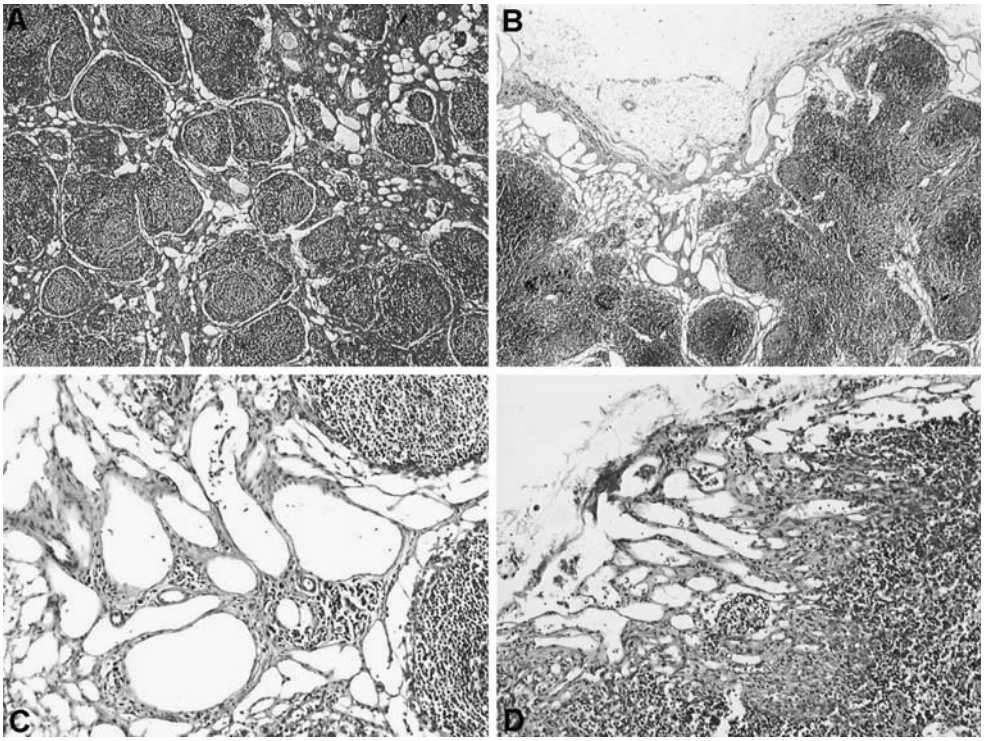

Fig. 2 Vascular transformation of lymph node sinuses in PVOD and PCH: diffuse parenchymal involvement associated with nodular lymphoid hyperplasia (**A**), broad sub capsular sinuses with multiple vascular channels (**B**), high magnification showing spindle cells in intrasinusal vascular walls (**C**), localised subcapsular lesion with spindle cells and vascular lumens (**D**)

tochemical study was performed with antigen retrieval by way of microwave and with HRP/AEC Kit (Microm, Francheville, France). The primary antibodies were directed against the following antigens: smooth muscle actin (Microm, MS113P), CD34 (Microm, MS363P) and factor VIII related antigen (DAKO, Trappes, France, A08202). For statistical analysis, p value was established with Fisher's exact test.

Results

The review of pulmonary parenchyma showed that diagnostic lesions of PVOD were constant in the 19 cases. PCH was absent or minimal in six cases but was the predominant feature in two others. There was no arterial plexiform lesion.

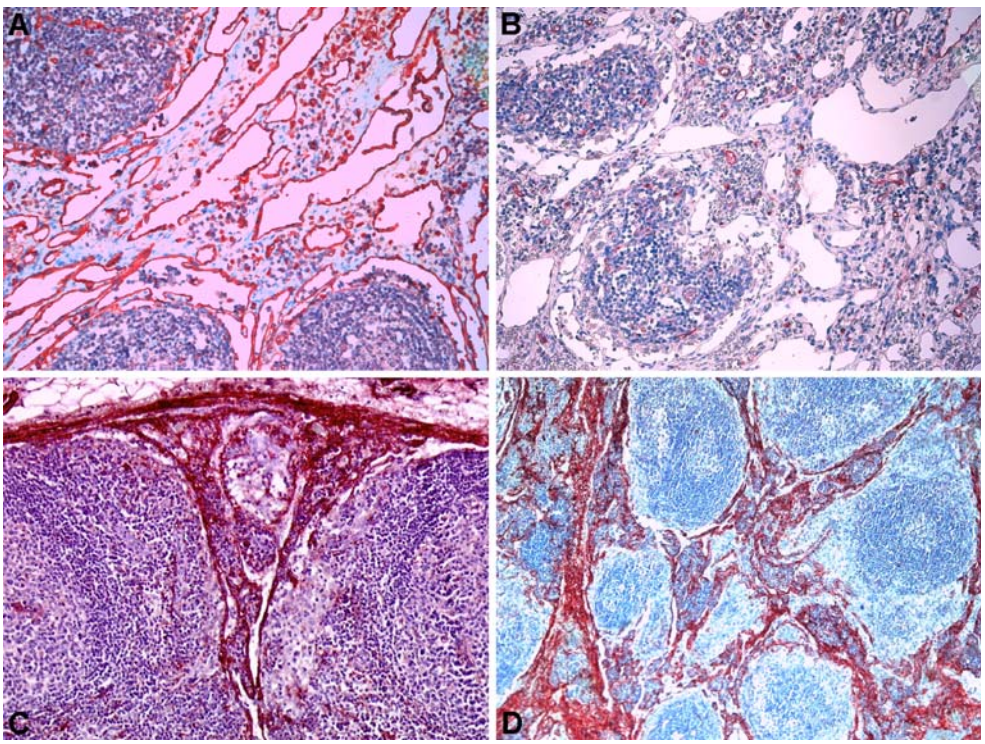

Fig. 3 Immunohistochemistry: endothelial cells expressing CD34 in dilated sinuses (**A**), factor VIII related antigen expression restricted to rare small vessels and mostly negative dilated sinuses (**B**), smooth muscle actin expression in a subcapsular localised form of vascular transformation of sinuses (**C**) and in a diffuse form associated with lymphoid hyperplasia (**D**)

Subcarinal lymph nodes with a short-axis measuring 1.1, 1.4 and 1.4 cm had been resected in three cases. In each of the 19 cases, two to 15 (mean =8.3±3.6) sections of hilar or lobar lymph nodes were present, and the largest had a short axis ranging from 0.8 to 1.8 cm (mean =1.1±0.3). There were 0 to 16 (mean=6.9±4.5) segmental or subsegmental lymph nodes per case. Lastly, subpleural or intrapulmonary lymph nodes have been sampled in four cases. In total, seven of the 19 patients (27%) had both more than 16 lymph nodes routinely sampled and hilar/lobar lymph nodes with short axis measuring at least 1.2 cm. Only one of the 33 control cases (3%) fulfilled both these criteria (Table 1).

Central (subcarinal, hilar and lobar) and peripheral (segmental, subsegmental and pulmonary) lymph nodes formed two groups showing similar histology. Nodal lymphatic congestion (Fig. 1) was characterised by ectasic sinuses appearing almost empty on histological sections. This lymphatic congestion was prominent (n=4, 21%), moderate (n=11, 58%), discreet (n=3, including the two with predominant PCH) or absent (n=1). In each case, this congestion was often more obvious in peripheral lymph nodes where it was the main lesion, but it was equally present in central lymph nodes. Such congestion was prominent and moderate in only 3% and 12% of the control cases, respectively.

Vascular transformation of sinuses (Fig. 2) was characterised by replacement of subcapsular, interfollicular or medullary sinuses by vascular channels with spindle cells and sometimes fibrosis. Involvement of central lymph nodes was diffuse or multifocal (n=8), discreet or focal (n=8) or absent (n=3). Peripheral lymph nodes were involved only in nine cases and mostly discreetly (n=7). In total, lesions were present in 16 of the 19 cases (84%). Immunohistochemistry (Fig. 3) showed that vascular channels were lined by endothelial cells expressing factor VIII related antigen and rarely CD34. Associated spindle cells often expressed smooth muscle actin. For comparison, vascular transformation of sinuses was diffuse or multifocal in 6%, discreet or focal in 36% and absent in 58% of control cases.

Intrasinusal haemorrhage with erythrophagocytosis and often haemosiderosis (Fig. 4) was prominent (n=2), moderate (n=4), discreet (n=8) or absent (n=5) in central lymph nodes. Peripheral lymph nodes were moderately (n=5) or discreetly (n=4) involved. This lesion was present but always discreet in only 24% of control cases.

In the case associated with CREST syndrome, follicular hyperplasia was prominent in central lymph nodes. Nine other cases, all associated with prominent or moderate pulmonary capillary haemangiomatosis, showed moderate follicular hyperplasia in hilar and lobar lymph nodes. Follicular hyperplasia was only discreet in segmental and subsegmental lymph nodes.

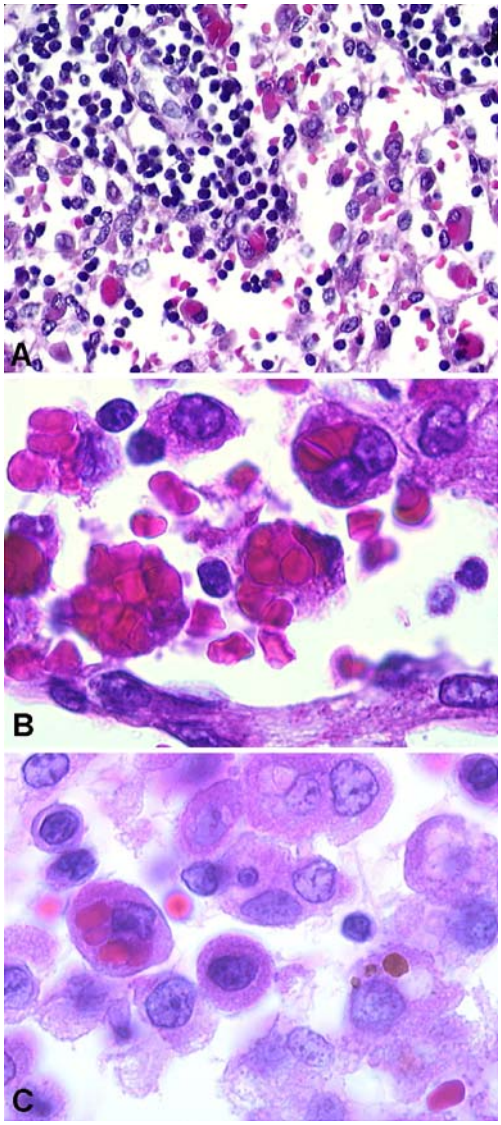

Fig. 4 Erythrophagocytosis in lymph node sinuses in PVOD and PCH: numerous histiocytes with large eosinophilic cytoplasmic containing red cells in a lymph node sinus (**A**), high magnification showing cytoplasms of histiocytes crammed with red cells (**B**), histiocytes containing phagocytosed red cells (*left*) and haemosiderin (*right*) in a sinus (**C**)

Moderate or prominent histiocytosis with anthracosis was present in peribronchial lymph nodes in eight patients. This appeared age-related, with the eight patients' age ranging from 37 to 60 years (mean 49) and seven of them being among the nine patients older than 38 years (p=0.005477).

A combination of lesions was often observed. Diffuse or multifocal vascular transformation of sinuses was associated with prominent or moderate follicular hyperplasia in six cases. In each case, lesions also had a rather heterogeneous distribution, with some lymph nodes showing no significant abnormality. One only case, with three sampled lymph nodes, showed no other lesion than histiocytosis and anthracosis.

Discussion

Our study demonstrates that lymph nodes histological abnormalities are common in PVOD and PCH as compared with other forms of pulmonary hypertension. Lesions occurred not only in enlarged lymph nodes but also in small peripheral ones. Lymph nodes also appeared abnormally numerous.

Nodal lymphatic congestion with sinusal dilatations was an expected lesion, since lymphatic vessel congestion in pulmonary interlobular oedematous septae is a characteristic feature of PVOD [10]. It was indeed often an obvious feature in peripheral peribronchial lymph nodes and also in subpleural and intrapulmonary lymph nodes. However, it was not the only lesion especially in central and mediastinal lymph nodes.

Vascular transformation of lymph node sinuses was a frequent finding in our series. This lesion is characterised by conversion of nodal sinuses into capillary-like channels, often accompanied by fibrosis [1]. This lesion has been described in various anatomic sites, often in association with lymphatic or venous occlusion and with malignant neoplasms [2]. Few mediastinal cases have been reported in association with congestive heart failure or constrictive pericarditis [1] and with chronic thromboembolic pulmonary hypertension [12]. A single case has been previously described in PCH [4], and capillaries seen in hilar and mediastinal lymph nodes in two other cases of PCH [3, 7] could in fact represent vascular transformation of sinuses. This histological lesion is known to simulate Kaposi's sarcoma [1, 2], and this diagnosis might indeed be suspected in a case of pulmonary hypertension associated with HIV infection. However, when examining pulmonary or mediastinal lymph nodes in the setting of pulmonary disease, one could rather consider lymphangioleiomyomatosis in the differential diagnosis. Lymph node involvement is frequent in lymphangioleiomyomatosis. It results in spindle cells nodules with vascular channels [11], which may resemble the nodular spindle-cell form of vascular transformation of sinuses made up of smooth muscle actin-positive myoid cells surrounding vessels [2]. Analysis of pulmonary histological lesions and immunostaining with HMB45 could be helpful in doubtful cases.

Vascular transformation of sinuses usually occurs in lymph nodes showing lymphoid depletion [1]. On the contrary, lymphoid hyperplasia often with germinal centres was present in many of our cases. This could be related to the interstitial lymphocytic infiltrate commonly seen in pulmonary capillary haemangiomatosis [8]. The association of germinal centre hyperplasia and diffuse vascular transformation of sinuses could, at low magnification, simulate an angio-follicular lymphoid hyperplasia or Castleman disease.

Angiogenic factors have been suspected to play a role in the occurrence of vascular transformation of sinuses in association with cancer [2]. Such factors are also likely in PVOD and especially in cases with PCH.

Erythrophagocytosis by histiocytes in the sinuses of lymph nodes has especially been described in axillary lymph nodes associated with breast carcinoma [9]. As in our cases, haemosiderosis and free red cells were also present. These lesions were presumably caused by trauma (breast biopsy), allowing large numbers of erythrocytes to enter the lymphatic channels and become phagocytosed in lymph node sinuses. In PVOD/PCH, this lesion probably indicates an important flow through shunts between obliterated blood vessels and lymphatic channels. Such erythrophagocytosis is supposed to be a reactive process with no clinical significance in absence of systemic haemophagocytic syndrome [9].

In conclusion, pathologists who may have to examine lymph node biopsy from patients with pulmonary arterial hypertension and lymphadenomegaly should suggest diagnoses of PVOD or PCH in the presence of the non-specific but suggestive lesions that we have observed.

Acknowledgements The authors thank Miss Dominique Gimont, Mrs Magalie Guerini and Miss Sylvie Planté for their technical assistance and Mrs Marylaure Legentil and Mrs Angélique Roggia for their secretarial work.

Conflict of interest statement We declare that we have no conflict of interest.

References

1. Chan JK, Warnke RA, Dorfman R (1991) Vascular transformation of sinuses in lymph nodes. A study of its morphological spectrum and distinction from Kaposi's sarcoma. Am J Surg Pathol 15:732–743
2. Cook PD, Czerniak B, Chan JK et al (1995) Nodular spindle-cell vascular transformation of lymph nodes. A benign process occurring predominantly in retroperitoneal lymph nodes draining carcinomas that can simulate Kaposi's sarcoma or metastatic tumor. Am J Surg Pathol 19:1010–1020
3. Domingo C, Encabo B, Roig J, López D, Morera J (1992) Pulmonary capillary hemangiomatosis: report of a case and review of the literature. Respiration 59:178–180
4. Dufour B, Maître S, Humbert M, Capron F, Simonneau G, Musset D (1998) High-resolution CT of the chest in four patients with pulmonary capillary hemangiomatosis or pulmonary venoocclusive disease. Am J Roentgenol 171:1321–1324
5. Frazier AA, Franks TJ, Mohammed TL, Ozbudak IH, Galvin JR (2007) From the archives of the AFIP: pulmonary veno-occlusive disease and pulmonary capillary hemangiomatosis. Radiographics 27:867–882
6. Holcomb BW, Loyd JE, Ely EW, Johnson J, Robbins IM (2000) Pulmonary veno-occlusive disease. A case series and new observations. Chest 118:1671–1679
7. Ishii H, Iwabuchi K, Kameya T, Koshino H (1996) Pulmonary capillary haemangiomatosis. Histopathology 29:275–278

8. Lantuéjoul S, Sheppard MN, Corrin B, Burke MM, Nicholson AG (2006) Pulmonary veno-occlusive disease and pulmonary capillary hemangiomatosis: a clinicopathologic study of 35 cases. Am J Surg Pathol 30:850–857
9. Listinsky CM (1988) Common reactive erythrophagocytosis in axillary lymph nodes. Am J Clin Pathol 90:189–192
10. Mandel J, Mark EJ, Hales CA (2000) Pulmonary veno-oclusive disease. Am J Respir Crit Care Med 162:1964–1973
11. Matsui K, Tatsuguchi A, Valencia J et al (2000) Extrapulmonary lymphangioleiomyomatosis (LAM): clinicopathologic features in 22 cases. Hum Pathol 31:1242–1248
12. Meysman M, Diltoer M, Raeve HD, Monsieur I, Huyghens L (1997) Chronic thromboembolic pulmonary hypertension and vascular transformation of the lymph node sinuses. Eur Respir J 10:1191–1193
13. Resten A, Maitre S, Humbert M et al (2004) Pulmonary hypertension: CT of the chest in pulmonary venoocclusive disease. Am J Roentgenol 183:65–70
14. Scully RE, Mark EJ, McNeely WF, McNeely BU (1993) Case records of the Massachusetts General Hospital. Weekly clinicopathological exercises. Case 48-1993. A 27-year-old woman with mediastinal lymphadenopathy and relentless cor pulmonale. N Engl J Med 329:1720–1728

Virchows Arch (2008) 453:177–188
DOI 10.1007/s00428-008-0627-4

ORIGINAL ARTICLE

Ultrastructure of myoepithelial cells as a target cell in sialoadenitis of submandibular glands of lupus-prone female NZBxNZWF_1 mice

Toshiharu Hayashi · Hideyuki Hayashi · Taeko Fujii · Chie Adachi · Keiko Hasegawa

Received: 6 February 2008 / Revised: 14 April 2008 / Accepted: 6 May 2008 / Published online: 19 June 2008

Abstract The changes of myoepithelial cells of sialoadenitis in submandibular glands in lupus-prone female NZB × NZWF_1 (B/WF_1) mice, a model for human secondary Sjögren's syndrome (sSS), were examined ultrastructurally. Inflammatory foci consisting of mainly lymphoid cells (lymphocytes and plasma cells) in the interlobular interstitium began to develop from 18 weeks of ages, and those were found within acini from the age of 25 weeks. These were paralleled with the production of anti-double-stranded deoxyribonucleic acid and anti-Ro/SS-A antibodies with age. Infiltrated lymphoid cells consisted of $CD4^+$ T cells and Ig^+ (or $IgG2a^+$) cells. Electron microscopy revealed destruction of myoepithelial cells with lysis of basement membranes contacted with either lymphocytes or plasma cells. These led to the destruction (degeneration and necrosis) of the epithelium in striated and intercalated ducts and acinar epithelium. Further destruction of those cells occurred by the invasion of lymphocytes into the epithelial layers. Small numbers of apoptotic myoepithelium and duct epithelium from the age of 25 to 36 weeks and an increase of those cells in survived mice at 44 weeks of age were observed. The present study suggests that the myoepithelium may be one of the target cells and that the destruction of myoepithelial cells by infiltrated lymphoid cells may precede the destruction of acinar ducts and epithelium in sialoadenitis in sSS.

Keywords Sjögren's syndrome · Myoepithelial cell · Target · Sialoadenitis · B/WF_1 mouse

T. Hayashi (✉) · H. Hayashi · T. Fujii · C. Adachi · K. Hasegawa
Laboratory of Veterinary Pathology, Faculty of Agriculture,
Yamaguchi University,
1677-1, Yoshida,
Yamaguchi 753-8515, Japan
e-mail: hayasi@yamaguchi-u.ac.jp

Introduction

Human Sjögren's syndrome (SS) is a chronic autoimmune disorder of unknown etiology including the potential roles of endogenous retroviruses as triggers [16, 30] and multiple factors (e.g., environmental stress, genetic factors, and hormonal imbalance) may be involved in the development of SS [29]. There are two types of SS, such as primary SS (pSS) and secondary SS (sSS) accompanying with other autoimmune diseases especially systemic lupus erythematosus (SLE) and rheumatoid arthritis [7, 32]. Most patients with SS complain of dry mouth and eyes with significant functional impairments of the salivary and lacrimal glands [28]. This autoimmune exocrinopathy is characterized by the mononuclear cell infiltration, which consisted of $CD4^+$ cells and B cells [24], in these glands associated with the production of several autoantibodies against autoantigens such as Ro/SS-A and La/SS-B [8, 24, 37], α-fodrin [10, 42], double-stranded deoxyribonucleic acid (dsDNA) [20], and nuclei and ductal epithelia in salivary and lacrimal glands [2].

In patients with SLE, the development of immune complex-mediated glomerulonephritis leads to death [5, 26] without treatment of corticosteroids, dialysis, or transplant. Female NZB × NZW(B/W)F_1 mice, one of animal models for human SLE [19], are also known to develop lesions in salivary and lacrimal glands from approximately 4 months of age similar to those in human sSS [3, 4, 41]. Recently, Mitsias et al. [24] have proposed the expression "autoimmune epithelitis" as an alternative for SS based on data pointing out the central role of the epithelial cell (e.g., antigen presentation in the initiation and perpetuation of the autoimmune lesion) in the pathogenesis of the syndrome, and the epithelial components of the other organs such as kidneys, liver, lungs, or thyroids are

commonly affected, resulting in various extraglandular manifestations. However, lesions of salivary and lacrimal glands develop not only in salivary and lacrimal ducts of interlobular interstitial tissues but also in acini. In addition, myoepithelial cells are present in salivary and lacrimal glands [36, 44], and the activation of ductal epithelial cells but also myoepithelial cells in the salivary glands of patients with SS has been reported [27]. Moreover, autoantibodies against myoepithelial cells appeared in autoimmune sialoadenitis model mice [34]. These raise questions that myoepithelial cells may play a role in the development of acinar tissues of SS. Thus, the present study focused on the changes of myoepithelial cells of striated and intercalated ducts and acinar epithelium in sialoadenitis of submandibular glands by electron microscopy in lupus-prone female B/WF_1 mice.

Materials and methods

Animals

Specific pathogen-free 8-week-old female BWF_1 mice were obtained (SLC Japan, Shizuoka, Japan). The number of mice used in each set of experiment is given in parenthesis. They were kept in metal cages and given autoclaved pellets (CE-2, Clea Japan, Tokyo, Japan) and water freely. They were kept at 25±2°C room temperature, 55±10% humidity, and a 12-h light/dark cycle (lighting time 08:00–20:00). The animal experiments were approved by the Animal Research Ethics Board of Faculty of Agriculture, Yamaguchi University.

Sampling

Samples for histopathology, immunohistochemistry, apoptotic assays, and electron microscopy (left and right sides of submandibular glands and blood) at the age of 8, 10,12, 16, 20, 22, 23, and 25 weeks (n=5 in each time point) before mice begin to die at the age of approximately 30 weeks [14] were obtained. Among salivary and lacrimal glands, submandibular glands were selected, because the development of inflammation in submandibular glands was the same degree as that in lacrimal glands with age and inflammatory lesions appearing earlier compared to parotid and sublingual salivary glands in B/WF_1 mice [15]. Furthermore, at the age of 36 and 44 weeks, submandibular glands from some survived mice were examined histologically (n=5, respectively). Tissues from 25-, 36- and 44-week-old mice were provided for the apoptotic assay, and those of histopathology at 25 weeks of age also were examined by immunohistochemistry (n=5). For electron microscopy, a part of tissues from mice at 8, 20, 25, and 36 weeks old (n=3, respectively) were examined.

Histology, apoptotic assays, and immunohistochemistry

For histology, immunohistochemistry and apoptotic assays, submandibular glands were fixed in 10% neutral buffered formalin (pH 7.4), and 4-μm-thick sections were prepared from paraffin wax-embedded tissues and stained with hematoxylin and eosin (H&E), periodic acid methenamin-silver for basement membrane and methyl green pironin for plasma cells.

Apoptotic cells were detected by the terminal deoxynucleotidyl transferase (TdT)-mediated deoxyuridine triphosphate nick end labeling (TUNEL) method in paraffin-embedded sections using the in situ TUNEL kit (Roche Diagnostics, Penzberg, Germany) according to manufacturer's instruction. In brief, deparaffinized sections were incubated with proteinase K working solution (20 μg/ml in 10 mM Tris/HCl, pH 7.6) for 30 min at 37°C. These sections were presoaked in TdT buffer for 2 h. Then, they were incubated with 0.3% H_2O_2 in methanol to block endogenous peroxidase and incubated with converter peroxidase for 30 min at 37°C and reacted with peroxidase buffer containing diaminobenzidine (DAB) for 5 min at 37°C. Nuclei was counterstained with hematoxylin for 1 min.

The presence of B and $CD4^+$ T cells was detected by immunohistochemistry. In brief, deparaffinized submandibular sections were treated with 5% bovine serum albumin (Sigma-Aldrich, St. Louis, MO, USA) to block nonspecific binding of antibody and those were treated with 0.3% H_2O_2 methanol to eliminate endogenous peroxidase activity for 10 min at 37°C, respectively. Then, sections were reacted with horseradish peroxidase (HRP)-conjugated goat anti-mouse IgG2a (Bethyl, Montgomery, TX, USA) or goat anti-mouse Ig (ICN Biomedicals, Aurora, OH, USA) for 24 h at 4°C. In addition, to detect $CD4^+$ T cells, firstly, samples were reacted with rat monoclonal antibody against mouse $CD4^+$ T cells (clone: RM4-5, BD, Biosciences, CA, USA) for 24 h at 4°C and, secondly, reacted with HRP-conjugated antibody to rat IgG (Cappel, Ohio, USA) for 10 min at 37°C. Thereafter, samples were reacted with peroxidase buffer containing DAB (Roche Diagnostics) for 10 min at 37°C. Nuclei were counterstained slightly with methyl green.

For the direct immunoperoxidase assay, blocking tests were performed as follows. Sections were reacted either with nonlabeled goat anti-mouse IgG2a (Bethyl) or nonlabeled goat anti-mouse Ig (Bethyl). The reaction without the primary antibody served as a negative control.

Electron microscopy

A part of the submandibular glands was immersed in glutaraldehyde at 4°C for 2 h. The tissues were then

postfixed in 2% osmium at 4°C for 2 h, dehydrated in graded ethanols at 4°C, and embedded in araldite. The orientation of the blocks was achieved by examining 1-μm sections stained with toluidin blue. Ultrathin sections were made and stained with uranyl acetate and lead nitrate and observed using electron microscopy (JEM-100CX II, Tokyo, Japan).

Scoring

The presence or absence of focal inflammatory cell infiltration was graded on a 0–3 scale by a modification of the method described by Greenspan et al. [9]. This grading system has four steps, with grade 0 representing a salivary gland free of lymphoid cell infiltration and grades 1 to 3 denoting the presence of focal lymphoid cell infiltration, as follows: grade 1, 25 cells; grade 2, 25–50 cells; grade 3, greater than 50 cells. The grade of cell infiltration in a mouse was expressed as the average score calculated by the following equation: score index=total score/number of foci.

Detection of anti-dsDNA and anti-Ro/SS-A antibodies

Concentrations of IgG anti-dsDNA and anti -Ro/SS-A antibodies in the serum were examined by enzyme-linked immunosorbent assay (ELISA). ELISA kits for mouse IgG anti-dsDNA and anti-Ro/SS-A(60 kDa) antibodies were purchased from Alpha Diagnostic International (Texas, USA). Each concentration of sera was assayed according to the manufacturer's instructions.

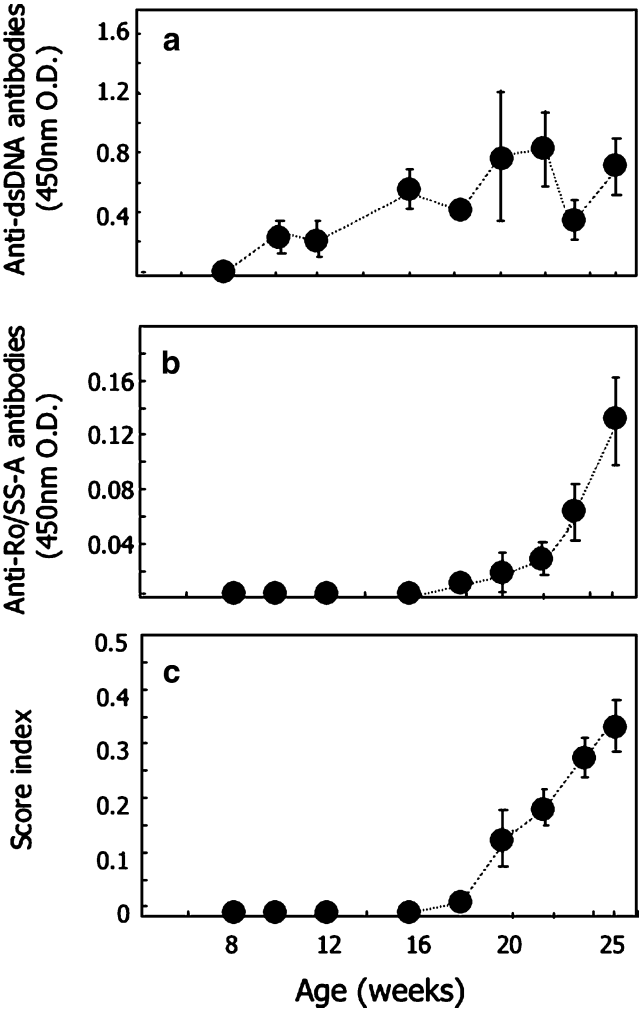

Fig. 1 Production of anti-dsDNA (**a**) and anti-Ro/SS-A (**b**) antibodies and score index (severity of lesions) (**c**) with age in BWF_1 mice. Each point represents of the mean±standard error

Results

Development of anti-dsDNA and anti-Ro/SS-A antibodies and inflammatory lesions (score index) in submandibular glands

Anti-dsDNA antibodies were found at 10 weeks of age and increased gradually until the age of 25 weeks (Fig. 1a). On the other hand, anti-Ro/SS-A antibodies were found at 18 weeks of age and increased lineally until 25 weeks of age (Fig. 1b). The development of the score index (severity of inflammation) in salivary glands was found 18 weeks of age and increased lineally until 25 weeks of age (Fig. 1c).

Light microscopy in submandibular glands

Until the age of 16 weeks, there were no lesions in submandibular glands. At the age of 18 weeks, initial lesions were observed at the site of excretory ducts. Lymphocytes were detected in the lumen of lymphatic and filled the lumen, and thereafter, lymphoid cells (lymphocytes and plasma cells; dominance of each type of cells varies) infiltrated around arterioles, ducts, and venules. These changes were mainly found in the interlobular interstitum. In mice at the age of 25 weeks and some survived mice at the age of 36 weeks, inflammatory foci often extended to acinar tissues (Fig. 2a–f), and small lymphoid cell accumulation with degeneration of epithelial cells in acini was found (Fig. 2a–f). Involved ducts, arterioles, and veins and acinar epithelium showed degenerative changes. At the age of 44 weeks, some survived mice showed severe atrophy of acini with intense infiltration of lymphoid cells, and these cells occupied most parts of submandibular glands (Fig. 3a). In these lesions, there were swelling, degeneration, destruction, and loss of ductal epithelial and acinar cells (Fig. 3b–g) of ducts and degeneration of small blood vessel walls. In addition, some arterioles showed hyaline degeneration (Fig. 3b) and/or

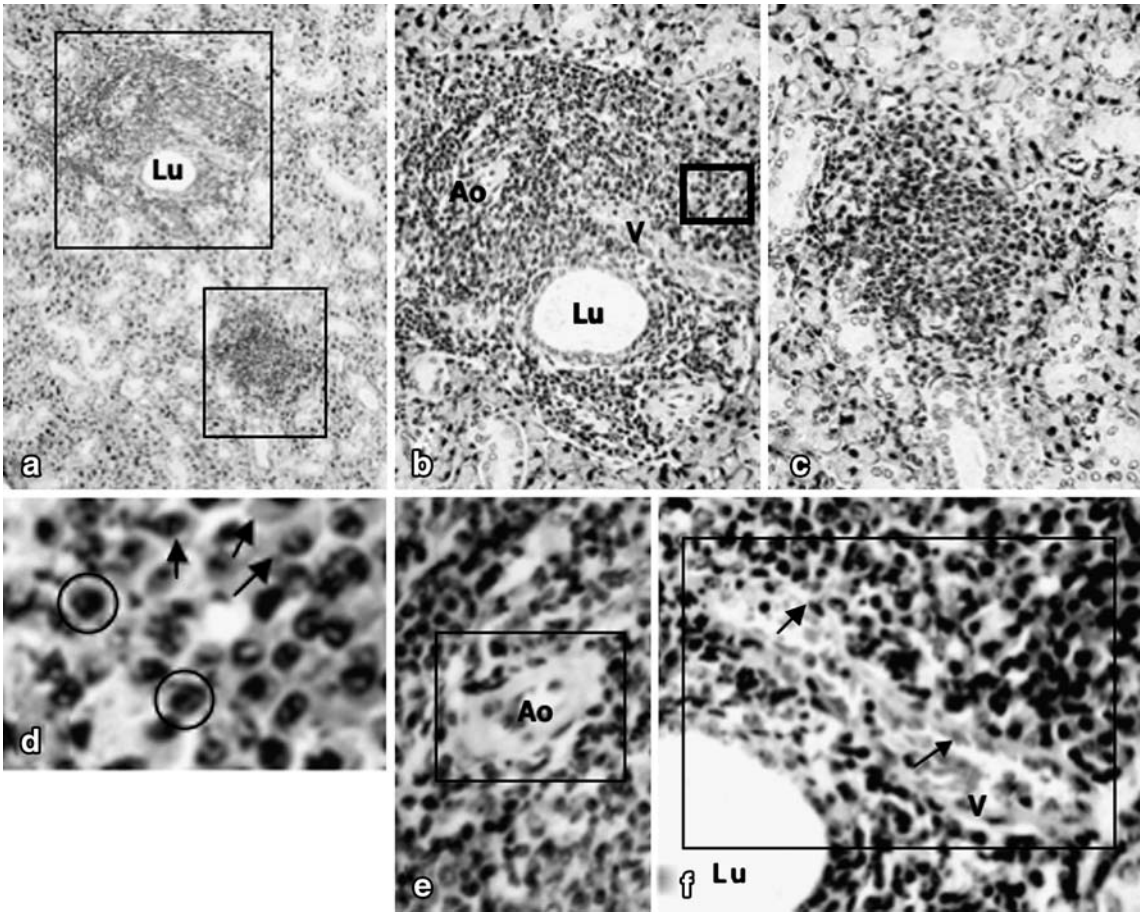

Fig. 2 Infiltration of lymphoid cells (lymphocytes and plasma cells) is seen (**a**) around excretory ducts (*Lu*), acinar tissues, and blood vessels (**b**, **c** higher magnification of *rectangles* of **a**). *Arrows* indicate plasma cells, and *circles* indicate lymphocytes in **d** (higher magnification of a *rectangle* of **b**). Degeneration of an arterioles (*Ao*; **e**) and a vein (*V*; **f**; *arrows* indicate destruction of wall) is shown (higher magnification of **b**). **a** ×20, **b** and **c** ×40, **d** ×800, and **e** and **f** ×400 (original magnification). 25 weeks of age. H&E

fibrinoid necrosis with (Fig. 3d) or without endothelial cell proliferation, and an accumulation of secretory fluids and a leak of them from destroyed epithelium were sometimes found (Fig. 3d).

At the age of 25 and 36 weeks, a few $TUNEL^+$ apoptotic cells were detected in some duct epithelial and myoepithelial cells (Fig. 4a,b) including some infiltrating lymphoid cells. In addition, there were no evidences in apoptotic duct epithelial cells contacted with lymphocytes. At the age of 44 weeks in some survived mice, there were many $TUNEL^+$ apoptotic epithelial cells in excretory (Fig. 4c), striated, and intercalated ducts including the acinar epithelium, myoepithelium, and infiltrated lymphoid cells.

At the age of 25 weeks, many $CD4^+$ (5A), Ig^+ (5B), and $IgG2a^+$ cells in infiltrated lymphoid cells in the interlobular interstitium and acini were observed. In addition, in basement membranes around ducts, acini, and capillaries, the binding of Ig and IgG2a was also observed at the part with or without inflammatory cell infiltration (Fig. 5c).

Electron microscopy

Striated and intercalated duct changes in acini

Myoepithelial cells were located at intercalated and striated ducts, being interposed between the base of epithelial cells in those areas and the basement membranes, and there were no degenerative changes of epithelial cells without lymphoid cell infiltration at the age of 8 weeks (Fig. 6a). From the age of 20 weeks, there was infiltration of different-sized lymphocytes (e.g., small lymphocytes, medium sized and large lymphocytes) with scanty cytoplasm and organelles and plasma cells having a well-developed rough endoplasmic reticulum. Myoepithelial cells in contact with lymphoid cells via basement membranes showed increased myofilaments with pyknotic nuclei and degeneration of organelles of the cytoplasm (Fig. 6b,e). In such areas, duct epithelial cells showed relatively intact cells (Fig. 6b,c) or degeneration and/or escape from intercalated ducts (Fig. 6d,e).

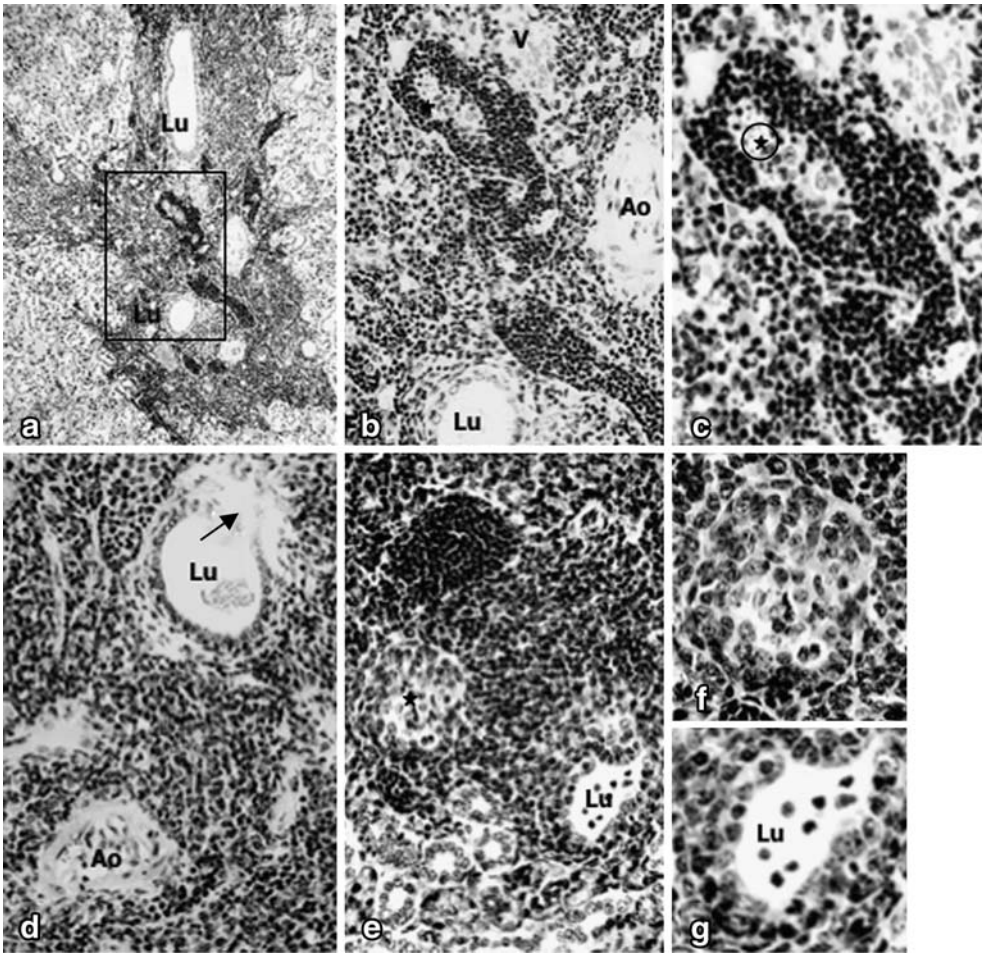

Fig. 3 Numerous lymphoid cells around excretory (*Lu*, **a**–**d**) and intercalated ducts (*Lu*, **e**, **g**) are shown. **b** and **c** are higher magnification of **a** and degenerated vein (*V*) and arteriole (*Ao*) in **b** and **d**, and destructed (an *arrow* in **d**) and desquamated (a *star mark* in **c**) ductal epithelium in the lumen are seen. *A star mark* in **e** and **f** (higher magnification of **e**) indicates hyperplasia of epithelial cells, and degenerated duct epithelium in **e** and **g** (higher magnification of **e**) are seen. **a** ×20, **b** ×40, **c**, **d**, and **e** ×250, and **f** and **d** ×800 (original magnification). 44 weeks of age. H&E

In addition, hypertrophic myoepithelial cells with swelled nuclei and increased cytoplasm in contact with lymphoid cells were observed, and they lost connection with the epithelium (Fig. 7a,b). At this site, thickness, discontinuity, irregularity, or lysis of basement membranes (Fig. 7a–d) and destruction of myoepithelium with (Figs. 7a,b,d) or without (Fig. 7c) the degeneration of duct epithelium were observed.

In addition, epithelial cells showing prominent vacuolar degeneration or clear cytoplasm by invaded lymphocytes but not plasma cells into epithelial layers were observed (Fig. 8a,b).

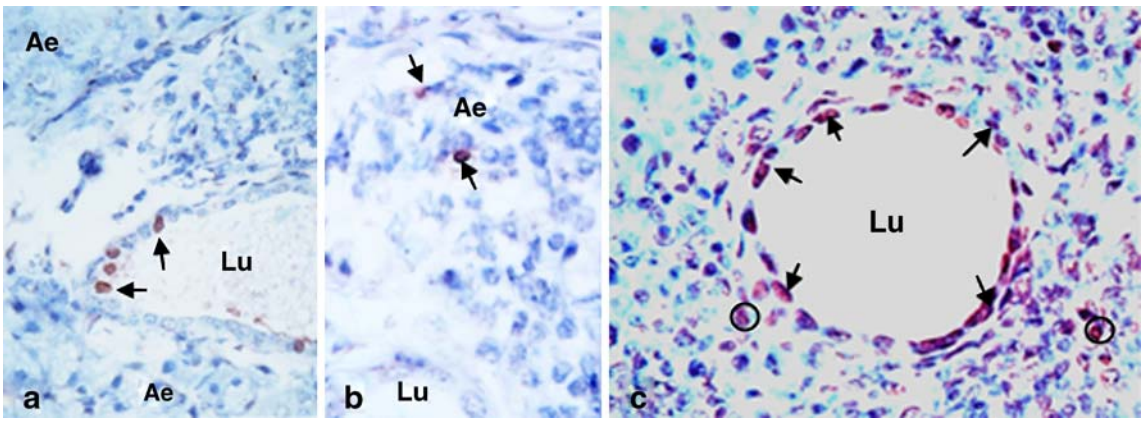

Fig. 4 *Arrows* in **a** indicate apoptotic epithelial cells in the excretory ducts (*Lu*), and *arrows* of **b** indicate apoptotic myoepithelial cells around acinar epithelium (*Ae*). *Arrows* indicate many apoptotic excretory duct epithelium (*Lu*), and *circles* indicate infiltrated apoptotic lymphoid cells (**c**). **a**, **b** 25 weeks of age and **c** 44 weeks of age. **a**, **b** ×350 and **c** ×250 (original magnification). Tunnel assays. Nuclei are stained slightly with hematoxylin

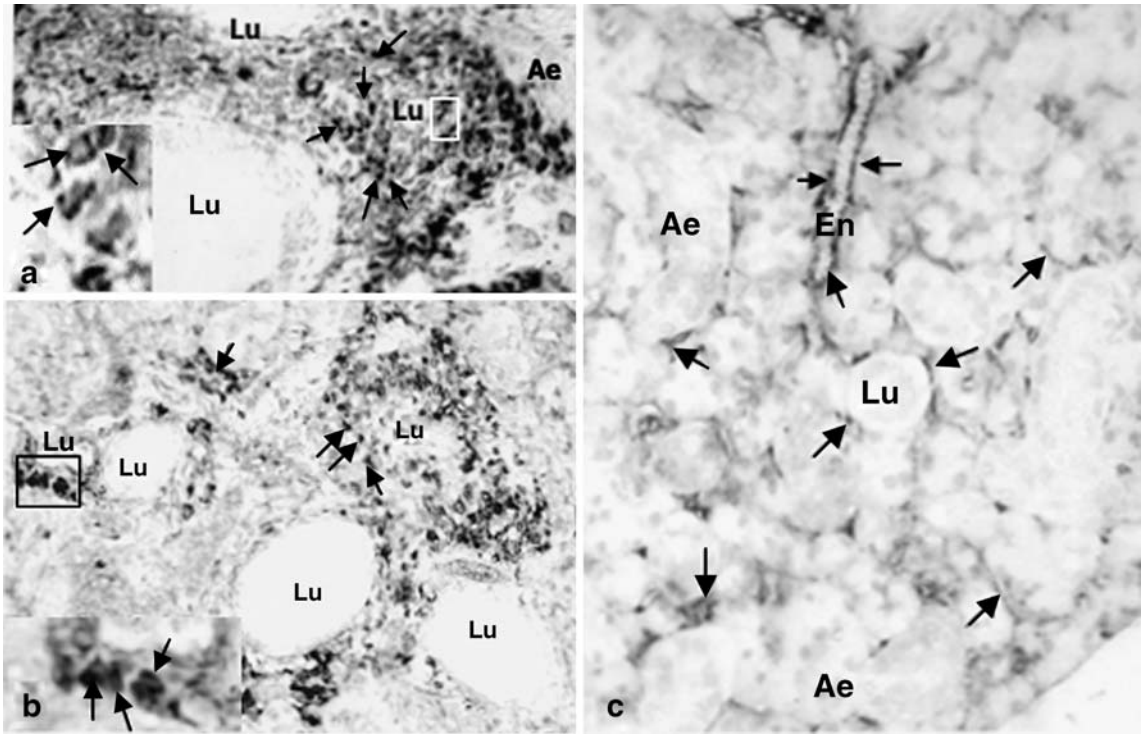

Fig. 5 Infiltration of many $CD4^+$ T cells (*dots*: *arrows*) around the excretory duct (*Lu*) in **a**, and *insert* shows higher magnification of a *white rectangle* (*arrows* indicate $CD4^+$ T cells). Infiltration of many Ig^+ cells (*dots*: *arrows*) around excretory ducts (*Lu*) in **b**, and an *insert* shows higher magnification of a *black rectangle* (*arrows* indicate Ig^+ cells). *Arrows* of **c** indicate binding of Ig to basement membranes showing thin and discontinuous meshwork around intercalated ducts (*Lu*), capillaries (*En*), and acinar tissues (*Ae*). 25 weeks of age. **a**–**c** ×100 and *inserts*, ×750 (original magnification). Nuclei are stained slightly with methyl green. Immunoperoxidase

Hyperplasia of duct epithelium

Other than destructive changes of duct epithelium, there was epithelial cell hyperplasia of intercalated, striated, and excretory ducts with intraepithelially infiltrated lymphocytes at 36 weeks of age (Fig. 8c,d). In these lesions, duct epithelium with or without degeneration were observed. In addition, destruction and/or thickening of the basement membrane around ducts and capillaries were observed (Fig. 8d).

Acinar epithelium changes

Myoepithelial cells around the acinar epithelium without cell infiltration showed relatively normal appearance at the age of 8 weeks (Fig. 9a). From the age of 20 weeks, myoepithelial cells showed degeneration by the attachment of lymphoid cells (Fig. 9b–d). Degeneration of the acinar epithelium by infiltration of lymphocytes in and around the acini (Fig. 9c) and that by infiltration of plasma cells around the acini (Fig. 9d) were observed. Severely affected acini showed atrophy (Fig. 9e,f) and destruction of basement membranes and the myoepithelium with infiltration of lymphoid cells, and some macrophages were recognized.

Discussion

The present study demonstrated that sialoadenitis in submandibular glands developed with age in B/WF_1 mice. This was associated with the production of anti-dsDNA and anti-Ro/SS-A antibodies in B/WF_1 mice. The ultrastructure revealed the destruction of myoepithelial cells in intercalated and striated ducts and acini. Thereafter, epithelium destruction progressed. In addition, there was no destruction of myoepithelial cells and epithelium in case of the lacking infiltration of lymphoid cells. These suggest that myoepithelial cells may be one of important target cells in acinar tissues.

There may be, at least, two types of pathogenetic (nonimmune or immune-mediated) mechanisms working in damages of intercalated and striated ductal epithelia and acinar epithelium. Firstly, lymphoid cells (lymphocytes and/or plasma cells) attached to myoepithelial cells may induce the destruction of myoepithelial cells. Through this process, epithelial cell damage may occur mechanically. It is possible, since myoepithelial cells are located between the basement membranes and the acinar and duct epithelial cells, and myeoepithelial cells may have a complex role, such as a part of a contractile apparatus that supports the

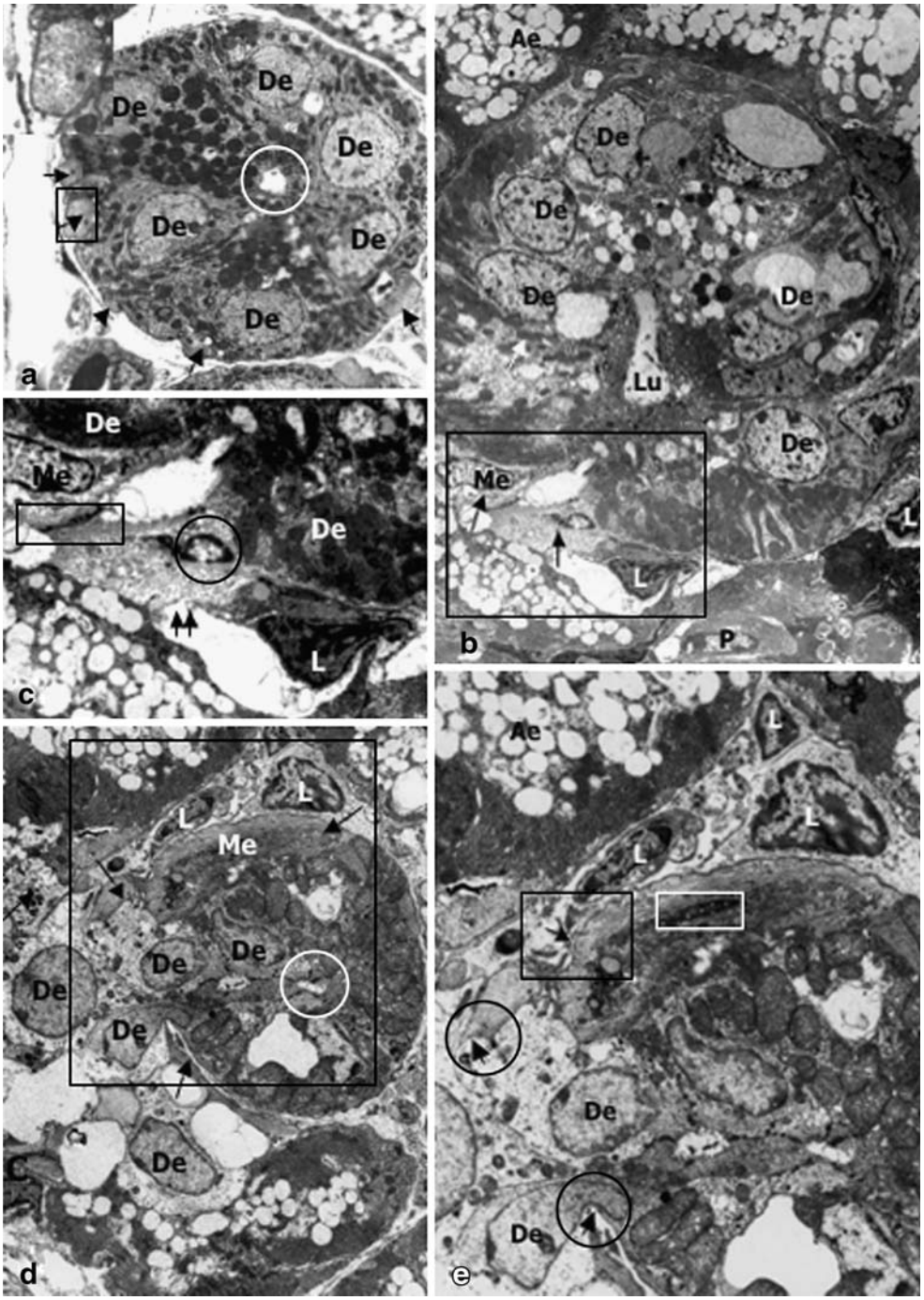

Fig. 6 *Arrows* (*insert*: higher magnification of a *rectangle* of **a**) indicate cross-sectioned myoepithelial cells with myofilaments in a striated duct (*De*), and a *white circle* indicates lumen. A *rectangle* of **b** shows close contact of one lymphocyte (*L*) to one degenerated myoepithelial cell showing shrinkage nucleus, and *arrows* indicate bundles of myofilaments with relatively intact duct epithelium (*De*). A *rectangle* of **c** (enlargement of *rectangle* of **b**) indicates thick basement membrane, and *arrows* indicate disappearance of basement membranes. In addition, at this part, pyknotic nucleus of myoepithelial cell can be seen (a *circle*). A *rectangle* of **d** indicates close contact of two lymphocyte (*L*) to basement membranes, and at this part myoepithelial cell (*Me*: *arrows* indicate myofilaments) showing degenerative change with shrunken nucleus (a *white rectangle* of **e**; enlargement of *rectangle* of **d**) and discontinuation or disappearance of basement membranes (*arrows in* **a** *circle*) are visible. In addition, escape of degenerated duct epithelial cells (*De*) from the intercalated duct is seen. **a** 8 weeks of age, **b**–**e** 36 weeks of age. **a**, **d** ×750, **b**, **e** ×1,200, and **c** ×2,400 (original magnification)

expulsion of saliva [36] but also the preservation of structural integrity of the modulation of glandular secretory function [44]. Secondly, epithelial damages may be induced by the migrated and penetrated lymphocytes into the intraepithelial layer (epitheliotropism), which is known to be the key process in autoimmune reaction [31], and also epitheliotropism is related to a specific and efficient function of lymphocytes in the target tissue being responsible for epithelial cell damage [43]. The present study demonstrated the infiltration of $CD4^+$ cells in interlobular and intralobular ducts and acinar tissues. There are a lot of reports that $CD4^+$ T cells including autoreactive T cells expressing $CD4^+V\beta8^+$ [12] infiltrate in SS. Thus, the presence of $CD4^+$ T cells strongly suggests the involvement of cellular immunity in the damage of the myoepithelium, and duct and acinar epithelia [34].

At first, the infiltration and trap of lymphoid cells into the duct and acinar tissues may occur, and these may be due to the interaction of adhesion molecules between basement membranes and lymphoid cells. The components of the

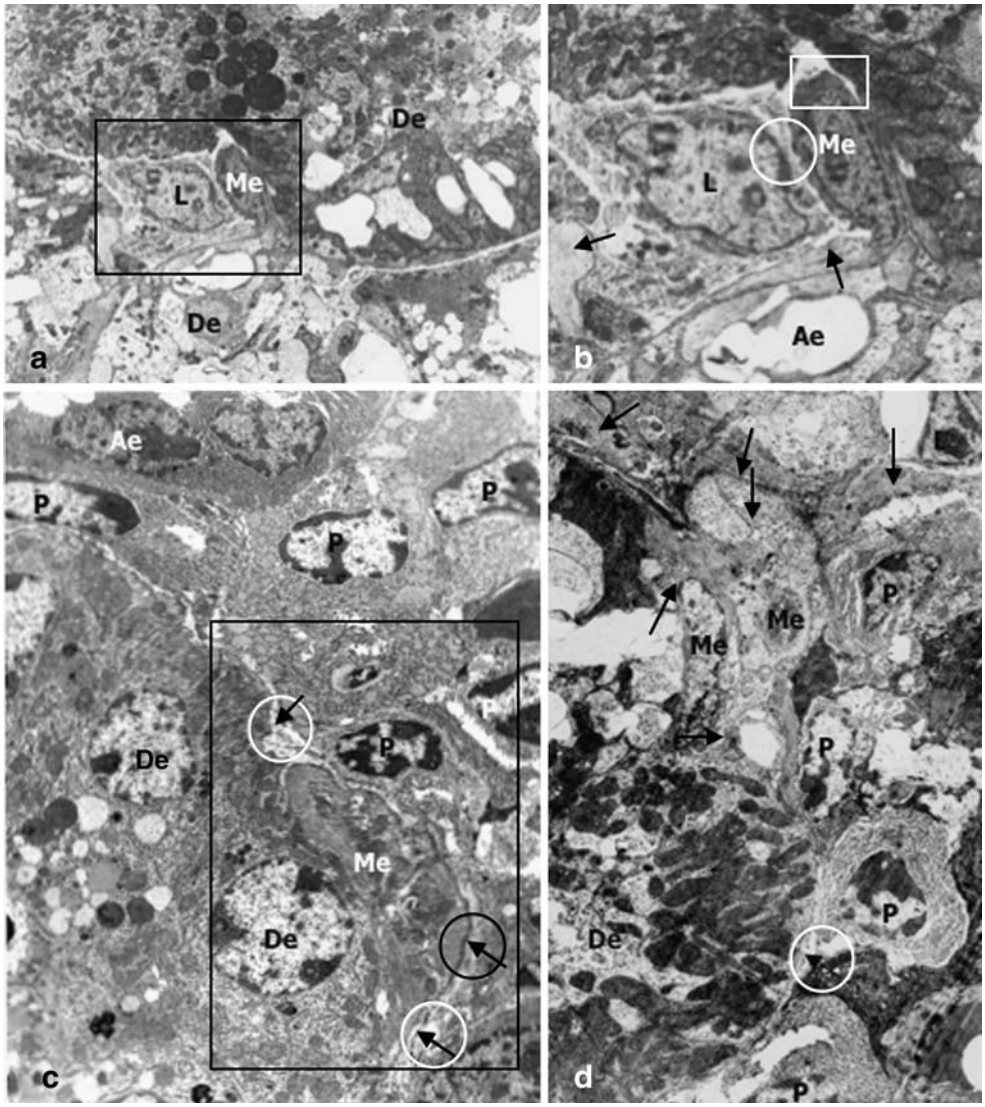

Fig. 7 A *rectangle* of **a** indicates the adherence of a large lymphocyte (*L*) to a hypertrophic myoepithelial cell (*Me*) with degenerated duct epithelium (*De*). *Arrows* of **b** (enlargement of *rectangle* of **a**) indicate bundles of myofilaments, and lysis of basement membrane is seen (a *white circle*). A *white rectangle* shows detach of a myoepithelial cell (*Me*) from a duct epithelial cell (*De*). **c** shows infiltration of plasma cells (*P*) around striated ducts and plasma cells closely contacted with basement membranes (a *rectangle*). An *arrow of a black circle* indicates thick basement membranes, and *arrows of white circles* indicate lysis of basement membranes where degenerated and disorganized myoepithelial cells (*Me*) can be seen, whereas duct epithelium (*De*) are relatively intact. In **d**, myoepithelial cells (*Me*; *arrows* indicate myofilaments) and duct epithelium (*De*) show severe degeneration with infiltration of plasma cells (*P*) around striated ducts, and discontinuity of basement membrane are seen (an *arrow in a white circle*). 36 weeks of age. **a** ×750, and **b**–**d** ×1,200 (original magnification)

basement membrane are mainly collagen type IV, proteoglycan, fibronectin, and laminin; of these, laminin is the most abundant glycoprotein molecule in salivary and lacrimal glands [6]. Upregulated expression of very late antigen-6, which is a ligand for laminin [40], on infiltrating lymphoid cells may facilitate the interaction of lymphoid cells with laminin of basement membranes of duct and acinar epithelia [12, 23, 25]. These may lead to destruction, disorganization, or lysis of basement membranes [27]. Thereafter, the interaction of lymphoid cells and myoepithelial cells may occur. In addition, an in vitro study demonstrated that activated myoepithelial cells expressed adhesion molecules such as intercellular adhesion molecule (ICAM)-1[21], which is the receptor of lymphocyte function-associated antigen-1 on lymphoid cells [40]. These may be responsible for the attachment of lymphoid cells to myoepithelial cells. As demonstrated here, hypertrophic myoepithelial cells may reflect the morphologic expression of cell activation. In addition, we have reported previously intense ICAM-1 expression on capillary endothelium in the dermis, which was associated with the systemic production of interleukin-1, tumor necrosis factor-α, and interferon-γ, in B/WF$_1$ mice [13, 14, 40], suggesting those cytokines may induce ICAM-1 expression on myoepithelium. Moreover, it has been suggested that chemokines are key regulators in these process [24]. For example, CXCL13 (or B cell attractant, BCA1) attracts naïve B cells and certain T cells through the receptor CXCR5 (or BLR1), and epithelial cells as well as capillary endothelial cells are implicated in the production of CXCL13 [1, 38], resulting in the allowance of invasion of lymphoid cells into the epithelial lining layer. On the other hand, the mechanisms of how to access of circulating cytokines, which activate the myoepithelial cells, are unknown. As demonstrated here, veins or venules in the interlobular interstitum were damaged by infiltrated lymphoid cells. Thus, one possibility is a leak from damaged blood vessels, and leaked cytokines and chemokines may activate myoepithelial cells

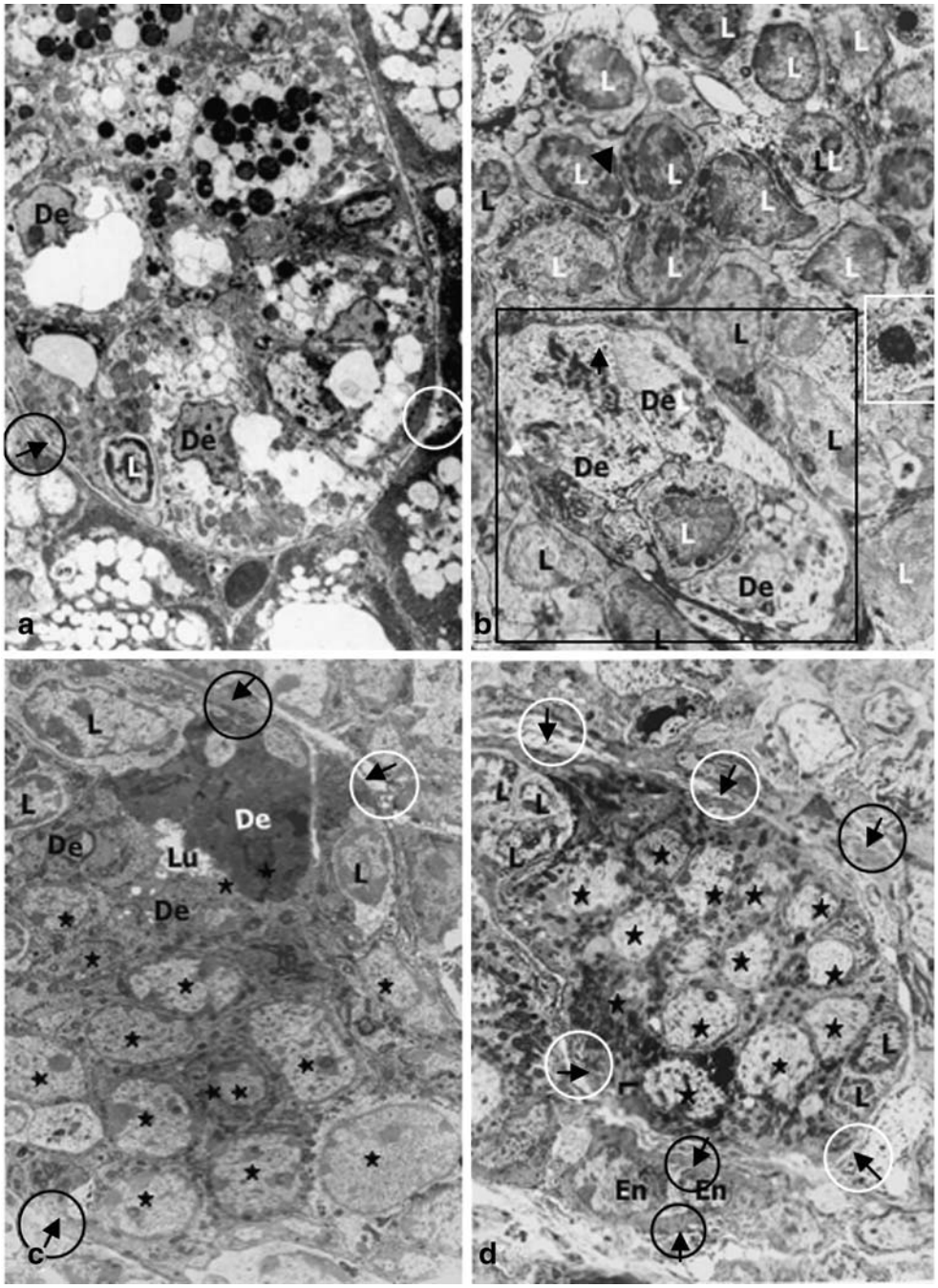

Fig. 8 **a** shows intraepithelial invasion of one lymphocyte (*L*) with degenerated striated ductal epithelial cells (*De*), and thick (an *arrow of a black circle*) and lytic (a *white circle*) basement membranes are visible. A *rectangle* of **b** shows one lymphocyte (*L*) infiltrated into epithelial layer and degenerated duct epithelial cells (*De*) with many lymphocytes (*L*) around duct. **c** shows degenerated ductal epithelial cells (*white De*) and relatively normal ductal epithelium (*black De*) of intercalated ducts, and proliferating epithelial cells (*star marks*) with lymphocytes infiltrated into epithelial layer (*L*) are seen. In addition, *arrows in black circle* indicate myofilaments, and *an arrow in white circle* indicates lytic basement membranes. In **d**, proliferation of duct epithelium (*star marks*) without degeneration of epithelium and intraepithelial infiltration of lymphocytes (*L*) are seen. *Arrows in white circles* indicate lytic basement membranes, and *an arrow in a black circle* indicate destructed myoepithelium. Furthermore, swelled capillary endothelium (*En*) with thick basement membranes (*arrows in black circles*) are seen. **a**–**d** 36 weeks of age. **a** ×1,000 and **b**–**d** ×1,500 (original magnification)

adjacent to inflammatory foci. It seems likely, since we have reported previously a leak of macromolecules from damaged vessels in the dermis in B/WF$_1$ [13]. The activation of myoepithelial cells in acinar areas apart from interlobular interstitial tissues [36] may also occur by increased permeability of capillaries other than the destruction of them. It seems likely, since thick basement membranes around capillaries are observed. This will lead to dysfunction of capillaries. Further studies are needed to clarify this point including vascular changes (e.g., hyaline or fibrinoid degeneration and lymphocytic perivasculitis in arterioles).

The present study demonstrated the binding of IgG2a to basement membranes of ducts, acini, and capillaries. IgG2a-type autoantibodies, which is a nephritogenic IgG subclass composing immune complexes deposited in glomeruli and class switched by the presence of helper T cytokines (e.g., interferon-γ [11, 14]), may be derived from the blood stream and also produced locally by infiltrated plasma cells. These autoantibodies may play a role in the destruction of basement membranes, since it has been reported that autoantibodies reacting in salivary glands, and IgG and C3 were detected in the basement membranes [34]. However, at present, we cannot conclude their roles in the

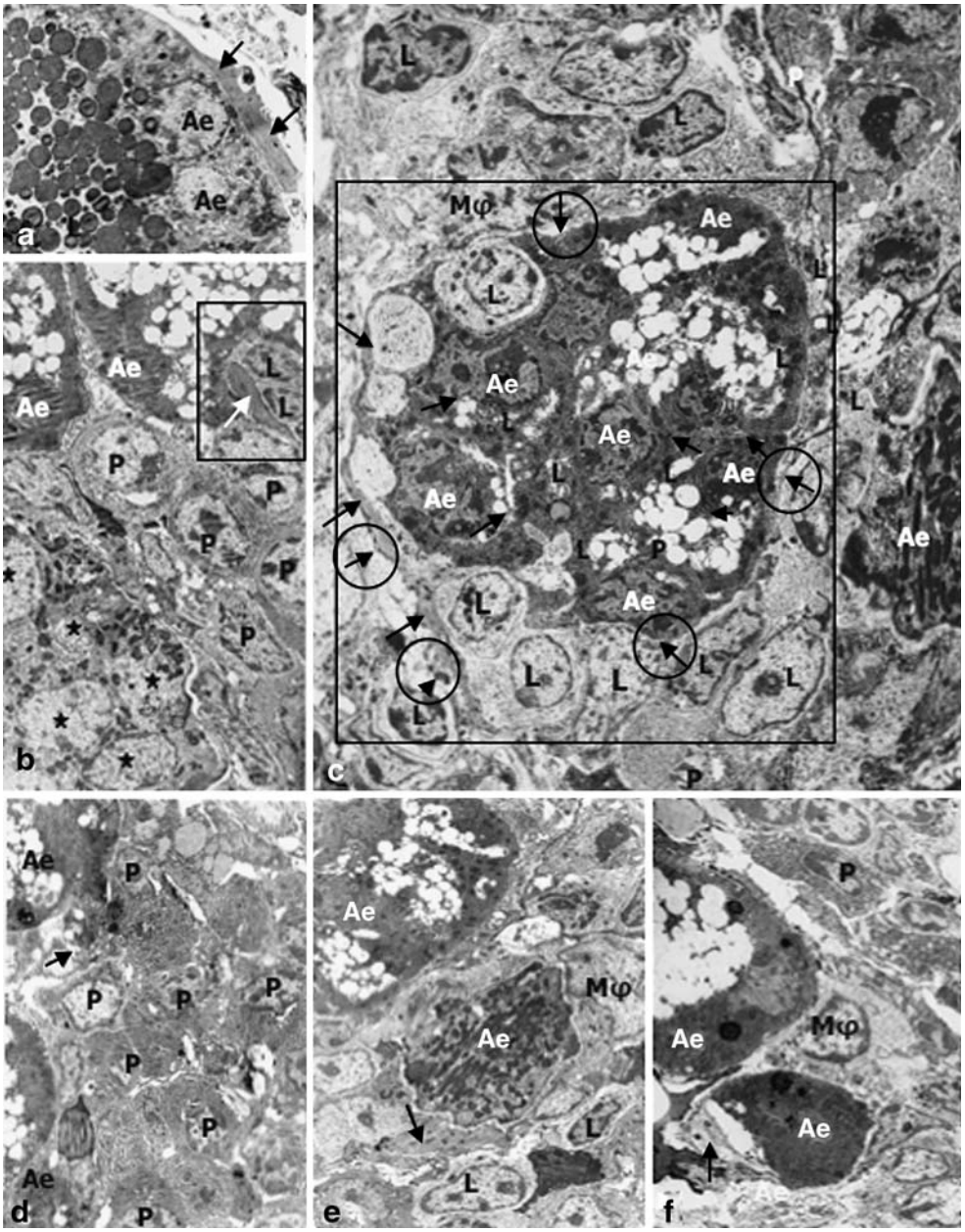

Fig. 9 *Arrows* of **a** indicate longitudinal myofilaments around acinar epithelium (*Ae*). Attachment of two lymphocytes (*L*) to myoepithelial cell (a *white arrow in rectangle*) and infiltration of plasma cells between acini (*Ae*) and proliferating intercalated ductal epithelium (*star marks*) are visible in **b**. **c** shows infiltration of lymphocytes (*L*) into acinar epithelium (*rectangle*) and dark atrophic acinar epithelium (*Ae*) with degeneration. *Arrows in circles* indicate basement membranes, and *arrows* indicate myofilaments, and infiltration of lymphocytes (*L*) and plasma cells (*P*) with some macrophages (*Mφ*) having many phagozomes and lysosomes around atrophic acini is seen. **d**–**f** shows severely degenerated acinar epithelium (*Ae*) with infiltration of plasma cells (*P*), lymphocytes (*L*), and some macrophages (*Mφ*). In **d**, there is infiltration of many plasma cells, and *arrows* in **d**, **e**, and **f** indicate myofilaments. **a** 8 weeks of age, **b**–**f** 36 weeks of age. **a** ×700, **b**, **c** ×1,500, and **d**–**e** ×1,000 (original magnification)

destruction of epithelium, since destructive changes of those cells were observed mainly at the sites of lymphoid cell infiltration.

The present study demonstrated hyperplasia of the epithelium of excretory, striated, and intercalated ducts. This suggests that basal cells in those ducts may be intact, since they are reserve cells for physiological regeneration of luminal columnar cells and for a pluridirectional differentiation into several types of reactive epithelial metaplasia [17]. However, intercalated ducts, which lack basal cells, also showed reactive epithelial hyperplasia. It is possible, since Ihrler et al. have reported that mature intercalated ducts may have a capacity to proliferate [17]. In addition, hyperplastic duct epithelium accompanies intraepithelial infiltration of lymphocytes. This suggests that intraepithelial infiltration of lymphocytes may contribute not only the destruction of epithelial cells but also the regeneration of duct epithelium. Further study is needed to clarify this point.

In the present study, degenerative and necrotic changes rather than apoptosis of duct and acinar epithelium and myoepothelial cells were mainly observed from the age of 18 to 36 weeks. Then, apoptotic changes of those cells increased at the age of 44 weeks. It has been reported that apoptosis associated with Fas expression play a role in developing of sialoadenitis in human SS and animal models [18, 35, 39]. Contradictorily, some study has showed that Fas-induced apoptosis of epithelium was a rare event in human patients

with pSS or sSS [33]. In addition, small numbers of apotoses were seen in acinar and intercalated duct cells in chronic sialoadenitis in humans [17]. Alternatively, the Fas antigen was strongly expressed on duct epithelial cells from patients with severe sialoadenitis but not from patients with mild sialoadenitis [22]. At present, the reasons for these controversial reports are unknown. On the other hand, it has been suggested that the expression of FAS and FASL did not increase the incidence of apoptosis [33], and they have suggested that the expression of CD40, CD154, Bax, and Bcl-2 in the salivary gland may contribute to inhibit apoptosis. If that is the case, the balance (increased or decreased expression of those proteins) may be determined to induce apoptosis or necrosis.

In conclusion, the present study stresses the significance of myoepithelial cells as one of the target cells during the development of sialoadenitis in sSS.

Conflict of interest statement We declare that we have no conflict of interest.

References

1. Amft N, Curnow SJ, Scheel-Toellner D, Devadas A, Oates J, Crocker J, Hamburger J, Ainsworth J, Mathews J, Salmon M, Bowman Sj, Buckley CD (2001) Ectopic expression of the B cell-attracting chemokine BCA-1 (CXCL13) on endothelial cells and within lymphoid follicles contributes to the establishment of germinal center-like structure in Sjögren's syndrome. Arthritis Rheum 44:2633–2641
2. Atkinson JC, Royce LS, Wellner R, Pillemer SR, Bermudez D, Fox PC (1995) Anti-salivary antibodies in primary Sjögren's syndrome. J Oral Pathol Med 24:206–212
3. Carlsöö B, Ostberg Y (1978) Ultrastructural observations on the parotitis autoimmunica in the NZB/NZW hybrid mice. Acta Otalaryngol 85:298–306
4. Chandrasekar B, McGuff S, Aufdermorte TB, Troyer DA, Talal N, Dernande G (1995) Effects of calorie restriction on transforming growth factor β1 and proinflammatory cytokines in murine Sjögren's syndrome. Clin Immunol Immunopathol 76:291–296
5. Croker JA, Kimberly RP (2005) Challenge and candidates in human disease. Trends Immunol 26:580–586
6. Defilippi P, Silengo L, Tarone G (1992) α6/β1 integrin (laminin receptor) is down-regulated by tumor necrosis factor α and interleukin-1b in human endothelial cells. J Biol Chem 267: 18303–18307
7. Delaleu N, Jonsson R, Köller MM (2005) Sjögren's syndrome. Eur J Oral Sci 113:101–113
8. Gal I, Lakos G, Zeher M (2000) Comparison of the anti-Ro/SSA autoantibody profile between patients with primary and secondary Sjögren's syndrome. Autoimmunity 32:89–92
9. Greenspan JS, Daniels TE, Talal N, Sylvester RA (1974) The histology of Sjögren's syndrome in labial salivary gland biopsies. Oral Surg 37:217–229
10. Haneji N, Nakamura T, Takio K, Yanagi K, Higashiyama H, Saito I, Noji S, Sugino H, Hayashi Y (1997) Identification of alpha-fodrin as a candidate autoantigen in primary Sjogren's syndrome. Science 276:604–607
11. Hasegawa K, Hayashi T (2003) Synthetic CpG olygodeoxynucleotides accelerate the development of lupus nephritis during preactive phase in NZB/NZWF_1 mice. Lupus 12:838–845
12. Hayashi Y, Hamano H, Haneji N, Ishimaru N, Yanagi K (1995) Biased T cell receptor V beta gene usage during specific stages of the development of autoimmune sialadenitis in the MRL/lpr mouse model of Sjögren's syndrome. Arthirtis Rheum 38:1077–1084
13. Hayashi T, Hasegawa K, Ichinohe N (2005) ICAM-1 expression on endothelium and systemic cytokine production in cutaneous neutrophilic lekocytoclastic vasculitis in NZB/NZWF_1 mice. Histol Histopathol 20:45–52
14. Hayashi T, Hasegawa K, Sasaki Y, Mori T, Adachi C, Maeda K (2007) Systemic administration of interleukin-4 expressing DNA delays the development of glomerulonephritis and prolongs survivals in lupus-prone female NZB/NZWF_1 mice. Nephrol Dial Transplant 22:3131–3138
15. Hayashi T, Shirachi T, Hasegawa K (2001) Relationship between sialoadenitis and periductal laminin expression in the submandibular salivary gland of NZB/NZW F_1 Mice. J Comp Pathol 125: 110–116
16. Hishikawa T, Ogasawara H, Kaneko H, Shirasawa T, Matsuura Y, Sekigawa I, Takasaki Y, Hashimoto H, Hirose S, Handa S, Nagasawa R, Maruyama N (1997) Detection of antibodies to a recombinant gag protein derived from human endogenous retrovirus clone 4-1 in autoimmune disease. Viral Immunol 10: 137–147
17. Ihrler S, Blasenbreu-Vogt S, Sendelfofert A, Rössle M, Harrison JD, Löhrs U (2004) Regeneration in chronic sialadenitis: an analysis of proliferation and apoptosis based on double immunohistochemical labeling. Virchows Arch 444:356–361
18. Ishimaru N, Yoneda T, Saegusa T, Yanagi K, Haneji N, Moriyama K, Saito I, Hayashi Y (2000) Severe destruction of autoimmune lesions with aging in murine Sjögren's syndrome through Fas-mediated apoptosis. Am J Pathol 156:1557–64
19. Izui S, Elder JH, McConahey PJ, Dixon FJ (1981) Identification of retroviral gp70 and anti-gp70 antibodies involved in circulating immune complexes in NZBNZW mice. J Exp Med 153:1151–1160
20. Jacob L, Lety M-A, Monterio RC, Jacob F, Bach J-F, Louvard D (1987) Altered cell-surface proteins, crossreactive with DNA, on spleen cells of autoimmune lupic mice. Proc Natl Acad Sci USA 84:1361–1363
21. Kapsogeorgou EK, Dimitriou ID, Abu-Helu RF, Moutsopoulos HM, Manoussakis MN (2001) Activation of epithelial and myoepithelial cells in the salivary glands of patients with Sjögren's syndrome: high expression of intercellular adhesion molecule-(ICAM-1) in biopsy specimens and cultured cells. Clin Exp Immunol 124:126–133
22. Matsumura R, Umemiya K, Kagami M, Tomioka H, Tanabe E, Sugiyama T, Sueishi M, Nakajima A, Azuma M, Okumuea K, Sumida T (1998) Glandular and extraglandular expression of the Fas–Fas ligand and apoptosis in patients with Sjögren's syndrome. Clin Exp Rheumatol 16:561–568
23. McArhtur CP, Fix NW, Kragel P (1993) Monoclonal antibody detection of laminin in minor salivary glands of patients with Sjögren's syndrome. J Autoimmun 6:649–661
24. Mitsias DI, Kapsogeorgou EK, Moutsopoulos HM (2006) Sjögren's syndrome: why autoimmune epithelitis? Oral Dis 12:523–532
25. Miyake S, Sakurai T, Okumura k, Yagita H (1994) Identification of collagen and laminin receptor integrins on murine T lymphocytes. Eur J Immunol 24:2000–2005
26. Mok CC, Lau CS (2003) Pathogenesis of systemic lupus erythematosus. J Clin Pathol 56:481–90
27. Molina C, Alliende C, Aguilera S, Kwon YJ, Leyton L, Martinez B, Leyton C, Perez P, Gonzalez MJ (2006) Basal lamina disorganization of the acini and ducts of labial salivary gland from patients

with Sjögren's syndrome: association with mononuclear cell infiltration. Ann Rheum Dis 65:178–183
28. Nagler RM (2004) Salivary glands and the aging process: mechanistic aspects, health-status and medicinal-efficacy monitoring. Biogerontology 5:223–233
29. Nakamura H, Kawakami A, Eguchi K (2006) Mechanisms of autoantibody production and the relationship between autoantibodies and the clinical manifestations in Sjögren's syndrome. Transl Res 148:281–288
30. Nakagawa K, Leonard CH (1996) The potential roles of endogenous retroviruses in autoimmunity. Immunol Rev 152:193–236
31. Nakanuma Y, Tsuneyama K, Harada K (2001) Pathology and pathogenesis of intrahepatic bile duct loss. J Hepatobiliary Pancreat Surg 8:303–315
32. Nossent JC, Swaak AJ (1998) Systemic lupus erythematosus VII: frequency and impact of secondary Sjögren's syndrome. Lupus 7:231–234
33. Ohlsson M, Skatstein K, Bolstad AI, Johannessen AC, Jonsson R (2001) Fas-induced apoptosis is a rare event in Sjögren's syndrome. Lab Invest 81:95–105
34. Ohno K, Hattori T, Kagami H, Ueda M (2007) Effects of preceding sialoadenitis on the development of autoimmunity against salivary gland. Oral Dis 13:158–162
35. Ping L, Ogawa N, Sugai S (2005) Novel role of CD40 in Fas-dependent apoptosis of cultured salivary epithelial cells from patients with Sjögren's syndrome. Arthritis Rheum 52:573–581
36. Raubenheimer EJ (1987) The myoepithelial cell: embryology, function, and proliferative aspects. Crit Rev Clin Lab Sci 25:161–193
37. Reichlin M (1998) Antibodies to Ro and La. Ann Med Intern 149:34–41
38. Salmonson S, Larsson P, Tengner P, Mellquist E, Hjelmstrom P, Wahren-Herlenius M (2002) Expression of the B cell-attracting chemokine CXCL13 in the target organ and autoantibody production in ectopic lymphoid tissue in the chronic inflammatory disease Sjögren's syndrome. Scand J Immunol 55:336–342
39. Shibata Y, Hishikawa Y, Izumi S, Fujita S, Yamaguchi A, Koji T (2002) Involvement of Fas/Fas ligand in the induction of apoptosis in chronic sialoadenitis of minor salivary glands including Sjögren's syndrome. Hum Cell 15:52–60
40. Shimizu Y, Van Seventer GA, Horgan KJ, Shaw S (1990) Costimulation of proliferative response of VLA-4 and VLA-5 with fibronectin or VLA-6 with laminin. J Immunol 21:35–42
41. Van Blokland SCA, Versnel MA (2002) Pathogenesis of Sjögren's syndrome: characteristics of different mouse models for autoimmune exocrinopathy. Clin Immunol 103:111–124
42. Witte T, Matthias T, Arnett FC, Peter HH, Hartung K, Sachse C, Wigand R, Braner A, Kaldon JR, Lakomok HJ, Schmidt RE (2000) IgA and IgG autoantibodies against alpha-fodrin as markers for Sjögren's syndrome. J Rheumatol 27:2617–2620
43. Yasoshima M, Tsuneyama K, Harada K, Sasaki M, Gershwin ME, Nakanuma Y (2000) Immunohistochemical analysis of cell–matrix adhesion molecules and their ligands in the portal tracts of primary biliary cirrosis. J Pathol 190:93–99
44. Zelles T, Boros I, Varga G (1999) Membrane stretch and salivary glands—facts and theories. Arch Oral Biol 44:S67–S571

Virchows Arch (2008) 453:189–196
DOI 10.1007/s00428-008-0610-0

ORIGINAL ARTICLE

Intermitochondrial cement (nuage) in a spermatocytic seminoma: comparison with classical seminoma and normal testis

Manrico Morroni · Angela Maria Cangiotti · Daniela Marzioni · Antonella D'Angelo · Rosaria Gesuita · Michele De Nictolis

Received: 29 January 2008 / Revised: 19 March 2008 / Accepted: 21 March 2008 / Published online: 19 April 2008

Abstract The nuage, an ultrastructural marker of normal human germ cells (spermatogonia type A and primary spermatocytes), may be found associated with mitochondria (intermitochondrial cement) and/or free in the cytoplasm. Eight specimens from germ cell-related tumours were reviewed to assess whether the nuage could have diagnostic significance in testicular neoplasms. The nuage of neoplastic cells from seven classical seminomas and one spermatocytic seminoma was compared with that from two normal testes. The ultrastructural study demonstrated that only spermatocytic seminoma cells contained both types of nuage and that significantly fewer spermatocytic seminoma cells (28%) contained intermitochondrial cement compared with control spermatogonia type A (81.1%) and primary spermatocytes (47.6%). The data indicate that (1) the detection of the nuage confirms that the phenotype of spermatocytic seminoma is more differentiated than that of classical seminoma; (2) the intermitochondrial cement is an additional example of how a distinctive organelle of a normal cell is preserved in its neoplastic counterpart and (3) if the intermitochondrial cement were found in other cases of spermatocytic seminoma, this organelle of the normal germ cell lineage could be considered as a new ultrastructural marker of the neoplasm.

Keywords Nuage · Spermatocytic seminoma · Classical seminoma · Normal germ cells · Transmission electron microscopy

M. Morroni (✉) · D. Marzioni
Institute of Normal Human Morphology, School of Medicine,
Polytechnic University of Marche,
Ancona, Italy
e-mail: m.morroni@univpm.it

M. Morroni · A. M. Cangiotti
Electron Microscopy Unit, University Hospital,
Ancona, Italy

A. D'Angelo
Department of Pathological Anatomy and Histopathology,
General Hospital,
Ascoli Piceno, Italy

R. Gesuita
Center of Epidemiology and Biostatistics, School of Medicine,
Polytechnic University of Marche,
Ancona, Italy

M. De Nictolis
Department of Pathological Anatomy and Histopathology,
School of Medicine, Polytechnic University of Marche,
Ancona, Italy

Introduction

In a wide variety of animals, germ cells exhibit particular structures called nuage [15], the French word for cloud. The nuage is a discrete, dense fibrous cytoplasmic organelle lacking a surrounding membrane. It is often associated with the mitochondrial cluster (intermitochondrial cement/material/bar or nuage–mitochondrial complex) or is closely adjacent to the germ cell nuclear envelope. It has been interpreted as a cytoplasmic marker of the germplasm or as the earliest stage of differentiation of the mammalian germ cell lineage [13, 16, 28, 58, 61] and could be related to the germ granules described in many lower animals [52].

Despite its wide diffusion in the animal kingdom, the molecular properties and function of the mammalian nuage remain largely unknown. Ultrastructural cytochemical studies have described basic proteins and ribonucleoproteins in

nuage material from human spermatogonia and spermatocytes [40]. Vasa protein, a class of proteins believed to act as RNA chaperones [55], has been detected in the nuage of animals ranging from nematodes to vertebrates [43]. More recently, tudor-related proteins [5, 6, 25] and a moonlighting protein, phospholipid hydroperoxide glutathione peroxidase [22], have been described in the germline nuage.

The human adult testis is affected by three epidemiologically, clinically and histologically diverse groups of testicular germ cell tumours: teratomas and yolk sac tumours of infants and children, seminomas and non-seminomatous germ cell tumours of postpubertal patients and spermatocytic seminoma. We examined a spermatocytic seminoma where nuage-like material was both free in the cytoplasm and in close association with the mitochondrial cluster of neoplastic cells, as seen in normal human germ cells (spermatogonia type A and primary spermatocytes) [23]: this ultrastructural finding has not been previously described in testicular germ cell tumours.

In this study, the ultrastructural features of seven classical seminomas and a spermatocytic seminoma were reviewed to assess whether nuage-like material may have diagnostic value in these germ cell-derived tumours.

Materials and methods

Patients

We reviewed material from eight germ cell-derived tumours, seven classical seminomas (patient age 31–43 years; mean 39 years) and one spermatocytic seminoma (63-year-old man). One of the seven classical seminoma specimens was a metastasis to the colon. Control tissue came from the otherwise normal testes of a 26-year-old man with bilateral varicocele. All biopsies were performed with fully informed patient consent as part of routine histological investigations.

Light and transmission electron microscopy

Specimens were processed for light and electron microscopy. For light microscopy, the specimens were fixed in 10% buffered formalin, processed according to standard protocols and embedded in paraffin. Sections 4 μm in thickness were stained with haematoxylin and eosin (H and E).

For electron microscopy, the material was fixed in 2% glutaraldeyde/2% paraformaldehyde in 0.1 M phosphate buffer for 3 h at 4°C, postfixed in 1% osmium tetroxide in the same buffer solution, dehydrated in graded alcohols and embedded in an Epon–Araldite mixture. Semithin sections (2 μm) were obtained with a MICROM HM 355 microtome (Zeiss, Oberkochen, Germany) and stained with toluidine blue. Thin sections were obtained with an MTX ultramicrotome (RMC, Tucson, AZ, USA), stained with lead citrate and examined with a CM10 transmission electron microscope (Philips, Eindhoven, The Netherlands).

Immunohistochemistry

For the immunohistochemical study, we used the avidin–biotin complex method with antibodies directed against the following antigens: cytokeratin CAM 5.2 (prediluted; Becton Dickinson, Milan, Italy), vimentin (1:1,000), CD117 (1:50), α-inhibin (1:25), CD30 (1:25), EMA (1:100), leucocyte common antigen (LCA; 1:20), α-fetoprotein (prediluted), human chorionic gonadotropin (hCG; prediluted), carcinoembryonic antigen (1:50), S-100 protein (1:500), calretinin (1:200), actin (1:400), desmin (1:75), neuron-specific enolase (1:1,000) and placental-like alkaline phosphatase (PLAP; 1:250); all from Dako Cytomation A/S, Glostrup, Denmark.

Statistical analysis

The cell was considered as the unit of observation. The proportions of cells containing intermitochondrial cement and 95% confidence intervals (95%CI) were estimated in the eight specimens and in germ cells (spermatogonia type A and primary spermatocytes) from the control testes, whose ultrastructural appearance was normal [23] despite the varicocele. The percentage of spermatocytic seminoma and control germ cells containing intermitochondrial cement was compared using the Z test; differences were estimated by means of CI. A level of 5% was considered significant.

Results

Classical seminomas

Histologically, the seven classical seminoma specimens contained uniformly round or polyhedral cells with the nucleus in central position, one or two prominent nucleoli and clear cytoplasm. Neoplastic cells had a distinct cell membrane and were arranged into lobules or cords separated by thin fibrovascular septa containing infiltrates of small lymphocytes and plasma cells. Mitotic figures were rare. The immunohistochemical pattern was characteristic of classical seminoma: the PLAP reaction was positive, whereas CD30, cytokeratin CAM 5.2, hCG and carcinoembryonic antigen were all negative.

All specimens had fairly typical ultrastructural features [10, 11, 17, 24, 35, 50]. In brief, they displayed round or oval nuclei containing finely dispersed chromatin, prominent and multiple nucleoli with open nucleolonema and

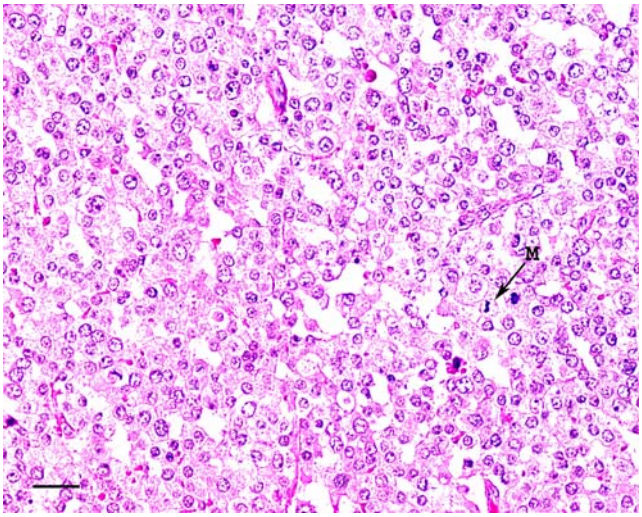

Fig. 1 Histological appearance of spermatocytic seminoma. *M* mitosis. Scale bar=50 μm

scarce cytoplasmic organelles that contained large amounts of glycogen. Free ribosomes, polyribosomes and lipid droplets were always evident. Annulate lamellae were found in six of the seven cases. Small primitive junctions were often observed between neoplastic cells. Neither free nuage nor intermitochondrial cement was detected in any of the specimens.

Spermatocytic seminoma

The tumour consisted of sheets of round cells that were grouped into clusters due to extensive oedema. Cells varied in size and were composed of three cell types: small, intermediate and large (Fig. 1). Intermediate cells predominated. In all three cell populations, the nuclei were spherical. In the smaller cells, chromatin was dense and amorphous, whilst in intermediate cells, it had a filamentous appearance. Sometimes large cells had multiple nuclei and filamentous chromatin. Large nucleoli were common, particularly in larger cells. Mitotic figures were also abundant. Neoplastic cells were frequently detected in seminiferous tubules and were identical to those in the tumour.

On immunohistochemistry, tumour cells showed dot-like positivity for cytokeratin CAM 5.2 (Fig. 2) and were negative for PLAP, vimentin, CD117, α-inhibin, CD30,

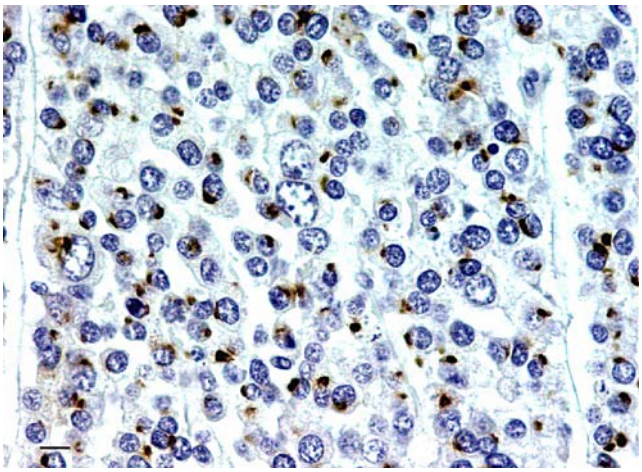

Fig. 2 Immunohistochemical expression of cytokeratin CAM 5.2 in spermatocytic seminoma. Neoplastic cells show dot-like staining. Scale bar=15 μm

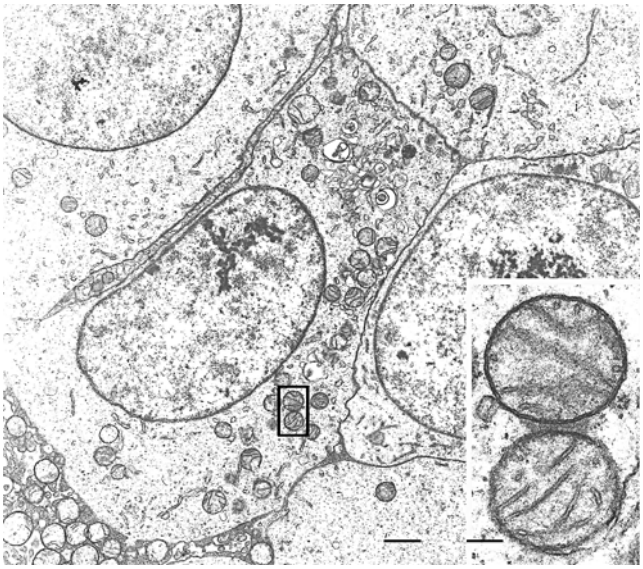

Fig. 3 Spermatocytic seminoma. Neoplastic cells show a simplified nuclear and cytoplasmic morphology. Note the characteristic prominent nucleolus with open nucleolonema. *Inset* enlargement of *boxed area* showing intermitochondrial cement between two mitochondria. Scale bar=1 μm; inset scale bar=0.15 μm

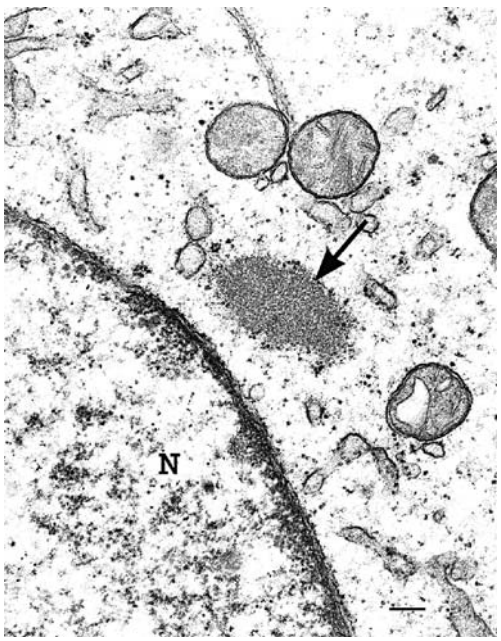

Fig. 4 Spermatocytic seminoma. Nuage-like material (*arrow*) free in the cytoplasm. *N* nucleus. Scale bar=0.18 μm

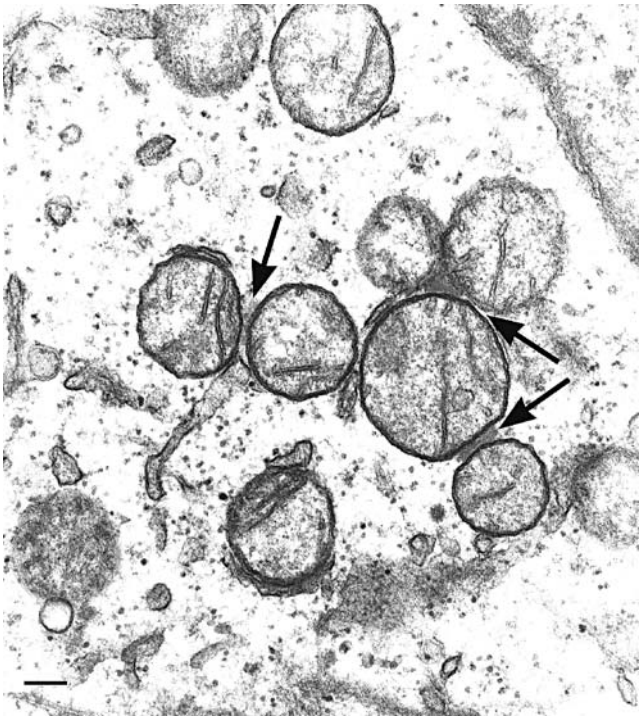

Fig. 5 Spermatocytic seminoma. Portion of the cytoplasm of a neoplastic cell showing three nuage–mitochondrial complexes (*arrows*) in a mitochondrial cluster. Scale bar=0.18 μm

EMA, LCA, hCG, α-fetoprotein, carcinoembryonic antigen, S-100 protein, calretinin, actin, desmin and neuron-specific enolase.

At the ultrastructural level, neoplastic cells (Fig. 3) had round or oval nuclei. Chromatin was homogeneously distributed. Nuclei contained a large nucleolus with open nucleolonema; some cells had multiple nucleoli. The amount of cytoplasm varied from cell to cell. Rough endoplasmic reticulum was scarce and characterised by short cisternae. Numerous free ribosomes were uniformly distributed throughout the cytoplasm. A developed Golgi apparatus was detected in rare neoplastic elements and was arranged in the vicinity of the nucleus. Mitochondria were numerous, round and dispersed in the cytoplasm or arranged in clusters. Glycogen and lipid droplets were scarce or absent. Some cells contained annulate lamellae. In some elements, cytoplasmic organelles were clustered on one side of the cytoplasm. Intermediate junctions were observed between cells. Rarely, pairs of cells containing nuclei in the resting phase displayed intercellular communications, suggesting incomplete cytoplasmic division.

A peculiar ultrastructural feature in the cytoplasm of the neoplastic spermatocytic seminoma cells was a dense fibrous material consistent with nuage that was found in two forms: (1) free in the cytoplasm and (2) between mitochondria (nuage–mitochondrial complexes). The former (Fig. 4), measuring 0.55 to 1.25 μm in diameter, was rarer (approximately 5% of cells). Nuage–mitochondrial complexes lay between two (Fig. 3, inset) or a maximum of three mitochondria (Fig. 5) and were more frequent (approximately 28% of cells, 95%CI=20.4–38.9; Table 1). With the exception of rare cells containing two or three complexes (Fig. 5), the majority contained a single complex per cell. These complexes were identical to those observed in normal human spermatogenetic cells.

Control testes

In spermatogonia type A (Fig. 6), mitochondria usually formed clusters (one to six per cell) that were generally constituted of two to three mitochondria (range=2–8). Nuage-like material was seen between neighbouring mitochondria in 81.1% (95%CI=64.8–92.0) of cells (Table 1). The nuage was always found between two mitochondria (Fig. 6, inset); cells contained on average one or two nuage–mitochondrial complexes, up to maximum of five.

Primary spermatocytes (Fig. 7), particularly from the zygotene stage onwards, also contained mitochondrial clusters; however, they were less numerous than in spermatogonia type A and were usually made up of two to three mitochondria. Altogether, 47.6% (95%CI=32.0–63.6; Table 1) of these cells contained nuage–mitochondrial complexes (Fig. 7, inset). As in spermatogonia type A, nuage-like material was found between two or three mitochondria and cells contained on average one or two nuage–mitochondrial complexes.

Table 1 Proportion of cells containing intermitochondrial cement and 95%CI in spermatocytic seminoma, spermatogonia type A and primary spermatocytes

	Cells				
	Total	Intermitochondrial cement	Percentage	95%CI	*p* values[a]
Spermatocytic seminoma	100	28	28.0	20.4–38.9	
Spermatogonia type A	37	30	81.1	64.8–92.0	<0.001
Primary spermatocytes	42	20	47.6	32.0–63.6	0.012

[a] Spermatocytic seminomatous cells vs spermatogonia type A vs primary spermatocytes

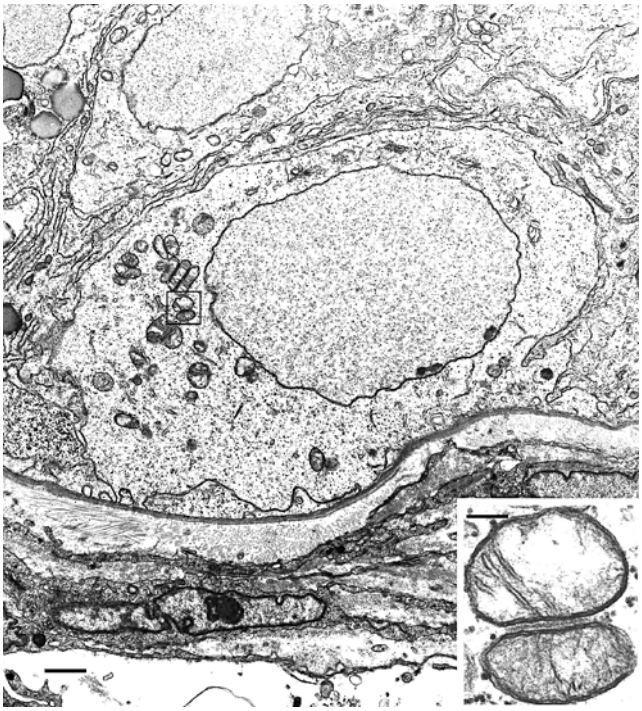

Fig. 6 Control testis. A spermatogonium type A containing some mitochondrial clusters. *Inset* enlargement of *boxed area* showing intermitochondrial cement between two mitochondria. *bm* basal membrane. Scale bar=1.1 μm; inset scale bar=0.16 μm

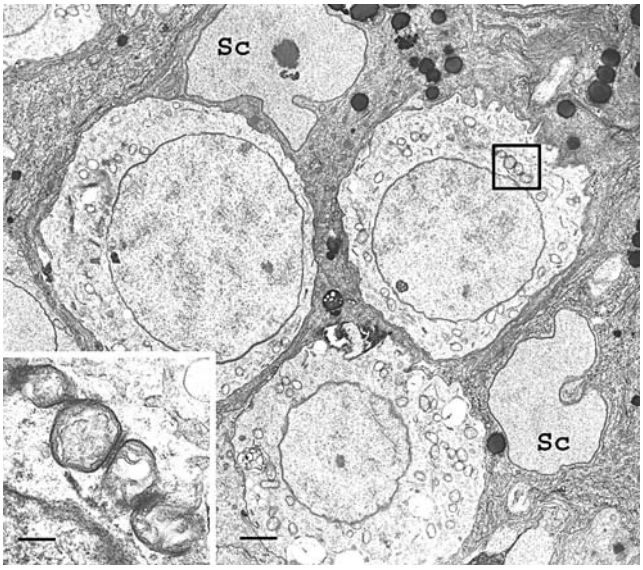

Fig. 7 Control testis. One of the three primary spermatocytes displays a nuage–mitochondrial complex (*boxed area*) enlarged in the *inset*. *Sc* Sertoli cells. Scale bar=1.9 μm; inset scale bar=0.3 μm

Statistical results

Free nuage was detected in <5% of spermatogonia type A and primary spermatocytes. Significantly fewer spermatocytic seminoma cells contained intermitochondrial cement compared with normal spermatogonia type A ($p<0.001$) and primary spermatocytes ($p=0.012$; Table 1). The percentage difference between spermatocytic seminomatous cells and primary spermatocytes containing intermitochondrial cement (19.6%, 95%CI=2.1–37.1) was significantly lower than the difference between spermatocytic seminomatous cells and spermatogonia type A (53.1%, 95%CI=37.7–68.5; Table 2).

Discussion

This is the first ultrastructural study describing intermitochondrial cement in spermatocytic seminoma. Such a feature has never been detected in classical seminoma.

The nuage, also called nucleolus-like body due to its morphological resemblance to the nucleolus [21], mainly differs from it in location, as the latter is found in the nucleus, whilst the nuage occurs in the cytoplasm matrix or is associated with mitochondria [21]. There is substantial evidence that the nuage contains RNA [40, 48] and that nucleolar material is sometimes extruded from the nucleus into the cytoplasm [21]. Nuage constituents might also arise from mitochondria [44].

In humans, nuage has been detected in normal and pathological conditions. In normal conditions, it has been described in placental cytotrophoblasts [27, 32] and in both male (spermatogonia type A and primary spermatocytes) and female germ cells [23, 36, 39, 40]. In germ cells, it has been described not only free in the cytoplasm but also in close association with mitochondria, forming the so-called intermitochondrial cement. According to some authors, the nuage of spermatogonia and spermatocytes develops into the spermatid chromatoid body, whose function seems to be to form the spermatozoon tail annulus [18, 23, 40, 41].

Nuage-like material has also been demonstrated in a variety of tumour cells. Albrechtsen et al. [2] detected membraneless granular structures, which they denominated nuages, in a carcinoma in situ of the testis. Carlson and Sibley [4] identified nuage-like structures in unspecified (as to type) seminomas. Erlandson [17] described cytoplasmic nuage-like structures in cells from a presumed atypical retroperitoneal seminoma. In a seminoma, Ghadially [21] noted features suggesting nucleolar material escaping from the nucleolus, but found no nuage in the cell cytoplasm; he

Table 2 Percentages of cells containing intermitochondrial cement and 95%CI: difference between spermatocytic seminoma and spermatogonia type A and between spermatocytic seminoma and primary spermatocytes

Spermatocytic seminoma minus	*D*	95%CI
Spermatogonia type A	53.1	37.7–68.5
Primary spermatocytes	19.6	2.1–37.1

concluded that the escaped material dispersed rapidly once outside the nucleus. Nuage-like material has also been found in other non-germinal cancers such as hepatocellular carcinoma [49], metastatic carcinoid tumour of the colon [12] and rhabdomyosarcoma [21]. It has also been described in a non-neoplastic condition, i.e. striated muscle cells of reducing body myopathy [3, 26, 38].

In all such neoplastic and non-neoplastic diseases, the nuage-like material was always free in the cytoplasm and was never associated with mitochondria as in normal germ cells (spermatogonia type A and primary spermatocytes) [23, 36, 39, 40] or in the spermatocytic seminoma described in this paper. In line with previous reports [10, 11, 17, 24, 35, 50], none of our seven seminoma specimens contained intermitochondrial cement or free nuage. Similarly, intermitochondrial cement has not been encountered in the neoplastic counterpart of primitive germ cells of the ovary (dysgerminoma) [19].

Few spermatocytic seminomas have been studied at the ultrastructural level [1, 34, 46, 54, 60]. The general ultrastructural features of the neoplastic cells of the specimen described in this paper confirm previous reports, except for the presence in the cytoplasm of both intermitochondrial cement and free nuage. Significantly fewer neoplastic cells contained intermitochondrial cement compared with normal germ cells (spermatogonia type A and primary spermatocytes). Nevertheless, it is interesting to note that the percentage difference between spermatocytic seminomatous cells and primary spermatocytes containing intermitochondrial cement was significantly smaller than the difference between spermatocytic seminomatous cells and spermatogonia type A. Intermitochondrial cement has never been described in spermatocytic seminoma; although in the paper by Rosai et al. (Fig. 8, upper panel [46]), two mitochondria appear to be connected by material similar to nuage, and in the report by Talerman et al. [54], the same feature seems to be depicted in some mitochondrial clusters (Fig. 4). In both cases, however, magnification is too low for a positive identification.

Spermatocytic seminoma is a specific and unique germ cell neoplasm. It is the only testicular germ cell tumour to lack a homologous counterpart in the ovary and to be found at none of the extragonadal locations where germ cell tumours are known to arise. It is also the sole germ cell tumour that always occurs in pure form and is not admixed with other neoplastic germ cell elements, including seminoma. Spermatocytic seminoma may be confused with classical seminoma; the distinction is important from the clinical standpoint because spermatocytic seminoma virtually never metastasises [20, 29, 56] and requires no treatment besides orchiectomy [7, 14, 33, 45, 47, 53, 57]. Recent immunohistochemical and molecular studies [42, 51, 59] have demonstrated a different origin for seminoma/dysgerminoma and spermatocytic seminoma. Seminoma/dysgerminoma originates from an embryonic germ cell, whilst the cell of origin of spermatocytic seminoma is at least capable of maturing to the stage of spermatogonia-pachytene spermatocyte. Genome-wide analyses of genomic changes and expression profiling confirm the origin of spermatocytic seminoma from primary spermatocytes that have at least initiated prophase meiosis [30, 31]. In this respect, it is interesting to note that the percentage of spermatocytic seminoma cells containing intermitochondrial cement was nearer that of primary spermatocytes than that of spermatogonia type A.

We interpreted the intermitochondrial cement observed in our specimen as reflecting a more differentiated phenotype than seminoma.

In conclusion, review of our cases of germ cell-derived tumours demonstrated that (1) detection of intermitochondrial cement in spermatocytic seminoma confirms a more differentiated phenotype compared with seminoma; (2) intermitochondrial cement assumes a role of some importance in ultrastructural biology as a further example of how a distinctive organelle of normal human cells is preserved in their neoplastic counterparts [8 9, 37] and (3) finally, if intermitochondrial cement were found in other cases of spermatocytic seminoma, this organelle of the normal germ cell lineage could be considered as a new ultrastructural marker of the neoplasm.

Acknowledgements We are grateful to Drs. Mariella Marelli, Maria Cristina Zingaretti and Camilla Latini for their excellent technical assistance. We are also grateful to Prof. Giorgio Barbatelli for his help in selecting the control testes and Dr. Michele Bisceglia (Dept. Pathology, IRRCCS-CSS Hospital, San Giovanni Rotondo, Italy) for his critical reading and comments on the manuscript. The study was supported by a Polytechnic University of Marche grant (2007 FAR, formerly 60%) to M. M.

Conflict of interest statement The authors declare they have no conflict of interest.

References

1. Albores-Saavedra J, Huffman H, Alvarado-Cabrero I, Ayala AG (1996) Anaplastic variant of spermatocytic seminoma. Human Pathol 27:650–655
2. Albrechtsen R, Nielsen MH, Skakkebaeck NE, Wewer U (1982) Carcinoma in situ of the testis. Some ultrastructural characteristic of germ cells. Acta Pathol Microbiol Immunol Scand A 90:301–303
3. Brooke MH, Neville HE (1972) Reducing body myopathy. Neurology 22:829–840
4. Carlson G, Sibley RK (1988) Electron microscopy of testicular and paratesticular neoplasms. In: Russo J (ed) Tumor diagnosis by electron microscopy. vol. 2. Field and Wood, Philadelphia, pp 123–164
5. Chuma S, Hiyoshi M, Yamamoto A, Hosokawa M, Takamune K, Nakatsuji N (2003) Mouse tudor repeat-1 (MTR-1) is a novel

component of chromatoid bodies/nuages in male germ cells and forms a complex with snRNPs. Mech Dev 120:979–990
6. Chuma S, Hosokawa M, Kitamura K, Kasai S, Fujioka M, Hiyoshi M, Takamune K, Noce T, Nakatsuji N (2006) Tdrd1/Mtr-1, a tudor-related gene, is essential for male germ-cell differentiation and nuage/germinal granule formation in mice. Proc Natl Acad Sci U S A 103:15894–15899
7. Chung PWM, Bayley AJS, Sweet J, Jewett MAS, Tew-George B, Gospodarowicz MK, Warde PR (2004) Spermatocytic seminoma: a review. Eur Urol 45:495–498
8. Cinti S, Ferretti M, Amati S, Balercia G, Vecchi A, Osculati F (1983) Electron microscopy applied to fine-needle aspiration. A report of six cases from various sites. Tumori 69:423–435
9. Cinti S (1985) Ultrastructural pathology of solid tumors. Biomed Pharmacother 39:115–122
10. Dickersin GR (1987) The ultrastructure of selected gynaecologic neoplasms. Clin Lab Med 7:117–156
11. Dickersin GR (ed) (2000) Dysgerminoma (Seminoma). In: Diagnostic electron microscopy. A text/atlas. Springer, New York, pp 451–461
12. Dingemans KP (1983) Metastasizing tumor of the colon with cellular inclusions. Ultrastruct Pathol 4:265–268
13. Dvorák M, Tesarík J (1980) Ultrastructure of human ovarian follicles. In: Motta PM, Hafez ESE (eds) Biology of the ovary. Developments in obstetrics and gynecology. Martinus Nijhoff, The Hague, pp 121–137
14. Eble JN (1994) Spermatocytic seminoma. Human Pathol 25:1035–1042
15. Eddy EM (1975) Germ plasm and the differentiation of the germ cell line. Int Rev Cytol 43:229–280
16. Eddy EM (1996) The germ line and development. Dev Genet 19:287–289
17. Erlandson RA, Seminoma (1994) Diagnostic transmission electron microscopy of tumors. Raven, New York, pp 719–726
18. Fawcett DW, Eddy EM, Phillips DM (1970) Observations on the fine structure and relationships of the chromatoid body in mammalian spermatogenesis. Biol Reprod 2:129–153
19. Ferenczy A (1987) Electron microscopy of histologically difficult to diagnose gynaecologic neoplasms. Ultrastruct Pathol 11: 335–360
20. Floyd C, Ayala AG, Logothetis CJ, Silva EG (1988) Spermatocytic seminoma with associated sarcoma of the testis. Cancer 61: 409–414
21. Ghadially FN (ed) (1997) Intracytoplasmic nucleolus-like bodies. In: Ultrastructural pathology of the cell and matrix, 4th edn. Boston: Butterworth-Heinemann, pp 1084–1089
22. Haraguchi CM, Mabuchi T, Hirata S, Shoda T, Yamada AT, Hoshi K, Yokota S (2003) Spatiotemporal changes of levels of a moonlighting protein, phospholipid hydroperoxide glutathione peroxidase, in subcellular compartments during spermatogenesis in the rat testis. Biol Reprod 69:885–895
23. Holstein AF, Roosen-Runge EC (eds) (1981) Atlas of human spermatogenesis. Grosse, Berlin, pp 32–85
24. Holstein AF, Roosen-Runge EC, Schirren C (eds) (1988) Tumor cells in the testis. In: Illustrated pathology of human spermatogenesis. Grosse, Berlin, pp 239–264
25. Hosokawa M, Shoji M, Kitamura K, Tanaka T, Noce T, Chuma S, Nakatsuji N (2007) Tudor-related proteins TDRD1/MTR-1, TDRD6 and TDRD7/TRAP: domain composition, intracellular localization, and function in male germ cells in mice. Dev Biol 301:38–52
26. Hübner G, Pongratz D (1981) Reducing body myopathy—ultrastructure and classification. Virchows Arch A Pathol Anat Histopathol 392:97–104
27. Jones CJ, Ockleford CD (1985) Nematosomes in the human placenta. Placenta 6:355–361
28. Kellokumpu-Lehtinen PL, Söderström KO (1978) Occurrence of nuage in fetal germ cells. Cell Tissue Res 194:171–177
29. Kraggerud SM, Berner A, Bryne M, Pettersen EO, Fossa SD (1999) Spermatocytic seminoma as compared to classical seminoma: an immunohistochemical and DNA flow cytometric study. APMIS 107:297–302
30. Looijenga LHJ, Hersmus R, Gillis AJM, Pfundt R, Stoop HJ, van Gurp RJHLM, Veltman J, Beverloo HB, van Drunen E, van Kessel AG, Pera RR, Schneider DT, Summersgill B, Shipley J, McIntyre A, van der Spek P, Schoenmakers E, Oosterhuis JW (2006) Genomic and expression profiling of human spermatocytic seminomas: primary spermatocyte as tumorigenic precursor and DMRT1 as candidate chromosome 9 gene. Cancer Res 66:290–302
31. Looijenga LHJ, Stoop HJ, Hersmus R, Gillis AJM, Oosterhuis JW (2007) Genomic and expression profiling of human spermatocytic seminomas: pathogenetic implications. Int J Androl 30:328–336
32. Martin BJ, Spicer SS (1973) Ultrastructural features of cellular maturation and aging in human trophoblast. J Ultrastruct Res 43: 133–149
33. Masson P (1946) Etude sur le séminome. Rev Can Biol 5:361–387
34. Matoška J, Ondruš D, Horňák M (1988) Metastatic spermatocytic seminoma. A case report with light microscopic, ultrastructural, and immunohistochemical findings. Cancer 62:1197–1201
35. Min K-W, Scheithauer BW (1990) Pineal germinomas and testicular seminoma: a comparative ultrastructural study with special references to early carcinomatous transformation. Ultrastruct Pathol 14:483–496
36. Motta PM, Nottola SA, Makabe S, Heyn R (2000) Mitochondrial morphology in human fetal and adult female germ cells. Hum Reprod 15:129–147
37. Mrak RE (2002) The Big Eye in the 21st century: the role of electron microscopy in modern diagnostic neuropathology. J Neuropathol Exp Neurol 61:1027–1039
38. Ohsawa M, Liewluck T, Ogata K, Iizuka T, Hayashi Y, Nonaka I, Sasaki M, Nishino I (2007) Familial reducing body myopathy. Brain Develop 29:112–116
39. Paniagua R, Nistal M (1984) Morphological and histometric study of human spermatogonia from birth to the onset of puberty. J Anat 139:535–552
40. Paniagua R, Nistal M, Amat P, Rodriguez MC (1985) Presence of ribonucleoproteins and basic proteins in the nuage and intermitochondrial bars of human spermatogonia. J Anat 143:201–206
41. Phillips DM (1974) Spermiogenesis. Academic, New York, p 52
42. Rajpert-De Meyts E, Jacobsen GK, Bartkova J, Aubry F, Samson M, Bartek J, Skakkebaek NE (2003) The immunoistochemical expression pattern of Chk2, p53, $p19^{INK4d}$, MAGE-A4 and other selected antigens provides new evidence for the premeiotic origin of spermatocytic seminoma. Histopathology 42:217–226
43. Raz E (2000) The function and regulation of vasa-like genes in germ-cell development. Genome Biol 1:10171–10176
44. Reunov A, Isaeva V, Au D, Wu R (2000) Nuage constituents arising from mitochondria: is it possible? Dev Growth Differ 42: 139–143
45. Rosai J, Silber I, Khodadoust K (1969) Spermatocytic seminoma. I. Clinicopathologic study of six cases and review of the literature. Cancer 24:92–102
46. Rosai J, Khodadoust K, Silber I (1969) Spermatocytic seminoma. II. Ultrastructural study. Cancer 24:103–116
47. Scully RE (1961) Spermatocytic seminoma of the testis. A report of 3 cases and review of the literature. Cancer 14:788–794
48. Shinde A, Nakano S, Kusaka H, Nakaya Y, Sawada H, Kohara N (2004) Nucleolar characteristic of reducing bodies in reducing body myopathy. Acta Neuropathol 107:265–271
49. Smetana K, Gyorkey F, Gyorkey P, Busch H (1972) Studies on nucleoli and cytoplasmic fibrillar bodies of human hepatocellular carcinomas. Cancer Res 32:925–932

50. Srigley JR, Mackay B, Toth P, Ayala A (1988) The ultrastructure and histogenesis of male germ neoplasia with emphasis on seminoma with early carcinomatous features. Ultrastruct Pathol 12: 67–86
51. Stoop H, van Gurp R, de Krijger R, Geurts van Kessel A, Köberle B, Oosterhuis W, Looijenga L (2001) Reactivity of germ cell maturation stage-specific markers in spermatocytic seminoma: diagnostic and etiological implications. Lab Invest 81:919–928
52. Strome S, Garvin J, Paulsen J, Capowski E, Martin P, Beanan M (1994) Specification and development of the germline in *Caenorhabditis elegans*. Ciba Found Symp 182:31–45
53. Talerman A (1980) Spermatocytic seminoma. Clinicopathological study of 22 cases. Cancer 45:2169–2176
54. Talerman A, Fu YS, Okagaki T (1984) Spermatocytic seminoma. Ultrastructural and microspectrophotometric observations. Lab Invest 51:343–349
55. Tanner NK, Linder P (2001) DExD/H box RNA helicases: from generic motors to specific dissociation functions. Mol Cell 8:251–262
56. True LD, Otis CN, Delprado W, Scully RE, Rosai J (1988) Spermatocytic seminoma of the testis with sarcomatous transformation. A report of five cases. Am J Surg Pathol 12:75–82
57. Ulbright TM (2005) Germ cell tumors of the gonads: a selective review emphasizing problems in differential diagnosis, newly appreciated, and controversial issues. Mod Pathol 18:S61–S79
58. Van Blerkom J, Motta P (eds) (1979) Fertilization and preimplantation embryogenesis. In: The cellular basis of mammalian reproduction. Urban and Schwarzenberg, Munich, pp 165–189
59. Zeeman A-M, Stoop H, Boter M, Gillis AJM, Castrillon DH, Oosterhuis JW, Looijenga LHJ (2002) VASA is a specific marker for both normal and malignant human germ cells. Lab Invest 82: 159–166
60. Walter P (1980) Spermatocytic seminoma. Study of 8 case and review of the literature. Virchows Arch A Pathol Anat Histopathol 386:175–187
61. Weakley BS (1971) Basic protein and ribonucleic acid in the cytoplasm of the ovarian oocyte in the golden hamster. Z Zellforsch Mikrosk Anat 112:69–84

Virchows Arch (2008) 453:197–201
DOI 10.1007/s00428-008-0624-7

CASE REPORT

Mixed-type liposarcoma: clinicopathological, immunohistochemical, and molecular analysis of a case arising in deep soft tissues of the lower extremity

Thomas Mentzel · Gabriele Palmedo · Markus Hantschke · Jörg Woziwodzki · Christian Beck

Received: 7 April 2008 / Revised: 5 May 2008 / Accepted: 5 May 2008 / Published online: 13 June 2008

Abstract A rare case of mixed-type liposarcoma arising in deep soft tissue of the right thigh of a 45-year-old female patient is reported. The neoplasm was completely excised and was composed of an irregular admixture of areas of atypical lipomatous tumor/well-differentiated liposarcoma of the lipoma-like subtype with areas of myxoid/round cell liposarcoma. An amplification of the *MDM2* and *CDK4* genes respectively in the atypical lipomatous tumor/well-differentiated liposarcoma areas was detected by fluorescence in situ hybridization (FISH) analysis, and translocations of the *CHOP* and *FUS* genes were detected by FISH analysis in the myxoid/round cell liposarcoma areas.

Keywords Liposarcoma · Mixed-type liposarcoma · MDM2 · CDK4 · CHOP · FUS · Immunohistochemistry · Cytogenetics

Introduction

Liposarcoma represents the most common soft tissue sarcoma in adults, accounting for approximately 20% of all sarcomas. Liposarcoma is currently subclassified into four main subtypes, including *atypical lipomatous tumor/well-differentiated liposarcoma* (lipoma-like, sclerosing, inflammatory, and spindle-cell variants), *dedifferentiated liposarcoma*, which represents the morphological form of progression of atypical lipomatous tumor/well-differentiated liposarcoma, *myxoid liposarcoma*, which forms a continuous spectrum with round cell liposarcoma, and rare *pleomorphic liposarcoma*. Cytogenetic and molecular genetic studies contributed substantially to this classification, and specific chromosomal abnormalities have been detected for all types of liposarcoma. Atypical lipomatous tumors/well-differentiated liposarcomas are characterized by supernumery ring and/or giant marker chromosomes containing amplified material of the q13–15 regions of chromosome 12, myxoid liposarcomas show a specific reciprocal chromosome translocation t(12;16)(q13.3;p11.2) with fusion of the *CHOP* and *FUS* genes as the primary chromosomal aberration, and pleomorphic liposarcomas often have multiple, complex structural rearrangements without consistent and specific abnormalities. Very rare cases show a combination of morphological types (mixed-type liposaroma), and we present such a case arising in deep soft tissues of an adult patient.

T. Mentzel (✉) · G. Palmedo · M. Hantschke
Dermatopathologische Gemeinschaftspraxis,
Siemensstrasse 6/1,
88048 Friedrichshafen, Germany
e-mail: mentzel@dermpath.de
URL: www.dermpath.de

J. Woziwodzki
Department of Pathology,
Aurich, Germany

C. Beck
Department of Surgery,
Varel, Germany

Materials and methods

The tissue was fixed in 4% buffered formalin, routinely processed and embedded in paraffin; 4-μm-thick sections were stained with hematoxylin and eosin. In addition, representative sections were stained immunohistochemically by the labeled streptavidin biotin technique using commercially available antibodies; antigen retrieval was used for all antibodies. Stainings for CD68 (clone=PG-M1; dilution=

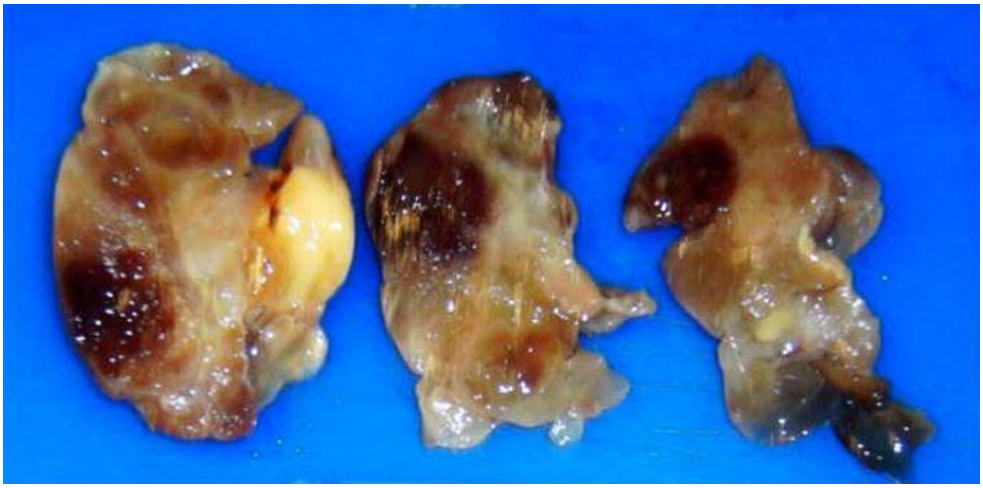

Fig. 1 Grossly, a nodular neoplasm with myxoid, gelatinous as well as yellow, lipomatous areas is seen

1:200; DAKO, Glostrup, Denmark), MDM2 (IF2; 1:200; Invitrogen, Carlsbad, CA, USA), CDK4 (DC9-31; 1:400; Biosource, Nivelles, Belgium), and S-100 protein (polyclonal, 1:4,000; DAKO, Glostrup, Denmark) were available. Appropriate positive and negative controls were used. For the detection of a translocation of the *FUS* and *CHOP* genes, a directly labeled spectrum orange/spectrum green dual color break-apart probe (Abbott, Wiesbaden, Germany) was used for hybridization to a region distal and proximal to the *FUS* and *CHOP* genes, respectively. Amplification of the *CDK4* and *MDM2* genes was detected by hybridization of DIG-labeled bacterial artificial chromosomes (BACs) followed by binding to fluorescein isothiocyanate (FITC) anti-DIG. Fluorescence in situ hybridization was performed on 3-μM sections of formalin-fixed, paraffin-embedded tissue after baking at 65°C for 16 h, deparaffinization with xylene, and dehydration with ethanol. All tissue sections were pretreated with a 30% solution of pretreatment solution and digested with Proteinase K following the instructions of the suppliers (Q-Biogene, Heidelberg, Germany). Digestion times were optimized on a case-by-case basis. After a second dehydration step, the probes were applied to the sections and the covered slides were sealed with rubber cement, heat-denatured, and hybridized at 37°C for 16 h. After stringent washing with 50% formamide in 2× SSC and treating with FITC anti-DIG in the case of indirectly labeled probes, the sections were counterstained with DAPI II in mounting medium (125 ng/ml, Vysis Bergisch Gladbach, Germany) and visualized under a Zeiss Axioplan 2 microscope using a HBO103 lamp and the appropriate filters for the three fluorescence dyes.

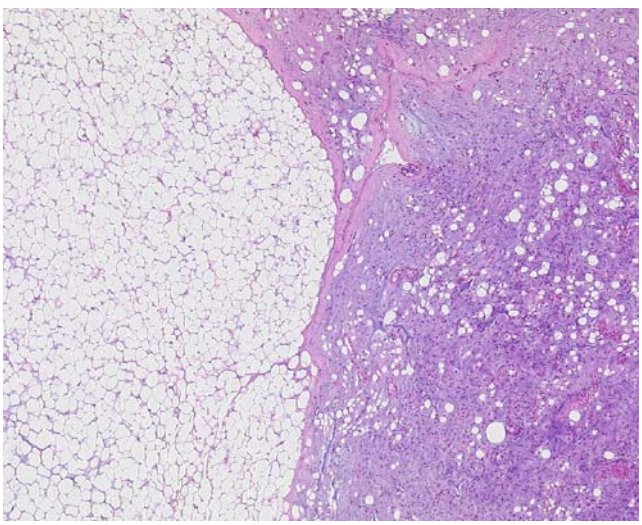

Fig. 2 Low-power view shows lipogenic (*left*) and myxoid tumor areas (*right*)

Results

A 45-year-old female patient complained about an increasing soft tissue swelling in the upper third of the anterior part

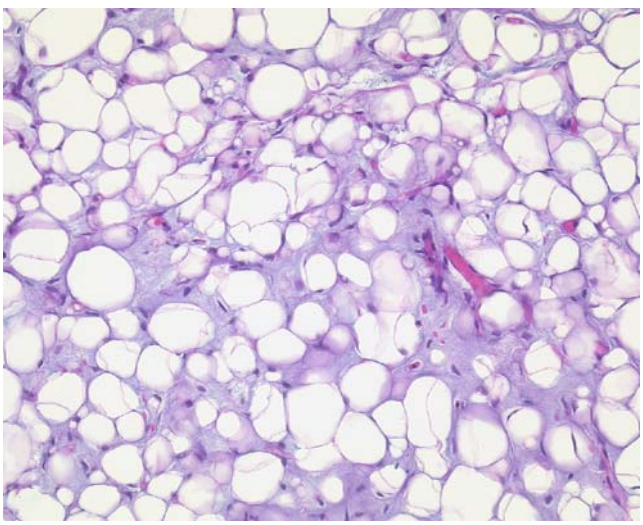

Fig. 3 Lipogenic tumor areas are composed of atypical lipogenic cells showing variations in size and shape. In addition, scattered enlarged tumor cells with enlarged and hyperchromatic nuclei and multivacuolated lipoblasts are seen. The stroma shows focal myxoid changes

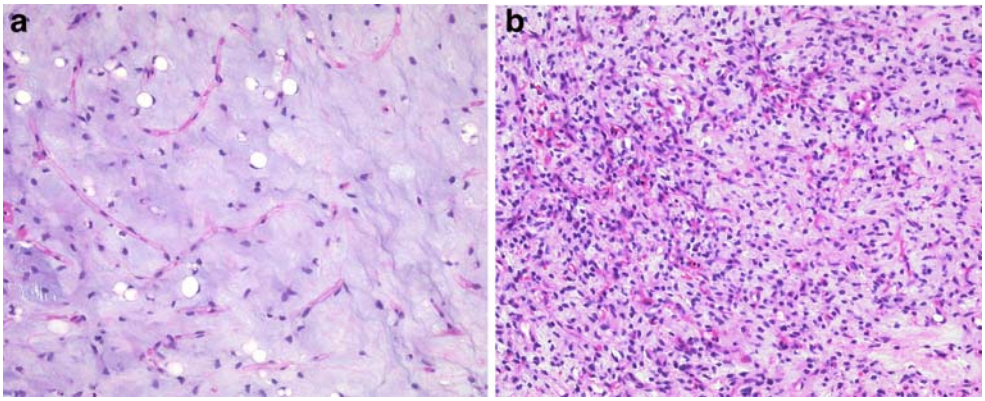

Fig. 4 In myxoid tumor areas, small undifferentiated cells admixed with scattered atypical lipogenic cells and lipoblasts are set in a prominent myxoid stroma with thin-walled and branching blood vessels (**a**). Note focal transition to more cellular tumor areas containing enlarged tumor cells with enlarged, round nuclei (**b**)

of the right thigh within 3 months. Ultrasound investigations showed an intramuscular, lobular, and relatively homogenous lipogenic lesion, and an atypical lipoma was suspected. Intraoperatively, an intramuscular neoplasm measuring 8 cm in largest diameter was found and marginally excised, and after the diagnosis was established a wide tumor excision with tumor-free margins was performed. Grossly, a heterogeneous neoplasm with myxoid, gelatinous areas irregularly associated with lipomatous areas was seen (Fig. 1); no areas of tumor necrosis were evident.

Histologically, two irregularly admixed components were found (Fig. 2). Lipomatous tumor areas did not show lobulation and were composed of mature appearing adipocytic cells showing considerable variations in size and shape. In addition, cells with slightly enlarged and hyperchromatic nuclei as well as scattered lipoblasts in perivascular location were found (Fig. 3). The tumor stroma contained numerous dilated vessels with slightly fibrosed walls and revealed focal myxoid changes. Immunohistochemically, no clear nuclear expression of MDM2 and CDK4, respectively and no increased number of CD68

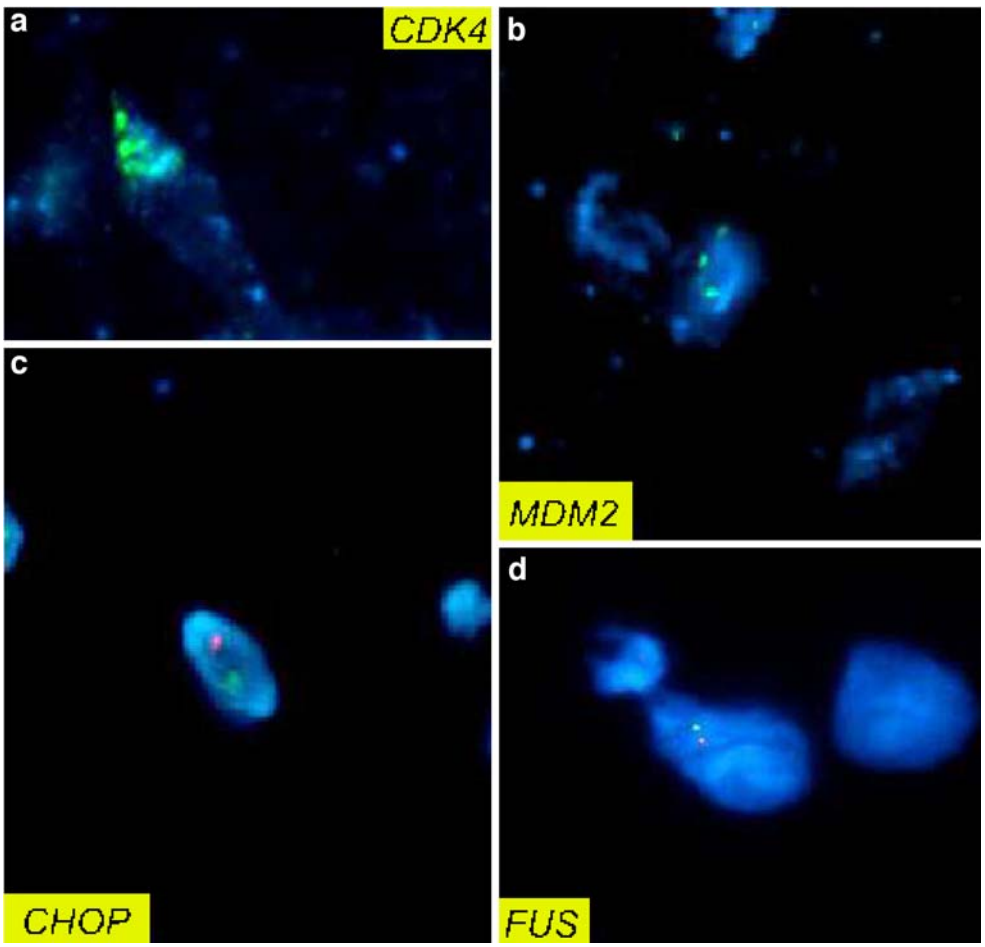

Fig. 5 Amplification of *CDK4* (**a**) and *MDM2* (**b**) detected by hybridization of two FITC-labeled BACs. Translocations of the *CHOP* (**c**) and *FUS* (**d**) genes. Split-apart signals were detected by two break-apart probes

positive histiocytes were present. Molecular analysis by FISH technique showed a *MDM2* amplification in 21 out of 53 analyzed nuclei and a *CDK4* amplification in 14 out of 61 analyzed nuclei (Fig. 5). No *CHOP* and *FUS* gene translocations have been detected in this tumor area by FISH analysis. These findings were consistent with atypical lipomatous tumor/well-differentiated liposarcoma of the lipoma-like subtype.

The myxoid tumor component was composed of small, undifferentiated mesenchymal cells associated with uni- and multivacuolated lipoblasts set in a prominent myxoid stroma with mucin pools and a prominent network of thin-walled and branching capillaries. Focally, more cellular areas containing round to oval tumor cells with enlarged round and hyperchromatic nuclei were noted (Fig. 4). No nuclear expression of MDM2 or CDK4 was detected in this tumor component immunohistochemically. Molecular analysis by FISH technique showed a translocation of the *CHOP* gene in 21 out of 53 analyzed nuclei and a translocation of the *FUS* gene in 23 out of 62 analyzed nuclei (Fig. 5). No *MDM2* and *CDK4* amplifications have been detected by FISH analysis. These findings were consistent with myxoid/round cell liposarcoma, and the final diagnosis of mixed-type liposarcoma, composed of atypical lipomatous tumor/well-differentiated liposarcoma and myxoid/round cell liposarcoma, was made.

Discussion

Mixed-type liposarcoma represents the rarest subtype of liposarcoma with only a few cases reported in the English literature. Mixed-type liposarcoma is defined as a liposarcoma showing either features of combined myxoid/round cell liposarcoma and atypical lipomatous tumor/well-differentiated liposarcoma/dedifferentiated liposarcoma or of myxoid/round cell liposarcoma and pleomorphic liposarcoma. The few reported cases arose predominantly in elderly patients and were seen in retroperitoneal or intra-abdominal locations; more rarely, cases arising in the mediastinum and deep soft tissues of the extremities have been documented [3, 7–9, 12]. The few karyotyped cases showed the presence of ring or giant marker chromosomes as the sole chromosomal abnormality or in association with complex rearrangements [1, 2, 11]. There is only one case of true mixed-type liposarcoma arising in subcutaneous tissue of the thigh in a 29-year-old male patient that metastasized to the supraclavicular region, in which a mixed genotype corresponding to atypical lipomatous tumor/well-differentiated liposarcoma and myxoid liposarcoma has been illustrated in the primary neoplasm as well as in the metastasis [9].

The reported case represents an exceedingly rare example of true mixed-type liposarcoma arising in deep soft tissue of the lower extremity in an adult patient, in which both tumor components were irregularly admixed. The atypical lipomatous tumor/well-differentiated liposarcoma component did not show tumor progression into dedifferentiated liposarcoma, whereas in the myxoid areas, foci of round cell differentiation were found, consistent with progression to grade two of malignancy. The characteristic molecular changes of both tumor components were found and emphasize the presence of polyclonal neoplastic development in rare instances. Interestingly, no nuclear expression of MDM2 and CDK4 was detected immunohistochemically, whereas clear amplification of both genes was seen by FISH technique. This phenomenon most likely reflects a well-differentiated atypical lipomatous tumor with low copy numbers of the amplified genes.

There are a number of cases of so-called mixed-type liposarcoma in the literature, in which no molecular evidence of the two tumor components was given [3–8, 13, 14]. However, at least some of these cases most likely represent examples of atypical lipomatous tumor/well-differentiated liposarcoma or of dedifferentiated liposarcoma with focal prominent myxoid changes, what represents a well-recognized phenomenon especially in long-standing lipogenic neoplasms in retroperitoneal and intraabdominal locations. Very rarely, dedifferentiation has been reported in myxoid liposarcoma, and a close relationship between atypical lipomatous tumor/well-differentiated liposarcoma and myxoid liposarcoma was proposed [10]. Unfortunately, it was impossible to prove true dedifferentiation in myxoid liposarcoma cytogenetically in these three cases, and it can be speculated that these neoplasms represent probably examples of mixed-type liposarcoma showing a combination of myxoid/round cell liposarcoma and dedifferentiated liposarcoma as a form of progressive atypical lipomatous tumor/well-differentiated liposarcoma.

In summary, a rare case of true mixed-type liposarcoma has been reported, emphasizing the broad spectrum of malignant lipogenic neoplasms and the need for careful sampling of large mesenchymal neoplasms.

Conflict of interest statement We declare that we have no conflict of interest

References

1. Fletcher CDM, Akerman M, Dal Cin P, de Wever I, Mertens F, Mitelman F, Rosai J, Rydholm A, Sciot R, Tallini G, van den Berghe H, van den Ven W, Vanni R, Willen H (1996) Correlation between clinicopathological features and karyotype in lipomatous

tumours. A report of 178 cases from the chromosomes and morphology (CHAMP) collaborative study group. Am J Pathol 148:623–630
2. Gisselsson D, Höglund M, Mertens F, Johansson B, Dal Cin P, van den Berghe H, Earnshaw WC, Mitelman F, Mandahl F (1999) The structure and dynamics of ring chromosomes in human neoplastic and nonneoplastic cells. Hum Genet 104:315–325
3. Hashimoto H, Enjoji M (1982) Liposarcoma. A clinicopathologic subtyping of 52 cases. Acta Pathol Jpn 32:933–948
4. Irie T, Hatori M, Watanabe M, Ehara S, Kokubun S (2003) Radiologically and histologically mixed liposarcoma: a report of two biphasic cases. Jpn J Clin Oncol 33:482–485
5. Kato T, Motohara T, Kaneko Y, Shikishima H, Takahashi T, Okushiba S, Kondo S, Kato H (1999) Case of retroperitoneal dedifferentiated mixed-type liposarcoma: comparison of proliferative activity in specimens from four operations. J Surg Oncol 72:32–36
6. Kim JI, Choi KU, Lee IS, Moon TY, Lee CH, Kim HW, Kim JY, Park DY, Sol MY (2006) Gene expression in mixed type liposarcoma. Pathology 38:114–119
7. Kindblom LG, Angervall L, Svendsen P (1975) Liposarcoma. A clinicopathologic, radiographic, and prognostic study. APMIS 253 (Suppl.):5–71
8. Klimstra DS, Moran CA, Perino G, Koss MN, Rosai J (1995) Liposarcoma of the anterior mediastinum and thymus. A clinicopathologic study of 28 cases. Am J Surg Pathol 19:782–791
9. Meis-Kindblom JM, Sjögren H, Kindblom LG, Peydro-Mellquist A, Röijer E, Aman P, Stenman G (2001) Cytogenetic and molecular genetic analysis of liposarcoma and its soft tissue simulators: recognition of new variants and differential diagnosis. Virchows Arch 439:141–151
10. Mentzel T, Fletcher CDM (1997) Dedifferentiated liposarcoma: a clinicopathological study suggesting a closer relationship between myxoid and well-differentiated liposarcoma. Histopathology 30:457–463
11. Schneider-Stock R, Walter H, Radig K, Rys J, Bosse A, Kuhnen C, Hoang-Vu C, Roessner A (1998) MDM2 amplification and loss of heterozygosity at Rb and p53 genes: no simultaneous alterations on the oncogenesis of liposarcomas. J Cancer Res Clin Oncol 124:532–540
12. Sreekantaiah C, Karakousis CP, Leong SP, Sandberg AA (1991) Trisomy 8 as a nonrandom secondary change in myxoid liposarcoma. Cancer Genet Cytogenet 51:195–205
13. Tan GY, Chong YL, Ramesh K, Walford NQ, Tan JK (2004) Giant mixed-type perinephric liposarcoma. Int Urol Nephrol 36:319–322
14. Yamaguchi T, Suzuki H, Ishii N, Nakada T, Onmura Y, Matsushita S (1991) Retroperitoneal mixed type liposarcoma: a case report. Hinyokiki Kiyo 37:141–145

Virchows Arch (2008) 453:203–207
DOI 10.1007/s00428-008-0630-9

CASE REPORT

Visceral manifestations of hypochondrogenesis

Helen Wainwright · Peter Beighton

Received: 21 January 2008 / Revised: 8 April 2008 / Accepted: 9 May 2008 / Published online: 19 July 2008

Abstract Autopsy of a stillborn neonate with hypochondrogenesis revealed severe cardiac abnormalities and extensive diverticulosis of the proximal region of the small intestine. Visceral ramifications are unusual in hypochondrogenesis; they may reflect heterogeneity of the intramolecular defect in the COL2A1 gene that codes for the achondrogenesis type II–hypochondrogenesis spectrum of disorders.

Keywords Bone dysplasia · Cardiac defects · Diverticulosis · Genetics

Introduction

Hypochondrogenesis (OMIM 200610) is a potentially lethal genetic skeletal dysplasia that presents in the neonate with limb shortening. Micrognathia and palatal clefts are inconsistent features [8]. The diagnosis is made by recognition of the characteristic radiographic manifestations [3] and confirmed by demonstration of typical histological changes in the zones of endochondrial ossification. Stillbirth or early death from cardiorespiratory failure is usual.

Although hypochondrogenesis is rare, autopsy findings have been featured in several published reports. The only significant visceral ramification that has been documented is cardiac septal defects [9].

Autopsy in a South African neonate with hypochondrogenesis revealed a complex cardiac malformation and extensive diverticulae of the proximal region of the small intestine. This latter abnormality has not previously been reported in the condition. Our observations are described, depicted, and discussed in this article.

H. Wainwright (✉)
Division of Anatomical Pathology, Faculty of Health Sciences,
University of Cape Town,
Observatory 7925,
Cape Town, South Africa
e-mail: Helen.Wainwright@uct.ac.za

P. Beighton
Division of Human Genetics, Faculty of Health Sciences,
University of Cape Town,
Observatory 7925,
Cape Town, South Africa

Clinical history

A stillborn female infant of European stock was delivered in Cape Town on 19th November 1998 after the ultrasonic recognition of symmetrical shortening of the limb bones and induction at the 21st week of pregnancy. The mother was aged 30 years; no other family history was available. The neonate was hydropic, with a post-nuchal cyst, a flat dysmorphic facies, and short straight limbs (Fig. 1). In the feet, toes 2–5 were very hypoplastic or absent (Fig. 2).

Radiographs of the deceased baby revealed a broad chest and short straight tubular bones that lacked ossification centers (Fig. 3). The vertebral bodies were ovoid, and ossification was deficient in the cervical and sacral regions. The ilia were rounded, the pubis was unossified, and the scapulae were small. The fibulae were hypoplastic.

Materials, methods, and results

Autopsy revealed the following cardiac malformations:

- Persistent left superior vena cava that drained into the right auricle via the coronary sinus
- Hypoplastic pulmonary trunk

Fig. 1 The neonate; whole-body external view showing hydrops, a flat dysmorphic facies and short straight limbs

- Aberrant origin of the right pulmonary artery from the aorta
- Right-sided aortic arch
- Left-sided ductus arteriosus to the left subclavian artery
- Separate origin of the right subclavian artery from the aorta

The duodenum and proximal 190 mm of small intestine contained more than 26 small outpouchings on the antimesenteric serosal surface (Fig. 4). The diverticulae measured 1 mm in length. The distal 220 mm of small intestine had a smooth uninvolved serosal surface. The colon measured 150 mm in length and appeared normal.

Microscopy revealed abnormal crypts embedded in stroma with lymphoid hyperplasia and small vessels (Fig. 5). The overlying muscularis propria was markedly atrophic, and it was not possible to identify two separate layers.

The only other visceral abnormality was right hemi-uterus, with two ovaries. The right umbilical artery was absent.

In the skeleton, histological studies of the chondro-osseous junction in the vertebral bodies and long bones revealed matrix deficiency and ballooned chondrocyte lacunae (Fig. 6). Cytoplasmic inclusions were evident in the chondrocytes (Fig. 4). These observations were consistent with the diagnosis of hypochondrogenesis.

For logistical reasons, it was not possible to undertake cytogenetic and molecular investigations.

Discussion

Hypochondrogenesis is a member of the type II collagen group of bone dysplasias [11]. The condition is allelic with

Fig. 2 The feet are dysplastic, with hypoplasia or absence of toes 2–5

◀ **Fig. 3** Antero-posterior radiograph, stillbirth at 21 weeks gestation. The limb bones are short, and the fibulae are hypoplastic. The thorax is broad, the ilia and scapulae are small, and the pubis is unossified. Ossification in the cervical and sacral regions is delayed

achondrogenesis type II and results from heterozygosity for a new mutation of the COL2A1 gene situated at the chromosomal locus 12q13.1. Hypochondrogenesis–achondrogenesis type II is regarded as a continuum [2], but in view of the disparity in severity at the ends of the phenotypic range, these conditions are recognized as separate entities at the phenotypical level. Either way, the phenotypic spectrum reflects intramolecular heterogeneity [6]. The clinical, radiographical and histological features of the stillborn infant whom we have documented were consistent with the diagnosis of hypochondroplasia, and this designation has been used in this article.

The diagnosis of hypochondrogenesis was made on a basis of the characteristic radiological features, notably short limb bones with hypoplastic fibulae, a broad thorax, ovoid vertebral bodies with coronal clefts, delayed ossification in the cervical and sacral regions, small ilia and scapulae, and lack of ossification of the pubis [7]. As with other lethal infantile bone dysplasias, diagnosis of this spectrum can usually be made by radiography alone in the clinical setting, and an expensive molecular confirmation is of little value [5]. At the histological level, the diagnosis is supported by the demonstration of chondrocytes containing ballooned lacunae in the zones of endochondrial ossification [12].

There are very few reports of visceral involvement in hypochondrogenesis, possibly because of the paucity of documented autopsies (Table 1). For instance, there was no mention of visceral abnormalities in a review of 23 infants with the achondrogenesis–hypochondrogenesis spectrum of disorders [12]. Nevertheless, the presence of cardiac malformations appears to be genuine if very inconsistent with the feature of hypochondrogenesis. Maroteaux et al. [8] documented a heart murmur in an affected infant, and

Fig. 4 Proximal 190 mm of small intestine with multiple small diverticulae on the serosal surface

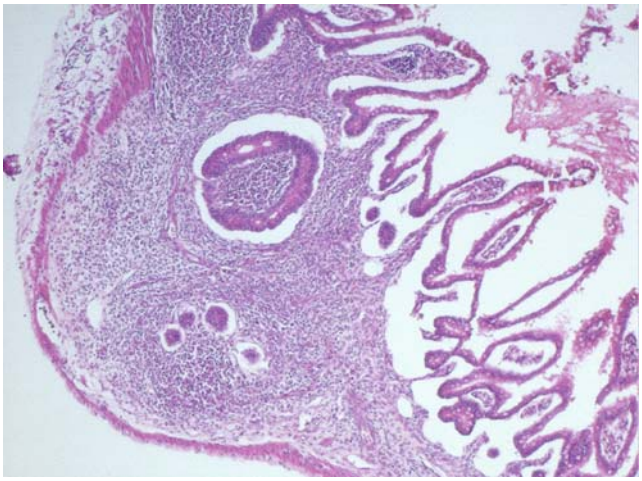

Fig. 5 Abnormal crypts, vessels, and lymphoid tissue with overlying thinned muscularis mucosa at ×10 magnification

Potocki et al. [9] described an affected neonate with a complete arterio-venous canal defect and another with a secundum type of atrial septal defect. These latter authors commented that type II collagen was not present in the myocardium and suggested that the determinant COL2A1 gene may have an indirect effect on embryogenesis. In this context, it may be relevant that teratogenic drugs such as dimethadione in pregnant rats have produced both heart and skeletal malformations. Similarly, several genes that are involved in both heart development and formation of the axial skeleton have been demonstrated in genetically modified mice [13].

The detection of extensive diverticulae in the proximal small intestine of the affected neonate was unforeseen. Diverticulosis at this site is unusual, and it seems likely that this anomaly is a syndromic component rather than a chance concomitant. The pathogenesis of the diverticulae is uncertain, but it may be relevant that similar abnormalities have been reported in a family with immunological incompetence [1] and in the Ehlers–Danlos syndrome type IV, in which type III collagen is involved. Diverticulae of the bowel have also been documented in another connective tissue disorder, the Marfan syndrome [4]. It is possible that mechanical factors are involved, but it is unlikely that the diverticulae in the infant with hypochondrogenesis were the consequence of this process. As with the cardiac abnormalities, defective embryogenesis may be responsible. Another alternative would be a contiguous gene effect in which a chromosomal microdeletion has involved adjacent genes; this remains unproven.

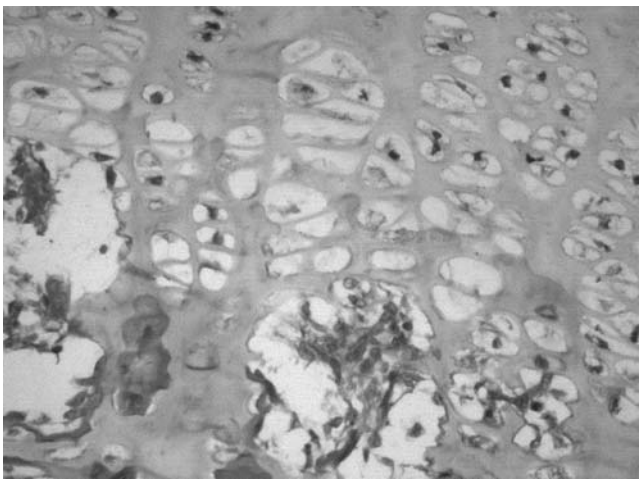

Fig. 6 High-power histological view of the chondro-osseous junction in a vertebral body showing matrix deficiency and ballooned chondrocytic lacunae

Table 1 Visceral manifestations of hypochondrogenesis

Manifestation	Reference
Cardiac arterio-venous canal defect	Potocki et al. [9]
Atrial septal defect	Potocki et al. [9]
Cardiac murmur	Maroteaux et al. [8]
Intestinal diverticulosis	Present patient
Hemi-uterus	Present patient
Complex cardiac defect	Present patient

The significance of the absent toes in the affected baby is uncertain; postaxial polydactyly has been reported in achondrogenesis type II [10], and these abnormalities may be another reflection of intragenic heterogeneity in the phenotypic spectrum of this disorder.

Further documentation of non-skeletal abnormalities in hypochondrogenesis will facilitate genotype–phenotype correlations and advance understanding of the pathogenesis of this disorder.

Acknowledgment We are grateful to Professor Judy Hall of Vancouver for her guidance and to Professor A. Superti-Furga of Freiburg for his assistance with the diagnostic process. We are grateful for the support from the National Research Foundation and the Medical Research Council of South Africa.

Conflict of interest statement We declare that we have no conflict of interest.

References

1. Andersen LP, Schjoldager B, Halver B (1988) Jejunal diverticulosis in a family. Scand J Gastroent 23:672–674
2. Borochowitz A, Ornoy A, Lachman R, Rimoin RL (1986) Achondrogenesis II–hypochondrogenesis: variability versus heterogeneity. Am J Med Genet 24:273–288
3. Castori M, Brancati F, Scanderbeg AC, Dallapiccola B (2006) Hypochondrogenesis. Pediatr Radiol 36(5):460–461
4. Clunie GJA, Mason JM (1962) Visceral diverticula and the Marfan syndrome. Brit J Surg 50:51–51
5. Kapur RP (2007) Achondrogenesis. Pediatr Dev Pathol 10:253–255

6. Korkko J, Cohn DH, Ala-Kokko L, Krakow D, Prockop DJ (2000) Widely distributed mutations in the COL2A1 gene produce achondrogenesis type II/hypochondrogenesis. Am J Med Genet 92(2):95–100
7. Lachman RS, Tiller GE, Graham JM Jr, Rimoin DL (1992) Collagen, genes and the skeletal dysplasias on the edge of a new era: a review and update. Eur J Radiol 14:1–10
8. Maroteaux P, Stanescu V, Stanescu R (1983) Hypochondrogenesis. Eur J Pediatr 141:14–22
9. Potocki L, Abuelo DN, Oyer CE (1995) Cardiac malformation in two infants with hypochondrogenesis. Am J Med Genet 59:295–299
10. Rittler M, Orioli IM (1995) Achondrogenesis type II with polydactyly. Am J Med Genet 59:157–160
11. Superti-Furga A, Unger S (2007) Nosology and classification of genetic skeletal disorders: 2006 revision. Am J Med Genet 143(1):1–18
12. Van der Harten HJ, Brons JTJ, Dijkstra F, Niermeyer MF, Meijer CJLM, Van Giejn HP, Arts NFTH (1988) Achondrogenesis–hypochondrogenesis: the spectrum of chondrogenesis imperfecta. Pediatr Pathol 8:571–597
13. Weston AD, Ozolins TR, Brown NA (2006) Thoracic skeletal defects and cardiac malformation: a common epigenetic link? Birth Defects Res C Embryo Today 78(4):354–370

Virchows Arch (2008) 453:209–216
DOI 10.1007/s00428-008-0632-7

CASE REPORT

Heterozygous nonsense SCN5A mutation W822X explains a simultaneous sudden infant death syndrome

Emanuela Turillazzi · Giampiero La Rocca · Rita Anzalone · Simona Corrao · Margherita Neri · Cristoforo Pomara · Irene Riezzo · Steven B. Karch · Vittorio Fineschi

Received: 25 March 2008 / Revised: 4 May 2008 / Accepted: 13 May 2008 / Published online: 13 June 2008

Abstract The sudden, unexpected, and unexplained death of both members of a set of healthy twins (simultaneous sudden infant death syndrome (SSIDS)) is defined as a case in which both infants meet the definition of sudden infant death syndrome individually. A search of the world medical literature resulted in only 42 reported cases of SSIDS. We report the case of a pair of identical, male, monozygotic twins, 138 days old, who suddenly died, meeting the full criteria of SSIDS and where a genetic screen was performed, resulting in a heterozygous nonsense SCN5A mutation (W822X) in both twins. Immunohistochemistry was performed on cardiac tissue samples utilizing polyclonal antibodies anti-Na^+ CP type Vα (C-20) and a terminal deoxynucleotidyl transferase deoxyuridine triphosphate nick end labeling assay. The cellular localization of the Na^+ CP type Vα (C-20) demonstrated by confocal microscopy on staining pattern of myocytes was concentrated in the intercalated disks of ventricular myocytes. These findings suggest that defective ion channels represent viable candidates for the pathogenesis of SIDS and, obviously, of SSIDS, supporting a link between sudden infant death syndrome and cardiac channelopathies.

Keywords Simultaneous sudden infant death syndrome · SCN5A gene mutation · W822X mutation · Na^+ channel function · $Na_v1.5$ protein function

E. Turillazzi · M. Neri · C. Pomara · I. Riezzo · V. Fineschi (✉)
Department of Forensic Pathology, University of Foggia,
Ospedale Colonnello D'Avanzo, Viale degli Aviatori 1,
71100 Foggia, Italy
e-mail: vfinesc@tin.it

G. La Rocca · R. Anzalone · S. Corrao
Department of Experimental Medicine,
Human Anatomy Section, University of Palermo,
Palermo, Italy

S. B. Karch
PO Box 5139, Berkeley, CA 94705, USA

Introduction

Sudden infant death syndrome (SIDS) is defined as the sudden unexpected death of an infant <1 year of age, with onset of the fatal episode apparently occurring during sleep, that remains unexplained after a thorough investigation, including performance of a complete autopsy and review of the circumstances of death and the clinical history [3]. SIDS may occur in singleton or in one member of a twin pair. The sudden unexpected and unexplained death of both members of a set of healthy twins (simultaneous sudden infant death syndrome—SSIDS) is defined as a case in which both infants meet the definition of SIDS individually; infants must be either monozygotic or dizygotic pairs; death must occur within 24 h of each other [9]. SSIDS occurs very rarely; a search of the world medical literature resulted in only 42 reported cases of SSIDS [4, 9].

We have analyzed a pair of identical, male, monozygotic twins, 138 days old, who suddenly died, meeting the full criteria of SSIDS and in which the molecular postmortem analysis showed a mutation of *SCN5A* gene described as W822X [8]. Cellular localization of the Na^+ CP type Vα (C-20) visualized by confocal laser microscopy on staining pattern of myocytes demonstrated reduction in Na^+ channels expression in ventricular myocytes in respect to control cases.

Clinical history

A pair of identical, white Caucasian male, monozygotic twins, 138 days old, who were thriving and in good health, were found cyanotic and breathless by their mother in the crib. She brought them into the living room and placed them on a sofa to attempt resuscitation, which was unsuccessful. Circumstantial data revealed that the night the deaths occurred, the infants coslept in prone position with a blanket in the same crib; in the early morning, at 7 AM, they were fed by the mother herself. When the mother woke up about at 8.30 AM, she found the babies in the prone position and unresponsive. The medical history showed that the infants had mild respiratory symptoms (cough, mucus production, respiratory difficulties) a few days before their death. Mother's medical history during pregnancy was negative for alcohol consumption, and therapeutic drugs and drugs of abuse; it was positive for cigarette abuse. No history of SIDS was present in extended family.

Materials and methods

A complete autopsy was performed according to the autopsy protocol usually followed at our Institute of Forensic Pathology in case of sudden infant death, including careful examination of the cardiac conduction system and of the central and peripheral autonomic nervous structures involved in cardiorespiratory reflexogenesis [15]. Each internal organ was sectioned, and slides were stained with hematoxylin and eosin, Bielschowsky, and Klüver–Barrera stains. After excluding the presence of gross cardiac malformations, the origin of the coronary arteries was carefully inspected. The heart chambers were regularly examined for pathologic changes in the atria, septa, ventricles, pericardium, endocardium, and coronary arteries. Samples of the myocardium and the major coronary arteries were stained with hematoxylin–eosin and trichromic Heidenhain (Azan). The cardiac conduction system was removed in two blocks: The first included the sinoatrial node and the crista terminalis, while the second contained the atrioventricular node, from the His bundle down to the bifurcation and bundle branches. These two blocks were serially cut at intervals of 40 μm (levels) and stained alternately with hematoxylin–eosin and Azan [15]. Parents declined the genetic screening. On twins, a genetic screen was performed on cardiac sections from formalin-fixed and paraffin-embedded samples. Each sample was constituted by three 30-μm sections.

DNA extraction After paraffin removal, DNA extraction was carried out using Nucleon HT Hard Tissues Extraction Kit (Amersham Biosciences), following manufacturers' instructions. The kit is designed specifically for difficult samples like formalin-fixed paraffin-embedded tissues. After the extraction procedure, extracted DNA was resuspended in DNAse free water and quantified spectrophotometrically (A_{260}/A_{280}).

Double PCR Since polymerase chain reaction (PCR) starting from formalin-fixed paraffin-embedded tissues is a complex task due to the extensive modification induced on dsDNA by formalin itself; a double PCR protocol has been carried out, with some modification with respect to published protocols [5–7, 12, 23]. Two microgram of DNA extracted for each sample has been used to carry out PCR reactions, which were accomplished using Phusion High-Fidelity PCR Kit (Finnzymes), following manufacturer's instructions. The reactions were performed in a MyCycler Thermal Cycler (Bio-Rad) with an initial step of denaturation (98°C, 30 s), followed by 35 cycles of denaturation (98°C, 10 s), annealing (47–52°C, depending from the primers used, 30 s), and extension (72°C, 1 min), with a subsequent final extension step (72°C, 10 min). Primers used for this study are indicated below. In particular, SCN5A exons have been amplified using published intron primers [32, 33]. After first PCR, 5 μl of the first amplified reaction were used to carry out a second PCR protocol, using the same primers and the same cycle steps. After the second PCR reactions, the PCR products were evaluated by electrophoresis on 2.5% high-resolution agarose gel. In order to better estimate the molecular weight of the PCR products, two types of molecular weight ladders were used, a 100 bp (Amersham Biosciences) and a 50 bp one (Sigma).

Beta actin forward	AAACTGGAACGGTGAAGGTG
Beta actin reverse	TCAAGTTGGGGGACAAAAAG
Exon 9 forward	GGGAGACAAGTCCAGCCCAGCAA
Exon 9 reverse	AGCCCACACTTGCTGTCCCTTG
Exon 12 forward	GCCAGTGGCTCAAAAGACAGGCT
Exon 12 reverse	CCTGGGCACTGGTCCGGCGCA
Exon 16 forward	GAGCCAGAGACCTTCACAAGGTCCCCT
Exon 16 reverse	CCCTTGCCACTTACCACAAG
Exon 21 forward	TCCAGGCTTCATGTCCACCTGTCT
Exon 21 reverse	TCTCCCGCACCGGCAATGGT
Exon 22 forward	AGTGGGGAGCTGTTCCCATCCT
Exon 22 reverse	GGACCGCCTCCCACTCC

DNA purification from agarose gels The PCR products of the expected molecular weight were cut from the gel and purified using GFX PCR DNA And Gel Band Purification Kit (Amersham Biosciences), following manufacturers' instructions. The DNA obtained was eluted in diethylpyrocarbonate-treated water and used for incubation with appropriate restriction enzymes.

RFLP analysis Each amplified fragment, cut and purified from the gel, was incubated with appropriate restriction enzyme in order to verify the presence of a mutation resulting in the loss or in the gain of a restriction site in its sequence. The enzymes used in this work were: Van 91I (Roche), Hae II (Promega), MspA1I (Promega), RCA I (Roche), and BstOI (Promega; Table 1). Restriction reactions were carried out following manufacturers' instructions. Proper control experiments were performed in order to ensure enzyme specificity and to avoid overdigestion of the bands. Control experiments comprised also DNA extracted from healthy volunteers and from human cell lines not bearing mutations on the gene of interest.

Electrophoresis on agarose gel The restriction products were electrophoresed on 2.5% agarose gel. The molecular weight of the cutting products has been compared to the molecular weight of the uncut DNA fragment and to negative controls.

Immunohistochemistry was performed on cardiac tissue samples utilising polyclonal antibodies anti-Na^+ CP type Vα (C-20; Santa Cruz, CA, USA) and a terminal deoxynucleotidyl transferase deoxyuridine triphosphate nick end labeling (TUNEL) assay (Chemicon, Temecula, CA, USA). We used 4-μm-thick paraffin sections mounted on slides covered with 3, amminopropyl-triethoxysilane (Fluka, Buchs, Switzerland). A pretreatment was necessary to facilitate antigen retrieval and to increase membrane permeability to antibodies boiling slides in 0.1-M citric acid buffer for 14 min. The primary antibody was applied in a 1:500 ratio for 120 min at 20°C. The detection system utilized was the LSAB+ kit (Dako, Copenhagen, Denmark), a refined avidin–biotin technique in which a biotinylated secondary antibody reacts with several peroxidase-conjugated streptavidin molecules. The sections were covered with the TdT enzyme, diluted in a ratio of 30% in reaction buffer (Apotag Plus Peroxidase In Situ Apoptosis Detection Kit, Chemicon) and incubated for 60 min at 38°C. The positive reaction was visualized by 3.3 diaminobenzidine (DAB) peroxidation, according to standard methods. The sections were counterstained with Mayer's hematoxylin, dehydrated, coverslipped, and observed in a Leica DM5000B optical microscope (Leica, Cambridge, UK).

In order to obtain the determination of the fraction of myocyte nuclei labeled by TUNEL, the number of myocyte nuclei per unit area of tissue was determined by counting an average of ten fields, 1.4 mm^2 each, at a magnification of ×10 in each area of myocardium sampled. The percentage of apoptotic myocyte nuclei was determined. Cardiac myocytes were viewed using a confocal imaging system (CLSM SPE Leica) equipped with a krypton–argon laser beam and mounted on a Leica DM5000B microscope. A ×60 oil immersion objective with a 1.4 numerical aperture was used. Confocal laser scanning microscopy is able to produce thin and unblurred optical sections, offering the prospect of three-dimensional spatial reconstruction of the parameters of interest. We used a 506-nm beam of an argon-ion laser and the fluorescence was acquired at wavelengths of >531 nm in the line scan mode of the confocal system at rate of 5 ms per scan. A sequence of these sections collected along the z-axis can be used to render and quantitatively analyze the structure three-dimensionally.

Results

A thorough death scene investigation was conducted, showing a normal ambient air temperature; a very low carbon monoxide level was detected in the apartment. Complete autopsies were performed 24 h after death. External examination was unremarkable: no signs of traumatic injuries neither of compression of the nose or mouth or upper airway obstruction were detected. Intense cyanosis on lips and nails were observed. The results of the autopsies (body measurements, biological features, and organs' weight) are summarized in Table 2.

Internal examination failed to show congenital abnormalities and revealed epicardial petechiae and heavy lungs presenting abundant white foam on the main bronchi. Complete microscopic examinations were also conducted. Histological examination revealed polivisceral hemostasis and mild cerebral edema. Acute pulmonary edema mixed

Table 1 List of the exon mutations investigated in this study, with indication of the restriction enzymes used in RFLP analysis and restriction sites for wild-type and mutated exons

Exon number	Investigated mutation	Restriction enzyme	Restriction pattern for wild-type exon	Restriction pattern for mutated exon	Reference
9	R376H	HaeII	One site	Restriction site lost	Rossenbacker et al. 2004
12	A551T	MspA1I	Two sites	One site lost	Lai et al. 2005
16	W822X	Van91I	One site	Restriction site lost	Keller et al. 2005
21	G1319V	RcaI	No restriction site	One site inserted	Smits et al. 2002
22	V1405L	BstOI	Two sites	One site inserted	Smits et al. 2002

Table 2 Body measurements and organs' weight

	Twin A	Twin B
Birth weight (g)	1,760	1,550
APGAR		
1 min	7	7
5 min	8	8
Body measurement (cm)		
Crown-heel	59	61
Crown rump	35	35
Head circumference	37	37
Chest circumference	35	35
Abdominal circumference	33	32.5
Organ weight (g)		
Thymus (10 normal value)	28	18
Thyroid	5	4
Heart (27 normal value)	25	25
Lungs (37 normal value)	55	55
Liver (160 normal value)	138	157
Spleen (16 normal value)	15	29
Kidneys (22 normal value)	16	16
Brain (540 normal value)	530	530

with areas of acute pulmonary emphysema were recorded. Histological examination of the cardiac conduction system was unremarkable.

Toxicological analyses conducted on blood and urine samples were negative for drugs of abuse. Microbiologic studies, including bacterial and viral cultures of blood, heart, and lungs, were negative. Radiology, vitreous chemistry, and metabolic screening were negative.

In conclusion, death scene investigation, macroscopic and microscopic findings, toxicological and microbiologic analyses, radiology, vitreous chemistry, and metabolic screening did not yield any specific cause of death.

The results of our genetic analyses showed that between the exons investigated, the mutated genotype was assessed in exon 16. Figure 1 shows the restriction pattern of exon 16 amplified from the investigated patients and subjected to restriction fragment length polymorphism analysis. The PCR product of exon 16 is a 400-bp band, which was successfully amplified in the investigated subjects and in the control genome coming from cultured human cells, negative for this mutation. As visible, while the PCR product coming from control DNA (Fig. 1b) was cut from the restriction enzyme (Van 91I), showing the band of 400 bp and the 350-bp band indicative of the cut at position 26 of the exon sequence. The DNA fragment coming from the investigated subjects resulted unrestricted from the restriction enzyme (Fig. 1a), therefore lacking the restriction product of 350 bp. Lack of this restriction site is a feature introduced by the mutation described as W822X [8] which results in a nonsense mutation generating a truncated form of the channel protein. The mutation is due to a point substitution of a guanine with an adenine residue, (G2466A). As a control, an overnight digestion reaction, as well as an overdigest with modified enzyme substrate was performed (not shown), resulting in the absence of restriction products indicative of enzyme cutting.

The immunohistochemical study revealed an intensive positive result to TUNEL assay (Fig. 2a) approximately 38±

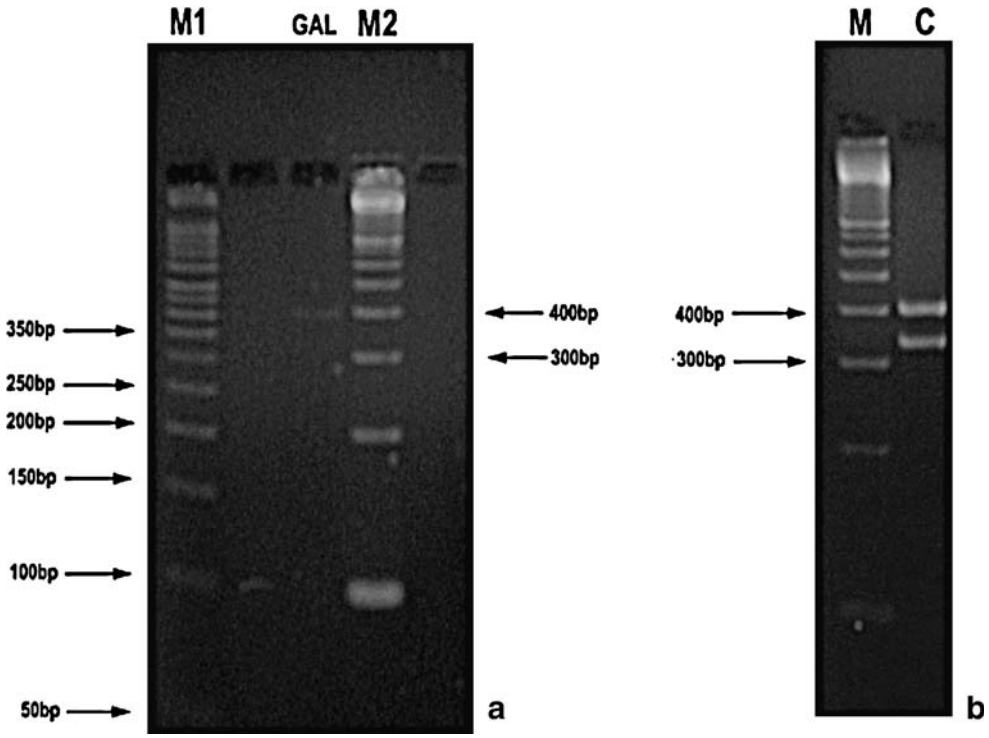

Fig. 1 Restriction pattern of exon 16 of *SCN5A* gene in investigated patients and in control DNA from cultured human cells. **a** Restriction pattern of exon 16 in the investigated subject; *M1* 50-bp ladder; *M2* 100-bp ladder; *GAL* restriction product of exon 16, revealing only the unrestricted fragment. **b** Restriction pattern of exon 16 amplified from control DNA of a human cell line; *M* 100-bp ladder; *C* restriction products of exon 16, showing the presence of both the unrestricted band (400 bp) and the cleavage product at about 350 bp

18% apoptotic cells were observed compared to 3±1% in control hearts. This result is questionable because its low specificity questions the diagnostic value of this method in autopsy pathology practice; apoptosis is also present as the effect of nonspecific triggers, such as the increase in wall stress. The cellular localization of the Na^+ CP type Vα (C-20) demonstrated by confocal laser microscopy on staining pattern of myocytes was concentrated in the intercalated disks of ventricular myocytes (Fig. 2b–c). Our results confirm the specific localization of this subtype of sodium channels to the intercalated disk (Fig. 2d). Heterozygote expression in twins hearts showed a nearly 50% reduction in Na^+ channels expression in ventricular myocytes in respect to control cases (Fig. 3).

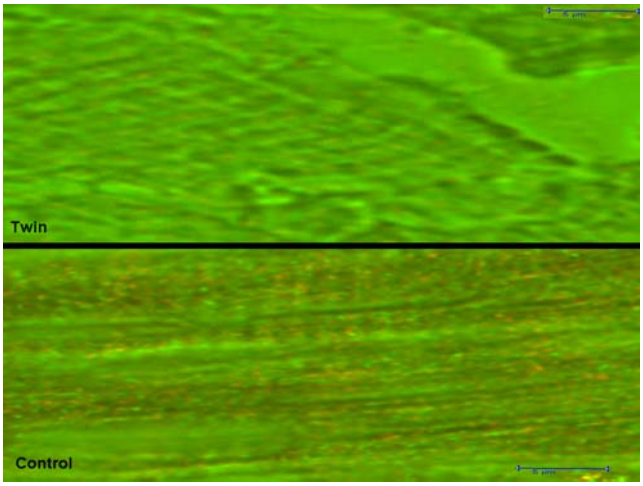

Fig. 3 Confocal laser scanning microscope: heterozygote expression in twin's heart shows a nearly 50% reduction in Na^+ channels expression (orange punctate positiveness) in ventricular myocytes in respect to control case

Discussion

In both twins, the molecular analysis showed a heterozygous nonsense SCN5A mutation (W822X) generating a truncated form of the cardiac channel protein (SCN5A gene mutation associated with Brugada syndrome (BS) phenotype). The mutation was firstly reported by Keller et al. [8] in a family with BS and was present in the index patient diagnosed with BS after surviving a sudden cardiac arrest, in his brother who had a typical BS phenotype and in their father who transmitted the mutation and was a silent mutation carrier without the BS phenotype. This mutation generates a truncated form of the channel protein and a loss of $Na_v1.5$ protein function. The W822X mutation was predicted to cause premature Na^+ channel protein truncation, with parts of domains II, III, and IV missing. Although the truncated protein was localized at the membrane surface, it was functionally an inactive channel [8]. This mutation results in a loss of Na^+ channel function. Alterations in sodium channel expression and function are known to have severe effects on excitability. In the heart, mutations in the gene encoding Nav1.5 cause inherited hyperexcitability syndromes, including long QT syndrome

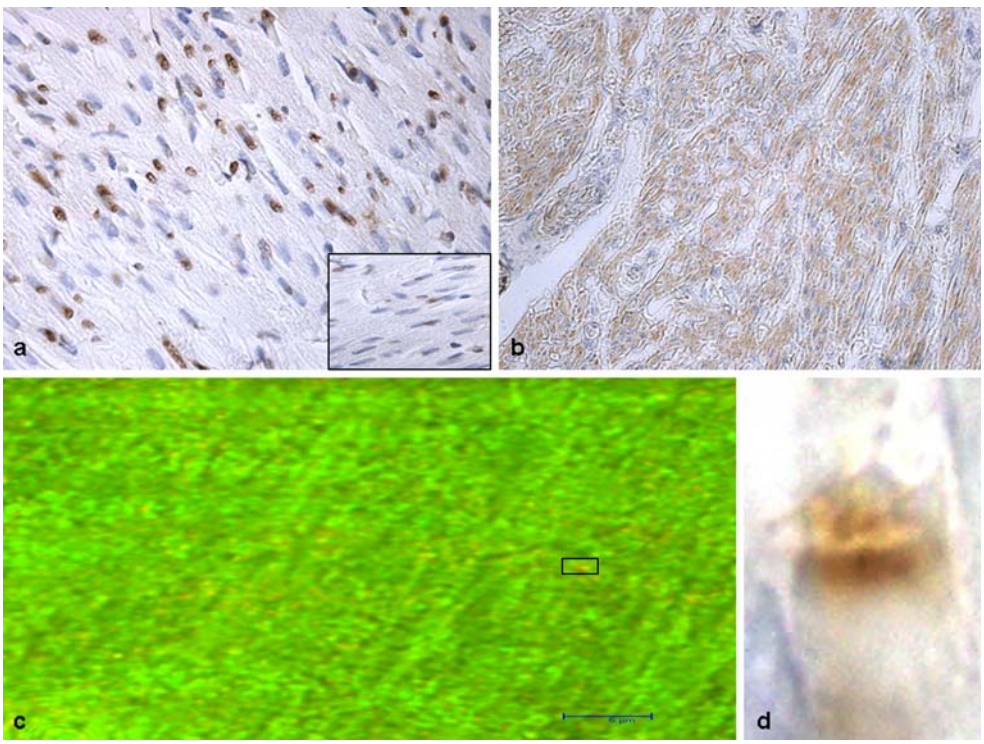

Fig. 2 **a** Determination of apoptotic cardiomyocytes nuclei by TUNEL assay: intensive positive result (brown nuclei) compared to normal bleu nuclei (*insert*: negative control) ×60. **b** Immunolocalization of Na^+ CP type Vα (C-20) in ventricular myocytes (brown reaction) ×40. **c** Confocal laser scanning microscope: staining for Na^+ CP type Vα (C-20) shows punctate positiveness (orange) along the z-lines (*insert* in **d**). **d** High magnification of a portion of a ventricular myocyte labeled for Na^+ CP type Vα (C-20; brown), demonstrating localization of Na^+ CP type Vα (C-20) at an intercalated disk

type III and Brugada syndrome, which can lead to sudden cardiac death. Differential expression and localization of sodium channel subunits are likely to be important determinants of electric excitability of cardiac myocytes [11, 13, 19, 25]. Cardiac ion channel genes, particularly SCN5A, have been hypothesized as candidate gene(s) for SIDS [29].

SIDS deaths among twins have received a little attention in the medical community and very limited information was provided in the literature. As referred by Koehler et al. [9], in the first worldwide review of cases, the medical literature has mainly focused in the deaths of single infants while the topic of SSIDS has been directly assessed in only a few articles [6, 10, 18, 26]. The study found that only 12 pairs of twins met all the three criteria (29.2%), nine pairs met two criteria (21.9%), alternative cause of death was offered in five pairs of twins (121%), and in the remaining 15 pairs (36.6%) only limited information was available. In 2007, a case of simultaneous infant death syndrome [4] was described in which both infants were healthy and did not have any serious medical history, except for the fact that 2 days prior to deaths the twins had received the second dose of oral polio, DPT, and the first dose of hepatitis B vaccines. Death scene investigation, judicial investigation, parental assessment, macroscopic and microscopic autopsy findings, and toxicological analysis were consistent for SIDS.

The statement that forensic investigation of SSIDS involves a thorough death scene investigation, detailed review of clinical history, and complete autopsy, toxicology, radiology, pathology, and microbiology studies to determine the cause and manner of death and the contributory factors is no more adequate. Clinical, epidemiological, and/or neuropathological observations have strongly supported a genetic basis for SIDS [27], with subsequent pursuit of candidate genes in five categories: (a) genes for ion channel proteins based on electrocardiographic evidence of prolonged QT intervals in SIDS victims, (b) gene for serotonin transporter based on decreased serotonergic receptor binding in brainstems of SIDS victims, (c) genes pertinent to the early embryology of the autonomic nervous system (ANS; and with a link to the 5-HT system) based on reports of ANS dysregulation in SIDS victims [15], (d) genes for nicotine-metabolizing enzymes based on evidence of cigarette smoking as a modifiable risk factor for SIDS [14], and (e) genes regulating inflammation, energy production, hypoglycemia, and thermal regulation based on reports of postnatal infection, low birth weight, and/or overheating in SIDS victims [36]. Cardiac ion channel genes, particularly SCN5A, have been hypothesized as candidate gene(s) for SIDS [29]. Heterozygous mutations in the cardiac voltage-gated sodium channel α-subunit gene (SCN5A) have been implicated in rare, familial types of cardiac arrhythmogenic disorders, involving long QT syndrome variant type 3 (LQT3), Brugada syndrome, and progressive cardiac conduction defect (PCCD) or Lev–Lenegre disease syndrome [16]. The SCN5A gene encodes the α-subunit of human cardiac voltage-dependent sodium channel, hNa_v 1.5. This channel produces a depolarizing inward sodium current I_{Na} and subsequently inactivates within milliseconds. The mechanisms of how SCN5A mutations lead to different cardiac electrical diseases are still under investigation. In general, SCN5A mutations leading to the BS phenotype are associated with a loss of channel function with a reduction of the Na^+ current. Maier et al. [13] proposed that the Nav1.5 channels in intercalated disks are involved primarily in initiation and propagation of the cardiac action potential from cell to cell.

Each channelopathy is capable of causing sudden unexpected death during infancy [28]. Data from the literature evidence that molecular aberrations in cardiac ion channels implicated in these heritable arrhythmia syndromes account for a significant proportion (10–15%) of SIDS [30]. Since 1998, Schwartz et al. [20] provided evidence to support the QT hypothesis in the pathogenesis of SIDS; several report of the literature provide strong evidence of a link between mutations in sodium-channel-interacting protein gene and SIDS. In 2000, Schwartz et al. [21] reported a spontaneous mutation on the SCN5A in an infant who nearly died of SIDS. Several reports identified mutation in the SCN5A gene in infants with aborted or experienced SIDS [17, 21, 22, 35]. Defects in the SCN5A gene were discovered in 2% of infants from a 2-year population-based cohort of SIDS by Ackerman [1] in the first systematic survey of autopsied SIDS or unexplained infant death cases. SCN5A mutations were identified in cases of sudden unexplained nocturnal death syndrome, a disease allelic to Brugada syndrome [31]. A near-miss case of SIDS due to Brugada syndrome has been reported in 2005 by Skinner et al. [24] who discovered a heterozygous mutation in position 3578 of the SCN5A coding sequence in a 19-day-old male who experienced a ventricular fibrillation successfully treated with DC cardioversion. In a recent study, Wang et al. [34] greatly expanded the spectrum of functionally characterized SCN5A variants associated with SIDS. Arnestad et al. [2] reported data which provide strong evidence that overt or latent functional LQTS gene variants are associated with 9.5% of SIDS cases. The case for cardiac channelopathies in SIDS has been extended recently to cardiac potassium channels as Schwartz et al. [22] presented a case involving a de novo mutation in KVLQT1, the gene most frequently associated with LQT syndrome. In 2007, Van Norstrand et al. [30] reported a novel mutation in the glycerol-3-phosphate dehydrogenase-1-like gene (GPD1-L), a gene associated with Brugada (BrS2), in three victims of SIDS.

Conclusions

Taken together, all these findings suggest that defective ion channels represent viable candidates for the pathogenesis of SIDS and, obviously, of SSIDS, supporting a link between sudden infant death syndrome and cardiac channelopathies. Heterozygous nonsense SCN5A mutation W822X explained this simultaneous sudden infant death syndrome: does it make mandatory the genetic screening for channelopathies in such cases? Given the diversity of results to date, genetic studies support the clinical impression that SSIDS is heterogeneous with more than one entity and with more than one possible genetic etiology. Future studies should consider expanded phenotypic features that might help clarify the heterogeneity and improve the predictive value of the identified genetic factors [3, 36].

Conflict of interest statement We declare that we have no conflict of interest.

References

1. Ackerman MJ, Siu BL, Sturner WQ, Tester DJ, Valdivia CR, Makielski JC, Towbin JA (2001) Postmortem molecular analysis of SCN5A defects in sudden infant death syndrome. JAMA 286:2264–2269
2. Arnestad M, Crotti L, Rognum TO, Insolia R, Pedrazzini M, Ferrandi C, Vege A, Wang DW, Rhodes TE, George AL Jr, Schwartz PJ (2007) Prevalence of long-QT syndrome gene variants in sudden infant death syndrome. Circulation 115:361–367
3. Bajanowski T, Brinkmann B, Vennemann M (2006) The San Diego definition of SIDS: practical application and comparison with the GeSID classification. Int J Legal Med 120:331–336
4. Balci Y, Tok M, Kocaturk BK, Yenilmez C, Yirulmaz C (2007) Simultaneous sudden infant death syndrome. J Forensic Leg Med 14:87–91
5. Cao W, Hashibe M, Rao J-Y, Morgenstern H, Zhang Z-F (2003) Comparison of methods for DNA extraction from paraffin-embedded tissues and buccal cells. Cancer Detect Prev 27:397–404
6. Guyer B, Martin JA, MacDorman MF, Anderson RN, Strobino DM (1997) Annual summary of vital statistics—1996. Pediatrics 100:905–918
7. Jackson PJ, Hugh-Jones ME, Adair DM, Green G, Hill KK, Kuske CR, Grinberg LM, Abramova FA, Keim P (1998) PCR analysis of tissue samples from the 1979 Sverdlovsk anthrax victims: the presence of multiple *Bacillus anthracis* strains in different victims. Proc Natl Acad Sci USA 95:1224–1229
8. Keller DI, Barrane FZ, Gouas L, Martin J, Pilote S, Suarez V, Osswald S, Brink M, Guicheney P, Schwick N, Chahine M (2005) A novel nonsense mutation in the SCN5A gene leads to Brugada syndrome and a silent gene mutation carrier state. Can J Cardiol 21:925–931
9. Koehler SA, Ladham S, Shakir A, Wecht CH (2001) Simultaneous sudden infant death syndrome: a proposed definition and worldwide review of cases. Am J Forensic Med Pathol 22:23–32
10. Ladham S, Koehler SA, Shakir A, Wecht CH (2001) Simultaneous sudden infant death syndrome: a case report. Am J Forensic Med Pathol 22:33–37
11. Lai LP, Su YN, Hsieh FJ, Chiang FT, Juang JM, Liu YB, Ho YL, Chen WJ, Yeh SJ, Wang CC, Ko YL, Wu TJ, Ueng KC, Lei MH, Tsao HM, Chen SA, Lin TK, Wu MH, Lo HM, Huang SK, Lin JL (2005) Denaturing high-performance liquid chromatography screening of the long QT syndrome-related cardiac sodium and potassium channel genes and identification of novel mutations and single nucleotide polymorphisms. J Hum Genet 50:490–496
12. Lehmann U, Kreipe H (2001) Real-time PCR analysis of DNA and RNA extracted from formalin-fixed and paraffin-embedded biopsies. Methods 25:409–418
13. Maier SK, Westenbroek RE, McCormick KA, Curtis R, Scheuer T, Catterall WA (2004) Distinct subcellular localization of different sodium channel alpha and beta subunits in single ventricular myocytes from mouse heart. Circulation 109:1421–1427
14. Matturri L, Ottaviani G, Lavezzi AM (2006) Maternal smoking and sudden infant death syndrome: epidemiological study related to pathology. Virchows Arch 449:697–706
15. Matturri L, Ottaviani G, Lavezzi AM (2008) Guidelines for neuropathologic diagnostics of perinatal unexpected loss and sudden infant death syndrome (SIDS)—a technical protocol. Virchows Arch 452:19–25
16. Moric E, Herbert E, Trusz-Gluza M, Filipecki A, Mazurek U, Wilczok T (2003) The implications of genetic mutations in the sodium channel gene (SCN5A). Europace 5:325–334
17. Priori SG, Napolitano C, Giordano U, Collisani G, Memmi M (2000) Brugada syndrome and sudden cardiac death in children. Lancet 355:808–809
18. Ramos V, Hernandez AF, Villanueve E (1997) Simultaneous death of twins. Am J Forensic Med Pathol 18:75–78
19. Rossenbacker T, Carroll SJ, Liu H, Kuipéri C, de Ravel TJ, Devriendt K, Carmeliet P, Kass RS, Heidbüchel H (2004) Novel pore mutation in SCN5A manifests as a spectrum of phenotypes ranging from atrial flutter, conduction disease, and Brugada syndrome to sudden cardiac death. Heart Rhythm 5:610–615
20. Schwartz PJ, Stramba-Badiale M, Segantini A, Austoni P, Bosi G, Giorgetti R, Grancini F, Marni ED, Perticone F, Rosti D, Salice P (1998) Prolongation of the QT interval and the sudden infant death syndrome. N Engl J Med 338:1709–1714
21. Schwartz PJ, Priori SG, Dumaine R, Napolitano C, Antzelevitch C, Stramba-Badiale M, Richard TA, Berti MR, Bloise R (2000) A molecular link between the sudden infant death syndrome and the long-QT syndrome. N Engl J Med 343:262–267
22. Schwartz PJ, Priori SG, Bloise R, Napolitano C, Ronchetti E, Piccinini A, Goj C, Breithardt G, Schulze-Bahr E, Wedekind H, Nastoli J (2001) Molecular diagnosis in victims of sudden infant death syndrome. Lancet 358:1342–1343
23. Shedlock AM, Haygood MG, Pietsch TW, Bentzen P (1997) Enhanced DNA extraction and PCR amplification of mitochondrial genes from formalin-fixed museum specimens. Biotechniques 22:394–396
24. Skinner JR, Chung SK, Montgomery D, McCulley CH, Crawford J, French J, Rees MI (2005) Near-miss SIDS due to Brugada syndrome. Arch Dis Child 90:528–529
25. Smits JP, Eckardt L, Probst V, Bezzina CR, Schott JJ, Remme CA, Haverkamp W, Breithardt G, Escande D, Schulze-Bahr E, LeMarec H, Wilde AA (2002) Genotype–phenotype relationship in Brugada syndrome: electrocardiographic features differentiate SCN5A-related patients from non-SCN5A-related patients. J Am Coll Cardiol 40:350–356
26. Spiers PS (1974) Estimated rates of concordance for the sudden infant death syndrome in twins. Am J Epidemiol 100:1–7
27. Task Force on Sudden Infant Death Syndrome (2005) The changing concept of sudden infant death syndrome: diagnostic coding shifts, controversies regarding the sleeping environment, and new variables to consider in reducing risk. Pediatrics 116:1245–1255

28. Tester DJ, Ackerman MJ (2005) Sudden infant death syndrome: how significant are the cardiac channelopathies? Cardiovasc Res 67:388–396
29. Towbin JA, Friedman RA (1998) Prolongation of the QT interval and SIDS. N Engl J Med 338:1760–1761
30. Van Norstrand DW, Valdivia CR, Tester DJ, Ueda K, London B, Makielski JC, Ackerman MJ (2007) Molecular and functional characterization of novel glycerol-3-phosphate dehydrogenase 1 like gene (GPD1-L) mutations in sudden infant death syndrome. Circulation 116:2253–2259
31. Vatta M, Dumaine R, Varghese G, Richard TA, Shimizu W, Aihara N, Nademanee K, Brugada R, Brugada J, Veerakul G, Li H, Bowles NE, Brugada P, Antzelevitch C, Towbin JA (2002) Genetic and biophysical basis of sudden unexplained nocturnal death syndrome (SUNDS), a disease allelic to Brugada syndrome. Hum Mol Genet 11:337–345
32. Wang Q, Shen J, Splawski I, Atkinson D, Li Z, Robinson JL, Moss AJ, Towbin JA, Keating MT (1995) SCN5A mutations associated with an inherited cardiac arrhythmia, long QT syndrome. Cell 80:805–811
33. Wang Q, Li Z, Shen J, Keating MT (1996) Genomic organization of the human SCN5A gene encoding the cardiac sodium channel. Genomics 34:9–16
34. Wang DW, Desai RR, Crotti L, Arnestad M, Insolia R, Pedrazzini M, Ferrandi C, Vege A, Rognum T, Schwartz PJ, George AL Jr (2007) Cardiac sodium channel dysfunction in sudden infant death syndrome. Circulation 115:368–376
35. Wedekind H, Smits JP, Schulze-Bahr E, Arnold R, Veldkamp MW, Bajanowski T, Borggrefe M, Brinkmann B, Warnecke I, Funke H, Bhuiyan ZA, Wilde AA, Breithardt G, Haverkamp W (2001) De novo mutation in the SCN5A gene associated with early onset of sudden infant death. Circulation 104:1158–1164
36. Weese-Mayer DE, Ackerman MJ, Marazita ML, Berry-Kravis EM (2007) Sudden infant death syndrome: review of implicated genetic factors. Am J Med Genet A 143:771–788

Virchows Arch (2008) 453:217–219
DOI 10.1007/s00428-008-0623-8

LETTER TO THE EDITOR

Chronic lymphedema due to morbid obesity: an exceptional cause of abdominal wall angiosarcoma

Sebastien Salas · Nathalie Stock · Eberhard Stoeckle · Michele Kind · Binh Bui · Jean-Michel Coindre

Received: 15 April 2008 / Accepted: 28 April 2008 / Published online: 17 June 2008

Sir,

Angiosarcomas are rare malignant soft tissue tumors that show differentiation toward endothelial cells occurring in various clinical settings, including lymphedema-associated angiosarcoma, idiopathic angiosarcoma on the head and neck in elderly people, angiosarcoma arising on chronically sun-damaged skin and post-irradiation angiosarcoma [4]. Chronic lymphedema secondary to mastectomy and axillary lymphadenectomy for breast cancer, and more rarely to infectious disease, congenital disease and traumatism, is a known predisposing condition for cutaneous and superficial soft tissue angiosarcoma. We report a new case of high-grade abdominal wall angiosarcoma in a chronically lymphedematous abdominal panniculus due to morbid obesity.

A 44-year-old morbidly obese man presented with a skin lesion in the periumbilical region. Clinical examination revealed a 10-cm papular lesion on a post-operative abdominal wall hernia. There was a clinical history of Crohn's disease diagnosed 34 years previously. Treatment included many abdominal operations. A contrast-enhanced computed tomography scan of the abdomen revealed extensive heterogeneous thickening of the skin and subcutaneous fat, with infiltration of the abdominal musculature (Fig. 1). In October 2006, a dermolipectomy was performed. Histologically, the tumor involved the whole dermis, subcutaneous fat with an infiltrative pattern and margins. Beside the tumor, many ectatic vessels lined by a normal appearing endothelium were noted (Fig. 2a). Cell proliferation consisted of solid sheets of fusiform cells with

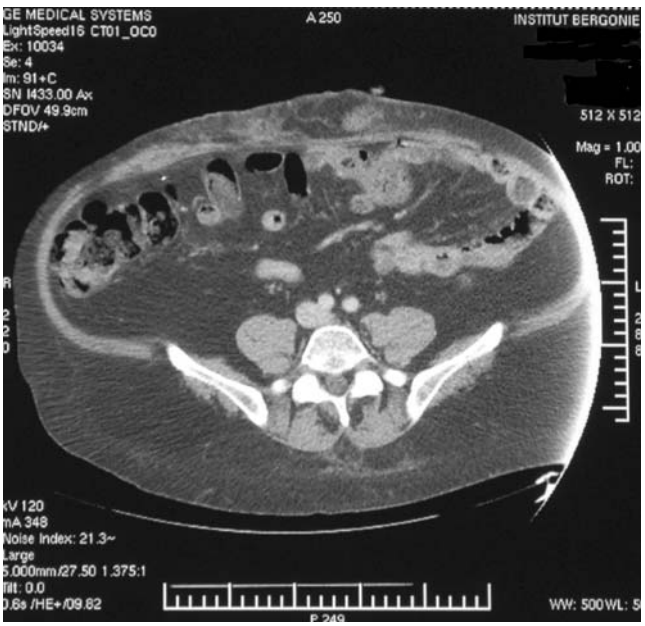

Fig. 1 Contrast-enhanced computed tomography scan of abdomen: extensive heterogeneous thickening of the skin and subcutaneous fat, with infiltration of the abdominal musculature

S. Salas · N. Stock · J.-M. Coindre
Departments of Pathology, Institut Bergonié. 229, cours de l'Argonne,
33076 Bordeaux Cedex, France

E. Stoeckle
Departments of Surgery, Institut Bergonié,
Bordeaux, France

M. Kind
Departments of Radiology, Institut Bergonié,
Bordeaux, France

B. Bui
Departments of Oncology, Institut Bergonié,
Bordeaux, France

N. Stock · J.-M. Coindre (✉)
University Victor Ségalen,
Bordeaux, France
e-mail: coindre@bergonie.org

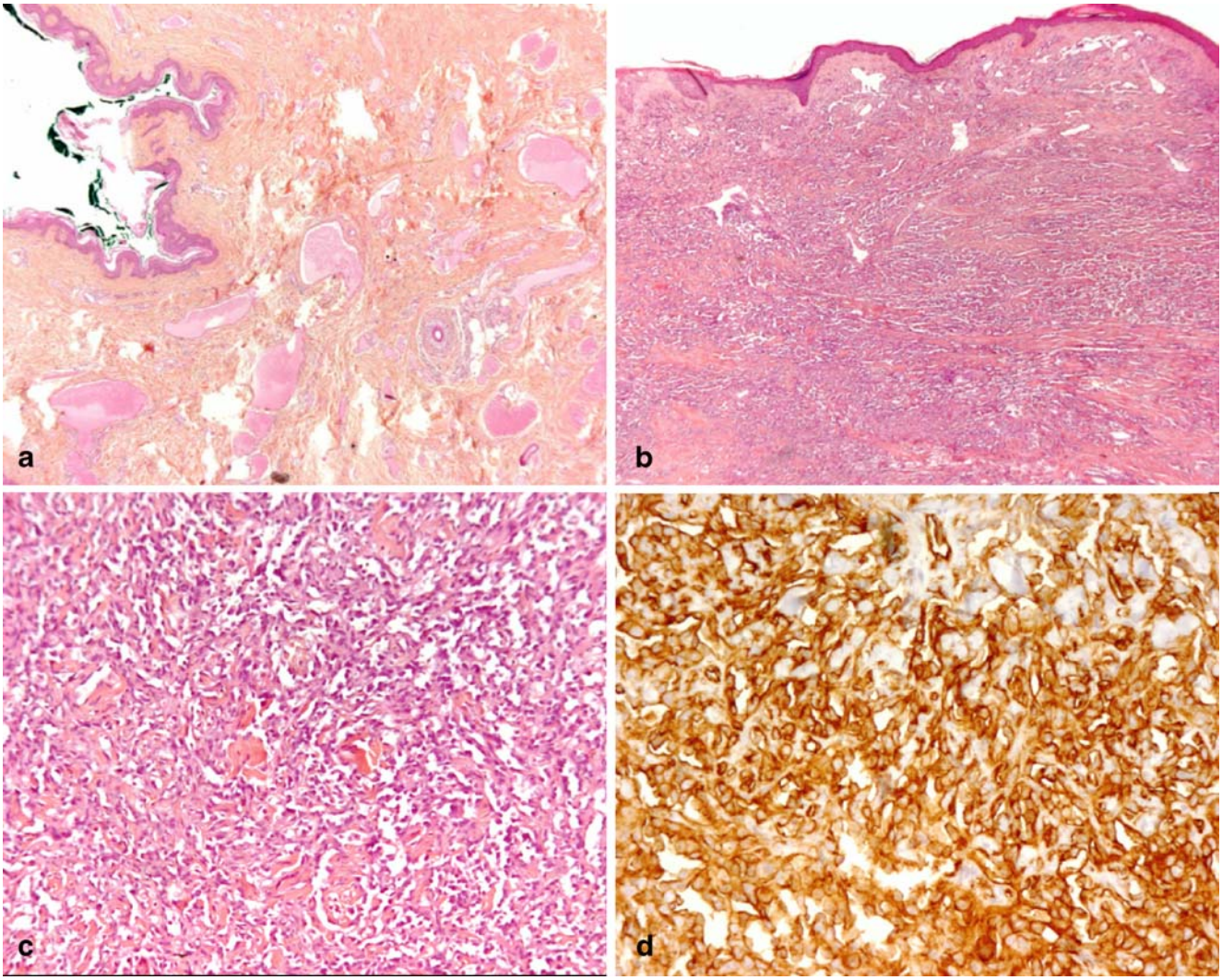

Fig. 2 Histological features of the angiosarcoma. **a** Chronic lymphedema of the abdominal wall with ectatic lymphatic vessels in the dermis at the periphery of the tumor (Hematoxylin eosin safran (HES), ×40). **b** Angiosarcoma with spindle cells infiltrating the whole dermis and subcutis and dissociating collagen bundles (HES, ×40). **c** Irregular vascular channels lined by atypical cells with irregular and hyperchromatic nuclei (HES, ×200). **d** Strong cytoplasmic staining of neoplastic cells by anti-CD31 antibody (×400)

branching irregular vascular channels infiltrating between collagen bundles and adipocytes (Fig. 2b). These structures were lined by a neoplastic endothelium with an irregular, round-to-oval, hyperchromatic nucleus and prominent nucleolus. Anisocaryosis was discrete and pleomorphic cells were not seen (Fig. 2c). Mitotic count was 19 per 10 high-power fields. Immunohistochemistry showed a diffuse and strong positivity of tumor cells for CD34, CD31 and D2–40 (Fig. 2d). The patient had microscopically incomplete tumor resection. From November 2006 to February 2007, he received four cycles of MAID (Mesna 2,500 mg/m^2/day, days 1 to 4; Doxorubicin 20 mg/m^2/day, days 1 to 3; Ifosfamide 2,500 mg/m^2/day, days 1 to 3; and Dacarbazine 300 mg/m^2/day days 1 to 3, every 3 weeks) owing to the aggressiveness and the metastatic potential of the tumor. Despite three surgical re-excisions, it was not possible to obtain microscopically complete tumor resection. Postoperative radiotherapy could not be performed because of his Crohn's disease history and the voluminous abdominal wall hernia. In June 2007, an early multifocal recurrence was observed so he was treated with paclitaxel. Disease progression occurred after eight cycles and he died 11 months after the diagnosis.

Since 1984, 90 angiosarcomas have been collected in the French Sarcoma Group clinical database, including three located in the abdominal wall. Only one patient presented morbid obesity. The two others had a previous history of abdominal radiotherapy. Since 1986, only four cases of abdominal angiosarcoma in morbidly obese patients have been reported in the literature, usually with rapid disease progression [1–3, 5]. Our case is the first demonstration of histological lymphedema in this rare setting. In all the

cases, morbid obesity and subsequent chronic lymphedema of the abdominal wall were postulated to be the etiological factors implicated in the development of angiosarcoma. Only one other case had a previous history of abdominal surgery [1]. Thus, we postulate that the combination of surgical treatment and morbid obesity, which both impair lymphatic flow, may be the cause of abdominal wall angiosarcoma. Angiosarcoma in this location has a very aggressive clinical course, even after complete ablation. Although the reports vary, as a whole the prognosis of angiosarcomas associated with chronic lymphedema is dismal, with an overall expected survival of 1 to 2 years. Abdominal wall angiosarcomas in morbidly obese patients are extremely rare, despite the increasing prevalence of obesity in the general population. However, any suspicious cutaneous lesion should be biopsied in order to establish a prompt diagnosis.

Acknowledgement Dr Ray Cooke is thanked for reviewing and editing the manuscript.

Conflict of interest statement We declare that we have no conflict of interest.

References

1. Aguiar Bujanda D, Camacho Galan R, Bastida Inarrea J, Aguiar Morales J, Conde Martel A, Rivero Suarez P, de Armas Diaz F, Bohn Sarmiento U, Cabrera Suarez MA (2006) Angiosarcoma of the abdominal wall after dermolipectomy in a morbidly obese man. A rare form of presentation of Stewart-Treves syndrome. Eur J Dermatol 16:290–292
2. Azam M, Saboorian H, Bieligk S, Smith T, Molberg K (2001) Cutaneous angiosarcoma complicating morbid obesity. Arch Pathol lab Med 125:531–533
3. Krause KI, Hebert AA, Sanchez RL, Solomon AR (1986) Anterior abdominal wall angiosarcoma in a morbidly obese woman. J Am Acad Dermatol 15:327–330
4. Naka N, Ohsawa M, Tomita Y, Kanno H, Uchida A, Aozasa K (1995) Angiosarcoma in Japan. A review of 99 cases. Cancer 75:989–996
5. Shehan JM, Ahmed I (2006) Angiosarcoma arising in a lymphedematous abdominal pannus with histologic features reminiscent of Kaposi's sarcoma: report of a case and review of the literature. Int J Dermatol 45:499–503

Virchows Arch (2008) 453:221–222
DOI 10.1007/s00428-008-0628-3

LETTER TO THE EDITOR

Estrogen receptors alpha and beta in adrenal cortical neoplasia: heterogeneity and physiological implications

Despina Georgiadou · Theodoros N. Sergentanis · Akrivi Kostopoulou · George N. Zografos · George Papastratis

Received: 20 March 2008 / Revised: 5 May 2008 / Accepted: 7 May 2008 / Published online: 13 June 2008

Dear Editor,

In a recently published article in *Virchows Archiv*, Barzon et al. thoroughly examined the expression of estrogen receptors in human adrenocortical tumors [1]. Given the lack of systematic evidence in the literature, we had independently hypothesized that estrogen receptor alpha-to-beta ratio might be an important counterpart in adrenal cortical neoplasia [2].

Following our initial hypothesis, we have immunohistochemically evaluated the expression of ER-alpha and ER-beta in 38 adrenal adenomas, 7 adrenal cortical carcinomas (ACCs), and 23 normal adrenal tissue samples from unrelated patients. Among the 38 adenomas, 20 were nonfunctioning adenomas (NFA), 9 were cortisol-producing adenomas (CPAs), and 9 were aldosterone-producing adenomas (APAs). For ER-alpha and ER-beta immunohistochemical assessment, the monoclonal mouse anti-human ER-alpha clone1D5 (DakoCytomation, Glostrup, Denmark) and the AR385-5R anti ER-beta antibody (Biogenex, San Ramon, CA, USA) were respectively used.

Statistical analysis was performed with STATA 8.0 statistical software (Stata Corp, College Station, TX, USA). To avoid multiple comparison adjustments versus the control (normal tissue) group, which would diminish the study power given the small sample size, the analysis is principally oriented within the adenoma subpopulation, which is at any case the main focus of this Letter. We believe that the results below come to complement those reported by Barzon et al., as the latter have not performed immunohistochemistry upon the adrenocortical adenoma subpopulation, proceeding directly to reverse transcriptase-polymerase chain reaction (RT-PCR) assessment therein.

Regarding ER-alpha expression within the adenoma subpopulations, 10 out of 20 NFA exhibited occasional positivity (defined as <1% cells), whereas the occasional positivity rate was 4 out of 9 in CPA, decreasing to 0% (0 out of 9) in APA. The documented variability in the occasional positivity rate was statistically significant (p= 0.032, Fisher's exact test). Noticeably, the occasional positivity rate in normal adrenal tissue was 2 out of 23.

By means of quantitative RT-PCR, Barzon et al. demonstrated that there is significant heterogeneity in ER-alpha mRNA content, pointing to lesser expression in NFAs. On the one hand, our finding confirms that there is considerable variability in ER-alpha expression between the different adenoma subtypes. On the other hand, however, our results are suggestive of lower expression in APAs. Surprisingly enough, the absolute immunohistochemical negativity in APAs is in line with physiological data: estrogen attenuates the angiotensin–aldosterone pathway acting on the adrenal zona glomerulosa [3]; consequently, diminished estrogen receptor protein expression may be in favor of excessive aldosterone production.

Regarding ER-beta immunohistochemical evaluation, the occasional positivity rate did not exhibit statistically significant heterogeneity, as it was equal to 10 out of 19 in NFAs (in one case 20% of cells were ER-beta positive, far beyond the occasional threshold; as a result, the case was thus not included in the calculation), 3 out of 9 in CPAs, and seven out of nine in APAs (p=0.385, Fisher's exact

D. Georgiadou (✉) · T. N. Sergentanis · G. N. Zografos · G. Papastratis
3rd Surgical Clinic, "George Gennimatas" General Hospital,
154, Mesogeion Avenue,
Athens 156 69, Greece
e-mail: desangeor@yahoo.gr

A. Kostopoulou
Department of Pathology,
"George Gennimatas" General Hospital,
Athens, Greece

test). This is indirectly in agreement with the results by Barzon et al., who reported no significant deviation from the control group. In our control group, ER-beta were positive in 6 out of 23 samples (2–5% of cells stained), occasionally positive in 11 out of 23 samples and negative in 6 out of 23 samples.

Concerning ACC, the ER-alpha occasional positivity rate was two out of seven, comparable to that reported by Barzon et al. (1 out of 16; $p=0.209$, Fisher's exact test). With respect to ER-beta, a rather fainter profile arose (Barzon et al. reported 12 out of 16 percentage of immunoreactivity); we detected 1 out of 7 cases exhibiting 10% positivity, 4 out of 7 cases exhibiting occasional positivity, and 2 out of 7 cases being negative. With respect to the control-versus-ACC comparison in our study, statistically significant differences emerged neither for ER-alpha (2 out of 23 vs. 2 out of 7 occasional positivity rate; $p=0.225$, Fisher's exact test) nor for ER-beta (6 out of 23 vs. 1 out of 7 positivity rate; $p=0.653$, Fisher's exact test). Nevertheless, because of the limited power of the present study, the emergence of differences in larger studies cannot be excluded.

In conclusion, further studies on larger samples are needed, focusing on the different adenoma subtypes. The present letter is of suggestive nature, given that: (1) the expression of estrogen receptors was in general minimal and (2) immunohistochemistry has to be complemented and verified by quantitative methods. Indeed, in this letter, the discrepancies were noted principally at the level of occasional immunohistochemical positivity; the precise quantitative aspects and implications of such discrepancies remain to be assessed on large adenoma series. Intra-subtype and inter-subtype variability in ER expression are issues that should ideally be addressed.

Slight though, differences in estrogen receptor expression may reveal discrepancies in the physiological behavior of adrenal adenomas, which remain to be clarified in the future.

References

1. Barzon L, Masi G, Pacenti M, Trevisan M, Fallo F, Remo A, Martignoni G, Montanaro D, Pezzi V, Palù G (2008) Expression of aromatase and estrogen receptors in human adrenocortical tumors. Virchows Arch 452:181–191
2. Georgiadou D, Sergentanis TN, Papastratis G (2008) Estrogen receptor alpha to beta ratio: A counterpart also in adrenal cortical neoplasia? Med Hypotheses 70:1225
3. Wu Z, Maric C, Roesch DM, Zheng W, Verbalis JG, Sandberg K (2003) Estrogen regulates adrenal angiotensin AT1 receptors by modulating AT1 receptor translation. Endocrinology 144:3251–3261

Virchows Arch (2008) 453:223–231
DOI 10.1007/s00428-008-0650-5

REVIEW AND PERSPECTIVE

The endometrial hyperplasias revisited

Efthimios Sivridis · Alexandra Giatromanolaki

Received: 28 May 2008 / Revised: 28 July 2008 / Accepted: 29 July 2008 / Published online: 23 August 2008

Abstract The proliferating lesions in the endometrium form a morphological continuum extending from benign to malignant, through a transitional pre-invasive stage. Within this spectrum, several classifications of endometrial hyperplasia have been developed over the years in which the precancerous lesions gained a substantial distinction, although not without inconsistencies in definitions and terminology. The revised WHO 1994 classification explicitly recognizes cytological atypia as the defining feature for distinguishing genuine hyperplastic lesions (simple and complex endometrial hyperplasia) from those that are potentially precancerous (simple and complex atypical endometrial hyperplasia) and puts an end to the verbal anarchy by adopting a common language of communication. This taxonomy, however, was criticized for complexity and low level of reproducibility. Thus, in the name of improved reproducibility a new classification was recently proposed which (a) combines simple and complex endometrial hyperplasia within one diagnostic category known as endometrial hyperplasia and (b) defines new criteria for recognising the precancerous lesions: a monoclonal growth, known as endometrial intraepithelial neoplasia (EIN), comprising clusters of crowded glands, greater than 1 mm in diameter, having a cytologically altered epithelium. The EIN concept was challenged of not being independently tested and received with great enthusiasm by some scholars and relative skepticism by others.

Keywords Endometrial hyperplasia · Precancerous lesions · WHO · EIN

E. Sivridis (✉) · A. Giatromanolaki
Department of Pathology, Democritus University of Thrace,
and University General Hospital of Alexandroupolis,
P.O. Box 128, Alexandroupolis 68100, Greece
e-mail: esivrid@med.duth.gr

Introduction

Hyperplasia is, in general terms, an increase in the size of an organ or tissue as a result of an increase in the number of its constituent cells per unit volume. In the endometrium, there are several forms of hyperplasia, some of which progress to carcinoma. Indeed, the most common type of endometrial carcinoma, endometrioid adenocarcinoma, frequently develops from pre-existing areas of hyperplasia—a concept originally described by Thomas Cullen in 1900 [1]. In addition, the morphological continuum endometrial hyperplasia/endometrioid adenocarcinoma shares in common many genotypic alterations, including microsatellite instability, PTEN and K-ras gene mutations [2–8]. As a consequence, the form of hyperplasia which is related to endometrial adenocarcinoma (EA) with unusual frequency is considered precancerous and should be treated accordingly. It is mandatory, therefore, to distinguish the endometrial hyperplasias into those that progress into malignancy and those that do not.

Classification schemes of endometrial hyperplasia: from anarchy to WHO

Several classification schemes of endometrial hyperplasia have been introduced over the years. These were essentially biased by inadequate long-term follow up data and inconsistency in definitions and terminology. As Gore (1973) characteristically stated, "not only are different names applied to the same lesion, but the same name is applied to different lesions, presumably of different malignant potential" [9].

Thus, many scholars in the field employed the term "atypical" hyperplasia for all hyperplastic lesions of the endometrium with a presumed malignant potential [10–12].

Others used the designation "adenomatous" hyperplasia in a similar way [13–19], and still others used the two terms interchangeably [20, 21]. Interestingly, morphological distinction between "atypical" and "adenomatous" hyperplasia was exercised by a number of investigators [22–26], but they did not all use the same criteria. Beutler et al. recognized two distinct forms of hyperplasia with some malignant potential: one with atypical glandular proliferation, the other with atypical epithelial proliferation [27]. Scully and Blaustein (1980) applied the term "complex" hyperplasia [28, 29] and Hall "irregular" hyperplasia to include every form of non-invasive proliferating lesion of the endometrium other than "simple" endometrial hyperplasia [30]. Earlier workers made no attempt to differentiate endometrial hyperplasia into any form [31–33].

This era of communication failure was succeeded by the 1975 WHO (World Health Organization) classification which recognized three main forms of endometrial hyperplasia: the cystic, the adenomatous and the atypical hyperplasia [34]. In this taxonomy, cystic endometrial hyperplasia corresponds to diffuse proliferation of both glands and stroma, most commonly with cystically dilated glands. Adenomatous hyperplasia represents focal glandular proliferation with crowding and complexity. Atypical endometrial hyperplasia reflects conspicuous proliferation of glands with apparent cytological atypia.

Kurman and associates found progression to carcinoma in fewer than 3% of cases of hyperplasia without atypia (cystic and adenomatous), compared with 22% of patients with atypia (atypical hyperplasia) [35]. Comparable results reported by Ferenczy and Gelfand with progression to carcinoma was 0% versus 25% for endometrial hyperplasias lacking cytological atypia and those having this feature, respectively [36].

The aforementioned classical studies demonstrated quite clearly that the absolute criterion for differentiating the genuine hyperplastic endometrial lesions from those that are potentially precancerous is the presence of cytological atypia. In view of this development, the revised WHO94 classification provided a scheme primarily dividing hyperplasias into those with and those without cytological atypia, while the degree of glandular crowding (simple versus complex) received secondary importance (Table 1) [37]. The ambiguous term "adenomatous" was abolished since a lesion cannot be neoplastic and hyperplastic at the same time.

In the new classification, simple endometrial hyperplasia indicates lesions formerly designated as cystic hyperplasia; complex endometrial hyperplasia refers to lesions with marked glandular complexity, usually with glandular crowding [38]. Cytological atypia is characterized by nuclear changes (see under "The WHO94 criteria").

Lacey et al., classifying endometrial hyperplasia according to nuclear atypia and the severity of glandular crowding, predicted the subsequent relative risk for developing endometrial adenocarcinoma [39]. They reported progression risks RR=2.0 for simple endometrial hyperplasia, RR=2.8 for complex endometrial hyperplasia and RR=14 to 48 for atypical hyperplasia. The study included 138 cases initially diagnosed as endometrial hyperplasia and subsequently evolved to carcinoma (1970–2003). Using the same classification scheme, Horn et al. found that 2% of the cases with complex endometrial hyperplasia (eight of 390) progressed into carcinoma as compared to 52% of the atypical hyperplasia cases (58 of 112) [40]. There were also a percentage of cases (10.5%) which from complex endometrial hyperplasia transformed into atypical hyperplasia.

Table 1 The WHO75 and WHO94 classifications

WHO 1975 classification	WHO 1994 classification
Cystic glandular hyperplasia	Endometrial hyperplasia
Adenomatous hyperplasia	Simple
Atypical endometrial hyperplasia	Complex
	Atypical endometrial hyperplasia
	Simple
	Complex

The WHO94 classification: criticism and simplification

The WHO94 classification scheme, however, based on Kurman and Norris' earlier suggestions [35, 41], was criticized for complexity and low level of reproducibility [42–44]. There were indeed several challenging reports. Thus, Skov et al. found considerable intra- and inter-observer variation using both the WHO1975 and the WHO1994 classifications of endometrial hyperplasia [42]. Bergeron et al. centered on the revised WHO94 taxonomy and reported comparable results [43]. There is also the recent report of the Gynecologic Oncology Group on 306 women who were diagnosed with atypical endometrial hyperplasia (AEH) and referred for further treatment (the study was initiated to assess the efficacy of hormonal therapy); however, after re-examination of the slides by a panel of three gynecologic pathologists who used WHO criteria, significant discrepancies were identified between review and original diagnoses in 62% of the cases [44].

Skov et al. improved reproducibility of the WHO classifications by reducing the four categories to two with clinical importance: atypical endometrial hyperplasia versus others—1975 classification, and atypical endometrial hyperplasia (complex) versus others—1994 classification [42]. Bergeron et al. succeeded in increasing the reproducibility of the WHO94 classification by introducing a combined category for simple and complex hyperplasia,

called "hyperplasia", and a combined category for atypical hyperplasia and well-differentiated adenocarcinoma, called "endometrioid neoplasia" (EN) [43]. Mutter and the Endometrial Collaborative Group (ECG) in a series of articles argued for the simplification of the WHO classification by entertaining two, rather than four, categories—"benign endometrial hyperplasia" (replacing simple and complex hyperplasia) and "endometrial intraepithelial neoplasia" (EIN), representing the immediate precursor of endometrioid adenocarcinoma with a 45-fold increased cancer risk [45–50].

The EIN classification

The EIN criteria

According to Mutter's group [46], an EIN lesion, presumed to be distinct from atypical endometrial hyperplasia, should only be diagnosed if it fulfils the following molecular, morphometric and morphological criteria: (a) monoclonal growth; (b) size greater than 1 mm in diameter or more than ten glands; (c) closely packed glands with a gland area (combined epithelium and lumens) greater than stroma area (volume percentage stroma <55%); (d) cytological change that is always different from that of the adjacent normal endometrium. There should be exclusion of cancer and a variety of benign conditions with overlapping features, including basal, secretory and menstrual endometrium, polyps and cystic endometrial atrophy [45, 47, 50–52]. The above diagnostic criteria should be met in their entirety.

Some pathologists subscribed enthusiastically to these views [53]. However, before a new classification system is adopted into clinical practice, it is expected to satisfy two basic requirements: reliability and reproducibility. In this context, it is worth investigating whether or not these conditions are fulfilled in the EIN taxonomy.

Reliability of EIN

Monoclonality and neoplastic growth How strong is such an association in the endometrium? Yilmaz et al. have shown that six out of 17 (35.3%) simple endometrial hyperplasias and four out of six (66.6%) complex endometrial hyperplasias were monoclonal in the absence of cytological atypia [54]. In contrast, three of 12 (25.0%) atypical hyperplasias (complex) were polyclonal. Similarly, Sun et al. have demonstrated monoclonality in 17 of 31 (55%) complex endometrial hyperplasias without atypia, whereas two of 15 (13%) cases of endometrial hyperplasia with atypia were polyclonal [55]. In the small sample of the study by Mutter et al., another troublesome matter emerged; only two of the four atypical endometrial hyperplasias were positive, whilst the remaining two were inconclusive [56]. In the study by Jovanovic et al., a polyclonal process was noted in two of nine (22.2%) atypical hyperplasias but also in seven of 22 (31.8%) endometrial adenocarcinomas [2]. These data indicate that clonality, a major feature of the EIN lesion [2, 45], is suggestive but not conclusive of endometrial neoplasia. It is of some interest that monoclonality has also been recorded in endometrial polyps [2] and endometriotic cysts [57, 58].

Lesion size and volume percentage stroma Clusters of crowded glands confined to an area of less than 1 mm^2 in diameter (fewer than ten glands) are not suitable for evaluation. Yet, such lesions of only microscopic size may well represent the earliest stage of endometrial carcinogenesis.

If, however, the lesion is greater than 1 mm in size, as indeed most are, the gland area should exceed that of stroma (volume percentage stroma <55%) in order to qualify as a precancerous endometrial lesion. There has been an overriding importance attached to this criterion, for as Prat [59], quoting the classical paper by Kurman et al. [35], pointed out that complex non-atypical endometrial hyperplasias often contain greater than 45% glandular component, despite their proven benign nature. Besides, many well-differentiated endometrial adenocarcinomas do not conform to this criterion and display an exceedingly high volume percentage stroma without being detracted from the diagnosis of malignancy [60].

The altered epithelium This is an important criterion which is expected from any precancerous lesion. It is vaguely defined by the Endometrial Collaborative Group as an epithelium "different from that of the adjacent normal endometrium". Such a definition does not preclude a morphological similarity of the EIN epithelium with that of atypical hyperplasia (WHO94). Cytological atypia is, of course, not peculiar to WHO94 classification and may be found in any EIN lesion. According to ECG [61], 78% of the endometrial biopsies which were originally diagnosed as atypical hyperplasia were reclassified as EIN.

Exclusion of conditions with overlapping features This is self evident and should be always exercised in any classification system.

Reproducibility of EIN

Within the last few years, a considerable number of studies have been reported on the subject of endometrial hyperplasia describing an "apparent" advantage of the EIN taxonomy over the WHO94 classification (these are listed in the references). However, it should be noted that many reviews and reproducibility studies that can be cited in support of the EIN concept were designed and performed by collaborating

and not independent research groups [44, 47, 50, 51, 61–63]. No exception to that is the absence of an independent assessment of the gland-to-stroma ratio by routine light microscopy [59]. Furthermore, by advocating a computerized morphometric analysis, the so-called D-score, rigidity was introduced into the EIN system. The D-score (volume percentage stroma, standard deviation of the shortest nuclear axis and gland outer surface density) needs special equipment and specifically trained personnel [63], and it is not, at present, applicable to everyday laboratory practice. Equally impractical for routine clinical work is the application of molecular assays for clonal analysis [47].

At present, there are no adequate follow up data to indicate whether the presence of clonality or the quantitative evaluation of the gland–stroma ratio is associated with short- or long-term development of invasive carcinoma [59].

Reliability of the study of Bergeron et al.

It is worth mentioning here that the study of Bergeron et al. [43], while criticizing the WHO94 classification for low level of reproducibility, suffered itself from a number of flaws [59, 64]. In particular, the study was based on 16 cases of well-differentiated endometrioid adenocarcinoma and only six cases of atypical hyperplasia. An inadequately documented methodology was preferred [59] with omissions in regard to the cases used; were they consecutive or cases with perceived diagnostic difficulties [64]? There were no photomicrographs or adequate histological descriptions.

The lack of any justification for combining the four existing categories of endometrial hyperplasia into the proposed two are presented in some detail under the "need not" subtitles ("Simple endometrial hyperplasia need not be combined with complex endometrial hyperplasia"; "AEH need not be combined with EA"; see below).

The WHO94 classification at a second look

The WHO94 criteria

These are, in essence, two: atypia and complexity. The former refers to cytology (hyperplasia with and without cytological atypia), the latter refers to architectural abnormality, that is, the degree of glandular crowding (simple versus complex hyperplasia; Table 1) [35, 37]. These features have been described in the preceding section "Classification schemes of endometrial hyperplasia: from anarchy to WHO", and are discussed further under the "need not" subtitles (see below: "Simple endometrial hyperplasia need not be combined with complex endometrial hyperplasia" and "AEH need not be combined with EA). Here it will suffice to comment on the criterion of cytological atypia.

Cytological atypia In the WHO94 classification, the diagnosis of a precancerous endometrial lesion is resting principally upon the presence of cytological atypia: round and, often, enlarged nuclei, prominent nucleoli, chromatin clearing or clumping, and a tendency for epithelial stratification with a loss of nuclear polarity [38, 65–67]. Despite claims to the contrary, these morphological features could be recognized and reproduced with a fair degree of precision by several independent groups of workers [35, 36, 39, 40, 68].

Reliability and reproducibility of WHO

Kendall et al., examining endometrial biopsy specimens, found a satisfactory reproducibility for the diagnoses of hyperplasia (both simple and complex), atypical hyperplasia and well-differentiated adenocarcinoma [68]. Further support for this conclusion was obtained by Horn et al. [40] who, after using the WHO94 classification, reached an overall (interobserver) correlation of 90% which is far better than the overall interobserver agreement of the study of Bergeron et al. (70–82%) [40]. Kurman et al. [35], Ferenczy and Gelfand [36] and Lacey et al. [39] reported comparable results, as these have been analysed in "Classification schemes of endometrial hyperplasia: from anarchy to WHO".

"Complexity" or is there a need for simplification?

Simple endometrial hyperplasia need not be combined with complex endometrial hyperplasia

There is no apparent justification for amalgamating simple and complex hyperplasia into a single diagnostic category, as suggested by the EIN proponents [45–50], Skov et al. [42] and Bergeron et al. [43]. For, indeed, simple hyperplasia is unique among the endometrial hyperplasias in involving diffusely both glands and stroma, with mitoses in both endometrial components. These features, by depriving pathologists of any morphological alternatives, make the diagnosis of simple endometrial hyperplasia straightforward.

Complex endometrial hyperplasia, on the other hand, as a focal lesion affecting, exclusively, glands, shows glandular complexity and glandular crowding. As a consequence, complex endometrial hyperplasia should be differentiated from a normal late proliferative endometrium, irregular

proliferative endometrium or anovulatory endometrium [65, 69–71]. It could be also confused with atypical endometrial hyperplasia if it was not for the presence of cytological atypia, but definitely, complex endometrial hyperplasia can not be mistaken with simple endometrial hyperplasia.

AEH need not be combined with EA

In contrast to Bergeron et al. views [43], Kendall and his colleagues indicated that the major problem in the differential diagnosis of proliferating endometrial lesions was the distinction between complex hyperplasia and atypical hyperplasia and not between atypical hyperplasia and well-differentiated adenocarcinoma [68]. It is true that the two lesions often co-exist [72–74] and share common genetic alterations, including microsatellite instability, PTEN and K-ras mutations, beta-catenin and MLH1 changes [6, 75–78], which may offer an explanation for the increased risk of progression from atypical hyperplasia to endometrial adenocarcinoma [35, 36, 79–82]. Yet, the two lesions should clearly be distinguished from each other for a hypothetical acceptance of the endometrioid neoplasia concept [43] will lead to overtreatment.

Atypical endometrial hyperplasia, very much like complex endometrial hyperplasia, is restricted to the glandular component of the endometrium, and it is usually focal rather than multifocal or diffuse [38]. The lesion usually, though not invariably, shows crowding and architectural complexity of the glands, but above all, it shows the features of nuclear and cytological atypia. These tend to be exuberant in atypical hyperplasia and less so in endometrial adenocarcinoma, whilst crowding and irregularity of glands is the dominant feature in adenocarcinomas and not in precancerous lesions [83, 84]. Furthermore, endometrial adenocarcinomas are commonly diffuse lesions and may show stromal fibrosis (stromatogenesis), stromal necrosis or stromal infiltration by polymorphonuclear leucocytes—features which are indicative of stromal invasion [38, 83, 85] and are particularly useful in curettage specimens [86, 87].

There has been one study which gives another dimension to the issue. Jacques et al. [88] found that determination of certain histopathological features of the endometrial adenocarcinoma, such as the histological type of the tumour and the degree of tumour differentiation, was a greater problem than differentiating adenocarcinoma from atypical hyperplasia.

Where do we stand?

The aforementioned studies, with all their discrepancies and shortcomings, demonstrate quite clearly that the endometrial hyperplasias form a spectrum of proliferating diseases ranging from benign (simple and complex hyperplasia) to malignant (well-differentiated adenocarcinoma) through a transitional pre-invasive stage. This has been designated as simple and complex atypical endometrial hyperplasia or, more recently, endometrial intraepithelial neoplasia without necessarily having the same meaning.

Irrespective of nomenclature, these lesions can be considered precancerous and should be definitely recognized as such, for they progress to malignancy with an unusual frequency and often coexist with well-differentiated endometrial adenocarcinoma with which they share common genetic abnormalities.

In the name of improved reproducibility, there is a tendency for combining subcategories of endometrial hyperplasia in generic groupings: the European Group combined simple and complex hyperplasia into endometrial hyperplasia, and atypical hyperplasia and well differentiated adenocarcinoma into endometrioid neoplasia [43]; the Endometrial Collaborative Group followed a similar approach with regard to simple and complex hyperplasia but differentiated endometrial adenocarcinomas from the precancerous endometrial lesions, which they call EIN, as distinct, though not convincingly so, from atypical hyperplasia [45, 46].

By combining diagnostic groups, the objective could be reached to a certain extent, but it would compromise the evolution of the scientific knowledge [64]. Such a contraction of the number of diagnostic choices seems simplistic rather than simple and bring us back to the early 1930s when no attempt was made to differentiate endometrial hyperplasia into any form [31, 32]. Certainly, a combined EH and EN category would improve reproducibility even further at the expense of the patient care [59]. Equally, the proposed EIN lesion, despite its molecular and morphometric basis, is not adequately supported by reproducible histological criteria, and the EIN concept, as a whole, has not been independently tested. Besides, it would be impracticable for everyday use in pathology labs.

There is no compelling evidence that the WHO94 classification is less reproducible than other classification systems, although the occasional equivocal case may cause difficulties; these should be faced by improving the young pathologists' diagnostic skills [64]. Thus, cytological atypia, the histologic feature most commonly in diagnostic dispute [89], should be endorsed when large epithelial cells with large rounded nuclei, either dense or vacuolated, and abundant cytoplasm, often with a tendency to stratification, are seen in the context of disorganized endometrial glands.

Finally, if there was some phrasal complexity in the WHO94 classification, this would ease by introducing the descriptive terms "atypical hyperplasia with glandular crowding" and "atypical hyperplasia without glandular

crowding", instead of complex and simple atypical hyperplasia, respectively, and retain the time-honoured terms "simple" and "complex" for the genuine endometrial hyperplasias.

Treatment

Several factors are taken into account in order to determine the best course of treatment for the woman with endometrial hyperplasia. The two most commonly considered are the specific type of hyperplasia and the patient's reproductive status.

Simple and complex endometrial hyperplasia can safely be treated with progestins [40, 90–92]. Lindahl and Willen presented the 5-year follow-up of 82 patients with endometrial hyperplasia without cytological atypia treated with 500 mg medroxyprogesterone acetate (MPA) i.m. twice weekly for 3 months [93]. No carcinoma developed, although bleeding problems often led to surgery (13 cases).

Atypical endometrial hyperplasia is traditionally treated by hysterectomy [40, 90, 92]. Yet, medical treatment (high-dose MPA) may be offered to patients with a contraindication to surgery and to young women who wish to retain fertility [92, 94, 95]. In this case, treatment should be continued for no less than 6 months [96]. The main obstacles to this object, of course, remain the lack of large prospective randomized trials, the poor standardization of dose and the frequent coexistence of an occult endometrial adenocarcinoma. Jobo et al. reported the clinical outcome of 53 women with atypical hyperplasia after receiving different treatments [97]. Thirty of 53 patients with atypical hyperplasia of the endometrium were treated by hysterectomy, and 20 of 53 were treated with MPA alone as a primary therapy: two of the 12 patients who were treated with low-dose MPA progressed to endometrial adenocarcinoma. Three of the eight patients treated with high-dose MPA conceived after treatment, having three healthy infants. The authors concluded that primary treatment with high-dose MPA is a safe and effective therapy for women with atypical hyperplasia who wish to preserve their fertility [97]. This benefit would have been lost, resulting in overtreatment, had Bergeron's concept of endometrioid neoplasia [43] been accepted.

Conclusions

Cytological atypia remains the defining feature in differentiating precancerous from genuine hyperplastic endometrial lesions. This, in a way, stands true not only for the WHO94 classification but also for the recently proposed EIN classification which, among other criteria, requires a "cytologically altered epithelium" for detecting precursors to endometrial adenocarcinoma. It is, therefore, necessary for the students of endometrial pathology to recognize cellular atypia.

The endometrial hyperplasias have been the subject of many proffered classifications over the years; the EIN classification is the latest. After a critical review of the literature on the topic, it appeared to us that the EIN concept is impractical and not adequately supported by reliable and reproducible criteria and that the WHO94 classification is reasonably good and has a considerable merit in the everyday routine practice. This, of course, should not discourage research on the various forms of endometrial hyperplasia, particularly in relation to molecular pathology, for as Scully [98], and Fox and Langley [99] stated, "it is our belief that the greater our understanding of the true nature of a lesion the greater, essentially, will be the possibility of a rational therapy".

Conflict of interest statement We declare that we have no conflict of interest.

References

1. Cullen TS (1900) Cancer of the uterus. Its pathology, symptomatology, diagnosis, and treatment. Henry Kimpton, London
2. Jovanovic AS, Boynton KA, Mutter GL (1996) Uteri of women with endometrial carcinoma contain a histopathological spectrum of monoclonal putative precancers, some with microsatellite instability. Cancer Res 56:1917–1921
3. Mutter GL, Boynton KA, Faquin WC, Ruiz RE, Jovanovic AS (1996) Allelotype mapping of unstable microsatellites establishes direct lineage continuity between endometrial precancers and cancer. Cancer Res 56:4483–4486
4. Sun H, Enomoto T, Shroyer KR, Ozaki K, Fujita M, Ueda Y, Nakashima R, Kuragaki C, Ueda G, Marata Y (2002) Clonal analysis and mutations in the PTEN and the K-ras in endometrial hyperplasia. Diagn Mol Pathol 11:204–211
5. Orbo A, Nilsen MN, Arnes MS, Pettersen I, Larsen K (2003) Loss of expression of MLH1, MSH2, MSH6, and PTEN related to endometrial cancer in 68 patients with endometrial hyperplasia. Int J Gynecol Pathol 22:141–148
6. Taranger-Charpin C, Carpentier S, Dales JP, Garcia S, Djemli A, Andrac L, Lavaut MN, Sferlazzo K, Boubli L (2004) Immunohistochemical expression of PTEN antigen: a new tool for diagnosis of early endometrial neoplasia. Bull Acad Natl Med 188:415–427
7. Baak JP, Van Diermen B, Steinbakk A, Janssen E, Skaland I, Mutter GL, Fiane B, Lovslett K (2005) Lack of PTEN expression in endometrial intraepithelial neoplasia is correlated with cancer progression. Hum Pathol 36:555–561
8. Kanaya T, Kyo S, Sakaguchi J, Maida Y, Nakamura M, Takakura M, Hashimoto M, Mizumoto Y, Inoue M (2005) Association of mismatch repair deficiency with PTEN frameshift mutations in endometrial cancers and the precursors in a Japanese population. Am J Clin Pathol 124:89–96
9. Gore H (1973) Hyperplasia of the endometrium. In: Norris HJ, Hertig AT, Abell MR (eds) The uterus. Williams & Wilkins Co. International Academy of Pathology, Baltimore, pp 255–275

10. Copenhaver EH (1959) Atypical endometrial hyperplasia. Obstet Gynecol 13:264–268
11. Campbell PE, Barter RA (1961) The significance of atypical endometrial hyperplasia. J Obstet Gynecol Brit Emp 68:668–672
12. Gray LA, Robertson RW, Christopherson WM (1974) Atypical endometrial changes associated with carcinoma. Gynecol Oncol 2:93–100
13. Gusberg SB (1947) Precursors of corpus carcinoma. Estrogens and adenomatous hyperplasia. Am J Obstet Gynecol 54:905–927
14. Gusberg SB (1976) The individual at high risk for endometrial carcinoma. Am J Obstet Gynecol 126:535–542
15. Gusberg SB, Hall RE (1961) Precursors of corpus cancer. III. The appearance of cancer of the endometrium in estrogenically conditioned patients. Obstet Gynecol 17:397–412
16. Gusberg SB, Kaplan AL (1963) Precursors of corpus cancer. IV. Adenomatous hyperplasia as Stage O carcinoma of the endometrium. Am J Obstet Gynecol 87:662–678
17. Gusberg SB, Moore DB, Martin F (1954) Precursors of corpus cancer. II. A clinical and pathological study of adenomatous hyperplasia. Am J Obstet Gynecol 68:1472–1481
18. Way S (1954) The aetiology of carcinoma of the body of the uterus. J Obstet Gynecol Brit Emp 61:46–58
19. Ritzmann H (1978) Types of endometrial hyperplasia and their relationship to carcinoma of the endometrium. In: Brush MG, King RJB, Taylor RW (eds) Endometrial cancer. Bailliere Tindall, London, pp 118–123
20. Speert H (1952) The premalignant phase of endometrial carcinoma. Cancer 5:927–994
21. Chamlian DL, Taylor HB (1970) Endometrial hyperplasia in young women. Obstet Gynecol 36:659–666
22. Hertig AT, Sommers SC (1949) Genesis of endometrial carcinoma. I. Study of prior biopsies. Cancer 2:946–956
23. Hertig AT, Gore H (1968) Tumors of the female sex organs. Supplement to part 2. Tumours of the vulva, vagina and uterus. Atlas of tumor pathology. Armed Forces Institute of Pathology, Washingston DC, pp 312–326
24. Vellios F (1974) Endometrial hyperplasia and carcinoma in-situ. Gynecol Oncol 2:152–161
25. Wentz WB (1974) Progestin therapy in endometrial hyperplasia. Gynecol Oncol 2:362–367
26. Tavassoli F, Kraus FT (1978) Endometrial lesions in uteri resected for atypical endometrial hyperplasia. Am J Clin Pathol 70:770–779
27. Beutler HK, Dockerty MB, Randall LM (1963) Precancerous lesions of the endometrium. Am J Obstet Gynecol 86:433–443
28. Scully RE (1981) Definition of precursors in gynecologic cancer. Cancer 48:531–537
29. Blaustein A (1980) Interpretation of biopsy of endometrium. Raven, New York
30. Hall KV (1957) Irregular hyperplasias of the endometrium. Acta Obstet et Gynecol Scand 36:306–321
31. Taylor HC Jr (1932) Endometrial hyperplasia and carcinoma of the body of the uterus. Am J Obstet Gynecol 23:309–332
32. Novak E, Yui E (1936) Relation of endometrial hyperplasia to adenocarcinoma of the uterus. Am J Obstet Gynecol 32:674–698
33. Greene RR, Roddick JW Jr, Milligan M (1959) Estrogens, endometrial hyperplasia, and endometrial carcinoma. Ann NY Acad Sci 75:586–600
34. Poulsen HE, Taylor CW, Sobin LH (1975) Histological typing of female genital tract tumours. World Health Organization, Geneva
35. Kurman RJ, Kaminski PF, Norris HJ (1985) The behaviour of endometrial hyperplasia. Along-term study of "untreated" hyperplasia in 170 patients. Cancer 56:403–412
36. Ferenczy A, Gelfand M (1989) The biological significance of cytologic atypia in progestogen-treated endometrial hyperplasia. Am J Obstet Gynecol 160:126–131
37. Scully RE, Bonfiglio TA, Kurman RJ, Silverberg SG, Wilkinson EJ (1994) Histological typing of female genital tract tumors. Springer, Berlin
38. Buckley CH, Fox H (2002) Biopsy pathology of the endometrium, 2nd edn. Arnold, London
39. Lacey JV Jr, Ioffe OB, Ronnett BM, Rush BB, Richesson DA, Chatterjee N, Langholz B, Glass AG, Sherman ME (2008) Endometrial carcinoma risk among women diagnosed with endometrial hyperplasia: the 34-year experience in a large health plan. Br J Cancer 98:45–53
40. Horn LC, Schnurrbusch U, Bilek K, Hentschel B, Einenkel J (2004) Risk of progression in complex and atypical endometrial hyperplasia: clinicopathologic analysis in cases with and without progestogen treatment. Int J Gynecol Cancer 14:348–353
41. Kurman RJ, Norris HJ (1986) Endometrium. In: Henson DE, Albores-Saavedra J (eds) The pathology of incipient neoplasia. Saunders, Philadelphia, pp 265–277
42. Skov BG, Broholm H, Engel U, Franzmann MB, Nielsen AL, Lauritzen AF, Skov T (1997) Comparison of the reproducibility of the WHO classifications of 1975 and 1994 of endometrial hyperplasia. Int J Gynecol Pathol 16:33–37
43. Bergeron C, Nogales FF, Masseroli M, Abeler V, Duvillard P, Muller-Holzner E, Pickartz H, Wells M (1999) A multicentric European study testing the reproducibility of the WHO classification of endometrial hyperplasia with a proposal of a simplified working classification for biopsy and curettage specimens. Am J Surg Pathol 23:1102–1108
44. Zaino RJ, Kauderer J, Trimble CL, Silverberg SG, Curtin JP, Lim PC, Gallup DG (2006) Reproducibility of the diagnosis of atypical endometrial hyperplasia: a Gynecologic Oncology Group study. Cancer 106:804–811
45. Mutter GL (2000) Histopathology of genetically defined endometrial precancers. Int J Gynecol Pathol 19:301–309
46. Mutter GL (2000) Endometrial intraepithelial neoplasia (EIN): will it bring order to chaos? The Endometrial Collaborative Group. Gynecol Oncol 76:287–290
47. Mutter GL, Baak JPA, Crum CP, Richart RM, Ferenczy A, Faquin WC (2000) Endometrial precancer diagnosis by histopathology, clonal analysis, and computerized morphometry. J Pathol 190:462–469
48. Zaino RJ (2000) Endometrial hyperplasia : is it time for a quantum leap to a new classification? Int J Gynecol Pathol 19:314–321
49. Baak JP, Mutter GL (2005) EIN and WHO94. Considering the classification of endometrial hyperplasia. J Clin Pathol 58:1–6
50. Mutter GL, Zaino RJ, Baak JP, Brentley RC, Robboy SJ (2007) Benign endometrial hyperplasia sequence and endometrial intraepithelial neoplasia. Int J Gynecol Pathol 26:103–114
51. Baak JP, Mutter GL, Robboy S, van Diest PJ, Uyterlinde AM, Orbo A, Palazzo J, Fiane B, Lovslett K, Burger C, Voorhorst F, Verheijen RH (2005) The molecular genetics and morphometry-based endometrial intraepithelial neoplasia classification system predicts disease progression in endometrial hyperplasia more accurately than the 1994 World Health Organization classification system. Cancer 103:2304–2312
52. Mutter GL (2002) Diagnosis of premalignant endometrial disease. J Clin Pathol 55:326–331
53. Dietel M (2001) The histological diagnosis of endometrial hyperplasia. Is there a need to simplify? Virchows Arch 439:604–608
54. Yilmaz I, Baloglu H, Haholu A, Berber U, Yildirim S, Ergur AR (2007) Objective risk definition for endometrial lesion spectrum: a diagnostic algorithm. Gynecol Oncol 105:451–456
55. Sun H, Enomoto T, Shroyer KR, Ozaki K, Fujita M, Ueda Y, Nakashima R, Kuragaki C, Ueda G, Murata Y (2002) Clonal

analysis and mutations in PTEN and the K-ras genes in endometrial hyperplasia. Diagn Mol Pathol 11:204–211
56. Mutter GL, Chaponot ML, Fletcher JA (1995) A polymerase chain reaction for non-random X chromosome inactivation identifies monoclonal endometrial cancers and precancers. Am J Pathol 146:501–508
57. Tamura M, Fukaya T, Murakami T, Uehara S, Yajima A (1998) Analysis of clonality in human endometriotic cysts based on evaluation of X chromosome inactivation in archival formalin-fixed, paraffin-embedded tissue. Lab Invest 78:213–218
58. Wu Y, Basir Z, Kajdacsy-Balla A, Strawn E, Macias V, Montgomery K, Guo SW (2003) Resolution of clonal origins for endometriotic lesions using laser capture microdissection and the human androgen receptor (HUMARA) assay. Fertil Steril 79:710–717
59. Prat J (2002) Histologic diagnosis of endometrial hyperplasia. Virchows Arch 441:306–307
60. Baak JPA, Nauta JJP, Wisse-Brekelmans ECM, Bezemer PD (1988) Architectural and nuclear morphometrical features together are more important prognosticators in endometrial hyperplasias than nuclear morophometrical features alone. J Pathol 154:335–341
61. Hecht JL Ince TA, Baak JP, Baker HE, Ogden MW, Mutter GL (2005) Prediction of endometrial carcinoma by subjective endometrial intraepithelial neoplasia diagnosis. Mod Pathol 18:324–330
62. Orbo A, Baak JP, Kleivan I, Lysne S, Prytz PS, Broeckaert MA, Slappendel A, Tichelaar HJ (2000) Computerised morphometrical analysis in endometrial hyperplasia for the prediction of cancer development. A long-term retrospective study from northern Norway. J Clin Pathol 53:697–703
63. Baak JP, Orbo A, van Diest PJ, Jiwa M, de Bruin P, Broeckaert M, Snijders W, Boodt PJ, Fons G, Burger C, Verheijen RH, Houben PW, The HS, Kenemans P (2001) Prospective multicenter evaluation of the morphometric D-score for prediction of the outcome of endometrial hyperplasias. Am J Surg Pathol 25:930–935
64. Scully RE, Young RH (2000) Endometrioid neoplasia retrogressive terminology. Am J Surg Pathol 24:753–754
65. Silverberg SG, Kurman RJ (1992) Tumors of the uterine corpus and gestational trophoblastic disease. Armed Forces Institute of Pathology, Washington DC
66. Ferency A, Bergeron C (1992) Endometrial hyperplasia. In: Lowe D, Fox H (eds) Advances in gynaecological pathology. Churchill Livingstone, Edinburgh, pp 207–234
67. Clement PB, Young RH (2000) Atlas of gynecological surgical pathology. W.B. Saunders Company, Philadelphia
68. Kendall BS, Ronett BM, Isacson C, Cho KR, Hedrick L, Diener-West M, Kurmam RJ (1998) Reproducibility of the diagnosis of endometrial hyperplasia, atypical hyperplasia, and well-differentiated carcinoma. Am J Surg Pathol 22:1012–1019
69. Robertson WB (1981) The endometrium. Butterworths, London
70. Clement PB, Young RH (1993) Tumors and tumorlike lesions of the uterine corpus and cervix. Churchill Livingstone, New York
71. Clement PB, Young RH (2002) Endometrioid carcinoma of the uterine corpus: a review of its pathology with emphasis on recent advances and problematic aspects. Adv Anat Pathol 9:145–184
72. Gucer F, Reich O, Tamussino K, Bader AA, Pieber D, Scholl W, Haas J, Petru E (1998) Concomitant endometrial hyperplasia in patients with endometrial carcinoma. Gynecol Oncol 69:64–68
73. Shutter J, Wright TC Jr (2005) Prevalence of underlying adenocarcinoma in women with atypical endometrial hyperplasia. Int J Gynecol Pathol 24:313–318
74. Trimble CL, Kauderer J, Zaino R, Silverberg S, Lim PC, Burke JJ 2nd, Alberts D, Curtin J (2006) Concurrent endometrial carcinoma in women with a biopsy diagnosis of atypical endometrial hyperplasia: a Gynecologic Oncology Group study. Cancer 106:812–819
75. Duggan BD, Felix JC, Muderspach LI, Tsao JL, Shibata DK (1994) Early mutational activation of the c-Ki-ras oncogene in endometrial carcinoma. Cancer Res 54:1604–1607
76. Sherman ME (2000) Theories of endometrial carcinogenesis: a multidisciplinary approach. Mod Pathol 13:295–308
77. Matias-Guiu X, Catasus L, Bussaglia E, Lagarda H, Garcia A, Pons C, Munoz J, Arguelles R, Machin P, Prat J (2001) Molecular pathology of endometrial hyperplasia and carcinoma. Hum Pathol 32:569–577
78. Moreno-Bueno G, Hardisson D, Sarrio D, Sanchez C, Cassia R, Prat J, Herman JG, Esteller M, Matias-Guiu X, Palacios J (2003) Abnormalities of E- and P-cadherin and catenin (beta-, gamma-catenin, and p120ctn) expression in endometrial cancer and endometrial atypical hyperplasia. J Pathol 199:471–478
79. Deligdisch L, Cohen CJ (1985) Histopathologic correlation and virulence implications of endometrial carcinoma associated with adenomatous hyperplasia. Cancer 56:1452–1455
80. Janicek MF, Rosenhein NB (1994) Invasive endometrial cancer in uteri resected for atypical endometrial hyperplasia. Gynecol Oncol 52:373–378
81. Ambros RA, Sheehan CE, Kallakury BV, Ross JS, Malfetano J, Paunovich E, Figge J (1996) MDM2 and p53 protein expression in the histologic subtypes of endometrial carcinoma. Mod Pathol 26:1165–1169
82. Sivridis E, Giatromanolaki A (2001) Prognostic aspects on endometrial hyperplasia and neoplasia. Virchows Arch 439:118–126
83. Fox H, Buckley CH (1982) The endometrial hyperplasias and their relationship to endometrial neoplasia. Histopathology 6:493–510
84. Kurman RJ, Norris HJ (1982) Endometrial neoplasia: hyperplasia and carcinoma. In: Blaustein A (ed) Pathology of the Female Genital Tract, 2nd edn. Springer, New York, pp 311–351
85. Silverberg SG (2000) Problems in the differential diagnosis of endometrial hyperplasia and carcinoma. Mod Pathol 13:309–327
86. Jesadapatrakul S, Tangjitgamol S, Manusirivitaya S (2005) Histopathologic consistency between endometrial hyperplasia diagnosis from endometrial curettage and pathologic diagnoses from hysterectomy specimens. J Med Assoc Thai 88(Suppl 2): S16–S21
87. Indermaur MD, Shoup B, Tebes S, Lancaster JM (2007) The accuracy of frozen pathology at time of hysterectomy in patients with complex atypical hyperplasia on preoperative biopsy. Am J Obstet Gynecol 196:40–42
88. Jacques SM, Qureshi F, Munkarah A, Lawrence WD (1998) Interinstitutional surgical pathology review in gynecologic oncology: I. Cancer in endometrial curettings and biopsies. Int J Gynecol Pathol 17:36–41
89. Allison KH, Reed SD, Voigt LF, Jordan CD, Newton KM, Garcia RL (2008) Diagnosing endometrial hyperplasia: why is it so difficult to agree? Am J Surg Pathol 32:691–698
90. Novac L, Grigore T, Cernea N, Niculescu M, Cotarcea S (2005) Incidence of endometrial carcinoma in patients with endometrial hyperplasia. Eur J Gynaecol Oncol 26:561–563
91. Rattanachaiyanont M, Angsuwathana S, Techatrisak K, Tanmahasamut P, Indhavivadhana S, Leerasiri P (2005) Clinical and pathological responses of progestin therapy for non-atypical endometrial hyperplasia: a prospective study. J Obstet Gynaecol Res 31:98–106
92. Brun JL, Descat E, Boubli B, Dallay D (2006) Endometrial hyperplasia: A review. I Gynecol Obstet Biol Reprod (Paris) 35:542–550
93. Lindahl B, Willen R (1994) Spontaneous endometrial hyperplasia. A 5 year follow-up of 82 patients after high-dose gestagen treatment. Anticancer Res 14(6B):2831–2834

94. Ushijima K, Yahata H, Yoshikawa H, Konishi I, Yasugi T, Saito T, Nakanishi T, Sasaki H, Saji F, Iwasaka T, Hatae M, Kodama S, Saito T, Terakawa N, Yaegashi N, Hiura M, Sakamoto A, Tsuda H, Fukunaga M, Kamura T (2007) Multicenter phase II study of fertility-sparing treatment with medroxyprogesterone acetate for endometrial carcinoma and atypiocal hyperplasia in young women. J Clin Oncol 25:2798–2803
95. Randall TC, Kurman RJ (1997) Progestin treatment of atypical hyperplasia and well-differentiated carcinoma of the endometrium in women under age 40. Obstet Gynecol 90:434–440
96. Wheeler DT, Bristow RE, Kurman RJ (2007) Histologic alterations in endometrial hyperplasia and wel-differentiated carcinoma treated with progestins. Am J Surg Pathol 31:988–998
97. Jobo T, Kawaguchi M, Imai M, Kuramoto H (2001) Treatment for complex atypical hyperplasia of the endometrium. Eur J Gynaecol Oncol 22:365–368
98. Scully RE (1973) The need for uniform terminology. Hum Pathol 4:602–603
99. Fox H, Langley FA (1976) Tumours of the ovary. William Heinemann Medical Books Limited, London

Virchows Arch (2008) 453:233–241
DOI 10.1007/s00428-008-0652-3

ORIGINAL ARTICLE

Endomyocardial fibrosis: pathological and molecular findings of surgically resected ventricular endomyocardium

Silvia D'Andretta Iglezias · Luiz Alberto Benvenuti · Fiorella Calabrese · Vera Maria Cury Salemi · Ana Maria Gonçalves Silva · Elisa Carturan · Sergio Almeida de Oliveira · Gaetano Thiene · Thales De Brito

Received: 17 June 2008 / Revised: 7 August 2008 / Accepted: 8 August 2008 / Published online: 2 September 2008

Abstract Endomyocardial fibrosis (EMF) is a restrictive cardiomyopathy of unknown etiology prevalent in tropical regions affecting the inflow tract and apex of one or both ventricles, which show fibrous thickening of the endocardium and adjacent myocardium. Surgical treatment is recommended for patients in functional classes III or IV (New York Heart Association). The gross and histological features of the heart have been comprehensively studied in autopsies, but studies in surgical samples are still lacking. Histological and immunohistochemical features of EMF in surgical samples collected from 32 patients were described and correlated with clinical data. Polymerase chain reaction (PCR) and reverse transcription-PCR, performed on formalin fixed endomyocardial samples, were used retrospectively to detect genomes of certain cardiotropic viruses and *Toxoplasma gondii*. Ventricular endocardium was thickened by superficial acellular hyaline collagen fibers type I and III, with predominance of the former type. Besides fibrosis, a chronic inflammatory process and an anomalous lymphatic rich vascular pattern were observed in the deep endocardium, connected to the terminal coronary circulation of the myocardium, which might be an important pathological finding concerning EMF pathogenesis. Molecular analysis of the endomyocardium revealed high incidence of cardiotropic infective agents (6/12, 50%); however, their role in the disease pathogenesis is still controversial.

Keywords Endomyocardial fibrosis · Immunohistochemistry · Lymphatic vessels · Surgical pathology · Polymerase chain reaction

S. D. Iglezias (✉)
Department of Pathology, University of São Paulo Medical School, São Paulo, Brazil
e-mail: silviaiglezias@uol.com.br

L. A. Benvenuti · V. M. C. Salemi · S. A. de Oliveira
Heart Institute (InCor), University of São Paulo Medical School, São Paulo, Brazil

F. Calabrese · E. Carturan · G. Thiene
Department of Pathology, University of Padua Medical School, Padua, Italy

A. M. G. Silva · T. De Brito
LIM 06, Institute of Tropical Medicine, University of São Paulo Medical School, São Paulo, Brazil

Introduction

Endomyocardial fibrosis (EMF) is a restrictive cardiomyopathy of unknown etiology, first described in Africa by Jack N.P. Davies in 1948 [1]. It occurs almost exclusively in tropical and subtropical countries, especially in Uganda, Nigeria, Ivory Coast, India, and Brazil. EMF predominates in children and young adults in Africa and India; however, in Brazil the disease affects predominantly middle-aged adults, particularly women. The disease involves the inflow tract and apex of one or both ventricles, which show fibrous thickening of the endocardium and granulation tissue at the myocardial border. Superimposed thrombosis and calcification are common at advanced stages of the disease [2]. Restriction of the ventricular filling always takes place and may lead either to left- or right-sided cardiac failure. Surgical resection of the fibrous and thickened endocardium is recommended to patients with advanced heart disease in functional class III or IV (New York Heart Association (NYHA)) [3, 4]. Even though the standard gross and histological features of the heart itself have been thoroughly

studied at autopsy [2], detailed descriptions of the pathology as seen in surgical samples are limited to endomyocardial biopsies of a few cases [5, 6].

EMF etiology remains unknown although a relation with systemic or heart infection or parasitism, previous blood eosinophilia, or nutritional deprivation had been suggested [7, 8]. Some data indicate an infectious cause such as high prevalence in humid parts of tropical countries, association with eosinophilia and markers of poverty, endocardial inflammatory infiltrate, and so on [9]. Many authors, Davies included, have sought a more direct connection between EMF and infectious agents such as viruses, protozoa, nematodes, and others [10–12] with no success.

The polymerase chain reaction (PCR) is a potent tool for detecting infective agents, originally described in 1985 [13]. Since then, viral genomes have been detected in heart samples of several cardiomyopathies, indicating viral participation in their etiopathogenesis [14–19].

This study was conducted to: (1) evaluate the histomorphological changes in EMF observed in surgical samples, using both routine and immunohistochemical methods, with clinical correlation; (2) compare histological data from surgical and autopsy samples as previously described in the literature; and (3) evaluate the occurrence of certain cardiotropic viruses and *Toxoplasma gondii* protozoa genomes in heart samples of patients presenting EMF using molecular analysis in formalin fixed paraffin-embedded surgical samples.

Material and methods

Patients and sample selection

This retrospective study included 32 patients presenting typical EMF (Fig. 1a and b) confirmed by clinical, echocardiographic, and cineventriculographic findings. All the patients were submitted to surgical resection of the thickened endocardium at the Heart Institute (InCor), University of São Paulo Medical School, between 1991 and 2005.

All available clinical and surgical reports were reviewed. Gender, age, presence of blood eosinophilia (number of eosinophils $\geq 450\ \mu l^{-1}$), time between onset of symptoms and surgery, presence of significant associated diseases, NYHA functional class at time of surgery, cineangiocardiographic data, ventricle affected by EMF, surgical procedures, and postsurgical evolution were all recorded.

Histology and immunohistochemistry

After formalin fixation, representative samples of the resected tissue were cut and submitted to routine procedure for embedding in paraffin. When necessary, previous decalcification treatment of the samples was performed. In 32 cases, 3–4 μm thickness sections were realized and stained with hematoxylin–eosin (H & E), Masson's trichrome, reticulin (Wilder's stain), Verhoeff's elastic stain or submitted to immunohistochemistry. All samples were required to contain myocardial tissue for inclusion in the study.

Immunohistochemical screening methods comprised detection of collagen fibers types I, III, and IV, T- and B-lymphocytes, macrophages, and lymphatic endothelium in order to study the collagen of the thickened endocardium and to characterize the inflammatory cells and the lymphatics in the EMF plaque. We used EnVision (Dako, USA) and LSAB-based immunohistochemical methods and chromogen 3.3′diaminobenzidin or alkaline phosphatase were used to develop the reactions. All sections were lightly counterstained with Harris' hematoxylin. The source, clone, and titer of the primary antibodies are summarized in Table 1.

In 21 cases from patients presenting atypical chest pain and/or with blush detected during coronary cineangiocardiography, the vessel number per unit of area of endocardium (square millimeter) was counted under medium power magnification (×200) using a computerized image analysis system (Quantimet, Leica). The data were compared using the t test, and differences were considered statistically significant when $p \leq 0.05$.

Molecular analysis

Retrospective PCR and reverse transcription (RT)-PCR for detection of certain cardiotropic viruses and *T. gondii* genomes were performed in formalin fixed paraffin-embedded samples of 16 cases. Samples previously submitted to severe chemical decalcification were excluded from the study. Additionally, the same procedures were performed in myocardial samples of 20 patients (mean age—53.3±5.6 years old, 12 males) presenting non-inflammatory cardiac disease. Those patients did not come from geographical areas where EMF occurs and comprised the control group of previous published work [16].

The dried tissue pellets obtained after deparaffinization with xylene were resuspended in two different digestion solutions for RNA [20] and DNA [21]. The oligonucleotides used to ascertain the quality of extracted RNA or DNA were complementary to the mRNA glyceraldehyde-3-phosphate dehydrogenase (3GPDH) [22] and β-globin gene, respectively [13].

RT-PCR was used to evaluate the following RNA viruses: enteroviruses (EV), influenza A, and influenza B [17]. RT-PCR for the late gene of cytomegalovirus (CMV) was used to detect not only the presence of CMV but also

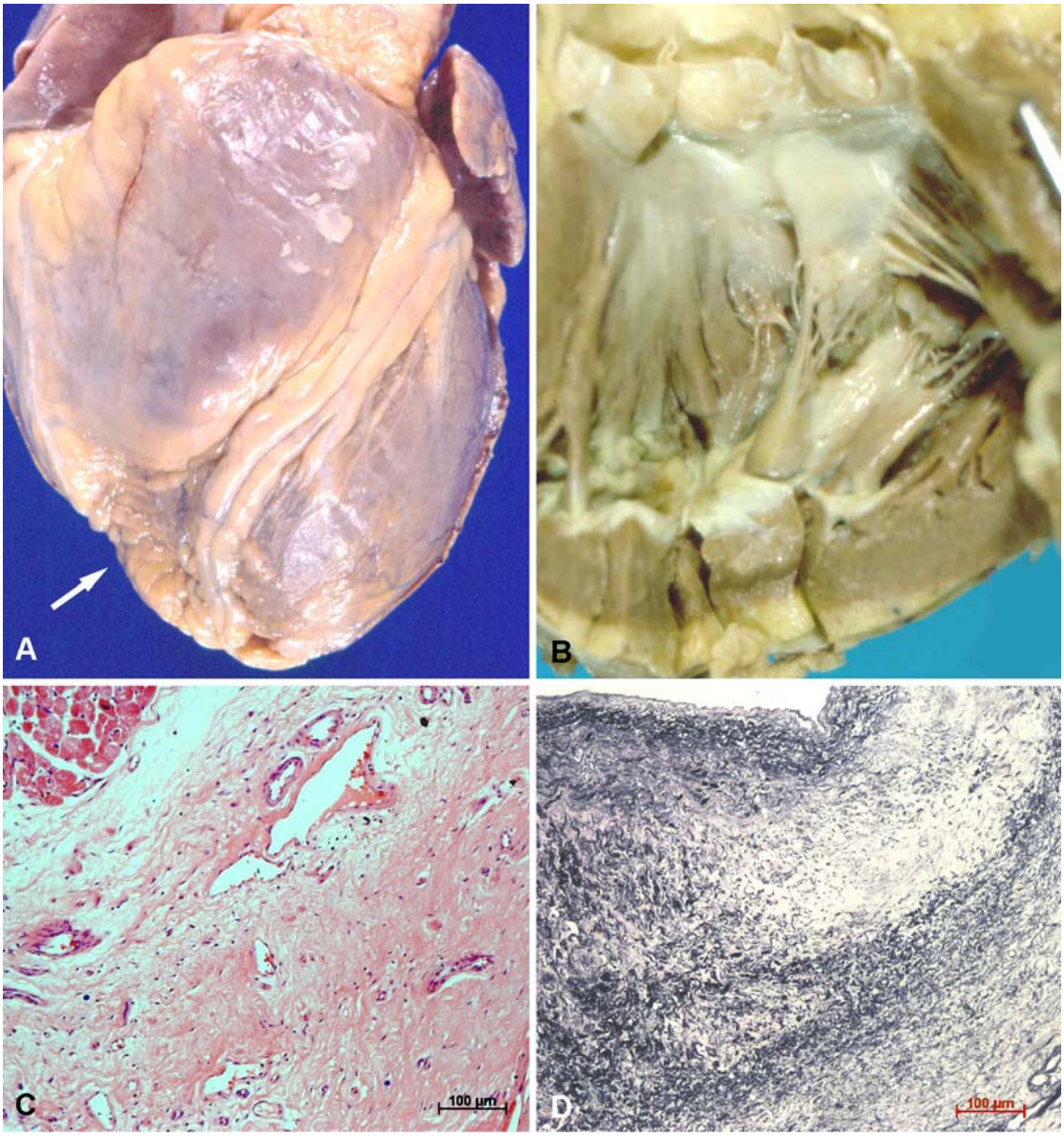

Fig. 1 **a**, **b** gross appearance of EMF. **a** *Arrow* points to the right border "notch", a characteristic external feature when EMF involves and contracts the right ventricle; **b** a patch of white fibrotic endocardium at the apex of the left ventricle. **c** Fibrotic ventricular endocardium showing a superficial layer of acellular fibrous tissue and a deep zone of moderately cellular fibrous tissue with a rich vascular net (H & E); **d** proliferated elastic fibers at the superficial layer of the thickened endocardium (Verhoeff elastic stain)

Table 1 Immunohistochemical protocols

Antigen	Code/clone	Source	Primary serum titer
Collagen I	2150–0020 policlonal	Biogenesis	1/2200
Collagen III	2150–0100 policlonal	Biogenesis	1/2200
Collagen IV	M0785 monoclonal	Dako	1/200
T Cell, CD3	A0452 policlonal	Dako	1/30
B Cell, CD20	M75 monoclonal	Dako	1/80
Macrophages CD68	M0814 monoclonal	Dako	1/1000
Lymphatics D2–40	M3619 monoclonal	Dako	1/100

its active infection [23]. PCR was used to evaluate *T. gondii* protozoa and the following DNA viruses: adenovirus, herpes simplex, Epstein–Barr [17], and parvovirus B19 [24]. Fifteen microliters of each reaction was analyzed on a 3% Nu-sieve agarose containing 0.03 μg/ml ethidium bromide. The gels were placed under UV light for visualization of the amplified products. Positive and negative control reactions were performed simultaneously. All the samples were analyzed without prior knowledge of patient clinical data and all PCR-positive products were repeated to eliminate false positives. The sensitivity of exams performed in our laboratory has been previously described and quoted at 1800 single RNA molecules/PFU [16].

The specificity of the PCR or RT-PCR products was confirmed by automated sequencing using BIG DYE dideoxy-terminator chemistry (ABI PRISM 310, Applied Biosystems). The sequence comparison was performed by Basic Local Alignment Sequencing Tool search of Gene Bank databases [17].

Results

Clinical data

Of the 32 patients included in the histopathological study, 26 were women and six men, aged between 27 and 72 years old (mean—49.40±11.87). In 30 cases, the clinical records were available for review.

Most patients showed initial symptoms between the age of 30 and 50 years old, but two of them reported symptoms of the disease before the age of 20. The predominant clinical picture was an insidious and progressive heart failure. In nine cases, the clinical picture was sudden (four with atypical chest pain, three with arrhythmia, and two with pulmonary embolism). Other symptoms during the clinical follow-up were arrhythmia, paroxysmal dyspnea, cerebral hemorrhage, and atypical chest pain. The last symptom occurred in 15/30 patients (50%), showed no relation to physical efforts, and was sometimes intense, lasting for several minutes up to a few days. Relapsing blood eosinophilia above 6% was observed in 15/30 (50%) patients during the clinical follow-up and ranged from 564 to 1,932 cells/mm^3. Conditions possibly associated with blood eosinophilia included allergy to medications, asthma or allergic rhinitis (2/15), multiple intestinal parasitism (3/15), and hepatosplenic schistosomiasis (2/15). One patient was previously treated for hypereosinophilic syndrome 4 years before the cardiac symptoms.

All patients underwent coronary cineangiocardiography, but only 16 were available for review. All of them presented characteristic ventricular lesions. In 9/16 cases (56%), vascular blush (or neovascularization) was observed, five related to the right and four to the left coronary artery (Fig. 3d).

The period between the onset of symptoms and surgery ranged from 6 months to 31 years (mean—11.2±8.9). All patients presented heart failure functional class III or IV (NYHA) at the time of surgery and were submitted to surgical treatment as described by Oliveira et al. [4]. EMF involved the left ventricle in 15/32 (46.8%), the right ventricle in 4/32 (12.5%), and both in 13/32 (40.6%) patients. Mitral valve annuloplasty, mitral valve replacement, and tricuspid valve annuloplasty were performed in 22, two, and 21 patients, respectively.

Of the 26/32 patients (81%) who survived surgery, postoperative follow-up occurred in 21, and ranged from 6 months to 11 years (mean—5.1±3.4). All patients experienced clinical improvement and were CF I or II (NYHA) 6 months after surgery. Severe deterioration of cardiac function after 6 months to 4 years of follow-up was detected in 6/21 patients (28.6%). Three of them died and the others were resubmitted for surgery within 3 to 6 years of the initial operation.

Histopathology and immunohistochemistry

Typical histological findings of EMF were present in all cases. The fibrous layer in the endocardium was composed of a dense hyaline tissue alternating with deep edematous areas (Fig. 1c). Facing the ventricular cavity, the endocardium showed dense packed hyaline collagen that was poorly vascularized and on the myocardial side, an edematous collagen was present, with a rich net of small- and medium-sized blood vessels and mild inflammatory infiltrate. Elastic fibers were present in considerable numbers close to the myocardium and covering the inner ventricular cavity. Usually, they were arranged disorderly and presented variable thickness (Fig. 1d), but sometimes, they appeared orderly with condensed parallel elastic fibers. Masson's trichrome showed intense blue stain corresponding to dense collagen, but superficial orange stained areas were detected in many cases (Fig. 2a,b). Recent superficial deposits of fibrin with a few inflammatory cells were frequently seen on the fibrous plaque. Calcification of the fibrous layer occurred in 11/32 (34.4%) samples, with bone metaplasia in three cases. Reticulin fibers were short and immunohistochemistry showed interlaced fibers of types I and III collagen, with predominance of type I fibers. Fibers of type IV collagen were seen only around blood vessels.

Deep within the endocardium, focal chronic inflammatory infiltrate occurred, usually around blood vessels (Fig. 2c), with predominance of T-lymphocytes and macrophages. Eosinophils were rarely seen in the endocardium,

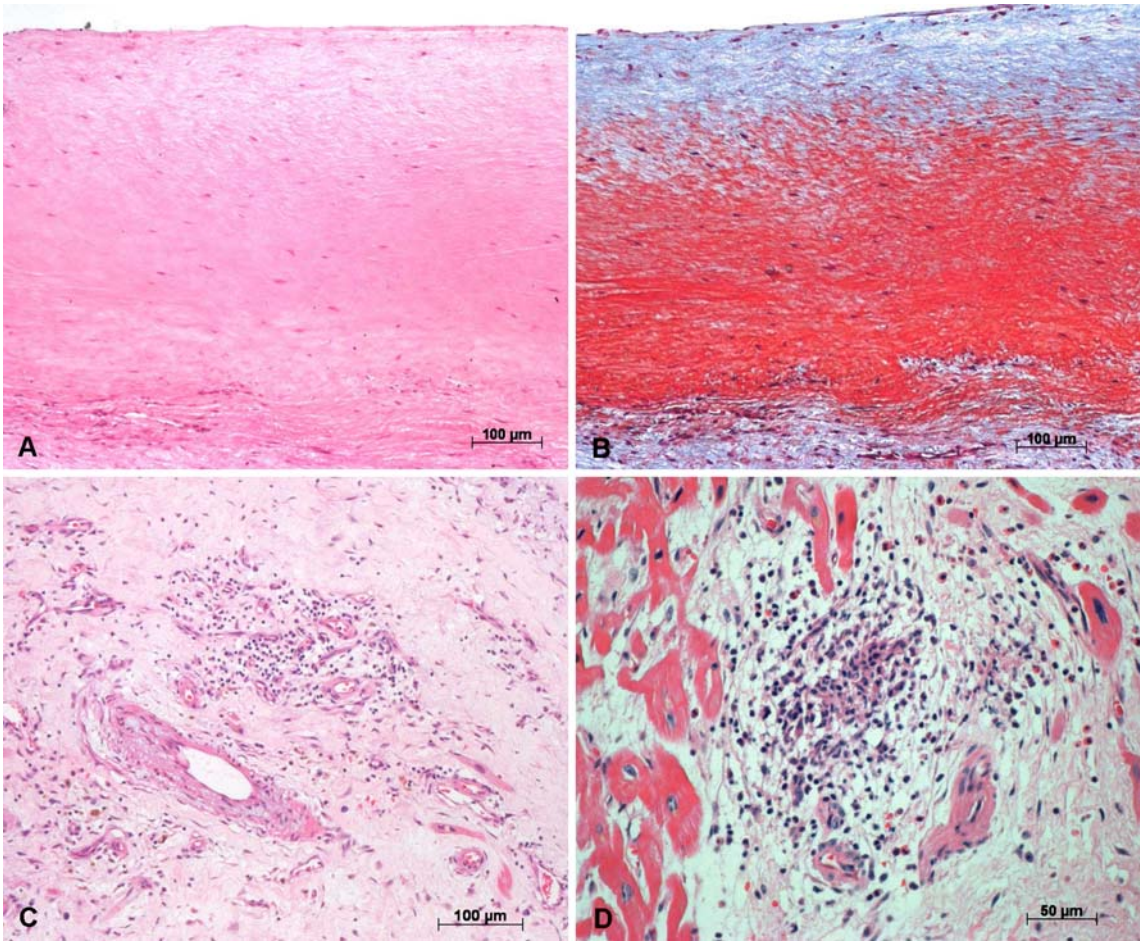

Fig. 2 **a** superficial dense collagen (H & E) and **b** orange areas of dense collagen (Masson trichrome) were seen in the endocardium; **c** prominent perivascular chronic inflammatory infiltrate (H & E); **d** poorly defined granuloma with a few eosinophils in the endomyocardium interface (H & E)

except in one case where a small and poorly defined granuloma presenting numerous eosinophils and few epithelioid cells was present at the endomyocardial interface (Fig. 2d). Samples from 4/32 (12.5%) patients showed granulation tissue with prominent inflammatory infiltrate in the endomyocardium, characterized by linear, superficial thrombosis, hemosiderin deposits, numerous proliferated small blood vessels, and marked inflammatory infiltrate with plasma cells and few eosinophils in an edematous loose connective tissue.

Many irregular blood vessels were present under the fibrous scar (Fig. 1c). Arterioles with thickened walls, usually due to fibrous proliferation and mucus degeneration of the intima, were observed close to vessels with delicate walls. Proliferating vessels were occasionally observed permeating the adjacent myocardium in connection with the local terminal coronary web (Fig. 3a). In some areas the vascular pattern suggested arteriovenous shunts (Fig. 3b). Immunohistochemistry showed that at least 30% of the vessels were lymphatic, which predominate at the endomyocardial interface (Fig. 3c). Recent thrombi were not found in the proliferated vessels, but recanalized thrombi were occasionally present.

No statistical difference in the number of endocardial vessels occurred between patients with (n=9; mean—66.77±24.60 vessels/mm^2) or without coronary blush (n=7; mean—58.67±27.78 vessels/mm^2) and between patients with (n=15; mean—68.43±23.80 vessels/mm^2) or without atypical chest pain (n=5; mean—53.56±20.58 vessels/mm^2).

The subendocardial myocardium showed moderate hypertrophy of isolated fibers. Both routine histology and immunohistochemistry revealed few interstitial inflammatory cells, with predominance of macrophages and T-lymphocytes, without aggression to the myocardial fibers (borderline myocarditis) [25].

Molecular findings

The presence of sufficient nucleic acids for PCR analysis was confirmed by amplification of both β-globin for DNA

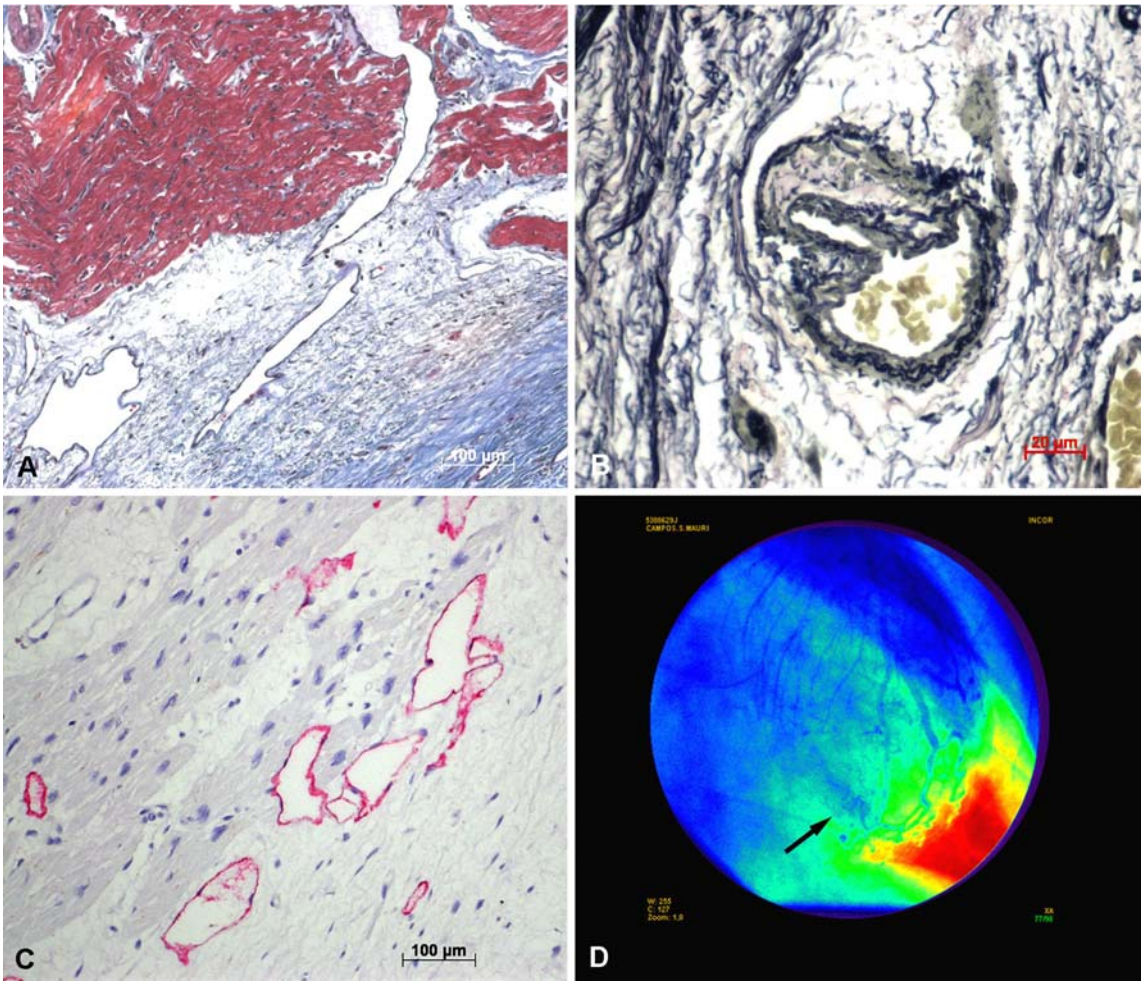

Fig. 3 Vascular aspects of EMF in endocardium. **a** dilated thin-walled blood vessels in the deep vascular layer permeating the adjacent myocardium seen at the top (Masson stain); **b** small vessel showing delicate elastic wall on the right and an irregular muscular thick wall on the left. This aspect may be interpreted either as a vessel division or an arteriovenous shunt because the wall of the right-sided vessel looks like a vein and the left-sided one appears to be a small artery (Verhoeff stain); **c** lymphatics seen in the endomyocardium interface; the myocardium is shown on the *left* (immunohistochemistry for podoplanin/D2-40); **d** left coronary angiogram in right anterior oblique: a vascular blush is shown in the region of septal branch (*arrow*)

and 3GPDH for RNA in 12/16 (75%) samples. Infective genomes were identified by PCR in 6/12 (50%) positive extracted cardiac samples. Two patients were positive for EV, two for CMV, one for both EV and CMV, and one for *T. gondii*. The RT-PCR or PCR were always repeated to confirm the initial positive amplification. Sequencing analysis of the viral CMV PCR products showed the follow homology: AF413626—human herpesvirus 5 strain 17A putative glycoprotein (UL20a) gene (identity 99.8%), X17403—human cytomegalovirus strain AD169 complete genome (identity 95.7%), and AF413627—human herpesvirus 5 strain 19A putative glycoprotein (UL20a) gene (98.3% identity). The EV PCR products showed the homology comprised between 85% and 90% for different enteroviral serotypes (i.e., coxsackievirus, echovirus, poliovirus, enterovirus). It was not possible to perform sequencing analysis on the *T. gondii* PCR products. None of the control samples showed positive amplification for any of the viruses investigated. No association occurred between the clinicopathological characteristics and the presence of infective genomes in the endomyocardium (Table 2).

Discussion

This study showed that surgical specimens are not only representative but also diagnostic of EMF, since all the histological criteria previously described in the literature were present [2].

The thickened fibrous endocardium showed three zones as previously described by Davies and Ball [11]. The superficial zone, presenting elastic and reticulin fibers, showed an arrangement reminiscent of endocardial reconstruction. Surprisingly, Masson's trichrome showed orange-stained

Table 2 Clinicopathological characteristics of patients positive and negative for infective genomes

Clinicopathological characteristic	Patients positive for infective genomes	Patients negative for infective genomes
Female gender	4/6 (67%)	4/6 (67%)
Age (years)	48±10	49±12
Blood eosinophilia	4/6 (67%)	2/6 (33%)
Δt of disease (years)	9.5±6.8	10.9±9.5
Bilateral EMF	4/6 (67%)	3/6 (50%)
Sudden death after surgery	2/6 (33%)	0/6 (0%)
HF	1/4 (25%)	2/6 (33%)
Prominent inflammatory infiltrate in the endomyocardium	2/6 (33%)	1/6 (17%)

Δt Elapsed time between onset of symptoms and surgery, *EMF* endomyocardial fibrosis, *HF* severe deterioration of cardiac function 3 to 4 years after surgery.

areas among the intense blue-stain characteristic of dense collagen, perhaps indicating collagen structural alterations. The immunohistochemical data showed the predominance of collagen type I over type III, in agreement with the gel electrophoretic studies of Rhadakumary et al. [26]. Deep within the endocardium, a second zone was observed containing a nonspecific inflammatory infiltrate, with predominance of macrophages and T-lymphocytes. It could be speculated that cytokine liberation by these cells might contribute both to fibrogenesis and to angiogenesis [27]. A small and poorly defined epithelioid granuloma was detected in only one case, with the presence of eosinophils, suggesting a Th2 immunological response. Although scarce, the presence of B-lymphocytes might be probably related to neolymphangiogenesis [28].

Blood hypereosinophilia led some authors to associate EMF with the Löeffler syndrome, in which hypereosinophilia and endocardial fibrosis may be present [29]. Eosinophils are found in many different diseases where collagen deposits are frequent, such as sclerosing cholangitis and Hodgkin's disease [30]. Although a large number of intact eosinophils were not observed in the present cases, degranulated eosinophils cannot be detected by routine staining [31] and might have been present in the cellular infiltrate.

It has been speculated that hypereosinophilia followed by eosinophil degranulation in the ventricular myocardium at early stages of EMF might promote local necrosis, inflammation, and thrombosis that culminate in scar tissue formation and endocardial thickening [32]. Hypereosinophilic syndrome was diagnosed in only one patient from the current series; however, relapsing blood eosinophilia during the follow-up was present in almost half of the patients. Other systemic manifestations are present in Löeffler syndrome chiefly in the respiratory tract, which are not observed in EMF. The current tendency is to consider EMF and Löeffler syndrome as separate entities.

Next to the myocardium, a third zone of blood vessels occurs, denominated "the granulation tissue layer" by Davies and Ball [11]. In 1973, Andrade and Teixeira [33] had already described intramyocardial coronary lesions in EMF and suggested that they might be important for disease progression. It is noteworthy that arterioles, small veins, and capillaries may be seen side by side, sometimes in an arrangement suggestive of arteriovenous shunt. Evidence for communication between this endocardial vascular net and the intramyocardial coronary circulation was observed in this work. For the first time, immunohistochemistry revealed a lymphatic net among the endocardial vessels which also communicate with those of the myocardium. Taken together, the lymphovascular pattern might contribute to a relative local impairment of the blood return circulation.

The vascular layer probably originates from the granulation tissue at the base of the initial lesion and presents a vascular morphology altered by different causes including hemodynamic factors. The presence of an active circulation beneath the fibrous plaque is probably important for the maintenance of the lesion.

Atypical chest pain in EMF has been mentioned by some authors and was linked to pathological alterations in the left ventricle [34–36]. Chest pain was present in 50% of the patients studied, sometimes during the follow-up, all of them presenting left ventricular disease. Balakrishnan et al. described "blush" (or neovascularization) in the terminal coronary circulation in 54.2% of patients, using coronary cineangiocardiography [37]. This image might correspond to the vascular lesions described above since it is not present in healthy individuals with preserved terminal coronary circulation. In the present series, 9/16 (56%) patients showed "blush" during the coronary cineangiocardiography, seven of them involving precordial pain not related to physical effort. Although it was not possible to identify any statistical association between chest pain, "blush" and vascular lesions, the clinical impression is that in EMF "blush" might be a manifestation of an altered microcirculation, occasionally associated with chest pain.

EMF etiology remains obscure even 60 years after its description [38]. Besides its association with hypereosinophilic syndromes, EMF has been linked to nutritional disturbances [9], geochemical factors [39], parasitism and infections [10].

As initially suggested by Davies and Ball [11], cardiotropic viral agents could trigger local endomyocardial inflammation evolving to scar tissue formation. In Nigeria, one previous report investigating cardiotropic infective agents (coxsackie B virus, arboviruses, and *T gondii*) in

patients presenting EMF reported higher positive blood serology for *T. gondii* but not for viruses compared to controls [12]. This study is the first one to investigate the occurrence of cardiotropic infective agents directly in the endomyocardium of patients presenting EMF. Despite the use of formalin-fixed paraffin-embedded samples which can underestimate the positivity of molecular analysis [40], half of the patients with EMF showed infective genomes in the ventricular endomyocardium. Cardiotropic viruses (EV and CMV) were present in 5/12 (42%) and *T. gondii* in 1/12 (8%) patients. Although that rate is exceedingly high compared to the control group and also to the previously published data concerning noninflammatory myocardium [16, 41], we have to keep in mind that the control samples were obtained of patients that did not come from geographical areas where EMF occurs.

Both experimental and human studies have already detected viral persistence in several chronic heart diseases, such as endocardial fibroelastosis and idiopathic dilated cardiomyopathy [42, 43]. The persistence of this so-called defective virus is often associated with slight cytolysis and consequently with mild inflammatory infiltrate. In the current small series, the lack of any association between the clinicopathological characteristics of the patients and the presence of infective genomes in the endomyocardium suggests that they may not be primarily related to the etiopathogenesis of EMF. However, the long-standing disease of the patients could mask the pathogenetic role of infective agents. Moreover, the injured endomyocardium would be more prone to secondary infection with infective agents, and their presence might contribute to aggravate the injury.

Acknowledgements The authors would like to thank Marcia Martins Reis for her excellent technical assistance in immunohistochemistry. This work was partially supported by the Fundação de Amparo a Pesquisa do Estado de São Paulo, process number 03/08052-8, and LIM 06, University of São Paulo Medical School.

Conflitct of interest statement We declare that we have no conflict of interest.

References

1. Davies JNP (1948) Endocardial Fibrosis in Africans. East Afr Med J 25:10–14
2. Connor DH, Somers K, Hutt MSR et al (1967) (1968). Endomyocardial fibrosis in Uganda (Davies' disease) Review. Part 1: Am Heart J 74: 687–709. Part 2: Am Heart J 75:107–124
3. Mady C, Pereira Barreto AC, de Oliveira SA et al (1989) Effectiveness of operative and non operative therapy in endomyocardial fibrosis. Am J Cardiol 63:1281–1282
4. Oliveira SA, Pereira-Barreto ACP, Mady C et al (1990) Surgical treatment of endomyocardial fibrosis: a new approach. J Am Coll Cardiol 16:1246–1251
5. Chopra P, Narula J, Talwar KK et al (1990) Histomorphologic characteristics of endomyocardial fibrosis: an endomyocardial biopsy study. Hum Pathol 21:613–616
6. Somers K, Hutt MSR, Patel AK et al (1971) Endomyocardial biopsy in diagnosis of cardiomyopathies. Br Heart J 33:822–832
7. Mayosi BM (2007) Contemporary trends in the epidemiology and management of cardiomyopathy and pericarditis in sub-Saharan Africa. Heart 93(10):1176–1183
8. Sliwa K, Damasceno A, Mayosi BM (2005) Epidemiology and etiology of cardiomyopathy in Africa. Circulation 112:3577–3583
9. Rutakingirwa M, Ziegler JL, Newton R et al (1999) Poverty and eosinophilia are risk factors for endomyocardial fibrosis (EMF) in Uganda. Trop Med Int Health 4(3):229–235
10. Andy JJ (2001) Aetiology of endomyocardial fibrosis (EMF). West Afr J Med 20(3):199–207
11. Davies JNP, Ball JD (1955) The pathology of endomyocardial fibrosis in Uganda. Br Heart J 17:337–359
12. Ijaola O, Falase AO (1990) Distribution of antibodies against coxsackie B viruses, arboviruses and *Toxoplasma gondii* among patients with endomyocardial fibrosis (EMF) compared with normal subjects from EMF endemic and non-endemic zones of Nigeria. Afr J Med Med Sci 19:93–103
13. Saiki RK, Scharf S, Faloona F et al (1985) Enzymatic amplification of beta-globin genomic sequences and restriction site analysis for diagnosis of sickle-cell anemia. Science 230:1350–1354
14. Bowles NE, Ni J, Kearney DL et al (2003) Detection of viruses in myocardial tissues by polymerase chain reaction: evidence of adenovirus as a common cause of myocarditis in children and adults. J Am Coll Cardiol 42:466–472
15. Bowles NE, Ni J, Marcus F et al (2002) The detection of cardiotropic viruses in the myocardium of patients with arrhythmogenic right ventricular dysplasia/cardiomyopathy. J Am Coll Cardiol 39:892–895
16. Calabrese F, Angelini A, Thiene G et al (2000) No detection of enteroviral genome in the myocardium of patients with arrhythmogenic right ventricular cardiomyopathy. J Clin Pathol 53:382–387
17. Calabrese F, Rigo E, Milanesi O et al (2002) Molecular diagnosis of myocarditis and dilated cardiomyopathy in children: clinicopathologic features and prognostic implications. Diagn Mol Pathol 11:212–221
18. Kytö V, Vuorinen T, Saukko P et al (2005) Cytomegalovirus Infection of the heart is common in patients with fatal myocarditis. Clin Infect Dis 40:683–688
19. Li Y, Peng T, Yang Y et al (2000) High prevalence of enteroviral genomic sequences in myocardium from cases of endemic cardiomyopathy (Keshan disease) in China. Heart 83:696–701
20. Stanta G, Schneider C (1991) RNA extracted from paraffin-embedded human tissue is amenable to analysis by PCR amplification. Biotechniques 11:304–308
21. Shibata DK (1992) The polymerase chain reaction and the molecular genetic analysis of tissue biopsies. In: Herrington CS, McGee O'D (eds) Diagnostic molecular pathology. A practical approach. Oxford University Press, New York, pp 85–111
22. Ercolani L, Florence B, Denaro M et al (1988) Isolation and complete sequence of a functional human glyceraldehyde-3-phosphate dehydrogenase gene. J Biol Chem 263:1535–1541
23. Lam KM, Oldenburg N, Khan MA et al (1998) Significance of reverse transcription polymerase chain reaction in the detection of human cytomegalovirus gene transcripts in thoracic organ transplant recipients. J Heart Lung Transplant 17:555–565
24. Schowengerdt KO, Ni J, Denfield SW et al (1997) Association of parvovirus B19 genome in children with myocarditis and cardiac allograft rejection: diagnosis using the polymerase chain reaction. Circulation 96:3549–3554
25. Aretz HT (1987) Myocarditis:The Dallas Criteria. Hum Pathol 18 (6):619–624

26. Radhakumary C, Kumari TV, Kartha CC (2001) Endomyocardial fibrosis is associated with selective deposition of type I collagen. Indian Heart J 53:486–489
27. Adams DH, Lloyd AR (1997) Chemokines: leucocyte recruitment and activation cytokines. Lancet 349:490–495
28. Angeli V, Ginhoux F, Llodra J et al (2006) B cell-driven lymphangiogenesis in inflamed lymph nodes enhances dendritic cell mobilization. Immunity 24:203–215
29. Brockington IF, Olsen EGJ (1973) Loeffler's endocarditis and Davies' endomyocardial fibrosis. Am Heart J 85:308–322
30. Noguchi H, Kephart GM, Colby TV et al (1992) Tissue eosinophilia and eosinophil degranulation in syndromes associated with fibrosis. Am J Pathol 140(2):521–528
31. Spry CJF (1986) Eosinophils in eosinophilic endomyocardial disease. Postgrad Med J 62:609–613
32. Olsen EGJ, Spry CJF (1985) Relation between eosinophilia and endomyocardial disease. Prog Cardiovasc Dis 27(4):241–254
33. Andrade ZA, Teixeira ARL (1973) Changes in the coronary vasculature in endomyocardial fibrosis and their possible significance. Am Heart J 86(2):152–158
34. Gupta PN, Valiathan M, Balakrishnan KG et al (1989) Clinical course of endomyocardial fibrosis. Br Heart J 62:450–454
35. Pereira Barretto AC, Mady C, Pileggi F (1996) Longitudinal follow-up of patients not treated by surgery. Arq Bras Cardiol 67 (4):285–288
36. Bestetti RB, Corbucci H, Fornitano L et al (2005) Angina-like chest pain and syncope as the clinical presentation of left ventricular endomyocardial fibrosis: a case report. Angiology 56 (3):339–342
37. Balakrishnan KG, Sasidharan K, Venkitachalam CG et al (1983) Coronary angiographic features in endomyocardial fibrosis. Cardiology 70:121–126
38. Bukhman G, Ziegler J, Parry E (2008) Endomyocardial fibrosis: still a mystery after 60 years. PLoS Negl Trop 2(2):e97 doi:10.1371/journal.pntd.0000097
39. Valiathan SM, Kartha CC (1990) Endomyocardial fibrosis—the possible connexion with myocardial levels of magnesium and cerium—review. Int J Cardiol 28(1):1–5
40. Hunt JL (2008) Molecular pathology in anatomic pathology practice. A review of basic principles. Arch Pathol Lab Med 132: 248–260
41. Ueno H, Yokota Y, Shiotani H et al (1995) Significance of detection of enterovirus RNA in myocardial tissue by reverse transcription-polymerase chain reaction. Int J Cardiol 51:157–164
42. Ni J, Bowles NE, Kim Y-H et al (1997) Viral infection of the myocardium in endocardial fibroelastosis. Molecular evidence for the role of mumps virus as an etiologic agent. Circulation 95:133–139
43. Keeling PJ, Tracy S (1994) Link between enteroviruses and dilated cardiomyopathy: serological and molecular data. Br Heart J 72(6 suppl):S25–29

Virchows Arch (2008) 453:243–248
DOI 10.1007/s00428-008-0646-1

ORIGINAL ARTICLE

AMACR expression in colorectal cancer is associated with left-sided tumor localization

Andreas Marx · Philipp Simon · Ronald Simon · Martina Mirlacher · Jakob R. Izbicki · Emre Yekebas · Jussuf T. Kaifi · Luigi Terracciano · Guido Sauter

Received: 2 May 2008 / Revised: 30 June 2008 / Accepted: 12 July 2008 / Published online: 19 August 2008

Abstract Alpha-methylacyl-CoA racemase (AMACR) is an enzyme playing an important role in the β-oxidation of branched-chain fatty acids and fatty acid derivatives. Altered expression levels of AMACR have been described in various cancers including colorectal cancer (CRC). To determine the potential prognostic impact of AMACR expression, we analyzed 1,315 CRC on a tissue microarray (TMA) by immunohistochemistry (IHC). Clinical follow-up data were available from all cancer patients. Positive AMACR staining was observed in 1,074 (81.7%) of the 1,315 cases including 276 cancers with weak (21.0%) and 798 cancers with strong staining (60.7%). AMACR IHC was significantly associated with tumor grade, stage, non-mucinous phenotype, and left-sided tumor localization ($p<0.0001$ each). AMACR positivity was observed in 65.8% of cancers from the right-sided colon, in 73.2% of cancers from the colon transversum, in 81.1% of cancers from the colon descendens, and in 88.9% of the distal left-sided cancers (sigma and rectum; $p<0.0001$). However, AMACR staining results were unrelated to clinical outcome. It is concluded that AMACR cannot serve as a prognostic marker in CRC. We hypothesize that the association of AMACR expression with tumor localization may be related to differences in the metabolism/exposure to fatty acids occurring along the colon.

Keywords AMACR · Colorectal cancer

A. Marx (✉) · P. Simon · R. Simon · M. Mirlacher · G. Sauter
Institute for Pathology,
University Medical Center Hamburg-Eppendorf,
Martinistr. 52,
20246 Hamburg, Germany
e-mail: a.marx@uke.de

J. R. Izbicki · E. Yekebas · J. T. Kaifi
Department of Surgery,
University Medical Center Hamburg-Eppendorf,
20246 Hamburg, Germany

L. Terracciano
Institute of Pathology, University Hospital Basel,
Basel, Switzerland

Introduction

Alpha-methylacyl-CoA racemase (AMACR) is a mitochondrial and peroxisomal enzyme playing an important role in the β-oxidation of branched-chain fatty acids and fatty acid derivatives. It catalyzes the conversion of 2*R*-fatty acids into their *S*-stereoisomeres, which can further be metabolized and degraded [4, 5, 9, 22, 23]. The frequent overexpression in prostate cancer has first pointed to a role of AMACR in cancer biology, and AMACR expression analysis has soon become a routine tool in prostate cancer diagnosis [6, 7, 10, 15, 17, 18, 21, 29]. Subsequent studies have revealed that AMACR is also over-expressed in many other tumor types [9, 14, 16, 20, 27, 28, 30]. The potential utility of AMACR analysis in the diagnosis of dysplasia is currently widely studied, especially in gastrointestinal tract pathology [3].

Several studies have shown that increased AMACR protein levels can be found in about 45–83% of colorectal carcinomas [2, 8, 13, 20, 25, 27, 30]. It was recently suggested that AMACR over-expression may be associated with favorable histological grade and good prognosis in colorectal cancer (CRC) [2, 13, 25, 30]. Chen et al. have further suggested, that AMACR protein may serve as a tool to distinguish CRC from cancers derived from the small intestine [2]. These data are of potential interest; however, the existing studies were done on relatively small numbers

Table 1 Clinical and pathological features of colorectal cancers

Clinical/pathological features	*n*
Gender	
Female	646
Male	669
Tumor grade	
G1	16
G2	1,118
G3	181
Tumor stage	
pT1	55
pT2	213
pT3	846
pT4	201
Nodal status	
pN0	690
pN1	353
pN2	272
Tumor type	
Tubular carcinoma	1,223
Mucinous carcinoma	89
Signet cell carcinoma	3
Localization	
Cecum	164
Colon ascendens	155
Colon transversum	108
Colon descendens	53
Colon sigmoideum	266
Rectosigmoid	76
Rectum	493
Total number	1,315

of cancers of fewer than 200 patients each. To further expand our knowledge on the relevance of AMACR expression in CRC, we analyzed a series of 1,315 cancers with follow-up data on a set of tissue microarrays.

Materials and methods

Patients and tissue microarray construction Two different tissue microarrays (TMA) with a total of 1,800 CRC samples were included in this study. The first TMA was manufactured from resection specimens of 1,420 CRC patients at the Institute of Pathology of the University Hospital of Basel. Raw survival data were obtained from the responsible physicians for all of the 1,420 patients. The median follow-up time was 38.4 months (range 1–144 months).

The second TMA included samples from 380 CRC patients, whose tumor resection specimens were examined at the Institute of Pathology of the University Medical Center Hamburg-Eppendorf. Also for this TMA, raw survival data were available for all of the 380 patients with a median follow-up period of 42.8 month (range 1–180 month).

TMA construction was as described [26]. In brief, hematoxylin and eosin-stained sections were made from each block to define representative tumor regions. Tissue cylinders with a diameter of 0.6 mm were then punched

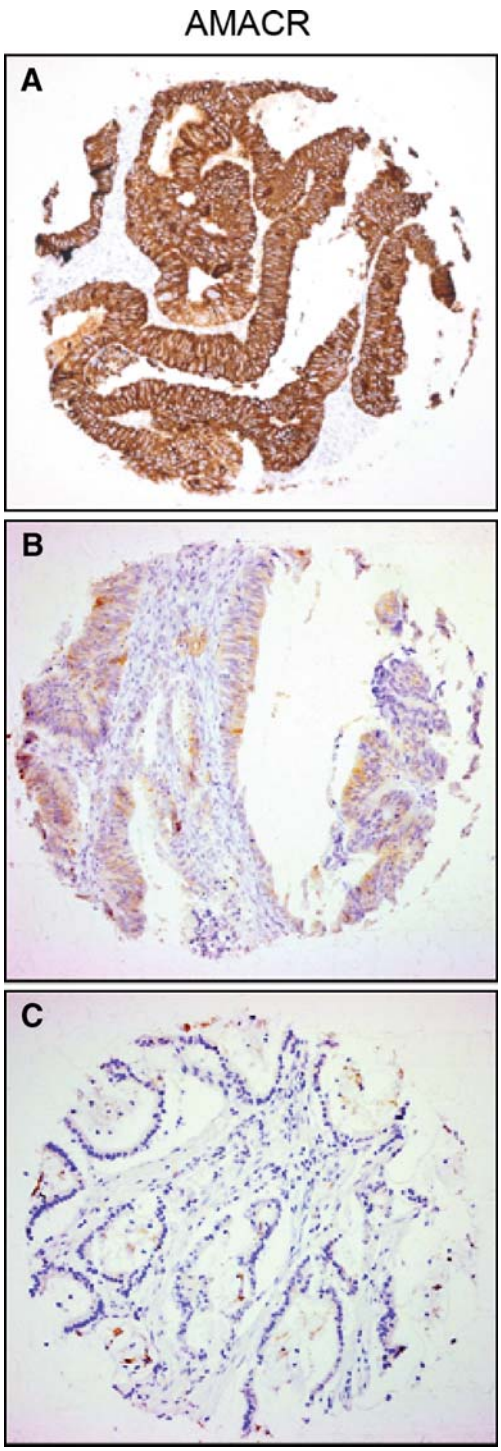

Fig. 1 TMA samples of colorectal cancers show strong (**a**), weak (**b**), or negative (**c**) immunostaining for AMACR

Table 2 AMACR IHC, clinical and pathological features

	n	AMACR IHC			*p* value[a]
		Negative	Weak	Strong	
		%	%	%	
Tumor grade					
G1	16	18.75	31.25	50.00	
G2	1,118	13.60	21.74	64.67	
G3	181	47.51	15.47	37.02	<0.0001
Tumor stage					
pT1	55	16.36	29.09	54.55	
pT2	213	10.80	22.07	67.14	
pT3	846	17.38	21.16	61.47	
pT4	201	30.85	16.92	52.24	<0.0001
Nodal status					
pN0	690	15.94	20.43	63.62	
pN1	353	19.55	22.66	57.79	
pN2	272	22.79	20.22	56.99	0.087
Tumor type					
Tubular	1,223	16.11	21.01	62.88	
Mucinous	89	46.07	21.35	32.58	
Signet cell	3	100.00	0	0	<0.0001
Tumor localization					
Cecum + ascendens	319	34.17	21.32	44.51	
Transversum	108	26.85	25.00	48.15	
Descendens	53	18.87	16.98	64.15	
Sigmoid + rectum	835	11.14	20.60	68.26	<0.0001
Total	1,315				

[a] Chi-square *p* value

from tumor areas of each "donor" tissue block using a homemade semi-automated precision instrument and brought into empty recipient paraffin blocks. Four-micrometer sections of the resulting TMA blocks were transferred to an adhesive coated slide system (Instrumedics Inc., Hackensack, NJ, USA). Patient information and clinical data as age, sex, localization and type of the tumor, pTNM-stage, and carcinoma grade were retrospectively retrieved from clinical and pathological databases (Table 1). All tumors were reclassified by two pathologists (LT, AM). Follow-up data were obtained from local cancer register boards or via attending physicians. For statistical analyses, tumor localizations were grouped as follows: right-sided cancer (cecum, ascendens), cancer from the colon transversum, cancer from the colon descendens, and distal left-sided cancer (sigma, rectum).

Immunohistochemistry After deparaffinization, the tissue sections were pretreated for 25 min in a Sharp™ microwave oven (approximately 98°C) for heat-induced epitope retrieval at pH 9.0 [tris(hydroxymethyl)aminomethane–ethylenediamine tetraacetic acid buffer]. Standard indirect immunoperoxidase procedures were used for visualization of bound antibody (Envision System, DAKO, Glostrup, Denmark). The monoclonal rabbit anti-human p504s antibody (clone 13H4; DAKO, Glostrup, Denmark) was used at a dilution of 1:200 (61.3 mg/l). Diaminobenzidine was used as the chromogen. Only cytoplasmatic staining was considered. For tumor tissues, the percentage of positive cells was estimated, and the staining intensity was recorded as 1+, 2+, or 3+. For statistical analyses, the staining results were categorized into three groups. Tumors without any staining were considered AMACR "negative." Tumors showing at least weak AMACR staining were considered "positive." Tumors with 1+ or 2+ positivity in up to 50% of cells or 3+ positivity in up to 20% of cells were considered "weakly positive." Tumors with 2+ staining in >50% or 3+ staining in >20% were considered "strongly positive."

Statistics Contingency tables and chi-square analyses were used to analyze associations between immunohistochemistry (IHC) results and entity subgroups with the aid of the JMP software package (SAS Institute Inc, version 5.0.1a).

Overall survival was estimated by the Kaplan–Meier method and evaluated by log-rank testing for univariate and likelihood ratio testing for multivariate analysis.

Results

AMACR immunohistochemistry A total of 485 from 1,800 tissue samples (26.9%) were non-informative due to either absence of unequivocal cancer tissue or complete loss of tissue. AMACR immunostaining was seen in 1,074 of the remaining 1,315 CRC (81.7%). Immunostaining was typically cytoplasmatic with coarse granularity. Representative examples of AMACR-stained cancers are shown in

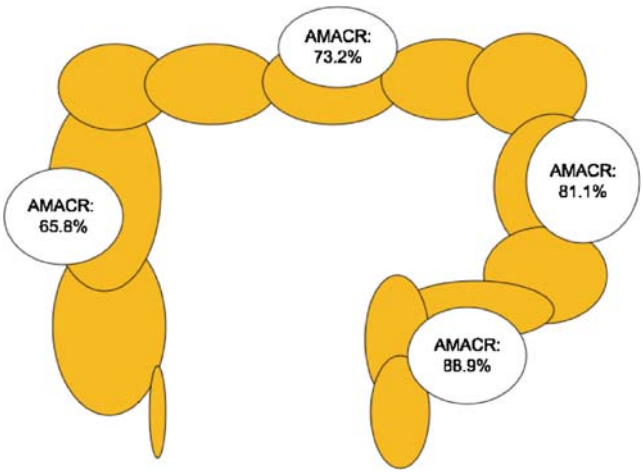

Fig. 2 AMACR immunostaining of colorectal cancer depends on tumor localization

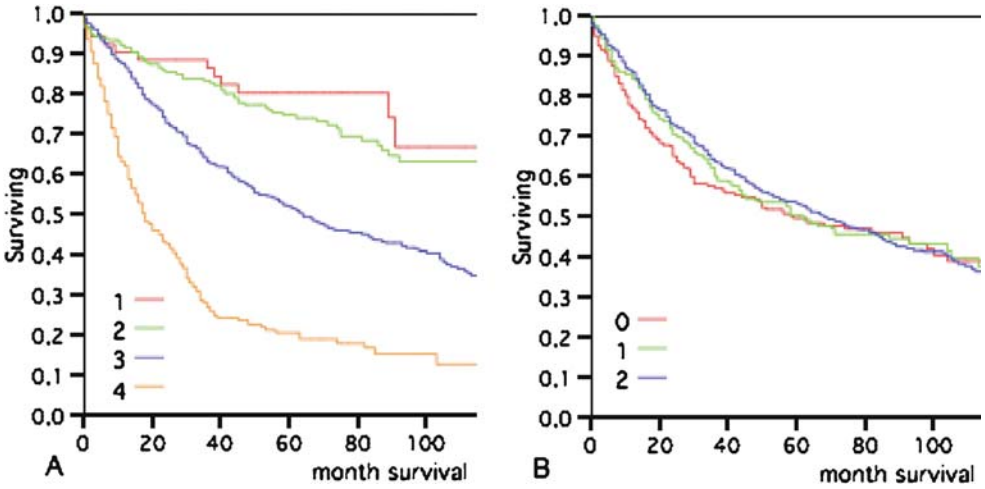

Fig. 3 Patient survival is related to tumor stage (**a**) but not to AMACR IHC (**b**). **a** Tumor stage vs survival; *red* T1, *green* T2, *blue* T3, *orange* T4; $p<0.0001$. **b** AMACR IHC vs survival; *red* negative, *green* weak, *blue* strong AMACR IHC; $p=0.1669$

Fig. 1. AMACR staining was considered weak in 276 (21.0%) and strong in 798 cases (60.7%). The relationship between AMACR staining, tumor phenotype, and clinical parameters is shown in Table 2.

Decreased AMACR expression was significantly associated with high tumor grade ($p<0.0001$) and high tumor stage ($p<0.0001$), but there was no correlation to the nodal status ($p=0.087$). AMACR staining was more frequent in tubular carcinoma than in the less frequent histological subtypes (mucinous, signet cell; $p<0.0001$). Moreover, AMACR expression levels were significantly related to the tumor localization. AMACR expression was lowest in carcinomas from the right colon (65.8%), intermediate in carcinomas from the colon transversum (73.2%) and colon descendens (81.1%), and highest in carcinomas from the distal left-sided colon (sigma and rectum; 88.9%); Table 2 and Fig. 2.

Survival analysis

As expected, high tumor grade and stage as well as advanced nodal status were associated with poor patient survival (Fig. 3a; $p<0.0001$), while histological tumor type was unrelated to clinical outcome (Table 2). Left-sided CRC (distal to the left colon flexur) were associated with a better prognosis ($p=0.0014$). AMACR IHC status of all CRC was unrelated to patient survival ($p=0.1669$; Fig. 3b). These associations held true also in the subset of tubular carcinomas only (data not shown). Also, the inclusion of tumors with weak positivity into the AMACR negative group (as in the study by Lin et al [13]) did not lead to significant survival differences between AMACR positive and negative tumors (data not shown).

Multivariate analysis Multivariate analysis including tumor stage, tumor grade, tumor location, nodal status, and AMACR expression did not also reveal any prognostic impact of AMACR expression. In this analysis, only pT ($p<0.0001$), grade ($p=0.0019$), and pN ($p<0.0001$) had significance but not tumor localization ($p=0.5252$) or AMACR expression ($p=0.1857$; Table 3).

Discussion

The frequency of immunohistochemical AMACR positivity found in this study on 1,315 CRC patients (81.7%) was comparable to previous results. Other investigators described 45% to 83% AMACR positive CRC, but all of these studies were performed on patient numbers smaller than 200 [2, 8, 13, 20, 25, 27, 30]. The association found with non-mucinous tumor type, tumor grade, and tumor stage was also in line with the results of a previous study [13]. Based on the high frequency of AMACR positivity seen in this study and the concordance of our results with previous data, it appears unlikely that the use of TMA containing only limited amounts of tumor tissue per patient (one spot of 0.6 mm diameter per patient) has led to a significant number of false negative cases.

Table 3 Multivariate analysis

Parameter	Variable	Risk ratio	95%CI	*p* value
Tumor stage	pT1/2 vs 3/4	0.70	0.61–0.79	<0.0001
Grade	G1/2 vs 3/4	0.83	0.74–0.93	0.0019
Nodal status	N0 vs N1/2	0.66	0.61–0.72	<0.0001
Tumor localization	Right- vs left-sided	1.03	0.94–1.12	0.5252
AMACR IHC	Positive vs negative	0.93	0.84–1.03	0.1857

Lin et al. have previously reported a striking independent association between AMACR expression and patient survival in their study on 163 CRC and discussed the potential use of AMACR as a prognostic marker [13]. As their study was also executed on a TMA, focal AMACR expression cannot serve as an explanation for the discrepancies as compared to our study. The biological significance of focal AMACR expression, which we sometimes observe on large sections, remains to be clarified.

Comparable to Shi et al., no significant association between AMACR expression and prognosis could be found in our study, despite other features such as tumor grade and tumor stage which were highly significant for the outcome in this patient cohort [25]. However, the differences in AMACR expression between tumors of different grade and stage were quite small in terms of absolute numbers. The strong p value seems to be caused by the high number of analyzed cases in our study (n=1,315) providing strong statistical power. The strong association between classical prognostic features such as tumor stage, tumor grade, and nodal status and prognosis in our patient set provides indirect proof for the validity of our clinical data. Therefore, we believe that our findings strongly argue against a clinical utility of AMACR immunostaining as a prognostic biomarker in colorectal cancer patients.

The AMACR expression level was significantly higher in the left-sided than in the right-sided CRC. The reason for this observation is unclear. It could be hypothesized that pathways leading to increased AMACR expression are less often activated in patients with hereditary non-polyposis colon cancer syndromes or sporadic colorectal cancers exhibiting microsatellite instability (MSI), which are more often localized in the right colon. This hypothesis obtains support from a report by Chen et al. showing that colon cancers with MSI have reduced AMACR expression [2]. This observation does not rule out other causes for the left colon preference of AMACR over-expression. In fact, it is expected that every alteration occurring more frequently in the left colon than in the right colon should be statistically associated with lower MSI frequency as MSI is known to preferably occur in the right colon [2]. Given the known function of AMACR as a fat metabolizer, it could also be speculated that the localization-dependent expression could be related to a different exposition to branched-chain fatty acids and fatty acid derivatives in the distal colon as compared to the more proximal intestine [19]. Branched-chain fatty acids are, for example, found in meat products, especially red meat [13, 15]. Epidemiological studies have indicated that consumption of red meat is associated with a higher risk of developing colon cancer, especially in the distal portion of the large intestine [1, 11, 12, 24].

In summary, our data show that AMACR expression occurs frequently in colorectal cancers with a clear preference for left-sided tumors. The cause for this obvious association is unclear. Despite a mild relationship between AMACR expression and unfavorable tumor phenotype, previous reports on a possible prognostic role of AMACR in colon cancer could not be confirmed.

Conflicts of interest We declare that we have no conflict of interest.

References

1. Chao A, Thun MJ, Connell CJ, McCullough ML, Jacobs EJ, Flanders WD, Rodriguez C, Sinha R, Calle EE (2005) Meat consumption and risk of colorectal cancer. JAMA 293:172–182
2. Chen ZM, Ritter JH, Wang HL (2005) Differential expression of alpha-methylacyl coenzyme A racemase in adenocarcinomas of the small and large intestines. Am J Surg Pathol 29:890–896
3. Dorer R, Odze RD (2006) AMACR immunostaining is useful in detecting dysplastic epithelium in Barrett's esophagus, ulcerative colitis, and Crohn's disease. Am J Surg Pathol 30:871–877
4. Ferdinandusse S, Denis S, Ijlst L, Dacremont G, Waterham HR, Wanders RJ (2000) Subcellular localization and physiological role of alpha-methylacyl-CoA racemase. J Lipid Res 41:1890–1896
5. Ferdinandusse S, Overmars H, Denis S, Waterham HR, Wanders RJ, Vreken P (2001) Plasma analysis of di- and trihydroxycholestanoic acid diastereoisomers in peroxisomal alpha-methylacyl-CoA racemase deficiency. J Lipid Res 42:137–141
6. Hameed O, Humphrey PA (2005) Immunohistochemistry in diagnostic surgical pathology of the prostate. Semin Diagn Pathol 22:88–104
7. Humphrey PA (2007) Diagnosis of adenocarcinoma in prostate needle biopsy tissue. J Clin Pathol 60:35–42
8. Jiang Z, Fanger GR, Banner BF, Woda BA, Algate P, Dresser K, Xu J, Reed SG, Rock KL, Chu PG (2003) A dietary enzyme: alpha-methylacyl-CoA racemase/P504S is overexpressed in colon carcinoma. Cancer Detect Prev 27:422–426
9. Jiang Z, Fanger GR, Woda BA, Banner BF, Algate P, Dresser K, Xu J, Chu PG (2003) Expression of alpha-methylacyl-CoA racemase (P504s) in various malignant neoplasms and normal tissues: a study of 761 cases. Human Pathol 34:792–796
10. Jiang Z, Woda BA, Rock KL, Xu Y, Savas L, Khan A, Pihan G, Cai F, Babcook JS, Rathanaswami P, Reed SG, Xu J, Fanger GR (2001) P504S: a new molecular marker for the detection of prostate carcinoma. Am J Surg Pathol 25:1397–1404
11. Larsson SC, Rafter J, Holmberg L, Bergkvist L, Wolk A (2005) Red meat consumption and risk of cancers of the proximal colon, distal colon and rectum: the Swedish Mammography Cohort. Int J Cancer 113:829–834
12. Larsson SC, Wolk A (2006) Meat consumption and risk of colorectal cancer: a meta-analysis of prospective studies. Int J Cancer 119:2657–2664
13. Lin A, Weiser MR, Klimstra DS, Paty PB, Tang LH, Al-Ahmadie H, Hoo Park S, Guillem JG, Temple L, Wong WD, Gerald WL, Shia J (2007) Differential expression of alpha-methylacyl-coenzyme A racemase in colorectal carcinoma bears clinical and pathologic significance. Human Pathol 38:850–856
14. Martignoni G, Brunelli M, Gobbo S, Remo A, Ficarra V, Cossu-Rocca P, Pea M, Chilosi M, Menestrina F, Cheng L (2007) Role of molecular markers in diagnosis and prognosis of renal cell carcinoma. Anal Quant Cytol Histol 29:41–49
15. Mobley JA, Leav I, Zielie P, Wotkowitz C, Evans J, Lam YW, L'Esperance BS, Jiang Z, Ho SM (2003) Branched fatty acids in

dairy and beef products markedly enhance alpha-methylacyl-CoA racemase expression in prostate cancer cells in vitro. Cancer Epidemiol Biomark Prev 12:775–783
16. Molinie V, Balaton A, Rotman S, Mansouri D, De Pinieux I, Homsi T, Guillou L (2006) Alpha-methyl CoA racemase expression in renal cell carcinomas. Human Pathol 37:698–703
17. Molinie V, Herve JM, Lugagne PM, Yonneau L, Ellard S, Lebret T, Botto H (2005) Value of new prostate cancer markers: alpha methylacyl CoA racemase (P504S) and p63. Prog Urol 15:611–615
18. Mubiru JN, Valente AJ, Troyer DA (2005) A variant of the alpha-methyl-acyl-CoA racemase gene created by a deletion in exon 5 and its expression in prostate cancer. Prostate 65:117–123
19. Narisawa T, Takahashi M, Masuda T, Niwa M (1986) Dietary factors to induce and suppress colon cancer development. Gan No Rinsho 32:674–679
20. Nassar A, Amin MB, Sexton DG, Cohen C (2005) Utility of alpha-methylacyl coenzyme A racemase (p504s antibody) as a diagnostic immunohistochemical marker for cancer. Appl Immunohistochem Mol Morphol 13:252–255
21. Rubin MA, Bismar TA, Andren O, Mucci L, Kim R, Shen R, Ghosh D, Wei JT, Chinnaiyan AM, Adami HO, Kantoff PW, Johansson JE (2005) Decreased alpha-methylacyl CoA racemase expression in localized prostate cancer is associated with an increased rate of biochemical recurrence and cancer-specific death. Cancer Epidemiol Biomark Prev 14:1424–1432
22. Schmitz W, Albers C, Fingerhut R, Conzelmann E (1995) Purification and characterization of an alpha-methylacyl-CoA racemase from human liver. Eur J Biochem 231:815–822
23. Setchell KD, Heubi JE, Bove KE, O'Connell NC, Brewsaugh T, Steinberg SJ, Moser A, Squires RH Jr (2003) Liver disease caused by failure to racemize trihydroxycholestanoic acid: gene mutation and effect of bile acid therapy. Gastroenterology 124:217–232
24. Shannon J, White E, Shattuck AL, Potter JD (1996) Relationship of food groups and water intake to colon cancer risk. Cancer Epidemiol Biomark Prev 5:495–502
25. Shi X, Gong E, Wu X (2007) Alpha-methylacyl-CoA racemase/P504S overexpression in colorectal carcinoma is correlated with tumor differentiation. Appl Immunohistochem Mol Morphol 15:175–180
26. Simon R, Mirlacher M, Sauter G (2005) Tissue microarrays. Methods Mol Med 114:257–268
27. Went PT, Sauter G, Oberholzer M, Bubendorf L (2006) Abundant expression of AMACR in many distinct tumour types. Pathology 38:426–432
28. Witkiewicz AK, Varambally S, Shen R, Mehra R, Sabel MS, Ghosh D, Chinnaiyan AM, Rubin MA, Kleer CG (2005) Alpha-methylacyl-CoA racemase protein expression is associated with the degree of differentiation in breast cancer using quantitative image analysis. Cancer Epidemiol Biomark Prev 14:1418–1423
29. Xu J, Stolk JA, Zhang X, Silva SJ, Houghton RL, Matsumura M, Vedvick TS, Leslie KB, Badaro R, Reed SG (2000) Identification of differentially expressed genes in human prostate cancer using subtraction and microarray. Cancer Res 60:1677–1682
30. Zhou M, Chinnaiyan AM, Kleer CG, Lucas PC, Rubin MA (2002) Alpha-Methylacyl-CoA racemase: a novel tumor marker over-expressed in several human cancers and their precursor lesions. Am J Surg Pathol 26:926–931

Virchows Arch (2008) 453:249–255
DOI 10.1007/s00428-008-0642-5

ORIGINAL ARTICLE

IL-1B −31T>C promoter polymorphism is associated with gastric stump cancer but not with early onset or conventional gastric cancers

R. Sitarz · W. W. J. de Leng · M. Polak · F. H. M. Morsink · O. Bakker · W. P. Polkowski · R. Maciejewski · G. J. A. Offerhaus · A. N. Milne

Received: 6 February 2008 / Revised: 4 June 2008 / Accepted: 3 July 2008 / Published online: 8 August 2008

Abstract It has been reported that interleukin-1beta (IL-1B) genes play a crucial role in the genetic predisposition to gastric cancer although there is no information about their role in different subtypes of gastric cancer. We performed single nucleotide polymorphism analysis of IL-1B in 241 gastric cancers including early onset gastric cancers (EOGC), conventional gastric cancers, and gastric stump cancers (GSCs) as well as 100 control patients, using real-time polymerase chain reaction and sequence analysis. The C allele was present in 60% of EOGCs, 59% of conventional gastric cancers, and 90% of GSCs, compared to 62% in the control group. Interestingly, there was no difference between early onset and conventional gastric cancer with respect to the *IL-1B* −31T>C polymorphism distribution. A statistically significant difference in the presence of the C allele compared to the control group was found in patients with gastric stump cancer (p= 0.008) with the T allele conferring protection against gastric stump cancer. In summary, we have shown that the *IL-1B* −31C allele promoter polymorphism is significantly associated with gastric stump cancer compared to the control group. Although several molecular differences have been identified between conventional gastric cancer and early onset gastric cancer, the *IL-1B* −31 allele distribution is similar between these two groups.

Keywords *IL-1B* 31T>C polymorphism · Early onset gastric cancer · Gastric stump cancer · Conventional gastric cancer

R. Sitarz · W. W. J. de Leng · F. H. M. Morsink · G. J. A. Offerhaus · A. N. Milne (✉)
Department of Pathology, H04-312,
University Medical Center Utrecht,
Postbox 85500, 3508 GA Utrecht, The Netherlands
e-mail: a.n.a.milne@umcutrecht.nl

R. Sitarz · R. Maciejewski
Department of Human Anatomy, Medical University of Lublin,
Lublin, Poland

M. Polak · G. J. A. Offerhaus
Department of Pathology, Academic Medical Centre,
Amsterdam, The Netherlands

O. Bakker
Department of Endocrinology, Academic Medical Centre,
Amsterdam, The Netherlands

W. P. Polkowski
Department of Surgical Oncology, Medical University of Lublin,
Lublin, Poland

Introduction

Although gastric cancer incidence decreases worldwide, it is still the second most common cause of cancer-related death in the world [35]. According to the Lauren classification [24], gastric cancer is divided into two main histological types, diffuse and intestinal. Gastric cancer results from a combination of environmental factors and accumulation of specific genetic alterations. In conventional gastric cancer (presenting >45 years old), environmental factors play a more important role, compared to early onset gastric cancer (EOGC, presenting at ≤45 years old) where it is postulated that genetic factors may be more important [20]. We have previously shown that molecular differences exist between conventional gastric cancer and EOGC [4–6, 29–32]. Apart from cases of hereditary gastric cancer, it remains unclear what predisposes the young patients to gastric cancer at such an early age.

Helicobacter pylori, is a class I carcinogen [16] and is the main environmental factor causing gastric cancer [11,

36]. *H. pylori* infection has been shown to range from approximately 60% in the general population to approximately 84% in patients with gastric cancer [36]. Only a few papers about *H. pylori* infection in gastric cancer patients younger than 40 years have been published, all showing an association between gastric cancer and *H. pylori* infection [21, 28, 37]. *H. pylori* is involved in both intestinal and diffuse types of gastric cancer, the latter type being more common in EOGC [37].

Interleukin-1beta (IL-1B) is a key pro-inflammatory cytokine, which regulates the expression of several genes involved in inflammation. IL-1B is an endogenous inhibitor of gastric acid secretion and is important in initiating and enhancing the inflammatory response to *H. pylori* infection [34, 43]. Although the production of IL-1B depends on several factors, there is increasing evidence that the genetic background plays a major role. Therefore, single nucleotide polymorphisms (SNPs) in the *IL-1B* gene may be of importance in gene transcriptional activity.

Several single nucleotide polymorphisms in *IL-1B* have been studied, but many of these seem to be functionally insignificant and not associated with predisposition to cancer [7]. There are two biallelic polymorphisms at positions −31 and −511 in the promoter region of *IL-1B*, of which the −31C allele and the −511T allele are in positive linkage disequilibrium and associated with gastric cancer risk. It has been reported that carriers of the *IL-1B* −31C allele, showed higher plasmatic concentrations of IL-1B than subjects with wild-type *IL-1B* genotype [14]. Upregulation of IL-1B is involved in tumor-promoting effects such as invasiveness [40], angiogenesis [38], and metastasis [45] and has been recognized as negative prognostic factor, mainly in metastatic cancer [27]. Conversely, an association between peptic ulcer and the *IL-1B* −31T polymorphism has been described [8, 9]. Bearing this information in mind, the IL-1B status of patients with EOGC is of great interest. Whether these patients have a genetic predisposition for the carcinogenic pathway in response to *H. pylori* infection has never been investigated.

Several independent groups have found an association between partial gastrectomy (mostly after gastroduodenal ulcers) and increased risk for development of gastric cancer [33, 39]. These so-called gastric stump cancers (GSCs) are carcinomas occurring in the gastric remnant at least 5 years after surgery for a benign disease [42]. This represents a novel group in terms of *IL-1B* polymorphisms in that they are patients who have a predisposition for gastroduodenal ulcers yet have also developed gastric cancer. The *IL-1B* status of gastric stump cancers has never been studied to date.

In this study, we examined the distribution of the *IL-1B* −31T>C polymorphism in 241 gastric cancers including EOGC, conventional gastric cancer and GSC using real-time polymerase chain reaction (PCR) and sequence analysis and we investigated the relationship of *IL-1B* status with histology and location of the tumor.

Materials and methods

Patients

We used 96 conventional gastric cancers (>45 years old) obtained from the Academic Medical Centre, Amsterdam diagnosed between 1993 and 2003. One hundred and fifteen early onset gastric cancers (≤45 years old) diagnosed between 1980 and 2002, were obtained from 24 different institutions throughout The Netherlands through the nationwide database system and from the Department of Pathology at the Jorvi Hospital (Espoo, Finland) and 30 gastric stump cancers from the Amsterdam post-gastrectomy cohort [41]. The control group consisted of 100 DNA samples from the Department of Endocrinology at the Academic Medical Center, Amsterdam as published previously [44]. The tumors were classified by an experienced gastrointestinal pathologist (GJAO) according to the Lauren classification, as can be seen in Table 1. *H. pylori* vacA s region genotype and the presence of the cagA gene were known for 29 of the EOGC

Table 1 Patients' characteristics

	No. of patients	Age (range)	Histology	Location
Early onset gastric cancer (EOGC)	115	≤45 (21–45 years)	Intestinal—25 (22%) Diffuse—80 (70%) Mixed—10 (9%)	Cardia—9 (8%) Non-cardia—66 (57%) Unknown—40 (35%)
Conventional gastric cancer	96	>45 (47–86 years)	Intestinal—49 (51%) Diffuse—36 (38%) Mixed—11 (11%)	Cardia—49 (51%) Non-cardia—41 (43%) Unknown—6 (6%)
Gastric stump cancer (GSC)	30	(54–85 years)	Intestinal—26 (87%) Diffuse—2 (7%) Mixed—2 (7%)	Unknown
Control group	100	(22–52 years)	None	None

cases as detected by PCR followed by agarose gel electrophoresis and as published previously [6]. *H. pylori* infection was detected in 11 of 29 (37.9%) of these cases, a percentage which is in accordance with published data concerning The Netherlands population [25].

DNA isolation

DNA was isolated from formalin-fixed tissue using the QIAamp DNA mini kit (Qiagen, Venlo, The Netherlands) or the Puregene DNA isolation kit (Gentra, Minneapolis, USA) according to the manufacturer's instructions. Normal tissue was obtained from a tumor-free lymph node, or where necessary, from tissue with a small component of neoplastic cells. DNA concentrations were measured using the NanoDrop spectrophotometer (Isogen Life Science, IJsselstein, The Netherlands).

Real-time PCR

The polymorphism −31T>C in the promoter region of *IL-1B* was detected using the LightCycler 2.0 (Roche, Mannheim, Germany) with 5′-ccccttccctttaacttgattgtgaaatc-3′ and 5′-aggtttggtatctgccagtttctc-3′ (Applied Biosystems, Foster City, USA) as primers and the fluorescent probes 6-FAM-5′-CTGTTTTTATAGCTTTCA-3-MBG′, and VIC-5′-CTGTTTTTATGGCTTTCA-3′-MGB (Applied Biosystems) in a 20-µl reaction mixture containing 10 µl QuantiTect Probe PCR Kit (Qiagen, Leusden, The Netherlands), 10 pmol forward and reverse primer, 2 pmol of each probe, and 50 ng genomic DNA. PCR conditions were as follows: 94°C for 15 min followed by 45 cycles of 94°C for 15 s and 60°C for 30 s. In each run, three positive control samples (TT, TC, and CC allele) as confirmed twice on sequencing were used together with water as a negative control.

Sequencing

To confirm the results from the real-time PCR, 10% of the samples were sequenced. The promoter region was amplified using the primers (forward) 5′-ccccttccctttaacttgattgtgaaatc-3′ and (reverse) 5′-aggtttggtatctgccagtttctc-3′ (Applied Biosystems). PCR products were purified using the QIAquick PCR purification kit (Qiagen), according to the manufacturer's instructions. The sequences were analyzed on an ABI 3100 automated sequencer (Applied Biosystems) using the ABI Big Dye Terminator Cycle Sequence Kit (Applied Biosystems) and the Genescan 2.1 software.

Statistics

The SPSS 14.0 software package was used for statistical analysis. A chi-squared test was applied to determine whether there was a statistical difference between the presence of the C and T allele ($p<0.05$). The Hardy–Weinberg equilibrium was assessed using the chi-squared test. A multinominal logistic regression model was used to calculate the odds ratio for developing gastric cancer depending on SNP status, and also for adjusting for histological type and location (proximal versus distal only for EOGC and conventional gastric cancer).

Results

The identification of a genetic risk profile for gastric cancer could help the populations most at risk. Therefore, we evaluated the role of *IL-1B* −31T>C promoter polymorphism in different subtypes of gastric cancer. The distribution of the *IL-1B* −31T>C polymorphism was examined by real-time PCR (see Fig. 1) in 241 cases of gastric cancer, including 96 conventional gastric cancers, 115 EOGCs, and 30 GSCs as well as in 100 healthy control cases, and these results can be seen in Table 2, where the number of each specific genotype can be seen for each subtype of gastric cancer. In terms of carriage of the C allele, this was found in 60% of EOGCs, 59% of conventional gastric cancer, 90% of GSCs, and 62% of controls, as seen in the bottom row of Table 2. The *IL-1B* polymorphism status was confirmed in 10% of our study populations, using sequence analysis, an example of which can be seen in Fig. 1. All genotypic distributions were in Hardy–Weinberg equilibrium ($p\geq0.05$).

A logistic regression model was used to determine the statistical likelihood of developing different subtypes of gastric cancer depending on the *IL-1B* SNP status. In this regression model, carriage of the C allele was compared between the different types of gastric cancer, with adjustments made for both histology and location of the tumor (for the categories of EOGC and conventional gastric cancer) and corrected for histology only in the case of stump cancers. In patients with GSC, carriage of the C allele conferred a significant increased risk of the development of gastric cancer with respect to the controls ($p=0.008$, OR=5.52, 95% confidence interval 1.57–19.43). Carriage of the C allele (genotypes CT and CC) in both EOGC and conventional gastric cancer did not confer an increased risk of gastric cancer with respect to the control group ($p=0.76$, OR 0.92, 95% confidence interval 0.53–1.59 and $p=0.71$, OR 0.9, 95% confidence interval 0.51–1.59, respectively).

Using a logistic regression model, the genotype distribution was also compared between EOGC, conventional gastric cancer, GSC, and the control group. In the gastric stump cancer group, the CC and CT genotypes predisposed to gastric cancer with an OR of 5.33 ($p=0.022$, 95% confidence interval 1.27–22.44) and 5.6 ($p=0.009$, 95% confidence interval 1.54–20.40), respectively. No difference was found

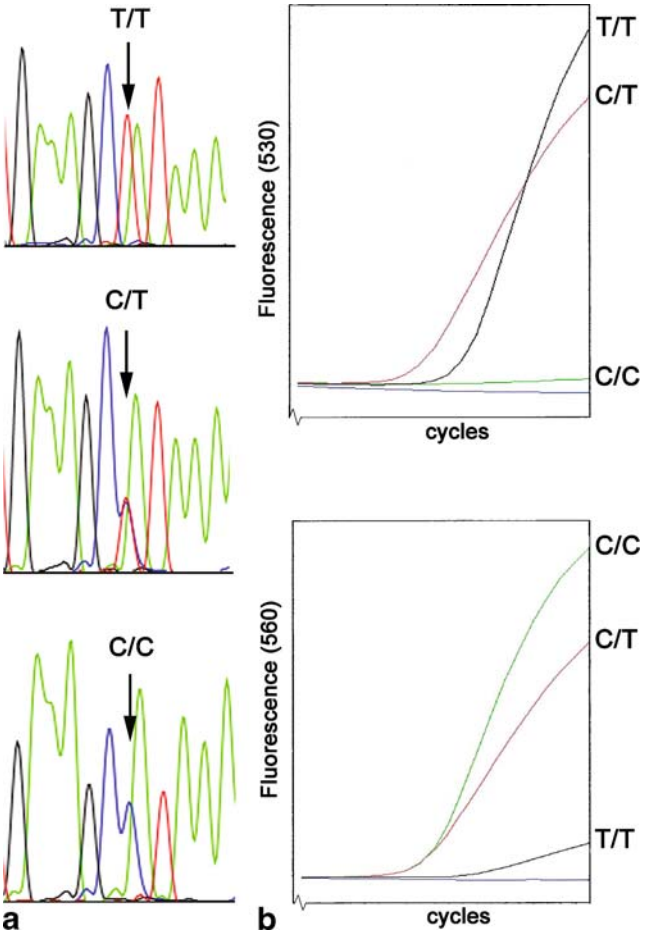

Fig. 1 Result of sequencing and LightCycler analysis. **a** An example of the sequence analysis of the CC, CT, and TT *IL-1B* polymorphism. **b** LightCycler analysis of CC, CT, and TT SNP genotypes at the −31 position of the promoter region of *IL-1B* using MGB probes. *Upper panel* shows the FAM-labeled probe, visualized at 530 nm for detection of the T allele; *lower panel* shows the VIC-labeled probe, visualized at 560 nm for detection of the C allele

in genotype distribution between EOGCs and conventional gastric cancers and the control group.

In addition, the *IL-1B* −31T>C genotype or carriage of the C allele did not predispose to a specific location of gastric cancer (cardia versus non-cardia, applicable to EOGC and conventional gastric cancers only) or to a histological type.

Discussion

Inflammation is a central component of several chronic diseases. *IL-1B* is an inducible gene that plays an important role in both inflammation and carcinogenesis. The expression of *IL-1B* depends on varying individual susceptibility, geographical location, and genetic factors. Genetic polymorphisms that alter the levels of IL-1B may have substantial influence on cancer activity. In the present study, we focused on the distribution of the −31T>C promoter polymorphism of the human *IL-1B* gene in conventional gastric cancer, EOGC, and GSC.

The *IL-1B* −31C allele is reported to be associated with higher risk of gastric cancer [8, 9]. Interestingly, we did not find an association between the pro-inflammatory genotype of *IL-1B* −31 and predisposition to conventional or early onset gastric cancer. The role of *IL-1B* −31T>C polymorphism in gastric cancer has been variable and the literature is inconclusive. Positive associations between pro-inflammatory genotypes of *IL-1B* −31 and higher risk of gastric cancer have been previously reported in populations from Poland, Scotland, and Mexico [8, 9, 12]. This is in contrast to studies in Finland [18] and Brazil [13], and our current findings are also in line with two published meta-analyses about the association of *IL-1B* polymorphisms with gastric cancer in a Caucasian population [3, 19]. It does appear that not all Asian or white populations have demonstrated a predisposition for gastric cancer in association with pro-inflammatory *IL-1* polymorphisms and in some instances, studies found that there was a positive association, but with novel markers of the *IL-1B* gene [1]. So far, there is no clear explanation for these conflicting results although the relatively small number of gastric cancer cases (211) included in this particular study may provide an explanation for the negative association between the IL-1B marker and risk of GC. Zeng et al. [46] reported that the *IL-1B*-genotype-dependent risk of gastric cancer was limited to specific areas where the prevalence of gastric cancer was low. This hypothesis, however, conflicts with data showing an association between the *IL-1B* −31C allele and gastric cancer in Poland and Portugal, two countries both with high prevalence rates of gastric cancer [8, 9, 35]. The effect of differing genetic and environmental

Table 2 Prevalence of *IL-1B* −31T>C genotype

Genotype of *IL-1B* −31T>C	Early onset gastric cancer	Conventional gastric cancer	Gastric stump cancer	Controls
CC	17/115 (15%)	21/96 (22%)	8/30 (27%)	19 (19%)
TC	52/115 (45%)	36/96 (37%)	19/30 (63%)	43 (43%)
TT	46/115 (40%)	39/96 (41%)	3/30 (10%)	38 (38%)
Carriage of the C allele	60%	59%	90%	62%

All percentages rounded to the nearest digit.

factors on different populations may provide an explanation for these conflicting reports. The importance of haplotype context has been highlighted in recent literature where polymorphisms in metabolic genes and in CDH1 have been shown to act in combination with smoking, alcohol consumption, and *H. pylori* infection in the development of gastric cancer [2, 17].

EOGC is a separate entity within gastric cancer and may result from different genetic alterations that accumulate more rapidly compared to conventional gastric cancer [6]. This is the first study that investigates the pro-carcinogenic background of EOGC by evaluating the role of the *IL-1B* −31T>C polymorphism in predisposition to EOGC. We demonstrated that the distribution of the *IL-1B* −31T>C polymorphism is not different between EOGC and the control group and that there is no difference between conventional gastric cancer and EOGC for the *IL-1B* −31 polymorphism. Thus, once infected by *H. pylori* (which appears to occur at the same rate as in conventional gastric cancers [6]), the IL-1B status does not explain the increased risk of gastric cancer in these young patients.

An intriguing subtype of gastric cancer is gastric stump cancer, due to its gastroduodenal ulcer and partial gastrectomy history and subsequent gastric cancer development. It is described that gastric cancer and duodenal peptic ulcer disease are inversely associated, have distinct gastric acid secretion [10], and possess a distinct *IL-1B* −31T>C genotype distribution. It is believed that subjects who develop duodenal ulcers are actually protected from developing gastric cancer, suggesting that the two outcomes are mutually exclusive [15].

In the GSC patients, who developed peptic ulcer and gastric cancer, we found a statistically significant difference in *IL-1B* −31T>C polymorphism compared to the control group, with the C allele being associated with cancer. These findings are surprising as although the patients in this unique subgroup have a strong history of gastroduodenal ulcer, they do not have the polymorphism reportedly associated with ulcers but rather have a predilection for the C allele, which may explain the increased cancer risk in these patients. Although our gastric stump cancer group is small (30 patients), it seems that the *IL-1B* −31T>C polymorphism influences the prognosis of patients after partial gastrectomy. Although individuals with duodenal ulcers generally do not have the C polymorphism, the minority does appear to be at risk of developing gastric stump cancer. Surgery removes the inflamed and *H. pylori*-ridden antrum and induces acid suppression, thus converting these from an antrum-predominant into a corpus-predominant phenotype (to some extent comparable to the pharmacological acid suppression group) [22, 23]. In addition, these patients with the C genotype are known to have an associated high IL-1B output which further increases the acid suppression thus increasing their risk of subsequent development of gastric cancer.

Researchers have reported significant associations between *IL-1B* promoter region polymorphisms and the anatomic site of the tumor and histology. Machado et al. reported that the *IL-1B* −511T (−31C) genotype is associated with an intestinal type of gastric cancer in a Portuguese population [26] and Garza-Gonzalez et al. described the association between the *IL-1B* −31C genotype and the risk of distal gastric cancer in a Hispanic population [12]. We examined the associations between *IL-1B* −31T>C polymorphisms and location of the tumor or the histology and found no relation. This discrepancy is most likely due to study size, as in our study, where we have assessed a total of 241 gastric cancers, in contrast to the 152 and 63 used by Machado et al. and Garza-Gonzalez et al., respectively, and thus, it is likely that there is no correlation between histology and IL-1B genotype. On the other hand, the high rate of *H. pylori* infection in countries such as Portugal may result in the IL-1B polymorphism playing a more important role in the development of intestinal gastric cancer in this particular population.

In summary, this is the first study describing the role of the *IL-1B* −31T>C polymorphism in EOGC and GSC. Although EOGC appears to have a different genetic background compared to conventional gastric cancer, we did not find any differences in the *IL-1B* −31T>C polymorphism distribution. Interestingly, our study has shown that the *IL-1B* −31C genotype can contribute significantly to the development of GSC.

Acknowledgments The authors thank Sjoerd Repping from the Endocrinology Department, Academic Medical Centre, Amsterdam, for provision of the control group. Robert Sitarz, first author, is funded by the Stella Major Foundation.

Conflict of interest statement We declare that we have no conflict of interest.

References

1. Amieva MR, El-Omar EM (2008) Host–bacterial interactions in *Helicobacter pylori* infection. Gastroenterology 134:306–323
2. Boccia S, Sayed-Tabatabaei FA, Persiani R, Gianfagna F, Rausei S, Arzani D, La Greca A, D'Ugo D, La Torre G, van Duijn CM, Ricciardi G (2007) Polymorphisms in metabolic genes, their combination and interaction with tobacco smoke and alcohol consumption and risk of gastric cancer: a case–control study in an Italian population. BMC Cancer 7:206
3. Camargo MC, Mera R, Correa P, Peek RM Jr, Fontham ET, Goodman KJ, Piazuelo MB, Sicinschi L, Zabaleta J, Schneider BG (2006) Interleukin-1beta and interleukin-1 receptor antagonist gene polymorphisms and gastric cancer: a meta-analysis. Cancer Epidemiol Biomarkers Prev 15:1674–1687

4. Carvalho R, Milne AN, Polak M, Corver WE, Offerhaus GJ, Weterman MA (2005) Exclusion of RUNX3 as a tumour-suppressor gene in early-onset gastric carcinomas. Oncogene 24:8252–8258
5. Carvalho R, Milne AN, Polak M, Offerhaus GJ, Weterman MA (2006) A novel region of amplification at 11p12-13 in gastric cancer, revealed by representational difference analysis, is associated with overexpression of CD44v6, especially in early-onset gastric carcinomas. Genes Chromosomes Cancer 45:967–975
6. Carvalho R, Milne AN, van Rees BP, Caspers E, Cirnes L, Figueiredo C, Offerhaus GJ, Weterman MA (2004) Early-onset gastric carcinomas display molecular characteristics distinct from gastric carcinomas occurring at a later age. J Pathol 204:75–83
7. Chen H, Wilkins LM, Aziz N, Cannings C, Wyllie DH, Bingle C, Rogus J, Beck JD, Offenbacher S, Cork MJ, Rafie-Kolpin M, Hsieh CM, Kornman KS, Duff GW (2006) Single nucleotide polymorphisms in the human interleukin-1B gene affect transcription according to haplotype context. Hum Mol Genet 15:519–529
8. El-Omar EM, Carrington M, Chow WH, McColl KE, Bream JH, Young HA, Herrera J, Lissowska J, Yuan CC, Rothman N, Lanyon G, Martin M, Fraumeni JF Jr, Rabkin CS (2000) Interleukin-1 polymorphisms associated with increased risk of gastric cancer. Nature 404:398–402
9. El-Omar EM, Carrington M, Chow WH, McColl KE, Bream JH, Young HA, Herrera J, Lissowska J, Yuan CC, Rothman N, Lanyon G, Martin M, Fraumeni JF Jr, Rabkin CS (2001) The role of interleukin-1 polymorphisms in the pathogenesis of gastric cancer. Nature 412:99
10. El-Omar EM, Oien K, El-Nujumi A, Gillen D, Wirz A, Dahill S, Williams C, Ardill JE, McColl KE (1997) *Helicobacter pylori* infection and chronic gastric acid hyposecretion. Gastroenterology 113:15–24
11. Forman D, Newell DG, Fullerton F, Yarnell JW, Stacey AR, Wald N, Sitas F (1991) Association between infection with *Helicobacter pylori* and risk of gastric cancer: evidence from a prospective investigation. BMJ 302:1302–1305
12. Garza-Gonzalez E, Bosques-Padilla FJ, El-Omar E, Hold G, Tijerina-Menchaca R, Maldonado-Garza HJ, Perez-Perez GI (2005) Role of the polymorphic IL-1B, IL-1RN and TNF-A genes in distal gastric cancer in Mexico. Int J Cancer 114:237–241
13. Gatti LL, Burbano RR, de Assumpcao PP, Smith Mde A, Payao SL (2004) Interleukin-1beta polymorphisms, *Helicobacter pylori* infection in individuals from northern Brazil with gastric adenocarcinoma. Clin Exp Med 4:93–98
14. Hall SK, Perregaux DG, Gabel CA, Woodworth T, Durham LK, Huizinga TW, Breedveld FC, Seymour AB (2004) Correlation of polymorphic variation in the promoter region of the interleukin-1 beta gene with secretion of interleukin-1 beta protein. Arthritis Rheum 50:1976–1983
15. Hunt RH (1996) The role of *Helicobacter pylori* in pathogenesis: the spectrum of clinical outcomes. Scand J Gastroenterol Suppl 220:3–9
16. IARC Working Group (1994) Schistosomes, liver flukes and *Helicobacter pylori*. IARC Working Group on the evaluation of carcinogenic risks to humans. Lyon, 7–14 June 1994. IARC Monogr Eval Carcinog Risks Hum 61:1–241
17. Jenab M, McKay JD, Ferrari P, Biessy C, Laing S, Capella Munar GM, Sala N, Pena S, Crusius JB, Overvad K, Jensen MK, Olsen A, Tjonneland A, Clavel-Chapelon F, Boutron-Ruault MC, Kaaks R, Linseisen J, Boeing H, Bergmann MM, Trichopoulou A, Georgila C, Psaltopoulou T, Mattiello A, Vineis P, Pala V, Palli D, Tumino R, Numans ME, Peeters PH, Bueno-de-Mesquita HB, Lund E, Ardanaz E, Sanchez MJ, Dorronsoro M, Navarro Sanchez C, Quiros JR, Hallmans G, Stenling R, Manjer J, Regner S, Key T, Bingham S, Khaw KT, Slimani N, Rinaldi S, Boffetta P, Carneiro F, Riboli E, Gonzalez C (2008) CDH1 gene polymorphisms, smoking, *Helicobacter pylori* infection and the risk of gastric cancer in the European Prospective Investigation into Cancer and Nutrition (EPIC-EURGAST). Eur J Cancer 44:774–780
18. Kamangar F, Abnet CC, Hutchinson AA, Newschaffer CJ, Helzlsouer K, Shugart YY, Pietinen P, Dawsey SM, Albanes D, Virtamo J, Taylor PR (2006) Polymorphisms in inflammation-related genes and risk of gastric cancer (Finland). Cancer Causes Control 17:117–125
19. Kamangar F, Cheng C, Abnet CC, Rabkin CS (2006) Interleukin-1B polymorphisms and gastric cancer risk—a meta-analysis. Cancer Epidemiol Biomarkers Prev 15:1920–1928
20. Kikuchi S, Nakajima T, Nishi T, Kobayashi O, Konishi T, Inaba Y, Wada O, Satou H, Ishibashi T, Ichikawa S, Okamoto N, Hirata T, Kubo T, Sato N, Miki K, Myoga A (1996) Association between family history and gastric carcinoma among young adults. Jpn J Cancer Res 87:332–336
21. Koshida Y, Koizumi W, Sasabe M, Katoh Y, Okayasu I (2000) Association of *Helicobacter pylori*-dependent gastritis with gastric carcinomas in young Japanese patients: histopathological comparison of diffuse and intestinal type cancer cases. Histopathology 37:124–130
22. Kuipers EJ, Lee A, Klinkenberg-Knol EC, Meuwissen SG (1995) Review article: the development of atrophic gastritis—*Helicobacter pylori* and the effects of acid suppressive therapy. Aliment Pharmacol Ther 9:331–340
23. Kuipers EJ, Lundell L, Klinkenberg-Knol EC, Havu N, Festen HP, Liedman B, Lamers CB, Jansen JB, Dalenback J, Snel P, Nelis GF, Meuwissen SG (1996) Atrophic gastritis and *Helicobacter pylori* infection in patients with reflux esophagitis treated with omeprazole or fundoplication. N Engl J Med 334:1018–1022
24. Lauren P (1965) The two histological main types of gastric carcinoma: diffuse and so-called intestinal-type carcinoma. An attempt at a histo-clinical classification. Acta Pathol Microbiol Scand 64:31–49
25. Lunet N, Barros H (2003) *Helicobacter pylori* infection and gastric cancer: facing the enigmas. Int J Cancer 106:953–960
26. Machado JC, Pharoah P, Sousa S, Carvalho R, Oliveira C, Figueiredo C, Amorim A, Seruca R, Caldas C, Carneiro F, Sobrinho-Simoes M (2001) Interleukin 1B and interleukin 1RN polymorphisms are associated with increased risk of gastric carcinoma. Gastroenterology 121:823–829
27. Mahmoud FA, Rivera NI (2002) The role of C-reactive protein as a prognostic indicator in advanced cancer. Curr Oncol Rep 4:250–255
28. Masuda G, Tokunaga A, Shirakawa T, Togashi A, Kiyama T, Kato S, Matsukura N, Bou H, Watanabe M, Tajiri T (2007) *Helicobacter pylori* infection, but not genetic polymorphism of CYP2E1, is highly prevalent in gastric cancer patients younger than 40 years. Gastric Cancer 10:98–103
29. Milne AN, Carvalho R, Jansen M, Kranenbarg EK, van de Velde CJ, Morsink FM, Musler AR, Weterman MA, Offerhaus GJ (2008) Cyclin E low molecular weight isoforms occur commonly in early-onset gastric cancer and independently predict survival. J Clin Pathol 61:311–316
30. Milne AN, Carvalho R, Morsink FM, Musler AR, de Leng WW, Ristimaki A, fferhaus GJ (2006) Early-onset gastric cancers have a different molecular expression profile than conventional gastric cancers. Mod Pathol 9:564–572
31. Milne AN, Sitarz R, Carvalho R, Carneiro F, Offerh, aus GJ (2007) Early onset gastric cancer: on the road to unraveling gastric carcinogenesis. Curr Mol Med 7:15–28
32. Milne AN, Sitarz R, Carvalho R, Polak MM, Ligtenberg M, Pauwels P, Offerhaus GJ, Weterman MA (2007) Molecular analysis of primary gastric cancer, corresponding xenografts, and 2 novel gastric carcinoma cell lines reveals novel alterations in gastric carcinogenesis. Hum Pathol 38:903–913
33. Nicholls JC (1979) Stump cancer following gastric surgery. World J Surg 3:731–736

34. Noach LA, Bosma NB, Jansen J, Hoek FJ, van Deventer SJ, Tytgat GN (1994) Mucosal tumor necrosis factor-alpha, interleukin-1 beta, and interleukin-8 production in patients with *Helicobacter pylori* infection. Scand J Gastroenterol 29:425–429
35. Parkin DM, Bray F, Ferlay J, Pisani P (2005) Global cancer statistics, 2002. CA Cancer J Clin 55:74–108
36. Parsonnet J, Friedman GD, Vandersteen DP, Chang Y, Vogelman JH, Orentreich N, Sibley RK (1991) *Helicobacter pylori* infection and the risk of gastric carcinoma. N Engl J Med 325:1127–1131
37. Rugge M, Busatto G, Cassaro M, Shiao YH, Russo V, Leandro G, Avellini C, Fabiano A, Sidoni A, Covacci A (1999) Patients younger than 40 years with gastric carcinoma: *Helicobacter pylori* genotype and associated gastritis phenotype. Cancer 85:2506–2511
38. Saijo Y, Tanaka M, Miki M, Usui K, Suzuki T, Maemondo M, Hong X, Tazawa R, Kikuchi T, Matsushima K, Nukiwa T (2002) Proinflammatory cytokine IL-1 beta promotes tumor growth of Lewis lung carcinoma by induction of angiogenic factors: in vivo analysis of tumor–stromal interaction. J Immunol 169:469–475
39. Sinning C, Schaefer N, Standop J, Hirner A, Wolff M (2007) Gastric stump carcinoma—epidemiology and current concepts in pathogenesis and treatment. Eur J Surg Oncol 33:133–139
40. Song X, Voronov E, Dvorkin T, Fima E, Cagnano E, Benharroch D, Shendler Y, Bjorkdahl O, Segal S, Dinarello CA, Apte RN (2003) Differential effects of IL-1 alpha and IL-1 beta on tumorigenicity patterns and invasiveness. J Immunol 171:6448–6456
41. Tersmette AC, Offerhaus GJ, Giardiello FM, Brand R, Tersmette KW, Tytgat GN, Vandenbroucke JP (1991) Long-term prognosis after partial gastrectomy for benign conditions. Survival and smoking-related death of 2633 Amsterdam postgastrectomy patients followed up since surgery between 1931 and 1960. Gastroenterology 101:148–153
42. Thorban S, Bottcher K, Etter M, Roder JD, Busch R, Siewert JR (2000) Prognostic factors in gastric stump carcinoma. Ann Surg 231:188–194
43. Wallace JL, Cucala M, Mugridge K, Parente L (1991) Secretagogue-specific effects of interleukin-1 on gastric acid secretion. Am J Physiol 261:G559–G564
44. Westerveld H, Visser L, Tanck M, van der Veen F, Repping S (2008) CAG repeat length variation in the androgen receptor gene is not associated with spermatogenic failure. Fertil Steril 89:253–259
45. Yano S, Nokihara H, Yamamoto A, Goto H, Ogawa H, Kanematsu T, Miki T, Uehara H, Saijo Y, Nukiwa T, Sone S (2003) Multifunctional interleukin-1beta promotes metastasis of human lung cancer cells in SCID mice via enhanced expression of adhesion-, invasion- and angiogenesis-related molecules. Cancer Sci 94:244–252
46. Zeng ZR, Hu PJ, Hu S, Pang RP, Chen MH, Ng M, Sung JJ (2003) Association of interleukin 1B gene polymorphism and gastric cancers in high and low prevalence regions in China. Gut 52:1684–1689

Virchows Arch (2008) 453:257–265
DOI 10.1007/s00428-008-0641-6

ORIGINAL ARTICLE

The role of VEGF-C staining in predicting regional metastasis in melanoma

Barbara Boone · Willeke Blokx · Dirk De Bacquer · Jo Lambert · Dirk Ruiter · Lieve Brochez

Received: 10 April 2008 / Revised: 10 June 2008 / Accepted: 5 July 2008 / Published online: 5 August 2008

Abstract Sentinel lymph node status is the most important prognostic factor in primary melanoma. The number of melanoma-associated lymphatic vessels has been associated with sentinel lymph node status and survival. Vascular endothelial growth factor-C (VEGF-C) is found to promote tumour-associated lymphatic vessel growth. In many human neoplasms, VEGF-C expression in neoplastic cells or tumour-associated macrophages (TAMs) has been linked to lymphatic dissemination of tumour cells. Recent studies have suggested a correlation between VEGF-C expression in primary melanoma and the presence of lymph node metastasis. We performed VEGF-C immunohistochemical staining on melanoma tissues of 113 patients with known sentinel lymph node status. We showed that both high VEGF-C expression in melanoma cells and TAMs are positively associated with the presence of a positive sentinel lymph node. No correlation with Breslow thickness, Clark invasion level or ulceration could be detected. VEGF-C expression in melanoma cells was predictive of a shorter overall and disease-free survival, without being an independent predictor of survival. Our results confirm that VEGF-C expression in primary cutaneous melanoma plays a role in the lymphatic spread of the tumour.

Keywords Skin · Melanoma · Lymphangiogenesis · Sentinel lymph node · VEGF-C · TAMs · Immunohistochemistry

B. Boone (✉) · J. Lambert · L. Brochez
Department of Dermatology, University Hospital Ghent,
De Pintelaan 185,
9000 Ghent, Belgium
e-mail: barbara.boone@ugent.be

W. Blokx · D. Ruiter
Department of Pathology, UMC Sint-Radboud,
Geert Grooteplein-Zuid 10,
6525 GA Nijmegen, The Netherlands

D. De Bacquer
Department of Public Health, University Hospital Ghent,
De Pintelaan 185,
9000 Ghent, Belgium

Introduction

Tumour thickness and ulceration are powerful prognostic markers in localised melanoma [1, 2]. However, sentinel lymph node status is the single most significant independent clinicopathological determinant of patient survival even when primary tumour thickness and ulceration status are included in the analysis [12, 24, 52]. Since the identification of vascular endothelial growth factor receptor-3 (VEGFR-3) or Flt4, podoplanin, LYVE-1 and Prox1 as lymphatic markers [6, 49, 53], the role of lymphangiogenesis has been investigated in multiple tumours. Earlier studies presumed lymphatic endothelium to play a passive role during tumour metastasis and lymphatic invasion to occur via tumour cells infiltrating pre-existing lymphatic vessels [5, 35]. However, recent experimental and clinical evidence suggest that active lymphangiogenesis is induced by primary cutaneous melanoma [43] and that the extent of tumour-associated lymphangiogenesis can be used as a powerful prognostic tool [7, 8, 29, 41, 46, 50].

Recently vascular endothelial growth factor-C (VEGF-C) has been identified as an activator of lymphangiogenesis by binding vascular endothelial growth factor receptor-3 expressed on lymphatic endothelium [21, 23]. VEGF-C belongs to the PDGF/VEGF family. In 1996, the protein

was purified and its cDNA cloned from human prostatic carcinoma cells [19, 25]. VEGF-C is found to be secreted not only by tumour cells, but also by macrophages, dendritic cells, endothelial cells, platelets, basophilic granulocytes and lymphocytes [17]. The gene coding for VEGF-C is located on chromosome 4q34 [4, 33]. VEGF-C is synthesised as a prepropeptide and undergoes stepwise proteolytic processing generating several VEGF-C isoforms with varying affinities for VEGFR-3. The fully processed VEGF-C can also activate VEGFR-2, which is expressed both on the endothelial cells of blood vessels and lymphatic vessels. However, VEGF-C has greater affinity for VEGFR-3 than for VEGFR-2 [20, 30, 32, 36]. Upon binding to its receptor, VEGF-C activates the extracellular signal-regulated kinase 1/2, the phosphatidylinositol 3-kinase/AKT and the c-Jun NH_2-terminal kinase 1/2 pathways leading to proliferation, migration and survival of the lymphatic endothelial cells [54]. VEGF-C and its receptor VEGFR-3 play an important role in the development of the lymphatic vascular system during embryogenesis and are postulated to intervene in the maintenance of lymphatic endothelial differentiation in adults [13, 21, 23, 27]. Overexpression of VEGF-C in the skin of transgenic mice was shown to result in hyperplasia of the lymphatic vasculature [18]. The lymphangiogenic capacity of VEGF-C via VEGFR-3 binding has been confirmed in various studies [9, 31, 51].

Research in animal tumour models has shown that overexpression of VEGF-C promotes tumour lymphangiogenesis and lymphatic spread to regional lymph nodes [22, 28, 44]. This effect can be suppressed by blocking VEGFR-3 signalling [15, 26, 42]. VEGF-C expression has been observed in several human melanoma cell lines in vitro [37, 38, 43]. A375 melanoma cells expressing VEGF-C were found to induce lymphatic vessel growth and invasion of lymphatic vessels in the avian chorioallantoic membrane [34]. Skobe et al. demonstrated the occurrence of intratumoral lymphangiogenesis in VEGF-C overexpressing MeWo melanoma xenotransplants [43]. A number of clinicopathological studies have shown a direct correlation between VEGF-C expression and regional metastatic tumour spread in human cancers [14, 45, 48]. Recent data show that VEGF-C is not only expressed by tumour cells, but also by a subfraction of TAMs and that the latter is also related to lymphangiogenesis and lymph node metastasis [39, 40].

In melanoma, the association between VEGF-C and lymphatic metastasis has only been investigated in limited series [8, 7, 29, 38, 41]. In the present study, we investigated the correlation between VEGF-C expression in primary melanoma cells/TAMs and the presence of sentinel lymph node metastasis in a large series of patients with known sentinel lymph node status and follow-up.

Materials and methods

Specimen selection

Patients were identified retrospectively from the melanoma unit database, Department of Dermatology, Ghent University Hospital, Belgium. In total, 113 patients, who were diagnosed with melanoma between January 1996 and August 2005 and who were subjected to a sentinel lymph

Table 1 Clinicopathological characteristics

	Number (%)	Mean (95% CI)
Clinical characteristics		
Sex (n=113)		
Male	45 (39.8)	
Female	68 (60.2)	
Age at time of diagnosis (years) (n=)		49.88 (46.89–52.88)
Location of primary melanoma (n=113)		
Head, neck	8 (7.1)	
Trunk	39 (34.5)	
Extremities	66 (58.5)	
Disease progression during follow-up (n=112)		
Absent	93 (83)	
Present	19 (17)	
Mortality (n=113)		
Alive	102 (90.3)	
Dead	11 (9.7)	
Disease-free survival (months) (n=112)		31.19 (26.89–35.48)
Follow-up time (months) (n=112)		33.88 (29.72–38.03)
Pathological characteristics		
Breslow (n=113)		
pT1 ≤1.00 mm	11 (9.7)	
pT2 1.01–2.00 mm	57 (50.4)	
pT3 2.01–4.00 mm	38 (33.6)	
pT4 >4.00 mm	7 (6.2)	
Clark (n=110)		
Levels II, III	62 (56.4)	
Levels IV, V	48 (43.6)	
Ulceration (n=112)		
Absent	81 (72.3)	
Present	31 (27.7)	
Sentinel lymph node (n=113)		
Negative	88 (77.9)	
Positive	25 (22.1)	
Number of positive lymph nodes at time of diagnosis (n=113)		
None	88 (77.9)	
1	15 (13.3)	
>1	10 (8.8)	

node biopsy, agreed upon participation. The collection of skin biopsies was performed after written informed consent. The study was approved by the Institutional Ethical Committee (project number: 2004/041).

In total, 113 Caucasian patients treated for primary cutaneous melanoma with known sentinel lymph node status were included. One patient was lost during follow-up. The database consisted of 45 (39.8%) males and 68 (60.2%) females with a mean (95% confidence interval) age at time of diagnosis of 49.88 (46.89–52.88) years. The location of the primary cutaneous melanoma was variable and more often seen at extremities (58.5%) than on the trunk (34.5%) or in the head and neck region (7.1%). According to the TNM classification [1], 11 (9.7%) melanomas presented as pT1 (Breslow <1 mm), 57 (50.4%) melanomas as pT2 (Breslow 1–2 mm), 38 (33.6%) melanomas as pT3 (Breslow 2–4 mm) and seven (6.2%) melanomas as pT4 (Breslow >4 mm). Ulceration of the cutaneous melanoma was present in 31 (27.7%) patients. Sentinel lymph node biopsy was performed in all patients and revealed metastatic invasion in 25 (22.1%) patients. Subsequent radical lymphadenectomy showed more than one lymph node to be invaded in ten of 25 (40%) of these patients. In three patients, in-transit metastasis were noted at the time of diagnosis without the presence of a metastatically invaded sentinel lymph node (N2c). Disease progression was observed in 19 (17%) patients with a mean (95% confidence interval) follow-up time of 33.88 (29.72–38.03) months. At the end of the follow-up period, 11 (9.7%) patients had died. Active disease was present in eight of the 102 patients that were still alive at the end of the study (Table 1).

Immunohistochemistry

Since VEGF-C is found to be expressed by tumour cells and TAMs, we distinguished VEGF-C expression in melanoma cells from that in TAMs. Therefore, three consecutive sections were prepared per melanoma sample. The first section was stained with an antibody directed against MelanA, a melanosomal differentiation antigen which is expressed in melanoma tissue and is routinely used by the pathologist in the diagnostic approach of melanoma. The second section was stained with an anti-VEGF-C antibody. In the third section, we examined the presence of TAMs by the use of an anti-CD68 antibody. With the aid of the three consecutive sections, VEGF-C positivity in melanoma cells or TAMs was estimated as a percentage of the MelanA-positive melanoma cells or CD68-positive TAMs within the primary tumour (Fig. 1).

Immunohistochemistry was carried out on 4-μm-thick serial paraffin sections. Sections were dewaxed in toluene and hydrated with a graded series of ethanol concentrations and water. Subsequently, antigen retrieval was obtained by

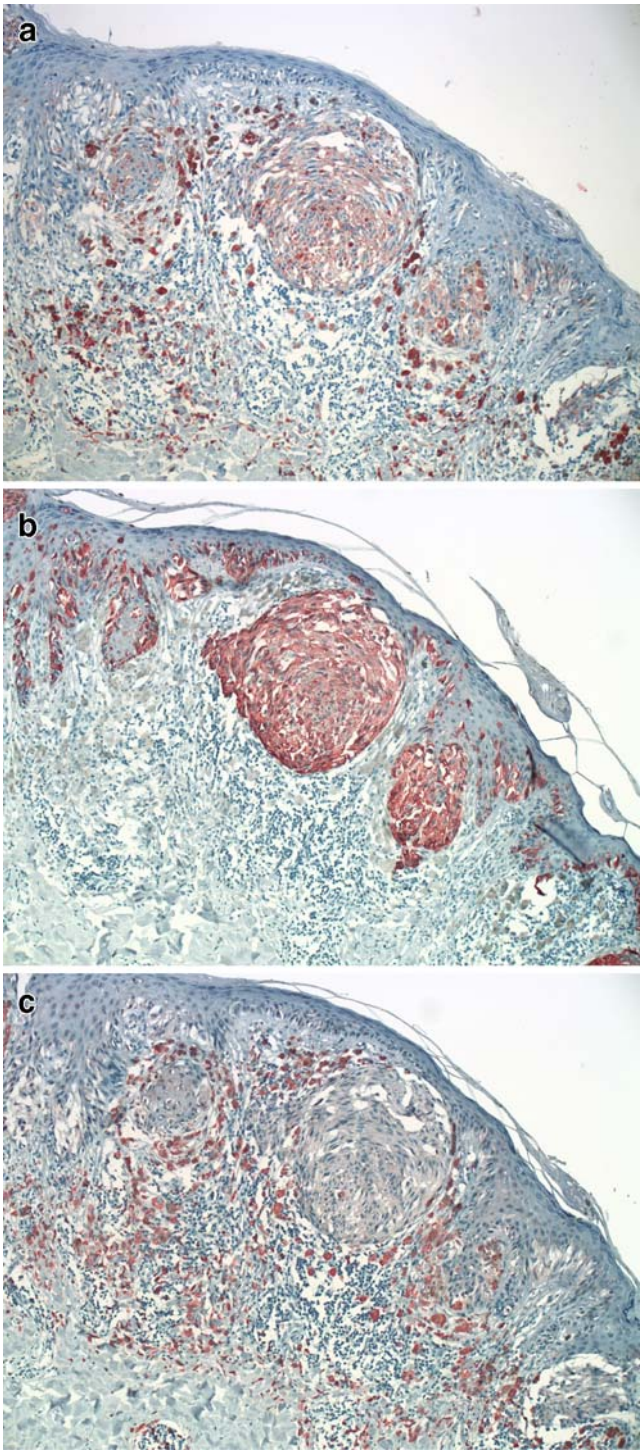

Fig. 1 Three consecutive sections of a melanoma sample immunostained with anti-VEGF-C (**a**), anti-MelanA (**b**) and anti-CD68 (**c**) antibodies. MelanA is strongly expressed in melanoma cells (**b**), whereas strong CD68 positivity is observed in TAMs (**c**). VEGF-C expression in melanoma cells and TAMs (**a**) has been estimated as a percentage of the MelanA-positive melanoma cells (**b**) or CD68-positive TAMs (**c**) within the primary tumour

Table 2 Antibodies used for immunohistochemistry

Primary antibody	Reference	Type	Conditions	Secondary antibody	Reference	Conditions
VEGF-C	Sc-7133, Santa Cruz Epitope location: N-terminus	Goat polyclonal IgG	1/50, 1 h pH 6	Rabbit anti-goat IgG	E0466 Dako	1:400 30 min
MelanA	NCL-L MelanA NovoCastra	Mouse monoclonal IgG	1/20, 30 min pH 9	Link antibody (goat anti-mouse IgG)	K0675 Dako	– 15 min
CD68	M0814 Dako	Mouse monoclonal IgG	1/300, 30 min pH 9	Link antibody (goat anti-mouse IgG)	K0675 Dako	– 15 min

using hot water bath incubation of sections in a pH 6 or 9 buffer for 30 min. Endogeneous peroxidase activity was quenched by incubating the section for 10 min with 3% hydrogen peroxide. Using a DAKO Autostainer device (Dako, Heverlee, Belgium), separate subsequent sections were incubated at room temperature with MelanA (NCL-L-MelanA, Novocastra, Menarini Diagnostics, Zaventem, Belgium), VEGF-C (sc-7133, Santa Cruz, TebuBio, Boechout, Belgium) and CD68 (M0814, Dako, Heverlee, Belgium) primary antibodies, respectively (Table 2). Staining was performed using a streptavidin–peroxidase complex technique with a LSAB2 System-HRP kit (K0675, Dako, Heverlee Belgium) and using 3-amino-9-ethylcarbazole or AEC as chromogene. Finally, nuclei were counterstained

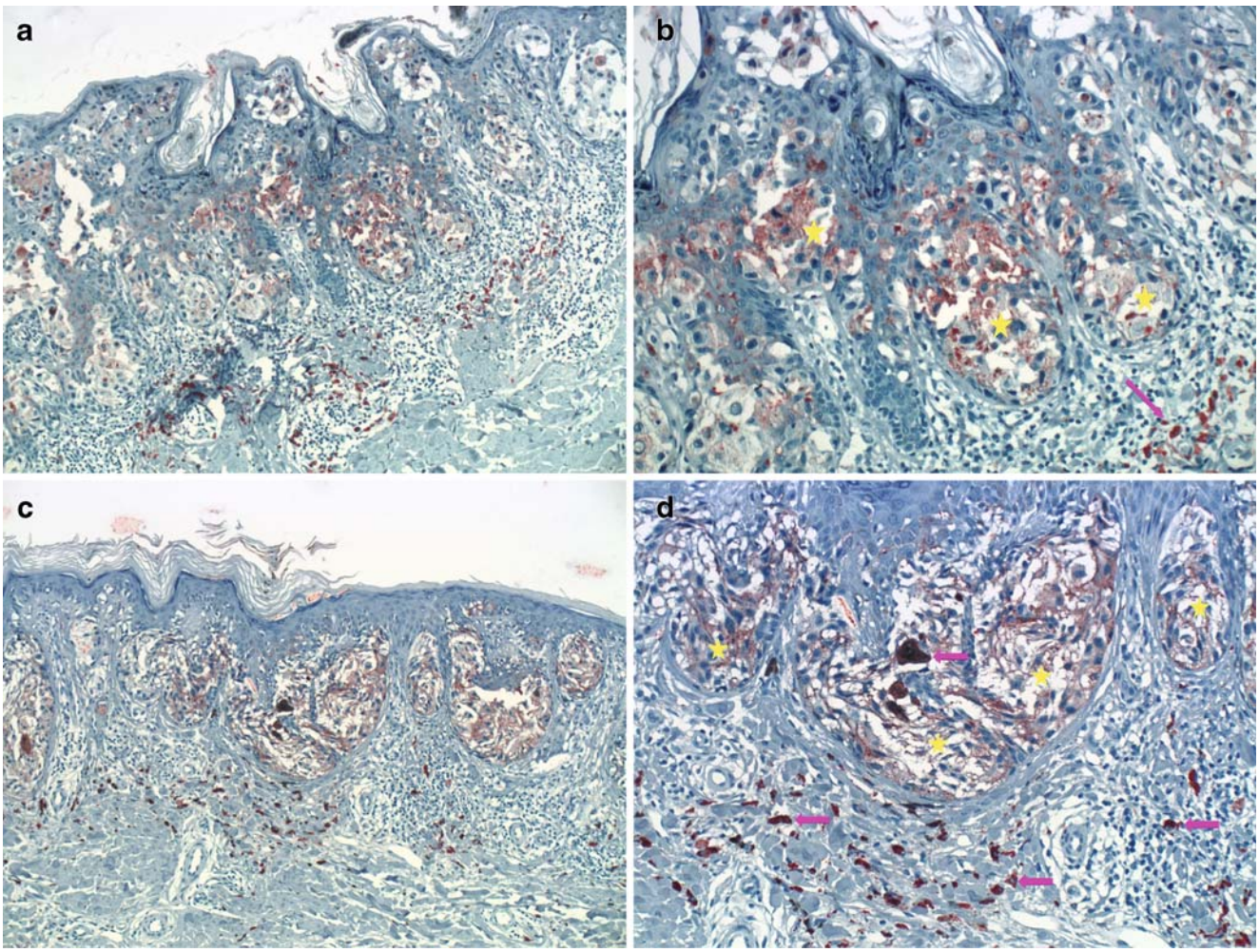

Fig. 2 VEGF-C staining in two different (**a**, **b** and **c**, **d**) melanoma tissues at different magnifications (**a**, **c**: ×100 and **b**, **d**: ×200) shows a diffuse, weak to moderate cytoplasmic pattern in intra- and subepidermal melanoma cell nests (*yellow asterisks*) versus a strong cytoplasmic pattern in TAMs (*purple arrows*)

with hematoxylin. Negative controls were performed by substituting the primary antibody with non-immune IgG. VEGF-C staining of the hair follicle bulbs, sweat and sebaceous glands were used as an internal positive control.

Immunostained sections were assessed by two independent observers (WB and BB) who were blinded to the clinicopathological information of the patient. With the aid of the three consecutive sections, VEGF-C expression in melanoma cells or TAMs was estimated as a percentage of the MelanA-positive melanoma cells or CD68-positive TAMs within the primary tumour. Staining intensity was scored semiquantitatively as weak, moderate or strong. There was a good agreement between the observations of both investigators (WB and BB), and contrasting results were discussed until an agreement was reached.

Statistical analysis

Possible associations between VEGF-C staining and sentinel lymph node status or other clinicopathological parameters were analysed using the Mann–Whitney *U*, Kruskal–Wallis and Pearson's chi-square tests. Kaplan–Meier survival analysis was used to obtain overall and disease-free survival curves that were compared using the log rank test. Cox proportional hazards model was used to identify variables with an independent effect on overall and disease-free survival. Linear correlations between continuous variables were analysed by the Spearman's rho test.

Results

Immunostaining

VEGF-C expression in primary cutaneous melanoma tissue was observed in melanoma cells and TAMs, with a higher staining intensity in the TAMs. VEGF-C was also expressed in the hair follicle bulb, sweat and sebaceous glands, which was used as an internal positive control. Positive VEGF-C specimens demonstrated a cytoplasmic staining pattern with sometimes a coarse granular distribution in melanoma cells (Figs. 2 and 3).

Positive staining in melanoma cells or TAMs was observed in 93 (82.3%) sections. VEGF-C expression was more frequently observed in TAMs (70.8%) than in melanoma cells (60.2%). The median estimated percentage of VEGF-C staining in melanoma cells was 5%, whereas in TAMs it amounted up to 40% (Table 3). When comparing the percentages of VEGF-C-positive melanoma cells with the percentages of VEGF-C-positive TAMs within melanoma tissue, a positive correlation was found (Spearman's rho, $r=0.485$, $p=0.000$).

Prognostic significance

VEGF-C expression in melanoma cells was higher in the sentinel lymph node-positive tumours compared to the sentinel lymph node-negative tumours (median 30% versus 3.5%, Mann–Whitney *U*, $p=0.018$). In total, 80% (20/25) of the sentinel lymph node-positive melanomas revealed melanoma cells expressing VEGF-C compared to only 54% (48/88) of the sentinel lymph node-negative melanomas (Pearson's chi-square, $p=0.022$). In addition, the presence of VEGF-C expression in melanoma cells was predictive of a shorter overall (log rank, $p=0.035$) and disease-free (log rank, $p=0.028$) survival. However, Cox regression analysis showed VEGF-C expression in melanoma cells not to be an independent predictor of survival, but its effect on survival could be explained by its correlation with the sentinel lymph node status. VEGF-C expression in melanoma cells

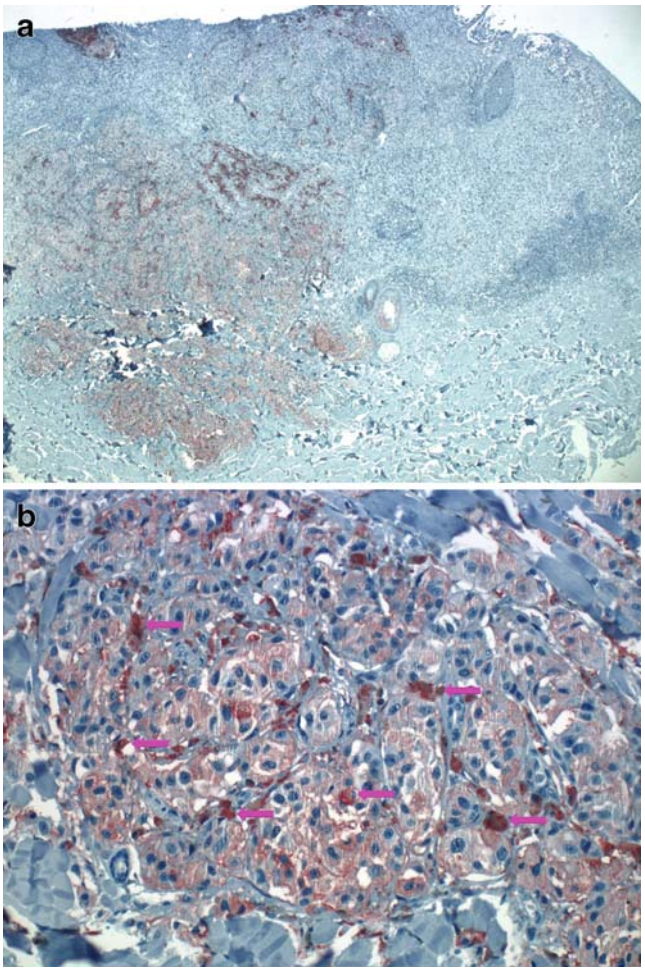

Fig. 3 VEGF-C staining in the primary tumour of a sentinel lymph node-positive patient demonstrates a pronounced positivity especially in the deeper part of the dermal melanoma component. **b** Moderate VEGF-C staining in the melanoma cells and intense staining in the TAMs that are scattered within the tumour (*purple arrows*). Magnification: ×25 (**a**), ×200 (**b**)

Table 3 VEGF-C immunostaining

Immunostaining			Positivity percentage				Staining intensity	
	Melanoma cells				Melanoma cells	TAMs	Melanoma cells	TAMs
	Absent	Present						
TAMs			Median (P_{25}–P_{75})		5% (0–40%)	40% (0–70%)	Weak to moderate	Strong
Absent	20	13	Categories	0%	45 samples (39.8%)	33 samples (29.2%)		
Present	25	55		1–10%	24 samples (21.2%)	10 samples (8.8%)		
				11–20%	8 samples (7.1%)	12 samples (10.6%)		
				21–50%	12 samples (10.6%)	10 samples (8.8%)		
				>50%	24 samples (21.2%)	48 samples (42.5%)		

was not associated with Breslow thickness, Clark level or ulceration of the primary cutaneous melanoma.

Analogous to VEGF-C expression in melanoma cells, VEGF-C expression in TAMs was strongly associated with the sentinel lymph node status. The median percentage of VEGF-C-positive TAMs was higher in the sentinel lymph node-positive tumours compared to the sentinel lymph node-negative tumours (median 80% versus 20%, Mann–Whitney U, p=0.003). VEGF-C expression in TAMs was not associated with pathological characteristics of the primary tumour such as Breslow thickness, Clark level or ulceration, nor with disease-free or overall survival (Table 4, Fig. 4).

Discussion

An increasing number of clinicopathological studies has shown a direct correlation between tumour expression of VEGF-C and lymphatic metastatic tumour spread in human cancers [14, 45, 48]. In melanoma, the association between immunohistochemical VEGF-C expression in the primary tumour and lymphatic metastasis has been investigated in limited series. Based on VEGF-C immunostaining on ten primary melanoma tissues of patients with positive lymph nodes, Schietroma and colleagues were the first to suggest that VEGF-C expression in cutaneous melanoma may be predictive of lymph node metastasis dissemination [38]. Dadras and colleagues further investigated this hypothesis. In a first study, 19 patients with non-metastatic primary melanoma and 18 patients who had documented early lymph node metastasis were matched for gender, age at diagnosis, tumour thickness, Clark's level of invasion, histological type and presence of ulceration. Focal cytoplasmic VEGF-C expression was found more frequently in metastatic melanomas (50.0%) than in non-metastatic melanomas (31.6%); however, these differences did not

Table 4 VEGF-C expression and clinicopathological parameters

	VEGF-C expression in melanoma (%)			VEGF-C expression in TAM (%)		
	Median	P_{25}–P_{75}	P value	Median	P_{25}–P_{75}	P value
Breslow						
≤1.00 mm	10	0–70		60	10–80	
1.01–2.00 mm	5	0–27		40	0–70	
2.01–4.00 mm	5	0–30		25	0–80	
>4.00 mm	60	5–70		80	0–90	
			0.362[a]			0.769[a]
Clark						
II, III	5	0–26.25		20	0–70	
IV, V	5	0–60		50	0–80	
			0.372[b]			0.567[b]
Ulceration						
Absent	5	0–40		40	5–70	
Present	5	0–30		20	0–80	
			0.694[b]			0.547[b]
Sentinel lymph node						
Negative	3.5	0–28.75		20	0–67.5	
Positive	30	3.5–60		80	10–90	
			0.018[b]			0.003[b]

[a] Kruskal–Wallis test, Sig <0.05

[b] Mann–Whitney U test, Sig <0.05

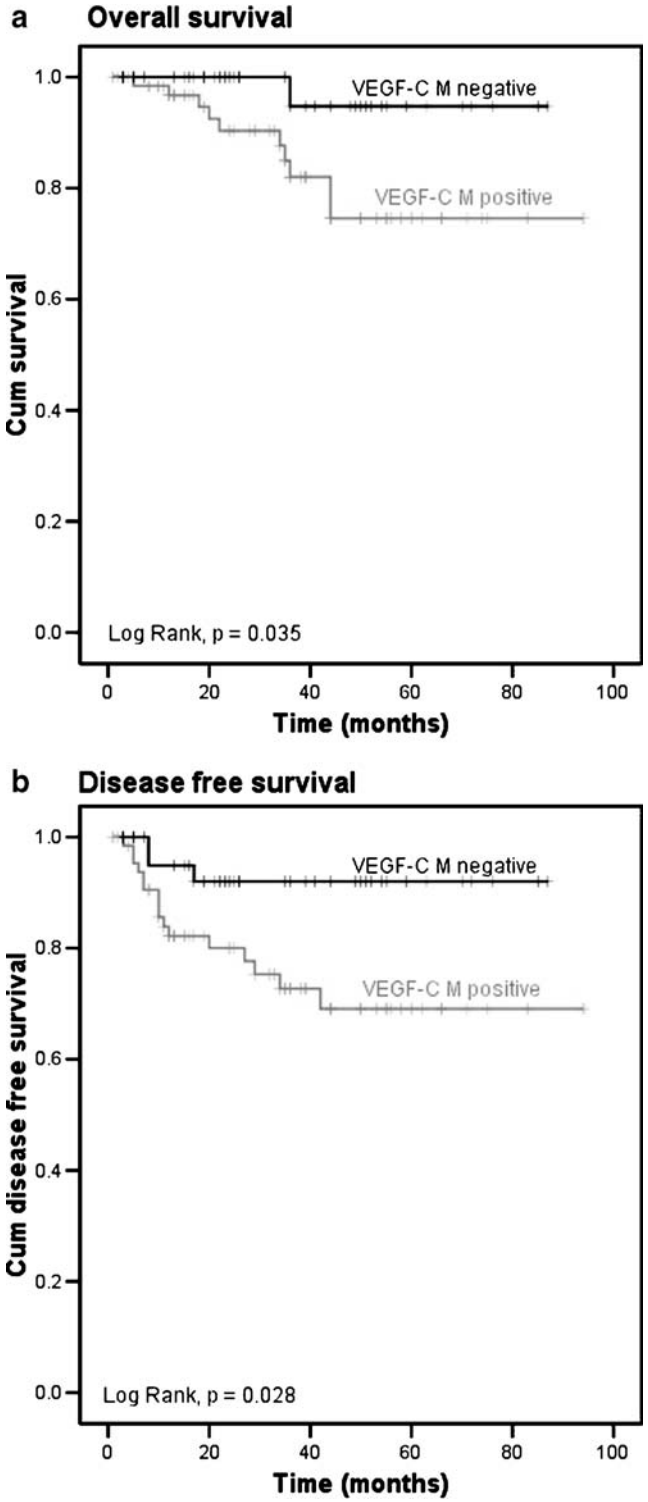

Fig. 4 VEGF-C expression in melanoma cells (VEGF-C M) versus overall (**a**) and disease-free (**b**) survival

reach statistically significant levels [8]. A small study on 21 melanoma samples revealed no qualitative differences in the intensity of VEGF-C staining in metastatic (13 patients) versus non-metastatic (eight patients) melanoma [41]. Dadras and colleagues performed a second study on 45 melanoma patients who underwent sentinel lymph node biopsy. Eighteen patients were sentinel lymph node positive. Sentinel lymph node-positive and -negative patients were similar in terms of tumour histological type, presence and degree of ulceration, anatomic sites, signs of regression and peritumoral inflammation. In total, 88.2% of the sentinel lymph node-positive melanomas revealed moderate to high levels of cytoplasmic VEGF-C compared to only 44.0% of sentinel lymph node-negative melanomas. This difference was statistically significant (p=0.00818) [7]. Recently, a case–control study was performed in 45 melanoma specimens of 15 sentinel lymph node-positive and 30 sentinel lymph node-negative patients. VEGF-C overexpression was more frequently observed in melanomas metastatic to the sentinel lymph node, but this did not reach significance. No significant correlation was found between VEGF-C expression and other clinicopathological parameters [29]. Based upon these studies, VEGF-C expression in primary cutaneous melanoma seems to be associated with lymphatic spread. However, most studies are not able to reach statistically significant results, which can be due to the relatively small sample sizes.

We found VEGF-C expression in melanoma cells to be significantly associated with the presence of a metastatically invaded sentinel lymph node. This study did not only score VEGF-C expression in melanoma cells but also in TAMs. It has been shown in human cervical cancer [39], oral squamous cell carcinoma [11], pancreatic ductal adenocarcinoma [10], breast cancer [40] and non-small cell lung cancer [47] that a subfraction of TAMs is a major source of VEGF-C production and that these macrophageal expression levels correlate with regional lymphatic neoangiogenesis and lymphatic metastasis. VEGF-C expression in melanoma-associated macrophages has already been observed [7, 8, 29]. Moreover VEGF-C is known to induce macrophage recruitment in melanoma [43]. In this study, we found TAMs to be an important source of VEGF-C production. Compared to VEGF-C expression in melanoma cells, VEGF-C positivity in TAMs was observed more frequently and the percentage and intensity of staining were higher. Moreover, VEGF-C-expressing TAMs appeared to be predictive of sentinel lymph node status. Although the accumulation of inflammatory cells at tumour sites has previously been considered a mechanism of host defence, these findings indicate that the inflammatory reaction around a developing neoplasm can contribute to tumour progression and metastasis [3].

Recently, it has been shown that VEGF-C induces growth of the lymphatics within the sentinel lymph node even before onset of metastasis. Upon arrival of the metastatic cells, further extension of lymphangiogenesis within the sentinel lymph node and metastatic spread to distant organs was observed [16]. Therefore VEGF-C and its receptor could be

interesting targets to slow or even prevent the onset of metastasis. Several agents, such as anti-VEGFR-3 antibodies, small interfering RNA's blocking VEGF-C expression, small molecule kinase inhibitors and recombinant adeno-associated virus expressing soluble VEGFR-3 have been tested in mouse tumour models where they have shown their ability to efficiently block the VEGFR-3 pathway with inhibition of lymph node metastasis as a consequence [54]. These findings suggest that VEGF-C staining in the primary cutaneous melanoma could predict the metastatic capacity of the tumour even before the presence of a microscopically invaded sentinel lymph node offering new possible targets for adjuvant treatment.

Acknowledgements The authors thank Mrs. R. Heyse and Mrs. S. D'Hont for their technical support and assistance in completing this study. This study was supported by the National Fund for Scientific Research-Flanders, grant number G.0128.06.

Barbara Boone is a research fellow of the National Fund for Scientific Research-Flanders, grant number G.0128.06.

Conflict of interest statement We declare that we have no conflict of interest.

References

1. Balch CM, Buzaid AC, Soong SJ, Atkins MB, Cascinelli N, Coit DG, Fleming ID, Gershenwald JE, Houghton A Jr., Kirkwood JM, McMasters KM, Mihm MF, Morton DL, Reintgen DS, Ross MI, Sober A, Thompson JA, Thompson JF (2001) Final version of the American Joint Committee on Cancer staging system for cutaneous melanoma. J Clin Oncol 19:3635–3648
2. Balch CM, Soong SJ, Gershenwald JE, Thompson JF, Reintgen DS, Cascinelli N, Urist M, McMasters KM, Ross MI, Kirkwood JM, Atkins MB, Thompson JA, Coit DG, Byrd D, Desmond R, Zhang Y, Liu PY, Lyman GH, Morabito A (2001) Prognostic factors analysis of 17,600 melanoma patients: validation of the American Joint Committee on Cancer melanoma staging system. J Clin Oncol 19:3622–3634
3. Bingle L, Brown NJ, Lewis CE (2002) The role of tumour-associated macrophages in tumour progression: implications for new anticancer therapies. J Pathol 196:254–265
4. Chilov D, Kukk E, Taira S, Jeltsch M, Kaukonen J, Palotie A, Joukov V, Alitalo K (1997) Genomic organization of human and mouse genes for vascular endothelial growth factor C. J Biol Chem 272:25176–25183
5. Clarijs R, Ruiter DJ, de Waal RM (2001) Lymphangiogenesis in malignant tumours: does it occur. J Pathol 193:143–146
6. Cueni LN, Detmar M (2006) New insights into the molecular control of the lymphatic vascular system and its role in disease. J Invest Dermatol 126:2167–2177
7. Dadras SS, Lange-Asschenfeldt B, Velasco P, Nguyen L, Vora A, Muzikansky A, Jahnke K, Hauschild A, Hirakawa S, Mihm MC, Detmar M (2005) Tumor lymphangiogenesis predicts melanoma metastasis to sentinel lymph nodes. Mod Pathol 18:1232–1242
8. Dadras SS, Paul T, Bertoncini J, Brown LF, Muzikansky A, Jackson DG, Ellwanger U, Garbe C, Mihm MC, Detmar M (2003) Tumor lymphangiogenesis: a novel prognostic indicator for cutaneous melanoma metastasis and survival. Am J Pathol 162:1951–1960
9. Enholm B, Karpanen T, Jeltsch M, Kubo H, Stenback F, Prevo R, Jackson DG, Yla-Herttuala S, Alitalo K (2001) Adenoviral expression of vascular endothelial growth factor-C induces lymphangiogenesis in the skin. Circ Res 88:623–629
10. Esposito I, Menicagli M, Funel N, Bergmann F, Boggi U, Mosca F, Bevilacqua G, Campani D (2004) Inflammatory cells contribute to the generation of an angiogenic phenotype in pancreatic ductal adenocarcinoma. J Clin Pathol 57:630–636
11. Feng HC, Song YF, Wen YM (2004) [Correlation between expression of vascular endothelial growth factor-C in tumor-associated macrophages and lymphatic metastasis in oral cancer]. Ai Zheng 23:278–281
12. Gershenwald JE, Thompson W, Mansfield PF, Lee JE, Colome MI, Tseng CH, Lee JJ, Balch CM, Reintgen DS, Ross MI (1999) Multi-institutional melanoma lymphatic mapping experience: the prognostic value of sentinel lymph node status in 612 stage I or II melanoma patients. J Clin Oncol 17:976–983
13. Goldman J, Le TX, Skobe M, Swartz MA (2005) Overexpression of VEGF-C causes transient lymphatic hyperplasia but not increased lymphangiogenesis in regenerating skin. Circ Res 96:1193–1199
14. He Y, Karpanen T, Alitalo K (2004) Role of lymphangiogenic factors in tumor metastasis. Biochim Biophys Acta 1654:3–12
15. He Y, Kozaki K, Karpanen T, Koshikawa K, Yla-Herttuala S, Takahashi T, Alitalo K (2002) Suppression of tumor lymphangiogenesis and lymph node metastasis by blocking vascular endothelial growth factor receptor 3 signaling. J Natl Cancer Inst 94:819–825
16. Hirakawa S, Brown LF, Kodama S, Paavonen K, Alitalo K, Detmar M (2007) VEGF-C-induced lymphangiogenesis in sentinel lymph nodes promotes tumor metastasis to distant sites. Blood 109:1010–1017
17. Jackowski S, Janusch M, Fiedler E, Marsch WC, Ulbrich EJ, Gaisbauer G, Dunst J, Kerjaschki D, Helmbold P (2007) Radiogenic lymphangiogenesis in the skin. Am J Pathol 171:338–348
18. Jeltsch M, Kaipainen A, Joukov V, Meng X, Lakso M, Rauvala H, Swartz M, Fukumura D, Jain RK, Alitalo K (1997) Hyperplasia of lymphatic vessels in VEGF-C transgenic mice. Science 276:1423–1425
19. Joukov V, Pajusola K, Kaipainen A, Chilov D, Lahtinen I, Kukk E, Saksela O, Kalkkinen N, Alitalo K (1996) A novel vascular endothelial growth factor, VEGF-C, is a ligand for the Flt4 (VEGFR-3) and KDR (VEGFR-2) receptor tyrosine kinases. EMBO J 15:1751
20. Joukov V, Sorsa T, Kumar V, Jeltsch M, Claesson-Welsh L, Cao Y, Saksela O, Kalkkinen N, Alitalo K (1997) Proteolytic processing regulates receptor specificity and activity of VEGF-C. EMBO J 16:3898–3911
21. Karkkainen MJ, Haiko P, Sainio K, Partanen J, Taipale J, Petrova TV, Jeltsch M, Jackson DG, Talikka M, Rauvala H, Betsholtz C, Alitalo K (2004) Vascular endothelial growth factor C is required for sprouting of the first lymphatic vessels from embryonic veins. Nat Immunol 5:74–80
22. Karpanen T, Egeblad M, Karkkainen MJ, Kubo H, Yla-Herttuala S, Jaattela M, Alitalo K (2001) Vascular endothelial growth factor C promotes tumor lymphangiogenesis and intralymphatic tumor growth. Cancer Res 61:1786–1790
23. Kukk E, Lymboussaki A, Taira S, Kaipainen A, Jeltsch M, Joukov V, Alitalo K (1996) VEGF-C receptor binding and pattern of expression with VEGFR-3 suggests a role in lymphatic vascular development. Development 122:3829–3837
24. Landi G, Polverelli M, Moscatelli G, Morelli R, Landi C, Fiscelli O, Erbazzi A (2000) Sentinel lymph node biopsy in patients with primary cutaneous melanoma: study of 455 cases. J Eur Acad Dermatol Venereol 14:35–45

25. Lee J, Gray A, Yuan J, Luoh SM, Avraham H, Wood WI (1996) Vascular endothelial growth factor-related protein: a ligand and specific activator of the tyrosine kinase receptor Flt4. Proc Natl Acad Sci U S A 93:1988–1992
26. Lin J, Lalani AS, Harding TC, Gonzalez M, Wu WW, Luan B, Tu GH, Koprivnikar K, VanRoey MJ, He Y, Alitalo K, Jooss K (2005) Inhibition of lymphogenous metastasis using adeno-associated virus-mediated gene transfer of a soluble VEGFR-3 decoy receptor. Cancer Res 65:6901–6909
27. Makinen T, Veikkola T, Mustjoki S, Karpanen T, Catimel B, Nice EC, Wise L, Mercer A, Kowalski H, Kerjaschki D, Stacker SA, Achen MG, Alitalo K (2001) Isolated lymphatic endothelial cells transduce growth, survival and migratory signals via the VEGF-C/D receptor VEGFR-3. EMBO J 20:4762–4773
28. Mandriota SJ, Jussila L, Jeltsch M, Compagni A, Baetens D, Prevo R, Banerji S, Huarte J, Montesano R, Jackson DG, Orci L, Alitalo K, Christofori G, Pepper MS (2001) Vascular endothelial growth factor-C-mediated lymphangiogenesis promotes tumour metastasis. EMBO J 20:672–682
29. Massi D, Puig S, Franchi A, Malvehy J, Vidal-Sicart S, Gonzalez-Cao M, Baroni G, Ketabchi S, Palou J, Santucci M (2006) Tumour lymphangiogenesis is a possible predictor of sentinel lymph node status in cutaneous melanoma: a case–control study. J Clin Pathol 59:166–173
30. Nicosia RF (1998) What is the role of vascular endothelial growth factor-related molecules in tumor angiogenesis. Am J Pathol 153:11–16
31. Oh SJ, Jeltsch MM, Birkenhager R, McCarthy JE, Weich HA, Christ B, Alitalo K, Wilting J (1997) VEGF and VEGF-C: specific induction of angiogenesis and lymphangiogenesis in the differentiated avian chorioallantoic membrane. Dev Biol 188:96–109
32. Olofsson B, Jeltsch M, Eriksson U, Alitalo K (1999) Current biology of VEGF-B and VEGF-C. Curr Opin Biotechnol 10:528–535
33. Paavonen K, Horelli-Kuitunen N, Chilov D, Kukk E, Pennanen S, Kallioniemi OP, Pajusola K, Olofsson B, Eriksson U, Joukov V, Palotie A, Alitalo K (1996) Novel human vascular endothelial growth factor genes VEGF-B and VEGF-C localize to chromosomes 11q13 and 4q34, respectively. Circulation 93:1079–1082
34. Papoutsi M, Siemeister G, Weindel K, Tomarev SI, Kurz H, Schachtele C, Martiny-Baron G, Christ B, Marme D, Wilting J (2000) Active interaction of human A375 melanoma cells with the lymphatics in vivo. Histochem Cell Biol 114:373–385
35. Pepper MS (2001) Lymphangiogenesis and tumor metastasis: myth or reality? Clin Cancer Res 7:462–468
36. Saaristo A, Veikkola T, Enholm B, Hytonen M, Arola J, Pajusola K, Turunen P, Jeltsch M, Karkkainen MJ, Kerjaschki D, Bueler H, Yla-Herttuala S, Alitalo K (2002) Adenoviral VEGF-C overexpression induces blood vessel enlargement, tortuosity, and leakiness but no sprouting angiogenesis in the skin or mucous membranes. FASEB J 16:1041–1049
37. Salven P, Lymboussaki A, Heikkila P, Jaaskela-Saari H, Enholm B, Aase K, von Euler G, Eriksson U, Alitalo K, Joensuu H (1998) Vascular endothelial growth factors VEGF-B and VEGF-C are expressed in human tumors. Am J Pathol 153:103–108
38. Schietroma C, Cianfarani F, Lacal PM, Odorisio T, Orecchia A, Kanitakis J, D'Atri S, Failla CM, Zambruno G (2003) Vascular endothelial growth factor-C expression correlates with lymph node localization of human melanoma metastases. Cancer 98:789–797
39. Schoppmann SF, Birner P, Stockl J, Kalt R, Ullrich R, Caucig C, Kriehuber E, Nagy K, Alitalo K, Kerjaschki D (2002) Tumor-associated macrophages express lymphatic endothelial growth factors and are related to peritumoral lymphangiogenesis. Am J Pathol 161:947–956
40. Schoppmann SF, Fenzl A, Nagy K, Unger S, Bayer G, Geleff S, Gnant M, Horvat R, Jakesz R, Birner P (2006) VEGF-C expressing tumor-associated macrophages in lymph node positive breast cancer: impact on lymphangiogenesis and survival. Surgery 139:839–846
41. Shields JD, Borsetti M, Rigby H, Harper SJ, Mortimer PS, Levick JR, Orlando A, Bates DO (2004) Lymphatic density and metastatic spread in human malignant melanoma. Br J Cancer 90:693–700
42. Shimizu K, Kubo H, Yamaguchi K, Kawashima K, Ueda Y, Matsuo K, Awane M, Shimahara Y, Takabayashi A, Yamaoka Y, Satoh S (2004) Suppression of VEGFR-3 signaling inhibits lymph node metastasis in gastric cancer. Cancer Sci 95:328–333
43. Skobe M, Hamberg LM, Hawighorst T, Schirner M, Wolf GL, Alitalo K, Detmar M (2001) Concurrent induction of lymphangiogenesis, angiogenesis, and macrophage recruitment by vascular endothelial growth factor-C in melanoma. Am J Pathol 159:893–903
44. Skobe M, Hawighorst T, Jackson DG, Prevo R, Janes L, Velasco P, Riccardi L, Alitalo K, Claffey K, Detmar M (2001) Induction of tumor lymphangiogenesis by VEGF-C promotes breast cancer metastasis. Nat Med 7:192–198
45. Stacker SA, Williams RA, Achen MG (2004) Lymphangiogenic growth factors as markers of tumor metastasis. APMIS 112:539–549
46. Straume O, Jackson DG, Akslen LA (2003) Independent prognostic impact of lymphatic vessel density and presence of low-grade lymphangiogenesis in cutaneous melanoma. Clin Cancer Res 9:250–256
47. Takizawa H, Kondo K, Fujino H, Kenzaki K, Miyoshi T, Sakiyama S, Tangoku A (2006) The balance of VEGF-C and VEGFR-3 mRNA is a predictor of lymph node metastasis in non-small cell lung cancer. Br J Cancer 95:75–79
48. Thiele W, Sleeman JP (2006) Tumor-induced lymphangiogenesis: a target for cancer therapy? J Biotechnol 124:224–241
49. Tobler NE, Detmar M (2006) Tumor and lymph node lymphangiogenesis—impact on cancer metastasis. J Leukoc Biol 80:691–696
50. Valencak J, Heere-Ress E, Kopp T, Schoppmann SF, Kittler H, Pehamberger H (2004) Selective immunohistochemical staining shows significant prognostic influence of lymphatic and blood vessels in patients with malignant melanoma. Eur J Cancer 40:358–364
51. Veikkola T, Jussila L, Makinen T, Karpanen T, Jeltsch M, Petrova TV, Kubo H, Thurston G, McDonald DM, Achen MG, Stacker SA, Alitalo K (2001) Signalling via vascular endothelial growth factor receptor-3 is sufficient for lymphangiogenesis in transgenic mice. EMBO J 20:1223–1231
52. Wagner JD, Corbett L, Park HM, Davidson D, Coleman JJ, Havlik RJ, Hayes JT 2nd (2000) Sentinel lymph node biopsy for melanoma: experience with 234 consecutive procedures. Plast Reconstr Surg 105:1956–1966
53. Was H (2005) [Characterization of markers and growth factors for lymphatic endothelium]. Postepy Biochem 51:209–214
54. Wissmann C, Detmar M (2006) Pathways targeting tumor lymphangiogenesis. Clin Cancer Res 12:6865–6868

Virchows Arch (2008) 453:267–274
DOI 10.1007/s00428-008-0649-y

ORIGINAL ARTICLE

Cadherin–catenin complex and transcription factor Snail-1 in spindle cell carcinoma of the head and neck

Nina Zidar · Nina Gale · Nika Kojc · Metka Volavšek · Antonio Cardesa · Llucia Alos · Heinz Höfler · Kareen Blechschmidt · Karl-Friedrich Becker

Received: 2 May 2008 / Revised: 29 June 2008 / Accepted: 23 July 2008 / Published online: 19 August 2008

Abstract Spindle cell carcinoma (SpCC) is a biphasic tumor composed of squamous cell carcinoma (SCC) and a malignant spindle cell component. There is mounting evidence that SpCC is a monoclonal neoplasm originating from a stem cell giving rise to both components. We tested the hypothesis that spindle cell phenotype might be related to the cadherin–catenin complex, which forms adherens junctions between cells. We analyzed the immunohistochemical expression of E- and N-cadherin, α-, β- and γ-catenin, and Snail-1, a transcription repressor of E-cadherin, in 30 cases of SpCC, and 30 cases of SCC of the head and neck. In SpCC, cadherin and catenin expression was similar in the SCC component, whereas in the spindle cell component, loss of E-cadherin and neo-expression of N-cadherin was found in 19 cases, loss of cadherins in seven, and their co-expression in four cases. Catenin expression were altered in 18 SpCCs. Snail-1 was found in 19 SpCC cases. In SCC, E-cadherin and catenins were expressed in all cases, and N-cadherin focally in five cases. Snail-1 was observed in the stroma. To summarize, in SpCC, there is an altered expression of the cadherin–catenin complex, associated with morphological transition from epithelial to spindle cell phenotype. These features are reminiscent of epithelial–mesenchymal transition (EMT). Our study thus indicates that EMT might play an important role in the pathogenesis of SpCC. This conclusion is further supported by our finding of Snail-1 expression, a potent inducer of EMT, in more than half SpCC cases.

Keywords Spindle cell carcinoma · Pathogenesis · E-cadherin · N-cadherin · α-Catenin · β-Catenin · γ-Catenin · Snail-1

N. Zidar (✉) · N. Gale · N. Kojc · M. Volavšek
Institute of Pathology, Medical Faculty, University of Ljubljana,
Korytkova 2,
1000 Ljubljana, Slovenia
e-mail: nina.zidar@mf.uni-lj.si

A. Cardesa · L. Alos
Department of Pathology, Hospital Clinic, IDIBAPS,
University of Barcelona,
Villaroel 170,
08036 Barcelona, Spain

H. Höfler · K. Blechschmidt · K.-F. Becker
Institute of Pathology, Technical University of Munich,
Trogerstrasse 18,
81675 Munich, Germany

H. Höfler
Institut für Pathologie, Helmholtz Zentrum München,
Deutsches Forschungszentrum für Gesundheit
und Umwelt, GmbH,
Neuherberg 85764, Germany

Introduction

Spindle cell carcinoma (SpCC) is a biphasic tumor composed of conventional squamous cell carcinoma (SCC) and a malignant spindle cell component [8]. It has been described in various sites of the body including the upper and lower respiratory tracts, breast, skin, urogenital and gastrointestinal tracts, and salivary glands [3]. In the head and neck, SpCC occurs most frequently in the larynx and oral cavity, followed by the skin, tonsil, sinonasal tract, and pharynx [15].

Microscopically, SpCC consists of a SCC component and a spindle cell component. The former is represented by in situ carcinoma or by an invasive SCC, whereas the latter usually forms the bulk of the tumor. Sometimes,

only spindle cells are present. Immunohistochemically, tumor cells often express epithelial and mesenchymal markers [8].

Histogenesis of SpCC is controversial, but there is mounting evidence that this is a monoclonal neoplasm originating from a single stem cell giving rise to both epithelial and mesenchymal components [10, 31]. It has not been elucidated why tumor cells exhibit the spindle cell morphology, but there is evidence to suggest that phenotype of cells might be related to the cadherin–catenin complex [20, 22, 23, 34].

Cadherins constitute a large family of cell adhesion molecules which form and maintain adhesive contacts between cells. More than 80 cadherins have been described, the most commonly studied cadherins in human development and disease being E-cadherin and N-cadherin, also known as classical (type I) cadherins. E-cadherin is present in epithelial tissues and N-cadherin in the central nervous system and in the heart. Cadherin-mediated adhesion is controlled by catenins: the cadherin cytoplasmic domain possesses a binding site for either β-catenin or γ-catenin (plakoglobin), which in turn, associates with α-catenin and links cadherin–catenin complexes to the actin-based cytoskeleton. The cadherin–catenin complex forms a typical cell–cell junction referred to as the adherens junction. Adherens junctions are essential during embryogenesis, whereas in later life they form and maintain cellular and tissue integrity. They also play a vital role in various pathological conditions, including cancer [11, 18, 25, 26].

β-Catenin has a double function and can thus play different roles in the carcinogenesis [37]. If localized to the cell membrane, it functions as an adhesion molecule being a component of the adherens junction. Reduced expression of membranous β-catenin has been found to be associated with a worse outcome in a variety of malignancies [35]. If localized to the nucleus, it functions as a signaling molecule inducing expression of target genes, such as cyclin D1 [6] playing an important role in the pathogenesis of some malignancies, such as colorectal carcinoma [5], hepatocellular carcinoma [12], and malignant melanoma [29]. γ-Catenin (plakoglobin) has also a double function: it is a component of both adherens junctions and desmosomes [37].

The aim of our study was to test the hypothesis that spindle cell phenotype in SpCC might be related to an altered expression of the components of adherens junctions. For this purpose, we analyzed the immunohistochemical expression of E- and N-cadherin, and α-, β-, and γ-catenin in SpCC, in comparison to "conventional" moderately differentiated SCC of the head and neck, using commercially available antibodies. We also analyzed the immunohistochemical expression of Snail-1, a transcription repressor of E-cadherin, using an antibody which was recently established, enabling the analysis of Snail-1 protein in human tissues [28].

Materials and methods

Our study included 30 patients with SpCC of the head and neck, and 30 patients with moderately differentiated SCC of similar locations. Among patients with SpCC, there were 25 men and five women, aged 39 to 91years (mean 66.2 ± 12.1). Tumors were located in the larynx (14 cases), hypopharynx (four cases), oropharynx (four cases), oral cavity (four cases), skin (two cases), and paranasal sinuses (two cases). In 21 cases, tumors consisted of both SCC and spindle cell components whereas in nine cases, tumors were composed of spindle cells only.

Among patients with SCC, there were 24 men and six women, aged 38 to 84years (mean 55.4 ± 8.8). Tumors were located in the larynx (14 cases), hypopharynx (four cases), oropharynx (five cases), oral cavity (five cases), and skin (two cases).

Tissue samples were fixed in 10% buffered formalin, embedded in paraffin, and cut at 4μm for H&E slides. For immunohistochemistry, additional sections were cut. Antigen retrieval and staining with monoclonal antibodies against cadherins, catenins, and Snail-1 was performed in an automatic immunostainer (Discovery, Ventana, Tucson, AZ, USA). Overview of source and clone, pretreatment conditions, and dilution of the primary antibodies used in this study is summarized in Table 1. Sections were treated with biotinylated secondary antibody, followed by incubation with peroxidase-conjugated streptavidin. Visualization of the immunoreaction was carried out with 3.3′ diaminobenzidine. Finally, sections were counterstained with hematoxylin.

Normal structures within tissue samples served as positive controls for cadherins and catenins showing a membranous reaction (squamous epithelium for E-cadherin and catenins, and nerves for N-cadherin). Fibrosarcoma served as a positive control for Snail-1 exhibiting nuclear reaction in the majority of tumor cells [14]. Negative controls omitting the primary antibodies were also included.

The percentage of positive cells was estimated using an image analysis system (Cell and Tissue Analysis, Leica, Germany), and graded as 0: no staining, 1: up to 10% of positive cells, 2: 11–50% of positive cells, 3: 51–80%, and 4: more than 80% of positive cells.

Statistical analysis

Spearman correlation coefficient was used to analyze the relationship between expression of cadherins, catenins, and Snail-1. Correlation was considered to be statistically significant at $p \leq 0.05$.

Table 1 Overview of source and clone, pretreatment conditions, and dilution of the primary antibodies used in this study

Antigen	Source	Clone	Pretreatment	Dilution
Keratin, wide spectrum	DAKO	Z0622	Citrate buffer + protease 2	1:1,200
Vimentin	DAKO	V9	EDTA	1:300
E-Cadherin	Labvision	SPM471	EDTA	1:20
N-Cadherin	DAKO	6G11	EDTA	1:20
α-catenin	Novocastra	25B1	EDTA	1:20
β-Catenin	Novocastra	17C2	EDTA	1:15
γ-Catenin	Novocastra	11B6	EDTA	1:20
Snail-1	Dr. E. Kremmer (GSF—National Research Centre for Environment and Health, Munich)	Sn9H2	Citrate buffer	1:20

Results

Keratin and vimentin in spindle cell carcinoma

Vimentin was expressed in malignant spindle cells in all patients, whereas keratin was found in spindle cells in 18/30 patients with SpCC.

Cadherins and catenins in spindle cell carcinoma

In SCC components, if present, E-cadherin and catenins exhibited similar patterns of immunostaining than in SCC. Results of immunohistochemistry for cadherins and catenins in the spindle cell components of the SpCC is summarized in Table 2. Cadherin switch (loss of E-cadherin and expression of N-cadherin) was found in 19 cases (Fig. 1), whereas co-expression of both cadherins was found in four cases. Reaction for both cadherins was negative in seven cases.

Catenin expression was altered in 18 SpCCs, with partial or complete loss of one catenin in ten cases, two catenins in seven cases, and all three catenins in one case. γ-Catenin was lost most frequently (in 17 cases; Fig. 2b), followed by α-catenin and β-catenin, which were lost in six and four cases, respectively.

Cadherins and catenins in SpCC exhibited mostly a membranous pattern of reaction. When the staining intensity was weak, it was almost impossible to distinguish between membranous and cytoplasmic patterns. No nuclear reaction was found.

Snail-1 in spindle cell carcinoma

Positive immunohistochemical reaction for Snail-1 was found in 19 cases of SpCC exhibiting a nuclear reaction (Fig. 3b). Positive reaction was mostly found in spindle cells, and only exceptionally in the SCC component.

Snail-1 was also expressed in the endothelial cells in blood vessels within the tumors, in some myofibroblasts and mononuclear inflammatory cells.

Cadherins and catenins in squamous cell carcinoma

E-cadherin was expressed in all cases of SCC, exhibiting a membranous pattern of reaction. In four cases, small clusters of negative cells were found at the invasive front. The vast majority of SCCs were negative for N-cadherin. N-cadherin was focally expressed in five cases, in up to 10% of the tumor cells. α-Catenin expression was similar to E-cadherin; it was found in all cases of SCC, exhibiting a membranous pattern of reaction.

β-Catenin was expressed in all cases of SCC and exhibited a similar pattern of reaction to E-cadherin. No nuclear reaction was found. A different reaction was observed in apoptotic cells, which were recognized by characteristic morphology and appeared either as scattered solitary cells within the tumor islands or in the areas of (para) keratinization. In apoptotic cells, expression of β-catenin was either faint or completely lost.

γ-Catenin was expressed in all cases, exhibiting an almost diffuse membranous pattern. A different reaction was observed in apoptotic cells where γ-catenin exhibited a strong cytoplasmic and occasionally also a nuclear reaction.

Normal structures in adjacent mucosa served as positive control: E-cadherin and all catenins were found in the squamous epithelium and salivary glands. N-cadherin and β-catenin were expressed in the nerves, whereas catenins were present in endothelial cells.

Snail-1 in squamous cell carcinoma

In the vast majority of SCCs, tumor cells did not stain with Snail-1 antibody. Only in four cases, Snail-1 was focally

Table 2 Results of immunohistochemistry for keratin, vimentin, cadherins, catenins, and Snail-1 in 30 patients with spindle cell carcinoma of the head and neck

Site	Keratin	Vimentin	E-cadherin	N-cadherin	α-Catenin	β-Catenin	γ-Catenin	Snail-1
Larynx	4	4	4	1	4	4	4	1
Larynx	2	4	0	3	4	4	3	1
Oropharynx	3	4	4	4	4	4	4	0
Hypopharynx	0	4	0	4	4	4	0	2
Larynx	0	4	0	1	0	3	0	2
Hypopharynx	0	4	0	1	0	0	0	1
Oral cavity	0	4	0	0	0	4	0	3
Maxillary sinus	1	4	0	0	0	3	0	0
Larynx	1	4	0	3	3	4	0	2
Oropharynx	1	4	1	3	4	4	4	0
Oropharynx	0	4	0	1	4	4	0	1
Larynx	2	4	0	4	0	4	3	0
Larynx	0	4	0	0	3	3	0	1
Oropharynx	0	4	0	2	2	0	0	0
Hypopharynx	0	4	0	0	3	4	3	1
Larynx	0	4	0	3	4	4	0	1
Larynx	1	4	0	3	2	4	0	2
Hypopharynx	4	4	0	0	4	4	4	0
Oral cavity	1	4	0	4	0	4	0	1
Skin	1	4	0	4	3	4	1	2
Larynx	0	4	0	2	3	4	0	1
Oral cavity	3	4	0	0	3	4	3	0
Skin	4	4	0	4	4	4	4	0
Oral cavity	3	4	0	0	4	4	0	2
Larynx	3	4	0	3	4	3	4	2
Maxillary sinus	0	4	0	3	3	0	0	0
Larynx	2	4	0	3	3	0	0	3
Larynx	0	4	0	1	3	3	3	0
Larynx	3	4	1	3	3	3	3	0
Larynx	1	4	0	1	4	4	0	3

Only results for the spindle cell components are shown in the table.
The percentage of positive cells was estimated using an image analysis system and graded as 0: no staining, 1: up to 10% of positive cells, 2: 11–50% of positive cells, 3: 51–80%, and 4: more than 80% of positive cells.

expressed in occasional tumor cells, mostly at the invasive front. Positive reaction was also observed in some myofibroblasts, mostly at the invasive front (Fig. 3a), whereas myofibroblasts in the central part of the tumor were usually negative. Snail-1 was also found in the endothelial cells in the majority of blood vessels within the tumor, and in mononuclear inflammatory cells. In the surrounding mucosa, endothelial and inflammatory cells did not stain with antibodies against Snail-1.

Statistical analysis

The frequency of Snail-1 expression was significantly higher in SpCC than in SCC ($p = 0.0001$). In SpCC, a negative correlation was found between Snail-1 and γ-catenin expression ($p = 0.047$), and between keratin and γ-catenin expression ($p = 0.030$).

Discussion

In this study, we found an altered expression of the cadherin–catenin complex components in the vast majority of SpCCs: one or more components of the cadherin–catenin complex forming adherens junctions normally present in epithelial tissue and SCC were lost. The varying patterns of cadherin expression were observed, the most common being the loss of E-cadherin and neo-expression of N-cadherin (also called the cadherin switch), followed by the loss of both cadherins, and by co-expression of both cadherins. An altered expression of catenins was detected in two thirds of SpCCs, with partial or complete loss of one catenin or two catenins, and exceptionally of all three catenins.

In contrast, moderately differentiated SCC of the head and neck exhibited rather regular patterns of cadherin–

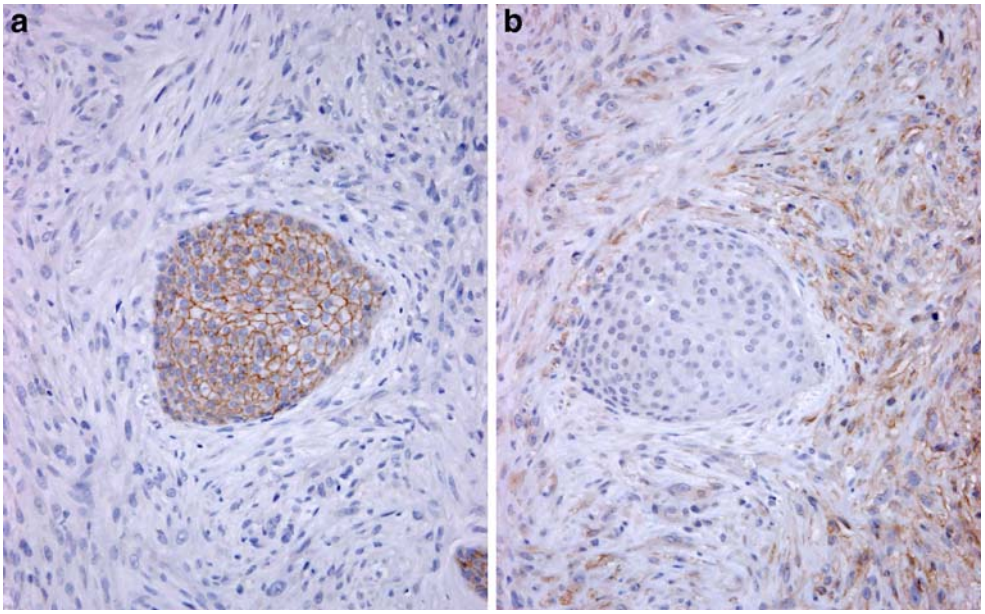

Fig. 1 Cadherin switch in spindle cell carcinoma: loss of immunohistochemical expression of E-cadherin (**a**), and neo-expression of N-cadherin (**b**). An island of normal squamous epithelium within the tumor serves as a positive control for E-cadherin. Original magnification ×20

catenin immunohistochemistry, which were similar to normal squamous epithelium. Positive reaction for E-cadherin was found in all tested cases of SCC; it was associated with positive reactions for α-, β-, and γ-catenin. E-cadherin and catenins exhibited a membranous pattern of reaction. No nuclear staining of β-catenin was observed suggesting that β-catenin functions mainly as an adhesion molecule in SCC of the head and neck as previously reported [35]. Occasionally, E-cadherin was lost in small clusters of tumor cells, mostly at the invasive front. These cells have been postulated to represent epithelial–mesenchymal transition (EMT) at the invasive tumor front and are believed to play a vital role in progression and metastasizing [32].

To summarize, in SpCC there is an altered expression of the cadherin–catenin complex, associated with morphological transition from epithelial to spindle cell phenotype, loss of epithelial markers and expression of mesenchymal markers, or co-expression of both. These features are reminiscent of epithelial–mesenchymal transition. EMT is a fundamental process governing morphogenesis during embryonal development. It is also reactivated in a variety of pathologic conditions in adult life including wound healing, fibrosis, and progression of carcinoma [1, 4, 19, 24, 27, 30, 33]. Our results indicate that EMT might also play an important role in the pathogenesis of SpCC of the head and neck.

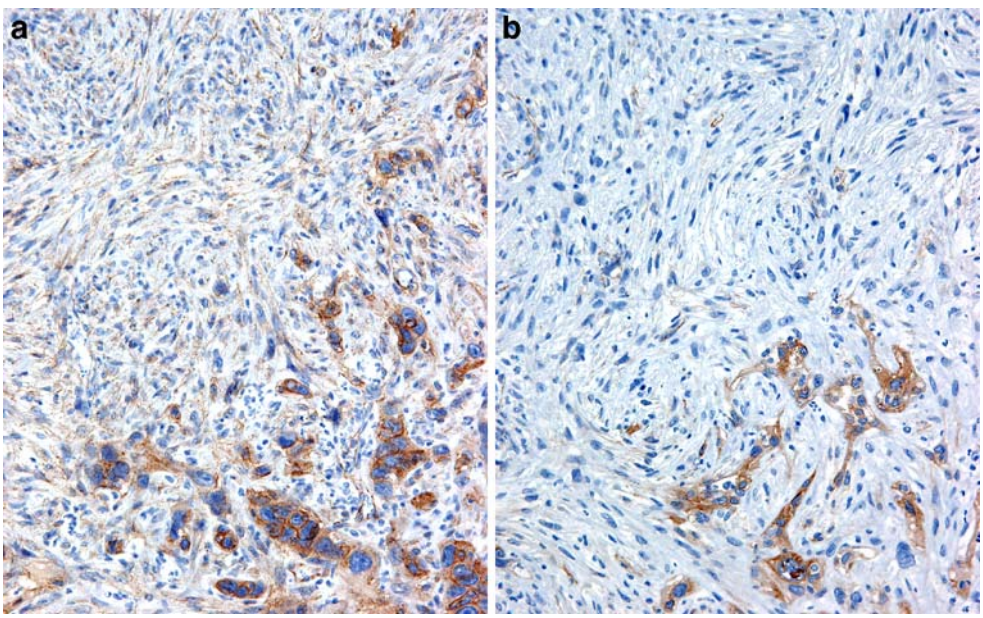

Fig. 2 Catenins in spindle cell carcinoma. Positive immunohistochemical reaction for β-catenin in islands of squamous cell carcinoma and in malignant spindle cells (**a**). Loss of γ-catenin in malignant spindle cells; positive reaction for γ-catenin in islands of squamous cell carcinoma and in vascular endothelial cells (**b**). Original magnification ×20

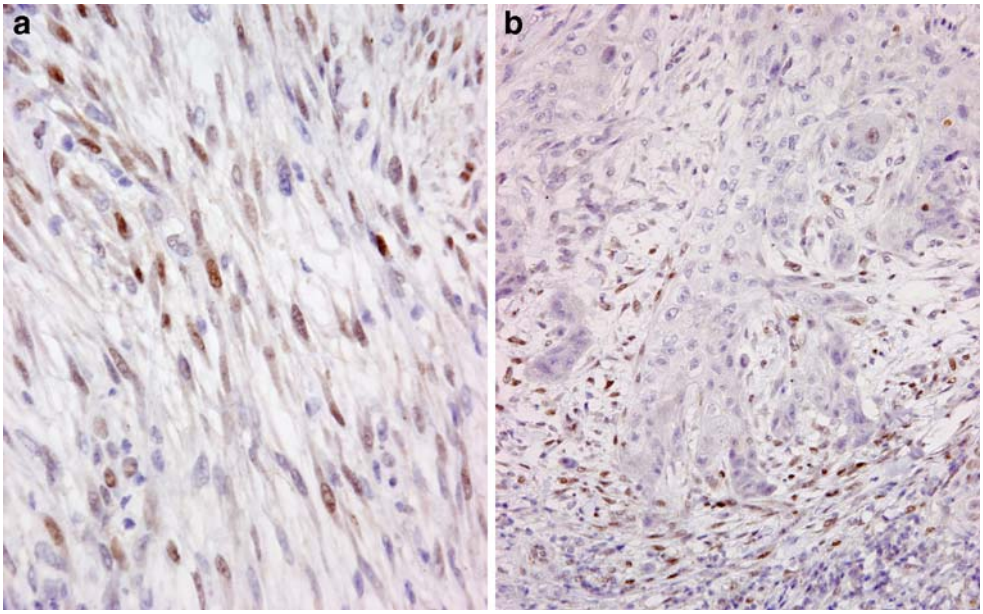

Fig. 3 Snail-1 in squamous cell carcinoma: positive reaction in myofibroblasts and endothelial cells particularly at the invasive front (**a**). Snail-1 in spindle cell carcinoma: positive reaction in tumor cells (**b**). Original magnification ×20

This is further supported by our finding of Snail-1 being expressed in almost two thirds of SpCCs. Snail belongs to the Snail family of Zinc-finger transcription factors. It represses the transcription of E-cadherin by binding to E-box elements in E-cadherin promoter, thus producing changes in cell phenotype consistent with EMT [2, 7]. Snail-1 is expressed in most developmental processes in which EMT is required, as well as in many pathologic conditions including malignant tumors [1, 4, 19, 24, 33].

Much attention has been recently paid to the significance of Snail-1 in malignant tumors, and it appears that it depends on the tumor type and location [4]. In our study, we found a differential expression of Snail-1 in SpCC compared to SCC. In SpCC, it was mostly expressed in the tumor cells possibly resulting in the spindle cell morphology. Interestingly, correlation between Snail-1 and E-cadherin expression was not statistically significant. This may be due to the small number of patients included in this study. In contrast, a statistically significant correlation was found between Snail-1 and γ-catenin expression, and between γ-catenin and keratin expression. As γ-catenin is a component of both adherens junctions and desmosomes, and keratin is the major desmosome-linked intermediate filament [16, 37], this finding might suggest that desmosomal proteins also play an important role in EMT in general, and in the pathogenesis of SpCC in particular.

In SCC, Snail-1 was rarely found in the tumor cells, but was often pronounced in endothelial cells and myofibroblasts, particularly at the invasive front, as already described in SCC of the uterine cervix [14]. The significance of these stromal changes at the invasive tumor front are not understood yet, but may confirm a recent suggestion that EMT and endothelial–mesenchymal transition are important mechanisms of myofibroblast formation in malignant tumors [36].

In EMT, epithelial cells turn off epithelial genes and turn on mesenchymal genes. They lose the apical–basal polarity, tight junctions and adherens junctions, reorganize the actin cytoskeleton, redistribute the organelles, and change to a highly motile fibroblastoid, mesenchymal phenotype allowing them to move through extracellular matrix [30]. It appears that the term EMT comprises a wide spectrum of changes, with a common denominator being a spindle cell phenotype [21, 33]. At one end of this spectrum are cells with characteristic phenotypical changes (i.e., fibroblastoid shape, loss of epithelial polarity), associated with a reduced expression of epithelial genes but which failed to turn on a mesenchymal gene expression program [17, 21]. At the other end of the spectrum is complete EMT, characterized by a complete loss of epithelial markers and gain of mesenchymal markers [17]. Similarly, in the SpCC, the common denominator is a spindle cell phenotype, with a wide spectrum of immunophenotypes, ranging from a complete cadherin switch, loss of epithelial markers, and expression of mesenchymal markers, to co-expression of both cadherins and epithelial and mesenchymal markers. The prognostic significance of cadherin–catenin immunophenotypes in SpCC remains to be determined. Because of the rarity of SpCC of the head and neck, we were only able to collect a diverse group of patients regarding the tumor location and stage. Analysis of the prognostic significance of immunophenotypes in such conditions was not possible.

In conclusion, our study indicates that EMT might play an important role in the pathogenesis of SpCC. This is further supported by our finding of transcription factor Snail-1, a well-known inducer of EMT, in many SpCCs.

Apart from Snail-1, there are other transcriptional repressors, and apart from transcriptional repression, there are other mechanisms triggering EMT, including gene mutation, promoter hypermethylation, enhanced degradation, chromatin rearrangements, and post-translational truncation or modification [9, 13, 28]. It remains to be determined whether any of these mechanisms are involved in the pathogenesis of SpCC.

Conflict of interest statement We declare that we have no conflict of interest.

References

1. Barrallo-Gimeno A, Nieto MA (2005) The Snail genes as inducers of cell movement and survival: implications in development and cancer. Development 132:3151–3161
2. Batlle E, Sancho E, Francí C, Domínguez D, Monfar M, Baulida J, García De Herreros A (2000) The transcription factor snail is a repressor of E-cadherin gene expression in epithelial tumour cells. Nat Cell Biol 2:84–89
3. Batsakis JG, Suarez P (2000) Sarcomatoid carcinomas of the upper aerodigestive tracts. Adv Anat Pathol 7:282–293
4. Becker KF, Rosivatz E, Blechschmidt K, Kremmer E, Sarbia M, Höfler H (2007) Analysis of the E-cadherin repressor Snail in primary human cancers. Cells Tissues Organs 185:204–212
5. Bienz M, Clevers H (2000) Linking colorectal cancer to Wnt signaling. Cell 103:311–320
6. Cadigan KM, Nusse R (1997) Wnt signaling: a common theme in animal development. Genes Dev 11:3286–3305
7. Cano A, Pérez-Moreno MA, Rodrigo I, Locascio A, Blanco MJ, del Barrio MG, Portillo F, Nieto MA (2000) The transcription factor snail controls epithelial–mesenchymal transitions by repressing E-cadherin expression. Nat Cell Biol 2:76–83
8. Cardesa A, Zidar N (2005) Spindle cell carcinoma. Larynx, hypopharynx and trachea. In: Barnes L, Eveson JW, Reichart PA, Sidransky D (eds) Pathology and genetics of tumours of the head and neck. WHO Classification of Tumours. IARC, Lyon, pp 11–113
9. Castro Alves C, Rosivatz E, Schott C, Hollweck R, Becker I, Sarbia M, Carneiro F, Becker KF (2007) Slug is overexpressed in gastric carcinomas and may act synergistically with SIP1 and Snail in the down-regulation of E-cadherin. J Pathol 211: 507–515
10. Choi HR, Sturgis EM, Rosenthal DI, Luna MA, Batsakis JG, El-Naggar AK (2003) Sarcomatoid carcinoma of the head and neck. Molecular evidence for evolution and progression from conventional squamous cell carcinoma. Am J Surg Pathol 27:1216–1220
11. Conacci-Sorrell M, Zhurinsky J, Ben-Ze'ev A (2002) The cadherin–catenin adhesion system in signaling and cancer. J Clin Invest 109:987–991
12. de La Coste A, Romagnolo B, Billuart P, Renard CA, Buendia MA, Soubrane O, Fabre M, Chelly J, Beldjord C, Kahn A, Perret C (1998) Somatic mutations of the beta-catenin gene are frequent in mouse and human hepatocellular carcinomas. Proc Natl Acad Sci U S A 95:8847–8851
13. de Moraes RV, Oliveira DT, Landman G, de Carvalho F, Caballero O, Nonogaki S, Nishimoto I, Kowalski LP (2008) E-cadherin abnormalities resulting from CPG methylation promoter in metastatic and nonmetastatic oral cancer. Head Neck 30:85–92
14. Francí C, Takkunen M, Dave N, Alameda F, Gómez S, Rodríguez R, Escrivà M, Montserrat-Sentís B, Baró T, Garrido M, Bonilla F, Virtanen I, García de Herreros A (2006) Expression of Snail protein in tumor–stroma interface. Oncogene 25:5134–144
15. Gale N, Zidar N (2006) Benign and potentially malignant lesions of the squamous epithelium and squamous cell carcinoma. In: Cardesa A, Menzel T, Rudolf P (eds) Head and neck, soft tissues, retroperitoneum and skin. Pathologie, 3rd edn. Springer, Berlin, pp 1–38
16. Gotzmann J, Mikula M, Eger A, Schulte-Hermann R, Foisner R, Beug H, Mikulits W (2003) Molecular aspects of epithelial plasticity: implications for local tumor invasion and metastasis. Mut Res 566:9–20
17. Grünert S, Jechlinger M, Beug H (2003) Diverse cellular and molecular mechanisms contribute to epithelial plasticity and metastasis. Nat Rev 4:657–665
18. Gumbiner BM (2005) Regulation of cadherin-mediated adhesion in morphogenesis. Nat Rev Mol Cell Biol 6:622–634
19. Hardy RG, Vicente-Dueñas C, González-Herrero I, Anderson C, Flores T, Hughes S, Tselepis C, Ross JA, Sánchez-García I (2007) Snail family transcription factors are implicated in thyroid carcinogenesis. Am J Pathol 171:1037–1046
20. Islam S, Carey TE, Wolf GT, Wheelock MJ, Johnson KR (1996) Expression of N-cadherin by human squamous carcinoma cells induces a scattered fibroblastic phenotype with disrupted cell-cell adhesion. J Cell Biol 135:1643–1654
21. Janda E, Lehmann K, Killisch I, Jechlinger M, Herzig M, Downward J, Beug H, Grünert S (2002) Ras and TGF beta cooperatively regulate epithelial cell plasticity and metastasis: dissection of Ras signaling pathways. J Cell Biol 156:299–313
22. Kim JB, Islam S, Kim YJ, Prudoff RS, Sass KM, Wheelock MJ, Johnson KR (2000) N-Cadherin extracellular repeat 4 mediates epithelial to mesenchymal transition and increased motility. J Cell Biol 151:1193–1206
23. Navarro P, Lozano E, Cano A (1993) Expression of E- or P-cadherin is not sufficient to modify the morphology and the tumorigenic behaviour of murine spindle carcinoma cells. J Cell Sci 105:923–934
24. Peinado H, Portillo F, Cano A (2004) Transcriptional regulation of cadherins during development and carcinogenesis. Int J Dev Biol 48:365–375
25. Peinado H, Olmeda D, Cano A (2007) Snail, ZEB and bHLH factors in tumour progression: an alliance against epithelial phenotype? Nat Rev Cancer 7:415–428
26. Perez-Moreno M, Jamora C, Fuchs E (2003) Sticky business: orchestrating cellular signals at adherens junctions. Cell 112:535–548
27. Radisky DC, Kenny PA, Bissell MJ (2007) Fibrosis and cancer: do myofibroblasts come also from epithelial cells via EMT? J Cell Biochem 101:830–839
28. Rosivatz E, Becker KF, Kremmer E, Schott C, Blechschmidt K, Höfler H, Sarbia M (2006) Expression and nuclear localization of Snail, an E-cadherin repressor, in adenocarcinoma of the upper gastrointestinal tract. Virchows Arch 448:277–287
29. Rubinfeld B, Robbins P, El-Gamil M, Albert I, Porfiri E, Polakis P (1997) Stabilization of beta-catenin by genetic defects in melanoma cell lines. Science 75:1790–1792
30. Thiery JP (2003) Epithelial–mesenchymal transitions in development and pathologies. Curr Opinion Cell Biol 15:740–746
31. Thompson L, Chang B, Barsky SH (1996) Monoclonal origins of malignant mixed tumors (carcinosarcomas). Evidence for a divergent histogenesis. Am J Surg Pathol 20:277–285
32. Tran NL, Nagle RB, Cress AE, Heimark RL (1999) N-cadherin expression in human prostate carcinoma cell lines: an epithelial–mesenchymal transformation mediating adhesion with stromal cells. Am J Pathol 155:787–798
33. Usami Y, Satake S, Nakayama F, Matsumoto M, Ohnuma K, Komori T, Semba S, Ito A, Yokozaki H (2008) Snail-associated

epithelial–mesenchymal transition promotes oesophageal squamous cell carcinoma motility and progression. J Pathol 215:330–339
34. Yokoyama K, Kamata N, Hayashi E, Hoteiya T, Ueda N, Fujimoto R, Nagayama M (2001) Reverse correlation of E-cadherin and snail expression in oral squamous cell carcinoma cells in vitro. Oral Oncol 37:67–71
35. Yu Z, Weinberger PM, Provost E, Haffty BG, Sasaki C, Joe J, Camp RL, Rimm DL, Psyrri A (2005) beta-catenin functions mainly as an adhesion molecule in patients with squamous cell cancer of the head and neck. Clin Cancer Res 11:2471–2477
36. Zeisberg EM, Potenta S, Xie L, Zeisberg M, Kalluri R (2007) Discovery ofendothelial to mesenchymal transition as a source for carcinoma-associated fibroblasts. Cancer Res 67:10123–10128
37. Zhurinsky J, Shtutman M, Ben-Ze'ev A (2000) Plakoglobin and beta-catenin: protein interactions, regulation and biological roles. J Cell Sci E113:3127–3139

Virchows Arch (2008) 453:275–282
DOI 10.1007/s00428-008-0648-z

ORIGINAL ARTICLE

Detection of Epstein–Barr virus-encoded small RNA-expressed myofibroblasts and IgG4-producing plasma cells in sclerosing angiomatoid nodular transformation of the spleen

Satoko Kashiwagi · Toshio Kumasaka · Nobukawa Bunsei · Yuki Fukumura · Shigetaka Yamasaki · Keiko Abe · Keiko Mitani · Hiroshi Abe · Toshiharu Matsumoto · Koichi Suda

Received: 15 August 2007 / Revised: 23 April 2008 / Accepted: 23 July 2008 / Published online: 12 August 2008

Abstract Sclerosing angiomatoid nodular transformation (SANT) of the spleen is a rare inflammatory tumor-like lesion composed of vascular nodules and non-neoplastic stroma including spindle cells and inflammatory cells. The focus of our study was on the stromal proliferating process in SANT. Nine cases of SANT were examined. All cases showed α-smooth muscle actin (α-SMA) and vimentin on the spindle cells but not CD21, CD31, CD34, CD68, desmin, S100, human herpes virus-8, or anaplastic lymphoma kinase-1. In one case, 20–30% of the myofibroblasts in Epstein–Barr-virus (EBV)-positive spindle cells were detected using double-labeling immunohistochemistry for α-SMA and EBV-encoded small RNA in situ hybridization. A quantitative analysis of IgG and IgG4-positive plasma cells (pPCs) in SANT was performed. The median densities of IgG-pPCs and IgG4-pPCs in SANT were approximately four-fold and 13-fold higher than those in the normal spleens, respectively. In addition, there was a statistically significant increase of IgG4/IgG-pPCs ratio in SANT in comparison to the control specimens. In conclusion, the fibrogenesis in a subset of SANT may be associated with EBV-infected myofibroblasts in an overlapping immune reaction indicated by the presence of infiltrating IgG4-pPCs. Further investigation is needed to elucidate the association between SANT and IgG4-related sclerosing disease.

Keywords Inflammatory pseudotumor · Follicular dendritic cell tumor · EBER in situ hybridization · Bone-marrow-derived stem cells · IgG4-related sclerosing disease

S. Kashiwagi · T. Kumasaka (✉) · N. Bunsei · Y. Fukumura · K. Mitani · H. Abe · T. Matsumoto · K. Suda
Department of Human Pathology,
Juntendo University Graduate School of Medicine,
2-1-1, Hongo, Bunkyo-Ku,
113-8421 Tokyo, Japan
e-mail: kumasaka@med.juntendo.ac.jp

S. Yamasaki
Department of Pathology,
Tokyo Rinkai Hospital,
1-4-2, Rinkai-Cho, Edogawa-Ku,
134-0086 Tokyo, Japan

K. Abe
Department of Histopathology,
Tohoku University Graduate School of Medicine,
2-1, Seiryo-Cho, Aoba-Ku,
980-8575 Sendai, Japan

Introduction

Martel et al. [14] first described sclerosing angiomatoid nodular transformation (SANT) of the spleen as altered red pulp tissue that had been entrapped by a non-neoplastic stromal proliferative process, and that was distinguished from splenic vascular tumors. However, it is unclear whether the pathogenesis of this splenic lesion is a de novo lesion or the end stage of a variety of benign splenic conditions including inflammatory pseudotumor (IPT), hamartoma, or hematoma [14]. Weinreb et al. [19] reported both the expression of CD30 in endothelial cells and EBV-encoded small RNA (EBER) in spindle cells in SANT, thus implying that SANT might be associated with a cytokine-mediated inflammatory process induced by EBV. Accord-

ing to the proliferation of myofibroblasts in the IPT-like areas in SANT, the myofibroblasts, as one of the fibrogenic cell types, may play a pivotal role in the fibrotic process of SANT [14, 19]. It has recently become known that myofibroblasts are derived from various progenitor cells such as locally residing fibroblasts, hepatic stellate cells, smooth muscle cells, epithelial cells, endothelial cells, and bone marrow (BM)-derived circulating stem cells [8, 20]. A proliferation of the myofibroblasts arising from these various progenitor cells occurs in the miscellaneous fibrosclerotic disorders, or in the fibrotic-tumor-like lesions in organs [18]. Therefore, understanding the phenotype of the fibrogenic cells in SANT is quite important in elucidating the mechanisms responsible for the emergence of SANT in the spleen.

Recently, Kamisawa et al. [10, 11] proposed IgG4-related sclerosing disease to be a multiorgan fibrosclerotic disorder which is characterized by a high serum level of IgG4 and a large number of IgG4-producing plasma cells infiltrating the fibrosclerotic lesions, including autoimmune pancreatitis, sclerosing cholangitis, retroperitoneal fibrosis, and sclerosing sialoadenitis. They also noted that a part of IPT might be associated with IgG4-related sclerosing disease. Accordingly, the characteristic histology of IPT-like lesions in SANT is therefore very close to the histology of IgG4-related sclerosing disease, as well as IPT, thus indicating that they may have a common fibrogenetic pathway.

We, therefore, evaluated EBV infection in fibrogenic cells and IgG4-producing plasma cells in SANT of the spleen by performing EBER in situ hybridization and immunohistochemistry with a morphometrical analysis.

Materials and methods

Nine cases were collected from the archives of the Division of Diagnostic Pathology at Juntendo University Hospital, the Division of Clinical Pathology at Juntendo University Urayasu Hospital, the Division of Clinical Pathology at Juntendo University Shizuoka Hospital, the Division of Clinical Pathology at Yamanashi Prefectural Central Hospital, the Division of Clinical Pathology at Kanto Industrial Hospital, and the Division of Clinical Pathology at Tokyo Metropolitan Otsuka Hospital. Two cases (cases 4 and 7, Table 2) were diagnosed as SANT, while the other cases were diagnosed as IPT.

Appropriately trimmed specimens were fixed in 10% formaldehyde in phosphate-buffered saline, processed into paraffin-embedded tissues, serially cut to 4 μm thickness, and stained with hematoxylin–eosin, Elastica van Gieson, Azan–Mallory, and Reticulin's silver. Immunohistochemical examinations were performed using the primary antibodies for α-smooth muscle actin (α-SMA), vimentin, desmin, S-100, CD21, CD31, CD34, CD68, anaplastic lymphoma kinase-1 (ALK-1), human herpes virus-8, immunoglobulin IgG, and IgG4 (Table 1). Briefly, deparaffinized, 4-μm-thickened paraffin-embedded tissue sections with or without pretreatment were incubated with ALK-1 antibody at 4°C for 17 h, or with the other antibodies at room temperature for an hour. The EnVision®+ System (Peroxidase; Dako, Glostrup, Denmark) and 3, 3′-diaminobenzidine tetrahydrochloride as the chromogen were utilized to detect the antibody binding. EBER in situ hybridization was performed on all nine cases. The EBV EBER probe was purchased from Research Genetics (Huntsville, AL). Briefly, deparaffinized, 4-μm-thickened paraffin-embedded tissue sections were incubated with 0.04% pepsin in 0.01 M HCl at room temperature for 30 min. After washing, the sections were incubated with an EBV EBER probe at 95°C for 7 min and then at 45°C for 17 hours. The sections were washed in sodium chloride citrate (2× SCC) at 38°C for 5 min twice and then were incubated with streptavidin–alkali phosphatase conjugate (Dako) at room temperature for 1 h followed by development with Fast red (Research Genetics).

Table 1 Summary of antibodies and pretreatment for immunohistochemistry

Antibodies	Clone	Companies	Dilution	Pretreatment
α-SMA	1A4	Dako, Glostrup, Denmark	1:200	N/A
Vimentin	V9	Dako	1:500	HIER
Desmin	D33	Dako	1:100	HIER
S-100	Polyclonal	Dako	1:400	N/A
CD21	1F8	Dako	1:100	Protease
CD31	JC70A	Dako	1:100	HIER
CD34	QBEnd/10	Novocastra, Newcastle, UK	1:200	HIER
CD68	KP-1	Dako	1:400	HIER
ALK protein (CD246)	ALK-1	Dako	1:50	HIER
HHV8	13B10	Novocastra Newcastle UK	1:50	HIER
IgG	polyclonal	Dako	1:800	Protease
IgG4	polyclonal	The Binding Site, Bindingham, UK	1:500	HIER

N/A Not applicable, *HIER* heat-induced epitope retrieval

Double-labeling immunohistochemistry for α-SMA and EBER in situ hybridization were also performed on one EBV-positive case (case 8). TACS-Blue (R&D Systems, Minneapolis, MN) as the chromogen was utilized for detecting α-SMA when performing double-labeling immunohistochemistry.

The number of IgG-positive plasma cells and IgG4-positive plasma cells were counted on ten fields in each specimen of the splenic tumors and the control spleens using a digital microscopic system (DP71 and AX80, Olympus, Tokyo, Japan). The control spleens were obtained from six men and four women, who underwent a splenectomy due to other diseases: six were associated with gastric carcinoma, two with pancreatic carcinoma, one with esophageal carcinoma, and one with adrenal cortical carcinoma, with a range from 53 to 84 years (mean 69.7± 10.6). To obtain the standardized value of each case and control, the total numbers of IgG and IgG4-positive plasma cells were divided by the total tissue area (0.55 mm^2) from which the plasma cells were counted. The number of IgG and IgG4-positive plasma cells, or the ratio of the number of IgG4 to IgG-positive plasma cells in the splenic tumors, was compared with the control spleens.

The Mann–Whitney *U* test (StatMate III for Windows, ATMS Co., Ltd., Tokyo, Japan) was used to compare the number of IgG and IgG4-positive plasma cells and the ratio of the number of IgG4/IgG-positive plasma cells. A *P* value less than 0.05 was considered to be statistically significant.

Results

Clinical features

The clinicopathological features of the cases are summarized in Table 2. There were nine patients, including five men and four women ranging from 31 to 72 years of age (mean 48.8±14.3). Seven of nine cases were asymptomatic in terms of the spleen and the other two had epigastralgia or back discomfort. Two of the eight cases had malignant neoplasm and two had cholelithiasis. The white blood cell count and serum C reactive protein (CRP) were within the normal limit in all cases except for case 6, which had an elevated serum CRP. The serum levels of IgG, or IgG4, were not measured in all cases because of no hypergammaglobulinemia. Follow-up information was available in five of nine cases that were alive without local recurrence or inflammatory disorders in their other organs, with a median follow up of 37 months (range, 3 to 113 months).

Macroscopic findings

The weight of the spleen ranged from 80 to 500 g and the tumor size ranged from 2 to 11 cm in diameter. The case that presented an elevated serum CRP showed the largest spleen and also the largest tumor in the study group (Table 2). Grossly, all cases had a solitary tumor in the spleen showing a well-demarcated, unencapsulated, dark brown or tan mass. All tumors, except for one (case 8), were composed of various-sized multinodular lesions. Four of nine cases had a large stellate fibrotic scar (Fig. 1). No case demonstrated either hemorrhaging or necrosis.

Microscopic findings

All cases had a demarcated tumor composed of round or oval-shaped vascular lesions surrounded by fibrous tissue (Fig. 2a). A histological characteristic of the tumors was the existence of vascular lesions surrounded by fibrosis which was composed of lamellar, dense collagen fibers (Fig. 2b). Dense collagen fibers intermingled with spindle cells and inflammatory cells around multinodular lesions were

Table 2 Summary of the clinical and pathologic features of sclerosing angiomatoid nodular transformation of the spleen

Case	Age	Sex	Clinical presentation		Spleen		Follow up (months)	Original diagnosis
			Presenting symptoms/concomitant disease	CRP (mg/dl)	Weight (g)	Tumor size (cm)		
1	31	F	Discovered incidentally/none	0.3	230	5.5	Lost to follow up	IPT
2	34	M	Back discomfort/none	0.2	N/A	7.0	3	IPT
3	37	M	Epigastralgia/none	0.1	80	3.0	79	IPT
4	44	F	None/cholelithiasis	0.01	N/A	3.5	25	SANT
5	46	M	None/chronic hepatitis	0.4	110	6.5	Lost to follow up	IPT
6	50	M	Discovered incidentally/none	5.7	500	11.0	Lost to follow up	IPT
7	60	M	None/gastric cancer	1.0	100	2.5	37	SANT
8	65	F	None/cholelithiasis	0.1	N/A	5.1	Lost to follow up	IPT
9	72	F	None/colon cancer	0.3	N/A	2.0	113	IPT

N/A Not applicable, *SANT* sclerosing angiomatoid nodular transformation, *IPT* inflammatory pseudotumor

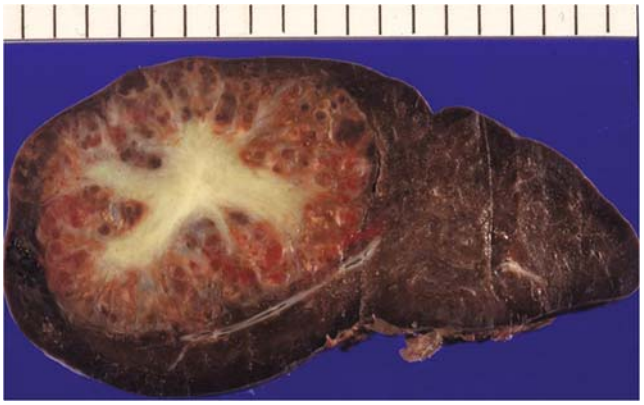

Fig. 1 Cut surface of the resected spleen. The splenic tumor showed solitary, well-demarcated and red–brown-colored small nodules around the central, stellate-shaped scar

observed (Fig. 2c). Case 8 had severe and diffuse fibrosis and a few angiomatoid nodules (Fig. 2d). In all cases, either plasma cells or lymphocytes and a much smaller number of eosinophils infiltrated the angiomatoid nodules and a large number of plasma cells mainly infiltrated the internodular lesions. All cases showed hemosiderin deposits or hemosiderin-laden macrophages, while five of them had Gamna–Gandy bodies. In addition, seven cases had obliterative phlebitis.

Immunohistochemistry

The spindle cells in the internodular lesions in all cases were immunopositive for α-SMA (Fig. 3a) and vimentin, but not for desmin, S-100, or CD34. No immunopositivity among

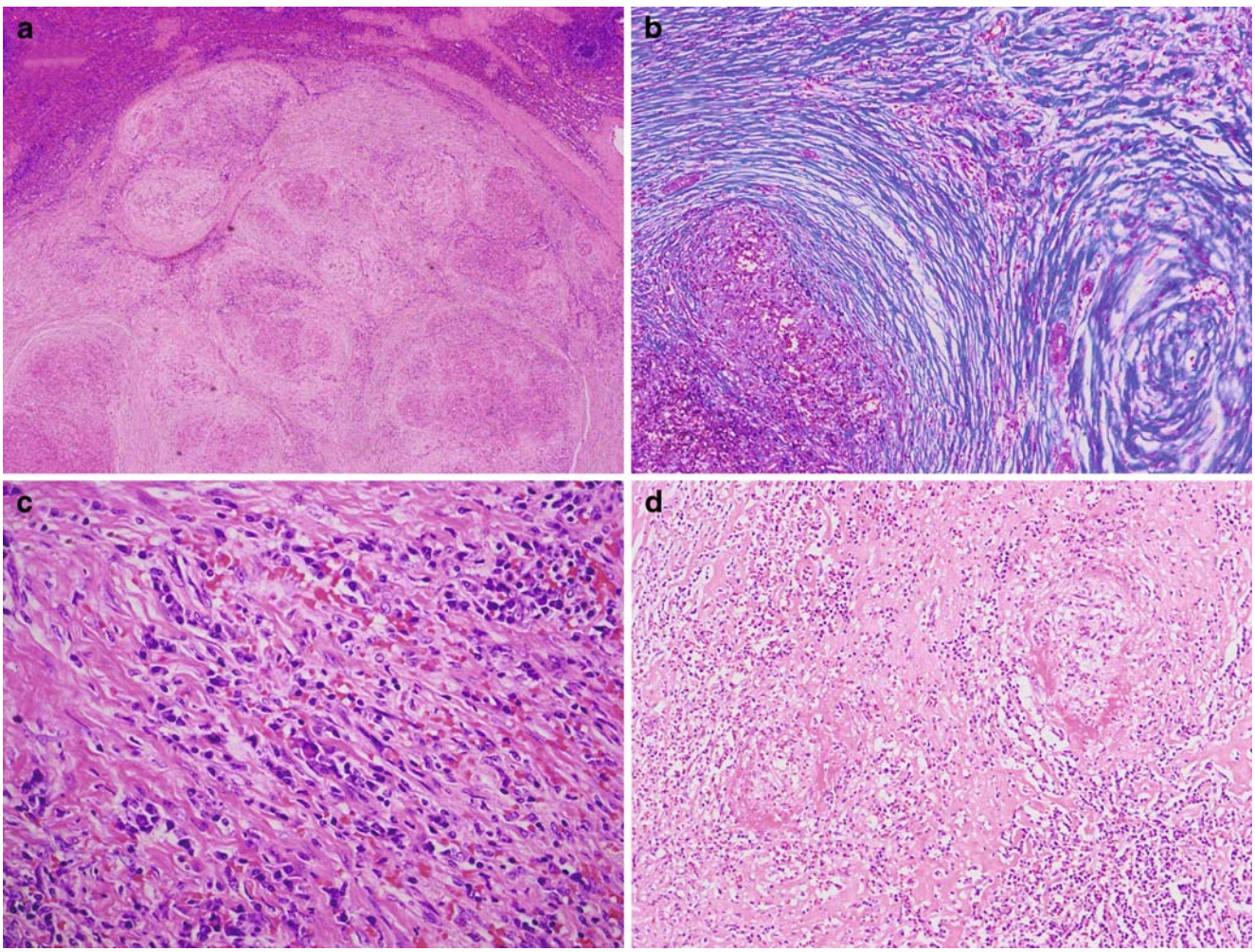

Fig. 2 Histological findings of SANT. SANT was well demarcated and consisted of fibrous nodules (HE stain; **a**). Concentric fibrosis surrounded by small angiomatoid areas (Azan stain; **b**). Plasma cells markedly infiltrated in the fibrotic area in SANT, and some of them had large, atypical, or binuclear cells (HE stain; **c**). In case 9, a few angiomatoid lesions were identified in the peripheral area of the tumor, although it had histological similarity to an inflammatory pseudotumor (HE stain; **d**)

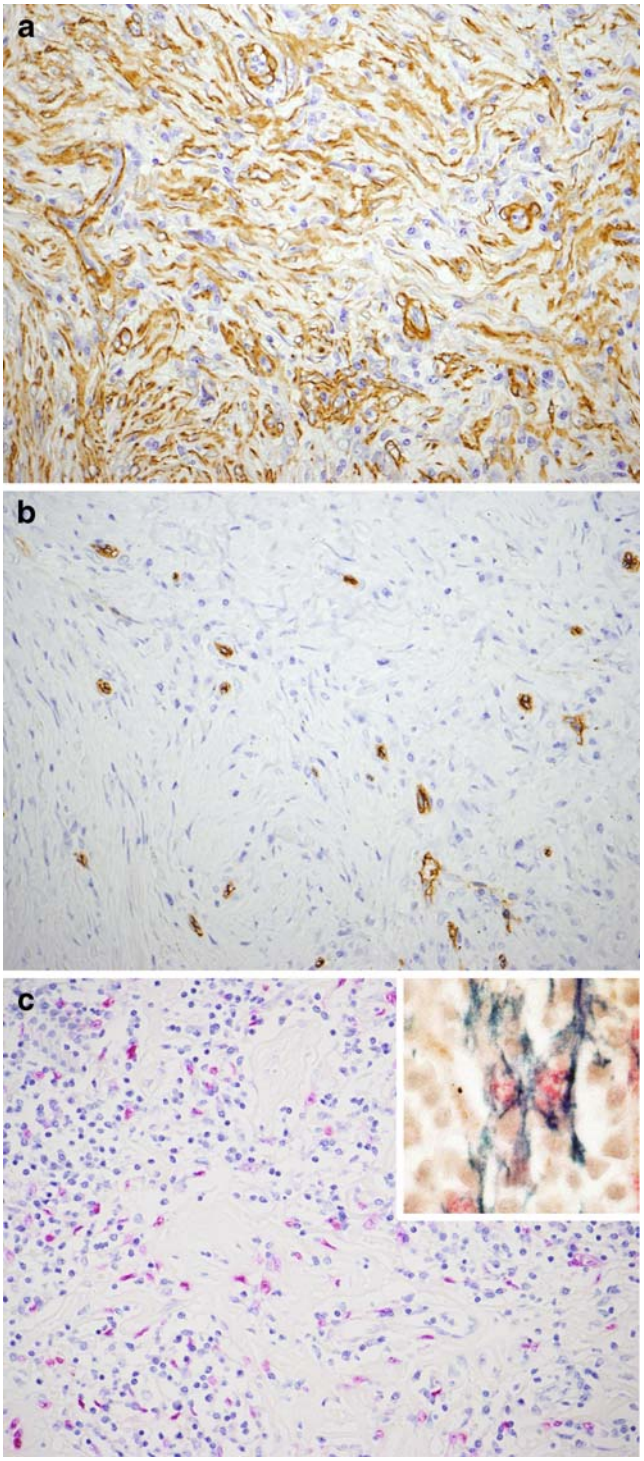

Fig. 3 Immunohistochemical findings of SANT. Many spindle cells in the fibrotic area were immunopositive for α-SMA (**a**); A few blood vessels in the internodular area were immunopositive for CD34 (**b**); Many EBER-expressed spindle cells proliferated in the internodular area (EBER, *red color*. *Inset* double staining for α-SMA immunostaining and EBER *in situ* hybridization; α-SMA, blue color; EBER, *red color* (**c**)

CD21, ALK-1, or HHV-8 was seen in any of the cases. The internodular lesions had very few vessels that were highlighted by immunostaining for CD31 and CD34 (Fig. 3b). All cases had many macrophages, with or without hemosiderin, that were immunopositive for CD68. Only Case 8 showed many spindle cells with nuclear expression for EBER in the internodular lesions. Double-labeling immunohistochemistry for α-SMA and EBER in situ hybridization demonstrated approximately 20–30% of the EBER-positive cells to be immunopositive for α-SMA (Fig. 3c).

To determine the densities of infiltrating IgG4 and IgG-positive plasma cells and the ratio of IgG- to IgG4-positive plasma cells infiltrating in the tumors in comparison to those plasma cells in the normal spleens as a control, we counted the number of IgG- and IgG4-positive plasma cells using a digital microscopic system (Fig. 4). The density of the IgG-positive plasma cells in the splenic tumors ranged from 1,507 to 6,535 cells/mm^2 (median, 3,470) and the median density in the splenic tumors was approximately four-fold higher than that in the normal spleens. In addition,

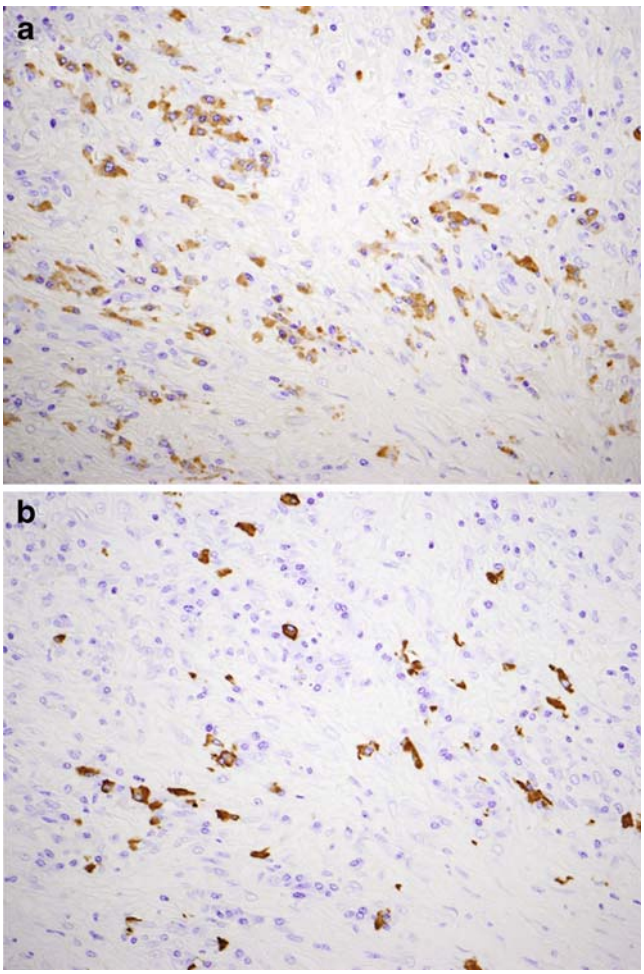

Fig. 4 Many IgG and IgG4-positive plasma cells infiltrated in the internodular area of SANT; IgG (**a**), IgG4 (**b**)

the density of the IgG4-positive plasma cells in the splenic tumors ranged from 305 to 3,482 (median, 602), and it was approximately 13-fold higher than that observed in the normal spleens. Both of the densities of the IgG4- and IgG-positive plasma cells between the splenic tumors and the normal spleens had significant differences ($P<0.0002$, $P<0.0008$, respectively). The percentage of the number of IgG4-positive plasma cells in the IgG-positive plasma cells in the splenic tumors ranged from 12.2% to 53.3% (mean 26.1%), while the percentage of IgG4/IgG in the normal spleen ranged from 0% to 13.0% (mean, 7.2%). Therefore, the difference between the splenic tumors and the normal spleen, in the percentage of IgG4/IgG-positive plasma cells, was found to be statistically significant ($P<0.0003$; Fig. 5).

Discussion

The present study focused on the non-neoplastic stromal proliferative process of sclerosing angiomatoid nodular transformation (SANT) of the spleen. Martel et al. [14] first demonstrated that the angiomatoid nodules in SANT were composed of small blood vessels of three immunophenotypical types: cord capillaries (CD34+/CD8−/CD31+); sinusoids (CD34−/CD8+/CD31+); small veins (CD34−/CD8−/CD31+), thus indicating that the normal splenic red pulp was entrapped by a non-neoplastic stromal proliferative process. They also noted that SANT had an internodular lesion histologically indistinguishable from IPT associated with EBV [1, 16]. In the present study, all cases had moderate to severe internodular fibrosis composed of proliferating spindle cells and the deposition of collagen with various degrees of inflammatory cell infiltration. Immunohistochemistry revealed that the proliferating spindle cells were strongly positive for vimentin and α-SMA, but not for CD21, CD31, CD34, or CD68. These results revealed that the internodular lesions of SANT histologically resembled IPT, as described in the previous reports [14, 19]. In addition, we determined that the myofibroblasts in the IPT-like area of SANT had a subpopulation of EBV-infected myofibroblasts in one of nine cases. Weinreb et al. [19] first investigated EBV in SANT, and detected EBV RNA in one of six cases that had diffuse areas resembling IPT, and noted that SANT might be associated with EBV infection. However, there was no data regarding the immunophenotype of the EBER-positive spindle cells in SANT in their description. One of our cases showed many EBER-expressed spindle cells in the IPT-like area that contained a subpopulation of EBER-expressed spindle cells (20–30%), identified as myofibroblasts by double-labeling immunohistochemistry for α-SMA and EBER in situ hybridization. The existence of the EBV RNA in the myofibroblasts of SANT supports the concept that a subgroup of SANT may be indistinguishable from IPT. We, therefore, propose that the proliferation of EBV-infected myofibroblasts may be a common pathway of a fibrosclerotic process in splenic inflammatory tumor-like lesions, including SANT.

It is unclear where the myofibroblasts in SANT are derived. Recently, splenic IPT has been immunophenotypically subdivided into three categories, such as IPT, inflammatory myofibroblastic tumor (IMT), and follicular dendritic cell tumor (FDCT) [1–3, 5, 9, 12, 13, 16, 17, 21]. However, it was not reported that the splenic IMT had expression of the ALK protein, which is involved in the neoplastic process of the pulmonary or soft tissue IMT [4, 6, 7, 12, 16]. Therefore the splenic IMT is both histologically and immunophenotypically identical to splenic IPT. Accordingly, the splenic inflammatory tumor-like lesions may subdivide

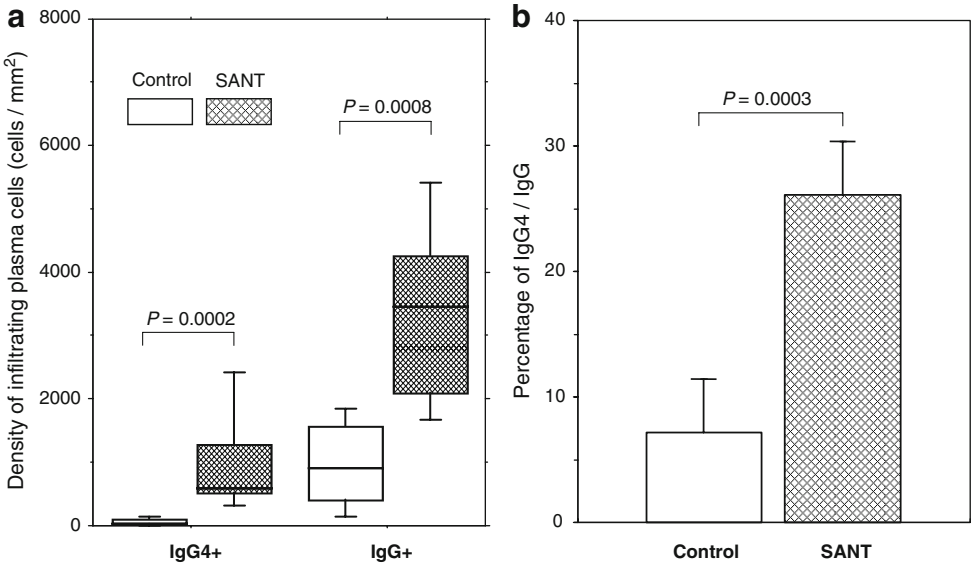

Fig. 5 Both of the cellular densities of IgG4- and IgG-positive plasma cells between SANT and the normal spleens as a control had significant differences ($P=0.0002$, $P=0.0008$, respectively; **a**). The difference of the percentage of IgG4/IgG-producing plasma cells between SANT and the control was also statistically significant ($P=0.0003$; **b**)

into two categories: IPT/IMT and IPT-like FDCT. Lewis et al. [13] proposed that a mesenchymal stem cell might differentiate into myofibroblasts, follicular dendritic cells, or no specific cells to develop each splenic inflammatory tumor-like lesion. Moreover, recent evidence confirms that follicular dendritic cells may arise from BM-derived circulating stem cells, and may be able to differentiate into myofibroblasts [15]. Therefore, a progenitor cell of myofibroblasts in these inflammatory tumor-like lesions of the spleen may arise from blood-borne cells, i.e., BM-derived circulating stem cells, because the splenic-resident cells, including fibroblasts, vascular smooth muscle cells, or endothelial cells cannot be directly infected with EBV. All things considered, a common pathway of the inflammatory stromal proliferative process associated with EBV-infected BM-derived circulating stem cells in splenic inflammatory tumor-like lesions, including SANT, may exist. However, before reaching this conclusion, additional studies with a larger series of SANT are necessary because of EBV being detected in only two cases with SANT in two series, including ours [19].

The aspect of the combination of a proliferating stromal process and infiltration of inflammatory cells, such as plasma cells and lymphocytes in SANT, thus provided important insight into IgG4-related sclerosing disease. Kamisawa et al. [11] described IgG4-related sclerosing disease to be a systemic disease that is histopathologically characterized by extensive IgG4-producing plasma cell infiltration of various organs, and tissue fibrosis with obstructive phlebitis, and also the occurrence of inflammatory pseudotumors in some cases of this disease. In our series, all cases met the histologic criteria of IgG4-related sclerosing disease, and seven of nine cases also had obliterative phlebitis similar to IgG4-related sclerosing disease. A quantitative analysis in this study also supported the premise that SANT might be associated with IgG4-producing plasma cells. Weinreb et al. [19] noted that SANT might be associated with an immune reaction because of the expression of CD30 on endothelial cells. Zen et al. [22] reported that some of the fibrotic lesions associated with IgG4-related sclerosing disease might be induced by an immune reaction regulated by T-regulatory cells. Therefore, the possibility that SANT is associated with IgG4-related sclerotic disease cannot be ruled out. However, our data were quite limited because of a lack of serum data of IgG4. In addition, there was no case demonstrating either a multiorgan fibrosclerotic disorder concomitant with SANT or a recurrent fibrosclerotic disorder of other organs after a splenectomy in our series. In fact, no case with recurrent inflammatory fibrosclerotic disorder in the other organs after a splenectomy for SANT has yet been reported [14, 19]. As a result, further evaluation is required to establish a clear association between SANT and IgG4-related sclerosing disease. The preoperative serum level of IgG4 is, therefore, considered to be helpful in determining whether or not SANT is associated with IgG4-related sclerosing disease.

Acknowledgements The authors gratefully acknowledge Drs. Toshimasa Uekusa, Hiroyuki Kato, Toshio Oyama, Saori Shiono, Fujihiko Suzuki, and Ryo Wada for their useful advice.

References

1. Arber DA, Kamel OW, van de Rijn M, Davis RE, Medeiros LJ, Jaffe ES, Weiss LM (1995) Frequent presence of the Epstein–Barr virus in inflammatory pseudotumor. Hum Pathol 26:1093–1098
2. Arber DA, Weiss LM, Chang KL (1998) Detection of Epstein–Barr Virus in inflammatory pseudotumor. Semin Diagn Pathol 15:155–160
3. Brittig F, Ajtay E, Jakso P, Kelenyi G (2004) Follicular dendritic reticulum cell tumor mimicking inflammatory pseudotumor of the spleen. Pathol Oncol Res 10:57–60
4. Cessna MH, Zhou H, Sanger WG, Perkins SL, Tripp S, Pickering D, Daines C, Coffin CM (2002) Expression of ALK1 and p80 in inflammatory myofibroblastic tumor and its mesenchymal mimics: a study of 135 cases. Mod Pathol 15:931–938
5. Chen TC, Kuo TT, Ng KF (2001) Follicular dendritic cell tumor of the liver: a clinicopathologic and Epstein–Barr virus study of two cases. Mod Pathol 14:354–360
6. Coffin CM, Hornick JL, Fletcher CD (2007) Inflammatory myofibroblastic tumor: comparison of clinicopathologic, histologic, and immunohistochemical features including ALK expression in atypical and aggressive cases. Am J Surg Pathol 31:509–520
7. Cook JR, Dehner LP, Collins MH, Ma Z, Morris SW, Coffin CM, Hill DA (2001) Anaplastic lymphoma kinase (ALK) expression in the inflammatory myofibroblastic tumor: a comparative immunohistochemical study. Am J Surg Pathol 25:1364–1371
8. Hinz B, Phan SH, Thannickal VJ, Galli A, Bochaton-Piallat ML, Gabbiani G (2007) The myofibroblast: one function, multiple origins. Am J Pathol 170:1807–1816
9. Horiguchi H, Matsui-Horiguchi M, Sakata H, Ichinose M, Yamamoto T, Fujiwara M, Ohse H (2004) Inflammatory pseudotumor-like follicular dendritic cell tumor of the spleen. Pathol Int 54:124–131
10. Kamisawa T, Funata N, Hayashi Y, Tsuruta K, Okamoto A, Amemiya K, Egawa N, Nakajima H (2003) Close relationship between autoimmune pancreatitis and multifocal fibrosclerosis. Gut 52:683–687
11. Kamisawa T, Okamoto A (2006) Autoimmune pancreatitis: proposal of IgG4-related sclerosing disease. J Gastroenterol 41:613–625
12. Kutok JL, Pinkus GS, Dorfman DM, Fletcher CD (2001) Inflammatory pseudotumor of lymph node and spleen: an entity biologically distinct from inflammatory myofibroblastic tumor. Hum Pathol 32:1382–1387
13. Lewis JT, Gaffney RL, Casey MB, Farrell MA, Morice WG, Macon WR (2003) Inflammatory pseudotumor of the spleen associated with a clonal Epstein–Barr virus genome. Case report and review of the literature. Am J Clin Pathol 120:56–61
14. Martel M, Cheuk W, Lombardi L, Lifschitz-Mercer B, Chan JK, Rosai J (2004) Sclerosing angiomatoid nodular transformation (SANT): report of 25 cases of a distinctive benign splenic lesion. Am J Surg Pathol 28:1268–1279
15. Munoz-Fernandez R, Blanco FJ, Frecha C, Martin F, Kimatrai M, Abadia-Molina AC, Garcia-Pacheco JM, Olivares EG (2006) Follicular dendritic cells are related to bone marrow stromal cell progenitors and to myofibroblasts. J Immunol 177:280–289

16. Neuhauser TS, Derringer GA, Thompson LD, Fanburg-Smith JC, Aguilera NS, Andriko J, Chu WS, Abbondanzo SL (2001) Splenic inflammatory myofibroblastic tumor (inflammatory pseudotumor): a clinicopathologic and immunophenotypic study of 12 cases. Arch Pathol Lab Med 125:379–385
17. Oz Puyan F, Bilgi S, Unlu E, Yalcin O, Altaner S, Demir M, Cakir B (2004) Inflammatory pseudotumor of the spleen with EBV positivity: report of a case. Eur J Haematol 72:285–291
18. Powell DW, Mifflin RC, Valentich JD, Crowe SE, Saada JI, West AB (1999) Myofibroblasts. I. Paracrine cells important in health and disease. Am J Physiol 277:C1–9
19. Weinreb I, Bailey D, Battaglia D, Kennedy M, Perez-Ordonez B (2007) CD30 and Epstein–Barr virus RNA expression in sclerosing angiomatoid nodular transformation of spleen. Virchows Arch 451:73–79
20. Wynn TA (2008) Cellular and molecular mechanisms of fibrosis. J Pathol 214:199–210
21. Yamaguchi M, Yamamoto T, Tate G, Matsumoto T, Matsumiya A, Kuzume M, Sanada Y, Kumada K (2000) Specific detection of Epstein–Barr virus in inflammatory pseudotumor of the spleen in a patient with a high serum level of soluble IL-2 receptor. J Gastroenterol 35:563–566
22. Zen Y, Fujii T, Harada K, Kawano M, Yamada K, Takahira M, Nakanuma Y (2007) Th2 and regulatory immune reactions are increased in immunoglobin G4-related sclerosing pancreatitis and cholangitis. Hepatology 45:1538–1546

Virchows Arch (2008) 453:283–290
DOI 10.1007/s00428-008-0645-2

ORIGINAL ARTICLE

Asthma induction in mice leads to appearance of α2–3- and α2–6-linked sialic acid residues in respiratory goblet-like cells

Svend Kirkeby · Niels-Erik Viby Jensen · Ulla Mandel · Steen Seier Poulsen

Received: 9 April 2008 / Revised: 26 June 2008 / Accepted: 10 July 2008 / Published online: 6 August 2008

Abstract Allergic asthmatic inflammation in mice was induced by sensitization with ovalbumin and lipopolysaccharide from *Escherichia coli* and visualized in the airways of asthmatic mice by spatial and temporal changes of carbohydrates containing sialic acid residues. Immunohistochemistry was used to demonstrate binding of lectins and antibodies that detect α2–3- and α2–6-linked sialic acid residues. After sensitization and challenge, the histology of the lung changed markedly, and goblet-like cells appeared, most likely caused by Clara cell metaplasia. Normal Clara cells showed no reaction after incubation with the sialic acid detecting agents, while the goblet-like cells expressed both α2–3- and α2–6-linked sialic acid residues in the asthmatic animals. The lectins but not the antibodies reacted with intestinal goblet cells. Instead, an antibody recognizing a disialoganglioside, stained large mononuclear cells in the submucosa, indicating a difference in sialylation between goblet cells in the intestine and goblet-like cells developed from Clara cells.

S. Kirkeby · U. Mandel
Dental School, University of Copenhagen,
Copenhagen, Denmark

N.-E. V. Jensen · S. S. Poulsen
Department of Biomedical Sciences,
University of Copenhagen,
Copenhagen, Denmark

S. Kirkeby (✉)
Department of Oral Medicine, Dental School,
University of Copenhagen,
Nørre Allé 20,
2200 Copenhagen N, Denmark
e-mail: sk@odont.ku.dk

Keywords Asthma · Mouse · Clara cells · Goblet cells · Glycosylation · Sialic acid

Abbreviations

MAA	*Maackia amurensis* agglutinin
SNA	*Sambacus nigra* agglutinin
PAS	periodic acid Schiff

Introduction

Mouse models for asthma share many pathological and immunological features with human asthma. After sensitization and respiratory tract challenges, wild-type mice develop a syndrome that closely resembles allergic asthma characterized by cellular lung inflammation, increased IgE, mucus hypersecretion, and eventually airway remodeling [4].

A difference between the cellular compartments of human and rodent airways is that, in normal mice, Clara cells represent the most abundant secretory cell type of both proximal and distal airways, while no goblet cells are present in the intrapulmonary bronchi or bronchioles [6]. However, goblet cell hyperplasia is a prominent feature of chronic airway diseases associated with mucus hypersecretion, and a number of stimuli significantly increase goblet cell numbers in the airways of experimental rodents [11, 13].

Goblet cells are often identified in tissue sections with periodic acid Schiff (PAS) protocols [4, 11, 12], which detects adjacent glycols in neutral sugars, uronic, and sialic acids, and some *N*-acetylamino sugars [9], but little is known of the detailed sugar specificity in the cells. In a number of studies, receptors for sialic acid (a nine-carbon

monosaccharide) have been demonstrated in the respiratory tract of both humans and laboratory animals, and changes in their expression are often associated with pathological changes in lung morphology and/or function [1, 3, 7, 16, 18].

This investigation aims to detect a possible change in expression of sialic acids caused by the allergic immune response. We have therefore used lectin and antibody histochemistry to study the in situ binding to specific sialic acid groups in the lung of normal mice and in mice sensitized to develop an asthma syndrome.

Materials and methods

Animals

Ten female C57/Bl6 8 weeks of age were used. The animals were housed in the animal facilities of the Panum Institute, University of Copenhagen, Copenhagen, Denmark, with temperature (21°C)- and humidity (55%)-controlled rooms with a light–dark cycle of 12 h each. They had access to water and chow (no. 1314, Altromin, Lage, Germany) ad libitum. The experimental studies were approved by the Danish National Committee of Animal Studies.

Induction of asthma

Pellets of ovalbumin were made by coagulating 100 ml of egg white in a water bath at 100°C for 60 min; the coagulate was cut into smaller sections that were dehydrated in 96% alcohol and stored at 5°C. Before use, the coagulate pieces were resuspended in phosphate-buffered saline for 24 h and homogenized by pushing the coagulate through a syringe. The animals were sensitized by injecting 0.1 ml of the heat-coagulated hen's egg white homogenate subcutaneously in the back of the neck.

Following a 14-day sensitization period, the animals were challenged with solutions of ovalbumine (OVA) 20 mg/ml in saline (Albumin from Hens egg white, crude powder, Fluka, Germany) and lipopolysaccharide (LPS) 2.5 mg/ml in saline (lipopolysaccharide from *Escherichia coli* 055:B5, Sigma-Aldrich, Germany) for 30 min a day on alternate days for a total of 6 days. The challenge was done by exposing the animals to an aerosol of the solutions generated by an aeroneb nebulizer (4.0–6.0 μm VMD, Aerogen, Ireland) in an airtight box (volume, 15 l) with an air turnover rate of 2.5 l per minute. Groups of two animals were sacrificed 1, 2, 4, 6, and 8 days after the first aerosol challenge; thus, the animals received between one and six aerosol challenges. The animals were sacrificed after the last challenge, and the lungs were retrieved for histological sampling. Further samples from the intestine were also collected in order to compare glycosylation in mucin producing cells from different sites.

Histological samples

The mice were sacrificed by cervical dislocation. For fixation of the lungs, the abdomen was opened and a little incision made in the diaphragm on both sides, whereafter the lungs were fixated by injecting 4% paraformaldehyde (PF) through a cannula placed in the trachea, thereby fixating the lungs in situ from the luminal side. The lungs were stored in 4% PF at 5°C for 24 h and then switched to 70% alcohol before being embedded in paraffin; hereafter, they were cut in 4-μm sections.

Lectins and antibodies

The lectins used to detect sialic acid residues were *Maakia amurensis* agglutinin (MAA; detects sialic acid α2–3Gal) and *Sambucus nigra* agglutinin (SNA; detects sialic acid α2–6Gal; EY laboratories; San Mateo, CA, USA). MAA consists of two isolectins that both bind to sialylated glycans but have distinct oligosaccharide specificity. The isolectin known as MAH is a hemagglutinin that binds to O-linked glycans, whereas the MAL isolectin is a leukoagglutinin and binds to N-linked glycans [14]. In this investigation, we have used the commercially available *Maackia amurensis* lectin that is a mixture of the two isoforms. The lectins were biotinylated as follows: 1 mg lectin was dissolved in 1 ml $NaHCO_3$ (0.1 M, pH 8.2) and mixed with biotin-NHS dissolved in 0.2 ml dimethylformamide. The mixture was stirred for 2 h at room temperature and dialyzed in 5 l 0.05 Tris/0.15 M NaCl (pH 7.2) overnight at 4°C.

Three different monoclonal antibodies were used to identify sialic acid residues in the sections. To detect the presence of disialoganglioside, we used a mouse monoclonal antibody, NUH2, that was raised after immunization of mice with the disialoganglioside fraction of human colonic adenocarcinoma [17]. The antibody FH6 is a monoclonal IgM antibody that recognizes the sialyl dimeric Lewis-X glycolipid with the structure NeuAcα2–3Galβ1–4(Fucα1–3)GlcNAcβ1–3Galβ1–4(Fucα1–3)GlcNAcβ1–3Galβ1–4Glcβ1–1Cer. The monosialo derivate of the difucosyllactonorhexaosyl-ceramide was obtained from human adenocarcinomas. The antibody has proven specific since it lacks reactivity with other glycolipids having a closely related structure such as Sialosyl–Lewis A and Sialosyl 2–6 fucoganglioside [5]

The antibody 3F1 directed against sialyl-Tn (NeuAcα2–6GalNAc-O-Thr/Ser) is of IgG1 type and has been generated by Dr. H. Clausen, Copenhagen, Denmark

(unpublished). It has proved specific to detect the sialyl-Tn glycans by van Leeuwen et al. [22].

Incubation

Before incubation, the sections were deparaffinized and subjected to microwave oven treatment for antigen retrieval. The sections were incubated for 24 h at 4°C with lectin diluted 1:200 in Tris-buffered saline (TBS) containing 20 mM $CaCl_2$ and $MgCl_2$. After a 3×5 rinse in TBS, the sections were immersed in Alexa Fluor 594 streptavidin conjugate (Molecular Probes, Eugene OR, USA) for 30 min. After a rinse in TBS, the sections were mounted in a fluorescence mounting medium S3023 (DAKO).

Controls

To ensure the specificity of the histochemical reaction, a number of control incubations were performed. (1) To block non-specific staining, the washing solutions contained TBS with 5% Triton-X 100 or 1% BSA. (2) To avoid detection of endogenous biotin in the tissue, the sections were quenched in an avidin/biotin blocking kit (Zymed Laboratories) before they were incubated with a biotinylated probe. (3) Sections were incubated in medium without lectin or primary antibody. (4) Sections were incubated in medium with irrelevant IgM or IgG monoclonal antibodies. To decide the specificity of the sialic-binding probes, some sections were digested with neuraminidase from *Vibrio cholera* (Sigma) for 2 h and processed according to the method described by Reid et al. [19].

Results

Morphology

The murine airway cell distribution is markedly different from human airways, which are lined by ciliated pseudostratified columnar epithelium containing goblet cells down to the level of the bronchioles. Mucoserous glands are situated in the submucosa. The bronchiolar epithelium is cuboidal, ciliated, and contains Clara cells. The primary features seen in asthma are hyperplasia of the submucosal glands and goblet cells, thickening of the basement membrane, and increased number of leukocytes primarily eosinophiles.

In comparison, the conductive airways of the mouse lung are lined by ciliated epithelium in the same way as in the human lung, but there is a complete lack of submucosal glands and goblet cells. The primary secretory cells are the Clara cells.

After exposure to either OVA or LPS, the histology of the lung changes markedly. Goblet cell-like cells appear,

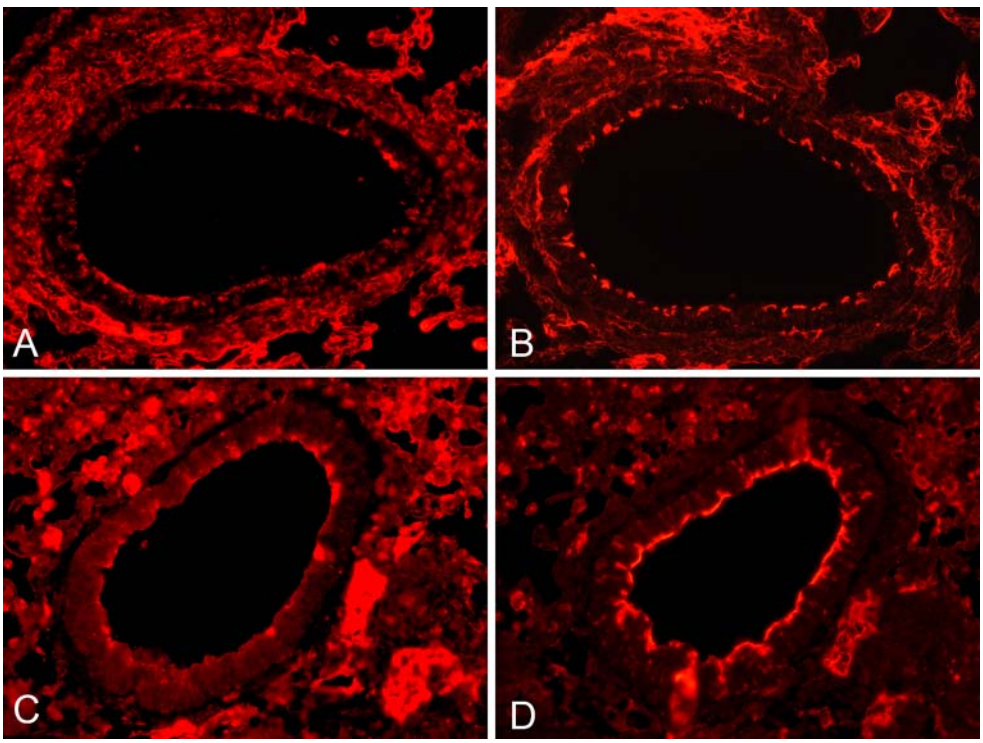

Fig. 1 **A**–**D** Incubation of lung sections with lectins and antibodies. **A** SNA, **B** MAA, **C** FH6, **D** NUH2. The *micrographs* show reactions in the bronchioles and surrounding respiratory tissue obtained from an untreated mouse. **A** and **B** illustrate two close by sections with a bronchiole having only a weak, unevenly distributed lectin reaction on the luminal surface of the epithelial cells. The bronchiole in **C** also show a weak and uneven staining pattern when incubated with FH6, while, as shown in **D**, incubation with NUH2 resulted in a stronger and continuous distribution at the luminal surface of the bronchiolar epithelial cells. **C** and **D** illustrate two close by sections. The lectin and antibody reactions as shown in Fig. 1 had not changed significantly 1–2 days after the asthmatic stimulus

most likely because of Clara cell metaplasia. The number of immune cells greatly increases primarily with concentrations of cells around the larger blood vessels and to a lesser degree around the bronchioles and bronchia.

The type of inflammatory cells appearing varies with the type of exposure. OVA-challenged lungs primarily contain eosinophiles and neutrophiles, while LPS-challenged lungs contain macrophages and neutrophiles. Prolonged airway challenging will cause airway remodelling as seen in human asthma, but these features do not occur in the protocol presently used because of the short exposure time of 6 days.

Histochemistry: lung

The staining reactions obtained after incubation of the lung tissue from the untreated mice were much alike with the staining achieved from mice 1–2 days after challenge. Incubation with the two lectins and with FH6 resulted in a meagre discontinuous reaction on the apical cell membrane of the epithelial cells lining the bronchi and bronchioles (Fig. 1A–C). A more continuous staining at the apical cell membrane appeared with NUH2 (Fig. 1D), while no reaction was noticed with the sialyl-Tn detecting antibody 3F1. Thus, in the lung tissue from the normal mice or from recently challenged mice, none of the sialic acid detecting probes used in this study reacted with Clara cells or other epithelial cells in the lower airways

Four to 6 days after challenge, many of the surface epithelial cells were stained with the sialic detecting probes. Not only did the number of reacting lung epithelial cells increase but also showed a change in the cellular staining since most of the supranuclear cytoplasm of the epithelial

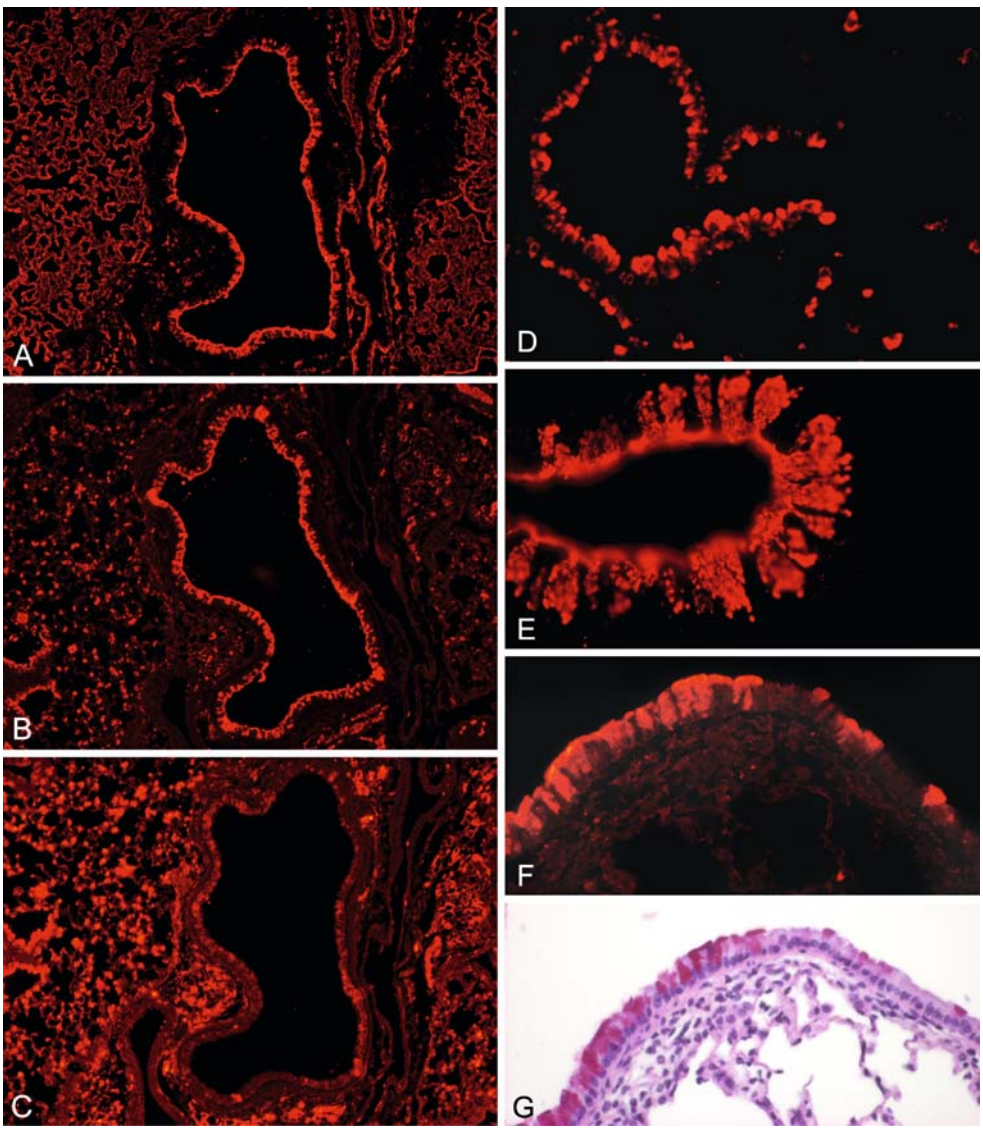

Fig. 2 **A**–**G** Incubation of lung sections 6 days after asthmatic treatment. **A**–**C** show three close by sections incubated with MAA (**A**), NUH2 (**B**), and FH6 (**C**). Almost all the epithelial cells lining the lumen in the small bronchus react strongly after incubation with MAA and NUH2, while only a few epithelial cells are stained after incubation with FH6. However, other parts of the respiratory tree may possess many epithelial cells that express sialyl Lewis X after FH6 incubation as shown in **D** that illustrates the reaction in a terminal bronchiole. Six days after the stimulus, many of the epithelial cells lining the bronchi and bronchioles have become columnar and show a goblet-like shape as in **E**, which shows a section incubated with NUH2. **F** and **G** are serial sections of a bronchus from an asthmatic mouse 6 days after stimulus, incubated with either SNA (**F**) or PAS (**G**). The two sections indicate that the columnar cells that are stained by the sialic acid-detecting lectin also are PAS positive

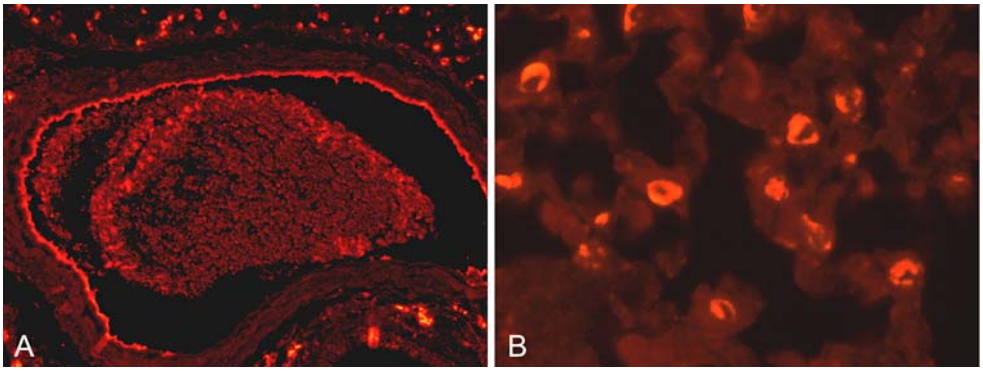

Fig. 3 **A**, **B** Sections obtained from a mouse 6 days after asthmatic treatment. In **A**, the endothelial cells in a large blood vessel show reaction after incubation with FH6. The mononuclear cells in the alveolar septa are visualized after incubation with 3F1 (**B**)

cells lining the large bronchi now showed staining after lectin incubation and after incubation with NUH2 (Fig. 2A,B,E, and F). These cells proved also to be PAS positive (Fig. 2G). A similar cytoplasmic reaction was present in many of the cells forming the respiratory epithelium of the bronchioles. While incubation with MAA, SNA, and NUH2 resulted in a rather consistent reaction in the epithelial cells, a more variable staining pattern was obtained after incubation with FH6. In some bronchi and bronchioles, only a few epithelial cells were stained with the sialyl Lewis-X detecting antibody (Fig. 2C), while in others, almost all epithelial cells were marked (Fig. 2D). Only a few bronchial cells showed a positive reaction after incubation with the sialyl-Tn detecting antibody 3F1. The reaction in the cells stained with the various sialic-recognizing probes was located either in the apical cytoplasm or in the entire cytoplasm, often displaying a goblet-like appearance (Fig. 2E and F).

In addition to their binding to bronchial/bronchiolar epithelial cells, FH6 also reacted with endothelial cells in pulmonary blood vessels in asthmatic mice, while 3F1 detected large mononuclear cells located in the alveolar septa (Fig. 3).

Histochemistry: intestine

In sections incubated with the lectins, the goblet cells in the intestine were stained with both SNA and MAA (Fig. 4A,B).

Dispersed cells in the villi were reacting in sections incubated with the antibody NUH2 (Fig. 4C). A large magnification revealed that the NUH2-positive intestinal

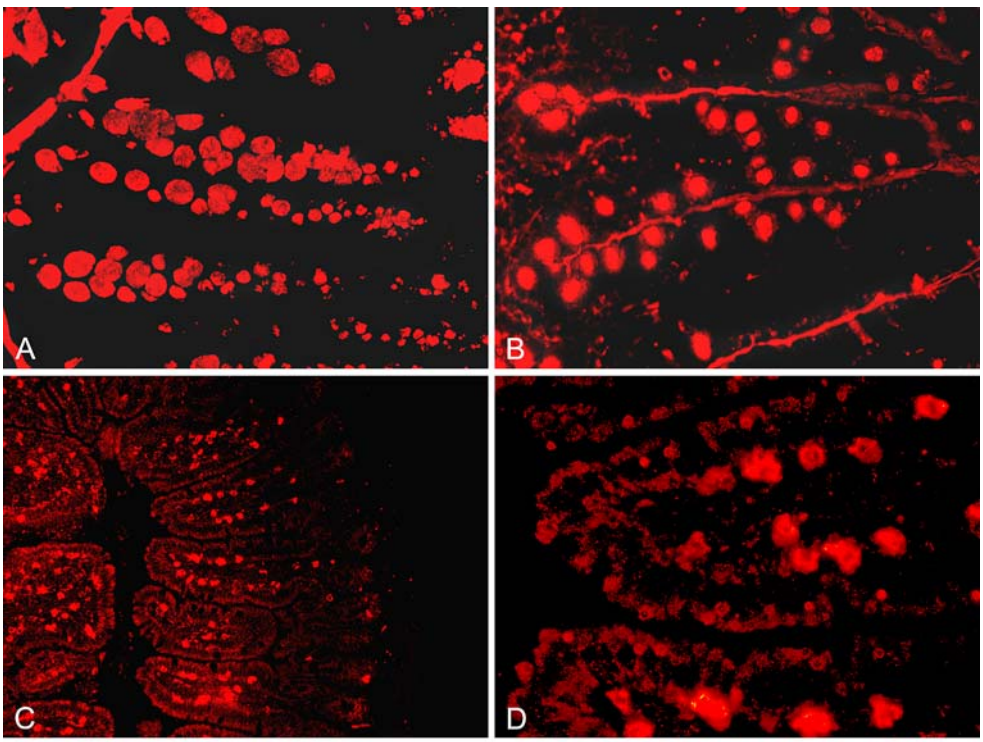

Fig. 4 **A**–**C** Sections from the intestine incubated with lectins and antibodies. **A**: SNA and **B**: MAA both detect the glycocalyx and goblet cells in the mucosa, while no submucosal cells are marked by the lectins. The sections shown in **C** and **D** were incubated with NUH2. The survey section (**C**) shows antibody-positive cells in the villi, while there is no reaction in the glycocalyx. A higher magnification as shown in **D** reveals that the antibody-positive cells are located in the submucosal connective tissue

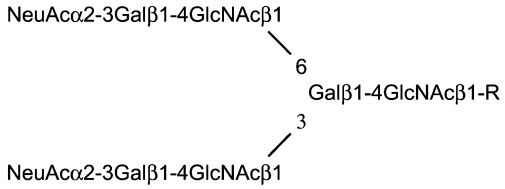

Fig. 5 Structure of the disialoganglioside that is recognized by NUH2

cells were not located in the surface epithelium but were large mononuclear cells located in the underlying connective tissue (Fig. 4D). There was no reaction in neither goblet cells or large mononuclear cells in sections incubated to visualize the presence of sialyl Lewis-X or sialyl-Tn antigens.

Controls

No reaction was found in sections incubated in medium without lectin or primary antibody, or in sections incubated with irrelevant immunoglobulin. A strong inhibition in expression of the sialic detecting probes were observed in sections subjected to neuraminidase treatment.

Discussion

The result obtained with both lectin and antibody showed that glycans containing sialic acid are present in normal mice lungs at the luminal surface of the epithelial cells lining the bronchi and bronchioles. The airway sialoglycoproteins may have different functions: mediators of adherence by a negative charge, serve as cell-surface receptors for bacteria and viruses, and influence viscoelastic properties [23]. Sialic acid can be attached to penultimate galactose, *N*-acetylglucosamine, or *N*-acetylgalactosamine sugars of glycoproteins, glycolipids, or mucins. In intestinal mucins, the glycans sequences most commonly found are NeuAcα2–6 GalNAc, NeuAcα2–6Gal, and NeuAcα2–3Gal [2].

PAS staining is frequently used to demonstrate the mucus hypersecretion in lung sections from asthmatic mice, but a positive PAS reaction gives little information on the sugar specificity. To obtain further information on the glycosylation pattern in normal and asthmatic mouse airways, we have shown that binding of sialic used α2–3-(MAA, NUH2, and FH6) and α2–6-linked sialic acid-recognizing (SNA and 3F1) probes. In untreated mice, the scattered reaction for sialic acid at the apical cell membranes is probably caused by binding to the glycocalyx of the epithelial cells lining the bronchi or bronchioles. No cytoplasmic staining was recorded in the Clara cells using lectins, antibody, or PAS protocols, confirming that goblet cells are absent in the distal airways of normal mice [6]. One to 2 days after ovalbumin inhalation, there was no major change in the location of the fluorescence reaction product after incubation of the lung sections.

Four to 6 days after inhalation, there was a dramatic difference in the staining pattern since a large number of epithelial cells in the bronchi and bronchioles reacted after incubation with the lectins and antibodies. These cells had the appearance of goblet cells with a basal nucleus, and often, their content of cytoplasmic granules was evident. The cells are probably metaplastic Clara cells. In normal lungs, Clara cells are cuboidal non-ciliated secretory cells associated with lung homeostasis [24], but exposure to ovalbumin in mice provokes hypertrophy of the cells, which acquire a mucous cell phenotype [21]. Comparison of SNA and PAS staining showed that the same columnar epithelial cells reacted with both agents.

Both the α2–3sialic and the α2–6sialic-recognizing lectins have previously been used to detect sialyl epithelial cell receptors for human and avian influenza viruses in the airways [10, 16]. We here suggest that metaplastic Clara cells in mouse airways develop sialyl α2–3 and sialyl α2–6 glycoconjugates after being exposed to experimental asthma.

NUH2 was raised after immunization with the disialoganglioside fraction of human colonic adenocarcinoma, and it is a highly specific anti-sialosyl IgM. The antibody reacts specially with disialogangliosides having the structure shown in Fig. 5. The antibody does not detect structures lacking the sialic acid at either the β1–3 or β1–6 side chain, and it does not recognize binary disialostructures having unequal chain lengths nor with a binary type 2 chain structure having a trimannosyl core as found in the side chain of *N*-linked complex type oligosaccharides [17]. The antigen is present in low quantity in some normal human cells such as erythrocyte and highly in some colon cancers, placental trophoblasts, and sperm. The target carbohydrate for NUH2 is the sialylated I-antigen, which is produced by activity of a β-1,6-*N*-acetylglucosaminyltransferase (IGnT) that converts the small i-antigen (Galβ1–4GlcNAc1–3Galβ1–4GlcNAc-R into the branched large I-antigen [15]; Fig. 6). In human

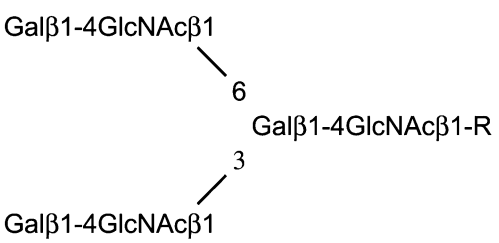

Fig. 6 Structure of the branched *N*-acetyllactosamine

RBC, the fetal i-antigen is replaced by the adult I-antigen, while during mouse embryogenesis, the I-antigen is expressed throughout the preimplantation period. The i-antigen in the 5-day embryo and the succeeding increase in the i-antigen is associated with a decrease in the I-antigen [8]. In the adult mouse, Magnet and Fukuda [15] detected expression of the large I-antigen forming β-IGnT in various tissues. In the intestine, the enzyme was present in the serosa and in the surface epithelium. In the mouse lung, the I-antigen was located to the alveoli, whereas the unbranched carbohydrate i-antigen was located to the bronchioles.

The sialyl Lewis-X-recognizing antibody FH6 showed variable epithelial cell staining in the bronchi/bronchioles and in pulmonary endothelial cells from asthmatic mice. An increased expression of sialyl Lewis-X epitopes is found in mucin from patients with CF or chronic bronchitis, leading to the suggestion that expanded sialyl Lewis-X in airway mucins correlates with severe lung infection or inflammation [20]. The reaction with the endothelial cells is probably caused by sialyl Lewis-X binding to E-selectin involved in the inflammatory response in which leucocytes are connected to sites of infection or injury.

The sialyl-Tn-recognizing antibody 3F1 detected a few scattered epithelial cells in the asthmatic airways and numerous large mononuclear cells in the alveolar walls. Sialyl-Tn is a mucin-associated antigen carried by apomyosins and is overexpressed in several epithelial cancers.

This study thus show appearance of α2–3 and α2–6 linked sialic acid residues in metaplastic Clara cells, and it may be suggested that sialylation of branched *N*-acetyllactosamine takes place in the bronchial epithelial cells after asthmatic sensitization and challenge. Furthermore, no enterocytes were stained when sections from the small intestine were incubated with any of the antibodies, but NUH2 gave rise to a strong reaction in scattered, large submucosal, mononuclear cell. Since the antibodies FH6 and NUH2 strongly reacted with the goblet-like cells in the asthmatic bronchi and bronchioles, it can also be concluded that there is a difference in sialic acid residues in the goblet cells of the intestine and in the goblet-like cells developed from Clara cells in the asthmatic mouse.

Conflict of interest statement We declare that we have no conflict of interest.

References

1. Castells MT, Ballesta J, Madrid JF, Aviles M, Martinez-Menarguez JA (1991) Characterization of glycoconjugates in developing rat respiratory system by means of conventional and lectin histochemistry. Histochemistry 95:419–426
2. Dai D, Nanthahakumar NN, Savidge TC, Newburg DS, Walker AW (2002) Region specific ontogeny of α-2,6-sialyltransferase during normal and cortisone-induced maturation in mouse intestine. Am J Physiol 282:G480–G490
3. Davril M, Degroote S, Humbert P, Galabert C, Dumur V, Lafitte JJ, Lamblin G, Roussel P (1999) The sialylation of bronchial mucins secreted by patients suffering from cystic fibrosis or from chronic bronchitis is related to the severity of airway infection. Glycobiology 9:311–321
4. Epstein MM (2004) Do mouse models of allergic asthma mimic clinical disease? Int Arch Allergy Immunol 133:84–100
5. Fukushi Y, Nudelman E, Levery SB, Hakomori SI, Rauvala H (1984) Novel fucolipids accumulating in human adenocarcinoma. J Biol Chem 259:10511–10517
6. Hayashi T, Ishii A, Nakaio S, Hasegawa K (2004) Ultrastructure of goblet-cell metaplasi from Clara cell in allergic asthmatic airway inflammation in a mouse model of asthma in vivo. Virchows Arch 444:66–73
7. Ibricevic A, Pekosz A, Walter MJ, Newby C, Battaile JT, Brown EG, Holzman MJ, Brody SL (2006) Influenza virus receptor specificity and cell tropism in mouse and human airway epithelial cells. J Virol 80:7469–7480
8. Kapadia A, Feizi T, Evans MJ (1981) Changes in the expression and polarization of blood group I and I antigens in post-implantation embryos and teratocarcinomas of mouse associated with cell differentiation. Exp Cell Res 131:185–195
9. Kiernan JA (1990) Histological and histochemical methods: theory and practice, 2nd edn. Pergamon, Oxford, UK
10. Kogure T, Suzuki T, Takahashi T, Miyamoto D, Hidari K, Guo CT, Ito T, Kawaoka Y, Suzuki Y (2006) Human trachea primary epithelial cells express both sialyl(α2–3)Gal receptor for human parainfluenza virus type 1 and avian influenza viruses, and sialyl (α2–6)gal receptor for human influenza viruses. Glycoconj J 23:101–106
11. Komori M, Inoue H, Matsumoto K, Koto H, Fukuyama S, Aizawa H, Hara N (2001) PAF mediates cigarette smoke-induced goblet cell metaplasia in guinea pig airways. Am j Physiol Cell Mol Physiol 280:L436–L441
12. Kouznetsova I, Chwiealski CE, Bälder R, Hinz M, Braun A, Krug N, Hoffmann W (2007) Induced trefoil factor family 1 expression by trans-differentiating Clara cells in a murine asthma model. Am J Respir Cell Mol Biol 36:286–295
13. Lamb D, Reid L (1968) Mitotic rates, goblet cell increase and histochemical changes in mucus in rat bronchial epithelium during exposure to sulphur dioxide. J Pathol Bacteriol 96:97–111
14. Macher BA, Yen TY (2007) Proteins at membrane surfaces—a review of approaches. Mol BioSyst 3:705–713
15. Magnet AD, Fukuda M (1997) Expression of the large I antigen forming β1,6-*N*- acetylglucosaminyltransferase in various tissues of adult mice. Glycobiology 7:285–295
16. Nichols JM, Bourne AJ, Chen H, Guan Y, Peiris JS (2007) Sialic receptor detection in the detection in the human respiratory tract: evidence for widespread distribution of potential binding sites for human and avian influenza viruses. Respir Res 8:73–83
17. Nudelman ED, Mandel U, Levery SB, Kaizu T, Hakomori SI (1989) A series of disialogangliosides with binary 2–3 sialosyllactosamine structure, defined by monoclonal antibody NUH2, are oncodedevelopmentally regulated antigens. J Biol Chem 264:18719–1825
18. Pastor LM, Frutos MJ, Grana L, Ramos D, Gallego-Huidobro J, Calvo A (1992) Histochemical study of glycoconjugates in the nasal mucosa of the rat and guinea pig. Histochem J 24:727–736
19. Reid PE, Arratoon C, Owen DA (1988) Applications of the selective periodate oxidation of sialic acids III. Identification of neuraminidase-sensitive and neuraminidase-resistant sialic acids and their side chain O-cyl variants. Histochem J 20:645–650

20. Rose MC, Voynow JA (2006) Respiratory tract mucin glycoproteins in health and disease. Physiol Rev 86:245–278
21. Roth FD, Quintar AA, Echevarria EMU, Torres AI, Aoki A, Maldonado CA (2007) Budesonide effects on Clara cell under normal and allergic inflammatory condition. Histochem Cell Biol 127:55–68
22. van Leeuwen EMB, Cloosen S, Senden-Gijsbers BLMG, Agervig Tarp M, Mandel U, Clausen H, Havenga MJE, Duffour M-T, Garcia-Vallejo JJ, Germeraad WTV, Boss GMJ (2006) Expression of aberrantly glycosylated tumor mucin-1 on human DC after transduction with a fiber-modified adenoviral vector. Cytotherapy 8:24–35
23. Yoon JH, Kim KS, Kim SS, Lee JG (1998) Sialoglycoproteins and penultimate sugar expression pattern in developing murine olfactory and respiratory mucosa. Yonsei Med J 39:20–26
24. Zuber C, Taatjes DJ, Roth J (2007) Recent progress in histochemistry. Histochem Cell Biol 128:557–594

Virchows Arch (2008) 453:291–300
DOI 10.1007/s00428-008-0651-4

ORIGINAL ARTICLE

Splenomegaly, hypersplenism and peripheral blood cytopaenias in patients with classical Anderson–Fabry disease

João Paulo Oliveira · Carmen Valbuena · António Baldaia Moreira · Elsa Fonseca · Carlos Soares · Elisa Leão Teles · Stephen Waldek

Received: 4 June 2008 / Accepted: 7 August 2008 / Published online: 2 September 2008

Abstract A 39-year-old male with classical Anderson–Fabry disease (AFD) and long-standing idiopathic splenomegaly, who had been on haemodialysis since the age of 24, was splenectomised for symptomatic pancytopaenia. Spleen enlargement was first noted at clinical presentation, at age 16, but despite thorough investigation its cause remained unclear. Anaemia, leukopaenia and thrombocytopaenia were first observed a few years thereafter, but well before the start of dialytic treatment. On gross pathological examination the spleen weighed 700 g and had a fibro-congestive appearance. Histologically, it showed expansion of the red pulp and decreased white pulp. Some histiocytes and many of the endothelial cells lining the sinusoids had vacuolated cytoplasm with argyrophilic material within, suggesting their involvement in the storage pathology of AFD. In a retrospective review of our cohort of patients with classical AFD (n=10), complete blood counts showing anaemia, leukopaenia or thrombocytopaenia were found in five, two and four patients, respectively, including a 6-year-old boy, whose spleen was also enlarged. Data from AFD international registries show that peripheral blood cytopaenias, particularly anaemia, are prevalent among these patients. Sinusoidal endothelial involvement resulting in compromise of splenic blood flow may be the cause of congestive splenomegaly and hypersplenism in classical AFD.

Keywords Anderson–Fabry disease · Splenomegaly · Hypersplenism · Thrombocytopaenia

J. P. Oliveira
Department of Medical Genetics, Faculty of Medicine, Porto, Portugal

J. P. Oliveira · A. Baldaia Moreira · C. Soares
Department of Nephrology, Hospital São João, Porto, Portugal

C. Valbuena · E. Fonseca
Department of Pathology, Faculty of Medicine and Hospital São João, Porto, Portugal

E. Leão Teles
Department of Paediatrics, Hospital São João, Porto, Portugal

S. Waldek
Adult Inherited Metabolic Diseases, Hope Hospital, Salford, United Kingdom

J. P. Oliveira (✉)
Serviço de Genética Médica, Faculdade de Medicina, Universidade do Porto, 4200-319 Porto, Portugal
e-mail: jpo@med.up.pt

Introduction

Anderson–Fabry disease (AFD) is a rare X-linked inherited sphingolipidosis due to deficient activity of the lysosomal enzyme α-galactosidase (α-Gal) [1]. The α-Gal defect results in multi-systemic accumulation of neutral glycosphingolipids containing terminal α-galactosyl residues, mostly globotriaosylceramide (Gb3).

Classical AFD is clinically characterised at the early stages by acroparesthesias, decreased sweating and a distinctive skin rash of angiokeratomas, followed later by progressive chronic kidney disease (CKD), hypertrophic and/or ischaemic cardiac disease and premature cerebrovascular disease [1]. Involvement of endothelial, perithelial

and smooth-muscle cells of blood vessels, as well as of cardiomyocytes, dorsal root ganglia and cells of the autonomic nervous system are regarded as the major factors in the pathogenesis of the classical AFD phenotype [1].

Storage of Gb3 in cells of the reticuloendothelial system also occurs in AFD [1] and has been known since the original bone marrow aspirate and autopsy studies of patients with AFD demonstrated the presence of vacuolated or lipid-laden cells in the bone marrow, lymph nodes, spleen and liver [2, 3]. Data on the histopathology of the spleen is limited to a few early studies of autopsy specimens [2] and of biopsies taken at laparotomy [4].

In contrast to Gaucher disease—a sphingolipidosis in which glucosylceramide accumulates within macrophages, leading to massive hepatosplenomegaly and hypersplenism, often resulting in anaemia and thrombocytopaenia [5]—the reticuloendothelial involvement in patients with AFD is usually asymptomatic. Only a small number of cases have been reported who had enlargement of lymph nodes, spleen or liver as presenting sign(s) [3, 4, 6–11]. Liver enlargement, however, has been mostly regarded as a manifestation of congestive heart failure [3]. Anaemia is recognised as a common complication of AFD [3, 12], even in patients with normal renal function, and its pathogenesis has been ascribed to impaired renal function, heart failure, inflammation or to chronic bleeding [3, 12].

Herein, we report a classically affected AFD patient who had clinically evident reticuloendothelial involvement at diagnosis and describe the histopathological findings in his spleen, which had to be surgically removed 22 years later to treat symptomatic hypersplenism. In addition, a retrospective study of our series of patients with the classical AFD phenotype and analyses of the Fabry Registry database suggest that the prevalence of peripheral blood cytopaenias other than anaemia in AFD patients may be higher than previously recognised. Therefore, we propose that mild to moderate hypersplenism may be a relatively frequent subclinical manifestation of AFD.

Case report

At the age of 39 years, a male patient with the classical phenotype of AFD underwent splenectomy to treat symptomatic hypersplenism (see Table 1 for a summary of the patient's past clinical history). He had been for almost 15 years on maintenance haemodialysis and asymptomatic chronic Hepatitis B Virus (HBV) infection was known for more than 10 years. Although splenomegaly and hypersplenism had been recognised several years before reaching end-stage renal failure (ESRF), frequent epistaxis and recurrent cellulitis of the legs, along with platelet counts below 50×10^9/l and neutrophil counts below 1.0×10^9/l (see Table 2), eventually justified the surgical indication.

The patient was of slight build (height=1.52 m, "dry weight"=47.0 kg) and had the coarse facial features of AFD [3]. Blood pressure was normal without medication. Multiple 1.0–1.5 cm lymphadenopathies were palpable in

Table 1 Summary of the patient's clinical history

Age	Clinical events and laboratory data
10 y	No clinical evidence of disease on family screening, following the diagnosis of AFD in an older brother
16–17 y	Sought medical attention because of recurrent diarrhoea. Generalised lymphadenopathy, liver and spleen enlargement noted on physical examination. No evidence of a primary haematologic disorder
	Diagnosis of CKD and referral for further evaluation
17 y	Multiple angiokeratomas with the typical distribution of AFD noted on skin examination. A skin biopsy showed the typical histological features of AFD angiokeratomas
	Electron microscopy study of a cervical lymph node biopsy showed the distinctive lamellated appearance of Gb3 deposits within histiocytic cells
	CrCl=47.7 ml/min/1.73 m^2, sCr=1.7 mg/dl; urinalysis: trace proteinuria, normal sediment. Normocytic, normochromic anaemia (Hg=10.4 g/dl)
17–24 y	Progressive deterioration of renal function with proteinuria reaching nephrotic level (= 3.6 g/day).
	First notice of low WBC and platelet counts
24 y	ESRF and start of maintenance HD
25–28 y	Acute hepatitis B, progressing to asymptomatic chronic infection
29–38 y	Worsening of all blood cytopaenias with recurrent nose and gum bleeding
	No residual enzyme activity demonstrated on α-Gal leukocyte assay
	GLA gene mutation identified as p.C94S
39 y	Therapeutic splenectomy

y Age in full years, *AFD* Anderson–Fabry disease, *CKD* chronic kidney disease. *CrCl* creatinine clearance, *sCr* serum creatinine, *Hg* haemoglobin *WBC* white blood cell, *ESRF* end-stage renal failure, *HD* haemodialysis, *α-Gal* α-galactosidase, *GLA* α-galactosidase gene

Table 2 Evolution of the relevant haematological parameters along follow-up of the index patient

Clinical event	Date	Hg (g/dl)	WBC ($\times 10^9$/l)	N ($\times 10^9$/l)	P ($\times 10^9$/l)
1st values in the nephrology clinic	Nov./1976	10.4[a]	6.4[a]	4.16[a]	150[a]
1st evidence of hypersplenism	Mar./1979	11.4[a]	4.8[a]	3.70[a]	72[a]
Lowest values observed before starting HD	1979–1983	9.8[a]	3.1[a]	2.17[a]	70[a]
Last values before the beginning of HD	Jun./1983	9.9[a]	4.0[b]	3.40[b]	120[a]
Lowest values observed on chronic HD	1983–1997	5.4[a]	1.3[b]	0.87[b]	19[a]
Last values prior to splenectomy	22/Feb./1998	9.1[a]	1.2[b]	0.72[b]	60[a]
2nd postoperative day	25/Feb./1998	10.9[a]	9.38[b]	8.37[b]	138[a]

Hg Haemoglobin, *WBC* white blood cells, *N* neutrophils; *P* platelets. *HD* haemodialysis
[a] Normal reference ranges, Hg=16±2 g/dl; WBC=5–10×10^9/l, N=3.0–5.8×10^9/l; P=290±150×10^9/l
[b] Normal reference ranges, WBC=7±3×10^9/l, N=2.0–7.5×10^9/l.

the neck, axillary and inguinal chains, the liver was palpable 2–3 cm below the right costal margin and the spleen was palpable 7–8 cm below the left costal margin. There were no clinical signs of portal hypertension and on ultrasound scan the liver size was at the upper limit of the normal range. Chronic lymphoedema was present in both legs. All three haematopoietic cell lines were represented in the bone marrow aspirate, with a ratio of myeloid to erythroid precursors of 1.5/1; many histiocytic cells showing a "foamy" cytoplasmic appearance were also noted.

At laparotomy, the spleen was described as greatly enlarged and congestive, with multiple capsular adhesions to the greater omentum, but no other abnormalities were recognised during the surgical exploration of the abdomen. On the second postoperative day, the white blood cell (WBC) and neutrophil counts had normalised and the platelet count had more than doubled as compared to the baseline preoperative control (see Table 2).

Methods, subjects and definitions

To assess the prevalence of generalised lymphadenopathy, hepatomegaly and splenomegaly, as well as of peripheral blood cytopaenias in male patients with classical AFD, we have retrieved all past and current clinical files of male patients with the diagnosis of AFD who have ever been admitted to, or followed-up at our hospital, since the first case was diagnosed in 1967 [13]. We have selected, for further review, only the files of patients which fulfilled the following criteria: (1) presentation with the classical AFD cutaneous phenotype and known or presumed hemizygosity for an α-Gal gene (*GLA*) mutation associated with residual α-Gal enzyme activity in plasma or in leukocytes less than 5% of the normal average (demonstrated in at least one affected male of the same family); and (2) clinical follow-up at our hospital for a minimum of 12 months with, at least, one complete blood count (CBC) available for review. Clinical and laboratory data obtained after the eventual start of enzyme replacement therapy (ERT) were excluded. These medical files were further analysed in detail for any record of the following clinical and haematologic features: generalized lymphadenopathy, palpable spleen or splenomegaly, palpable liver or hepatomegaly; anaemia, leukopaenia, neutropaenia or thrombocytopaenia. Any clinical events or circumstances that might have determined or contributed to those findings were also noted.

Adult age was defined as 18 or more years. Generalised lymphadenopathy was defined as enlarged lymph nodes palpable in two or more distinct anatomic regions [14]. Assessment of liver and of spleen size was done according to standard clinical [15–18] and sonographic criteria [19–22]. CKD stages were defined according to current clinical practice recommendations [23]. Glomerular filtration rate was estimated (eGFR) from sCr levels using standard algorithms [24, 25]. In adults, chronic renal insufficiency (CRI) was defined as a sCr value above 1.5 mg/dl, corresponding to stage 3 CKD or higher in most patients. In adult males, anaemia was defined as a haemoglobin level below 13 g/dl [26], leukopaenia was defined as a total WBC count below 4.3×10^9/l [27] and neutropaenia was defined as a neutrophil count below 1.5×10^9/L [28]. Appropriate age-related norms were used to define anaemia, leukopaenia and neutropaenia in children [26, 29]. Irrespective of age, thrombocytopaenia was defined as a platelet count below 150×10^9/l [30].

In addition, the prevalence of peripheral blood cytopaenias among adult patients enrolled at the Fabry Registry—a worldwide observational and voluntary programme tracking the natural course and outcomes of patients with AFD (https://www.lsdregistry.net/fabryregistry/)—was assessed using the above definitions for anaemia, leukopaenia and thrombocytopaenia. These prevalences were all reported as stratified by CKD stage, to allow for the confounding effect of advanced chronic renal failure upon haemoglobin levels [12, 31].

Results

Pathology findings in the spleen removed from the index patient

Grossly, the spleen measured 18.5×13.5×4.0 cm and weighed 700 g. The cut surface was homogeneous and of deep-red colour. On light microscopy examination, the parenchyma showed congestion and expansion of the red pulp, decreased white pulp and focal areas of fibrosis (Fig. 1). There were precursors of all haematopoietic cell lines, indicating extramedullary haematopoiesis (Fig. 2). Numerous macrophages had iron in the cytoplasm (Fig. 3) and a few showed cytoplasmic vacuolation (Fig. 4). A few scattered foci of haemophagocytosis were also observed (Fig. 5). Many endothelial cells of the sinusoids showed a reactive aspect with vacuolation and argyrophilic material within the cytoplasm (Fig. 6).

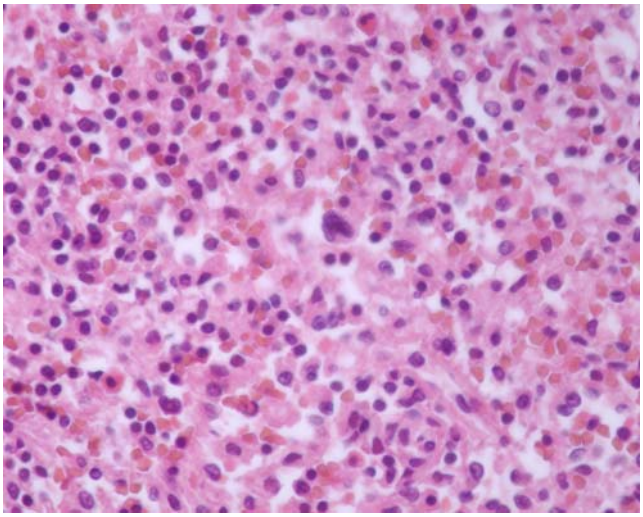

Fig. 2 Megakaryocyte in the red pulp; haematoxylin–eosin stain, ×400

Generalised lymphadenopathy, splenomegaly, hepatomegaly and peripheral blood cytopaenias in our patient cohort

We identified a total of 15 male patients with the diagnosis of AFD who have been admitted to our Hospital, or seen at outpatient clinics, at least once, during the last 40 years. Three patients were excluded from further analysis because they had a non-classical phenotype: one patient had presented at age 55 with a mild cardiac variant and other two, who had reached ESRF, respectively, at ages 58 and 61 years, were identified in a screening program of AFD among haemodialysis patients. At the time of this review, these latter two patients had already died. Two of the patients presenting with the typical cutaneous phenotype were excluded from further analysis because they had a total follow-up at our Hospital shorter than 12 months: one of them had been transplanted in another Hospital and the other refused dialysis and died in ESRF shortly after AFD diagnosis.

Demographic and relevant clinical data of the patients selected for review are presented in Table 3. Patient F1 had died at our hospital in 1976, of uraemic complications. Patient R1 was referred to another hospital after the beginning of chronic haemodialysis, received a kidney transplant a few years later and has recently died, but this review was limited to the data available in our hospital files.

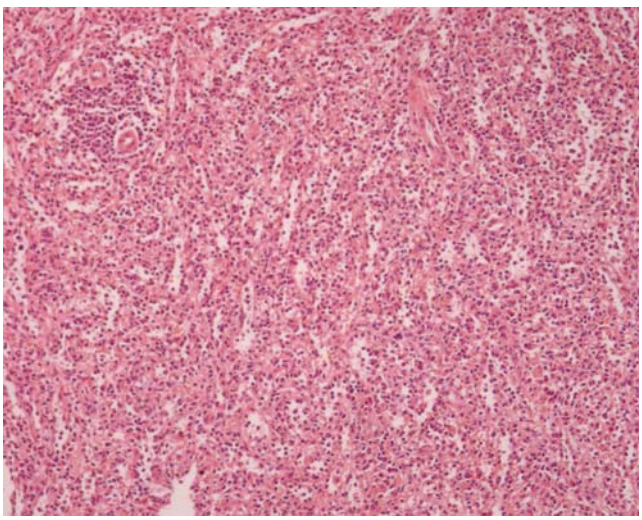

Fig. 1 Congestion and expansion of red pulp, reduced white pulp and focal fibrotic areas of the red pulp; haematoxylin–eosin stain, ×100

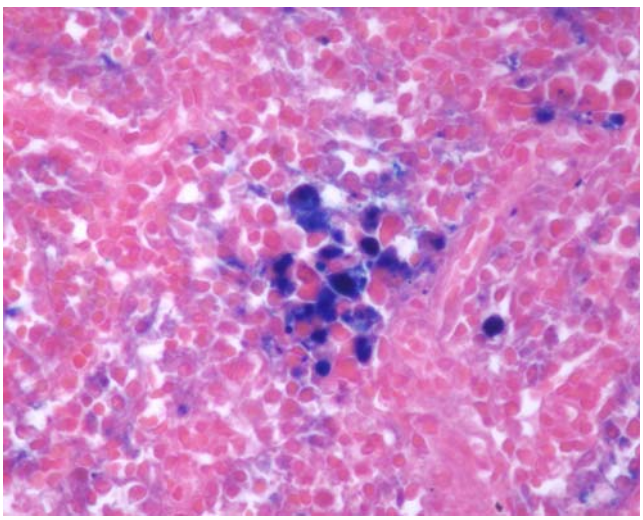

Fig. 3 Macrophages containing iron in the cytoplasm; Perls' Prussian blue stain, ×400

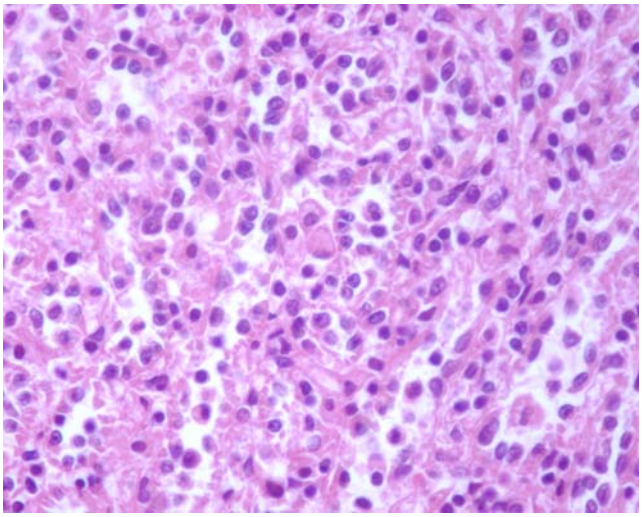

Fig. 4 Vacuolated histiocytes and reactive appearance of sinusoidal endothelial cells; haematoxylin–eosin stain, ×400

The liver was palpable only in the index patient (F2), but its size was not above the normal range. Enlarged lymph nodes were also found in patient R1 at age 27, in both axillary regions, when he was admitted for a kidney biopsy. Splenomegaly was incidentally diagnosed by ultrasonography in patient F3, at age 6, on the investigation of recurrent abdominal pain. Anaemia was found in all four adult patients with CRI but also in the 6-year-old child, whose eGFR was normal. Leukopaenia and/or neutropaenia were seen only in the two patients who had splenomegaly. Thrombocytopaenia was detected in the two relatives of the index patient, as well as in a third case of another family, adding up to a total prevalence of 40% in this cohort.

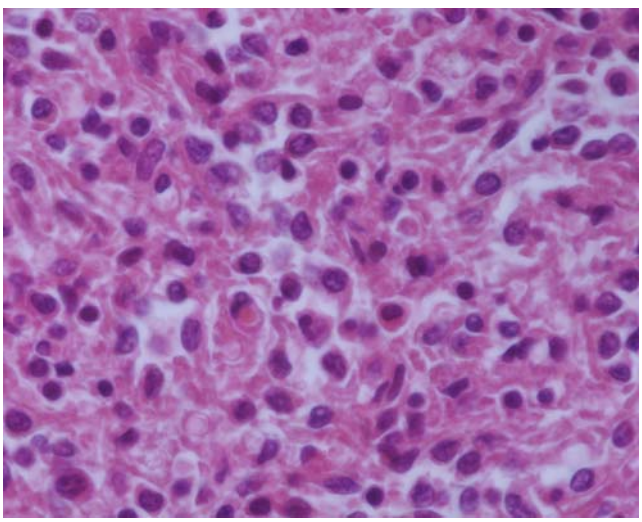

Fig. 5 Haemophagocytosis; haematoxylin–eosin stain, ×1,000

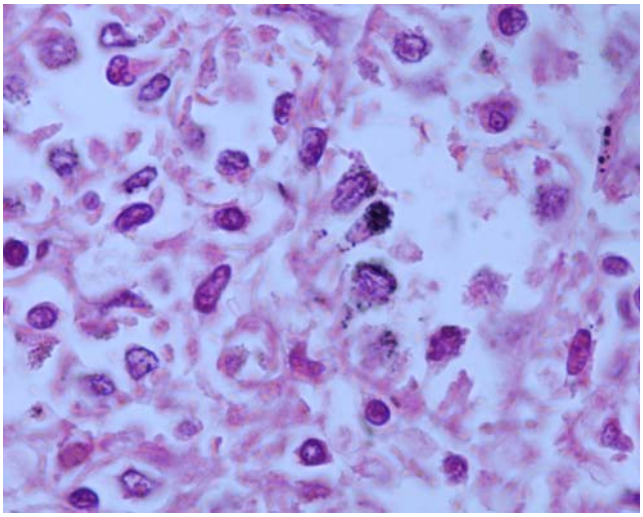

Fig. 6 Reactive endothelial cells containing argyrophilic material in the cytoplasm; methenamine silver stain, ×1,000

Peripheral blood cytopaenias in the Fabry Registry adult male cohort

The prevalences of anaemia, leukopaenia and thrombocytopaenia in adult males enrolled at the Fabry Registry, as stratified by CKD stage, are shown in see Table 4.

Discussion

Symptomatic involvement of the reticuloendothelial system in patients with AFD, manifesting by generalised lymphadenopathy and/or splenomegaly, although infrequently reported, has been recognised since long (see Table 5 for a summary of earlier case reports) [3, 4, 6–11, 32, 33]. Common to all previously published cases, as to our index patient, is male gender, the classical AFD phenotype, presentation up to the age of 35 years, and the absence of a more obvious clinical explanation for the splenomegaly or the lymphadenopathy. Additionally, there was evidence of Gb3 deposits in the lymph nodes and the spleen of all the patients who had biopsies taken for histological examination. However, while AFD is a recognised aetiology of generalised lymphadenopathy, even in the general medical literature [14], a recent review in a major textbook on metabolic diseases explicitly states that AFD is not a cause of splenomegaly [1].

In our patient, anaemia was first noted at age 17, when the eGFR was about 55 ml/min/1.73 m^2, a CKD stage where haemoglobin values below 12 g/dl are rarely found [31]. In addition, low platelet and WBC counts were recurrently observed since the age of 20, several years before the start of hemodialysis and of HBV infection. The development of peripheral blood cytopaenias in a patient

Table 3 Demographic and clinical data of the male patients with classic Anderson–Fabry disease selected for analysis

Case #	α-Gal activity	Age at diagnosis	Length of follow-up	Clinical outcome	Age at outcomes	Organ enlargement			Cytopaenia			
						L	LN	S	RBC	WBC	N	P
F1	NA	20 y	9 y	D (ESRF)	29 y				X			X
F2	0	17 y	32 y	HD>ER	24 y>43 y		X	X	X	X	X	X
F3	0	PN	7 y	ER	7 y			X	X	X		X
R1	0.1	27 y	5 y	HD	31 y		X		X			
T1	1.2	19 y	4 y 11 m	ER	20 y							
C1	0.4	20 y	3 y 11 m	ER	22 y							
P1	0.1	18 y	3 y 10 m	ER	20 y							X
P2	0.6	20 y	3 y 3 m	ER	21 y							
G1	1.1	52 y	1 y 9 m	HD>ER>D	52 y≫53 y				X			
G2	0.6[a]	18 y	2 y 6 m									

Each capital letter in the case identifiers denotes a different family; F2 is the patient reported herein. *α-Gal* α-Galactosidase activity measured in leukocytes (normal range: 36–80 nmol/h/mg), *y* Ages in full years, *m* months, Length of follow-up to a clinical outcome or to the last outpatient clinic visit, in full years and months up to 5 years, then in full years, *LN* lymph node, *L* liver, *S* spleen. *RBC* red blood cells, *WBC* white blood cells, *N* neutrophils, *P* platelets, *NA* data not available, *PN* prenatal diagnosis, *D* death, *HD* haemodialysis, *ER* enzyme replacement therapy, *ESRF* end-stage renal failure, *X* manifestation present.

[a] α-Galactosidase activity measured in plasma (normal range: 8.3–35.6 nmol/h/ml).

with an enlarged spleen and normal bone marrow cytology led to the clinical diagnosis of hypersplenism [34]. In patients with splenomegaly, thrombocytopaenia and/or leukopaenia are frequently associated with liver pathology [18, 21, 35, 36]. However, even after long-standing chronic HBV infection, our patient remained without any clinical or laboratory evidence of liver dysfunction or fibrosis.

The protracted dependence on haemodialysis may have contributed to the worsening of thrombocytopaenia as in these patients megakaryocytopoiesis decrease over time, regardless of increased plasma thrombopoietin levels, by an as yet unknown mechanism [37]. Peripheral destruction and splenic sequestration of platelets may have an additional role in the pathogenesis of haemodialysis-associated thrombocytopaenia [37, 38].

Notwithstanding the thorough diagnostic investigations and prolonged clinical follow-up, the underlying cause of splenomegaly in our patient could not be determined before surgery. According to a surgical classification [39], the removed spleen had a moderately increased size, and its gross appearance was essentially congestive and fibrotic. On histological examination, there was no evidence of any of the haematologic, infectious or inflammatory diseases most commonly associated with spleen enlargement [21, 40, 41]. The diagnostic yield of splenectomy is very high [40, 41] and, as occurred in our patient, up to 40% of all

Table 4 Prevalence of peripheral blood cytopaenias in adult males enrolled at the Fabry Registry, stratified by renal function

Cytopaenia	Estimated glomerular filtration rate (eGFR, ml/min/1.73 m^2)			
	≥90	≥60 to <90	≥30 to <60	<30
Anaemia[a]	80/250 (32%)	68/198 (34.3%)	80/142 (56.3%)	108/136 (79.4%)
Leukopaenia[b]	11/96 (13.1%)	12/80 (15%)	4/46 (8.7%)	8/46 (17.4%)
Thrombocytopaenia[c]	4/84 (4.8%)	6/67 (9%)	8/40 (20%)	13/41 (31.7%)

In these analyses, a patient was only represented once at each eGFR stage, using the smallest haemoglobin level, WBC or platelet count available at that particular level of renal function. The same patient may be represented in more than one eGFR stage, if renal function deteriorated during the course of follow-up. As patients have not been stratified by the level of α-Gal activity, nor by age ranges above 18 years, and the mean patient ages increased from the group with eGFR >=90 ml/min/1.73 m^2 to the groups with eGFR <60 ml/min/1.73 m^2, the apparent increase in the prevalence of thrombocytopaenia with decreasing eGFR could also be due to the severity of α-Gal deficiency, cumulative exposure to AFD, or any combination of these factors.

[a] Haemoglobin level <13 g/dl; data source: Steven Waldek, Fabry Registry Data Request Report, FDR-051025-01, 13Dec05.

[b] White blood cell count $<4.3\times10^9$ /l; data source: João P. Oliveira, Fabry Registry Data Request Report, FDR-060103-01, 13Jan06.

[c] Platelet count $<150\times10^9$ /l; data source: João P. Oliveira: Fabry Registry Data Request Report, FDR-060103-01, 12Jun06.

Table 5 Summary of previous case reports of patients with Anderson–Fabry disease and symptomatic reticuloendothelial organ involvement or thrombocytopaenia

Ref. #	Age	Organ enlargement			Thrombocytopaenia[a]	Additional notes
		L	LN	S		
[48]	22		X		45.0×10^9/l	Platelet count normalised following splenic X-ray irradiation.
[48]	18		X		72.0×10^9/l	Platelet count normalised following splenic X-ray irradiation.
[50]	32	X		X	29.8×10^9/l	
[8]	30			X		Splenomegaly later confirmed at laparotomy for appendicitis and at autopsy [49].
[46]	28		X			LNBx showing lipid deposits in macrophages.
[46]	25		X			
[43, 44]	23		X	X		Surgical mesenteric LNBx and SBx showing vacuolated cells.
[27]	18		X			LNBx showing typical lamellated Gb3 deposits in EM examination.
[17, 22]	10	X	X	X		LNBx showing histiocytes with foamy cytoplasmic appearance.

Ref. # Reference number, *Age* age in years, *LN* lymph node, *L* liver; *S* spleen, *X* manifestation present, *Bx* biopsy, *EM* electron microscopy.
[a] Platelet count, in patients with thrombocytopaenia.

cases will have a final diagnosis of "congestive splenomegaly" [41].

Spleens removed from patients with hypersplenism characteristically show prominent marginal zones of the malpighian corpuscles [42], a feature that may have been obscured in our patient by the atrophy of the white pulp. Although hypersplenism can result in splenic iron deposition, this rarely appears heavy and tends to be restricted to the sinusoidal lining cells [43]. Notably, massive siderosis was found in the spleens of the first two patients with AFD who underwent post-mortem pathological studies [44]. As the iron overload was not observed in any other site, including in the Kupffer cells of the liver, its pathogenesis was unclear. Reactive extramedullary haematopoiesis, as indicated by the increased number of haematopoietic cell precursors, has already been described in association with fibrocongestive splenomegaly [45].

The interpretation of the splenic pathology in our patient is potentially confounded by his chronically haemodialysed condition: before the availability of erythropoiesis stimulators to treat anaemia, the spleens removed from such patients were frequently enlarged and showed variable degrees of siderosis [43, 46]. However, even in haemodialysis-dependent patients that were splenectomised because of clinical hypersplenism, the weight of the spleen rarely exceeded 500 g [43, 46, 47]. The prominence of the red pulp in our patient was consistent with the red pulp hyperplasia previously described in haemodialysed patients [48], but we have not observed the lymphoid hyperplasia that was ascribed to chronic hepatitis in the same patient population [48].

Cytoplasmic vacuolation was seen in many of the endothelial cells lining the splenic sinusoids and in a small proportion of the macrophages, but the global burden of Gb3 accumulation, as histologically evaluated, could not account for the more than four-fold increase in spleen weight. This is similar to Gaucher disease, in which the amount of pathological lipid storage in the affected macrophages accounts for less than 2% of the increase in liver and spleen mass [49]. The argyrophilic material observed in sinusoidal endothelial cells probably corresponds to the trisaccharide side-chain of Gb3, which remains within the lysosomes despite removal of the ceramide moiety by the paraffin-inclusion procedure for histological analysis.

The improvement of all peripheral blood cytopaenias after splenectomy was a further argument to confirm the clinical diagnosis of hypersplenism in our patient [34]. Splenectomy was reported to resolve the cytopaenias in all patients with idiopathic splenomegaly and hypersplenism [40]. Splenectomy was also effective to decrease the blood transfusion requirements of chronically haemodialysed patients with evidence of increased splenic sequestration of red blood cells (RBC) [47, 50]; furthermore, the WBC and platelet counts also rose, reaching twice the pre-splenectomy values [50].

Taken together, these data strongly suggest that the most plausible aetiology of the generalised lymphadenopathy, splenomegaly and hypersplenism observed in our index patient was AFD or directly related to it. The hypersplenism may have been aggravated by the long-standing haemodialysis status. We hypothesise that partial or complete obstruction of the splenic sinusoids by the hypertrophied Gb3-laden endothelial cells is the basic mechanism leading to congestive splenomegaly in AFD. An identical mechanism has been proposed as the underlying cause of idiopathic fibrocongestive splenomegaly, in patients who had evidence of splenic platelet sequestration prior to splenectomy [51]. The increased RBC pooling in

the spleen could also explain the iron overload described in AFD patients, in the absence of Kupffer cell involvement [44].

In our cohort, anaemia was prevalent only among patients with CRI. However, low haemoglobin levels were observed since relatively early stages of renal dysfunction, at which the general CKD male patient population rarely develops anaemia [31]. In addition, the two patients with anaemia detected at early CKD stages also had thrombocytopaenia, an association that is even harder to explain in this clinical setting. The two other patients with thrombocytopaenia had normal renal function and no additional cytopaenias. One of these (and the only child included in our series) also had splenomegaly. Thrombocytopaenia, either alone or in combination, was the most frequent of the peripheral blood cytopaenias associated with hypersplenism among inpatients and outpatients seen in general hospital [35].

In our cohort, thrombocytopaenia—and, to a lower extent, generalized lymphadenopathy and splenomegaly—seemed to be associated with the lowest α-Gal enzyme activity levels, suggesting that it may only be a manifestation of severe α-Gal deficiency. However, given the small number of patients and families in our cohort, it cannot be excluded that other genetic factor(s) co-segregating within the index patient's family may be the real cause of these findings.

In a recent cross-sectional study of the Fabry Outcome Survey (FOS), a European AFD observational database, anaemia has been recognised as a highly prevalent complication of AFD [12]. Analyses of the adult male cohort of the Fabry Registry confirmed the high prevalence of anaemia, but have additionally shown that leukopaenia and thrombocytopaenia are also frequent. The real prevalence of generalised lymphadenopathy and splenectomy in the AFD population may have been underestimated so far, as they may be missed on a less than thorough and systematic physical examination. Asymptomatic enlarged lymph nodes are frequently palpable in healthy people [14] and their presence in AFD patients may be difficult to accept as a clinical sign of the disease. Furthermore, retrospective medical-record-based estimates of the prevalence of splenomegaly in hospitalised patients have consistently been more than two-fold lower than in prospectively oriented series and show a predominance of cases of massive splenomegaly [18, 21]. These observations suggest that mild spleen enlargements may pass unnoticed in the usual hospital clinical practice setting.

Given the wide range of normal values and the Gaussian distributions of haemoglobin levels and of WBC, neutrophil and platelet counts, the use of cut offs to identify cytopaenias may overlook disease processes which may affect haematopoiesis or the survival of peripheral blood cells, but are not of enough magnitude to be systematically recognised by such criteria. Of note, even in our index patient, who had clinically apparent splenomegaly, some of the CBC results were above the threshold levels for cytopaenias. Therefore, the most effective approach to demonstrate that AFD is associated with peripheral blood cytopaenias would be to compare the distributions of haemoglobin, and of WBC, neutrophil and platelet counts, in appropriately matched cohorts of AFD patients and of healthy subjects. The significantly lower ($p<0.0001$) haemoglobin levels in adult males with normal renal function enrolled at the Fabry Registry, as compared to large population databases of healthy individuals [52], seems to support this view, but similar comparisons of WBC, neutrophil and platelet counts are still lacking. The same reasoning should be applied to the sonographic evaluation and comparison of spleen dimensions in AFD patients and healthy individuals. Finding a correlation between peripheral blood cell counts and the sonographic size of spleen could be an approach to demonstrate that hypersplenism is the mechanism behind the development of peripheral blood cytopaenias in AFD.

In conclusion, the data presented and discussed herein suggest that AFD may be a cause of congestive splenomegaly and hypersplenism in males with the classical phenotype, plausibly related to endothelial Gb3 accumulation in the splenic sinusoids. It is possible that peripheral blood cytopaenias—most frequently anaemia and thrombocytopaenia—observed in a significant number of patients, are a sign of subclinical hypersplenism. These hypotheses need to be tested in larger patient cohorts. Screening for lymphadenopathy and for spleen and liver enlargement on physical examination, CBC and sonography evaluation of spleen size should be performed as part of the routine assessment of AFD patients.

Acknowledgements JPO and SW are members of the European Board of Advisors of the Fabry Registry, a global registry of patients with Fabry disease sponsored by Genzyme Corporation.

We thank Selena Freisens and Inês Oliveira for their help in the retrieval of old bibliographic references.

Conflict of interest statement We declare that we have no conflict of interest.

References

1. Desnick RJ, Ioannou YA, Eng CM (2001) α-galactosidase A deficiency: Fabry disease. In: Scriver CR, Beaudet AL, Sly WS et al (eds) The metabolic and molecular bases of inherited disease, 8th edn. McGraw-Hill, New York, pp 3733–3774
2. de Groot WP (1964) Angiokeratoma corporis diffusum Fabry (Thesaurismosis hereditaria Ruiter–Pompen–Wyers). Dermatologia 128:321–349

3. Wise D, Wallace HJ, Jellinek EH (1962) Angiokeratoma corporis diffusum, a clinical study of eight affected families. Quart J Med 31:177–206
4. Urbain G, Peremans J, Philippart M (1967) Fabry's disease without skin lesions? (Letter). Lancet i:1111
5. Charrow J, Andersson HC, Kaplan P et al (2000) The Gaucher registry. Demographics and disease characteristics of 1698 patients with Gaucher disease. Arch Intern Med 160:2835–2843
6. Weicksel J (1925) Angiokeratosis universalis. Dtsch Med Wochenschr 51:898–905, [Article in German]
7. Wöhnlich H (1949) Zur Symptomatologie multipler Angiome. Arch Derm Syph (Berl) 187:528–536, [Article in German]
8. Brown A, Milne JA (1952) Diffuse angiokeratoma: report of two cases with diffuse skin changes, one with neurological symptoms and splenomegaly. Glasg Med J 33:361–367
9. Wallace RD, Cooper WJ (1965) Angiokeratoma corporis diffusum universale (Fabry). Am J Med 39:656–661
10. Mayou SC, Kirby JD, Morgna SH (1989) Anderson–Fabry disease: an unusual presentation with lymphadenopathy. J R Soc Med 82:555–556
11. Garcia-Consuegra J, Padrón M, Jaureguizar E et al (1990) Priapism and Fabry disease: a case report. Eur J Pediatr 149:500–501
12. Kleinert J, Dehout F, Schwarting A et al (2005) Anemia is a new complication in Fabry disease: data from the Fabry Outcome Survey. Kidney Int 67:1955–1960
13. Faria V (1970) Doença de Fabry, tesaurismose rara (a propósito de um caso clínico). Jornal do Médico 72:5–11, [Article in Portuguese]
14. Bazemore AW, Smucker DR (2002) Lymphadenopathy and malignancy. Am Fam Physician 66:2103–2110
15. Yang JC, Rickman LS, Bosser SK (1991) The clinical diagnosis of splenomegaly. West J Med 155:47–52
16. Grover SA, Barkun AN, Sackett DL (1993) The rational clinical examination. Does this patient have splenomegaly? JAMA 270:2218–2221
17. Naylor CD (1994) The rational clinical examination. Physical examination of the liver. JAMA 271:1859–1865
18. O'Reilly RA (1998) Splenomegaly in 2,505 patients at a large university medical center from 1913 to 1995. 1913 to 1962: 2,056 patients. West J Med 169:78–87
19. Rosenberg HK, Markowitz RI, Kolberg H et al (1991) Normal splenic size in infants and children: sonographic measurements. AJR Am J Roentgenol 157:119–121
20. Konuş OL, Ozdemir A, Akkaya A et al (1998) Normal liver, spleen, and kidney dimensions in neonates, infants, and children: evaluation with sonography. AJR Am J Roentgenol 171:1693–1698
21. O'Reilly RA (1998) Splenomegaly in 2,505 patients at a large university medical center from 1913 to 1995. 1963 to 1995: 449 patients. West J Med 169:88–97
22. Megremis SD, Vlachonikolis IG, Tsilimigaki AM (2004) Spleen length in childhood with US: normal values based on age, sex, and somatometric parameters. Radiology 231:129–134
23. National Kidney Foundation (2002) K/DOQI clinical practice guidelines for chronic kidney disease: evaluation, classification, and stratification. Am J Kidney Dis 39(2 Suppl 1):S1–S266
24. Schwartz GJ, Haycock GB, Edelmann CM, Spitzer A (1976) A simple estimate of glomerular filtration rate in children derived from body length and plasma creatinine. Pediatrics 58:259–263
25. Levey AS, Bosch JP, Lewis JB et al (1999) A more accurate method to estimate glomerular filtration rate from serum creatinine: a new prediction equation. Modification of Diet in Renal Disease Study Group. Ann Intern Med 130:461–470
26. World Health Organization (2001) Assessment of anaemia. In: Iron deficiency anaemia assessment, prevention and control: a guide for programme managers. World Health Organization, Geneva, pp 33–45
27. Holland SM, Gallin JI (2008) Disorders of granulocytes and monocytes. In: Fauci AS, Braunwald E, Kasper DL et al (eds) Harrison's principles of internal medicine, 17th edn. McGraw-Hill, New York, pp 375–384
28. Hsieh MM, Everhart JE, Byrd-Holt DD et al (2007) Prevalence of neutropenia in the U.S. population: age, sex, smoking status, and ethnic differences. Ann Intern Med 146:486–492
29. Ryan DH (2001) Examination of the blood. In: Beutler E, Lichtman MA, Coller BS et al (eds) William's hematology, 6th edn. McGraw-Hill, New York, pp 9–16
30. Warkentin TE, Roberts RS, Hirsh J, Kelton JG (2003) An improved definition of immune heparin-induced thrombocytopenia in postoperative orthopedic patients. Arch Intern Med 163:2518–2524
31. Hsu C-Y, McCulloch CE, Curhan GC (2002) Epidemiology of anemia associated with chronic renal insufficiency among adults in the United States: results from the third national health and nutrition examination survey. J Am Soc Nephrol 13:504–510
32. Urbain G, Philippart M, Peremans J (1969) Fabry's disease with hypogammaglobulinemia and without angiokeratomas. Arch Intern Med 124:72–76
33. Jaureguizar Monereo E, López Pereira P, Cabo J et al (1990) Priapismo associado con la Enfermedad de Fabry. Cir Pediatr 3:138–140, [Article in Spanish]
34. Chapman WC, Newman M (1999) Disorders of the spleen. In: Richard Lee G, Foerster J, Lukens J et al (eds) Wintrobe's clinical hematology, 10th edn. Lippincot Williams and Wilkins, Philadelphia, pp 1969–1989
35. O'Reilly RA (1996) Splenomegaly at a United States county hospital: diagnostic evaluation of 170 patients. Am J Med Sci 312:160–165
36. Adinolfi LE, Giordano MG, Andreana A et al (2001) Hepatic fibrosis plays a central role in the pathogenesis of thrombocytopenia in patients with chronic viral hepatitis. Br J Haematol 113:590–595
37. Ando M, Iwamoto Y, Suda A et al (2001) New insights into the thrombopoietic status of patients on dialysis through the evaluation of megakaryocytopoiesis in bone marrow and of endogenous thrombopoietin levels. Blood 97:915–921
38. Verzola A, Scapoli GL, Risichella IS et al (2000) "Isolated" thrombocytopenia by splenic sequestration in hemodialyzed patients. (Letter) Nephron 86:184–185
39. Targarona EM, Espert JJ, Balagué C et al (1998) Splenomegaly should not be considered a contraindication for laparoscopic splenectomy. Ann Surg 228:35–39
40. Carr JA, Shurafa M, Velanovich V (2002) Surgical indications in idiopathic splenomegaly. Arch Surg 137:64–68
41. Pottakkat B, Kashyap R, Kumar A et al (2006) Redefining the role of splenectomy in patients with idiopathic splenomegaly. ANZ J Surg 76:679–682
42. Leffler RJ (1952) The spleen in hypersplenism. Am J Pathol 28:303–313
43. Murray JA, Slater DN, Parsons MA et al (1984) Splenic siderosis and parenteral iron dextran in maintenance haemodialysis patients. J Clin Pathol 37:59–64
44. Pompen AW, Ruiter M, Wyers HJ (1947) Angiokeratoma corporis diffusum (universale) Fabry, as a sign of an unknown internal disease; two autopsy reports. Acta Med Scand 128:234–255
45. O'Malley DP, Kim YS, Perkins SL et al (2005) Morphologic and immunohistochemical evaluation of splenic hematopoietic proliferations in neoplastic and benign disorders. Mod Pathol 18:1550–1561
46. Ali M, Fayemi AO, Rigolosi R et al (1980) Hemosiderosis in hemodialysis patients. An autopsy study of 50 cases. JAMA 244:343–345

47. Asaba H, Bergström J, Lundgren G et al (1977) Hypersequestration of 51Cr-labelled erythrocytes as a criterion for splenectomy in regular hemodialysis patients. Clin Nephrol 8:304–307
48. Neiman RS, Bischel MD, Lukes RJ (1973) Hypersplenism in the uremic hemodialyzed patient: pathology and proposed pathophysiologic mechanisms. Am J Clin Pathol 60:502–511
49. Cox TM (2001) Gaucher disease: understanding the molecular pathogenesis of sphingolipidoses. J Inherit Metab Dis 24(Suppl 2): 106–121, discussion 87–88
50. Bengmark S, Henrikson H, Lindholm T et al (1976) Effect of splenectomy on anemia in patients on regular dialysis treatment. Scand J Urol Nephrol 10:63–69
51. Burger T, Kelényi G, Kett K et al (1976) Platelet storage in the spleen in idiopathic thrombocytopenic purpura and congestive splenomegaly. Acta Med Acad Sci Hung 33:13–24
52. Beutler E, Waalen J (2006) The definition of anemia: what is the lower limit of normal of the blood hemoglobin concentration? Blood 107:1747–1750

Virchows Arch (2008) 453:301–306
DOI 10.1007/s00428-008-0634-5

CASE REPORT

Oncocytic adrenal cortical tumor with cytoplasmic inclusions and hyaline globules

Tariq Al-Zaid · Joseph Alroy · Rolf Pfannl · Katherine J. Strissel · James F. Powers · Andrey Layer · Gennaro Carpinito · Arthur S. Tischler

Received: 28 March 2008 / Revised: 5 May 2008 / Accepted: 16 May 2008 / Published online: 8 August 2008

Abstract Adrenal cortical tumors, particularly oncocytic tumors, have been reported to contain a variety of intracytoplasmic and intramitochondrial inclusions. Oncocytic cortical tumors can also morphologically mimic pheochromocytomas. We report an unusual, partially oncocytic cortical neoplasm with nesting architecture, intranuclear inclusions, and hyaline globules reminiscent of pheochromocytoma, together with numerous, small, brightly eosinophilic, periodic acid-Schiff-positive cytoplasmic inclusions and typical cytoplasmic lipid droplets. Ultrastructural study revealed oncocytes containing numerous mitochondria with intramitochondrial crystals and lipid droplets. Immunohistochemistry and immunoblots were utilized to further characterize the tumor. Immunohistochemistry demonstrated immunoreactivity of both the eosinophilic inclusions and the hyaline globules for adipose differentiation-related protein (ADRP), which is one of a group of proteins associated with storage of neutral lipids in many cell types. Immunoblots confirmed the presence of ADRP and demonstrated an imbalance between ADRP and perilipin, another neutral lipid-associated protein, in tumor tissue compared to normal adrenal cortex. The findings suggest that mitochondrial dysfunction in oncocytic cortical tumors may lead to abnormal processing of proteins related to the lipid-storing functions of the adrenal cortex, resulting in unusual cytoplasmic inclusions and extracellular globules resembling the globules in pheochromocytomas. The finding of ADRP as a constituent of inclusions in adrenal cortical tumors has not been previously reported.

Keywords Adrenal cortex · Oncocytoma · Inclusions · Adipose differentiation-related protein (ADRP)

T. Al-Zaid · J. Alroy (✉) · R. Pfannl · J. F. Powers · A. S. Tischler
Department of Pathology, Tufts Medical Center,
#802, 750 Washington Street,
Boston, MA 02111, USA
e-mail: joseph.alroy@tufts.edu

J. F. Powers
e-mail: jpowers1@tuftsmedicalcenter.org

A. Layer · G. Carpinito
Department of Urology, Tufts Medical Center,
Boston, MA, USA

J. Alroy
Section of Pathology, Cummings School of Veterinary Medicine,
Tufts University,
Grafton, MA, USA

K. J. Strissel
Obesity and Metabolism Laboratory,
Human Nutrition Research Center, Tufts University,
Boston, MA, USA

Introduction

Adrenal cortical tumors can be wholly or partly oncocytic. Tumors in which all, or almost all, of the cells are oncocytic are defined as oncocytomas. These tumors are rare, slightly more than 30 cases having been described, and most are nonfunctional. We report an unusual, large, apparently benign, and clinically nonfunctional tumor in which essentially all of the cells exhibited both oncocytic and steroidogenic features. In addition, the tumor contained unusual cytoplasmic and intramitochondrial inclusions and extracellular hyaline globules that mimicked the globules in pheochromocytomas. Both the cytoplasmic inclusions and hyaline globules were found to be immunoreactive for adipose differentiation-related protein (ADRP), also known as adipophilin. Lipid droplet proteins of the perilipin family, including ADRP, play important roles in regulating the storage of lipid, coordinating lipid droplet metabolism,

and directing lipid metabolites to specific cellular destinations and signaling pathways in adrenal cortical and other cell types [7].

Clinical history

A 51-year-old male presented with history of low back pain for approximately 1 month. Magnetic resonance imaging (MRI) revealed a 10-cm left adrenal mass with heterogeneous enhancement (Fig. 1a). There was no clinical evidence of an endocrinologically active tumor, and hormone assays were not performed. Serum potassium and glucose were within normal limits. The patient underwent adrenalectomy. Clinical follow-up at the time of manuscript submission 8 months postoperatively (chest radiograph, MRI liver function tests and endocrinological evaluation) showed no evidence of metastatic disease or endocrinological abnormality.

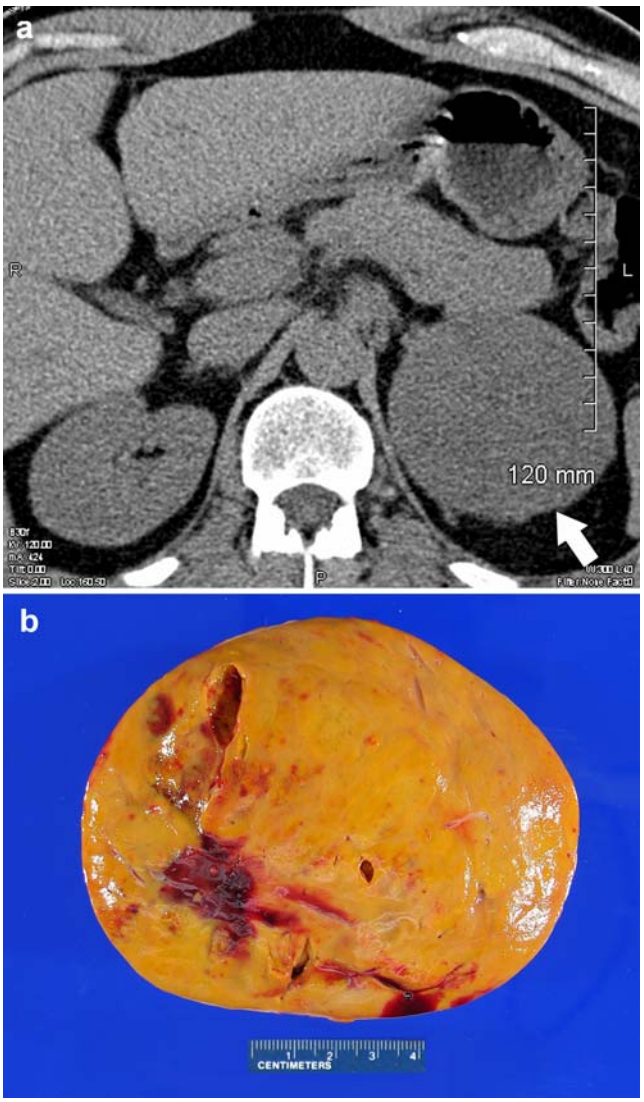

Fig. 1 **a** MRI image showing the large left-side adrenal tumor (*arrow*). **b** Gross cross-section of the tumor specimen shows a golden brown color that differs from the tan brown characteristic of a completely oncocytic tumor

Materials and methods

Immunohistochemical staining of paraffin sections was performed for chromogranin A (mouse monoclonal antibody LK2H10), inhibin alpha (mouse monoclonal), Melan-A (mouse monoclonal), calretinin (rabbit polyclonal IgG), and Ki67 (mouse monoclonal MIB-1) on a Ventana immunostainer after antigen retrieval in citrate buffer, pH 6.0, according to the Ventana protocols. All antibodies were optimally prediluted by Ventana for use on the Benchmark immunostainer. In order to further characterize the cytoplasmic granular inclusions and hyaline droplets, sections were also stained for ADRP (adipophilin) using guinea pig antiadipophilin (Research Diagnostics) with antiguinea pig secondary antibody and for perilipin A using a rabbit antimouse antibody generated as previously described [10]. The antibodies have been previously characterized and used to demonstrate the presence of these proteins in normal adrenal cortex [10]. Immunoblots for ADRP and perilipin A were performed with the same antibody solutions. Proteins were resolved in a 4–15% precast polyacrylamide gradient minigel, transferred to a PVDF membrane, and probed with primary antibody followed by alkaline phosphate-conjugated secondary. Bands were detected by chemiluminescence with CDP-star (Tropix, Bedford, MA, USA) as the alkaline phosphatase substrate. Luminescence was digitally recorded using a Kodak Image Station. For electron microscopy, formalin-fixed tissue was postfixed in 1% OsO_4 in Na cacodylate buffer for 3 h at 20°C, then stained en bloc with 5% aqueous uranyl acetate, dehydrated in a graded ethanol series, and embedded in Epon-812 resin. Thick sections (1 μm) stained with toluidine blue were used to select areas of tumor that contained inclusions and globules. Thin sections were cut at 50–70 nm, stained with uranyl acetate and lead citrate, and photographed with a Phillips EM201 transmission electron microscope.

Results

A well-circumscribed tumor measuring 11.2×9×6 cm and weighing 364 g was attached to the left adrenal. The cut surface was yellow to tan with some hemorrhagic foci but no necrosis (Fig. 1b). The adjacent cortex appeared normal or slightly atrophic. Light microscopic examination of

paraffin-embedded sections showed essentially the entire tumor composed of large, polygonal cells with abundant, granular eosinophilic cytoplasm growing as sheets or in a pattern of poorly defined nests separated by fine vascular network (Fig. 2a). The same cells contained numerous brightly eosinophilic small granular inclusions and scattered clear vacuoles. Scattered extracellular and intracellular hyaline globules resembling those in pheochromocytomas were also present (Fig. 2b). Rare clear cells with foamy cytoplasm were interspersed among the eosinophilic cells. Nuclei were hyperchromatic and pleomorphic, often showing prominent nucleoli and occasionally intranuclear invaginations of cytoplasm (Fig. 2b and d). Periodic acid-Schiff (PAS) stains demonstrated very intense, diastase-resistant PAS positivity of the extracellular hyaline globules (Fig. 2d) and weak or absent staining of the small eosinophilic granules. Extensive sampling showed no mitoses, no necrosis, and no evidence of vascular or transcapsular invasion.

Immunohistochemical studies demonstrated the tumor to be negative for chromogranin A and positive for inhibin (Fig. 2b), consistent with adrenal cortical origin. The tumor was also immunoreactive for Melan-A (not shown). Staining for Ki67 with antibody MIB-1 revealed only extremely rare positive tumor cell nuclei, consistent with the absence of mitoses.

Immunoreactive ADRP was seen as a thin rim at the periphery of the cytoplasmic granular inclusions and throughout the hyaline globules (Fig. 2c). In contrast, the tumor was negative for perilipin. There was no staining of the granular inclusions or globules with irrelevant IgG controls. Immunoblots showed abundant adipophilin and barely detectable perilipin in tumor tissue, while both adipophilin and perilipin were highly expressed in normal cortex (Fig. 3).

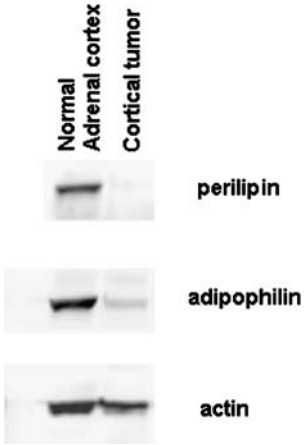

Fig. 3 Immunoblot of proteins from the oncocytic cortical tumor and normal adrenal cortex from a different specimen, probed for adipophilin and perilipin. Both proteins are sparse in the tumor compared to normal adrenal, consistent with the relative sparsity of lipid in the tumor. The tumor also shows an imbalance between adipophilin and perilipin compared to normal adrenal. Actin serves as a loading control

Electron microscopy revealed neoplastic cells occasionally joined by poorly developed adherens cell junctions (Fig. 4a). The tumor cell cytoplasm was packed with numerous mitochondria and contained relatively inconspicuous smooth and rough endoplasmic reticulum. In addition, varying numbers of lipid droplets were present in both the cytoplasm and the mitochondria. Cytoplasmic droplets often had a relatively light appearance while those in the

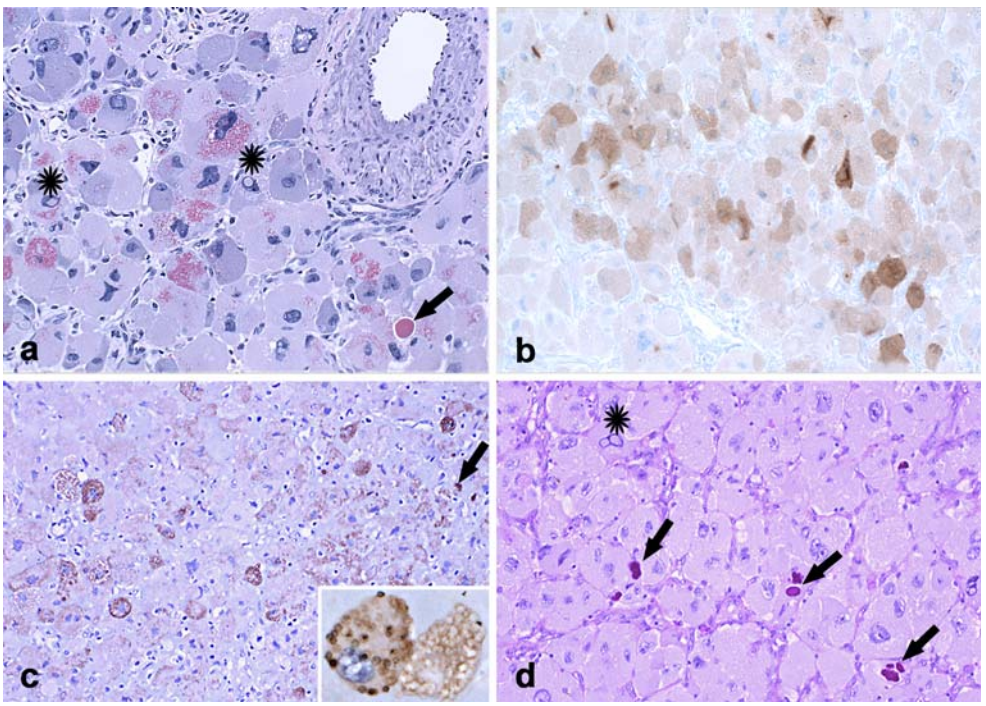

Fig. 2 Photomicrographs of neoplastic cells illustrating large oncocytic cells that contain large pleomorphic nuclei ith prominent intranuclear invaginations of cytoplasm ("inclusions", *asterisks*), brightly eosinophilic granular cytoplasmic granules, and extracellular hyaline globules (*arrows*). **a** H&E, **b** inhibin, **c** adipophilin, **d** PAS diastase (original magnification ×50, *inset* in **c** ×200)

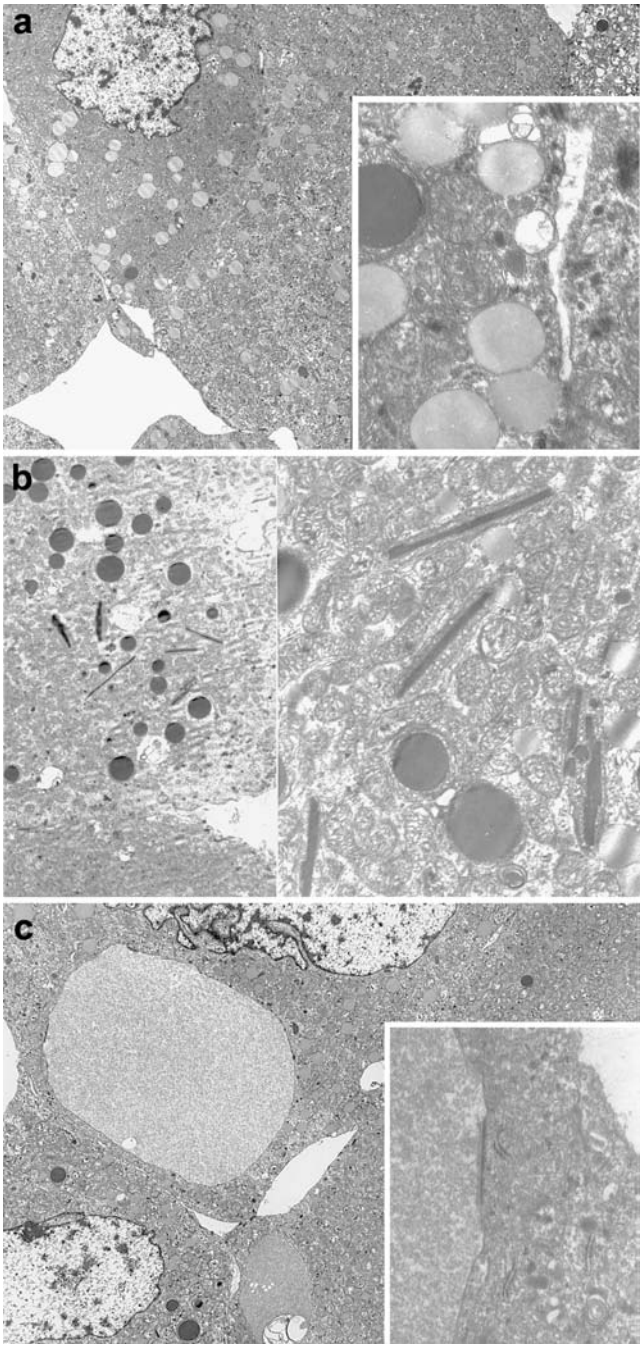

Fig. 4 **a** Low-magnification electron micrograph showing numerous mitochondria and sparse lipid droplets (original magnification ×3,860). *Inset* higher magnification is showing adherens junctions, light cytoplasmic lipid droplets, and a dark intramitochondrial lipid droplet (original magnification ×17,550). **b** Low-magnification electron micrograph showing multiple lipid droplets and crystalline structures(original magnification ×3,860). High-magnification *inset* shows that the crystals and lipid droplets are intramitochondrial (original magnification ×17,550). **c** Low-magnification electron micrograph showing multiple lipid droplets and crystalline structures (original magnification ×3,860). High-magnification *inset* shows that the crystals and lipid droplets are intramitochondrial (original magnification ×17,550)

mitochondria were electron-dense (Fig. 4b and c). A prominent tendency was that cells with conspicuous light cytoplasmic lipid droplets only rarely contained dark intramitochondrial lipid and vice versa (Fig. 4b and c). In addition, cells with dark intramitochondrial lipid contained nearby mitochondria with intramitochondrial crystals (Fig. 4c). Hyaline globules seen by light microscopy appeared as fine fibrillar material ultrastructurally (Fig. 4c).

Discussion

Oncocytomas have been described in different organs including salivary glands, thyroid and parathyroid glands, kidneys, adrenals [14], lung, and pituitary [12]. They have distinctive morphological features that include abundant eosinophilic granular cytoplasm containing numerous mitochondria. Adrenal cortical oncocytomas are rare benign tumors. Most are nonfunctional [22], although a case of a woman with cosecretion of testosterone and cortisol by an adrenal cortical oncocytoma was recently reported [16].

True oncocytomas are characterized by uniform expression of oncocytic features throughout the tumor. Gradations of oncocyte-like features can be seen focally or diffusely in other tumors, and oncocytic carcinomas, both functional [1, 11] and nonfunctional, have been reported. The present case is an unusual example of an apparently benign, clinically nonfunctional tumor that diffusely exhibited both well-developed oncocytic features and steroidogenic features in the same cells. It, therefore, does not fit the usual definition of oncocytoma or of focal oncocytic differentiation in conventional tumor types. In addition to appearing oncocytic, the tumor cells contained unusual cytoplasmic and intramitochondrial inclusions and extracellular hyaline globules.

By light microscopy, the most striking feature of this tumor was the presence of eosinophilic cytoplasmic granular inclusions. Apparently similar inclusions in a tumor, illustrated in the 2004 WHO Bluebook *Tumours of Endocrine Organs* [4], describe the inclusions as lipid droplets. However, lipid droplets per se typically appear as empty spaces in paraffin sections. The intense eosinophilia of these inclusions suggested to us that there must be an additional component. We hypothesized that such a component might be related to lipid-storing functions and, therefore, tested for ADRP and perilipin, which are proteins associated with storage of neutral lipids in many cell types [7, 10, 19, 25]. Our findings suggest that the eosinophilia of the inclusions is at least in part attributable to the presence of ADRP, which was also localized to the extracellular hyaline globules. The osmiophilia of the inclusions indicate that they consist of a mixture of lipid and proteins, while

the greater PAS positivity of the hyaline globules is consistent with a higher degree of glycosylation. The findings suggest that mitochondrial dysfunction in oncocytic cortical tumors may lead to abnormal processing and accumulations of proteins related to lipid-storing functions of the adrenal cortex, in turn resulting in unusual cytoplasmic inclusions and extracellular globules that can resemble the globules in pheochromocytomas.

So far, the ultrastructure of 17 cases of adrenocortical neoplasms with oncocytic features has been described [3, 8, 9, 12, 14, 17, 18, 20, 22, 23]. Three were carcinomas [8, 18, 23]and the malignancy of two others was uncertain [14]. None was associated with abnormal hormone levels [3, 8, 9, 12, 14, 17, 18, 20, 22, 23]. Several different unusual structures were described in seven cases. In one oncocytoma and one oncocytic carcinoma, elongated crystals were noted within the rough endoplasmic reticulum [23]. In one tumor, similar crystals were described in the smooth endoplasmic reticulum [17] and, in another, membrane-bound crystals were reported [14]. Intramitochondrial electron-dense, round, lipid-like inclusions were seen in one oncocytoma [3] and in one oncocytic carcinoma [8]. It is noteworthy that the oncocytic carcinoma also contained intramitochondrial crystals [8] as in the present case. Mitochondria are dynamic organelles that are essential for cell life and death [6]. A recent review highlighted the complexity of mitochondrial membrane assembly and lack of knowledge of how mitochondria adapt to physiological function during development and life of the cell [6]. The nature of intramitochondrial crystals and the causes of their formation are speculative. They have been reported in mitochondrial myopathies and in patients with severe chronic obstructive pulmonary disease (COPD) [15]. It has been suggested that mitochondrial crystals that are formed in skeletal muscle from creatine-depleted rats are result from cocrystallization of creatine kinase with another component within the intermembrane space [21]. In different species intramitochondrial crystals are formed in hepatocytes following exposure to lead acetate, ammonium intoxication, and levamisole, a drug that blocks the formation of adenosine triphosphate [24].

Adrenal cortical tumors, particularly oncocytic tumors, can be mistaken for pheochromocytomas [2]. Intranuclear cytoplasmic invaginations, as seen in the present case, occur frequently in pheochromocytomas [5], as do extracellular hyaline globules. The nested architecture of areas of this tumor is also reminiscent of pheochromocytomas. From a practical perspective, this case serves as a reminder that these findings are nonspecific and their use in differential diagnosis of adrenal tumors should be undertaken with caution. This point was recently also emphasized by Lack [13] who illustrates a functional adrenal cortical adenoma with hyaline globules similar to those in the present case.

Acknowledgments The authors thank Inna Lomakina for her technical help with the electron microscopic sample.

Conflict of Interest Statement We declare that we have no conflict of interest.

References

1. Ali AE, Raphael SJ (2007) Functional oncocytic adrenocortical carcinoma. Endocr Pathol 18:187–189
2. Alsabeh R, Mazoujian G, Goates J, Medeiros LJ, Weiss LM (1995) Adrenal cortical tumors clinically mimicking pheochromocytoma. Am J Clin Pathol 104:382–390
3. Begin LR (1992) Adrenocortical oncocytoma: case report with immunocytochemical and ultrastructural study. Virchows Arch A Pathol Anat Histopathol 421:533–537
4. DeLellis RA, Lloyd RV, Heitz PU, Eng C (2004) World health organization classification of tumors. IARC, Lyon
5. DeLellis RA, Suchow E, Wolfe HJ (1980) Ultrastructure of nuclear "inclusions" in pheochromocytoma and paraganglioma. Human Pathol 11:205–207
6. Dimmer KS, Scorrano L (2006) (De)constructing mitochondria: what for? Physiology (Bethesda) 21:233–241
7. Ducharme NA, Bickel PE (2008) Lipid droplets in lipogenesis and lipolysis. Endocrinology 149:942–949
8. el-Naggar AK, Evans DB, Mackay B (1991) Oncocytic adrenal cortical carcinoma. Ultrastruct Pathol 15:549–556
9. Erlandson RA, Reuter VE (1991) Oncocytic adrenal cortical adenoma. Ultrastruct Pathol 15:539–547
10. Fong TH, Yang CC, Greenberg AS, Wang SM (2002) Immunocytochemical studies on lipid droplet-surface proteins in adrenal cells. J Cell Biochem 86:432–439
11. Golkowski F, Buziak-Bereza M, Huszno B, Baldys-Waligorska A, Stefanska A, Budzynski A, Okon K, Chrzan R, Urbanik A (2007) The unique case of adrenocortical malignant and functioning oncocytic tumour. Exp Clin Endocrinol Diabetes 115:401–404
12. Kakimoto S, Yushita Y, Sanefuji T, Kondo A, Fujishima N, Kishikawa M, Matsumoto K (1986) Non-hormonal adrenocortical adenoma with oncocytoma-like appearances. Hinyokika Kiyo 32:757–763
13. Lack EE (2007) Tumors of the adrenal gland and extraadrenal paraganglia. American Registry of Pathology, Washington, DC
14. Lin BT, Bonsib SM, Mierau GW, Weiss LM, Medeiros LJ (1998) Oncocytic adrenocortical neoplasms: a report of seven cases and review of the literature. Am J Surg Pathol 22:603–614
15. Lloreta-Trull J, Serrano S (1998) Biology and pathology of the mitochondrion. Ultrastruct Pathol 22:357–367
16. Logasundaram R, Parkinson C, Donaldson P, Coode PE (2007) Co-secretion of testosterone and cortisol by a functional adrenocortical oncocytoma. Histopathology 51:418–420
17. Macadam RF (1970) Fine structure of a functional adrenal cortical adenoma. Cancer 26:1300–10
18. Mackay B, el-Naggar A, Ordonez NG (1994) Ultrastructure of adrenal cortical carcinoma. Ultrastruct Pathol 18:181–190
19. Miura S, Gan JW, Brzostowski J, Parisi MJ, Schultz CJ, Londos C, Oliver B, Kimmel AR (2002) Functional conservation for lipid storage droplet association among Perilipin, ADRP, and TIP47 (PAT)-related proteins in mammals, *Drosophila*, and *Dictyostelium*. J Biol Chem 277:32253–32257

20. Nguyen GK, Vriend R, Ronaghan D, Lakey WH (1992) Heterotopic adrenocortical oncocytoma. A case report with light and electron microscopic studies. Cancer 70:2681–2684
21. O'Gorman E, Fuchs KH, Tittmann P, Gross H, Wallimann T (1997) Crystalline mitochondrial inclusion bodies isolated from creatine depleted rat soleus muscle. J Cell Sci 110(Pt 12):1403–1411
22. Sasano H, Suzuki T, Sano T, Kameya T, Sasano N, Nagura H (1991) Adrenocortical oncocytoma. A true nonfunctioning adrenocortical tumor. Am J Surg Pathol 15:949–956
23. Seo IS, Henley JD, Min KW (2002) Peculiar cytoplasmic inclusions in oncocytic adrenal cortical tumors: an electron microscopic observation. Ultrastruct Pathol 26:229–235
24. Simpson CF, Bradley RE, Jackson RF (1974) Crystalloid inclusions in hepatocyte mitochondria of dogs treated with levamisole. Vet Pathol 11:129–137
25. Xu G, Sztalryd C, Lu X, Tansey JT, Gan J, Dorward H, Kimmel AR, Londos C (2005) Post-translational regulation of adipose differentiation-related protein by the ubiquitin/proteasome pathway. J Biol Chem 280:42841–42847

Virchows Arch (2008) 453:307–308
DOI 10.1007/s00428-008-0655-0

LETTER TO THE EDITOR

Parathyroid tissue in an adult's cervical bronchogenic cyst

Haridimos Markogiannakis · Bill Fleming · Roberto Dina

Received: 19 July 2008 / Accepted: 12 August 2008 / Published online: 1 September 2008

Dear Editor,

Bronchogenic cysts are rare, benign, congenital lesions that occur due to aberrant tracheobronchial tree development during embryogenesis [1–3]. They usually present in childhood, in the lungs or mediastinum, while cervical cysts are infrequent [1, 2]. Neither parathyroid gland absorption by a bronchogenic cyst nor parathyroid tissue in such a lesion has been reported. An adult's cervical bronchogenic cyst containing parathyroid tissue, incidentally found during thyroidectomy in the right superior parathyroid gland location, is presented.

A 52-year-old man presented with a multinodular goitre. Thyroid function, parathormone and calcium were normal. Ultrasound demonstrated a multinodular goitre with a 3-cm dominant nodule in the left and a 4-cm dominant nodule in the right thyroid lobe; no lymphadenopathy or additional abnormal findings were identified. Fine-needle aspiration cytology of both nodules revealed follicular cells with microfollicular pattern, occasionally showing oncocytic changes and nuclear pleomorphism but no malignant changes (Thy3 according to the Classification of the Royal College of Physicians [4]). Intraoperatively, a big multinodular goitre and a cyst in the right superior parathyroid gland location, interpreted as parathyroid cyst, were identified. No lymphadenopathy was observed. Total thyroidectomy and cyst excision were performed. The other three parathyroid glands were preserved.

The thyroid gland (10×8×3 cm, 87.5 g) consisted of an enlarged (8×5.5×3 cm) multinodular right and an enlarged (4.5×3×3.5 cm) nodular left lobe. The latter lobe was almost entirely replaced by a well-circumscribed, encapsulated nodule (3.5×2.4×3 cm), which consisted of follicles with microfollicular and solid architecture and, focally, Hürthle cell changes. A focus of capsular and few foci of vascular invasion were noted. No papillary pathology features were found. Ki-67 proliferative index was <1%. Minimally invasive follicular thyroid carcinoma with capsular and vascular invasion diagnosis was offered.

The cyst (0.8×0.4×0.3 cm, 0.16 g) was thin-walled, unilocular. Microscopically, the inner surface was lined by ciliated, pseudostratified, cuboidal to columnar epithelium with goblet cells. The cystic wall contained smooth muscle, seromucous glands and islands of parathyroid tissue (Fig. 1). This was confirmed by immunohistochemical parathormone demonstration (Fig. 2). There was no evidence of malignancy. A diagnosis of benign bronchogenic cyst with parathyroid tissue in its wall was made.

Cervical bronchogenic cysts are infrequent, usually diagnosed in children but can rarely be encountered in adults; such aberrant location could be explicable by migration of abnormal tracheobronchial tree buds during embryogenesis [1–3]. They are often asymptomatic, frequently found incidentally during radiologic evaluation or, seldom, thyroidectomy as in our patient [5]. Although rare, they should be included in the differential diagnosis of cervical masses.

Characteristic histologic findings are a ciliated, respiratory-type, pseudostratified epithelial lining with smooth muscle cells, mucous glands, cartilage and fibrous connec-

H. Markogiannakis · B. Fleming
Endocrine Surgery Unit, Hammersmith Hospital,
Imperial College Healthcare NHS Trust,
Du Cane Road,
London, UK

R. Dina (✉)
Department of Histopathology,
Imperial College School of Medicine,
Hammersmith Hospital, Du Cane Road,
London W12 0HS, UK
e-mail: r.dina@imperial.ac.uk

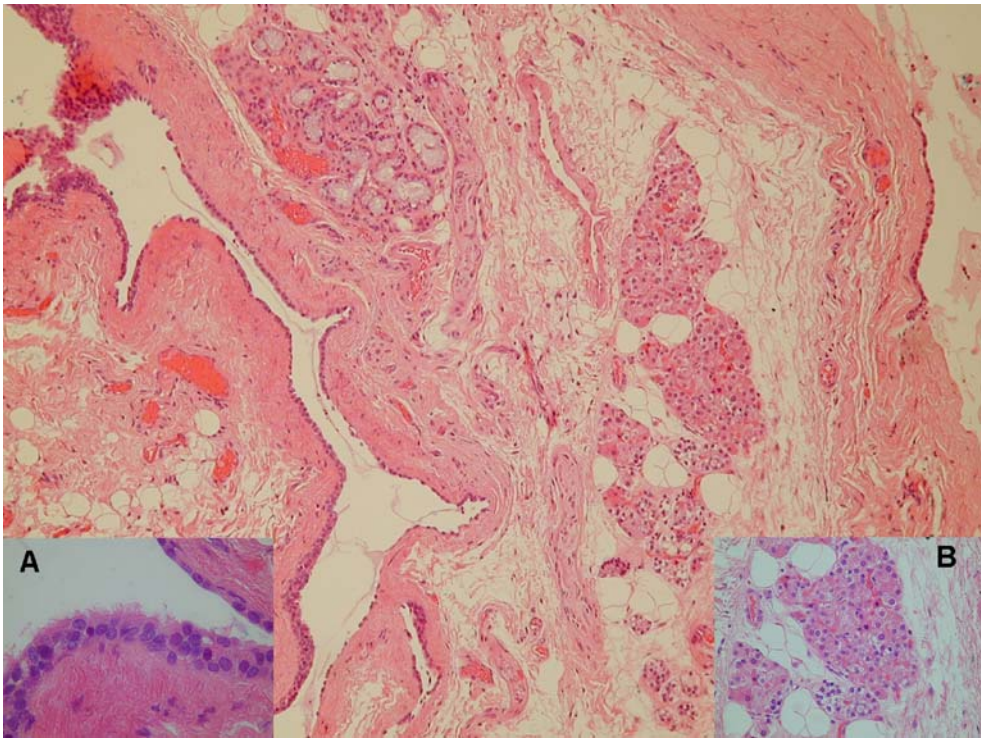

Fig. 1 The cyst with seromucinous glands and a portion of the parathyroid tissue are also visible on the right (H & E, ×100). *Inset A*: ciliated epithelium lining the cyst (H & E, ×1,000). *Inset B*: parathyroid tissue (H & E, ×400)

tive tissue [1–3]. Heterotopic tissue, however, has been rarely identified; a cyst containing pancreatic tissue [3] and another gastric mucosa [6] have been reported while parathyroid tissue has not been described. Parathyroid tissue in the cystic wall and the absence of the right upper parathyroid gland in our case might be embryologically explained by compression of a hypoplastic parathyroid gland by the cyst leading to absorption of the gland into the cystic wall.

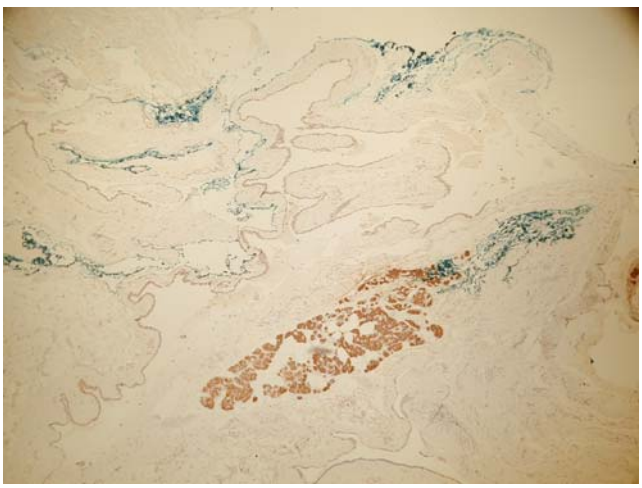

Fig. 2 The parathyroid tissue is expressing PTH (Novocastra 1:25, 10' microwave antigen retrieval) while the remaining tissue is negative (PTH, ×200)

References

1. Bocciolini C, Dall'olio D, Cunsolo E et al (2006) Cervical bronchogenic cyst: asymptomatic neck mass in an adult male. Acta Otolaryngol 126(5):553–556
2. Hadi UM, Jammal HN, Hamdan AL et al (2001) Lateral cervical bronchogenic cyst: an unusual cause of a lump in the neck. Head Neck 23(7):590–593
3. Langlois NE, Krukowski ZH, Miller ID (1997) Pancreatic tissue in a lateral cervical cyst attached to the thyroid gland—a presumed foregut remnant. Histopathology 31(4):378–380
4. Perros P (ed) (2007) British Thyroid Association, Royal College of Physicians. Guidelines for the management of thyroid cancer, 2nd edn. Report of the thyroid cancer guidelines update group. Royal College of Physicians, London
5. Lokey JS, Palmer RM, Macfie JA (2005) Unexpected findings during thyroid surgery in a regional community hospital: a 5-year experience of 738 consecutive cases. Am Surg 71(11):911–913; discussion 913–915
6. Vlodavsky E, Czernobilsky B, Bar Y et al (2005) Gastric mucosa in a bronchogenic cutaneous cyst in a child: case report and review of literature. Am J Dermatopathol 27(2):145–147

Virchows Arch (2008) 453:309–312
DOI 10.1007/s00428-008-0656-z

REVIEW AND PERSPECTIVE

Systems pathology—or how to solve the complex problem of predictive pathology

Manfred Dietel · Reinhold Schäfer

Received: 12 February 2008 / Revised: 14 August 2008 / Accepted: 15 August 2008 / Published online: 13 September 2008

Abstract To understand the extreme complexity of biological events requires a systemic approach. This holds particularly for the disordered biological interactions that are characteristic of disease, the subject of pathology. Which options are available to untie the Gordian knot? In this contribution, the potential role of systems biology and, as a further development, systems pathology will be discussed.

Keywords Systems biology · Systems pathology · Molecular pathology · Hypercomplexity · Omics technology · Integrated networks · Virtual microscopy

Defining the problem

In a Buddhist tale, a group of blind men touches an elephant to learn what it is like (Fig. 1a). Each man touches a different part of the animal but they only touch one part, such as the flank or the tusk. When the men discuss what they felt, they discover that they are in complete disagreement. Apparently, reality may be perceived differently depending upon one's perspective, and what appears to be the objective truth may be relative. Do scientists behave like the blind men (Fig. 1b) by focusing on myriads of details and forgetting the entire picture? Already in 1860, T.H. Huxley stated that the appearance of new characteristics of a whole thing cannot be deduced from the knowledge of the components. [1] Do we need a new way of thinking before we get lost in a mass of details? Are the structures of *systems biology*, or in our case *systems pathology*, helpful in obtaining a systematic order, given the incalculable number of interactions?

Systems biology–pathology can be defined as the scientific approach to understanding the hypercomplex mechanisms underlying biological processes, such as evolution, reproduction, cellular interactions, or carcinogenesis, through holistic or global thinking.

Though he was not the only one, others being Matthias Schleiden (1804–1881) [2], Theodor Schwann (1810–1882) [3], and Robert Remak (1815–1865) [4], Rudolf Virchow (1821–1902) was the first to describe the cell as the smallest living unit with self-reproducing potential—*omnis cellula a cellula* [5]. At that time, Virchow and others (Arnold Adolf Berthold (1803–1861) [6], Moritz Schiff (1823–1896) [7], and Charles-Edouard Brown-Séquard (1818–1894) [8]) already realized that cells communicate with each other. Changes in these functions within and between cells appeared to be the cause of major diseases such as cancer [9]. This was an early attempt towards a holistic view of disease and the first expression of systems-based thought, naturally, without any knowledge of molecular details. During the last century, we have acquired a huge amount of data on many aspects of cellular functions, such as intracellular pathways and intercellular communication. However, we currently face the fundamental problem that no convincing comprehensive systematic concept of homeostasis and pathogenesis has been developed [10]. Biological investigations are based to a large extent on an oversimplification, i.e., the idea that one or a few alterations cause complex diseases. In reality, this is often not the case. For example, the p53 tumor suppressor protein encoded by the most commonly mutated gene in human malignancy was selected "*Molecule of the Year*" in

M. Dietel (✉) · R. Schäfer
Department of Pathology, Charité—University Medicine Berlin,
Charitéplatz 1,
10117 Berlin, Germany
e-mail: manfred.dietel@charite.de

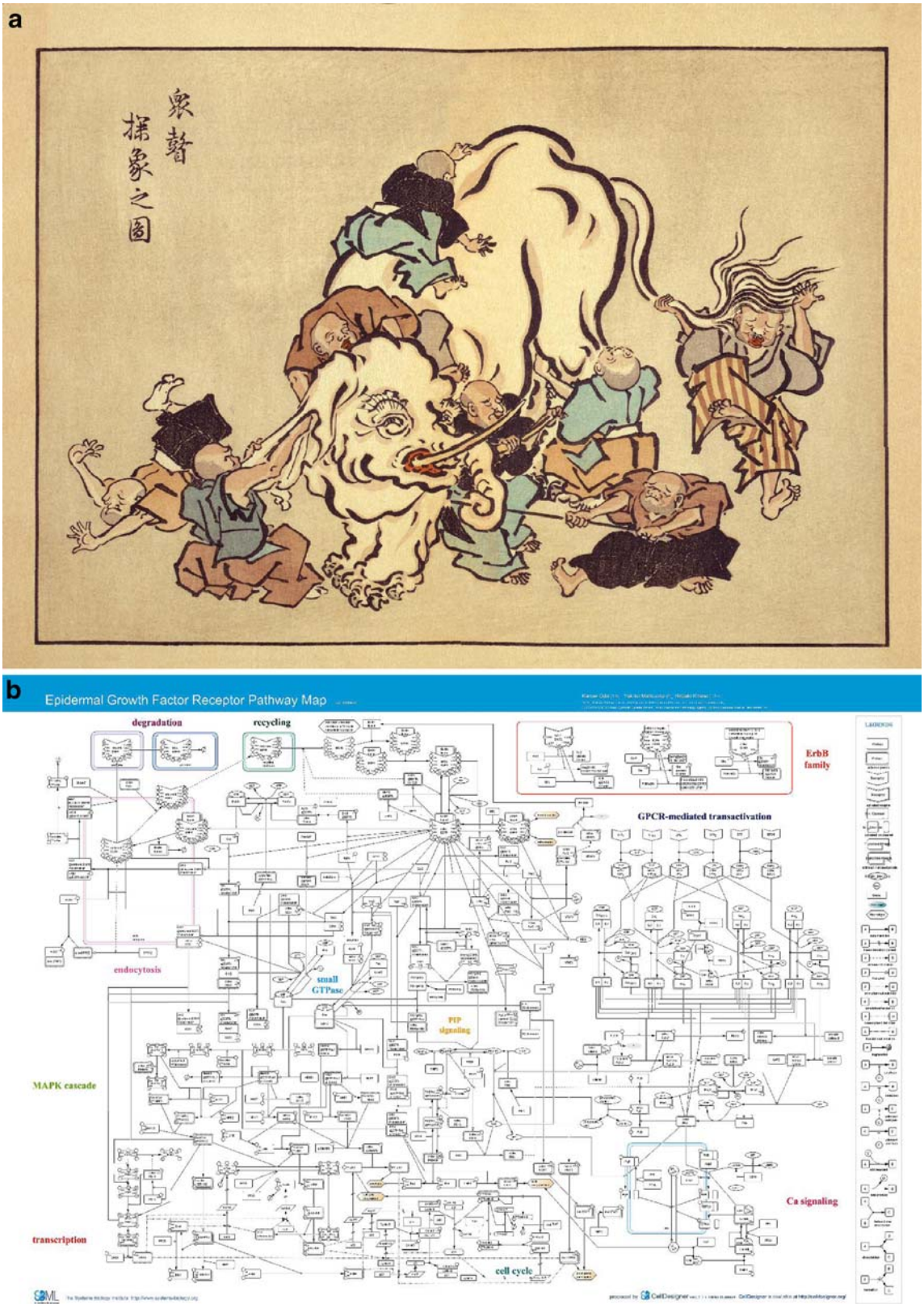

Fig. 1 **a** "Blind monks examining an elephant" by Itcho Hanabusa [17] and **b** modern scientist's concept of the "Epidermal growth factor receptor map" [18]. Is there really a fundamental difference between the (re-)searchers on the left and right with regard to the "objective truth" of the systems?

1993 and was heralded as *the* key to cancer [11]. This, however, turned out to be a too simplistic interpretation of the significance of p53 as a cancer gene. The concept "one disease–one target–one drug" was deduced from such overly simple conclusion.

Intensive, highly qualified scientific research assisted by extraordinary technical developments has enhanced the understanding of molecular mechanisms of disorders. This holds particularly for infectious diseases, in which a causative agent, i.e., a bacterium, can be eliminated by an antibiotic. This great success in the 1930s and 1940s paved the way towards medical reductionism. However, this approach is insufficient for coping with more complex diseases, such as immunological disorders or cancer. Most malignant tumors do not have monocausal origins. Rather, they are triggered by multiple genetic and epigenetic processes with a highly variable time course, dynamics, and penetrance. The biological, chemical, and physiological conditions that cause cancer in one individual but not in others remain unclear. Once the disease has become manifest, the challenge of finding the optimum treatment for the individual patient is a similarly complex issue. The concept of systems biology holds the promise of new strategic tools to enable the resolution of these issues.

We may continue for decades to accumulate details of molecular and functional interactions, separated networks, and new biomarkers (which are often of limited relevance, if not devoid of any clinical impact) without achieving an understanding of the complex processes. The promise of systems analysis is to define crucial structures in cellular networks whose modulation has the greatest chance to induce a profound change. Systems biology may offer computational models [12] by integrating various hierarchical and dynamic interactions creating probabilistic generalizations. The thus uncovered "biological laws" may best reflect reality and may therefore be useful for predicting biological effects, e.g., the antitumor activity of a certain drug in an individual patient.

During the last decade, systems biology has attracted a great deal of attention as a new partner discipline of medical science. This concerns particularly human pathology since it deals with the complexity and variability of diseases. S*ystems pathology* would then be the discipline to overcome the problems of biological complexity by describing and defining the interacting alterations in disease states.

What can scientific and diagnostic pathology learn from systems biology?

The interpretation of macroscopic and microscopic tissue alterations is a complex, experience-based, and somewhat subjective process. Pathologists are the physicians in the medical community who are "closest" to the tissue, particularly to that of tumors. Based on a "mental database" acquired over years of training [13], pathologists are able to classify benign or malignant lesions at the level of only a few morphological criteria. However, the functional complexity of biology is only partially mirrored by morphology. A systemic approach is necessary to recognize the tissue-based functional changes and to extract the information needed to understand the disease and designing an optimum therapy. This means that all essential features, e.g., mutations, gene expression patterns, protein or metabolic modifications, etc., should be analyzed by a heuristic approach to ultimately reach as complete an understanding of the tumor and its behavior as possible and to set up tumor-associated algorithms. Only this strategy will provide a basis for an individualized or personalized therapy.

Model systems such as the *virtual cell* may open the door to novel systems-based intervention strategies, to more efficient and rapid drug development, and consequently to better therapeutic options. A systems approach using a *virtual tumor cell* is of special importance in cancer therapy, in particular for defining major hub structures (nodes with a large number of connections or edges [14]) of the networks that are essential for cellular survival and for finding specific drugs for intervention. New anticancer drugs may converge on these hubs ("Achilles' heel of cancer") as the major target for therapy.

Academic and industrial cancer research face dramatically increasing costs and decreasing output when it comes to drug development, and accordingly the theoretical and experimental prediction of valuable target structures will become an increasingly important issue [15]. Since anticancer research will have to focus on combinatorial drug intervention for optimal drug effects, systems pathology may acquire incredible value.

A future view of pathology

How can a "systems biology" approach become a reality in pathology research and daily diagnostic work? One solution may be to use computationally based fuzzy logics [16] supplemented by neuronal network technology. This approach is a form of multivalued logic derived from fuzzy set theory to deal with reasoning that is approximate rather than precise. In fuzzy logic, the degree of truth of a statement can range between 0 and 1 and is not constrained by the two truth values (true versus false) as in classic predicate logic. In biology and pathology, there always exist several separate membership functions defining particular activity ranges, e.g., those of enzymes needed to properly control cellular functions. The "fuzzy approach"

characterizes this situation much closer than a "yes-or-no system." In addition, fuzzy logic has the advantage of being able to integrate a number of different states of information, e.g., inactive, slightly active, and very active states, when mapping the function of an enzyme, and to permit reliable conclusions to be drawn from this analysis.

To mirror the complex uniqueness of each individual tumor, a systems-based platform that will deliver information on carcinogenesis, prognosis, potential to metastasize, and therapy response is necessary. To define a conceptual framework, we suggest the application of the following procedures in a workflow:

1. The basis remains macroscopy and microscopy, immunohistochemistry (IHC), in situ hybridization (ISH), and molecular techniques, such as polymerase chain reaction sequencing, etc., as well as combinations thereof.
2. As new imaging tools, multicolor (fluorescence) IHC and multiplexed ISH combined with digitized and (semi) quantitative morphological analyses obtained by automated image processing using virtual microscopy and intelligent multiplex bio-optical–bioinformatic platforms including machine learning will be established. These will have the capability to reliably detect, differentiate, and quantify multiple structures, color–reaction products, and processes, each indicating a particular quality and/or function of the tissue/cells investigated.
3. Advanced platform-based high-throughput molecular technologies analyzing transcriptomics, proteomics, epigenomics, metabolomics, glycomics, and toponomics will help to define system response profiles for the tissue. These will define disease-specific and therapy-specific alterations and in so doing far exceed the predictive information currently obtained from conventional single biomarkers.
4. The large datasets generated by the technologies outlined above will have to be integrated into a systemic network, presumably based on or influenced by fuzzy logics. This will help to develop user-friendly algorithms for diagnosis and prediction of the individual behavior of tumors (prognosis, drug response, etc.) and nontumorous diseases.

The workflow introduced here may become the basis of a systems-pathology-driven morphological diagnostic procedure. The key to achieving at least some steps towards "truth" is integration of the disciplines involved and the will and understanding of the scientific community to tackle diseases by systems approaches.

Independent of the expected progress, the intellectual authority in the procedure will still be *the* pathologist. He remains responsible for the correct diagnosis and ultimately for the patient's well-being.

Acknowledgements The authors would like to thank C. Denkert, Christine Sers, and W. Weichert from the Department of Pathology, Charité Berlin, as well as Prof. Dr. Gunter Kloppel and Mrs. Kay Dege and Dagmar Schmöe from the Department of Pathology, Univ.-Klinikum UK-SH Campus Kiel, for their helpful advice and discussion of the manuscript. The paper was supported by the Bundesministerium für Bildung und Forschung in connection with the project MedSys-ColoNet, Charité and Humboldt-University, Berlin.

Conflict of interest statement We declare that we have no conflict of interest.

References

1. Huxley TH (1860) The origin of species. Westminster Review 17:541–570
2. Schleiden M (1842) Grundzüge der wissenschaftlichen Botanik nebst einer methodologischen Einleitung als Anleitung zum Studium der Pflanze. Tle. Leipzig
3. Schwann T (1839) Mikroskopische Untersuchungen über die Uebereinstimmung in der Struktur und dem Wachsthum der Thiere und Pflanzen, Frankfurt am Main, Berlin, Sander, [2006, Nachdr. der 1. Ausg.]
4. Remak R (1838) Observationes anatomicae et microscopicae de systematis nervosi structura. Dissertation der Universität Berlin
5. Virchow R, Cellularpathologie (1855) Arch path Anat und Physiol u. klin. Medizin 8:3–39
6. Berthold AA (1829) Lerhbuch der Physiologie der Menschen und Thiere. 2 Bde. Gött. 8
7. Schiff M (1855) Untersuchungen zur Physiologie des Nervensystems mit Berücksichtigung der Pathologie. Literarische Anstalt, Frankfurt
8. Brown-Séquard C-E (1856) Recherches expérimentales sur la physiologie et la pathologie des capsules surrénales. Acad Sci 8:422–425
9. Virchow R (1863) Die krankhaften Geschwülste. August Hirschwald, Berlin
10. Pomerening JR (2008) Uncovering mechanisms of bistability in biological systems. Curr Opin Biotechnol (in press) Jul 14 [Epub ahead of print]
11. Koshland DE Jr (1993) p53—molecule of the year. Science 262 (5142):1953
12. Kitano H (2002) Computational systems biology. Nature 421:573
13. Saidi O, Cordon-Cardoso C, Costa J (2007) Technology insight: will systems pathology replace the pathologist? Nat Clin Pract 4:39–45
14. Greef vd J, McBurney RN (2000) Rescuing drug discovery: in vivo systems pathology and systems pharmacology. Nat Rev Drug Discov 4:961–967
15. Dietel M (2007) Predictive medicine: incipient reality or fata morgana. J Pathol 212:353–355
16. Zimmermann H (2001) Fuzzy set theory and its applications. Kluwer Academic, Boston
17. Hanabusa I (1652–1724) An Ukiyo-e print illustration taken from the US Library of Congress's Prints and Photographs Division under the digital ID cph.3g08725. No known restrictions on publication
18. Oda K, Matsuoka Y, Funahashi A, Kitano H (2005) A comprehensive pathway map of epidermal growth factor receptor signaling. Mol Syst Biol 1:2005.0010

Virchows Arch (2008) 453:313–319
DOI 10.1007/s00428-008-0661-2

ORIGINAL ARTICLE

End-stage kidney disease: gains of chromosomes 7 and 17 and loss of Y chromosome in non-neoplastic tissue

Ondřej Hes · Radek Šíma · Jana Němcová · Milan Hora · Stela Bulimbasic · Dmitry V. Kazakov · Tomáš Ürge · Tomáš Reischig · Miroslav Dvořák · Michal Michal

Received: 26 March 2008 / Revised: 5 July 2008 / Accepted: 19 August 2008 / Published online: 16 September 2008

Abstract The aim of this study was to determine the copy number changes of chromosomes 7, 17, 3p, and Y in a non-neoplastic tubular epithelium in end-stage kidney disease (ESKD). Seventeen kidneys from 11 patients with ESKD were retrieved from the archive files. Non-neoplastic kidney tissue in these cases was examined separately. Tissues containing papillary adenomas (PA), clear (CRCC) and papillary renal cell carcinomas (PRCC), and myxoid liposarcoma (LPS) were examined using the same probes and compared with non-neoplastic tissue. Tubular changes in the kidney parenchyma were classified into three types: (1) The vast majority of tubules were entirely atrophic; (2) Several tubules were hyperplastic, i.e., tubules with undifferentiated large epithelial cells, in which it was impossible to establish the specific type of a renal tubulus; (3) Dysplastic tubules were dilated, sometimes wrinkled. The basal membranes were lined by large eosinophilic epithelial cells with polymorphic nuclei and pseudostratification. Nucleoli were clearly visible. These tubular changes were multifocal with a haphazard distribution within the atrophic parenchyma. PA were detected in nine patients, of whom eight patients also revealed an additional tumor type(s) (4x CRCC, 3x PRCC, 1x PRCC, and CRCC). One patient had a CRCC only, another had a combination of PRCC and LPS. Chromosomal abnormalities were found in the second and third group of tubular changes, i.e., in hyperplastic and dysplastic tubules. Trisomy of chromosome 7 was detected in six cases, whereas trisomy of chromosome 17 in eight cases. A combination of both trisomies was found in five cases. Loss of chromosome Y was found in two cases. Fluorescence in situ hybridization on tissues containing papillary adenomas, renal cell carcinomas, and liposarcoma revealed expected results, i.e., trisomy of chromosomes 7 and 17 in all PAs and PRCC. No gains were present in CRCC and LPS. Loss of Y was found in six PA, five PRCC, and one LPS; loss of X was found in two CRCCs. We suggest that chromosomal changes typical of the papillary renal cell lesions, i.e., trisomies of chromosomes 7 and 17, are very frequent in non-neoplastic parenchyma of the end-stage kidney, and they have a tendency to a multifocal occurrence.

Keywords End-stage kidney · Premalignant lesion · Dysplastic tubules · Gain · Trisomy · Chromosomes 7 and 17 · FISH

O. Hes · R. Šíma · J. Němcová · D. V. Kazakov · M. Michal
Department of Pathology, Faculty of Medicine Plzen,
Charles University Prague,
Plzen, Czech Republic

M. Hora · T. Ürge
Department of Urology, Faculty of Medicine Plzen,
Charles University Prague,
Plzen, Czech Republic

S. Bulimbasic
Department of Pathology, University Hospital Dubrava,
Zagreb, Croatia

T. Reischig
Department of Internal Medicine, Faculty of Medicine Plzen,
Charles University Prague,
Plzen, Czech Republic

M. Dvořák
Department of Forensic Medicine, Faculty of Medicine Plzen,
Charles University Prague,
Plzen, Czech Republic

O. Hes (✉)
Department of Pathology, Laboratore Spec. Diagnostiky,
Medical Faculty and University Hospital,
Alej Svobody 80, 304 60 PLZEN,
Pilsen, Czech Republic
e-mail: hes@medima.cz

Introduction

It is well known that patients with end-stage kidney disease (ESKD) have an increased risk of renal cell carcinoma. There have been several types of renal cell tumors reported in patients with ESKD [5, 6, 8, 10, 18, 19]. Papillary renal cell carcinoma (PRCC), clear renal cell carcinoma (CRCC), and papillary adenoma (PA) are the most frequent types of tumors occurring in ESKD [4, 7, 8]. Trisomy of chromosome 7 has been found in non-neoplastic proximal tubulus epithelias of normal kidney and lymphocytes infiltrating kidney tumors or surrounding parenchyma [2, 3, 11]. Little data are available on chromosomal alterations of tubular changes in ESKD. The aim of this study was to determine the copy number changes of chromosomes 7, 17, 3p, and Y in histologically non-neoplastic-looking tubular epithelium in ESKD.

Materials and methods

Seventeen kidneys from 11 patients with ESKD were retrieved from the files of the Departments of Pathology and Urology, Charles University in Plzen. Histologic sections of formalin-fixed, paraffin-embedded tissue were stained with hematoxylin and eosin. The number of blocks from each kidney varied from seven to 18 from one patient (mean 13). Both neoplastic and non-neoplastic tissues were available for analysis. Non-neoplastic renal parenchyma was examined separately from tumorous tissues. The number of examined hyperplastic and dysplastic tubules varied from two to six per one patient (mean 4).

Tissues containing papillary adenomas, renal cell carcinomas, and liposarcoma were studied separately under the same conditions.

As a negative control group, ten healthy donor kidney tissue samples and ten end-stage kidneys without any tumorous mass were examined to set the cutoff levels for fluorescence in situ hybridization (FISH) evaluation.
All patients from this control group have been dialyzed for a long-term.

FISH

FISH was carried out on 5-μm paraffin sections. Tissues were deparaffinized in xylene 3×5 min, washed 2×2 min in 100% ethanol, 1×2 min in 95% ethanol, and 1×5 min in deionized water. Then, the slides were incubated in the Epitope Retrieval Solution (DAKO, Glostrup, Denmark) for 40 min at 95°C and subsequently cooled at room temperature (RT) for 20 min in the Epitope Retrieval Solution. The slides were washed 5 min in deionized water, and tissues were covered with the Proteinase K Ready-to-Use (DAKO) solution for 3–5 min. Then, the slides were immediately washed twice for 2 min in deionized water, dehydrated in 70%, 85%, and 100% ethanol for 2 min each and air dried.

Afterward, the mixtures of CEP7, CEP17, CEP3 + TelVysion 3p (Vysis, Downers Grove, IL, USA), or SE X/Y (Kreatech, Amsterdam, Netherlands) probes were applied on the samples and covered with coverslips. Slides were denatured at 85°C for 5 min and incubated in humidified box at 37°C overnight. Then, the slides were washed for 2 min in 0.4× SSC/0.3% NP-40 at 73°C and for 1 min in 2× SSC/0.1% NP-40 at RT. After that, the slides were counterstained with DAPI II (Vysis) and examined.

Fluorescent signals from non-neoplastic tubular epithelium nuclei were counted. Only nonoverlapping intact nuclei were scored, split centromere signals were counted as one. Cutoff levels for gain and loss of a signal (chromosome) were set at 3× SD of the mean number of variants seen in normal control nuclei and were as more than 10% for an interpretation of gain of chromosomes 7 and 17 and more than 20% for loss of chromosome Y.

Results

The basic clinicopathological data are summarized in Table 1. The patients were one woman and ten men, with ages ranging from 41 to 67 years (mean, 51.9 years). All but one patient lost kidney function because of chronic glomerulonephritis, the exception being a case of renal complete insufficiency due to diabetic nephropathy. Eight patients were treated by hemodialysis and subsequent renal transplantation, while the remaining three individuals were only dialyzed. The duration of hemodialyzation ranged from 0.6 to 6 years (mean, 2.5 years). The patients had functional renal grafts from 2 to 9 years (mean, 5.75 years). Renal tumors were found in all but one patient, using ultrasonography or computed tomography (CT) during periodic clinical examinations. All pathologic findings were located in the native kidneys. No tumors were detected in renal grafts. Unusual scarring of the kidney parenchyma was misinterpreted as a tumorous mass in one patient (case 10) on CT. Unilateral nephrectomy was performed in five patients, bilateral in six patients.

Papillary adenomas were detected in nine patients, of whom eight patients also revealed an additional tumor type (s) (4× CRCC, 3× PRCC, 1× PRCC, and CRCC). All but two patients had multiple PAs. One patient had a CRCC only; another had a combination of PRCC and low-grade myxoid liposarcoma.

Tubular changes in the kidney parenchyma were present in all examined cases and were classified into three major types:

1. The vast majority (>95%) of tubules were entirely atrophic.

Table 1 Clinical characteristics

	Sex/age	Renal disease	Dialysis	Transplantation	Nephrectomy/side	Type of tumor
Case 1	F/67	GN NOS	1 year	2 years	Unilateral/left	CRCC
Case 2	M/46	DM	1 year	0	Bilateral	PAs, 2 CRCC
Case 3	M/57	GN NOS	8 months	6 years	Bilateral	PAs, PRCC
Case 4	M/41	GN NOS	2 years	0	Bilateral	PAs, PRCC
Case 5	M/52	GN NOS	1 year	2 years	Unilateral/right	PA, PRCC
Case 6	M/49	FSGS	1 year	4 years	Unilateral/left	PA, CRCC
Case 7	M/55	GN NOS	4 years	9 years	Bilateral	PAs, PRCC, CRCC
Case 8	M/54	GN NOS	6 years	8 years	Unilateral/right	PA, CRCC
Case 9	M/59	GN NOS	4 years	0	Unilateral/left	PAs, CRCC
Case 10	M/50	MP GN	3 years	9 years	Bilateral	PAs
Case 11	M/41	MP GN	4 years	6 years	Bilateral	PRCC, myx liposa

F female, *M* male, *GN* glomerulonephritis, *NOS* not other specified, *DM* diabetes mellitus, *FSGS* focal and segmental glomerulosclerosis, *MP GN* membranous-proliferative glomerulonephritis, *PA* papillary adenoma, *CRCC* clear renal cell carcinoma, *PRCC* papillary renal cell carcinoma, *myx liposa* myxoid liposarcoma

2. Several (<4%) tubules were hyperplastic, i.e., tubules with undifferentiated large epithelial cells, in which it was impossible to establish the specific type of renal tubulus (Fig. 1). Diameter of the hyperplastic tubules varied between 0.1 and 0.4 mm.
3. Dysplastic tubules (individual tubules). These were dilated, sometimes wrinkled. The basal membranes were lined by large eosinophilic epithelial cells with polymorphic nuclei and pseudostratification. Nucleoli were clearly visible (Fig. 2a,b). These tubular changes were multifocal with a haphazard distribution within the atrophic parenchyma. Diameter of the hyperplastic tubules varied between 0.1 and 0.8 mm.

Normal tubules and tubules with undifferentiated features (where it was impossible to establish the position in the nephron) were seen only very rarely.

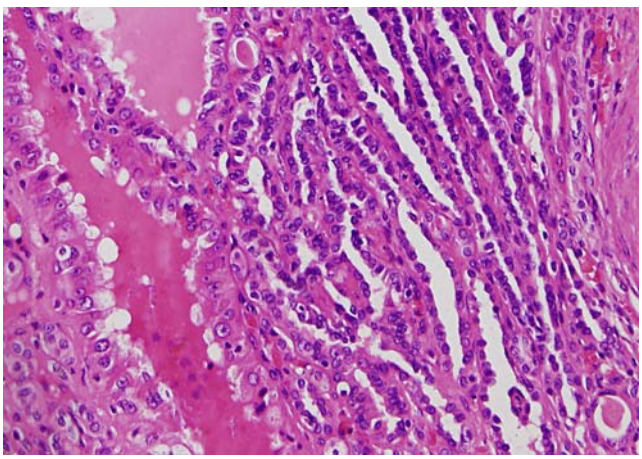

Fig. 1 Several tubules were hyperplastic: i.e., tubules were lined by undifferentiated large epithelial cells. Structures of papillary adenoma can be seen on the *right*

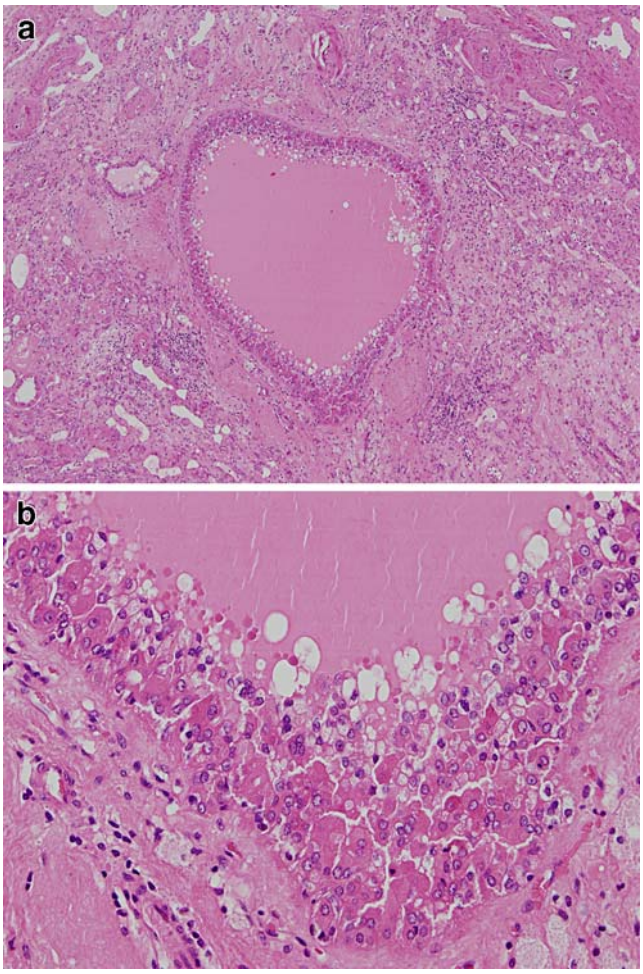

Fig. 2 **a** Several tubules were dysplastic. These tubules were dilated, sometimes wrinkled. Such tubular changes were multifocal with a haphazard distribution within the atrophic parenchyma. **b** The basal membranes of dysplastic tubules were lined by large eosinophilic epithelial cells with polymorphic nuclei and pseudostratification. Nucleoli were clearly visible

Table 2 FISH results

Parameter	Side	Chromosome 7		Chromosome 17		Chromosomes XY	
		Total nuclei	Status	Total nuclei	Status	Total nuclei	Status
Case 1							
Non-neoplastic tissue	Left	105	Disomic	102	Disomic	NA	XX
CRCC	Left	101	Disomic	101	Disomic	100	73% X0
Case 2							
Non-neoplastic tissue	Right	103	Disomic	100	Disomic	103	XY
CRCC	Right	113	Disomic	100	Disomic	100	15% 0Y
Non-neoplastic tissue	Left	100	Disomic	105	Disomic	NA	NA
Case 3							
Non-neoplastic tissue	Right	100	Disomic	101	25% trisomy	100	XY
PA	Right	116	61% trisomy	101	72% trisomy	100	89% X0
PA	Right	105	50% trisomy	101	70% trisomy	100	89% X0
Non-neoplastic tissue	Left	100	Disomic	111	26% trisomy	102	XY
PRCC	Left	101	55% trisomy	100	72% trisomy	100	74% X0
Case 4							
Non-neoplastic tissue	Right	100	32% trisomy	146	12% trisomy	100	XY
PA	Right	100	78% trisomy	102	48% trisomy	100	81% X0
Non-neoplastic tissue	Left	100	Disomic	100	Disomic	115	XY
PRCC	Left	100	51% trisomy	100	61% trisomy	100	83% X0
Case 5							
Non-neoplastic tissue	Right	56	Disomic	52	38% trisomy	100	XY
PA	Right	100	58% trisomy	100	43% trisomy	100	76% X0
PRCC	Right	118	65% trisomy	108	68% trisomy	100	73% X0
Case 6							
Non-neoplastic tissue	Left	10	Disomic	109	Disomic	106	XY
CRCC	Left	109	Disomic	116	Disomic	100	58% 0Y
Case 7							
Non-neoplastic tissue	Right	101	32% trisomy	104	31% trisomy	100	XY
Non-neoplastic tissue	Left	47	60% trisomy	55	16% trisomy	100	24% X0
PRCC	Left	106	58% trisomy	100	63% trisomy	100	86% X0
PA	Left	37	Disomic	72	26% trisomy	100	39% X0
Case 8							
Non-neoplastic tissue	Right	63	45% trisomy	102	28% trisomy	100	XY
CRCC	Right	101	Disomic	100	Disomic	100	XY
PA	Right	102	71% trisomy	112	62% trisomy	NA	NA
Case 9							
Non-neoplastic tissue	Left	20	Disomic	31	Disomic	5	XY
PRCC	Left	100	50% trisomy	100	38% trisomy	100	72% X0
PA	Left	104	Disomic	102	Disomic	100	XY
PA	Left	100	44% trisomy	102	41% trisomy	100	36% X0
CRCC	Right	103	Disomic	105	Disomic	100	XY
Case 10							
Non-neoplastic tissue	Right	107	Disomic	106	Disomic	65	XY
PA	Right	124	Disomic	101	24% trisomy	NA	NA
Non-neoplastic tissue	Left	100	Disomic	52	Disomic	106	XY
Case 11							
Non-neoplastic tissue	Right	18	39% trisomy	101	Disomic	81	52% X0
PRCC	Right	115	57% trisomy	101	80% trisomy	100	XY
Non-neoplastic tissue	Left	47	40% trisomy	106	16% trisomy	102	XY
Myxoid liposarcoma	Left	100	Disomic	102	Disomic	100	44% X0

NA not analyzable

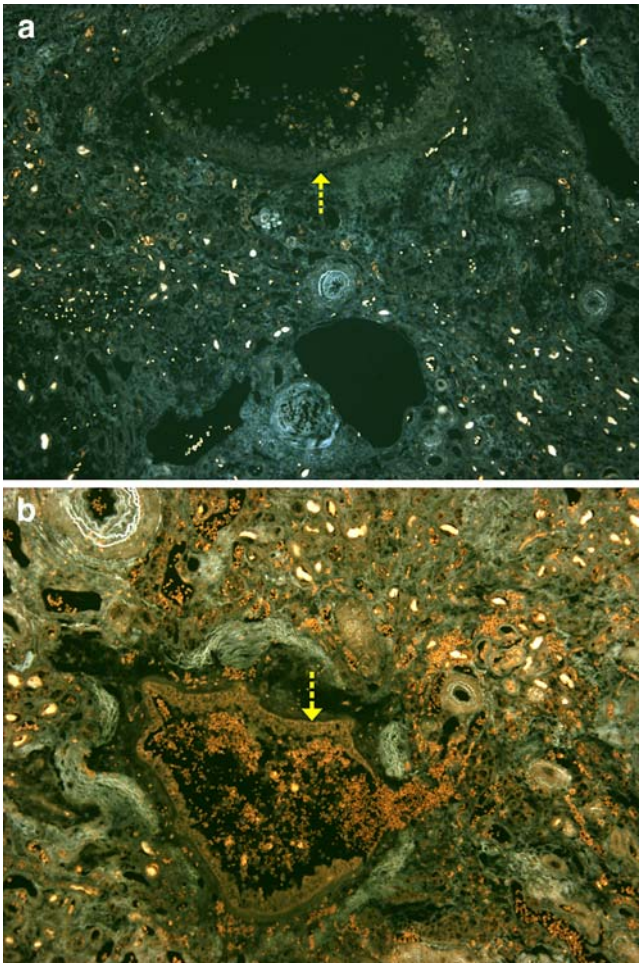

Fig. 3 FISH was carried out on paraffin sections. A low-power appearance of dysplastic tubulus (*arrow*) in the dark field. **a** Analysis of chromosome 7. **b** Analysis of chromosome 17 (*arrow*)

The results of the FISH analysis are summarized in Table 2. In a majority of cases, at least 100 nonoverlapping nuclei were examined. In some cases, the total number of nuclei was lower than 100 because some tubules did not contain more cells. Chromosomal abnormalities were found in the second and third group of tubular changes, i.e., in hyperplastic and dysplastic tubules (Fig. 3a,b). Trisomy of chromosome 7 was detected in six (Fig. 4), trisomy of chromosome 17 in eight cases (Fig. 5). A combination of both trisomies was found in five cases. Loss of chromosome Y was found in two cases. Then, the FISH for 3p loss detection was performed using telomeric probe for the 3p25 chromosomal region. Unfortunately, this 3p25 chromosomal region examination failed in all studied cases, especially due to a weak signal of telomeric probe. 3p25 telomeric probe worked well on a control (non-fixed metaphase lymphocytes).

FISH on tissues containing papillary adenomas, renal cell carcinomas, and liposarcoma revealed expected results (see Table 2). Papillary adenomas and papillary renal cell carcinomas showed both trisomies of chromosomes 7 and 17. Some papillary adenomas were not analyzable because of limited volume of the paraffin tumorous material. There were no significant differences in chromosome 7 and 17 status in papillary adenomas and carcinomas. Result of analysis of chromosomes 7 and 17 was not significant in papillary adenoma in case 7 because of limited volume of analyzed tissue. No trisomy of chromosomes 7 and 17 was noted in clear RCC. Loss of chromosome Y was seen in one case of well-differentiated liposarcoma. Loss of chromosome X was seen in two cases of clear RCC (one female patient and one male patient).

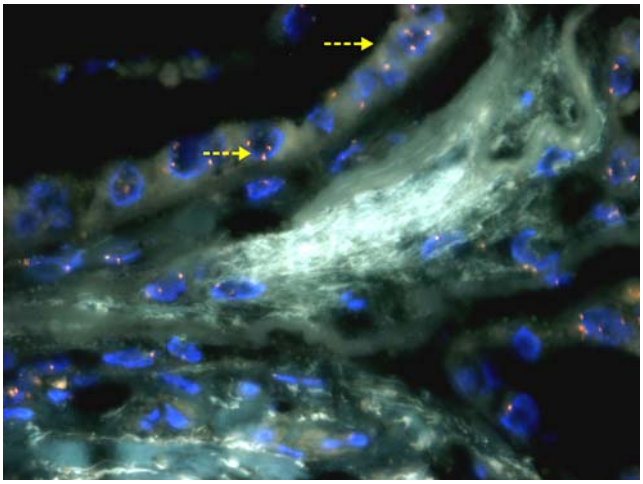

Fig. 4 Two cells with three signals (*arrows*) are clearly visible in the epithelial cells lining a dysplastic tubulus (analysis of chromosome 7)

Discussion

In our study we found that (1) chromosomal changes such as gains of chromosomes 7 and 17 and loss of Y

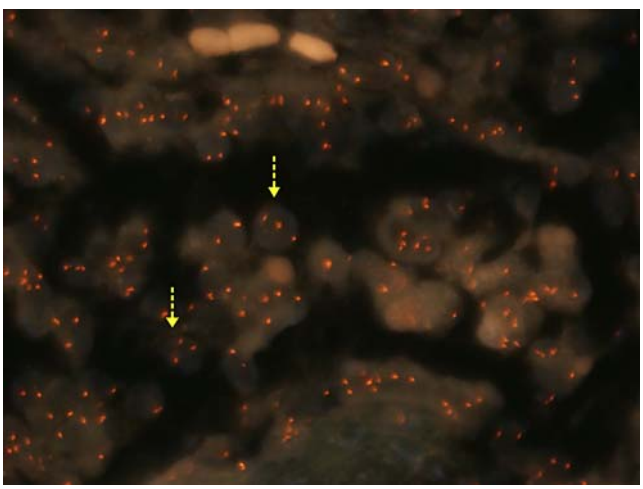

Fig. 5 Analysis of chromosome 17. At least two cells (*arrows*) showed three nuclear signals in dysplastic tubulus

chromosome may be found in non-neoplastic tissue of the end-stage kidney diseases and (2) these chromosomal abnormalities tend to have a multifocal occurrence.

Tumors in ESKD have been extensively studied by Hughson et al. The authors have proposed that papillary RCC is the most frequent type of renal cell carcinoma found in these patients. Moreover, the genetic changes of these tumors are similar to those seen in sporadic cases [7–9]. Specific and probably new types of renal tumors occurring in the setting of ESKD have recently been published. The typical features of these tumors are a frequent papillary pattern, presence of oxalate crystals, and clear to eosinophilic cytoplasm [18, 19]. We were not able to find similar tumors in our series of patients. Moreover, no significant amount of oxalate deposits was present in the kidney parenchyma in our cases.

There is no reference in the literature on premalignant lesions in ESKD. Precursors of sporadic RCC in non-atrophic kidney have been described by Mourad et al., who examined non-neoplastic tissue surrounding RCC (mainly clear RCC and sarcomatoid NOS RCC) and found dysplastic changes located mainly in the cortex or in a periglomerular distribution. However, the authors found intratubular epithelial dysplasia in 30 out of 110 patients with RCC [15].

Similar findings have been published recently. Dysplastic changes in normal kidneys have been identified in 23% of the kidneys harboring RCC. Dysplastic changes were focal and located adjacent to the tumor mass in ten cases, whereas a diffuse distribution was a rare finding [20]. On the contrary, tubular changes in our series were always multifocal with a haphazard distribution spread within the entire atrophic parenchyma.

A study dealing with chromosomal changes in tubular abnormalities in clear RCC has been published recently. Premalignant lesions and tumor tissues in this study had the same genotypic changes (LOH or microsatellite instability) in more than 85% [16].

Chromosomal changes of PA and PRCC are characterized mainly by trisomy of chromosomes 7 and 17 and loss of chromosome Y [12, 13, 17]. However, trisomy of chromosome 7 was found in majority of RCC, the combination of trisomy of chromosomes 7 and 17 and loss of Y chromosome is rather specific for papillary neoplasms [14]. We tried to identify these chromosomal changes in hyperplastic and dysplastic renal tubules. Interestingly, trisomy of chromosome 7 was detected in six, trisomy of chromosome 17 in eight cases. A combination of both trisomies was found in five cases. Loss of chromosome Y was found only in two cases.

Trisomy of chromosome 7 has been studied in non-neoplastic tissue of normal, non-atrophic kidney surrounding RCC. Cells with trisomy of chromosome 7 were mainly epithelial tubular cells [3, 11] or a combination of lymphocytes infiltrating tumor tissue and tubular cells [2]. Our study was concerned of ESKD, and all positive tubules for trisomies of chromosomes 7 and 17 were abnormal. As was mentioned above, positive tubules harbored hyperplastic or dysplastic changes. No abnormalities were noted in atrophic or undiferentiated tubules without hyperplastic or dysplastic features. However, some non-neoplastic cells showed trisomy of chromosome 7 or 17; the number of trisomies was under the cutoff level.

Brunelli et al. showed that both PA and PRCC share similar chromosomal changes, i.e., gains of chromosomes 7, 17, 16, 12, and 20 and loss of Y chromosome [1]. Loss of the Y chromosome was observed in nine of ten PA from males. It was concluded that gains of chromosomes 7, 17, 16, 12, and 20 and loss of Y chromosome occur early in the neoplastic evolution of papillary renal cell neoplasia. On the contrary, we have found only two of nine male cases with loss of Y chromosome. However, the loss of chromosome Y was found in all analyzed cases of PA and PRCC. Loss of chromosome Y was interestingly seen in one case of well-differentiated liposarcoma. Loss of chromosome X was seen in two cases of clear RCC (one female patient and one male patient).

An interesting fact is that trisomies of chromosomes 7 and 17 were noted in the kidneys with different tumors (besides papillary adenomas and papillary RCC). Our findings point to the fact that chromosomal changes typical of the papillary renal cell lesions are very frequent in non-neoplastic-looking parenchyma of the end-stage kidney and that they have a tendency to a multifocal occurrence.

Acknowledgment The study was supported by MSM 0021620819 replacement of and support to some vital organs.

Conflict of interest statement We declare that we have no conflict of interest.

References

1. Brunelli M, Eble JN, Zhang S, Martignoni G, Cheng L (2003) Gains of chromosomes 7, 17, 12, 16, and 20 and loss of Y occur early in the evolution of papillary renal cell neoplasia: a fluorescent in situ hybridization study. Mod Pathol 16:1053–1059
2. Dal Cin P, Aly MS, Delabie J, Ceuppens JL, van Gool S, van Damme B, Baert L, van Poppel H, van den Berghe H (1992) Trisomy 7 and trisomy 10 characterize subpopulations of tumor-infiltrating lymphocytes in kidney tumors and in the surrounding kidney tissue. Proc Natl Acad Sci USA 89:9744–9748
3. Elfving P, Aman P, Mandahl N, Lundgren R, Mitelman F (1995) Trisomy 7 in nonneoplastic epithelial kidney cells. Cytogenet Cell Genet 69:90–96
4. Gronwald J, Baur AS, Holtgreve-Grez H, Jauch A, Mosimann F, Jichlinski P, Wauters J-P, Cremer T, Guillou L (1999) Chromosomal abnormalities in renal cell neoplasms associated with

acquired renal cystic disease. A series studied by comparative genomic hybridization and fluorescence in situ hybridization. J Pathol 187:308–312
5. Farivar-Mohseni H, Perlmutter AE, Wilson S, Shingleton WB, Bigler SA, Fowler JE (2005) Renal cell carcinoma and end-stage renal disease. J Urol 175:2018–2021
6. Hoshida Y, Nakanishi H, Shin M, Satoh T, Hanai J, Aozasa K (1999) Renal neoplasms in patients receiving dialysis and renal transplantation: clinico-pathological features and p53 gene mutations. Transplantation 68:385–390
7. Hughson MD, Meloni AM, Silva FG, Sandberg AA (1996) Renal cell carcinoma in an end-stage kidney of patient with a functional transplant: cytogenetic and molecular genetic findings. Cancer Genet Cytogenet 89:65–68
8. Hughson MD, Schmidt L, Zbar B, Daugherty S, Meloni AM, Silva FG, Sandberg AA (1996) Renal cell carcinoma of end-stage renal disease: a histopathologic and molecular genetic study. J Am Soc Nephrol 7:2461–2468
9. Hughson MD, Bigler S, Dickman K, Kovacs G (1999) Renal cell carcinoma of end-stage renal disease: an analysis of chromosome 3, 7, and 17 abnormalities by microsatellite amplification. Mod Pathol 12:301–309
10. Junker K, Thrum K, Schlichter A, Müller G, Hindermann W, Schubert J (2002) Clonal origin of multifocal renal cell carcinoma as determined by microsatellite analysis. J Urol 168:2623–2636
11. Knuutila S, Larramendy ML, Elfving P, el-Rifai W, Miettinen A, Mitelman F (1995) Trisomy 7 in non-neoplastic tubular epithelial cells of the kidney. Hum Gen 95:149–156
12. Kovacs G, Fuzesi L, Emanuel A, Kung H-F (1991) Cytogenetics of papillary renal cell tumors. Genes Chromosomes Cancer 3:249–255
13. Kovacs G, Akhtar M, Beckwith JB, Bugert P, Cooper CS, Delahunt B, Eble JN, Fleming S, Ljunberg B, Medeiros LJ, Moch H, Reuter VE, Ritz E, Roos G, Schmidt D, Srigley JR, Storkel S, van den Berg E, Zbar B (1997) The Heidelberg classification of renal cell tumours. J Pathol 183:131–133
14. Moch H, Sauter G, Gasser TC, Bebendorf L, Richter J, Presti JC Jr, Waldman FM, Mihatsch MJ (1998) EGF-r gene copy number changes in renal cell carcinoma detected by fluorescence in situ hybridization. J Pathol 184:424–429
15. Mourad WA, Nestok BR, Saleh GY, Solez K, Power RF, Jewell LD (1994) Dysplastic tubular epithelium in "normal" kidney associated with renal cell carcinoma. Am J Surg Pathol 18:117–1124
16. Pehlivan S, Koyuncuoglu M, Pehlivan M, Izzetoglu S, Mater Y, Cabuk M, Kirkali Z (2004) Premalignant lesions of the kidney share the same genetics changes as conventional renal cell carcinoma. World J Urol 22:120–123
17. Sanjmyatav J, Rubtsov N, Starke H, Schubert J, Hindermann W, Junker K (2005) Identification of tumor entities of renal cell carcinoma using interphase fluorescence in situ hybridization. J Urol 174:731–735
18. Sule N, Yakupoglu U, Shen SS, Krishnan B, Yang G, Lerner S, Sheikh-Hamad D, Truong LD (2005) Calcium oxalate deposition in renal cell carcinoma associated with acquired cystic kidney disease: a comprehensive study. Am J Surg Pathol 29:443–451
19. Tickoo SK, dePeralta-Venturina M, Lara H, Worcester HD, Salama M, Young A, Moch H, Amin M (2006) Spectrum of epithelial neoplasms in end-stage renal disease: an experience from 66 tumor-bearing kidneys with emphasis on histologic patterns distinct from those in sporadic adult renal neoplasia. Am J Surg Pathol 30:141–153
20. Yörükoglu K, Aktas S, Mungan MU, Kirkali (1999) Tubular dysplasia and carcinoma in situ: precursors of renal cell carcinoma. Urology 53:684

Virchows Arch (2008) 453:321–328
DOI 10.1007/s00428-008-0647-0

ORIGINAL ARTICLE

What is the significance of CD34 immunostaining in the extraglomerular and intraglomerular mesangium?

Cristina Gluhovschi · Gheorghe Gluhovschi · Elena Potencz · Diana Herman · Ligia Petrica · Silvia Velciov · Gheorghe Bozdog · Flaviu Bob · Corina Vernic · Daniel Cioca

Received: 31 March 2008 / Revised: 17 June 2008 / Accepted: 17 July 2008 / Published online: 8 August 2008

Abstract CD34, traditionally a marker of hematopoietic stem cells (HSCs), was found on endothelial cells and fibroblasts as well. At the level of the extraglomerular or intraglomerular mesangium, CD34 may signal either the presence of HSCs or, conversely, may be a marker of transdifferentiation. CD34-positive cells of the extraglomerular mesangium could migrate into the intraglomerular mesangium and participate in reparative processes at this level. The aim of our study was to analyze the presence of CD34 at the level of the extraglomerular and intraglomerular mesangium and its relationship with histological markers of activity and chronicity, as well as with other immunohistochemical markers in glomerulonephritis (GN). A cross-sectional study of 36 patients with GN was conducted. Conventional stains: hematoxylin–eosin, periodic acid Schiff, and Trichrome Gömöri, as well as immunohistochemistry: CD34, alpha smooth muscle actin (alpha SMA), vimentin, and proliferating cell nuclear antigen (PCNA) were employed. Activity and chronicity of GN were evaluated according to a scoring system initially used for lupus nephritis and antineutrophil-cytoplasmic-antibody-associated vasculitis. Immunohistochemistry was assessed using a semiquantitative score. The mean age was 46.44±12.97 years; 22 were male and14 were female. The extraglomerular mesangium was visible on specimens in 30 patients. CD34 was present in the extraglomerular mesangium in 15 patients: 11 of these patients showed concomitant intraglomerular and extraglomerular mesangial CD34 immunostaining, while four showed only extraglomerular mesangial immunostaining. In three patients, CD34 immunostaining was present only in the intraglomerular mesangium. Twelve patients showed negative immunostaining in both the extraglomerular and the intraglomerular mesangium. Overall, there was a fair degree of relationship, which did not reach statistical significance between CD34 in the extraglomerular mesangium and CD34 in the intraglomerular mesangium across the 36 patients. In the intraglomerular mesangium, CD34 did not significantly correlate with mesangial alpha SMA, vimentin, PCNA, and activity or chronicity index. In the extraglomerular mesangium, CD34 did not show a significant correlation with alpha SMA, vimentin, or PCNA. The activity index and the chronicity index showed a good correlation with serum creatinine. Mesangial cell proliferation correlated well with the mesangial matrix increase, while interstitial vimentin showed a good correlation with interstitial alpha SMA. We demonstrated the presence of CD34 in the extraglomerular mesangium, which could be related to transdifferentiated mesangial cells or to HSCs in the absence of blood vessels at this level. Our study shows the value of histological indices

C. Gluhovschi · G. Gluhovschi · L. Petrica · S. Velciov · G. Bozdog · F. Bob
Division of Nephrology,
University of Medicine and Pharmacy "V. Babes",
Timisoara, Romania

E. Potencz · D. Herman
Division of Pathology,
University of Medicine and Pharmacy "V. Babes",
Timisoara, Romania

C. Vernic
Department of Medical Informatics and Biostatistics,
University of Medicine and Pharmacy "V. Babes",
Timisoara, Romania

D. Cioca
Immunology, Austrian Academy of Sciences,
Innsbruck, Austria

C. Gluhovschi (✉)
Calea Aradului No. 8 Ap.16,
300088 Timisoara, Romania
e-mail: gluhovschi@yahoo.com

for evaluating GN but cannot assign significance to CD34 immunolabeling for the assessment of GN.

Keywords Glomerular disease · Pathology · CD34

Introduction

The extraglomerular mesangium is a region of the juxtaglomerular apparatus whose role and function are incompletely understood. It is strategically located between the two arterioles, the macula densa and the vascular pole of the glomerulus. The extraglomerular mesangium, which forms a syncytium, is connected to the intraglomerular mesangium via gap junctions at the level of the vascular pole of the glomerulus [1]. It is important to note that blood vessels are absent at the level of the extraglomerular mesangium. While analyzing a group of patients with GN, we observed the presence of the CD34 marker in the extraglomerular mesangium. As the presence of mesangial cells bearing the CD34 marker is rarely referred to in the literature and the presence of the CD34 marker in the extraglomerular mesangium has not been reported, our objective was to document this observation. CD34 is found on endothelial cells, hematopoietic stem cells (HSCs), and also on glomerular mesangial cells that have undergone a process of transdifferentiation [2–5]. As blood vessels are absent at the level of the extraglomerular mesangium, the presence of CD34 at this level cannot be attributed to the presence of endothelial cells. It is unclear whether the finding of the CD34 marker represents HSCs or transdifferentiated mesangial cells.

Because the extraglomerular mesangium participates in reparative processes of the intraglomerular mesangium and HSCs could be involved in this process, the presence of cells bearing the CD34 marker could suggest HSCs. Conversely, cells bearing the CD34 marker could represent transdifferentiated mesangial cells.

CD34 is a single-chain heavily glycosylated transmembrane protein of approximately 116 kDa [6]. Shortly after isolation, it was termed QBEnd. First identified in a myeloid leukemia cell line (KG1a) and originally characterized as a marker for hematopoietic progenitor cells and endothelial cells, immunohistological reactivity with anti-CD34 antibodies is encountered in addition to immature leukemias and vascular tumors, in a histologically diverse subset of nonhematolymphoid neoplasms including angiosarcoma, solitary fibrous tumors, epithelioid sarcomas, spindle cell lipomas, dermatofibrosarcoma protuberans, and myofibroblastomas. Although a variety of neoplasms displays immunological reactivity with anti-CD34, this immunophenotype is restricted and can aid in distinguishing specific tumors from histological mimics in their differential diagnoses [6].

The observed CD34 immunohistological reactivity in disparate neoplasms raised the question of whether the CD34 protein was expressed in diverse cell types or if shared epitopes among different proteins could explain this finding.

Immunohistological reactivity for CD34 in HSCs and endothelial cells was shown to correspond to CD34 protein expression. Natkunam et al. [6] demonstrated by immunoblotting that immunohistological reactivity of six different unrelated tumors was due to the expression of the same molecular weight CD34 protein and not to shared epitopes on unrelated proteins.

Subsequently, it became apparent that CD34 was shared by multiple lineages, being expressed on immature hematopoietic stem–progenitor cells, capillary endothelial cells, both embryonic and adult fibroblasts, and rare glial cells in nervous tissue. It is stage specific, rather than lineage specific, as demonstrated by the reconstruction of genealogies of clonally derived CD34 progeny [1–3, 6].

CD34 at the level of the extraglomerular or intraglomerular mesangium may signal either the presence of HSCs [7] or, conversely, may be a marker of transdifferentiation [4, 5]. According to Naruse, CD34 is more effective than alpha smooth muscle actin (SMA) in detecting transformation or activation of mesangial cells and in diagnosing mesangial proliferative glomerular diseases [4].

The presence of stem cells in either location does not automatically portend a good prognosis. For example, some forms of focal and segmental glomerulosclerosis (FSGS), IgA nephropathy, and systemic lupus erythematosus are stem cell disorders [8]; furthermore, FSGS has been transferred by means of HSCs that have localized to the extraglomerular mesangium in rodents [9, 10].

HSCs and the extraglomerular mesangium participate in regenerative processes at the level of the glomerulus and, thus, could be involved in pathological processes in GN.

Objectives

The aim of the study was to analyze the presence of CD34 at the level of the extraglomerular and intraglomerular mesangium and its relationship with histological markers of activity and chronicity, as well as with other immunohistochemical markers (alpha SMA, vimentin, and proliferating cell nuclear antigen (PCNA)) in GN.

Materials and methods

Subjects

A cross-sectional study of 36 patients hospitalized in the Division of Nephrology, University of Medicine and

Pharmacy "V. Babes" Timisoara, Romania during 2003–2004 was performed. Thirty-three of the patients had chronic GN, and three had rapidly progressive GN.

All patients underwent a thorough clinical examination (history, physical exam), diagnostic procedures (chest X-rays, electrocardiogram, abdominal ultrasound), and standard laboratory evaluation (complete blood count, erythrocyte sedimentation rate, fasting glucose levels, serum urea, serum creatinine, lipid profile, total serum protein levels with electrophoresis, liver enzymes, urinalysis, urinary protein excretion, and urine cultures) for their underlying disease. Patient examination was extended for diagnostic purposes and associated comorbidities on a case-by-case basis. Every attempt was made to rule out secondary diseases (malignancy, infection, or autoimmune disease) by ordering antinuclear antibodies, extractable nuclear antigen profile, lupus erythematosus cells, antineutrophil cytoplasmic antibody (ANCA; enzyme-linked immunosorbent assay and/or indirect immunofluorescence), C3, serum immunoglobulin levels, rheumatoid factor, Bence-Jones protein, and cryoglobulin test. All patients underwent percutaneous kidney biopsies after providing informed consent.

Histology

Routinely fixed and processed kidney sections were processed for light microscopy and stained with hematoxylin–eosin, periodic acid Schiff, and Gömöri's trichrome technique using routine methods.

Kidney biopsy evaluation

All biopsy specimens were assessed by two pathologists. Activity as expressed by the activity index and chronicity as expressed by the chronicity index were gauged according to a scoring system proposed by Neumann and coworkers [11] for ANCA-associated vasculitis based on the standardized scoring system for activity and chronicity developed for lupus nephritis. According to this scoring system, the glomeruli, tubuli, and vessels were independently assessed for inflammatory (active) and sclerotic–fibrotic (chronic) lesions.

The glomeruli were divided into eight segments, and each segment was evaluated for mesangial cell proliferation, intracapillary proliferation–infiltration, fibrinoid necrosis, extracapillary proliferation, mesangial matrix increase, segmental sclerosis, and fibrosed crescents–adhesions. The number of segments was employed to compute the percentage of glomeruli affected by the abovementioned abnormalities, and points were attributed as follows: 1 point was given for less than 20% involvement, 2 points for an involvement between 21% and 40%, 3 points for 41–60% involvement, 4 points for 61–80% involvement, and 5 points for 81–100% involvement.

At the tubulointerstitial level, inflammatory lesions (edema and interstitial infiltrate), and sclerotic–fibrotic lesions (interstitial fibrosis, tubular atrophy, and vascular hyalinosis–fibrosis) were assessed.

To evaluate the tubulointerstitial lesions, a semiquantitative scoring system was used as follows: 1 point was attributed for an involvement of less than 30% (mild) of the tubules or the interstitial area, 2 points for involvement between 31% and 60% (moderate), and 3 points for involvement in the 61–100% range (severe). Results were used to compute the activity index and chronicity index. Immunohistochemistry was graded for statistical evaluation using a semiquantitative intensity scale from 0 to 3 (absent, mild, moderate, intense). Only sections containing more than six glomeruli, estimated as optimal [12], were considered.

Immunohistochemistry

The detection of CD34, alpha SMA, vimentin, and PCNA was performed on 6-μm-thick, routinely formalin-fixed paraffin-embedded sections using the horseradish-peroxidase-labeled streptavidin–biotin (LSAB2-HRP) method. The primary antibodies used were: CD34 Class II (Clone QBEnd 10, 581, DAKO), monoclonal mouse anti-alpha-SMA (Clone 1A4, DAKO), monoclonal mouse antivimentin (Clone Vim 3B4, DAKO), and monoclonal mouse anti-PCNA (Clone PC10, DAKO). The LSAB2-HRP technique was employed as specified by the manufacturer's protocol. Briefly, sections were deparaffinized and rehydrated with distilled water, pretreated with Tris–ethylenediaminetetraacetic acid buffer (pH 9.0) until the temperature reached 95°C. (For vimentin, enzymatic digestion with the proteolytic enzyme RTU code 3007, DAKO was performed). The next step was serum blocking, followed by incubation with the primary antibodies diluted 1:50 for anti-CD34, 1:1,000 for anti-alpha-SMA, 1:400 for antivimentin, and 1:1,500 for anti-PCNA. Following peroxidase blocking, sections were incubated sequentially with a biotinylated secondary antibody and peroxidase-labeled streptavidin. Labeling was completed by incubating the sections with the chromogenic substrate solution 3-3′ diaminobenzidine (DAB). After this, sections were counterstained with Mayer's hematoxylin, rinsed in running tap water, and dehydrated. Sections were then cleared in two changes of toluene and mounted using Eukit.

Normal-appearing tissue from three patients who underwent nephrectomy for suspected kidney tumors was used as a control.

Statistical analysis

Statistical analysis was performed using the EpiInfo 6.04, Epi 3.2.2, and SPSS 10 packages and consisted in

Table 1 Histological and clinical diagnosis of the study subjects

Histological diagnosis	Clinical diagnosis	Number of patients
Crescentic GN	Rapidly progressive GN (two primary, one vasculitis)	3
Focal and segmental glomerulosclerosis	All primary	11
Membranous nephropathy	Four primary, one SLE	5
Mesangiocapillary GN	Lymphoma	1
Mesangial proliferative GN	All primary	11
Minimal change disease	All primary	5

computing the frequency counts and percentages for the qualitative variables, the means, medians, and standard deviations for the quantitative variables, and Spearman's rank correlation coefficient. We used Colton's [13] interpretation for Spearman's rank correlation coefficient as follows:

- 0–0.25 little or no correlation
- 0.25–0.5 fair degree of relationship
- 0.5–0.75 moderate to good correlation
- 0.75–1 very good to excellent correlation

A p value<0.05 was considered to be statistically significant.

Results

The mean age was 46.44±12.97 years with an age range of 18–74. Twenty-two patients were male and 14 were female. The clinicopathological diagnoses of the study subjects are shown in Table 1.

Regarding the underlying histopathological forms, a concomitant CD34 immunoreactivity in the extraglomerular mesangium and intraglomerular mesangium was observed in two cases of crescentic GN, three cases of FSGS, one case of membranous nephropathy (MN), three cases of mesangial proliferative glomerulonephritis (MPGN), and two cases of minimal change disease (MCD).

CD34 immunoexpression in the extraglomerular mesangium alone was found in three cases of FSGS and one case of MPGN.

CD34 immunostaining in the glomerular mesangium alone was observed in one case of FSGS, one case of MN, and one case of MCD.

Negative CD34 immunoreactivity in either compartment (extraglomerular mesangium or intraglomerular mesangium) was observed in three cases of FSGS, one case of MN, six cases of MPGN, one case of MCD, and in one case of mesangiocapillary GN.

The relationship between the immunohistochemical localization of CD34 in the extraglomerular and intraglomerular mesangium for the different histopathological forms is presented in Table 2.

CD34 immunohistochemical localization was observed in the endothelial cells of the glomerular capillary tuft, as well as in the endothelium of the other nephron vessels. CD34+ cells in the interstitium did not correlate with the investigated parameters. An analysis of CD34 at the level of the interstitium and endothelium is beyond the scope of this paper. We did not encounter CD34+ cells at tubular level.

An example of CD34 immunohistochemical localization is shown in Fig. 1 and at a higher magnification in Fig. 2.

Overall, across the entire group of 36 patients, Spearman's rank correlation coefficients between the immuno-

Table 2 Relationship between the immunohistochemical localization of CD34 in the extraglomerular and intraglomerular mesangium, detailed for each underlying histopathological form

Histopathological form	Both extraglomerular and intraglomerular mesangium	Extraglomerular mesangium only	Intraglomerular mesangium only	Neither compartment
Crescentic GN 2/3[a]	2	0	0	0
FSGS 10/11[a]	3	3	1	3
MN 3/5[a]	1	0	1	1
Mesangiocapillary GN 1/1[a]	0	0	0	1
Mesangial proliferative GN 10/11[a]	3	1	0	6
MCD 4/5[a]	2	0	1	1

[a] Extraglomerular mesangium visible on specimens

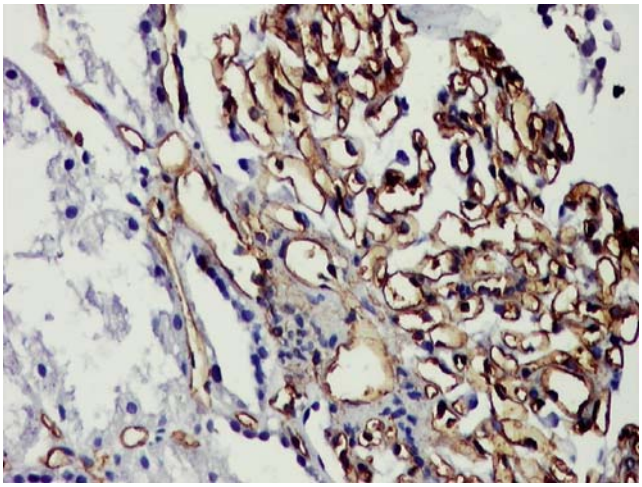

Fig. 1 Glomerulus with variable CD34-positive expression. Capillaries and rare cells of the vascular pole with CD34-positive staining. CD34 stain–LSAB2–DAB, ×200

histochemical CD34 expression and the main variables were as follows:

- CD34 intraglomerular mesangium and CD34 extraglomerular mesangium: $r=0.42$, $p>0.05$
- CD34 intraglomerular mesangium and alpha SMA intraglomerular mesangium: $r=0.09$, $p>0.05$
- CD34 intraglomerular mesangium and vimentin intraglomerular mesangium: $r=0.08$, $p>0.05$
- CD34 intraglomerular mesangium and PCNA intraglomerular mesangium: $r=0.22$, $p>0.05$
- CD34 intraglomerular mesangium and mesangial cell proliferation (%): $r=-0.27$, $p>0.05$
- CD34 intraglomerular mesangium and mesangial cell proliferation: $r=-0.27$, $p>0.05$

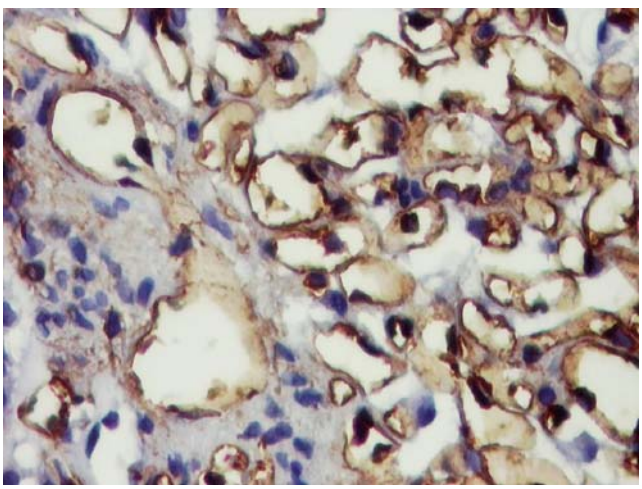

Fig. 2 Vascular pole with capillaries and scanty cells with CD34 positive staining. CD34 stain–LSAB2–DAB, ×400

- CD34 intraglomerular mesangium and mesangial matrix increase: $r=-0.13$, $p>0.05$
- CD34 intraglomerular mesangium and segmental sclerosis: $r=0.06$, $p>0.05$
- CD34 intraglomerular mesangium and interstitial fibrosis: $r=-0.002$, $p>0.05$
- CD34 intraglomerular mesangium and tubular atrophies: $r=-0.06$, $p>0.05$
- CD34 intraglomerular mesangium and activity index: $r=-0.005$, $p>0.05$
- CD34 intraglomerular mesangium and chronicity index: $r=-0.02$, $p>0.05$
- CD34 intraglomerular mesangium and serum creatinine: $r=-0.03$, $p>0.05$
- CD34 extraglomerular mesangium and alpha SMA extraglomerular mesangium: $r=0.35$, $p>0.05$
- CD34 extraglomerular mesangium and vimentin extraglomerular mesangium: $r=0.21$, $p>0.05$
- CD34 extraglomerular mesangium and PCNA extraglomerular mesangium: $r=0.33$, $p>0.05$.

Overall, across the entire group of 36 patients, Spearman's rank correlation coefficients and significances between the other studied variables were as follows:

- Activity index and serum creatinine: $r=0.69$, $p<0.05$
- Chronicity index and serum creatinine: $r=0.50$, $p<0.05$
- Interstitial fibrosis and serum creatinine: $r=0.44$, $p>0.05$
- Mesangial cell proliferation (%) and mesangial matrix increase: $r=0.57$, $p<0.05$
- Mesangial cell proliferation and mesangial matrix increase: $r=0.61$, $p<0.05$
- Mesangial cell proliferation (%) and serum creatinine: $r=0.11$, $p>0.05$
- Mesangial cell proliferation and serum creatinine: $r=0.15$, $p>0.05$
- Mesangial matrix increase and interstitial fibrosis: $r=0.46$, $p>0.05$
- Mesangial matrix increase and activity index: $r=0.56$, $p<0.05$
- Segmental sclerosis and serum creatinine: $r=0.31$, $p>0.05$
- Interstitial vimentin and interstitial alpha SMA: $r=0.64$, $p<0.05$.

Discussion

The most likely explanation for CD34 localization at the level of the extraglomerular and intraglomerular mesangium is either the presence of stem cells or cells that have undergone a process of transdifferentiation. The extraglomerular mesangium provides access to the intraglomerular

mesangium; thus, the reconstruction process of the intraglomerular mesangium could take place by any of the following: cells migrating from the extraglomerular mesangium into the intraglomerular mesangium [14, 15], bone-marrow-derived or local stem cells [16–21], or the division of mesangial cells [22].

The participation of extraglomerular mesangium cells in the reconstruction of the intraglomerular mesangium is well documented [14, 15]. Experimental studies in the anti-Thy 1.1. model of mesangial proliferative GN have shown that the intraglomerular mesangium is repopulated postlesion by mesangial-like cells that migrate from the extraglomerular mesangium at the level of the juxtaglomerular apparatus. These cells may contribute to the repair of the mesangial lesion [14, 15]. The reparative role of CD34 cells at the level of the glomerulus has been documented in a series of other studies [23–25]. Alternatively, transdifferentiation could start in the extraglomerular mesangium. At present, there is no single reliable marker of "stemness"[26], encumbering studies aimed at examining CD34 immunohistochemical localization.

In brief, CD34 immunoexpression at the level of the extraglomerular and intraglomerular mesangium could represent four distinct possibilities:

(a) Transdifferentiation in both the extraglomerular and the intraglomerular mesangium;
(b) Concomitant presence of stem cells in both compartments;
(c) Transdifferentiation and presence of stem cells in both locations or one process taking place in one location and the second in the other one;
(d) Transdifferentiation and presence of stem cells in one location, and absence of either process in the other one.

We found only a fair degree of relationship between CD34 immunoreactivity in the extraglomerular mesangium and CD34 immunoexpression in the intraglomerular mesangium, which did not reach statistical significance. CD34 cells could already have migrated from the extraglomerular mesangium into the intraglomerular mesangium by the time the biopsy was performed, or CD34 cells could represent transdifferentiated cells rather than stem cells. Regardless, a focus on the extraglomerular mesangium, given its strategic location, is warranted.

In contrast to Naruse, we did not find a relationship between CD34 and alpha SMA in the intraglomerular mesangium. According to Naruse, CD34 is more effective than alpha SMA in detecting transformation or activation of mesangial cells and diagnosing mesangial proliferative glomerular diseases [4].

Regarding the extraglomerular mesangium, a fair degree of relationship that did not reach statistical significance was observed between extraglomerular mesangium CD34 immunoreactivity and either extraglomerular mesangium alpha SMA or extraglomerular mesangium PCNA expression. No correlation was found between extraglomerular mesangium CD34 and extraglomerular mesangium vimentin. The usage of monoclonal anti-CD34 antibodies from a panel of antibodies (anti-alpha-SMA, antivimentin, anti-PCNA) did not provide any significant yield in our model. Further studies are needed to address the issue of CD34 immunohistochemical localization in the extraglomerular and intraglomerular mesangium.

We analyzed the relationship between CD34 in the intraglomerular mesangium and morphological indices evaluated by conventional stains according to a scoring system adapted from Neumann and between CD34 and other immunohistochemical markers (alpha SMA, vimentin, and PCNA). A fair degree of inverse relationship that did not reach statistical significance was observed between mesangial CD34 immunoexpression and mesangial cell proliferation. No correlations were found between CD34 immunoexpression in the intraglomerular mesangium and any of the following: intraglomerular mesangium alpha SMA, intraglomerular mesangium vimentin, intraglomerular mesangium PCNA, mesangial matrix increase, segmental sclerosis, interstitial fibrosis, tubular atrophies, activity index, chronicity index, or serum creatinine.

Our study illustrates the value of histological indices in the evaluation of glomerulonephritis. A good correlation was found between the activity index and serum creatinine, chronicity index and serum creatinine, mesangial cell proliferation and mesangial matrix increase, and mesangial matrix increase and activity index.

CD34 expression at vascular level was frequently ring-shaped. In the investigated GN patients, a loss of CD34 at the level of the glomerular and interstitial capillaries was evident in fibrotic lesions and was probably related to a loss of glomerular microvasculature and interstitial vasculopathy [27–34].

CD34-positive cells in the interstitium did not correlate with the investigated parameters. Okon, El Kossi, Baddour, and El Nahas described the CD34 marker on spindle-shaped and round cells in the interstitium of GN patients, while Iwano showed that bone-marrow-derived fibroblasts bear a CD34-negative phenotype [23, 35–38]. We did not encounter CD34-positive cells at tubular level. Data from several reports [17, 18, 39] suggested that HSCs have renotropic, multiplastic, and tubulogenic capacities and represent regenerative potential in acute kidney injury.

Conclusions

The concomitant expression of CD34 in the extraglomerular and intraglomerular mesangium could account for the extraglomerular site of origin of intraglomerular mesangial

cells. These would pass from one compartment into the other, as shown by Hugo et al. [14] and Haseley et al. [15].

The finding of CD34-positive cells could signal the presence of HSCs. Transdifferentiation of resident cells into a CD34-positive phenotype could represent an alternative explanation.

The concomitant expression of CD34-positive cells in the extraglomerular and intraglomerular mesangium warrants further study regarding the relationship between the two compartments in GN. We demonstrated the presence of the CD34 marker in the extraglomerular mesangium, which could be in relationship with transdifferentiated mesangial cells or with HSCs in the absence of blood vessels at this level. Our study shows the value of histological indices for evaluating GN but cannot assign significance to CD34 immunolabeling for the assessment of GN.

Acknowledgements Preliminary data from this study were presented in a poster session at the Congress of the European Society of Nephrology, European Dialysis, and Transplant Association, July, 2006, Glasgow, UK.

Conflict of interest statement We declare that we have no conflict of interest.

References

1. Goligorsky MS, Iijima K, Krivenko Y et al (1997) Role of mesangial cells in macula densa to afferent arteriole information transfer. Clin Exp Pharmacol Physiol 24(7):527–531
2. Nishio H, Tada J, Hashiyama M et al (1997) MC7. CD34 workshop panel report. In: Kishimoto T, Kitukani H, von dem Borne AEG et al (eds) Leucocyte typing VI. White cell differentiation antigens. Proceedings of the 6th International Workshop and Conference; 1996 Nov 10–14; Kobe, Japan. Garland Publishing Inc, New York, pp 974–976
3. Krause DS, Fackler MJ, Civin CI et al (1996) CD34: structure, biology and clinical utility (Review). Blood; 87:1–13
4. Naruse K, Fujieda M, Hayashi Y et al (1999) CD34 expression as a novel marker of transformed mesangial cells in biopsied glomerular diseases. J Pathology 189(1):105–111
5. Chebotareva NV, Proppe D, Rudolf P et al (2002) Clinical significance of expression of the smooth muscle-actin alpha and CD34 antigen in mesangial cells in glomerulonephritis (Article in Russian). Ter Arkh 74(6):27–31
6. Natkunam Y, Rouse R, Zhu S et al (2000) Immunoblot analysis of CD34 expression in histologically diverse neoplasms. Am J Pathol 156:21–27
7. Imasawa T, Utsunomiya Y, Kawamura T et al (2001) The potential of bone marrow-derived cells to differentiate into glomerular mesangial cells. J Am Soc Nephrol 12(7):1401–1409
8. Nishimura M, Toki J, Sugiura K et al (1994) Focal segmental glomerular sclerosis, a type of intractable chronic glomerulonephritis, is a stem cell disorder? J Exp Med 179(3):1053–1058
9. Cornacchia F, Fornoni A, Plati AR et al (2001) Glomerulosclerosis is transmitted by bone marrow-derived mesangial cell progenitors. J Clin Invest 108(11):1649–1656
10. Striker GE (2002) BM-derived progenitors deliver both their genotype and phenotype. Syllabus. ASN Renal Week; PGE Course: Advances in Cell and Molecular Biology: Integration with Renal Medicine. October 30–31, Philadelphia, Pennsylvania
11. Neumann I, Kain R, Regele H et al (2005) Histological and clinical predictors of early and late renal outcome in ANCA-associated vasculitis. Nephrol Dial Transpl 20(1):96–104
12. Davison A, Cameron JS, Grunfeld JP et al (eds) (2005) Oxford textbook of clinical nephrology. 3rd edn. Oxford University Press, Oxford, pp 169–182
13. Dawson B, Trapp RG (2004) Basic and clinical biostatistics. Lange, New York, p 48
14. Hugo C, Shankland SJ, Bowen-Pope DF et al (1997) Extraglomerular origin of the mesangial cell after injury. J Clin Invest 100(4):786–794
15. Haseley LA, Hugo C, Reidy MA et al (1999) Dissociation of mesangial cell migration and proliferation in experimental glomerulonephritis. Kidney Int 56:964–972
16. Poulsom R, Alison MR, Cook T et al (2003) Bone marrow stem cells contribute to healing of the kidney. J Am Soc Nephrol 14 (Suppl 1):S48–S54
17. Lin F, Cordes K, Li L et al (2003) Hematopoietic stem cells contribute to the regeneration of renal tubules after renal ischemia-reperfusion injury in mice. J Am Soc Nephrol 14:1188–1199
18. Lin F, Igarashi P (2003) Searching for stem/progenitor cells in the adult mouse kidney. J Am Soc Nephrol 14:3290–3292
19. Schena FP, Abbattista MR (2003) Stem cells: reparative medicine and nephrology (review). J Nephrol 16(Suppl 7):S1–S5
20. Ricardo SD, Deane JA (2005) Adult stem cells in renal injury and repair (review). Nephrology 10(3):276–282
21. Ito T (2003) Stem cells of the adult kidney:where are you from? Nephrol Dial Transplant 18(4):641–644
22. Julian B (2005) IgA Nephropathy. An update on pathogenesis. In: Clinical Nephrology Conferences. ASN Renal Week Philadelphia. Syllabus, pp 477–490
23. Baddour N, Adam AG, El Koraie AH et al (2002) The reparative role of stem cells in human glomerulonephritis. XXXIX Congress of the European Renal Association European Dialysis and Transplant Association July 14–17, 2002 Copenhagen Denmark. Nephrol Dial Transplant 17(Suppl 1):9–10 Abstracts
24. Guo J, Schedl A, Krause DS (2004) Bone marrow transplantation attenuates progression of mesangial sclerosis in mouse. In ASN Congress, October 27–November 1, 2004, St. Louis, MO SA FC 098 J Am Soc Nephrol Abstracts Issue
25. Yokoo T, Ohoshi Y, Utsunomiya Y et al (2003) Gene delivery using human cord blood-derived CD34+ cells into inflamed glomeruli in NOD/SCID mice. Kydney Int 64(1):102–109
26. Goligorsky MS, Rabelink T (2006) Meeting report: ISN forefronts in nephrology on endothelial biology and renal disease: from bench to prevention (review). Kidney Int 70(2):258–264
27. Kang DH, Kanellis J, Hugo C et al (2002) Role of the microvascular endothelium in progressive renal disease. J Am Soc Nephrol 13:806–816
28. Kitamura H, Shimizu A, Masuda Y et al (1998) Apoptosis in glomerular endothelial cells during the development of glomerulosclerosis in a remnant kidney model. Exp Nephrol 6:328–336
29. Ohashi R, Kitamura H, Yamanaka N (2000) Peritubular capillary injury during the progression of experimental glomerulonephritis in rats. J Am Soc Nephrol 11:47–56
30. Bottinger EP, Bitzer M (2002) TGF-beta signaling in renal disease. J Am Soc Nephrol 13:2600–2610
31. Wada Y, Morioka T, Oyanagi-Tanaka Y et al (2002) Impairment of vascular regeneration precedes progressive glomerulosclerosis in anti-Thy 1.1. glomerulonephritis. Kidney Int 61:432–443
32. Bohle A, Mackensen-Haen S, Wehrmann M (1996) Significance of postglomerular capillaries in the pathogenesis of chronic renal failure. Kidney Blood Press Res, 19(3–4):191–195

33. Remuzzi A, Gagliardini E, Sangalli F et al (2006) ACE inhibition reduces glomerulosclerosis and regenerates glomerular tissue in a model of progressive renal disease. Kidney Int 69(7):1124–1130 April (1)
34. Adamczak M, Gross ML, Amann K et al (2004) Reversal of glomerular lesions involves coordinated restructuring of glomerular microvasculature. J Am Soc Nephrol 15:3063–3072
35. Okon K, Szumera A, Kuzniewski M (2003) Are CD34+ cells found in renal interstitial fibrosis? Am J Nephrol 23(6):409–414
36. El Kossi MM, El Nahas AM (2003) Stem cell factor and crescentic glomerulonephritis. Am J Kidney Dis 41(4):785–795
37. El Nahas AM (2003) Plasticity of kidney cells: role in kidney remodeling and scarring. Kidney Int 64(5):1553–1465
38. Iwano M, Plieth D, Danoff TM et al (2002) Evidence that fibroblasts derive from epithelium during tissue fibrosis. J Clin Invest 110:341–350
39. Cantley LG (2005) Adult stem cells in the repair of the injured renal tubule (review). Nat Clin Prac Nephrol 1(1):22–32

Virchows Arch (2008) 453:329–338
DOI 10.1007/s00428-008-0653-2

ORIGINAL ARTICLE

Kidney biopsy findings in heterozygous Fabry disease females with early nephropathy

Carmen Valbuena · Elísio Carvalho · Manuela Bustorff · Mariana Ganhão · Sandra Relvas · Rosete Nogueira · Fátima Carneiro · João Paulo Oliveira

Received: 12 February 2008 / Revised: 9 July 2008 / Accepted: 7 August 2008 / Published online: 4 September 2008

Abstract Fabry disease is an X-linked glycosphingolipidosis caused by deficiency of alpha-galactosidase. Progressive chronic kidney disease (CKD) is a major cause of morbidity and mortality in males. Although 40% of heterozygous females may develop renal involvement, pathologic data on Fabry nephropathy in heterozygotes are scarce. We reviewed the kidney biopsies of four affected females who had normal to slightly sub-normal renal function, two of them with overt proteinuria. Chronic non-specific degenerative lesions and glycosphingolipid accumulation per cell type were semi-quantitatively assessed by light and electron microscopy. Cellular distribution of glycosphingolipid deposits was best assessed on semithin sections. Podocyte effacement was seen only in proteinuric patients. Combined analysis of our data with those of two earlier series showed that glomerular sclerosis and tubulointerstitial fibrosis are predictors of proteinuria and CKD stage. There was no histopathological evidence supporting a major role of vascular damage in the early pathogenesis of Fabry nephropathy in females.

Keywords Fabry disease · Heterozygous females · Kidney pathology

C. Valbuena · M. Ganhão · S. Relvas · F. Carneiro
Department of Pathology, Hospital São João,
Porto, Portugal

C. Valbuena · F. Carneiro
Department of Pathology, Faculty of Medicine,
University of Porto,
Porto, Portugal

E. Carvalho · M. Bustorff · J. P. Oliveira
Department of Nephrology, Hospital São João,
Porto, Portugal

R. Nogueira
Department of Pathology, Centro Hospitalar de Gaia,
Vila Nova de Gaia, Portugal

F. Carneiro
Department of Pathology,
Institute of Molecular Pathology and Immunology (IPATIMUP),
University of Porto,
Porto, Portugal

J. P. Oliveira
Department of Genetics, Faculty of Medicine, University of Porto,
Porto, Portugal

C. Valbuena (✉)
Serviço de Anatomia Patológica, Hospital São João,
Alameda Hernâni Monteiro,
4200-319 Porto, Portugal
e-mail: valbuena@med.up.pt

Introduction

Fabry disease is a rare X-linked lysosomal storage disease due to deficiency of α-galactosidase (αGal) enzyme activity. This metabolic defect results in multi-systemic accumulation of neutral glycosphingolipids with terminal α-galactosyl residues, predominantly globotriaosylceramide (Gb3) [1]. Complications of renal, cardiac and cerebrovascular involvement are the major causes of late morbidity and mortality [1–3].

The severity of clinical expression in males is inversely correlated with αGal residual activity and the classical phenotype of Fabry disease typically develops in individuals with <1% residual enzyme activity [2]. In these patients, chronic kidney disease (CKD) is an invariable complication, usually progressing to end-stage renal failure (ESRF) in the third to fifth decades of life. Low-grade proteinuria precedes deterioration of renal function in most cases, and the prevalence and degree of proteinuria increase

with CKD stage [4]. Before the availability of effective renal replacement therapies, ESRF was the main cause of death of classically affected patients [1, 2].

In females, the expression of Fabry disease is modulated by the effect of X chromosome inactivation [5] and the resulting proportions of normal and enzyme-deficient cells in individual organs. Heterozygous women may be completely asymptomatic or only have mild symptoms [1], but the majority ultimately develop substantial clinical manifestations [6, 7] and are at higher risk of premature death [8]. Evidence of renal involvement, including proteinuria and decreased renal function, may be found in up to 40% of known adult heterozygotes [4, 6]. A small proportion of female patients can be as severely affected as males with the classical phenotype [1, 9], reaching ESRF approximately at the same age [4].

The kidneys are major sites of glycosphingolipid deposition in Fabry disease and electron microscopy (EM) shows inclusions in all types of kidney cells, despite their normal appearance by conventional histology, even in patients with normal renal function and no proteinuria [10, 11]. As Gb3 deposits are dissolved by the paraffin-embedding procedure, the most characteristic finding on routine light microscopy (LM) of kidney biopsies is vacuolation of podocytes, of parietal epithelial cells and of Henle's loop and distal tubular cells [10, 12–14]. Mesangial widening, segmental and global glomerular sclerosis, tubular atrophy, interstitial fibrosis and other non-specific lesions are additionally seen, even at the early stages of Fabry disease nephropathy [10, 12, 13].

The sub-cellular mechanisms linking glycosphingolipid accumulation to the clinical manifestations of Fabry disease are not clearly understood. The main pathogenic theory of the classical phenotype assigns its complications predominantly to ischaemic tissue damage resulting from microvascular endothelial disease and/or necrosis of vascular smooth muscle cells and/or pericyte injury [1–3].

The development of proteinuria and of late-onset renal dysfunction in patients with the cardiac phenotypic variant, who have significant renal Gb3 deposits confined to podocytes [2, 15], suggests that these cells may have a role in the pathogenesis of Fabry nephropathy. Lethal injury to Gb3-overloaded podocytes, through the formation of focal adhesions between the glomerular tuft and the Bowman's capsule [12, 16], or increased hydraulic stress upon endothelial cells in the vicinity of damaged podocytes [17] are other possible mechanisms of glomerular sclerosis in Fabry nephropathy. By causing tubular injury, proteinuria has a direct role in CKD progression and may provide a link between the aforementioned primarily glomerular pathologic processes and the development of tubulointerstitial disease [18]. Mesangial cell necrosis [10], direct toxic injury to tubular cells [12] and diffuse involvement of interstitial cells [17] have also been suggested to be relevant in the pathogenesis of Fabry nephropathy progression.

Most of the current concepts and pathologic description of the Fabry nephropathy have been derived from autopsy and biopsy studies of affected males [19–24], but it has been recognised since long that affected females develop the same type of kidney lesions described in males [20, 25]. However, data on kidney pathology in heterozygous females are scarce and the largest published series describing kidney biopsy findings in affected females included only three [10] or five patients [13].

As in other chronic nephropathies, the progression of Fabry nephropathy is characterised by segmental and global glomerular sclerosis, tubular atrophy and interstitial fibrosis [10–14, 17]. In males, the presence of glomerular segmental or global sclerosis is the only significant pathologic association of proteinuria at early stages of Fabry nephropathy [10, 27]. Furthermore, negative correlations could be demonstrated between inulin clearance and LM composite scores of either chronic glomerular pathology or tubulointerstitial pathology [26, 27]. Contrastingly, a composite score of Gb3 inclusions did not correlate with either renal function or LM pathology scores [27]. Whether these findings also apply to females with Fabry disease is not known.

We have reviewed the kidney biopsies of four females with Fabry disease, with normal or mildly sub-normal renal function, using a specifically developed approach to assess Gb3 accumulation in different cell types and to quantify chronic non-specific degenerative lesions. The latter findings were combined with similar data of previously published series [10, 13] and correlated with proteinuria and renal function.

Subjects, materials and methods

Following approval by the institutional Health Ethics Board, retrospective clinical details and laboratory data were retrieved from each patient's hospital files. Hypertension was diagnosed and classified according to recommended criteria [28]. Serum creatinine (sCr) and proteinuria values reported as at the time of kidney biopsy were those obtained on protocol evaluation prior to the biopsy. Proteinuria was expressed as the concentration ratio of total protein to creatinine (mg/g) in routine 24-h urine samples. Glomerular filtration rate was estimated (eGFR) as the creatinine clearance calculated by the Cockcroft–Gault equation [29], adjusted for tubular creatinine secretion and normalised to the body surface area (BSA) of 1.73 m^2 [30, 31]. BSA was derived from height and weight [32]. CKD was staged by eGFR [33].

Leukocyte αGal activity was measured according to a standard method [34]. Mutations of the αGal gene (*GLA*)

were identified by amplifying all its seven exons and respective intronic boundaries, using routine polymerase chain reaction (PCR) methods, followed by automatic sequencing of each PCR amplicon.

Case summaries

Case 1 had proteinuria first detected on a routine medical checkup, at the age of 30 years. She was asymptomatic, reported no relevant past medical history and had normal blood pressure. Two of her brothers, followed elsewhere, had received kidney transplants as young adults, for ESRF attributed to "focal glomerular sclerosis". Her sCr was 0.8 mg/dl, proteinuria was quantified as 1,400 mg/day and the urine sediment was normal. A comprehensive diagnostic workup for proteinuria showed no abnormalities and an angiotensin-converting enzyme inhibitor (ACEI) was eventually prescribed. She stayed asymptomatic and normotensive but her sCr increased to 1.1 mg/dl and proteinuria reached nephrotic level (4.5 g/day) within 2 years of the first observation, prompting a diagnostic kidney biopsy.

The other three patients were known heterozygotes for Fabry disease and underwent kidney biopsy on protocol baseline evaluation for enzyme replacement therapy (ERT) with recombinant human αGal (agalsidase). Case 2, sister of case 1, was identified on family screening. Case 3 asked for genetic screening at the age of 48 years, after a maternal first cousin died with complications of Fabry disease. Two years before, she had been diagnosed stage 2 hypertension and medicated accordingly including with an ACEI. Case 4 was identified following the diagnosis of Fabry disease nephropathy in her two young adult sons. She was not aware of previous cases of CKD in the family.

Kidney biopsy procedure and processing

Tissue samples had all been obtained by percutaneous kidney biopsy according to routine clinical procedures [35, 36]. Two or three core samples were taken in each case, which were appropriately processed for LM, EM and immunofluorescence (IF) study, according to standard histopathology protocols [37, 38].

Fragments selected for LM were fixed in 10% buffered formalin, embedded in paraffin, and 3-μm thick serial sections were cut from the paraffin block and stained with haematoxylin and eosin, periodic acid Schiff and modified trichrome.

Fragments selected for EM were fixed in 3% glutaraldehyde, post-fixed in osmium tetroxide and embedded in epoxy resin (Epon™). Methylene blue or toluidine blue-stained 1-μm semithin (ST) sections were prepared from the Epon™ embedded fragments. Ultrathin sections (80 nm) for EM examination were stained with uranyl acetate and lead citrate. Photographs encompassing glomerular capillary loops and mesangial areas were taken at various magnifications.

Fragments selected for IF were snap-frozen in isopentane at −80°C. Tissue sections thereof were cut at 5 μm in a cryostat and processed for indirect IF staining, with a panel of antibodies directed to immunoglobulins (IgG, IgA, IgM), complement factors (C3, C1q) and fibrinogen.

Kidney biopsy reading, scoring and interpretation

Archive LM and ST slides, as well as IF and EM photographs, were reviewed by a single nephropathologist (CV). Available LM and ST slides were re-stained and/or new sections were prepared from the original paraffin blocks as needed. Counting of a minimum of ten "scorable glomeruli" was prerequisite for further biopsy reading. The total number of "scorable glomeruli" in each biopsy was the sum of the highest number counted in any of the conventional LM sections with the number counted in the ST section. Glomeruli showing less than three fourths of the Bowman's capsule circumference and void Bowman's capsules were not counted. In each case, two glomeruli were reviewed ultra-structurally.

The biopsies were read using standard criteria for glomerular, tubulointerstitial and vessel morphology evaluation [37–39]. The total numbers of scorable glomeruli showing segmental sclerosis or global sclerosis were counted and their proportions calculated for each biopsy. Interstitial fibrosis and tubular atrophy were estimated in LM sections as the proportion of cut section affected, scored to the nearest 5%.

Arterial sclerosis, arteriolar or arterial hyalinosis and hypertrophy of the smooth muscle layer of arteries and arterioles were recorded as present or absent in LM sections. Arterial sclerosis was further assessed according to the ratio of vessel wall thickness to lumen diameter [40].

Specific Fabry disease changes—i.e. vacuoles in LM sections, dark blue cytoplasmic inclusions in ST sections and electrondense osmiophilic intracellular deposits in EM (Fig. 1) [10, 11, 13, 24] —were recorded as present or absent in different types of glomerular, tubular, interstitial and vascular cells. The extension of glycosphingolipid accumulation was further graded in the ST sections according to the proportion of cells of the specified type that showed any deposits.

The histopathological findings were compared among the four patients and related to CKD progression and blood pressure history as well as to renal function and proteinuria at the time of biopsy. Furthermore, in an attempt to establish significant correlations between CKD stage and proteinuria level and specific LM histopathological parameters, we have statistically analysed our data in combination

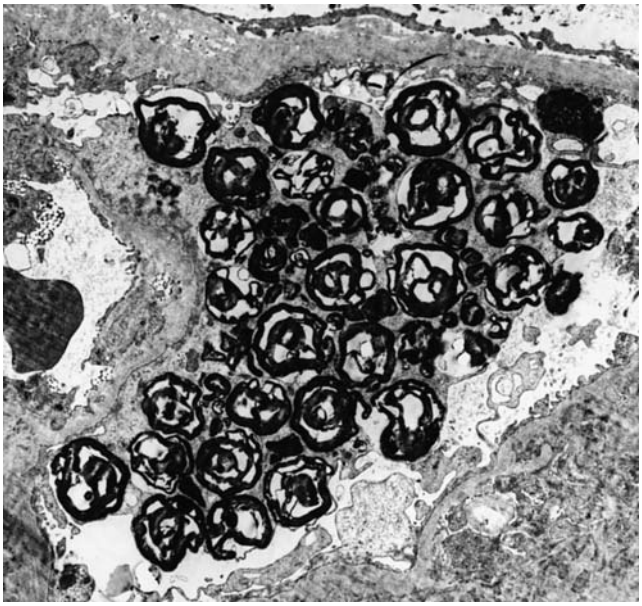

Fig. 1 Multiple large Gb3 inclusions in a podocyte, with the typical concentric lamellated ultra-structural appearance—"myelin figures" (case 1; EM, 1,800×3)

with those of previous series [10, 13]. Non-parametric correlations and stepwise regression analyses were performed with the SPSS for Windows® statistics software.

Results

Demographic and other relevant clinical and laboratory data of the four patients included in this study are shown in Table 1. Mutation p.R220X is known to cause the classical phenotype of Fabry disease [41]. Mutation p.239ΔI has not been previously described, but a deceased first cousin of case 3 had the classical Fabry disease phenotype. Although in case 4 no exonic *GLA* mutation was found and the pathogenic role of the double intronic molecular variants identified on sequence analysis is uncertain, her two sons, who share the same genotype, presented with the classical Fabry disease phenotype. In all cases, residual leukocyte αGal activity was between 30% to 35% of the normal mean. At the time of kidney biopsy, all patients had eGFR in the slightly sub-normal or the low normal range, but only in case 1 was a significant increase in sCr retrospectively documented. Overt proteinuria (>300 mg/day) was present in two patients (cases 1 and 2), reaching nephrotic level in case 1; cases 3 and 4 had proteinuria below 300 mg/day. Hypertension was diagnosed in a single patient (case 3) but two others had pre-hypertensive blood pressure levels.

All biopsies were of good quality and the minimum number of scorable glomeruli was 12 (Table 2). In case 3, the IF study was not performed.

Results of LM and ST assessment of chronic non-specific glomerular and tubulointerstitial lesions and of arteriolar and arterial lesions are respectively presented in Tables 2 and 3. The degrees of interstitial fibrosis, tubular atrophy and the percentage of sclerotic glomeruli seemed to correlate with eGFR, and the percentage of segmentally sclerotic glomeruli roughly correlated with the degree of proteinuria. The degrees of interstitial fibrosis and of tubular atrophy observed in each biopsy were identical in three of the patients. However, case 3 had a disproportionately higher degree of interstitial fibrosis; of note, she was the eldest patient in this series and the only one with systemic hypertension and hypercholesterolaemia. The presence of vascular hyalinisation and/or of medial hypertrophy did not appear to correlate with either renal function or proteinuria: these lesions were not observed in case 1, who had the severest renal involvement, with CKD progression, but were present in case 4, who had the mildest clinical presentation of Fabry nephropathy.

Podocyte and tubular cell vacuolation was a universal finding on conventional LM—although in case 1 (Fig. 2) and case 4 it was scarce and focally distributed. Vacuolated interstitial cells were observed only in case 1.

Assessment of Gb3 deposits in ST sections is summarised in Table 4. ST sections allowed a more accurate identification of glycosphingolipid deposits in glomerular (Fig. 3),

Table 1 Clinical and laboratory data at the time of kidney biopsy

Case	Age	Mutation	αGal (L)	sCr	eGFR	uProt/Cr	Urine sediment	BP status	Medication
1	32y	p.R220X	20	1.1	74	2,002	Normal	Pre-hypertension	ACEI, OC
2	45y	p.R220X	18	0.9	79	721	E=27.6/μl, L=22.3/μl[b]	Pre-hypertension	
3	50y	p.239ΔI	20	0.9	76	184	Normal	Hypertension, stage 1	TD, ACEI, S, OC
4	42y	Intronic[a]	18	0.7	92	139	Normal	Normal	

Age in full years

BMI body mass index, in kg per square meter, *αGal (L)* α-galactosidase residual activity in leukocytes (normal laboratory range, 36–80 nMol/h/mg), *sCr* serum creatinine, in mg/dl, *eGFR* estimated glomerular filtration rate, in ml/min/1.73 m^2, *uProt/Cr* urine total protein to creatinine concentration ratio, in mg/g, *BP* blood pressure, *E* erythrocytes, *L* leukocytes, *ACEI* angiotensin-converting enzyme inhibitor, *TD* thiazide diuretic, *S* statin, *OC* oral contraceptive

[a] Intronic *GLA* mutations: IVS4+1703A→G/IVS6+249C→T

[b] Erythrocytes/leukocytes; as counted by flow cytometry (normal values—E<27.1/μl, L<20.5/μl)

Table 2 Glomerular global and focal sclerosis and chronic non-specific tubulointerstitial lesions

Histological parameter	Cases			
	1	2	3	4
Conventional light-microscopy sections				
Number of glomeruli, *N*	7	17	13	17
Glomeruli with global sclerosis, *N* (%)	3 (43%)	0	2 (15%)	1 (6%)
Glomeruli with focal sclerosis, *N* (%)	3 (43%)	5 (29%)	2 (15%)	1 (6%)
Tubular atrophy, %[a]	30%	10%	5%	5%
Interstitial fibrosis, %[a]	30%	10%	20%	5%
Semithin sections				
Number of glomeruli, *N*	5	12	4	14
Glomeruli with global sclerosis, *N* (%)	1 (20%)	1 (8%)	0	0
Glomeruli with focal sclerosis, *N* (%)	2 (40%)	1 (8%)	0	0
Combined LM + ST total				
Number of glomeruli, *N*	12	29	17	31
Glomeruli with global sclerosis, *N* (%)	4 (33%)	1 (3%)	2 (12%)	1 (3%)
Glomeruli with focal sclerosis, *N* (%)	5 (42%)	6 (21%)	2 (12%)	1 (3%)
Glomeruli with any sclerosis, *N* (%)	9 (75%)	7 (24%)	4 (24%)	2 (6%)

LM light microscopy, *ST* semithin

[a] Tubular atrophy and interstitial fibrosis were estimated to the nearest 5%, by assessing the relative degree of involvement in each cortical field, at ×200 magnification, and averaging all available fields

interstitial and capillary endothelial cells (Fig. 4) and disclosed the presence of Gb3 deposits in cells without apparent vacuolation on conventional LM sections. The extension of glycosphingolipid deposition did not seem to correlate with the patient's age in none of the cell types analysed. Glomerular parietal epithelial cells were the most extensively affected in all cases, with more than one third of these cells showing at least one toluidine blue-stained deposit in ST sections. Podocytes, vascular smooth muscle cells and distal tubular cells were also involved in all cases. Distal tubules were affected in all cases but not all distal tubules were affected nor did every cell in affected distal tubules have Gb3 deposits (Fig. 5). The extension of

Table 3 Arteriolar and arterial lesions (light-microscopy sections)

Histological parameter	Cases			
	1	2	3	4
Hyalinisation	No	No	Yes	Yes
Intimal fibrosis	No	No	+++[a]	No
Hypertrophy of muscle layer	No	No	Yes	Yes

[a] Graded according to the criteria of Remuzzi et al. [40]

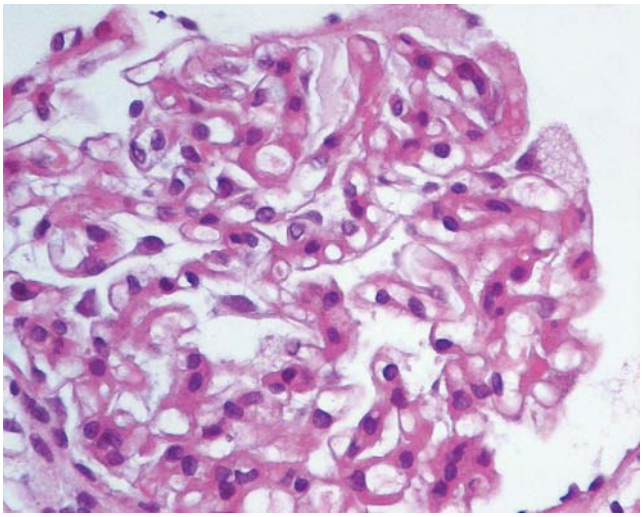

Fig. 2 Cytoplasmic vacuolation observed in a single podocyte (case 1; LM, haematoxylin and eosin, ×200)—in fact, this was the sole vacuolated podocyte observed in the entire biopsy

podocyte glycosphingolipid deposition in ST sections was broadly related with the degree of proteinuria: only the two patients with baseline proteinuria/creatinine concentration ratio above 500 mg/g had more than one third of podocytes affected. Furthermore, glomerular endothelial and proximal tubular cell deposits were exclusively seen in these two patients with moderate to severe proteinuria, who also showed the highest degrees of vascular smooth muscle cell involvement. Involvement of interstitial cells was a distinctive histological feature in case 1 (Fig. 4), who had the severest presentation of Fabry nephropathy, including

Table 4 Fabry disease intracellular glycosphingolipid inclusions as assessed in semithin sections under light microscopy

Cell types	Cases			
	1	2	3	4
Podocytes	++	++	+	+
Parietal glomerular cells	+++	++	+++	+++
Mesangial cells	+	+	+	0
Glomerular endothelial cells	+	+	0	0
Proximal tubular cells	+	+	0	0
Distal tubular cells	+++	+	+	+
Arterial endothelial cells	++	+	−	−
Arteriolar endothelial cells	0	0	+	0
Vascular smooth muscle cells	+++	+++	+	++
Vascular fibroblasts	++	+++	−	0
Peritubular capillary cells	++	0	+	+[a]
Interstitial cells	++	0	0	0

0 No deposits, + deposits present in few cells (according to the tertiles of the proportion of affected cells), ++ deposits present in some cells (according to the tertiles of the proportion of affected cells), +++ deposits present in many cells (according to the tertiles of the proportion of affected cells), − cell type not sampled

[a] Limited to a single vessel

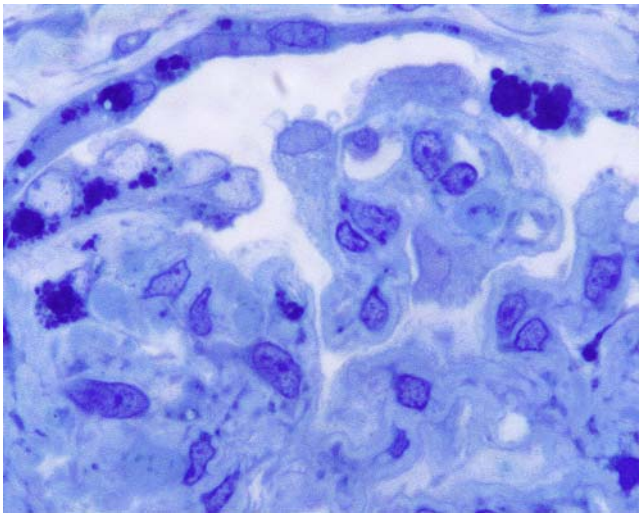

Fig. 3 Gb3 deposits in glomerular parietal and visceral epithelial cells (case 1; ST section, methylene blue-stained, ×400)

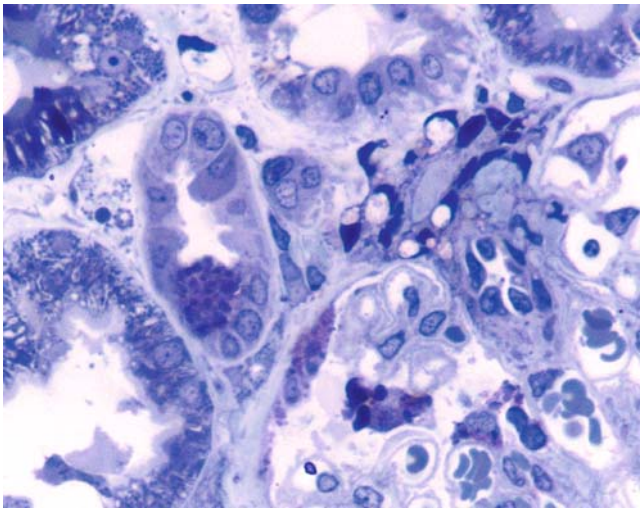

Fig. 5 Heavy Gb3 storage is visible in a single cell of a distal tubule (case 3; ST section, toluidine blue-stained, ×200)

nephrotic proteinuria and a significant increase in sCr along a short-term follow-up period. This patient also showed the highest degree of distal tubular as well as of peritubular capillary cell involvement. Case 4, who had normal renal function and minimal proteinuria, had relatively extensive vascular smooth muscle cell involvement.

EM features are shown in Table 5. EM revealed small glycosphingolipid deposits within mesangial cells in case 4 and within glomerular endothelial cells in cases 3 and 4, two cell types that seemed uninvolved in the corresponding ST sections. Podocyte effacement (Fig. 6) was a morphological feature in the two patients with moderate (case 2) or severe (case 1) proteinuria and was not seen in the remaining two patients, who had milder degrees of proteinuria. Additional notable EM findings in case 4 were the presence of extracellular membranofibrillary deposits in the mesangium (Fig. 7), as well as of electrondense immune deposits in sub-endothelial and mesangial location. The latter one stained intensively with IgA anti-serum in IF study. None of the other patients had immune deposits seen in EM or a positive IF study.

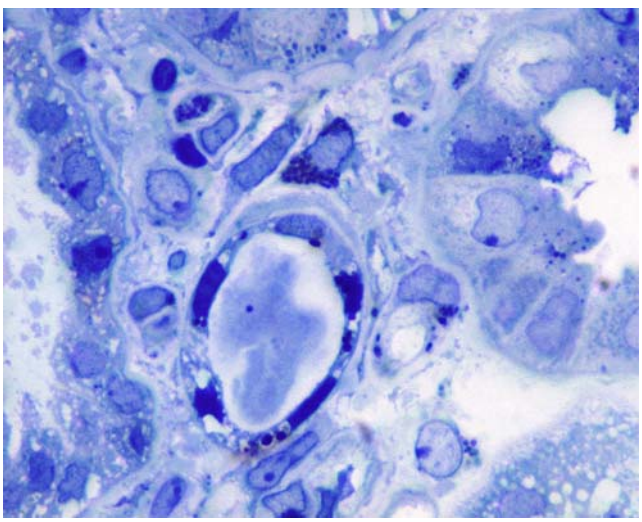

Fig. 4 Gb3 deposits in interstitial, peritubular capillary endothelial and tubular epithelial cells (case 1; ST section, methylene blue-stained, ×200)

Table 6 combines clinical and histopathological data of our patients and of those of previously reported series [10, 13]. Statistical analyses of these data demonstrated highly significant correlations ($p<0.005$) between proteinuria and glomerular sclerosis, between CKD stage and glomerular sclerosis and tubulointerstitial fibrosis, as well as between glomerular sclerosis and tubulointerstitial fibrosis. On stepwise logistic regression, glomerular sclerosis emerged as the most important predictor of proteinuria ($R^2=0.76$; $p<0.0005$), while tubulointerstitial fibrosis was the most important predictor of CKD stage ($R^2=0.69$; $p=0.002$).

Table 5 Non-specific cell lesions and intracellular glycosphingolipid deposits as assessed by electron microscopy

Cell types	Cases			
	1	2	3	4
Non-specific lesions				
Podocyte effacement	Focal	Focal	No	No
Osmiophilic intracellular deposits				
Podocytes	+	++	++	++
Parietal glomerular cells	++	+++	+++	+
Mesangial cells	+	+	+	+
Glomerular endothelial cells	+	+	+	+

+ Deposits present in few cells (according to the tertiles of the percentage of affected cells), ++ deposits present in some cells (according to the tertiles of the percentage of affected cells), +++ deposits present in many cells (according to the tertiles of the percentage of affected cells)

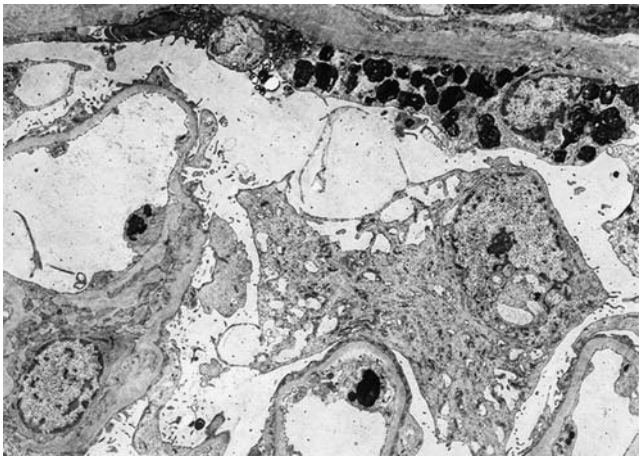

Fig. 6 Focal areas of podocyte effacement; amorphous Gb3 deposits are visible in glomerular parietal epithelial cells and in endothelial cells (case 2; EM, 1,800×3)

Discussion

To compare the severity of the kidney lesions observed in our patients and to identify meaningful clinicopathologic correlations, we defined a set of histopathologic and ultra-structural criteria for systematic reading and semi-quantification of glomerular, tubulointerstitial and vascular lesions, as well as the burden of glycosphingolipid accumulation in each kidney cell type. The items selected for biopsy reading and scoring were based on clinicopathologic correlations derived from published biopsy series [10, 13, 26] and on the hypotheses regarding the involvement of different types of cells on the pathogenesis of Fabry nephropathy [2, 10, 12, 17].

In clinical trials of agalsidases, the effect of ERT on the kidney was assessed by protocol repeat biopsies, but the scoring systems used in those settings [26, 42–44] were specifically designed to quantify treatment-induced changes and are not useful for broader general use. The usefulness of protocol kidney biopsies and of a scoring system to evaluate histologic markers of progressive Fabry nephropathy has been formerly suggested [12, 45], and a clinically oriented scoring system for quantitative analysis of kidney biopsies of patients with Fabry disease is currently undergoing validation [27].

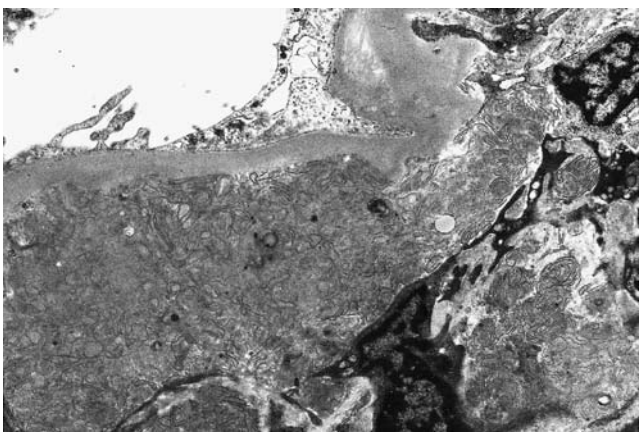

Fig. 7 Mesangial membranofibrillary deposits in sub-endothelial location (case 4; EM, 2,700×3)

Assessment of chronic non-specific glomerular and tubulointerstitial degenerative lesions

We searched for clinicopathologic correlations of chronic non-specific glomerular and tubulointerstitial lesions using the data shown in Table 6. In these 12 patients, the clinical expression of Fabry nephropathy as related to age is in accordance with cross-sectional data from a worldwide Fabry disease registry [4]. The series reported by Gubler et al. [10] included a child with very mild disease and an asymptomatic young adult without any pathologic evidence of Fabry nephropathy. Contrastingly, all females reported by Fischer et al. [13] had clinically severe nephropathy and the youngest patient in their series was 30 years old. In our patients, the severity of clinical expression of Fabry nephropathy stands between that of the two former series. The overall results of our statistical analyses of these data are entirely concordant with previous findings in males [27].

Assessment of arterial and arteriolar degenerative lesions

In our patients, the severity of the clinical expression of Fabry nephropathy or the degrees of interstitial fibrosis, tubular atrophy or glomerular sclerosis did not relate to the presence of intimal fibrosis, vascular hyalinosis or hypertrophy of the muscle layer (Tables 2 and 3). None of those vascular lesions were observed in case 1, who had the severest renal involvement and CKD progression, but were present in case 4, who had the mildest clinical presentation of Fabry nephropathy. Only case 3 had atherosclerotic intimal vascular lesions, in agreement with her clinical history of systemic hypertension and high serum cholesterol levels [46]. Non-concordant tubulointerstitial fibrosis and tubular atrophy scorings (20% vs. 5%, respectively) were the exclusive findings in this latter patient. A possible explanation could be the combined effects of hypertension and hypercholesterolaemia [46]. However, in patients with benign as well as malignant hypertensive nephrosclerosis, the degree of tubular atrophy has been reported to be higher than the degree of interstitial fibrosis [47].

Assessment of intracellular glycosphingolipid accumulation

Although usually referred to as a distinctive sign of Fabry nephropathy [10–14], diffuse cytoplasmic vacuolation of

Table 6 Comparison of the three largest kidney biopsy series reporting pathology findings in females with Fabry disease

	Gubler et al. [10]			Fischer et al. [13]					Present series			
Age at kidney biopsy (years)	8	22	51	30	37	54	55	73	32	42	45	50
CKD stage	0	0	2	?	2	4	5	4	2	1	2	2
Proteinuria	0	0	0	+++	+++	+++	++++	++++	++++	++	0	0
No. of evaluated glomeruli	8	15	25	2	4	17	23	5	12	31	29	17
No. of sclerotic glomeruli	0	0	5	1	2	17	22	3	9	2	7	4
% of sclerotic glomeruli	0%	0%	20%	50%	50%	100%	96%	60%	75%	31%	24%	24%
Tubular atrophy/interstitial fibrosis	0	0	+	0	+	++	+++	+	+/++	+	+	+

No. of sclerotic glomeruli is the total number of evaluated glomeruli that showed either segmental or global sclerosis. CKD stages: 0—no evidence of kidney disease, 1—eGFR≥90 ml/min/1.73 m^2, 2—eGFR=89–60 ml/min/1.73 m^2, 3—eGFR=59–30 ml/min/1.73 m^2, 4—eGFR=29–15 ml/min/1.73 m^2, 5—eGFR<15 ml/min/1.73 m^2. Proteinuria was graded as: 0=no overt proteinuria, +=0.3–0.5 /day, ++=0.5–1.0 g/day, +++=1.0–3.5 g/day, ++++≥3.5 g/day. Tubular atrophy/interstitial fibrosis graded as: 0=absent, +=mild, ++=moderate, +++=severe

podocytes and tubular cells was not evident in some of our patients and also was not related to the amount or the volume of Gb3 deposits, as evaluated on the ST sections (Figs. 2 and 3). As patchy cytoplasmic vacuolation of glomerular and tubular cells is a non-specific kidney pathology feature of massive proteinuria and Alport syndrome [48, 49], its diagnostic value for Fabry nephropathy in females is limited.

In line with Gubler et al. findings in male patients [10], EM showed the presence of Gb3 deposits in every glomerular cell type, even in those that seemed to be spared on ST sections. This disparity is most probably dependent on the size of the Gb3 deposits, which would be below the resolution of the light microscope in the apparently unaffected cells on the ST sections. Comparing data on Tables 4 and 5 for differences between EM and ST findings in the glomeruli, the semi-quantification of Gb3 deposits on ST sections seemed to be better related with the degree of proteinuria. In addition, the absence of deposits in mesangial cells and in glomerular endothelial cells was a feature exclusive of the patient with the mildest clinical expression of Fabry nephropathy.

In our patients, the epithelial cells of the Bowman's capsule showed the severest burden of Gb3 accumulation of all kidney cell types, as seen in ST as well as in EM evaluation. This finding is consistent with a recent report describing the presence of Gb3 deposits in 84% of glomerular parietal epithelial cells, as compared to only 42% of podocytes, in the ultra-structural study of the kidney biopsies of two affected sisters [50]. However, it is at odds with the more traditional view that podocytes are the earliest and most severely affected kidney cells in Fabry nephropathy, with the epithelial cells of Bowman's capsule becoming involved as the disease progresses [10–14]. Therefore, it might be speculated that predominant involvement of glomerular parietal as compared to glomerular visceral epithelial cells is a singular feature of Fabry nephropathy in females.

Tubular involvement was expected at the early stages of Fabry nephropathy [10–14]. Distal tubules were affected heterogeneously in all cases (Fig. 5). Although in females this could be the histological expression of X chromosome inactivation, as suggested before as an explanation for similar biopsy findings [10], this same pattern of distal tubular Gb3 storage has also been described in biopsies of affected males [10]. In proximal tubules, Gb3 deposits were exclusively observed in the two patients with overt proteinuria.

The finding of Gb3 deposits on peritubular capillaries grossly related to the clinical severity of Fabry nephropathy but did not correlate with the vascular arteriolar or arterial lesions and, in contrast to previous observations [51], did seem to occur as an early pathologic event. Although clearance of peritubular capillary Gb3 deposits in serial kidney biopsies has been used as a marker of ERT efficiency [44], the pathophysiologic relevance of this treatment outcome needs further demonstration.

Involvement of interstitial cells was seen only in case 1, who had the severest clinical and pathological expression of Fabry nephropathy. Thus, it might be speculated that Gb3-related interstitial cell damage could somehow contribute to, or be an aggravating factor of, the tubulointerstitial fibrosis seen in kidney biopsies of patients with Fabry disease, even before significant deterioration of renal function has occurred.

Additional findings

Podocyte effacement was apparent on EM sections only in the two patients with overt proteinuria, an observation that is consistent with previous data [10, 13] and adds to the hypothesis that in the early stages of Fabry nephropathy, the relative preservation of the fine structures of the podocyte foot processes and of the slit diaphragms is a major determinant of the amount of proteinuria [11, 14]. The membranofibrillary deposits observed in case 4 were

identical to those already described by Gubler et al. [10] and by Fischer et al. [13] in hemizygous males and might be the remnants of Gb3 inclusions of dead cells. We postulate that the rupture of Gb3 overloaded lysosomes into the cytoplasm of affected cells could be a crucial event leading to cell death. In podocytes and parietal glomerular epithelial cells, this would eventually set in motion the pathogenic cascade that ultimately result in focal adhesions of the glomerular tuft to the Bowman's capsule, synechiae and focal segmental sclerosis [52–55].

Mesangial deposition of IgA in case 4 was totally asymptomatic. Clinically overt IgA nephropathy has been reported as a coincidental diagnosis in males [56] as well as in females [57, 58] with Fabry disease, but in recently reported series, asymptomatic IgA deposits were identified in about 15% of patients [44, 59], a frequency that is significantly higher than in non-selected autopsy cases [60]. This may not be merely coincidental [57] and deserve further study.

In conclusion, despite the potential confounding effect of X chromosome inactivation, the overall findings in kidney biopsies of females with Fabry disease are not significantly different from those described in males, validating kidney biopsy as an important diagnostic tool for Fabry nephropathy also in heterozygotes. The more robust pathological predictors of proteinuria and CKD stage are non-specific chronic lesions identified in LM, respectively glomerular sclerosis and tubulointerstitial fibrosis. The cellular distribution and the burden of Gb3 accumulation per cell type are best determined in ST sections. Finally, in our series of patients, we could not find evidence supporting a major role of vascular damage in the early pathogenesis of Fabry nephropathy in females. Instead, we suggest that damage to visceral and parietal glomerular epithelial cells may be more relevant at this stage.

Acknowledgements Carmen Valbuena and João Paulo Oliveira were equal contributors to this article. Carmen Valbuena is recipient of a non-restricted research grant from Genzyme Portugal. David G. Warnock provided encouragement and strongly supported this project.

Conflict of interest statement The authors declare that they have no conflict of interest.

References

1. Desnick RJ, Ioannou YA, Eng CM (2001) α-Galactosidase A deficiency: Fabry disease. In: Scriver CR, Beaudet AL, Sly WS et al (eds) The metabolic and molecular bases of inherited disease. 8th edn. McGraw Hill, New York, pp 3733–3774
2. Desnick RJ, Wasserstein MP, Banikazemi M (2001) Fabry disease (α-Galactosidase A deficiency): renal involvement and enzyme replacement therapy. In: Schieppati A, Daina E, Sessa A, Remuzzi G (eds) Rare kidney diseases (contributions to nephrology, vol 136). Karger, Basel, pp 174–192
3. Desnick RJ, Brady R, Barranger J et al (2003) Fabry disease, an under-recognized multisystemic disorder: expert recommendations for diagnosis, management, and enzyme replacement therapy. Ann Intern Med 138:338–346
4. Ortiz A, Oliveira JP, Waldek S et al (2008) Nephropathy in males and females with Fabry disease: cross-sectional description of patients before treatment with enzyme replacement therapy. Nephrol Dial Transplant 23:1600–1607
5. Lyon MF (1962) Sex chromatin and gene action in the mammalian X chromosome. Am J Hum Genet 14:135–418
6. Deegan PB, Baehner AF, Barba Romero M-Á et al (2006) Natural history of Fabry disease in females in the Fabry outcome survey. J Med Genet 43:347–352
7. Wilcox WR, Oliveira JP, Hopkin RJ et al (2008) Females with Fabry disease frequently have major organ involvement: lessons from the Fabry registry. Mol Genet Metab 93:112–128
8. MacDermot KD, Holmes A, Miners AH (2001) Anderson–Fabry disease: clinical manifestations and impact of disease in a cohort of 60 obligate carrier females [Letter]. J Med Genet 38:769–775
9. Thadhani R, Wolf M, West ML et al (2002) Patients with Fabry disease on dialysis in the United States. Kidney Int 61:249–255
10. Gubler M-C, Lenoir G, Grünfeld J-P et al (1978) Early renal changes in hemizygous and heterozygous patients with Fabry's disease. Kidney Int 13:223–235
11. Sessa A, Tosoni A, Nebuloni M et al (2002) Renal ultrastructural findings in Anderson–Fabry disease. J Nephrol 15:109–112
12. Alroy J, Sabnis S, Kopp JB (2002) Renal pathology in Fabry disease. J Am Soc Nephrol 13:S134–S138
13. Fischer EG, Moore MJ, Lager DJ (2006) Fabry disease: a morphologic study of 11 cases. Mod Path 19:1295–1301
14. Sessa A, Meroni M, Battini G et al (2003) Renal involvement in Anderson–Fabry disease. J Nephrol 16:310–313
15. Meehan SM, Junsanto T, Rydel JJ, Desnick RJ (2004) Fabry disease: renal involvement limited to podocyte pathology and proteinuria in a septuagenarian cardiac variant. Pathologic and therapeutic implications. Am J Kidney Dis 43:164–171
16. Warnock DG (2005) Fabry disease: diagnosis and management, with emphasis on the renal manifestations. Curr Opin Nephrol Hypertens 14:87–95
17. Sessa A, Meroni M, Battini G et al (2003) Evolution of renal pathology in Fabry disease. Acta Paediatr Suppl 443:6–8
18. Palmer BF (2007) Proteinuria as a therapeutic target in patients with chronic kidney disease. Am J Nephrol 27:287–293
19. Pompen AWM, Ruiter M, Wyers HJG (1947) Angiokeratoma corporis diffusum (universale) Fabry, as a sign of an unknown internal disease; two autopsy reports. Acta Med Scand 128:234–255
20. Colley JR, Miller DL, Hutt MSR et al (1958) The renal lesion in angiokeratoma corporis diffusum. Brit M J 1:1266–1268
21. Bethune JE, Landrigan PL, Chipman CD (1961) Angiokeratoma corporis diffusum universale (Fabry's disease) in two brothers. New Engl J Med 264:1280–1285
22. Henry EW, Rally CR (1963) The renal lesion in angiokeratoma corporis diffusum (Fabry's disease). Can Med Assoc J 89:206–213
23. Groot WP (1964) Angiokeratoma corporis diffusum Fabry (Thesaurismosis hereditaria Ruiter–Pompen–Wyers). Dermatologica 128:321–349
24. Hartley MW, Miller RE, Dempsey HJ, Carroll JF (1964) Dysphospholipidosis in Fabry's disease: a light and electron microscopic study. Ala J Med Sci 1:361–367
25. Burda CD, Winder PR (1967) Angiokeratoma corporis diffusum universale (Fabry's disease) in female subjects. Am J Med 42:293–301

26. Branton MH, Schiffmann R, Sabnis SG et al (2002) Natural history of Fabry renal disease: influence of alpha-galactosidase A activity and genetic mutations on clinical course. Medicine (Baltimore) 81:122–138
27. Oliveira JP (2007) Staging of Fabry disease using renal biopsies. Clin Ther 29(Suppl A):S15–S16
28. Chobanian AV, Bakris GL, Black HR et al (2003) Seventh report of the joint national committee on prevention, detection, evaluation, and treatment of high blood pressure. Hypertension 42:1206–1252
29. Cockcroft DW, Gault MH (1976) Prediction of creatinine clearance from serum creatinine. Nephron 16:31–41
30. Rule AD, Larson TS, Bergstralh EJ et al (2004) Using serum creatinine to estimate glomerular filtration rate: accuracy in good health and in chronic kidney disease. Ann Intern Med 141:929–937
31. Vervoort G, Willems HL, Wetzels JFM (2002) Assessment of glomerular filtration rate in healthy subjects and normoalbuminuric diabetic patients: validity of a new (MDRD) prediction equation. Nephrol Dial Transplant 17:1909–1913
32. Gehan EA, George SL (1970) Estimation of human body surface area from height and weight. Cancer Chemother Rep 54:225–235
33. National Kidney Foundation (2002) K/DOQI clinical practice guidelines for chronic kidney disease: evaluation, classification and stratification. Am J Kidney Dis 39(Suppl.1):S1–S266
34. Desnick RJ, Allen KY, Desnick SJ et al (1973) Fabry's disease: enzymatic diagnosis of hemizygotes and heterozygotes. Alpha-galactosidase activities in plasma, serum, urine, and leukocytes. J Lab Clin Med 81:157–171
35. Wiseman DA, Hawkins R, Numerow LM, Taub KJ (1990) Percutaneous renal biopsy utilizing real time, ultrasonic guidance and a semiautomated biopsy device. Kidney Int 38:347–349
36. Whittier WL, Korbet SM (2004) Renal biopsy: update. Curr Opin Nephrol Hypertens 13:661–665
37. Furness PN (2000) ACP best practice No 160: renal biopsy specimens. J Clin Pathol 53:433–438
38. Walker PD, Cavallo T, Bonsib SM, Ad Hoc Committee on Renal Biopsy Guidelines of the Renal Pathology Society (2004) Practice guidelines for the renal biopsy. Mod Path 17:1555–1563
39. Sternberg SS (ed) (1992) Histology for pathologists. Raven, New York
40. Remuzzi G, Grinyò J, Ruggenenti P et al (1999) Early experience with dual kidney transplantation in adults using expanded donor criteria. J Am Soc Nephrol 10:2591–2598
41. Meaney C, Blanch LC, Morris CP (1994) A nonsense mutation (R220X) in the α-galactosidase A gene detected in a female carrier of Fabry disease. Hum Mol Genet 3:1019–1020
42. Eng CM, Guffon N, Wilcox WR et al (2001) Safety and efficacy of recombinant human alpha-galactosidase A-replacement therapy in Fabry's disease. N Engl J Med 345:9–16
43. Schiffmann R, Kopp JB, Austin HA 3rd et al (2001) Enzyme replacement therapy in Fabry disease: a randomized controlled trial. JAMA 285:2743–2749
44. Thurberg BL, Rennke H, Colvin RB et al (2002) Globotriaosylceramide accumulation in the Fabry kidney is cleared from multiple cell types after enzyme replacement therapy. Kidney Int 62:1933–1946
45. Svarstad E, Bostad L, Kaarbøe O et al (2005) Focal and segmental glomerular sclerosis (FSGS) in a man and a woman with Fabry's disease. Clin Nephrol 63:394–401
46. Chade AR, Lerman A, Lerman OL (2005) Kidney in early atherosclerosis. Hypertension 45:1042–1049
47. Caetano ERSP, Zatz R, Saldanha LB, Praxedes JN (2001) Hypertensive nephrosclerosis as a relevant cause of chronic renal failure. Hypertension 38:171–176
48. Olson JL, Schwartz MM (1998) The nephrotic syndrome: minimal change disease, focal segmental glomerulosclerosis, and miscellaneous causes. In: Jennette JC, Olson JL, Schwartz MM, Silva FG (eds) Heptinstall's pathology of the kidney, 5th edn. Lippincott-Raven, Philadelphia, pp 187–257
49. Pirani CL (1994) Evaluation of kidney biopsy specimens. In: Tisher CG, Brenner BM (eds) Renal pathology with clinical and functional correlations, 2nd edn. Lippincott, Philadelphia, pp 85–115
50. Tosoni A, Nebuloni M, Zerbi P et al (2005) Ultrastructural study of renal involvement in two females with Anderson–Fabry disease. Ultrastruct Pathol 29:203–207
51. Faraggiana T, Churg J, Grishman E et al (1981) Light- and electron-microscopic histochemistry of Fabry's disease. Am J Pathol 103:247–262
52. Kriz W, Gretz N, Lemley KV (1998) Progression of glomerular diseases: is the podocyte the culprit? Kidney Int 54:687–697
53. Kriz W, Lemley KV (1999) The role of the podocyte in glomerulosclerosis. Curr Opin Nephrol Hypertens 8:489–497
54. Mundel P, Shankland SJ (2002) Podocyte biology and response to injury. J Am Soc Nephrol 13:3005–3015
55. Ichikawa I, Ma J, Motojima M, Matsusaka T (2005) Podocyte damage damages podocytes: autonomous vicious cycle that drives local spread of glomerular sclerosis. Curr Opin Nephrol Hypertens 14:205–210
56. Kawamura O, Sakuraba H, Itoh K et al (1997) Subclinical Fabry's disease occurring in the context of IgA nephropathy. Clin Nephrol 47:71–75
57. Yoshida A, Morozumi K, Takeda A et al (1994) Fabry-like laminated myelin body associated with IgA nephropathy. Nippon Jinzo Gakkai Shi 36:1303–1307
58. Whybra C, Schwarting A, Kriegsmann J et al (2006) IgA nephropathy in two adolescent sisters heterozygous for Fabry disease. Pediatr Nephrol 21:1251–1256
59. Breunig F, Weidemann F, Strotmann J et al (2006) Clinical benefit of enzyme replacement therapy in Fabry disease. Kidney Int 69:1216–1221
60. Waldherr R, Rambausek M, Duncker WD, Ritz E (1989) Frequency of mesangial IgA deposits in a non-selected autopsy series. Nephrol Dial Transplant 4:943–946

Virchows Arch (2008) 453:339–345
DOI 10.1007/s00428-008-0654-1

ORIGINAL ARTICLE

Secondary sclerosing cholangitis after intensive care unit treatment: clues to the histopathological differential diagnosis

Irene Esposito · Andrea Kubisova · Adolf Stiehl · Hasan Kulaksiz · Peter Schirmacher

Received: 16 April 2008 / Revised: 4 July 2008 / Accepted: 7 August 2008 / Published online: 4 September 2008

Abstract Secondary sclerosing cholangitis (SSC) is a chronic cholestatic disorder caused by mechanical, infectious, toxic, or ischemic factors. A new variant of SSC occurring after long-term treatment in intensive care units (ICU) has been recently described and characterized from the clinical point of view. The aim of this study was the histomorphological characterization of ICU-treatment-related SSC (ICU-SSC) and the definition of histological changes occurring over time based on the morphological findings. Liver biopsies of ten patients affected by ICU-SSC obtained at different time points (1.5 to 57 months) after the initial injury were analyzed. The main morphological alterations included degenerative changes of portal bile ducts, portal edema, inflammation, and fibrosis as well as biliary interface activity and bilirubinostasis. Perivenular necroses and bile infarcts were found in eight and six patients, respectively. Bile duct loss was not observed. No correlation between morphological features of biopsies and liver chemistry tests or outcome could be established. Based on the morphological observation, a possible disease-progression model starting with an initial damage of portal bile ducts (primary insult) with associated portal/periportal changes (inflammation, ductular reaction) and resulting in secondary parenchymal changes is proposed.

Keywords Secondary sclerosing cholangitis · Intensive care · Cholestasis · Sepsis

I. Esposito
Institute of Pathology, Helmholtz Zentrum München-German Research Center for Environmental Health, Oberschleissheim, Germany

I. Esposito
Institute of Pathology, Technische Universität München, Munich, Germany

I. Esposito · A. Kubisova · P. Schirmacher (✉)
Institute of Pathology, University of Heidelberg, Im Neuenheimer Feld 220, 69120 Heidelberg, Germany
e-mail: peter_schirmacher@med.uni-heidelberg.de

A. Stiehl
Department of Internal Medicine, Division of Gastroenterology, University of Heidelberg, Heidelberg, Germany

H. Kulaksiz
Department of Internal Medicine, University of Ulm, Ulm, Germany

Introduction

Sclerosing cholangitis is a chronic, variably progressive cholestatic disease affecting the extra- and/or intrahepatic biliary tree with evolution into biliary cirrhosis and cholestatic liver failure [1]. A primary or idiopathic form and a less common secondary, acquired form of sclerosing cholangitis are known, which share similar radiological, morphological, and clinical features. In addition, primary sclerosing cholangitis (PSC) and some forms of secondary sclerosing cholangitis (SSC) belong to the spectrum of liver diseases associated with progressive intrahepatic bile duct loss or ductopenia, usually developing over decades. Most common causes of SSC include infectious, toxic, or ischemic injuries of the biliary tree. Long-standing biliary obstruction of diverse etiologies (stones, benign strictures), often with superimposed suppurative cholangitis, also causes morphological alterations that resemble PSC and may rarely

evolve into secondary biliary cirrhosis [2]. Furthermore, autoimmune pancreatocholangitis is an immune-mediated disorder characterized by a PSC-like involvement of the extra- and intrahepatic biliary tract [3]. Recently, a new variant of SSC occurring after long treatment in intensive care units has been described and characterized, mostly from the clinical point of view [4–9]. In the present study, the histomorphological features of rapid-onset secondary sclerosing cholangitis after long-term intensive care unit (ICU) treatment are described. A possible progression model is suggested, and criteria for the histopathological differential diagnosis are proposed.

Materials and methods

Ten patients (nine men, one woman; median age at diagnosis 52.5, range 16–68 years) affected by ICU-SSC with available needle biopsies of the liver were retrospectively analyzed in this study. The main clinical data are summarized in Table 1. All patients were treated in an intensive care unit for septic shock after an initial insult, and they all required long-term ventilation, catecholamines, total parenteral nutrition, and antibiotics. The alterations in the liver function did not resolve despite successful treatment of the sepsis. The complete clinical characterization of the patients' collective has been previously published [9]. None of the patients showed elevation of the cholestasis parameters [bilirubin, serum alkaline phosphatase, and γ-glutamyltransferase (GGT)] prior to their admission or on the initial laboratory tests in the ICU.

Liver biopsies had been obtained at admission to the Department of Gastroenterology of the University of Heidelberg 1.5 to 6.5 months (median, 2 months) after injury from patients 1 and 3–10. The liver biopsy of patient 2 was obtained 57 months after injury. A follow-up biopsy was obtained from patient 5 2 weeks after the first one.

Tissue sections obtained from the liver biopsies were retrieved from the archive of the Institute of Pathology of the University of Heidelberg and analyzed for the purposes of the present study by two pathologists (I.E. and P.S.) experienced in biliary and hepatic pathology blinded to detailed clinical information. In addition to conventional hematoxylin and eosin sections, periodic acid–Schiff (PAS)-diastase staining, Gomori's silver impregnation for reticulin, and Van Gieson's or Masson's trichrome staining for connective tissue were available in all cases. Rhodamine-staining for copper was used as a marker of chronic cholestasis. For better demonstration of bile duct status (ductular reaction and metaplasia), immunostaining for cytokeratin (CK) 7 (Dakocytomation, Glostrup, Denmark) was performed according to standard protocols.

Table 1 Patients' demographic and clinical data

Patient	Age	Gender	Cause of ICU treatment	Duration of ICU treatment (days)	Time interval injury–biopsy (months)	Total follow-up (months)	Total bilirubin[a] (mg/dl)	AP[a] (U/l)	GGT[a] (U/l)	ALT[a] (U/l)	AST[a] (U/l)	Outcome (cause of death)
1	68	M	Vascular surgery	32	6.5	10	15.6	372	577	213	161	Death (liver failure)
2	16	M	Burn injury	15	57	92	2.2	1677	396	n.a.	n.a.	Ltx 8 years after injury
3	55	F	Cardiac surgery	27	3.5	8	18.8	1986	346	203	269	Death (multiorgan failure)
4	60	M	Bacterial infection	28	2	8	11.9	1184	1476	265	149	Alive, severe cholestasis
5	28	M	Accident	53	1.75	3	18	1500	1554	83	165	Death (liver failure)
6	47	M	Cardiac surgery	45	1.5	5	9.7	443	360	53	83	Death (circulatory failure)
7	50	M	Cardiac surgery	18	1.5	2	26.7	1390	1274	164	126	Alive, severe cholestasis
8	68	M	Cardiac surgery	42	5	10	7.7	1806	462	n.a.	n.a.	Death (cerebral ischemia)
9	57	M	Cardiac surgery	35	2	2	41.7	1002	588	124	112	Death (circulatory failure)
10	48	M	Vascular surgery	48	2	4	1.8	512	1009	59	59	Alive, severe cholestasis

Normal values for men: AST <38 U/l, ALT <41 U/l, GGT <66 U/l, AP 40–129 U/l, total bilirubin <1.1 mg/dl; normal values for women: AST <32 U/l, ALT <31 U/l, GGT <39 U/l, AP 35–104 U/l, total bilirubin <1.1 mg/dl

LTX Liver transplantation, *n.a.* not available

[a] Laboratory values at the time of biopsy

The following parameters were taken into account for the histopathological evaluation: total numbers of portal tracts (PT), number of affected PT, portal changes (edema, inflammation, bile duct changes, and fibrosis), acinar changes (hepatocellular changes, necrosis, inflammation, cholestasis, and fibrosis).

All morphological parameters were semiquantitatively assessed on a three-point scale (0 = absent; + = mild/weak; ++ = moderate; +++ = heavy/strong). Continuous variables were stratified according to their median and percentile values for comparison purposes.

Results

Morphological spectrum of ICU-related SSC

The quality of the biopsy material was good in all but one case (patient 3), where significant autolytic changes were present. The median number of portal tracts was 20 (3–28), and in all cases, the majority of them (76–100%) showed histopathological changes. In all cases, mild to moderate portal inflammation was observed. The inflammatory infiltrate mostly consisted of lymphocytes, less frequently of plasma cells and neutrophil granulocytes, which showed preferential periductal localization. In four cases, eosinophils were present. Portal inflammation was accompanied in all cases by edema with portal enlargement, as well as by a number of alterations of the interlobular bile duct epithelium, which included cytoplasmic vacuolization, loss of cellular polarity, cellular drop-out, and irregularities of the basal membrane. Mild to heavy ductular reaction—that is, the presence of numerous ductular-shaped structures at the margins of the portal tracts—was found in all cases, together with a mostly mild to moderate ductular metaplasia of the periportal hepatocytes [10], as demonstrated in eight of ten cases by means of immunostaining for CK7. Mild to moderate portal fibrosis was present in all cases, but it was never concentric around ducts or ductules. There was no evidence of definite bile duct loss or even ductopenia. Lymph follicles, granulomas, or lymphocytic interface activity was not observed. Portal changes were associated with mild to strong hepatocellular bilirubinostasis in nine of ten cases, canalicular bilirubinostasis in six of ten cases, perivenular hepatocyte ballooning in four of ten cases, focal perivenular necroses in eight of ten cases, and preferentially periportal bile infarcts in six of ten cases. Periportal hepatocytes showed morphological features of cholate stasis. However, rhodamine staining did not show copper accumulation (not shown). Broad fibrous septa linking portal tracts were found in four of ten cases. No patient showed overt liver cirrhosis. The observed changes are shown in detail in Table 2 and are illustrated in Fig. 1.

Table 2 Morphological changes of secondary sclerosing cholangitis after ICU treatment

	Portal tracts						Bile ducts		Cholestasis		Necrosis		Other Changes
Case	Number	Inflammation	Neutrophils	Eosinophils	Lymphocytes	Fibrosis	Fibrotic bridges	Cytological changes	Proliferation	hepatocellular	canalicular	Ductular metaplasia	Perivenular necrosis	Bile infarct	
1	10	++	++	0	+	+	0	+++	+++	+++	0	++	+	+	Cell ballooning
2	24 (3 normal)	++/+++	++	0	+++	++	+	+++	++	0	0	+/-	0	0	
3	3	+	+	0	++	+	0	++	++	+++	++	n.a.	+	0	
4	11	+	+	+	+	++	0	++	+++	++	++	+	++	+	
5	21 (3 normal)	++	+	+	+	++	0	++	++	++	++	0	+	0	Cell ballooning
5[a]	20	++	++	+	++	++	+	+++	+++	+	+++	+	+	+	Cell ballooning
6	17 (4 normal)	+	++	+	+	+	0	++	++	+	+	+	+	+	
7	27 (3 normal)	++	+	0	++	+	0	++	+	++	0	+	+	0	Cell ballooning
8	28	+++	++	0	++	++	+	+++	+++	+	+	++/+++	0	0	
9	15	++	++	++	+	++	+	+/++	++/+++	++	0	+	+	+	Cell ballooning
10	20	++	++	0	+	++	0	++	++	+++	++	+	+	+	

[a] Second biopsy of patient 5 performed 14 days after the first one

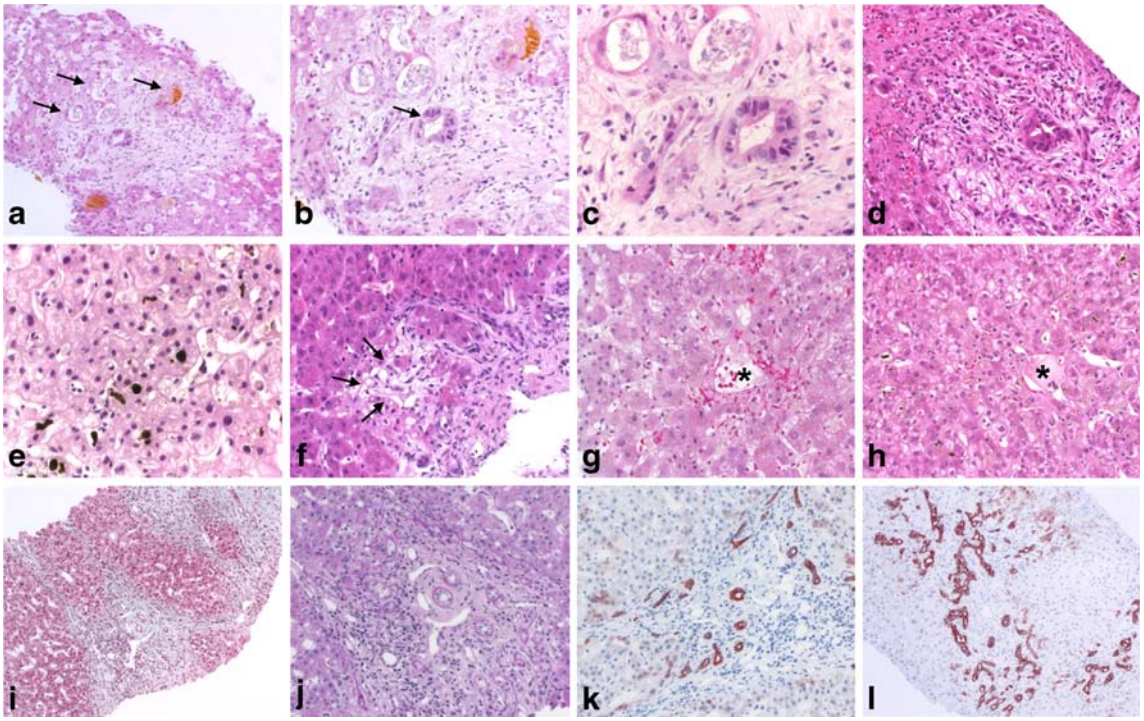

Fig. 1 Morphological characteristics of ICU-associated secondary sclerosing cholangitis. **a**–**d** Portal changes. **a** (Case 5) Low-power view of a portal tract showing marked enlargement due to edema, mild inflammation, and mild fibrosis. At the periphery of the portal tract, dilated cholangioli are seen (*arrows*), some of them containing yellow bile plugs (×25). **b** (Case 5) Higher magnification of a portal tract illustrating the relatively mild inflammatory infiltrate contrasting with the striking degenerative changes of the interlobular bile duct (*arrow*; ×100). **c** (Case 5) Degenerative changes of the bile duct epithelium are shown in detail (×400). **d** (Case 4) Another example of portal tract changes in ICU-related SSC. Portal tract expansion with mild inflammation, degenerative changes of the interlobular bile duct, and beginning ductular reaction are shown (×100). **e**–**h** Parenchymal changes. **e** (Case 3) Hepatocellular and canalicular cholestasis (×200). **f** (Case 6) Periportal bile infarct (arrows; ×100). **g** and **h** (Cases 5 and 7) Perivenular loss of hepatocytes. The central vein is indicated with an *asterisk* (×100). **i**–**l** Later stages. **i**–**k** (Case 2) Extensive fibrosis with bridges linking portal tracts is evident in the Masson's trichrome staining (**i** ×25). The prominent ductular reaction is highlighted in the PAS staining (**j** ×100) and in the immunostaining for CK7 (**k** ×100). **l** (Case 8) Immunostaining for CK7 showing extensive ductular reaction and ductular metaplasia of periportal hepatocytes (×25)

Clinicopathological correlations

First, possible correlations between liver chemistry values and morphological changes were analyzed. Liver chemistry tests suggested a predominant cholestatic or a mixed cholestatic/hepatocellular damage [11]. In general, no definitive correlation was observed between serological cholestasis parameters and the morphological representation of cholestasis. For instance, patient 2 had a strong increase in the serum levels of alkaline phosphatase but no morphological evidence of cholestasis, whereas patient 10 had only a modest to moderate increase in the level of total bilirubin and alkaline phosphatase, but the liver biopsy showed a moderate to severe hepatocellular and canalicular cholestasis. Also, no evident correlation was found between the hepatocellular damage expressed by the elevation in the serum transaminases and the morphological evidence of liver cell damage (ballooning, necrosis). For instance, patients 6 and 10 had the lowest transaminase levels of the whole cohort at the time of biopsy, but the examination of the liver tissue revealed the presence of perivenular necroses and bile infarcts in both cases. On the other hand, patient 3 had a significant increase in the serum transaminases [alanine aminotransferase (ALT) seven times the upper limit of the normal value] but only mild (+) perivenular necroses.

Since biopsies from different patients were obtained at different time intervals from the injury event that caused ICU treatment, we next sought to determine if a correlation between morphological changes and clinical progression/outcome existed. For this purpose, liver biopsies were classified as "early" when obtained <1.8 months from the injury event (<25th percentile, patients 5, 6, and 7), as "intermediate" when obtained between 1.8 and 4.6 months from the injury event (26–74th percentile, patients 3, 4, 9, and 10) and as "late" when obtained later than 4.6 months from the injury event (>75th percentile, patients 1, 2, and 8). All patients displayed evident alterations of the portal bile ducts and some degree of portal inflammation, together with mild to moderate portal fibrosis. Instead, morphological evidence of cholestasis and necrosis was not a constant finding, but no clear correlation with the clinical

evolution and/or the outcome was found. However, most of the tissue probes were obtained between 1.5 and 6.5 months from the injury event, a time span which could be too short to detect any clear morphological markers of disease progression and outcome. Nevertheless, the analysis of the liver tissues of patient 5, which were obtained with a 2-week interval from each other, revealed signs of progression in the cholestatic and necrotic features (appearance of ductular metaplasia, as shown in the CK7 staining, and of bile infarcts) as well as in the fibrotic reaction (bridges) in the later biopsy. Moreover, the analysis of a "very late" biopsy, like that of patient 2, which was obtained almost 6 years after the injury event, shows that slow progression to liver cirrhosis of biliary type can be one possible outcome of the disease, which otherwise rapidly progresses to cholestatic liver insufficiency.

Discussion

Secondary sclerosing cholangitis occurring in critically ill patients after ICU treatment is a recently described, still not well-characterized entity [5–8] that has to be included in the differential diagnosis of chronic cholestatic diseases. In the reported series, including our present, patients affected by ICU-SSC have a history of long-term intensive care treatment with necessity of mechanical ventilation and catecholamine therapy as a consequence of trauma, severe burning, cardiovascular accidents, or major cardiovascular and abdominal surgery. Hypoxic/ischemic, toxic (infectious and drug-related), and obstructive factors are likely to play a role in the multifactorial pathogenesis of ICU-SSC [12], but the contribution of primary and secondary causative factors remains difficult and eventually impossible to evaluate in a given case. The formation of biliary casts with subsequent bacterial infection has been reported as one of the earliest events in ICU-SSC, but its cause remains still elusive. One of the most accredited hypotheses identifies the hypoxic/ischemic damage of the intrahepatic biliary tree, following hypotension, reduced arterial blood oxygenation, and infusion of high doses of vasoconstrictors as the most probable etiologic factor [6, 8]. All these factors are also involved in the pathogenesis of sepsis-associated cholestasis, which is attributed to functional alterations of the hepatocytes and/or the bile ducts and is reversible after successful therapy [12]. ICU-SSC is instead a progressive disease, where an anatomical—and not merely functional—damage of the biliary tree is possibly perpetuated by (auto)immunological mechanisms that become activated only in a subset of patients. Since ICU-SSC has been described only in recent years, it is possible that modern measures of intensive care treatment play a role in the etiopathogenesis of this disorder, but specific factors have not been identified yet [8].

In this study, we focused on the morphological characterization of ICU-SSC, aiming at defining criteria supporting the histopathological differential diagnosis, a possible progression model, and potential clinicopathological correlations that may be of relevance for the clinical management. The observed morphological changes can be divided in those affecting the portal/periportal and the acinar areas. The portal alterations include: (1) inflammatory-degenerative changes of the bile duct; (2) mild to moderate, often periductal inflammatory infiltrate; (3) portal edema with moderate portal enlargement; (4) cholestatic features with ductular reaction and cholate stasis; and (5) mild to moderate fibrosis without a specific periductal pattern. The acinar changes appear to be secondary and include: hepatocellular and/or canalicular cholestasis, perivenular necroses potentially attributable to ischemia, and bile infarcts. The alterations of portal bile ducts, together with a certain degree of portal inflammation and ductular reaction, were a constant finding, being already detectable in early biopsies and uniformly distributed within a biopsy. On the other hand, periportal and acinar changes, such as cholate stasis, bilirubinostasis, necroses, and (bridging) fibrosis were more inconstant and possibly (for example in patient 5) progressive events. Based on this morphological observation, a disease-progression model, starting with an initial damage of portal bile ducts (primary insult) with associated portal/periportal changes (inflammation, ductular proliferation) and evolving with secondary cholestatic parenchymal changes, is suggested (Fig. 2). However, larger numbers of patients and examination of tissue specimens at different time points in the evolution of ICU-SSC are surely needed to give further support to this hypothesis.

Some morphologic characteristics associated with ICU-SSC have in part been described in previous studies and correlate well with our findings. In two of the three cases reported by Scheppach et al., a liver biopsy was performed 8 and 11 months after initial symptoms, respectively, and in both cases, ductular proliferation and bridging fibrosis were present. The third patient underwent liver transplantation, and the examination of the explanted organ showed PSC-like changes, including ulceration of the epithelium of large intrahepatic bile ducts, which were filled with bile plugs [4]. Engler et al. reported ductular proliferation, minimal portal inflammatory infiltrates, and portal fibrosis in the biopsies of seven patients; in three of them, micronodular cirrhosis was found [5]. Liver biopsies were performed at different time points in the series of Benninger et al. Four to 6 months after clinical presentation, morphological signs of chronic cholestasis and fibrosis were present, whereas later biopsies (12–24 months after injury) showed overt cirrhosis in two out of three patients [6]. Changes consistent with chronic bile duct obstruction have been described in four patients already 1–3 months after clinical presentation by

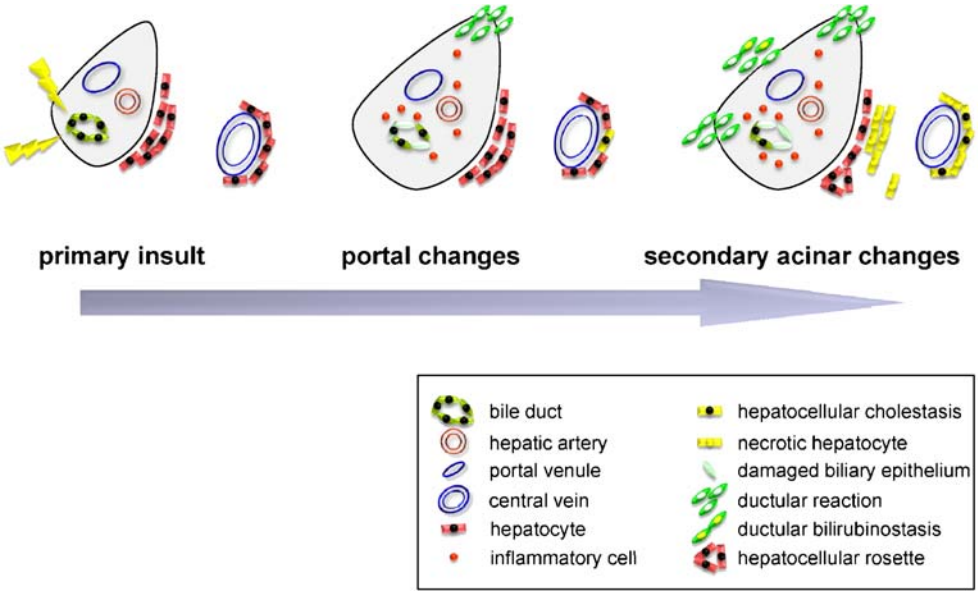

Fig. 2 Schematic representation of the proposed disease progression model. An initial insult to the portal bile ducts (*flash*) causes degenerative changes of the bile duct epithelium (e.g., cytoplasmic vacuolization, loss of nuclear polarization) and portal changes (enlargement due to edema and inflammation, ductular proliferation) and progresses to secondary parenchymal changes, such as bilirubinostasis, hepatocellular rosette formation, and cholestatic necroses

Gelbmann et al., and incomplete liver cirrhosis was present in one of two patients, who were biopsied >12 months after injury. Moreover, liver explants examined 1, 2, 9, and 16 months after injury showed morphological alterations suggesting secondary biliary cirrhosis [8]. All together, our and previous data show that morphological changes associated with ICU-SSC are comparable, with signs of bile duct damage and chronic cholestasis being already evident shortly after the clinical presentation. The evolution of the disease remains, however, quite unpredictable, with some cases rapidly developing into cholestatic liver failure and death and others more slowly progressing into secondary biliary cirrhosis. The factors that influence the outcome are not completely clarified, but comorbidities surely play an important role in these seriously ill patients. The absence of a correlation between laboratory values and morphological evidence of cholestasis is a known phenomenon in primary biliary diseases, such as PSC or primary biliary cirrhosis, where—especially in early stages—morphological changes can be focal and unevenly distributed.

Patients' history and clinical presentation are certainly fundamental for the diagnosis of ICU-SSC and for the exclusion of pre-existent liver disease (e.g., PSC) as well as of other systemic conditions (e.g., AIDS, neoplastic diseases) that can cause SSC. Nevertheless, morphology is helpful in distinguishing ICU-SSC from other disorders. Septicemia-associated cholestasis is an important differential diagnosis of ICU-SSC, since the clinical context of the two conditions can be the same. Histological changes associated with sepsis-induced cholestasis can be unspecific (portal inflammation, perivenular bilirubinostasis) and therefore indistinguishable from early stages of ICU-SSC, as those described by Gelbmann et al. [8]. However, the so-called *cholangiolitis lenta*, arising in patients with severe septic/endotoxic shock, usually shows a predominantly peri- and intraductular neutrophilic infiltrate and a rapid and extensive ductular reaction with prominent ductular bilirubinostasis [13], features that are usually not observed in ICU-SSC. Large bile duct obstruction also shares similar morphological features with ICU-SSC, but the primary bile duct damage (i.e., with no or only mild inflammation) is usually not as prominent as in ICU-SSC, while portal edema and ductular reaction are typical, and suppurative cholangitis of pre-existing bile ducts may occur. Drug-induced bile duct injury may be difficult to distinguish from ICU-SSC, since drugs may actually contribute to the severity and progression of this disorder. An accurate clinical evaluation of ICU patients with signs of cholestasis should therefore always take into consideration the possibility of drug-induced bile duct damage.

Other chronic cholestatic conditions that might be distinguished from ICU-SSC are autoimmune pancreatocholangitis/IgG4-hepatopathy and idiopathic adulthood ductopenia. Intrahepatic manifestations of autoimmune pancreatocholangitis/IgG4-hepatopathy, in particular those patterns with features of large bile duct obstruction or canalicular cholestasis [14], can be excluded by the absence of an infiltrate rich in IgG4-bearing plasma cells and of prominent periductal sclerosis. Idiopathic adulthood ductopenia is characterized by bile duct loss, a feature that is not observed early on in ICU-SSC.

In conclusion, ICU-SSC is a chronic cholestatic disease characterized by relatively specific morphological changes of the liver, consisting of degenerative changes of the interlobular bile duct epithelium with only mild accompanying chronic inflammatory reaction and usually severe cholestasis. Liver biopsy is useful in the differential diagnosis of ICU-SSC in the appropriate clinical context. Possible correlation

between morphological changes and outcome should be verified on a larger number of patients.

Conflict of interest statement We declare that we have no conflict of interest.

References

1. Maggs JR, Chapman RW (2007) Sclerosing cholangitis. Curr Opin Gastroenterol 23:310–316
2. Abdalian R, Heathcote EJ (2006) Sclerosing cholangitis: a focus on secondary causes. Hepatology 44:1063–1074
3. Bjornsson E, Chari ST, Smyrk TC et al (2007) Immunoglobulin G4 associated cholangitis: description of an emerging clinical entity based on review of the literature. Hepatology 45:1547–1554
4. Scheppach W, Druge G, Wittenberg G et al (2001) Sclerosing cholangitis and liver cirrhosis after extrabiliary infections: report on three cases. Crit Care Med 29:438–441
5. Engler S, Elsing C, Flechtenmacher C et al (2003) Progressive sclerosing cholangitis after septic shock: a new variant of vanishing bile duct disorders. Gut 52:688–693
6. Benninger J, Grobholz R, Oeztuerk Y et al (2005) Sclerosing cholangitis following severe trauma: description of a remarkable disease entity with emphasis on possible pathophysiologic mechanisms. World J Gastroenterol 11:4199–4205
7. Jaeger C, Mayer G, Henrich R et al (2006) Secondary sclerosing cholangitis after long-term treatment in an intensive care unit: clinical presentation, endoscopic findings, treatment, and follow-up. Endoscopy 38:730–734
8. Gelbmann CM, Rummele P, Wimmer M et al (2007) Ischemic-like cholangiopathy with secondary sclerosing cholangitis in critically ill patients. Am J Gastroenterol 102:1221–1229
9. Kulaksiz H, Heuberger D, Engler S et al (2008) Poor outcome in progressive sclerosing cholangitis after septic shock. Endoscopy 40:214–218
10. Van Eyken P, Sciot R, Desmet VJ (1989) A cytokeratin immunohistochemical study of cholestatic liver disease: evidence that hepatocytes can express 'bile duct-type' cytokeratins. Histopathology 15:125–135
11. Green RM, Flamm S (2002) AGA technical review on the evaluation of liver chemistry tests. Gastroenterology 123:1367–1384
12. Geier A, Fickert P, Trauner M (2006) Mechanisms of disease: mechanisms and clinical implications of cholestasis in sepsis. Nat Clin Pract Gastroenterol Hepatol 3:574–585
13. Lefkowitch JH (1982) Bile ductular cholestasis: an ominous histopathologic sign related to sepsis and "cholangitis lenta". Hum Pathol 13:19–24
14. Umemura T, Zen Y, Hamano H et al (2007) Immunoglobin G4-hepatopathy: association of immunoglobin G4-bearing plasma cells in liver with autoimmune pancreatitis. Hepatology 46:463–471

Virchows Arch (2008) 453:347–357
DOI 10.1007/s00428-008-0662-1

ORIGINAL ARTICLE

Expression of hepatocyte growth factor activator inhibitor type 1 on the epithelial cell surface is regulated by hypoxic and oxidative stresses

Wataru Komaki · Tsuyoshi Fukushima · Hiroyuki Tanaka · Hiroshi Itoh · Etsuo Chosa · Hiroaki Kataoka

Received: 23 April 2008 / Revised: 7 July 2008 / Accepted: 20 August 2008 / Published online: 4 September 2008

Abstract Hepatocyte growth factor activator inhibitor type 1 (HAI-1)/*spint-1* is a membrane-bound protease inhibitor that is thought to regulate the activities of hepatocyte growth factor activator, matriptase, hepsin, and prostasin. In this study, we show that the membrane form of HAI-1 was significantly upregulated immunohistochemically in epithelial cells under adverse conditions including tissue injury, necroinflammatory reactions, and invasion of carcinomas. To analyze the mechanism underlying these in vivo observations, we examined the effects of hypoxia and oxidative stress on HAI-1 expression in vitro, using three human cell lines, HLC-1, WiDr, and HeLa. Hypoxic condition significantly enhanced the expression of HAI-1 in these cells. Oxidative stress also enhanced HAI-1 expression. Promoter analyses of the human *HAI-1*/*spint-1* gene revealed overlapping binding site for Egr-1-3 and Sp1 near the transcription start site as the key domain for *HAI-1*/*spint-1* transcription. This site was also critical in both hypoxic- and oxidative stress-induced HAI-1 upregulation. In fact, in vivo immunohistochemical studies indicated that areas with HAI-1 upregulation tended to express markers associated with hypoxia and oxidative stress. These observations suggest that the tissue microenvironment regulates the cell surface expression of HAI-1, and thereby may regulate proteolysis and processing of bioactive molecules on the cellular surface.

Keywords HAI-1 · Hypoxia · Oxidation · Cell surface proteolysis · Protease inhibitor

W. Komaki · T. Fukushima · H. Tanaka · H. Kataoka (✉)
Section of Oncopathology and Regenerative Biology, Department of Pathology, Faculty of Medicine, University of Miyazaki, 5200 Kihara, Kiyotake, Miyazaki 889-1692, Japan
e-mail: mejina@fc.miyazaki-u.ac.jp

W. Komaki · E. Chosa
Section of Orthopaedic Surgery, Department of Medicine of Sensory and Motor Organs, Faculty of Medicine, University of Miyazaki, Miyazaki, Japan

H. Itoh
Department of Pathological Sciences, Faculty of Medical Sciences, University of Fukui, Fukui, Japan

Introduction

Regulation of proteolysis in the pericellular microenvironment has important roles in development, normal homeostasis, reactions to various stimuli, and cellular responses to pathological phenomena. Proteolysis occurs during the remodeling of the extracellular matrix, coagulation and fibrinolytic cascades, and processing of cytokines, growth factors, and other bioactive mediators. Excess protease activity must be tightly regulated by the cognate inhibitor to avoid deleterious effects. Hepatocyte growth factor activator inhibitor type 1 (HAI-1) is a cell surface serine protease inhibitor initially identified as a potent inhibitor of hepatocyte growth factor (HGF) activator, a serum protease that converts the proform of HGF (pro-HGF) into its mature active form [14, 27]. HAI-1 also regulates some membrane-bound serine proteases, such as matriptase, hepsin, and prostasin [14, 15, 19]. Matriptase is a type II transmembrane protein with critical roles in epidermal maturation and thymic function and is thought to be involved in carcinogenesis and tumor progression [31]. It activates pro-urokinase and protease-activated receptor 2, and can

degrade extracellular matrix proteins [31]. Hepsin is also a type II transmembrane serine protease and is abundantly expressed in the liver [32]. Recent studies have indicated that hepsin is involved in metastatic tumor progression [2, 32]. Notably, both matriptase and hepsin are also potent activators of pro-HGF [14, 15, 17]. Prostasin is a glycosylphosphatidylinositol linkage serine protease on the cell surface, which activates the epithelial sodium channel of the plasma membrane and also regulates keratinization of the epidermis [5, 18]. HAI-1 also inhibits certain kallikrein 1-related peptidases (tissue kallikreins) [21]. Taken together, HAI-1 appears to be critical for regulation of pericellular proteolysis and processing of various bioactive molecules on the cellular surface. Therefore, the regulation of HAI-1 expression is important to many processes occurring at the level of cells and tissues. The importance of HAI-1 has been confirmed in mutant mice. Deletion of the *HAI-1*/*spint-1* gene in mice resulted in embryonic lethality due to impaired development of the placenta labyrinth, indicating its non-redundant function in certain cells [6, 30].

Previously, we showed that HAI-1 is expressed on the basolateral surface of various types of epithelial cells [11]. Endothelial and mesothelial cells also expressed HAI-1 on their surfaces [1]. Of interest was the observation that the expression of membrane-bound HAI-1 was significantly augmented in cells in injured and inflamed tissues [11, 12]. This augmented expression was also observed in cancer cells at the invasion front [22]. These observations suggest that the expression of HAI-1 is regulated by specific features of the tissue microenvironment. We further suggest that the pathologic environment associated with injured tissue may augment the expression of this cell surface inhibitor. For example, we have shown that inflammatory cytokines and oxidative stress upregulate the expression of HAI-1 in colon carcinoma cells and biliary epithelial cells, respectively, in vitro [12, 26]. However, the precise molecular mechanism regulating the expression of HAI-1 remains to be determined. The *HAI-1* gene (gene name: *spint-1*) has been mapped to chromosome 15q15 and consists of 11 exons spanning 12 kbp [9]. The major transcription start site is 207 bp upstream from the start codon, and neither a TATA box nor a CAAT box is present in the promoter regions of mouse and human *HAI-1*/*spint-1* genes [9, 10].

In this study, we examined the expression patterns of HAI-1 in various pathologic epithelial tissues including carcinomas. Based on the results obtained, we hypothesized that hypoxia and oxidative stress may upregulate HAI-1 expression. To investigate this possibility, we tested the effects of hypoxia and oxidative stress on the expression of HAI-1 in cultured epithelial cell lines and analyzed the promoter region responsible for the expression. The data indicate that both hypoxia and oxidative stress induced HAI-1 expression, which was mediated by an Egr-1-3/SP1 binding region near the transcription start site within the HAI-1 promoter.

Materials and methods

Immunohistochemistry

Formalin-fixed paraffin-embedded tissue specimens were sectioned (4 μm) and stained with hematoxylin and eosin (HE). For immunohistochemical detection for HAI-1, hypoxia-inducible factor (HIF-1α), and 4-hydroxy-2-nonenal (4-HNE), the sections were processed for antigen retrieval (autoclaving in 10 mM citrate buffer, pH 6.0, or 1 mM EDTA, pH 8.0, for 5 min), followed by treatment with 3% H_2O_2 in phosphate-buffered saline (PBS) for 10 min and washed in PBS twice. After blocking in 3% bovine serum albumin (BSA) and 10% normal goat serum in PBS for 1 h at room temperature, the sections were incubated with primary antibodies for 16 h at 4°C. The preparation of anti-human HAI-1 monoclonal antibody has been reported previously [11]. Anti-human HIF-1α and anti-4-HNE mouse monoclonal antibodies were purchased from Novus Biologicals (Littleton, CO, USA) and the Japan Institute for the Control of Aging (Shizuoka, Japan), respectively. Negative controls consisted of omission of the primary antibody. The sections were then washed in PBS and incubated with Envision-labeled polymer reagent (DAKO, Glostrup, Denmark) reagent for 45 min at 37°C. The reaction was revealed with nickel, cobalt-3,3′-diaminobenzidine (metal enhanced DAB substrate kit; Pierce, Rockford, IL, USA), and the sections were counterstained with hematoxylin. Surgically resected specimens of two cases of gastrointestinal ulcer (gastric ulcer and jejunal ulcer), two cases of colon cancer, and 20 cases of lung cancer (11 cases of adenocarcinoma, seven cases of squamous cell carcinoma, and two cases of large cell carcinoma) were immunostained with the informed consent of the patients. Strong membranous immunoreactivity of HAI-1 in more than 10% of cancer cells was judged as positive. For HIF-1α and 4-HNE, immunoreactivity in more than 20% of cancer cells was judged as positive.

Cell lines and cell culture

A human lung adenocarcinoma cell line (HLC-1), human colon carcinoma cell line (WiDr), and human uterine cervix carcinoma cell line (HeLa) were cultured in RPMI 1640 medium supplemented with 10% fetal bovine serum, at 37°C in a humidified atmosphere containing 5% CO_2. For hypoxia treatment, subconfluent cells (60% to 80% confluent) in 24-well or six-well culture plates were maintained in

serum-free medium with 20% O_2 (normoxia) or 1% O_2 (hypoxia) using modular incubator chambers (APM-30D, ASTEC, Fukuoka, Japan), with or without $CoCl_2$ (Nakalai, Kyoto, Japan). For oxidation treatment, cells were grown to 60% to 80% confluence in 24-well or six-well plates and maintained in serum-free medium under normoxic (20% O_2) conditions with or without H_2O_2. All cell lines were routinely tested for mycoplasma contamination.

Reverse transcription-polymerase chain reaction (RT-PCR)

Total cellular RNA was extracted using Trizol reagent (Invitrogen, Carlsbad, CA, USA) according to the manufacturer's instructions. For RT-PCR, 2 μg of total RNA was reverse-transcribed with Superscript II reverse transcriptase (Invitrogen), and the resultant cDNA was used for conventional RT-PCR and quantitative real-time RT-PCR. The following primers were used: HAI-1, forward 5′-TCCATTTCCCCAGTGACA-3′, reverse 5′-TGCCATAACAACCACCATAG-3′, and TaqMan FAM-ACTGCGTGGACCTGCCAGACACA-TAMRA. Conventional PCR was carried out using the hot start Taq enzyme (Hotstar™; Qiagen, Valencia, CA, USA) with a thermal cycle profile of 30 s at 95°C, 1 min at 55°C, and 1 min at 72°C, using a thermal cycler. The PCR products were analyzed by 1.5% agarose gel electrophoresis. The quantitative real-time RT-PCR for HAI-1 was performed according to methods previously described [2] using LightCycler (Roche Diagnostics, Mannheim, Germany). The amount of messenger RNA (mRNA) in each sample was calculated as the number of copies per 10^2 copies of β-actin (Roche Diagnostics).

Immunoblot analysis

HLC-1 cells were cultured in six-well plates, and cells at 60% confluency were used for the experiments. Cultured HLC-1 cells were treated with 1 μM phorbol 12-myristate 13-acetate (PMA) (Sigma, Saint Louis, MO, USA) for indicated periods at 37°C for 1 h in 2 mL of serum-free medium. Then, the cells were incubated under conditions of normoxia (20% O_2), hypoxia (1% O_2 with or without 100–600 μM $CoCl_2$), or with oxidative stress (100–600 μM H_2O_2) in serum-free conditions and incubated for 2 to 24 h. For immunoblot analysis of HAI-1, the cultured cells were washed with ice-cold PBS and extracted in 100 μL of 50 mM Tris–HCl, pH 7.5, 150 mM NaCl, 0.2% NP-40 supplemented with 0.3 μL of protease inhibitor cocktail (Sigma) on ice. Then, 10 μL of 20% NP-40 and 10 μL of 20% Triton X-100 were added, and the extraction was incubated for 10 min on ice before clarification by centrifugation at $10^4 \times g$ at 4°C for 5 min. Protein concentration was measured by the Bradford method (BioRad, Hercules, CA, USA). Sodium dodecyl sulfate-polyacrylamide gel electrophoresis was performed under reducing condition using a NuPAGE 4–12% gradient gel (Invitrogen). After electrophoresis, the proteins were transferred electrophoretically onto Immobilon-P membranes (Millipore, Billerica, MA, USA). After blocking the non-specific binding sites with 5% skim milk in 50 mM Tris–HCl (pH 7.5), 150 mM NaCl, and 0.05% Tween 20 (TBS-T), the membrane was incubated with anti-HAI-1 monoclonal antibody, 1N7 (1 μg/mL) or anti-β-actin mouse monoclonal antibody, AC-74 (Sigma; 1 μg/mL) for 1 h at room temperature, followed by four washes with TBS-T and incubation with horseradish peroxidase-conjugated goat anti-mouse IgG (DAKO), diluted 1:3,000 in TBS-T with 1% BSA, for 1 h at room temperature. The labeled proteins were visualized with a chemiluminescence reagent (Perkin Elmer Life Sciences, Boston, MA, USA).

Cloning and site-directed mutagenesis of the HAI-1/spint-1 promoter

Promoter constructs containing the indicated nucleotide sequences of the human *HAI-1*/*spint-1* 5′-flanking region were made by PCR and subcloned into the *Mlu*I/*Bgl*II site of the promoterless luciferase pGL3 basic vector (Promega, Madison, WI, USA). Each sequence between 2,034, 543, 211, 79, or 30 bp upstream of the transcription start site (designated as +1) and 43 bp downstream of the transcription site of the *HAI-1*/*spint-1* gene was subcloned and the resultant plasmid was designated as pHAI(−2034/+43)-, pHAI(−543/+43)-, pHAI(−211/+43)-, pHAI(−79/+43)-, or pHAI(−30/+43)-Luc, respectively. Using pHAI(−211/+43)-Luc as a template, the mutant promoter of HAI-1/spint-1 gene was prepared by replacing the nucleotide sequence of GGGC (−52 to −49) to AATT within the potential binding site of a complex of Egr-1-3 and Sp1 using a PCR-based method previously described [13]. The resultant reporter plasmid with the mutant promoter was designated as pHAI (−211/+43 mut)-Luc.

Transfections and reporter assays

Cells were plated 24 h before transfection in 24-well plates and cultured to 70% to 90% confluency. The reporter plasmid (0.25 μg) was transfected in Opti-MEM I reduced-serum medium (Invitrogen) using FuGENE6 transfection reagent (Roche) according to the manufacturer's instructions. After transfection, the cells were maintained under normoxic conditions (20% O_2), hypoxic conditions (1% O_2 with 150 μM $CoCl_2$) or in oxidative stress (normoxia with 300 μM H_2O_2) for the indicated periods in serum-free RPMI 1640 medium. Reporter assays

were performed using a dual luciferase reporter assay system (Promega) according to the manufacturer's instructions. The corresponding empty vector (pGL3 basic vector) was used as a control. After incubation of the cells for the indicated periods, the cellular lysates were prepared. Luciferase activity was measured by a luminometer (Turner Biosystems, Sunnyvale, CA, USA) as relative light units adjusted for efficiency of transfection standardized by co-transfection with 0.05 μg Renilla luciferase plasmid pRL-TK (Promega) as an internal control. The results of promoter activity assays were expressed as a percentage of luciferase activity compared to cells transfected with the maximal promoter construct driven by SV-40 promoter and enhancer (pGL3 control). All transfection experiments were done in triplicate.

Statistical analysis

Data were analyzed with the StatView 4.0 program (Brainpower, Calabasas, CA, USA). Comparisons between unpaired groups were conducted with the Mann–Whitney *U* test. Comparisons between time-course groups were conducted by two-way repeated measure analysis of variance. *P* values of <0.05 were regarded as statistically significant. Results are expressed as means ± standard deviation (SD).

Results

Augmented expression of membrane form of HAI-1 in adverse environmental conditions

Previously, we reported that the membrane form of HAI-1 was expressed on the surface of epithelial cells and that immunoreactivity for membranous HAI-1 was upregulated in injured or regenerating epithelium [11]. Initially in this study, we preliminarily examined the expression of HAI-1 in epithelia in adverse, pathologic tissue microenvironments using two cases each of gastrointestinal ulcer and advanced colon cancer, and four cases of advanced lung cancer, and found a fairly consistent tendency of enhanced HAI-1 immunoreactivity in epithelial cells, including tumor cells, in significantly adverse tissue microenvironments. For example, desquamating epithelial cells on a severely inflamed, injured mucosa (Fig. 1a) and tumor cells undergoing central necrosis (Fig. 1b) showed significantly upregulated HAI-1 immunoreactivity.

Effects of hypoxia on the expression of HAI-1 in vitro

Based on the preceding observations, we hypothesized that pathologic microenvironments may upregulate HAI-1, and hypoxia and/or oxidative stress may be inducible factor(s)

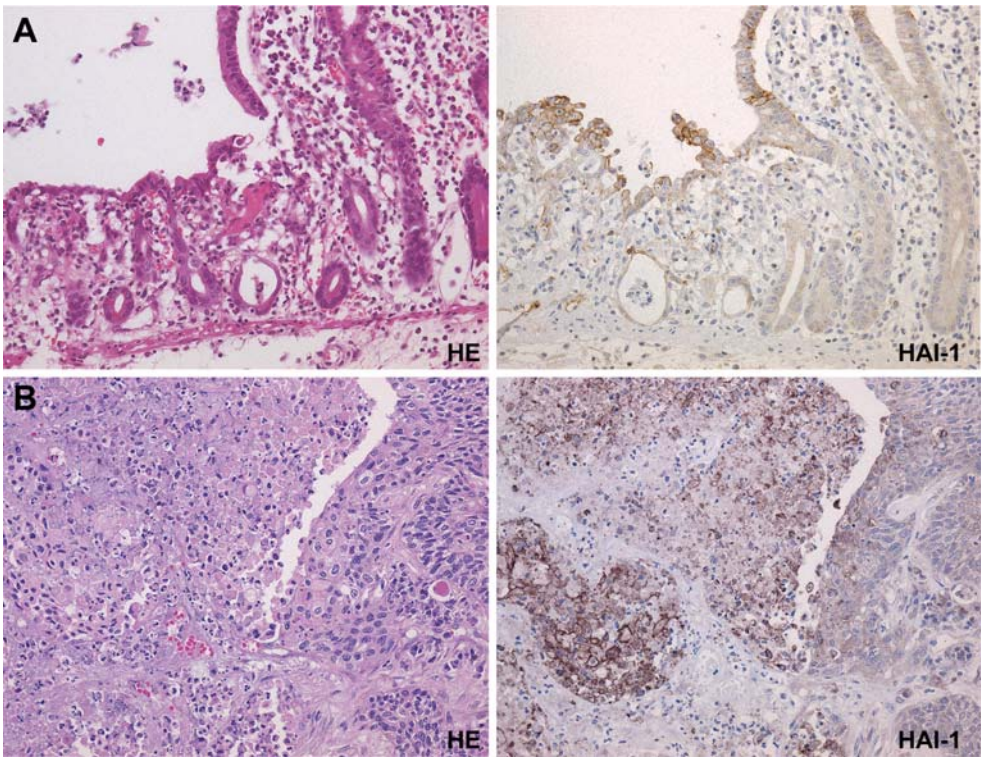

Fig. 1 Enhanced expression of the membrane form of HAI-1. **a** Regenerating ulcer in the jejunum. HAI-1 immunoreactivity is significantly upregulated in desquamating epithelial cells and also in the cells covering severely injured tissue. **b** HAI-1 expression in cancer cells in necrotic portion (squamous cell carcinoma of the lung). Degenerative cancer cells in necrotic lesion shows significantly enhanced membranous immunoreactivity of HAI-1

for the expression of the membrane form of HAI-1 in epithelial cells and carcinoma cells. To test this hypothesis, we examined the effects of hypoxia on the expression of HAI-1 in vitro. As shown in Fig. 2a, all three human epithelial cell lines examined (HLC-1, HeLa, and WiDr) expressed HAI-1 mRNA. The expression level was low in HeLa compared with HLC-1 and WiDr. We used the HLC-1 human lung adenocarcinoma cell line to examine the effects of hypoxia on HAI-1 mRNA levels (Fig. 2b). In this experiment, HLC-1 cells were incubated in serum-free conditions with or without hypoxic treatment. Under normoxic conditions (20% O_2 without $CoCl_2$), serum starvation initially resulted in a significant decrease in HAI-1 mRNA levels for the first 6 h after the starvation. The level of HAI-1 mRNA recovered gradually and was modestly upregulated after 24 h of serum-free conditions (Fig. 2b). In contrast, under hypoxic conditions (1% O_2+ 150 μM $CoCl_2$), the level of HAI-1 was upregulated even 3 to 6 h after serum starvation and the time-course difference between normoxic conditions and hypoxic treatment was statistically significant (repeated measure two-way analysis of variance test, $p<0.01$; Fig. 2b). The hypoxia-induced upregulation of HAI-1 mRNA was also observed in WiDr human colon adenocarcinoma cells (Fig. 2c). In this cell line, the peak induction was observed 3 to 6 h after treatment.

We then checked the level of membrane form of the mature HAI-1 protein. Cells were pretreated with PMA in order to remove pre-synthesized HAI-1 from the cell surface (PMA induced ectodomain shedding via cellular protease activity) [12]. One hour after PMA treatment, the cells were washed and subjected to hypoxic treatment. A preliminary time-course study (3, 6, 9, 12, and 24 h of hypoxia) indicated that the most significant difference in protein level occurred at 9 h. In Fig. 2d, a representative result following 9-h hypoxia is shown. It should be noted that after PMA treatment, relatively little cell surface HAI-1 remained. Hypoxic stress (1% O_2) increased HAI-1 protein modestly (1.4-fold) and $CoCl_2$ treatment also increased the protein in a dose-dependent manner with peak stimulation at 150 μM. At 600 μM $CoCl_2$, the synthesis of HAI-1 was

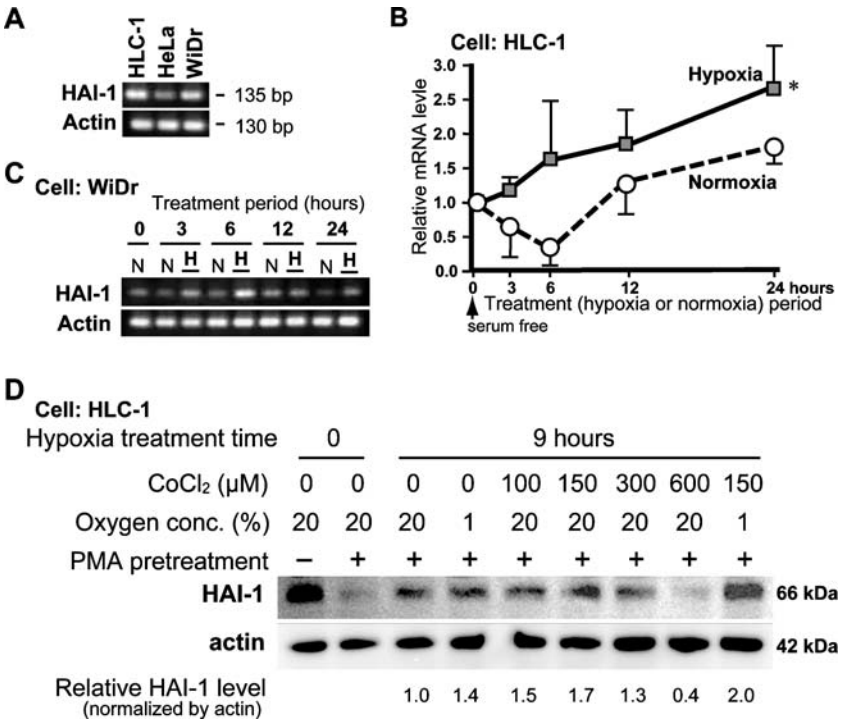

Fig. 2 Upregulation of HAI-1 in response to hypoxia. **a** Expression of HAI-1 mRNA in human epithelial cell lines (HLC-1, HeLa, WiDr) evaluated by conventional RT-PCR. **b** Quantitative real-time RT-PCR for HAI-1 mRNA expression in response to hypoxia treatment. HLC-1 cells were cultured under normoxia (20% O_2) or hypoxia (1% O_2+ 150 μM $CoCl_2$) in serum-free condition for 24 h. The level of HAI-1 mRNA normalized to the actin mRNA level was measured at each time point. The values are means ± SD (2× triplicate experiments). *p <0.01 compared with normoxia control (repeated measure two-way analysis of variance test). **c** Effects of hypoxia on HAI-1 mRNA expression in WiDr cells. A representative result of conventional RT-PCR is shown. *N* Normoxia (20% O_2), *H* hypoxia (1% O_2+150 μM $CoCl_2$). **d** Effects of hypoxia on the expression of HAI-1 protein. The cells were pretreated with PMA to remove cell surface HAI-1 by ectodomain shedding, and the effects of low oxygen concentration (1% O_2) and/or $CoCl_2$ on the levels of the mature membrane form of HAI-1 in serum-free condition were analyzed by immunoblot

rather suppressed. The most significant stimulatory effect was achieved by combined treatment with 1% O_2 and 150 μM $CoCl_2$, showing a twofold enhancement of the mature membrane form of HAI-1 compared with control cells. Following 12 to 24 h of treatment, the level of cell surface HAI-1 reached a plateau, probably due to establishment of an equilibrium between synthesis and ectodomain shedding of the membrane form of HAI-1. After 24 h, the protein levels did not significantly differ between the hypoxia-treated cells and normoxic controls (data not shown).

Effect of oxidative stress on the expression of HAI-1

We also examined the effect of oxidative stress on the expression of HAI-1 (Fig. 3). HLC-1 cells were pretreated with PMA to remove the preexisting membrane form of HAI-1 as described above, and the cells were incubated with varying concentrations of H_2O_2 (150–900 μM) in serum-free conditions, and the level of the membrane form of HAI-1 was analyzed. The oxidative stress enhanced the level of HAI-1, and the most significant difference was observed 4 h after H_2O_2 treatment with peak stimulation at 300 μM H_2O_2 (Fig. 3a). The level of HAI-1 mRNA was also increased upon H_2O_2 treatment. Quantitative real-time RT-PCR study revealed that the time-course difference between H_2O_2-treated cells and control cells was statistically significant (repeated measure two-way analysis of variance test, $p<0.01$). At 2 and 6 h of H_2O_2 treatment, HAI-1 mRNA increased approximately threefold compared with corresponding control cells (Fig. 3b).

Analysis of the promoter region responsible for hypoxic stress- and oxidative stress-induced HAI-1 transcription

For a better understanding of the regulation of HAI-1 expression, we analyzed the promoter activity of the *HAI-1*/*spint-1* gene with a dual luciferase assay. Figure 4 shows the schematic representation of the prepared constructs and the results of the reporter assay. Experiments were limited to HLC-1 and HeLa cells, because the transfection efficiency for WiDr cells was too low. In agreement with our observation that HLC-1 expressed more HAI-1 than HeLa cells (Fig. 2a), the promoter activity was higher in HLC-1 compared with HeLa (Fig. 4). In both HLC-1 and HeLa cell lines, the key promoter activities were identified in the 5′-flanking regions −79 to −30 from the transcription start site of *HAI-1*/*spint-1* gene. This region contained a potential overlapping binding site for Egr-1-3/Sp1, which was well conserved between human and mouse [10]. Indeed, mutation in the Egr-1-3/SP1 binding sites resulted in significantly reduced luciferase activity in both cell lines (Fig. 5).

Next, we tested the effects of hypoxia and oxidative stress on the promoter activity using the above luciferase constructs. Both hypoxic (1% O_2+150 μM $CoCl_2$) and oxidative (300 μM H_2O_2) treatments enhanced luciferase activity in HLC-1 cells in a statistically significant level (Fig. 6). Again, the 5′-flanking region −79 to −30 appeared to be the key promoter region. Notably, the hypoxia- or oxidation-induced response was not observed when the mutant promoter (−211/+43 mut) was used, indicating that the overlapping Egr-1-3/Sp1 binding site (−42 to −58) was in fact responsible for the stress-induced upregulation of HAI-1 transcription (Fig. 6). HeLa cells showed similar results (data not shown).

Expression of HAI-1 in areas of hypoxic and/or oxidative microenvironment in vivo

Finally, we stained serial tissue sections with antibodies against HAI-1, HIF-1α (hypoxia marker), and 4-HNE (oxidation marker) using human lung cancer tissues. Membrane form HAI-1-positive cases (i.e., strong immuno-

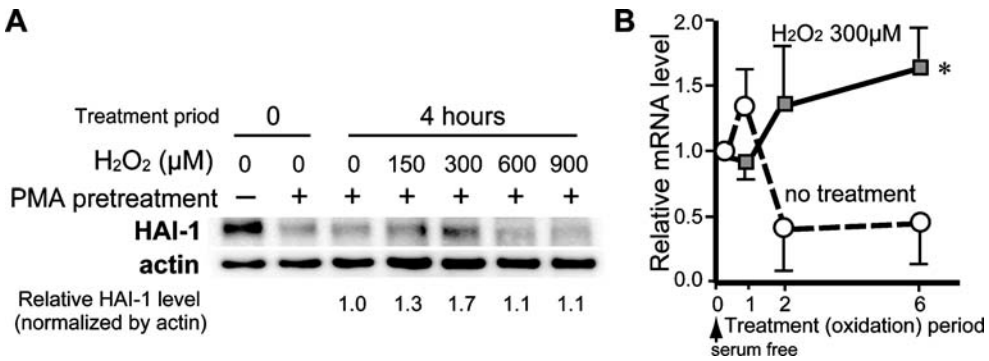

Fig. 3 Upregulation of HAI-1 in response to oxidation stress. **a** Effects of oxidative stress by H_2O_2 on the expression of HAI-1 protein by HLC-1 cells. The cells were pretreated with PMA to remove cell surface HAI-1 by ectodomain shedding. Immunoblots analyzed the effects of H_2O_2 (150–900 μM) on the expression of the mature membrane form of HAI-1 in serum-free medium. **b** Quantitative real-time RT-PCR for HAI-1 mRNA expression in response to H_2O_2 treatment. HLC-1 cells were cultured with or without 300 μM H_2O_2 in serum-free condition for 6 h. The level of HAI-1 mRNA normalized to the actin mRNA level was measured at each time point. The values are means ± SD (triplicate experiments). *$p<0.01$ compared with control (repeated measure two-way analysis of variance test)

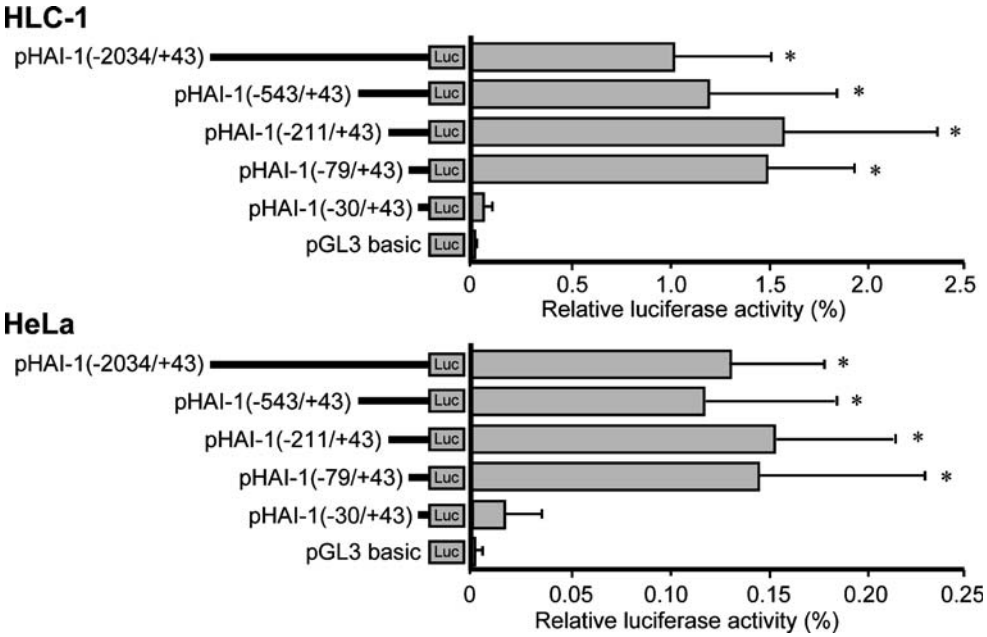

Fig. 4 Analysis of the human *HAI-1*/*spint-1* gene promoter in HLC-1 and HeLa cells. Transient transfection assays were performed with a dual luciferase reporter assay. Promoter constructs containing the indicated nucleotide sequences of the *HAI-1*/*spint-1* 5′-flanking region are indicated. The activity was measured as relative light units adjusted for efficiency of transfection standardized by co-transfection with pRL-TK. Promoter activities were expressed as a percentage of the luciferase activity compared to cells transfected with the maximal promoter construct driven by SV-40 promoter and enhancer. *$p<0.05$, compared with pHAI-1 (−30/+43; Mann–Whitney *U* test)

reactivity of membrane form HAI-1 in more than 10% of the cancer cells) were observed in 4/11 of adenocarcinoma, 3/7 of squamous cell carcinoma, and 1/2 of large cell carcinoma cases. In addition, strong cytoplasmic immunoreactivity was seen in two cases of adenocarcinoma and one large cell carcinoma, without apparent membranous localization. Positive HIF-1α immunoreactivity and 4-HNE was observed in 50% and 80% of the lung carcinoma cases, respectively. Most (7/8) of the HAI-1-positive cases were 4-HNE positive, and 60% (5/8) of the HAI-1-positive cases were also HIF-1α positive. As shown in Fig. 7a–d, the areas showing enhanced 4-HNE and HIF-1α immunoreactivity tended to accompany enhanced HAI-1 expression. However, HAI-1-positive cells were not necessarily positive for these hypoxia and oxidation markers (Fig. 7e), suggesting the complexity of the regulation of HAI-1 expression in vivo.

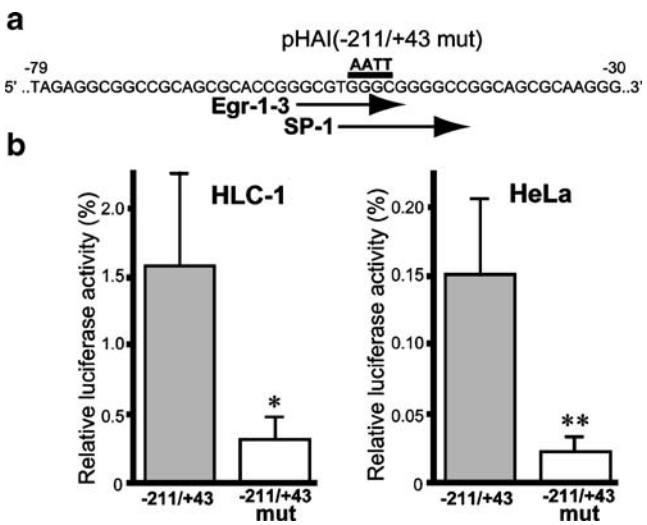

Fig. 5 Functional analysis of the key promoter region of the *HAI-1*/*spint-1* gene. **a** Nucleotide sequence of the presumptive key promoter region. This region contains an overlapping Egr-1-3/Sp-1 site. Specific base-pair substitution used to mutate the Egr-1-3/Sp-1 site is indicated. **b** Effect of the mutation on reporter activities in HLC-1 and HeLa cells. Values are means ± SD of triplicate assays. *$p<0.05$; **$p<0.01$, compared with wild-type promoter (Mann–Whitney *U* test)

Discussion

Data presented here demonstrate that HAI-1 expression is enhanced in response to hypoxic and oxidative stresses. Furthermore, the key promoter region for this response can now be assigned to the 5′-flanking region −79 to −30 of the *HAI-1*/*spint-1* gene. Although the biological significance of this response remains to be clarified, HAI-1 may have crucial roles in cells under hypoxic and/or oxidative stresses. These findings are compatible with previous immunohistochemical observations that showed enhanced epithelial expression of HAI-1 at sites of severe injury or carcinoma cells at the invasion front [11, 12, 22] because those areas are likely under oxidative or hypoxic stresses [4, 28]. Indeed, areas showing 4-HNE immunoreactivity or upregulated HIF-1α expression often showed enhanced HAI-1 immunoreactivity in vivo, suggesting that the microenvironments with upregulated HAI-1 may be subject to hypoxic and/or oxidative stresses.

HAI-1 is predominantly expressed on the surface of epithelial cells and is thought to be functioning on the cell surface [12]. However, its role in epithelial biology is poorly understood at present. The key promoter region of the *HAI-1*/*spint1* gene assigned in this study is composed of an overlapping Egr-1-3/Sp1 binding site, and this site is in

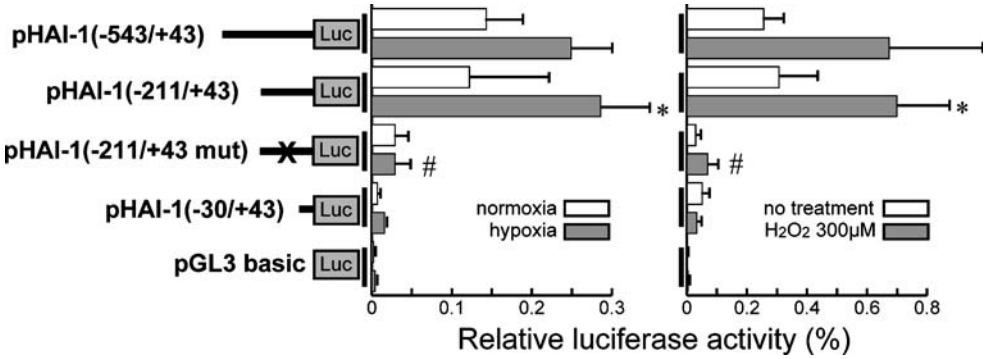

Fig. 6 Functional analysis of the key promoter region in hypoxia and oxidation-induced HAI-1 upregulation (HLC-1 cells). Mutation in the overlapping Egr-1-3/Sp-1 site resulted in impaired responses to hypoxic and oxidative stresses. Luciferase activities were measured 16 h after the treatment. *$p<0.05$ compared to the corresponding non-treated control; #$p<0.01$ compared to the wild-type promoter with hypoxia or H_2O_2 treatment

fact responsible for the stress-induced transcription of *HAI-1/spint1*. The molecule(s) which binds to this domain and activates *HAI-1/spint-1* transcription in responses to stress remains to be determined. However, it is known that Egr-1 plays a role in cellular responses to hypoxia and oxidative stress. This suggests that the hypoxic stress- and oxidative stress-induced upregulation of HAI-1 observed here may be mediated by Egr-1 [23, 33, 34]. In addition, SP-1 is reportedly induced by hypoxia in brain tissue [25]. To further confirm the molecule(s) interacting with key promoter element(s) of *HAI-1/spint-1* gene, rigorous electrophoretic mobility shift assay will be required.

The functional role of upregulated HAI-1 in cells subjected to hypoxia and/or oxidative stress remains to be determined. HGF and its receptor MET are known to be upregulated in the hypoxia [29], and upregulation of HGF/MET signaling in hypoxia may be an important tissue reaction for survival in such conditions [3, 20]. Since HAI-1 is a potent inhibitor of HGF-activating enzymes such as HGF activator, matriptase, and hepsin [14, 15], our present observation showing hypoxia-induced HAI-1 upregulation is rather surprising. However, HAI-1 regulates the activation of matriptase and is required for the trafficking of matriptase to the cell surface even though it can inhibit matriptase activity [16, 24]. Without HAI-1, activation and trafficking of matriptase appear to be significantly impaired [16, 24]. Such paradoxical effects of HAI-1 are also observed in the case of HGF activator. HAI-1 inhibits HGF activator, but paradoxically, serves as a reservoir of HGF activator on the cell surface [12]. Therefore, the membrane form of HAI-1 may be a critical molecule for the optimal activity of HGF-activating proteases in the pericellular microenvironment, thereby ensuring HGF/MET signaling that might be required for cellular survival. An alternative possibility is that HAI-1 may suppress excess protease activities on the cellular surface and may protect the cells from a cascading protease reaction.

Recently, another membrane-bound serine protease inhibitor, HGF activator inhibitor type 2 (HAI-2) was reported to be upregulated in response to hypoxia in breast cancer [7]). Interestingly, the expression of HAI-2 in breast carcinoma correlates with aggressiveness of the tumor in vivo [7]. HAI-2 shows a molecular structure similar to HAI-1, having two extracellular Kunitz domains, but lacking an LDL receptor-like domain and an N-terminal MANSC (motif at N terminus with seven cysteines) domain [8, 14]. Although little is known regarding the mechanism underlying hypoxia-induced HAI-2 upregulation and the function of HAI-2 in tumors, this evidence suggests that membrane-bound Kunitz-type serine protease inhibitors, HAI-1 and HAI-2, could have protective roles in epithelial cells under hypoxic and oxidative conditions. Further detailed clinico-pathological analyses of the HAI-1 expression in various tumors and injured tissues may lead to a better understanding of the biological roles of HAI-1 in vivo.

In summary, our results indicate that the tissue microenvironment regulates the expression of cell surface HAI-1 which in turn may modulate protease activities at the epithelial cell surface. Further work is needed to identify the cognate protease(s) and functional roles of the membrane form of HAI-1 under various pathologic conditions. Such studies might open new avenues for unraveling the

Fig. 7 Comparative immunohistochemical analysis of HAI-1 and hypoxia/oxidation markers in pulmonary cancer tissues. Serial sections were simultaneously stained with anti-HAI-1, HIF-1α, and 4-HNE antibodies. **a** Well-differentiated adenocarcinoma showing stromal invasion. **b** Dysplastic respiratory epithelium observed in a case of pulmonary squamous cell carcinoma. Note that the lumen is filled with necrotic tissue. **c** Invasive cancer cells (poorly differentiated adenocarcinoma cells) in fibrotic tissue with concomitant immunoreactivities to both HAI-1 and 4-HNE. **d** Well-differentiated squamous cell carcinoma. Cells adjacent to keratinizing degeneration (cancer pearl) show enhanced immunoreactivity to both HAI-1 and HIF-1α. **e** Well-differentiated adenocarcinoma. Cancer cells with membranous HAI-1 expression in this portion show immunoreactivities to neither HIF-1α nor 4-HNE

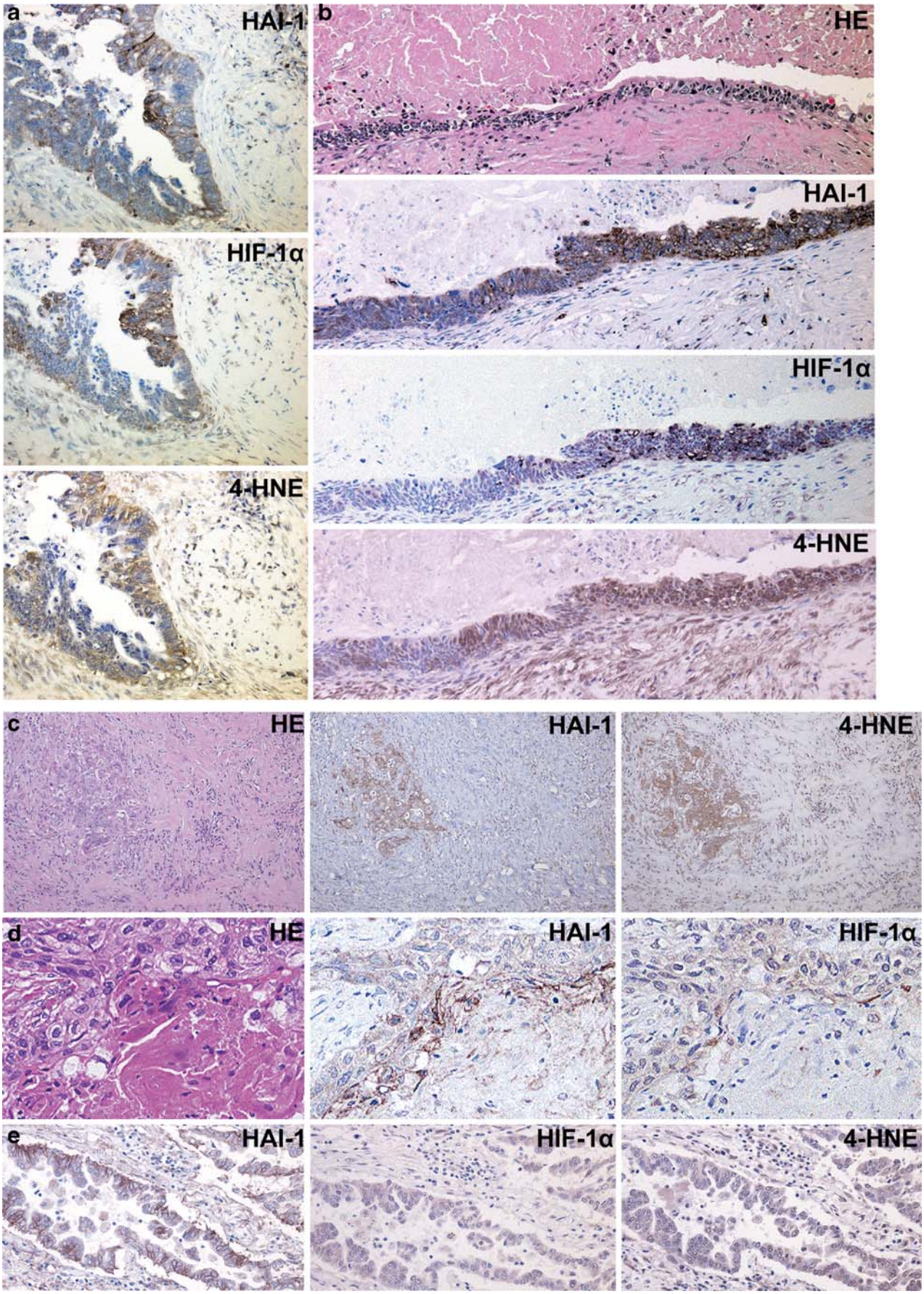
a
HAI-1
HIF-1α
4-HNE
b
HE
HAI-1
HIF-1α
4-HNE
c
HE
HAI-1
4-HNE
d
HE
HAI-1
HIF-1α
e
HAI-1
HIF-1α
4-HNE

molecular complexities of epithelial responses under challenging physiological conditions.

Acknowledgments This work was supported in part by grants-in-aid for scientific research (B) no. 17390116, 20390114 and the Miyazaki Prefecture Collaboration of Regional Entities for the Advancement of Technological Excellence, Japan Science and Technology Agency.

Conflict of interest statement We declare that we have no conflict of interest.

References

1. Akiyama Y, Nagai M, Komaki W, Marutsuka K, Asada Y, Kataoka H (2006) Expression of hepatocyte growth factor activator inhibitor type 1 in endothelial cells. Hum Cell 19:91–97
2. Betsunoh H, Mukai S, Akiyama Y, Fukushima T, Minamiguchi N, Hasui Y, Osada Y, Kataoka H (2007) Clinical relevance of hepsin and hepatocyte growth factor activator inhibitor type 2 expression in renal cell carcinoma. Cancer Sci 98:491–498
3. Cai L, Johnstone BH, Cook TG, Liang Z, Traktuev D, Cornetta K, Ingram DA, Rosen ED, March KL (2007) Suppression of hepatocyte growth factor production impairs the ability of adipose-derived stem cells to promote ischemic tissue revascularization. Stem Cells 25:3234–3243
4. Christofori G (2006) New signals from the invasive front. Nature 441:444–450
5. Donaldson SH, Hirsh A, Li DC, Holloway G, Chao J, Boucher RC, Gabriel SE (2002) Regulation of the epithelial sodium channel by serine proteases in human airways. J Biol Chem 277:8338–8345
6. Fan B, Brennan J, Grant D, Peale F, Rangell L, Kirchhofer D (2007) Hepatocyte growth factor activator inhibitor-1 (HAI-1) is essential for the integrity of basement membranes in the developing placental labyrinth. Dev Biol 303:222–230
7. Generali D, Fox SB, Berruti A, Moore JW, Brizzi MP, Patel N, Allevi G, Bonardi S, Aguggini S, Bersiga A, Campo L, Dogliotti L, Bottini A, Harris AL (2007) Regulation of hepatocyte growth factor activator inhibitor 2 by hypoxia in breast cancer. Clin Cancer Res 13:550–558
8. Guo J, Chen S, Huang C, Chen L, Studholme DJ, Zhao S, Yu L (2004) MANSC: a seven-cysteine-containing domain present in animal membrane and extracellular proteins. Trends Biochem Sci 29:172–174
9. Itoh H, Yamauchi M, Kataoka H, Hamasuna R, Kitamura N, Koono M (2000) Genomic structure and chromosomal localization of the human hepatocyte growth factor activator inhibitor type 1 and 2 genes. Eur J Biochem 267:3351–3359
10. Itoh H, Kataoka H, Meng JY, Hamasuna R, Kitamura N, Koono M (2001) Mouse hepatocyte growth factor activator inhibitor type 1 (HAI-1) and type 2 (HAI-2)/placental bikunin genes and their promoters. Biochim Biophys Acta 1519:92–95
11. Kataoka H, Suganuma T, Shimomura T, Itoh H, Kitamura N, Nabeshima K, Koono M (1999) Distribution of hepatocyte growth factor activator inhibitor type 1 (HAI-1) in human tissues. Cellular surface localization of HAI-1 in simple columnar epithelium and its modulated expression in injured and regenerative tissues. J Histochem Cytochem 47:673–682
12. Kataoka H, Shimomura T, Kawaguchi T, Hamasuna R, Itoh H, Kitamura N, Miyazawa K, Koono M (2000) Hepatocyte growth factor activator inhibitor type 1 is a specific cell surface binding protein of hepatocyte growth factor activator (HGFA) and regulates HGFA activity in the pericellular microenvironment. J Biol Chem 275:40453–40462
13. Kataoka H, Itoh H, Nuki Y, Hamasuna R, Naganuma S, Kitamura N, Shimomura T (2002) Mouse hepatocyte growth factor (HGF) activator inhibitor type 2 lacking the first Kunitz domain potently inhibits the HGF activator. Biochem Biophys Res Commun 290:1096–1100
14. Kataoka H, Miyata S, Uchinokura S, Itoh H (2003) Roles of hepatocyte growth factor (HGF) activator and HGF activator inhibitor in the pericellular activation of HGF/scatter factor. Cancer Metastasis Rev 22:223–236
15. Kirchhofer D, Peek M, Lipari MT, Billeci K, Fan B, Moran P (2005) Hepsin activates pro-hepatocyte growth factor and is inhibited by hepatocyte growth factor activator inhibitor-1B (HAI-1B) and HAI-2. FEBS Lett 579:1945–1950
16. Lee MS, Kiyomiya K, Benaud C, Dickson RB, Lin CY (2005) Simultaneous activation and hepatocyte growth factor activator inhibitor 1-mediated inhibition of matriptase induced at activation foci in human mammary epithelial cells. Am J Physiol Cell Physiol 288:C932–941
17. Lee SL, Dickson RB, Lin CY (2000) Activation of hepatocyte growth factor and urokinase/plasminogen activator by matriptase, an epithelial membrane serine protease. J Biol Chem 275:36720–36725
18. Leyvraz C, Charles RP, Rubera I, Guitard M, Rotman S, Breiden B, Sandhoff K, Hummler E (2005) The epidermal barrier function is dependent on the serine protease CAP1/Prss8. J Cell Biol 170:487–496
19. Lin CY, Anders J, Johnson M, Dickson RB (1999) Purification and characterization of a complex containing matriptase and a Kunitz-type serine protease inhibitor from human milk. J Biol Chem 274:18237–18242
20. Moumen A, Patane S, Porras A, Dono R, Maina F (2007) Met acts on Mdm2 via mTOR to signal cell survival during development. Development 134:1443–1451
21. Mukai S, Fukushima T, Naka D, Tanaka H, Osada Y, Kataoka H (2008) Activation of hepatocyte growth factor activator zymogen (pro-HGFA) by human kallikrein 1-related peptidases. FEBS J 275:1003–1017
22. Nagaike K, Kohama K, Uchiyama S, Tanaka H, Chijiiwa K, Itoh H, Kataoka H (2004) Paradoxically enhanced immunoreactivity of hepatocyte growth factor activator inhibitor type 1 (HAI-1) in cancer cells at the invasion front. Cancer Sci 95:728–735
23. Nose K, Ohba M (1996) Functional activation of the egr-1 (early growth response-1) gene by hydrogen peroxide. Biochem J 316:381–383
24. Oberst MD, Chen LY, Kiyomiya K, Williams CA, Lee MS, Johnson MD, Dickson RB, Lin CY (2005) HAI-1 regulates activation and expression of matriptase, a membrane-bound serine protease. Am J Physiol Cell Physiol 289:C462–470
25. Salminen A, Liu PK, Hsu CY (1995) Alteration of transcription factor binding activities in the ischemic rat brain. Biochem Biophys Res Commun 212:939–944
26. Sasaki M, Ikeda H, Kataoka H, Nakanuma Y (2006) Augmented expression of hepatocytes growth factor activator inhibitor type 1 (HAI-1) in intrahepatic small bile ducts in primary biliary cirrhosis. Virchows Arch 449:462–471
27. Shimomura T, Denda K, Kitamura A, Kawaguchi T, Kito M, Kondo J, Kagaya S, Qin L, Takata H, Miyazawa K, Kitamura N (1997) Hepatocyte growth factor activator inhibitor, a novel Kunitz-type serine protease inhibitor. J Biol Chem 272:6370–6376
28. Sivridis E, Giatromanolaki A, Koukourakis MI (2005) Proliferating fibroblasts at the invading tumour edge of colorectal adenocarcinomas are associated with endogenous markers of hypoxia, acidity, and oxidative stress. J Clin Pathol 58:1033–1038

29. Sullivan R, Graham CH (2007) Hypoxia-driven selection of the metastatic phenotype. Cancer Metastasis Rev 26:319–331
30. Tanaka H, Nagaike K, Takeda N, Itoh H, Kohama K, Fukushima T, Miyata S, Uchiyama S, Uchinokura S, Shimomura T, Miyazawa K, Kitamura N, Yamada G, Kataoka H (2005) Hepatocyte growth factor activator inhibitor type 1 (HAI-1) is required for branching morphogenesis in the chorioallantoic placenta. Mol Cell Biol 25:5687–5698
31. Uhland K (2006) Matriptase and its putative role in cancer. Cell Mol Life Sci 63:2968–2978
32. Wu Q, Parry G (2007) Hepsin and prostate cancer. Front Biosci 12:5052–5059
33. Yan SF, Lu J, Zou YS et al (1999) Hypoxia-associated induction of early growth response-1 gene expression. J Biol Chem 274:15030–15040
34. Zhang P, Tchou-Wong KM, Costa M (2007) Egr-1 mediates hypoxia-inducible transcription of the NDRG1 gene through an overlapping Egr-1/Sp1 binding site in the promoter. Cancer Res 67:9125–913

Virchows Arch (2008) 453:359–367
DOI 10.1007/s00428-008-0664-z

ORIGINAL ARTICLE

Angiogenesis in salivary carcinomas with and without myoepithelial differentiation

A. F. Costa · A. P. D. Demasi · V. L. L. Bonfitto · J. F. L. Bonfitto · C. Furuse · V. C. Araújo · K. Metze · A. Altemani

Received: 4 March 2008 / Revised: 18 August 2008 / Accepted: 20 August 2008 / Published online: 16 September 2008

Abstract To investigate whether salivary carcinomas with and without myoepithelial differentiation could present differences regarding degree of angiogenesis, we compared tumor vascularization between adenoid cystic (31 cases) and epithelial-myoepithelial carcinomas (14) versus mucoepidermoid (37) carcinoma. The expression of peroxiredoxin I was also studied to verify the potential relationship between cellular metabolism and microvascular density. Microvascular density for CD34 and CD105 were significantly lower in carcinomas with myoepithelial differentiation. However, no correlation was found between degree of angiogenesis and amounts of myoepithelial cells. High-grade peroxiredoxin I expression was found in 73.7% of mucoepidermoid carcinomas, whereas 85.1% of carcinomas with myoepithelial differentiation presented low-grade expression. In conclusion, carcinomas with myoepithelial differentiation, regardless of the amounts of myoepithelial cells, are associated to a significantly lower vascular density. The reasons for this lower angiogenic activity remain to be determined but could be related to metabolic characteristics of the cancer cells.

A. F. Costa · V. L. L. Bonfitto · J. F. L. Bonfitto · K. Metze · A. Altemani
Department of Pathology, Faculty of Medical Sciences, University of Campinas (UNICAMP), Campinas, Sao Paulo, Brazil

A. P. D. Demasi · C. Furuse · V. C. Araújo
São Leopoldo Mandic Dental Research Institute, Campinas, Sao Paulo, Brazil

A. Altemani (✉)
Departamento de Anatomia Patológica, Faculdade de Ciências Médicas, UNICAMP, Rua Tessália Vieira de Camargo 126, ZIP Code 13084-971 Campinas, Sao Paulo, Brazil
e-mail: aaltemani@uol.com.br

Keywords Angiogenesis · Adenoid cystic carcinoma · Mucoepidermoid carcinoma · Epithelial-myoepithelial carcinoma · Myoepithelial cell and microvessel density

Introduction

Tumor growth and metastasis are dependent on angiogenesis [8]. The properties of the tumor cells to release and induce angiogenic and anti-angiogenic factors are considered an essential mechanism for tumor-induced angiogenesis [15]. However, for a tumor itself to become neovascularized, not all cells must switch to the angiogenic phenotype [9], and different types of neoplastic cells vary regarding their abilities to release angiogenic and anti-angiogenic factors. In this context, comparing human myoepithelial and non-myoepithelial cells, the former are reported to present a multifaceted anti-angiogenic phenotype [24].

Myoepithelial cells normally surround ducts and acini of glandular organs such as the breast and salivary glands. However, in contrast to the breast, where tumors with myoepithelial component are not common, in salivary glands many of the neoplasms contain myoepithelial cells in their composition [14]. These tumors with myoepithelial component usually exhibit low ability to metastasize and/or slow progression [14, 25]. In terms of angiogenesis, we have recently reported that carcinomas with myoepithelial differentiation arising in pleomorphic adenoma presented lower microvessel density (MVD) for CD105 than those without such differentiation [28]. CD105 (endoglin), an accessory component of the transforming growth factor β receptor complex, plays a pivotal role in tumor-induced angiogenesis [1, 10, 23] and has been reported as a powerful marker of neovascularization [22].

Drawing from this background, we hypothesized that other types of salivary carcinomas (non-expleomorphic adenoma) with and without myoepithelial differentiation could also show differences regarding tumor-induced angiogenesis, which has been considered a putative target for cancer therapy [10, 22]. Thus, we compared MVD for CD34 (a pan-endothelial marker) and for CD105 (a neoangiogenesis marker) in intratumoral and peritumoral regions of adenoid cystic (ACC) and epithelial-myoepithelial carcinomas (EMC) versus mucoepidermoid (MEC) carcinomas. The latter is the most frequent salivary carcinoma without myoepithelial differentiation, whereas ACC and EMC represent those with myoepithelial differentiation.

However, tumor-induced angiogenesis is not only determined by the net balance between angiogenic inductors and inhibitors but also by nonangiogenic factors. Therefore, in an attempt to investigate the potential relationship between factors related to cellular metabolism and microvascular density, we verified the spatial relationship between proliferating tumor cells and closeness to vessels and the expression of peroxiredoxin I (Prdx-1) in carcinoma cells. Prdx-1 expression can be associated with cellular metabolism in view of its ability to decompose hydrogen peroxide (H_2O_2) [30], one of the harmful species generated as secondary products by metabolic reactions utilizing molecular oxygen. Among them, mitochondrial oxidative phosphorylation, the oxygen-dependent process responsible for the highest energy yield in the cells, is recognized as the primary endogenous source of H_2O_2 [7]. Prdx-1 is an enzyme that presents a high degree of affinity for H_2O_2 and its peroxidase activity, which requires electrons from the thioredoxin system and relies on a cysteine residue in the N-terminal region [30].

Materials and methods

The present study was approved by the Committee of Ethics of the University of Campinas, Brazil and was performed on 82 human salivary carcinomas samples (31 ACC, 14 EMC, and 37 MEC) which were retrieved from the files of the Department of Pathology of the University of Campinas (diagnosed between 1991 and 2007). Hematoxylin–eosin-stained slides from each tissue block were reviewed to confirm the pathological diagnosis and select a representative section for analysis. Demographic and clinical information was obtained from the patients' medical records.

Immunohistochemistry

One paraffin block from each case was chosen for the immunohistochemical study [27], and the following antibodies were used (Table 1): CD34 and CD105 for detection of blood vessels, α-smooth-muscle actin (α-SMA), and vimentin for detection of myoepithelial cells and Prdx-1 for cellular metabolism. The 5-μm sections were deparaffinized and hydrated, and endogenous peroxidase activity was quenched by immersion of the slides in 3% hydrogen peroxide. For all antibodies, except for α-SMA and anti-CD105, antigen retrieval (AR) was achieved by boiling in a steamer immersed in citrate buffer (pH6.0, for 30min). For CD105, AR was performed using 0.4% pepsin for 30min (Table 1). Only the sections for CD105 were incubated at 37°C with protein block serum free (code x0909, Dako, SA, Denmark) for 30min. Subsequently, for all antibodies, the sections were incubated overnight at 4°C with the primary antibody and afterwards with the EnVision polymer HRP and Envision+ (code K1491, DAKO, SA, Denmark) for 1h at 37°C. Sections were stained for 5min at 37°C with 3,3′-diaminobenzidine tetrahydrochloride (DAB) and counter-stained with hematoxylin.

Table 1 Details of the antibodies used for immunohistochemistry

Specificity	Clone	Dilution	Source	Buffer (AR)
CD34	QBEnd 10	1:50	Dako[a]	Citrate
CD105	SN6h	1:10	Dako[a]	Pepsin
Vimentin	V9	1:100	Dako[a]	Citrate
α-SMA	1A4	1:200	Dako[a]	None
Ki67	MIB1	1:150	Dako[a]	Tris–EDTA
Prdx-1	Polyclonal	1:450	Alexis[b]	Citrate

[a] Dako, SA, Denmark
[b] Aléxis, Lausen, Switzerland

Double-labeling immunohistochemical staining (EnVision doublestain, code K1395, Dakopatts S/A, Denmark) was performed for Ki67/CD34. Briefly, a monoclonal antibody anti-Ki67 (Table 1) was applied after antigen retrieval using Tris–EDTA buffer (pH8.9) and incubated overnight at 4°C; detection was achieved using the EnVision polymer HRP and DAB to visualize the binding of the first antibody. The sections were then incubated with a second antibody against CD34 (Table 1) at 4°C overnight. EnVision polymer linked to alkaline phosphatase and fast red as substrate chromogen system were used to complete the second immunostaining.

Negative controls were run by omitting primary antibodies.

Evaluation of staining

Microvessel counting

Immunohistochemical reactions for CD34 and CD105 were interpreted by two authors (AFC and VB) using a double-headed microscope. Two distinct sets of measurements

were performed in each tumor-stained section, in which the most vascularized areas at low power magnification (hotspots) were chosen for vessel counting at ×40 magnification: (a) three fields within the tumor mass (intratumoral vascular density) and (b) three fields within a high power field area from the tumor border (peritumoral vascular density). Microvessel density for CD34 as well as for CD105 were considered the mean number of vessels in these areas in each sample. Single endothelial cells or clusters of these cells, with or without lumen, were considered individual vessels. Vessels with muscular walls were excluded.

We also evaluated whether there was invasion of CD34- and/or CD105-positive vessels by carcinoma cells (tumor emboli).

Myoepithelial cell quantification

The relative numbers of stained cells for α-SMA and vimentin were considered in relation to all neoplastic cells seen for each stained section. The immunoreactivity was assessed using a two-tiered scale: <50% and ≥50% of positive cells.

Quantification of peroxiredoxin I expression in carcinoma cells

Prdx-1 immunostaining was semiquantified by a visual grading system in which the intensity of staining was categorized as negative (total absence of Prdx-1 immunostaining), low Prdx-1 expression (<25% of the tumor cells were positive), and high Prdx-1 expression (≥25% of positive cells; Fig. 5). The intensity of staining of tumor cells was classified as faint or intense in comparison to that of epithelial cells of ductal structures of salivary glands.

Distribution of proliferating carcinoma cells in relation to tumor vasculature

In order to verify the spatial relationship between proliferating tumor cells and closeness to vessels, the amounts of Ki67-positive carcinoma cells within an area of 100μm of radius around the vessels were subjectively compared with those beyond these limits in double-stained sections for Ki67/CD34.

Statistical analysis

Normal distribution of the values was evaluated by Kolmorogov–Smirnov test. The comparison between the three different tumor groups was done by analysis of variance (ANOVA) followed by the least square differences post hoc test. Microvessel density in different regions of the tumor was compared by ANOVA for dependent groups. Data were presented as mean ± SD, and the results with $p < 0.05$ were considered significant. All the statistical procedures were performed using WinSTAT, version 3.1.

Results

In ACC group, 79.4% were women, average age was 44 (19–65years), and lesions were located in parotid glands in four cases, submandibular glands in eight, and minor salivary glands in 19. ACCs were classified according to histological patterns [14] as tubular/cribriform, 19 cases, and solid, 12. In EMC group, 57% were women, average age was 55 (37 to 79), and lesions were located in parotid glands in seven cases, submandibular glands in two, and minor salivary glands in four. In MEC group, 62% were women, average age was 42 (7–68years), and lesions were located in parotid glands in nine cases, submandibular glands in five, and minor salivary glands in 23 cases. MECs were classified according to histological grades [14] as low/intermediate grade, 29 cases, and high grade, eight cases.

Microvascular density for CD34 and CD105

Figures 1 and 2 illustrate MVD for CD105 and CD34 in all groups. Comparing ACC and EMC (carcinomas with myoepithelial differentiation) with MEC (carcinoma without myoepithelial differentiation), a significant difference regarding CD34-MVD as well as CD105-MVD was detected in the intratumoral regions but not in the peritumoral areas (Table 2). MEC showed a significantly higher CD34-MVD and CD105-MVD in intratumoral regions where the positive vessels usually formed a rim of

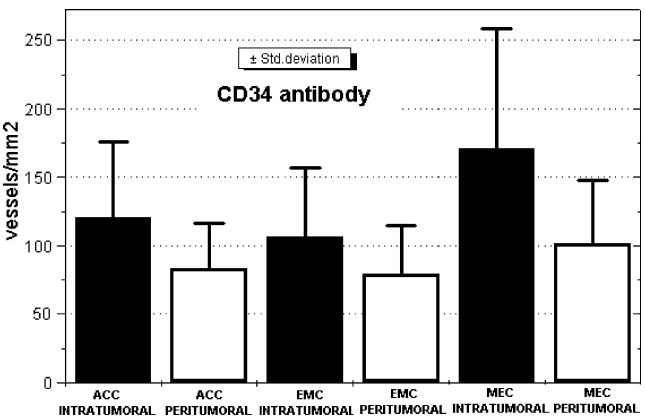

Fig. 1 CD34-MVD in intratumoral and peritumoral regions in adenoid cystic (*ACC*), epithelial-myoepithelial (*EMC*), and mucoepidermoid (*MEC*) carcinomas. ACC and EMC presented significantly lower CD34-MVD in intratumoral regions than MEC. Comparing intratumoral with peritumoral regions, the former exhibited significantly higher CD34-MVD in MEC and ACC

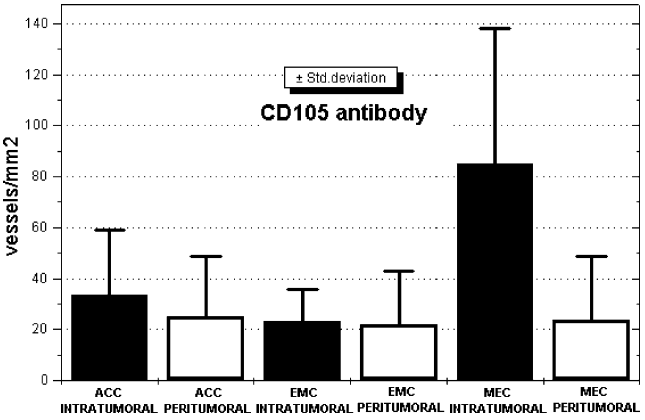

Fig. 2 CD105-MVD in intratumoral and peritumoral regions in adenoid cystic (*ACC*), epithelial-myoepithelial (*EMC*), and mucoepidermoid (*MEC*) carcinomas. ACC and EMC presented significantly lower CD105-MVD in intratumoral regions than MEC. Comparing intratumoral with peritumoral regions, the former exhibited significantly higher CD105-MVD only in MEC

capillaries immediately adjacent to the carcinomatous aggregates. In contrast, in ACC and EMC, both CD34-MVD and CD105-MVD were significantly lower, particularly CD105-positive vessels (Fig. 3).

Comparing intratumoral with peritumoral regions, in MEC, the former presented significantly higher CD34-MVD as well as CD105-MVD. In ACC, only CD34-MVD was significantly increased in intratumoral regions, whereas CD105-MVD was equally low in intratumoral and peritumoral areas. In EMC, intratumoral and peritumoral regions did not show significant differences regarding CD34-MVD as well as CD105-MVD (Figs. 1 and 2, Table 2).

Follow-up information, which ranged from 5 to 60months, was available in 30 patients (16 with ACC and 14 with MEC), and distant metastases were detected in five out of 16 patients with ACC and none of the 14 with MEC. In ACC group, comparing tumors from patients with and without distant metastases, neither intratumoral CD34-MVD (mean 17.1 versus 17.4) nor CD105-MVD (mean 4.7 versus 4.3) were increased in the metastatic group.

In sections stained by CD34 and CD105, vessels with tumor emboli were not found.

Myoepithelial cells

α-SMA and vimentin have been considered useful markers for identification of neoplastic myoepithelial cells [12]. In our series, α-SMA- and vimentin-positive cells consistent with myoepithelial cells were observed only in ACC and EMC cases. The findings regarding CD34-MVD and CD105-MVD in ACC group, subdivided according to the amount of α-SMA and vimentin-positive cells, are shown in Table 3. Tumors composed of ≥50% of α-SMA- or vimentin-positive cells did not present lower intratumoral CD34-MVD and/or CD105-MVD when compared to those containing <50% of positive cells (Fig. 4). In EMC, all tumors were composed of ≥50% of α-SMA or vimentin-positive cells.

Prdx-1 expression in carcinoma cells

In MEC, Prdx-1 expression was observed in 100% of 19 cases studied, in which 73.7% presented high Prdx-1 expression (Fig. 5). In contrast, in 22 cases of ACC, 9.0% showed high Prdx-1 expression, 36.3% low, and 54.5% were negative. In five cases of EMC, 40% presented high and 60% low Prdx-1 expression. The intensity of staining between myoepithelial and epithelial cells were compared in ACC and EMC. In the myoepithelial cells, the intensity was usually faint.

Distribution of proliferating carcinoma cells in relation to tumor vasculature

Comparing the amounts of Ki67-positive carcinoma cells within an area of 100μm of radius around the vessels with those beyond these limits, a spatial relationship between proliferating tumor cells and closeness to vessels was not identified in MEC, ACC, or EMC (Fig. 6).

Table 2 Microvascular densities by CD34 and CD105 antibodies in intratumoral and peritumoral regions of adenoid cystic (ACC), epithelial-myoepithelial (EMC) and mucoepidermoid (MEC) carcinomas

Groups	CD34-MVD intratumoral region (mean ± SD)	CD34-MVD peritumoral region (mean ± SD)	*p*	CD105-MVD intratumoral region (mean ± SD)	CD105-MVD peritumoral region (mean ± SD)	*p*
ACC	18.3±8.4	12.6±4.9	0.0143	5.1±3.8	4.0±3.5	0.34
EMC	16.2±7.6	11.7±5.7	0.0962	3.5±1.9	3.3±3.2	0.09566
MEC	26.0±13.2	15.4±7.0	0.0003	12.9±8.1	3.4±3.8	0.0001
p	0.0065	0.097		0.00003	0.61	

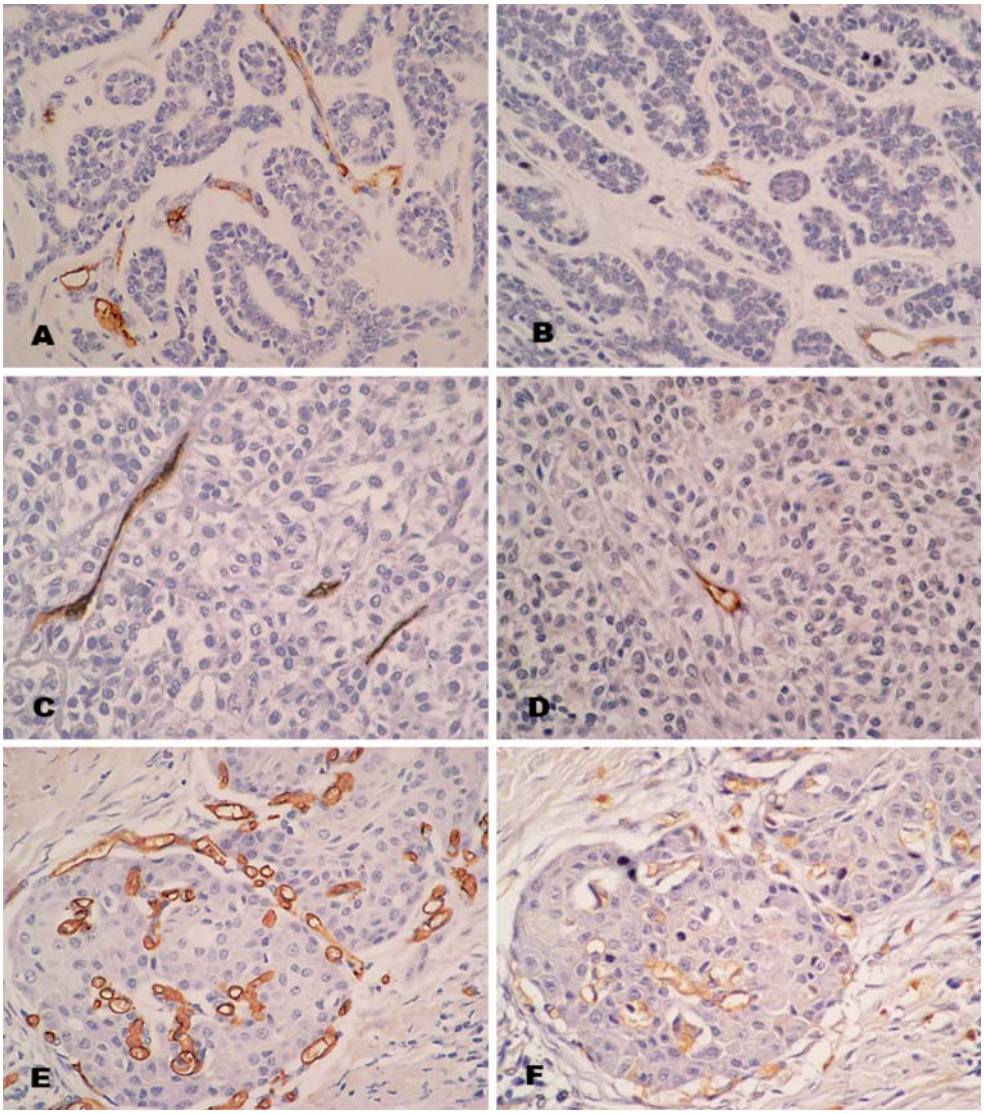

Fig. 3 CD34 (*left*) and CD105 (*right*)-positive vessels: in adenoid cystic carcinoma (**a**, **b**), in epithelial-myoepithelial carcinoma (**c**, **d**), and in mucoepidermoid carcinoma (**e**, **f**). In mucoepidermoid carcinoma, numerous CD34 and CD105 capillaries form a rim adjacent to carcinomatous aggregates whereas adenoid cystic and epithelial-myoepithelial carcinomas show few vessels stained by CD34 and CD105

Discussion

Several lines of evidence have shown that tumors with myoepithelial phenotype can be considered a distinct entity [25]. Compared to common malignant cell lines, myoepithelial cells (a) secrete high amounts of proteinase inhibitors and inhibitors of angiogenesis but low amounts of proteinases and of angiogenic factors; and (b) present increased expression of genes for angiogenic inhibitors and decreased expression in those for angiogenic factors. Furthermore, myoepithelial tumor xenografts compared to non-myoepithelial tumor xenografts exhibit minimal angiogenesis [2, 24]. Based on these findings, Barsky and Karlin [2] suggested that the myoepithelial tumor microenvironment would be inhibitory to angiogenesis. In line with this assumption, we recently showed that salivary carcinomas with myoepithelial differentiation arising in pleomorphic adenoma presented lower neoangiogenesis than those without such differentiation [28].

Thus, in the current study, to verify whether other salivary carcinomas present differences regarding the degree of tumor vascularization, we compared the most frequent carcinomas with and without myoepithelial differentiation (ACC and EMC versus MEC). In ACC and EMC,

Table 3 Microvascular densities by CD34 and CD105 antibodies in adenoid cystic carcinomas subdivided in two groups according to the amount of myoepithelial cells

Antibody	Amount of myoepithelial cells	CD34-MVD (mean)	CD105-MVD (mean)
α-SMA-positive cells	<50% (19 cases)	18.13	4.45
	≥50% (7 cases)	20.12	7.24
Vimentin-positive cells	<50% (20 cases)	18.85	4.41
	≥50% (6 cases)	18.05	7.85

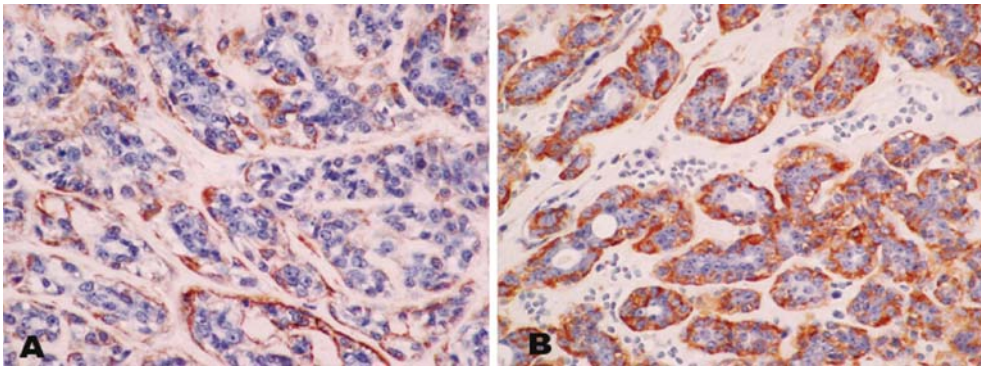

Fig. 4 Myoepithelial cells in adenoid cystic carcinomas: **a** tumor with a small number of myoepithelial cells (<50% of tumor cells) and **b** another with numerous cells (≥50% of tumor cells). CD34-MVD and CD105-MVD were higher in the latter (15.3 and 3.3 versus 8.3 and 2.0, respectively)

we detected significantly lower intratumoral CD34-MVD and CD105 MVD than in MEC. In contrast to CD34, which highlights the entire tumor-associated vessels and normal vessels, CD105 is over-expressed in the activated endothelial cells participating in neoangiogenesis but reacts weakly in normal tissues [3, 5, 20, 29]. As expected, we found that all tumors presented lower numbers of CD105-positive vessels in comparison to CD34-positive ones. This finding was particularly marked in ACC and EMC where CD105-positive vessels were usually scarce.

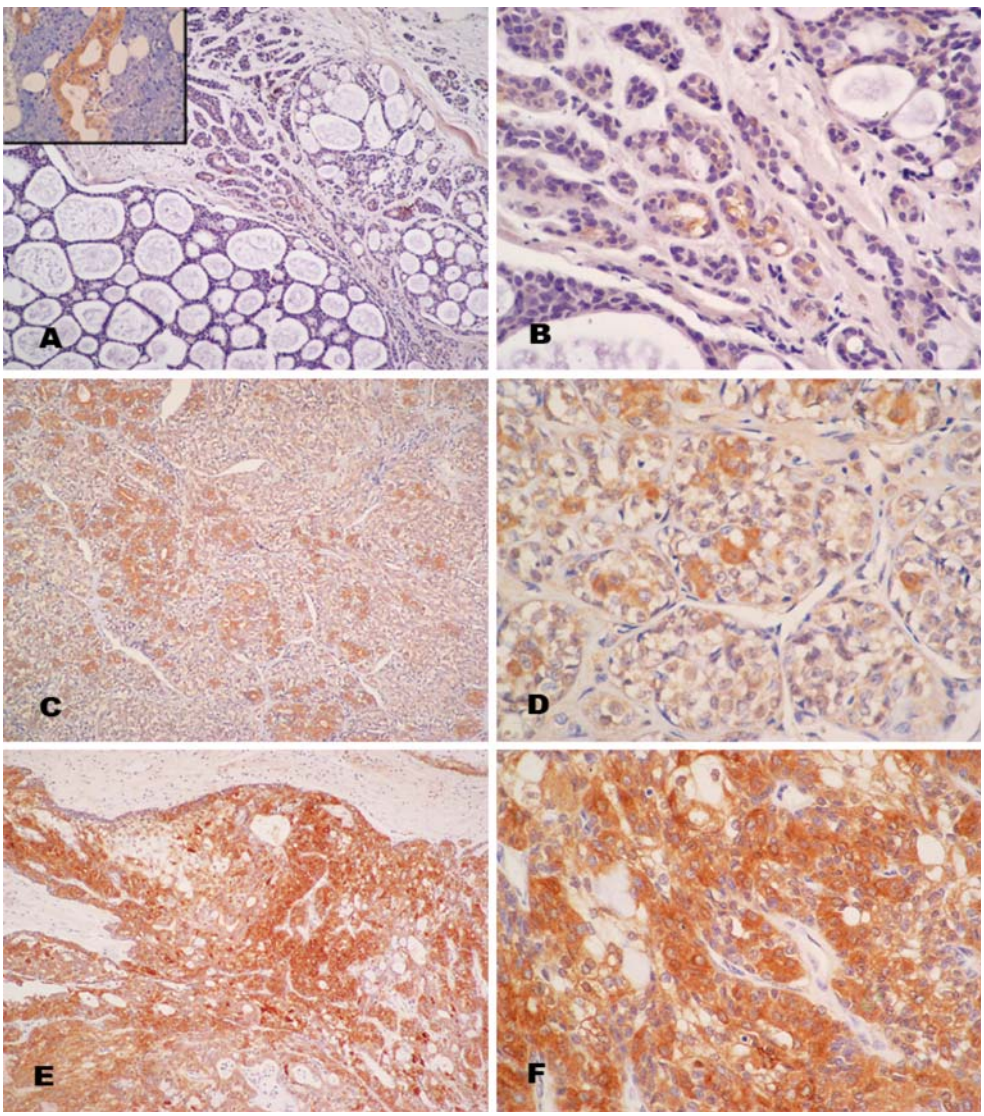

Fig. 5 Prdx-1 expression in carcinoma cells. Low Prdx-1 expression (<25% of positive cells) in ACC (**a**, **b**); high Prdx-1 expression (≥25% of positive cells) in EMC (**c**, **d**) and in MEC (**e**, **f**). The intensity of staining of tumor cells was classified as faint or intense in comparison to that of epithelial cells of ductal structures of salivary glands (*inset*), and in myoepithelial cells, the intensity was usually faint

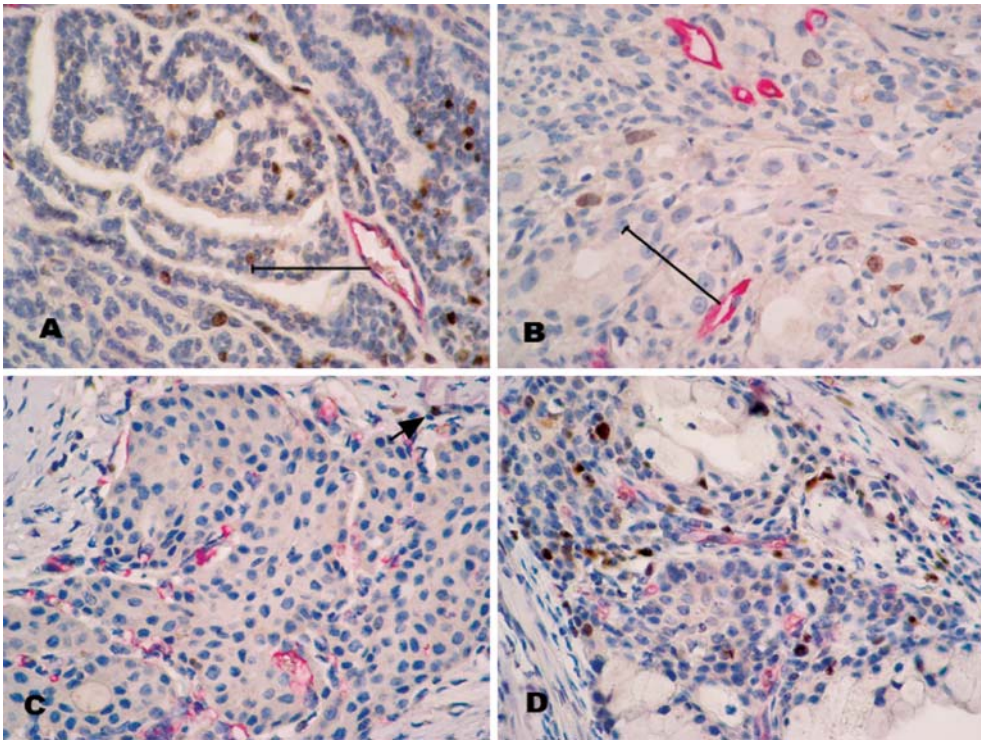

Fig. 6 Distribution of proliferating carcinoma cells in relation to tumor vasculature in double-stained sections for Ki67 (*brown*)/CD34 (*red*). A spatial relationship between proliferating tumor cells and closeness to vessels was not identified in ACC (**a**), EMC (**b**), or MEC (**c**, with rare Ki67+ cells [*arrow*], and **d** with numerous cells). *Bars* 100 μm

These results in ACC and EMC are in agreement with those in carcinomas with myoepithelial differentiation arising in pleomorphic adenomas [28] and reinforce that salivary carcinomas with myoepithelial component can be associated with lower angiogenesis in comparison to those without such differentiation. However, in the current series, some findings suggest that the anti-angiogenic phenotype of myoepithelial cells [24] may not play a pivotal role in the lower angiogenesis of these tumors. Among these findings are: (a) in carcinomas with myoepithelial differentiation, intratumoral regions (in which vessels are closer to the tumor cells) did not show lower level of MVD than peritumoral regions and (b) ACCs containing greater amount of myoepithelial cells were not associated with reduction of vascular density.

Studies have shown that microvessel density is not only determined by the net balance between angiogenic factors and inhibitors but also by nonangiogenic factors related to tumor metabolic demand [17]. The higher expression of Prdx-1 in MEC than in ACC and EMC suggests that salivary carcinomas without myoepithelial differentiation could present marked metabolic differences in relation to tumors with myoepithelial cells. As a function of the MVD and the consequent oxygen availability, it could be suggested that the relative contribution of mitochondrial oxidative phosphorylation and glycolysis for cellular energy supply is divergent among the tumors studied. The higher level of oxygen afforded by elevated MVD in MEC could lead to a sequential augment in the levels of mitochondrial activity, H_2O_2 formation, and Prdx-1 expression. Opposite effects could be expected to occur in ACC and EMC, which present diminished MVD. In these tumors, the low Prdx-1 expression levels could characterize a low rate of oxidative metabolism indicating that possibly they meet their energy demands predominantly via glycolysis, an oxygen-independent process. The absence of spatial relationship between proliferating cells (Ki67+) and closeness to vessels in carcinomas with myoepithelial differentiation, despite the low vascular density of these tumors, also reinforces that glycolysis could be an important metabolic pathway in these tumors. Considering that partial pressure of oxygen decreases to near zero at distance greater than 100μm from a vessel [4, 16], the marked cellular proliferation observed beyond this limit suggests that possibly these tumors maintain their metabolic activities predominantly via an oxygen-independent process.

The histological assessment of tumor vascularity can be used to broaden our understanding of the angiogenic process in neoplasia. It has been proposed that angiogenesis is generally most active at the tumor periphery, making it important to include the normal tissue/tumor interface in the area to be assessed [11]. In lung and breast carcinomas, it was shown that vascular density was high at the tumor periphery but decreased gradually towards the inner areas [18, 19]. However, in our series of salivary carcinomas, in which two sets of measurements (within

the tumor and at the invading front) were performed, the tumor periphery presented lower or similar microvascular density in comparison to intratumoral regions. The reasons for these variations in salivary carcinomas in relation to other types of cancer (such as lung and breast carcinomas) still need to be clarified. We believed that tissue-specific tumor features and/or growth rate of the tumors (lower in ACC, EMC and MEC and faster in lung and breast cancers) might be responsible for these findings. In terms of quantifying tumor angiogenesis, our results show that in salivary carcinomas, microvessel density should be measured in intratumoral regions, where angiogenesis is most active.

Tumors of high vascular density have been reported to be associated with an increased metastatic potential [13]. The angiogenic process is considered to increase the opportunity of development of metastases in many malignant tumors [26, 31]. Among salivary carcinomas, MEC and ACC are known to present important differences in terms of metastatic behavior. Lymph node involvement is more common in MEC whereas ACC is characterized by high incidence of distant metastases [14]. A recent in vitro study has suggested that ACC cells with higher metastatic potential might present greater stimulus to angiogenesis [32]. However, our findings did not support this assumption because comparison of ACCs with and without distant metastases did not reveal increase of CD34-MVD nor of CD105-MVD in the group with metastases. Another explanation for variations in the metastatic potential of ACCs might be differences in intrinsic properties of cancer cells themselves and/or of the tumor microenvironment [21]. The latter includes proteolytic modification of the extracellular matrix, allowing malignant cells better access to vessels [21].

Finally, the recognition of distinct patterns of tumor vascularization in carcinomas with and without myoepithelial differentiation may have implications in the field of anti-angiogenic therapy. CD105 promoter is predominantly active in proliferating endothelial cells, and this molecule is currently being evaluated as an ideal target for antiangiogenic therapies that aim to prevent the development of neovasculature [6]. Thus, this therapy should be preferentially directed towards the highly angiogenic tumors without myoepithelial differentiation, such as MEC, which presented numerous CD105-positive vessels. In contrast, this vascular targeting agent might be less effective in ACCs and EMC, where neoangiogenesis is usually low.

In conclusion, carcinomas with myoepithelial differentiation, regardless of the amounts of myoepithelial cells, are associated to a significantly lower vascular density, particularly in terms of CD105-positive vessels (neoangiogenesis). The reasons for this lower angiogenic activity remain to be determined but could be related to metabolic characteristics of the cancer cells.

Acknowledgements We thank Fundação de Amparo à Pesquisa do Estado de São Paulo (FAPESP) for supporting this study (grant number 07/55336-2).

All experiments comply with the current laws of Brazil.

We declare that we have no conflict of interest.

References

1. Barbara NP, Wrana JL, Letarte M (1999) Endoglin is an accessory protein that interacts with the signaling receptor complex of multiple members of the transforming growth factor-beta superfamily. J Biol Chem 274:584–594
2. Barsky SH, Karlin NJ (2005) Myoepithelial cells: autocrine and paracrine suppressors of breast cancer progression. J Mammary Gland Biol Neoplasia 10:249–260
3. Bodey B, Bodey B, Siegel SE, Kaiser HE (1998) Over-expression of endoglin (CD105): a marker of breast carcinoma-induced neovascularization. Anticancer Res 18:3621–3628
4. Dewhirst MW, Secomb TW, Ong ET, Hsu R, Gross JF (1994) Determination of local oxygen consumption rates in tumors. Cancer Res 54:3333–3336
5. Ding S, Li C, Lin S, Yang Y, Liu D, Han Y, Zhang Y, Li L, Zhou L, Kumar S (2006) Comparative evaluation of microvessel density determined by CD34 or CD105 in benign and malignant gastric lesions. Hum Pathol 37:861–866
6. Duff SE, Li C, Garland JM, Kumar S (2003) CD105 is important for angiogenesis: evidence and potential applications. FASEB J 17:984–992
7. Finkel T, Holbrook NJ (2000) Oxidants, oxidative stress and the biology of ageing. Nature 408:239–247
8. Folkman J (1990) Endothelial cells and angiogenic growth factors in cancer growth and metastasis. Introduction. Cancer Metastasis Rev 9:171–174
9. Folkman J (2003) Angiogenesis and apoptosis. Semin Cancer Biol 13:159–167
10. Fonsatti E, Del Vecchio L, Altomonte M, Sigalotti L, Nicotra MR, Coral S, Natali PG, Maio M (2001) Endoglin: an accessory component of the TGF-beta-binding receptor-complex with diagnostic, prognostic, and bioimmunotherapeutic potential in human malignancies. J Cell Physiol 188:1–7
11. Fox SB, Harris AL (2004) Histological quantitation of tumour angiogenesis. APMIS 112:413–430
12. Furuse C, Sousa SO, Nunes FD, Magalhães MH, Araújo VC (2005) Myoepithelial cell markers in salivary gland neoplasms. Int J Surg Pathol 13:57–65
13. Gasparini G, Harris AL (1995) Clinical importance of the determination of tumor angiogenesis in breast carcinoma: much more than a new prognostic tool. J Clin Oncol 13:765–782
14. Goode RK, El-Naggar AK, Huvos AG (2005) Chapter 5. In: Barnes L, Eveson JW, Reichart P, Sidransky P (eds) World health organization classification of tumours. Head and neck tumours. Pathology and genetics. IARC, Albany, US, pp 219–222
15. Gupta MK, Qin RY (2003) Mechanism and its regulation of tumor-induced angiogenesis. World J Gastroenterol 9:1144–55
16. Helmlinger G, Netti PA, Lichtenbeld HC, Melder RJ, Jain RK (1997) Solid stress inhibits the growth of multicellular tumor spheroids. Nat Biotechnol 15:778–783
17. Hlatky L, Hahnfeldt P, Folkman J (2002) Clinical application of antiangiogenic therapy: microvessel density, what it does and doesn't tell us. J Natl Cancer Inst 94:883–893
18. Kakolyris S, Fox SB, Koukourakis M, Giatromanolaki A, Brown N, Leek RD, Taylor M, Leigh IM, Gatter KC, Harris AL (2000)

Relationship of vascular maturation in breast cancer blood vessels to vascular density and metastasis, assessed by expression of a novel basement membrane component, LH39. Br J Cancer 82:844–851
19. Kakolyris S, Giatromanolaki A, Koukourakis M, Kaklamanis L, Kouroussis CH, Bozionelou V, Georgoulias V, Gatter KC, Harris AL (2001) Assessment of vascular maturation in lung and breast carcinomas using a novel basement membrane component, LH39. Anticancer Res 21:4311–4316
20. Kumar P, Wang JM, Bernabeu C (1996) CD 105 and angiogenesis. J Pathol 178:363–366
21. Kumar V, Abbas AK, Fausto N (2005) Chapter 7. In: Robbins, Cotran (eds) Pathologic basis of disease. Elsevier Saunders, Philadelphia, US, pp 269–342
22. Li C, Guo B, Bernabeu C, Kumar S (2001) Angiogenesis in breast cancer: the role of transforming growth factor beta and CD105. Microsc Res Tech 52:437–449
23. Li C, Issa R, Kumar P, Hampson IN, Lopez-Novoa JM, Bernabeu C, Kumar S (2003) CD105 prevents apoptosis in hypoxic endothelial cells. J Cell Sci 116:2677–85
24. Nguyen M, Lee MC, Wang JL, Tomlinson JS, Shao ZM, Alpaugh ML, Barsky SH (2000) The human myoepithelial cell displays a multifaceted anti-angiogenic phenotype. Oncogene 19:3449–3459
25. Ogawa Y (2003) Immunocytochemistry of myoepithelial cells in the salivary glands. Prog Histochem Cytochem 38:343–426
26. Romani AA, Borghetti AF, Del Rio P, Sianesi M, Soliani P (2006) The risk of developing metastatic disease in colorectal cancer is related to CD105-positive count. J Surg Oncol 93:446–455
27. Sabattini E, Bisgaard K, Ascani S, Poggi S, Piccioli M, Ceccarelli C, Pieri F, Fraternali-Orcioni G, Pileri SA (1998) The EnVisionTM+ system: a new immunohistochemical method for diagnostics and research. Critical comparison with the APAAP, ChemMateTM, CSA, LABC and SABC techniques. J Clin Pathol 51:506–511
28. Soares AB, Juliano PB, Araujo VC, Metze K, Altemani A (2007) Angiogenic switch during tumor progression of carcinoma ex-pleomorphic adenoma. Virchows Arch 451:65–71
29. Wang JM, Kumar S, Pye D, van Agthoven AJ, Krupinski J, Hunter RD (1993) A monoclonal antibody detects heterogeneity in vascular endothelium of tumours and normal tissues. Int J Cancer 54:363–370
30. Wood ZA, Poole LB, Karplus PA (2003) Peroxiredoxin evolution and the regulation of hydrogen peroxide signaling. Science 300:650–653
31. Yue L, Wei-qun Y, Lu G-w, Wei Wang H (2006) Correlation between CD105 expression and postoperative recurrence and metastasis of hepatocellular carcinoma. BMC Cancer 6:110
32. Zhang J, Peng B (2007) In vitro angiogenesis and expression of nuclear factor kappaB and VEGF in high and low metastasis cell lines of salivary gland adenoid cystic carcinoma. BMC Cancer 7:95 doi:10.1186/1471-2407-7-95

Virchows Arch (2008) 453:369–375
DOI 10.1007/s00428-008-0666-x

ORIGINAL ARTICLE

Delivering a pathology curriculum in an integrated medical course

Norman J. Carr · Martin Olmos · John Bushnell

Received: 19 May 2008 / Revised: 21 August 2008 / Accepted: 23 August 2008 / Published online: 13 September 2008

Abstract Modern integrated medical curricula usually do not include a separate pathology course. Consequently, there is a risk that important pathological principles may be omitted. We aimed to ensure that pathology is properly represented by developing a core pathology curriculum created in consultation with local pathologists. Appropriate information technology to track the delivery of this material within the integrated curriculum structure was developed using a learning content management system in which a metadata schema was constructed. This allows a sophisticated view of where and how pathology appears in the course and can also increase the visibility of the subject by demonstrating the central place of pathology in medicine. In conclusion, a core curriculum in pathology that can be tracked by information technology with sufficient power and flexibility is a solution to the potential loss of pathology from integrated medical courses. We believe the result is superior to a stand-alone pathology course.

Keywords Medical education · Pathology teaching · Curriculum development · Learning content management

Pathology is a core subject, the link between basic science and clinical medicine [1]. Its importance to medical students is emphasised in the Australian Medical Council's goals and objectives of basic medical education [2] and is made explicit by the General Medical Council in the statement that medical graduates 'must know about and understand…abnormal structure and function, including the natural history of human diseases' [3].

However, there is widespread concern amongst pathologists that medical students learn in sufficient pathology in modern medical courses [4–6]. In general, medical educators have moved away from traditional discipline-based curricula towards integrated curricula. Such courses are considered to help students see the clinical relevance of the basic sciences, to make links with other subjects and to learn the complex process of clinical decision-making [1, 7–10]. Nevertheless, the loss of the dedicated 'pathology course' in such integrated curricula is often considered a retrograde step resulting in students encountering insufficient pathology. Not only could students fail to learn pathology in sufficient depth but they might also have insufficient experience of pathology to consider choosing it as a career [4–6].

The new medical curriculum at the University of Wollongong is an example of an integrated course. One of the challenges in creating the new curriculum was to address the problems of incorporating the teaching of pathology. This paper describes how appropriate information technology (IT) allows a core curriculum in pathology to be delivered and assessed. The IT database can be interrogated easily to demonstrate exactly how and when the pathology curriculum has been included in the course. In this way, a 'virtual pathology course' can be tracked within the integrated curriculum. We believe this addresses many of the fears that pathologists might otherwise entertain about integrated medical courses.

Setting

The Graduate School of Medicine at the University of Wollongong is a new medical school which has an

Electronic supplementary material The online version of this article (doi:10.1007/s00428-008-0666-x) contains supplementary material, which is available to authorized users.

N. J. Carr (✉) · M. Olmos · J. Bushnell
Graduate School of Medicine, University of Wollongong,
New South Wales 2522, Australia
e-mail: ncarr@uow.edu.au

integrated curriculum leading to the award of the MB BS. It is based on 93 clinical problems around which the content is arranged (Electronic supplementary material, Fig. 1). The clinical competencies and underpinning knowledge that a newly qualified doctor would need to deal with each problem are clearly defined in a 'blueprint' cross-referenced to the course learning outcomes. Pathology is fully integrated into the curriculum, and there is no separate pathology course. From the perspective of pathology as a discipline, there are risks associated with this curriculum structure: if an important pathological principle happens not to be addressed directly by any of the clinical problems, it may be missed out entirely. Anecdotally, this is one of the objections that pathologists often raise when an integrated curriculum is developed without a separately identifiable pathology course.

We decided to develop a core curriculum in pathology so we could ensure that all important pathological principles would be included in the course. We wanted to link this pathology curriculum to our information management system so we could track exactly where the material was being delivered and assessed.

Developing the core curriculum

One of us (NJC) devised a core curriculum comprising a syllabus in general and systematic pathology based on a combination of what is included in standard undergraduate textbooks, previous experience in teaching pathology to undergraduates and national guidelines [5]. The resulting draft was then circulated to practicing pathologists in the region for comment—not only histopathologists but also clinical and general pathologists. The initial draft was modified as a result of this feedback. A second circulation resulted in the working version of the core curriculum. We believe this process has produced a better result than if we had just taken a curriculum produced elsewhere and tried to use it. The reason is that each course is unique, and some aspects of a core curriculum may be applicable to one course but not another. Our pathology curriculum is tailored to our course, is up to date and takes into account the opinion of local practicing pathologists.

In one study, circulating drafts of checklists of pathology content to pathologists tended to result in an increase in the number of topics, and the authors of that study 'exercised vigilance in trying to ensure that imbalance of scope and emphasis did not occur' [11]. Our experience was similar—topics and disease entities were added at each iteration of the circulated draft. We found that starting with a lean original draft was helpful in preventing a final version that was too large and unwieldy. Trying to be too comprehensive from the start may have resulted in a syllabus too long to be useful. Our aim was to produce a list of core material essential to understanding the pathology relevant to the 93 clinical problems that comprise the course rather than a comprehensive list of all the pathology a medical student might conceivably encounter.

Part of the core curriculum is shown in Table 1. However, we do not suggest that what we have developed would be suitable for all medical schools, because it has been tailored to our particular needs. For example, microbiology and genetics have limited representation because these fields are separate science entities in our course. On the other hand, we stray into the borderland with sociology and ethics in considering the definition and nature of 'disease' because this topic is not covered in the social sciences in our medical school.

Information technology

The educational design of the course required a number of characteristics from the technology. In particular, in order to allow pathology content in the course to be identified, content must be tracked within the curriculum using a metadata schema, which is a system resembling the cataloguing of items used by libraries. Metadata is structured information describing the characteristics of an item; the individual elements together with their meaning form a schema. For example, the National Library of Medicine uses a metadata schema that includes such characteristics as keywords and MeSH headings that are used when searching the database [12]. Having constructed a metadata schema for the course, the various components, including the pathology core curriculum, can be mapped to it as described later. Other requirements of the technology include: the ability to hold many large digital resources; user access to content via the metadata schema and the multiple taxonomies it generates; availability of content throughout the course; cohort-specific content persistence (e.g. a cohort in fourth year has access to the content they covered in their first year, not what the current first year cohort is covering), with minimum duplication; permission control over content, to allow specific subgroups access to specific content and version control of content.

A learning content management system called Equella (The Learning Edge, Hobart, Australia) was selected to meet these requirements. It was extensively customised with the creation of XSL templates, reports and power searches. It was integrated with version 4 of Blackboard Vista (Blackboard Inc, Washington D.C., USA) through its PowerLink tool, as the online environment and portal to all content for students and staff.

A curriculum metadata schema was created, describing the clinical problems, learning outcomes, body systems,

Table 1 This is an extract from the core curriculum

General Pathology
Place of pathology in medical practice
Scientific basis of medicine
Medicine in the "Western" tradition is based on scientific principles (i.e. testable hypotheses)
Pathological processes are central to the scientific understanding of disease
However, there are other ways in which people think about disease (e.g. patient-centred vs. doctor-centred concepts)
Using the laboratory (*also relevant to working in a multidisciplinary team*)
Sending specimens to the lab
Interacting with lab staff
Writing request forms
Lab request as professional consultation
Death and post mortem issues
The autopsy: its role, indications, basic procedures and reconstruction
Ethical/spiritual issues for practitioners and relatives
Writing death certificates
Public health data are derived from death certificates
Interpreting laboratory data
Concept of the reference range and normal distribution
The laboratory disciplines (microbiology, immunology, haematology, clinical genetics, clinical chemistry)
Common electrolyte problems—hyper/hyponatraemia, hyper/hypokalaemia, hypercalcaemia
Abnormal lipid profile
Laboratory techniques
Histology
Gross observations, tissue processing and staining
Electron microscopy
Immunohistochemistry
Cytology
Genetics
Cytogenetics—karyotyping; spectral karyotyping
In situ hybridisation (e.g. FISH)
PCR and principal applications
Southern blotting (also Northern?)
DNA microarray analysis and principal applications
Immunology
Immunoassay
Western blotting
ELISA
Methods based on antibody precipitation
Microbiology
Microbiology culture and sensitivity
Principles of diagnostic methods (morphology, biochemistry, immunology, PCR)
Clinical Biochemistry
Enzyme assays
Protein separation techniques (electrophoresis, chromatography)
Analytical techniques used for
Substances in body fluids (sugars, lipoproteins, hormones)
Drug testing
Haematology
Flow cytometry
Blood smear
Basic concepts in pathology
What is a "disease"?
Disease classification
Why do doctors classify disease into diagnoses?
Use of jargon in medicine
Causes and mechanisms of disease
Aetiology vs. pathogenesis
Immediate aetiology as agent of underlying sociopolitical cause
Categories of aetiological agents (useful when dealing with a diagnostic dilemma): genetic, metabolic, toxic, vascular, physical, infectious, neoplastic, etc.
Abnormal structure and abnormal function are related
Abnormalities in structure can cause symptoms
Abnormalities in structure are useful diagnostically (clinical examination, radiology, operative findings and macroscopic and microscopic pathology)
Congenital disease—definition; examples
Agenesis
Hypoplasia
Ectopia
Screening for disease
Principles and controversies
Examples (cervical cytology, PSA, colon)
Responses of cells to changes in their environment
Hypoxic cell damage
Pathogenesis
Causes of ischaemia
Consequences for the cell
Reversible vs. irreversible injury
Morphological consequences of ischaemia
Changes in organelles
Infarction (*link to necrosis*)
Physical and chemical agents causing cell damage
Heat, cold, electricity, trauma, radiation, pressure
Drugs and toxins
Free radicals
Cell death
Necrosis
Types, and significance when encountered in a path report (*link to infarction*)
Apoptosis
Pathological and physiological causes
Stimulation and inhibition of apoptosis
Caspase cascade
Basic morphology and its relation to intracellular processes
Autolysis
Term used by pathologists
Potentially reversible structural adaptations of tissues
Hypertrophy and hyperplasia
Definition
Pathogenesis of illustrative examples
Hyperplasia can predispose to neoplasia
Atrophy
Definition
Pathogenesis of illustrative examples

Table 1 (continued)

General Pathology
Metaplasia
Definition
Pathogenesis of illustrative examples
Abnormal accumulations
Definition, main causes and significance (when encountered in a path report) of:
Calcification
Haemosiderin
Fatty change
Lipofuscin
Amyloid
Crystals (gout)
Inflammation
Inflammation has evolved because it has survival advantage, but can produce disease out of proportion to the cause (*links with immunology and host defence*)
Chemical mediators
Endogenous
Histamine
Serotonin
Cytokines
Prostaglandins, leucotrienes and lipoxins
Nitric oxide
Exogenous (all cascade systems)
Kinins
Complement
Clotting factors *(link to haemostasis)*
Fibrinolytic system
Acute inflammation
Definition
Cardinal signs
Vascular and cellular components
The "acute inflammatory cell" and macrophages
Recruitment of neutrophils to the site of inflammation
Phagocytosis
Intracellular killing
Mast cells
Haemodynamic changes
Morphology
Pus, suppuration
Inflammation of serous and mucous membranes
Gangrene
Use of term by doctors
Pathogenesis
Morphology
Sequelae
Resolution
Granulation tissue and scarring (*link to wound healing and necrosis*)
Components of granulation tissue
collagen deposition=fibrosis=scarring
Abscess/empyema
Fistula and sinus formation
Chronic inflammation
Chronic inflammation
Definition and causes
Cells
Macrophages
Lymphocytes and plasma cells
Eosinophils
Granulomas and giant cells
Nature
Significance when encountered
Wound healing
Keloid
First and second intention
Factors inhibiting wound healing
Fracture healing and potential complications
Systemic effects of inflammation
Systemic inflammatory response syndrome
Pyrexia, acute phase reactants, malaise, etc
Host defence and immunopathology
Innate vs. adaptive immunity *(link to immunopathology)*
Examples and how they may be breached:
Mechanical barriers
Secretion contents and currents
Commensal bacteria
Cells of the innate immune system
T-cells and B-cells
Function
Organisation into lymphoid tissue
Antigen-presenting cells and the MHC
Types of antibody and their main characteristics
Cytotoxic, helper and suppressor T-cells
NK cells
Response of the adaptive immune system to antigens
Specificity
Diversity
Memory
Recognition of self
Principles of: hypersensitivity types I–IV
Autoimmunity
Principles
Organ specific
Non-organ specific
Transplant rejection
Immunodeficiency
Inherited
Drugs
AIDS
Diabetes and other systemic diseases
Vitamin and mineral deficiency
Neoplasia
Definition; benign vs. malignant
Metastasis
Classification of neoplasms by line of differentiation
Tumour nomenclature
Diagnosis by line of differentiation (*link to histopathological techniques*)
Grading (*link to prognostic features*)
Basic epidemiology
Common neoplasms and their incidence
Leading causes of death

Table 1 (continued)

General Pathology
Neoplasia is due to genetic alterations
Oncogenes and proto-oncogenes
Tumour suppressor genes
p53
Inherited vs. acquired genetic abnormalities
Carcinogenesis
Chemical agents
Ionising radiation
Viruses
Loss of immune surveillance
As genetic alterations accumulate, morphological changes occur
Dysplasia/intraepithelial neoplasia
Tumour markers and their use in diagnosis and management
Prognostic features
Stage
TNM system
Grade
Oedema
Basic pathophysiology
Pulmonary oedema
Pleural effusion
Ascites
Haemostasis, thrombosis and embolism
Formation of thrombus
Platelets
Clotting factors and fibrinolysis
Lab tests of haemostatic function
Diseases in which clotting is abnormal
Haemophilia
DIC
Thrombosis
Definition
Virchow's triad
Outcomes of thrombosis (*link to infarction*)
Embolism
Different materials that may embolise
Pulmonary thromboemboli (*link to DVT*)
Systemic thromboemboli
Shock
Definition
Pathogenesis and distinguishing features of
Hypovolaemic shock
Cardiogenic shock
Septic shock
Neurogenic shock
Anaphylactic shock
Multi-organ failure (*links to ARDS*, *acute tubular necrosis*, *adrenal haemorrhage*, *Sheehan's syndrome*, *ischaemic enterocolitis*, *etc.*)
Stone formation
Use example(s) to illustrate
Physical chemistry of precipitation
Varieties of stone
Pathogenesis
Complications

Comprises the General Pathology section

science specialties and clinical specialties that each item is associated with. This overlays multiple taxonomies on the content and allows detailed searching and interlinking via each of these fields. For example, students and staff can search across the entire course for resources, readings, lecture slides, etc. related to a particular specialty such as pathology. Further, navigation through the clinical problems' blueprints via these descriptors forms a 'curriculum web'. An example of how this can work in practice is shown in Supplementary Figs. 1 and 2 (Electronic supplementary material).

Student assessment is aligned with teaching via the learning outcomes that are stated for each learning activity. These outcomes are part of the metadata schema and represent the link between the pathology curriculum and assessment practices.

Since the 93 problem blueprints form the skeleton of our curriculum, navigating through these makes evident to students the integrated nature of the curriculum, as the blueprints are extensively interconnected through shared schema elements such as learning outcomes, specialties and body systems [13]. For example, they can easily see how pathology is integral to understanding the many problems and is not seen as an isolated subject. Furthermore, since students use this curriculum web to navigate through to resources, the curriculum becomes a usable everyday framework rather than a course outline document that is received in week one and never consulted again.

Detailed reports and charts can be generated using the metadata to track coverage of the specialties, problems, learning outcomes, and body systems in the course. An example of one such chart is shown in Supplementary Fig. 3 (Electronic supplementary material). These visualisations are very helpful in identifying coverage patterns and exceptions, as well as comparing the images from year to year for evaluation purposes. They suggest not only *where* in the course pathology is covered, but *how*. For example, Supplementary Fig. 3 (Electronic supplementary material) shows that pathology is covered consistently throughout the phase, suggesting the specialty is well integrated into the curriculum. Similar visualisations can be generated to show the coverage of pathology across the clinical problems and learning outcomes.

Staff and students have evaluated the school's online learning environment, and the comments have been encouraging and favourable. A typical student comment: 'It is a tremendous asset to both students and faculty. Not only does it allow you to revisit material remotely, but more importantly it systematically organises it for you, allowing you to go back and access material from previous weeks or months in mere seconds.' Moreover, this online learning environment has won international awards. It recently received an Australasian Society for Computers in Learning

in Tertiary Education award and was the top-ranked Platinum Learning Impact Award recipient from IMS Global, which recognises the use of learning technology in context world-wide.

Discussion

The fear that the absence of pathology as a separate subject in integrated curricula leads to insufficient pathology content in modern medical courses is widespread [4–6]. This paper has described a way in which these potential problems can be addressed by firstly developing a core curriculum and then using IT to tag the corresponding course content in a metadata schema to ensure the curriculum is properly delivered. We believe this two-fold approach is essential. Without a core pathology curriculum, the incorporation of pathology topics in the course as a whole might otherwise become a matter of chance. On the other hand, in an integrated curriculum, sophisticated IT is the only practical way of tracking the various components of the pathology core curriculum to ensure they appear in appropriate contexts.

There is another advantage to this system. Students use the metadata schema on a daily basis to find teaching material. Consequently, students to see the central place of pathology in medicine as they navigate the online environment. This can address the problem of lack of exposure of pathology in integrated curricula, since the loss of pathology courses may cause pathology to lose its visibility to students as a discipline, leading to problems of recruitment into the specialty [4–6]. Ensuring that pathology is properly represented in the curriculum by methods such as those described in this paper will at least allow students to adequately encounter the subject.

There are few other descriptions of core pathology curricula in the literature. In the field of oral pathology, the British Society for Oral and Maxillofacial Pathology (BSOMP) have published a minimum curriculum similar in style to ours [14]. They were prompted to do so because, like the General Medical Council, the General Dental Council (GDC) have guidelines for teaching students expressed as generic outcomes that do not identify specific pathology topics. Their solution was to produce a consensus minimum through the BSOMP Teachers Group and cross-reference the topics not only with the GDC guidelines but also the Quality Assurance Agency for Higher Education benchmark statements for dentistry. BSOMP, when constructing their minimum curriculum, took it to 'include elements of… epidemiology, aetiology, genetics, microbiology and transmission, immunology, innate host defences, pathogenesis, structural changes at the macroscopic and microscopic levels, sequelae, complications and the interrelationship between disease processes, diagnosis, management and prognosis'. This list is similar in scope to ours, but we also included use of the clinical laboratory and the place of pathology in medical practice.

At the College of Medicine, University of Iowa, a core list of morphological entities was constructed. All the morphological entities from a standard text (Robbins Pathologic Basis of Disease) were listed and circulated to faculty members. The selection criterion was that a 'physician in training should recognise classical examples or a diagrammatic representation of the following lesions, and distinguish them from each other.' The result was a list of 608 lesions that were considered core entities [15]. We did not use this method on the basis that it emphasised recognition of appearances at the expense of deep understanding of important principles. There are also guidelines for oral pathology from the United States, although their content and validity have been questioned on the basis that they emphasise an excess of factual knowledge [16].

If pathologists wish to see pathology flourish in modern curricula, they need to engage in the process of change and become involved in curriculum development, rather than romanticising the past [5, 6, 17]. If they do not, they are likely to become increasingly irrelevant in the development of medical education. As Marshall et al. succinctly put it: 'while the medical education train accelerates away, pathologists are at risk of being left on the platform arguing the benefits of steam' [18]. We believe that pathologists have the opportunity to make a significant contribution to medical education in the era of the integrated curriculum by developing well-designed core curricula and tracking delivery using appropriate IT.

Conflict of Interest Statement We declare that we have no conflict of interest.

References

1. Du Boulay C (1997) Learning pathology: why? how? when. J Clin Pathol 50:623–624
2. Australian Medical Council (2008) Goals and objectives of basic medical education. http://www.amc.org.au/accredgoals.asp Accessed 21 Apr 2008
3. General Medical Council (2002) Tomorrow's doctors: Recommendations on undergraduate medical education. GMC, London, p 6
4. Weedon D (2003) Whither pathology in medical education. Med J Aust 178:200–202
5. Royal College of Pathologists of Australasia (2003) Learning objectives for pathology in medical curricula. RCPA, Surry Hills, pp 3–9
6. Mattick K, Marshall R, Bligh J (2004) Tissue pathology in undergraduate medical education: atrophy or evolution. J Pathol 203:871–876

7. Albanese M, Mitchell S (1993) Problem based learning - a review of the literature on its outcomes and implementation. Acad Med 68:52–81
8. Bligh J (2000) Problem based learning - the story continues to unfold. Med Educ 34:688–689
9. Vernon D, Blake R (1993) Does problem based learning work? A meta-analysis of evaluative research. Acad Med 68:550–563
10. Bouhuijs PAJ, Schmidt HG, Berkel H (1993) Problem-based learning as an educational strategy. Network, Maastricht
11. Vernon-Roberts B, Cleary EG, Vernon-Roberts J (1997) Graded check lists to assist undergraduate students in self-directed learning and assessment in general and systematic anatomical pathology. Pathology 29:370–373
12. United States National Library of Medicine (2004) NLM metadata schema. http://www.nlm.nih.gov/tsd/cataloging/metafilenew.html Accessed 8 Aug 2008
13. Harden RM (2001) AMEE Guide No. 21: Curriculum mapping: a tool for transparent and authentic teaching and learning. Med Teach 23:123–137
14. Odell EW, Farthing PM, High A et al (2004) British Society for Oral and Maxillofacial Pathology, UK: minimum curriculum in oral pathology. Eur J Dent Educ 8:177–184
15. Dick F, Leaven T, Dillman D et al (1998) Core morphological concepts of disease for second-year medical students. Hum Pathol 29:1017–1020
16. Allen CM (1996) Oral and maxillofacial pathology: what should we teach and how should we teach it. Oral Surg Oral Med Oral Pathol 82:235
17. Domizio P, du Boulay C (2006) Working smarter. Career choices and career progression in the pathology specialties: national surveys of UK medical graduates. Bull Royal Coll Pathol 134:31–35
18. Marshall R, Cartwright N, Mattick K (2004) Teaching and learning pathology: a critical review of the English literature. Med Educ 38:302–313

Virchows Arch (2008) 453:377–386
DOI 10.1007/s00428-008-0670-1

ORIGINAL ARTICLE

The microscopic (optical and SEM) examination of putrefaction fluid deposits (PFD). Potential interest in forensic anthropology

P. Charlier · P. Georges · F. Bouchet · I. Huynh-Charlier · R. Carlier · V. Mazel · P. Richardin · L. Brun · J. Blondiaux · G. Lorin de la Grandmaison

Received: 17 July 2008 / Revised: 25 August 2008 / Accepted: 28 August 2008 / Published online: 16 September 2008

Abstract This article describes the potential interest in physical and forensic anthropology of the microscopic analysis of residues of putrefaction fluid, a calcified deposit frequently found associated with bone rests. Its sampling and analysis seem straightforward and relatively reproducible. Samples came from archeological material (Monterenzio Vecchia, an Etruscan necropolis from the north of Italy dated between the fifth and third century B.C.; body rests of Agnès Sorel, royal mistress died in 1450 A.D.; skull and grave of French King Louis the XI and Charlotte of Savoy dated from 1483 A.D.). All samples were studied by direct optical microscope and scanning electron microscopy. Many cytological, histological, and elemental analysis were possible, producing precious data for the identification of these remains and, in some cases, the cause of death.

Keywords Putrefaction · Decomposition · Forensic anthropology · Microscopy · Paleopathology

Introduction

After death, the whole body is subject to modifications related to its decomposition. Putrefaction, in its usual course, leads to liquefaction of tissues and to the formation of putrefaction fluid deposit (PFD). The fluid resulting from this process were mixed with different blood transudates

P. Charlier (✉) · G. Lorin de la Grandmaison
Department of Forensic Medicine and Pathology,
University Hospital R. Poincaré (AP-HP, UVSQ),
92380 Garches, France
e-mail: ph_charlier@yahoo.fr

P. Charlier
HALMA-IPEL (UMR 8164, CNRS), Lille 3 University,
Villeneuve d'Ascq, France

P. Georges
INRAP,
Saint-Orens-de-Gameville, France

F. Bouchet
Paleoparasitology Laboratory, Pharmacy Faculty,
Reims, France

I. Huynh-Charlier
Department of Radiology,
University Hospital La Pitié Salpétrière (AP-HP),
75013 Paris, France

R. Carlier
Department of Radiology,
University Hospital R. Poincaré (AP-HP, UVSQ),
92380 Garches, France

V. Mazel · P. Richardin
C2RMF, Louvre Museum,
Paris, France

L. Brun
Department of Pathology, University Hospital,
Parakou, Benin

J. Blondiaux
CEPN,
Walincourt-Selvigny, France

[1]. Such putrefaction fluid, initially present in the anatomical cavities or regions (thorax, abdomen, skull, limbs), is secondarily released all around the body when the skin barrier is broken [2–4]. This liquid, viscous and fatty, with a sharp red color, made up of more or less degraded cellular and tissue residues, is accompanied by multiple fatty acids [5–9]. Its pH is acid, with a value ranging between 5 and 6 (in our experience). It surrounds the corpse and "bathes" the bones (it settles in those cavities left empty, like the sloping and concave part of the skull vault; parietal–occipital area for a body lying on the back: Fig. 1) [10–12]. With time, sedimentation and calcification occur, precipitating the decomposition liquid. This can be seen, for example, on the internal table of the skull vault in a particular point corresponding at the hydroaeric level [13–15].

We submitted several archeological samples of decomposition liquid to a classical optic microscope (OM) and scanning electronic microscopic (SEM) analysis in order to try to identify any tissue or, at least, cellular fragments still present in this substance. It consisted in a direct application of microscopic examination coupled with an elemental surface analysis.

Material and methods

The material included six archeological samples, half analyzed with a SEM and half with an OM.

Almost all of the skeletons from the Etruscan–Celtic necropolis of Monterenzio Vecchia (MV; made up of 40 subjects, close to Bologna, Italy; archeological researches under the authority of Prof. Daniele Vitali and Thierry Lejars) presented comparable deposits of reddish color on the sloping and endocranial part of the occipital bone [16], but, due to conservative reasons, only three of them were sampled (tombs MV 15, MV 25, and MV 26). These 1-cm-long fragments of PFD were sampled directly into the skull during archeological and paleopathological survey.

Fig. 1 Macroscopic sight of a calcified deposit of fluid of putrefaction on the endocranium of the subject MV 12

They were then cleaned by a fine scraping with non-contaminating plastic instruments and a delicate vaporization of pressured air on all the faces during 10 min. No gold covering was realized in order to be able to perform elemental analysis on the surface. Environmental SEM examination of each sample was directly performed on a Philips XL30 CP with X-ray microanalysis (energy-dispersive X-ray spectroscopy). The resolution of the microscope was 3.5 nm at 30 kV using the secondary electron detector. All images were stored using a standard resolution digital frame store.

A study with optical microscope was also carried out on other samples: PFD taken from the funeral urn of Agnès Sorel (buried in the Saint-Ours collegial of Loches, Indre-and-Loire, France in 1450), PFD recovered on the interior slopes of French King Louis the XI's sarcophagus (buried in the Notre-Dame basilica of Cléry-Saint-André, Loiret, France, in 1483), PFD sampled on the endocranium of French Queen Charlotte of Savoy (second wife of French King Louis the XI, buried at his side in 1483). Due to conservative reasons, an SEM examination was not possible for these last three samples.

The protocol followed for optical microscope sample preparation was as follows:

- The first step consisted in a very fine fragmentation of the sample. This was justified by the fact that the PFD has no architecture of it own and that this fragmentation does not consist in a loss of information (since we worked in a microscopic scale). In addition, this reduction allowed for a better penetration of the fixative substances.
- In order to rehydrate and fix the samples, they were immersed in 20% diluted acetic acid for 48 h, in order to slowly decalcify the fragments of PFD.
- Our solution was obtained using the following two phases: a liquid phase made of the PFD in suspension and a solid-phase slope. These two phases will be studied separately.
- The cytological analysis of the PFD in suspension began with the sampling of 200 μL from the supernatant. This liquid was then centrifuged (800 turns per minute for 10 min) in order to obtain two spots per slide. Four slides were produced by sample: two slides were colored by the technique of Papanicolaou after a fixing of the spots with a lacquer; the two other blades were colored by the technique of the May–Grünwald–Giemsa (MGG) after fixing of the spots to the air.
- The study of the remaining solid phase (base of centrifugation) was carried out after a new centrifugation (3,500 turns per minute for 10 min). The supernatant was kept in reserve (for a later possible

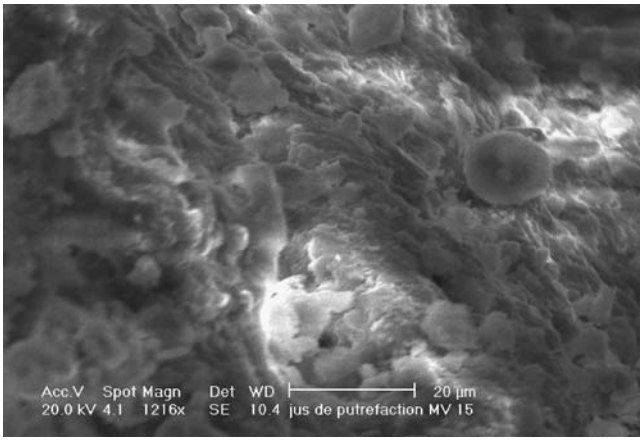

Fig. 2 Red blood cells observed within the PFD of the subject MV 15 (SEM, magnification ×1,200)

cytological study) while the base was recuperated then fixed 24 h in the AFA (acetic acid, formaldehyde, alcohol). As soon after fixation and decalcification, the sample was put in cassette on a foam, followed by the traditional circuit of inclusion (dehydration in xylene and increasing alcohol baths, then inclusion in liquid paraffin, cooling, section with the microtome (from 6 to 10 µm), deposit on an albumenized slide, air-drying free, dewaxing and rehydration by immersion in xylene then in decreasing alcohol baths to distilled water). Several colorations were carried out for each sample: periodic acid Schiff, Gram, toluidine blue, and hematoxylin, eosin, saffron (HES).

Results

Monterenzio Vecchia 15

Two fragments of 5- and 7-mm length were studied successively. The microscopic examination highlighted, at the level of the faces of fracture (i.e., at the contact between the PFD and the bone surface, not on the external surface), several biconcave circular formations measuring between 7 and 10 µm, strongly suggesting red blood cells (Fig. 2).

Some crystalline structures, on the surface, corresponded to postmortem contaminations or crystallizations of biological products. The laminated organization of the liquid of decomposition was apparent on certain zones of rupture, where up to six layers could be identified with a thickness from 2 to 4 µm.

The whole sample showed many cavities testifying to the semifluid (and bullous) character of the putrefaction liquid at the moment of its sedimentation and solidification (cavities corresponding to bubbles of fermentation or fat gaps microscopically empty). Many mycelia clusters could be highlighted, the size of the mycelium lying between 5 and 8 µm.

An elemental analysis (Fig. 3) was carried out on several sectors of the sample, showing similar aspects, i.e., a clear prevalence of three elements (calcium, silicon, and oxygen) and traces of carbon, aluminum, magnesium, phosphorus, potassium, titanium, and iron.

Monterenzio Vecchia 25

The analysis of this subject's PFD was of particular interest because of a paleopathological lesion diagnosed on the inner part of the skull: a 1-cm-long parasagittal left frontal osteolytic lesion interpreted as an angioma or, more generally, a vascular malformation that eroded (at the time of its development and due to its pulsatile character) the young bone close in contact (i.e., the cranial vault).

The surface of the sample was voluntarily incompletely cleaned in order to let appear the differences of composition and structure between the ground gangue of filling of the cadaver and the PFD itself. This ground gangue had an irregular marbled aspect in which no organic structure was identifiable. Many crystals were observed, of variable size and form. An elemental analysis was carried out in several

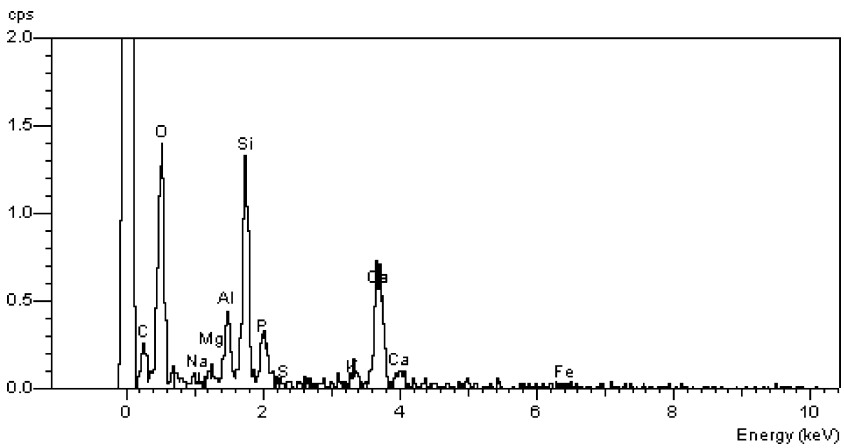

Fig. 3 Elemental spectrum of the PFD of the subject MV 15

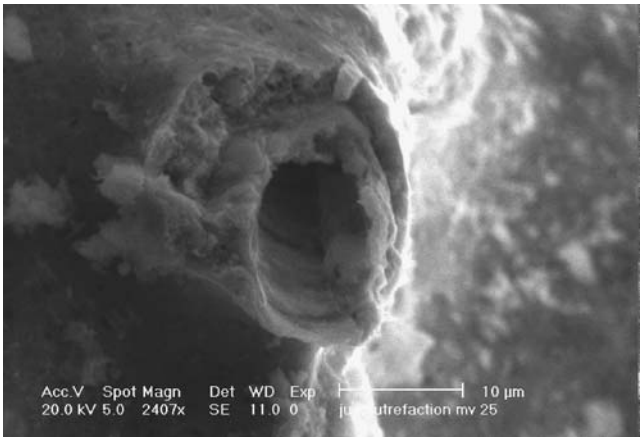

Fig. 4 Vascular structure observed in the PFD of the subject MV 25 (SEM, magnification ×2,400)

zones of the surface, giving comparable results (Fig. 3): an important high content in silicon, oxygen, and aluminum, corresponding according to all probabilities to a telluric alumina–silicate. Scarcity of calcium and magnesium within the sample was found. Traces of carbon, sodium, magnesium, phosphorus, sulfur, chlorine, potassium, calcium, titanium, and iron were also found. It was thus necessary henceforth to regard these elemental ratios as those of the ground.

The PFD itself showed a notably different laminated aspect characterized by the presence of several superimposed successive layers (lamellate aspect). Some structures could be highlighted, in particular a hollow cylindrical formation of 15-µm diameter, whose microscopic aspect was compatible with that of a capillary vascular wall (Fig. 4).

In addition, when examining with very high magnification (at least ×2,000), the surface of the PFD presented a sifted aspect, consecutive with the solidification of the liquid of decomposition in a semifluid bullous state; these cavities corresponded to bubbles of fermentation or fat gaps, as previously observed on the sample MV 15. The elemental analysis carried out on the PFD highlighted a very clear concentration of iron, associated with the presence of silica in a much smaller quantity (this last being postmortem contamination) and traces of carbon, sodium, magnesium, aluminum, phosphorus, sulfur, chlorine, potassium, calcium, and titanium (Fig. 5).

Monterenzio Vecchia 26

The studied sample measured nearly 3 cm in length and was examined under SEM on all its surface. A formation of 1-mm length for 0.6 mm of broad, observable with the binocular lenses, of translucent wrinkled yellow aspect, was charted. The coarsely planes had a very fine thickness of less than 5 µm (Fig. 6).

Some globulus protuberances were present on the visible face of approximately 5 µm, corresponding to cellular cores (Fig. 7).

In some rare places, it was possible to distinguish some biconcave circular 7- to 8-µm-long formations, corresponding to isolated red blood cells.

An elemental analysis was carried out on this formation. Its organic nature was confirmed by its important content in carbon and oxygen. Traces of copper, magnesium, aluminum, silicon, phosphorus, sulfur, potassium, calcium, and chlorine were also detected.

The elemental analysis of the adjacent zones of the sample gave us the total composition of this PFD from this individual. We noted a clear prevalence of silicon and oxygen, average concentrations of aluminum and calcium, and carbon traces, coppers, magnesium, phosphorus, sulfur, chlorine, potassium, and iron.

Agnès Sorel

The remains of Agnès Sorel were recently analyzed [17–18]. The first French King's official mistress died in

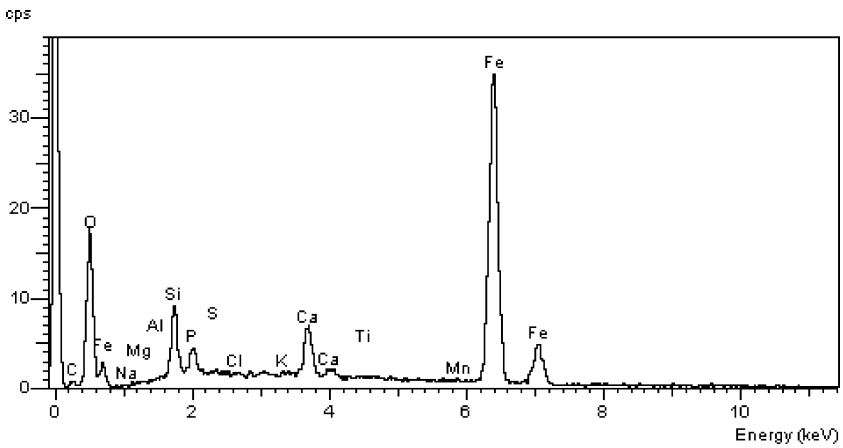

Fig. 5 Elemental spectrum of the PFD of the subject MV 25

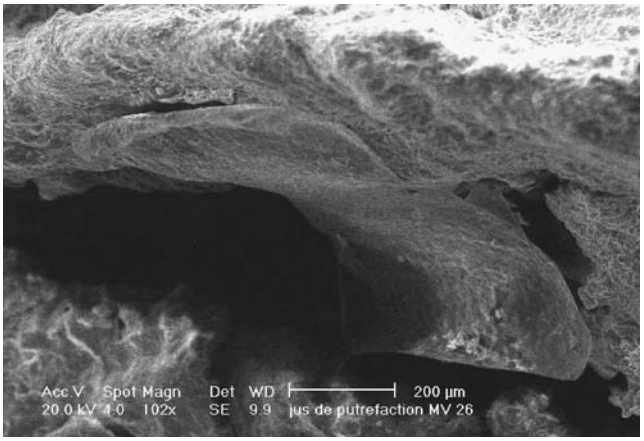

Fig. 6 Fragment of dura mater present in the PFD of the subject MV 26 (SEM, magnification ×100)

Fig. 8 Detail of the liquid of decomposition solidified in contact with the lead coffin (binocular magnifying lenses, magnification ×10)

February 1450 in Jumièges (Normandy) of an acute mercury intoxication with the waning of a antiworm drug treatment for *Ascaris lumbricoides*. Her body was the subject of a delicate embalming. The body was opened; then, the heart and the entrails were extracted and immediately buried; the abdominal and thoracic cavities were then filled with spices and vegetable matters (black pepper of West Africa, rhizomes, seeds and sheets of white mulberry tree, etc.). After a long transport to Loches (center of France, close to Loire river), the body was buried there in a triple coffin of lead, oak, and cedar.

Our study [19] showed that the effectiveness of the embalming was only temporary, as the decomposition of the corpse had already begun. The putrefaction fluid, particularly its acidic components, interacted with the lead of the sarcophagus and formed a lead oxide precipitate, which was then deposited on the remains of Agnès Sorel and stopped the autolysis process. Amalgams of PFD in contact with scraps of the lead coffin (Fig. 8) were analyzed under the optical microscope and SEM; in addition, an elemental analysis was carried out in order to confirm their organic and mineral mixed nature.

The hairs, originally from a Venetian blond, had a disconcerting brown color related to the postmortem deposit of PFD on its surface (Fig. 9). When some hairs were in contact, one with the other, this deposit was absent, and the natural structure of the hair was then visible without any surface deposit, in particular the presence of cuticles organized in fish scales (Fig. 10).

The elemental analysis of the hair surface indeed showed a high content in lead (from the PFD that interacted with the metal coffin: Fig. 11), while the surface of clean hairs presented an elemental profile characteristic of uncontaminated hair (Fig. 12).

The systematic study of nearly 40 g of residues of PFD showed the persistence of many cellular and tissue

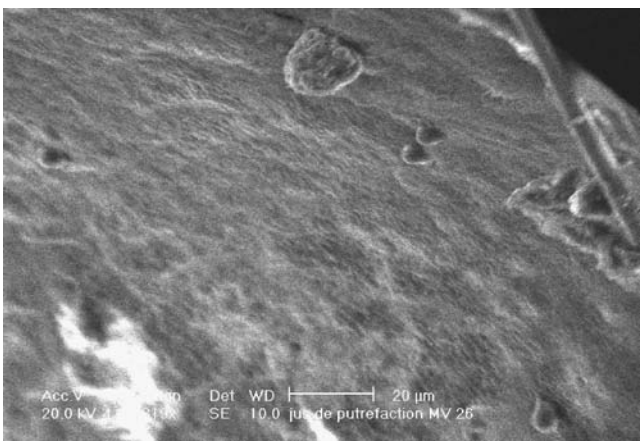

Fig. 7 Cellular cores on the surface of a dura mater fragment present in the PFD of the subject MV 26 (SEM, magnification ×820)

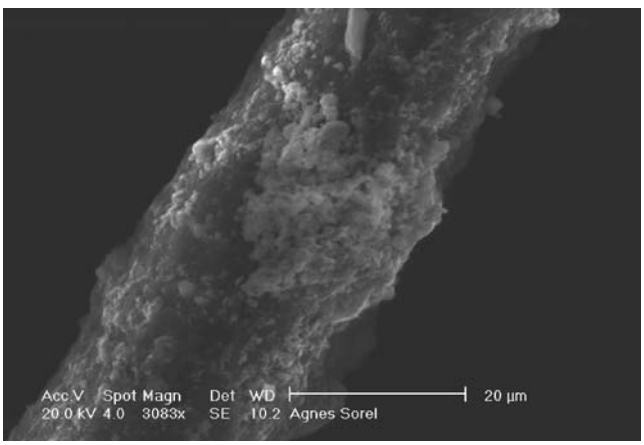

Fig. 9 Detail of the surface of a hair from Agnès Sorel covered with PFD (SEM, magnification ×3,100)

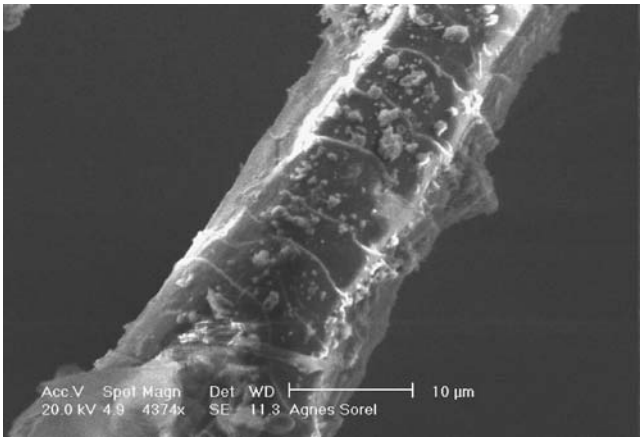

Fig. 10 Detail of the surface of a "clean" hair from Agnès Sorel with the still visible cuticle (SEM, magnification ×4,400)

elements. First of all, many hair formations (fragments of skull hairs, pubic hairs, and axillary hairs) were included in the PFD. Under an MGG coloration, many mycelium filaments were highlighted, mainly of aspergilla type; multiple bacterial colonies were also present, mainly of negative Gram type (without prevalent species). Clusters of platelets from red blood cells were observed, recognizable with their biconcave form and their variable 5- to 7-µm-long diameter but characterized by a clear chestnut color. Not one intracellular parasite was highlighted on almost the 6,000 examined red blood cells.

Still in the PFD, many eggs of *A. lumbricoides*, a human and intestinal parasitic worm, were seen (Fig. 13), associated with many cellulose remains of male fern.

Louis the XI

A systematic anthropological [20–21] and forensic [22] examination of the skeleton did not find any PFD on the bones of King Louis the XI, particularly on the skull vault. Important deposits (Fig. 14) were still present on the sides of its stone sarcophagus, in the crypt of the Notre-Dame Basilica in Cléry-Saint-André (close to Orléans, Loiret).

As for the samples of the lead coffin from Agnès Sorel's grave, the microscopic observation of this deposit appeared as informative as that of deposits taken on the surface of bone remains. The bottom was occupied by an eosinophilic acellular substance without any recognizable anatomical structure; it was just punctuated with some bacterial or mycelium elements without any characteristics.

Some epithelial elements with a majority of keratinized Malpighian cells were highlighted and were of relatively limited interest (Fig. 15). One can just notice the visible nuclear conservation in the form of a central basophilic granulation and the notable absence of atypical aspect (within the limits of the representativity of these rarely found cells).

Much more interesting was the description of a short hair (1.3-cm length) of white aspect, completely included in the PFD. The optical microscopic examination confirmed its human nature according to its morphological characteristics [15, 23–25]. It also highlighted canities characterized by a complete white coloring to the screen of the hair; indeed, the Fontana coloration did not highlight melanin persistence of pigment on the totality of the preserved capillary segment (Fig. 16).

Charlotte of Savoy

The samples of PFD from Charlotte of Savoy were taken from the posterior part of her skull, in the deepest part of the occipital pit (Fig. 17), just near a zone of sawing (contemporary of the embalming of the queen in 1483).

The elements highlighted were mainly represented by leucocytes and red blood cells whose conservation appeared excellent (Figs. 18 and 19), without particular anomaly, in particular without intracytoplasmic parasite.

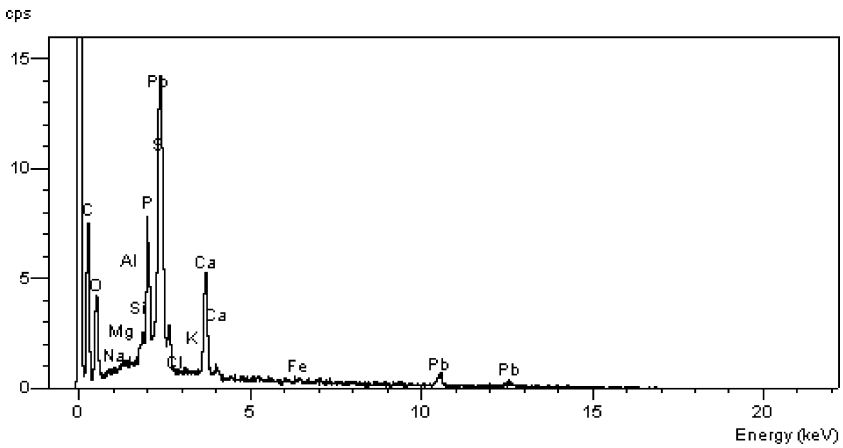

Fig. 11 Elemental spectrum of the surface of a hair from Agnès Sorel covered with PFD

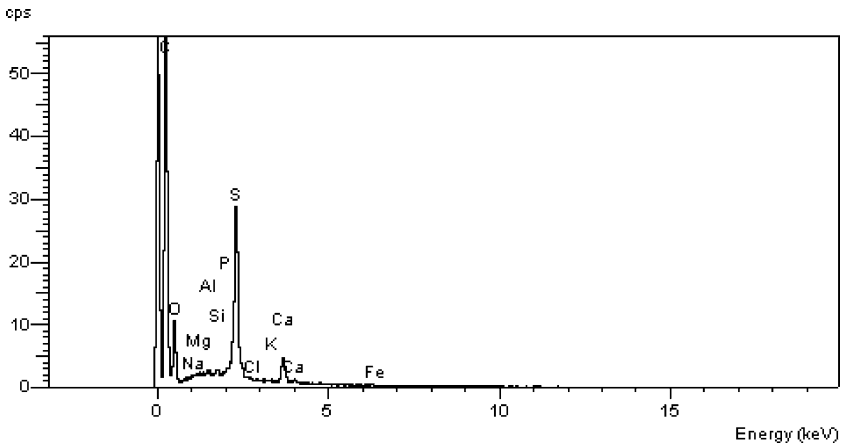

Fig. 12 Elemental spectrum of the surface of a "clean" hair from Agnès Sorel

Discussion

Monterenzio Vecchia 15

SEM examination showed the presence of multiple mycelia. Their deposit in the putrefaction fluid was probably contemporary with cadaver autolysis and contamination of the body by thanatophages fauna and flora. As has been shown by elemental analysis, they have been more or less completely mineralized.

Monterenzio Vecchia 25

The extraordinary high content of iron shown by the elemental analysis of the PFD raised the question of its origins: was it the consequence of a postmortem contamination (rust coming from an oxidation near a metallic object)? Was this iron concentration secondary to an intracranial hemorrhagic process having led to an accumulation of blood which secondarily formed a deposit?

The study of the funerary furniture revealed the complete absence of any metallic object (in particular a lack of iron), in the tomb of the subject MV 25. There was no sign of disturbance to the grave which could explain a violation (i.e., a disappearance of any metallic object) has been detected. On the other hand, the paleopathological study highlighted the presence of a 1-cm-long parasagittal left frontal osteolytic lesion (Figs. 20 and 21) interpreted as an angioma or, more generally, a vascular malformation. Could this malformation have constituted, without any antemortem rupture, a blood pocket responsible for this excessive iron concentration in the PFD? We do not think so, considering that the blood volume probably did not exceed 2 cm^3, taking into account the size of the lesion (this value seems too weak to substantially modify any elemental concentration of the PFD). On the other hand, if one holds account of the macroscopic lesions and the elemental proportioning carried out on the intracranial PFD, we can better propose, for this 10- to 11-year-old child, the assumption of a death caused by meningeal hemorrhage

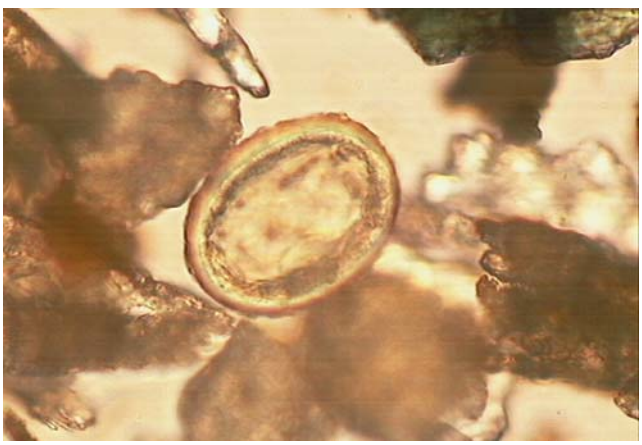

Fig. 13 One of the many eggs of *A. lumbricoides* observed in the PFD of Agnès Sorel after cytocentrifugation (HES coloration)

Fig. 14 PFD still present on the sides of the French King Louis the XI's sarcophagus in Cléry-Saint-André.

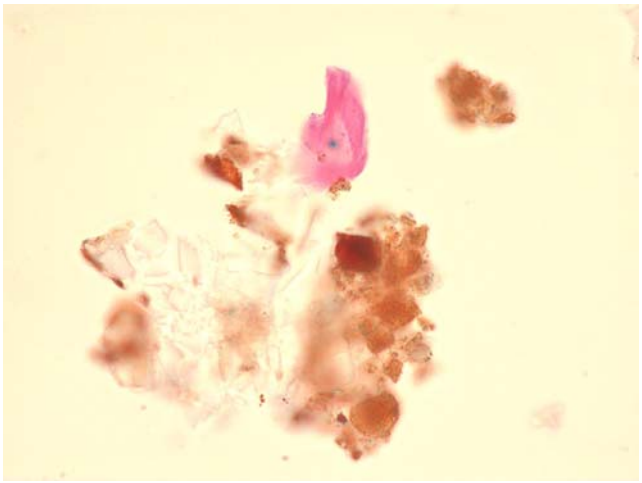

Fig. 15 Keratinized Malpighian cell in the French King Louis the XI's sarcophagus PFD after cytocentrifugation (HES coloration)

related to the rupture of its left frontal intracranial vascular malformation. It should so be possible to consider the skull as a tank with moderate to quite absent communication with external structures during the formation of the PFD.

Monterenzio Vecchia 26

SEM morphological and elemental analysis showed that the observed tissue fragment was "mummified" in the PFD (explaining its organic composition). Its morphological aspect and its localization in the skull were evocative of a tissue diagnosis of dura mater, without notable particular anomaly.

Scarcity of iron in the PFD was important to note, confirming the exceptionally rich nature in this metal of the sample coming from the subject MV 25 (see supra).

Fig. 16 Section of a hair found in the PFD of the French King Louis the XI's sarcophagus. Its natural white color (canities) was confirmed by a Fontana coloration not objectifying any residual melanin pigment

Fig. 17 View of the PFD in the occipital part of French Queen Charlotte of Savoy's skull

Agnès Sorel

The fauna (mycelia of aspergilla type and bacterial colonies) observed in the PFD corresponded to a traditional cadaver fauna, particularly in an archeological wet atmosphere (hiding under ground).

The clear chestnut color of red blood cells was due to a discoloration of the cytoplasm by the lead from the sarcophagus, a well-known observation of pathologists working on old remains [26–30]. The absence of any parasites (for example *Plasmodium*) in this kind of cells was an important negative observation according to the strong malarial frequency in France during the fifteenth century.

Taking into account the fact that the *Ascaris* eggs were deeply included in the PFD and not simply present on the surface, it seems possible to assert that they were initially present in the body of Agnès Sorel during the early stages

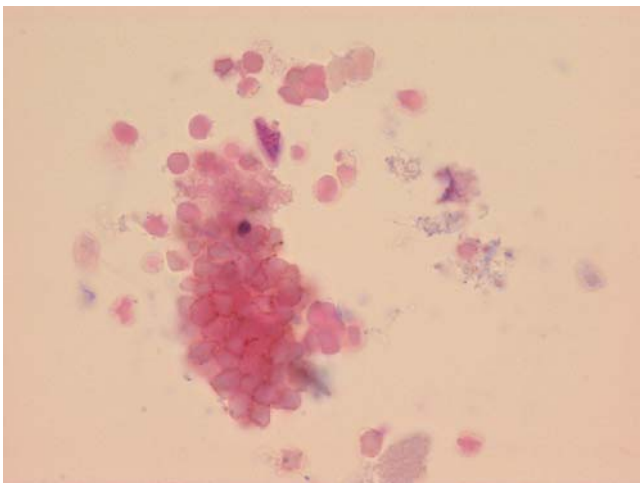

Fig. 18 Group of red blood cells (deformed) observed in the PFD of French Queen Charlotte of Savoy after cytocentrifugation (HES coloration)

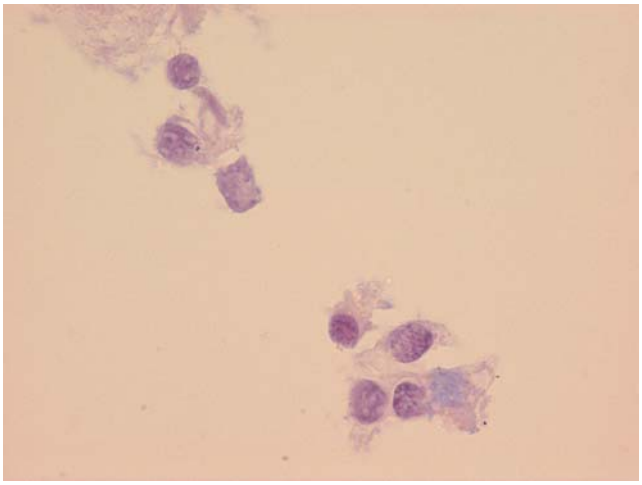

Fig. 19 Group of leucocytes observed in the PFD of French Queen Charlotte of Savoy after cytocentrifugation (HES coloration)

Fig. 21 Detail of the precedent intracranial bone lesion on the left frontal of the subject MV 25

of putrefaction. Moreover, due to the funeral urn having been bought new at the time of the reduction of the body in 1777, a postmortem contamination by animal meat charged with parasites present in the vase before the human remains cannot be proposed.

Male fern fragments correspond to a vegetable species currently used in medieval pharmacopoeia as an antiworm drug. Its presence in the PFD is explained by the absorption of a therapeutic decoction of male fern a short time before death, and a release of these vegetable remains at the time of the cadaver autolysis; they then could be mixed with the remains of tissues and cellular structures during decomposition and putrefaction.

Louis the XI

Of particular interest was the observation of this hair included in the PFD, characterized by complete canities. In addition, we note (see for example the historical chronicle by Philippe de Commynes) that French King Louis the XI died, an almost bald person with white hair, at 60 years of age in 1483. This element could find its place in an identification process of the dead or, at least, as an important data for the age determination.

Fig. 20 General view of the frontal bone with the intracranial lesion diagnosed on the subject MV 25, a 11- to 11-year-old child. Note the presence of a deposit of solidified PFD close to the lesion

Charlotte of Savoy

As for Agnès Sorel's and Louis the XI's PFD, the microscopic examinations of numerous red blood cells did not show the presence of any parasite.

Synthesis

The study under optical microscope and scanning electronic microscope (SEM) of the putrefaction fluid deposits (PFD), a new cytological method gave interesting data.

One of its advantages is in not destroying the sample examined without any preparation with the SEM as soon as the sample is taken. It makes it possible to observe many biological structures still present in these calcified formations (dura mater, red blood cells, mycelium filaments, bacterial colonies, capillary vascular walls, etc.), but this diagnosis only remains morphological (the cytological or histological diagnosis becomes certain only thanks to elemental determinations or by confronting these observations with those of a traditional preparation colored by HES).

On the other hand, the technique in standard cytology (optical microscopy) appears destructive but supports direct diagnoses; the histological morphological observations remain impossible because of the fragmentation of the sample.

It appears necessary in all cases to carry out an examination and elemental determination of the adjacent sediment in order to check if the recorded values testify to an external contamination or one from the original source. The nature even of the liquid of decomposition results from a mixture between the environment and the catabolism of the cadaver (decomposition and putrefaction). Within the framework of the intracranial liquid of decomposition, the external contamination seems to be definitely less (comparatively with the samples carried out on the long bones, for example), for obvious anatomical reasons.

Before any utilization of such techniques in forensic anthropology, complementary analysis needs to be performed on comparable modern cases.

Conflict of interest statement We declare that we have no conflict of interest.

References

1. Cabirol N, Pommier MT, Gueux M et al (1998) Comparison of lipid composition in two types of human putrefactive liquid. Forensic Sci Int 94(1–2):47–54
2. Charlier P (2006) Apports de la paléopathologie humaine à l'archéo-zoologie: l'exemple de Monterenzio Vecchia. In: Curci A, Vitali D (eds) Animali tra uomini e dei. Archeozoologia del mondo preromano Ante Quem, Studi e Scavi, Bologna, pp 153–162
3. Doran GH, Dickel DN, Ballinger WE et al (1986) Anatomical, cellular and molecular analysis of 8000 year old human brain tissue from the Windover archaeological site. Nature 323:803–806
4. Gill-King H (1997) Chemical and ultrastructural aspects of decomposition. In: Haglund WH, Sorg LH (eds) Forensic taphonomy. CRC, London, pp 93–108
5. Hauswirth WH, Dickel C, Doran GH et al (1991) 8000-year-old brain tissue from the Windover site. Anatomical, cellular and molecular analysis. In: Ortner DJ, Aufderheide AC (eds) Human paleopathology. Current syntheses and future options. Smithsonian Institution Press, Washington, pp 60–72
6. Léry N, Payen G, Martin G (1988) La décomposition des corps en sépulture étanche. Essai d'une approche méthodologique. Acta Med Leg Soc (Liège) 38(1):133–143
7. Maat GJR (1991) Ultrastructure of normal and pathological fossilized red blood cells compared with pseudopathological biological structures. Int J Osteoarchaeol 3–4(1):209–214
8. Mazel V, Richardin P, Charlier P (2006) Restes biologiques dans les patines rituelles de la statuaire Dogon (Mali). In: Charlier P (ed) 1er Colloque International de Pathographie (Loches, Avril 2005). De Boccard, Paris, pp 137–150
9. Micozzi MS (1991) Post-mortem change in human and animal remains. A systematic approach. Charles C. Thomas, Springfield
10. Payen G, Léry N, Rimoux L et al (1988) La décomposition des corps en sépulture étanche. Modifications macroscopiques des cadavres et contaminations. Acta Med Leg Soc (Liège) 38 (1):145–151
11. Payen G, Rimoux L, Gueux M et al (1988) La décomposition des corps en sépulture étanche. Aspects microbiologiques et environnementaux. Acta Med Leg Soc (Liège) 38(1):153–163
12. Rimoux L, Gueux M, Boujet C et al (1988) La décomposition des corps en sépulture étanche. Biochimie des effluents liquides et gazeux. Acta Med Leg Soc (Liège) 38(1):165–184
13. Maat GJR (1993) Bone preservation, decay and its related conditions in ancient human bone from Kuwait. Int J Osteoarchaeol 3:77–86
14. Reichs KJ (1986) Forensic osteology. Advances in the identification of human remains. Charles C. Thomas, Springfield
15. Charlier P (2008) Ostéo-archéologie et techniques médico-légales: tendances et perspectives. Pour un 'Manuel pratique de paléopathologie humaine'. De Boccard, Paris
16. Charlier P (2005) Ostéo-archéologie de deux nécropoles étrusco-celtiques: Monte Bibele et Monterenzio Vecchia (Bologne, Italie). Reconstitution d'une pathocénose à l'échelle de la vallée de l'Idice. PhD, EPHE, IVème section, Sciences Historiques et Philologiques, La Sorbonne, Paris
17. Charlier P (2005) Death of a beauty. Paleopathology Newsletter 132:18–23
18. Charlier P (2005) Vie et mort de la Dame de Beauté. L'étude médicale des restes d'Agnès Sorel.. Rev Prat (Monographie) 15 (55):1734–1737
19. Charlier P (2006) Qui a tué la Dame de Beauté ? Étude scientifique des restes d'Agnès Sorel (1422–1450). Hist Sci Med 3(40):255–263
20. Georges P, Acquaviva C, Bruzek J et al. (2005) Étude du caveau royal et des sépultures de la chapelle des Dunois-Longueville de l'église Notre-Dame de Cléry-Saint-André (Loiret). Approche critique des données anciennes et récentes. Rapport d'étude et perspectives de recherches nouvelles. INRAP, SRA du Centre Orléans
21. Georges P (2006) L'embaumement et le prélèvement du cœur au Moyen-Age: le sciage du sternum. In: Charlier P (ed) 1er Colloque international de pathographie (Loches, Avril 2005). De Boccard, Paris, pp 99–112
22. Charlier P (2006) Les procédures d'embaumement aristocratique en France médiévale et moderne (Agnès Sorel, le Duc de Berry, Louis XI, Charlotte de Savoie, Louis XIII, Louis XIV et Louis XVIII). Med nei Secoli 18(3):777–798
23. Durigon M (1999) Pratique médico-légale. Masson, Paris
24. Krogman WM, Iscan MY (1986) The human skeleton in forensic medicine. Charles C. Thomas, Springfield
25. Rathburn TA, Buikstra J (1984) Human identification. Charles C. Thomas, Springfield
26. Thillaud PL, Glon Y, Charlier P et al (2003) La momie du Fin-Renard (Bourges). In: Gourevitch D, Moirin A, Rouquet N (eds) Maternité et petite enfance dans l'Antiquité romaine. Muséum d'Histoire Naturelle, Bourges, pp 102–110
27. Thillaud PL, Glon Y, Charlier P et al (2004) Les secrets de la momie de Bourges. Rev Prat (Monographie) 54:691–293
28. Ciranni R, Fornaciari G (2004) Juvenile cirrhosis in a 16th century Italian mummy. Current technologies in pathology and ancient human tissues. Virchows Arch 445(6):647–650
29. Waldron HA (1981) Postmortem absorption of lead by the skeleton. Am J Phys Anthropol 55(3):395–398
30. Schultz M (2001) Paleohistopathology of bone: a new approach to the study of ancient diseases. Am J Phys Anthropol Suppl 33:106–147

Virchows Arch (2008) 453:387–400
DOI 10.1007/s00428-008-0658-x

ORIGINAL ARTICLE

Placental protein 13 (galectin-13) has decreased placental expression but increased shedding and maternal serum concentrations in patients presenting with preterm pre-eclampsia and HELLP syndrome

Nandor Gabor Than · Omar Abdul Rahman · Rita Magenheim · Balint Nagy · Tibor Fule · Beata Hargitai · Marei Sammar · Petronella Hupuczi · Adi L. Tarca · Gabor Szabo · Ilona Kovalszky · Hamutal Meiri · Istvan Sziller · Janos Rigo Jr. · Roberto Romero · Zoltan Papp

Received: 22 May 2008 / Revised: 31 July 2008 / Accepted: 15 August 2008 / Published online: 13 September 2008

Abstract Placental protein 13 (PP13) is a galectin expressed by the syncytiotrophoblast. Women who subsequently develop preterm pre-eclampsia have low first trimester maternal serum PP13 concentrations. This study revealed that third trimester maternal serum PP13 concentration increased with gestational age in normal pregnancies ($p < 0.0001$), and it was significantly higher in women presenting with preterm pre-eclampsia ($p = 0.02$) and hemolysis, elevated liver enzymes, and low platelet count (HELLP) syndrome ($p = 0.01$) than in preterm controls. Conversely, placental PP13 mRNA ($p = 0.03$) and protein, as well as cytoplasmic PP13 staining of the syncytiotrophoblast ($p < 0.05$) was decreased in these pathological pregnancies compared to controls. No differences in placental expression and serum

N. G. Than (✉) · B. Nagy · P. Hupuczi · G. Szabo · I. Sziller · J. Rigo Jr. · Z. Papp
First Department of Obstetrics and Gynecology,
Semmelweis University,
27 Baross Street,
1088 Budapest, Hungary
e-mail: nthan@med.wayne.edu

O. Abdul Rahman
Department of Medical Chemistry, Molecular Biology and Pathobiochemistry, Semmelweis University,
9 Puskin Street,
1088 Budapest, Hungary

R. Magenheim
First Department of Internal Medicine,
Semmelweis University,
2/a Korányi S. Street,
1083 Budapest, Hungary

T. Fule · B. Hargitai · I. Kovalszky
First Department of Pathology and Experimental Cancer Research,
Semmelweis University,
26 Üllői Street,
1085 Budapest, Hungary

M. Sammar · H. Meiri
Diagnostic Technologies Ltd,
2 Hacarmel Street,
20692 Yokneam, Israel

A. L. Tarca · R. Romero
Perinatology Research Branch,
NICHD/NIH/DHHS,
Wayne State University/Hutzel Women's Hospital,
3990 John R,
Detroit, MI 48201, USA

Present address:
N. G. Than
Perinatology Research Branch,
NICHD/NIH/DHHS,
Wayne State University/Hutzel Women's Hospital,
3990 John R,
Detroit, MI 48201, USA

concentrations of PP13 were found at term between patients with pre-eclampsia and control women. In contrast, the immunoreactivity of the syncytiotrophoblast microvillous membrane was stronger in both term and preterm pre-eclampsia and HELLP syndrome than in controls. Moreover, large syncytial cytoplasm protrusions, membrane blebs and shed microparticles strongly stained for PP13 in pre-eclampsia and HELLP syndrome. In conclusion, parallel to its decreased placental expression, an augmented membrane shedding of PP13 contributes to the increased third trimester maternal serum PP13 concentrations in women with preterm pre-eclampsia and HELLP syndrome.

Keywords Brush border membrane · Galectin · Syncytiotrophoblast microparticle · Trafficking · Virtual microscopy

Introduction

Pre-eclampsia is a syndrome associated with shallow trophoblast invasion and abnormal spiral artery remodeling [1–4], uteroplacental ischemia, and anti-angiogenic state [5–8], generalized endothelial cell dysfunction and increased maternal systemic inflammatory response [9–12]. Early-onset pre-eclampsia often has a severe clinical presentation that is associated with increased perinatal morbidity and mortality, and high incidence of hemolysis, elevated liver enzymes, and low platelet count (HELLP) syndrome [2, 13, 14]. Moreover, the rates of uteroplacental vascular insufficiency, lesions of the villous tissues and increased syncytiotrophoblast microparticle (STBM) shedding are higher in early-onset than in late-onset pre-eclampsia [1, 15–19]. These differences led to the proposal that early-onset pre-eclampsia is a placental disease, while late-onset pre-eclampsia is a maternal disease [16, 20].

Placental-derived proteins, such as soluble vascular endothelial growth factor receptor-1, placental growth factor, endoglin, inhibin A and activin A have been implicated in the pathophysiology and prediction of pre-eclampsia [5–8, 21]. Recently, four nested case–control studies have demonstrated that patients who subsequently developed preterm pre-eclampsia had a significantly lower median maternal serum placental protein 13 (PP13) concentration in the first trimester than those women who had normal delivery at term [22–25]. The combined measurements of serum PP13 concentrations and uterine artery Doppler pulsatility indexes had even better value in the risk assessment of preterm pre-eclampsia [22]. However, PP13 is a less valuable marker for term pre-eclampsia [23, 25].

PP13 was purified and cloned from the placenta [26–28], localized to the syncytiotrophoblast brush border membrane [29], and detected in maternal and cord blood [30]. It was designated galectin-13 as it belongs to the galectin family [29, 31], whose members share similar topology, carbohydrate recognition domain, and specificity for *N*-acetyllactosamine-containing glycoconjugates [32]. Indeed, an in vitro study proved its lectin activity and favored binding to sugar residues widely expressed on placental microvillous surfaces [29]. Of importance, the *LGALS13* gene encoding for PP13 is uniquely expressed by the placenta as shown by Northern blot [28], GNF SymAtlas (http://wombat.gnf.org/SymAtlas/) and GenBank (www.ncbi.nlm.nih.gov) gene expression data.

The unique placental expression and localization at the maternal–fetal interface might suggest that PP13 is related to the pathophysiology of pre-eclampsia and HELLP syndrome. To test this hypothesis, we investigated the placental expression and localization of PP13 in parallel with its maternal serum concentrations in patients with pre-eclampsia and HELLP syndrome.

Materials and methods

Study design, patient groups and clinical definitions

Samples were collected at the First Department of Obstetrics and Gynecology, Semmelweis University (Budapest, Hungary), a national referral center for high-risk pregnancies, between October 2003 and March 2006. Pregnancies were dated according to ultrasound measurements between 8–12 weeks of gestation (GW). Patients with multiple pregnancies or with fetuses having congenital or chromosomal abnormalities were excluded. The collaborative research was approved by Regional Research Ethics Committee, and informed consent was obtained from women prior to sample collection; specimens and data were stored anonymously.

This cross-sectional study aimed (1) to determine maternal serum PP13 concentrations in normal pregnant women in the third trimester and (2) to compare maternal serum and placental PP13 concentrations and *LGALS13* gene expression in women with pre-eclampsia with or without HELLP syndrome as well as in gestational age matched controls at the time of delivery.

Maternal sera were collected from a first subset of control women with normal pregnancy between GW24–40. Enrollment and blood draw took place at routine laboratory sampling during prenatal care visits. Women were included in this control group ($n = 46$) if they (1) had no medical, obstetrical or surgical complications; (2) had no labor and did not deliver at the time of blood draw; and (3) delivered at term (GW $\geq$ 37), a neonate with a birth-weight appropriate for gestational age [33].

Maternal sera and placentas were also collected from women at the time of delivery. Women were enrolled at

the Labor and Delivery Unit upon admission, and those who had blood drawn prior to any medication were included in the analysis in the following gestational age matched groups: (1) pre-eclampsia with (n = 12) or (2) without HELLP syndrome (n = 20) and (3) a second subset of controls (n = 30), which consisted of term (n = 20) and preterm controls (n = 10). Term controls had no medical or obstetrical complications and delivered at term (GW ≥ 37) a newborn with birth-weight appropriate for gestational age [33]. Preterm controls included women with spontaneous preterm (GW < 37) delivery without any clinical or histological signs of chorioamnionitis. Control women underwent Caesarean section secondary to previous Caesarean section or malpresentation. Pre-eclampsia was defined as hypertension that developed after GW20 (systolic or diastolic blood pressure ≥140 or ≥90 mmHg, respectively, measured at two different time points, 4 h to 1 week apart) coupled with proteinuria (≥300mg in a 24 h urine collection, or two random urine specimens obtained 4 h to 1 week apart containing ≥1+ by dipstick or one dipstick of ≥2+ protein) [2, 34]. Severe pre-eclampsia was defined as systolic blood pressure ≥160 mmHg or diastolic blood pressure ≥110 mmHg and/or proteinuria greater than 5g in a 24 h collection or ≥3+ protein on dipstick, and it was also diagnosed in the presence of multi-organ involvement [2, 34]. HELLP syndrome was defined as hemolysis (serum LDH >600IU/l; bilirubin >1.2mg/dl; presence of schistocytes in peripheral blood), elevated liver enzymes (serum ALT and/or AST >70IU/l) and thrombocytopenia (platelet count <100,000/mm^3) [35]. In preterm pre-eclampsia with or without HELLP syndrome, delivery was necessitated by the symptoms before term (GW < 37).

Samples

Blood samples were immediately centrifuged (10 min at 2,500 rpm) after draw; sera were separated and stored at −80°C. Villous tissue samples were excised from central cotyledons after separation of the placentas from the choriodecidual layer. Native (for protein determination) and RNAlater®–ICE (Ambion Inc., St. Austin, TX, USA) soaked (for quantitative real-time polymerase chain reaction (qRT-PCR)) samples were deep frozen and stored at −80°C. Whole placentas were formalin-fixed, and representative tissue blocks were paraffin-embedded. Not all specimens were available from every patient.

Placental tissue preparations for protein determination

Deep frozen placental villous tissues (500mg; n = 52) were pulverized in liquid nitrogen and homogenized on ice in 500 μl RIPA lysis buffer (50 mM Tris–HCl pH = 7.4; 150 mM NaCl; 1% NP40; 0.25% Na deoxycholat, 1 mM EDTA, and 1 mM PMSF). Homogenates were centrifuged (15 min at 10,000 rpm) to pellet non-soluble debris; supernatants containing soluble or solubilized cytoplasmic, membrane and nuclear proteins were collected, and their total protein contents were measured by the Bradford assay and equalized for 1mg/ml. These protein extracts were then used for ELISA, immunoprecipitation, or immunoblotting.

Immunoprecipitation

Placental protein extracts (1mg; n = 52) were pre-cleared on protein A agarose (Sigma-Aldrich Co., St. Louis, MO, USA) (1 h at 4°C) and centrifuged (5 min at 2,500 rpm), and supernatants were transferred into fresh tubes and incubated with an excess (2 μg) of anti-PP13 antibody (overnight at 4°C). Protein A agarose (30 μl) was added to each tube and mixtures were incubated (1 h at 4°C). Precipitated immunocomplexes were collected by centrifugation (5 min at 2,500 rpm), repeatedly washed in RIPA buffer containing 0.1% detergent, and centrifuged (5min at 2,500 rpm) four times. Pellets were resuspended in Laemmli buffer, boiled (5 min), and centrifuged (1 min at 10,000 rpm), and supernatants were applied to sodium dodecyl sulphate (SDS)-polyacrylamide gel electrophoresis (PAGE).

SDS-PAGE and Western blot analysis

Initially, placental protein extracts (30 μg) were used for Western blot analysis; however, many of the samples did not contain detectable amounts of PP13. Thus, immunoprecipitates (30 μl) were subsequently run on 15% SDS-PAGE along with recombinant PP13 (rPP13) (5–50ng) as positive control (Diagnostic Technologies Ltd., Yokneam, Israel). Proteins were electroblotted to nitrocellulose membranes (Invitrogen Corporation, Carlsbad, CA, USA) and blocked (30 min at 25°C) with phosphate-buffered saline (PBS) containing 0.1% Tween-20 and 5% skim milk powder. Membranes were incubated with biotinylated anti-PP13 monoclonal antibody (Diagnostic Technologies Ltd., Yokneam, Israel) (2 μg/ml; overnight at 4°C) and then with horseradish peroxidase (HRP)-conjugated streptavidin (Jackson Immunoresearch Laboratories Inc., West Grove, PA, USA) (1:10,000; 1 h at room temperature), and developed by Super Signal West Pico ECL reagent (Pierce Biotechnology Inc., Rockford, IL, USA). Band visualization, signal quantification and molecular weight determination were performed by a Fluorchem SP (Alpha Innotech Corporation, San Leandro, CA, USA) or a Las3000 (Fuji Film, Tokyo, Japan) CCD imaging system. The sensitivity of both systems was 200 pg PP13/lane.

ELISA

PP13 concentrations of placental protein extracts and maternal sera were determined using a solid-phase sandwich ELISA kit (Diagnostic Technologies Ltd., Yokneam, Israel). Optical density was measured at 450 nm and translated into quantitative amounts using a calibration curve consisting of rPP13 standards (0–500 pg/mL). The lower limit of detection was 5 pg/mL. The intra- and inter-assay variations in our laboratory were 5.4% and 9.4%, respectively.

RNA isolation

Deep frozen placental tissues (n = 23) were thawed and homogenized. After centrifugation at 12,000 rpm, RNA-later®–ICE was removed. Total RNA was isolated with Eppendorf ® perfect RNA eukaryotic kit (Eppendorf AG, Hamburg, Germany) and treated with Dnase I. Total RNA quality and integrity were determined by measuring the OD260/280 and OD260/230 ratios.

Quantitative real-time RT-PCR

cDNA was synthesized using 0.5 μg Dnase-I-treated total RNA and First Strand cDNA Synthesis Kit (Roche Diagnostics Co., Indianapolis, IN, USA). Primers (*LGALS13* forward: GCAAACAATTTGAGCTGTG, reverse: CACTGAGGTCAGGGAGA; *YWHAZ* forward: TCCTTTGCTTGCATCCCAC, reverse: AAGGCAGACAATGACAGACCA; *HPRT* forward: GGCAGTATAATCCAAAGATGGTC reverse: GTCTGGCTTATATCCAACACTTG) were designed using the LightCycler Probe Design Software 1.0 (Hoffmann-La Roche Ltd, Basel Switzerland) and synthesized by Sigma-Genosys Ltd. (Haverhill, UK). PCR reactions consisted of 9 μl DNA Master SYBR Green I mix (Hoffmann-La Roche Ltd., Basel, Switzerland), 1 μl cDNA and 2.5pmol primers, and a negative control without cDNA template was run simultaneously with every assay. The PCRs were run in duplicate on LightCycler thermal cycler, and the average was used in the calculations. Standard curves were obtained using serial dilutions of the β-globin reference gene, and the concentration of each gene product was determined by a kinetic approach with the LightCycler software. The expression of phospholipase A2 (*YWHAZ*) and hypoxanthine phosphoribosyltransferase (*HPRT*) housekeeping genes that have great expression stability in the placenta significantly correlated in all samples, and *HPRT* was used for normalization.

Histopathology

Placentas were fixed and histopathologically evaluated in 38/62 cases due to temporarily limited personal and laboratory conditions. Specimens were examined according to a standard protocol by two pathologists (BH, TF) blinded to clinical details. The topography and size of all macroscopic lesions were described, and the ratio of these lesions and viable placental tissue was estimated. Seven representative histological blocks were taken from each placenta to include both ends of the umbilical cord, placental membranes, and three macroscopically normal central/paracentral areas of the placental disc. An en face block of the basal plate was taken for the best representation of uteroplacental arteries [36]. In addition, macroscopic lesions were also sampled. All tissue blocks were paraffin-embedded; 4 μm sections were cut and mounted on SuperFrost/Plus slides (Fisherbrand, Loughborough, UK). After deparaffination and rehydration, slides were stained with hematoxylin-eosin (HE) and evaluated in ten randomly chosen microscopic fields [37]. Macroscopic and microscopic lesions were defined according to published criteria [37–39], quantified and statistically analyzed.

Immunohistochemistry

Four μm sections were cut from full thickness blocks (n = 38) of a macroscopically normal central area of each placenta. Sections were incubated with 10 mM Tris (pH = 9, 1 mM EDTA) (30 min at 100°C) to expose antigens. After inhibition of endogenous peroxidases with 3% H_2O_2, unspecific antibody binding was blocked with 3% BSA in PBS containing 10% goat serum (Vector Laboratories, Burlingame, CA, USA) (30 min at room temperature). Sections were incubated (90 min at 37°C, then overnight at 4°C) with monoclonal anti-PP13 antibody (1:20) in PBS containing 1% BSA. After washing, the second incubation (1 h at room temperature) was performed with HRP-conjugated anti-mouse IgG (1:100). Slides were developed with DAB Substrate Kit (Vector Laboratories, Burlingame, CA, USA) and counterstained with hematoxylin (H) or HE. In negative controls, the primary antibody was omitted or preabsorbed with a tenfold excess of rPP13.

Evaluation of immunostaining

Visual evaluation of immunostainings was performed microscopically (Carl Zeiss MicroImaging GmbH, Gottingen, Germany) by two pathologists (BH and TF). All slides (n = 38) were digitally scanned by a high resolution scanner (Mirax Scan, Carl Zeiss MicroImaging GmbH, Gottingen, Germany), deposited to a virtual laboratory (www.pathonet.com), and used for virtual microscopic evaluation by a third examiner (NGT) applying Mirax Viewer 1.8.3.0 (Carl Zeiss MicroImaging GmbH, Gottingen, Germany and 3DHistech Ltd., Budapest, Hungary). All examiners were blinded to the clinical information. Immunostainings were semi-

quantitatively scored by BH and NGT with a modified immunoreactive score [40]. Immunostaining intensity was graded as follows: 0 = negative, 1 = weak, 2 = intermediate, and 3 = strong. The percentage of cells staining positive was assessed as follows: 0 = negative, 1 = 1–10%, 2 = 11–50%, 3 = 51–80%, and 4 = 81–100%. The final composite score for PP13 immunoreactivity was obtained by multiplying the intensity and percentage scores, giving a range of 1–12, in which a score of 1–4 = weak, 5–8 = moderate, and 9–12 = strong. Each slide was evaluated three times in ten random fields by both examiners; the average of the scores was determined as the representative data for that sample.

Statistical analysis

Maternal serum and placental PP13 concentrations were $\log_{10}$ transformed to improve data normality. The association between the log transformed PP13 concentrations or *LGALS13/HPRT* gene expression ratio and two explanatory variables (gestational age and disease status) were tested using a linear model strategy. In these models, the main effects and the interaction of gestational age and disease status (presence of pre-eclampsia) were estimated, while their significance was tested via *t*-tests. The models were fitted under the *R* statistical environment (www.r-project.org) using specialized functions. All other analyses were run by SPSS 12.0 (SPSS Inc., Chicago, IL, USA); comparisons among the groups were performed using Chi-square test and Fisher's exact test for proportions and Kruskal–Wallis test followed by Mann–Whitney test for non-normally distributed continuous variables. A p value of <0.05 was considered statistically significant.

Results

Demographic and clinical data

The 46 Caucasian women in the first subset of controls had a mean maternal age of 30 ± 4.9 years; the mean gestational age at delivery was GW39.1 ± 1.3. Demographic and clinical characteristics as well as placental histopathological findings of women in the second subset of controls and patients with pre-eclampsia with or without HELLP syndrome are displayed in Tables 1 and 2, respectively. Severe pre-eclampsia was diagnosed in 61.5% (8/13) of women with preterm and 57.1% (4/7) of patients with term pre-eclampsia. All patients with HELLP syndrome had pre-eclampsia. Neonatal birth-weight was lower in pre-eclampsia with or without HELLP syndrome than in controls. Primiparity was higher in pre-eclampsia than in controls at term; however, this was not the case before term. Maternal body mass index (BMI) was higher in preterm pre-eclampsia, and placental weight was lower in preterm pre-eclampsia with or without HELLP syndrome than in preterm controls (Table 1). From the 22 investigated macroscopic and histological placental lesion types, those consistent with maternal and fetal vascular underperfusion were more frequent in pre-eclampsia with or without HELLP syndrome than in controls, especially in patients who delivered preterm (Table 2).

Maternal serum PP13 concentrations

The analysis of the first subset of control women revealed that $\log_{10}$ PP13 concentration increased as a function of gestational age in their sera taken at routine prenatal care visits ($p < 0.0001$) (Fig. 1a). When analyzing the second subset of control women, $\log_{10}$ PP13 concentrations in maternal serum taken at the time of delivery increased similarly as a function of gestational age ($p = 0.02$). In contrast, maternal serum PP13 concentrations did not correlate with gestational age in patients with pre-eclampsia with or without HELLP syndrome (Fig. 1a).

Since neither the mean $\log_{10}$ maternal serum PP13 concentrations at any given GW nor their rate of increase with gestational age were different between the two subsets of controls, these groups were pooled together to increase the statistical power. For the same reasons, the groups of pre-eclampsia with or without HELLP syndrome were also combined. Then, $\log_{10}$ PP13 concentrations ($\widehat{Y}$) were calculated and a linear regression model was fitted to the results as a function of gestational age (expressed in GW), disease status (DS; control = 0; pre-eclampsia = 1) and their interaction. The following equation gives the estimated $\log_{10}$ PP13 concentrations:

$$\widehat{Y}_{PP13} = 0.85 + (0.037 \cdot \mathrm{GW}) + (1.75 \cdot \mathrm{DS}) + (-0.045 \cdot \mathrm{GW} \cdot \mathrm{DS}) \quad (1)$$

The slopes of the regression lines for $\log_{10}$ PP13 concentrations were significantly different between controls and patients with pre-eclampsia ($p = 0.02$) and the difference between the two groups decreased with advancing gestational age (Fig. 1b and Table 3).

Subsequently, women were sub-divided into term and preterm subgroups to reveal the differences in maternal serum PP13 concentrations that may exist between the second subset of control women and patients with distinct subforms of pre-eclampsia at the time of onset of disease. Median maternal serum PP13 concentrations in preterm pre-eclampsia without (250.0 pg/ml (range: 52–462), $p = 0.02$) and with HELLP syndrome (213.0 (74–571), $p = 0.01$) were significantly higher than in preterm controls (109.6 (31–203)) (Fig. 1c). There was no difference

Table 1 Demographic and clinical characteristics of the study groups

Groups	Preterm controls	Preterm pre-eclampsia	Preterm HELLP	Term controls	Term pre-eclampsia
Number of cases[a]	10	13	12	20	7
Maternal age (years)[b]	26.5 (5.5)	30.9 (5.6)	28.4 (4.5)	32.2 (4.9)	28.3 (3.0)
Gestational age at delivery (weeks)[b]	32.5 (2.8)	30.9 (2.1)	31.42 (2.8)	38.7 (0.8)	37.6 (0.8)
Primiparity[c]	50	38.5	58.3	15	85.7**
Smoking[c]	30	15.4	0	5	0
Systolic blood pressure (mmHg)[b, d]	115.6 (7.2)	162.3 (16.0)*	162.9 (10.5)*	120.3 (11.9)	163.1 (15.8)*
Diastolic blood pressure (mmHg)[b, d]	75.0 (8.7)	95.5 (11.7)*	105.0 (13.8)*	74.8 (5.8)	103.0 (11.2)*
Maternal BMI (kg/m^2)[b]	25.6 (4.3)	32.4 (8.4)***	26.6 (3.4)	26.2 (4.0)	28.3 (1.1)
Neonatal birth-weight (g)[b]	2246 (709.1)	1391.5 (446.9)**	1445.8 (421.8)**	3317 (470)	2714 (498)***
Placental weight (g)[b]	410.5 (65.8)	261.5 (63.1)***	262.6 (51.7)***	504.0 (81.9)	379.8 (110.9)
Caesarean section[c]	50	100	100	100	100

All women were Caucasian
*$p<0.001$; **$p<0.01$; ***$p<0.05$ compared to gestational age matched controls
[a] Values are presented as number
[b] Values are presented as mean (+SD)
[c] Values are presented as percentage
[d] Highest blood pressure values measured before delivery

between the term pre-eclampsia (211.1 (100–226)) and term control (218.0 (52–685)) groups.

Placental PP13 concentrations

Placental PP13 concentrations did not correlate with gestational age in any of the groups (Fig. 2a). Median placental PP13 concentrations in preterm pre-eclampsia without (7.5 ng/mg total protein (range, 0.7–23.8, $p = 0.13$)) and with HELLP syndrome (5.6 (1.9–29.3, $p = 0.15$)) were lower than in preterm controls (24.7 (3.0–35.8)) (Fig. 2b). There was no difference between the pre-eclampsia (14.3 (3.2–19.6)) and control (12.1 (4.3–92.1)) groups at term.

Placental *LGALS13* gene expression

The mean *LGALS13/HPRT* gene expression ratio decreased with advancing gestational age in the second subset of controls ($p = 0.01$); however, this did not change in patients with pre-eclampsia (Fig. 3a). In addition, the mean *LGALS13/HPRT* gene expression ratio was higher in controls than in the pre-eclampsia group ($p = 0.02$). The *LGALS13/HPRT* gene expression ratios were fitted to a linear regression model:

$$\widehat{Y}_{\mathrm{LGALS13}} = 16.4 + (-0.39 \cdot \mathrm{GW}) + (-15.33 \cdot \mathrm{DS}) + (0.39 \cdot \mathrm{GW} \cdot \mathrm{DS}). \quad (2)$$

Table 2 Histopathological findings

	Preterm and term controls	Preterm pre-eclampsia	Preterm HELLP	Term pre-eclampsia
Number of placentas[a] (*n*)	14	9	10	5
Distal villous insufficiency (%)	0	55.6**	50**	40***
Increased syncytial knots (%)	57.2	88.9	70	100
Increased perivillous fibrin (%)	0	55.6**	20	40***
Recent villous infarct (%)	0	55.6**	30***	0
Remote villous infarct (%)	7.2	33.4	70**	40
Remote villous infarct, extensive (%)	7.2	44.4***	80*	40
Small placenta (%)	0	66.7*	66.7*	60**
Uteroplacental vessel thrombosis (%)	0	22.3	55.6**	0
Uteroplacental vessel adaptation problem[b] (%)	0	25	44	25
Villous stromal fibrosis (%)	7.2	66.7**	60**	60***
Villous dysmaturity (%)	7.2	77.8**	80*	40

The Pearson's chi-square test and the Fisher's exact test were used for statistical analysis. Values are presented as number or percentage
*$p<0.001$; **$p<0.01$, ***$p<0.05$ compared to controls
[a] Three macroscopically normal central and paracentral areas of the placental discs, an *en face* block of the basal plates, and all blocks of the macroscopic lesions were microscopically evaluated in each placenta
[b] Fibrinoid necrosis with or without acute atherosis

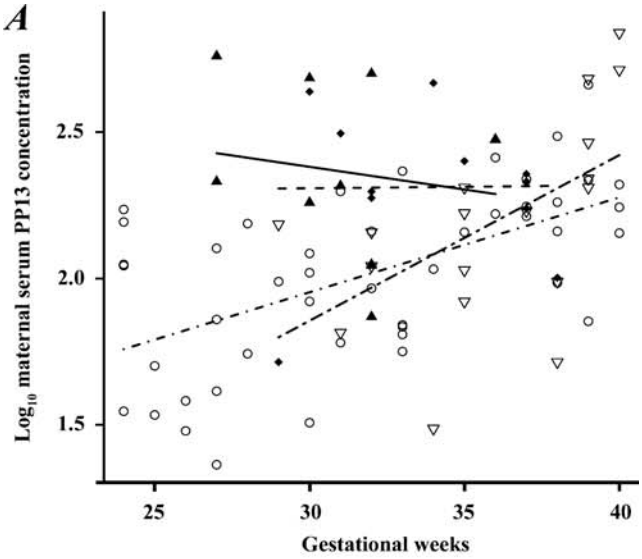

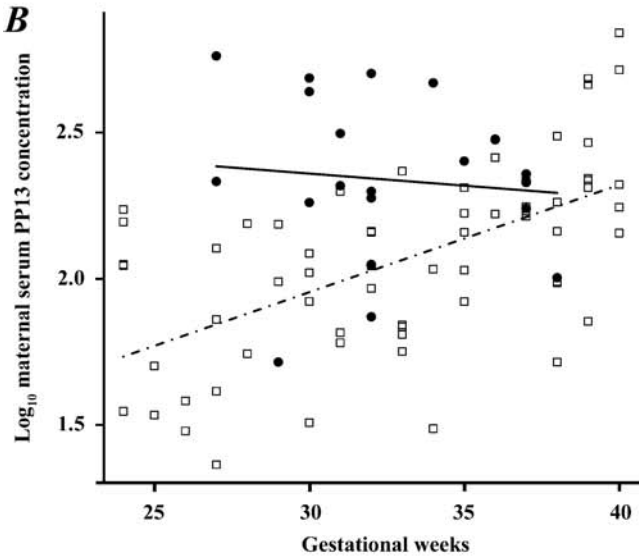

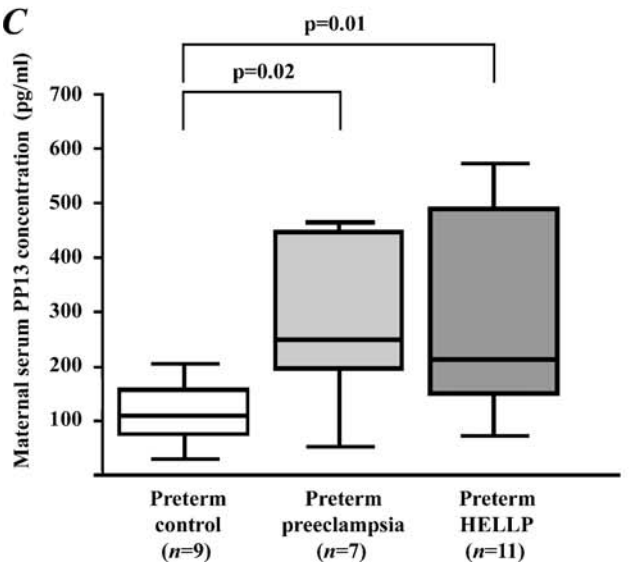

◀ **Fig. 1** Maternal serum PP13 concentrations. **a** Log_{10} PP13 concentration increased as a function of gestational age in sera of normal pregnant women taken at routine prenatal care visits (n=46; ○ – • –) and in preterm and term controls taken at the time of delivery (n=18; ▽ — - —); however, did not correlate with gestational age in patients with pre-eclampsia with (n=11; ▲ ——) or without HELLP syndrome (n=12; ♦ – –) at the time of delivery. **b** The regression line for log_{10} serum PP13 concentrations was different in the pooled group of controls (n=64; □ – • –) from the pooled group of pre-eclampsia (n=23; • ——). **c** Median maternal serum PP13 concentrations were significantly higher in women with preterm pre-eclampsia with or without HELLP syndrome than in preterm controls. *Boxes* represent the median±25th percentiles, *whiskers* the extreme values

Not surprisingly, the median *LGALS13/HPRT* gene expression ratio was significantly lower in patients with preterm pre-eclampsia than in preterm controls (3.45-fold; p = 0.03) (Fig. 3b); however, no difference was detected between the term pre-eclampsia and term control groups (1.02-fold).

Molecular size of PP13

To verify the specificity of the antibody, we performed Western blots on immunoprecipitated placental protein extracts. Recombinant, His-tagged PP13 was recognized as a 18 kDa band, while placental-derived PP13 migrated as a 16 kDa band in all investigated samples (Fig. 4). These

Table 3 Maternal serum PP13 concentrations adjusted to the linear regression model

Maternal serum PP13 concentrations (pg/ml)[a]		
Gestational weeks	Control[b]	Preeclampsia[b]
24	53.8	NA
25	58.5	NA
26	63.7	NA
27	69.3	239.9
28	75.4	235.4
29	82.0	230.9
30	89.2	226.6
31	97.1	222.3
32	105.6	218.2
33	114.9	214.1
34	125.0	210.0
35	136.0	206.1
36	148.0	202.2
37	161.0	198.4
38	175.1	194.7
39	190.6	191.0
40	207.3	NA

[a] The equation of the linear model was used for the intrapolation of gestational age-specific maternal serum PP13 concentrations in control women and in patients with preeclampsia

[b] Each value represents an intersection on the regression lines for the given gestational week

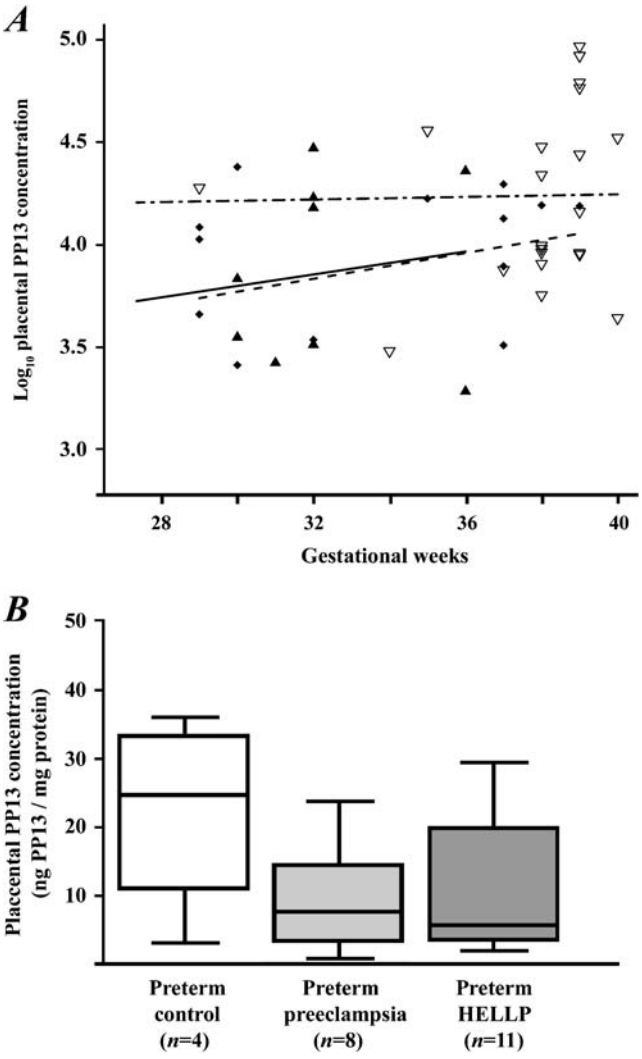

Fig. 2 Placental PP13 concentrations. **a** Log_{10} placental PP13 concentrations did not correlate with gestational age either in control women (n=22; ▽— - —) or in patients with pre-eclampsia with (n=11; ▲ ——) or without HELLP syndrome (n=14; ◆ – –). **b** Median placental PP13 concentrations were lower in women with pre-eclampsia without (3.3-fold) or with (4.4-fold) HELLP syndrome than in controls. *Boxes* represent the median±25th percentiles, *whiskers* the extreme values

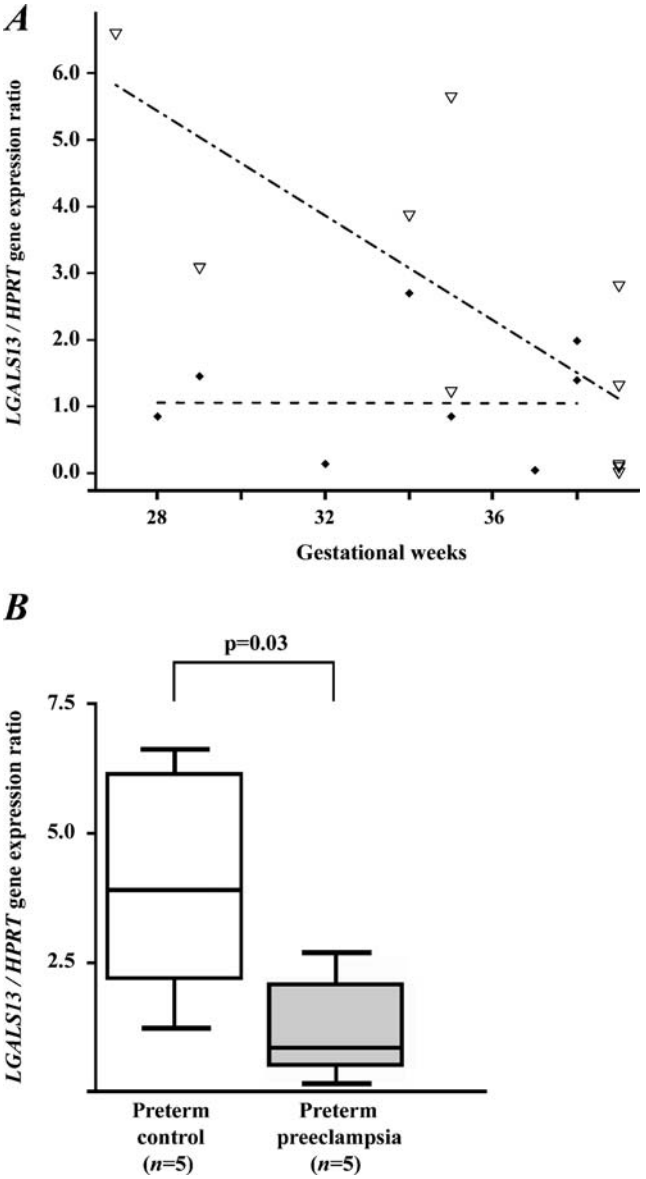

Fig. 3 Placental *LGALS13* gene expression. **a** The regression line for the *LGALS13/HPRT* gene expression ratio decreased with advancing gestational age in control women (n=10; ▽— - —), while it did not change in patients with pre-eclampsia (n=9; ◆ – –). **b** The *LGALS13/HPRT* gene expression ratio was 3.5-fold lower in women with preterm pre-eclampsia than in preterm controls. *Boxes* represent the median±25th percentiles, *whiskers* the extreme values

results provided the biochemical evidence for the nature of the immunostained protein and revealed that the same molecular size PP13 was detectable in all control and pathological placentas.

Placental PP13 immunostaining

The intensity of cytoplasmic staining of the syncytiotrophoblast was significantly weaker in central cotyledons in preterm pre-eclampsia without (mean composite score ± SD, 3.7 ± 0.4; p = 0.04) and with HELLP syndrome (3.5 ± 0.7, p = 0.02) compared to preterm controls (5.0 ± 1.2). However, there was no significant difference between pre-eclampsia (4.3 ± 0.7) and controls (4.9 ± 1.7) at term (Figs. 5a–e and 6a). The coefficients of variation (CVs) between the scores provided by the two examiners for cytoplasmatic and membrane staining were 10.53% (p = 0.13) and 8.68% (p = 0.1), respectively.

Because of the extensive loss of the brush border membrane in pre-eclamptic placentas, it was only possible to evaluate the membrane intensity score. Staining of the microvillous membrane was uniform in term (membrane

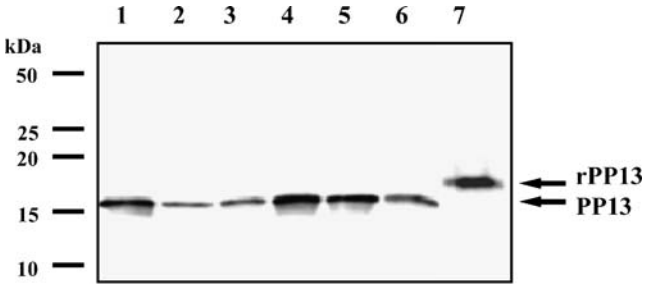

Fig. 4 Identification of recombinant and placental expressed PP13 by Western blotting. The His-tagged rPP13 (7) migrated as a 18 kDa band, while immunoprecipitated placental PP13 was recognized as an immunologically identical 16 kDa band in all samples (*1–2* term controls, *3* term pre-eclampsia, *4* preterm control, *5* preterm pre-eclampsia, *6* preterm HELLP syndrome). The positions of molecular mass markers are signed in the *left*

intensity score ± SD, 1.8 ± 0.4) and preterm (1.6 ± 0.4) controls (Figs. 5a,b and 6b), while it was stronger in term pre-eclampsia (2.2 ± 0.3, $p = 0.04$) and preterm pre-eclampsia without (2.2 ± 0.6) and with HELLP syndrome (2.3 ± 0.4, $p = 0.01$). Syncytial cytoplasm protrusions, membrane blebs and shed membrane particles stained intensely; however, there was no PP13 staining at the sites of membrane loss (Figs. 5c–e and 6c). The villous capillary endothelium was weakly immunoreactive in all sections (Figs. 5a–e and 6c).

Discussion

PP13 localizes to the syncytiotrophoblast microvillous membrane and villous endothelium

Our previous [29] and present studies localized PP13 to the cytoplasm and brush border membrane of the syncytiotrophoblast, which is a highly polarized cell-layer with distinct proteomic and glycomic profiles on its apical and basement membranes [41, 42]. The brush border membrane contains an abundance of *N*-acetyl-galactosamine [42], the strongest carbohydrate ligand for PP13 [29], which may suggest a causal link between the binding specificity and sublocalization of PP13. As other galectins, PP13 lacks a secretion signal peptide but may accumulate directly below the plasma membrane and can be secreted to the cell surface via non-classical pathways, such as through the extrusion of membrane blebs or exovesicle shedding [43]. Indeed, syncytiotrophoblast membrane blebs were immunopositive for PP13 in this study and exovesicles generally contain annexin-II [44], a ligand for PP13 at the syncytiotrophoblast apical membrane [29]. Of note, annexin-II is a major component of lipid rafts in microvillous surfaces and it functions as an interface between lipid rafts and the actin cytoskeleton [44]. As a high similarity of the syncytiotrophoblast microvillous membrane to lipid rafts has recently been identified [41] and galectins bear an important role in lipid rafts on microvillous surfaces [44], it would be intriguing to verify whether PP13 has a placenta-specific role in membrane trafficking and organization of the microvillous membrane through its interaction with annexin-II and β/γ-actin [29].

As a novel finding of this study, the villous endothelium was immunopositive for PP13 in all investigated placentas, which is in accord with a previous report that showed comparable amounts of PP13 in maternal and cord blood [30]. Thus, it would be important to test whether differences exist in cord blood PP13 concentrations in healthy and pathological pregnancies.

The localization and expression of PP13 is altered in pre-eclampsia and HELLP syndrome

This study has shown first that PP13 staining of the syncytiotrophoblast microvillous membrane is increased in pre-eclampsia with or without HELLP syndrome, irrespective of gestational age, suggesting a shift in the intracellular trafficking of PP13 in these syndromes. In contrast, cytoplasmic PP13 staining of the syncytiotrophoblast is decreased in preterm pre-eclampsia with or without HELLP syndrome when compared to gestational age-matched controls. In accordance with these, placental *LGALS13* gene expression and PP13 protein content were lower in preterm pre-eclampsia than in gestational age-matched controls, and a similar decrease in placental PP13 protein content was found in preterm HELLP syndrome. The impairment of *LGALS13* gene expression in preterm pre-eclampsia and HELLP syndrome is underlined by the following: (1) spatial and temporal gene expression differences within the placental disks might have had only minimal impact on our expression data as only central cotyledons were investigated, and patients with pre-eclampsia and control women were matched for gestational age; (2) the immunostaining of the syncytiotrophoblast was also significantly weaker in these central cotyledons in preterm pre-eclampsia with or without HELLP syndrome when compared to controls.

Our previous [29] and present studies localized PP13 to the syncytiotrophoblast but not to cytotrophoblasts, suggesting that the regulation of the *LGALS13* gene expression is related to syncytialization [49–51]. Of note, recent studies have provided evidence that syncytin-1, a major regulator of syncytialization [45], was abnormally localized to the apical microvillous membrane in pre-eclampsia [46]; moreover, its placental expression was significantly decreased in preterm but not in term pre-eclampsia and

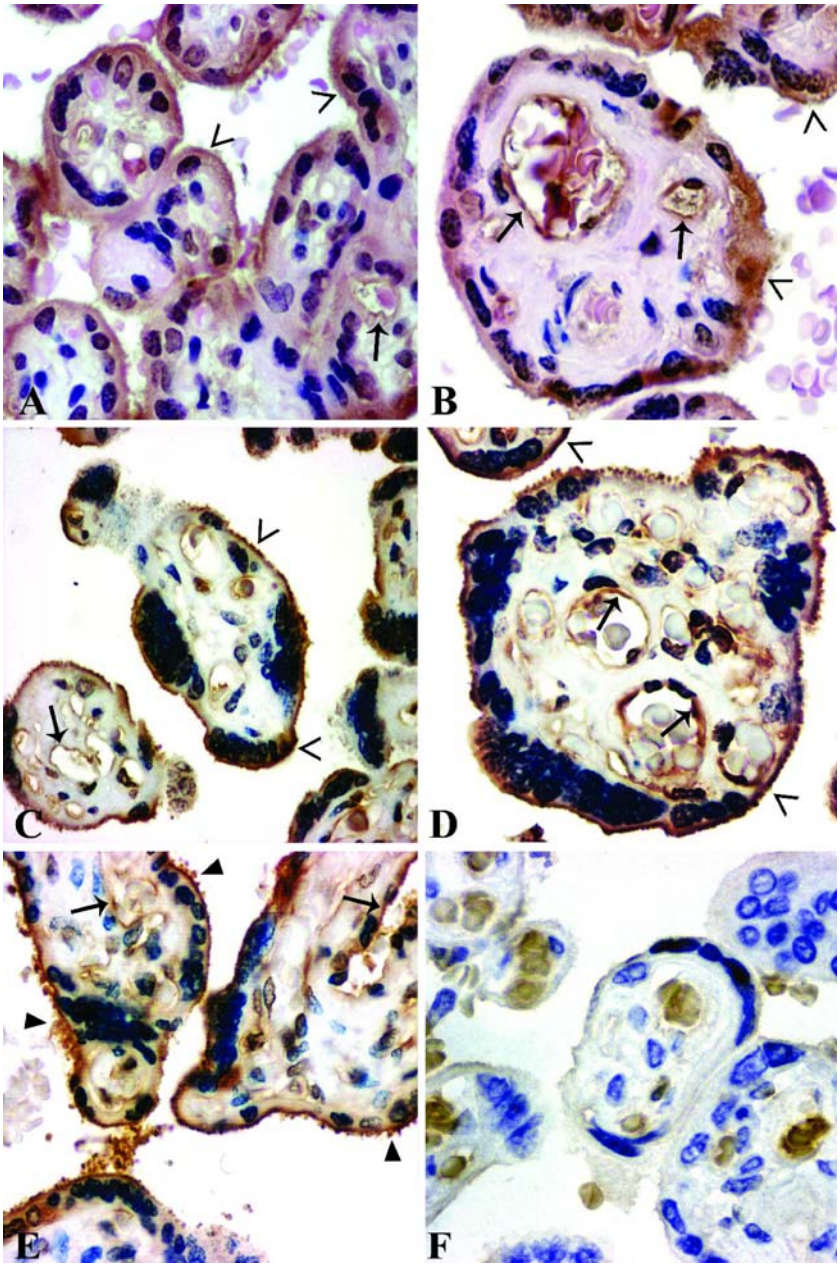

Fig. 5 Placental immunolocalization of PP13. Syncytiotrophoblastic immunostaining was moderate in preterm controls (**a** GW 35), and weak in term controls (**b** GW 38), preterm (**c** GW 29) and term pre-eclampsia (**d** GW 37) and HELLP syndrome (**e** GW 36). The brush border membrane (*open arrowheads*) stained moderately in controls (**a**, **b**), and strongly in pre-eclampsia without (**c**, **d**) or with HELLP syndrome (**e**). Cytoplasm protrusions, membrane blebs and shed membrane particles were PP13 positive (*filled arrowheads*) (**c**–**e**). The villous endothelium (*arrows*) was immunopositive in all sections (**a**–**e**). Negative control*:* isotype-matched IgG staining (**f**). HE (**a**, **b**) or hematoxilin (**c**–**f**) counterstain. 500× (**a**, **c**, **e**) or 700× (**b**, **d**, **f**) magnifications

HELLP syndrome [46–48]. The altered *Syncytin* gene expression and protein localization was suggested to impair cell-fusion and syncytiotrophoblast formation [46–48], which may lead to decreased *LGALS13* gene expression in preterm pre-eclampsia. Further functional studies are warranted to elucidate the regulation of *LGALS13* gene expression and its relation to syncytin-1 and villous trophoblast differentiation.

Shedding of PP13 immunopositive membrane particles is enhanced in preterm pre-eclampsia and HELLP syndrome

Syncytiotrophoblast cytoplasm protrusions, microvillous membrane blebs, and shed membrane particles were strongly PP13 immunopositive, which is a novel finding. Previous studies revealed that early- rather than late-onset pre-eclampsia is

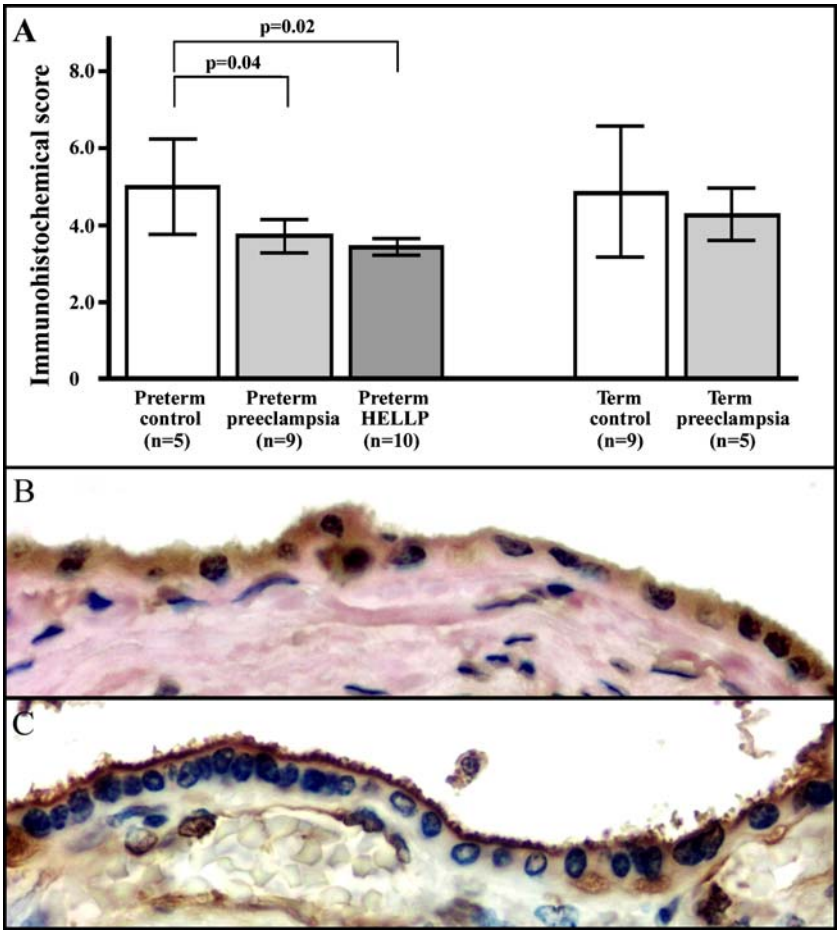

Fig. 6 IHC score analysis and immunolocalization of PP13 in the syncytiotrophoblast. The composite IHC score of the syncytiotrophoblast was higher in preterm controls than in preterm pre-eclampsia with or without HELLP syndrome (**a**). High magnification (800×) images show uniformly moderate cytoplasmic and brush border membrane staining in a preterm control (**b**), while weak cytoplasmic and strong membrane staining in a preterm HELLP syndrome placenta (**c**). Cytoplasm protrusions, membrane blebs and shed membrane particles stained intensely for PP13 (**c**). HE (**b**) or hematoxilin (**c**) counterstain

characterized by frequent placental lesions and increased STBM shedding [15–19]. An intensive loss of the brush border membrane, cytoplasm protrusions and microvillous blebs [52–54] were implicated as sources of the large quantities of STBMs in preterm pre-eclampsia [18, 55]. These morphological changes were suggested to be the consequence of placental vascular underperfusion and ischemia [48, 52, 54]. We observed that (1) the frequency of characteristic changes in placental histopathological findings consistent with placental vascular underperfusion, (2) the magnitude of syncytiotrophoblast brush border distortions and (3) the extent of microvillous membrane shedding were highest in preterm pre-eclampsia with or without HELLP syndrome. Moreover, shed membrane particles were strongly immunopositive for PP13, which may lead to an increase in maternal serum PP13 concentrations in these cases.

Maternal serum PP13 concentrations are elevated in preterm pre-eclampsia and HELLP syndrome in the third trimester

Maternal serum PP13 concentrations increased as a function of gestational age in the control groups, similar to the increase in maternal serum concentrations of syncytiotrophoblastic proteins localized to the brush border membrane, such as PP5/TFPI-2, heat-stable alkaline phosphatase (PLAP) and pregnancy-specific beta$_1$-glycoprotein (SP1) [27]. This rise in serum PP13 concentrations with advancing gestation was also similar to the increase in trophoblast cell volumes as assessed by stereological methods [56]. Thus, concentrations of PP13 in maternal serum are dependent on the volume of its origin, the trophoblast, in normal pregnancies.

Of importance, no difference was detected in serum PP13 concentrations in preterm controls presenting with labor that led to preterm delivery when compared to normal pregnant women who delivered at term. In contrast, maternal serum PP13 concentrations were higher in women presenting with preterm pre-eclampsia with or without HELLP syndrome than in preterm controls; however, no such difference was found between patients and controls at term. Furthermore, characteristic changes were also detected in placental histopathology, PP13 content and immunostaining in preterm pre-eclampsia, but no similar differences were found between patients and controls at term. These findings may underline the different mechanisms of disease in term and preterm pre-eclampsia [14, 16, 20]. Moreover, as placentas in preterm pre-eclampsia with or without HELLP syndrome showed a PP13 pattern more typical of term than preterm controls, this phenomenon might be considered as a biochemical correlate of the accelerated maturation of the villous tree, represented by our frequent findings of distal villous insufficiency in cases of preterm pre-eclampsia.

Our study did not show differences in maternal serum and placental PP13 concentrations and immunostainings between preterm pre-eclampsia alone or coupled with HELLP syndrome, suggesting a common pathway for the dysregulation of PP13 production and placental shedding in the two syndromes. This finding is in accord with the current view that although pre-eclampsia and HELLP syndrome might have distinct familial segregation and genetic background [57–61], independent genes and mechanisms in various subsets of these syndromes may initiate shared pathophysiological pathway(s), common clinical symptoms and placental dysfunction [61, 62].

What is the cause of the high maternal serum PP13 concentrations in preterm pre-eclampsia? (1) The *LGALS13* gene is predominantly expressed by the placenta [28]; therefore, this organ is the probable source for the elevated amounts of PP13 in the maternal circulation. (2) There is a lower placental *LGALS13* gene expression in preterm pre-eclampsia, which obviously cannot account for an increased placental PP13 production. (3) Thus, our data suggest that the excess syncytiotrophoblastic shedding of PP13 is probably the major source of its increased third trimester maternal serum concentrations in preterm pre-eclampsia and HELLP syndrome, which is similar to that observed with other brush border localized proteins, such as PLAP and PP5/TFPI-2 [27, 40].

We suggest that a constitutionally decreased *LGALS13* gene expression throughout pregnancy might account for the low first trimester maternal serum PP13 concentrations in patients destined to develop early-onset/preterm pre-eclampsia [22–25]; however, PP13 concentrations increase parallel with the augmented shedding of STBMs in these subset of patients in the third trimester [18].

Conclusions

Our combined approach has shed new light on the behavior of PP13 in pre-eclampsia and HELLP syndrome at the onset of clinical symptoms. Essential differences in placental histopathology, PP13 expression, and apical membrane shedding of PP13 in preterm pre-eclampsia and HELLP syndrome have been demonstrated, and the latter might contribute to the increased maternal serum PP13 concentrations in these cases. Our findings may reflect a different mechanism of disease between term and preterm pre-eclampsia.

Acknowledgements The authors are grateful to Dr. Zsolt Csapo and Dr. Katalin Hertelendy for their support in the Histopathological and Chemistry Laboratories; to Dr. Timea Kovats, Dr. Julia Dienes, Dr. Maria Lengyel, Katalin Karaszi, Krisztina Mekli, and Istvan Szabo for their helpful technical assistance; to Julia Olah, Katalin Lang, Katalin Raum, and all the colleagues in the laboratories, operating theatres and Labor and Delivery Unit of the First Department of Obstetrics and Gynecology for their help with the specimens. The authors thank Dr. Offer Erez, Dr. Chong Jai Kim, Dr. Derek Wildman, and Sara Tipton for their critical reading of the manuscript and valuable advices.

The Fluorchem SP CCD imaging system was a generous donation of the Hungarian Terry Fox Foundation to the First Department of Obstetrics and Gynecology. N.G.T. is grateful to the Hungarian Academy of Sciences for the János Bolyai Scholarship.

Funding This research was funded by the Hungarian Országos Tudományos Kutatási Alapprogramok (T/046473 to N.G.T.) and by grants from the European Union (FP6, "Pregenesys - 037244" to H.M. and N.G.T.) and the Israel Chief Scientist (31851, 37324, 14128 to H.M.).

Conflict of interest statement We declare that we have no conflict of interest.

References

1. Myatt L (2002) Role of placenta in preeclampsia. Endocrine 19:103–111
2. Sibai B, Dekker G, Kupferminc M (2005) Pre-eclampsia. Lancet 365:785–799
3. Lyall F (2005) Priming and remodelling of human placental bed spiral arteries during pregnancy—a review. Placenta 26(Suppl A):S31–S36
4. Espinoza J, Romero R, Mee KY et al (2006) Normal and abnormal transformation of the spiral arteries during pregnancy. J Perinat Med 34:447–458
5. Torry DS, Wang HS, Wang TH et al (1998) Preeclampsia is associated with reduced serum levels of placenta growth factor. Am J Obstet Gynecol 179:1539–1544
6. Maynard SE, Min JY, Merchan J et al (2003) Excess placental soluble fms-like tyrosine kinase 1 (sFlt1) may contribute to endothelial dysfunction, hypertension, and proteinuria in pre-eclampsia. J Clin Invest 111:649–658

7. Chaiworapongsa T, Romero R, Espinoza J et al (2004) Evidence supporting a role for blockade of the vascular endothelial growth factor system in the pathophysiology of preeclampsia. Young Investigator Award. Am J Obstet Gynecol 190:1541–1547
8. Venkatesha S, Toporsian M, Lam C et al (2006) Soluble endoglin contributes to the pathogenesis of preeclampsia. Nat Med 12:642–649
9. Roberts JM, Taylor RN, Musci TJ et al (1989) Preeclampsia: an endothelial cell disorder. Am J Obstet Gynecol 161:1200–1204
10. Redman CW, Sacks GP, Sargent IL (1999) Preeclampsia: an excessive maternal inflammatory response to pregnancy. Am J Obstet Gynecol 180:499–506
11. Gervasi MT, Chaiworapongsa T, Pacora P et al (2001) Phenotypic and metabolic characteristics of monocytes and granulocytes in preeclampsia. Am J Obstet Gynecol 185:792–797
12. Jauniaux E, Poston L, Burton GJ (2006) Placental-related diseases of pregnancy: involvement of oxidative stress and implications in human evolution. Hum Reprod Updat 12:747–755
13. Myatt L, Miodovnik M (1999) Prediction of preeclampsia. Semin Perinatol 23:45–57
14. von Dadelszen P, Magee LA, Roberts JM (2003) Subclassification of preeclampsia. Hypertens Pregnancy 22:143–148
15. Moldenhauer JS, Stanek J, Warshak C et al (2003) The frequency and severity of placental findings in women with preeclampsia are gestational age dependent. Am J Obstet Gynecol 189:1173–1177
16. Redman CW, Sargent IL (2005) Latest advances in understanding preeclampsia. Science 308:1592–1594
17. Sebire NJ, Goldin RD, Regan L (2005) Term preeclampsia is associated with minimal histopathological placental features regardless of clinical severity. J Obstet Gynaecol 25:117–118
18. Goswami D, Tannetta DS, Magee LA et al (2006) Excess syncytiotrophoblast microparticle shedding is a feature of early-onset pre-eclampsia, but not normotensive intrauterine growth restriction. Placenta 27:56–61
19. Egbor M, Ansari T, Morris N et al (2006) Morphometric placental villous and vascular abnormalities in early- and late-onset pre-eclampsia with and without fetal growth restriction. BJOG 113:580–589
20. Ness RB, Roberts JM (1996) Heterogeneous causes constituting the single syndrome of preeclampsia: a hypothesis and its implications. Am J Obstet Gynecol 175:1365–1370
21. Zwahlen M, Gerber S, Bersinger NA (2007) First trimester markers for pre-eclampsia: placental vs. non-placental protein serum levels. Gynecol Obstet Invest 63:15–21
22. Nicolaides KH, Bindra R, Turan OM et al (2006) A novel approach to first-trimester screening for early pre-eclampsia combining serum PP-13 and Doppler ultrasound. Ultrasound Obstet Gynecol 27:13–17
23. Spencer K, Cowans NJ, Chefetz I et al (2007) First-trimester maternal serum PP-13, PAPP-A and second-trimester uterine artery Doppler pulsatility index as markers of pre-eclampsia. Ultrasound Obstet Gynecol 29:128–134
24. Chafetz I, Kuhnreich I, Sammar M et al (2007) First-trimester placental protein 13 screening for preeclampsia and intrauterine growth restriction. Am J Obstet Gynecol 197:35–37
25. Romero R, Kusanovic JP, Than NG et al (2008) First trimester maternal serum PP13 in the risk assessment for preeclampsia. Am J Obstet Gynecol 199(2):122.e1–122.e11
26. Bohn H, Kraus W, Winckler W (1983) Purification and characterization of two new soluble placental tissue proteins (PP13 and PP17). Oncodev Biol Med 4:343–350
27. Than GN, Bohn H, Szabo DG (1993) Advances in pregnancy-related protein research. CRC, Boca Raton
28. Than NG, Sumegi B, Than GN et al (1999) Isolation and sequence analysis of a cDNA encoding human placental tissue protein 13 (PP13), a new lysophospholipase, homologue of human eosinophil Charcot-Leyden Crystal protein. Placenta 20:703–710
29. Than NG, Pick E, Bellyei S et al (2004) Functional analyses of placental protein 13/galectin-13. Eur J Biochem 271:1065–1078
30. Burger O, Pick E, Zwickel J et al (2004) Placental protein 13 (PP-13): effects on cultured trophoblasts, and its detection in human body fluids in normal and pathological pregnancies. Placenta 25:608–622
31. Visegrady B, Than NG, Kilar F et al (2001) Homology modelling and molecular dynamics studies of human placental tissue protein 13 (galectin-13). Protein Eng 14:875–880
32. Barondes SH, Castronovo V, Cooper DN et al (1994) Galectins: a family of animal beta-galactoside-binding lectins. Cell 76:597–598
33. Papp Cs, Szabo G, Toth-Pal E et al (1991) Fetal growth rate and its variations 1988/89. Orv Hetil 132:1865–1870
34. ACOG (2002) ACOG practice bulletin: Diagnosis and management of preeclampsia and eclampsia. Number 33, January 2002. Obstet Gynecol 99:159–167
35. Barton JR, Sibai BM (2004) Diagnosis and management of hemolysis, elevated liver enzymes, and low platelets syndrome. Clin Perinatol 31:807–833 vii
36. Khong TY (2001) A topographical and clinical approach to examination of the placenta. Pathology 33:174–186
37. Redline RW, Boyd T, Campbell V et al (2004) Maternal vascular underperfusion: nosology and reproducibility of placental reaction patterns. Pediatr Dev Pathol 7:237–249
38. Langston C, Kaplan C, Macpherson T et al (1997) Practice guideline for examination of the placenta: developed by the Placental Pathology Practice Guideline Development Task Force of the College of American Pathologists. Arch Pathol Lab Med 121:449–476
39. Hargitai B, Marton T, Cox PM (2004) Best practice no 178. Examination of the human placenta. J Clin Pathol 57:785–792
40. Ogawa M, Yanoma S, Nagashima Y et al (2007) Paradoxical discrepancy between the serum level and the placental intensity of PP5/TFPI-2 in preeclampsia and/or intrauterine growth restriction: possible interaction and correlation with glypican-3 hold the key. Placenta 28:224–232
41. Paradela A, Bravo SB, Henriquez M et al (2005) Proteomic analysis of apical microvillous membranes of syncytiotrophoblast cells reveals a high degree of similarity with lipid rafts. J Proteome Res 4:2435–2441
42. Jones CJ, Carter AM, Aplin JD et al (2007) Glycosylation at the fetomaternal interface in hemomonochorial placentae from five widely separated species of mammal: is there evidence for convergent evolution? Cells Tissues Organs 185:269–284
43. Nickel W (2005) Unconventional secretory routes: direct protein export across the plasma membrane of mammalian cells. Traffic 6:607–614
44. Danielsen EM, Hansen GH (2006) Lipid raft organization and function in brush borders of epithelial cells. Mol Membr Biol 23:71–79
45. Aplin JD, Straszewski-Chavez SL, Kalionis B et al (2006) Trophoblast differentiation: progenitor cells, fusion and migration—a workshop report. Placenta 27(Suppl A):S141–S143
46. Knerr I, Beinder E, Rascher W (2002) Syncytin, a novel human endogenous retroviral gene in human placenta: evidence for its dysregulation in preeclampsia and HELLP syndrome. Am J Obstet Gynecol 186:210–213
47. Lee X, Keith JC Jr, Stumm N et al (2001) Downregulation of placental syncytin expression and abnormal protein localization in pre-eclampsia. Placenta 22:808–812
48. Langbein M, Strick R, Strissel PL et al (2008) Impaired cytotrophoblast cell-cell fusion is associated with reduced Syncytin and increased apoptosis in patients with placental dysfunction. Mol Reprod Dev 75:175–183

49. Benirschke K, Kaufmann P (2000) Pathology of the human placenta, 4th edn. Springer, New York
50. Gude NM, Roberts CT, Kalionis B et al (2004) Growth and function of the normal human placenta. Thromb Res 114:397–407
51. Bischof P, Irminger-Finger I (2005) The human cytotrophoblastic cell, a mononuclear chameleon. Int J Biochem Cell Biol 37:1–16
52. Jones CJ, Fox H (1980) An ultrastructural and ultrahistochemical study of the human placenta in maternal pre-eclampsia. Placenta 1:61–76
53. de Luca Brunori I, Battini L, Brunori E et al (2005) Placental barrier breakage in preeclampsia: ultrastructural evidence. Eur J Obstet Gynecol Reprod Biol 118:182–189
54. Crocker I (2007) Pre-eclampsia and villous trophoblast turnover: perspectives and possibilities. Placenta 28(Suppl A):S4–S13
55. Redman CW, Sargent IL (2007) Microparticles and immunomodulation in pregnancy and pre-eclampsia. J Reprod Immunol 76:61–67
56. Mayhew TM, Wadrop E, Simpson RA (1994) Proliferative versus hypertrophic growth in tissue subcompartments of human placental villi during gestation. J Anat 184(Pt 3):535–543
57. Rigo J Jr, Nagy B, Fintor L et al (2000) Maternal and neonatal outcome of preeclamptic pregnancies: the potential roles of factor V Leiden mutation and 5,10 methylenetetrahydrofolate reductase. Hypertens Pregnancy 19:163–172
58. Lachmeijer AM, Arngrimsson R, Bastiaans EJ et al (2001) A genome-wide scan for preeclampsia in the Netherlands. Eur J Hum Genet 9:758–764
59. van Dijk M, Mulders J, Poutsma A, Könst AA et al (2005) Maternal segregation of the Dutch preeclampsia locus at 10q22 with a new member of the winged helix gene family. Nat Genet 37:514–519
60. Sziller I, Babula O, Hupuczi P et al (2007) Mannose-binding lectin (MBL) codon 54 gene polymorphism protects against development of pre-eclampsia, HELLP syndrome and pre-eclampsia-associated intrauterine growth restriction. Mol Hum Reprod 13:281–285
61. Oudejans CB, van DM, Oosterkamp M et al (2007) Genetics of preeclampsia: paradigm shifts. Hum Genet 120:607–612
62. Cross JC (2003) The genetics of pre-eclampsia: a feto-placental or maternal problem? Clin Genet 64:96–103

Virchows Arch (2008) 453:401–406
DOI 10.1007/s00428-008-0657-y

ORIGINAL ARTICLE

The pre-lymphatic pathway, the rooths of the lymphatic system in breast tissue: a 3D study

Sofia Asioli · Vincenzo Eusebi · Laura Gaetano · Luisa Losi · Gianni Bussolati

Received: 13 February 2008 / Accepted: 14 August 2008 / Published online: 4 September 2008

Abstract Three-dimensional (3D) visualisation of microscopic structures provides useful information about their configuration and the spatial (hence functional) relationship between different components in tissues. This paper describes 3D dynamic reconstructions of the pre-lymphatic labyrinth in two cases of "normal" breast core biopsies and one case of pseudoangiomatous stromal hyperplasia. Direct anastomoses between pre-lymphatic channels and true lymphatics of the breast were demonstrated. It is concluded that pre-lymphatics are a way of communication between breast epithelial/stromal structures and the main lymphatic system. The present findings suggest that the existence of pre-lymphatics has to be taken in consideration in the intramammary spread of malignant tumours.

Keywords Pre-lymphatics · Lymphatic labyrinth · 3D · Normal breast · PASH

S. Asioli (✉) · G. Bussolati
Department of Biomedical Sciences and Human Oncology,
Molinette Hospital, University of Turin,
Via Santena 7,
10126 Turin, Italy
e-mail: sofia.asioli@unito.it

V. Eusebi
Section of Anatomic Pathology "M. Malpighi",
University of Bologna, Bellaria Hospital,
Bologna, Italy

L. Gaetano
Department of Mechanics, Polytechnic of Turin,
Turin, Italy

L. Losi
Department of Pathology and Forensic Medicine,
University of Modena and Reggio Emilia,
Modena, Italy

Introduction

The lymphatic vascular network differs from that of the blood vessels as it is an "open" system to the stromal environment [1]. Lymphatic capillaries are structurally similar to blood capillaries [1], and both are composed of endothelial cells with intercellular junctions, adhesion plates, isolated vesicles, deep caveolae, flat nuclei and a well-formed basal lamina. Nevertheless, in normal tissues, there are spaces within the connective tissue that end directly at a lymphatic junction [2]. The spaces are mostly evident when tracers are injected in tissues and become particularly prominent when the oedema forces the cells and fibre bundles apart [2]. Openings of lymphatic capillaries into stromal spaces have been documented at ultrastructural level by Casley-Smith and Florey [1]. Artefacts were excluded, as no similar openings were seen in neighbouring blood capillaries, and were interpreted as consequent to poorly developed adhesion plates [1]. These spaces were named "pre-lymphatics" by Casley-Smith [2] and in the breast are so numerous and so often interconnected as to deserve the name of "lymphatic labyrinth" [3]. Spaces are lined by flattened attenuated cells that are vimentin- and CD-34-positive. CD 31 and D2-40 are consistently negative [4]. The same cells at ultrastructural level show scattered intermediate filaments and lack basal lamina [4] as to deserve the name of "delimiting fibroblasts" by Ozzello [5]. Pre-lymphatics are present around ducts and within the specialised stroma of lobules, but are hardly visible in normal breast because they are collapsed [4], a phenomenon described by Hartveit as the "missing" lymphatic system [3]. Whenever lymph needs to be drained, especially in inflammatory situations, pre-lymphatics open on demand [3]. Although Vuitch et al. [6] believed that these spaces were artefact, Badve and

Sloane [7] demonstrated that these same spaces are real, as they are visible in frozen sections as well as at ultrastructural level [4]. In addition, neoplastic cells were found to spread through them, highlighting the labyrinth structure of these same spaces [8].

Most of the above observations were obtained indirectly from conventional haematoxylin and eosin staining (H&E) or electron microscopy. Direct visualisation of spaces entering into lymphatics would be obtained only by the use of the 3D reconstruction of histological tissue.

We reconstructed from two cases of normal breast core biopsies and a case of pseudoangiomatous stromal hyperplasia (PASH) through a 3D model, the complex labyrinth arrangement of pre-lymphatics and their connection into lymphatic channels.

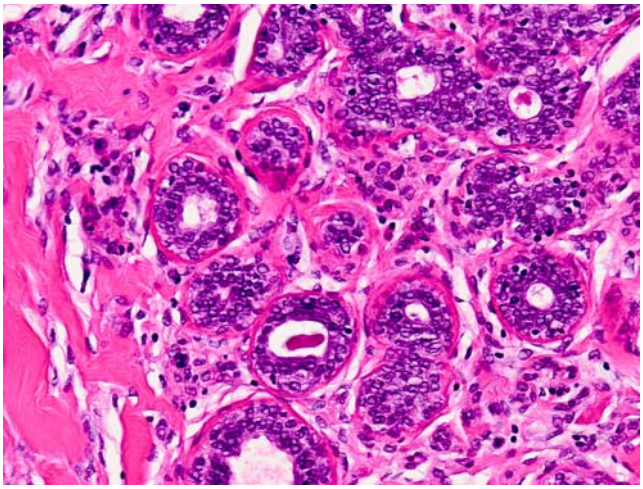

Fig. 1 Case 1: spaces present within the inter acinar stroma. The spaces have elongated shape, are lined by flattened spindle cells and are characteristically devoid of red blood cells

Materials and methods

Cases

Cases 1 and 2 were core biopsies from 48- and 39-year-old women. These were obtained from the files of the Department of Pathology and Forensic Medicine of the University of Modena and Reggio Emilia. Both patients had undergone biopsy as a screening procedure for familiar breast cancer.

Case 3 is of a 51-year-old lady who presented with a 6-month story of a lump in the lower external quadrant of the left breast. The lump was excised. The tissue removed consisted of a 4.5 cm across nodule with smooth surface. The cut surface was homogeneous and grey in colour.

Tissues were embedded in paraffin and stained with H&E as routine.

Histologically, cases 1 and 2 were selected among several others and were constituted by numerous lobules where dilated easily visible spaces were present within the intra-acinar stroma (Fig. 1). Case 3 had the typical feature of PASH [6], being a fibroepithelial lesion in which lobules appeared architecturally distorted, immersed in a stroma showing elongated empty spaces (Fig. 2a,b).

For immunohistochemistry, all cases were stained for D2-40 monoclonal antibody (clone D2-40, diluted 1:100; Signet Laboratories); CD 34 (clone QB-END10, diluted 1:400, Neomarkers) and CD31 (clone yc/70A, diluted 1:20, Cell Marque) employing an automated immunostainer (Ventana BenchMark AutoStainer; Ventana Medical Systems).

The cells that lined the spaces in all cases were CD-34-positive, but negative for CD 31 and D2-40.

For 3D analysis, serial sections obtained from the paraffin blocks were immunohistochemically stained for D2-40. Sections (50 sections, 4 μm thick) then were all photographed. For 3D reconstruction, one lobule from cases 1 and 2 showing numerous widely open spaces were selected (Fig. 1). In case 3, one glandular/stromal area was selected (Fig. 2).

The contours of the spaces of two normal lobules from cases 1 and 2 as well as of one distorted lobule from case 3 were shadowed with the painter tool (red colour) in order to better visualise their shapes. In addition, all the acini of the selected lobule and the perilobular lymphatic channels stained by D2-40 antibody were also shadowed with the painter tool (blue and green colours, respectively).

Three-dimensional procedure

To realign serially cut sections correctly, we created external fiducial markers in the paraffin-embedded specimen using a tissue arrayer instrument (ATA-100; Chemicon International, Temecula, CA, USA) before obtaining serial sections (Fig. 3). Accordingly, four cores removed from an anthracotic lymph node by the tissue arrayer were inserted as reference markers into the ‘recipient’ paraffin block of breast tissue, near the area to be serially cut, and 3D-reconstructed [9]. As already stated, 50 sections, 4 μm thick, were serially cut from the recipient block. Digital pictures of D2-40-stained sections were serially captured at the selected magnification with an OLYMPUS_ DP11 digital camera mounted on an OLYMPUS_ VANOX T microscope. The semi-movable stage of the microscope allowed orientation of the images because the reference markers were set in the same position.

Three-dimensional reconstruction

Using the serial images obtained, 3D models of selected channels, lymphatics and acini were obtained employing

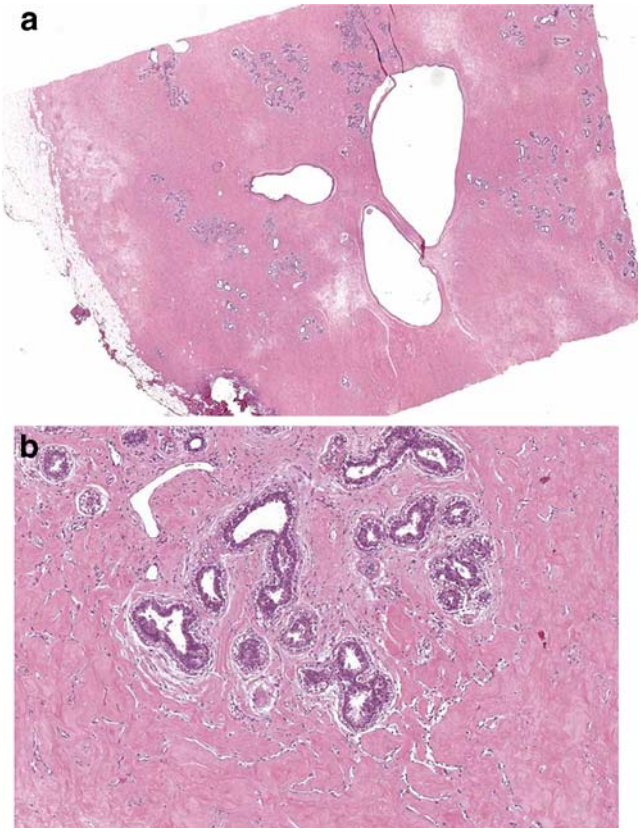

Fig. 2 Case 3 shows typical features of pseudoangiomatous stromal hyperplasia (**a**) in which lobules appear architecturally distorted, immersed in a stroma showing elongated empty spaces (**b**)

Amira 4.0, advanced 3D visualisation and volume modelling software (TGS Template Graphics Software, http://www.tgs.com). In order to have the studied structures unchanged through sections, we previously included the anthracotic lymph node in four points of the paraffin-embedded sample as fiducial tissue markers (see above) [9]. Then, we could manually align serial sections by matching these reference points with the software tools. Finally, AMIRA allowed to segment automatically the regions of interest which were interpolated and finally 3D-reconstructed.

Results

At low magnification, as seen at H&E level, the spaces situated among the acini and around the lobules have an elongated shape, were characteristically devoid of red blood cells and lined by flattened spindle cells (Figs. 1 and 2). Serial sections, stained for D2-40, highlighted lymphatics that were observed around the lobules, whilst the empty spaces were consistently unstained (Fig. 4). Depending on the plane of sectioning, spaces appeared round or ovoid in shape, with some of them laying very close to lymphatic vessels (positive for D2-40) present in the perilobular stroma (Fig. 5).

Three-dimensional modelling

The spatial organisation of the empty spaces (channels), as reconstructed on serial sections, was very complex, but similar in all three cases. The channels were of various size, shape and length and were frequently interconnected. Most spaces were tortuous, elongated and showed small calibre. A minority was short, had irregular profile and large calibre. Intermediate combinations were seen. In general, the caliber of the channels of the PASH case was larger than that seen in normal lobules. Some spaces were linear and followed almost parallel planes of growth as seen in modelling field (level) 31 of case 1 (Fig. 6). Other

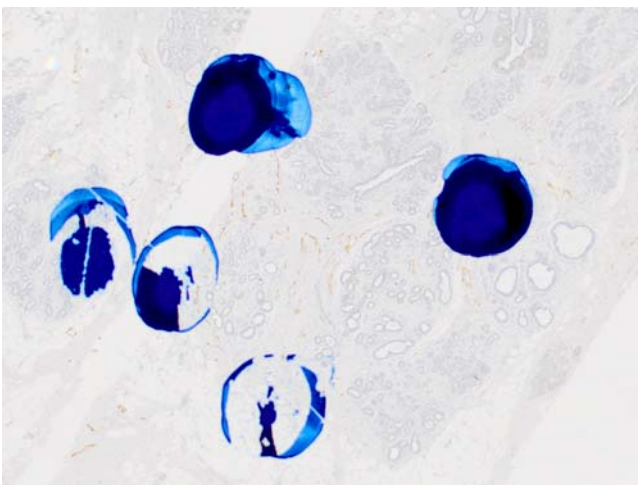

Fig. 3 In order to align serial sections, antracotic lymph node arrays were included as fiducial markers in four points of the paraffin-embedded tissue block

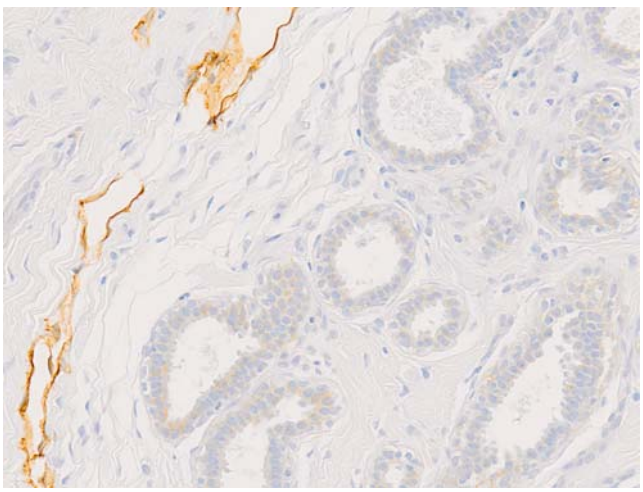

Fig. 4 Stain for D2-40 highlights occasional lymphatics around the lobules, whilst the empty spaces scattered among the acini are consistently unstained

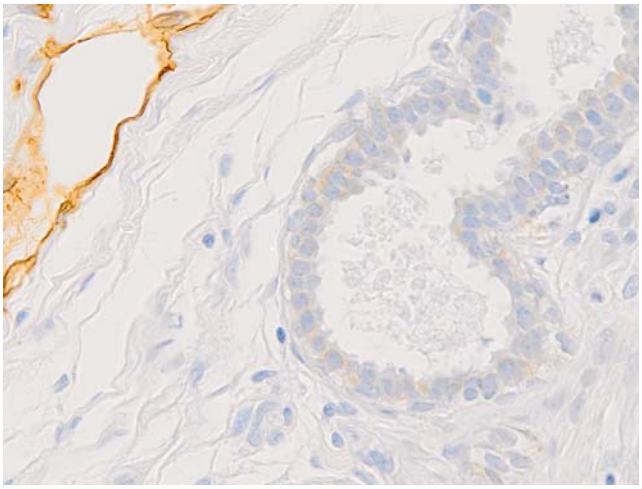

Fig. 5 Spaces appear round to ovoid in shape. One of them is very close to a lymphatic vessel (positive for D2-40) present in the perilobular stroma

modelling fields (levels), especially in PASH, showed spaces with convoluted cavities. Most of the spaces were present within the acinar stroma, but others, especially in the case of PASH, were observed in the perilobular stroma as to build up a complex scaffolding around the lobule (Fig. 7a, modelling field 27, case 2, and b, modelling field 46, case 3). Spaces present within the lobule frequently showed a circumferential distribution around acini (Fig. 8, modelling field 15, case 1).

In no fewer that seven modelling fields, spaces in different cases connected directly to the D2-40-stained perilobular lymphatic vessel (Figs. 8 and 9a, modelling field 10, case 3, and b, modelling field 5, case 3). The

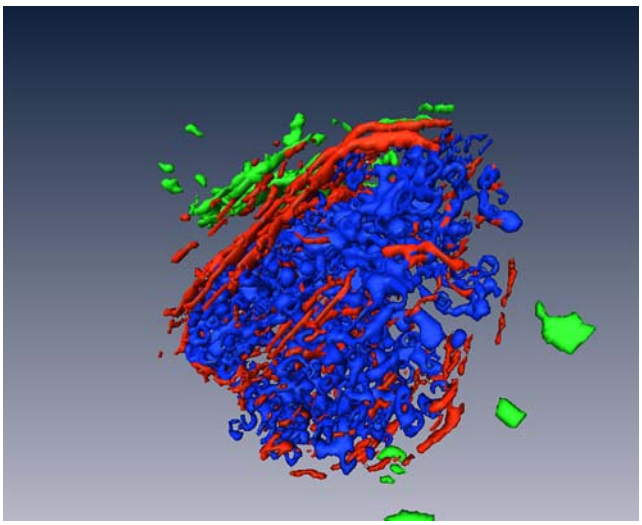

Fig. 6 The spatial organisation of the empty spaces (channels), as reconstructed on serial sections, is very complex, but similar in all three cases. Some spaces are linear and follow almost parallel planes of growth as seen in modelling field (level) 31 of case 1 (*red*: channels; *blue*: acini; *green*: lymphatics)

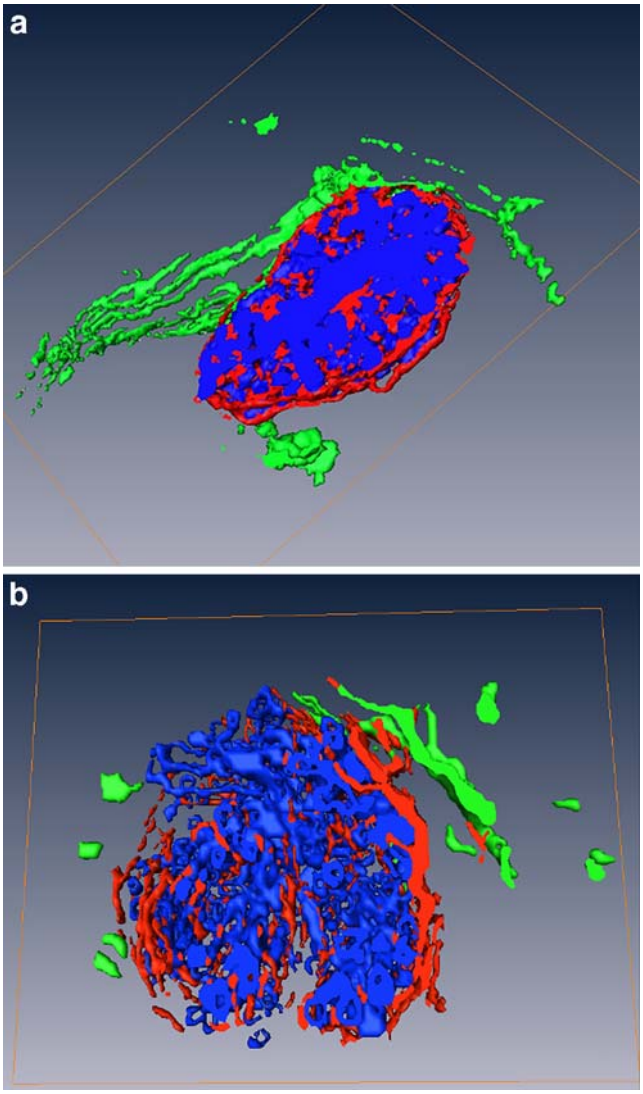

Fig. 7 Most of the spaces are localised within the lobular stroma. When in perilobular location, they build up a complex scaffolding around the lobule. **a** Modelling field 27, case 2. **b** Modelling field 15, case 1. In **b**, perivascular channels connect with a lymphatic in the upper outer corner

3D profile of the three cases can be directly visualised in the motion images stored in the web site of this journal (www.sprigerlink.com).

Discussion

Three-dimensional reconstruction provides useful information about the configuration of microscopic structures, and it offers a useful tool to examine the spatial (hence functional) relationship between different components in tissues. Three-dimensional studies, especially in breast tissues, were based on diafanisation of paraffin blocks of large sections that were examined directly at stereomicroscopic level [10–13]. More recently, the use of the computer that allows the 3D

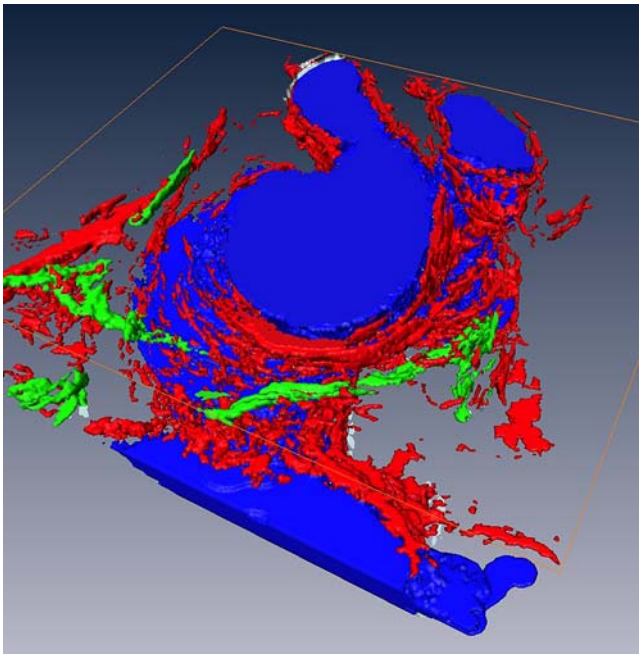

Fig. 8 Spaces frequently show a circumferential distribution around acini in PASH and appear of large caliber (modelling field 46, case 3)

reconstruction of normal structures and of specific lesions from the analysis of multiple histological sections (static 3D) has proven to be a valuable technique in different areas of pathology such as normal distribution of microcirculation of retina [14], para-trabecular pattern of infiltration of non-Hodgkin's lymphoma in bone marrow [15], angiogenesis in the bone marrow of children with leukemia [16], distribution of microvessels in prostate cancer [17], evaluation and reconstruction of spinal cord injury [18], relationship between functional and structural changes of glomerular capillary networks in normal kidney [19], distribution and organisation of microvascular structure of cardiac coronary vascular tree [20], distribution of the vessels in normal and neoplastic thyroid [10] and distributions of vessels in oligodendrogliomas [21]. In breast, Ohtake et al. [22, 23], in a 3D reconstruction of intraductal extension of invasive breast carcinoma, have highlighted the presence of occasional intralobar and extralobar anastomoses which allowed the spread of in situ duct carcinoma through different lobes. These same data were not confirmed by Foschini et al. [11] and Going and Moffat [24]. The similarity between tubular and tubulo-lobular carcinomas has been defined [25], and the size and extent of lobes has been illustrated [24].

A novel approach to the use of computerised 3D techniques is the dynamic reconstruction of specific areas in which the area itself rotate and can be visualised from many angles. In this way, the convoluted shape of the nuclei of papillary thyroid carcinoma was highlighted [26].

In the present study, the lobules that were selected contained several spaces within the specialised stroma. Spaces were seen also in perilobular location where lymphatics were also visible, and these features were consistent with the description of the pre-lymphatic labyrinth depicted by Hartveit [3]; in fact, spaces appeared round to ovoid, some were elongated, devoid of red blood cells, lined by flat "attenuated" cells that were negative for D2-40 stain and invested the acini. Lymphatics were present only around the lobules, showed dilated lumens that were also devoid of red blood cells and lined by flattened cells that were positive for D2-40. The difference between normal lobules and PASH consisted in the larger

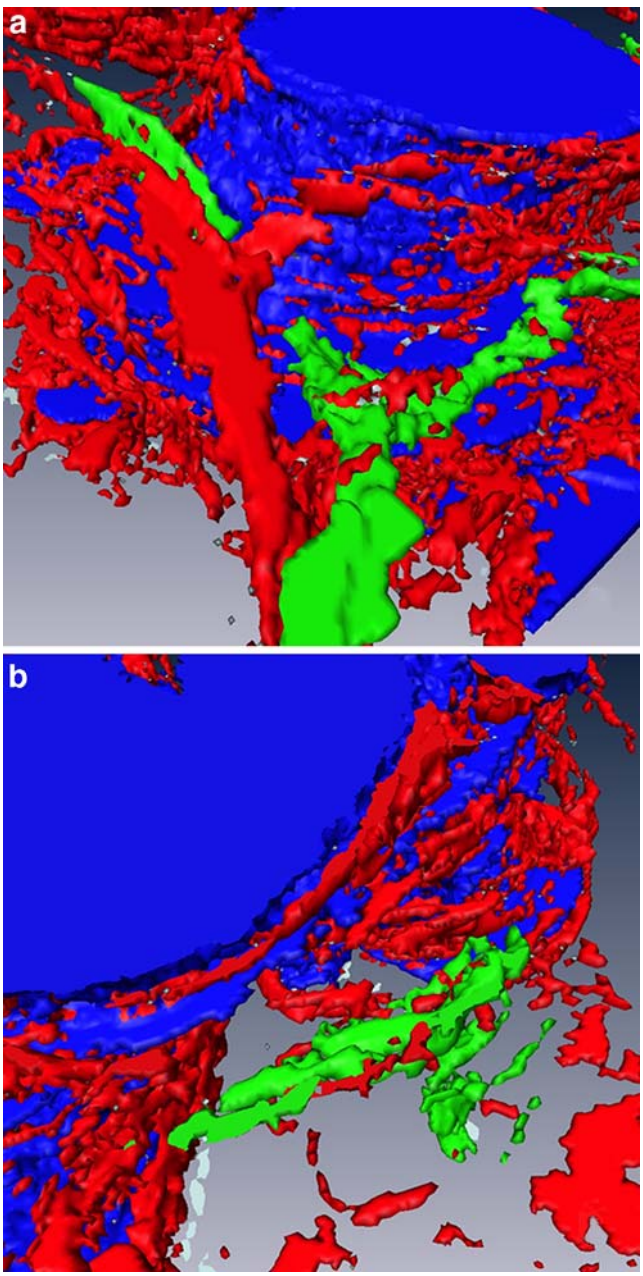

Fig. 9 Channels connect directly to the perilobular lymphatic vessel. **a** Modelling field 10, case 3. **b** Modelling field 5, case 3

caliber of channels D2-40-negative that were characteristic of pseudoangiomatous stromal hyperplasia and by the larger number of channels in perilobular stroma.

The dynamic 3D reconstruction of the lobules from all cases showed evidence that the spaces were intimately interconnected and proved the existence of an intralobular labyrinth, and the distribution of the spaces around the lobules indicated the existence of a sort of scaffolding. Shape, distribution and connection of the interstitial spaces, as traced in serial sections, concur in defining the nature of such pre-lymphatic spaces as real structures, and not as shrinkage artifacts. It was also found that at least one space in each lobule anastomosed directly with a lymphatic, also proving the previous theories of the existence of a pre-lymphatic network of which most of the credit goes to Casley-Smith and Florey and to Hartveit [1, 3]. Whether larger caliber of channels as mostly seen in PASH is the result of higher pressure in the stroma than lymphatics is still open to question.

The pre-lymphatic network cannot certainly any longer be disregarded as a way of spread of inflammatory and neoplastic cells. As the channels appear located around the acini, it is possible [4] that they can be the easiest way of spreading non-cohesive neoplastic cells such as lymphomas and invasive lobular carcinomas [4, 8]. It is pertinent to remind that one of the cases reported by Damiani et al. [8] consisted of a lymphoma that spread along the channels of PASH.

Conflict of interest statement We declare that we have no conflict of interest.

References

1. Casley-Smith JR, Florey HW (1961) The structure of normal small lymphatics. Q J Exp Physiol Cogn Med Sci 46:101–106
2. Casley-Smith JR (1973) The lymphatic system in inflammation. In: Zweifach BW, Grant L, McCluskey RT (eds) The inflammatory process. Academic, New York, pp 161–203
3. Hartveit F (1990) Attenuated cells in breast stroma: the missing lymphatic system of the breast. Histopathology 16:533–543
4. Eusebi V, Tavassoli FA (2008) Tumors of the breast. American Registry of Pathology/AFIP, Washington
5. Ozzello L, Sanpitak P (1970) Epithelial-stromal junction of intraductal carcinoma of the breast. Cancer 26:1186–1198
6. Vuitch MF, Rosen PP, Erlandson RA (1986) Pseudoangiomatous hyperplasia of the mammary stroma. Hum Pathol 17:185–191
7. Badve S, Sloane JP (1994) Pseudoangiomatous hyperplasia of male breast. Histopathology 26:463–466
8. Damiani S, Peterse JL, Eusebi V (2002) Malignant neoplasms infiltrating "pseudoangiomatous" stromal hyperplasia of the breast: an unrecognized pathway of tumor spread. Histopathology 41:208–215
9. Bussolati G, Marchiò C, Volante M (2005) Tissue array as fiducial markers for section alignment in 3-D reconstruction technology. J Cell Mol Med 9:438–445
10. Foschini MP, Papotti M, Parmeggiani A et al (2004) Three-dimensional reconstruction of vessel distribution in benign and malignant lesions of thyroid. Virchows Arch 445:189–198
11. Foschini MP, Righi A, Cucchi MC et al (2006) The impact of large sections and 3D technique on the study of lobular in situ and invasive carcinoma of the breast. Virchows Arch 448:256–261
12. Foschini MP, Tot T, Eusebi V (2002) Large-section (macro-section) histologic slides. In: Silverstein MJ (ed) Ductal carcinoma in situ of the breast. Lippincott, Philadelphia, pp 249–254
13. Wellings SR, Jensen HM (1973) On the origin and progression of ductal carcinoma in the human breast. J Natl Cancer Inst 50:1111–1118
14. Foreman DM, Bagley S, Moore J et al (1996) Three-dimensional analysis of the retinal vasculature using immunofluorescent staining and confocal laser scanning microscopy. Br J Ophthalmol 80:246–251
15. Salisbury JR, Deverell MH, Seaton JM et al (1997) Three-dimensional reconstruction of non-Hodgkin's lymphoma in bone marrow trephines. J Pathol 181:451–454
16. Perez-Atayde AR, Sallan SE, Tedrow U et al (1997) Spectrum of tumor angiogenesis in the bone marrow of children with acute lymphoblastic leukaemia. Am J Pathol 150:815–821
17. Kay PA, Robb RA, Bostwick DG (1998) Prostate cancer micro-vessels: a novel method for three-dimensional reconstruction and analysis. Prostate 37:270–277
18. Duerstock BS, Bajaj CL, Pascucci V et al (2000) Advances in three-dimensional reconstruction of the experimental spinal cord injury. Comput Med Imaging Graph 24:389–406
19. Antiga L, Ene-Iordache B, Remuzzi G et al (2001) Automatic generation of glomerular capillary topological organization. Microvasc Res 62:346–354
20. Brey EM, King TW, Johnston C et al (2002) A technique for quantitative three-dimensional analysis of microvascular structure. Microvasc Res 63:279–294
21. Cassoni P, Gaetano L, Senetta R et al (2008) Histology far away from Flatland: 3D roller-coasting into grade-dependent angiogenetic patterns in oligodendrogliomas. J Cell Mol Med 12:564–568
22. Ohtake T, Abe R, Kimijima I et al (1995) Intraductal extension of primary invasive breast carcinoma treated by breast conservative surgery. Cancer 76:32–45
23. Ohtake T, Kimijima I, Fukushima T et al (2001) Computer-assisted complete three-dimensional reconstruction of the mammary ductal/lobular systems. Cancer 91:2263–2272
24. Going JJ, Moffat DF (2004) Escaping from flatland: clinical and biological aspects of human mammary duct anatomy in three dimensions. J Pathol 203:538–544
25. Marchiò C, Sapino A, Arisio R et al (2006) A new vision of tubular and tubulo-lobular carcinomas of the breast, as revealed by 3-D modelling. Histopathology 48:556–562
26. Papotti M, Manazza AD, Chiarle R et al (2004) Confocal microscope analysis and tridimensional reconstruction of papillary thyroid carcinoma nuclei. Virchows Arch 444:350–355

Virchows Arch (2008) 453:407–411
DOI 10.1007/s00428-008-0621-x

CASE REPORT

Mantle cell lymphoma with partial involvement of the mantle zone: an early infiltration pattern of mantle cell lymphoma?

Assia Bassarova · Anne Tierens · Grete Fossum Lauritzsen · Alexander Fosså · Jan Delabie

Received: 6 December 2007 / Revised: 14 April 2008 / Accepted: 16 April 2008 / Published online: 12 August 2008

Abstract Most patients with mantle cell lymphoma present with a diffuse or nodular infiltration of the involved organs at diagnosis. We present two patients with a rare morphological variant, displaying a partial involvement of the mantle zone. Patient 1 presented with an enlarged inguinal lymph node, which showed marked follicular hyperplasia with singly spread Cyclin D1+ small lymphoid cells in the mantle zones. An additional lymph node biopsy taken 3 months later showed the same pattern. Patient 2 presented with a classical mantle cell lymphoma with lymph node, bone marrow and gastro-intestinal involvement. However, revision of an appendectomy specimen taken 4 years earlier showed pronounced follicular hyperplasia with singly spread Cyclin D1+ small lymphoid cells in the mantle zones. Mantle cell lymphoma with partial involvement of the mantle zone has rarely been reported and many represent an early manifestation of mantle cell lymphoma. Our cases also illustrate that the inclusion of an anti-cyclin D1 antibody in the diagnostic panel of antibodies to study unexplained follicular hyperplasia, might be advised.

Keywords Mantle cell · Lymphoma · "In situ" Variant

A. Bassarova (✉) · A. Tierens · J. Delabie
Pathology Clinic, The National Hospital-
The Norwegian Radium Hospital,
Montebello,
0310 Oslo, Norway
e-mail: assia.bassarova@rr-research.no

G. F. Lauritzsen · A. Fosså
Department of Oncology, The National Hospital-
The Norwegian Radium Hospital,
Montebello,
0310 Oslo, Norway

Introduction

Mantle cell lymphoma comprises approximately 3–10% of non-Hodgkin lymphomas. Most patients present with stage III or stage IV disease, and in at least 25% of the cases peripheral blood involvement is also found [5]. Gastrointestinal tract, bone marrow and Waldeyer's ring are the most commonly involved extranodal sites. Mantle cell lymphoma is characterized by a variable clinical course with a median survival of 3–5 years [5]. Prognosis is tightly correlated with lymphoma cell proliferation [1, 2, 5].

Classical mantle cell lymphoma is characterized by a diffuse, nodular or mantle zone growth pattern. The lymphoma cells are small- to medium-sized with slightly to markedly irregular nuclear contours, moderately dispersed chromatin but inconspicuous nucleoli [1]. Immunophenotypically, mantle cell lymphoma is characterized by the expression of CD5 and cyclin D1. Cyclin D1 overexpression is due to a recurrent cytogenetic abnormality, t (11; 14)(q13;q32) involving CCND1 and immunoglobulin heavy chain genes [9].

Recently, some cases of mantle cell lymphoma with a peculiar "in situ" growth pattern and apparent indolent clinical course have been reported [4, 6, 7]. Microscopic examination in all cases revealed follicular hyperplasia. The germinal centres were conspicuous and surrounded by an apparently normal or mildly expanded mantle zone. However, immunostaining for cyclin D1 revealed singly spread positive small lymphoma cells in the mantle zones [4, 6, 7]. In two of the reported cases, peripheral blood and bone marrow were also involved [4, 6].

In this paper we present two additional patients with a similar variant of mantle cell lymphoma.

Clinical history

Patient 1

The 42-year-old female patient had noted a slowly growing mass in the groin. On physical examination a moderately enlarged lymph node was detected. Computer tomography and PET-CT further revealed moderately enlarged cervical, axillar, iliacal and inguinal lymph nodes with increased fluorodeoxyglucose (FDG) uptake. All relevant blood tests, including complete blood counts and LDH were normal. Further staging procedures including GI tract endoscopic biopsies and bone marrow trephine biopsy ultimately revealed Ann Arbor stage IVA lymphoma. Treatment was initiated according to the Nordic Mantle Cell Lymphoma III protocol, i.e. high-dose chemotherapy and retuximab with stem cell rescue; see http://www.Nordic-lymphoma.org.

Patient 2

A 65-year-old male patient presented with a 6-month history of mild coughing and moderately enlarged cervical lymph nodes. PET-CT revealed generalized lymph node involvement. Complete blood counts and other relevant blood tests, including LDH were normal. Surgical lymph node biopsy, endoscopic stomach biopsy and bone marrow biopsy showed Ann Arbor stage IVA lymphoma. The patient was also treated according to the Nordic Mantle Cell Lymphoma III protocol, i.e. high-dose chemotherapy and retuximab with stem cell rescue; see http://www. Nordic-lymphoma.org. Four years earlier, the patient underwent appendectomy for acute appendicitis. At that time, no clinical suspicion for lymphoma was reported.

Materials and methods

Immunohistochemistry The paraffin blocks were cut at 4–6 μm, dried overnight at 60°C and dewaxed in xylene. A standard panel with the following primary antibodies was used in both cases: CD20, CD10, BCL-6, BCL-2, CD3, CD5, CD21, CyclinD1, IgM and IgD. Heat-induced epitope retrieval was used for all stainings. Visualization was performed using the EnVision® method (DakoCytomation, Glostrup, Denmark) according to the manufacturer's instructions. Appropriate positive and negative controls were used.

Flow cytometry A four-color flow cytometric analysis was performed on whole bone marrow specimens, anticoagulated with heparin. Fifty microliters of whole bone marrow containing between 0.5 and 1×10^6 cells were stained for surface antigens with the following antibody combinations: fluorescein isothyocyanate (FITC)/peridininchlorophyll cyanine 5.5 (PercPCY5.5)/allophycocyanine (APC)—(1) CD20/CD5/CD19/CD43; (2) FMC7/CD23/CD19/CD5; (3) Simultest κ/λ/CD20/CD19. Flow cytometry analysis was performed on a Facscalibur, using Cell Quest Pro software.

FISH analysis Fluorescent in situ hybridization (FISH) analysis was performed on formalin-fixed tissue specimens, using LSI IGH/CCND1 dual fusion DNA probe (Vysis, Downers Grove, IL, USA). The slides were deparaffinized, immersed in citric buffer for 60 min at 80°C, followed by pepsin pretreatment and dehydrated in ethanol. After denaturation step for 5 min at 73°C, hybridization was performed at 37°C overnight. The next day the slides were washed in sodium chloride-sodium citrate (SSC) buffer, counterstained with DAPI and evaluated using an Olympus BX61 microscope.

PCR analysis DNA was extracted from both fresh snap frozen and FFPE tissue using BioRobot M48 (Qiagen, Hilden, Germany). The quantity and quality of the extracted DNA were then checked and DNA was used for polymerase chain reaction (PCR) analysis of Ig heavy chain (IgH). BIOMED-2-based PCR protocol and three sets of VH primers corresponding to the three VH FR regions (FR1, FR2 and FR3) were used [8]. The results were analysed using ABI Prism® 3100 Genetic analyser.

Cytogenetics Fresh tissue samples were manually minced and enzymatically treated until a suitable suspension of cells and cell clumps was obtained. After 5–7 days culturing colchicines was added for the last 4 h and the short-term cultures were harvested according to standard protocols. The chromosomes in the dividing cells were then G-banded and a karyotype established in accordance with the recommendations of the International System for Human Cytogenetic Nomenclature.

Results

Patient 1

Axillary and inguinal lymph node biopsies were performed and showed the same picture. The overall architecture was preserved, with intact sinuses, B- and T-zones. Prominent follicular hyperplasia was noted with hyperplastic germinal centres and mantle zones. Because of the clinical suspicion of lymphoma, an extended investigation with a panel of antibodies for immunohistochemistry was performed. Surprisingly, anti Cyclin D1 immunostaining showed a rim of

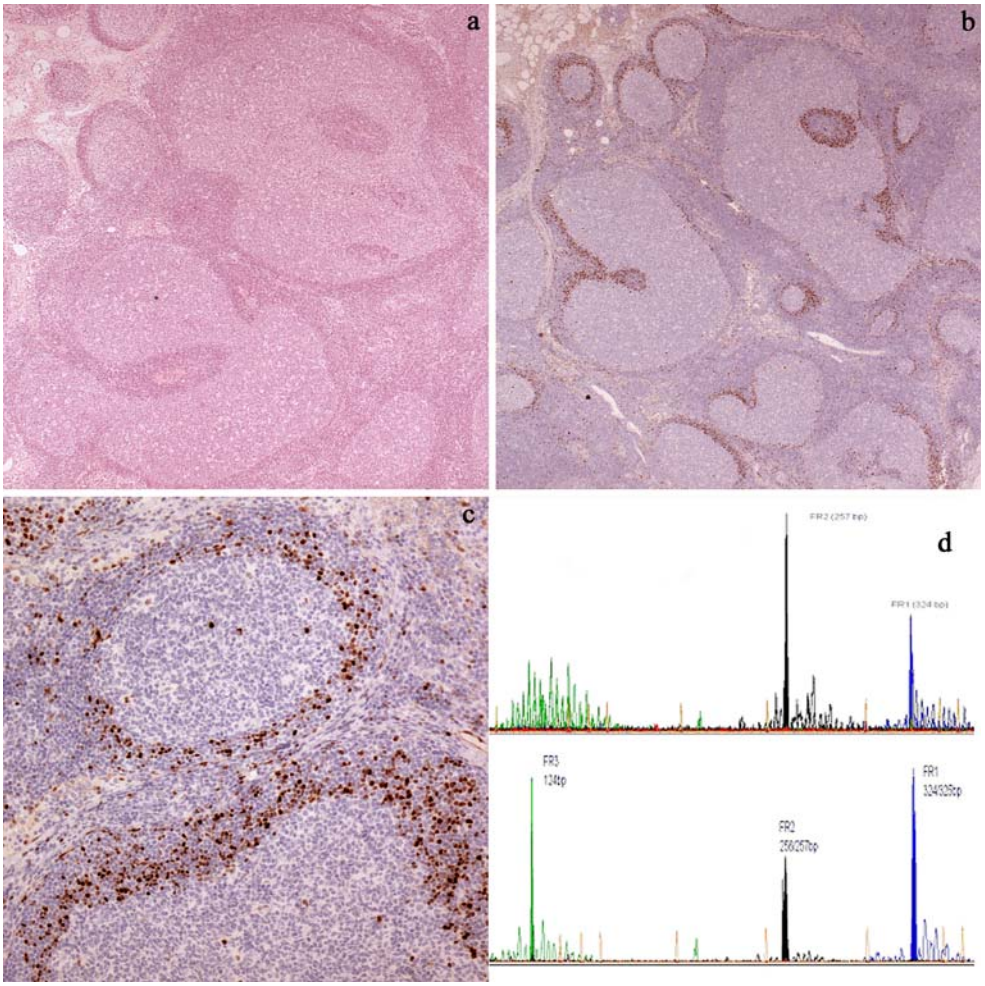

Fig. 1 Patient 1: **a** Lymph node biopsy with prominent follicular hyperplasia (H&E, ×20). **b** Cyclin D1 staining showing a rim of positive cells in the mantle zones (×20). **c** Cyclin D1 staining showing a rim of positive cells in the mantle zones (×100). **d** PCR results from inguinal lymph node and from axillary lymph node showing the same monoclonal immunoglobulin heavy chain gene rearrangement in a polyclonal background

positive cells in the mantle zones (Fig. 1). PCR analysis was performed on two consecutive biopsies using snap frozen and formalin-fixed tissue and demonstrated the same monoclonal immunoglobulin heavy chain gene rearrangement (Fig. 1). FISH analysis revealed spread single cells with t(11;14)(q13; q32.3) translocation. Cytogenetic analysis of the lymph node showed normal karyotype, 46, XX. The bone marrow biopsy showed a normal histology, CyclinD1 staining was negative, but flow cytometric analysis of bone marrow aspirate identified minimal (1%) mantle cell lymphoma infiltration. Minimal involvement by lymphoma was also observed in the endoscopic biopsies from the stomach.

Patient 2

Cervical lymph node biopsy showed mantle cell lymphoma with mixed nodular and diffuse growth pattern. Cytogenetic analysis of the lymph node demonstrated an abnormal karyotype: 46, XY, t(11;14)(q13;q32). Endoscopic biopsies from the stomach and duodenum revealed minimal infiltration. Bone marrow trephine and flow cytometry showed bone marrow involvement. The pattern of infiltration in the bone marrow was diffuse, interstitial and intrasinusoidal with approximately 10–12% atypical lymphocytes (Fig. 2). The immunophenotype of the lymphoma was: CD5+, CD23−, CD19+, CD20+, CD79B+, immunoglobulin light chain kappa +, cyclin D1+.

A reexamination of the appendectomy specimen removed 4 years earlier revealed acute appendicitis with marked lymphoid hyperplasia. Many secondary lymphoid follicles with expanded mantle zones were noted in submucosa. Cyclin D1 staining revealed accentuated, expanded mantle zones in some follicles and small groups of positive cells in other areas (Fig. 2). FISH analysis revealed spread single cells with t(11;14)(q13; q32.3) translocation (Fig. 2).

Discussion

Four cases of mantle cell lymphoma with an unusual morphology and indolent clinical course have recently been described [4, 6, 7]. A common feature of those cases was the

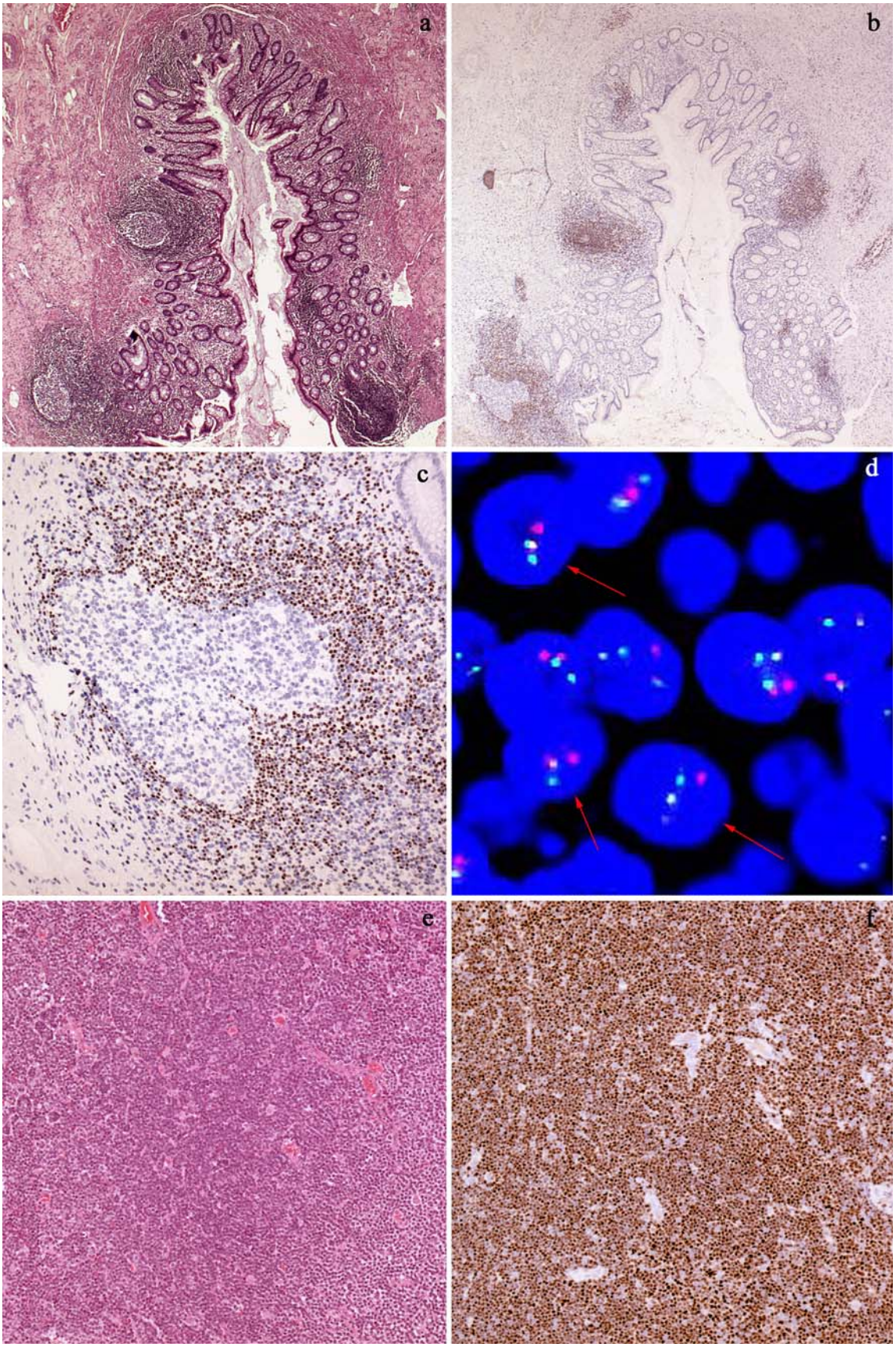
a
b
c
d
e
f

◀ **Fig. 2** Patient 2: **a** Appendix biopsy showing marked lymphoid hyperplasia (H&E, ×20). **b** Cyclin D1 staining of the appendix revealed accentuated, expanded mantle zones in some follicles and small groups of positive cells in other areas (×20). **c** Cyclin D1 staining showing a rim of positive cells in the mantle zones (×100). **d** FISH analysis of the appendix showing single nuclei with one or two fusion signals and single red (native CCND1) and single green (native IgH) signals (arrows) (×600). **e** Lymph node biopsy showed mantle cell lymphoma with mixed-nodular and diffuse growth pattern (H&E, ×20). **f** Cyclin D1 staining of the lymph node (×20)

pronounced follicular hyperplasia with reactive germinal centres and normal or mildly expanded mantle zones. Cyclin D1 staining revealed singly spread or a thin rim of positive neoplastic cells in the mantle zones. Based on the unusual histological picture Richard et al. introduced the term 'in situ-like' mantle cell lymphoma [7], in parallel with the in situ variant of follicular lymphoma [3]. The cases presented here show the same morphological characteristics. In one of the patients two consecutive lymph node biopsies showed marked follicular hyperplasia with single cyclin D1 positive lymphoid cells in the mantle zones. The second patient presented with classical mantle cell lymphoma, but re-examination of an appendectomy specimen removed 4 years earlier demonstrated cyclin D1 positive cells in the mantle zones of the follicles present in the wall of the appendix. At the time of the appendectomy, there were no clinical signs of lymphoma. Whether the minimal lymphoma localization in the appendix with concurrent follicular hyperplasia may have contributed to the acute inflammation, is a matter of speculation. At clinical presentation with lymphoma, both of our patients were diagnosed with Ann Arbor stage IVA disease based on the involvement of multiple lymph nodes, gastrointestinal tract and bone marrow. In two of the reported cases peripheral blood and bone marrow involvement was noted [4, 6] while in the two other patients only nodal disease was documented [7].

Histological examination alone does not raise suspicion of mantle cell lymphoma in the two cases of 'in situ' mantle cell lymphoma reported here. Only cyclinD1 staining can reveal this diagnosis. In view of the fact that these cases closely resemble reactive follicular hyperplasia on histologic examination, we suggest that cyclin D1 staining should be added to the analysis of unexplained follicular hyperplasia, either when occurring in elderly patients or when there is genuine clinical suspicion for lymphoma as in one of our patients. Whether the pattern of mantle cell lymphoma involvement presented here represents an early manifestation of mantle cell lymphoma, meriting the use of the term "in situ" mantle cell lymphoma, as previously defined, remains to be confirmed. However, the biopsy samples in our patient 2, showing first partial involvement of the mantle zone in the appendix, and then massive mantle cell lymphoma in the lymph node 4 years later, is consistent with this interpretation.

Conflict of interest statement We declare that we have no conflict of interest.

References

1. Argatoff LH, Connors JM, Klasa RJ, Horsman DE, Gascoyne RD (1997) Mantle cell lymphoma: a clinicopathologic study of 80 cases. Blood 89:2067–2078
2. Bosch F, López-Guillermo A, Campo E, Ribera JM, Conde E, Piris MA, Vallespí T, Woessner S, Montserrat E (1998) Mantle cell lymphoma: presenting features, response to therapy, and prognostic factors. Cancer 82:567–575
3. Cong P, Raffeld M, Teruya-Feldstein J, Sorbara L, Pittaluga S, Jaffe ES (2002) In situ localization of follicular lymphoma: description and analysis by laser capture microdissection. Blood 99:3376–3382
4. Espinet B, Sole F, Pedro C, Garcia M, Bellosillo B, Salidoa M, Florensa L, Camacho F, Baro T, Lloreta J, Serrano S (2005) Clonal proliferation of cyclin D1-positive mantle lymphocytes in an asymptomatic patient: an early-stage event in the development or an indolent form of a mantle cell lymphoma? Hum Pathol 36:1232–1237
5. Jaffe ES, Harris NL, Stein H, Vardiman JW ((ed)] (2001) World Health Organization Classification of Tumors. Tumours of Haematopoietic and Lymphoid Tissues. Lyon: IARC Press, pp 168–170
6. Nodit L, Bahler DW, Jacobs SA, Locker J, Swerdlow SH (2003) Indolent mantle cell lymphoma with nodal involvement and mutated immunoglobulin heavy chain genes. Hum Pathol 34:1030–1034
7. Richard P, Vassallo J, Valmary S, Missoury R, Delsol G, Brousset P (2006) "In situ-like" mantle cell lymphoma: a report of two cases. J Clin Pathol 59:995–996
8. van Dongen JJ, Langerak AW, Brüggemann M, Evans PA, Hummel M, Lavender FL, Delabesse E, Davi F, Schuuring E, García-Sanz R, van Krieken JH, Droese J, González D, Bastard C, White HE, Spaargaren M, González M, Parreira A, Smith JL, Morgan GJ, Kneba M, Macintyre EA (2003) Design and standardization of PCR primers and protocols for detection of clonal immunoglobulin and T-cell receptor gene recombinations in suspect lymphoproliferations: report of the BIOMED-2 Concerted Action BMH4-CT98–3936. Leukemia 17:2257–2317
9. Williams ME, Swerdlow SH, Meeker TC (1993) Chromosome t(11;14)(q13;q32) breakpoints in centrocytic lymphoma are highly localized at the bcl-1 major translocation cluster. Leukemia 7:1437–1440

Virchows Arch (2008) 453:413–415
DOI 10.1007/s00428-008-0663-0

LETTER TO THE EDITOR

Toxic hepatic injury mimicking ascending cholangitis: is *Pyrus amygdaliformis* to blame?

Despoina Televantou · Emmanouil Sinakos · Evangelos A. Akriviadis · Prodromos Hytiroglou

Received: 18 April 2008 / Revised: 16 July 2008 / Accepted: 20 August 2008 / Published online: 12 September 2008

Keywords Liver · *Pyrus amygdaliformis* · Toxic injury

Cholestatic hepatic injury can be caused by a number of drugs and herbal remedies [1, 3, 5]. Occasionally, drugs that cause cholestasis, such as amoxicillin-clavulanate, chlorpromazine, and erythromycin are associated with acute purulent inflammation of the intrahepatic bile ducts, mimicking acute (ascending) cholangitis [3]. We present a case of acute cholestatic toxic liver injury with histologic features of ascending cholangitis and a possible association with ingestion of forest fruit.

The patient is a 55-year-old man, who presented with a 3-day history of marked jaundice. There was no abdominal pain, fever, or history of medications, except for a 5-day course of a cephalosporin antibiotic taken 2 months prior to presentation. On physical examination, there were no findings apart from jaundice. The patient was carefully interviewed regarding potential toxins, and he admitted recent consumption of *Pyrus amygdaliformis* fruit (also known as "wild pears" in Greece). In detail, he admitted consuming approximately 0.5 kg of raw fruit daily, during the week prior to presentation. He also admitted previous exposure to the same fruit, but that was sporadic and in much smaller quantities.

Laboratory findings on his first day of hospitalization were as follows: hemoglobin, 15.4 g/dl; white blood cell count, 7,370 per milliliter; platelets, 275,000 per milliliter; glucose, 118 mg/dl; urea, 27 mg/dl; creatinine, 1.1 mg/dl; bilirubin, 10.6 mg/dl; direct bilirubin, 7.0 mg/dl; aspartate aminotransferase (AST), 195 U/L (normal, <37 U/L); alanine aminotransferase (ALT), 315 U/L (normal, <45 U/L); alkaline phosphatase (AP), 878 U/L (normal, <258 U/L); gamma-glutamine transpeptidase, 187 U/L (normal, <55 U/L); lactate dehydrogenase, 482 U/L (normal, <480 U/L); international normalized ratio, 1.05; and erythrocyte sedimentation rate (first hour), 39 mm. Viral and autoimmune markers, including HBsAg, anti-HBc IgM, anti-HAV IgM, anti-HCV, antinuclear antibodies, antimitochondrial antibodies, anti-smooth muscle antibodies, c-ANCA, and p-ANCA were negative.

Abdominal CT scan showed no abnormalities. Treatment with intravenous ceftriaxone (2 g daily) was initiated. An endoscopic retrograde cholangiopancreatography (ERCP) was performed. There were no strictures or other pathologic findings in the common bile duct and the main pancreatic duct, except for a small amount of bile sludge that was removed through the ampulla. During hospitalization there was no evidence of renal or pulmonary dysfunction. The patient underwent laparoscopic cholecystectomy on the third day of hospitalization. A needle liver biopsy was also obtained. Laboratory findings on the day of surgery included: AST, 207 U/L; ALT, 463 U/L; AP, 759 U/L; bilirubin, 11.5 mg/dl; and direct bilirubin, 8.1 mg/dl.

Histologic examination of the liver biopsy showed moderate portal inflammatory infiltrates consisting of

D. Televantou · P. Hytiroglou (✉)
Department of Pathology, Aristotle University Medical School, 54006 Thessaloniki, Greece
e-mail: phitir@med.auth.gr

E. A. Akriviadis
Department of Internal Medicine, Aristotle University Medical School, Thessaloniki, Greece

E. Sinakos · E. A. Akriviadis
Department of Internal Medicine, Interbalkan Medical Center, Thessaloniki, Greece

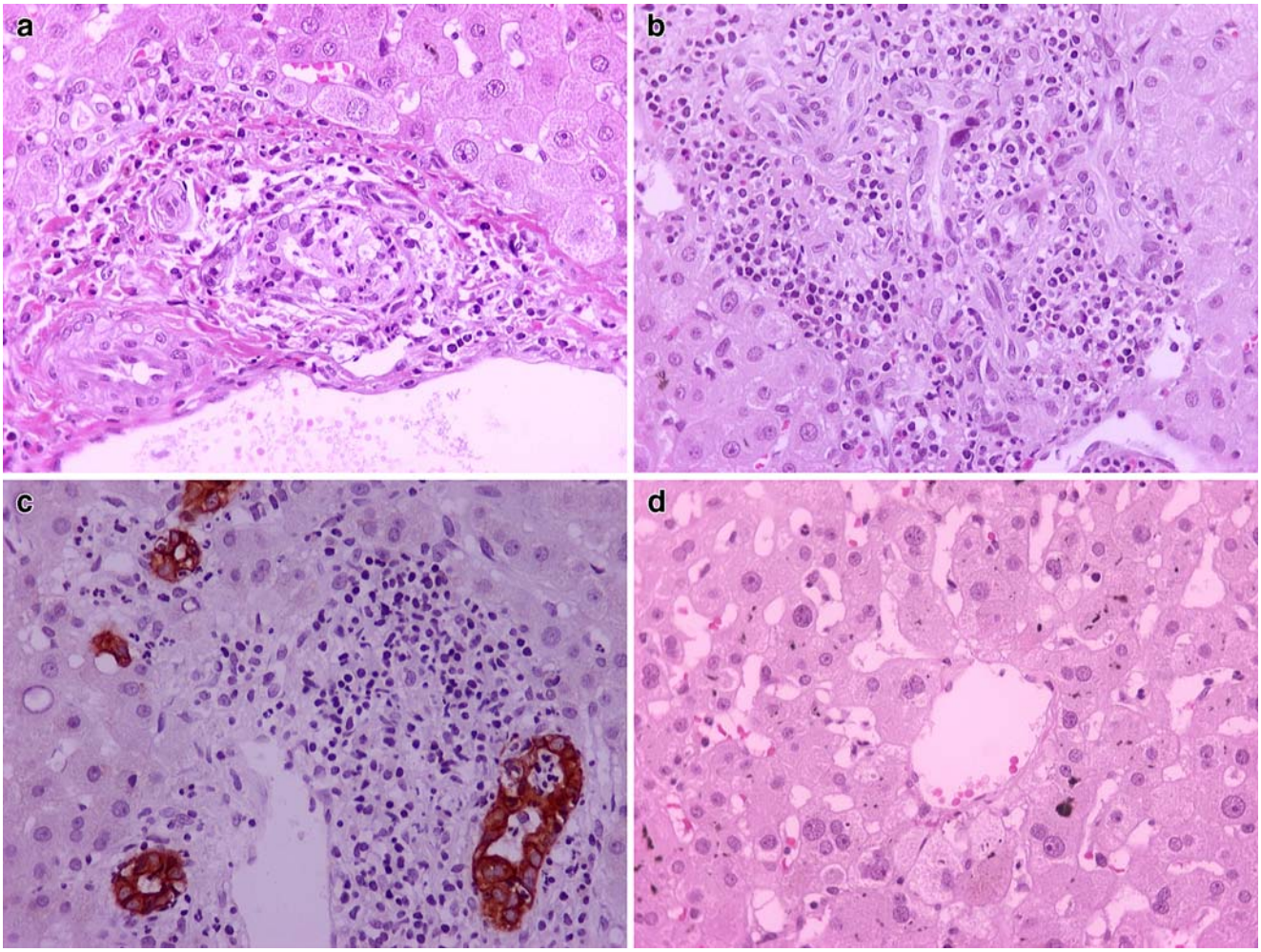

Fig. 1 Histologic findings in liver biopsy. **a** This portal tract has moderate inflammatory infiltrates, consisting of neutrophils, lymphocytes, few plasma cells and occasional eosinophils. The bile duct shows degenerative changes of the epithelium. **b** Another portal tract with severe degenerative changes of biliary epithelial cells and rare neutrophils in bile duct lumen. **c** Immunohistochemical stain for cytokeratin 7 showing minimal ductular reaction. A few neutrophlis are present in the bile duct lumen. **d** A centrilobular region with marked cholestasis, "feathery" degeneration of hepatocytes and a few inflammatory cells. (a–d, ×400)

lymphocytes, neutrophils, and occasional eosinophils. There was neutrophilic infiltration of bile ducts, accompanied by degenerative changes of the epithelial cells (Fig. 1a,b). A few neutrophils were present in bile duct lumens (Fig. 1a–c). There was no interface hepatitis, bile duct loss, or fibrosis. Minimal ductular reaction was seen on immunohistochemical stain for cytokeratin 7 (Fig. 1c). In the lobules, there was marked cholestasis, predominantly involving centrilobular regions, accompanied by "feathery" degeneration of hepatocytes (Fig. 1d). Mild steatosis was also present.

Table 1 Laboratory values following discharge from the hospital

	7 days	22 days	37 days	51 days	60 days	91 days
AST (U/L)	345	34	25	23	20	22
ALT (U/L)	621	110	38	28	24	31
AP (U/L)	293	169	93	115	–	72
γ-GT (U/L)	–	129	–	–	–	–
Bilirubin (mg/dl)	5.2	2.1	1.5	1	1.5	1.2
Direct bilirubin (mg/dl)	3.6	1.4	0.9	0.2	0.2	0.2

AST Aspartate aminotransferase, *ALT* alanine aminotransferase, *AP* alkaline phosphatase, *γ-GT* gamma-glutamyl transpeptidase

Histologic examination of the resected gallbladder showed moderate inflammatory infiltrates, mostly composed of lymphocytes. In focal areas, there were dense infiltrates of neutrophils.

The patient was discharged 1 day postoperatively with directions to continue antibiotic treatment for 5 days and to begin treatment with ursodeoxycholic acid (1,000 mg/day), which he continued for 6 months. His laboratory values following discharge from the hospital are shown in Table 1. The liver function tests normalized approximately 1 month after surgery. Since then, the patient has remained asymptomatic, with normal laboratory findings.

The histologic features of this case were suggestive of acute (ascending) cholangitis, because there was neutrophilic infiltration of bile ducts, with presence of neutrophils in duct lumens and degenerative changes of the epithelium. However, acute infection of the biliary tree is usually associated with large bile duct obstruction and, therefore, the histologic picture usually includes ductular reaction. Such reaction was not a feature of our case. Furthermore, CT scan and ERCP failed to demonstrate any evidence of large bile duct obstruction. Most importantly, our patient did not have the characteristic clinical findings of ascending cholangitis, including high fever, chills, and right upper quadrant pain. Finally, the inflammatory changes extended to the gallbladder, although no gallstones were present.

An alternative explanation for the clinical presentation and the histologic findings of our case is provided by toxic injury. Drugs and toxins can produce a wide spectrum of histologic changes, mimicking a variety of liver disorders. Although the clinical findings in our case were not specific for toxic injury, a thorough investigation of other possible causes, including ERCP, failed to provide any etiologic evidence. Since the patient was not on any medication, a careful history of dietary habits was taken, revealing the information of forest fruit consumption. *P. amygdaliformis* is a "wild" variety of pear tree. The fruit of this tree is not consumed widely, since it is only found in the wild. To our knowledge, it contains no chemical substances with known toxicity. Furthermore, we found no reported cases of hepatic or other toxicity in the literature.

A large number of drugs (e.g., anabolic and contraceptive steroids, angiotensin-converting enzyme inhibitors, chlorpromazine, erythromycin, benoxaprofen), toxins (e.g., paraquat), and herbal remedies (e.g., celandine, glycyrrhizin, chaparral) may cause cholestatic injury [1, 3, 5]. The only kind of fruit that we could identify as a cause of cholestasis in the literature is Ackee fruit, a native plant of Jamaica, which is also known to cause centrilobular necrosis [4]. Four types of drug-induced cholestatic injury have been described, namely, the canalicular, the hepatocanalicular, the ductal, and the cholangiodestructive type [5]. Occasionally, drug-induced cholestasis may be accompanied by histologic features of acute cholangitis [3]. In some of these cases, there may be actual destruction of bile ducts, resulting in a vanishing bile duct syndrome with prolonged cholestasis [2].

Although the clinical history and histologic findings suggest that some substance contained in *P. amygdaliformis* caused hepatic injury to our patient, a definite causative association is difficult to prove. Supportive of this association is the fact that the consumed fruits were unlikely to be contaminated by any toxic substance, since they are not cultivated, but are only found in the wild. Additionally, our patient was not exposed to other toxins (he is a merchant by profession) and he was alone when he consumed *Pyrus* fruit. Obviously, the patient is reluctant to get exposed to the possible deleterious effect of such fruit again. However, report of additional cases may be of importance, since this tree is widely distributed in the Mediterranean region. In the meanwhile, this case should remind pathologists that histologic features of acute cholangitis may in fact be due to toxic hepatic injury.

References

1. Chitturi S, Farrell GC (2001) Drug-induced cholestasis. Semin Gastrointest Dis 12:113–245
2. Degott C, Feldmann G, Larrey D et al (1992) Drug-induced prolonged cholestasis in adults: a histological semiquantitative study demonstrating progressive ductopenia. Hepatology 15:244–251
3. Goodman ZD (2002) Drug hepatotoxicity. Clin Liver Dis 6:381–397
4. Larson J, Vender R, Camuto P (1994) Cholestatic jaundice due to ackee fruit poisoning. Am J Gastroenterol 89:1577–1578
5. Zimmerman HJ, Ishak KG (2002) Hepatic injury due to drugs and toxins. In: MacSween RMN, Burt AD, Portmann BC, Ishak KG, Scheuer PJ, Anthony PP (eds) Pathology of the liver. 4th edn. Churchill Livingstone, London, pp 638–640

Virchows Arch (2008) 453:417–431
DOI 10.1007/s00428-008-0665-y

REVIEW AND PERSPECTIVE

KRAS mutation testing for predicting response to anti-EGFR therapy for colorectal carcinoma: proposal for an European quality assurance program

J. H. J. M. van Krieken · A. Jung · T. Kirchner · F. Carneiro · R. Seruca · F. T. Bosman · P. Quirke · J. F. Fléjou · T. Plato Hansen · G. de Hertogh · P. Jares · C. Langner · G. Hoefler · M. Ligtenberg · D. Tiniakos · S. Tejpar · G. Bevilacqua · A. Ensari

Received: 24 June 2008 / Accepted: 21 August 2008 / Published online: 18 September 2008

Abstract Novel therapeutic agents targeting the epidermal growth factor receptor (EGFR) have improved outcomes for patients with colorectal carcinoma. However, these therapies are effective only in a subset of patients. Activating mutations in the KRAS gene are found in 30–40% of colorectal tumors and are associated with poor response to anti-EGFR therapies. Thus, KRAS mutation status can predict which patient may or may not benefit from anti-EGFR therapy. Although many diagnostic tools have been developed for KRAS mutation analysis, validated methods and standardized testing procedures are lacking. This poses a challenge for the optimal use of anti-EGFR therapies in the management of colorectal carcinoma. Here we review the molecular basis of EGFR-targeted therapies and the resistance to treatment conferred by KRAS mutations. We also present guideline recommendations and a proposal for a European quality assurance program to help ensure accuracy and proficiency in KRAS mutation testing across the European Union.

Keywords Colorectal carcinoma · Anti-EGFR therapy · *KRAS* mutation testing · Practice guidelines · Quality assurance

J. H. J. M. van Krieken (✉) · M. Ligtenberg
Department of Pathology,
Radboud University Nijmegen Medical Centre,
PO Box 9101, Nijmegen 6500 HB, The Netherlands
e-mail: J.vanKrieken@pathol.umcn.nl

A. Jung · T. Kirchner
Department of Pathology, Ludwig-Maximilians Universität,
Munich, Germany

F. Carneiro · R. Seruca
Institute of Molecular Pathology and Immunology of the
University of Porto (IPATIMUP),
Porto, Portugal

F. Carneiro · R. Seruca
Medical Faculty of the of Porto,
Porto, Portugal

F. Carneiro
Department of Pathology, Hospital S. João,
Porto, Portugal

F. T. Bosman
University Institute of Pathology,
Lausanne, Switzerland

P. Quirke
Pathology and Tumour Biology,
University of Leeds,
Leeds, England

J. F. Fléjou
Department of Pathology, Saint-Antoine Hospital,
University Paris 6,
Paris, France

T. Plato Hansen
Department of Pathology, Odense University Hospital,
Odense, Denmark

G. de Hertogh
Department of Pathology, University Hospitals KU Leuven,
Leuven, Belgium

P. Jares
Department of Pathology,
Hospital Clinic,
Barcelona, Spain

C. Langner · G. Hoefler
Institute of Pathology, Medical University Graz,
Graz, Austria

Introduction

Novel classes of therapeutic agents for treating cancer are rapidly changing clinical practice. Several of these new drugs target specific molecules expressed by cancer cells. One group targets members of the human epidermal growth factor receptor (HER) family, namely, the epidermal growth factor receptor (EGFR) and the human epidermal growth factor receptor 2 (HER2). Both EGFR and HER2 contribute to the development and progression of several cancers and therefore have been explored as targets for cancer therapy. To apply targeted therapies optimally, it is important to recognize that their activity differs across patient populations and to understand the molecular mechanisms underlying these differences.

A well-defined example of how the efficacy of a targeted therapy can vary among patients with different molecular profiles is the use of trastuzumab (Herceptin®), an anti-HER2 monoclonal antibody, in the treatment of breast cancer. HER2 is overexpressed in 20–30% of malignant breast tumors as a result of amplification of the coding gene [1, 2]. HER2-positive status is associated with poor prognosis and is a strong predictor of response to trastuzumab therapy [1, 3]. Assessment of HER2 status has become standard practice to identify breast cancer patients most likely to benefit from trastuzumab therapy [3]. In parallel, substantial progress has been made to validate HER2 testing methods and implement quality assurance to ensure consistency and accuracy in HER2 testing [4].

Targeted therapeutic agents have also been developed for the treatment of colorectal cancer, a leading cause of cancer-related deaths worldwide [5]. The majority of patients with colorectal cancer are diagnosed with locally advanced or metastatic disease which responds poorly to conventional forms of treatment. The drugs recently introduced for treating colorectal cancer target the EGFR, which is overexpressed in 50–80% of colorectal tumors [6–10]. Although the advent of EGFR-targeted therapies has improved outcomes for colorectal cancer patients, they are effective in only a subset of patients [11]. Therefore, a major challenge in optimizing EGFR-targeted treatment options in colorectal cancer is to identify reliable biomarkers that can predict which patients will or will not respond to these targeted therapies.

It has become clear that mutations in the *Kirsten RAS* (*KRAS*) gene negatively predict success of anti-EGFR therapies. Gain-of-function *KRAS* mutations lead to EGFR-independent activation of intracellular signaling pathways, resulting in tumor cell proliferation, protection against apoptosis, increased invasion and metastasis, and activation of tumor-induced angiogenesis [12]. Unlike HER2 testing in breast cancer, however, there is a wide variety of testing methods and a lack of quality assurance schemes for the assessment of *KRAS* mutation status in colorectal cancer patients.

The objectives of this paper are threefold: (1) to review the molecular basis of EGFR-targeted therapies and the resistance to treatment conferred by *KRAS* mutations; (2) to summarize the different methods available for the detection of *KRAS* mutations; and (3) to propose guideline recommendations and a European quality assurance (QA) program for *KRAS* mutation testing in colorectal carcinoma.

Molecular basis of EGFR-targeted therapies

EGFR and cancer

EGFR is a 170-kDa transmembrane tyrosine kinase receptor that is present in most epithelial tissues and plays an important role in cell growth and function. Modulation of growth factor receptors, such as the EGFR, is a key strategy used by tumor cells to become self-sufficient and rely less on growth signals for their transformation, proliferation and survival. EGFR is overexpressed in many solid cancers and has been shown by many studies to be involved in the development and progression of human malignancies [12, 13]. Extensive research over the last few years has improved our understanding of the oncogenic role of the EGFR and the mechanisms of receptor activation and function. These advances have led to the development of new treatment modalities aimed at targeting the EGFR signaling system.

EGFR belongs to HER family of cell surface receptors (see Fig. 1a). The HER receptor family consists of four structurally related proteins: EGFR (also called HER1/ErbB1), HER2 (ErbB2), HER3 (ErbB3), and HER4 (ErbB4). Each receptor is composed of three domains: (1)

M. Ligtenberg
Department of Human Genetics,
Radboud University Nijmegen Medical Centre,
Nijmegen, The Netherlands

D. Tiniakos
Laboratory of Histology and Embryology,
Medical School University of Athens,
Athens, Greece

S. Tejpar
Digestive Oncology Unit, University Hospital Gasthuisberg,
Leuven, Belgium

G. Bevilacqua
Department of Oncology,
University of Pisa and Pisa University Hospital,
Pisa, Italy

A. Ensari
Department of Pathology,
Ankara University Medical School,
Ankara, Turkey

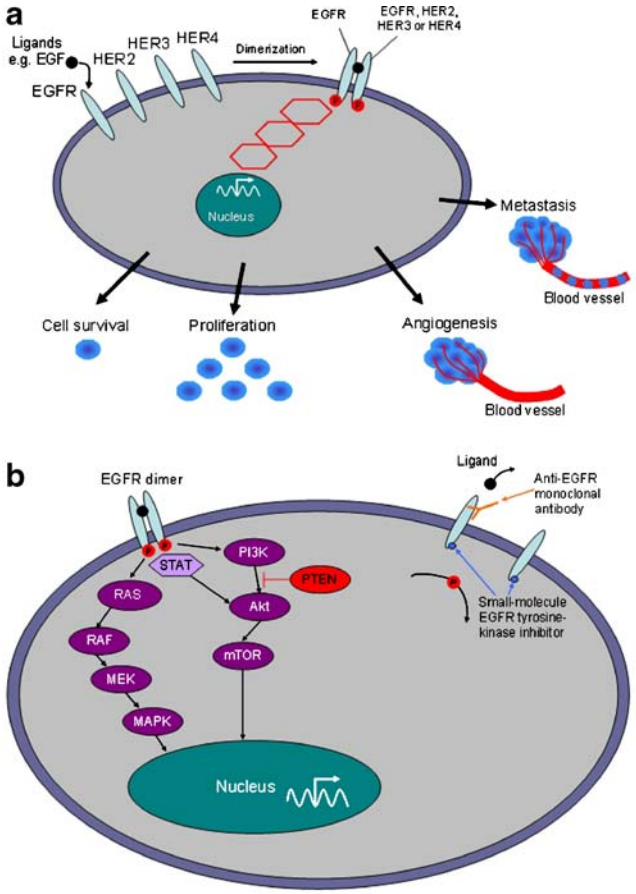

Fig. 1 **a** Cellular responses controlled by EGFR-dependent intracellular signaling. The binding of specific ligands to the extracellular portion of the EGFR results in the formation of a functionally active EGFR dimer with another ligand-bound EGFR or one of the EGFR-related receptors (HER2, HER3, or HER4). Receptor dimerization causes ATP-dependent phosphorylation of tyrosine kinase residues within the intracellular domain of the receptors. This tyrosine phosphorylation triggers activation of downstream signal transduction cascades which control cell growth, development, and function. Perturbations in EGFR-dependent intracellular signaling have been implicated in multiple aspects of the malignant process, including enhanced tumor cell survival and proliferation, tumor-induced angiogenesis, and metastasis. **b** Signal transduction pathways controlled by EGFR activation and two therapeutic approaches to block the EGFR. Ligand-induced stimulation of EGFR induces activation of three major signaling cascades: RAS-MAPK, PI3K-Akt, and STAT pathways. Together, these pathways control gene transcription, cell cycle progression, cell proliferation and survival, adhesion, angiogenesis, and cell migration. To suppress EGFR-dependent signaling, two classes of EGFR antagonists have been developed. First, anti-EGFR monoclonal antibodies bind specifically to the extracellular domain of the receptor and inhibit ligand binding, thus preventing ligand-induced EGFR activation. Second, small-molecule EGFR tyrosine kinase inhibitors bind to the intracellular catalytic domain of the receptor, thereby, inhibiting EGFR tyrosine phosphorylation and downstream signaling pathways

an extracellular domain that recognizes and binds ligands specifically, such as epidermal growth factor (EGF), transforming growth factor (TGF)-α and amphiregulin which bind specifically to EGFR; (2) a hydrophobic transmembrane domain that is involved in interactions between cell surface receptors; and (3) an intracellular domain that serves as a site of tryosine kinase activity. There are at least two exceptions to these general principles: HER2 has no known ligand and is constitutively active, and HER3 does not possess intrinsic tyrosine kinase activity. However, all receptors and their specific ligands interact to form an integrated system in which an initial signal can be amplified and diversified into multiple cellular responses.

To activate the EGFR signaling system, three sequential steps are generally required. First, specific ligands bind to the extracellular domain of EGFR, resulting in a conformational change. Second, this structural change allows the receptor to form a dimer with another ligand-bound EGFR (homodimer) or with one of the EGFR-related HER receptors (heterodimer). Finally, receptor dimerization causes autophosphorylation of tyrosine kinase residues within the intracellular domain of the receptors, leading to activation of signal transduction pathways. EGFR tyrosine phosphorylation triggers several signaling cascades, including the RAS-MAPK, PI3K-Akt and STAT pathways (Fig. 1b). Together, these EGFR-induced signaling pathways control gene transcription, cell cycle progression, cell proliferation and survival, adhesion, angiogenesis, migration, and invasion [14].

Activation of downstream signaling pathways without the involvement or modulation of cell surface receptors is another mechanism by which tumor cells can lose their dependence on growth factors. Perturbations in the EGFR signaling system may lead to the same effects as modulation of the EGFR alone: uncontrolled cell growth and proliferation, suppression of apoptosis, stimulation of angiogenesis, and increased metastatic spread (Fig. 1a). Consequently, the EGFR axis is thought to play a central role in the regulation of epithelial tumor cell growth, proliferation, and malignant transformation.

EGFR-blocking therapy

Given the important role of EGFR in tumorigenesis and disease progression, this receptor has become a relevant and promising target for anti-cancer therapies. *In vitro* and *in vivo* studies show that blocking EGFR and downstream signaling may lead to inhibition of carcinoma cell growth, resulting in potential benefits for cancer patients.

Two classes of EGFR antagonists have been developed and are currently used in cancer treatment (Fig. 1b). First, anti-EGFR monoclonal antibodies bind to the extracellular domain of the EGFR and compete with natural ligands for binding to the receptor, thus, blocking ligand-induced EGFR activation. Second, small-molecule inhibitors of EGFR tyrosine kinases compete with ATP for binding to the intracellular catalytic domain of the EGFR

tyrosine kinase. This competition inhibits EGFR tyrosine phosphorylation and hence suppresses downstream signaling pathways.

Two anti-EGFR antibodies (cetuximab and panitumumab) and two small-molecule EGFR tyrosine kinase inhibitors (gefitinib and erlotinib) have been evaluated extensively for the treatment of colorectal cancer, metastatic non-small-cell lung cancer, squamous-cell carcinoma of the head and neck, and pancreatic cancer where malignant transformation depends on EGFR signaling [12]. Additional EGFR-targeting agents, including monoclonal antibodies, small molecules and vaccines, are currently under investigation [15].

EGFR and colorectal cancer

Several lines of evidence have demonstrated a role for EGFR in colorectal tumorigenesis. Preclinical data suggest that EGFR mRNA expression and EGF levels are higher in malignant areas of colorectal tumors than in the surrounding benign mucosa (as reviewed by Lockhart and Berlin [16]). In experimental models of colon cancer, TGF-α expression and EGFR activation allow for increased tumor cell growth and survival [16]. Moreover, mice treated with EGFR tyrosine kinase inhibitors and mice deficient in EGFR develop fewer colorectal polyps compared with untreated and wild-type mice, respectively, after challenge with colon cancer-inducing agents [16].

In human colorectal cancer, EGFR is also associated with tumor development and progression. The mechanisms underlying the role of EGFR in colorectal cancer are not entirely clear. EGFR is overexpressed in up to 82% of colorectal cancers [6–10]. *EGFR* amplification, preferentially of a mutant allele, is correlated with but does not reliably predict EGFR overexpression [17]. Mutations in the *EGFR* gene are rare in colorectal cancer but occur regularly in other cancer types, such as lung cancer [18–21].

Based on the importance of the EGFR axis in colorectal cancer, drugs that interfere with various functional domains of the receptor have been developed, as mentioned above. Currently, two anti-EGFR monoclonal antibodies have been approved in several countries for the treatment of colorectal cancer [12, 22]. Cetuximab, a human–mouse chimeric IgG1 monoclonal antibody, was the first EGFR-targeted agent approved for the treatment of colorectal cancer [12, 23]. Panitumumab, a fully human IgG2κ monoclonal antibody, was recently approved in the US and Europe as third-line treatment of metastatic colorectal cancer [12, 24]. Both antibodies have been shown to reduce the risk of tumor progression and to improve overall survival (OS), progression-free survival (PFS) and quality of life in patients with refractory colorectal cancer [11, 23, 25–28]. However, only a small proportion (8–23%) of patients were observed to achieve an objective response with cetuximab [11, 23, 25] or panitumumab [26, 28]. Cetuximab or panitumumab therapy is costly and might cause side effects. To optimize benefits and reduce the risks as well as contain costs associated with anti-EGFR treatment, the EGFR has been evaluated as a potential marker of clinical outcomes.

EGFR overexpression is more common among tumors of more advanced stage, tumors with worse histological grades, and tumors with lymphovascular invasion [7, 29, 30]. Patients with colorectal carcinomas showing EGFR staining by immunohistochemistry (IHC) in >50% of tumor cells have a poor prognosis [8]. High EGFR expression correlates with lower response rates in patients with advanced rectal cancer undergoing preoperative radiotherapy [31]. These findings suggest that EGFR overexpression is associated with advanced disease, increased metastatic ability and poor prognosis, although its impact on patient survival is less conclusive [10]. However, these data came largely from studies in which colorectal cancer patients with refractory and/or metastatic disease were selected for anti-EGFR therapy on the basis of an EGFR-positive status. It is likely, with this selection bias in the population tested, that the frequency of EGFR overexpression and its relationship to colorectal cancer prognosis might have been overestimated in the literature thus far. Inter-laboratory variation in the detection of EGFR levels also contributed to uncertainty regarding the robustness of previous conclusions. Different methods for assessing EGFR expression have produced different results which may or may not correlate with tumor stage, metastatic potential, and patient outcome. There are also divergent EGFR expression patterns between primary and metastatic tumors, regardless of the testing method used. Taken together, the role of EGFR overexpression in colorectal cancer remains inconclusive and warrants further investigation.

While EGFR overexpression is common among colorectal tumors, several studies have shown that EGFR levels are a poor predictor of response to anti-EGFR therapies. In clinical trials evaluating the efficacy of cetuximab, treatment response was not related to levels of EGFR expression [11, 25, 28]. Cetuximab has shown efficacy in some patients with tumors negative for EGFR as assessed by IHC [32], while many patients with EGFR-expressing colorectal tumors fail to respond to cetuximab [11, 25]. Similarly, a number of patients with EGFR-expressing tumors do not benefit from panitumumab therapy [26–28]. More recently, increased *EGFR* gene copy number as detected by fluorescence in situ hybridization (FISH) was associated with response to cetuximab or panitumumab [33]. This has been contradicted by findings that FISH analysis of *EGFR* amplification does not select all colorectal cancer patients who may benefit from cetuximab therapy [34]. These discrepancies could be explained by

tumor heterogeneity, presence of heterogeneous EGFR populations with different levels of low- and high-affinity sites, lack of standardized EGFR testing methods, and poor correlation between EGFR protein and DNA levels [17, 35].

The *EGFR* gene is rarely mutated in colorectal cancer. Less than 1% of colorectal carcinomas show mutations in the *EGFR* gene, according to the Cosmic database on somatic mutations in cancer (www.sanger.ac.uk/genetics/CGP/cosmic/). For these reasons, *EGFR* mutations have limited to no prognostic power and also do not predict EGFR-targeted treatment outcomes in patients with colorectal cancer [19]. In non-small-cell lung cancer, however, *EGFR* mutations and gene amplification are closely linked with favorable response to small-molecule tyrosine kinase inhibitors [18, 20, 21, 36]. Of note, a recent study reported a strong correlation between *EGFR* mutation status and phosphorylation of the EGFR at tyrosine 992 (pEGFR-tyr992) as detected by IHC [37]. Importantly, the expression of pEGFR-tyr992 also correlates significantly with clinical responsiveness to gefitinib in pulmonary adenocarcinoma [37]. It remains to be determined if this approach using specific antibodies recognizing EGFR phosphorylated forms can predict responses to anti-EGFR therapies in colorectal carcinoma.

Biomarkers in colorectal cancer

A major challenge in selecting appropriate patients for treatment is to identify reliable biomarkers that can predict the outcome of anti-EGFR therapies. As discussed above, EGFR protein expression, gene amplification, and mutations have limited predictive value in colorectal cancer, although they remain useful markers of treatment response in lung cancer [10, 13, 18]. The search for predictive biomarkers in colorectal cancer is now directed mainly toward key signaling components downstream of the EGFR.

Potential markers of alterations in EGFR-induced signaling in colorectal cancer include mutations in *KRAS*, *BRAF*, and *PIK3CA* genes as well as PTEN protein expression. The role of *KRAS* mutations, which result in constitutive activation of downstream EGFR signaling pathways, as a determinant of colorectal cancer prognosis and treatment response is discussed below.

Mutations in the *BRAF* gene, which encodes a serine/threonine kinase that activates the RAS-MAPK pathway, have been found in 4–15% of colorectal cancers [38–40]. This frequency increases to 70% in colorectal cancers with a microsatellite instability (MSI) phenotype due to hypermethylation of the *MLH1* promoter [41–43]. In MSI colorectal carcinoma, *BRAF* mutations occur independently of *KRAS* mutations and provide proliferation and survival signals through activation of several signaling pathways [44, 45]. Cell lines with *RAS/BRAF* mutations are highly resistant to cetuximab *in vitro* compared with wild-type cells [46]. One study showed no relationship between *BRAF* mutations and median survival of patients with metastatic colorectal cancer receiving bevacizumab, an antibody against vascular endothelial growth factor-A (VEGF) [47]. However, there are no data available on the role of *BRAF* mutations in predicting clinical response to anti-EGFR agents. Lievre *et al*. screened 30 colorectal cancer patients receiving cetuximab for several mutations including *BRAF*, but none of these patients had a tumor with a *BRAF* mutation or a MSI phenotype [48].

The *PIK3CA* gene encodes the p110α catalytic subunit of phosphoinositide 3-kinase (PI3K) protein, a critical component of the PI3K-Akt signaling pathway downstream of ligand-induced EGFR activation (see Fig. 1b). This catalytic subunit can be activated by an interaction with RAS proteins. *PIK3CA* mutations have been found in 10–18% of colorectal cancers [38, 46, 49], but it is unclear whether these mutations can predict response to EGFR-targeted therapies. According to one *in vitro* study, cell lines with activating *PIK3CA* mutations are resistant to cetuximab compared with wild-type cell lines [46]. However, two studies failed to observe a link between *PIK3CA* mutation status and cetuximab response in patients with colon cancer [33, 48]. These data were based on only five patients with *PIK3CA* mutations, possibly precluding the ability to find a significant link between *PIK3CA* mutations and treatment response. The predictive value of *PIK3CA* mutations in colorectal cancer needs to be clarified in larger studies.

PTEN (phosphatase and tensin homolog) acts as a tumor suppressor protein by inhibiting the PI3K-Akt signaling pathway (see Fig. 1b). Cell lines deficient in PTEN expression are more resistant to cetuximab *in vitro* than those with normal PTEN expression [46]. The loss of PTEN protein expression negatively predicts efficacy of cetuximab therapy in patients with metastatic colorectal cancer [50]. In this study, 63% (10/16) of patients with tumors that showed normal PTEN expression were able to achieve a partial response whereas no response was documented in 11 patients with tumors that lacked PTEN expression [50]. Additional studies are warranted to evaluate PTEN as a marker in the selection of colorectal cancer patients for anti-EGFR therapies.

KRAS: a downstream target of EGFR signaling

The human *KRAS* oncogene is mutated in over 30% of colorectal cancers [51]. Over 3,000 *KRAS* point mutations in colorectal cancer have been reported thus far (www.sanger.ac.uk/genetics/CGP/cosmic/). Somatic missense

mutations in the *KRAS* gene lead to single amino acid substitutions and are generally independent of *EGFR* mutations [52]. The most frequent alterations are detected in codons 12 (~82% of all reported *KRAS* mutations) and 13 (~17%) in exon 2 of the *KRAS* gene. Mutations in other positions, such as codons 61 and 146, have also been reported [51]. However, these alterations account for a minor proportion (1–4%) of *KRAS* mutations and their clinical relevance in colorectal cancer is unclear [51, 53]. *KRAS* mutations in codons 12 and 13 appear to play a major role in the progression of colorectal cancer [54–56], while mutations in codons 12, 13, and 61 are potential biomarkers in lung cancer [57].

The *KRAS* gene encodes a small G-protein that functions downstream of EGFR-induced cell signaling. This G-protein belongs to the family of RAS proteins that are involved in coupling signal transduction from cell surface receptors to intracellular targets via several signaling cascades, including the RAS-MAPK pathway (Fig. 1b). RAS proteins normally cycle between active GTP-bound (RAS-GTP) and inactive GDP-bound (RAS-GDP) conformations (see Fig. 3). RAS proteins are activated by guanine nucleotide exchange factors (GEFs) which are recruited to protein complexes at the intracellular domain of activated receptors. Signaling is terminated when RAS-GTP is hydrolyzed to the RAS-GDP inactive complex by GTPase-activating proteins (GAPs). Under physiological conditions, levels of RAS-GTP *in vivo* are tightly controlled by the counterbalancing activities of GEFs and GAPs. Mutations in genes that encode RAS proteins disrupt this balance, causing perturbations in downstream signaling activities.

KRAS mutations result in RAS proteins that are permanently in the active GTP-bound form (Fig. 2) due to defective intrinsic GTPase activity and resistance to GAPs. Unlike wild-type RAS proteins which are inactivated after a short time, the aberrant proteins are able to continuously activate signaling pathways in the absence of any upstream stimulation of EGFR/HER receptors. Oncogenic activation of RAS signaling pathways has been implicated in many aspects of the malignant process, including abnormal cell growth, proliferation, and differentiation. *KRAS* mutations are, in most cases, an early event in the development and progression of colorectal cancers [56, 58, 59]. Consistent with this concept, several studies have demonstrated that *KRAS* mutation status is an important prognostic factor in colorectal cancer [55, 58–60]. *KRAS* mutations are associated with tumors of more advanced stage, increased metastatic potential, poor prognosis, and decreased PFS and OS of patients [55, 56, 58, 59]. The prognostic value of *KRAS* mutations in colorectal cancer is presently controversial and warrants further confirmation.

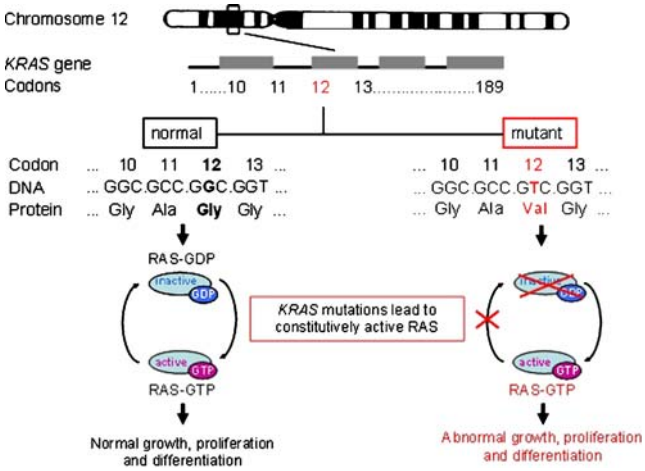

Fig. 2 Role of *KRAS* mutations in oncogenic activation of intracellular signaling. The human *KRAS* gene, located on chromosome 12, encodes a small G-protein that functions downstream of EGFR-induced cell signaling. This G-protein belongs to the family of RAS proteins involved in signal transduction pathways that regulate cell development and function. RAS proteins normally cycle between active (RAS-GTP) and inactive (RAS-GDP) conformations. Somatic missense mutations in codon 12 of the *KRAS* gene, leading to single amino acid substitutions such as p.Gly12Val, are the most common alterations found in colorectal tumors. These *KRAS* mutations result in RAS proteins that are constitutively in the active RAS-GTP conformation. Unlike wild-type RAS proteins which are deactivated after a short time, the mutated RAS proteins cause continuous activation of RAS signaling pathways in the absence of upstream stimulation of EGFR/HER receptors. This oncogenic activation of RAS signaling pathways leads to abnormal cell growth, proliferation and differentiation

KRAS mutation status may have a considerable impact on therapeutic decisions for colorectal cancer patients. Considering the molecular basis of EGFR-targeting agents, blocking EGFR at the receptor level will not ablate downstream signaling activities in tumors with *KRAS* mutations and hence constitutively active RAS proteins. Indeed, several studies have reported that *KRAS* mutations confer resistance to anti-EGFR monoclonal antibodies [24, 48, 61–65]. *KRAS* mutations are associated with poor responses to therapy, reduced PFS and shorter OS in colorectal cancer patients treated with cetuximab alone or in combination with chemotherapy [48, 62–65]. Similarly, an analysis of *KRAS* mutations in tumor samples from 92% of patients in a registrational clinical trial of panitumumab for the treatment of metastatic colorectal cancer predicted a lack of efficacy of panitumumab on PFS and OS in patients with *KRAS* mutant tumors [24]. Taken together, these results indicate that *KRAS* mutation status is an important parameter for selecting patients for therapy: patients with mutant tumors will not benefit from EGFR-targeted therapies. On the basis of these data, the European Medicines Agency (EMEA) has approved the use of cetuximab and panitumumab for the treatment of metastatic

colorectal cancer in patients who carry a normal, wild-type *KRAS* gene [12]. However, as only a fraction of patients with colorectal tumors that carry a wild-type *KRAS* allele can achieve a clinical response with EGFR-targeted therapies, the search for additional predictive parameters remains an important challenge.

Methods for *KRAS* mutation testing

PCR has become the cornerstone of molecular diagnostic tools, including those developed for *KRAS* mutation testing. PCR assays are highly sensitive and can be easily automated. PCR assays are thus well-suited for large-scale, high-throughput diagnostic testing. For *KRAS* mutation testing, however, standard PCR assays are not sufficient. The main requirement for conclusive *KRAS* genotyping by PCR assay is the ability to discriminate between different mutant alleles and wild type. There are two main challenges to achieving a conclusive result: one is the heterogeneity of the testing material, and the other is differences in the detection limits for distinct mutations. Depending on the tissue analyzed, the amount of tumor versus non-tumor area is variable and heterogeneous, resulting in a template mixture in which wild-type and mutant DNA are not present in equimolar amounts. Moreover, a cancer cell may carry a heterozygous or homozygous *KRAS* mutation, increasing the genetic heterogeneity of the tissue material used. Differences in PCR efficiencies for the detection of the different mutations can lead to a bias whereby certain mutations are detected preferentially over others.

A plethora of methods is available for the detection of mutations in the KRAS gene (see Table 1 for a non-exhaustive overview). Many of these methods are laboratory-based assays and are not commercially available for use in routine diagnostics. Other methods have been developed further and are available as commercial test kits not directly intended for diagnostic purposes. To date, two KRAS mutation test kits (TheraScreen® by DxS Ltd. and KRAS LightMix® by TIB MolBiol) have met the essential requirements of the relevant European Directives (CE-Mark) for diagnostic use in the European Union. Only one study, to our knowledge, has evaluated the concordance between different methods for KRAS mutation testing [66]. In this study, 40 colorectal tumor samples were tested for seven common mutations in codons 12 and 13 of the KRAS gene by four commercially available assays and by direct sequencing as a reference. Two allele-specific PCR-based methods and one PCR/direct sequencing method demonstrated high to good agreement with direct sequencing, whereas an oligonucleotide hybridization method showed poor agreement. Given the technical requirements for a conclusive KRAS test result and the potential for variability between different KRAS genotyping methods, a thorough analytical validation of testing methods together with a high standard of quality assurance are critical for accurate, reliable KRAS mutation testing in clinical practice. Such an initiative to validate and standardize KRAS mutation testing will also include the development of a website (http://esp-pathology.org) providing the latest information on current diagnostic methods and intended uses of KRAS mutation testing. Therefore, at present, no advice is given to which method is preferred. The advantage of commercially available tests is the validation process that these have gone through, but obviously the costs of these tests are higher that in-house developed methods. Most experience exists in different laboratories with sequencing after PCR, and this is a relatively inexpensive method, but requires validation on a large series of cases. For most other methods, it is too early to assess the advantages and disadvantages.

Recommended guidelines and European QA program

Guidelines for *KRAS* mutation testing in colorectal cancer

The optimal use of EGFR-targeted therapies requires accurate *KRAS* mutation testing. Testing for *KRAS* mutations generally comprises three stages: (1) referral for *KRAS* mutation testing; (2) selection of the tissue block containing the tumor area of interest; and (3) DNA extraction and *KRAS* mutation analysis. In the current clinical setting, colorectal cancer patients are not routinely screened for *KRAS* mutation status. Pathologists test for *KRAS* mutations only upon the specific request of a clinician. Clinicians, in turn, request *KRAS* genotyping only if the test results are intended to guide decisions on patient management. These practices might not be sufficient for optimal patient care. The process of requesting *KRAS* status testing, finding the original tissue block and reporting the test results is cumbersome, time-consuming, and prone to errors. Therefore, routine mutation testing at the time of initial diagnosis of stage II and III tumors should be considered. There is also a lack of validated testing methods and standardized operating procedures for the detection of *KRAS* mutations. There are very few studies that have systematically compared the sensitivity, specificity and reproducibility of the different techniques for *KRAS* genotyping. The concordance between different diagnostic methods is also largely unknown. Therefore, there is an urgent need to establish and implement clinical practice guidelines and standardized procedures for *KRAS* mutation testing in patients with colorectal cancer.

In recognition of the importance of accurate HER2 testing in breast cancer management, practice guidelines

Table 1 Overview of methods used for *KRAS* genotyping

Method	Intended use	Ref.
Gel electrophoresis assays		
Temporal temperature gradient electrophoresis	LBM	[67]
Denaturing gradient gel electrophoresis	LBM	[68]
Constant denaturant capillary electrophoresis	LBM	[69]
SSCP assay	LBM	[70]
Sequencing		
Dideoxy sequencing	LBM, RUO kit	[71]
Pyrosequencing	LBM	[72, 73]
PyroMark™ *KRAS*	RUO kit	
Allele-specific PCR assays[a]		
Allele discrimination based on primer design		
ARMS-PCR	LBM	[74, 75]
KRAS mutation test kit	RUO kit	
TheraScreen® kit	CE-Mark kit for clinical use	[76]
KRAS LightMix® kit	CE-Mark kit for clinical use	
REMS-PCR	LBM	[77]
FLAG assay	LBM	[78]
Enriched PCR-RFLP	LBM	[79]
Allele discrimination based allele-specific ligation detection reaction		
PCR-LDR	LBM	[80]
PCR-LDR spFRET assay	LBM	[81]
Allele discrimination based on discriminating amplification efficiencies at low melting temperatures		
COLD-PCR	LBM	[82]
Other methods		
Surface ligation reaction and biometallization	LBM	[83]
Multi-target DNA assay panel	LBM	[84]
Allele-specific oligonucleotide hybridization—Invigene®		
KRAS genotyping kit	LBM, RUO kit	

LBM Laboratory-based method, not commercially available, *RUO*: research use only, not validated for clinical applications
[a] Allele-specific assays are also used by vendors offering *KRAS* genotyping services

and a testing algorithm for HER2 testing have been formulated by the American Society of Clinical Oncology and the College of American Pathologists [3]. This expert panel has recommended validation of all laboratory assays or modifications, use of standardized operating procedures, and compliance with new testing criteria. Importantly, the panel has also recommended that HER2 testing be done in an accredited laboratory or in a laboratory that meets the quality assurance and proficiency requirements set forth in the practice guidelines.

To address the need for standardized *KRAS* mutation testing methods and procedures in colorectal carcinoma, two working groups of the European Society of Pathology (ESP), the Diseases of the Digestive Tract ESP Working Group and the Molecular Pathology ESP Working Group, convened an expert panel to develop guideline recommendations and a proposal for a European QA program for *KRAS* mutation testing. This expert panel consisted of European pathologists, molecular biologists, and oncologists with expertise in colorectal carcinoma and *KRAS* mutation analysis. A panel meeting was held during the Third Intercontinental Congress of Pathology in Barcelona in May 2008. The purpose of this meeting was for the panel members to refine and agree on draft guidelines and an organizational structure of a European QA program for *KRAS* mutation testing. Consensus recommendations and proposals are summarized here.

Target patient population for KRAS mutation testing

Activating mutations in codons 12 and 13 of the *KRAS* gene identify patients who have a poor clinical response to EGFR-targeted therapies. Ideally, a predictive test should distinguish between treatment responders and non-responders accurately and reliably. Such an ideal predictor is presently not available. The best option available today is a test that identifies patients who carry two wild-type *KRAS* alleles and excludes patients with mutant codon 12 or 13 alleles.

The anti-EGFR antibodies, cetuximab and panitumumab, currently available for clinical use have been approved in several countries for the treatment of patients

with *KRAS* wild-type metastatic colorectal cancer. In the European Union, cetuximab has been approved for use in combination with chemotherapy or as a single agent in patients who are refractory or intolerant to irinotecan-based chemotherapy. Similarly, panitumumab has been approved as third-line treatment for refractory metastatic colorectal cancer. Routine testing for *KRAS* mutations might not be beneficial for patients with stage I colorectal carcinoma. However, this expert panel recommends standard *KRAS* mutation testing for all patients with stage II to III colorectal carcinomas.

The role of the primary pathologist in KRAS mutation testing

The primary pathologist plays a central role in *KRAS* mutation testing. The pathologist can either perform the test at his/her laboratory if it has been accredited for *KRAS* mutation testing or send the tissue block to a reference laboratory for external testing. In both situations, the pathologist is responsible for at least three important procedures. First, the pathologist is responsible for choosing the most appropriate tissue block to be tested (see below for discussion on optimal material for testing). Second, the pathologist should ensure that the tissue block selected for *KRAS* genotyping contains sufficient quantity of invasive tumor cells needed for analysis. The minimum amount of tumor versus non-tumor area required will depend on the *KRAS* genotyping method. It is the pathologist's responsibility to evaluate the tumor content of the tissue block and to ensure that it fulfills the minimum criterion of the testing method. To evaluate tumor content, it is recommended that the pathologist assess a hematoxylin–eosin (HE) stained section of the tissue area of the paraffin block designated for DNA extraction and *KRAS* mutation analysis before and after DNA extraction. This will ensure that the tissue area has an adequate tumor density, preferably greater than 70% invasive carcinoma cells, needed for detection of *KRAS* mutations. Finally, the pathologist is responsible for documentation, which should include results from HE staining analysis as well as from *KRAS* mutation testing, and for preparation of the pathology report (see below on optimal reporting of *KRAS* test results). If the testing is performed by a reference laboratory, the pathologist should integrate the test results into the pathology report.

Optimal tissue material for KRAS mutation testing

Based on current knowledge, the most appropriate material for *KRAS* mutation testing is primary tumor tissue. This type of material is commonly archived and thus accessible, and typically contains sufficient amount of invasive carcinoma cells required for *KRAS* mutation testing. If an endoscopic biopsy of the primary tumor is performed, it is important that the material obtained contains adequate amount of adenocarcinoma cells in the area identified.

However, it is estimated that 20% of the target patient population will present with metastatic disease and will not have archival material from the primary tumor. This poses an important challenge for the pathologist in the selection of appropriate material for *KRAS* mutation testing. In this situation, the panel recommends that *KRAS* mutation testing is performed using material from the metastatic tumor, for example, from resected liver metastases or positive lymph nodes. The pathologist must ensure that the metastatic tissue block contains adequate amount of adenocarcinoma cells.

For some patients, both the primary tumor tissue as well as metastatic tissue specimens might be available for *KRAS* mutation testing. At present, there are insufficient data available to demonstrate the superiority of either primary or metastatic tissue material for *KRAS* mutation testing. In the experience of this expert panel, primary and metastatic tumor tissues from the same patient can give discordant results on *KRAS* mutation status. However, the true discordance in *KRAS* genotyping results between primary and metastatic tumor tissues is presently unknown. More studies are needed to better define which type of material can provide the most reliable results in patients with metastatic disease. Until such data are available, the panel recommends that, in accordance with existing literature data, primary tumor tissue is tested, but that, ideally, both primary and metastatic tumor tissues are analyzed for *KRAS* mutation status and that the results are collected in a central database to increase our knowledge. In case the results are discordant, presently no evidence is available to advise standard treatment and the patient needs to be discussed in a multidisciplinary team.

In general, a paraffin block containing only tissue from adenoma or non-invasive carcinoma should not be used for *KRAS* mutation analysis. If an endoscopic biopsy of the primary tumor or a biopsy of a metastatic site is performed, the pathologist should ensure that malignant cells are present in the biopsy material to be tested and clearly indicate which blocks or slides should be used for testing.

Optimal procedures for KRAS mutation testing

To ensure accurate *KRAS* mutation testing, the panel recommends that each laboratory develops standardized operating procedures and testing requirements for *KRAS* mutation analysis using available information that will be provided by either the vendors of a commercially available method or the ESP-website (see below). Recommendations for specific testing parameters, including method sensitivity

and specificity, method validation, analysis success rate, and documentation of costs, are summarized in Table 2. Some of these recommendations are compatible with ISO (International Organization for Standardization; http://www.iso.org) general requirements for the competence of testing and calibration laboratories (ISO/IEC 17025:2005). These requirements will become essential components of accreditation for *KRAS* mutation testing. Tests that have a detection sensitivity of 1% might detect subclones in a tumor that have acquired a mutation. It is presently unknown what the consequence of such a finding might be.

Optimal reporting of test results

Result reporting is an integral part of any diagnostic procedure, including *KRAS* mutation testing. All *KRAS* test results are to be reported to the primary pathologist who is responsible for preparation of the pathology report for a specific tissue block or biopsy material. Optimal reporting of *KRAS* test results should conform to the OECD Guidelines for Quality Assurance in Molecular Genetic Testing (http://www.oecd.org). In brief, the reports should include at minimum the following information: (1) identification of the patient and health care professional; (2) type of material and percentage of tumor cells present in the sample; (3) indication for testing and patient-specific medical data; (4) the testing method used, including its analytical sensitivity and specificity; and (5) test results (mutant or wild-type *KRAS* allele) and interpretation of results in the context of the indication for testing.

Proposal for a European quality assurance program

During the process of developing a European QA program for *KRAS* mutation testing, the expert panel considered the experience with HER2 testing as an informative example. While trastuzumab (Herceptin®) became available in 2002 for the treatment of breast cancer, it was another 5 years before clinical practice guidelines were established for optimal HER2 testing algorithm and proficiency requirements. Another problem encountered with the introduction of trastuzumab was the lack of adequate financial provisions for diagnostic testing, although some national authorities required mandatory HER2 testing in breast cancer patients prior to trastuzumab therapy. Today, molecular diagnostic tools, testing procedures and the reimbursement process for diagnostic tests linked to a specific medication differ greatly across countries in Europe. Clearly, there is a need to establish a standardized, evidence-based QA program for molecular diagnostics across the European Union.

Here, we propose to establish a European QA program for testing *KRAS* mutations in colorectal cancer. This program aims to ensure optimal accuracy and proficiency in *KRAS* mutation testing across all countries or institutions in the European Union. A potential framework for a European QA program for *KRAS* mutation testing is shown in Fig. 3. The program will be organized by the European Society of Pathology in close collaboration with existing regional and/or national QA programs. Laboratories can participate in the European QA program at the regional or

Table 2 Recommendations for *KRAS* mutation testing

Parameter	Recommendation
Sensitivity	The lower detection limit of mutant signal should be set at 1% of tumor cells for allele-specific PCR and 25–30% for direct sequencing.
Specificity	A specific test should be able to detect 7 common mutations in codons 12 and 13 of the *KRAS* gene and not detect mutations in codon 61. False negatives may occur because of test specificities (e.g. lack of an allele-specific PCR for codon 13 mutation).
Method validation[a]	The laboratory should use a validated method for *KRAS* mutation testing. The objectives of the validation are to: Determine the minimum tumor tissue area and section thickness for DNA extraction. Stipulate which fixatives are acceptable for use. Determine input DNA quantity, quality and concentration. Determine the cut-off values for discerning *KRAS* mutant alleles from wild-type alleles. Evaluate sensitivity of the test, for example by using dilution series cell lines. Compare the accuracy of test results against a pre-defined reference method (e.g. direct sequencing). Determine the reproducibility between different testing assays and equipment. Verify the robustness of the testing method. Robustness may be influenced by several factors, including varying DNA concentrations and the use of manual or automated protocols or equipment.
Analysis success rate	A laboratory should obtain the following success rates for accreditation: 95% of samples with successful DNA extraction 97% of samples with correct *KRAS* test results
Costs	Costs of *KRAS* mutation testing should be calculated and documented for national reimbursement schemes.

[a] Compatible with accreditation requirements of ISO/IEC 17025:2005

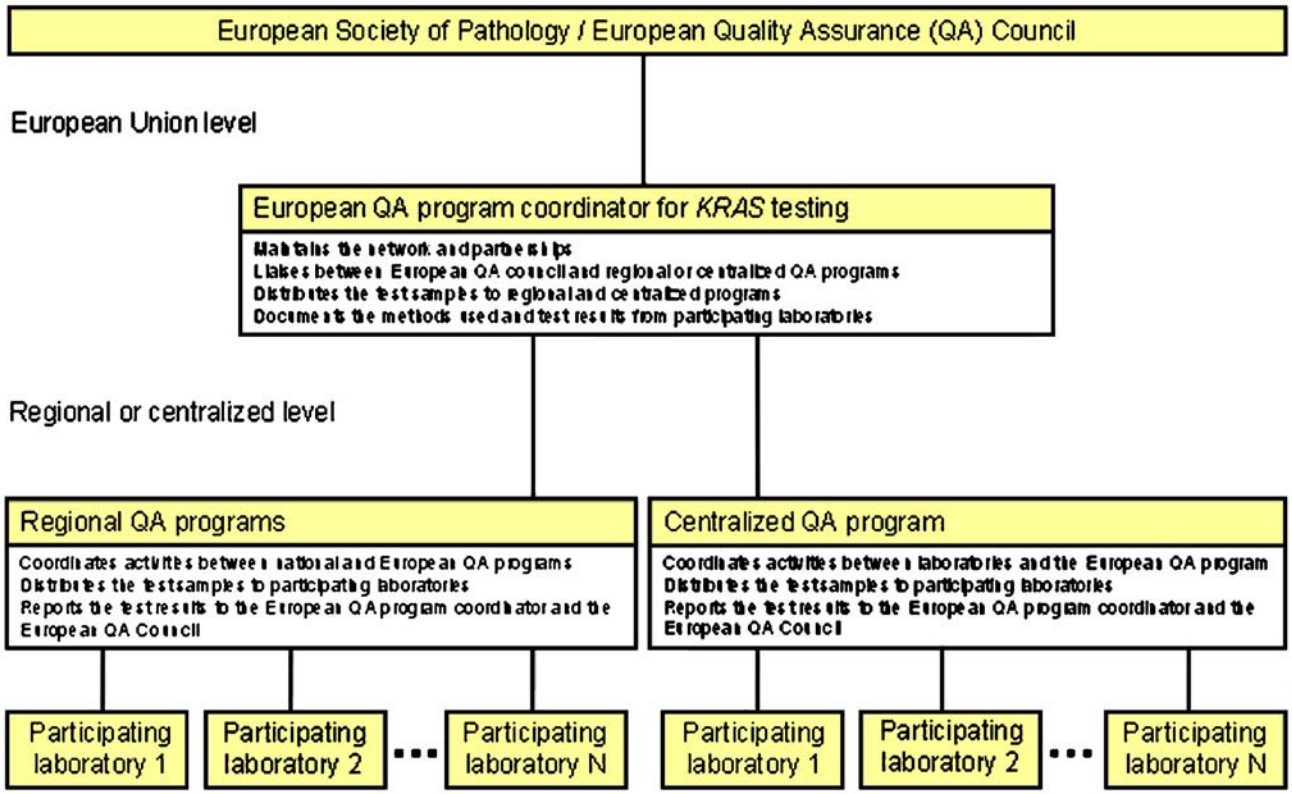

Fig. 3 Proposed framework for a European quality assurance (QA) program for *KRAS* mutation testing in colorectal cancer. The European QA program, under the direction of a QA council, will be organized by the European Society of Pathology in close collaboration with existing regional and/or national QA programs. The QA program, together with a designated coordinator, will be responsible for establishing QA guidelines and testing criteria, implementing the QA program and performing laboratory accreditation. Participating laboratories can attain accreditation at the regional or centralized level

centralized level, depending on the country's specific circumstances. Laboratories in countries with existing QA programs may attain accreditation at the regional level, whereas a centralized program will be created to coordinate QA activities for countries or institutions not yet engaged in a QA program.

The fundamental initiatives of the proposed European QA program are as follows:

1. The European QA program for *KRAS* mutation testing aims to provide timely, standardized, evidence-based guidelines for the performance of a diagnostic test for *KRAS* mutations on colorectal tumor tissues.
2. The European QA program intends to collaborate with existing regional and/or national QA programs to develop strategies and standardized procedures that help to ensure optimal performance, interpretation and reporting of *KRAS* mutation analysis. To achieve this, the European QA program will provide administrative and logistic support and networking opportunities for the development and implementation of standardized operating procedures and QA criteria for proficiency testing and competency assessments. The European QA program will also coordinate accreditation of participating laboratories at the European and regional level.
3. The European QA program will facilitate the administrative process and reimbursement discussions in each country in the European Union by providing the necessary documents and QA schemes for implementation and performance of diagnostic tests for *KRAS* mutation analysis.

To support these proposed initiatives, the European QA program intends to establish and maintain a website (http://esp-pathology.org) that will provide the latest recommendations, as well as, potentially, an overview of validated laboratory methods, standardized operating procedures, and accreditation criteria relevant for *KRAS* mutation testing.

As our understanding of the genetics and molecular biology of colorectal cancer advances, other parameters will hopefully be identified as predictors of treatment outcome. Presently, *KRAS* mutation status must be considered in the appropriate therapeutic context for each patient. The guideline recommendations and European QA program proposed here for *KRAS* mutation testing will help to ensure that all patients who may or may not benefit from EGFR-targeted therapies are identified in a timely and

consistent manner. Although the proposed QA program is intended for the standardization of *KRAS* mutation testing methods and procedures, this expert panel is of the opinion that such a program can potentially be adapted to incorporate other predictive biomarkers in colorectal cancer as they become available.

Conclusions

Colorectal cancer is a major cause of cancer-related mortality. The EGFR signaling pathway is frequently activated in colorectal cancer and has been extensively investigated as a target for cancer therapy. Therapeutic agents that target the EGFR have improved outcomes for patients with colorectal cancer, although they are effective in only a subset of patients. Point mutations in codons 12 and 13 of the *KRAS* oncogene are predictive of poor response to EGFR-targeted therapies. Testing for *KRAS* mutation status is, therefore, a potential strategy to select those patients who will or will not benefit from EGFR-targeted therapies. Although many robust techniques have been developed for *KRAS* genotyping, most of these techniques or testing procedures have not been validated in the clinical setting. Thus, there is an urgent need for validated methods and standardized testing procedures to ensure accurate testing of *KRAS* mutation status. Here we propose guideline recommendations and a European quality assurance program for *KRAS* mutation testing in patients with colorectal carcinoma.

Acknowledgements The panel meeting held during the Third Intercontinental Congress of Pathology in Barcelona, May 2008 was supported by Amgen Inc.

G. Hoefler: Project GZ 70420/0134-IV/B/12/2006 "Molecular Markers To Predict Clinical Outcome and Therapy Response in Stage II Colon Cancer" of the Austrian Ministry for Health, Family and Youth.

Writing assistance was provided by Archimed medical communication ag, Zofingen, Switzerland.

References

1. Owens MA, Horten BC, Da Silva MM (2004) HER2 amplification ratios by fluorescence in situ hybridization and correlation with immunohistochemistry in a cohort of 6,556 breast cancer tissues. Clin Breast Cancer 5:63–69
2. Dowsett M, Hanna WM, Kockx M, Penault-Llorca F, Ruschoff J, Gutjahr T, Habben K, van de Vijver MJ (2007) Standardization of HER2 testing: results of an international proficiency-testing ring study. Mod Pathol 20:584–591
3. Wolff AC, Hammond ME, Schwartz JN, Hagerty KL, Allred DC, Cote RJ, Dowsett M, Fitzgibbons PL, Hanna WM, Langer A, McShane LM, Paik S, Pegram MD, Perez EA, Press MF, Rhodes A, Sturgeon C, Taube SE, Tubbs R, Vance GH, van d V, Wheeler TM, Hayes DF (2007) American Society of Clinical Oncology/College of American Pathologists guideline recommendations for human epidermal growth factor receptor 2 testing in breast cancer. J Clin Oncol 25:118–145
4. Ellis IO, Coleman D, Wells C, Kodikara S, Paish EM, Moss S, Al-Sam S, Anderson N, Bobrow L, Buley I, Connolly CE, Dallimore NS, Hales S, Hanby A, Humphreys S, Knox F, Lowe J, Macartney J, Nash R, Parham D, Patnick J, Pinder SE, Quinn CM, Robertson AJ, Shrimankar J, Walker RA, Winder R (2006) Impact of a national external quality assessment scheme for breast pathology in the UK. J Clin Pathol 59:138–145
5. Jemal A, Siegel R, Ward E, Hao Y, Xu J, Murray T, Thun MJ (2008) Cancer statistics, 2008. CA Cancer J Clin 58:71–96
6. Hemming AW, Davis NL, Kluftinger A, Robinson B, Quenville NF, Liseman B, LeRiche J (1992) Prognostic markers of colorectal cancer: an evaluation of DNA content, epidermal growth factor receptor, and Ki-67. J Surg Oncol 51:147–152
7. Kluftinger AM, Robinson BW, Quenville NF, Finley RJ, Davis NL (1992) Correlation of epidermal growth factor receptor and c-erbB2 oncogene product to known prognostic indicators of colorectal cancer. Surg Oncol 1:97–105
8. Mayer A, Takimoto M, Fritz E, Schellander G, Kofler K, Ludwig H (1993) The prognostic significance of proliferating cell nuclear antigen, epidermal growth factor receptor, and mdr gene expression in colorectal cancer. Cancer 71:2454–2460
9. Salomon DS, Brandt R, Ciardiello F, Normanno N (1995) Epidermal growth factor-related peptides and their receptors in human malignancies. Crit Rev Oncol Hematol 19:183–232
10. Spano JP, Lagorce C, Atlan D, Milano G, Domont J, Benamouzig R, Attar A, Benichou J, Martin A, Morere JF, Raphael M, Penault-Llorca F, Breau JL, Fagard R, Khayat D, Wind P (2005) Impact of EGFR expression on colorectal cancer patient prognosis and survival. Ann Oncol 16:102–108
11. Saltz LB, Meropol NJ, Loehrer PJ Sr, Needle MN, Kopit J, Mayer RJ (2004) Phase II trial of cetuximab in patients with refractory colorectal cancer that expresses the epidermal growth factor receptor. J Clin Oncol 22:1201–1208
12. Ciardiello F, Tortora G (2008) EGFR antagonists in cancer treatment. N Engl J Med 358:1160–1174
13. Metro G, Finocchiaro G, Cappuzzo F (2006) Anti-cancer therapy with EGFR inhibitors: factors of prognostic and predictive significance. Ann Oncol 17 Suppl 2:ii42–ii45
14. Harari PM, Allen GW, Bonner JA (2007) Biology of interactions: antiepidermal growth factor receptor agents. J Clin Oncol 25:4057–4065
15. Ono M, Kuwano M (2006) Molecular mechanisms of epidermal growth factor receptor (EGFR) activation and response to gefitinib and other EGFR-targeting drugs. Clin Cancer Res 12:7242–7251
16. Lockhart AC, Berlin JD (2005) The epidermal growth factor receptor as a target for colorectal cancer therapy. Semin Oncol 32:52–60
17. Spindler KL, Lindebjerg J, Nielsen JN, Olsen DA, Bisgard C, Brandslund I, Jakobsen A (2006) Epidermal growth factor receptor analyses in colorectal cancer: a comparison of methods. Int J Oncol 29:1159–1165
18. Bonomi PD, Buckingham L, Coon J (2007) Selecting patients for treatment with epidermal growth factor tyrosine kinase inhibitors. Clin Cancer Res 13:s4606–s4612
19. Ogino S, Meyerhardt JA, Cantor M, Brahmandam M, Clark JW, Namgyal C, Kawasaki T, Kinsella K, Michelini AL, Enzinger PC, Kulke MH, Ryan DP, Loda M, Fuchs CS (2005) Molecular alterations in tumors and response to combination chemotherapy

with gefitinib for advanced colorectal cancer. Clin Cancer Res 11:6650–6656
20. Paez JG, Janne PA, Lee JC, Tracy S, Greulich H, Gabriel S, Herman P, Kaye FJ, Lindeman N, Boggon TJ, Naoki K, Sasaki H, Fujii Y, Eck MJ, Sellers WR, Johnson BE, Meyerson M (2004) EGFR mutations in lung cancer: correlation with clinical response to gefitinib therapy. Science 304:1497–1500
21. Pao W, Miller V, Zakowski M, Doherty J, Politi K, Sarkaria I, Singh B, Heelan R, Rusch V, Fulton L, Mardis E, Kupfer D, Wilson R, Kris M, Varmus H (2004) EGF receptor gene mutations are common in lung cancers from "never smokers" and are associated with sensitivity of tumors to gefitinib and erlotinib. Proc Natl Acad Sci U S A 101:13306–13311
22. Rocha-Lima CM, Soares HP, Raez LE, Singal R (2007) EGFR targeting of solid tumors. Cancer Control 14:295–304
23. Jonker DJ, O'Callaghan CJ, Karapetis CS, Zalcberg JR, Tu D, Au HJ, Berry SR, Krahn M, Price T, Simes RJ, Tebbutt NC, van HG, Wierzbicki R, Langer C, Moore MJ (2007) Cetuximab for the treatment of colorectal cancer. N Engl J Med 357:2040–2048
24. Amado RG, Wolf M, Peeters M, Van CE, Siena S, Freeman DJ, Juan T, Sikorski R, Suggs S, Radinsky R, Patterson SD, Chang DD (2008) Wild-type KRAS is required for panitumumab efficacy in patients with metastatic colorectal cancer. J Clin Oncol 26:1626–1634
25. Cunningham D, Humblet Y, Siena S, Khayat D, Bleiberg H, Santoro A, Bets D, Mueser M, Harstrick A, Verslype C, Chau I, Van CE (2004) Cetuximab monotherapy and cetuximab plus irinotecan in irinotecan-refractory metastatic colorectal cancer. N Engl J Med 351:337–345
26. Gibson TB, Ranganathan A, Grothey A (2006) Randomized phase III trial results of panitumumab, a fully human anti-epidermal growth factor receptor monoclonal antibody, in metastatic colorectal cancer. Clin Colorectal Cancer 6:29–31
27. Siena S, Peeters M, Van CE, Humblet Y, Conte P, Bajetta E, Comandini D, Bodoky G, van HG, Salek T, Wolf M, Devercelli G, Woolley M, Amado RG (2007) Association of progression-free survival with patient-reported outcomes and survival: results from a randomised phase 3 trial of panitumumab. Br J Cancer 97:1469–1474
28. Van CE, Peeters M, Siena S, Humblet Y, Hendlisz A, Neyns B, Canon JL, Van Laethem JL, Maurel J, Richardson G, Wolf M, Amado RG (2007) Open-label phase III trial of panitumumab plus best supportive care compared with best supportive care alone in patients with chemotherapy-refractory metastatic colorectal cancer. J Clin Oncol 25:1658–1664
29. Radinsky R, Risin S, Fan D, Dong Z, Bielenberg D, Bucana CD, Fidler IJ (1995) Level and function of epidermal growth factor receptor predict the metastatic potential of human colon carcinoma cells. Clin Cancer Res 1:19–31
30. Steele RJ, Kelly P, Ellul B, Eremin O (1990) Epidermal growth factor receptor expression in colorectal cancer. Br J Surg 77:1352–1354
31. Giralt J, Eraso A, Armengol M, Rossello J, Majo J, Ares C, Espin E, Benavente S, de T I (2002) Epidermal growth factor receptor is a predictor of tumor response in locally advanced rectal cancer patients treated with preoperative radiotherapy. Int J Radiat Oncol Biol Phys 54:1460–1465
32. Chung KY, Shia J, Kemeny NE, Shah M, Schwartz GK, Tse A, Hamilton A, Pan D, Schrag D, Schwartz L, Klimstra DS, Fridman D, Kelsen DP, Saltz LB (2005) Cetuximab shows activity in colorectal cancer patients with tumors that do not express the epidermal growth factor receptor by immunohistochemistry. J Clin Oncol 23:1803–1810
33. Moroni M, Veronese S, Benvenuti S, Marrapese G, Sartore-Bianchi A, Di NF, Gambacorta M, Siena S, Bardelli A (2005) Gene copy number for epidermal growth factor receptor (EGFR) and clinical response to antiEGFR treatment in colorectal cancer: a cohort study. Lancet Oncol 6:279–286
34. Italiano A, Follana P, Caroli FX, Badetti JL, Benchimol D, Garnier G, Gugenheim J, Haudebourg J, Keslair F, Lesbats G, Lledo G, Roussel JF, Pedeutour F, Francois E (2008) Cetuximab shows activity in colorectal cancer patients with tumors for which FISH analysis does not detect an increase in EGFR gene copy number. Ann Surg Oncol 15:649–654
35. Francoual M, Etienne-Grimaldi MC, Formento JL, Benchimol D, Bourgeon A, Chazal M, Letoublon C, Andre T, Gilly N, Delpero JR, Lasser P, Spano JP, Milano G (2006) EGFR in colorectal cancer: more than a simple receptor. Ann Oncol 17:962–967
36. Cappuzzo F, Hirsch FR, Rossi E, Bartolini S, Ceresoli GL, Bemis L, Haney J, Witta S, Danenberg K, Domenichini I, Ludovini V, Magrini E, Gregorc V, Doglioni C, Sidoni A, Tonato M, Franklin WA, Crino L, Bunn PA Jr, Varella-Garcia M (2005) Epidermal growth factor receptor gene and protein and gefitinib sensitivity in non-small-cell lung cancer. J Natl Cancer Inst 97:643–655
37. Hijiya N, Miyawaki M, Kawahara K, Akamine S, Tsuji K, Kadota J, Akizuki S, Uchida T, Matsuura K, Tsukamoto Y, Moriyama M (2008) Phosphorylation status of epidermal growth factor receptor is closely associated with responsiveness to gefitinib in pulmonary adenocarcinoma. Hum Pathol 39:316–323
38. Barault L, Veyrie N, Jooste V, Lecorre D, Chapusot C, Ferraz JM, Lievre A, Cortet M, Bouvier AM, Rat P, Roignot P, Faivre J, Laurent-Puig P, Piard F (2008) Mutations in the RAS-MAPK, PI(3)K (phosphatidylinositol-3-OH kinase) signaling network correlate with poor survival in a population-based series of colon cancers. Int J Cancer 122:2255–2259
39. Tan YH, Liu Y, Eu KW, Ang PW, Li WQ, Salto-Tellez M, Iacopetta B, Soong R (2008) Detection of BRAF V600E mutation by pyrosequencing. Pathology 40:295–298
40. Calistri D, Rengucci C, Seymour I, Lattuneddu A, Polifemo AM, Monti F, Saragoni L, Amadori D (2005) Mutation analysis of p53, K-ras, and BRAF genes in colorectal cancer progression. J Cell Physiol 204:484–488
41. Oliveira C, Pinto M, Duval A, Brennetot C, Domingo E, Espin E, Armengol M, Yamamoto H, Hamelin R, Seruca R, Schwartz S Jr (2003) BRAF mutations characterize colon but not gastric cancer with mismatch repair deficiency. Oncogene 22:9192–9196
42. Domingo E, Espin E, Armengol M, Oliveira C, Pinto M, Duval A, Brennetot C, Seruca R, Hamelin R, Yamamoto H, Schwartz S Jr (2004) Activated BRAF targets proximal colon tumors with mismatch repair deficiency and MLH1 inactivation. Genes Chromosomes Cancer 39:138–142
43. Ogino S, Cantor M, Kawasaki T, Brahmandam M, Kirkner GJ, Weisenberger DJ, Campan M, Laird PW, Loda M, Fuchs CS (2006) CpG island methylator phenotype (CIMP) of colorectal cancer is best characterised by quantitative DNA methylation analysis and prospective cohort studies. Gut 55:1000–1006
44. Rajagopalan H, Bardelli A, Lengauer C, Kinzler KW, Vogelstein B, Velculescu VE (2002) Tumorigenesis: RAF/RAS oncogenes and mismatch-repair status. Nature 418:934
45. Preto A, Figueiredo J, Velho S, Ribeiro AS, Soares P, Oliveira C, Seruca R (2008) BRAF provides proliferation and survival signals in MSI colorectal carcinoma cells displaying BRAF(V600E) but not KRAS mutations. J Pathol 214:320–327
46. Jhawer M, Goel S, Wilson AJ, Montagna C, Ling YH, Byun DS, Nasser S, Arango D, Shin J, Klampfer L, Augenlicht LH, Soler RP, Mariadason JM (2008) PIK3CA mutation/PTEN expression status predicts response of colon cancer cells to the epidermal growth factor receptor inhibitor cetuximab. Cancer Res 68:1953–1961
47. Ince WL, Jubb AM, Holden SN, Holmgren EB, Tobin P, Sridhar M, Hurwitz HI, Kabbinavar F, Novotny WF, Hillan KJ, Koeppen

H (2005) Association of k-ras, b-raf, and p53 status with the treatment effect of bevacizumab. J Natl Cancer Inst 97:981–989
48. Lievre A, Bachet JB, Le CD, Boige V, Landi B, Emile JF, Cote JF, Tomasic G, Penna C, Ducreux M, Rougier P, Penault-Llorca F, Laurent-Puig P (2006) KRAS mutation status is predictive of response to cetuximab therapy in colorectal cancer. Cancer Res 66:3992–3995
49. Velho S, Oliveira C, Ferreira A, Ferreira AC, Suriano G, Schwartz S Jr, Duval A, Carneiro F, Machado JC, Hamelin R, Seruca R (2005) The prevalence of PIK3CA mutations in gastric and colon cancer. Eur J Cancer 41:1649–1654
50. Frattini M, Saletti P, Romagnani E, Martin V, Molinari F, Ghisletta M, Camponovo A, Etienne LL, Cavalli F, Mazzucchelli L (2007) PTEN loss of expression predicts cetuximab efficacy in metastatic colorectal cancer patients. Br J Cancer 97:1139–1145
51. Edkins S, O'Meara S, Parker A, Stevens C, Reis M, Jones S, Greenman C, Davies H, Dalgliesh G, Forbes S, Hunter C, Smith R, Stephens P, Goldstraw P, Nicholson A, Chan TL, Velculescu VE, Yuen ST, Leung SY, Stratton MR, Futreal PA (2006) Recurrent KRAS codon 146 mutations in human colorectal cancer. Cancer Biol Ther 5:928–932
52. Kosaka T, Yatabe Y, Endoh H, Kuwano H, Takahashi T, Mitsudomi T (2004) Mutations of the epidermal growth factor receptor gene in lung cancer: biological and clinical implications. Cancer Res 64:8919–8923
53. Oliveira C, Westra JL, Arango D, Ollikainen M, Domingo E, Ferreira A, Velho S, Niessen R, Lagerstedt K, Alhopuro P, Laiho P, Veiga I, Teixeira MR, Ligtenberg M, Kleibeuker JH, Sijmons RH, Plukker JT, Imai K, Lage P, Hamelin R, Albuquerque C, Schwartz S Jr, Lindblom A, Peltomaki P, Yamamoto H, Aaltonen LA, Seruca R, Hofstra RM (2004) Distinct patterns of KRAS mutations in colorectal carcinomas according to germline mismatch repair defects and hMLH1 methylation status. Hum Mol Genet 13:2303–2311
54. Russo A, Bazan V, Agnese V, Rodolico V, Gebbia N (2005) Prognostic and predictive factors in colorectal cancer: Kirsten Ras in CRC (RASCAL) and TP53CRC collaborative studies. Ann Oncol 16 Suppl 4:iv44–iv49
55. Samowitz WS, Curtin K, Schaffer D, Robertson M, Leppert M, Slattery ML (2000) Relationship of Ki-ras mutations in colon cancers to tumor location, stage, and survival: a population-based study. Cancer Epidemiol Biomarkers Prev 9:1193–1197
56. Andreyev HJ, Norman AR, Cunningham D, Oates J, Dix BR, Iacopetta BJ, Young J, Walsh T, Ward R, Hawkins N, Beranek M, Jandik P, Benamouzig R, Jullian E, Laurent-Puig P, Olschwang S, Muller O, Hoffmann I, Rabes HM, Zietz C, Troungos C, Valavanis C, Yuen ST, Ho JW, Croke CT, O'Donoghue DP, Giaretti W, Rapallo A, Russo A, Bazan V, Tanaka M, Omura K, Azuma T, Ohkusa T, Fujimori T, Ono Y, Pauly M, Faber C, Glaesener R, de Goeij AF, Arends JW, Andersen SN, Lovig T, Breivik J, Gaudernack G, Clausen OP, De Angelis PD, Meling GI, Rognum TO, Smith R, Goh HS, Font A, Rosell R, Sun XF, Zhang H, Benhattar J, Losi L, Lee JQ, Wang ST, Clarke PA, Bell S, Quirke P, Bubb VJ, Piris J, Cruickshank NR, Morton D, Fox JC, Al-Mulla F, Lees N, Hall CN, Snary D, Wilkinson K, Dillon D, Costa J, Pricolo VE, Finkelstein SD, Thebo JS, Senagore AJ, Halter SA, Wadler S, Malik S, Krtolica K, Urosevic N (2001) Kirsten ras mutations in patients with colorectal cancer: the 'RASCAL II' study. Br J Cancer 85:692–696
57. Zerbe LK, Dwyer-Nield LD, Fritz JM, Redente EF, Shroyer RJ, Conklin E, Kane S, Tucker C, Eckhardt SG, Gustafson DL, Iwata KK, Malkinson AM (2008) Inhibition by erlotinib of primary lung adenocarcinoma at an early stage in male mice. Cancer Chemother Pharmacol 62:605–620
58. Keller JW, Franklin JL, Graves-Deal R, Friedman DB, Whitwell CW, Coffey RJ (2007) Oncogenic KRAS provides a uniquely powerful and variable oncogenic contribution among RAS family members in the colonic epithelium. J Cell Physiol 210:740–749
59. Wang JY, Wang YH, Jao SW, Lu CY, Kuo CH, Hu HM, Hsieh JS, Chong IW, Cheng TL, Lin SR (2006) Molecular mechanisms underlying the tumorigenesis of colorectal adenomas: correlation to activated K-ras oncogene. Oncol Rep 16:1245–1252
60. Castagnola P, Giaretti W (2005) Mutant KRAS, chromosomal instability and prognosis in colorectal cancer. Biochim Biophys Acta 1756:115–125
61. Benvenuti S, Sartore-Bianchi A, Di NF, Zanon C, Moroni M, Veronese S, Siena S, Bardelli A (2007) Oncogenic activation of the RAS/RAF signaling pathway impairs the response of metastatic colorectal cancers to anti-epidermal growth factor receptor antibody therapies. Cancer Res 67:2643–2648
62. De RW, Piessevaux H, De SJ, Janssens M, De HG, Personeni N, Biesmans B, Van Laethem JL, Peeters M, Humblet Y, Van CE, Tejpar S (2008) KRAS wild-type state predicts survival and is associated to early radiological response in metastatic colorectal cancer treated with cetuximab. Ann Oncol 19:508–515
63. Di FF, Blanchard F, Charbonnier F, Le PF, Lamy A, Galais MP, Bastit L, Killian A, Sesboue R, Tuech JJ, Queuniet AM, Paillot B, Sabourin JC, Michot F, Michel P, Frebourg T (2007) Clinical relevance of KRAS mutation detection in metastatic colorectal cancer treated by Cetuximab plus chemotherapy. Br J Cancer 96:1166–1169
64. Khambata-Ford S, Garrett CR, Meropol NJ, Basik M, Harbison CT, Wu S, Wong TW, Huang X, Takimoto CH, Godwin AK, Tan BR, Krishnamurthi SS, Burris HA III, Poplin EA, Hidalgo M, Baselga J, Clark EA, Mauro DJ (2007) Expression of epiregulin and amphiregulin and K-ras mutation status predict disease control in metastatic colorectal cancer patients treated with cetuximab. J Clin Oncol 25:3230–3237
65. Lievre A, Bachet JB, Boige V, Cayre A, Le CD, Buc E, Ychou M, Bouche O, Landi B, Louvet C, Andre T, Bibeau F, Diebold MD, Rougier P, Ducreux M, Tomasic G, Emile JF, Penault-Llorca F, Laurent-Puig P (2008) KRAS mutations as an independent prognostic factor in patients with advanced colorectal cancer treated with cetuximab. J Clin Oncol 26:374–379
66. Juan T, Suggs S, Wolf M, Sarosi I, Freeman D, Oliner K, Bakkar A, Patterson SD (2008) A comparability study of 4 commercial KRAS tests. American Association for Cancer Research (AACR) Annual Meeting, April 12–16, 2008, Abstract #1811
67. Kressner U, Bjorheim J, Westring S, Wahlberg SS, Pahlman L, Glimelius B, Lindmark G, Lindblom A, Borresen-Dale AL (1998) Ki-ras mutations and prognosis in colorectal cancer. Eur J Cancer 34:518–521
68. Hayes VM, Westra JL, Verlind E, Bleeker W, Plukker JT, Hofstra RM, Buys CH (2000) New comprehensive denaturing-gradient-gel-electrophoresis assay for KRAS mutation detection applied to paraffin-embedded tumours. Genes Chromosomes Cancer 29:309–314
69. Zhao C, Xu G, Shi X, Ma J, Lu S, Yang Q (2004) Detection of K-ras exon 1 mutations by constant denaturant capillary electrophoresis. Biomed Chromatogr 18:538–541
70. Chaubert P, Bautista D, Benhattar J (1993) An improved method for rapid screening of DNA mutations by nonradioactive single-strand conformation polymorphism procedure. Biotechniques 15:586
71. Khanna M, Park P, Zirvi M, Cao W, Picon A, Day J, Paty P, Barany F (1999) Multiplex PCR/LDR for detection of K-ras mutations in primary colon tumors. Oncogene 18:27–38
72. Ogino S, Kawasaki T, Brahmandam M, Yan L, Cantor M, Namgyal C, Mino-Kenudson M, Lauwers GY, Loda M, Fuchs CS (2005) Sensitive sequencing method for KRAS mutation detection by pyrosequencing. J Mol Diagn 7:413–421
73. Poehlmann A, Kuester D, Meyer F, Lippert H, Roessner A, Schneider-Stock R (2007) K-ras mutation detection in colorectal cancer using the pyrosequencing technique. Pathol Res Pract 203:489–497

74. Fox JC, England J, White P, Ellison G, Callaghan K, Charlesworth NR, Hehir J, McCarthy TL, Smith-Ravin J, Talbot IC, Snary D, Northover JM, Newton CR, Little S (1998) The detection of K-ras mutations in colorectal cancer using the amplification-refractory mutation system. Br J Cancer 77:1267–1274
75. van Heek NT, Clayton SJ, Sturm PD, Walker J, Gouma DJ, Noorduyn LA, Offerhaus GJ, Fox JC (2005) Comparison of the novel quantitative ARMS assay and an enriched PCR-ASO assay for K-ras mutations with conventional cytology on endobiliary brush cytology from 312 consecutive extrahepatic biliary stenoses. J Clin Pathol 58:1315–1320
76. Cross J (2008) DxS Ltd. Pharmacogenomics 9:463–467
77. Mixich F, Ioana M, Voinea F, Saftoiu A, Ciurea T (2007) Noninvasive detection through REMS-PCR technique of K-ras mutations in stool DNA of patients with colorectal cancer. J Gastrointestin Liver Dis 16:5–10
78. Amicarelli G, Shehi E, Makrigiorgos GM, Adlerstein D (2007) FLAG assay as a novel method for real-time signal generation during PCR: application to detection and genotyping of KRAS codon 12 mutations. Nucleic Acids Res 35:e131
79. Kimura K, Nagasaka T, Hoshizima N, Sasamoto H, Notohara K, Takeda M, Kominami K, Iishii T, Tanaka N, Matsubara N (2007) No duplicate KRAS mutation is identified on the same allele in gastric or colorectal cancer cells with multiple KRAS mutations. J Int Med Res 35:450–457
80. Hashimoto M, Barany F, Xu F, Soper SA (2007) Serial processing of biological reactions using flow-through microfluidic devices: coupled PCR/LDR for the detection of low-abundant DNA point mutations. Analyst 132:913–921
81. Wabuyele MB, Farquar H, Stryjewski W, Hammer RP, Soper SA, Cheng YW, Barany F (2003) Approaching real-time molecular diagnostics: single-pair fluorescence resonance energy transfer (spFRET) detection for the analysis of low abundant point mutations in K-ras oncogenes. J Am Chem Soc 125:6937–6945
82. Li J, Zhong W (2007) Typing of multiple single-nucleotide polymorphisms by a microsphere-based rolling circle amplification assay. Anal Chem 79:9030–9038
83. Zhang P, Chu X, Xu X, Shen G, Yu R (2008) Electrochemical detection of point mutation based on surface ligation reaction and biometallization. Biosens Bioelectron 23:1435–1441
84. Syngal S, Stoffel E, Chung D, Willett C, Schoetz D, Schroy P, Jagadeesh D, Morel K, Ross M (2006) Detection of stool DNA mutations before and after treatment of colorectal neoplasia. Cancer 106:277–283

Virchows Arch (2008) 453:433–440
DOI 10.1007/s00428-008-0674-x

REVIEW AND PERSPECTIVE

Current practices in performing frozen sections for thyroid and parathyroid pathology

Robert Y. Osamura · Jennifer L. Hunt

Received: 10 June 2008 / Revised: 4 September 2008 / Accepted: 8 September 2008 / Published online: 1 October 2008

Abstract In this review article, current trends in thyroid and parathyroid frozen sections are discussed. In Japan and other countries, the numbers of thyroid frozen sections have been dramatically decreasing over the past decade. The decline in the number of thyroid frozen sections has been attributed to two major factors: highly diagnostic preoperative fine needle aspiration for papillary carcinomas, the most frequent type of thyroid cancers, and the acknowledgment in the literature of the disadvantageous frozen sections for follicular tumors. Several authors have argued that the frozen section of thyroid nodules should be limited only to cases that have a preoperative cytology diagnosis as "atypical" or "suspicious". In contrast, frozen sections for parathyroid glands have been increasing in numbers. This increase is thought to be largely due to the high number of parathyroidectomies for secondary hyperplasia in dialysis patients. Frozen sections are usually performed to confirm the removal of parathyroid tissue for either cyropreservation or auto-transplantation. It is concluded that thyroid and parathyroid frozen section examination is restricted to selected situations.

A part of this study was presented at the 21st European Congress of Pathology, In the Symposium Frozen Section Diagnosis in Endocrine Tumors on September 9, 2007.

R. Y. Osamura (✉)
Department of Pathology, Tokai University School of Medicine,
143 Shimokasuya,
Isehara City, Kanagawa 259-1193, Japan
e-mail: osamura@is.icc.u-tokai.ac.jp

J. L. Hunt
Department of Anatomic Pathology, Cleveland Clinic,
Cleveland, OH, USA

Keywords Thyroid · Cancer · Parathyroid · Hyperparathyroidism · Frozen section

Introduction

Frozen sections are performed with the aim to provide a rapid diagnosis that has immediate impact on surgical decision making [1, 2]. Frozen section examinations in endocrine pathology have been most commonly used for intraoperative assessment of thyroid and parathyroid tumors and cervical lymph node metastases. In recent years, however, the number of frozen sections in thyroid surgery has been steadily decreasing worldwide [3–5]. This decline has been attributed to two major factors: the high diagnostic accuracy of fine needle aspiration (FNA) cytology for papillary thyroid carcinoma (PTC) and the low sensitivity of frozen section diagnosis for follicular lesions of the thyroid. Many institutions have therefore restricted the use of thyroid frozen sections to thyroid nodules with a preoperative cytology diagnosis of "atypical" or "suspicious."

In contrast, frozen sections for parathyroid diseases have been increasing in number. This is mainly due to an increase in the number of parathyroidectomies for secondary hyperplasia in chronic dialysis patients, while surgery for parathyroid adenomas has remained fairly constant. However, in some institutions, the use of rapid intraoperative determination of the serum level of parathyroid hormone has decreased the need to confirm the removal of a parathyroid adenoma by frozen section. Some authors believe that this serum test may eventually eliminate the need for frozen section examination in surgical treatment of parathyroid adenoma [6–8].

The arguments for and against performing frozen sections in thyroid and parathyroid surgery are not just economic and not just based on specificity and sensitivity rates. Artifacts induced by freezing can substantially alter the nuclear morphology, and the tissue can be largely wasted in the course of tissue sectioning. These factors are particularly important in small lesions, from which only one or two sections may be obtained.

This review will describe recent trends in frozen section diagnosis for thyroid and parathyroid lesions and provide some practical tips and techniques for approaching thyroid and parathyroid frozen section pathology.

Thyroid frozen sections

Incidence of frozen sections on thyroid glands

Several recent studies have reported a decrease in the number of frozen section diagnosis for thyroid lesions [3–5, 9]. To some degree, the number and type of thyroid frozen sections are likely to depend on the experience of the surgical team, the case volume, and on the prevalent types of surgeries being performed. To illustrate the trends in frozen section usage with reference to these variables, the incidence and practices around thyroid frozen sections at four different Japanese hospitals were analyzed.

Tokai University Hospital

Tokai University Hospital is a large teaching hospital. In 2006, 55 surgeries were performed for thyroid-related diseases, and no frozen sections were done. When analyzed as a trend over time, there was a decrease in frozen sections noted over the past 15 years (Fig. 1), despite a near-constant number of surgeries for a similar disease spectrum.

Itoh Hospital

Itoh Hospital is a specialized hospital that specializes almost entirely on thyroid management and surgery. In 2006, for a total of 1,358 cases of thyroid-related surgery performed (Fig. 2), no frozen sections were done.

Kuma Hospital

At Kuma Hospital, another thyroid-specialized facility in Japan, around 1,800 cases of thyroid-related surgery were performed in 2006. Approximately 10% of these cases did have frozen sections. The primary reason for these frozen sections was to evaluate for direct tracheal invasion by cancer or to evaluate potential parathyroid tissue for auto-transplantation during total thryoidectomy.

Isehara Kyodo Hospital

Isehara Kyodo Hospital is a community hospital in Japan with a limited number of thyroid resections. Between 2002 and 2006, 74 thyroid resections were performed, and of these, 53% had frozen sections. This series included 22 cases with follicular lesions, eight cases of PTC and seven cases with miscellaneous diagnoses. This represented 5% of all frozen sections done in that institution.

Aside from the differences in utilization of thyroid frozen sections because of experience level and case volume, there is likely also a contribution from better education of both surgeons and pathologists around the standard of care of preoperative FNA and the utility of thyroid frozen sections, especially regarding diagnostic sensitivity and specificity.

First, it has become the standard of care to approach most thyroid nodules with a preoperative FNA [10]. It is recognized that thyroid FNA cytology is highly sensitive and specific for a diagnosis of PTC, with diagnostic

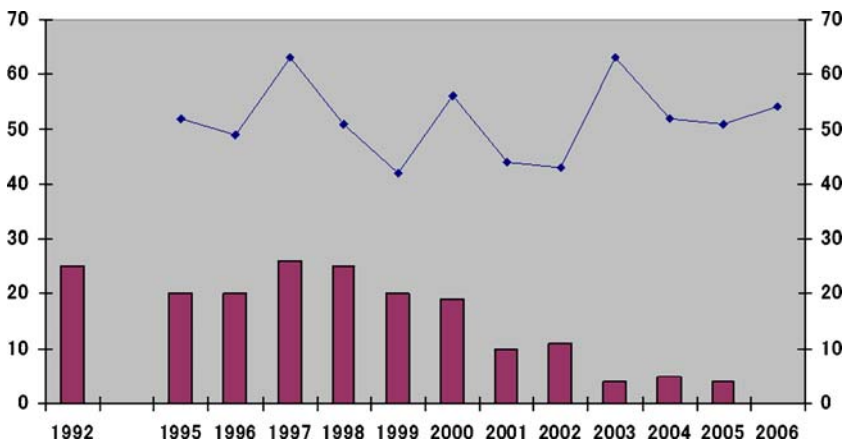

Fig. 1 Trend over 14-year period for the use of frozen section diagnosis for thyroid surgeries at Tokai University Hospital. The *red bars* demonstrate the number of frozen sections performed for thyroids each year, and the *blue line* indicates the number of surgeries performed for thyroid disease in each year. The number of frozen sections decreased dramatically, while the number of overall thyroid surgeries remained relatively constant

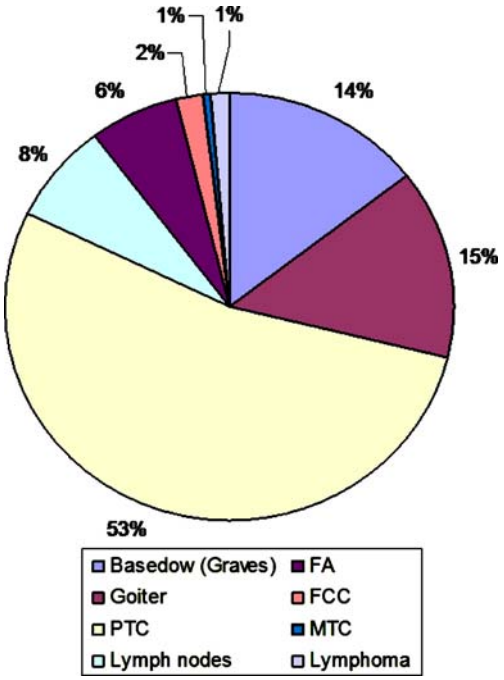

Fig. 2 Incidence of different diseases and diagnoses in surgical thyroid lesions at Itoh Hospital for Thyroid Diseases in 2006. None of these cases underwent frozen section

features including specific cytologic abnormalities such as intranuclear inclusions and nuclear grooves (Fig. 3) [11]. For example, between 2002 and 2006 at Tokai University Hospital, a diagnosis of PTC was made in 105 patients in which both FNA and histology diagnoses were performed. In these patients, the preoperative FNA diagnosis was "PTC" in 91 cases and "suggestive of PTC" in another six cases. This represents a sensitivity of 92.4% (97/105). Because of the high sensitivity and specificity of FNA, LiVolsi and Baloch [12] emphasized that the intraoperative frozen sections should no longer be performed on thyroid nodules with a definitive preoperative FNA diagnosis of PTC.

In contrast, for tumors that do not meet the criteria for a diagnosis of PTC on FNA but show some suspicious or worrisome features, there may be a distinct role for frozen section examination. Mittendorf et al. [13] refined the conditions in which frozen section can be the most useful. They reported 45 patients (7%) with preoperative FNA that was suspicious but not diagnostic of PTC. Eighteen of these patients (40%) later had histologically proven carcinoma, whereas the remainder had benign disease. Prominent nuclear inclusions and/or grooves, papillary formation, and the absence of colloid were features that were most highly associated with the final diagnosis of PTC ($P<0.05$). Rare intranuclear inclusions and/or grooves alone in an otherwise benign-appearing specimen were uniformly associated with benign disease. Importantly, no clinical features could reliably identify the patients that had true malignant disease. Frozen section examination was performed in 27 of the surgical patients, and the results of it altered treatment decision in 15 patients (56%). Therefore, frozen section examination was thought to be of value for

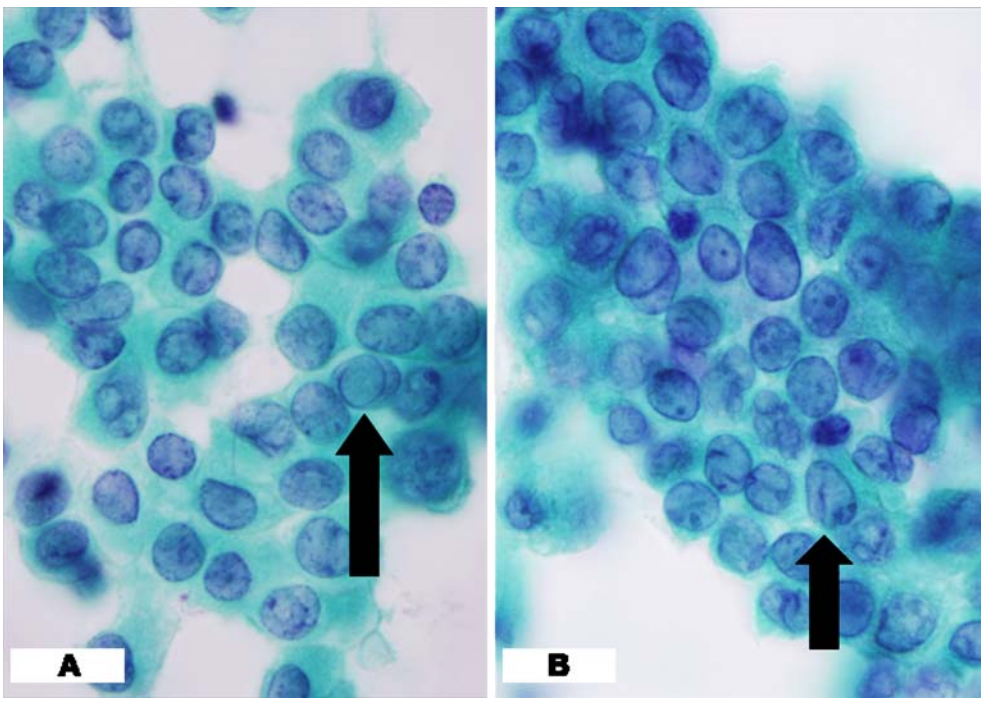

Fig. 3 Papanicolaou stain: Cytology smear preparations from a preoperative fine needle aspiration of papillary carcinoma. **a** An intra-nuclear inclusion (*arrow*); **b** nuclear grooves (*arrow*)

determining the extent of the thyroidectomy in these patients. The usefulness of thyroid frozen sections may also be extended to the cases with other malignancies, including anaplastic or medullary carcinomas or atypical lymphoid cells in the aspirated materials.

The second contributing factor to the decreasing rate of thyroid frozen sections is that both surgeons and pathologists have recognized that frozen section diagnosis has a very low sensitivity and specificity in most follicular tumors of the thyroid [3]. These tumors obviously require careful and complete sampling for an accurate diagnosis of invasion, and this is not a practical approach for frozen section examination in most routine pathology laboratories [12]. In addition to problems induced by incomplete sampling in frozen sections, another issue is the fact that nuclear details are obscured by artifacts in frozen sections (Table 1). Therefore, if only a frozen section is performed on follicular variant of PTC, it is very unlikely that the nuclear features of PTC will be recognized (Fig. 4). Performing intraoperative cytology, which is discussed below, will help to overcome this limitation (Fig. 5).

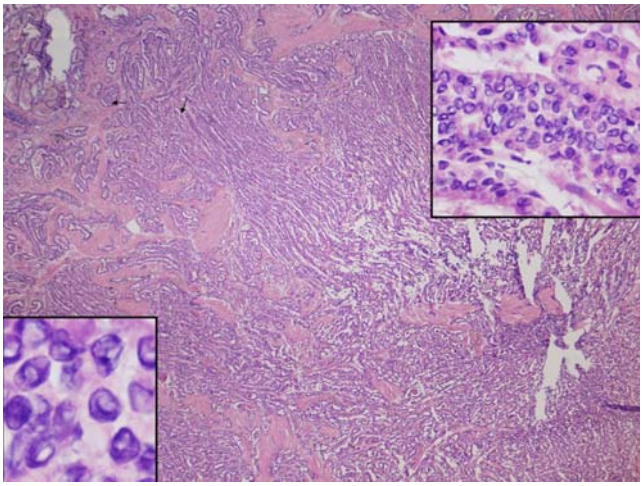

Fig. 4 H&E stained frozen sections: The background image shows a frozen section from a clearly invasive tumor with papillary growth. The *insets* demonstrate the nuclear artifacts from frozen section, which both show obscuring of classic nuclear features of papillary carcinoma

Handling of thyroid tissue for frozen sections

In general, we recommend the following procedure for handling a fresh thyroidectomy specimen. The specimen should be inspected for an intact capsule and then be inked along the external surface. Subsequently, the thyroid can be serially sectioned, usually from superior to inferior.

Recommendations for specific circumstances

Preoperative FNA was "suspicious" or "atypical"

The only way to adequately visualize the nuclear features of PTC in the intraoperative setting is to perform cytologic smears. We prefer the use of scrape preparations over touch preparations. Touch preparations can be heavily contaminated with colloid, and the cellular elements may be quite sparse. In contrast, by carefully blotting away excess colloid from the surface of a lesion and then gently scraping and smearing onto a blank slide, abundant cellular elements can usually be obtained for cytologic interpretation. Cellularity does not need to be assessed, as the purpose of the cytologic intraoperative preparation is only to look for the nuclear features of PTC (Fig. 5; Table 2).

Table 1 Advantages and disadvantages of frozen section examination

Advantages	Disadvantages
Diagnosis available for immediate decision making	Tissue wasting secondary to sectioning Preliminary nature of the diagnosis Sampling errors

Encapsulated nodules

When an encapsulated lesion is discovered, it is recommended that no frozen section is to be performed. The only diagnostic findings in encapsulated follicular lesions will come from assessing the nuclear features and from assessing the entire capsule. In some circumstances, scrape preparations can be performed on an encapsulated lesion. This would be most helpful for ruling out a well-defined follicular variant of PTC. It is important to recognize, however, that the follicular variant of PTC remains a difficult diagnosis intraoperatively even with good cytologic preparations.

Multinodular goiter

In the case of a multinodular goiter, frozen sections should not be performed unless one nodule is worrisome or suspicious based on the gross appearance.

Small lesions (<1 cm)

Lesions smaller than 1 cm should not be examined by frozen section. It is especially critical to absolutely avoid freezing an entire lesion. The resulting tissue alterations may make a diagnosis on permanent sections nearly impossible.

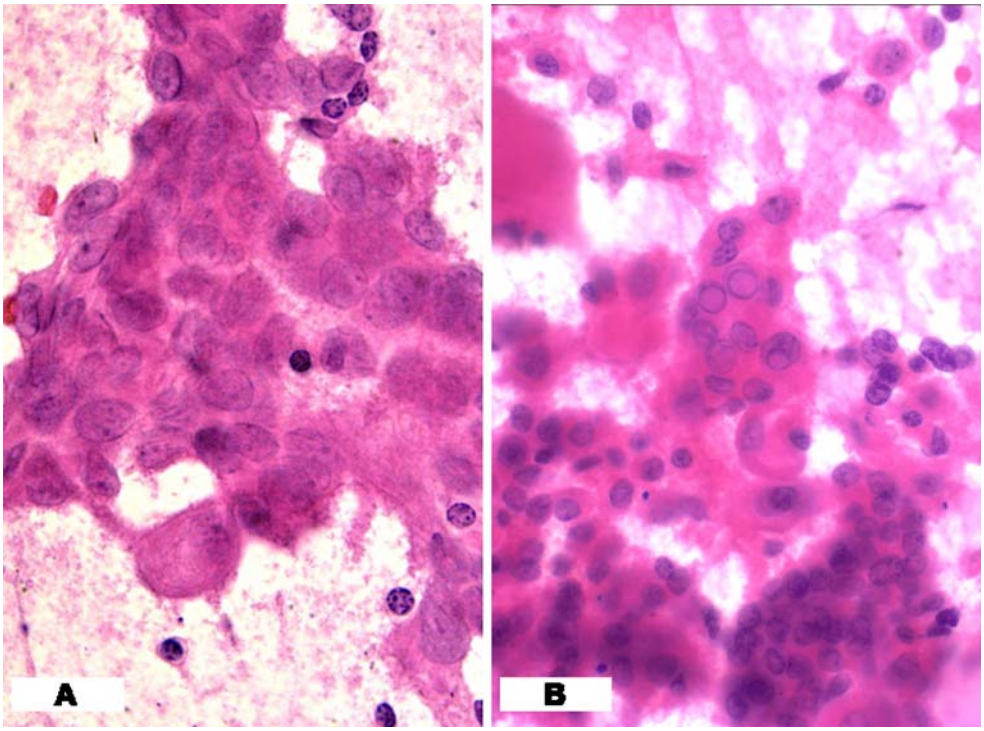

Fig. 5 H&E stain: Cytology scrape preparations from thyroid nodules obtained intraoperatively during frozen section. Note the easily identified features of papillary carcinoma, including grooves (**a**) and inclusions (**b**)

Pitfalls of thyroid frozen section

The most significant pitfall for frozen section in thyroid nodules is a papillary hyperplastic nodule. These lesions have papillary architecture, but the nuclear features are quite bland. Again, using a combination of frozen section and scrape preparation with cytology will enable the pathologist to recognize these lesions.

Parathyroid frozen sections

In contrast to the marked decrease in thyroid frozen sections, there appears to be an increase in the number of parathyroid frozen sections. Many of these cases are related to secondary hyperparathyroidism, where multiple glands are involved (Fig. 6).

At Tokai University Hospital, for example, the numbers of frozen sections for parathyroid adenomas have not changed, but the cases of secondary hyperparathyroidism have increased (Fig. 7). Surgery for secondary hyperparathyroidism, which is often done in the setting of long-standing dialysis for renal disease, includes a total parathyroidectomy with removal of all four glands as the standard of care. Generally, one gland is used for autotransplantation, with intramuscular reimplantation of minced parathyroid fragments of about 1 mm in size into the arm.

Parathyroid frozen sections are typically performed for several scenarios, including tissue identification in normal-sized glands for differentiating parathyroid from fat, thymus, thyroid, lymph node, and other tissue and identification of intra-thyroidal parathyroid gland.

Even in today's surgical practice, preoperative localization of enlarged parathyroid glands remains difficult. It has been estimated that the accuracy of preoperative imaging diagnosis for parathyroids is only about 70% by ultrasound or 75% by methoxyisobutyl isonitrile and CT [14]. The overall insensitivity of these imaging studies is partially responsible for the need for frozen section confirmation of parathyroid tissue during surgery. Frozen section for parathyroids remains an important diagnostic approach when parathyroid tissue is suspected, but the gross appearance is not diagnostic. Frozen sections of parathyroid suffer from

Table 2 Situations in which a thyroid frozen examination is likely or unlikely to be useful

Cytology diagnosis	Gross impression	Frozen potentially useful	Frozen unlikely to be useful
Any	Nodular goiter		X
Follicular or Hurthle cell lesion	Encapsulated nodule		X
Papillary carcinoma	Any		X
Atypical or suspicious for papillary carcinoma	Nodule or lesion	X	
Any	Nodule under 1 cm		X

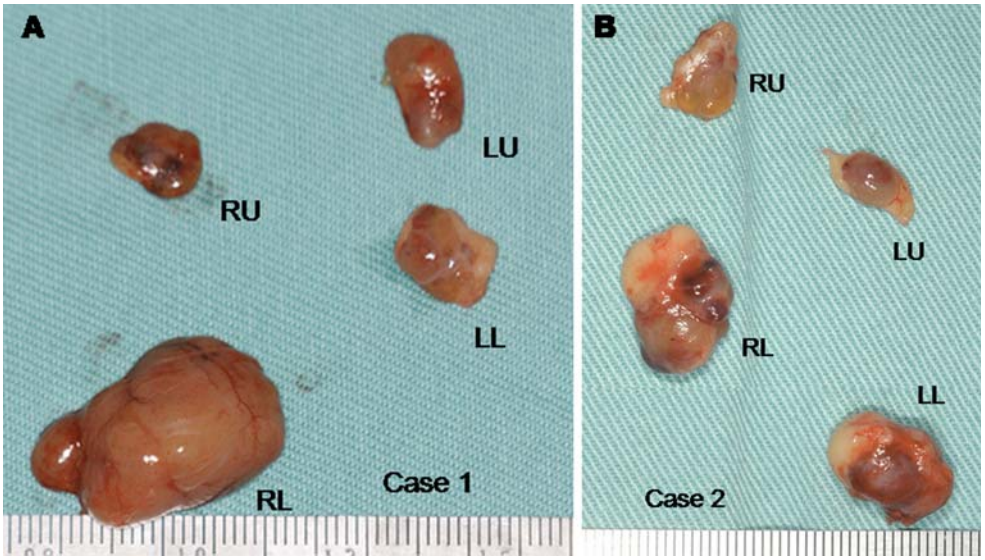

Fig. 6 Two separate cases of parathyroid gland hyperplasia. **a** A case where one gland is significantly more enlarged than the other three glands, which are still larger than normal. **b** A case of parathyroid hyperplasia in which the glands are equally enlarged

similar artifacts as do thyroid frozens (Fig. 8). However, the nuclear features are not used diagnostically for parathyroids, and therefore, the sensitivity and specificity of parathyroid frozens remain quite high.

Despite the increase in surgical interventions for hyperparathyroidism, one qualifying influence on the number of parathyroid frozen sections has been the incorporation of rapid intraoperative parathyroid hormone levels (RI-PTH) into surgical management. In parathyroid adenoma surgeries that are coupled with RI-PTH, frozen section confirmation of the hypercellular gland may therefore no longer be necessary [15–17]. Guarda et al. [16] studied 141 patients who underwent parathyroid surgery, 125 for adenoma, and 16 for secondary hyperplasia. Their results suggested that RI-PTH can be an essential guide for the surgeon performing focused parathyroid surgery. Frozen sections are no longer needed because a significant drop of PTH levels after resection of the largest gland is a far better indicator of adenoma removal and subsequent cure than histologic confirmation.

Handling of parathyroid tissue for parathyroid frozen sections

Parathyroids are characterized by assessing the size and the weight of the glands. Both of these measurements can be important for identifying enlarged and hypercellular glands. Representative sections can be frozen from larger glands,

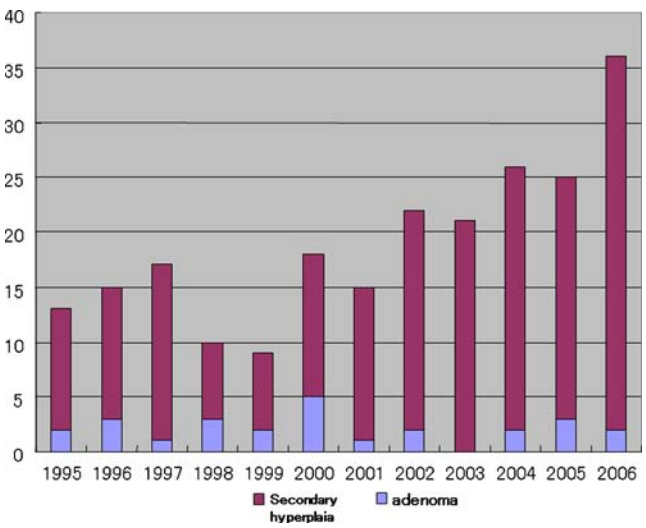

Fig. 7 This graph demonstrates the incidence of parathyroidectomy frozen sections requested for secondary hyperplasia and for parathyroid adenoma over an 11-year period at Tokai University Hospital

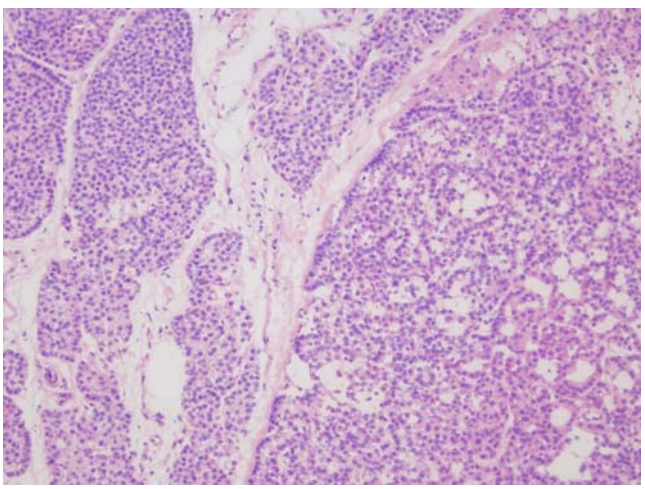

Fig. 8 H&E, frozen section: This image demonstrates the features of an enlarged hypercellular parathyroid gland at the time of frozen section. The chief cells (*left half of image*) and oxyphilic cells (*right half of image*) cannot be well seen because they are obscured by frozen section artifacts

particularly when there are no worrisome features. Particular attention should be paid if there are grossly visible broad fibrous bands or if the gland is found to be adherent to adjacent structures intraoperatively. These features should alert the pathologist to the possibility of a parathyroid carcinoma.

Recommendations for specific circumstances

Parathyroid surgery with the use of rapid intraoperative parathyroid hormone assays

In the setting of parathyroid adenoma surgery, frozen sections should be performed if rapid intraoperative testing of serum PTH level is not available or if the surgeon needs typing of the removed tissue. Frozen section does not need to be performed in conjunction with *RI-PTH* serum measurement, but it is recommended to keep fresh tissue until the results of the RI-PTH are available. If a significant drop in the PTH level is achieved, no freezing is necessary. If there is no significant drop, a frozen section should be performed in order to guide the surgeon.

Very small fragments

It used to be a standard practice for a surgeon to biopsy an unaffected parathyroid gland to assess for cellularity. With the advent of RI-PTH, this practice has become less important. When very small fragments are sent for freezing, the major pitfall is cutting through the tissue while sectioning. Only careful frozen section technique can reduce this risk.

Thymus sent to rule-out intrathymic parathyroid

There is no good solution to assess the cervical thymus intraoperatively because the fat tissue in the specimen will not freeze well. The best approach will be a careful gross inspection of serially sectioned tissue to identify any potential enlarged parathyroid glands.

Parathyroids with worrisome clinical or histologic features

It is particularly important to recognize the potential signs of malignancy in a parathyroid gland intraoperatively. These would include adherence to local structures, broad fibrous bands, increased mitotic activity, or increased pleomorphism. It is not essential to make a diagnosis of parathyroid carcinoma on frozen section, but it is important to alert the clinician to this possibility so that this gland is not used for autotransplantation. Obviously, it is devastating to re-implant a gland only to discover that the permanent sections reveal a carcinoma [18]. Furthermore, identification of the features of a potential carcinoma can enable the surgeon to perform an en bloc resection of the gland, which is considered to be the treatment of choice for parathyroid carcinoma [18].

Conclusions

The number of cases of thyroid frozen sections has decreased remarkably in recent years. This is, on the one hand, due to the excellent results of the preoperative diagnosis by FNA cytology, and on the other hand, the recognition of the low sensitivity of frozen section examination in case of a follicular thyroid lesion. However, it is particularly important to note that thyroid frozen sections are recommended in the cases "suspicious" for PTC or "atypical" by FNA. The number of cases of parathyroid frozen sections may be increasing, likely due to an increasing incidence of parathyroid hyperplasia in dialysis patients. The use of rapid intraoperative PTH testing has the potential to decrease the need for frozen sections for single gland disease. In order to obtain the full benefit of thyroid and parathyroid frozen sections, clear understanding between the surgeon and the pathologist of the pitfalls and risks of frozen section should be a priority in discussions.

Acknowledgment The authors thank Dr. Kaori Kameyama and Dr. Mitsuyoshi Hirokawa for providing pertinent data at Itoh Hospital and Kuma Hospital, respectively, and Professor Guenter Klöppel for reading the manuscript. The authors also thank Itoh Hospital, Kuma Hospital and Isehara Kyodo Hospital for providing pertinent data to pursue this study.

Conflict of interest statement We declare that we have no conflict of interest.

References

1. Novis DA, Gephardt GN, Zarbo RJ (1996) Interinstitutional comparison of frozen section consultation in small hospitals: a College of American Pathologists Q-Probes study of 18,532 frozen section consultation diagnoses in 233 small hospitals. Arch Pathol Lab Med 120:1087–1093
2. Gephardt GN, Zarbo RJ (1996) Interinstitutional comparison of frozen section consultations. A college of American Pathologists Q-Probes study of 90,538 cases in 461 institutions. Arch Pathol Lab Med 120:804–809
3. Miller MC, Rubin CJ, Cunnane M et al (2007) Intraoperative pathologic examination: cost effectiveness and clinical value in patients with cytologic diagnosis of cellular follicular thyroid lesion. Thyroid 17:557–565
4. Makay O, Icoz G, Gurcu B et al (2007) The ongoing debate in thyroid surgery: should frozen section analysis be omitted? Endocr J 54:385–390
5. Huber GF, Dziegielewski P, Matthews TW et al (2007) Intraoperative frozen-section analysis for thyroid nodules: a step toward clarity or confusion? Arch Otolaryngol Head Neck Surg 133:874–881

6. Iacobone M, Scarpa M, Lumachi F, Favia G (2005) Are frozen sections useful and cost-effective in the era of intraoperative qPTH assays? Surgery 138:1159–1164, (discussion 1164–1165)
7. Elliott DD, Monroe DP, Perrier ND (2006) Parathyroid histopathology: is it of any value today? J Am Coll Surg 203:758–765
8. Karakousis GC, Han D, Kelz RR et al (2007) Interpretation of intra-operative PTH changes in patients with multi-glandular primary hyperparathyroidism (pHPT). Surgery 142:845–850, (discussion 850 e1–e2)
9. Haymart MR, Greenblatt DY, Elson DF, Chen H (2008) The role of intraoperative frozen section if suspicious for papillary thyroid cancer. Thyroid 18:419–423
10. Anton RC, Wheeler TM (2005) Frozen section of thyroid and parathyroid specimens. Arch Pathol Lab Med 129:1575–1584
11. Basolo F, Ugolini C, Proietti A, Iacconi P, Berti P, Miccoli P (2007) Role of frozen section associated with intraoperative cytology in comparison to FNA and FS alone in the management of thyroid nodules. Eur J Surg Oncol 33:769–775
12. LiVolsi VA, Baloch ZW (2005) Use and abuse of frozen section in the diagnosis of follicular thyroid lesions. Endocr Pathol 16: 285–293
13. Mittendorf EA, Khiyami A, McHenry CR (2006) When fine-needle aspiration biopsy cannot exclude papillary thyroid cancer: a therapeutic dilemma. Arch Surg. 141:961–966, (discussion 966)
14. Mihai R, Gleeson F, Buley ID, Roskell DE, Sadler GP (2006) Negative imaging studies for primary hyperparathyroidism are unavoidable: correlation of sestamibi and high-resolution ultrasound scanning with histological analysis in 150 patients. World J Surg 30:697–704
15. Dewan AK, Kapadia SB, Hollenbeak CS, Stack BC Jr (2005) Is routine frozen section necessary for parathyroid surgery? Otolaryngol Head Neck Surg 133:857–862
16. Guarda LA (2004) Rapid intraoperative parathyroid hormone testing with surgical pathology correlations: the "chemical frozen section". Am J Clin Pathol 122:704–712
17. Carter AB, Howanitz PJ (2003) Intraoperative testing for parathyroid hormone: a comprehensive review of the use of the assay and the relevant literature. Arch Pathol Lab Med 127: 1424–1442
18. Rosen IB, Young JE, Archibald SD, Walfish PG, Vale J (1994) Parathyroid cancer: clinical variations and relationship to autotransplantation. Can J Surg 37:465–469

Virchows Arch (2008) 453:441–448
DOI 10.1007/s00428-008-0678-6

REVIEW AND PERSPECTIVE

Gastroenteropancreatic neuroendocrine tumors: indications for and pitfalls of frozen section examination

Anne Couvelard · Alain Sauvanet

Received: 1 July 2008 / Revised: 8 September 2008 / Accepted: 12 September 2008 / Published online: 7 October 2008

Abstract Gastroenteropancreatic neuroendocrine tumors constitute a heterogeneous group of neoplasms. Surgical resection remains the only curative treatment. Frozen section examination is requested by the surgeon in a large variety of surgical situations, but its use differs greatly according to the location of the tumor and the type of surgery performed. The objective of this review is to describe the main indications for and pitfalls of frozen section examination of gastroenteropancreatic neuroendocrine tumors.

Keywords Gastroenteropancreatic neuroendocrine tumors · Frozen section examination · Surgery · Pathology

Gastroenteropancreatic neuroendocrine tumors (GEP-NETs) are rare tumors that are mainly treated in tertiary referral centers, especially those in certain locations such as the pancreas or the liver. Surgical resection remains the best and the only curative treatment for patients [1]. The surgical goals are to: (1) prolong survival by resecting the primary tumor and any nodal or hepatic metastases, (2) control the symptoms related to hormonal secretion and (3) prevent or treat local complications. In the context of GEP-NETs, frozen section examination (FSE) is requested by surgeons in a variety of situations; its use depends mainly on the location of the tumor in the digestive system, on the type of surgery performed and on the presence or lack of hormonal symptoms. Indeed, small functioning tumors can be diagnosed clinically very early without an obvious lesion visualized by imaging techniques [1, 2]. The main reason then for calling for frozen section examination in the evaluation of GEP-NETs is to confirm that the tumor has been resected, to check the diagnosis and to evaluate the extent of the disease. In contrast to exocrine tumors (adenocarcinomas), the main purpose is, with few exceptions, not to evaluate the adequateness of the resection, since endocrine tumors are generally well delineated and require only a limited surgical margin.

It is difficult to analyze the management of frozen sectioning in GEP-NETs, since these tumors develop in different locations with very different surgical strategies and may show a heterogeneous prognosis, being either benign or malignant with aggressive behavior [3–7]. This review is based on a review of the pertinent literature and on the surgical and pathological experience of two authors from a single institution.

We will first discuss the main histological differential diagnoses which may be encountered in all locations in the digestive tract during FSE. Then, since the surgical management of digestive endocrine tumors and the role and value of FSE differ greatly according to the localization in the digestive system, we will discuss successively the main indications, differential diagnosis, and pitfalls in relation to the different locations (pancreas, ampulla of Vater, duodenum, small intestine, appendix, liver, peritoneum, and other rare locations).

A. Couvelard (✉)
Université Paris 7, UFR médicale,
Assistance Publique-Hôpitaux de Paris, Hôpital Beaujon,
Service d'Anatomie Pathologique,
100 Boulevard du Général Leclerc,
92110 Clichy, France
e-mail: anne.couvelard@bjn.aphp.fr

A. Sauvanet
Université Paris 7, UFR médicale,
Assistance Publique-Hôpitaux de Paris,
Hôpital Beaujon, Service de Chirurgie Hépatique et Pancréatique,
92110 Clichy, France

Frozen section examination: the main histological differential diagnosis

In most frozen sections, digestive endocrine tumors display a characteristic histology. Most surgically resected tumors are well-differentiated, easy to recognize on hematoxylin and eosin stained slides and accurately typed on frozen sections (Fig. 1a) [5, 8]. However, in some cases the histological diagnosis can be challenging. Diagnostic difficulties are related to both technical and morphological factors. One crucial differential diagnosis in any digestive location is versus adenocarcinomas. Aggressive endocrine tumors may be poorly delineated and contain irregular cells and thus mimic an adenocarcinoma. In addition, GEP-NETs may be accompanied by fibrosis, which can mimic the desmoplastic stroma that is the hallmark of most adenocarcinomas (Fig. 1b). Uncommon histological variants of GEP-NETs are also challenging during FSE. They include (1) clear cell endocrine tumors (Fig. 1c), which can be very difficult to recognize and whose differential diagnosis includes metastatic renal clear cell carcinoma and mucinous adenocarcinoma [9]; (2) oncocytic endocrine tumors that contain very irregular and atypical cells whose appearance does not reveal their endocrine nature (Fig. 1d) [10] and (3) endocrine tumors with a tubular component, especially somatostatin cell tumors, that may evoke a mistaken frozen section diagnosis of adenocarcinoma or, in pancreatic location, of chronic pancreatitis [11]. Other histological differential diagnoses depend highly on the location of the GEP-NETs and will be discussed successively in the corresponding sections below.

Very rarely, surgically resected tumors are poorly differentiated endocrine carcinomas. This is only occasional since they represent less than 5% of all digestive endocrine tumors, are mainly treated by chemotherapy and usually present as large, locally advanced and metastatic unresectable masses. Their differential diagnosis on frozen section would include poorly differentiated adenocarcinomas, metastases from an extrapancreatic primary and lymphomas [12, 13].

Pancreas

FSE is fairly frequently called for in the surgery of pancreatic endocrine tumors, since the histological diagnosis is sometimes not made preoperatively. Its use depends on the choice of surgical procedure, of which there are two main types: enucleation and radical hemi-pancreatectomy [14–17].

Tumor enucleation can be performed in cases in which the pancreatic endocrine tumor (PET) is single, capsulated, of limited size (less than 2 to 3 cm) and peripheral, situated at a distance from the main duct. It is mainly performed for insulinomas or incidentally discovered PET [16, 18]. FSE may be required for enucleation specimens for various reasons. One is to confirm that the tumor is resected, with the differential diagnosis including lobular pancreatic tissue (Fig. 2a), adipose tissue, or ectopic or accessory spleen

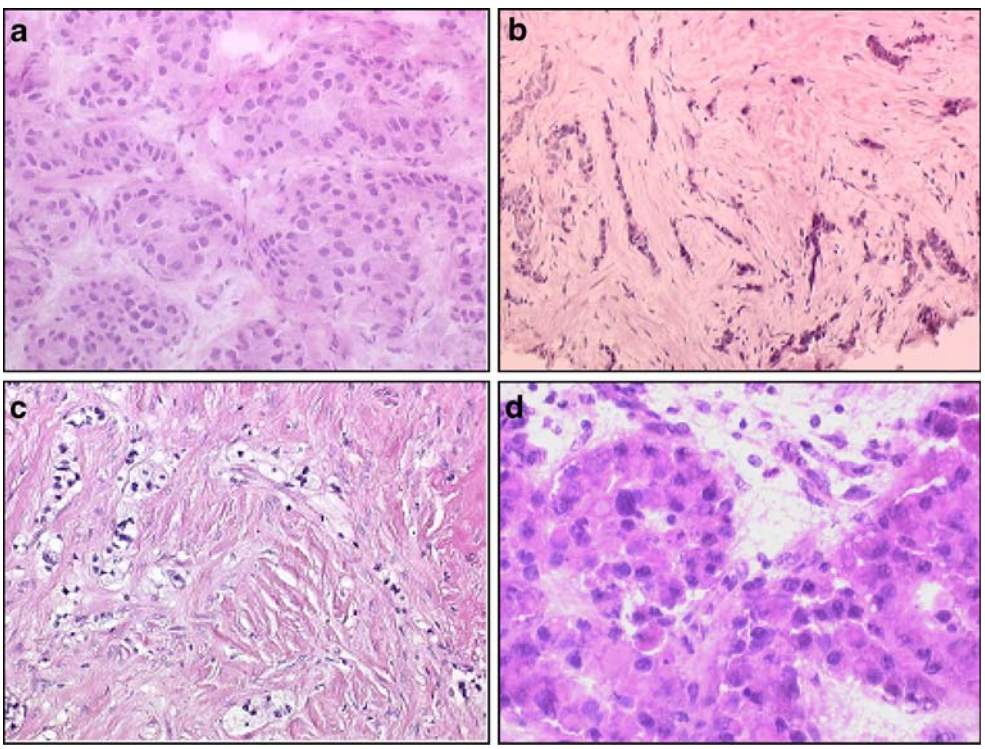

Fig. 1 Histological diagnosis and main differential diagnosis of digestive endocrine tumors on frozen sections. **a** This typical pancreatic neuroendocrine tumor is composed of regular cells arranged in small lobules. **b** A tumor with a fibrous stroma and a trabecular pattern, located in the head of the pancreas, mimicking an adenocarcinoma. **c** A clear cell pancreatic endocrine tumor with a fibrous stroma mimicking an adenocarcinoma in a patient with a von Hippel–Lindau disease (VHL). Frozen section examination was indicated to exclude a serous cystadenoma, which is not an indication for resection. The endocrine nature was highly suspected because of the high frequency of clear cell endocrine tumors in VHL disease. **d** An oncocytic pancreatic neuroendocrine tumor containing irregular atypical cells

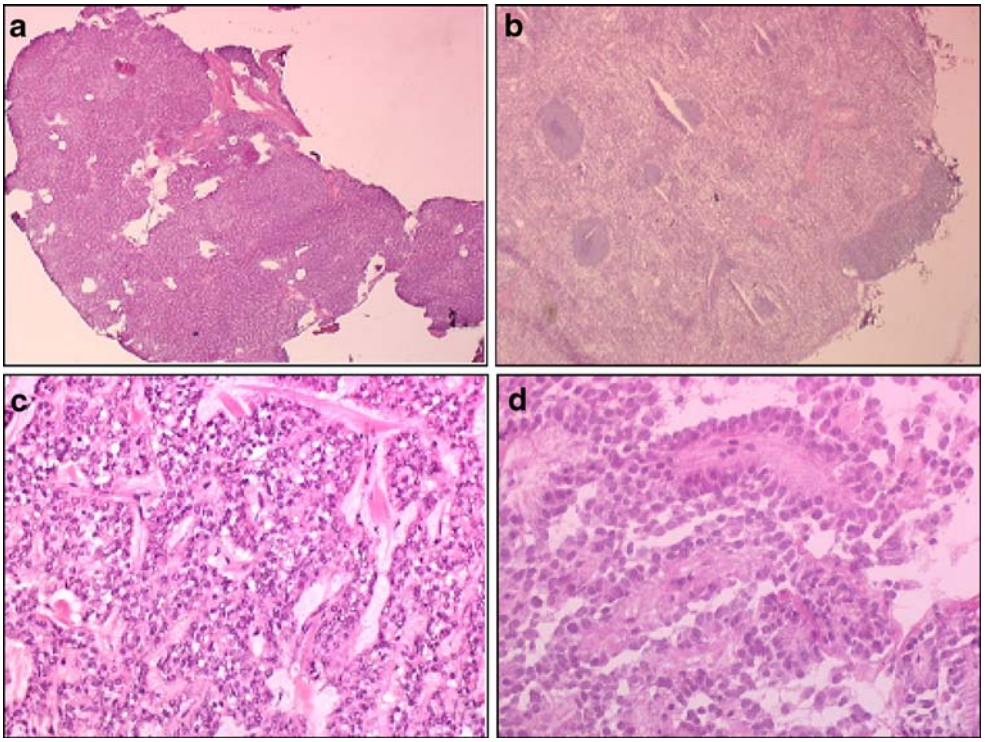

Fig. 2 Main differential diagnosis of endocrine tumors in the pancreas. Normal pancreatic lobule (**a**) or an accessory spleen (**b**). A solid pseudopapillary neoplasm (SPN) that was misdiagnosed as a pancreatic endocrine tumor at frozen section examination (**c**). The presence of pseudopapillae, when present, help to make the appropriate diagnosis in SPN (**d**)

(Fig. 2b). It is imperative for the surgeon to find and remove the tumor, especially if it is an insulinoma. A second reason is to confirm the diagnosis of well-differentiated endocrine tumor. Indeed, the gross examination of enucleated PETs, which can present as round and encapsulated, cystic, or poorly delineated fibrotic lesions (Fig. 3a and b), is not sufficient to confirm the diagnosis. The differential diagnosis includes solid pseudopapillary neoplasms (SPNs), acinar cell carcinomas, adenocarcinomas, and moderately to poorly differentiated endocrine tumors. In such cases, enucleation is contraindicated and a more radical resection is required. The presence of necrosis and cellular atypia and the number of mitoses should be evaluated for the differential diagnosis versus moderately differentiated PET. These tumors, which present cellular and structural atypia intermediate between those of well and poorly differentiated tumors are rare and are not reported in a separate category in the WHO classification [8]. Acinar cell carcinomas and pancreatic endocrine tumors can share characteristic histological features such as a solid, acinar, or glandular architecture, relatively minimal stroma and nuclear uniformity. The presence of eosinophilic cytoplasms, of numerous mitoses (greater than ten per ten high-power fields) and widespread acinar formations favor a diagnostic of acinar cell carcinoma [19]. The differential diagnosis versus SPN can be very difficult on frozen sections, especially for small SPNs which do not always reveal cystic or hemorrhagic changes. In these cases the pseudopapillary histological pattern is often lacking or may be present in only limited areas. Successive frozen sections

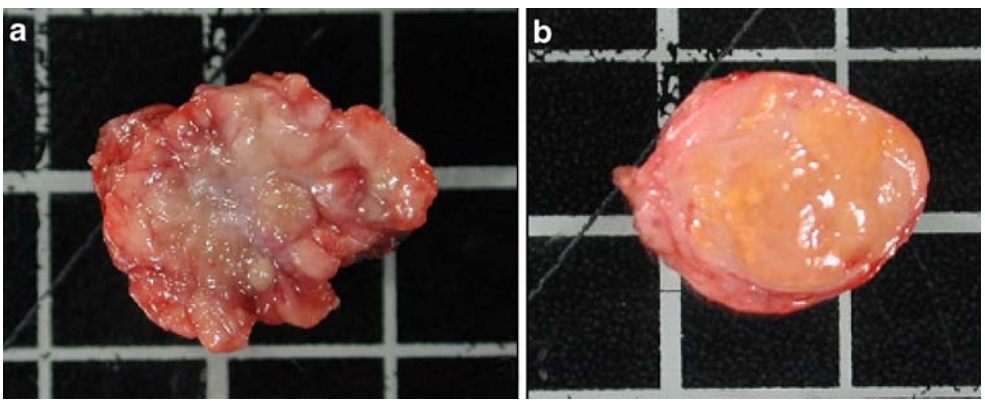

Fig. 3 Gross examination of pancreatic endocrine tumors. Gross examination showing different aspects, fibrous (**a**) and round well delimited (**b**), of two enucleated pancreatic endocrine tumors

could probably help to make the appropriate diagnosis (Fig. 2c and d). Absence of indented nuclei at a high magnification can also help in the diagnosis of PETs. It is still debated whether enucleation is contraindicated in cases of SPN, but their frequent infiltration through the tumor capsule and into the adjacent pancreatic parenchyma is the main argument for radically removing such type of tumor [20]. A third reason for frozen section evaluation is to confirm the presence of a lymph node metastasis or other tumor spread. Analysis of such lymph nodes is important because were metastasis found, enucleation would be contraindicated and a more radical resection required. Evaluation of margin resection by FSE is usually not performed. Indeed, a positive margin after enucleation of PET (mainly insulinomas) does not seem to increase the risk of tumor recurrence [21].

Unlike enucleation, FSE is rarely requested in the case of radical resections of PETs. Frozen sections can be useful for various reasons. One is to check the pancreatic margins, though this is rare. Although there is no data in the literature about the minimal margin to obtain during resection of PET, one can suggest that when the tumor is grossly well delimited, the margin can be very close. Indeed, in most cases, there is only a need for a small distance (a margin ranging from few millimeters to 1 cm is probably sufficient) between endocrine tumor and the surgical margin because of the well limitation at gross examination. Frozen sections are performed only in case of an infiltrative pattern. If it is infiltrated, an additional pancreatic resection is needed. A second reason is to confirm the endocrine nature of the tumor. The need for this has been reduced because of improved radiographic diagnostic techniques, including somatostatin-receptor scintigraphy and preoperative endoscopic ultrasonography-guided fine needle aspiration for cytological analysis [22]. However, when, for example, an extended resection is only achievable by the sacrifice of surrounding organs or by simultaneous vascular resection, a frozen section is indicated in order to justify the aggressive treatment if the diagnosis was not available before surgery [23]. It must be underlined that FSE of a lesion in the head of the pancreas after a pancreaticoduodenectomy is generally not advisable, since sampling a hard-to-find lesion may alter the macroscopic examination of the specimen after fixation [17]. A third reason for frozen section analysis is to confirm peritoneal involvement. This is the exception, and the surgeon is unlikely to change the planned procedure if there is limited involvement. A fourth reason is to confirm diffuse bilobar liver metastases if undiagnosed preoperatively. Indeed, this finding can contraindicate a synchronous resection if resection of the primary requires a pancreaticoduodenectomy, because of an excessively high operative risk [24].

In von Hippel–Lindau disease (VHL), patients can present with multiple pancreatic endocrine tumors and cysts. Pancreatic resection is not indicated for serous cystadenomas. Thus, FSE may be indicated in the differential diagnosis between endocrine tumor and atypical solid serous cystadenoma. Clear cell endocrine tumors, which are frequent in VHL disease, can be difficult to recognize, as pointed out above (Fig. 1c). Microadenomatosis has recently been demonstrated in VHL patients [personal observation; 11]. In such cases, as well as for multiple endocrine neoplasia type 1, frozen sections of the pancreatic margins may contain small microadenomas. However, such a finding should not lead the surgeon to modify the planned surgery.

In persistent hyperinsulinic hypoglycemia (PHH), if one insulinoma is detected before surgery, FSE is generally not necessary. Sometimes, the tumor is small and not easily visible at imaging and perioperative echography can help; in such cases, FSE can be requested to confirm that the tumor has been removed. However, in very rare cases (4% of cases of PHH according to a recent study) PHH can be secondary to diffuse adult nesidioblastosis [25]. It is almost impossible to diagnose nesidioblastosis clinically, biochemically, or with imaging. Indeed, only small nodules <5 mm are present and no tumor is found by the surgeon or by the pathologist's gross examination. Since the histological criteria (i.e., β-cell hypertrophy and islet hyperplasia) of diffuse nesidioblastosis vary in extent from case to case and are sometimes minimal, it is not recommended that the diagnosis be established on frozen sections [26]. The treatment is operative resection but the optimum pancreatic resection is difficult to define and multiple procedures may be necessary [27]. Nesidioblastosis in newborns, in which the role of frozen sectioning has been well established, will not be discussed in this review.

Ampulla of Vater

Endocrine tumors of the ampulla are very rare. They may be associated with von Recklinghausen disease and in this case they are almost exclusively somatostatin cell tumors [28, 29]. Small benign ampullary tumors can be resected by endoscopic or transduodenal ampullectomy. However, this is restricted to tumors less than 1 cm, without any detectable lymph node involvement at complete preoperative work-up [8]. In the case of surgical ampullary resection, which is an effective treatment in the management of noninvasive or minimally invasive exocrine adenomas of the ampulla, it is recommended to evaluate the surgical margins of the main pancreatic and bile ducts intraoperatively on frozen sections [30]. Local resection has been reported in some cases of small endocrine tumors [31–33], resulting in good long-term survival; and it seems

reasonable to recommend FSE of surgical margins in the management of ampullary endocrine tumors. However, it must be emphasized that the specimen must be handled carefully so that proper sampling and examination can be performed subsequently by conventional microscopy. Indeed, establishing the presence and depth of invasion of an ampullary lesion is essential for staging and to assess a prognosis. In addition, FSE is useful to confirm peripancreatic lymph node involvement, since metastatic disease would probably contraindicate a limited ampullary resection and lead to a pancreaticoduodenectomy.

Duodenum

FSE is frequently needed in cases of Zollinger–Ellison syndrome. Gastrinomas are usually small (less than 1 cm) and in some cases, imaging techniques are not able to visualize the tumor. In multiple endocrine neoplasia type 1, the duodenal gastrinomas are frequently multifocal with a high rate of spread and recurrence after excision [5, 34–35]. In this setting, indications for surgical resection are still a matter of debate [36]. Perioperative exploration includes palpation, trans-illumination (Fig. 4a), and longitudinal duodenotomy to allow complete examination of the entire mucosal surface. The smallest duodenal submucosal tumors can be removed by mucosal and submucosal dissection; larger tumors require full-thickness duodenal wall excision. Frozen sectioning is useful to confirm that the tumor is resected (Fig. 4b; the differential diagnosis includes Brunner's gland hyperplasia (Fig. 4c), pancreatic (Fig. 4d) or fundic heterotopia, adenomyoma, accessory papilla, and lymphangectasia). In some cases in which the functioning tumor is very small, several samples are successively submitted to the pathologist until the removal of the tumor is confirmed. A second reason is to confirm lymph node involvement (the differential diagnosis includes pancreatic lobules or adipose tissue). Due to the high rate of lymph node metastasis, surgery for gastrinomas should include clearance of periduodenopancreatic lymph nodes, which could be extended if a lymph node metastasis is confirmed by frozen sectioning.

Small intestine, jejunum–ileum

Ileal endocrine tumors, even if small, are malignant and frequently complicated by bowel obstruction, mesenteric invasion, or bleeding. The diagnosis is made in the great majority of cases before surgery. In this context, intraoperative exploration includes palpation of the whole intestine and enteroscopy to look for multiple, usually small, endocrine tumors which are associated with the main tumor in 30% of cases [37]. FSE may be necessary to determine whether small mucosal lesions are associated endocrine tumors. The differential diagnosis includes pancreatic heterotopia, lymphangioma, and lymphangectasia. Melanomas, adenocarcinomas, or gastrointestinal stro-

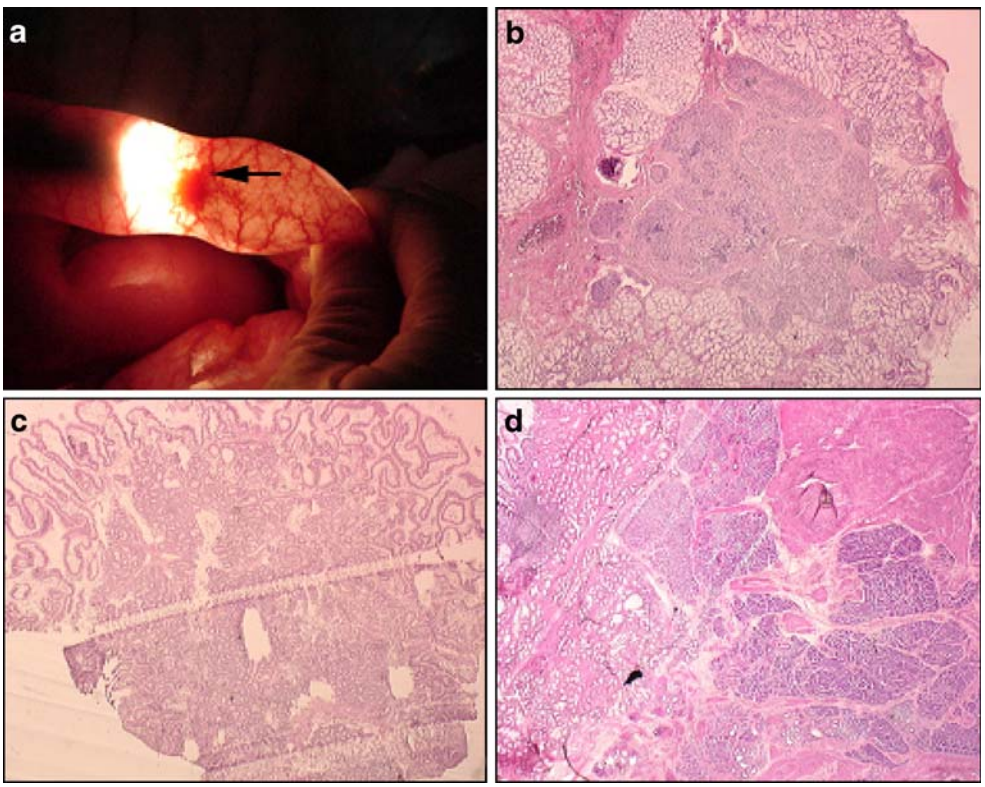

Fig. 4 Diagnosis and differential diagnosis of gastroenteropancreatic neuroendocrine tumor in the duodenum. **a** Transillumination of the duodenum showing a small endocrine tumor (*arrow*). The diagnosis is confirmed by frozen section examination (**b**) showing a small well delineated endocrine tumor embedded in Brunner's glands. In the duodenum, the differential diagnosis includes Brunner's gland hyperplasia (**c**) and pancreatic heterotopia (**d**)

mal tumors may also be found in the small intestine [38]. In the case of ileal endocrine tumors, FSE is rarely needed to evaluate the margins.

Appendix

The usual presentation of appendiceal tumors is acute appendicitis; consequently most of the patients are operated on an emergency basis. When possible, FSE should be requested whenever the appendiceal findings are atypical or if a tumor is suspected by the surgeon. It is required for the tumor diagnosis as well as for evaluation of the appendiceal margin, in contrast to most other sites [38]. Primary appendiceal tumors are of four main types (i.e., well-differentiated endocrine tumors, goblet cell carcinoids, mucinous cystadenomas, and adenocarcinomas), which can be recognized on frozen section [39–41]. The diagnosis of goblet cell carcinoid (Fig. 5a) or adenocarcinoma on frozen sections leads to a right hemicolectomy, even when the appendiceal margin is negative. It is important to evaluate this proximal margin for endocrine tumors; if the resection margin is positive, a more distal resection is required. However, the criteria for an additional right hemicolectomy are still controversial in some cases and are difficult to analyze for appendiceal endocrine tumors <2 cm. An analysis of the permanent sections is required to determine whether they are fulfilled, and a re-intervention should be performed in those cases. Other differential diagnoses encountered at frozen section include appendicitis (indeed the fibrosis may look like an infiltrative malignancy), endometriosis, and diverticulitis [38].

Liver

Liver metastases are evaluated for surgical resection or local ablation with the aim of reducing the tumor burden and alleviating a hormonal syndrome. The number of liver metastases is frequently underestimated by imaging [42]. Frozen sectioning is useful to confirm small liver metastases, in order to precisely evaluate the extension of an advanced metastatic disease. The differential diagnosis includes hyalinized nodules, von Meyenburg complexes (Fig. 5b), and foreign-body granulomas. It must be emphasized that artifacts can lead to difficulties in the analysis of a liver metastasis, especially when the nodules are small, depending on the type of resection. This is probably due to the presence of only a weak stroma in most endocrine tumors (Fig. 5c).

Liver transplantation may be an option in patients with metastases confined to the liver. Peritoneal carcinomatosis and distant lymph node metastasis, if confirmed by frozen section, are generally accepted as contraindication to liver transplantation.

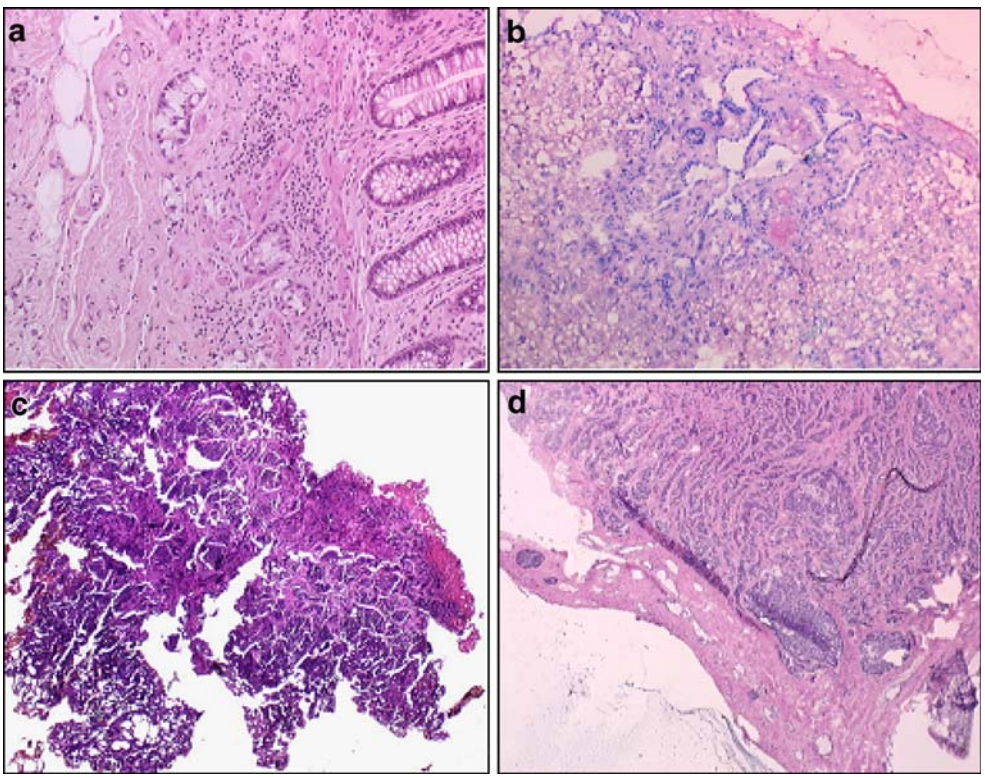

Fig. 5 Diagnosis and differential diagnosis of gastroenteropancreatic neuroendocrine tumors in the appendix (**a**), liver (**b**, **c**), and peritoneum (**d**). **a** A goblet cell carcinoid at the appendix margin that was detected on frozen section. **b** In the liver, a von Meyenburg complex can mimic a small endocrine metastasis. **c** In the liver, artifacts can lead to difficulties in the frozen section diagnosis of an endocrine metastasis, especially when the nodules are small, probably because there is no abundant stroma to rigidify the tumor. **d** Peritoneal metastatic endocrine tumors can be accurately diagnosed histologically on frozen sections

Peritoneum

FSE is usually performed in this location for the diagnosis of metastastic carcinoma during abdominal surgery for endocrine tumors (Fig. 5d). The main differential diagnosis is versus metastatic adenocarcinomas. Mimickers of tumor metastasis include fibrosis, fat necrosis, hyalinized nodule, and foreign-body granulomas [38].

Other locations

In other digestive locations, surgery for GEP-NETs is infrequent and frozen sections are rarely needed. Rectal tumors, for example, are often small and benign and are discovered fortuitously at the time of colonoscopic removal. Limited resections are often performed by endoscopy for small tumors [43–44]. In the stomach, hypergastrinemia-associated fundic type I or II ECL cell endocrine tumors, which are the most frequent gastric endocrine tumors, are of benign behavior and can be removed safely by minimally invasive techniques [5, 45–46].

Conclusion

In conclusion, the role and value of FSE of GEP-NETs vary greatly according to the location of the tumors. The main reasons for performing frozen sections are to identify an endocrine tumor in order to confirm that it has been resected, to evaluate the extent of disease (local spread, metastases, multiple tumors) and, less frequently, to evaluate the adequacy of resection. As for other tumor types, the pathologist needs information from the surgeon and must know what is expected from the FSE and what decision will be made on the basis of its results because the consequences can be considerable, particularly in pancreatic surgery [16].

Acknowledgment We are grateful to Professor Günther Klöppel for critical reading and editing the manuscript.

Conflict of Interest Statement We declare that we have no conflict of interest.

References

1. Plöckinger U, Rindi G, Arnold R et al (2004) Guidelines for the diagnosis and treatment of neuroendocrine gastrointestinal tumours. A consensus statement on behalf of the European Neuroendocrine Tumour Society (ENETS). Neuroendocrinology 80:394–424
2. Akerström G, Hellman P (2007) Surgery on neuroendocrine tumours. Best Pract Res Clin Endocrinol Metab 21:87–109
3. DeLellis RA, Lloyd RV, Heitz PU, Eng C (2004) World Health Organization classification of tumours, pathology and genetics of tumours of endocrine organs. IARC, Lyon
4. Hamilton SR, Aaltonen LA (2000) World Health Organization classification of tumours, pathology and genetics of tumours of the digestive system. IARC, Lyon
5. Klöppel G, Rindi G, Anlauf M et al (2007) Site-specific biology and pathology of gastroenteropancreatic neuroendocrine tumors. Virchows Arch 451:S9–S27
6. Rindi G, Klöppel G, Alhman H et al (2006) TNM staging of foregut (neuro) endocrine tumors: a consensus proposal including a grading system. Virchows Arch 449:395–401
7. Rindi G, Klöppel G, Couvelard A et al (2007) TNM staging of midgut and hindgut (neuro) endocrine tumors: a consensus proposal including a grading system. Virchows Arch 451:757–762
8. Solcia E, Klöppel G, Sobin LH (2000) Histological typing of endocrine tumours, 2nd edn. WHO International Histological Classification of Tumours. Springer-Verlag, Berlin Heidelberg New York
9. Abbey-Toby A, Vullierme MP, Sauvanet A et al (2006) A clear cell malignant gastrinoma of the pancreas with cytoplasmic accumulation of lipid droplets. Virchows Arch 448:105–106
10. Sugihara A, Nakasho K, Ikuta S et al (2006) Oncocytic non-functioning endocrine tumor of the pancreas. Pathol Int 56:755–759
11. Chetty R, Serra S, Asa SL et al (2006) Pancreatic endocrine tumour with ductules: further observations of an unusual histological subtype. Pathology 38:5–9
12. Ahlman H, Nilsson O, McNicol AM et al (2008) Poorly-differentiated endocrine carcinomas of midgut and hindgut origin. Neuroendocrinology 87:40–46
13. Nilsson O, Van Cutsem E, Delle Fave G et al (2006) Poorly differentiated carcinomas of the foregut (gastric, duodenal and pancreatic). Neuroendocrinology 84:212–215
14. Cioc AM, Ellison EC, Proca DM et al (2002) Frozen section diagnosis of pancreatic lesions. Arch Pathol Lab Med 126:1169–1173
15. Doucas H, Neal CP, O'Reilly K et al (2006) Frozen section diagnosis of pancreatic malignancy: a sensitive diagnostic technique. Pancreatology 6:210–213
16. Falconi M, Bettini R, Boninsegna L et al (2006) Surgical strategy in the treatment of pancreatic neuroendocrine tumors. JOP 7:150–156
17. Lechago J (2005) Frozen section examination of liver, gallbladder and pancreas. Arch Pathol Lab Med 129:1610–1618
18. Crippa S, Bassi C, Salvia R et al (2007) Enucleation of pancreatic neoplasms. Br J Surg 94:1254–1259
19. Hruban RH, Bishop Pitman M, Klimstra DS (eds) (2007) Tumors of the pancreas. (AFIP Atlas of tumor pathology, Fourth series, Fascicle 6) ARP, Washington
20. Salvia R, Bassi C, Festa L et al (2007) Clinical and biological behavior of pancreatic solid pseudopapillary tumors: report on 31 consecutive patients. J Surg Oncol 95:304–310
21. Nikfarjam M, Warshaw AL, Lloyd Axelrod L et al (2008) Improved contemporary surgical management of insulinomas a 25-year experience at the Massachusetts General Hospital. Ann Surg 247:165–172
22. Caudill JL, Humphrey SK, Salomão DR (2008) Islet cell tumor of the pancreas: increasing diagnosis after instituting ultrasonography-guided fine needle aspiration. Acta Cytol 52:45–51
23. Matthews BD, Heniford BT, Reardon PR et al (2000) Surgical experience with nonfunctioning neuroendocrine tumors of the pancreas. Am Surg 66:1116–1122, discussion 1122–1123
24. Kianmanesh R, Sauvanet A, Hentic O et al (2008) Two-step surgery for synchronous bilobar liver metastases from digestive endocrine tumors: a safe approach for radical resection. Ann Surg 247:659–665
25. Anlauf M, Wieben D, Perren A et al (2005) Persistent hyperinsulinic hypoglycemia in 15 adults with diffuse nesidioblastosis: diagnostic criteria, incidence, and characterization of β-cell changes. Am J Surg Pathol 29:524–533

26. Klöppel G, Anlauf M, Raffel A et al (2008) Adult diffuse nesidioblastosis: genetically or environmentally induced? Human Pathol 39:3–8
27. Raffel A, Krausch M, Anlauf M et al (2007) Diffuse nesidioblastosis as a cause of hyperinsulinic hypoglycemia in adults: a diagnosis and therapeutic challenge. Surgery 141:179–184
28. Hartel M, Wente MN, Sido B et al (2005) Carcinoid of the ampulla of Vater. J Gastroenterol Hepatol 20:676–681
29. Modlin IM, Lye KD, Kidd M (2003) A 5-decade analysis of 13,715 carcinoid tumors. Cancer 97:934–959
30. Grobmyer SR, Stasik CN, Draganov P et al (2008) Contemporary results with ampullectomy for 29 "benign" neoplasms of the ampulla. J Am Coll Surg 206:466–471
31. Clements WM, Martin SP, Stemmerman G et al (2003) Ampullary carcinoid tumors: rationale for an aggressive surgical approach. J Gastrointest Surg 7:773–776
32. Gilani N, Ramirez FC (2007) Endoscopic resection of an ampullary carcinoid presenting with upper gastrointestinal bleeding: a case report and review of the literature. World J Gastroenterol 13:1268–1270
33. Ricci JL (1993) Carcinoid of the ampulla of Vater. Local resection or pancreaticoduodenectomy. Cancer 71:686–690
34. Anlauf M, Garbrecht N, Bauersfeld J et al (2007) Hereditary neuroendocrine tumors of the gastroenteropancreatic system. Virchows Arch 451:S29–S38
35. Anlauf M, Perren A, Meyer CL et al (2005) Precursor lesions in patients with multiple endocrine neoplasia type 1-associated duodenal gastrinomas. Gastroenterology 128:1187–1198
36. Fendrich V, Langer P, Waldmann J et al (2007) Management of sporadic and multiple endocrine neoplasia type 1 gastrinomas. Br J Surg 94:1331–1341
37. Burke AP, Thomas RM, Elsayed AM et al (1997) Carcinoids of the jejunum and ileum: an immunohistochemical and clinicopathologic study of 167 cases. Cancer 79:1086–1093
38. Younes M (2005) Frozen section of the gastrointestinal Tract, appendix and peritoneum. Arch Pathol Lab Med 129:1558–1564
39. McGory ML, Maggard MA, Kang H et al (2005) Malignancies of the appendix: beyond case series reports. Dis Colon Rectum 48:2264–2271
40. O'Donnell ME, Carson J, Garstin WI (2007) Surgical treatment of malignant carcinoid tumours of the appendix. Int J Clin Pract 61:431–437
41. Plöckinger U, Couvelard A, Falconi M et al (2008) Consensus guidelines for the management of patients with digestive neuroendocrine tumours: well-differentiated tumour/carcinoma of the appendix and goblet cell carcinoma. Neuroendocrinology 87:20–30
42. Dromain C, de Baere T, Lumbroso J et al (2005) Detection of liver metastases from endocrine tumors: a prospective comparison of somatostatin receptor scintigraphy, computed tomography, and magnetic resonance imaging. J Clin Oncol 23:70–78
43. Bernick PE, Klimstra DS, Shia J et al (2004) Neuroendocrine carcinomas of the colon and rectum. Dis Colon Rectum 47:163–169
44. Schindl M, Niederle B, Häfner M et al (1998) Stage-dependent therapy of rectal carcinoid tumors. World J Surg 22:628–633
45. Modlin IM, Lye KD, Kidd M (2003) Carcinoid tumors of the stomach. Surg Oncol 12:153–172
46. Solcia E, Fiocca R, Villani L et al (1995) Hyperplastic, dysplastic, and neoplastic enterochromaffin-like-cell proliferations of the gastric mucosa. Classification and histogenesis. Am J Surg Pathol 19:S1–S7

Virchows Arch (2008) 453:449–455
DOI 10.1007/s00428-008-0676-8

ORIGINAL ARTICLE

Activated Akt as an indicator of prognosis in gastric cancer

Caterina Cinti · Carla Vindigni · Alessandra Zamparelli · Dario La Sala · Maria Carmela Epistolato · Daniele Marrelli · Gabriele Cevenini · Piero Tosi

Received: 1 September 2008 / Revised: 10 September 2008 / Accepted: 11 September 2008 / Published online: 8 October 2008

Abstract The immunohistochemical expression of phosphorylated (activated) Akt (pAkt) in 50 advanced gastric carcinomas has been analyzed and the results correlated with age, sex, location in the stomach, histotype, stage, survival, mitotic and apoptotic index, some cell cycle regulators (cyclin D1, cyclin E, p34/cdc2, p27/kip1), and cell proliferation. There was a statistically significant direct correlation between pAkt expression (both cytoplasmatic and nuclear) and depth of infiltration of the tumor, number of infiltrated lymph nodes and p34/cdc2 expression, and between prevalently nuclear pAkt and cyclin D1 and cyclin E. Conversely, there was a significant inverse correlation between nuclear pAkt and apoptotic index and between cytoplasmatic and nuclear pAkt and patient survival. No correlation was found between pAkt and sex, age, tumor location, histotype, mitotic index, and cell proliferation. These findings suggest that pAkt may be considered an indicator of tumor progression and patient survival in gastric cancer.

Keywords Gastric cancer · Akt · pAkt · Tumor progression · Survival

C. Cinti · D. La Sala
Institute of Clinical Physiology,
Consiglio Nazionale delle Ricerche, Siena Unit,
Siena, Italy

C. Vindigni · M. C. Epistolato · P. Tosi (✉)
Department of Human Pathology and Oncology,
Division of Pathological Anatomy and Histopathology,
University of Siena, Italy,
Via delle Scotte, 6,
53100 Siena, Italy
e-mail: tosi@unisi.it

A. Zamparelli
Institute of Molecular Genetics,
Consiglio Nazionale delle Ricerche, c/o IOR,
Bologna, Italy

D. Marrelli
Department of Human Pathology and Oncology,
Division of Surgical Oncology, University of Siena,
Siena, Italy

G. Cevenini
Department of Surgery and Bioengineering, University of Siena,
Siena, Italy

Introduction

Gastric cancer is one of the most common malignancies worldwide that originates through a multi-stage process involving multiple interacting genetic and environmental factors. It is known that chronic gastric infection due to *Helicobacter pylori* is associated with a six-fold greater risk of stomach cancer, although the molecular mechanism by which *H. pylori* predisposes to cancer is not well established [1]. As other cancers, gastric carcinoma develops through the accumulation of several genetic alterations, such as the inactivation of tumor suppressor genes and/or the activation of oncogenes [2, 3], however, the underlying critical molecular mechanism of its progression is largely not yet understood. It has recently been demonstrated that the proto-oncogene Akt/protein kinase B plays an important role in neoplastic transformation. Overexpression of Akt has an anti-apoptotic effect in many cell types, resulting in resistance to, or delay of, cell death. Akt regulates cell survival through the phosphorylation of downstream substrates that directly or indirectly control the apoptotic machinery [4–6]. Immunohistochemical studies using specific antibodies against the activated form, phosphorylated Akt (pAkt), have shown that Akt activity is detectable in

many tumors, such as myeloma and breast, colon, ovary, prostate, lung, kidney, and pancreatic cancers [7–9]. Activated Akt has been functionally linked to a poor prognosis in many cancers [10, 11] and it has been shown that it can promote resistance to chemo- and radiotherapy [12–14]. It has also recently been demonstrated that pAkt expression is associated with increased resistance to multiple chemotherapeutic agents in gastric cancer patients [15].

No gene mutation of Akt has been reported in cancer, even though its amplification has been found in many tumors [16–18]. The centrality of Akt to gastric physiology and neoplastic transformation has been suggested by the cloning of this oncogene from a gastric adenocarcinoma in which the gene was amplified and by its potent promitogenic action on gastric cancer cells in vitro [18, 19]. pAkt protein modulates the function of numerous substrates related to the regulation of cell proliferation, such as cyclin-dependent kinase inhibitors, p21/Waf1/Cip and p27/Kip1 [20, 21], and cyclin D1 and cyclin E [5]. p27/Kip1 is a cyclin-dependent kinase inhibitor that mainly binds cyclin D1/cdk4 and cyclin E/cdk2 complexes, thus blocking the G1/S transition necessary for cell cycle progression [22]. p27/Kip1 expression is mainly regulated through degradation by ubiquitin-dependent proteolysis and the protein level is up-regulated under stress conditions, leading to cell cycle inhibition and apoptosis [22, 23]. Additional roles for p27/Kip1 have also been proposed recently, including tumor suppression [24], regulation of cell migration [25], and mitosis [26]. It has been shown that Akt phosphorylates p21/Waf1 and p27/Kip1 and inhibits their anti-proliferative effects [27–29]. In particular, phosphorylated p27/Kip1 is exported from the nucleus to the cytoplasm and degraded by an ubiquitin system and is therefore no longer capable of inhibiting the activation of cyclin/cdk complexes.

In the present study, we examined pAkt by immunohistochemistry in a series of advanced gastric carcinomas and correlated its expression with clinicopathological parameters, mitotic and apoptotic index, cell cycle regulators (p27/Kip1, cyclin D1 and cyclin E, p34/cdc2) and cell proliferation (Mib1), with the aim of evaluating whether the expression of pAkt may be related to tumor progression and considered a prognostic indicator in gastric cancer.

Materials and methods

Patients

50 cases of advanced gastric cancer were analyzed. Patients had undergone curative resection (R0 gastrectomy with D2 lymphadenectomy) in the Division of Surgical Oncology, Siena University Hospital, Italy, between 1994 and 1997, and had been diagnosed at the Division of Pathological Anatomy and Histopathology, Siena University Hospital, Italy. None of the patients underwent pre- or post-operative chemotherapy or radiotherapy. Patients were followed up from the date of surgery to death or to 31 December 2005 (minimum follow-up period—5 years). The age of the patients (34 males and 16 females) ranged from 34 to 83 years. Tumor localization was in the gastric cardias (seven cases), gastric body (14 cases), and antrum (29 cases).

Histopathology

Samples of the surgical specimens were immediately fixed in 10% buffered formalin for 24 h and then processed for routine paraffin embedding. Five-micrometer-thick sections were stained with hematoxylin–eosin (HE) to determine the stage (TNM) [30] and the histotype according to Lauren [31].

According to the TNM classification, 23 cases (46%) were T2, 26 (52%) T3, and one case (2%) T4. Sixteen cases (32%) were negative for lymph node invasion and 34 (68%) were positive. In the positive cases, 12 (35%) were N1, eight (24%) were N2, and 14 (41%) were N3.

At the time of the study, further HE sections were examined to confirm stage and histotype: 31 cases (62%) were intestinal and 19 (38%) diffuse. Contiguous sections were stained with Azur A to count mitoses and apoptoses. Mitotic index (MI) and apoptotic index (AI) were calculated as the percentage of cancer cells in mitosis or apoptosis in 15–20 randomly selected fields at 400× [32].

Immunohistochemistry

Five-micrometer-thick sections were deparaffinized, rehydrated, immersed in citric acid buffer (pH6.0) and incubated in a 750 W microwave oven twice for 5 min. Primary monoclonal antibodies were used for phosphorylated Akt (Ser-473, New England Biolabs, Ipswich, MA, USA), Ki67/Mib1 (clone SP6, Neomarkers, Fremont, CA, USA), cyclin D1 (clone SP4, NeoMarkers, Fremont, CA, USA), cyclin E (clone CYE05, NeoMarkers, Fremont, CA, USA), p27/Kip1 (clone DCS-F2F6, NeoMarkers, Fremont, CA, USA) and p34/cdc2 serine/threonine kinase/cdk AB1 (clone A 17.1.1, NeoMarkers, Fremont, CA, USA). All slides were incubated with the primary antibody for 1 h and with the secondary antibody (Ultra Vision Large Volume Detection System, antipolyvalent, HRp, Lab Vision, Fremont, CA, USA) for 20 min. The binding reaction was detected using 3,3′-diaminobenzidine (DAB; DAKO Corporation, Carpinteria, CA, USA) and slides were then counterstained with hematoxylin.

In each case, ten high power (400×) fields were selected and at least 1,000 cells were evaluated. pAkt staining was detected in the cytoplasm (pAkt) or in the nuclei (pAktn) of cancer cells. pAkt expression was considered nuclear

(pAktn) when nuclear staining was prevalent. For Mib1, cyclin D1 and cyclin E, the localization had to be exclusively nuclear; for p27/Kip1, both nuclear and cytoplasmatic localization were considered for positivity; for p34/cdc2 the localization had to be cytoplasmatic.

Expression of pAkt, pAktn, and p34/cdc2 was graded on a semiquantitative scale, ranging from 0 to 3 (for pAkt and pAktn: 0=0, 1≤15%, 2=15–30%, 3>30%; for p34/cdc2: 0=0, 1≤25%, 2=25–50%, 3>50%). Cancers were also classified as pAkt/pAktn negative (<10% positive cells) or pAkt/pAktn positive (>10% positive cells).

For other markers, the positivity was calculated as the percentage of positive cancer cells out of the total amount of cancer cells. The staining patterns of cyclin D1 and cyclin E were classified as follows: negative (none or <5% of cells positive) or positive (>5% of cells positive). p27/Kip1 immunostaining was considered positive if 20% or more of cancer cells were stained.

Reproducibility

The reproducibility of all parameters was assessed by two independent observers in six cases, by repeating counts seven times. The correlation coefficient within and between the two observers was greater than 0.9 for all the parameters.

Statistics

Qualitative data were expressed as frequencies, organized into contingency tables and evaluated using the chi-square test to verify the dependence of observations on two or more categorical variables (Pearson's chi-square test or the Fisher exact test). Since the Kolmogorov–Smirnov normality test applied to the sample data determined that the quantitative variables could not be considered Gaussian distributed, all statistical analyses were carried out using non-parametric tests. The Mann–Whitney *U* test was used to compare data using quantitative variables. Survival curves were estimated using the Mantel–Cox test and differences between survival curves were determined using the log-rank test. The results were considered statistically significant for $p<0.05$.

Statistical analysis was performed using the SPSS 10.0 statistical software (SPSS, Chicago, IL, USA).

Results

Correlation of pAkt/pAktn expression with clinicopathological parameters

The data related to clinicopathological parameters are summarized in Table 1. pAkt immunostaining was detected in 34 (68%) of the 50 cases analyzed, 17 of which (50%) showed prevalently nuclear positivity (Fig. 1). Among these 34 positive cases, 21 were intestinal type cancers (61.8%) and 13 diffuse type cancers (38.2%). No significant correlation was found between pAkt and pAktn expression and sex, age, tumor location, and Lauren histotype ($p>0.05$).

Table 1 Clinicopathological parameters

Variables	No.	%
Sex		
F	34	68
M	16	32
Tumor location		
Cardias	7	14
Body	14	28
Antrum	29	58
Depth of invasion		
T2	23	46
T3+T4	27	54
Lymph node metastasis		
N0	16	32
N+	34	68
N1	12	35
N2	8	24
N3	14	41
Lauren histotype		
Intestinal	31	62
Diffuse	19	38
Total	50	100

On the other hand, a statistically significant direct correlation was found between pAkt and pAktn expression and depth of infiltration ($p=0.032$); patients with high expression of pAkt and pAktn were prevalently allocated in categories T3–T4.

There was also a significant direct correlation between pAkt and pAktn expression and the number of infiltrated lymph nodes (respectively $p=0.011$ and $p=0.025$; Fig. 2). More than 80% of pAkt/pAktn positive cases had lymph node metastases and 50% of them had more than 15 positive lymph nodes (category N3).

pAkt and pAktn expression had a significantly negative correlation with survival rate (respectively $p=0.039$ and $p=0.011$; Fig. 3). Five-year survival probability was 18% in patients with high pAkt/pAktn expression vs. 58% in negative cases.

Correlation between pAkt/pAktn expression, cell proliferation and apoptosis

pAktn was found to be inversely correlated with apoptotic index (AI; $p=0.043$; Fig. 4), while no significant correlation was found between pAkt expression and AI, and between pAkt and pAktn expression and mitotic index (MI) and Mib1 positive cells ($p>0.05$; not shown).

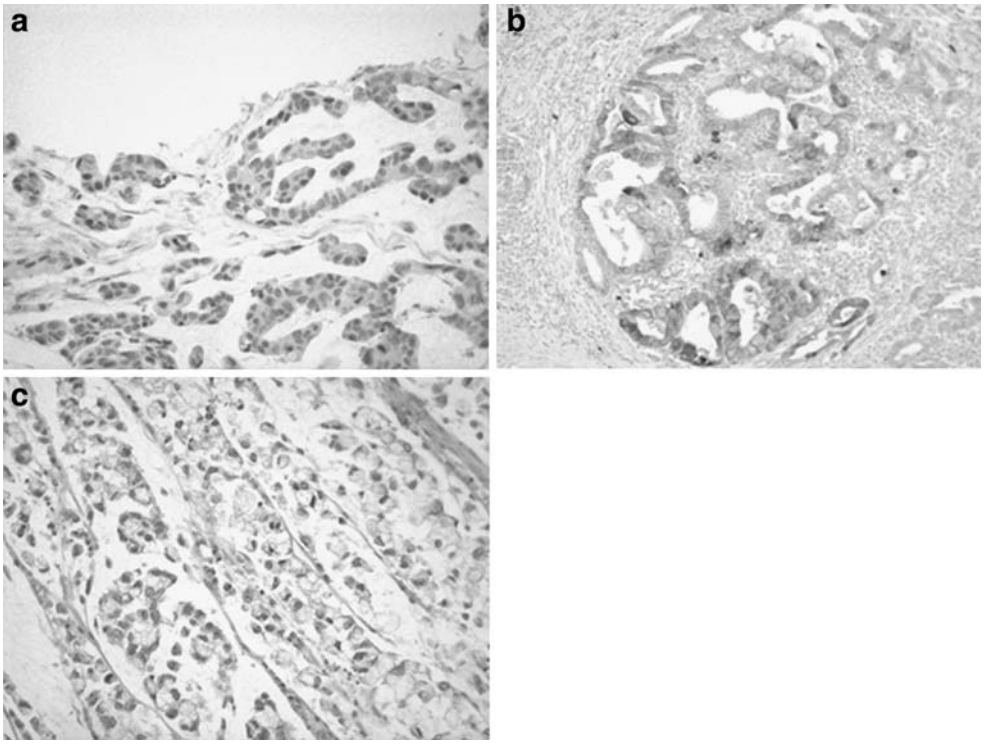

Fig. 1 Immunostaining of pAkt in gastric cancer: **a**–**b** cytoplasmatic and nuclear stains in a case of intestinal type cancer; **c** prevalently nuclear stain in a case of diffuse type cancer

p27/kip1 was positive in 19 (38%) of the 50 cases analyzed. Nuclear immunolocalization was detected in most of the cases (68.4%), while only 31.6% of them showed cytoplasmatic localization. Cases with high pAkt and pAktn expression showed higher values of p27/kip1 and of p27 cytoplasmatic overexpression, but the differences were not significant ($p>0.05$).

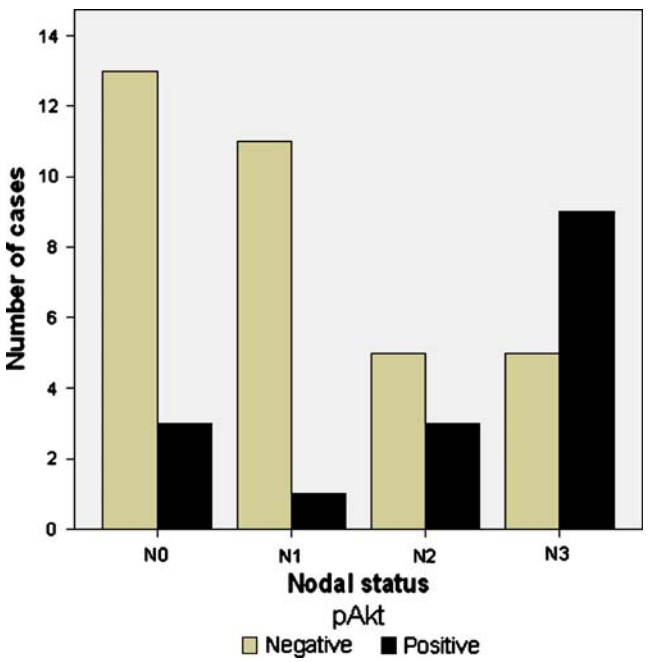

Fig. 2 Correlation between pAkt positivity and nodal status. The differences are statistically significant (Pearson's chi-square test: $p=0.011$)

Positive expression of cyclin D1 was detected in 12 of the 50 cases (24%) and of cyclin E in eight cases (16%). A significant correlation was found between pAktn and cyclin D1 ($p=0.018$) and cyclin E ($p=0.046$). High pAktn expression was associated with a strong positivity for cyclin D1 and cyclin E.

As regards p34/cdc2 expression, 26 cases out of 50 (52%) showed positivity in less than 25% of cells, 22 cases

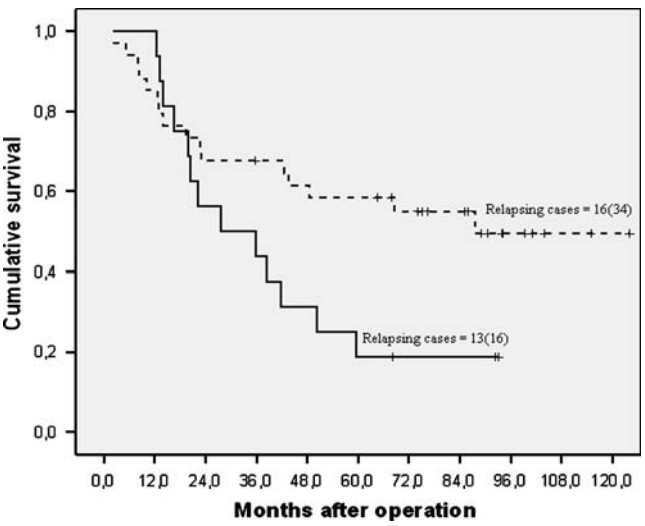

Fig. 3 Cumulative survival in relation to pAkt positivity. The difference between the pAkt-negative cases (*broken line*) and pAkt-positive cases (*solid line*) is statistically significant (log-rank test, $p=0.039$): number of relapsing (total) patients in pAkt negative=16 (34), number of relapsing (total) patients in pAkt positive=13(16)

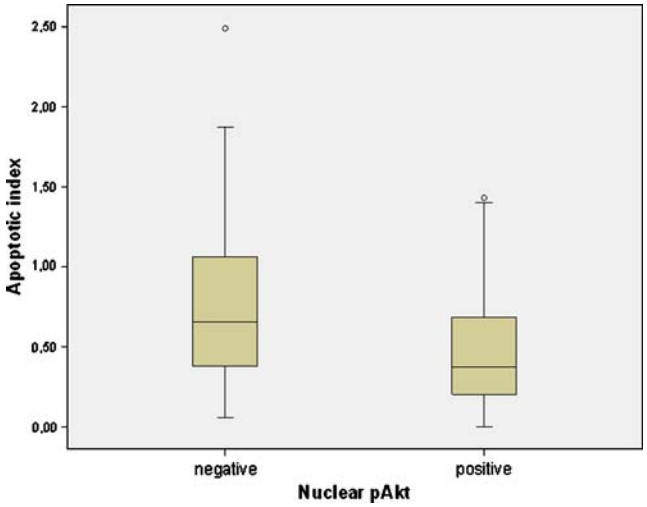

Fig. 4 Apoptotic index in relation to nuclear pAkt positivity. The difference between negative and positive cases is statistically significant (two independent samples *t* test: $p=0.043$)

(44%) positivity in 25% to 50% of cells, and two cases (4%) showed positivity in more than 50% of cells. A significant direct correlation ($p=0.019$) was found between pAkt and p34/cdc2 expression

Discussion

Akt modulates the function of numerous substrates related to the regulation of cell proliferation and apoptosis and is putatively involved in the development of some cancers. An elevated Akt activation, the phosphorylated Akt (pAkt), has been demonstrated in various malignancies [33] and often correlated with tumor progression, such as in colon (using western blotting and immunohistochemistry) [34], prostate [35], lung [36], and thyroid cancer [37]. It has been shown that Akt activation in cancer cells increases the motility required for tissue invasion and metastases [38] and is consequently related to poor prognosis in many cancers [10, 11, 39, 40]. pAkt can promote resistance to chemo- and radiotherapy in many tumors [12–14] and it has been found to be significantly correlated with cancer progression, cell proliferation and angiogenesis, as well as with chemoresistance in gastric cancer [32, 41–44]. The results of Han et al. [42] are obtained by using immunohistochemistry, western blotting, and polymerase chain reaction (PCR) analyzed on gastric cancer cell lines.

In the present study, pAkt was expressed in 34 (68%) of the 50 tumors analyzed, 50% of which showed a prevalently nuclear localization. pAkt/pAktn positivity was found to be directly correlated with the number of infiltrated lymph nodes and depth of tumor invasion of stomach wall, while it was inversely correlated with patient survival rate. Our data are in agreement with a previous study, reporting that Akt activation is related to a poor outcome in gastric cancer [41]. We also analyzed the relationship between pAkt expression and apoptotic index, because Akt has been reported to be a signal transduction protein capable of controlling the balance between cell survival and apoptosis [5, 45]. It is known that phosphorylation of Akt is promoted by phosphatidylinositides converted by PI3K products at the cytoplasmatic level. Phosphorylated Akt delivers anti-apoptotic survival signals by phosphorylating Bad and activating caspase-9 at the cytoplasmatic level [46, 47], as well as by inhibiting the function of some nuclear proteins at the nuclear level, such as forkhead transcription factors, which are involved in the apoptotic response. Akt-dependent phosphorylation of forkhead proteins leads to their exclusion from the nucleus and to loss of transcription targets such as Bim and Fas-ligand in the nucleus [6]. In the present study, we found that high expression of pAktn is correlated with a low apoptotic index, confirming that a nuclear localization of pAkt is necessary to negatively control the apoptotic response in cancer cells.

The Akt pathway has also been implicated in altering p27/Kip1 activity. The cyclin-dependent kinase inhibitor p27/kip1 is a putative tumor suppressor factor in human cancer. It has been demonstrated that the serine/threonine kinase Akt regulates cell proliferation in cancer by preventing p27/kip1-mediated growth arrest. p27/kip1 phosphorylation, induced by pAkt, causes retention of p27/kip1 in the cytoplasm and, thus, prevents cell cycle arrest induced by p27/kip1. Phosphorylated p27/kip1 accumulates in the cytoplasm of cancer cells in coincidence with Akt activation and is subsequently degraded by the ubiquitin system [5, 21, 29]. In this way, the growth inhibitory properties of p27/kip1 are functionally inactivated and the proliferation of cancer cells is sustained. Although we did not find a statistically significant correlation between pAkt/pAktn and p27/Kip1 expression in our study, we observed that cases with high pAkt/pAktn expression had a high level of cytoplasmatic p27/kip1 expression. This result is in agreement with previous studies [5, 27, 29] performed on breast cancer, in cell culture, by site-directed mutagenesis and transfection, by Akt immunoblotting activation, as well as by immunohistochemistry, BrdU incorporation, and indirect immunofluorescence.

pAkt is also implicated in controlling cyclin D1 and cyclin E activity, thus, contributing to the regulation of cell cycle progression. pAkt prevents the degradation of cyclins D1 and E, which is induced by an ubiquitin-dependent proteolysis pathway, because it inactivates GSK3, which is necessary for their phosphorylation, translocation from nucleus to cytoplasm and degradation [5]. Both cyclin D1 and cyclin E have been found to be deregulated and overexpressed in various types of cancers and seem to play an important role in the progression and biological behavior

of cancer. Overexpression of both these cyclins has also been found in gastric cancer, but their prognostic value is still controversial. For cyclin D1, no significant correlation has been found between its immunohistochemical expression and any of the more frequently considered clinicopathological parameters [48–50]. On the other hand, cyclin E overexpression was found to be directly correlated with the number of infiltrated lymph nodes and the low incidence of T1 and stage I tumors, as well as with p53 overexpression in early gastric cancer [49, 51, 52]. On the basis of these findings, it may be argued that cyclin E overexpression is a useful prognostic indicator in gastric carcinoma, quite the contrary to cyclin D1. In this study, a significant correlation was found between pAktn and both cyclin D1 and cyclin E expression, suggesting that the pAkt may promote also gastric cancer progression by controlling cyclins D1 and E, which are two critical players in the cell cycle.

In conclusion, our preliminary results indicate that pAkt controls the activation of p27/kip1, cyclins D1 and E and apoptosis, which play an important role in the cell cycle. Hence, it is not surprising that pAkt may be correlated with cancer progression and patient survival in gastric cancer, as it may be in other malignancies. However, to reach a conclusion, our results need to be confirmed in larger series of cases.

Conflict of interest statement We declare that we have no conflict of interest.

References

1. Axon A (2002) Review article: gastric cancer and *Helicobacter pylori* Alimet. Pharmacol Ther 16(4):83–88
2. Saegusa M, Takano Y, Kamata Y et al (1996) Bcl-2 expression and allelic loss of the p53 gene in gastric carcinomas. J Cancer Res Clin Oncol 122:427–432
3. Endoh Y, Sakata K, Tamura G et al (2000) Cellular phenotypes of differentiated-type adenocarcinomas and precancerous lesions of the stomach are dependent on the genetic pathways. J Pathol 191:257–263
4. Fresno Vara JA, Casado E, de Castro J et al (2004) PI3K/Akt signalling pathway and cancer. Cancer Treat Rev 30:193–204
5. Chang F, Lee JT, Navolanic PM et al (2003) Involvement of PI3K/Akt pathway in cell cycle progression, apoptosis, and neoplastic transformation: a target for cancer chemotherapy. Leukemia 17:590–603
6. Wang R, Brattain MG (2006) AKT can be activated in the nucleus. Cell Signaling 18:1722–1731
7. Roy HK, Olusola BF, Clemens DL et al (2002) AKT proto-oncogene overexpression is an early event during sporadic colon carcinogenesis. Carcinogenesis 23:201–205
8. Altomare DA, Tanno S, De Rienzo A et al (2003) Frequent activation of AKT2 kinase in human pancreatic carcinomas. J Cell Biochem 88:470–476
9. Alkan S, Izban KF (2002) Immunohistochemical localization of phosphorylated AKT in multiple myeloma. Blood 99:2278–2279
10. Yamamoto S, Tomita Y, Hoshida Y et al (2004) Prognostic significance of activated Akt expression in pancreatic ductal adenocarcinoma. Clin Cancer Res 10:2846–2850
11. Ermoian RP, Furniss CS, Lamborn KR et al (2002) Dysregulation of PTEN and protein kinase B is associated with glioma histology and patient survival. Clin Cancer Res 8:1100–1106
12. Clark AS, West K, Streicher S et al (2002) Constitutive and inducible Akt activity promotes resistance to chemotherapy, trastuzumab, or tamoxifen in breast cancer cells. Mol Cancer Ther 1:707–717
13. Brognard J, Clark AS, Ni Y et al (2001) Akt/protein kinase B is constitutively active in non-small cell lung cancer cells and promotes cellular survival and resistance to chemotherapy and radiation. Cancer Res 61:3986–3997
14. Tanno S, Yanagawa N, Habiro A et al (2004) Serine/threonine kinase AKT is frequently activated in human bile duct cancer and is associated with increased radioresistance. Cancer Res 64:3486–3490
15. Oki E, Baba H, Tokunaga E et al (2005) Aky phosphorylation associates with LOH of PTEN and leads to chemoresistance for gastric cancer. Int J Cancer 117:376–380
16. Bellacosa A, de Feo D, Godwin AK et al (1995) Molecular alterations of the AKT2 oncogene in ovarian and breast carcinomas. Int J Cancer 64:280–285
17. Cheng JQ, Ruggeri B, Klein WM et al (1996) Amplification of AKT2 in human pancreatic cells and inhibition of AKT2 expression and tumorigenicity by antisense RNA. Proc Natl Acad Sci USA 93(8):3636–3641
18. Staal SP (1987) Molecular cloning of the akt oncogene and its human homologues AKT1 and AKT2: amplification of AKT1 in a primary human gastric adenocarcinoma. Proc Natl Acad Sci USA 84:5034–5037
19. Rusnak DW, Lackey K, Affleck K et al (2001) The effects of the novel, reversible epidermal growth factor receptor/ErbB-2 tyrosine kinase inhibitor, GW2016, on the growth of human normal and tumor-derived cell lines in vitro and in vivo. Mol Cancer Ther 1:85–94
20. Diehl JA, Cheng M, Roussel MF et al (1998) Glycogen synthase kinase-3beta regulates cyclin D1 proteolysis and subcellular localization. Gen Dev 12:3499–3511
21. Liang J, Zubovitz J, Petrocelli T et al (2002) PKB/Akt phosphorylates p27, impairs nuclear import of p27 and opposes p27-mediated G1 arrest. Nat Med 8:1153–1160
22. Philipp-Staheli J, Payne SR, Kemp CJ (2001) p27(Kip1): regulation and function of a haplo-insufficient tumor suppressor and its misregulation in cancer. Exp Cell Res 264:148–168
23. Pagano M, Tam SW, Theodoras AM et al (1995) Role of the ubiquitin–proteasome pathway in regulating abundance of the cyclin-dependent kinase inhibitor p27. Science 269:682–685
24. Fero M, Randel E, Gurley KE et al (1998) The murine gene p27Kip1 is haplo-insufficient for tumor suppression. Nature 396:177–180
25. Besson A, Gurian-West M, Schmidt A et al (2004) p27Kip1 modulates cell migration through the regulation of RhoA activation. Genes Dev 18:862–876
26. Nakayama K, Nagahama H, Minamishima YA et al (2004) Skp2-mediated degradation of p27 regulates progression into mitosis. Dev Cell 6:661–672
27. Liang J, Slingerland JM (2003) Multiple roles of the PI3K/PKB (Akt) pathway in cell cycle progression. Cell Cycle 2:339–345
28. Shin I, Yakes FM, Rojo F et al (2002) PKB/Akt mediates cell-cycle progression by phosphorylation of p27 (kip1) at threonine 157 and modulation of its cellular localization. Nat Med 8:1145–1152
29. Viglietto G, Motti ML, Bruni P et al (2002) Cytoplasmic relocalization and inhibition of the cyclin-dependent kinase inhibitor p27(Kip1) by PKB/Akt-mediated phosphorylation in breast cancer. Nat Med 8:1136–1144
30. Greene FL, Page DL, Fleming ID et al (eds) (2002) American Joint Committee on Cancer Staging Manual, 6th ed. Springer, New York

31. Lauren T (1965) The two histologic main types of gastric carcinoma: diffuse and so called intestinal type. Acta Pathol Microbiol 64:31–49
32. Vindigni C, Miracco C, Spina D et al (1997) Cell proliferation, cell death and angiogenesis in early and advanced gastric cancer of intestinal type. Int J Cancer 74:637–641
33. Cicenas J (2008) The potential role of Akt phosphorylation in humane cancers. Int J Biol Markers 23:1–9
34. Itoh N, Semba S, Masafumi I et al (2002) Phosphorylation of Akt/PKB is required for suppression of cancer cell apoptosis and tumor progression in human colorectal carcinoma. Cancer 94:3127–3134
35. Liao Y, Grobholz R, Abel U et al (2003) Increase of AKT/PKB expression correlates with Gleason pattern in human prostate cancer. In J Cancer 107:676–680
36. Okudela K, Hayashi H, Ito T et al (2004) K-ras gene mutation enhances motility of immortalized airway cells and lung adenocarcinoma cells via Akt activation: possible contribution to non-invasive expansion of lung adenocarcinoma. Am J Pathol 164:91–100
37. Vasko V, Saji M, Hardy E et al (2004) Akt activation and localisation correlate with tumour invasion and oncogene expression in thyroid cancer. J Med Genet 41:161–170
38. Grille SJ, Bellicosa A, Upson J et al (2003) The protein kinase Akt induces epithelial mesenchymal transition and promotes enhanced motility and invasiveness of squamous cell carcinoma lines. Cancer Res 63:2172–2178
39. Schmitz KJ, Otterbach F, Callies R et al (2004) Prognostic relevance of activated Akt kinase in node-negative breast cancer: a clinicopathological study of 99 cases. Mod Pathol 17:15–21
40. Horiguchi A, Oya M, Uchida A et al (2003) Elevated Akt activation and its impact on clinicopathological features of renal cell carcinoma. J Urol 169:710–713
41. Murakami D, Tsujitani S, Osaki T et al (2007) Expression of phosphorylated Akt (pAkt) in gastric carcinoma predicts prognosis and efficacy of chemotherapy. Gastric Cancer 10:45–51
42. Han Z, Wu K, Shen H et al (2008) Akt1/protein kinase Bα is involved in gastric cancer progression and cell proliferation. Dig Dis Sci 53:1801–1810
43. Lee BL, Kim WH, Jung J, Cho SJ et al (2008) A hypoxia-independent up-regulation of hypoxia-inducible factor-1 by AKT contributes to angiogenesis in human gastric cancer. Carcinogenesis 29:44–51
44. Yu HG, Ai YW, Yu LL et al (2008) Phosphoinositide 3-kinase/Akt pathway plays an important role in chemoresistance of gastric cancer cells against etoposide and doxorubicin induced cell death. Int J Cancer 122:433–443
45. Kobayashi I, Semba S, Matsuda Y et al (2006) Significance of Akt phosphorylation on tumor growth and Vascular Endothelial Growth Factor expression in human gastric carcinoma. Pathobiology 73:8–17
46. Cardone MH, Roy N, Stennicke HR et al (1998) Regulation of cell death protease caspase-9 by phosphorylation. Science 282:1318–1321
47. Brunet A, Bonni A, Zigmond MJ et al (1999) Akt promotes cell survival by phosphorylating and inhibiting a Forkhead transcription factor. Cell 96:857–868
48. Takano Y, Kato Y, Masuda M et al (1999) Cyclin D2, but not cyclin D1, overexpression closely correlates with gastric cancer progression and prognosis. J Pathol 189:194–200
49. Aoyagi K, Koufuji K, Yano S et al (2000) Immunohistochemical study on the expression of cyclin D1 and E in gastric cancer. Kurume Med J 47:199–203
50. Chetty R, Sitti CW (2003) Cyclin E immunoexpression in gastric cancer does not correlate with clinicopathological parameters. Histopathology 42:66–69
51. Jiaqing L, Hokita S, Xiangming C et al (1998) Role of cyclin E and p53 expression in progression of early gastric cancer. Gastric Cancer 1:160–165
52. Bani-Hani KE, Almasri NM, Khader YS et al (2005) Combined evaluation of expressions of cyclin E and p53 proteins as prognostic factors for patients with gastric cancer. Clinical Cancer Research 11:1447–1453

Virchows Arch (2008) 453:457–464
DOI 10.1007/s00428-008-0660-3

ORIGINAL ARTICLE

Intratumoural lymphatics in benign and malignant soft tissue tumours

G. Mahendra · K. Kliskey · K. Williams · K. Hollowood · D. Jackson · N. A. Athanasou

Received: 30 May 2008 / Revised: 16 July 2008 / Accepted: 20 August 2008 / Published online: 24 September 2008

Abstract Soft tissue sarcomas do not generally metastasise via lymphatics, and the presence or absence of lymphatic vessels within sarcomas and benign soft tissue tumours is not known. In this study, we determined whether lymphatic vessels were present in a wide range of benign and malignant soft tissue lesions by examining intratumoural expression of the lymphatic endothelial cell markers, Lyve-1 and podoplanin. Intratumoural Lyve-1+/podoplanin+ lymphatics were not identified in sarcomas apart from all cases of epithelioid sarcoma (a tumour which is known to metastasise to lymph nodes) and a few cases of leiomyosarcoma, rhabdomyosarcoma and synovial sarcoma. Intratumoural lymphatics were also absent in most benign soft tissue tumours. Reparative and inflammatory soft tissue lesions contained lymphatics, as did all (pseudosarcomatous) proliferative myofibroblastic lesions including nodular, proliferative and ischaemic fasciitis, elastofibroma, nuchal fibroma and deep fibromatosis. Our results show that most soft tissue sarcomas do not contain intratumoural lymphatics, a finding which is consistent with the infrequent finding of sarcoma metastasis to lymph nodes. In contrast to fibrosarcoma and a number of other malignant spindle cell tumours, proliferative fibroblastic/myofibroblastic lesions of soft tissue contain intralesional lymphatic vessels.

Keywords Lymphatics · Sarcoma · Benign soft tissue tumours

G. Mahendra · K. Kliskey · K. Williams · N. Athanasou (✉)
Department of Pathology,
Nuffield Department of Orthopaedic Surgery,
University of Oxford, Nuffield Orthopaedic Centre,
Windmill Road, Headington,
Oxford OX3 7LD, UK
e-mail: nick.athanasou@noc.anglox.nhs.uk

K. Hollowood
Department of Cellular Pathology, John Radcliffe Hospital,
Headley Way, Headington,
Oxford OX3 9DU, UK

D. Jackson
Institute of Molecular Medicine, C/- John Radcliffe Hospital,
University of Oxford,
Headley Way, Headington,
Oxford OX3 9DU, UK

Introduction

The infrequent event of lymphatic metastasis in the natural history of soft tissue sarcomas is well documented, the reported incidence being 2.6–5% [1, 2]. In some series, certain histological subtypes of soft tissue sarcoma, such as epithelioid sarcoma, synovial sarcoma, angiosarcoma, clear cell sarcoma, rhabdomyosarcoma and leiomyosarcoma, have been shown to have a higher incidence of lymph node metastasis [2–4]. Intratumoural lymphatic vessels are known to be relatively uncommon in some primary epithelial malignancies [5, 6], but whether the infrequency of lymph node metastasis from soft tissue sarcomas can be explained by the absence of lymphatics in these tumours is not known as the presence of lymphatic vessels in soft tissue sarcomas (and their benign counterparts) has not been systematically analysed.

Lymphatic vessels are known to be present in many reactive lesions, such as in wound healing and infection [7–9]. Nodular and proliferative fasciitis are lesions in which there are numerous plump, proliferative spindle-shaped cells that lie in well-vascularised connective tissue reminiscent of reparative fibrous and granulation tissue [10, 11]; these lesions are thought by some observers to

represent a reactive proliferative response to trauma [12, 13]. These fibroblastic and myofibroblastic (Fb/MFb) lesions have been labelled 'pseudosarcomatous' as they can be misdiagnosed for a soft tissue sarcoma on account of their rapid clinical growth and worrisome histological features such as high cellularity and increased mitotic activity [10, 12]. Another proliferative Fb/MFb lesion which needs to be distinguished from fibrosarcoma and other malignant spindle cell tumours is deep musculoaponeurotic fibromatosis. The pathogenesis of deep fibromatosis is not known but an antecedent history of trauma is reported in 16% to 28% of cases [14, 15]. Fibromatosis has an infiltrative growth pattern and tends to recur but does not metastasise [14, 16]. Fibromatosis contains scattered prominent, thin-walled, evenly spaced vessels, but whether lymphatics are present within the vascular network of this and other Fb/MFb lesions of soft tissue is not known.

In this study, our aim has been to determine, using two highly specific markers of lymphatics endothelial cells, Lyve-1 and podoplanin [17, 18], whether the relative infrequency of lymph node metastasis from soft tissue sarcomas can be explained by the absence of lymphatic vessels within these tumours. In addition, as lymphatics are a known component of reparative and inflammatory lesions, we determined whether the presence of these vessels could be used as a diagnostic discriminant to distinguish proliferative Fb/MFb lesions, such as nodular fasciitis and fibromatosis, from fibrosarcoma and other malignant spindle cell tumours.

Materials and methods

One hundred eighty cases of benign and malignant soft tissue tumour were retrieved from the files of the histopathology departments of the Nuffield Orthopaedic Centre and the Oxford Radcliffe Hospital, Oxford. The cases were reviewed by three pathologists (GM, KH, NAA). The number and histological type of the benign and malignant soft tissue tumours and tumour-like lesions examined in this study are shown in Tables 1 and 2. The histological and other criteria used for tumour diagnosis are detailed in [19]. One case of epithelioid sarcoma and one case of leiomyosarcoma, both of which subsequently developed lymph node metastases, were included in the study. Two to five representative sections of each tumour were examined; these included one section of the tumour margin with surrounding soft tissue. Five-micrometer sections of formalin-fixed, paraffin-embedded tissue were cut onto silane-coated slides (Surgipath, UK); the sections were incubated at 37°C for 24 h prior to staining to improve tissue adhesion.

All immunohistochemical staining was performed using an indirect immunoperoxidase technique (ChemMate Envision, Dako, UK).

Tissue sections were dewaxed and re-hydrated by successive immersion in xylene, graded ethanol and water. Antigen retrieval was performed by microwave treatment (700 W, 2×4 min) in Target Retrieval Solution (Dako, UK). Endogenous peroxidase was blocked by 0.2% (*v*/*v*) hydrogen peroxide in 80% ethanol and protein block serum prior to 30 min incubation with mouse-anti-Lyve-1 and anti-podoplanin monoclonal antibodies [17, 18]. Immunohistochemistry was also carried out using the monoclonal antibodies JC70 and QBend10 (Dako, UK) directed against the vascular endothelial cell markers CD31 and CD34, respectively. Antigens were detected by incubation with labelled polymer and diaminobenzidine. The sections were then counterstained with haematoxylin, dehydrated, cleared and mounted. Sections of normal skin and lymph node

Table 1 The presence or absence of intralesional lymphatic vessels in soft tissue sarcomas

Type of sarcoma	Intralesional lymphatics present	Intralesional lymphatic absent
Leiomyosarcoma (total: 20; grade I—7; II—8; III—5)	3/20[a]	17/20
Fibrosarcoma (adult) (total: 8; grade II—7; III—1)	0/8	8/8
Myxofibrosarcoma (total: 4; grade II—2; III—1)	0/4	4/4
Low-grade fibromyxoid sarcoma (total: 3; grade I—2)	0/3	3/3
Malignant fibrous histiocytoma (total: 8; grade II—4; III—4)	0/8	8/8
Malignant peripheral nerve sheath tumour[b] (total: 7; grade I—2; II—3; III—2)	0/7	7/7
Rhabdomyosarcoma (total: 5; embryonal—2; alveolar—2; pleomorphic—1)	2/5	3/5
Epithelioid sarcoma (total: 4; classic—2; proximal—2)	4/4[a]	0/4
Soft tissue Ewing's sarcoma/PNET	0/3	3/3
Liposarcoma (total: 11; lipoma-like—4; sclerosing—1; myxoid/round cell—5; pleomorphic—1)	0/11	11/11
Synovial sarcoma (total: 13; biphasic—4; monophasic—9)	2/13	11/13

Total number of cases and their grading is shown in parenthesis.
[a] One case had histologically confirmed lymph node metastases.
[b] Three cases NF1-related.

Table 2 The presence or absence of intralesional lymphatic vessels in benign soft tissue tumours

Type of benign soft tissue tumour/lesion	Intralesional lymphatics present	Intralesional lymphatics absent
Angioleiomyoma (4)	1/4	3/4
Leiomyoma (2)	0/2	2/2
Lipoma (4)	0/4	4/4
Angiolipoma (3)	2/3	1/3
Intramuscular lipoma (2)	2/2	0/2
Spindle cell lipoma (1)	0/1	1/1
Chondroid lipoma (1)	0/1	1/1
Pleomorphic lipoma (1)	0/1	1/1
Hibernoma (3)	3/3	0/3
Myxoma (6)	0/6	6/6
Granular cell tumour (3)	2/3	1/3
Neurilemmoma (6)	0/6	6/6
Neurofibroma (7)	1/7	6/7
Plexiform neurofibroma (5)	5/5	0/5
Solitary fibrous tumour (2)	0/2	2/2
Nodular fasciitis (11)	11/11	0/11
Proliferative fasciitis (3)	3/3	0/3
Ischaemic fasciitis (1)	1/1	0/1
Elastofibroma (2)	2/2	0/2
Nuchal-type fibroma (1)	1/1	0/1
Fibroma of tendon sheath (3)	3/3	0/3
Superficial fibromatosis (3)	3/3	0/3
Deep (desmoid-type) fibromatosis (20)	20/20	0/20
Non-neoplastic Inflammatory/reparative lesions[a] (10)	10/10	0/10

Total number of cases is shown in parenthesis.
[a] 5 cases—granulomatous inflammation (TB, foreign body); 2 cases—pyogenic infection; 3 cases—healing wound

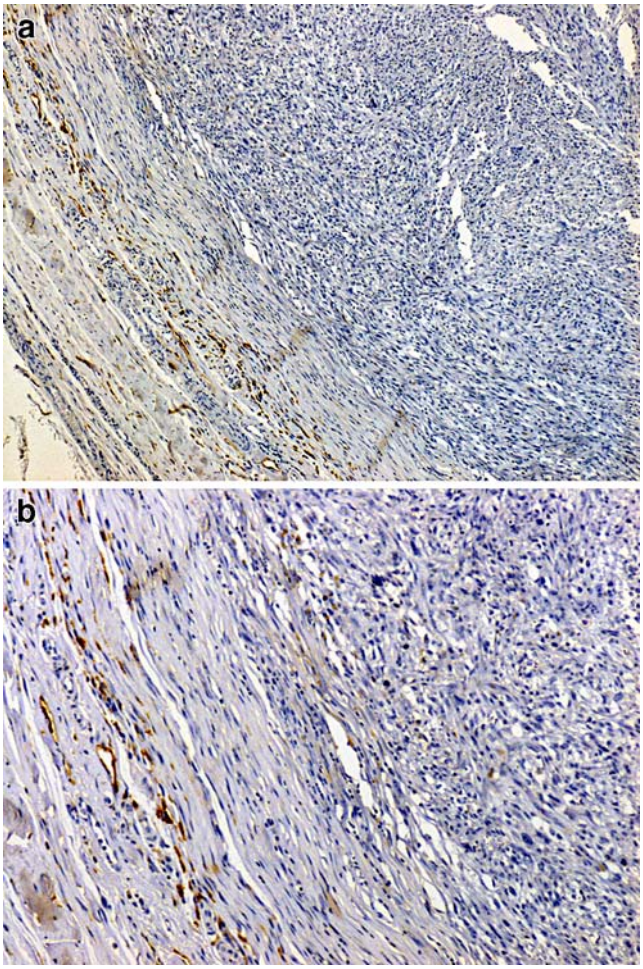

Fig. 1 Lyve-1 immunostaining of a leiomyosarcoma showing numerous extratumoural lymphatic vessels but no intralesional lymphatics. Original magnification: **a** ×100, **b** ×200

were used as positive control tissue; these contained both lymphatic and blood vessels. Negative controls consisted of sections of normal skin and lymph node stained by the above immunohistochemical technique using primary antibody diluent alone.

Results

Malignant soft tissue tumours

Vascular channels outlined by the lymphatic endothelial cell markers Lyve-1 and podoplanin were noted in the extralesional connective tissue around all 86 soft tissue sarcomas examined in the study (Fig. 1). These lymphatics varied in size from small capillaries to dilated vessels. Intratumoural Lyve-1+/podoplanin+ lymphatic vessels were noted only in a few sarcomas (Table 2). These included all four cases of epithelioid sarcomas examined, including one which developed lymph node metastases (Fig. 2). Intratumoural Lyve-

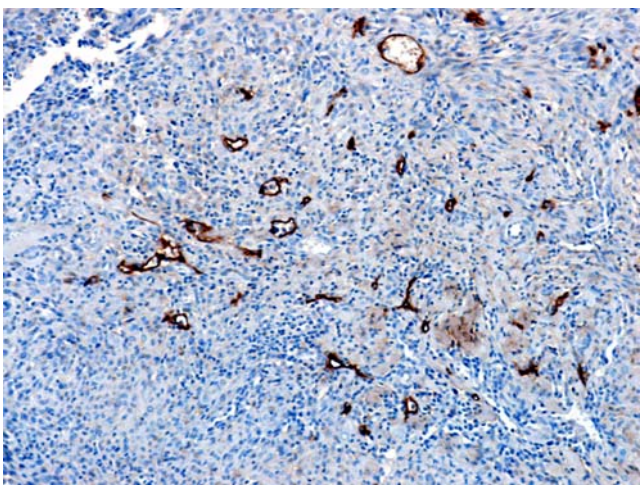

Fig. 2 Podoplanin-expressing intratumoural lymphatic vessels in an epithelioid sarcoma. Original magnification ×100

1+/podoplanin+ lymphatic vessels were also noted in three cases of leiomyosarcoma (including one which metastasised to lymph nodes), two cases of monophasic synovial sarcoma and two cases of rhabdomyosarcoma (Fig. 3). Intratumoural lymphatics within these sarcomas were scattered throughout the tumour and were mainly capillary in size. None of the intratumoural or extratumoural Lyve-1+/podoplanin+ vessels in the soft tissue sarcomas examined contained intraluminal tumour.

Benign soft tissue tumours

Lyve-1+/podoplanin+ vascular channels, ranging in size from small capillaries to dilated vascular channels, were seen in connective tissue around all benign soft tissue tumours. With the exception of a number of benign Fb/MFb proliferative lesions (discussed below), the majority of benign soft tissue tumours did not contain intratumoural Lyve-1+/podoplanin+ lymphatic channels (Table 2). The presence or absence of intratumoural lymphatics showed some variation between different benign tumour types and subtypes. For example, amongst the benign tumours of fat, with the exception of intramuscular lipoma, angiolipoma and hibernoma, none of the lipomatous tumours contained intratumoural lymphatic vessels (Fig. 4a). Fully encapsulated tumours, such as neurilemmoma, did not contain lymphatic vessels, as did most well-defined but unencapsulated neurofibromas; lymphatic vessels were, however, seen in one case of intraneural neurofibroma. Two cases of granular cell tumour and all cases of plexiform neurofibroma also contained lymphatic vessels; in the plexiform neurofibromas, there were numerous small to medium sized lymphatic vessels within neurofibromatous tissue that involved skin and subcutaneous tissue (Fig. 4b).

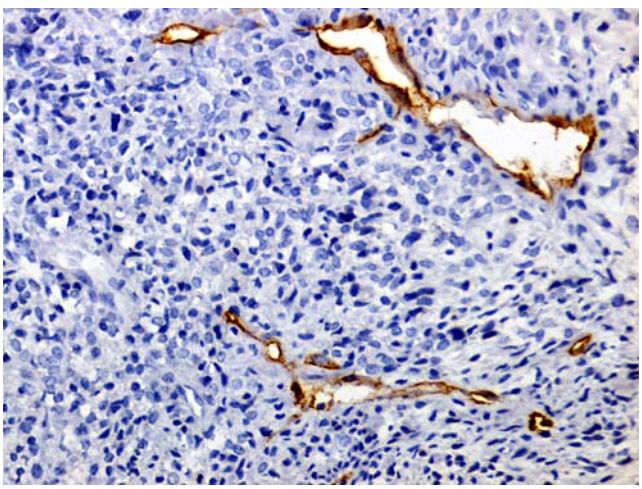

Fig. 3 Podoplanin-expressing intratumoural lymphatic vessels in a monophasic synovial sarcoma. Original magnification ×200

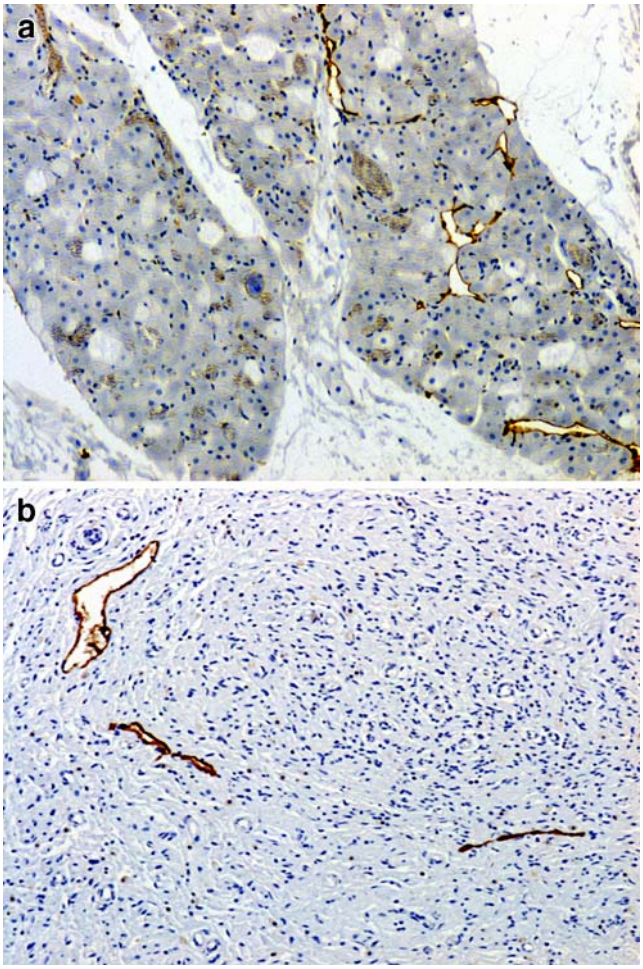

Fig. 4 Lyve-1 staining of benign soft tissue tumours showing focally scattered small intralesional lymphatics in **a** hibernoma. **b** Plexiform neurofibroma. Original magnification: **a** ×50, **b** ×100

Intralesional Lyve-1+/podoplanin+ lymphatic vessels were noted in all cases of benign Fb/MFb tumours examined including nodular fasciitis, proliferative fasciitis, ischaemic fasciitis, nuchal fibroma, elastofibroma, fibroma of tendon sheath and superficial and deep fibromatosis. Intralesional lymphatic vessels in nodular fasciitis and proliferative fasciitis were predominantly small, thin-walled, capillary-sized vessels that were scattered throughout the lesion with a relatively high density at the periphery; a few dilated lymphatic channels were also noted in some cases of proliferative fasciitis (Fig. 5a–c). In contrast to fibrosarcoma and MFH (Fig. 6a), all 20 cases of deep musculoaponeurotic fibromatosis contained intralesional lymphatic vessels. These lymphatics were mostly seen as scattered small capillary-sized vessels (Fig. 6b), but in three cases lymphatic vessels were numerous and included some small to medium sized lymphatic channels.

Reparative fibrous and granulation tissue in healing wounds of skin and subcutaneous tissue and foreign body granulomas and mycobacterial and pyogenic infections of

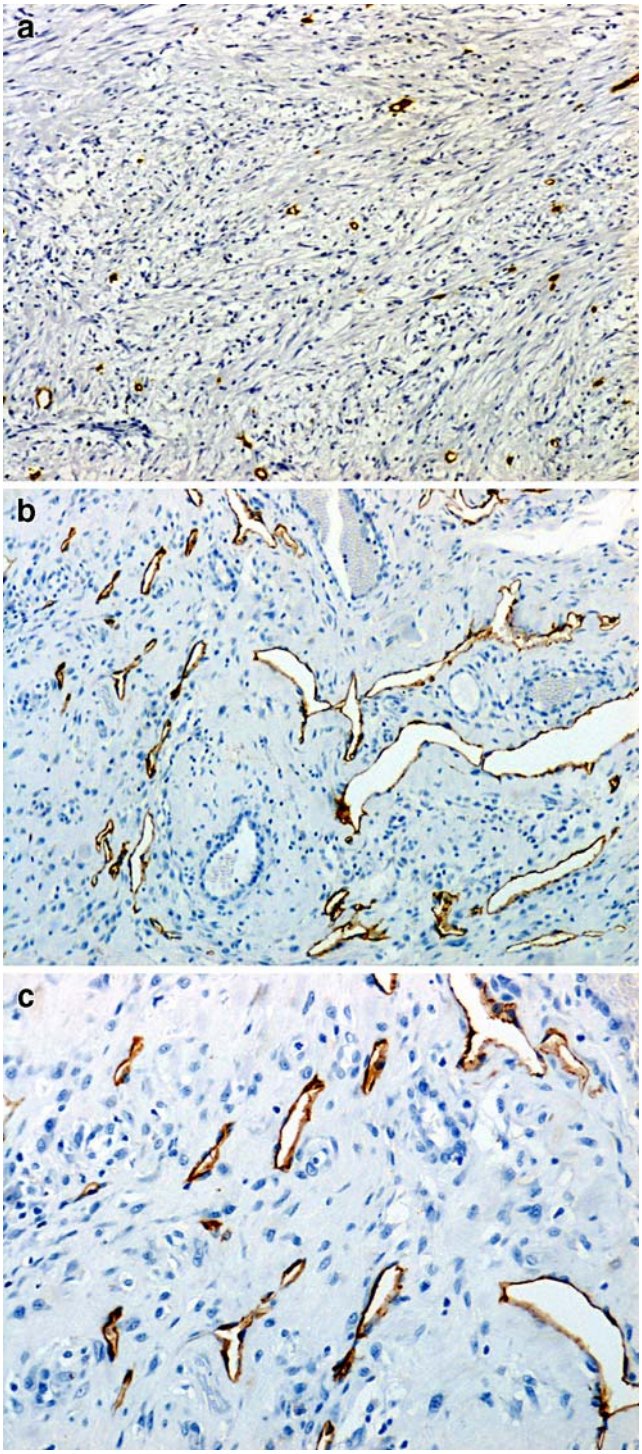

Fig. 5 Numerous Lyve-1-expressing intralesional lymphatic vessels of variable size in **a** nodular fasciitis, and **b**, **c** proliferative fasciitis. Original magnification: **a**, **b** ×100 and **c** ×200

soft tissue contained Lyve-1+/podoplanin+ vessels within areas of inflammation and surrounding connective tissue.

All benign and malignant soft tissue tumours contained vascular channels which were lined by CD31+/CD34+ endothelial cells, both within the tumour and in the surrounding connective tissue. CD31 and CD34 are both known to stain lymphatic endothelium and only a minority of these vessels were Lyve-1+/podoplanin+. Lyve-1+/podoplanin+ lymphatic vessels were morphologically similar to thin-walled CD31+/CD34+/Lyve-1−/podoplanin− blood vessels. It was notable that many of the vessels which did not contain red cells in the lumen were CD31+/CD34+ but not Lyve-1+/podoplanin+, indicating that the absence of red cells in the vessel lumen is an unreliable morphological criterion for distinguishing lymphatic vessels from blood vessels. Staining for Lyve-1 was generally weaker but more specific for lymphatic vessels compared with podoplanin, which also stained the neoplastic epithelial component of one biphasic synovial sarcoma, a finding noted in a previous study [20]. In addition to lymphatic channels, Lyve-1, as noted previously [9], also stained tumour-associated macrophages in connective tissue around some benign and malignant soft tissue tumours.

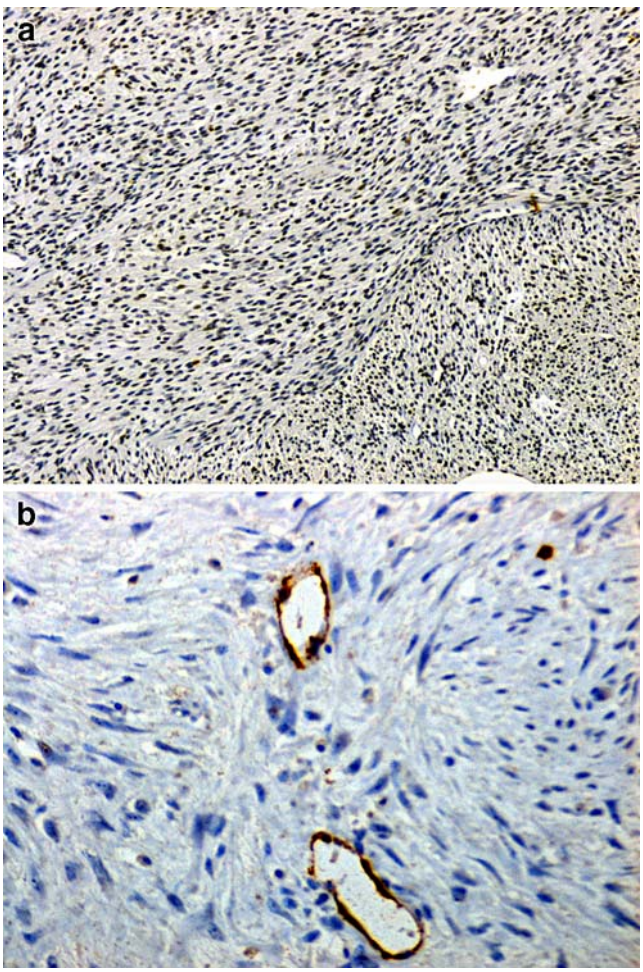

Fig. 6 Lyve-1 immunostaining of a well-differentiated fibrosarcoma showing absence of intratumoural lymphatics (**a**), in contrast to deep fibromatosis which shows multiple intralesional lymphatic vessels (**b**). Original magnification: **a**, **b** ×100

Discussion

In this study, we have shown that most soft tissue sarcomas do not contain intratumoural lymphatic vessels. Although extratumoural lymphatic vessels were found in the connective tissue around all malignant soft tissues tumours, only 12.7% of soft tissue sarcomas contained intralesional lymphatics. The absence of intratumoural lymphatics in the majority of the soft tissue sarcomas examined provides some rationale for the observation that most soft tissue sarcomas do not metastasise to lymph nodes. Some support for this conclusion comes from our finding that intratumoural lymphatics were present in two cases of sarcoma in which lymph node metastases of the primary sarcoma were documented. All four primary epithelioid sarcomas examined in this study were noted to contain lymphatics; this finding is in keeping with the reported relatively high incidence of lymph node metastasis of this tumour [21–23]. Other malignant soft tissue tumours which were noted to contain intratumoural lymphatics included rhabdomyosarcoma, synovial sarcoma and leiomyosarcoma; these tumours have been reported in some series to have a relatively high incidence of lymph node metastasis [2–4].

To our knowledge, there has been no systematic study of lymphatics in soft tissue sarcomas. Friedrichs et al. [24], in a small study, found that 50% of sarcomas contained lymphatic vessels. They analysed 32 sarcomas, including sarcomas of the uterus and bone; it is not clear how many soft tissue sarcomas were analysed in this study but, as in our study, they found lymphatic vessels in epithelioid sarcoma, leiomyosarcoma and synovial sarcoma but not in liposarcoma. Expression of vascular endothelial growth factor-C (VEGF-C), which promotes lymphangiogenesis, and its receptor VEGF-R3 was also noted in some sarcomas; however, there was no correlation between lymphatic microvessel density and expression of these markers.

Lymphatic metastasis is a well-recognised poor prognostic indicator in many tumours. There is controversy regarding whether lymph node metastasis by malignant tumours occurs primarily by invasion of pre-existing lymphatic vessels or by lymphangiogenesis within these tumours [25–27]. Some studies have suggested that only peritumoural lymphatics are sufficient for lymphatic metastasis [27–30]. Few intratumoural lymphatics and no active lymphangiogenesis were noted in primary human breast carcinomas which metastasise to lymph nodes, suggesting that lymphatic metastasis of this carcinoma proceeds via pre-existing peritumoural tissue lymphatics [5, 6]. In contrast, the presence of intratumoural lymphatics has been shown to be associated with a relatively poor outcome in squamous cell carcinoma of the head and neck, melanoma and papillary carcinoma of the thyroid, all tumours which frequently metastasise via lymphatics [31–33]. The findings of our study would suggest that peritumoural lymphatics alone are not sufficient for metastasis of sarcomas to lymph nodes as, although numerous Lyve-1+/podoplanin^{+} lymphatic vessels were found in connective tissues surrounding all the primary sarcomas we examined, only in two cases were lymph node metastases identified clinically and histologically. It could be argued that the finding of intralesional lymphatics in malignant tumours which did not exhibit lymph node metastasis contradicts this idea, but it is possible that, as in some murine sarcomas, there may be a paucity or absence of functional intratumoural lymphatics in these sarcomas [29].

The benign soft tissue tumours we examined showed some variation with regard to the presence or absence of lymphatic vessels. However, the majority of benign tumours did not contain intratumoural lymphatics in contrast to most benign Fb/MFb proliferative lesions. Benign tumours which were completely encapsulated, such as neurilemmoma, did not contain lymphatic vessels, as did many benign lesions that were well-defined but not encapsulated such as neurofibroma. Benign tumours that were relatively poorly defined such as granular cell tumour and hibernoma contained lymphatic vessels as did plexiform neurofibroma, a lesion with a frankly infiltrative growth pattern. The lymphatic vessels in these tumours may have represented pre-existing extratumoural lymphatics in the surrounding connective tissue which had become incorporated into the lesion as it continued to grow.

In contrast to most benign and malignant soft tissue tumours, intratumoural lymphatics were identified in all benign Fb/MFB proliferative lesions of soft tissue including nodular fasciitis, proliferative fasciitis, ischaemic fasciitis, nuchal fibroma, elastofibroma and superficial and deep fibromatosis. Granulation tissue formation and wound healing are two pathological processes where lymphangiogenesis is evident [7–9], and we noted lymphatics in all inflammatory and foreign body lesions of soft tissue. Although a direct association between the pathogenesis of reactive proliferative lesions such as nodular/proliferative fasciitis and trauma has not been established, several features are suggestive of this aetiology, including the natural course of regression of these lesions, their predominance in the upper extremity and their histological resemblance to healing wounds [10, 12]. Both nodular and proliferative fasciitis commonly contain inflammatory cells and it has been shown that macrophages recruited into inflammatory sites produce VEGF-C and VEGF-D, both of which are known to promote lymphangiogenesis by binding to VEGF-R3, which is expressed on lymphatic endothelial cells [7, 34].

Musculoaponeurotic fibromatosis is considered to be a lesion that has an intermediate biological behaviour between

benign Fb/MFb lesions and fibrosarcoma. Although it tends to recur locally, metastasis is not observed. Genetic, endocrine and physical factors such as trauma and irradiation have been implicated in its pathogenesis. An antecedent history of trauma has been reported in 16–28% of cases of deep fibromatosis [14, 15], and sporadic cases have been reported to regress spontaneously [35]. Inflammatory cells can be seen in some cases of fibromatosis and they may contribute to lymphangiogenesis in a manner similar to that postulated above for nodular and proliferative fasciitis. Our finding of Lyve-1+/podoplanin+ lymphatic vessels in superficial and deep fibromatosis would suggest that there may be a reactive component in these lesions. Similarly, the finding of intralesional lymphatics in all three cases of fibroma of tendon sheath is in keeping with the observation that this lesion initially resembles nodular fasciitis and that it may be at least in part reactive in nature [36].

Benign reactive and locally aggressive myofibroblastic lesions, such as nodular fasciitis and fibromatosis, are often difficult to distinguish from sarcomas histologically. Nodular fasciitis contains numerous plump, spindle-shaped cells with large, hyperchromatic ovoid or spindle-shaped nuclei; these cells contain prominent nucleoli and frequently show mitotic activity. Deep fibromatosis often presents as a large tumour which has a highly infiltrative pattern of growth that is suggestive of malignancy; it may contain spindle-shaped fibroblasts and myofibroblasts that show frequent mitotic activity. In this study, we found that all fibrosarcomas and fibrosarcoma variants, such as low-grade fibromyxoid sarcoma and myxofibrosarcoma, as well as all cases of MFH and malignant peripheral nerve sheath tumour, did not contain intratumoural lymphatic vessels. In contrast, we found intratumoural lymphatic vessels in all cases of nodular and proliferative fasciitis and in deep fibromatosis. Taken with other clinical, radiological and histological information, the identification of intratumoural lymphatics may be useful in identifying proliferative Fb/MFb lesions, and distinguishing them from fibrosarcoma and other malignant spindle cell tumours.

Acknowledgements The authors thank Mrs. C. Lowe for typing the manuscript. Dr. Mahendra was a Visiting Fellow funded by the government of Sri Lanka.

Conflict of interest statement We declare that we have no conflict of interest.

References

1. Sondak VK, Chang AE (2001) Clinical evaluation and treatment of soft tissue tumours. In: Weiss SW, Goldblum JR (eds) Enzinger and Weiss's soft tissue tumours. 4th edn. Mosby, St. Louis, pp 21–44
2. Fong Y, Coit DG, Woodruff JM et al (1993) Lymph node metastasis from soft tissue sarcoma in adults. Analysis of data from a prospective database of 1772 sarcoma patients. Ann Surg 217:72–77
3. Behranwala KA, A'Hern R, Omar A et al (2004) Prognosis of lymph node metastasis in soft tissue sarcoma. Ann Surg Oncol 11:714–719
4. Weingrad DN, Rosenburg SA (1978) Early lymphatic spread of osteogenic and soft-tissue sarcomas. Surgery 84:231–240
5. Williams CSM, Leek RD, Robson AM et al (2003) Absence of lymphangiogenesis and intratumoral lymph vessels in human metastatic breast cancer. J Pathol 200:195–206
6. Bono P, Wasenius V, Heikkilä P et al (2004) High Lyve-1 positive lymphatic vessels are associated with poor outcome in breast cancer. Clin Cancer Res 10:7144–7149
7. Hosking B, Makinen T (2007) Lymphatic vasculature: a molecular perspective. Bioessays 29:1192–1202
8. Ji RC (2005) Characteristics of lymphatic endothelial cells in physiological and pathological conditions. Histol Histopathol 20:155–175
9. Schledzewski K, Falkowski M, Moldenhauer G et al (2006) Lymphatic endothelium-specific hyaluronan receptor LYVE-1 is expressed by stabilin-1+, F4/80+, CD11b+ macrophages in malignant tumours and wound healing tissue in vivo and in bone marrow cultures in vitro: implication for the assessment of lymphangiogenesis. J Pathol 209:67–77
10. Montgomery EA, Meis JM (1991) Nodular fasciitis; its morphological spectrum and immunohistochemical profile. Am J Surg Pathol 15:942–948
11. Soule EH, Minn R (1975) Proliferative (nodular) fasciitis. Arch Pathol 73:17–24
12. Akerman M (1997) Benign fibrous lesions masquerading as sarcomas; clinical and morphological pitfalls. Acta Orthop Scand 68:37–40
13. Kim ST, Kim HJ, Park SW et al (2005) Nodular fasciitis in the head and neck: CT and MR imaging findings. Am J Neuroradiol 26:2617–2623
14. Pritchard DJ, Nascimento AG, Petersen IA (1996) Local control of extra-abdominal desmoid tumors. J Bone Joint Surg 78A:848–854
15. Lopez R, Kemalyan N, Moseley HS et al (1990) Problems in diagnosis and management of desmoid tumors. Am J Surg 159:450–453
16. De Wever I, Cin PD, Fletcher CDM et al (2000) Cytogenetics, clinical and morphological correlation in 78 cases of fibromatosis: a report from the CHAMP study group. Mod Pathol 13:1080–1085
17. Breiteneder-Geleff S, Soleiman A, Kowalski H et al (1999) Angiosarcomas express mixed endothelial phenotypes of blood and lymphatic capillaries: podoplanin as a specific marker for lymphatic endothelium. Am J Pathol 154:385–394
18. Banerji S, Ni J, Wang S et al (1999) LYVE-1, a new homologue of the CD44 glycoprotein, is a lymph-specific receptor for hyaluronan. J Cell Biol 144:789–801
19. Fletcher CDM, Unni KK, Mertens F (eds) (2002) World Health Organisation classification of tumours. pathology and genetics of tumours of soft tissue and bone. IARC, Lyon
20. Ordóñez NG (2005) D2-40 and podoplanin are highly specific and sensitive immunohistochemical markers of epithelioid malignant mesothelioma. Hum Pathol 36:372–380
21. De Visscher SAHJ, Ginkel RJV, Wobbes T et al (2006) Epithelioid sarcoma: still an only surgically curable disease. Cancer 107:606–612
22. Chase DR, Enzinger FM (1985) Epithelioid sarcoma: diagnosis, prognostic indicators and treatment. Am J Surg Pathol 9:241–263
23. Baratti D, Pennacchioli E, Casali PG et al (2007) Epithelioid sarcoma: prognostic factors and survival in a series of patients treated at a single institution. Ann Surg Oncol 12:3542–3551

24. Friedrichs N, Hahne JC, Pepper MS et al (2006) Immunohistochemical quantification of lymph vessels, VEGF-C and VEGF receptor 3 in human sarcomas. Histopathology 49:87–88
25. Beasley NJ, Prevo R, Banerji S et al (2002) Intratumoral lymphangiogenesis and lymph node metastasis in head and neck cancer. Cancer Res 62:1315–1320
26. Stacker SA, Baldwin ME, Achen MG et al (2002) The role of tumour lymphangiogenesis in metastatic spread. FASEB J 16:922–934
27. Pepper MS, Skobe M (2003) Lymphatic endothelium: morphological, molecular and functional properties. J Cell Biol 163: 209–213
28. Padera TM, Kadambi A, di Tomaso E et al (2002) Lymphatic metastasis in the absence of functional intratumoural lymphatics. Science 296:1883–1886
29. Leu AJ, Berk DA, Lymboussaki A et al (2000) Absence of functional lymphatics within a murine sarcoma: a molecular and functional evaluation. Cancer Res 60:4324–4327
30. Jain RK, Fenton BT (2002) Intratumoral lymphatic vessels: a case of mistaken identity or malfunction? J Natl Cancer Inst 94:417–421
31. Maula SM, Luukkaa M, Grénman R et al (2003) Intratumoral lymphatics are essential for the metastatic spread and prognosis in squamous cell carcinoma of the head and neck region. Cancer Res 63:1920–1926
32. Dadras SS, Paul T, Bertoncini J et al (2003) Tumor lymphangiogenesis: a novel prognostic indicator for cutaneous melanoma metastasis and survival. Am J Pathol 162:1951–1960
33. Hall FT, Freeman JL, Jackson DG et al (2003) Intratumoral lymphatics and lymph node metastasis in papillary thyroid carcinoma. Arch Otolaryngol Head Neck Surg 129:716–719
34. Cursiefen C, Chen L, Borges LP et al (2004) VEGF-A stimulates lymphangiogenesis and hemangiogenesis in inflammatory neovascularization via macrophage recruitment. J Clin Invest 113:1040–1050
35. Weiss SW, Goldblum JR (2001) Fibromatosis. In: Weiss SW, Goldblum JR (eds) Enzinger and Weiss's soft tissue tumours. 4th edn. Mosby, St. Louis, pp 309–346
36. Weiss SW, Goldblum JR (2001) Benign fibrous tissue lesions. In: Weiss SW, Goldblum JR (eds) Enzinger and Weiss's soft tissue tumours. 4th edn. Mosby, St. Louis, pp 247–307

Virchows Arch (2008) 453:465–471
DOI 10.1007/s00428-008-0677-7

ORIGINAL ARTICLE

Investigating differentiation mechanisms of the constituent cells of sex cord-stromal tumours of the ovary

Panagiotis Papanastasopoulos · Maria Repanti · Vasileia Damaskou · Vasiliki Bravou · Helen Papadaki

Received: 11 April 2008 / Revised: 13 August 2008 / Accepted: 4 September 2008 / Published online: 1 October 2008

Abstract SOX-9, an essential factor for male sexual development, can be induced by prostaglandin D2 in a Sry-independent mechanism. Recent data suggest that the hedgehog pathway is involved in the differentiation of normal Sertoli and Leydig cells. The purpose of our study was to investigate the mechanisms involved in the differentiation of ovarian sex cord-stromal tumour (SCST) cells. Two Sertoli–Leydig cell tumours and two granulosa cell tumours with a minor Sertoli element were studied using immunohistochemistry on paraffin-embedded tissue sections. Sertoli cells expressed anti-Mullerian hormone (AMH), SOX-9, prostaglandin D synthase (Pgds) and bcl-2 (in four of four cases); sonic hedgehog (Shh) and p53 (in three of four cases) and androgen receptors (AR; in one of four cases). Ki-67 index ranged from 10% to 50%. Leydig cells expressed Shh and AR (two of two cases), while they showed no expression of p53, bcl-2 and 0% Ki-67 index. Granulosa cells expressed AMH, Pgds, Shh, estrogen receptors, progesterone receptors, AR and bcl-2 (in two of two cases) and p53 (in one of two cases). Ki-67 index was 10% and 40%, respectively. Further investigation is required to clarify the role of the molecules outlined above in the histogenesis of ovarian SCST, as Pgds-mediated SOX-9 upregulation could provide a reasonable explanation for the presence of testicular differentiation in ovarian SCST.

Keywords Sex cord-stromal tumours · Differentiation mechanisms · SOX-9 · Prostaglandin D synthase · bcl-2

P. Papanastasopoulos · M. Repanti · V. Damaskou (✉) · V. Bravou
Department of Pathology, General Hospital "Agios Andreas", Patras, Greece
e-mail: vkdama@yahoo.gr

H. Papadaki
Laboratory of Anatomy, Histology and Embryology, Faculty of Medicine, University of Patras, Patras, Greece

Introduction

Sex-cord stromal tumours (SCST) are rare neoplasms of the ovary, accounting for 8% of all the histological types of ovarian tumours [1]. Sertoli–Leydig cell tumours constitute only 1% of ovarian sex-cord stromal tumours and less than 0.5% of all primary ovarian tumours [9]. Finally, granulosa cell tumours account for approximately 5% of all ovarian tumours [7].

Ovarian sex cord-stromal tumours may contain Sertoli cells, granulosa cells, Leydig cells, thecal cells or fibroblasts of gonadal stromal origin, either singly or in any combination and in any degree of differentiation [15].

One of the main questions that remain to be adequately answered is the origin of Sertoli- and Leydig-like cells as part of sex-cord stromal tumours. Much research has been conducted and several theories have been developed over the years in an attempt to provide a reasonable explanation. Electron microscopy studies have revealed significant ultrastructural similarities between Sertoli-like cells of ovarian sex-cord stromal tumours and follicular granulosa cells, especially neoplastic granulosa cells [8]. Furthermore, the same studies have recognised a similar morphological resemblance between Leydig-like cells in ovarian sex cord-stromal tumours and follicular thecal cells [8]. Research, using immunohistochemistry and several molecular biological tools, has provided evidence supporting a close

histogenetic relationship between Sertoli-like cells in ovarian sex-cord stromal tumours and granulosa cells or its precursors [8, 12]. Moreover, the origin of the Leydig-cell component of sex cord-stromal tumours seems to be controversial; several studies consider Leydig cells to be a reactive process caused by the presence of the surrounding neoplastic Sertoli-like cells [11, 12], while recent molecular genetic evidence supports the neoplastic nature of Leydig cells [5].

The purpose of this study is to investigate the mechanisms involved in the differentiation of the cells comprising ovarian sex cord-stromal tumours.

Materials and methods

Four sex cord-stromal tumours of the ovary were included in our study. Tissue sections were retrieved from archival material from the Department of Pathology of General Hospital, "Agios Andreas", Patras. The ovarian tumours were all primary and included two Sertoli–Leydig cell tumours—one well differentiated (Fig. 1) and one poorly differentiated—and two granulosa-cell tumours [with a minor (<10%) Sertoli-element] (Fig. 2). Haematoxylin- and eosin-stained sections were reviewed by two independent pathologists, and the diagnosis was confirmed.

Representative tumour tissue blocks were used for immunohistochemistry; 4-μm thick paraffin-embedded tissue sections were deparaffinized and rehydrated. Where necessary, for some of the antibodies, tissue sections were subjected to heat-induced epitope antigen retrieval using an electric pressure cooker and Trilogy TM (CELL MARQUE, Hot Springs, AR, 71913, USA). Endogenous peroxidase activity was blocked with the peroxidase-blocking solution (DAKO, Glostrup, Denmark). Immunohistochemical staining was performed using the ChemMateTM Dako EnVisionTM Detection System, Peroxidase/DAB, Rabbit/Mouse (DAKO, Glostrup, Denmark) in a Dako autostainer. After the incubation of primary antibodies for 30′–90′, the EnVision reagent—a peroxidase-conjugated polymer backbone, which also carries secondary antibody molecules directed against rabbit and mouse immunoglobulins—was applied and incubated for 20′. Diaminobenzidine was used as a color substrate and Mayer's haematoxylin as counterstain.

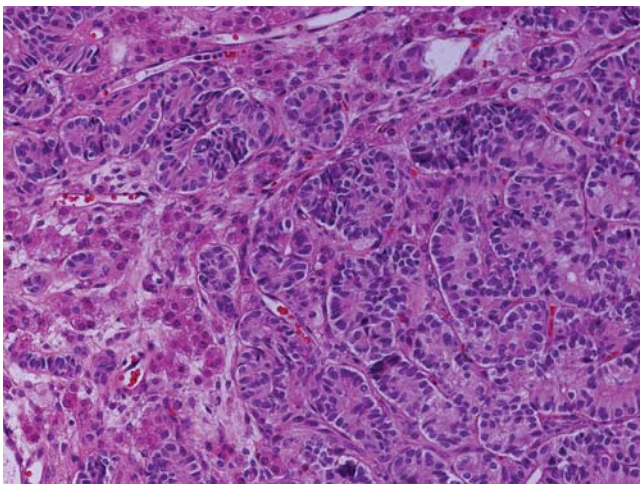

Fig. 1 Well-differentiated Sertoli–Leydig cell tumour. Solid and hollow tubules are separated by Leydig-cells with abundant eosinophilic cytoplasm (H&E stain)

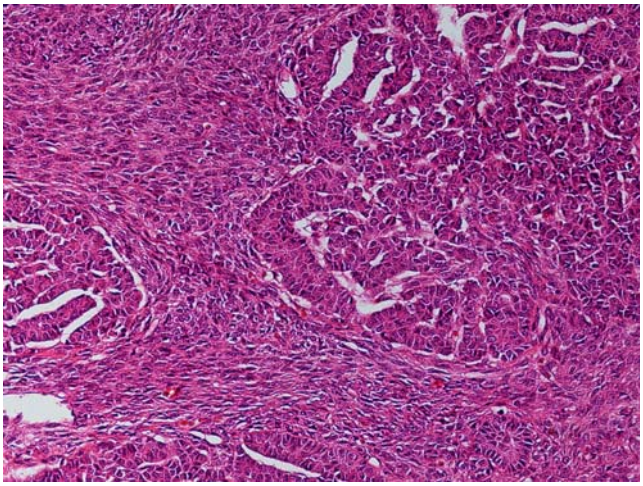

Fig. 2 Granulosa cell tumour with a minor sertoli element (<10%). Granulosa cells growing in a diffuse pattern, interspersed between Sertoli-form areas (H&E stain)

The following primary antibodies were used: anti-Mullerian hormone (AMH, CLONE 5/6, 1:15, Serotec, Kidlington,UK), SOX-9 (CLONE H-90, 1:50, Santa Cruz, CA, USA), prostaglandin D Synthase (Pgds, CLONE Lipocalin type; murine, 1:300, Cayman, Ann Arbor, MI, USA), sonic hedgehog (Shh, cross-reacting with indian and desert hedgehog, CLONE H-160, 1:20, Santa Cruz, CA, USA), estrogen receptors (CLONE 1D5, 1:50, DAKO, Glostrup, Denmark), progesterone receptors (PrR, CLONE PgR636^1, 1:50, DAKO, Glostrup, Denmark), androgen receptors (AR, CLONE AR441, 1:50, DAKO, Glostrup, Denmark), Ki-67 (CLONE MIB-1, 1:30, DAKO, Glostrup, Denmark), bcl-2 (CLONE 100, 1:50, Biogenex, SanRamon, USA) and p53 (CLONE DO7, 1:30, DAKO, Glostrup, Denmark).

Pretreatment with TrilogyTM (CELL MARQUE, Hot Springs, AR, 71913, USA) was used where appropriate. Furthermore, appropriate positive controls were used for each antibody. For negative controls, the primary antibody was omitted.

Staining intensity and the percentage of positive cells were taken into account in the immunoreactivity evaluation process. The degree of immunoreactivity was scored

semiquantitatively on a scale of 0–3+ (0: weak or moderate staining in <10% of cells, 1+: weak or moderate staining in 10–35%, 2+: weak staining in >70% or moderate staining in 35–70% or strong staining in 10–35%, 3+: moderate staining in >70% or strong staining in >35%.)

Results

Clinical details and gross findings

The patients ranged from 27 to 63 years of age. Each patient presented with a history or symptoms most probably related to estrogen or androgen overproduction. It is mention-worthy that one case presented with an acute abdomen due to an ovarian "cyst" rupture and another case with a synchronous benign (mature) cystic teratoma of the contralateral ovary. The tumours ranged from 3.5 to 12 cm. Surgery was the initial treatment for all four patients. At the time of diagnosis, as well as immediately post-operatively, no metastatic disease was identified in any of the patients. Basic clinical and gross pathologic data along with the final diagnosis are presented in Table 1.

Sertoli cell component

In all four cases studied, Sertoli-like cells were positive for AMH (cytoplasmic staining—Fig. 3), SOX-9 (mainly cytoplasmic staining, some positive nuclei—Fig. 4) and Pgds (cytoplasmic staining—Fig. 5). Furthermore, the Sertoli cell component was positive for Shh (cytoplasmic staining—Fig. 6) in three cases. Only the poorly differentiated Sertoli–Leydig cell tumour expressed AR (nuclear staining), while no immunoreactivity for any of the steroid-hormone receptors was noted in the well-differentiated tumour. The Sertoli cell component was strongly positive for bcl-2 (cytoplasmic staining—Fig. 7) in all four cases studied, while Ki-67 (nuclear staining) labeling index ranged from 10% of cells (well-differentiated Sertoli–Leydig cell tumour and one granulosa cell tumour) to 50% (poorly differentiated Sertoli–Leydig cell tumour). p53 (nuclear staining) was detected in three cases and showed stronger immunoreactivity in the poorly differentiated Sertoli–Leydig cell tumour. Immunohistochemical findings with regards to the Sertoli cell component are summarised in Table 2.

Leydig cell component

In both cases of Sertoli–Leydig cell tumour, Leydig-like cells were positive for Shh (cytoplasmic staining—Fig. 6). Only androgen receptors (nuclear staining) were expressed in the Leydig cell component of the tumours, which, in addition, showed no proliferative or anti-apoptotic index (no expression of p53, bcl-2 and 0% Ki-67 labeling index). The remaining markers used were not detected in the above tumours. Immunohistochemical findings with regard to the Leydig cell component are summarised in Table 3.

Table 1 Diagnosis, clinical and gross pathologic data

Case	Diagnosis	Age	Laterality	Size (cm)	Gross appearance	Symptoms/laboratory findings	Stage
1	Sertoli–Leydig cell tumour (well differentiated)	27	Left	3.5	Predominantly solid with focal cystic areas; lobulated; yellow	6-month history of amenorrhea; hirsutism; synchronous contralateral benign cystic teratoma	T1a N0 M0, FIGO Ia
2	Sertoli–Leydig cell tumour (poorly differentiated)	41	Right	12	Partially solid, partially cystic; focally lobulated; capsule rupture; yellowgray	Acute abdomen; 4-month history of amenorrhea; elevated 17-hydroxyprogesterone, testosterone	T1c, N0, M0 FIGO Ic
3	Granulosa cell tumour with a minor Sertoli element	61	Left	10	Partially solid, partially cystic; capsule rupture; grey	Abnormal vaginal bleeding; Synchronous complex endometrial hyperplasia and endometrial polyp	T1c N0 M0 FIGO Ic
4	Granulosa cell tumour with a minor Sertoli element	63	Right	11	Partially solid, partially cystic; capsule rupture; tan	Abnormal vaginal bleeding; History of atypical endometrial hyperplasia and synchronous endometrial adenocarcinoma (endometrioid type)	T1c N0 M0 FIGO Ic

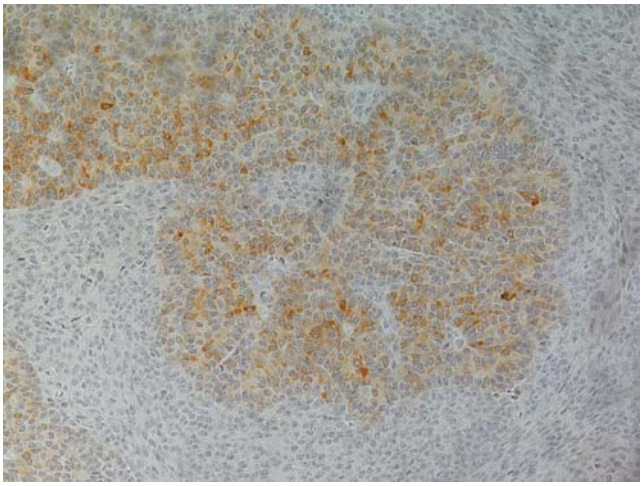

Fig. 3 Sertoli-form area of a granulosa-cell tumour with a minor (<10%) Sertoli element showing moderate cytoplasmic immunoreactivity for AMH (EnVision/DAB)

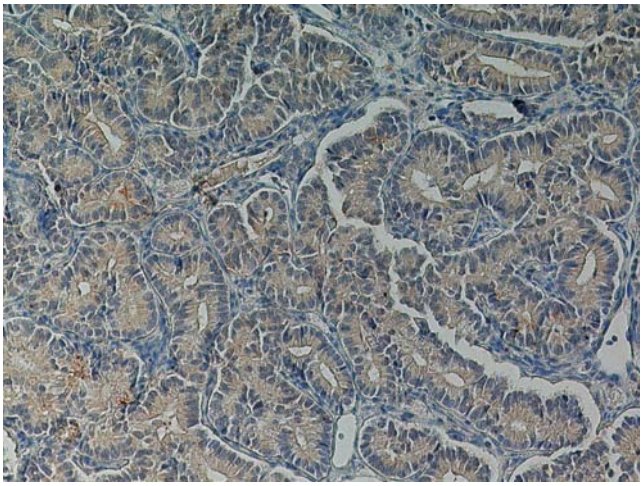

Fig. 5 Moderate cytoplasmic immunoreactivity for Pgds in a Sertoli–Leydig cell tumour, as opposed to the interspersed stroma (EnVision/DAB)

Granulosa cell component

In both cases of granulosa cell tumours, Granulosa-like cells showed immunoreactivity for AMH, Pgds and Shh (all cytoplasmic staining). Interestingly, weaker AMH expression was noted in the less-differentiated regions of the tumour (sarcomatoid). In both cases studied, the granulosa cell component expressed simultaneously all three types of steroid-hormone receptors (nuclear staining), as well as bcl-2 molecule (cytoplasmic staining—Fig. 7); p53 (nuclear staining) was positive in only one case, while Ki-67 (nuclear staining) was expressed by 10% and 40% of granulosa-like cells, respectively. The remaining markers used were not detected. Immunohistochemical findings with regard to the Granulosa cell component are summarised in Table 4.

Discussion

In this study, we investigated the expression of male sex-determination pathway molecules in ovarian sex cord-stromal tumours, focusing on the mechanisms involved in the differentiation of their constituent cells.

It is well known that the Y chromosome gene Sry encodes a transcription factor required to initiate testis development. The related autosomal gene *SOX-9* (SRY-box containing gene 9) is upregulated shortly after the onset of

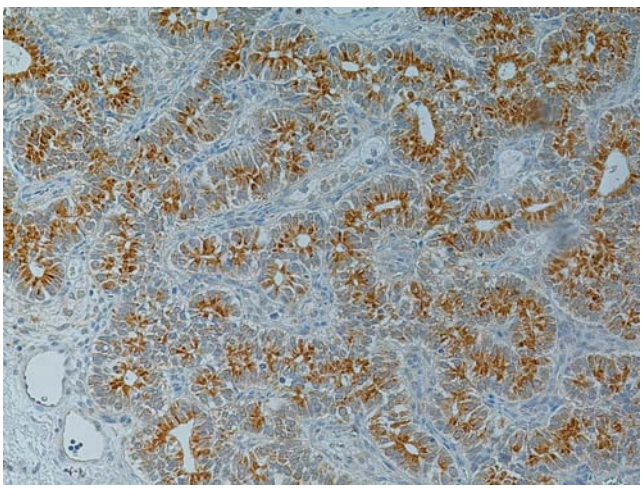

Fig. 4 Neoplastic Sertoli cells composing well-differentiated tubules in a Sertoli–Leydig cell tumour, showing strong cytoplasmic and occasionally nuclear immunoreactivity for SOX-9, as opposed to the interspersed stroma (EnVision/DAB)

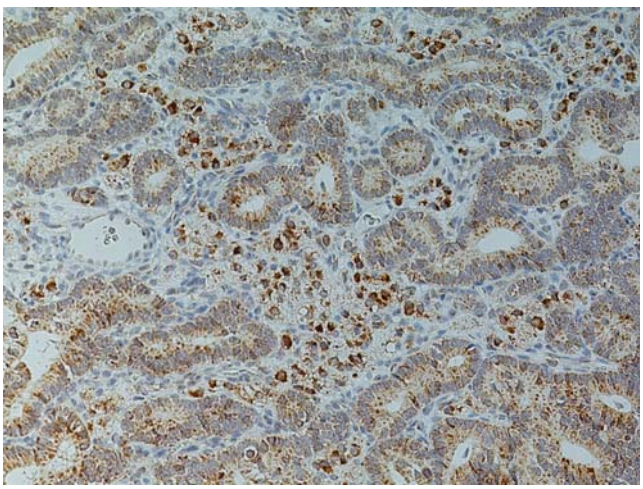

Fig. 6 Moderate granular cytoplasmic immunoreactivity for Shh in Sertoli cells of a Sertoli–Leydig cell tumour, while intervening Leydig cells show strong cytoplasmic immunoreactivity for Shh (EnVision/DAB)

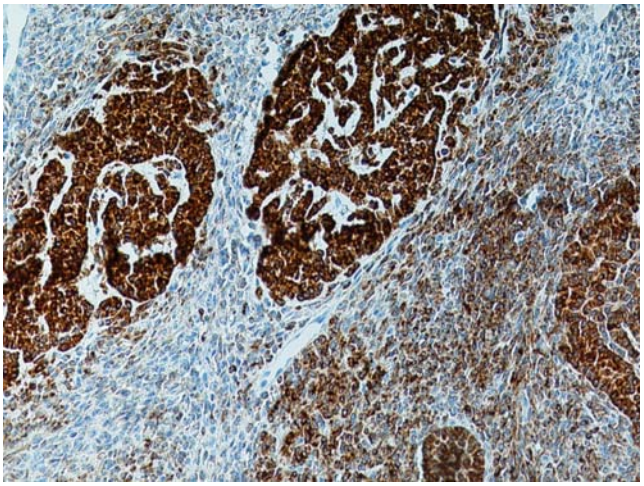

Fig. 7 Sertoli-form areas of a granulosa-cell tumour with a minor (<10%) Sertoli element and intervening granulosa cells growing in a diffuse pattern, showing strong and moderate cytoplasmic immunoreactivity for bcl-2, respectively (EnVision/DAB)

sex-determining region Y (Sry) transcription and is thought to be essential in the differentiation of Sertoli cells [16]. *SOX-9* is expressed first at low levels in the bipotent gonad of both sexes but becomes dramatically upregulated in the Sertoli cells immediately after the onset of *Sry*. However, in contrast to *Sry*, *SOX-9* expression is maintained in the Sertoli cell until after birth. Experiments using mice have shown that *SOX-9* is not only necessary but also sufficient on its own for male sexual development, as XX mice overexpressing *SOX-9* develop as males, suggesting that *SOX-9* is the only important target of *Sry* [19, 22]. Furthermore, AMH is one of the identified targets of SOX-9 [4].

In our study, SOX-9 expression was detected in all cases and was restricted to the neoplastic cells comprising the Sertoli-cell component. However, the upregulation of SOX-9 in the apparent absence of Sry still needs to be explained.

Sry-independent mechanisms of SOX-9 upregulation have been recently identified. In vitro cell mixing experiments have demonstrated that prostaglandin D2 (PGD2), produced and secreted by testicular Sertoli cells, is necessary and sufficient on its own to recruit cells that do not express *Sry* and enable them to express SOX-9 and differentiate into Sertoli cells [21, 22]. Furthermore, it has been proven recently that prostaglandin D synthase (Pgds) upregulates SOX-9 expression in human ovarian cancer cells, via the production of PGD2 [10].

In our study, Pgds was detected in every case studied and was expressed by both the Sertoli and the granulosa cell components. The authors cannot give a reasonable explanation for the cytoplasmic localization of SOX-9, as its role as a transcription factor would be expected to be mediated in the nucleus. Further investigation, involving a large number of cases and more sophisticated techniques, is required to find a possible correlation between Pdgs and SOX-9 expression in ovarian SCST. Pdgs-driven upregulation of SOX-9 could provide a reasonable explanation for the presence of neoplastic Sertoli and Leydig cells. Neoplastic granulosa cell expression of Pgds and SOX-9 cytoplasmic localisation are two further issues that need clarifying by further investigation. To our knowledge, previous to our study, Pgds has not been detected in Sertoli–Leydig cell tumours of the ovary.

Sertoli, Leydig and granulosa cell subpopulations showed immunoreactivity for the hedgehog family proteins. There are data available in the literature suggesting that hedgehog family members are normally produced and secreted by pre-sertoli and sertoli cells and that they act upon indifferent gonadal interstitial cells promoting their differentiation towards testicular Leydig cells [22]. Moreover, in experiments examining XX/XY chimeras, Sertoli

Table 2 Immunophenotype of Sertoli-like cells

Immunophenotype of Sertoli-like cells	SLCT well differentiated	SLCT poorly differentiated	Granulosa cell tumour	Granulosa cell tumour
AMH	2+	2+	2+	1+
SOX-9	3+	2+	2+	1+
Pgds	2+	1+	1+	2+
Shh	3+	1+	2+	0+
ER	0+	1+	1+	0+
PrR	0+	2+	1+	1+
AR	0+	2+	0+	0+
Ki-67 (%)	10	50	40	10
p53	1+	2+	0+	1+
Bcl-2	3+	2+	3+	3+

SLCT Sertoli–Leydig cell tumour, *SCST* sex cord-stromal tumour, *AMH* anti-Mullerian hormone, *SOX-9* SRY-box containing gene 9, *Pgds* prostaglandin D synthase, *Shh* sonic hedgehog homologue, *ER* estrogen receptors, *PrR* progesterone receptors, *AR* androgen receptors

Table 3 Immunophenotype of Leydig-like cells

Immunophenotype of Leydig-like cells	SLCT well differentiated	SLCT poorly differentiated
AMH	0+	0+
SOX-9	0+	0+
Pgds	0+	0+
Shh	3+	2+
ER	0+	0+
PrR	0+	0+
AR	1+	2+
Ki-67 (%)	0	0
p53	0+	0+
Bcl-2	0+	0+

SLCT Sertoli–Leydig cell tumour, *AMH* anti-Mullerian hormone, *SOX-9* SRY-box containing gene 9, *Pgds* prostaglandin D synthase, *Shh* sonic hedgehog homologue, *ER* estrogen receptors, *PrR* progesterone receptors, *AR* androgen receptors

cells were found to be the only type of cell in the testis that showed a strong bias for presence of the Y chromosome. This observation suggested that the Y-linked gene *Sry* is required only in the Sertoli cell lineage and that Leydig-cell differentiation can potentially be a Sry-independent phenomenon [13, 14]. Further studies will explore the potential role of hedgehog family proteins in the differentiation of testicular type cells in ovarian sex cord-stromal tumours. Immunoreactivity for hedgehog family proteins observed in the granulosa cell component of the tumours also remains unclear and needs further investigation. To our knowledge, previous to our study, no members of the hedgehog protein family have been detected in normal or neoplastic human granulosa or Leydig cells.

AMH was detected in the sertoli and granulosa cell components in each case studied. The authors, based on published data on the maturation of normal Sertoli cells [17], hypothesise that the strong immunoreactivity for AMH combined with the scarcity of AR expression observed in the Sertoli-cell component could potentially reflect a significant morphological immaturity of neoplastic Sertoli cells compared to their normal counterparts. Regarding the granulosa cell component, stronger AMH expression noted in the more differentiated regions of the tumours when compared to the sarcomatoid regions is consistent with the gradually increasing expression of AMH observed in the granulosa layer of the maturing primordial follicle [20]. Even so, the authors would like to state that due to the descriptive nature of this study, valid conclusions on the maturation status of the constituent cells of ovarian SCST will only be produced by studies involving a large number of cases.

Bcl-2 was significantly expressed in each case by both the Sertoli and the granulosa cell component. The relatively low Ki-67 labelling index combined with the high expression of bcl-2 observed in our study needs to be confirmed by studies involving a large number of cases. This could potentially serve as a reasonable explanation of the slow tumour progression and the late recurrences observed [3]. The role of p53 expression, as a potential additional anti-apoptotic mechanism in ovarian SCST, needs to be further investigated and clarified. To our knowledge, previous to this study, bcl-2 overexpression has been detected in only one case of Sertoli–Leydig cell tumours [18].

Leydig-like cells showed no proliferative activity or anti-apoptotic properties, as expressed by the Ki-67 labelling index and bcl-2 immunoreactivity, respectively. Interestingly, among the steroid-hormone receptors, only AR was found to be positive in the Leydig cell component of the tumours. Bearing in mind that a significant number of ovarian SCST cases are androgen-producing tumours, the authors believe that clarifying the mechanisms involved in the androgen-synthesis regulation could provide a better insight in the diagnosis and treatment of the above tumours. Furthermore, it is still not clear whether Leydig cells comprise of true neoplastic entities or just a reactive process.

In conclusion, we have investigated mechanisms involved in the differentiation of cells in ovarian sex cord-stromal tumours. We detected SOX-9 expression (a key-role molecule in the male sex determination pathway) in the Sertoli-cell component in every case studied. Furthermore, we demonstrated Pgds expression in the Sertoli-cell component of ovarian sex cord-stromal tumours. Sertoli-like and granulosa cells showed proliferative and high anti-apoptotic properties, as opposed to the Leydig-like cells. Finally, hedgehog family members were detected in all neoplastic cell subpopulations.

Table 4 Immunophenotype of granulosa-like cells

Immunophenotype of granulosa-like cells	Granulosa cell tumour	Granulosa cell tumour
AMH	1+	1+
SOX-9	0+	0+
Pgds	2+	2+
Shh	1+	1+
ER	2+	1+
PrR	2+	1+
AR	1+	1+
Ki-67 (%)	40	10
p53	0+	2+
Bcl-2	2+	2+

SCST sex cord-stromal tumour, *AMH* anti-Mullerian hormone, *SOX-9* SRY-box containing gene 9, *Pgds* prostaglandin D synthase, *Shh* sonic hedgehog homologue, *ER* estrogen receptors, *PrR* progesterone receptors, *AR* androgen receptors

Acknowledgments The authors would like to thank Dr Alexandra Jane Cooke for her invaluable help on reviewing, and correcting the manuscript where necessary.

The authors would like to declare that they have no conflict of interest.

References

1. Baker PM, Oliva E (2004) Immunohistochemistry as a tool in the differential diagnosis of ovarian tumors: an update. Int J Gynecol Pathol 24:39–55
2. Bishop CE, Whitworth DJ, Qin Y et al (2000) A transgenic insertion upstream of *Sox9* is associated with dominant XX sex reversal in the mouse. Nat Genet 26:490–494
3. Colombo N, Parma G, Franchi D (1999) An active chemotherapy regimen for advanced ovarian sex cord-stromal tumors. Gynecol Oncol 72:129–130
4. De Santa Barbara P, Bonneaud N, Boizet B et al (1998) Direct interaction of SRY related protein SOX9 and steroidogenic factor 1 regulates transcription of the human anti- müllerian hormone gene. Mol Cell Biol 18:6653–6665
5. Emerson RE, Wang M, Roth LM et al (2007) Molecular genetic evidence supporting the neoplastic nature of the Leydig cell component of ovarian Sertoli–Leydig cell tumors. Int J Gynecol Pathol 26(4):368–74
6. Genton CY (1980) Ovarian sertoli-leydig cell tumors. A clinical, pathological and ultrastructural study with particular reference to the histogenesis of these tumors. Arch Gynecol 230:49–75
7. Hirakawa M, Nagai Y, Yagi C et al (2007) Recurrent juvenile granulosa cell tumor of the ovary managed by palliative radiotherapy. Int J Gynecol Cancer 18(5): 913–915
8. Hittmair A, Zelger BG, Obrist P et al (1997) Ovarian Sertoli–Leydig cell tumor: a SRY gene-independent pathway of pseudo-male gonadal differentiation. Hum Pathol 28(10):1206–1210
9. Kostopoulou E, Talerman A (2003) Ovarian Sertoli–Leydig cell tumor of intermediate differentiation with immature skeletal muscle heterologous elements. Acta Obstet Gynecol Scand 82:197–198
10. Malki S, Bibeau F, Notarnicola C et al (2007) Expression and biological role of the prostaglandin D synthase/SOX9 pathway in human ovarian cancer cells. Cancer Lett 255:182–193
11. Mooney E, Man Y, Bratthauer G et al (1999) Evidence that Leydig cells in Sertoli–Leydig cell tumors have a reactive rather than a neoplastic profile. Cancer 86:2312–2319
12. Nouriani M, Felix JC, Dubeau L (2002) Histogenesis and histopathological characteristics of Sertoli–Leydig cell tumors. CME J Gynecol Oncol 7:114–120
13. Palmer SJ, Burgoyne PS (1991) In situ analysis of fetal, prepuberal and adult XX–XY chimaeric mouse testes: Sertoli cells are predominantly, but not exclusively, XY. Development 112:265–268
14. Ross AJ, Capel B (2005) Signaling at the crossroads of gonad development. Trends Endocrinol Metab 16(1):19–25
15. Scully RE (1982) Sex cord-stromal tumors. In: Blaustein A (ed) Pathology of the female genital tract. 2nd edn. Springer, New York, pp 581–601
16. Sekido R, Bar I, Narváez V et al (2004) SOX9 is up-regulated by the transient expression of SRY specifically in Sertoli cell precursors. Dev Biol 274:271–279
17. Sharpe RM, McKinnell C, Civlin C et al (2003) Proliferation and functional maturation of Sertoli cells, and their relevance to disorders of testis function in adulthood. Reproduction 125:769–784
18. Truss L, Dobin SM, Rao A et al (2004) Overexpression of the BCL2 gene in a Sertoli–Leydig cell tumor of the ovary: a pathologic and cytogenetic study. Cancer Genet Cytogenet 148:118–122
19. Vidal V, Chaboissier M, de Rooij D et al (2001) *Sox9* induces testis development in XX transgenic mice. Nat Genet 28:216–217
20. Weenen C, Laven JSE, von Bergh ARM et al (2004) Anti-Mullerian hormone expression pattern in the human ovary: potential implications for initial and cyclic follicle recruitment. Mol Hum Reprod 10(2):77–83
21. Wilhelm D, Martinson F, Bradford S et al (2005) Sertoli cell differentiation is induced both cell-autonomously and through prostaglandin signaling during mammalian sex determination. Dev Biol 287:111–124
22. Wilhelm D, Palmer S, Koopman P et al (2007) Sex determination and gonadal development in mammals. Physiol Rev 87:1–28

Virchows Arch (2008) 453:473–484
DOI 10.1007/s00428-008-0671-0

ORIGINAL ARTICLE

Exploration of the APC/β-catenin (WNT) pathway and a histologic classification system for pulmonary artery intimal sarcoma. A study of 18 cases

A. Gaumann · B. Bode-Lesniewska · D. R. Zimmermann · J. C. Fanburg-Smith · C. J. Kirkpatrick · F. Hofstädter · M. Woenckhaus · R. Stoehr · E. C. Obermann · W. Dietmaier · A. Hartmann

Received: 15 April 2008 / Revised: 3 September 2008 / Accepted: 5 September 2008 / Published online: 20 September 2008

Abstract APC, a tumor suppressor gene in the Wnt pathway, stabilizes β-catenin and controls cell growth. Mutation of APC or β-catenin leads to nuclear accumulation of β-catenin and transcription of cyclin D1/cyclin A. Pulmonary artery sarcoma (PAS) were studied by morphologic, immunohistochemical, and molecular genetic methods of the Wnt pathway. Eighteen cases were included: mean age 52 years, primary intraluminal location with typical clinical presentation. PAS were classified as epithelioid (n=4) or malignant fibrous histiocytoma (MFH; spindled/pleomorphic, n=4), myxofibrosarcoma (n=8), and one each hemangiopericytoma-like or malignant inflammatory myofibroblastic tumor-like. The tumor cells demonstrated vimentin, focal actins, and rare focal desmin positivity. All but one were grade 2 or 3 by FNCLCC grading. Alteration in chromosome 5q21 (APC) was found in 4/14 PAS by LOH, mostly epithelioid-type; an MFH-type case demonstrated microsatellite instability (MSI) and nuclear β-catenin. Cyclin D1 was expressed in seven tumors, all myxofibrosarcoma-type. No mutations were detected in APC or β-catenin. In summary, PAS are predominantly intermediate grade myxofibrosarcoma in middle-aged males, and fatal in two-thirds of patients. Despite myofibroblastic phenotype, APC/β-catenin pathway changes are rare. Cyclin D1, only expressed in the myxofibrosarcoma-type, is likely transcribed via factors other than β-catenin.

Keywords Pulmonary artery sarcoma · APC · β-catenin · Cyclin D1 · Cyclin A · LOH

A. Gaumann (✉) · F. Hofstädter · M. Woenckhaus · R. Stoehr · W. Dietmaier · A. Hartmann
Institute of Pathology, University of Regensburg,
Franz-Josef Strauss Allee 11,
D-93042 Regensburg, Germany
e-mail: andreas.gaumann@klinik.uni-regensburg.de

A. Gaumann · J. C. Fanburg-Smith
Department of Soft Tissue Pathology,
Armed Forces Institute of Pathology (AFIP),
6825 16th Street NW,
Washington, DC 20306-6000, USA

B. Bode-Lesniewska · D. R. Zimmermann
Institute of Surgical Pathology, University of Zürich,
Schmelzbergstr. 12,
CH-8091 Zürich, Switzerland

C. J. Kirkpatrick
Institute of Pathology,
University of Mainz,
Langenbeckstr. 1,
D-55101 Mainz, Germany

R. Stoehr · A. Hartmann
Institute of Pathology,
University of Erlangen,
Krankenhausstr. 12,
D-91054 Erlangen, Germany

E. C. Obermann
Institute of Pathology,
University of Basel,
Schönbeinstr. 40,
Ch-4056 Basel, Switzerland

Introduction

Primary sarcomas arising in major blood vessels, especially pulmonary artery sarcoma (PAS), are very rare. A PAS has been described first by Mandelstamm in 1923 [15]. Immunohistochemical and electron microscopy examinations suggest a myofibroblastic phenotype of intimal type [4, 17, 26], although at least partial differentiation along other cell lineages has been documented (e.g. osteocartilaginous, [4] smooth muscle, skeletal muscle or vascular (angiosarcoma) [8, 9, 11]). However, to date, morphologic classification of these tumors has not been systematically performed. PAS often show a rapid clinical progression reflected histologically by high proliferation rates and frequent areas of necrosis [4, 20]. Numerous cases reported in the literature were diagnosed at autopsy; many were thought originally to be blood clots. In recent years, an increasing number of publications have reported successful surgical treatment of these patients [16]. Although adjuvant chemotherapy and/or radiation were applied, most patients died within a few months.

Zhao and coworkers have reported that the pathogenesis of PAS may involve overexpression of platelet-derived growth factor α, as well as dysregulation of the cell cycle due to overexpression of mdm2 (an inhibitor of p53) and cdk4 (cyclin-dependent kinase 4, a regulator of Cyclin D1, a cell proliferation marker) [3, 28]. Despite these reports, the knowledge about the pathogenesis of PAS is very limited.

Since the transcription of Cyclin D1 and Cyclin A are induced by the Wnt-signaling pathway, we wanted to investigate its role in the pathogenesis of PAS. Wnt is one of the most important pathways in regulation of cell-cycle progression, c-myc, Cyclin D1 and Cyclin A, during embryonic development and cancer formation. The major signaling pathway of these secreted, transforming glycoproteins involve stabilization of cytoplasmic β-catenin by activation of Disheveled, which suppresses the negative regulation of β-catenin by glycogen synthase kinase 3-β (GSK-3β). Phosphorylation and ubiquitin-mediated degradation of β-catenin by GSK-3β are also dependent upon interactions with a protein complex involving the adenomatous polyposis coli (APC) protein. Stabilization leads to nuclear and cytoplasmatic accumulation of uncomplexed β-catenin, which binds to Tcf/Lef transcription factors, subsequently activating the expression of nuclear target genes (e.g., Cyclin D1 and c-myc) to establish the oncogenic transformation [10]. Since Alman et al. showed that mutation of APC frequently occurs in fibromatosis (so-called desmoid tumor), the exploration of the APC/β-catenin system in spindle cell neoplasms has attracted attention [1].

Thus, with our group of 18 PAS cases, we wanted to observe their morphology, determine a useful classification, and investigate possible involvement of the APC/β-catenin pathway in these spindle cell tumors.

Materials and methods

Inclusion criteria

Cases coded as "pulmonary artery sarcoma" were culled from the authors' files. Excluded were cases that did not meet the following inclusion criteria: The tumor had to be mesenchymal and found partially or completely within the pulmonary artery. The tumors had to show nuclear pleomorphism, necrosis, and increased mitotic activity, including the presence of atypical mitoses. Metastatic diseases from other organs or primary sites were ruled out by clinical and radiological examination. Patient data and follow-up were obtained from the patient records and clinical history.

Immunohistochemical examination

Immediately after surgery, all tissue samples were fixed in buffered formaldehyde (4%) and paraffin-embedded. Five-micrometer sections were cut from at least two representative tissue blocks from each tumor and tumor-free tissue. Immunostainings were performed as follows: antibodies against cytokeratin (1:250, Biomedicals AG Augst Switzerland), EMA (1:20 DAKO, Hamburg, Germany), vimentin (1:500, DAKO), desmin (1:20, DAKO), CD31 (1:10, DAKO), factor VIII (1:1000, DAKO), CD34 (1:20, Serotec Ltd. Oxford UK), α-smooth muscle actin (1:100, SIGMA-ALDRICH, Deisenhofen, Germany), HMB45 (1:50, Eurodiagnostics, NY, USA), S100 (1:500 DAKO), Ki-67 (1:50, DAKO), Cyclin A (1:100; Clone 6E6 Novocastra, UK), Cyclin D1 (1:50; Clone SP4, LabVision/NeoMarkers, UK), and β-catenin (1:50; BD Bioscience Inc; NJ, USA) were incubated overnight using an immunostainer (Ventana NexES IHC, Ventana, Medical Systems, Tucson, AZ). Microwave antigen retrieval was utilized (four times for 4 min at 800 W in 0.1 mol/l citrate buffer, pH 6.0). To improve staining sensitivity, a 3,3′-diaminobenzidine-enhanced detection kit (Ventana) and an amplification kit (Ventana) were applied. The tumor-free adjacent lung tissue with pulmonary artery vessels as well as tissues from colon carcinomas served as controls. For negative controls, primary antibodies were omitted or replaced by non-specific immunoglobulins.

Macrodissection

Matched normal and tumor DNA was isolated from formalin fixed, paraffin-embedded tissue sections (tumor and corresponding normal tissue, if available). Three representative 10-μm sections were cut, stained with methylene blue and

the tumor was dissected by scalpel scraping under an inverted microscope. Approximately 1 cm^2 of tumor tissue was digested with Proteinase K at 55°C for 24 h and the DNA was then purified by the MagnaPure procedure (Roche Diagnostics, Mannheim Germany).

LOH analysis at the 5q21.1 gene locus

The microsatellite marker used in this study and the location was taken from the Genome Database (http://gdbwww.gdb.org). The primers were obtained from Genset SA (Paris, France). Matched normal/tumor DNA samples were amplified by PCR in a 25 μl volume containing 0.2 mmol/l dNTP, 0.3 μmol/l primers, 1.5 mmol/l $MgCl_2$, 0.5 U Taq polymerase (Roche Diagnostics GmbH, Mannheim, Germany), using 100 ng isolated DNA as template. The reaction mixture was subjected to 3 min of denaturing at 95°C and 35 cycles of 95°C for 1 min, 55°C for 1 min and 72°C for 1 min, followed by a final extension step at 72°C for 10 min. PCR conditions were optimized by gradient PCR and was carried out in a MJ Research Thermocycler (PTC 100). Primer sequences were as follows: D5S346 (5q21): 5′ACTCACTCTAGTGATAAATCG3′ and 5′AGCAGATAAGACAGTATTACTAGTT3′. One microliter of amplified PCR product was applied to the ABI PRISM™ 310 genetic analyzer using POP6 polymer. Automatic fragment analysis was done using GeneScan™ 3.1.2 software (Applied Biosystems, Darmstadt, Germany).

Sequence analysis for β-catenin and APC

To screen for mutations in exon 3 of the β-catenin gene, extracted genomic DNA was amplified by PCR. The primers for exon 3 of the β-catenin gene (CTNNB1) were:

5′-GCTGATTTGATGGAGTTGGA-3′
5′GCTACTTGTTCTTGAGTGAA-3′.

The amplified PCR product included the "degradation box" shown to contain all mutations in colorectal cancer. The PCR reaction was performed under the following conditions: denaturation for 5 min at 94°C, 35 cycles of denaturation for 30 s at 94°C, 30 sec annealing at 55°C and 30 s elongation at 72°C, followed by a final elongation step for 7 min at 72°C. PCR products were purified by polyethylene glycol precipitation (equal volume of PCR product and PEG-Mix containing 26% PEG8000, 0.6 mol/l Na acetate, pH 5.5, 6.6 mmol/l $MgCl_2$). Purified DNA was sequenced in both directions:

forward-primer 5′GGAGTTGGACATGGCCATGG3′
reverse-primer 5′CCTGTTCCCACTCATACAGG3′

in a PTC 100 MJ Research thermocycler (initial incubation for 2 min at 96°C, 25 cycles of denaturation for 15 s at 96°C, 15-s annealing at 62°C and 4-min elongation at 60°C) using the PRISM Ready Dye Terminator Cycle Sequencing Kit (Applied Biosystems, Germany) and an Applied Biosystems 373 sequencer.

Codons 1260–1596 of the APC gene, containing the mutation cluster region [MCS] were amplified by PCR in all primary tumors showing LOH on chromosome 5q21:

codon 1260–1359 (5′CAGACTTATTGTGTAGAAGA3′/5′CTCCTGAAGAAAATTCAACA3′)
codon 1339–1436 (5′AGGGTTCTAGTTTATCTTCA3′ / 5′TCTGCTTGGTGGCATGGTTT3′),
codon 1417–1516 (5′GGCATTATAAGCCCCAGTGA3′/5′AAATGGCTCATCGAGGCTCA3′)
codon 1497–1596 (5′ACTCCAGATGGATTTTCTTG3′ / 5′GGCTGGCTTTTTGCTTTAC3′).

PCR conditions were as follows: denaturation for 3 min at 94°C, 35 cycles for denaturation for 1 min at 94°C, 1 min annealing at 54, 56, 60, 56°C, and 50-s elongation at 72°C, following a final step for 10 min at 72°C. Purified PCR products were sequenced directly in both directions, as described above, with primers and annealing temperatures used for PCR amplification. Mutations or polymorphisms detected were verified by sequencing both DNA strands of a second independently generated PCR amplicon.

Microscopical analysis

All specimens were analyzed by light microscopy [Zeiss Axioskop] by at least two of the authors (A.G. and B.B-L. and J.C.F-S.). The extent of immunohistochemical staining was estimated by counting the number of positive cells/ten high-power fields (HPF). Only nuclear staining was counted for Cyclin D1 and Cyclin A expression. Results were classified according to five categories: 0, negative; 1, between 1 and 25% of cells positive; 2, between 26% and 50% of cells positive; 3 between 51% and 75% of cells positive; 4, between 76% and 100% of cells positive.

Statistical analyses were performed using SigmaPlot 11 (SPSS Software, Germany) and GraphPadPrism 4.0 (USA). Continuous variables not following the normal distribution were compared between two or more groups with the Mann–Whitney rank sum test. Survival analysis of clinical parameters, APC, β-catenin, Cyclin A and Cyclin D1 were analyzed for overall survival (OS) and event-free survival (EFS). Univariate analyses of time to death due to the sarcomas or time of recurrence were established using the product-limit procedure (Kaplan–Meier method), with date of histological diagnosis as the starting point. Patients who died of other causes were censored at the time of death. Differences between categories were tested by the log-rank test. Statistically significant differences were considered with $p<0.05$.

Results

There were 11 males and seven females included in the study. The patient ages ranged from 30 to 71, with a median age of 52 years. Tumor sizes ranged from 1.5 to 19 cm. Clinical symptoms were non-specific including coughing, chest or back pain, and weight loss. No patients clinically had any other primary tumor. Patient follow-up time ranged from 1 to 77 months with a median time of 14 months. Three patients developed local recurrence over 15 months (mean), 11 developed metastases to the lung, one patient each to the brain, pleura, kidney, liver, and bone marrow, over 16 months (mean) and two patients were free of disease 42 months (mean) after primary surgery. Two patients were lost to follow-up. All but one tumor was completely excised. The exception was a biopsy-only case. Twelve patients received chemotherapy and/or radiation. The clinicopathological data are summarized in Table 1.

Macroscopically, all specimens had a polypoid intraluminal tumor mass in the main artery or pulmonary trunk extending distally along the branches of the pulmonary arteries. In the seven pneumonectomy specimens, lung infarctions at various stages of organization were present.

On histological examination, the intraluminal growth pattern of the tumors was confirmed by microscopic spreading of malignant spindle cells along the intima.

The neoplasms were morphologically categorized into different subtypes as follows: four cases, designated epithelioid type demonstrated predominantly pleomorphic epithelioid tumor cells with cytoplasmic clear cell change in three cases (Fig. 1a) and sclerosing features in one case (Fig. 1b). The other tumors demonstrated predominantly spindle cell morphology. Eight cases, designated myxofibrosarcoma-type, as these were morphologically comparable to the previously described extremity myxofibrosarcoma [18], revealed tumor lobules with myxoid change and prominent ropy vasculature, dripping with atypical tumor cells and observable mitoses (Fig. 1c). Four cases with high cellularity, mitotic activity and necrosis, and a storiform growth pattern, were designated as the malignant fibrous histiocytoma type (MFH-type; Fig. 1d). One of these cases had prominent myofibroblastic nodular whorls. One case, demonstrating perivascular hyalinization and staghorn vessels, was cellular with mitotic activity, reminiscent of a malignant hemangiopericytoma and designated malignant hemangiopericytoma-like (Fig. 1e) and another case showed prominent chronic inflammation composed of lymphocytes and a whorling myofibroblastic proliferation. This latter case was designated as malignant inflammatory myofibroblastic tumor-like (MIMFTlike, Fig. 1f). All sarcomas were graded by the FNCLCC grading scheme, introduced by Coindre et al. [6], a system based on differentiation, mitotic activity, and necrosis. These intimal sarcoma subtypes correlated with grade from low (MIMFTlike) to intermediate (myxofibrosarcoma-type and the one malignant hemangiopericytoma-like due to necrosis) to grade 2–3 (MFH-type) to high-grade (epithelioid-type). The types and their grades are found in Table 1.

The proliferation index ranged from 5% to 80% in Ki-67 staining (Fig. 3a). The mitotic activity ranged from 1 to 35/10 HPF. Excessive tumor necrosis (>50%) was present in four cases; necrosis was absent only in one case. One case that was subclassified as MFH-type sarcoma demonstrated focal osseous metaplasia. There was no neoplastic bone or cartilage in any of the tumors. Immunohistochemical stains showed consistent immunoreactivity for vimentin (18/18), rare to strong focal immunoreactivity for smooth muscle actin (11/18) and desmin (5/18). Smooth muscle actin and desmin were only both positive in three cases, but these had myofibroblastic rather than smooth muscle morphology and the markers were only focal and not diffuse (a MFH-type, the malignant hemangiopericytoma-like case, and a myxofibrosarcoma-type). No immunoreactivity was seen with EMA, factor VIII, CD34, HMB45, or S100 protein. One case was focally positive for cytokeratin but was also positive for SMA. In addition, this case had a typically hemangiopericytoma-like pattern showed clinically no evidence of a primary carcinoma. Immunostaining with CD31 was positive in tumor vessels, but one case also showed rare focal positivity in the tumor cell population. However, that case did not demonstrate any vasoformative features of angiosarcoma, was CD34- and factor VIII-negative, and the morphology was of an epithelioid-type intimal sarcoma. The immunohistochemical results are summarized in Table 2.

LOH Analysis of APC at 5q21.1 gene locus

DNA from all primary tumors and from matched normal tissues from 14 cases was successfully investigated for allelic deletion. Four cases without normal tissue were designated non-informative. Allelic loss in the APC gene locus was found in 4 out of 14 (28%) informative cases. The occurrence of LOH at chromosome 5q21was present in three epithelioid-type and one myxofibrosarcoma-type tumor (Fig. 2a). One high-grade MFH-type sarcoma displaying microsatellite instability (MSI; Fig. 2a) in this region showed a wild-type gene for the APC locus.

Sequence analysis of the APC gene

The genomic region spanning codons 1260–1596 was sequenced in all tumors that showed either allelic loss or MSI at chromosome 5q21. Common sequence variation was

Table 1 Clinical and pathological characteristics of the sarcomas

Patient no.	Age	Sex	Relation to vessel	Procedure	Histology (grading)	Follow-up	Additional treatment	Recurrence/metastasis time after diagnosis
#1	55	M	Pulmonary trunk pericardium	PT resection and reconstruction	MFS (G2)	Died 18 mo after diagnosis	XRT	Local (r) lung (m)/7 months
#2	49	F	Bifurcation right PA branch	Resection PA replacement	ET (G2)	Died 9 mo after diagnosis	None	Lung (m)/5 months
#3	59	M	Bifurcation right PA branch	Endarterectomy RPn	MFH (G3)	Died 7 mo after diagnosis	XRT doxorubicin/ dacarbacin 5 cycles	Local (r)/7 months
#4	30	M	RV outflow	RV outflow tract resection valve/trunk reconstruction	MFS (G2)	Alive 70 mo after diagnosis	adriamycin 5 cycles	None
#5	49	F	Pulmonary trunk	Resection failed	ET (G3)	Died 18 mo after diagnosis	Adriamycin 6 cycles	Local, lung(m) 6 months
#6	60	M	Pulmonary trunk luminal	Endarterectomy failed, LPn	MFS (G2)	Alive 45 mo after diagnosis	Adriamycin/ifosfamid 4 cycles	Lung (m)/5 months
#7	60	M	Pulmonary trunk luminal	PA resection reconstruction	MFH (G3)	Alive 77 mo after diagnosis	Adriamycin/ifosfamid 4 cycles	Lung 77 months
#8	41	F	RPA and mediastinum	Partial lung resection 5 mo palliative bypass VCI and right atrium	MFS (G2)	Died 30 mo after diagnosis	XRT 10x 30 Gy	Lung/local (r),15 months
#9	41	M	RPA	Endoluminal tumor resection and RPn	MFH (G3)	Died 9 mo after diagnosis	None	Not known
#10	68	M	LPA	LPn	ET (G3)	Died 8 mo after diagnosis	XRT 30 Gy of brain metastasis	Brain 4 months
#11	38	F	PT and LPA with obstruction of the RPA and the PV	Endoluminal tumor resection and resection of the PV	MFS (G2)	Died 35 mo after diagnosis	XRT 54 Gy	Local(r), liver local/ 24 months
#12	30	F	LPA	LPn	MFS (G2)	Died 24 mo after diagnosis	XRT 48 Gy CTX	Lung, cervical kidney (m)/22 months
#13	37	M	PT, LPA, RPA LLLartery and mediastinum	Biopsy of skull metastasis	MIMFT (G1)	Died 13 mo after diagnosis	CTX	Skull, lung 12 months
#14	63	M	PT, LPA, RPA	biopsy intraluminal	MFS (G2)	Died 6 mo after diagnosis	None	Not known
#15	67	F	LPA	LPn	MHPC (G2)	Died 1 mo after diagnosis	None	Pleura 1 month
#16	49	M	PT, PV, LPA, left lung	None	ET (G3)	Died 7 mo after diagnosis	CTX	Bone marrow
#17	61	F	RPA, RUL and RLL artery, pericardium	RPn, PA-reconstruction	MFH (G3)	Alive 14 mo after diagnosis	None	None
#18	71	M	PT and RPA/LPA	PT reconstruction	MFS (G2)	Not known	Not known	Not known

PT Pulmonary trunk, *PA* pulmonary artery, *RV* right ventricle, *PV* pulmonary valve (r) recurrence, *ET* epithelioid-type, *PAS MFS* myxofibrosarcoma-type, *PAS MFH* malignant fibrous histiocytoma Type PAS, *MHPC* malignant hemangiopericytoma-like PAS, *MIMFT* malignant inflammatory myofibroblastic tumor-like PAS, *m* metastasis, *XRT* radiation, *CTX* chemotherapy, *RPn* right pneumonectomy, *LPn* left pneumonectomy

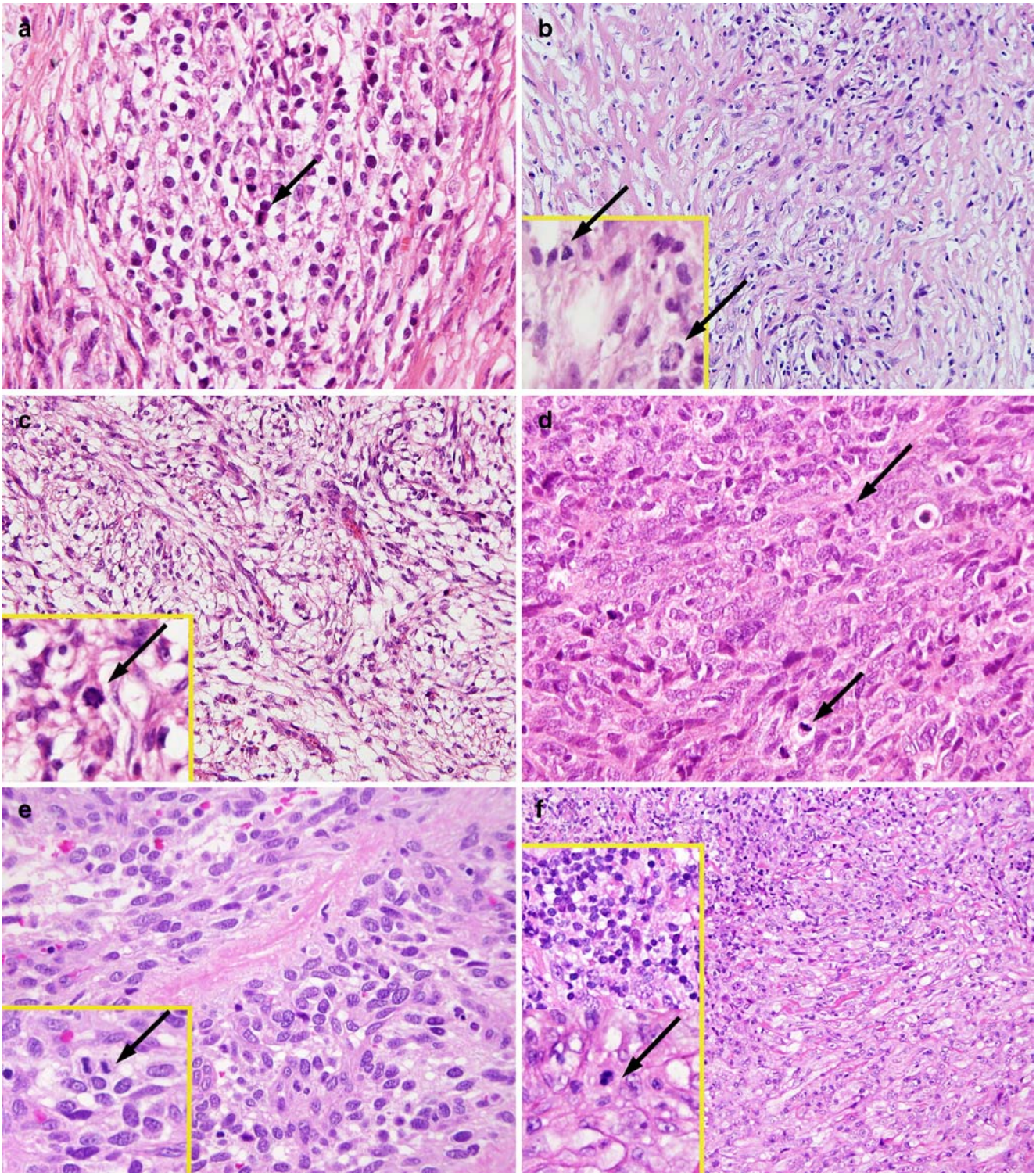

Fig. 1 Microphotographs (HE staining) of high-grade epithelioid-type PAS with clear cell features (**a**), and epithelioid-type PAS with sclerosing features; *inset* shows atypical mitotic figures (*arrow*) (**b**). An example of an intermediate grade myxofibrosarcoma-type PAS; inset shows a mitotic figure (*arrow*; **c**), a spindled pleomorphic malignant fibrous histiocytoma (MFH) type PAS with high cellularity, collagenized stroma, necrosis, and numerous mitotic figures (*arrow*; **d**). Another example of PAS with malignant hemangiopericytoma-like features with high cellularity, cytologic atypia, staghorn vasculature and prominent perivascular hyalinization and mitoses (*arrow*; **e**) and low-grade chronically inflamed malignant inflammatory myofibroblastic tumor-like PAS; *inset* shows dense inflammatory infiltration and a mitotic figure (*arrow*, **f**)

Table 2 Immunohistochemical characterization of the sarcomas of the pulmonary artery

Patient	Vimentin	CD31	CD34	FVIII	Desmin	SMA	Cytokeratin	Ki-67%
#1	+++	−	−	−	−	++	−	40
#2	+++	−	−	−	−	−	−	40
#3	++	−	−	−	++	−	−	10
#4	+	−	−	−	−	−	−	40
#5	++	−	−	−	+++	−	−	20
#6	++++	+	−	−	−	−	−	30
#7	+++	−	−	−	+	+	−	60
#8	+++	−	−	−	+	+	−	5
#9	+++	−	−	−	−	+	−	70
#10	+++	−	−	−/+++	−	+	−	80
#11	+++	−	−	−	−	+++	−	20
#12	+++	−	−	−	−	++	−	30
#13	+++	−	−	−	−	+	+	50
#14	+++	−	−	−	−	+	−	40
#15	+++	−	−	−	+	+	−	50
#16	++	−	−	−	−	−	−	40
#17	++	−	−	−	−	++	−	30
#18	+++	−	−	−	−	−	−	50

− Negative, + between 1 and 25% of tumor cells positive, ++ between 26% and 50% of tumor cells positive, +++ between 51% and 75% of tumor cells positive, ++++ between 76% and 100% of tumor cells positive

found in six tumors displaying a silent single nucleotide polymorphism (SNP) at codon 1493 [ACA/ACG] (see Table 3 and Fig. 2b). The allelic distribution (58% wild-type allele vs. 42% polymorphic allele) was very similar to that described by Davies and Snover [7]. No other mutations were detected in these cases.

Mutational analysis of the β-catenin gene and immunohistochemistry of the β-catenin protein

Direct sequencing was used to detect mutations in exon 3 of the β-catenin gene. No mutations were found in the 18 pulmonary artery sarcomas (see Table 3). In addition, immunohistochem-

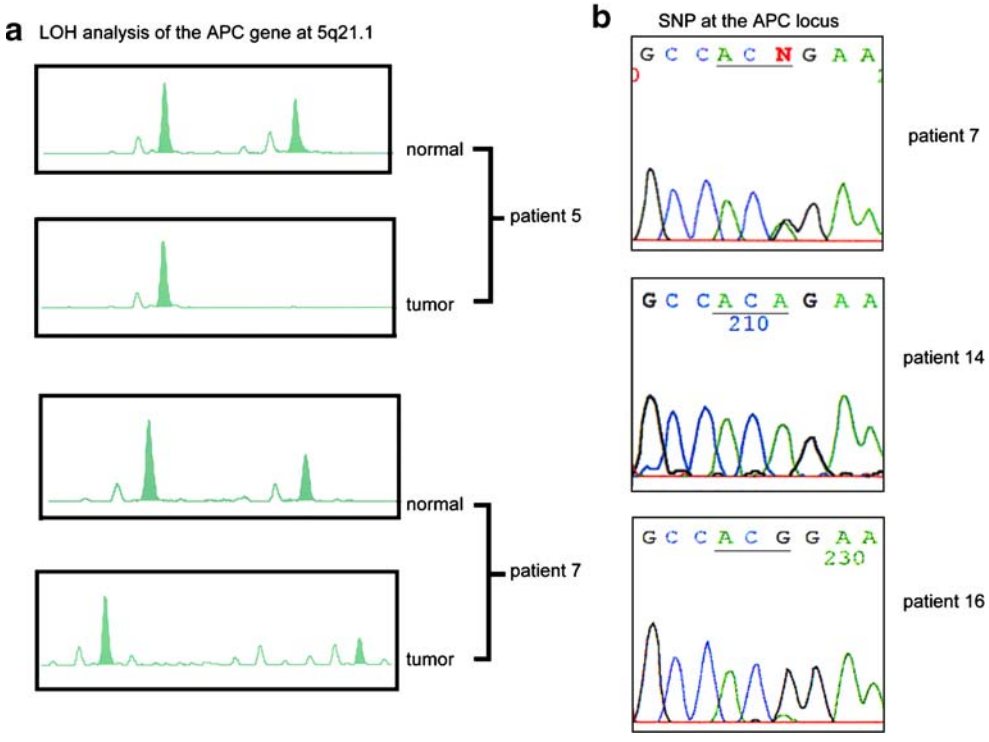

Fig. 2 Demonstration of LOH in an epithelioid-type PAS (case 5) and MSI in a MFH-type PAS (case 7) at the APC locus 5q21.1 (**a**). Sequence analysis at the MCS of the APC gene revealed no mutations but frequent single nucleotide polymorphism (**b**)

Table 3 Mutation analysis and expression of molecules involved in the ß-catenin pathway in sarcomas of the pulmonary artery

Patient	β-catenin nuclear/cytoplasm membrane	Cyclin A nuclear	Cyclin D1 nuclear	ß-catenin mutation	LOH/ MSI	APC mutation	Polymorphism codon ACA/ACG
#1	−/+	+	+	−	−	−	n.t.
#2	−/+	++	−	−	LOH	−	ACG homozygous
#3	−/+	+	−	−	−	−	n.t.
#4	−/+	+	+	−	−	−	n.t.
#5	−/++	−	−	−	LOH	−	ACG homozygous
#6	−/+	−	+	−	−	−	n.t.
#7	+/+	++	+	−	MSI	−	ACA/ACG heterozygous
#8	−/+	−	−	−	−	−	n.t.
#9	−/−	+	++++	−	−	−	n.t.
#10	−/+++	+++	−	−	−	−	n.t.
#11	−/−	+	+	−	n.i.	−	n.t.
#12	−/+	−	+	−	−	−	ACA homozygous
#13	−/−	−	−	−	n.i.	−	n.t.
#14	−/−	−	−	−	LOH	−	ACA homozygous
#15	−/+	+	−	−	n.i.	−	n.t.
#16	−/+	−	−	−	LOH	−	ACG homozygous
#17	−/+	+	−	−	n.i.	−	n.t.
#18	−/+	+	+	−	−	−	n.t.

− Negative; + between 1 and 25% of tumor cells positive, ++ between 26% and 50% of tumor cells positive, +++ between 51% and 75% of tumor cells positive, ++++ between 76% and 100% of tumor cells positive, *n.i.* not informative, *n.t.* not tested

istry of β-catenin was carried out to investigate the status of the Wnt-signaling pathway since inactivation of other components in the Wnt-signaling pathway, such as APC and Axin, is known to result in accumulation of β-catenin. The β-catenin protein was present in the cytoplasm in 14 cases and revealed in addition a partial membrane staining in three cases (cytoplasm, 77%; membrane, 16%). One MFH-type sarcoma had also scattered positivity in some nuclei of tumor cells (Fig. 3b). This case also showed nuclear staining of Cyclin D1 and A.

Immunohistochemistry of Cyclin D1 and Cyclin A

Immunohistochemistry with Cyclin D1 showed marked nuclear staining in 1 case and weak signal in seven cases (marked, 5%, weak, 39%; Fig. 3c) and none of these cases revealed cytoplasmic staining. Of note is that all myxofibrosarcoma-type tumors (grade 2/3) and two of the MFH-type (grade 3/3) variants expressed Cyclin D1, all associated with better outcome, either prolonged or complete survival, but none of the other tumors demonstrated Cyclin D1. We also performed immunohistochemistry, using antibodies to Cyclin A and demonstrated marked nuclear staining in three cases and weak staining in eight cases (marked, 16%, weak, 44%; Fig. 3d). There was no correlation found between Cyclin A and any of the defined morphologic subtypes. Neither Cyclin D1 nor Cyclin A co-located with any β-catenin expression.

Survival analysis

A correlation of overall (OS) and event-free survival (EFS) was performed for Cyclin D1, Cyclin A, APC, and clinical parameters. No significant difference in OS or EFS could be detected for Cyclin A (p=0.905; p=0.258). In addition, we did not observe a significant difference for APC p=0.79 and p=0.59), gender, age (<52 vs. >52 years) and grading (G3 vs. G2), concerning EFS and OS. However, OS and EFS were significantly greater in cases displaying at least some positive cells for Cyclin D1 (OS, p<0.0047; EFS, p< 0.01; Fig. 4a and b). Three patients with a tumor positive for Cyclin D1 were still alive without disease; four individuals had much longer survival than patients with other (Cyclin D1-negative) tumors. We also compared the predominant phenotype in our series, myxofibrosarcoma-like tumors with the other phenotypes of the classification. There was a tendency towards a better survival rate for MFS, but was not significant different (OS, p=0.113; EFS, p=0.117; Fig. 4c and d).

Discussion

Pulmonary artery sarcoma (PAS), generally fatal, has recently been treated surgically with some success and cases with long-term survival [16]. However, its morphology has not been systematically classified nor its patho-

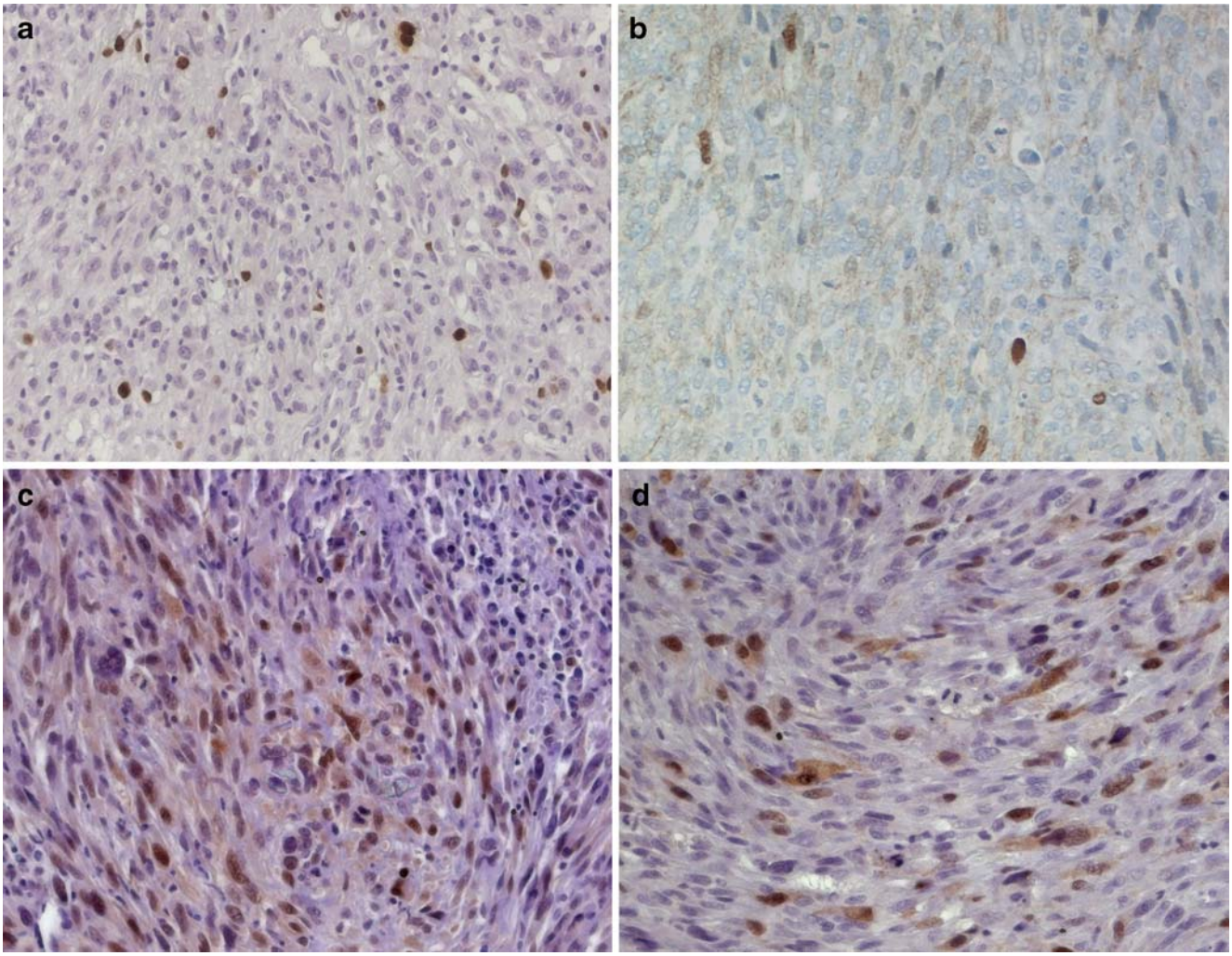

Fig. 3 Scattered tumor cells show nuclear positivity for the proliferation-associated molecule Ki-67 (case 5, **a**). Focal nuclear expression of β-catenin in the case displaying MSI at the APC locus (case 7, **b**) was observed. Marked nuclear Cyclin D1 expression is shown in a subset of tumor cells close to the invasion front (case 7, **c**). This patient was alive 77 months after diagnosis emphasizing the good outcome of these Cyclin D1 positive tumors; Similar results were observed with staining for the Cyclin A protein (case 7, **d**; ABC staining; DAB, magnification 20×)

genesis clearly understood. Our goal was to subclassify these PAS and explore its Wnt pathway to attempt to better understand the pathogenesis of the disease.

Based on morphology and the immunohistochemical expression of vimentin and partial presence of either smooth muscle actin or desmin, the tumors were designated intimal sarcomas with myofibroblastic differentiation. Although not specific, these findings are compatible with current knowledge about the morphology of PAS indicated in the literature [4, 13, 20]. Our findings are in line with the reported literature emphasizing that the majority of intimal sarcomas are poorly differentiated myxoid or pleomorphic sarcomas with immunohistochemical and ultrastructural signs of myofibroblastic differentiation [4, 13]. Myofibroblastic sarcomas comprise up to 80% of all reported intimal PAS. The remaining tumors are true osteosarcomas, chondrosarcomas, angiosarcomas, rhabdomyosarcomas or, very rarely, liposarcomas [4, 11, 13, 20, 21]. None of our cases contained malignant osteocartilaginous (one case did demonstrate benign metaplastic bone), vascular, or smooth muscle phenotype. This notion is also supported by the absence of endothelial markers (CD31, CD34, or factor VIII), as well as S100, in our pulmonary artery sarcomas. McGlennen concluded that polyphenotypic expression of several mesenchymal lineages suggests that the tumor progenitor cell has pluripotential properties with several possibilities of differentiation [17].

In addition, we could further subclassify our sarcomas into five subcategories with morphologic distinct growth patterns (clear cell/sclerotic epithelioid-type, pleomorphic malignant fibrous histiocytoma-type, myxoid myxofibrosarcoma-type, one case each malignant hemangiopericytoma-like and malignant inflammatory myofibroblastic-like). Except for previous reports of female predominance, the clinical

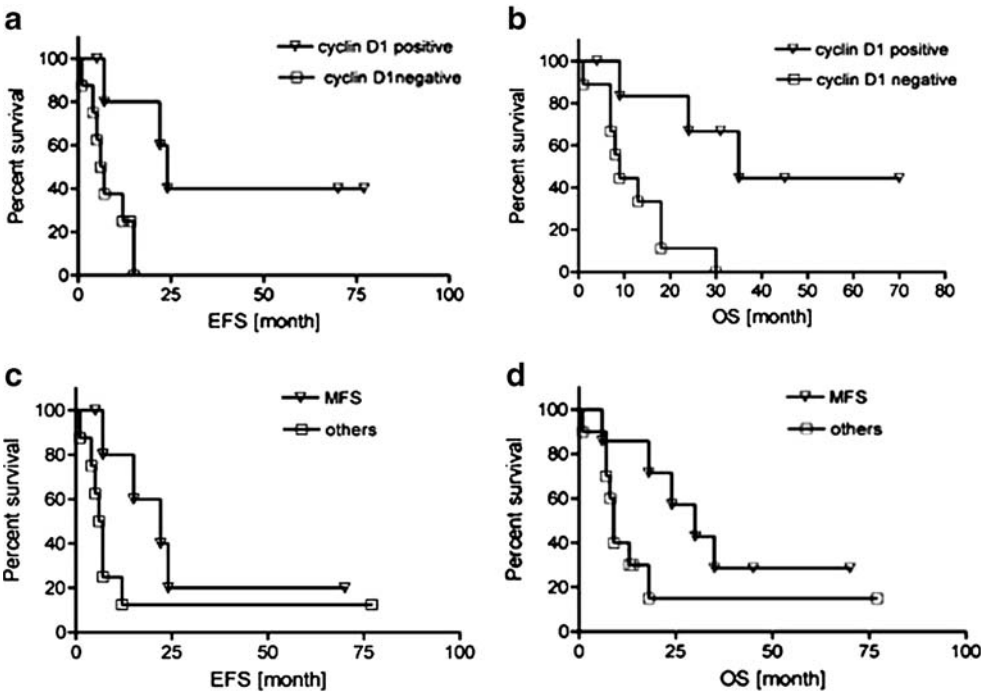

Fig. 4 Survival analysis revealed a significant correlation with overall survival (p=0.0047; **a**) and event-free survival (p=0.01; **b**) for Cyclin D1. Patients having a myxofibrosarcoma-like phenotype had a slightly better EFS and OS than the other MFH and epithelioid phenotypes which was not significant

features we found including demographics and symptoms were similar to those described for PAS [20].

The Wnt-signaling pathway, involving the tumor suppressor gene, APC, as well as β-catenin, plays an important role during embryogenesis and tumor formation. Since some genetic syndromes (e.g., Gardner syndrome) showed an association to polyposis and soft-tissue neoplasms, APC mutation has also been studied in those tumors. It has been shown that mutations of β-catenin are frequently observed in desmoid fibromatosis, a spindle cell tumor with aggressive local behavior [5, 24].

In our 18 PAS cases, examination for allelic loss at the APC locus revealed LOH in 28% of all tumors and only one case had MSI at this site. Subsequently, tumors with LOH showed a wild-type sequence (codon 1260 to 1596 containing the mutational cluster sequence) of the APC gene, [27] and no mutation in exon 3 of β-catenin gene was found. The only variant we found was a silent polymorphism at codon 1493 (ACA/ACG) of APC in six tumors. The frequency of this polymorphism matches that reported for the general population [7]. This is in line with Iwao et al. who analyzed β-catenin mutations in 73 benign and malignant bone and soft-tissue neoplasms showing mutations in only less than 5% of the tumors [12]. They demonstrated an accumulation of the β-catenin protein by Western blot analysis in their series. The PAS in our study revealed frequent cytoplasmic and membranous staining, indicating that the protein may be accumulated within the cell but is only transferred to the nucleus in the one case with MSI. Others have found β-catenin expression exclusively at the cell membrane of epithelioid sarcomas while genetic mutations of the β-catenin gene were absent [22]. These data support the view that genetic alterations of the β-catenin/APC pathway are rare events in spindle cell neoplasms, except for desmoid fibromatosis [2]. In a previous investigation, eight tumors from the current series were studied by CGH analysis, displaying no deletions at the long arm of chromosome 5 [3]. Results from the current study emphasize that the infrequent LOH at chromosome 5q21 and the absence of APC mutations, provide arguments against the involvement of the APC/β-catenin pathway in the pathophysiology of PAS.

Some proteins of the cyclin family such as Cyclin D1 and Cyclin A are known to be transcriptionally up-regulated by β-catenin [25]. The current study demonstrates nuclear expression for Cyclin D1 in eight PAS cases; all but one of these cases were myxofibrosarcoma-type and had no alteration of the APC gene, except the MSI case (MFH-like), which was also positive for Cyclin D1. This may emphasize that myxofibrosarcoma-type PAS, the most prevalent type in our series, is a distinct subset of intimal sarcoma. Cyclin D1 protein is known to be strongly associated with cyclin-dependent kinase 4 (cdk4) during cell-cycle progression [23]. Previously, we detected a gene amplification of the cdk4 gene in these sarcomas, supporting a possibility that expression of Cyclin D1 may be associated with cdk4 overexpression in our PAS series [28]. This warrants further study.

Cyclin D1 has not always been associated with a favorable prognosis. While Molendini et al. found a poor EFS and OS in patients with osteosarcoma lacking Cyclin D1 expression [19] others have shown that Cyclin D1 is correlated with a worse prognosis in a series of soft-tissue

sarcomas, supporting the view that Cyclin D1 overexpression may determine the evolution of an aggressive subset of soft-tissue sarcomas [14]. However, it is well known that Cyclin D1 is not only involved in cell-cycle progression from G1 to the S phase but also in apoptosis. For example, it has been shown that overexpression of Cyclin D1 sensitizes breast cancer cells to radiation or drug-induced apoptosis [29]. All except one of our patients, who were positive for Cyclin D1, received chemotherapy and/or radiation therapy. Therefore, it is likely that expression of this molecule may contribute to a better response to adjuvant therapy.

In summary, PAS in our series is mainly seen in adult men at the mean age of 52. These tumors are centrally located in the pulmonary trunk and extend luminally into the main pulmonary artery branches. Morphologically, they are usually intermediate- to high-grade epithelioid-type, MFH-type, or myxofibrosarcoma-type intimal sarcomas. Alternations of the Wnt/β-catenin pathway do not appear to be causally involved in the pathophysiology of PAS, although LOH at the APC locus occurs. Target genes of β-catenin such as Cyclin D1 are overexpressed particularly in the myxofibrosarcoma-type. The transcriptional activation of Cyclin D1, however, is most likely due to factors other than β-catenin.

Acknowledgements The authors wish to acknowledge the excellent technical support of Martina Waeber, Steffi Götz, Anja Vilberth, and Anne Pietryga-Krieger performing immunohistochemistry, LOH, and sequence analysis. We also thank Prof. E. Geissler for critical reading of the manuscript.

Conflict of interest statement We declare that we have no conflict of interest.

References

1. Alman BA, Li C, Pajerski ME, Diaz-Cano S, Wolfe HJ (1997) Increased beta-catenin protein and somatic APC mutations in sporadic aggressive fibromatoses (desmoid tumors). Am J Pathol 151:329–334
2. Bhattacharya B, Dilworth HP, Iacobuzio-Donahue C, Ricci F, Weber K, Furlong MA, Fisher C, Montgomery E (2005) Nuclear beta-catenin expression distinguishes deep fibromatosis from other benign and malignant fibroblastic and myofibroblastic lesions. Am J Surg Pathol 29:653–659
3. Bode-Lesniewska B, Zhao J, Speel EJ, Biraima AM, Turina M, Komminoth P, Heitz PU (2001) Gains of 12q13-14 and overexpression of mdm2 are frequent findings in intimal sarcomas of the pulmonary artery. Virchows Arch 438:57–65
4. Burke AP, Virmani R (1993) Sarcomas of the great vessels. A clinicopathologic study. Cancer 71:1761–1773
5. Cheon SS, Cheah AY, Turley S, Nadesan P, Poon R, Clevers H, Alman BA (2002) beta-Catenin stabilization dysregulates mesenchymal cell proliferation, motility, and invasiveness and causes aggressive fibromatosis and hyperplastic cutaneous wounds. Proc Natl Acad Sci USA 99:6973–6978
6. Coindre JM, Trojani M, Contesso G, David M, Rouesse J, Bui NB, Bodaert A, De Mascarel I, De Mascarel A, Goussot JF (1986) Reproducibility of a histopathologic grading system for adult soft tissue sarcoma. Cancer 58:306–309
7. Davies SM, Snover DC (1994) Frequent polymorphism in exon 15 of the adenomatous polyposis coli gene. Hum Genet 93:329–330
8. Goldblum JR, Rice TW (1995) Epithelioid angiosarcoma of the pulmonary artery. Hum Pathol 26:1275–1277
9. Hottenrott G, Mentzel T, Peters A, Schroder A, Katenkamp D (1999) Intravascular ("intimal") epithelioid angiosarcoma: clinicopathological and immunohistochemical analysis of three cases. Virchows Arch 435:473–478
10. Huelsken J, Behrens J (2002) The Wnt signalling pathway. J Cell Sci 115:3977–3978
11. Huo L, Moran CA, Fuller GN, Gladish G, Suster S (2006) Pulmonary artery sarcoma: a clinicopathologic and immunohistochemical study of 12 cases. Am J Clin Pathol 125:419–424
12. Iwao K, Miyoshi Y, Nawa G, Yoshikawa H, Ochi T, Nakamura Y (1999) Frequent beta-catenin abnormalities in bone and soft-tissue tumors. Jpn J Cancer Res 90:205–209
13. Johansson L, Carlen B (1994) Sarcoma of the pulmonary artery: report of four cases with electron microscopic and immunohistochemical examinations, and review of the literature [see comments]. Virchows Arch 424:217–224
14. Kim SH, Lewis JJ, Brennan MF, Woodruff JM, Dudas M, Cordon-Cardo C (1998) Overexpression of cyclin D1 is associated with poor prognosis in extremity soft-tissue sarcomas. Clin Cancer Res 4:2377–2382
15. Mandelstamm M (1923) Über primäre Neubildungen des Herzens. Virchows Arch 245:43–47
16. Mayer E, Kriegsmann J, Gaumann A, Kauczor HU, Dahm M, Hake U, Schmid FX, Oelert H (2001) Surgical treatment of pulmonary artery sarcoma. J Thorac Cardiovasc Surg 121:77–82
17. McGlennen RC, Manivel JC, Stanley SJ, Slater DL, Wick MR, Dehner LP (1989) Pulmonary artery trunk sarcoma: a clinicopathologic, ultrastructural, and immunohistochemical study of four cases. Mod.Pathol. 2:486–494
18. Mentzel T, Calonje E, Wadden C, Camplejohn RS, Beham A, Smith MA, Fletcher CD (1996) Myxofibrosarcoma. Clinicopathologic analysis of 75 cases with emphasis on the low-grade variant. Am J Surg Pathol 20:391–405
19. Molendini L, Benassi MS, Magagnoli G, Merli M, Sollazzo MR, Ragazzini P, Gamberi G, Ferrari C, Balladelli A, Bacchini P, Picci P (1998) Prognostic significance of cyclin expression in human osteosarcoma. Int J Oncol 12:1007–1011
20. Nonomura A, Kurumaya H, Kono N, Nakanuma Y, Ohta G, Terahata S, Matsubara F, Matsuda T, Asaka T, Nishino T (1988) Primary pulmonary artery sarcoma. Report of two autopsy cases studied by immunohistochemistry and electron microscopy, and review of 110 cases reported in the literature. Acta Pathol Jpn 38:883–896
21. Parish JM, Rosenow EC III, Swensen SJ, Crotty TB (1996) Pulmonary artery sarcoma. Clinical features. Chest 110:1480–1488
22. Saito T, Oda Y, Itakura E, Shiratsuchi H, Kinoshita Y, Oshiro Y, Tamiya S, Hachitanda Y, Iwamoto Y, Tsuneyoshi M (2001) Expression of intercellular adhesion molecules in epithelioid sarcoma and malignant rhabdoid tumor. Pathol Int 51:532–542
23. Tam SW, Theodoras AM, Shay JW, Draetta GF, Pagano M (1994) Differential expression and regulation of Cyclin D1 protein in normal and tumor human cells: association with Cdk4 is required for Cyclin D1 function in G1 progression. Oncogene 9:2663–2674
24. Tejpar S, Nollet F, Li C, Wunder JS, Michils G, dal Cin P, Van Cutsem E, Bapat B, van Roy F, Cassiman JJ, Alman BA (1999) Predominance of beta-catenin mutations and beta-catenin dysregulation in sporadic aggressive fibromatosis (desmoid tumor). Oncogene 18:6615–6620
25. Tetsu O, McCormick F (1999) Beta-catenin regulates expression of cyclin D1 in colon carcinoma cells. Nature 398:422–426
26. Van Damme H, Vaneerdeweg W, Schoofs E (1987) Malignant fibrous histiocytoma of the pulmonary artery. Ann Surg 205:203–207

27. Yashima K, Nakamori S, Murakami Y, Yamaguchi A, Hayashi K, Ishikawa O, Konishi Y, Sekiya T (1994) Mutations of the adenomatous polyposis coli gene in the mutation cluster region: comparison of human pancreatic and colorectal cancers. Int J Cancer 59:43–47
28. Zhao J, Roth J, Bode-Lesniewska B, Pfaltz M, Heitz PU, Komminoth P (2002) Combined comparative genomic hybridization and genomic microarray for detection of gene amplifications in pulmonary artery intimal sarcomas and adrenocortical tumors. Genes Chromosomes Cancer 34:48–57
29. Zhou Q, Hopp T, Fuqua SA, Steeg PS (2001) Cyclin D1 in breast premalignancy and early breast cancer: implications for prevention and treatment. Cancer Lett 162:3–17

Virchows Arch (2008) 453:485–489
DOI 10.1007/s00428-008-0667-9

ORIGINAL ARTICLE

$CD34^+$ fibrocytes in melanocytic nevi and malignant melanomas of the skin

Cordula Wessel · Christina C. Westhoff · Katharina Nowak · Ingrid Moll · Peter J. Barth

Received: 26 May 2008 / Revised: 1 August 2008 / Accepted: 26 August 2008 / Published online: 24 September 2008

Abstract $CD34^+$ fibrocytes are constitutive elements of the human connective tissue. The stroma associated with invasive carcinomas is characterized by a stereotypic loss of $CD34^+$ fibrocytes and a phenotype change towards $CD34^-$ α-Smooth muscle actin $(SMA)^+$ myofibroblasts. Secreted protein acidic and rich in cysteine (SPARC) is an important mediator of tumor-associated stromal remodeling. Melanocytic lesions of the skin have not been investigated as to this aspect up to now. Thus, we investigated a total of 20 malignant melanomas and 29 melanocytic nevi. The normal dermis and benign melanocytic nevi showed numerous $CD34^+$ fibrocytes, whereas malignant melanomas were devoid of this cell type. α-SMA-positive myofibroblasts were absent from the normal dermis, melanocytic nevi, and malignant melanomas. SPARC was positive in malignant melanoma cells and negative in their associated stroma, while all melanocytic nevi were completely negative. The stromal phenotype of malignant melanomas ($CD34^-$ α-SMA^-) differs from that of invasive carcinomas ($CD34^-$ α-SMA^+) suggesting different pathogenic mechanisms involved in tumor-associated stromal remodeling. SPARC expression appears to be closely related to malignancy in melanocytic lesions.

C. Wessel · I. Moll
Department of Dermatology and Venerology,
University Hospital Hamburg-Eppendorf,
Hamburg, Germany

C. C. Westhoff · K. Nowak · P. J. Barth (✉)
Institute of Pathology,
University Hospital Giessen and Marburg GmbH, Location Marburg, Medical Faculty of Philipps-University Marburg,
Baldingerstraße,
35033 Marburg, Germany
e-mail: barthp@med.uni-marburg.de

Keywords Melanocytic nevus · Malignant melanoma · Stroma · CD34 · α-SMA · SPARC

Introduction

$CD34^+$ fibrocytes are widely distributed within the stroma of the gastrointestinal [1–3], respiratory [4], and upper aerodigestive [5] and urogenital tract [6, 7]. The breast stroma is also mainly composed of $CD34^+$ fibrocytes [8–12]. The first descriptions of this cell type occurred in studies dealing with the immunohistochemical phenotype of the dermis and differential diagnosis of cutaneous appendage tumors and basal cell carcinomas [13–15]. At that time, the histogenesis of $CD34^+$ fibrocytes as well as their precise function in the dermal stroma remained unclear. In 1994, Bucala and coworkers showed that $CD34^+$ fibrocytes are derived from circulating CD14-positive monocytes and invade areas of stromal damage [16], where they are involved in tissue repair owing to their capability of collagen I and III synthesis as well as antigen presentation [17, 18]. In the stroma adjacent to and within invasive carcinomas, $CD34^+$ fibrocytes undergo morphologic and phenotypic alterations characterized by the adoption of a plump myofibroblast-like appearance and loss of CD34 expression accompanied by a gain of α-smooth muscle actin (SMA) expression [1, 5, 6, 8–12]. The underlying mechanisms precipitating this stromal phenotype change are far from being understood, but the matricellular secreted protein acidic and rich in cysteine (SPARC) has been claimed to play a pivotal role in tumor-associated stromal remodeling as well as in the regulation of tumor growth [9, 19, 20].

Stromal remodeling characterized by a loss of CD34 and gain of α-SMA expression virtually occurs in all primary tumor sites and histologic types of carcinoma [10]. Merely,

Table 1 Characteristics of malignant melanomas investigated (n=20)

Characteristics	Number
Histologic type	
SSM	10
LMM	3
NM	7
Clark level	
II	1
III	5
IV	7
V	7
Breslow index	
<1 mm	7
>1 and <2 mm	3
>2 and <4 mm	6
>4 mm	4

in diffuse gastric carcinomas and a subpopulation of invasive lobular carcinomas of the breast, stromal CD34 expression appears to be preserved [3, 11]. Nevertheless, it has been claimed that the analysis of the $CD34^+$ fibrocyte population might aid in distinguishing benign and malignant lesions of the breast such as radial scars and tubular carcinomas which may pose severe diagnostic challenges [21]. Moreover, it has been proposed that early stromal invasion in in situ carcinomas of the uterine cervix can be easily visualized by detection of a loss of $CD34^+$ fibrocytes [6]. However, the precise diagnostic impact of $CD34^+$ fibrocytes as well as the pathogenic mechanism underlying the tumor-associated stromal phenotype change requires further scrutiny. As we have stated, the first morphologic investigations on $CD34^+$ fibrocytes were done regarding skin appendage and epidermal tumors. Therefore, it is astonishing that studies pertaining to the $CD34^+$ fibrocyte population in benign and malignant melanocytic lesions of the skin have not been published up to now. Therefore, the present study was undertaken to explore benign and malignant melanocytic lesions as to the presence of CD34 fibrocytes and α-SMA-positive myofibroblasts. Moreover, it should be analyzed whether a stromal phenotype change, comparable to that observed in most invasive carcinomas, also occurs in melanocytic lesions. We further hypothesized that SPARC might be involved in the development of melanocytic nevi and malignant melanomas and thus we additionally investigated the expression of this matricellular protein in stromal, nevus, and melanoma cells.

Materials and methods

The present study comprises a total of 49 patients with benign and malignant cutaneous melanocytic lesions. Twenty-nine patients had benign melanocytic nevi, comprising of 21 dermal and eight compound nevi. The remaining 20 cases were malignant melanomas. Among these, ten were superficially spreading melanomas, three lentiginous melanomas and seven nodular melanomas. The major patient and tumor characteristics are summarized in Table 1. In all cases, tumor-free tissue was available for comparison as the lesions were completely excised with an appropriate rim of normal skin providing tumor-free surgical resection margins. After excision, tissues were fixed in a 10% formalin solution, embedded in paraffin, cut at a thickness of about 7 μm, and stained with hematoxylin and eosin for routine purposes.

Immunohistochemistry

CD34, α-SMA, and SPARC were detected immunohistochemically by means of the standard avidin biotin complex (ABC)-peroxidase method (ABC Elite Kit; Vector, Burlingame, CA, USA) using 3,3'-diaminobenzidine as chromogen and, separately, the standard ABC-alkaline phosphatase method (ABC-AP Kit; Vector, Burlingame, CA, USA) with Histo Red (Linaris, Wertheim—Bettingen, Germany) as chromogen. The latter method was chosen since it yields a bright red reaction product clearly distinct from melanin. Primary antibodies used and methods of tissue pretreatment are listed in Table 2. The sections were then seen by three independent observers with respect to the occurrence of CD34 and α-SMA-positive stromal cells. SPARC expression was separately assessed in stromal and tumor cells.

Results

Normal skin

The majority of dermal stromal cells were $CD34^+$ fibrocytes. In the reticular dermis, $CD34^+$ fibrocytes were numerous and exhibited a mostly bipolar shape with delicate cytoplasmic processes arranged in parallel to the adjacent epidermis. Sweat glands and hair follicles were surrounded by densely packed $CD34^+$ fibrocytes forming a

Table 2 Antibodies applied for immunohistochemistry and type of tissue pretreatment

Antibody (clone)	Source	Dilution	Tissue pretreatment
CD34 (Qbend 10)	Dako, Hamburg, Germany	1:50	Microwave 3×5 min, 600 W; 10-mM sodium citrate buffer (pH 6.0)
SPARC (15G12)	Novocastra, UK	1:40	Microwave 3×5 min, 600 W; 10-mM sodium citrate buffer (pH 6.0)
α-SMA (ASM-1)	Progen, Heidelberg, Germany	1:200	0.1% trypsin Tris–HCl 15 min 37°C

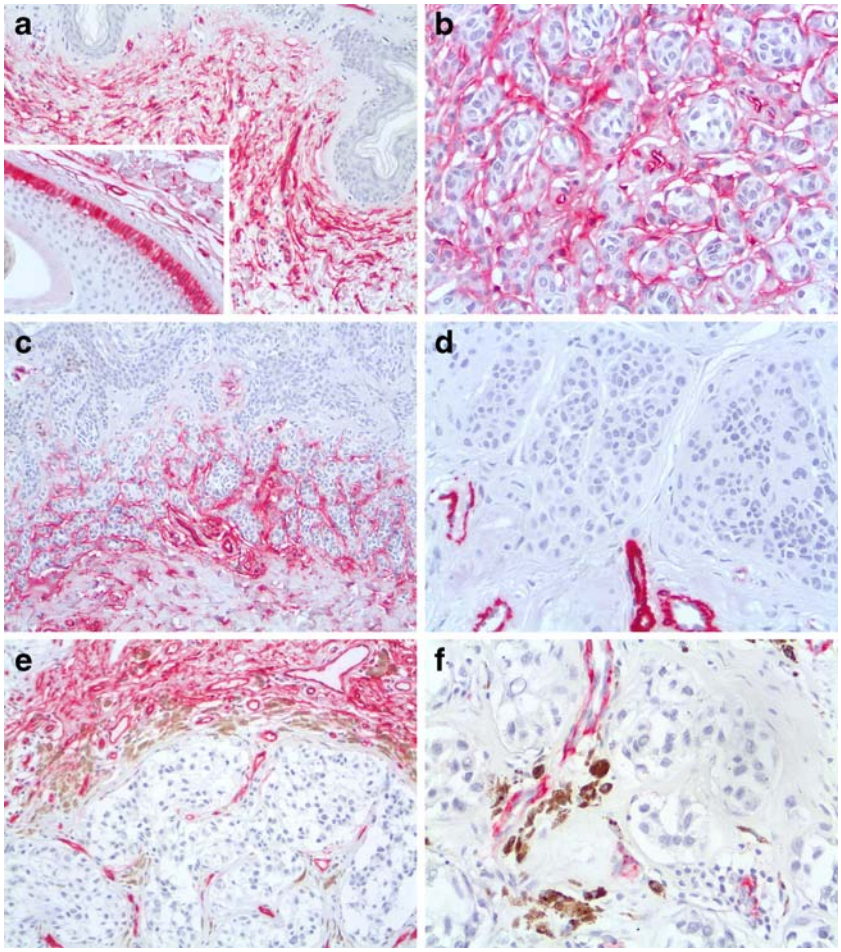

Fig. 1 The dermis harbors numerous $CD34^+$ fibrocytes (**a**). Epithelia of the external root sheath display strong CD34 immunoreactivity (**a**, *inset*). $CD34^+$ fibrocytes surround nests of nevus cells in a melanocytic nevus (**b**). Compound nevi show stromal $CD34^+$ fibrocytes in their deep portion located within the reticular dermis (*bottom*), whereas in the superficial portion $CD34^+$ fibrocytes are scarce (*top*, **c**). The stroma of melanocytic nevi is devoid of α-SMA-positive myofibroblasts. Note positive α-SMA staining of vessels (**d**). The interface between melanomas and tumor-free dermis displays an abrupt loss of $CD34^+$ fibrocytes (**e**). No α-SMA-positive myofibroblasts occur in melanomas. Note positive staining of vascular smooth muscle with α-SMA (**f**). In **e** and **f**, melanin pigment (*brown*) appears in histiocytes and melanoma cells

reticular network (Fig. 1a). The highest number of $CD34^+$ fibrocytes was found around the isthmus of the hair follicle where they were closely located to CD34-reactive epithelial cells of the external root sheath (Fig. 1a inset). Few $CD34^+$ fibrocytes were detected in the papillary dermis, predominantly neighboring capillaries and the infundibulum of hair follicles. α-SMA-positive stromal cells were absent from the normal dermis. SPARC expression was absent from the epidermis, normal melanocytes, skin appendages, and dermal stromal cells, but capillary endothelium displayed cytoplasmic SPARC immunoreactivity (Table 3).

Melanocytic nevi

The stroma adjacent to and within dermal nevi harbored $CD34^+$ fibrocytes at an amount equal to that observed in the normal dermis. Individual nevus cells and clusters of nevus cells were intimately surrounded by a delicate network of $CD34^+$ fibrocytes resulting in a nest-like appearance (Fig. 1b). Compound nevi displayed a more complex distribution of $CD34^+$ fibrocytes. The superficial portion of compound nevi showed scarce $CD34^+$ fibrocytes, whereas the nevus cells located in the reticular dermis were surrounded by densely packed $CD34^+$ fibrocytes (Fig. 1c). Morphologically, the $CD34^+$ fibrocytes associated with nevi resembled those occurring in the normal dermis. α-SMA-positive myofibroblasts were not observed in the stroma of melanocytic nevi (Fig. 1d). According to the normal skin, the stroma associated with melanocytic nevi displayed no SPARC expression (Fig. 2a). There was also no SPARC expression in the nevus

Table 3 $CD34^+$ fibrocytes, α-SMA-positive myofibroblasts, and SPARC expression in the normal dermis, melanocytic nevi, and malignant melanomas

		Normal dermis, $n=49$	Melanocytic nevi, $n=29$	Malignant melanoma, $n=20$
$CD34^+$ fibrocytes		49	29	0
α-SMA-positive myofibroblasts		0	0	0
SPARC	Stromal cells	0	0	0
	Nevus cells		0	
	Tumor cells			20

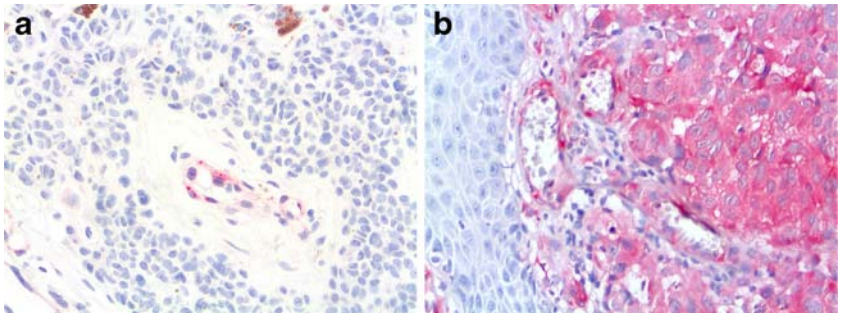

Fig. 2 Immunohistochemically, SPARC is not found in melanocytic nevi whereas the vascular endothelium is SPARC reactive (**a**). Melanomas show strong cytoplasmic SPARC staining. Stromal cells and the epidermis (to the *left*) are devoid of SPARC immunoreactivity (**b**)

cells, merely histiocytes located in the dermis and endothelial cells displayed SPARC reactivity (Table 3).

Malignant melanomas

The stroma of all melanomas investigated harbored neither CD34 (Fig. 1e) nor α-SMA-reactive stromal cells (Fig. 1f). In lesions infiltrating the reticular dermis, there was a clear-cut interface between the tumor and the adjacent tumor-free stroma characterized by an abrupt loss of CD34 expression within the tumor-associated stroma (Fig. 1e). CD34 immunoreactivity was not observed in the melanoma cells. Unlike the nevi, all malignant melanomas displayed strong SPARC expression in equal to or more than 50% of the tumor cells. In neither case was stromal SPARC expression observed (Fig. 2b, Table 3).

Discussion

In the last two decades, several authors reported on the presence of CD34-positive stromal cells within the dermis [13–15]. The first of these studies were purely descriptive and the histogenesis and putative function of this cell population remained enigmatic. Subsequent studies showed that dermal $CD34^+$ fibrocytes are derived at least partly from circulating fibrocytes being capable of tissue invasion and are implicated in wound healing [16]. $CD34^+$ fibrocytes also play an important role in diseases of the skin such as systemic sclerosis and nephrogenic fibrosing dermopathy [22]. Moreover, various cutaneous and subcutaneous tumors such as dermatofibrosarcoma protuberans [23], angiomyofibroblastomas and angiomyxomas [24], lipomatous tumors [25, 26], and trichodiscomas [27] have been claimed to be histogenetically linked to $CD34^+$ fibrocytes.

The present study is the first to give a description of $CD34^+$ fibrocytes in the normal dermis and benign and malignant melanocytic lesions. In the normal dermis, the distribution of $CD34^+$ fibrocytes closely resembles that observed in organs such as the breast and pancreas where $CD34^+$ fibrocytes are found in close vicinity to glands and ducts as well as vessels [1, 8–12, 21]. The skin recapitulates this distribution pattern as dermal $CD34^+$ fibrocytes are mostly found around hair follicles, skin appendages, and vessels. Merely, the papillary dermis displays only scarce $CD34^+$ fibrocytes.

The analysis of the dermal $CD34^+$ fibrocyte population has been shown to be a valuable tool in distinguishing benign and malignant skin appendage tumors such as trichoepithelioma and basal cell carcinomas [14, 15]. Herein, we show that this may also be true for melanocytic lesions as malignant melanomas show a loss of $CD34^+$ fibrocytes whereas this cell population is preserved in melanocytic nevi. However, the diagnostic utility of the stromal CD34 expression may be affected by the fact that a subpopulation of malignant melanoma cells may be CD34 reactive [28]. In the cited study, up to 30% of malignant melanomas harbored CD34-positive melanoma cells. Regarding the results of the present study in which no CD34-reactive melanomas cells were found, this value appears exceedingly high. Whatever the reasons of this apparent discrepancy, CD34-positive melanomas cells should be kept in mind when analyzing CD34 expression of malignant melanomas and their associated stroma by means of immunohistochemistry. On the other hand, the diagnosis of malignancy in a questionable melanocytic lesion should not be based on the sole loss of the stromal CD34 expression since in the superficial portion of dermal nevi CD34 fibrocytes are scarce.

Stromal remodeling associated with malignant melanomas differs from that observed in most invasive carcinomas as the loss of $CD34^+$ fibrocytes is not paralleled by a gain of stromal α-SMA-positive myofibroblasts. Differences were also observed concerning SPARC expression. In contrast to invasive ductal carcinomas of the breast [9] and urothelial carcinomas [7], stromal cells associated with malignant melanomas were devoid of SPARC expression. Vice versa, in all malignant melanomas investigated, at least 50% of the melanoma cells displayed strong SPARC expression which was not observed in the carcinoma cells [7, 9]. SPARC exerts a multitude of functions such as regulation of tumor cell growth and stromal deadhesion [18, 19]. Intracellular SPARC in melanoma cells plays a crucial role in the regulation of tumor cell proliferation whereas extracellular SPARC does not [29].

Moreover, downregulation of intracellular SPARC in melanomas has been shown to precipitate an inflammatory host response directed against the tumor [29]. In the cited study, stromal remodeling was also related to SPARC secretion by the tumor cells. These data are in keeping with our findings as all melanomas displayed cytoplasmic SPARC expression whereas melanocytic nevi did not. Thus, it appears justified to claim that SPARC plays a pivotal role in stromal remodeling associated with malignant melanoma. Additionally, SPARC expression in a melanocytic lesion apparently indicates malignancy.

Meanwhile, it has been well documented in a number of studies that the loss of stromal CD34 expression is a common feature of carcinomas irrespective of their primary site and histologic type. The present study documents that this is also the fact in malignant melanomas underlining the assumption that the stereotypic loss of CD34 might be of importance for the development of invasive tumors. However, the underlying and precipitating events of the stromal CD34 loss as well as their consequences for the course of a malignant tumor are far from being understood and should prompt further scrutiny.

Conflict of interest statement We declare that we have no conflict of interest.

References

1. Barth PJ, Ebrahimsade S, Hellinger A et al (2002) CD34$^+$ fibrocytes in neoplastic and inflammatory pancreatic lesions. Virchows Arch 440:128–133
2. Nakayama H, Enzan H, Miyazaki E et al (2000) Differential expression of CD34 in normal colorectal tissue, peritumoral inflammatory tissue, and tumour stroma. J Clin Pathol 53:626–629
3. Nakayama H, Enzan H, Miyazaki E et al (2001) CD34 positive stromal cells in gastric adenocarcinomas. J Clin Pathol 54:846–848
4. Nakayama H, Enzan H, Yamamoto M et al (2003) CD34-positive stromal cells in primary lung carcinomas. Oncol Rep 10:1313–1316
5. Barth PJ, Schenck zu Schweinsberg T, Ramaswamy A et al (2004) CD34$^+$ fibrocytes, α-smooth muscle antigen-positive myofibroblasts, and CD117 expression in the stroma of invasive squamous cell carcinomas of the oral cavity, pharynx, and larynx. Virchows Arch 444:231–234
6. Barth PJ, Ramaswamy A, Moll R (2002) CD34$^+$ fibrocytes in normal cervical stroma, cervical intraepithelial neoplasia III, and invasive squamous cell carcinoma of the cervix uteri. Virchows Arch 441:564–568
7. Nimphius W, Moll R, Olbert P et al (2007) CD34$^+$ fibrocytes in chronic cystitis and noninvasive and invasive urothelial carcinomas of the urinary bladder. Virchows Arch 450:179–185
8. Barth PJ, Ebrahimsade S, Ramaswamy A et al (2002) CD34$^+$ fibrocytes in invasive ductal carcinoma, ductal carcinoma in situ, and benign breast lesions. Virchows Arch 440:298–303
9. Barth PJ, Moll R, Ramaswamy A (2005) Stromal remodeling and SPARC (secreted protein acid rich in cysteine) expression in invasive ductal carcinomas of the breast. Virchows Arch 446:532–536
10. Barth PJ, Westhoff CC (2007) CD34$^+$ fibrocytes: morphology, histogenesis and function. Curr Stem Cell Res Ther 2:221–227
11. Ebrahimsade S, Westhoff CC, Barth PJ (2007) CD34$^+$ fibrocytes are preserved in most invasive lobular carcinomas of the breast. Pathol Res Pract 203:695–698
12. Kuroda N, Jin YL, Hamauzu T et al (2005) Consistent lack of CD34-positive stromal cells in the stroma of malignant breast lesions. Histol Histopathol 20:707–712
13. Narvaez D, Kanitakis J, Faure M et al (1996) Immunohistochemical study of CD34-positive dendritic cells of human dermis. Am J Dermatopathol 18:283–288
14. Kirchmann TT, Prieto VG, Smoller BR (1994) CD34 staining pattern distinguishes basal cell carcinoma from trichoepithelioma. Arch Dermatol 130:589–592
15. Humphreys TR, Monteiro MR, Murphy GF (2000) Mast cells and dendritic cells in basal cell carcinoma stroma. Dermatol Surg 26:200–203
16. Bucala R, Spiegel LA, Chesney J et al (1994) Circulating fibrocytes define a new leukocyte subpopulation that mediates tissue repair. Mol Med 1:71–81
17. Abe R, Donnelly SC, Peng T et al (2001) Peripheral blood fibrocytes: differentiation pathway and migration to wound sites. J Immunol 166:7556–7562
18. Chesney J, Bacher M, Bender A et al (1997) The peripheral blood fibrocyte is a potent antigen-presenting cell capable of priming naive T cells in situ. Proc Natl Acad Sci U S A 94: 6307–6312
19. Framson PE, Sage EH (2004) SPARC and tumor growth: where the seed meets the soil? J Cell Biochem 92:679–90
20. Murphy-Ullrich JE (2001) The de-adhesive activity of matricellular proteins: is intermediate cell adhesion an adaptive state? J Clin Invest 107:785–790
21. Ramaswamy A, Moll R, Barth PJ (2003) CD34$^+$ fibrocytes in tubular carcinomas and radial scars of the breast. Virchows Arch 443:536–540
22. Galan A, Cowper SE, Bucala R (2006) Nephrogenic systemic fibrosis (nephrogenic fibrosing dermopathy). Curr Opin Rheumatol 18:614–617
23. Haycox CL, Odland PB, Olbricht SM et al (1997) Immunohistochemical characterization of dermatofibrosarcoma protuberans with practical applications for diagnosis and treatment. J Am Acad Dermatol 37:438–444
24. Silverman JS, Albukerk J, Tamsen A (1997) Comparison of angiomyofibroblastoma and aggressive angiomyxoma in both sexes: four cases composed of bimodal CD34 and factor XIIIa positive dendritic cell subsets. Pathol Res Pract 193: 673–682
25. Silverman JS, Tamsen A (1997) Fibrohistiocytic differentiation in subcutaneous fatty tumors. Study of spindle cell, pleomorphic, myxoid, and atypical lipoma and dedifferentiated liposarcoma cases composed in part of CD34+ fibroblasts and FXIIIa+ histiocytes. J Cutan Pathol 24:484–493
26. Suster S, Fisher C (1997) Immunoreactivity for the human hematopoietic progenitor cell antigen (CD34) in lipomatous tumors. Am J Surg Pathol 21:195–200
27. Kutzner H, Requena L, Rütten A et al (2006) Spindle cell predominant trichodiscoma: a fibrofolliculoma/trichodiscoma variant considered formerly to be a neurofollicular hamartoma: a clinicopathological and immunohistochemical analysis of 17 cases. Am J Dermatopathol 28:1–8
28. Pisacane AM, Picciotto F, Risio M (2007) CD31 and CD34 expression as immunohistochemical markers of endothelial transdifferentiation in human cutaneous melanoma. Cell Oncol 29:59–66
29. Prada F, Benedetti LG, Bravo AI et al (2007) SPARC endogenous level, rather than fibroblast-produced SPARC or stroma reorganization induced by SPARC, is responsible for melanoma cell growth. J Invest Dermatol 127:2618–2628

Virchows Arch (2008) 453:491–499
DOI 10.1007/s00428-008-0675-9

ORIGINAL ARTICLE

Helicase-like transcription factor exhibits increased expression and altered intracellular distribution during tumor progression in hypopharyngeal and laryngeal squamous cell carcinomas

Aurélie Capouillez · Christine Decaestecker · Olivier Filleul · Dominique Chevalier · Frederique Coppée · Xavier Leroy · Alexandra Belayew · Sven Saussez

Received: 2 July 2008 / Revised: 31 August 2008 / Accepted: 9 September 2008 / Published online: 30 September 2008

Abstract The helicase-like transcription factor (HLTF) belongs to the SWI/SNF family of proteins that use the energy from adenosine triphosphate hydrolysis to remodel chromatin during a variety of cellular processes. HLTF is also involved in DNA repair. Using computer-assisted microscopy, the immunohistochemical expression of HLTF was determined using a series of 100 hypopharyngeal and 56 laryngeal squamous cell carcinomas (SCCs) compared to *tumor-free* epithelia (60 cases) and dysplasias (92 cases). In hypopharyngeal SCC tumor progression, increased HLTF expression was associated with the percentage of immunopositive epithelial tissue areas ($p=0.02$) and the staining intensity of the positive area ($p=0.0005$). In the cases of laryngeal lesions, the immunolabeling intensity of HLTF significantly decreased with malignancy ($p=0.01$). We also observed a significant shift of HLTF expression from the cytoplasm toward the nuclear compartment ($p=0.0007$). Our data reveal an association between the presence of HLTF and neoplastic progression of hypopharyngeal and laryngeal SCCs.

Keywords Head and neck carcinoma · HLTF · SWI/SNF protein · Dysplasia · Malignancy

Christine Decaestecker is a Senior Research Associate of the Belgian National Fund for Scientific Research. A. Capouillez held pre-doctoral fellowships from the Fonds de Recherche pour l' Industrie et l' Agriculture (FRIA, Belgium).

A. Capouillez · O. Filleul · S. Saussez (✉)
Laboratory of Anatomy, Faculty of Medicine and Pharmacy,
University of Mons-Hainaut,
Pentagone 1B-Avenue du Champ de Mars, 6,
7000 Mons, Belgium
e-mail: sven.saussez@umh.ac.be

A. Capouillez · F. Coppée · A. Belayew
Laboratory of Molecular Biology,
Faculty of Medicine and Pharmacy, University of Mons-Hainaut,
Mons, Belgium

C. Decaestecker
Laboratory of Toxicology, Institute of Pharmacy,
Université Libre de Bruxelles (ULB),
Brussels, Belgium

D. Chevalier
Department of Oto-Rhino-Laryngology, Faculty of Medicine,
Hôpital Claude Huriez and Centre de Biologie-Pathologie-CHRU,
Lille, France

X. Leroy
Department of Pathology, Faculty of Medicine,
Hôpital Claude Huriez and Centre de Biologie-Pathologie-CHRU,
Lille, France

Introduction

Perturbations in the regulation of gene expression, including changes at the level of DNA methylation and chromatin structure, are associated with carcinogenesis, and several oncogenes or tumor suppressor genes are affected by such alterations [1]. Mating type switching/sucrose non-fermenting proteins (SWI/SNF) are large protein complexes that contribute to chromatin remodeling by altering nucleosome positioning [1]. Their enzymatic activity is provided by SWI/SNF subunits that harbor a DNA helicase-like domain and function as DNA-dependent adenosine triphosphatases. Several studies have demonstrated that SWI/SNF proteins

may be linked to the development of human cancer and may function as tumor suppressors [2]. For example, the SNF5 subunit, which is present in all known variants of the SWI/SNF complex, is specifically inactivated or mutated in atypical teratoid and malignant rhabdoid tumors, two highly aggressive cancers of early childhood [3]. *HLTF*, a member of the SWI/SNF family, is involved in cancer progression in two ways involving either epigenetic silencing by DNA methylation or overexpression [1]. *HLTF* promoter methylation was first reported by Moinova et al. in colon cancer [2]. They demonstrated that all colon cancer cell lines lacking *HLTF* gene expression exhibited CpG methylation within the putative *HLTF* promoter and also that *HLTF* gene methylation was detected in 43% of primary colon cancers [2]. Several studies have confirmed *HLTF* promoter hypermethylation in human colorectal cancers [4–8], and other groups have described the same features in gastric [9–12], esophageal [13], and uterine cancers [14], suggesting that *HLTF* silencing may play a critical role in cancer. In esophageal squamous cell carcinoma (ESCC), *HLTF* methylation was detected in only one out of 40 samples, suggesting that *HLTF* was not a common target for methylation and epigenetic gene silencing in ESCC [13]. We recently investigated *HLTF* expression in a hamster model of kidney tumors induced by diethylstilbestrol (DES) and demonstrated that *HLTF* was induced very early during the tumor progression (after 2 months of DES treatment) in small pre-neoplastic buds [15]. Our data thus suggested that *HLTF* gene activation was linked to the initial steps of carcinogenesis and should be investigated in early stages (dysplasia) of other human cancers. HLTF therefore seemed to act as either a positive or negative regulatory factor in tumor development, depending on the histological type and stage of the tumor [1].

In the present study, we used quantitative immunohistochemistry to examine 100 cases of hypopharyngeal SCCs (HSCCs) and 56 cases of laryngeal SCCs (LSCCs) in comparison to normal controls [60 cases of *tumor-free* epithelium (TF_E)] and dysplastic tissues [92 cases grouping low-grade (Low_D) and high-grade (High_D) dysplasias] from peritumoral regions to answer the following questions: (1) Do *HLTF* expression levels change during the course of the disease? (2) Where is HLTF detected in the cell, and is this location altered during disease progression?

Materials and methods

Patient characteristics

The cases of 156 patients, 100 with HSCC and 56 with LSCC, who underwent surgery aimed at curative tumor resection, were studied. They were obtained by retrospective compilation (January 1989 to December 2001) from the records of the Ear–Nose–Throat Department of the Hôpital Claude Huriez (Lille, France). The description of the tumor status was based on the histopathological grade of tumor differentiation (criteria defined in [16] and the tumor–node–metastases (TNM) staging classification [17]). The 100 HSCCs and 56 LSCCS studied came from patients who did not undergo chemotherapy and/or radiotherapy before surgery (*see clinical data in* Table 1). Patients suffering from SCCs localized at other sites of the head and neck area were excluded from the study.

Table 1 Clinical data

Variable	High stage HSCCs, stage IV 100 cases	Low stage LSCCs, stages I & II 40 cases	High stage LSCCs, stage IV 16 cases
Age (years)			
Range	40–78	36–88	43–78
Average	55	57	57
Sex (cases)			
Male	90	40	16
Female	10		
Site (cases)			
Supraglottic area		5	9
Glottic area		30	
Supraglottic and glottic areas		5	4
Subglottic and glottic areas			3
Piriform sinus	80		
Postcricoid area	17		
Posterior wall	3		
Histological grade (cases)			
Well differentiated	52	34	10
Moderately differentiated	36	5	6
Poorly differentiated	12	1	
TNM stage (cases)			
T1N0M0		31	
T2N0M0		11	
T2N2M0	8		
T3N2M0	8		
T4N0M0	15		9
T4N1M0	9		3
T4N2M0	56		4
T4N3M0	4		
Tumor treatment (cases)			
Co_2 laser cordectomy		8	
Frontolateral laryngectomy		2	
Vertical partial laryngectomy		4	
Supracricoid partial laryngectomy		23	3
Supraglottic laryngectomy		3	
Total laryngectomy			13
Partial pharyngolaryngectomy	9		
Total pharyngolaryngectomy	71		
Circular pharyngolaryngectomy	10		
Esopharyngolaryngectomy	10		

In the vicinity of the tumor, we have also identified (with the help of XL, a head and neck pathologist) and analyzed 60 cases of tumor-free epithelium and 92 cases of dysplasia. The 60 cases of TF_E were composed of 27 hypopharyngeal cases and 33 laryngeal cases, whereas the 92 cases of dysplasia were composed of 48 hypopharyngeal cases (eight cases of low-grade dysplasia and 40 cases of high-grade dysplasia, defined below under "Definition of low- and high-grade epithelial dysplasias") and 44 laryngeal cases (11 cases of low-grade dysplasia and 33 cases of high-grade dysplasia). For the hypopharyngeal epithelia, we have compared 12 cases of healthy epithelium (these epithelia were cut off during a procedure of pharyngoplasty performed for snoring) and 15 cases of TF_E).

Anti-HLTF serum

Two human HLTF variants are expressed from the same open reading frame and differ only in the translation start site (Met1 or Met123) [18]. The rabbit antiserum (ART2) specific for the HLTFMet1 variant was raised against a peptide (VIPPDDFLTSDEEVD) from the amino-terminal sequence which is missing in the shorter Met123 variant (residues 42–56), as described by Debauve et al. [15].

Cell culture

Cell lines (HeLa, Detroit 562, FaDu, RPMI 2650, SCC9, SCC-VII, and RKO) were maintained at 37°C in an incubator with 5% CO_2. Cells were grown in T75-flasks (Orange Scientific, Braine-l'Alleud, Belgium) containing Dulbecco's modified essential medium for Detroit 562, FaDu, RPMI 2650, SCC9, and SCC-VII cell lines (DMEM, BioWhittaker Europe, Verviers, Belgium) or McCoy medium for the RKO cells. Media was supplemented with 10% fetal bovine serum (FBS, HyClone, Logan, Utah), 2 mM L-glutamine, 100 U/ml penicillin G, 100 μg/ml streptomycin, and 0.25 μg/ml amphotericin B (DMEM-FBS; supplements from Bio-Whittaker or Gibco-Invitrogen, Merelbeke, Belgium). Cell cultures were passaged once a week (split ratio 1:300) and fed fresh media every 2–3 days. For routine subculture and cell plating in preparation of immunofluorescence studies, cells were incubated with trypsin-ethylenediamine tetraacetic acid solution, suspended, and counted in a model Z1 Coulter counter.

Immunohistochemistry

All tumor samples were fixed for 24 h in 10% formaldehyde, dehydrated, and embedded in paraffin. Immunohistochemistry was performed on 5-μm-thick sections mounted on silane-coated glass slides [19]. Before starting the immunohistochemistry protocol, dewaxed tissue sections were briefly exposed to microwave pretreatment in a 0.01 M citrate buffer (pH 6.0) for 2×5 min at 900 W. The sections were then incubated with a solution of 0.4% hydrogen peroxide for 5 min, rinsed in phosphate-buffered saline (PBS; 0.04 M Na_2HPO_4, 0.01 M KH_2PO_4, 0.12 M NaCl, pH 7.4), and exposed for 20 min to solutions containing avidin (0.1 mg/ml in PBS) and biotin (0.1 mg/ml in PBS). After thorough washing with PBS, the sections were incubated for 20 min with 0.5% casein in PBS and sequentially exposed at room temperature to solutions of (1) the specific primary anti-HLTF antibody; (2) the corresponding biotinylated secondary antibody (polyclonal goat anti-rabbit IgG); and (3) the avidin–biotin–peroxidase complex (ABC kit). Incubation steps were alternated with washing steps to remove unbound proteins. Antigen-dependent presence of the peroxidase complex in the sections was visualized by incubation with chromogenic substrates containing diaminobenzidine and H_2O_2. After rinsing, the sections were counterstained with luxol fast blue and mounted with a synthetic medium. To exclude antigen-independent staining, the incubation step with primary/secondary antibodies was omitted from the protocol in controls. In all cases, these controls were negative. The biotinylated secondary antibodies and ABC kit came from DakoCytomation (Glostrup, Denmark). We defined a tumor exhibiting HLTF labeling exclusively in the cytoplasm of all the cells as having a cytoplasmic location and a tumor showing at least 5% of the cells with HLTF in the nucleus as having nuclear localization. In this latter group, most cells presented concomitant nuclear and cytoplasmic labeling.

Definition of low- and high-grade epithelial dysplasias

Morphological characteristics of dysplasia include increased cellular density associated with a large number of mitotic figures in the vicinity of the basal layer, irregular maturation, loss of polarity, and dyskeratosis. Cytologically, dysplasia is characterized by an increased ratio of nuclear to cytoplasmic area, anisocytosis, poikilocytosis, nuclear polymorphism, chromatin condensation, and large nucleoli, features sometimes associated with atypical mitotic figures. Low-grade dysplasia, comprising mild and moderate dysplasia, presents atypical features extending over the lower or middle third of the epithelium [20]. High-grade dysplasia, covering severe dysplasia and carcinoma in situ, extend over the entire thickness of the epithelium [20].

Computer-assisted microscopy

After the immunohistochemical steps, the levels of HLTF expression were quantitatively determined using a computer-assisted KS 400 imaging system (Carl Zeiss Vision, Hallbergmoos, Germany) connected to a Zeiss Axioplan

microscope [21]. For each microscopic field, we focused analysis on the epithelial region using computer-assisted morphometry after interactive identification. We scanned 15 fields covering a surface area ranging from 60,000 to 120,000 μm^2. Quantitative analysis of the immunohistochemical staining for a given marker yielded data on two variables: the labeling index (LI), i.e., the percentage of immunopositive tissue areas, and the mean optical density (MOD), i.e., staining intensity of positive cells [21]. For each case of dysplasia (low or high grade), an author (XL) specialized in this diagnostic procedure defined the respective fields within peritumoral areas.

Immunofluorescence staining of cultured cells

For cell immunostaining, 12-well plates containing sterile round glass coverslips (15-mm diameter) were seeded at a density of 5×10^3 cells/mm^2. After 3 days of growth, cell

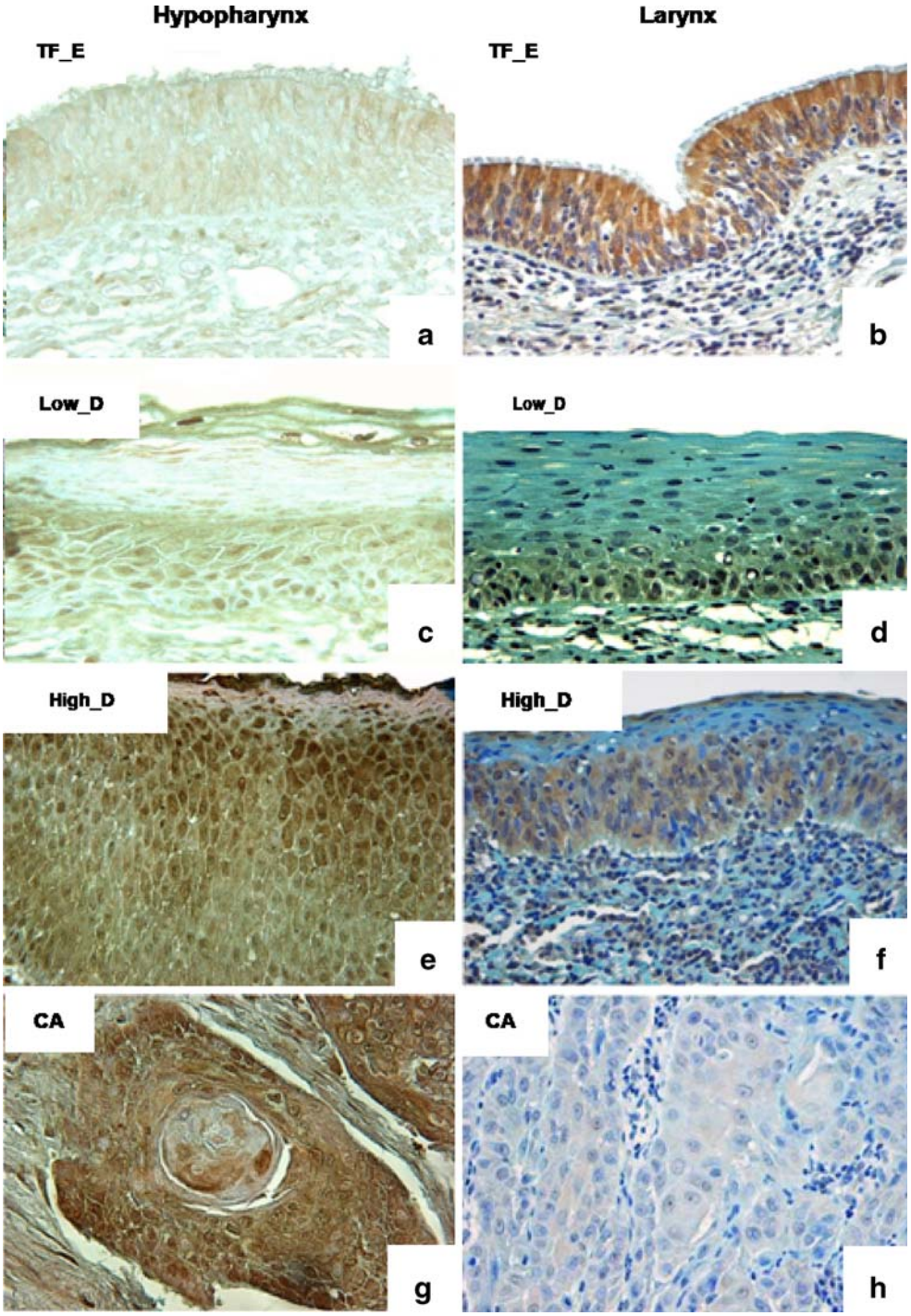

Fig. 1 **a**–**f** Immunohistochemical staining profile for HLTF in hypopharynx (**a**, **c**, **e**, **g**) and larynx (**b**, **d**, **f**, **h**), respectively. The antigen was localized in normal epithelium (*TF_E*, **a**), low-dysplasia (*Low_D*, **c**), and high-dysplasia (*High_D*, **e**) in areas surrounding hypopharyngeal carcinomas (*CA*, **g**). **b**, **d**, **f** HLTF staining demonstrated in TF_E (**b**), Low_D (**d**), and High_D (**f**) in areas surrounding laryngeal CA (**h**). Hematoxylin–eosin, magnification **a**–**h** ×320

cultures were rinsed with Dulbecco's PBS (DPBS) and fixed at 4°C in 4% paraformaldehyde in DPBS for 15 min. The fixative was replaced by DPBS, and cells were kept at 4°C until immunostaining was carried out. HLTF-containing immunocomplexes were demonstrated by incubating cell preparations with a mixture of biotinylated swine anti-rabbit immunoglobulin antibodies and fluorescein isothiocyanate-conjugated goat anti-rabbit immunoglobulin antibodies [F(ab)2 fragments; Dakocytomation, Glostrup, Denmark]. The preparations were mounted in Vectashield (Vector Laboratories, Burlingame, CA, USA). Immunostained sections were examined on a Leitz Orthoplan fluorescence microscope (Ploem system), and representative fields were recorded with a digital camera (Leica DC 300F).

Controls for the specificity of immunolabeling included the omission of the primary antibody or the substitution of non-immune sera for the primary antibodies. The specificity of anti-HLTF immunostaining was also examined with primary antibodies previously incubated with the synthetic peptide used as antigen. In each case, these controls were negative.

Data analysis

Independent groups of quantitative data were compared using the nonparametric Kruskall–Wallis (more than two groups). In the case of significant Kruskall–Wallis tests, post hoc tests (Dunn procedure) were used to compare pairs of groups (to avoid multiple comparison effects). The relationships between the qualitative (or ordinal) variables analyzed (e.g., cytoplasmic location vs. nuclear and cytoplasmic location) were studied by means of contingency tables. The significance of the potential associations was evaluated using the χ^2 or the exact Fisher test (in the 2×2 cases). All the statistical analyses were carried out with Statistica software (Statsoft, Tulsa, USA).

Results

Expression of HLTF during tumor progression of hypopharyngeal and laryngeal SCCs

The morphological examination of different tissue samples [including tumor-free epithelia, dysplasias, and carcinomas (CA)] revealed that the clinical course toward hypopharyngeal and laryngeal SCCs (HSCCs and LSCCs) was characterized by different patterns of HLTF immunolabeling (Fig. 1). In tumor-free epithelium, HLTF was found in the cytoplasm of the basal layer (65% of cases of HSCC TF_E and 97% of cases of LSCC TF_E; Fig. 1a, b). For hypopharyngeal epithelia, the comparison of the 12 healthy cases and the 15 TF_E revealed similar HLTF expression for both MOD and LI as well as nucleo-cytoplasmic distribution. Immunohistochemical staining of HLTF was clearly different in carcinomas (HSCCs and LSCCs) with respect to TF_E, Low_D, or High_D (Figs. 1 and 2). To clearly present our data, we first compared all groups (TF_E, Low_D, High_D, and CA) using the nonparametric

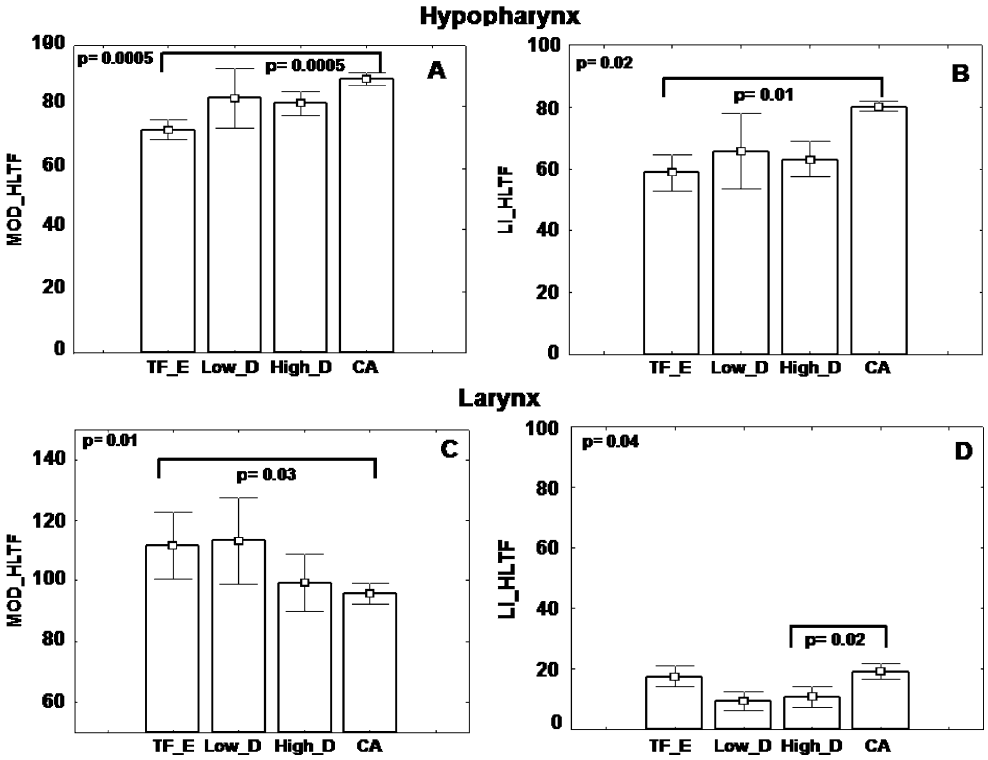

Fig. 2 Labeling index (**b**, **d**) and mean optical density (**a**, **c**) determined by computer-assisted microscopy for immunohistochemical HLTF expression in a series of 27 TF_E, eight Low_D, 40 High_D, and 100 H_CA (**a**, **b**), as well as in a series of 33 TF_E, 11 Low_D, 33 High_D, and 55 LSCCs (**c**, **d**). Data are expressed as means (*columns*) ±standard errors (*bars*). The significance level associated with the global multi-group comparison (Kruskall–Wallis test) is indicated in the *upper left corner of each frame*. Post hoc comparisons were used to compare the pairs of groups indicated by the *brackets*

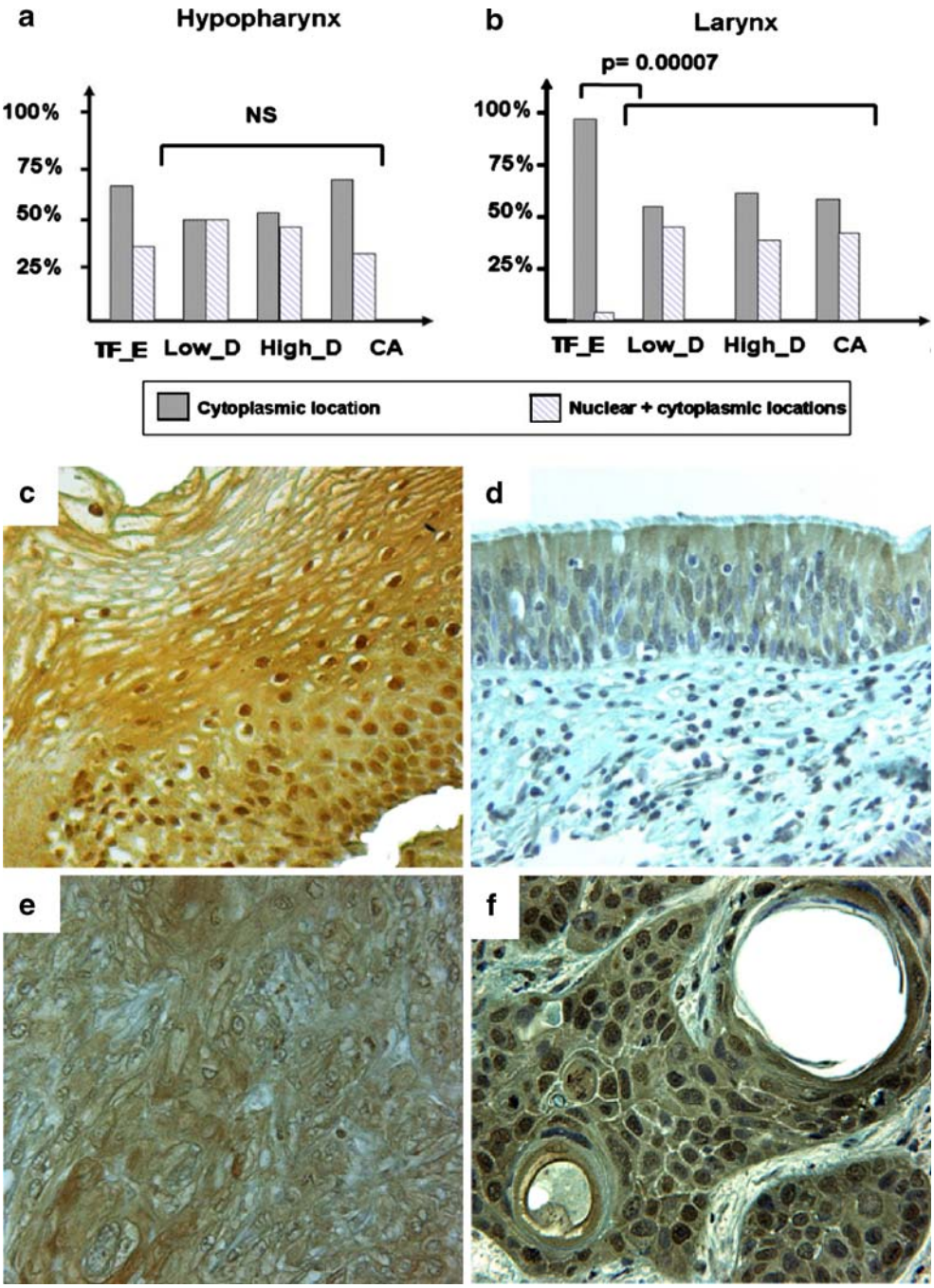

Fig. 3 Dysplasias (Low_D and High_D; **c**) presented an HLTF-dependent nuclear labeling that tended to decrease in hypopharyngeal CA (**a**, **c**, **e**). In LSCCs, dysplasias and CA revealed a significant shift of staining from the cytoplasm to the nucleus (**b**, **d**, **f**; χ^2 test was used after grouping Low_D, High_D, and CA groups)

Kruskall–Wallis test and then used post hoc comparisons for pairs of groups in Fig. 2. In the cases of hypopharyngeal CA, the use of two different quantitative variables revealed a similar relation to the clinical course. Increased HLTF expression was associated with both the percentage of immunopositive epithelial tissue area (LI variable, Kruskall–Wallis: $p=0.02$) and the staining intensity of the positive area (MOD variable, Kruskall–Wallis: $p=0.0005$; post hoc comparisons are detailed in Fig. 2a, b). Interestingly, the progression seemed to be associated with a slight shift in HLTF immunolabeling from the nucleus to the cytoplasmic compartment, exclusively when comparing dysplasias (grouping Low_D or High_D) to hypopharyngeal carcinomas (Fig. 3a, c, e). In quantitative terms, 50% of Low_D (four of eight) and 45% of High_D (18 of 40) cases displayed nuclear expression of HLTF. Although only 31% of HSCCs displayed nuclear expression of HLTF (28 of 90 cases), this variability is not statistically significant.

In the cases of laryngeal lesions, the MOD variable describing HLTF expression significantly decreased with malignancy (Kruskall–Wallis: $p=0.01$; Fig. 2c), whereas a slight increase in labeling index was observed between

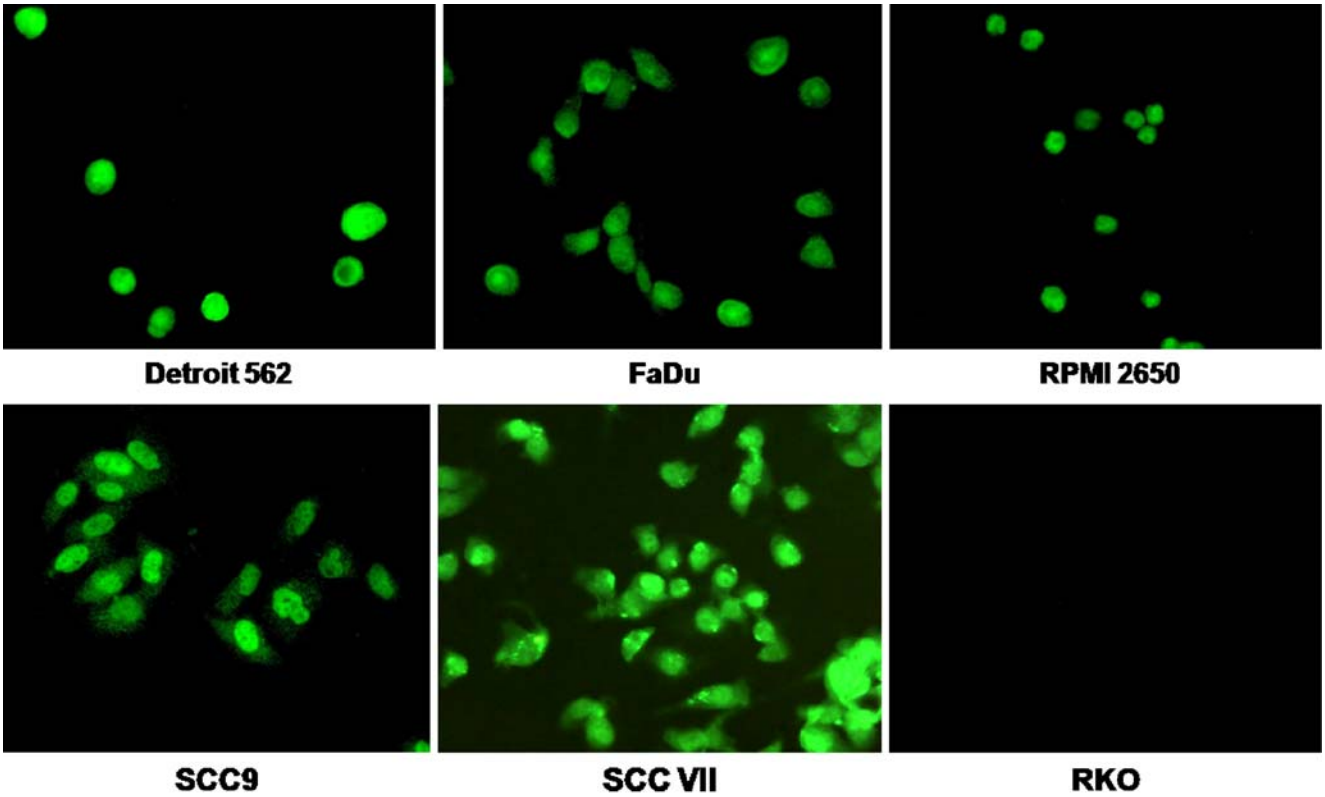

Fig. 4 Immunofluorescence detection of HLTF using ART2 antibody in Detroit 562, FaDu, RPMI 2650, SCC9, SCC-VII, and RKO cell lines. Magnification ×320

High_D and CA (post hoc test: p=0.02; Fig. 2d). We also observed a significant shift of HLTF expression from the cytoplasm to the nuclear compartment when comparing TF_E to dysplasias and LSCCs (Fig. 3). In fact, 3% of TF_E cases (one of 33) displayed nuclear expression of HLTF versus 45% (five of 11) of Low_D, 39% (13 of 33) of High_D, and 42% of LSCCs (23 of 55 cases). This difference was significant after grouping the latter three (preneoplastic and neoplastic) categories (Fisher test: p= 0.0007; Fig. 3b, d, f).

HLTF immunofluorescence staining pattern in five head and neck cell lines

The appearance of HLTF immunoreactivity during HSCC carcinogenesis suggests that it could be closely associated with neoplastic transformation and tumor progression. It indicates that HLTF production could be a phenotypic characteristic of at least one subpopulation of tumor cells. To further address this issue, HLTF expression was examined by immunofluorescence staining in the Detroit 562, FaDu, RPMI 2650, SCC9, and SCC-VII cell lines which were derived respectively from human pharyngeal carcinoma (Detroit 562 and FaDu), human nasal septum carcinoma, human tongue carcinoma, and human murine carcinoma. HLTF immunostaining of Detroit 562, FaDu, and RPMI 2650 cell lines resulted in weak to moderate nuclear and cytoplasmic fluorescence, whereas SCC9 and SCC-VII exhibited moderate to strong nuclear and cytoplasmic immunoreactivity (Fig. 4). The RKO cell line (derived from colon adenocarcinoma) was used as a negative control as its HLTF gene is hypermethylated and expressed at neither the RNA nor protein level (G. Debauve, unpublished data). These observations not only attest to the stability of HLTF expression in head and neck SCC cell lines but also indicate intercellular heterogeneity in the expression of these proteins.

Discussion

Our data reveal a significant up-regulation of HLTF expression throughout neoplastic progression of hypopharyngeal SCCs. This increased expression of HLTF in carcinomas seems to be accompanied by a shift from the nuclear compartment (N_E and dysplasias) to the cytoplasm. This is indicative of a switch in biological activity, such as the loss of chromatin/transcription regulation function or, more importantly in cancer progression, the lost of post-replication repair. In fact, Unk and co-authors have recently described that HLTF is required for error-free post-replication repair of damaged DNA [22]. They demonstrated that human HLTF functions together with

Rad6-Rad18 and Mms2-Ubc13 in proliferating cell nuclear antigen polyubiquitination and that it can complement the UV sensitivity of *rad5_* yeast cells [22]. These data strongly support a role for HLTF in promoting error-free DNA damage bypass. Thus, by preventing mutagenesis, HLTF DNA repair function would contribute to minimizing the incidence of carcinogenesis in humans.

Gong et al. have demonstrated that *HLTF* transcript levels were ~20-fold higher in a variety of transformed cell lines compared to non-transformed human fibroblast cells or human heart tissue [23]. They also showed that *HLTF* induction was associated with loss of *TP53* heterozygosity in Li-Fraumeni fibroblasts, suggesting a link between *HLTF* expression and cancer progression [23]. Our study, examining HLTF protein expression by immunohistochemistry in a hamster model of kidney tumors induced by DES allowed us to observe strong labeling in small preneoplastic tumor buds [15]. The latter, which were confirmed by our observations of a significant up-regulation of HLTF during hypopharyngeal carcinogenesis, led to the conclusion that *HLTF* gene activation was linked to the initial steps of carcinogenesis and should be investigated in early stages of cancers.

In a recent review focusing on the implications of HLTF in cancer progression, we hypothesized that HLTF overexpression could initiate cancerous transformation by changing the chromatin structure and activating the transcription of some target genes including *PAI1* [1,16]. However, as a further complexity, the expression of HLTF produces several protein variants, two of which (Met 1 and Met 123) were previously characterized and shown to diverge in transcriptional activity [1, 18]. Although no data are available about the role of the human HLTF RING domain, its rabbit orthologue binds an inner nuclear envelope protein (RFBP), which could play a role in subnuclear trafficking of factors with RING motifs [3,24].

We also reported that the levels of HLTF expression were very different during laryngeal tumor progression as compared to hypopharyngeal tumor progression. In fact, we showed that the MOD variable describing the intensity of HLTF immunolabeling significantly decreased with laryngeal malignancy. This point relates directly to the fact that cancers of the upper aerodigestive tract are heterogeneous in their neoplastic processes, each of which requires its own unique set of epidemiologic, anatomic, pathologic, and therapeutic considerations. Laryngeal and hypopharyngeal CAs present several significant clinical and biological differences which could be considered to partly explain the observed divergence in HLTF expression: (1) most hypopharyngeal CA patients (70–80% of cases) presented advanced stages (III and IV) at the time of diagnosis, whereas laryngeal CA patients were most frequently diagnosed at early stages (70–90% of cases presented stages I and II) [25]; (2) at a similar stage, hypopharyngeal CAs were associated with worse prognosis than laryngeal CAs, [25]; (3) well-differentiated CAs were common in larynx, whereas poorly differentiated tumors were more frequently located in hypopharynx [26], (4) in laryngeal CAs, there was a significant relationship between the presence of intratumoral lymphatics and nodal metastases which was not the case for hypopharyngeal CAs [27]; (5) the relationship of galectin-7 (an endogenous lectin with a wide range of extra- and intra-cellular functions mediated by protein–carbohydrate and protein–protein interactions) expression to aggressiveness appeared to depend on the location in the upper aerodigestive tracts: in hypopharyngeal CAs, galectin-7 overexpression was associated with worse prognosis, while this was not observed in laryngeal CAs [28, 29]. Previous studies described *HLTF* promoter hypermethylation in a significant number of cases of colorectal and gastric carcinomas, whereas only one case of esophageal carcinoma presented this silencing [4–13]. HLTF can thus act as either a positive or a negative regulatory factor in tumor development, depending on the histological type and the anatomical location.

Acknowledgements We thank the *Fondation pour la Recherche Médicale dans le Hainaut* (Hainaut, Belgium) for funding (S. Saussez and A. Belayew). We are also grateful to G. Ninfa for expert technical assistance.

Conflicts of interest The authors declare no conflict of interest relevant to this article.

References

1. Debauve G, Capouillez A, Belayew A et al (2008) HLTF and its implication in cancer progression. Cell Mol Life Sci 65:591–604
2. Moinova HR, Chen WD, Shen L (2002) HLTF gene silencing in human colon cancer. Proc Natl Acad Sci USA 99:4562–4567
3. Versteege I, Sevenet N, Lange J et al (1998) Truncating mutations of hSNF5/INI1 in aggressive paediatric cancer. Nature 394:203–206
4. Hibi K, Kodera Y, Ito K et al (2005) Aberrant methylation of HLTF, SOCS-1, and CDH13 genes is shown in colorectal cancers without lymph node metastasis. Dis Colon Rectum 48:1282–1286
5. Hibi K, Nakao A (2006) Highly-methylated colorectal cancers show poorly-differentiated phenotype. Anticancer Res 26:4263–4266
6. Hibi K, Nakao A (2006) Lymph node metastasis is infrequent in patients with highly-methylated colorectal cancer. Anticancer Res 26:55–58
7. Hibi K, Nakayama H, Kanyama Y et al (2003) Methylation pattern of HLTF gene in digestive tract cancers. Int J Cancer 104:433–436
8. Kim YH, Petko Z, Dzieciatkowski S et al (2006) CpG island methylation of genes accumulates during the adenoma progression step of the multistep pathogenesis of colorectal cancer. Genes Chromosomes Cancer 45:781–789
9. Hamai Y, Oue N, Mitani Y et al (2003) DNA hypermethylation and histone hypoacetylation of the HLTF gene are associated with reduced expression in gastric carcinoma. Cancer Sci 94:692–698

10. Kim JJ, Chung SW, Kim JH et al (2006) Promoter methylation of helicase-like transcription factor is associated with the early stages of gastric cancer with family history. Ann Oncol 17:657–662
11. Leung WK, Yu J, Bai AH (2003) Inactivation of helicase-like transcription factor by promoter hypermethylation in human gastric cancer. Mol Carcinog 37:91–97
12. Oue N, Mitani Y, Motoshita J et al (2006) Accumulation of DNA methylation is associated with tumor stage in gastric cancer. Cancer 106:1250–1259
13. Fukuoka T, Hibi K, Nakao A (2006) Aberrant methylation is frequently observed in advanced esophageal squamous cell carcinoma. Anticancer Res 26:3333–3335
14. Kang S, Kim JW, Kang GH et al (2006) Comparison of DNA hypermethylation patterns in different types of uterine cancer: cervical squamous cell carcinoma, cervical adenocarcinoma and endometrial adenocarcinoma. Int J Cancer 118:2168–2171
15. Debauve G, Nonclercq D, Ribaucour F et al (2006) Early expression of the helicase-like transcription factor (HLTF/SMARCA3) in an experimental model of estrogen-induced renal carcinogenesis. Mol Cancer 5:23
16. Hyams VJ, Batsakis JG and Michaels L eds. (1998) Tumors of the upper respiratory tract and ear. In: Atlas of Tumor Pathology, Armed Forces Institute of Pathology, Washington D.C.
17. Wittekind C, Greene FL, Hutter RRP et al (2004) TNM Atlas, 5th edn. UICC Springer, Berlin
18. Ding H, Descheemaeker K, Marynen P et al (1996) Characterization of a helicase-like transcription factor involved in the expression of the human plasminogen activator inhibitor-1 gene. DNA Cell Biol 15:429–442
19. Saussez S, Lorfevre F, Lequeux T et al (2008) The determination of the levels of circulating galectin-1 and -3 in HNSCC patients could be used to monitor tumor progression and/or responses to therapy. Oral Oncology 44:86–93
20. Galle N, Pilch Z, Sidransky D et al (2006) Head and neck tumours. IARC, Lyon, France
21. Saussez S, Decaestecker C, Lorfevre F et al (2008) Increased expression and altered intracellular distribution of adhesion/growth-regulatory lectins galectins-1 and -7 during tumour progression in hypopharyngeal and laryngeal squamous cell carcinomas. Histopathology 52:483–493
22. Unk I, Hajdú I, Fátyol K et al (2008) HLTF functions as a ubiquitin ligase for proliferating cell nuclear antigen polyubiquitination. Proc Natl Acad Sci USA 105:3768–3773
23. Gong X, Kaushal S, Ceccarelli E et al (1997) Developmental regulation of Zbu1, a DNA-binding member of the SWI2/SNF2 family. Dev Biol 183:166–182
24. Mansharamani M, Hewetson A, Chilton BS (2001) Cloning and characterization of an atypical type IV P-type ATPase that binds to the RING motif of RUSH transcription factors. J Biol Chem 276:3641–3649
25. Shah J (2003) Head and neck surgery and oncology. Mosby, London
26. Roland NJ, Caslin AW, Nash J et al (1992) Value of grading squamous cell carcinoma of the head and neck. Head Neck 14:224–229
27. Audet N, Beasly NJ, Mac Millan C et al (2005) Lymphatic vessel density, nodal metastases and prognosis in patients with head and neck cancer. Arch Otolaryngol Head Neck Surg 131:1065–1070
28. Saussez S, Cucu R, Decaesteker C et al (2006) Galectin-7 (p53-induced gene-1): a new prognostic predictor of recurrence and survival in stage IV hypopharyngeal cancer. Ann Surg Oncol 13:999–1009
29. Saussez S, Lorfebvre F, Cucu D et al (2007) High level of galectin-1 expression is a negative prognostic predictor of recurrence in laryngeal squamous cell carcinomas. Int J Oncol 30:1109–1117

Virchows Arch (2008) 453:501–509
DOI 10.1007/s00428-008-0673-y

ORIGINAL ARTICLE

Primary splenic diffuse large B-cell lymphoma manifesting in red pulp

Makoto Kashimura · Masahiro Noro · Bunshiro Akikusa · Atsushi Okuhara · Shuji Momose · Ikuo Miura · Masaru Kojima · Jun-ichi Tamaru

Received: 9 April 2008 / Revised: 4 September 2008 / Accepted: 5 September 2008 / Published online: 26 September 2008

Abstract We evaluated six cases of diffuse large B-cell lymphoma (DLBCL) involving the red pulp of the spleen. All had B symptoms and an aggressive clinical course. The lymphoma cells proliferated diffusely and non-cohesively in the cords of the red pulp. The lymphoma involved the bone marrow in four of the five patients and the liver in all four of the patients examined. However, lymph node (LN) involvement was rare at presentation, and systemic LN involvement was not observed even in the terminal phase. The lymphoma cells infiltrated the intrasinusoidal/intravascular and interstitial spaces of the involved tissues and were detected in the peripheral blood in two of the six patients. CD5-expressing lymphoma cells were detected in four of the five patients examined. Because these cases had some unique clinical features and occurred in distinct splenic sites, we proposed that primary splenic DLBCL manifesting in red pulp is a distinct clinicopathological entity.

Keywords Large B-cell lymphoma · Splenic red pulp · Intrasinusoidal lymphomatous infiltration · Bone marrow · Liver

M. Kashimura (✉)
Department of Hematology, Matsudo City Hospital,
4005 Kamihongo Matsudo,
Chiba 271-8511, Japan
e-mail: kasimura@mvi.biglobe.ne.jp

M. Noro · B. Akikusa
Department of Pathology, Matsudo City Hospital,
Matsudo, Japan

A. Okuhara
Laboratory of Hematology, Matsudo City Hospital,
Matsudo, Japan

S. Momose · J.-i. Tamaru
Department of Pathology, Saitama Medical Center,
Saitama Medical University,
Kawagoe, Japan

I. Miura
Department of Hematology and Oncology,
St Marianna University School of Medicine,
Kawasaki, Japan

M. Kojima
Department of Pathology and Clinical Laboratories,
Gunma Cancer Center Hospital,
Ohta, Japan

Introduction

Extranodal diffuse large B-cell lymphomas (DLBCLs) have specific clinicopathologic features that are dependent on the organ of origin [1]. Primary splenic DLBCL is a rare type of lymphoma. The majority of the DLBCLs are derived from the white pulp of the spleen and form one large, or multiple nodules [2]. Before the advent of immunohistological examination, the absence of mass formation and the diffuse infiltration of large neoplastic cells into the red pulp might have been diagnosed as malignant histiocytosis [3]. Kuratsune et al. [4] reported the first case of DLBCL that non-cohesively proliferated into the splenic red pulp and demonstrated clinicopathological features of malignant histiocytosis. Since their initial report, only 18 cases of DLBCLs non-cohesively infiltrating the splenic red pulp have been reported [4–13]. These reports support the existence of DLBCL manifesting in the splenic red pulp (DLBCLRP). Kroft et al. [8] identified two cases of DLBCLRP involving the bone marrow (BM) and the liver, and Morice et al. [10] reported two cases of DLBCLRP with prominent BM intravascular/intrasinusoidal lymphomatous infiltration.

Because there have been few case reports of DLBCLRP, there is no comprehensive list of its clinicopathological features. To clarify the features of this rare lymphoma, we describe six new cases of DLBCLRP and present an analysis of the clinicopathological features of an additional 18 previously reported cases [4–13]. After reviewing the data, we developed seven characteristic features of DLBCLRP. Based on these features, we propose that DLBCLRP is a distinct clinicopathologic entity. Moreover, we discuss the relationship between DLBCLRP and an Asian variant of intravascular lymphomatosis (IVL) with splenomegaly [14].

Materials and methods

Retrospective analyses were conducted for six patients clinicopathologically diagnosed with primary splenic large B-cell lymphoma manifesting in red pulp in our hospital from 2000 to 2007. Two hundred and ninety two patients were diagnosed with malignant lymphoma, including 228 with B-cell lymphomas (DLBCL 129, follicular lymphoma 58, marginal zone lymphoma 19, mantle cell lymphoma 6, etc), 45 with T-cell lymphomas, and 12 with Hodgkin's lymphomas during this 8-year period. Thirteen patients were diagnosed with primary splenic lymphoma, two with splenic marginal zone lymphoma, one with follicular lymphoma, and ten with DLBCL. Two patients were diagnosed as having DLBCL with a micronodular pattern. Eight patients were clinically diagnosed with DLBCLRP; however, two were excluded based on the unavailability of splenic tissues. All procedures were performed with informed consent of the patients.

Tissue specimens obtained from surgery, biopsy, or necropsy were fixed in formalin and embedded in paraffin. The paraffin-embedded sections were dewaxed with xylene. The sections were stained with hematoxylin–eosin (HE) for light microscopic examination, and by the streptavidin–biotin–peroxidase method (Nichirei Co., Tokyo, Japan) for immunohistochemical analysis. The panel of primary antibodies included L26 (CD20), JCB117 (CD79a), F7.2.38 (CD3), UCHL-1 (CD45RO), 1F8 (CD21), 124 (Bcl-2), PG-B6p (Bcl-6), MIB-1 (Ki-67), MUM1p (MUM1), IgM polyclonal (DAKO A/S, Glostrup, Denmark), MT1 (CD43), 4C7 (CD5), 56C6 (CD10), 1B12 (CD23), 1G12 (CD30), IgD polyclonal (Novocastra, Newcastle upon Tyne, UK), and SP4 (Cyclin D1, Lab Vision, Fremont, CA, USA). The primary antibodies were replaced with mouse or rabbit serum as a negative control.

Epstein–Barr virus (EBV)-encoded RNA (EBER) was detected by in situ hybridization (ISH). ISH was performed using the BioGenex Automated Staining System (i6000; BioGenex; San Ramon, CA, USA). The paraffin-embedded sections were dewaxed with xylene, treated with proteinase K, and hybridized with a fluorescein-conjugated oligonucleotide EBER probe (PR005-10X, BioGenex). To visualize the bound probe, a Super Sensitive polymer-HRP ISH Detection System (DF300-YCX, BioGenex) was used according to the manufacturer's instructions.

Karyotypes were obtained at the time of diagnosis from all six patients from spleen ($n=5$), and lymph node (LN; $n=1$) samples, as previously described [15]. Chromosomal abnormalities were described according to ISCN [16].

Serum samples were analyzed with an immunofluorescence kit using anti-EBV capsid antigen (VCA), early antigen, and EBV-encoded nuclear antigen (TFB Inc., Tokyo, Japan). Antibodies against the human immunodeficiency virus (HIV) and HTLV-1 were examined using chemiluminescent enzyme immunoassay kits (Abbot Japan and Fuji Rebio Inc., Tokyo, Japan).

We characterized the degree of extramedullary hematopoiesis in the splenic samples as erythropoietic (grade 1), granulopoietic (grade 2), and trilineage hematopoietic (grade 3). Hemophagocytosis of normal splenic histiocytes was characterized as grade 1 (<10) and grade 2 (>10) erythrophagocytes in 10 high power fields. In bone marrow samples, grade 1 indicated thrombophagocytosis and grade 2 indicated leukoerythrophagocytosis.

Results

Clinical features

In this series, five of the six patients were men (age, 64–81 years; median, 69 years). At presentation, all patients were febrile. Four patients (nos. 1, 3–5) had splenomegaly without lymphadenopathy. One patient (no. 2) had localized LN swelling at presentation and a second patient (no. 6) had localized LN swelling at the time of surgery, which suggested the presence of a primary splenic lymphoma. All patients had high levels of lactate dehydrogenase (LDH), soluble interleukin-2 receptor, hypoalbuminemia, and moderately elevated C-reactive protein (Table 1). Differential blood counts revealed the following: Marked lymphocytopenia was detected in all patients except 1 (no. 5), thrombocytopenia was detected in five patients (nos. 1–5), and anemia was detected in four patients (nos. 2, 4–6). In two patients (nos. 1 and 4), lymphoma cells were detected in the peripheral blood (Table 2). Cholestasis and hepatocellular damage with hepatomegaly was observed in four patients (nos. 1, 2, 5, and 6), suggesting hepatic involvement.

Characteristic clinical features of DLBCLRP (Table 2) included BM involvement in four of the five patients (nos. 1, 2, 5, and 6; determined at admission), and hepatic

Table 1 Laboratory data, clinical stage, and international prognostic index upon admission

	Patient 1	Patient 2	Patient 3	Patient 4	Patient 5	Patient 6
Age (years)/sex	75 M	68 M	70 M	81 M	64 F	65 M
White blood cell count, $\times 10^9$/L	2.4	3.9	7.6	7.4	2.3	2.9
Neutrophils, $\times 0^9$/L	1.8	3.3	6.6	4.4	0.9	2.2
Lymphocytes, $\times 10^9$/L	0.4	0.2	0.4	0.7	1.1	0.5
Hemoglobin level, g/L	140	116	133	100	87	91
Platelet count, $\times 10^9$/L	40	83	99	116	38	137
LDH	1,045	4,312	1,822	2,690	460	404
ALP	842	1,677	228	193	2,102	1,168
γ-GTP	489	374	120	26	191	153
LAP	131	225		80	161	138
AST	217	380	55	67	51	49
ALT	34	211	37	11	36	58
CRP	165	122	105	93	58	25
TP	56	53	65	56	60	49
Albumin	27	26	30	29	28	25
sIL-2R	4,050	5,060	5,250	7,790	19,500	15,800
Ferritin	847	na	710	na	276	2,110
Hemophagocytosis in BM[a]	+	+	+	na	+	++
Clinical stage	4B	4B	4B	4B	4B	4B
IPI	H	H	H	H	H	H

Abbreviation and normal level (in parentheses): *M* male, *F* female, *ALP* alkaline phosphatase (130–350 in cases 1, 4, 5, and 6; 66–220 in cases 2 and 3), *LDH* lactate dehydrogenase (80–200 in cases 1, 4, 5, and 6; 255–434 in cases 2 and 3), *LAP* leucin aminopeptidase (M 11–64, F 8–45), *AST* aspirate aminotransferase (0–31), *ALT* alanine aminotransferase (0–41), *CRP* C-reactive protein (less 3 mg/L), *sIL-2R* soluble interleukin-2 receptor (220–530 U/mL), *TP* total protein (67–83 g/L), albumin (38–53 g/L), ferritin (M 27–320, F 3.4–89 ng/mL), *BM* bone marrow, *na* not available, *IPI* international prognostic index, *H* high risk

[a] Grading of hemophagocytosis of normal histiocytes in bone marrow as grade + and ++ indicating thrombophagocytosis and leukoerythrophagocytosis

infiltration in four patients (nos. 1, 5, and 6, and no. 2 determined at biopsy and necropsy, respectively). Enlarged LN were rare and limited to localized areas. Systemic lymphadenopathy was not observed even during the terminal stage of the disease. Hemophagocytosis by normal histiocytes was observed in the spleen and BM of all six patients.

We assessed two treatment groups: (a) three patients (nos. 2–4) were treated with six courses of CHOP (combination of doxorubicin, vincristine, cyclophosphamide, and prednisolone), and (b) the remaining three patients (nos. 1, 5, and 6) were treated with six courses of rituximab and CHOP followed by two courses of rituximab, etoposide, and nimustine hydrochloride with intrathecal administration of methotrexate, Ara-C, and prednisolone for prophylaxis of central nervous system lymphoma.

Follow-up (1–75 months; median, 38 months) information was obtained for all six patients. Two patients (nos. 4 and 2) of

Table 2 Clinicopathological features of cases with primary splenic LBC lymphoma diffusely infiltrating the red pulp

			Spleen	Red pulp		HPC[a]	EMH[b]	BM	ISI	II	Liver	ISI	Portal	Lymph node		Blood
			Weight	Cord	Sinus									Splenic H	Syst	
Patient 1	75	M	525	+	+	++	+++	+	+	+	+	+	+	−	−	8%
Patient 2	68	M	na	+[c]	+[c]	+	+	+	−	+	+[c]	+[c]	+[c]	na	Inguinal	−
Patient 3	70	M	900	+	+	++	+	−	−	−	na	na	na	+	−	−
Patient 4	81	M	546	+	+	+	+	nd	na	na	na	na	na	−	−	16%
Patient 5	64	F	675	+	+	+	+++	+	−	+	+	+	+	+	−	−
Patient 6	65	M	220	+	+	+	+	+	−	+	+	+	+	−	Abdominal	−

ISI intrasinusoidal infiltration, *II* interstitial infiltration, *HPC* hemophagocytosis, *EMH* extramedullary hematopoiesis

[a] Grading of hemophagocytosis of normal histiocytes in spleens as + and ++ indicating less than ten and more than ten erythrophagocytes in 10 high power fields

[b] Grading of extramedullary hematopoiesis in spleens as +, ++, and +++ indicating erythropoiesis, granulopoiesis, and trilineage hematopoiesis, respectively

[c] Necropsy

the former group died of lymphoma, within 1 and 5 months of the onset of the disease, respectively. All three patients of the latter group survived following first complete remission.

All patients were negative for HIV and HTLV-1. Antibodies to EBV indicated an old infection. M-protein and autoantibodies, including Coombs' test, were not detected in any of the patients.

Pathologic features

Spleen size and weight were abnormally high in all informative cases (nos. 1, 3, 4, 5, and 6). In one patient (no. 2), spleen weight was not available (Table 2). The weight of the spleen, which is 80 to 120 g in healthy Japanese adults, was 220 to 900 g (median, 546 g) in the patients. Cut surfaces of the spleens showed beef red color and a lack of mass formation. In all six patients, the splenic red pulp was expanded and diffusely infiltrated by non-cohesive large lymphoma cells (nos. 1, 3, 4, 5, and 6 before therapy, and no. 2 at necropsy). Lymphoma cells were present in the cord and had infiltrated the sinuses to various degrees (Fig. 1a–c). In one patient (no. 5), a small number of large lymphoma cells were scattered among numerous T cells/histiocytes, and the patient was diagnosed with T-cell/histiocyte-rich B-cell lymphoma. All patients had extramedullary hematopoiesis of erythroblasts. Trilineage extramedullary hematopoiesis was observed in two patients (nos. 1 and 5). In all six patients, there were an abnormally high number of histiocytes, which were engaged in hemophagocytosis. In two (nos. 1 and 3) of these patients, there was intensive hemophagocytosis.

In one patient (no. 1), CD20 and CD34 immunohistochemistry revealed large lymphoma cells that were visible in the sinusoids and a few were present in the cords (Fig. 2a,b). In the remaining patients, the lymphoma cells had diffusely infiltrated the interstitial spaces (Fig. 2e). It is possible that the intravascular lymphomatous infiltration of this lymphoma disappeared due to the destruction of endothelial cells by lymphoma cells in the significantly infiltrated lesions. Thrombophagocytosis in the BM was observed in all patients, and leukoerythrophagocytosis was detected in one of the five patients examined (no. 6).

In four patients examined (nos. 1, 5, and 6 at biopsy, and no. 2 at necropsy), lymphoma cells had infiltrated into the sinusoidal and portal areas of the liver (Fig. 2c).

In one patient (no. 2), the lymph nodes were replaced completely by lymphoma cells. Intravascular infiltration of lymphoma cells was not visible in the HE-stained samples. However, diffuse infiltration into the vascular spaces was clearly detected by immunostaining for CD34 (Fig. 2d). Furthermore, in one patient (no. 4), intravascular infiltration of lymphoma cells was prominent in the adipose tissue of the splenic hilus (Fig. 2f), and in another patient (no. 1) infiltration into the subcutaneous vessels was observed. In three patients (nos. 2–4), lymphoma cells had infiltrated below the endothelial cells or into the vascular wall (Fig. 1d).

Immunohistochemistry of lymphoma cells

All patients had lymphoma cells positive for CD20 and Bcl-2 and negative for EBER, Cyclin D1, and CD23 (Table 3). The cells in two patients (nos. 3 and 6) were positive for CD10. Of the remaining four patients with CD10-negative lymphoma cells, the cells were negative for bcl-6 in three patients (nos.1, 4, and 5), and positive for bcl-6 and MUM1 in one patient (no. 2). CD5-positive cells were found in four of five patients by flow cytometry and three of five patients by immunohistochemistry. Cells of five patients examined were positive for surface membrane (sm) IgM and negative for smIgD (Table 3). Positive rate of Ki67 varied from 10% to 80%.

Chromosomal analysis

Chromosomes were analyzed in all six patients. Two patients (nos. 5 and 6) had normal karyotypes. The remaining four patients (nos. 1–4) were CD5-positive and carried complex chromosomal aberrations. One of these patients (no. 4) showed the 11q13 aberrations, whereas another (no. 2) showed the 3q27 abnormality (Table 4).

Discussion

Here, we have reported six cases of DLBCLRP. To further clarify the clinicopathological characteristics of DLBCLRP, we analyzed a total of 24 cases (Tables 5 and 6) of DLBCLRP, including six cases encountered by one of the authors (M. Kashimura). In the present series, 18 of the 24 patients were men and the age range of all the patients was 40–81 years (median, 64.5 years).

The size and weight of the spleens that were examined had increased in all informative cases. Spleen weight data were not available for five of the 24 patients. The weight of the spleen, which is 80–120 g and 110–170 g in healthy adults of Japan and western countries, respectively, was 220 to 2,600 g (median, 1,300 g) in the present cases.

We found that DLBCLRP has seven characteristic clinicopathological features as shown in Table 7 and a pattern of infiltration of the spleen. Lymphoma cells were present in the cord in all but one case of the 24 cases of splenic infiltration. In the remaining patient, the lymphoma cells were restricted to the sinusoids [7].

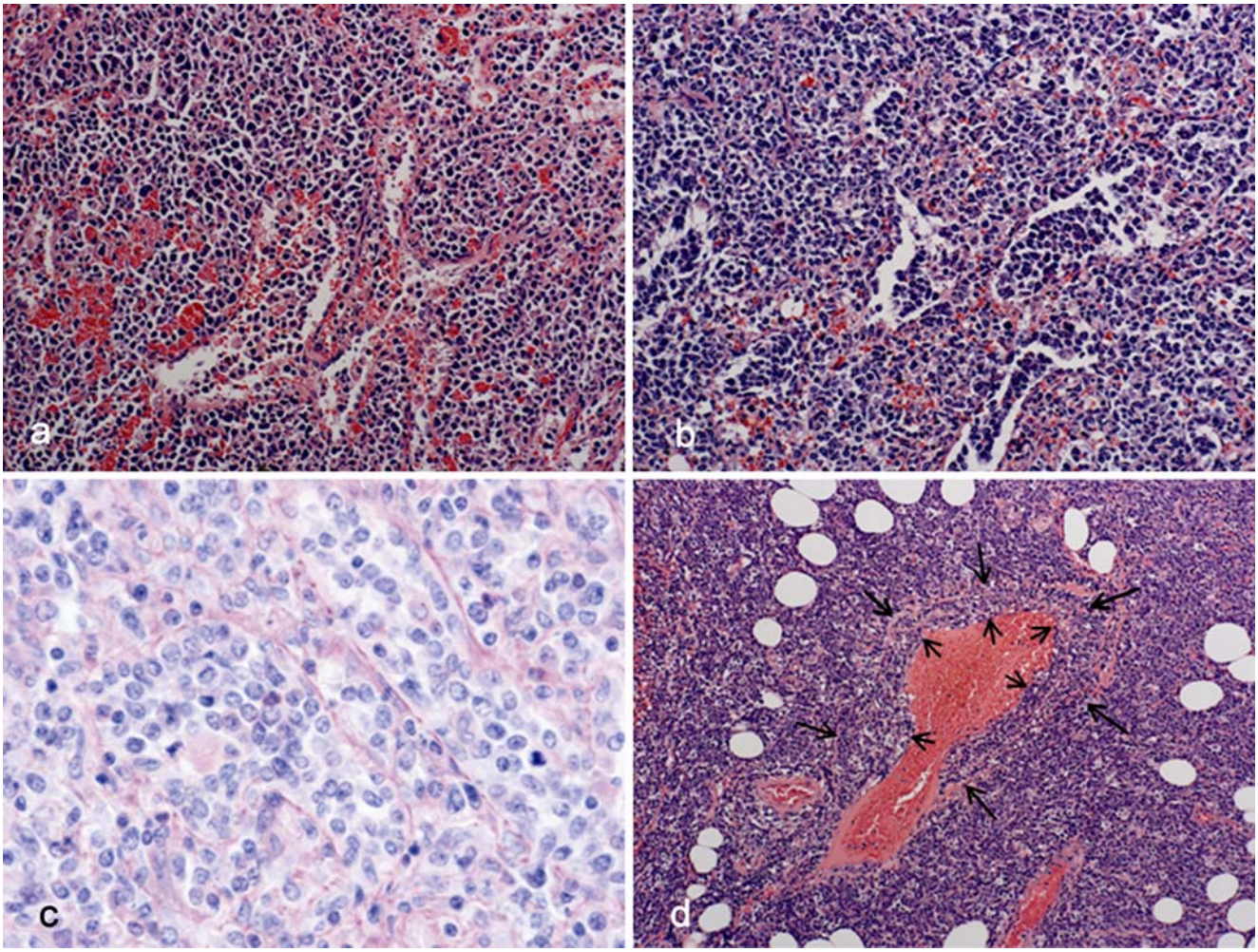

Fig. 1 Lymphoma cells infiltrate the Billroth's cords and sinuses of the splenic red pulp and the vascular wall. **a** Medium power field of the affected spleen. The tumor cells have diffusely infiltrated the Billroth's cords of red pulp, case 3 HE staining. Original magnification, ×100. **b** Medium power field of the affected spleen. Tumor cells have diffusely infiltrated the Billroth's cords as well as the sinusoid, case 4 HE staining. Original magnification, ×100. **c** High power magnification of PAS-stained sections showing the basement membrane of the sinusoid. Note the intrasinusoidal and extrasinusoidal lymphoma cell infiltrations, case 1. Original magnification, ×350. **d** Monomorphous lymphoma cell infiltration in the vascular wall. *Short arrows* indicate the vascular endothelial cells and *long arrows* indicate the arterial adventitia. Case 3 HE staining. Original magnification, ×40

At presentation, lymphoma cells were frequently found in the BM (13/20, 65%) and the liver (11/17, 65%). However, LN involvement was rare and limited to a localized area (10/21, 48%), and LN swelling was not significant. Systemic LN swelling was not observed, even during the terminal phase of the disease.

Another characteristic of DLBCLRP is an intrasinusoidal infiltration of lymphoma cells in the BM (3/7, 43%) and the liver (8/8, 100%) as well as interstitial infiltration of lymphoma cells in the BM (10/11, 91%) and the liver (7/8, 88%). Furthermore, we observed intravascular infiltration of lymphoma cells in the LN (no. 2) and the adipose tissue (nos. 1 and 4), and the presence of lymphoma cells in the peripheral blood (10/23, 43%). This rate appears higher than that observed for nodal DLBCL.

Moreover, we observed lymphoma cell surface expression of the CD5 antigen in eight of the ten patients (80%) [8, 10, 12], including four of our original six patients. Low intensity of the lymphoma cell CD5 antigen might not be detectable by immunohistochemistry (Tables 3 and 6).

None of the patients had a history of chronic lymphocytic leukemia. Transformation of splenic marginal zone lymphoma (SMZL) into DLBCL [17, 18], which might be associated with CD5-positive transformation, must be ruled out in order to diagnose DLBCLRP as the de novo DLBCL. Despite a careful study, we were unable to find proliferative lesions of medium-sized lymphoma cells in any of our cases, which is usually observed when DLBCL transforms from SMZL. Lymphoma cells of all five patients examined were positive for smIgM; however, they were

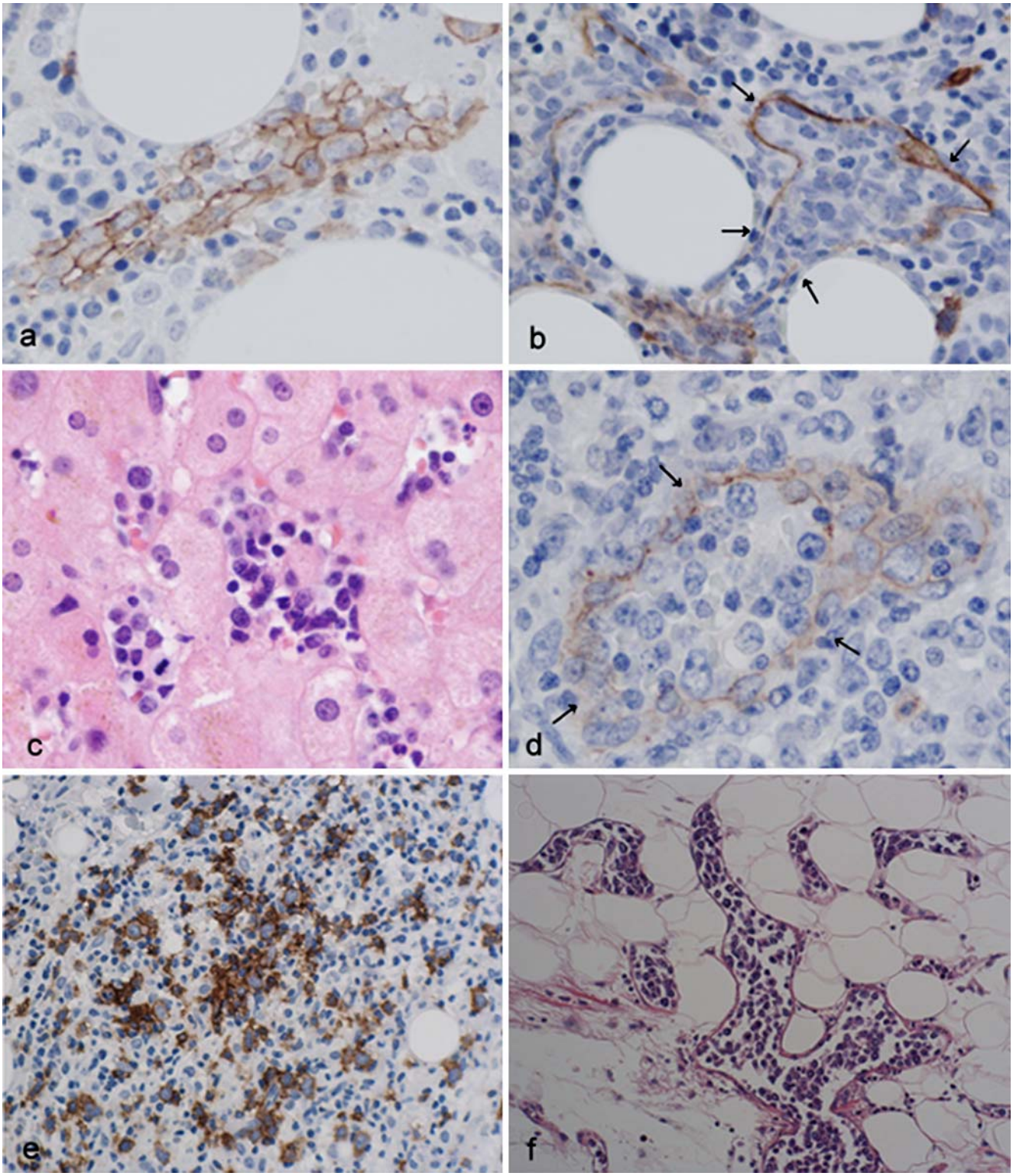

Fig. 2 Intrasinusoidal/intravascular lymphoma cell infiltration in the bone marrow, liver, lymph node, and adipose tissue. **a** CD20 immunostaining showing the predominantly intrasinusoidal pattern of marrow infiltration by large B-cell lymphoma, case 1. Original magnification, ×450. **b** CD34 immunoperoxidase staining of bone marrow sinusoidal cell lining (*arrow*). Large lymphoma cells are present in a sinus, case 1. Original magnification, ×350. **c** High power field of affected liver. Note an intrasinusoidal infiltration of large lymphoma cells, case 1 HE staining. Original magnification, ×350. **d** CD34 immunoperoxidase staining highlights the intravascular lymphoma cells from diffuse lymphomatous infiltration of lymph node parenchyma. *Arrows* show sinusoidal cell lining, case 2. Original magnification, ×400. **e** Medium power field of the affected BM. The tumor cells diffusely infiltrated in the cords of BM, case 6. Original magnification, ×100. **f** Perisplenic adipose tissue. Note the intravascular infiltrate of large lymphoma cells, case 4 HE staining. Original magnification, ×150

Table 3 Immunophenotype of primary splenic LBC lymphoma diffusely infiltrating the red pulp

	CD20	CD5: FCM	CD5: IHC	CD10	Cyclin D1	bcl-2	CD23	MUM1	Ki67 (%)	bcl-6	EBER-ISH	smIg FCM	IgM IHC	IgD IHC
Patient 1	+	+	Weak+	−	−	+	−	−	20	−	−	M-κ	+	−
Patient 2	+	+	+	−	−	+	−	+	20	+	−	κ	na	na
Patient 3	+	+	−	+	−	+	−	+	30	−	−	λ	+	−
Patient 4	+	+	+	−	−	+	−	−	10	−	−	M-λ	+	−
Patient 5	+	na	−	−	−	+	−	−	80	−	−	na	+	−
Patient 6	+	−	−	+	−	+	−	−	20	+	−	na	+	−

FCM flow cytometry, *IHC* immunohistochemistry, *ISH* in situ hybridization, *smIg* surface membrane immunoglobulin

negative for smIgD, which is unusual for SMZL cells [19, 20]. Although four of the six patients (nos. 1–4) showed complex chromosomal aberrations, none of them had trisomy 3 or allelic loss of 7q21-32, which is usually observed with SMZL [21, 22]. Clinically, autoimmune phenomena and the presence of M-protein have been frequently observed in SMZL patients [17, 20, 23–25], but these were not observed in our cases. Therefore, our cases are not likely to be associated with SMZL transformation.

Therefore, these four patients (nos. 1–4) were diagnosed with de novo CD5-positive DLBCL [26]. Two of these patients with complex chromosomal aberration had chromosome abnormalities involving 3q27 (no. 2) and 11q13 (no. 4), which have been previously reported in CD5-positive DLBCL [27]. Yamagichi et al. [28] recently reported four morphological variants of de novo CD5-positive DLBCL. Using the molecular classification system by Hans et al. [29], lymphoma cells of 82% of the patients were of the non-germinal center B-cell type and the others were germinal center B-cell type. Interestingly, intravascular and/or intrasinusoidal lymphomatous infiltration was observed in 38% of the cells. Although data were not shown, the bone marrow, liver, and spleen were reported to be the most frequently involved anatomical sites. De novo CD5-positive DLBCL is heterogeneous in morphological, molecular, and clinical aspects. A potion of the cases with de novo CD5-positive DLBCL with splenomegaly may be DLBCLRP. While lymphoma cells of two other patients (nos. 5 and 6) in this study were CD5 negative, clinicopathological features other than CD5 were identical in these six patients (Table 7).

This high rate of CD5-positive lymphoma cells may be an aberrant expression of the aggressive lymphoma cells [30–32]. In previous genetic studies, it was suggested that de novo CD5-positive DLBCL originates from somatically mutated CD5 progenitor B cells [33, 34]. The mechanism of expression of CD5 in this lymphoma remains unsolved.

The lymphoma cells positive for CD10 in two patients (nos. 3 and 6) were considered germinal center B-cell type. Of the remaining four patients that were negative for CD10, three were negative for bcl-6 (nos. 1, 4, and 5) and one was positive for bcl-6 and MUM1 (no. 2). Therefore, later these were considered non-germinal center B-cell type (Table 3) [29]. Clinicopathological features were not clearly distinguishable among patients with germinal center B-cell-like DLBCL and those with non-germinal center B-cell-type DLBCL, except for the appearance of the lymphoma cells in the peripheral blood. However, our limited sample size makes it difficult to regard this feature as significant.

Table 4 Chromosomal analysis of DLBCLRP

Patient 1	47, XY, der(1)del(1)(p?)dup(1)(q25q32), add(6)(q21), der(9)add(9)(p13)add(9)(q34), add(10)(q26),+16,−19,+r	20/20
Patient 2	44, XY, t(3;14)(q27;q32),−4, add(5)(p11),−9, −10,add(12)(p13),−13,−15, add(18)(p11), add(21)(p11), +der(?)t(?;13)(?;q12), der(?)t(?;15)(?;q11); +mar	5/20
	46, XY	15/20
Patient 3	48,X, −Y, add(2)(p23), del(6)(q?), +add(7)(q11), add(7)(q22)x2, +11, +add(18)(q21)	20/20
Patient 4	46, X, -Y, der(2)add(2)(p13)t(2;11)(q37;q13),add(4)(q35),del(6)(q?), add(8)(p11), add(11)(q13), +18	4/4
Patient 5	46,XX	20/20
Patient 6	46,XY, inv(9)(p12q13)	20/20

Table 5 Summary of the clinical findings DLBCLRP including our cases [4–13]

Age distribution (years)	40–81 (median 64.5)
Male/female	18:6
B symptom	14/15 (93%)
Weight of the spleen (g) (19 cases)	220–2,600 (median 1,300)
Appearance of tumor cells in peripheral blood	10/23 (43%)
Bone marrow involvement	13/20 (65%)
Liver involvement	11/17 (65%)
Lymph node involvement	
Splenic hilus	5/16 (31%)
Abdominal	6/21 (29%)
Other	4/21 (19%)
Systemic lymph node involvement	0/21 (0%)

Table 7 Clinicopathological characteristics of DLBCLRP

Lymphoma cells infiltrate diffusely and non-cohesively in the cords of splenic red pulp
Lymphoma cells frequently involve the bone marrow and the liver at presentation
Lymph node involvement is rare and limited to the local area, and lymph node swelling is not significant. Systemic lymph node swelling is not observed even in the terminal phase of the disease.
Intrasinusoidal as well as interstitial lymphomatous infiltration is observed in involved tissues
Lymphoma cells are often found in the peripheral blood
Lymphoma cells frequently express surface CD5 antigen
Hemophagocytosis of normal histiocytes is observed in the bone marrow and the splenic red pulp

DLBCLRP is a clinically highly aggressive lymphoma compared with conventional CD5-negative DLBCL and de novo CD5-positive DLBCL. The patients with de novo CD5-positive DLBCL showed more aggressive clinical features and parameters (LDH level, clinical stage, and international prognostic index (IPI) score) than those with CD5-negative DLBCL [26]. All six patients in this study had fever, high LDH levels, clinical stage 4B, and a high-risk IPI score.

Another characteristic feature of DLBCLRP is hemophagocytosis of normal histiocytes observed in all the BMs (intensive cases; 1/5, 20%) and spleens (intensive cases; 2/6, 33%). This might be due to the high cytokine concentrations produced by these aggressive lymphoma cells [35]. But none fulfilled the criteria for adult hemophagocytic syndrome [36–38]. Moreover, the frequent presence of B symptoms (14/15) was a characteristic of DLBCLRP. On the basis of these clinicopathological features, we propose that DLBCLRP is a distinct clinicopathological entity.

Table 6 Summary of pathological and phenotypic findings [4–13]

Pattern of splenic infiltration	
Splenic sinus	14/19 (74%)
Splenic cord	23/24 (96%)
Pattern of liver infiltration	
Intrasinusoidal	8/8 (100%)
Portal area	7/8 (88%)
Pattern of bone marrow infiltration	
Intrasinusoidal	3/7 (43%)
Interstitial	10/11 (91%)
Hemophagocytosis in spleen	11/12 (92%)
Hemophagocytosis in bone marrow	4/5 (80%)
Extramedullary hematopoiesis in spleen	7/10 (70%)
Tumor cell phenotype	
B-cell marker 24/24	24/24 (100%)
CD5 (FCM)	8/10 (80%)
CD5 (IHC)	3/12 (25%)
CD10 (IHC)	4/14 (29%)

The clinicopathological features of the cases of the Asian variant of IVL (AIVL) with splenomegaly are similar to those of DLBCLRP. Splenectomy samples from two patients with AIVL had cut surfaces that were beef red in color and there was a diffuse, large, B-cell lymphoma cell infiltrate in the red pulp [14]. However, the international consensus meeting of intravascular large B-cell lymphoma (IVLBCL) proposed a new definition of IVLBCL, which included cases from both western and Asian countries [39]. They added the criterion of a concomitant minimal extravascular location of the neoplastic cells [40] to the WHO criteria, which states that the neoplastic lymphocytes might only be present in the lumina of the small vessels, such as capillaries [41]. DLBCLRP produced interstitial infiltration as well as intrasinusoidal lymphomatous infiltration in the BM, liver, and LN (Fig. 2d and Table 5). The infiltration of DLBCLRP lymphoma cells into the liver and BM was a more characteristic feature of the SMZL than AIVL. However, further studies are required to clarify these relationships.

Briefly, DLBCLRP is an aggressive lymphoma with B symptoms. During the early phase, it spreads to the liver and/or BM via intrasinusoidal and/or interstitial infiltration. Because our characterization of DLBCLRP was based on the observations of a limited number of patients, further studies are required to confirm that DLBCLRP is a distinct clinicopathologic entity.

Conflict of interest statement The authors declare no competing financial interests.

References

1. Mann RB (1999) Are there site-specific differences among extranodal aggressive B-cell neoplasms? Am J Clin Pathol 111:S144–S150
2. Harris NL, Aisenberg AC, Meyer JE et al (1984) Diffuse large cell (histiocytic) lymphoma of the spleen. Clinical and pathologic characteristics of ten cases. Cancer 54:2460–2467
3. Burke JS (1981) Surgical pathology of the spleen: an approach to the differential diagnosis of splenic lymphomas and leukemias. Part II. Diseases of the red pulp. Am J Surg Pathol 5:681–694
4. Kuratsune H, Machii T, Aozasa K et al (1988) B cell lymphoma showing clinicopathological features of malignant histiocytosis. Acta Haematol 79:94–98
5. Betman HF, Vardiman JW, Lau J (1994) T-cell-rich B-cell lymphoma of the spleen. Am J Surg Pathol 18:323–324
6. Faravelli A, Gambini S, Perego D et al (1995) Splenic lymphoma: unusual case with exclusive red pulp involvement. Pathologica 87:692–695
7. Kobrich U, Falk S, Karhoff M et al (1992) Primary large cell lymphoma of the splenic sinuses: a variant of angiotrophic B-cell lymphoma (neoplatic angioendotheliomatosis)? Hum Pathol 2:1184–1187
8. Kroft SH, Howard MS, Picker LJ et al (2000) De novo CD5+ diffuse large B-cell lymphomas. A heterogeneous group containing an unusual form of splenic lymphoma. Am J Clin Pathol 114:523–533
9. Mollejo M, Algara P, Mateo MS et al (2003) Large B-cell lymphoma presenting in the spleen: identification of different clinicopathologic conditions. Am J Surg Pathol 27:895–902
10. Morice WG, Rodriguez FJ, Hoyer JD et al (2005) Diffuse large B-cell lymphoma with distinctive patterns of splenic and bone marrow involvement: clinicopathologic features of two cases. Mod Pathol 18:495–502
11. Palutke M, Eisenberg L, Narang S et al (1988) B lymphocytic lymphoma (large cell) of possible splenic marginal zone origin presenting with prominent splenomegaly and unusual cordal red pulp distribution. Cancer 62:593–600
12. Salgado C, Feliu E, Montserrat E et al (1993) B-type large-cell primary splenic lymphoma with massive involvement of the red pulp. Acta Haematol 89:46–49
13. Stroup RM, Burke JS, Sheibani K et al (1992) Splenic involvement by aggressive malignant lymphomas of B-cell and T-cell types. A morphologic and immunophenotypic study. Cancer 69:413–420
14. Murase T, Nakamura S, Tashiro K et al (1997) Malignant histiocytosis-like B-cell lymphoma, a distinct pathologic variant of intravascular lymphomatosis: a report of five cases and review of the literature. Br J Haematol 99:656–664
15. Hashimoto K, Miura I, Chyubachi A et al (1995) Correlations of chromosome abnormalities with histologic and immunologic characteristics in 49 patients from Akita, Japan with non-Hodgkin lymphoma. Cancer Genet Cytogenet 81:56–65
16. Mitelman F (ed) ISCN (1995). An international system for human cytogenetic nomenclature. Karger, Basel
17. Berger F, Felman P, Thieblemont C et al (2000) Non-MALT marginal zone B-cell lymphomas: a description of clinical presentation and outcome in 124 patients. Blood 95:1950–1956
18. Camacho FI, Mollejo M, Mateo MS et al (2001) Progression to large B-cell lymphoma in splenic marginal zone lymphoma: a description of a series of 12 cases. Am J Surg Pathol 25:1268–1276
19. Mollejo M, Menárguez J, Lloret E, Sánchez A, Campo E, Algara P, Cristóbal E, Sánchez E, Piris MA (1995) Splenic marginal zone lymphoma: a distinctive type of low-grade B-cell lymphoma. A clinicopathological study of 13 cases. Am J Surg Pathol 19:1146–1157
20. Van Huyen JP, Molina T, Delmer A et al (2000) Splenic marginal zone lymphoma with or without plasmacytic differentiation. Am J Surg Pathol 24:1581–1592
21. Dierlamm J, Michaux L, Wlodarska I et al (1996) Trisomy 3 in marginal zone B-cell lymphoma: a study based on cytogenetic analysis and fluorescence in situ hybridization. Br J Haematol 93:242–249
22. Mateo M, Mollejo M, Villuendas R et al (1999) 7q31-32 allelic loss is a frequent finding in splenic marginal zone lymphoma. Am J Pathol 154:1583–1589
23. Chacón JI, Mollejo M, Muñoz E et al (2002) Splenic marginal zone lymphoma: clinical characteristics and prognostic factors in a series of 60 patients. Blood 100:1648–1654
24. Franco V, Florena AM, Iannitto E (2003) Splenic marginal zone lymphoma. Blood 101:2464–2472
25. Iannitto E, Ambrosetti A, Ammatuna E et al (2004) Splenic marginal zone lymphoma with or without villous lymphocytes. Hematologic findings and outcomes in a series of 57 patients. Cancer 101:2050–2057
26. Yamaguchi M, Seto M, Okamoto M et al (2002) De novo CD5+ diffuse large B-cell lymphoma: a clinicopathologic study of 109 patients. Blood 99:815–821
27. Yoshioka T, Miura I, Kume M et al (2005) Cytogenetic features of de novo CD5-positive diffuse large B-cell lymphoma: chromosome aberrations affecting 8p21 and 11q13 constitute major subgroups with different overall survival. Genes Chromosomes Cancer 42:149–157
28. Yamaguchi M, Nakamura N, Suzuki R et al (2008) De novo CD5+ diffuse large B-cell lymphoma: results of a detailed clinicopathological review in 120 patients. Haematologica 93(8):1195–1202
29. Hans CP, Weisenburger DD, Greiner TC et al (2004) Confirmation of the molecular classification of diffuse large B-cell lymphoma by immunohistochemistry using a tissue microarray. Blood 103:275–282
30. Ballesteros E, Osborne BM, Matsushima AY (1998) CD5+ low-grade marginal zone B-cell lymphomas with localized presentation. Am J Surg Pathol 22:201–207
31. Ferry JA, Yang WI, Zukerberg LR et al (1996) CD5+ extranodal marginal zone B-cell (MALT) lymphoma. A low grade neoplasm with a propensity for bone marrow involvement and relapse.. Am J Clin Pathol 105:31–37
32. Tiesinga JJ, Wu CD, Inghirami C (2000) CD5+ follicle center lymphoma. immunophenotyping detects a unique subset of "floral" follicular lymphoma. Am J Clin Pathol 114:912–921
33. Katzenberger T, Lohr A, Schwarz S et al (2003) Genetic analysis of de novo CD5+ diffuse large B-cell lymphomas suggests an origin from a somatically mutated CD5+ progenitor B cell. Blood 101:699–702
34. Nakamura N, Hashimoto Y, Kuze T et al (1999) Analysis of the immunoglobulin heavy chain gene variable region of CD5-positive diffuse large B-cell lymphoma. Lab Invest 79:925–933
35. Imashuku S (1997) Differential diagnosis of hemophagocytic syndrome: underlying disorders and selection of the most effective treatment. Int J Hematol 66:135–151
36. Tsuda H (1997) Hemophagocytic syndrome in children and adults. Int J Hematol 65:215–226
37. Wong KF, Chan JK (1992) Reactive hemophagocytic syndrome—a clinicopathologic study of 40 patients in an Oriental population. Am J Med 93:177–180
38. Yao M, Cheng AL, Su IJ et al (1994) Clinicopathological spectrum of hemophagocytic syndrome in Epstein–Barr virus associated peripheral T-cell lymphoma. Br J Haematol 87:535–543
39. Ponzoni M, Ferreri AJ, Campo E et al (2007) Definition, diagnosis, and management of intravascular large B-cell lymphoma: proposals and perspectives from an international consensus meeting. J Clin Oncol 25:3168–3173
40. Ponzoni M, Arrigoni G, Gould VE et al (2000) Lack of CD 29 (beta1 integrin) and CD 54 (ICAM-1) adhesion molecules in intravascular lymphomatosis. Hum Pathol 31:220–226
41. Gatter KC, Warnke RA (2001) Intravascular large B-cell lymphoma. In: Jaffe ES, Harris NL, Stein H, Vardiman JW (eds) Tumors of haematopoietic and lymphoid tissues. IARC, Lyon

Virchows Arch (2008) 453:511–519
DOI 10.1007/s00428-008-0668-8

ORIGINAL ARTICLE

Integrin-linked kinase cytoplasmic and nuclear expression in laryngeal carcinomas

Anastasios K. Goulioumis · Vasiliki Bravou · John Varakis · Panos Goumas · Helen Papadaki

Received: 26 May 2008 / Revised: 27 August 2008 / Accepted: 27 August 2008 / Published online: 24 September 2008

Abstract Integrin-linked kinase (ILK) has been implicated in the development and progression of several human malignancies. Previous in vitro studies also implicate ILK in the activation of Akt and β-catenin as well as in the regulation of E-cadherin expression. However, the role of ILK in human laryngeal cancer and its possible in vivo downstream effectors in the disease are currently unknown. We examined by immunohistochemistry the protein expression of ILK, phosphorylated-Akt (p-Akt), E-cadherin, and β-catenin in 97 invasive squamous laryngeal carcinomas. Increased cytoplasmic and nuclear expression of ILK and p-Akt decreased membranous expression of E-cadherin and nuclear accumulation of β-catenin was found in 87.6%, 85.6%, 71.1%, and 43.3% of cases, respectively. Our results suggest that ILK expression may be implicated in human laryngeal carcinoma and its localization in the nucleus possibly proposes novel nuclear functions of this molecule. In addition, enhanced ILK expression correlates with activation of Akt but not with downregulation of E-cadherin and activation of β-catenin. Finally, in our material while activated Akt seems to characterize well-differentiated tumors, loss of E-cadherin and activation of β-catenin correlated with high grade carcinomas.

Keywords ILK · p-Akt · E-cadherin · β-catenin · Laryngeal carcinoma

A. K. Goulioumis · V. Bravou · J. Varakis · H. Papadaki (✉)
Department of Anatomy, School of Medicine,
University of Patras,
Patras 26500, Greece
e-mail: epetrou@upatras.gr

P. Goumas
Otorhinolaryngology–Head and Neck Surgery Department,
School of Medicine, University of Patras,
Patras, Greece

Introduction

Laryngeal carcinoma, classified as squamous cell carcinoma in 90% of the cases, is a common cause of morbidity and mortality worldwide, representing 2.4% of new cancer diagnoses annually in men [1]. As in other malignancies, identification of molecular mechanisms involved in laryngeal cancer progression contributes to the better understanding of its biological behavior and perhaps to the development of novel targeted anticancer therapies.

Integrin-linked kinase (ILK) which is normally located in the focal adhesion plaques is a cytoplasmic serine/threonine kinase implicated in integrin, growth factor, and Wnt signaling pathways [2–6]. ILK is known to have a nodal role in bidirectional cell–extracellular matrix signaling and to regulate several important biological processes such as cell proliferation, survival, cell adhesion, and angiogenesis [5]. Overexpression of ILK has been shown to induce tumor formation in nude mice [6]. Increased expression of ILK has also been reported in many types of tumors including melanoma, colon, prostate, anaplastic thyroid carcinoma, nonsmall cell lung cancer, and head and neck squamous cell carcinomas [5, 7–9]. To the best of our knowledge, there are no reports of ILK expression in human laryngeal carcinoma.

Several in vitro studies have implicated ILK in the regulation of E-cadherin expression as well as in the activation of Akt and β-catenin [3, 4, 10] signaling pathways. It has been well documented that downregulation of E-cadherin and activation of β-catenin, represent key molecular events in the development and progression of several human malignancies including laryngeal cancer [11, 12]. It is also known that the protein kinase Akt is involved in several processes thought to be critical in carcinogenesis, including aberrant cell proliferation, evasion from apoptosis, promotion of angiogenesis, and tumor cell invasiveness [13].

In a series of 97 invasive human laryngeal squamous cell carcinomas, we studied by immunohistochemistry the expression of ILK, phosphorylated-Akt (p-Akt; Ser 473), E-cadherin, and β-catenin and correlated our results with clinicopathological parameters such as tumor grade, stage, and location.

Materials and methods

Tissue specimens

The study was performed in accordance with the institutional ethical guidelines and has been approved by the Committee on Research and Ethics and the Scientific Committee of the University Hospital of Patras, Greece. Formalin-fixed paraffin-embedded tissue samples from 97 primary human invasive squamous laryngeal carcinomas (63 glottic and 34 supraglottic) were obtained from the Department of Pathology, Agios Andreas General Hospital, Patras, Greece. Adjacent nonneoplastic laryngeal tissue was used as control. Two of the patients were women and 95 were men. Ages ranged from 40 to 86 years, with an average age of 60 years. The WHO classification of tumors was used to determine the histological grade: 25/97 tumors (25.8%) were classified as grade I, 40/97 (41.2%) as grade II, and 32/97 (33%) as grade III [14]. Thirty-two out of 97 (33%) tumors were stage I, 26/97 (26.8%) stage II, 17/97 (17.5%) stage III, and 22/97 (22.7%) stage IV A according to tumor–node–metastasis (TNM) staging.

Immunohistochemistry

Immunohistochemistry was performed as previously described [15]. Antigen retrieval was enhanced by microwaving the slides in 0.01 M citrate buffer (pH=6). Primary antibody used were rabbit anti-ILK (Santa Cruz Biotechnology, CA, USA; dilution 1:500), rabbit anti-p-Akt (Ser473; Cell Signaling, Beverly, MA, USA; dilution 1:40), mouse anti-β-catenin (BD Biosciences, CA, USA; dilution 1:2,000), and mouse anti-E-cadherin (BD Biosciences, CA, USA; dilution 1:2,000). The antibody used for detection of p-Akt detects Akt1, Akt2, and Akt3 only when phosphorylated at Ser 473. Bound primary antibodies were detected with the biotin–streptavidin–peroxidase method (Envision detection kit, DAKO, Hamburg, Germany).

Immunohistochemical evaluation

All slides were assessed by one pathologist (H.P.) and one investigator (A.G.) independently and blinded to the case. Cytoplasmic, membranous, and nuclear staining for each protein was evaluated separately. Cytoplasmic staining of ILK, p-Akt, and β-catenin as well as membranous staining of β-catenin was homogenously distributed among tumor cells and it was scored based on the intensity of staining as follows: score 0—negative staining, 1—weak staining, 2—moderate staining, and 3—strong staining. Negative staining corresponds to complete absence of staining, strong corresponds to staining that can be easily recognized with light microscope at magnification (×4), weak corresponds to staining that can be recognized only at magnification (×20), and moderate is the staining with intensity values intermediate of weak and strong. Nuclear expression of ILK, p-Akt, and β-catenin and membranous expression of E-cadherin showed no significant variations in intensity of staining and the following scoring system was applied based on the percentage of positive cells: score 0—staining in less than 10% of tumor cells, 1—staining in 10-40% of tumor cells, score 2—staining in 40–70% of tumor cells, and score 3—staining in more than 70% of tumor cells. Cases with score 0 were considered negative and cases with scores 1, 2, or 3 were considered positive. In case of cytoplasmic β-catenin, increased cytoplasmic expression was defined as score >1 since in adjacent nonneoplastic laryngeal mucosa, expression of cytoplasmic β-catenin had a score 1. In case of membranous β-catenin and membranous E-cadherin, decreased membranous expression was defined as score <3 since adjacent nonneoplastic laryngeal mucosa had a score 3 for membranous localization of both proteins.

Statistical analysis

Statistical analysis was performed with the SPSS for Windows, release 15.0 (SPSS Inc., Chicago, IL, USA). Correlations of protein expression levels with clinicopathological parameters were analyzed with the nonparametric Kruskal–Wallis or Mann–Whitney tests for ordinal data and chi-square test for nominal data. Correlations between expression of proteins (immunohistochemical scores) were evaluated by the Spearman rank-order correlation coefficient. Parametric tests were performed with correction for ties. The significance level was defined as $p<0.05$.

Results

ILK is expressed in laryngeal cancer

Immunohistochemical staining for ILK was performed in 97 tumors and adjacent nonneoplastic laryngeal tissue. In adjacent nonneoplastic laryngeal tissue, none or weak cytoplasmic expression of ILK was detected in epithelial cells in accordance with previous reports of negative/low immunohistochemical staining of ILK in other normal

epithelia (Fig. 1a) [9, 15]. In contrast, 85/97 (87.6%) of laryngeal tumors were positive for ILK. Immunoreactivity for ILK was observed in the cytoplasm and/or the nucleus of cancer cells (Fig. 1b). Cytoplasmic localization of ILK was found in 79/97 (81.4%) carcinomas, while nuclear staining was detected in 56/97 (57.7%) cases with six out of 97 (6.2%) cases presenting sole nuclear staining and 29/97 (29.8%) cases presenting sole cytoplasmic staining. However, there was no statistically significant correlation between cytoplasmic or nuclear ILK expression and tumor grade, TNM stage, nodal metastases, or tumor location (Table 1).

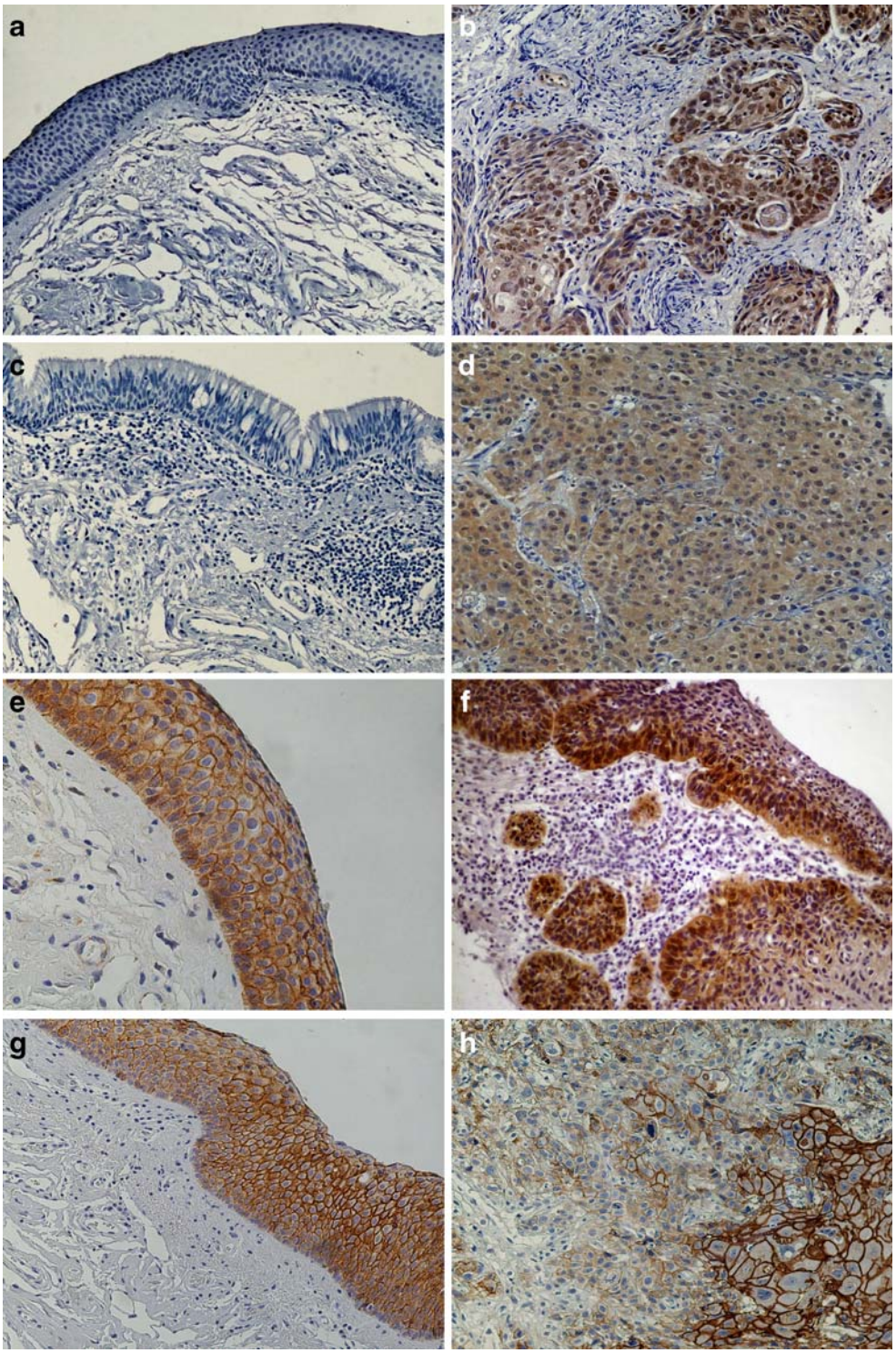

Fig. 1 Adjacent nonneoplastic laryngeal mucosa—negative immunostaining for ILK (**a**) and p-Akt (**c**) and membranous staining of β-catenin (**e**) and E-cadherin (**g**). Laryngeal squamous carcinoma—cytoplasmic and nuclear staining for ILK (**b**), p-Akt (**d**), and β-catenin (**f**) and loss of membranous E-cadherin (**h**) (×200)

Table 1 ILK expression in human laryngeal carcinomas

	Number	Cytoplasmic ILK[a]					Nuclear ILK[a]				
		0 *n* (%)	1 *n* (%)	2 *n* (%)	3 *n* (%)	*p* value[b]	0 *n* (%)	1 *n* (%)	2 *n* (%)	3 *n* (%)	*p* value[b]
Total	97	18 (18.6)	35 (36.1)	21 (21.6)	23 (23.7)		41 (42.3)	20 (20.6)	21 (21.6)	15 (15.5)	
Location						0.680					0.537
Glottic	63	11 (17.5)	26(41.2)	11 (17.5)	15 (23.8)		26 (41.2)	11 (17.5)	16 (25.4)	10 (15.9)	
Supraglottic	34	7 (20.6)	9 (26.5)	10 (29.4)	8 (23.5)		15 (44.1)	9 (26.5)	5 (14.7)	5 (14.7)	
Grade						0.774					0.906
I	25	2 (8)	12 (48)	5 (20)	6 (24)		11 (44)	3 (12)	6 (24)	5 (20)	
II	40	8 (20)	13 (32.5)	9 (22.5)	10 (25)		18 (45)	8 (20)	9 (22.5)	5 (15.5)	
III	32	8 (25)	10 (31.2)	7 (21.9)	7 (21.9)		12 (37.5)	9 (28.1)	6 (18.7)	5 (15.6)	
TNM						0.342					0.455
I	32	2 (6.3)	15 (46.9)	6 (18.8)	9 (28)		14 (43.7)	4 (12.5)	11 (34.4)	3 (9.4)	
II	26	6 (23.1)	11 (42.3)	4 (15.4)	5 (19.2)		10 (38.5)	5 (19.2)	5 (19.2)	6 (32.1)	
III	17	2 (11.8)	5 (29.4)	6 (35.3)	4 (23.5)		6 (35.3)	4 (23.5)	3 (17.6)	4 (23.4)	
IV	22	8 (36.4)	4 (18.2)	5 (22.7)	5 (22.7)		11 (50)	7 (31.8)	2 (9.1)	2 (9.1)	

Correlation with clinicopathological parameters

[a] ILK expression was scored as described in "Materials and methods".

[b] Kruskal–Wallis or Mann–Whitney test; $p<0.005$ was considered statistical significant.

Activation of Akt is higher in well-differentiated laryngeal carcinomas and strongly correlates with ILK expression

ILK has been shown in vitro to phosphorylate Akt at Ser 473 leading to its activation [10, 16]. Increased expression of phosphorylated Akt (ser 473) that is indicative of Akt activation has also been previously reported in human cancer [13, 15, 17]. We therefore examined expression of p-Akt (Ser 473) in our series of laryngeal carcinomas and adjacent nonneoplastic laryngeal tissue. Immunoreactivity for p-Akt in adjacent nonneoplastic laryngeal tissue was either absent or barely detectable consistent with absent/low expression levels observed in other normal epithelia (Fig. 1c) [15, 17]. In contrast, positive p-Akt immunostaining was found in 83/97 (85.6%) carcinomas examined. Immunoreactivity of tumor cells was cytoplasmic and nuclear (Fig. 1d). Cytoplasmic p-Akt was observed in 74/97 (76.3%) carcinomas and nuclear staining was also found in 74/97 (76.3%) cases. Cytoplasmic p-Akt expression significantly correlated with tumor grade with well-differentiated carcinomas showing higher p-Akt expression compared to moderately and poorly differentiated tumors ($p=0.01$; Fig. 2). There was no statistically significant correlation between cytoplasmic or nuclear p-Akt expression and other clinicopathological parameters under evaluation (Table 2). Notably cytoplasmic ILK expression significantly correlated with cytoplasmic p-Akt ($r=0.303$, $p=0.003$) and nuclear ILK correlated with nuclear p-Akt ($r=0.231$, $p=0.023$; Fig. 3). Finally, a marginally significant correlation was found between p-Akt (Ser 473) and E-cadherin expression ($r=0.175$, $p=0.086$), while cytoplasmic p-Akt (Ser 473) expression correlated with membranous β-catenin ($r=0.226$, $p=0.026$).

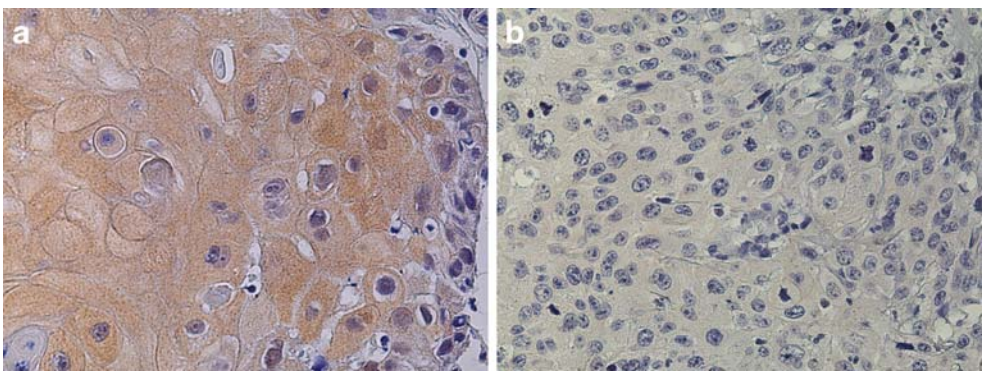

Fig. 2 P-Akt cytoplasmic expression in relation to tumor grade. **a** Low grade tumor showing strong immunoreactivity for p-Akt. **b** Negative p-Akt expression in a high grade tumor (×400)

Table 2 Expression of p-Akt in human laryngeal carcinomas

	Number	Cytoplasmic p-Akt[a]					Nuclear p-Akt[a]				
		0 *n* (%)	1 *n* (%)	2 *n* (%)	3 *n* (%)	*p* value[b]	0 *n* (%)	1 *n* (%)	2 *n* (%)	3 *n* (%)	*p* value[b]
Carcinomas total	97	23 (23.7)	18 (18.5)	25 (25.8)	31 (32)		23 (23.7)	32 (33)	19 (19.6)	23 (23.7)	
Location						0.649					0.122
Glottic	63	15 (23.8)	10 (15.9)	17 (27)	21 (33.3)		17 (27)	21 (33.3)	14 (22.2)	11 (17.5)	
Supraglottic	34	8 (23.5)	8 (23.5)	8 (23.5)	10 (29.5)		6 (17.6)	11 (32.4)	5 (14.7)	12 (35.3)	
Grade						0.01					0.241
I	25	2 (8)	2 (8)	10 (40)	11 (44)		5 (20)	7 (28)	10 (40)	3 (12)	
II	40	8 (20)	9 (22.5)	11 (27.5)	12 (30)		9 (22.5)	12 (30)	8 (20)	11 (27.5)	
III	32	13 (40.6)	7 (21.9)	4 (12.5)	8 (25)		9 (28.1)	13 (40.6)	1 (3.2)	9 (28.1)	
TNM						0.082					0.241
I	32	6 (18.7)	4 (12.5)	10 (31.3)	12 (37.5)		5 (15.6)	11 (34.4)	7 (21.9)	9 (28.1)	
II	26	9 (34.6)	8 (30.8)	4 (15.4)	5 (19.2)		5 (19.2)	11 (42.3)	4 (15.4)	6 (23.1)	
III	17	2 (11.8)	4 (23.5)	3 (17.7)	8 (47)		4 (23.5)	4 (23.5)	4 (23.5)	5 (29.5)	
IV	22	6 (27.3)	2 (9.1)	8 (36.3)	6 (27.3)		9 (40.9)	6 (27.3)	4 (18.2)	3 (13.6)	

Correlation with clinicopathological parameters

[a] p-Akt expression was scored as described in "Materials and methods".

[b] Kruskal–Wallis or Mann–Whitney test; $p<0.005$ was considered statistical significant.

Activation of β-catenin in laryngeal cancer correlates with advancing tumor grade

Immunohistochemical analysis of β-catenin protein expression in 97 laryngeal carcinomas revealed nuclear localization (score >0), cytoplasmic pooling (score >1), and diminished membrane expression (score <3) of β-catenin in 43.3%, 75.3%, and 77.3% of cases, respectively (Fig. 1f). Adjacent nonneoplastic laryngeal tissue showed strong membranous (score 3), weak cytoplasmic (score 1; Fig. 1e), and negative nuclear β-catenin localization (score 0) consistent with the role of β-catenin in adherens junctions in normal epithelial cells [18, 19]. Nuclear localization, cytoplasmic accumulation, and decreased membrane expression of β-catenin were all significantly correlated with advancing tumor grade ($p=0.008$, $p=0.002$,

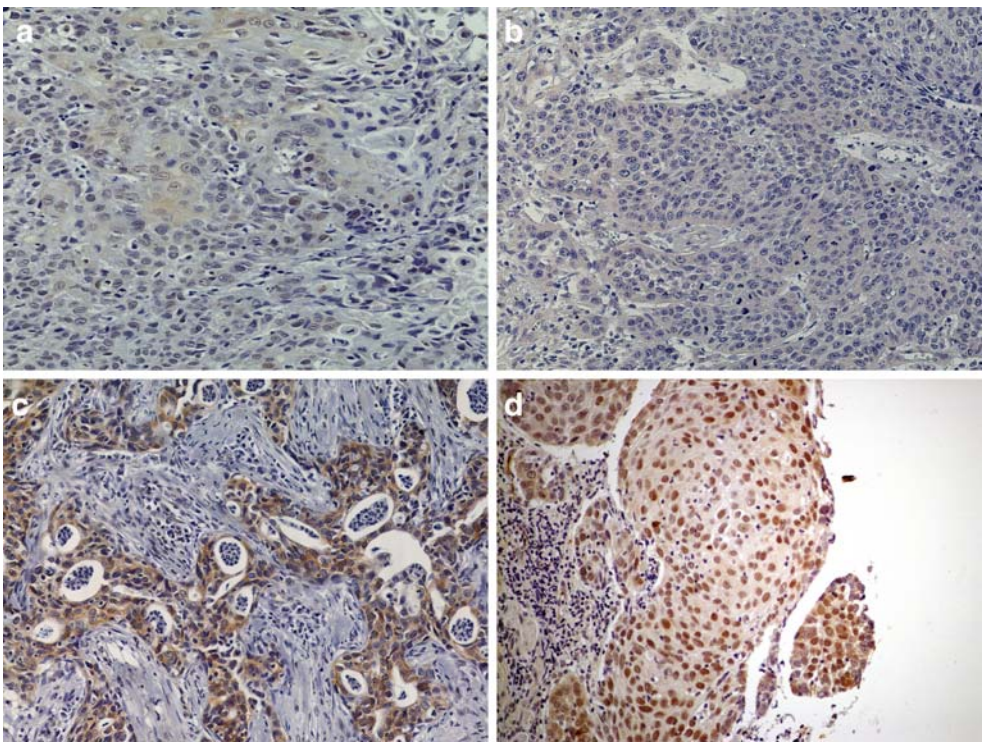

Fig. 3 ILK expression in laryngeal carcinomas correlates with activation of Akt. **a**, **b** Adjacent sections of a tumor showing weak immunoreactivity for ILK (**a**) and p-Akt (**b**). **c**, **d** Adjacent sections of a tumor with strong ILK (**c**) and p-Akt cytoplasmic expression (**d**) (×200)

and $p=0.001$, respectively). The expression of β-catenin did not correlate with other clinicopathological parameters (Table 3). Nuclear β-catenin expression also correlated with cytoplasmic ($r=0.494$, $p<0.001$) and membranous β-catenin ($r=-0.300$, $p=0.003$).

Downregulation of E-cadherin in laryngeal cancer correlates with advancing tumor grade and TNM stage

Expression of E-cadherin was evaluated in 97 laryngeal carcinomas and adjacent nonneoplastic tissue. Normal epithelial cells of adjacent nonneoplastic tissue showed fine membranous staining (score 3) consistent with the role of E-cadherin in adherens junctions in normal epithelia (Fig. 1g) [18, 19]. Reduced expression of E-cadherin (score <3) was detected in 69 of 97 tumors (71.1%) examined (Fig. 1h). Diminished membrane expression of E-cadherin correlated significantly with advancing tumor grade ($p<0.001$) and TNM stage ($p=0.014$), while no correlation with tumor location was observed (Table 4).

Activation of β-catenin in laryngeal carcinomas correlates with loss of E-cadherin but not with ILK expression

In the 97 cases of laryngeal carcinomas examined both nuclear and cytoplasmic localization of β-catenin correlated significantly with downregulation of E-cadherin ($r=0.344$, $p=0.001$, and $r=0.241$, $p=0.017$, respectively). In addition, a strong positive correlation was found between E-cadherin and membranous β-catenin staining ($r=0.353$, $p<0.001$). However, there was no statistically significant correlation of ILK expression with activation of β-catenin or downregulation of E-cadherin.

Discussion

ILK has been implicated in various aspects of the process of carcinogenesis particularly those concerning tumor progression [5]. The recent identification of small molecule ILK inhibitors that show encouraging results in suppression of tumor growth and invasion renders ILK a promising target for novel cancer therapies [5, 7, 9].

Although ILK is normally located in focal adhesions, our study showed none/weak immunohistochemical staining of ILK in adjacent nonneoplastic laryngeal mucosa. This finding has been previously reported in other normal epithelia including tongue, colon, and gastric epithelium [9, 15, 20]. In contrast to adjacent nonneoplastic laryngeal mucosa, we demonstrated overexpression of ILK in laryngeal squamous cell carcinomas. This finding suggests a possible role for ILK in laryngeal carcinoma. However, in contrast to studies in other human malignancies, ILK expression in our material was not correlated with tumor progression parameters such as grade and TNM stage [5].

Importantly, we found that ILK in addition to its cytoplasmic localization, in many instances (57.7%), was localized in the nucleus of laryngeal cancer cells. This finding is interesting since immunohistochemical studies in other human malignancies showed exclusively cytoplasmic expression of ILK [5, 7, 15]. Nuclear localization of ILK has, however, been recently reported in nonsmall cell lung

Table 3 Expression of β-catenin in human laryngeal carcinomas

	Number	Membranous β-catenin[a]					Nuclear β-catenin[a]				
		0 *n* (%)	1 *n* (%)	2 *n* (%)	3 *n* (%)	*p* value[b]	0 *n* (%)	1 *n* (%)	2 *n* (%)	3 *n* (%)	*p* value[b]
Carcinomas total	97	30 (30.9)	30 (30.9)	15 (15.5)	22 (22.7)		55 (56.7)	36 (37.1)	6 (6.2)	0 (0)	
Location						0.025					0.506
Glottic	63	14 (22.2)	21 (33.3)	12 (19.1)	16 (25.4)		37 (58.7)	23 (36.5)	3 (4.8)	0 (0)	
Supraglottic	34	16 (47.1)	9 (26.5)	3 (8.8)	6 (17.6)		18 (53)	13 (38.2)	3 (8.8)	0 (0)	
Grade						0.001					0.008
I	25	6 (24)	4 (16)	4 (16)	11 (44)		20 (80)	4 (16)	1 (4)	0 (0)	
II	40	7 (17.5)	16 (40)	9 (22.5)	8 (20)		23 (57.5)	15 (37.5)	2 (5)	0 (0)	
III	32	17 (53.1)	10 (31.2)	2 (6.3)	3 (9.4)		12 (37.5)	17 (53.1)	3 (9.4)	0 (0)	
TNM stage						0.146					0.654
I	32	7 (21.9)	11 (34.4)	3 (9.3)	11 (34.4)		20 (62.5)	11 (34.4)	1 (3.1)	0 (0)	
II	26	8 (30.8)	11 (42.3)	2 (7.7)	5 (19.2)		12 (46.2)	13 (50)	1 (3.8)	0 (0)	
III	17	4 (23.5)	5 (29.4)	3 (17.7)	5 (29.4)		11 (64.7)	4 (23.5)	2 (11.8)	0 (0)	
IV	22	11 (50)	3 (13.6)	7 (31.8)	1 (4.6)		12 (54.5)	8 (36.4)	2 (9.1)	0 (0)	

Correlation with clinicopathological parameters

[a] β-catenin expression was scored as described in "Materials and methods".

[b] Kruskal–Wallis or Mann–Whitney test; $p<0.005$ was considered statistical significant.

Table 4 E-cadherin expression in human laryngeal carcinomas

	Number	Membranous E-cadherin[a]				
		0 *n* (%)	1 *n* (%)	2 *n* (%)	3 *n* (%)	*p* value[b]
Carcinomas total	97	37 (38.1)	16 (16.5)	16 (16.5)	28 (28.9)	
Location						0.226
Glottic	63	21 (33.3)	10 (15.9)	13 (20.6)	19 (30.2)	
Supraglottic	34	16 (47.1)	6 (17.6)	3 (8.8)	9 (26.5)	
Grade						<0.001
I	25	3 (12)	3 (12)	7 (28)	12 (48)	
II	40	11 (27.5)	8 (20)	7 (17.5)	14 (35)	
III	32	23 (71.9)	5 (15.5)	2 (6.3)	2 (6.3)	
TNM stage						0.014
I	32	10 (31.3)	4 (12.5)	4 (12.5)	14 (43.7)	
II	26	7 (26.9)	8 (30.8)	5 (19.2)	6 (23.1)	
III	17	5 (29.4)	2 (11.8)	4 (23.5)	6 (35.3)	
IV	22	15 (68.2)	2 (9.1)	3 (13.6)	2 (9.1)	

Correlation with clinicopathological parameters

[a] E-cadherin expression was scored as described in "Materials and methods".

[b] Kruskal–Wallis or Mann–Whitney test; $p<0.005$ was considered statistical significant.

cancer, cell lines of esophageal squamous cell carcinoma, and in kidney-derived cell lines (COS-1) [8, 21, 22]. In the later instance, a mechanism involving ILK–caveolin-1 interaction has been suggested [21]. Recently, nuclear localization of ILK has also been reported in breast cancer cell lines and attributed to a mechanism involving activation of PAK-1 [23]. In this study, the presence of ILK nuclear localization was postulated to be implicated in the maintenance of nuclear integrity and also in the regulation of gene expression [23]. Additionally, ILK has been shown to be a member of a tubulin-based multiprotein complex at the centrosome regulating the organization of the mitotic spindle, a finding suggesting significant implications for ILK mitotic role in cancer [24, 25]. Taken together, these data indicate that ILK may exert novel yet unidentified nuclear functions in laryngeal cancer.

We also demonstrated enhanced expression of phosphorylated Akt in laryngeal carcinomas. There was a strong correlation of p-Akt expression with ILK suggesting that in laryngeal carcinomas ILK is probably implicated in the activation of Akt as it has been reported in other human malignancies [8, 13, 15]. Consistent with our findings, ILK has been shown to phosphorylate in vitro Akt at Ser 473 [5, 16]. Inhibition of ILK kinase activity and conditional knockout of ILK have also demonstrated an essential role of ILK in activation of the protein kinase Akt [5, 9, 10]. However, in contrast to other malignancies [8, 15], high levels of p-Akt were correlated with well-differentiated laryngeal carcinomas. It is interesting that similar findings were reported in the cases of non-small cell lung cancer and cholangiocarcinoma [26, 27]. There was no correlation between nuclear p-Akt and tumor grade in our material. This may be attributed to the fact that the various subcellular localization of p-Akt may differently influence laryngeal cancer biology. In this respect, it is of interest to note that an important role for the subcellular localization of Akt in determining downstream signalling and subsequent cellular events has been previously suggested [28].

As in previous studies, we demonstrated an activation of β-catenin and downregulation of E-cadherin which correlated with advancing tumor grade and TNM stage [11, 12]. We also documented a statistically significant correlation between downregulation of E-cadherin and nuclear accumulation of β-catenin. Apart from its role in E-cadherin-mediated cell adhesion, β-catenin is a central component of the Wnt signaling pathway [18, 19]. The catenin/cadherin adherence complex is known to play a significant role in cell adhesion, signaling, and cancer [18, 19]. In addition to mutations of Wnt signaling pathway components, loss of E-cadherin has also been shown to induce nuclear translocation of β-catenin and activation of its transcriptional activity [29]. Taken together, our findings probably indicate a causative relation between loss of E-cadherin and activation of β-catenin signaling in laryngeal cancer.

Although previous in vitro studies implicate ILK in the regulation of β-catenin signaling and E-cadherin expression, there was no significant in vivo correlation of ILK expression with β-catenin or E-cadherin in our material [3, 4]. This finding suggests that in laryngeal carcinogenesis mechanisms other than overexpression of ILK account for the observed deregulation of β-catenin and E-cadherin. In line with this hypothesis, we showed that activation of

β-catenin may due to the loss of E-cadherin [29]. Mutations of the Wnt signalling pathway components may also account for the nuclear accumulation of β-catenin in laryngeal carcinomas [18, 19, 30]. Moreover, loss of E-cadherin in laryngeal cancer may be attributed to genetic or epigenetic alteration of the E-cadherin gene [18, 19, 30, 31].

Our study shows a marginal correlation of cytoplasmic p-Akt with membrane E-cadherin ($p=0.086$) and a statistically significant correlation between cytoplasmic p-Akt and membrane β-catenin expression ($r=0.226$, $p=0.026$). The later finding is in contrast to previous studies [15, 32], but it is interesting to note that in our material, cytoplasmic p-Akt, membrane E-cadherin, and membrane β-catenin, they are all correlated with low tumor grade.

In conclusion, we demonstrated cytoplasmic and nuclear expression of ILK in human laryngeal squamous cell carcinomas suggesting a possible role for ILK in the development of these tumors. In addition, we found that ILK expression in laryngeal carcinomas correlates with p-Akt but not with the loss of E-cadherin or activation of β-catenin. Finally, we provided evidence that expression of p-Akt correlates with well-differentiated laryngeal tumors.

Acknowledgements We shall thank Dr. Maria Repandi, Director of Pathology Department of "Agios Andreas" General Hospital of Patras for providing us with the tissue samples of human squamous laryngeal cancer.

Conflict of interest The authors declare that they have no conflict of interest.

References

1. Parkin DM, Bray F, Ferlay J, Pisani P (2005) Global cancer statistics, 2002. CA Cancer J Clin 55:74–108
2. Dedhar S, Williams B, Hannigan G (1999) Integrin-linked kinase (ILK): a regulator of integrin and growth-factor signaling. Trends Cell Biol 9:319–323
3. Oloumi A, McPhee T, Dedhar S (2004) Regulation of E-cadherin expression and β-catenin/Tcf transcriptional activity by the integrin-linked kinase. Biochim Biophys Acta 1691:1–15
4. Novak A, Hsu SC, Leung-Hagesteijn C, Radeva G, Papkoff J, Montesano R, Roskelley C, Grosschedl R, Dedhar S (1998) Cell adhesion and the integrin-linked kinase regulate the LEF-1 and β-catenin signaling pathways. Proc Natl Acad Sci U S A 95:4374–4379
5. Hannigan G, Troussard AA, Dedhar S (2005) Integrin-linked kinase: a cancer therapeutic target unique among its ILK. Nat Rev Cancer 5:51–63
6. Wu C, Keightley SY, Leung-Hagesteijn C, Radeva G, Coppolino M, Goicoechea S, McDonald JA, Dedhar S (1998) Integrin-linked protein kinase regulates fibronectin matrix assembly, E-cadherin expression, and tumorigenicity. J Biol Chem 273:528–536
7. Younes MN, Kim S, Yigitbasi OG, Mandal M, Jasser SA, Dakak Yazici Y, Schiff BA, El-Naggar A, Bekele BN, Mills GB, Myers JN (2005) Integrin-linked kinase is a potential therapeutic target for anaplastic thyroid cancer. Mol Cancer Ther 4:1146–1156
8. Okamura M, Yamaji S, Nagashima Y, Nishikawa M, Yoshimoto N, Kido Y, Iemoto Y, Aoki I, Ishigatsubo Y (2007) Prognostic value of integrin β1-ILK-pAkt signaling pathway in non-small cell lung cancer. Human Pathol 38:1081–1091
9. Younes MN, Yigitbasi OG, Yazici YD, Jasser SA, Bucana CD, El-Naggar AK, Mills GB, Myers JN (2007) Effects of the integrin-linked kinase inhibitor QLT0267 on squamous cell carcinoma of the head and neck. Arch Otolaryngol Head Neck Surg 133:15–23
10. Troussard AA, Mawji NM, Ong C, Mui A, St-Arnaud R, Dedhar S (2003) Conditional knock-out of integrin-linked kinase demonstrates an essential role in protein kinase B/Akt activation. J Biol Chem 278:22374–22378
11. Rodrigo JP, Dominguez F, Suárez V, Canel M, Secades P, Chiara MD (2007) Focal adhesion kinase and E-cadherin as markers for nodal metastasis in laryngeal cancer. Arch Otolaryngol Head Neck Surg 133:145–150
12. Lopez-Gonzalez JS, Cristerna-Sanchez L, Vazquez-Manriquez ME, Jimenez-Orci G, Aguilar-Cazares D (2004) Localization and level of expression of β-catenin in human laryngeal squamous cell carcinoma. Otolaryngol Head Neck Surg 130:89–93
13. Nicholson KM, Anderson NG (2002) The protein kinase B/Akt signaling pathway in human malignancy. Cell Signal 14:381–395
14. Cardesa A, Gale N, Nadal A, Zidar N (2005) Squamous cell carcinoma. In: Barnes L, Eveson JW, Reichart P, Sidransky D (eds) World Health Organization classification of tumors. Pathology and genetics of head and neck tumors. IARC, Lyon, pp 118–121
15. Bravou V, Klironomos G, Papadaki E, Taraviras S, Varakis J (2006) ILK overexpression in human colon cancer progression correlates with activation of β-catenin, down-regulation of E-cadherin and activation of the Akt–FKHR pathway. J Pathol 208:91–99
16. Persad S, Attwell S, Gray V, Mawji N, Deng JT, Leung D, Yan J, Sanghera J, Walsh MP, Dedhar S (2001) Regulation of protein kinase B/Akt-serine 473 phosphorylation by integrin-linked kinase: critical roles for kinase activity and amino acids arginine 211 and serine 343. J Biol Chem 276:27462–27469
17. Massarelli E, Liu DD, Lee JJ, El-Naggar AK, Lo Muzio L, Staibano S, De Placido S, Myers JN, Papadimitrakopoulou VA (2005) Akt activation correlates with adverse outcome in tongue cancer. Cancer 104:2430–2436
18. Conacci-Sorrell M, Zhurinsky J, Ben-Ze'ev A (2002) The cadherin–catenin adhesion system in signaling and cancer. J Clin Invest 109:987–991
19. Hajra KM, Fearon ER (2002) Cadherin and catenin alterations in human cancer. Genes Chromosomes Cancer 34:255–268
20. Ito R, Oue N, Zhu X, Yoshida K, Nakayama H, Yokozaki H, Yasui W (2003) Expression of integrin-linked kinase is closely correlated with invasion and metastasis of gastric carcinoma. Virchows Arch 442:118–123
21. Driver GA, Veale RB (2006) Modulation of integrin-liked kinase (ILK) expression in human oesophageal squamous cell carcinoma cell lines by the EGF and TGFβ1 growth factors. Cancer Cell Int 6:12
22. Chun J, Hyun S, Kwon T, Lee EJ, Hong SK, Kang SS (2005) The subcellular localization control of integrin linked kinase 1 through its protein-protein interaction with caveolin-1. Cell Signal 17:751–760
23. Acconcia F, Barnes CJ, Singh RR, Talukder AH, Kumar R (2007) Phosphorylation-dependent regulation of nuclear localization and functions of integrin-linked kinase. Proc Natl Sci U S A 104:6782–6787
24. Fielding AB, Dobreva I, Dedhar S (2008) Beyond focal adhesions: integrin-linked kinase associates with tubulin and regulates mitotic spindle organization. Cell Cycle 7:1899–1906

25. Fielding AB, Dobreva I, McDonald PC, Foster LJ, Dedhar S (2008) Integrin-linked kinase localizes to the centrosome and regulates mitotic spindle organization. J Cell Biol 180:681–689
26. Shah A, Swain WA, Richardson D, Edwards J, Stewart DJ, Richardson CM, Swinson DE, Patel D, Jones JL, O'Byrne KJ (2005) Phospho-Akt expression is associated with favorable outcome in non-small cell lung cancer. Clin Cancer Res 11:2930–2936
27. Javle MM, Yu J, Khoury T, Chadha KS, Iyer RV, Foster J, Kuvshinoff BW, Gibbs JF, Geradts J, Black JD, Brattain MG (2006) Akt expression may predict favorable prognosis in cholangiocarcinoma. J Gastroenterol Hepatol 21:1744–1751
28. Saji M, Vasko V, Kada F, Allbritton EH, Burman KD, Ringel MD (2005) Akt1 contains a functional leucine-rich nuclear export sequence. Biochem Biophys Res Commun 332:167–173
29. Orsulic S, Huber O, Aberle H, Arnold S, Kemler R (1999) E-cadherin binding prevents β-catenin nuclear localization and β-catenin/LEF-1-mediated transactivation. J Cell Sci 112:1237–1245
30. Pećina-Slaus N, Kljaić M, Nikuseva-Martić T (2005) Loss of heterozygosity of APC and CDH1 genes in laryngeal squamous cell carcinoma. Pathol Res Pract 201:557–563
31. Dikshit RP, Gillio-Tos A, Brennan P, De Marco L, Fiano V, Martinez-Peñuela JM, Boffetta P, Merletti F (2007) Hypermethylation, risk factors, clinical characteristics, and survival in 235 patients with laryngeal and hypopharyngeal cancers. Cancer 110:1745–1751
32. Barandon L, Dufourcq P, Costet P, Moreau C, Allières C, Daret D, Dos Santos P, Daniel Lamazière JM, Couffinhal T, Duplàa C (2005) Involvement of FrzA/sFRP-1 and the Wnt/frizzled pathway in ischemic preconditioning. Circ Res 96:1299–1306

Virchows Arch (2008) 453:521–527
DOI 10.1007/s00428-008-0680-z

ORIGINAL ARTICLE

Aberrant expression of an "intestinal marker" Cdx2 in pyloric gland adenoma of the gallbladder

Yoji Wani · Kenji Notohara · Masayoshi Fujisawa

Received: 14 August 2008 / Revised: 8 September 2008 / Accepted: 23 September 2008 / Published online: 9 October 2008

Abstract The aim of this study was to survey Cdx2 expression in pyloric gland adenoma (PGA) of the gallbladder. We reviewed 29 PGA cases, ten (34.4%) and seven (24.1%) of which showed intestinal metaplasia (IM) and squamous morule (SM), respectively. The immunostaining for Cdx2, beta-catenin, MUC5AC, MUC2, MUC6, and M-GGMC-1 was performed and scored (0=negative, 1+=<10%, 2+=10% to <30%, 3+=30% to <50%, 4+=50% to <70%, 5+=70–100%). Although its scores were relatively low (1+ or 2+), Cdx2 was frequently expressed in 27 cases (93.1%). Not only goblet and/or Paneth cells were positive but also non-IM cells in PGAs, as opposed to the lack of staining in the background mucosa. Cdx2 scores were not correlated with those of IM (p=0.485) and MUC2 (p=0.868). Of note, Cdx2 was positive in foci of SM in all seven cases, and there was a significant difference in Cdx2 scores between PGAs with and without SM. Furthermore, the p value of scores between Cdx2 and beta-catenin was 0.051, and both mean labeling indices (LIs) were correlated (r=0.736). With Cdx2, higher morular LIs than glandular LIs were observed (p=0.001). Finally, we concluded that aberrant Cdx2 expression in PGAs is closely associated with nuclear beta-catenin expression and SM in contrast with IM.

Keywords Cdx2 · Beta-catenin · Pyloric gland adenoma · Gallbladder · Immunohistochemistry

Y. Wani (✉) · K. Notohara
Department of Pathology, Kurashiki Central Hospital, Kurashiki, Okayama, Japan
e-mail: yw7144@kchnet.or.jp

M. Fujisawa
Department of Pathology, Himeji Red Cross Hospital, Himeji, Japan

Introduction

The Cdx2 protein is an intestine-specific homeobox gene transcription factor that plays an important role in regulating the differentiation of the intestinal epithelium [1]. The expression in adult normal tissue is restricted to the nuclei of the intestinal epithelium from the duodenum to the rectum [2, 3]. Its expression, however, is not limited to normal mucosa because it has also been reported in colonic adenocarcinoma [2, 4]. Furthermore, Cdx2 expression has been documented in adenocarcinomas at other sites such as the stomach, pancreas, urinary bladder, and ovary; this expression has been interpreted as intestinal differentiation [4–8].

In gallbladder, Cdx2 expression has been observed in the mucosa in chronic cholecystitis, cholelithiasis, and adenocarcinoma and has been found to be related to MUC2 expression [9–12]. These phenomena have also been interpreted as intestinal differentiation. In tubular adenoma, the pyloric gland-type (or pyloric gland adenoma; PGA) of the gallbladder, which is composed of lobules that contain closely packed pyloric type tubular glands, only a report of Cdx2 has been published [13]. According to that, none of the 58 PGA cases showed Cdx2 expression.

We have clarified that Cdx2 protein is frequently aberrantly expressed in endometrial lesions with squamous differentiation, especially morular-type differentiation, and strongly correlates with nuclear expression of beta-catenin [14]. Furthermore, Saegusa et al. proved that in cell lines of endometrial carcinomas, overexpression of the active form of beta-catenin results in a significant increase in endogenous Cdx2 expression at both mRNA and protein levels [15]. They concluded that an association between Cdx2 and beta-catenin signaling might participate in an induction of transdifferentiation of endometrioid carcinoma cells. In

Table 1 Immunohistochemical panel

Primary antibody	Clone	Company	Dilution	Antigen retrieval
Cdx2	CDX2–88	BioGenex, San Ramon, CA, USA	1:100	MW (EDTA, pH 7.0)
Beta-catenin	17C2	Novocastra, Newcastle, UK	1:50	MW (citrate, pH 6.0) + PC
MUC2	Ccp58	Novocastra, Newcastle, UK	1:100	MW (citrate, pH 6.0)
MUC6	CLH5	Novocastra, Newcastle, UK	1:100	MW (citrate, pH 6.0)
M-GGMC-1	HIK1083	Kanto Chemical, Tokyo, Japan	1:25	MW
MUC5AC	CLH2	Novocastra, Newcastle, UK	1:100	MW (citrate, pH 6.0)

MW microwave, *PC* pressure cooker

PGA, squamous morules (or spindle cell metaplasias; SMs) are also present in 23% of cases [16]. SM is defined as having discrete nests or uniformly demarcated sheets of nonkeratinizing (immature) squamous cells, which are oval or spindle-shaped cells appearing bland and uniform and lacking prominent nucleoli [17–19]. These cells sometimes contain biotin-rich optically clear nuclei [18, 20]. Mitotic figures are usually not seen. Immunohistochemically, nuclear expression of beta-catenin, estrogen-beta receptor, p53, cyclin D1, and low MIB-1 index is shown in the foci of SM [18, 21] In addition, the gene mutation of beta-catenin in PGA has been established as well as in endometrial lesions [22, 23]. Given that PGA and endometrial lesions have SM in common, aberrant Cdx2 expression in PGA can also be presumed in a mode other than intestinal differentiation.

The aim of the present study was to survey Cdx2 expression in PGA of the gallbladder and to determine whether Cdx2 expression is related to intestinal differentiation, beta-catenin expression, or SM.

Materials and methods

We retrieved 29 cases of PGAs from the files of Kurashiki Central Hospital and Himeji Red Cross Hospital. We reviewed HE slides to note the size of the lesion and the presence or absence of IM and SM. With IM, a small number of admixed cells (Paneth cells and/or goblet cells) were also noted. In immunohistochemistry, paraffin-embedded sections cut at 4 μm were deparaffinized and rehydrated, and endogenous peroxidase was blocked in 3% hydrogen peroxidase. In all specimens, immunostainings were performed for beta-catenin and for mucin markers such as MUC5AC for gastric foveolar-type epithelium, MUC6, M-GGMC-1 for the pyloric-gland type, and MUC2 for the intestinal goblet-cell type, using suitable antigen retrieval for each, and detection was carried out with the Envision plus detection system (DAKO, Kyoto, Japan; Table 1). Diaminobenzidine was employed as a chromogen. The immunostaining was scored as follows: 0=negative, 1+=<10% positive cells, 2+=10% to <30%, 3+=30% to <50%, 4+=50% to <70%, 5+=70–100%. In a closer survey of the relationship between Cdx2 and beta-catenin, the number of positive nuclei for Cdx2 and beta-catenin was counted in the well-labeled high power fields (HPFs). The mean labeling indices (LIs; %) were calculated by counting 1,000 cells in three different HPFs. Moreover, with SM cases, morular and glandular LI (%) were also calculated by counting positive cells in all foci of SM and in the surrounding glandular cells (at least 1,000 cells per a focus of SM).

All statistical analyses were carried out using the SPSS software package version 15.0 (SPSS Inc., Chicago, IL, USA). Comparative data were analyzed using Pearson's chi square test, Linear-by-Linear association, Spearman's correlation coefficient, and the Mann–Whitney *U* test. A p value of <0.05 was considered statistically significant.

Table 2 Immunohistochemical results

Antibody	Score											
	0	%	1+	%	2+	%	3+	%	4+	%	5+	%
Cdx2	2	6.9	19	65.5	8	27.6	0	0.0	0	0.0	0	0.0
Beta-catenin	1	3.4	11	37.9	5	17.2	9	31.0	3	10.3	0	0.0
MUC6	0	0.0	0	0.0	2	6.9	5	17.2	3	10.3	19	65.5
M-GGMC-1	0	0.0	1	3.4	2	6.9	10	34.5	8	27.6	8	27.6
MUC2	24	82.8	5	17.2	0	0.0	0	0.0	0	0.0	0	0.0
MUC5AC	1	3.4	16	55.2	9	31.0	3	10.3	0	0.0	0	0.0

Results

PGA ranged in size from 3 to 16 mm (mean 8.2 mm). Seven cases (24.1%) contained foci of SM. Ten cases (34.4%) had small but distinct foci of goblet cells and/or Paneth cells. Of these, only two cases contained both metaplasias. The immunohistochemical results are listed in Table 2. In the background mucosa of all 18 cases assessable, Cdx2 expression was completely absent. Although its scores were low (1+ or 2+), Cdx2 was frequently expressed in 27 cases (93.1%). Not only goblet and/or Paneth cells, but also other cells in PGAs were found to be positive for the marker, in contrast with the absence of staining in the background mucosa (Figs. 1a–c, 2a–d). Of

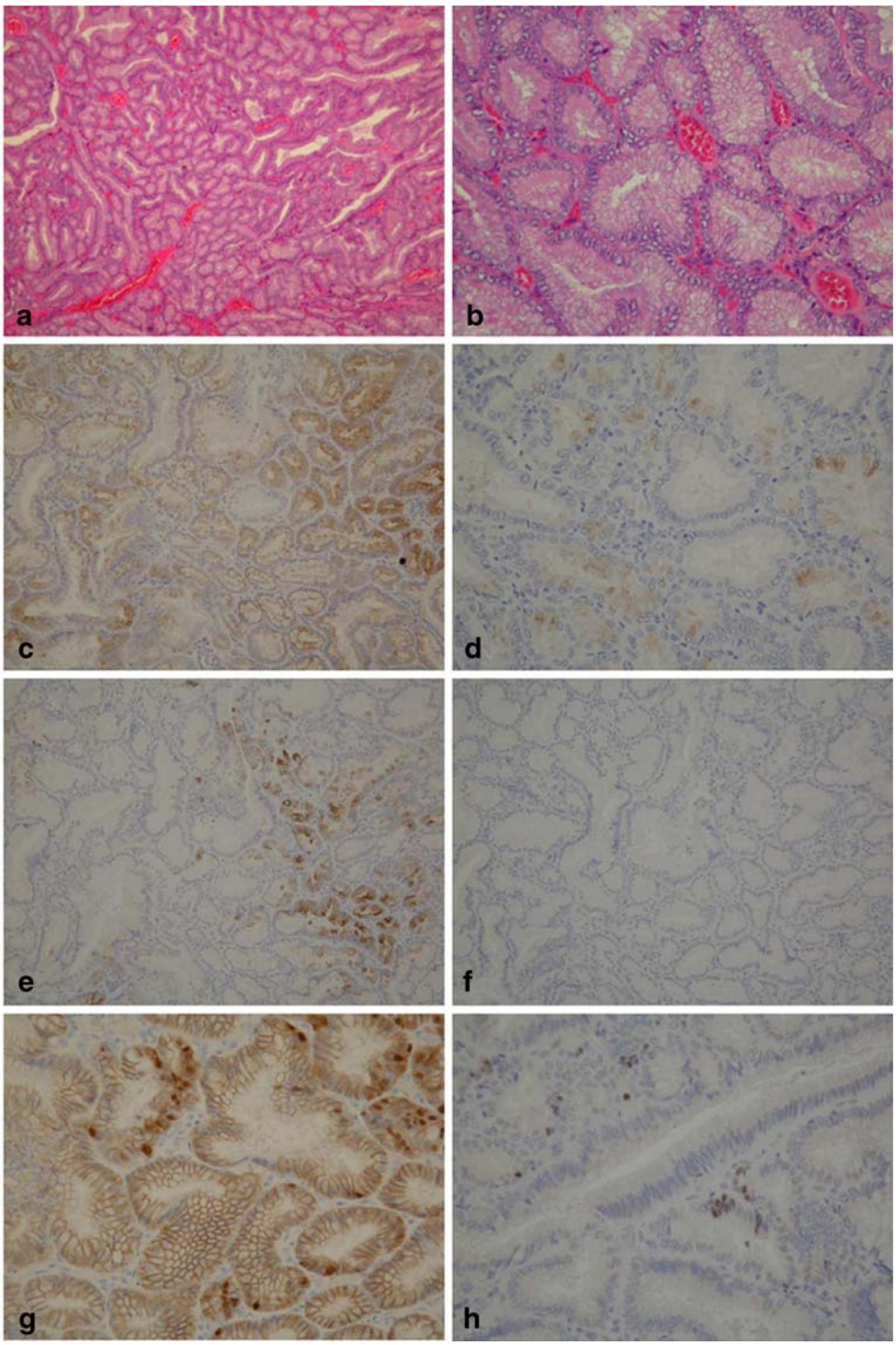

Fig. 1 PGA without IM (**A** HE ×100; **B** HE ×400). PGA showing the expression of mucin markers MUC6 (**C**, ×200), M-GGMC-1 (**D**, ×400), and MUC5AC (**E**, ×200), lacking MUC2 expression (**F**, ×200). Likewise, beta-catenin (**G**, ×400), nuclear Cdx2 expression (**H**, ×400) is identified in the minority of glandular cells

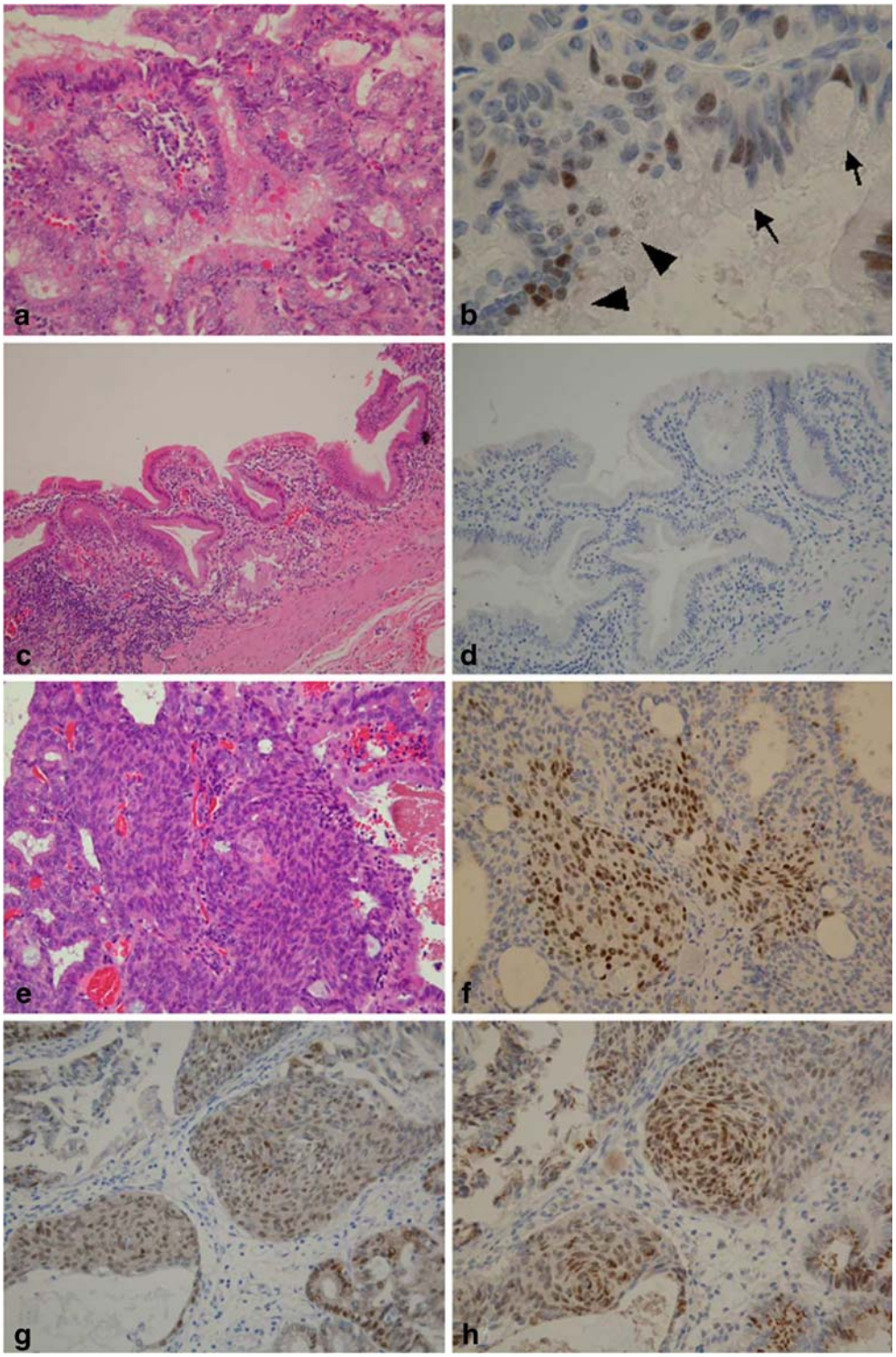

Fig. 2 PGA with IM (**A**–**D**) and SM (**E**–**H**). Cdx2 stain is seen in both Goblet (*arrow*) and Paneth cells containing granules (*arrow head*; **A** HE ×200; **B**, ×400), despite there being no staining in the background mucosa (**C** HE ×100; **D**, ×200). In morular foci (**E** HE ×200), Cdx2 expression (**F**, ×200; **H**, ×200) closely resembles nuclear expression of beta-catenin (**G**, ×200)

note, Cdx2 was also positive in foci of SM in all seven cases (100%; Fig. 2f,h). Statistically, Cdx2 scores were not correlated with those of IM (p=0.485) and MUC2 (p=0.868; Tables 3 and 4; Fig. 1g). However, only a small number of goblet and/or Paneth cells in five cases were positive for MUC2 (17.2%), where Cdx2-positive cells were also seen (Table 2; Fig. 2b). The Cdx2 score was not statistically correlated with that of MUC6 (p=0.871), M-GGMC-1 (p=0.878), and MUC5AC (p=0.499; Table 4; Fig. 1e,f,h). In contrast, there was a significant difference in

Table 3 Comparison of Cdx2 scores between PGA cases with and without metaplasia

	Cdx2			
	0	1	2	*p* Value
PGA with IM	0	8	2	0.485
PGA without IM	2	11	6	
PGA with SM	0	2	5	0.015*
PGA without SM	2	17	3	

Statistical analysis was performed with Pearson's chi square test ($p<0.05$)
PGA pyloric gland adenoma, *IM* intestinal metaplasia, *SM* squamous morule

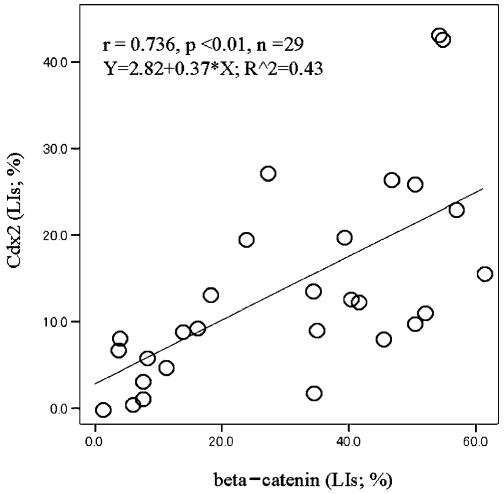

Fig. 3 Correlation between mLIs of Cdx2 and beta-catenin in PGA. Statistical analysis was performed with Spearman's correlation coefficient

Cdx2 scores between PGAs with and without SM (Table 3). Furthermore, the *p* value of scores between Cdx2 and beta-catenin was just around a cut-off level (0.051; Table 4; Fig. 1d); however, both of the mean LIs, which were counted in well-labeled fields, were correlated (r=0.736; Fig. 3). With both Cdx2 and beta-catenin in SM cases, the morular LIs were significantly higher than the glandular LIs (p=0.001, 0.038, respectively; Fig. 4).

Discussion

In gallbladder, Cdx2 expression, a well-known intestinal marker, has been observed in the mucosa in chronic cholecystitis, cholelithiasis, and adenocarcinoma and has been found to be related to MUC2 expression [9–12]. These phenomena have also been interpreted as intestinal differentiation. As to PGA, frequent Cdx2 expression (92%) has also been considered to be specific to PGA without any expression in the background mucosa of 18 cases. Our results were completely different from the data by Nagata et al., who described that no 58 PGA cases showed Cdx2 expression [13]. The reason for the dissociation of these results remains unclear. In their study, the number of PGA cases with SM or IM was not elucidated.

Table 4 Correlations of scores between Cdx2 and other markers

	Cdx2
Beta-catenin	p=0.051
MUC2	p=1.000
MUC6	p=0.871
M-GGMC-1	p=0.878
MUC5AC	p=0.499

Statistical analysis was performed with Linear-by-Linear Association

They might have experienced some PGA cases with a small number of Cdx2-positive cells, corresponding to our "Score 1" cases because they considered that Cdx2 expression was positive when the percentage of positively stained cells was 10% or more. In general, PGA contains tumor cells showing differentiation to goblet cells, Paneth cells, or endocrine cells, which are often admixed, and these admixed cells mean a kind of intestinal metaplasia of PGA [16]. It seems plausible that Cdx2 expression may correspond to the number of metaplastic cells. Indeed, in the present study, Cdx2 expression was focally identified in areas showing goblet and/or Paneth cell-type intestinal differentiation, but it was very limited. PGAs with Paneth cells or endocrine cells showed unquestionable positivity for Cdx2, whereas Cdx2 did not correlate to MUC2 expression (all but five were completely MUC2-negative). This miscorrelation between the two markers is unique and has never been reported in other gallbladder lesions (chronic cholecystitis or carcinoma) [10, 11]. In addition, Cdx2 expression was not confined to the areas or cases clearly showing intestinal metaplasia. Considering the identification of Cdx2 in most PGA cases without IM, Cdx2 expression in PGAs does not largely seem to indicate true intestinal differentiation. Furthermore, neither does it to correlate to expressions of MUC6 and M-GGMC-1 (pyloric phenotypes) nor MUC5AC (gastric foveolar phenotype).

Of note, Cdx2 was positive in foci of SM in all seven cases, and there was a significant difference in scores between cases with and without SM (p=0.015). The correlation of scores between Cdx2 and beta-catenin was just around a cutoff level value (p=0.051), and the correlation of mean LIs between Cdx2 and beta-catenin

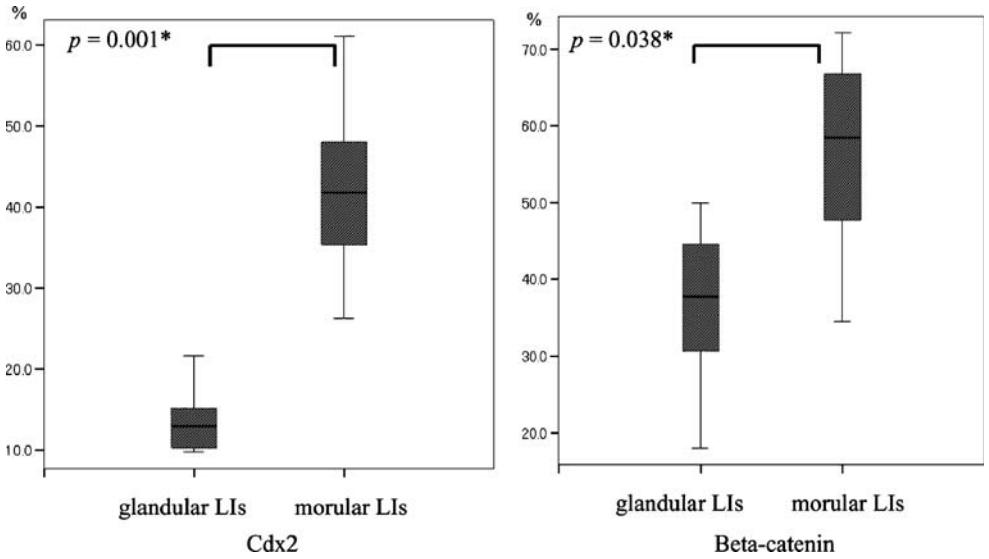

Fig. 4 Comparison of Cdx2 between glandular and morular LIs in PGA. The data are means ± SD values. Statistical analysis was performed with the Mann–Whitney *U* test

was also identified. Comparing the mean LIs for both markers, LIs of beta-catenin were likely to higher than those of Cdx2. However, foci of SM in all seven cases expressed both markers. In addition, morular LIs of Cdx2 were significantly higher than glandular LIs (p=0.001), as seen in beta-catenin (p=0.038). These observations in PGA have never been reported previously. Recently, we clarified that Cdx2 protein is aberrantly expressed in endometrial lesions with squamous differentiation, especially morular-type differentiation, and strongly correlates with nuclear expression of beta-catenin [14]. In addition to some previous reports with beta-catenin mutation in PGAs [22, 23], our results of the correlation of mean LIs between the two and their common expression in SM foci raise the intriguing possibility that the mutation of beta-catenin genes promotes Cdx2 expression, as Saegusa et al. indicated in endometrial lesions [15]. They proved that in cell lines of endometrial carcinomas, overexpression of the active form beta-catenin results in a significant increase in endogenous Cdx2 expression at both mRNA and protein levels. They concluded that an association between Cdx2 and beta-catenin signaling might participate in induction of transdifferentiation of endometrioid carcinoma cells. Further molecular study in PGAs will be necessary to confirm this speculation. In any event, Cdx2 expression has previously only been considered to be "intestinal differentiation" in gastrointestinal and pancreatobiliary systems. We will describe a new aspect of Cdx2 expression related to SM and stable beta-catenin, probably due to the latter gene mutation. Our study can also offer the expression of Cdx2 as one of the traits of PGA.

In summary, we documented frequent Cdx2 expression in PGA of the gallbladder. Unlike other gallbladder lesions (chronic cholecystitis, cholelithiasis, and adenocarcinoma), IM in itself plays a minor role of Cdx2 expression in PGA. Moreover, Cdx2 expression did not correlate to MUC2 expression. Besides, significantly high levels of Cdx2 expression in morular foci and a correlation of mean LIs between Cdx2 and beta-catenin are noteworthy. We, therefore, concluded that aberrant Cdx2 expression in PGAs is closely associated with beta-catenin expression and SM.

Acknowledgements The authors thank Mr. Hironori Kajitani and Ms. Akemi Minamimoto for their technical support. They also thank Mr. Yoshiharu Yamamoto, Clinical Research Center, Kurashiki Central Hospital, for providing assistance with the statistical analyses.

Disclosure/Conflict of Interest The authors have no conflict of interest to declare.

References

1. Suh E, Chen L, Taylor J et al (1994) A homeodomain protein related to caudal regulates intestine-specific gene transcription. Mol Cell Biol 14:7340–51
2. Barbareschi M, Murer B, Colby TV et al (2003) Cdx2 homeobox gene expression is a reliable marker of colorectal adenocarcinoma metastases to the lungs. Am J Surg Pathol 27:141–9
3. Silberg DG, Swain GP, Suh ER et al (2000) Cdx1 and Cdx2 expression during intestinal development. Gasteroenterology 119:961–71
4. Werling RW, Yaziji H, Bacchi CE et al (2003) CDX2, a highly sensitive and specific marker of adenocarcinoma of intestinal origin. Am J Surg Pathol 27:303–10
5. De Lott L, Morrison C, Suster S et al (2005) Cdx2 is a useful marker of intestinal-type differentiation. Arch Pathol Lab Med 129:1100–5
6. Kaimaktchiev V, Terracciano L, Tornillo L et al (2004) The homeobox intestinal differentiation factor CDX2 is selectively

expressed in gastrointestinal adenocarcinomas. Mod Pathol 17:1392–9
7. Mazziotta R, Borczuk A, Powell C et al (2005) CDX2 immunostaining as a gastrointestinal marker: expression in lung carcinomas is a potential pitfall. Appl Immunohistochem Mol Morphol 12:55–60
8. Moskaluk CA, Zhang H, Powell SM et al (2003) Cdx2 protein expression in normal and malignant human tissues: an immunohistochemical survey using tissue microarrays. Mod Pathol 16:913–9
9. Chang YT, Hsu C, Jeng YM et al (2007) Expression of the caudal-type homeodomain transcription factor CDX2 is related to clinical outcome in biliary tract carcinoma. J Gastroenterol Hepatol 22:389–4
10. Osawa H, Kita H, Satoh K et al (2004) Aberrant expression of CDX2 in the metaplastic epithelium and inflammatory mucosa of the gallbladder. Am J Surg Pathol 28:1253–4
11. Sakamoto H, Mutoh H, Ido K et al (2007) A close relationship between intestinal metaplasia and Cdx2 expression in human gallbladders with cholelithiasis. Hum Pathol 38:66–71
12. Wu XS, Akiyama Y, Igari T et al (2005) Expression of homeodomain protein CDX2 in gallbladder carcinomas. J Cancer Res Clin Oncol 131:271–8
13. Nagata S, Ajioka Y, Nishikura K et al (2007) Co-expression of gastric and biliary phenotype in pyloric-gland type adenoma of the gallbladder: immunohistochemical analysis of mucin profile and CD10. Oncol Rep 17:721–9
14. Wani Y, Notohara K, Saegusa M et al (2008) Aberrant Cdx2 expression in endometrial lesions with squamous differentiation: important role of Cdx2 in squamous morula formation. Hum Pathol 39:1072–9
15. Saegusa M, Hashimura M, Kuwata T et al (2007) Functional role of Cdx2 in beta-catenin signaling during transdifferentiation in endometrial carcinomas. Carcinogenesis 28:1885–92
16. Takei K, Watanabe H, Itoi T, Saito T (1996) p53 and Ki-67 immunoreactivity and nuclear morphometry of 'carcinoma-in-adenoma' and adenoma of the gall-bladder. Pathol Int 46:908–17
17. Crum C, Lee K (2005) Diagnostic gynecologic and obstetric pathology. Elsevier, Philadelphia, pp 525–529, 553–558
18. Nakatani Y, Masudo K, Nozawa A et al (2004) Biotin-rich, optically clear nuclei express estrogen receptor-beta: tumors with morules may develop under the influence of estrogen and aberrant beta-catenin expression. Hum Pathol 35:869–74
19. Saegusa M, Okayasu I (2001) Frequent nuclear β-catenin accumulation and associated mutations in endometrioid-type endometrial and ovarian carcinomas with squamous differentiation. J Pathol 194:59–67
20. Gamachi A, Kashima K, Daa T et al (2003) Aberrant intranuclear localization of biotin, biotin-binding enzymes, and beta-catenin in pregnancy-related endometrium and morule-associated neoplastic lesions. Mod Pathol 16:1124–31
21. Saegusa M, Hashimura M, Kuwata T et al (2004) β-catenin simultaneously induces activation of the p53-p21WAF-1 pathway and overexpression of cyclin D1 during squamous differentiation of endometrial carcinoma cells. Am J Pathol 164:1739–1749
22. Chang HJ, Jee CD, Kim WH (2002) Mutation and altered expression of beta-catenin during gallbladder carcinogenesis. Am J Surg Pathol 26:758–66
23. Yanagisawa N, Mikami T, Saegusa M et al (2001) More frequent beta-catenin exon 3 mutations in gallbladder adenomas than in carcinomas indicate different lineages. Cancer Res 61:19–22

Virchows Arch (2008) 453:529–534
DOI 10.1007/s00428-008-0659-9

CASE REPORT

Necrotic granulomatous pseudotumours in bilateral resurfacing hip arthoplasties: evidence for a type IV immune response

H. Pandit · M. Vlychou · D. Whitwell · D. Crook · R. Luqmani · S. Ostlere · D. W. Murray · N. A. Athanasou

Received: 29 March 2008 / Revised: 21 July 2008 / Accepted: 18 August 2008 / Published online: 4 September 2008

Abstract Clinical, radiological and histological findings were analysed in four patients who developed bilateral pseudotumours following metal-on-metal (MoM) resurfacing arthroplasties of both hips. Using a panel of monoclonal antibodies directed against HLA-DR, macrophages (CD14, CD68), dendritic cells (DC-SIGN, S100, CD11c), B cells (CD20), and T cells (CD3, CD4, CD8), the nature of the heavy inflammatory response seen in these cases was examined. Bilateral masses developed in periprosthetic soft tissues following the second MoM arthroplasty; these were characterised histologically by extensive coagulative necrosis, a heavy macrophage infiltrate and the presence of granulomas containing macrophages and giant cells; there was also a diffuse lymphocyte and variable plasma cell and eosinophil polymorph infiltrate. Immunohistochemistry showed strong expression of HLA-DR, CD14 and CD68 in both granulomatous and necrotic areas; lymphocytes were predominantly CD3+/CD4+ T cells. The clinical, morphological and immunophenotypic features of these necrotic granulomatous pseudotumours, which in all cases develop following a second resurfacing hip arthroplasty, is suggestive of a type IV immune response, possibly to MoM metal alloy components.

Keywords Metal-on-metal (MoM) resurfacing hip arthroplasty · Pseudotumours · Immunohistochemistry · Type IV immune response

H. Pandit · M. Vlychou · D. Whitwell · D. Crook · R. Luqmani · S. Ostlere · D. W. Murray · N. A. Athanasou (✉)
Nuffield Department of Orthopaedic Surgery,
Nuffield Orthopaedic Centre, University of Oxford,
Headington,
Oxford OX3 7LD, UK
e-mail: nick.athanasou@ndos.ox.ac.uk

Introduction

Resurfacing hip arthroplasties containing second-generation cobalt–chromium–molybdenum alloy metal-on-metal (MoM) components are now being increasingly employed in the treatment of arthritic disease. This component combination is particularly useful for the treatment of end-stage osteoarthritis of the hip in relatively young patients when conventional total hip replacement (THR) may not last a lifetime and the patient is likely to require revision surgery. The advantages of MoM resurfacing hip arthroplasty include relative conservation of bone, improved wear characteristics, lower dislocation rate and the ability to meet the higher demands and expectations of more active patients.

MoM articulations produce a high concentration of metal ions and wear particles that induce a foreign body macrophage response as well as a variable but often heavy infiltrate of lymphocytes and plasma cells, many of which are found around small vessels [5, 11, 18]; this inflammatory reaction has been termed an "aseptic lymphocyte-dominated vascular associated lesion" (ALVAL), and is considered by some investigators to develop as a result of a delayed hypersensitivity response to wear debris derived from the metal implant components [5, 9, 10]. However, several features characteristic of a type IV immune response, including a history of previous exposure to the antigen prior to development of the reaction and a granulomatous response [14], have not been documented in these cases.

In this study, we report a series of four patients who presented with an identical history of development of granulomatous pseudotumours following bilateral MoM resurfacing hip arthroplasty. The clinical, morphological and immunohistological findings in these cases would appear to provide evidence for a type IV hypersensitivity response being associated with the pathogenesis of these lesions.

Clinical history

Patient 01 This 50-year-old female patient presented with bilateral osteoarthritis (OA) secondary to hip dysplasia. She underwent staged hip resurfacings 34 months apart (left Birmingham hip resurfacing and right Conserve +). The patient experienced significant pain in her first hip resurfacing 6 weeks after the second hip resurfacing and subsequently sustained a fracture of the neck of the femur on that side after a trivial fall. At the time of revision surgery, a large mass was noticed posterior to the joint. The lesion was cystic; it contained fluid within thickened walls and communicated with the hip joint. The failed resurfacing was revised to a conventional THR and the patient made an uneventful recovery. The pain on the revised side settled completely. The patient has started experiencing pain on the right side for several months and magnetic resonance imaging (MRI) scans have confirmed the presence of a pseudotumour (similar to the contralateral side) posterior to the hip joint.

Patient 02 This 64-year-old female patient with bilateral primary OA underwent simultaneous bilateral resurfacings (Birmingham Hip Resurfacings). She was asymptomatic for 58 months, at which time she developed intermittent groin pain in the left hip and noticed a lump under the scar. This lump was a large fusiform cystic mass which was non-tender to touch and was not associated with any lymphadenopathy. Ultrasound examination confirmed bilateral pseudotumours—partly solid, partly cystic with thickened wall and a large fluid collection. Repeated aspirations of the hip joints have kept the symptoms under control but the patient may need revision surgery in future. Percutaneous biopsy has confirmed typical features of pseudotumour associated with MoM hip resurfacing (see below).

Patient 03 This 47-year-old female patient with bilateral OA secondary to trauma underwent staged hip resurfacings (both Birmingham hip resurfacings) 10 months apart. Following the second hip resurfacing, within 2 months the patient developed bilateral hip pain worse in the first hip resurfacing. An MRI scan of the pelvis revealed the presence of bilateral pseudotumours anterior to the hip joint. There was a fluid collection as well as the presence of thickened synovium. The patient underwent revision surgery on one side with uneventful recovery and complete resolution of symptoms. She is awaiting revision surgery on the other side.

Patient 04 This 65-year-old female patient with bilateral primary OA underwent staged resurfacings (bilateral Birmingham hip resurfacings) 4 months apart. Six months after the implantation of the second resurfacing, she presented with pain and femoral nerve palsy on the first hip resurfacing side. An MRI scan confirmed the presence of pseudotumour on both sides posterior to the hip joint. She underwent staged revision, which relieved her pain, but the nerve palsy did not recover. Subsequently, she developed pain on the contralateral side with inability to bear weight, this was also revised to a conventional THR and the patient made an uneventful recovery.

Materials and methods

The clinical, radiological and investigative findings in four female patients who had osteoarthritis and underwent bilateral MoM resurfacing arthroplasty employing second-generation metal components are summarised in Table 1.

Samples of the pseudotumour, the pseudocapsule and acetabular and femoral pseudomembrane were examined histologically. All samples were fixed in 10% neutral buffered formalin prior to processing and embedding in paraffin wax. Five-micrometer-thick tissue sections were stained with haematoxylin and eosin and examined by light microscopy.

Representative sections of the pseudotumours were analysed by immunohistochemistry using a large panel of antibodies to T lymphocytes (CD3, CD4, CD8), B lymphocytes (CD 20), macrophages (CD14, CD 68), plasma cells (VS38c), dendritic cells (DCSIGN) and HLA-DR to characterise the immunophenotype of inflammatory cells. Details of monoclonal antibodies used are shown in Table 2.

Results

With the exception of a raised ESR and CRP in one patient and a slight eosinophilia (0.5×10^9/l) in another patient, the white cell count, immunological and other investigations were normal. Radiological investigations, including MRI, computed tomography (CT) and ultrasound, showed the presence of a mass located posterolateral to the joint in three of the four patients; the other patient had a mass anterior to the joint, involving the psoas bursa and muscle (Fig. 1). Further imaging revealed a similar mass abnormality around the contralateral hip implant. No reactive lymph nodes were noted on imaging or at operation.

Three of the four patients (four hips, one being revised on both sides) underwent excision of the mass and revision to a conventional total hip replacement. Histology of these masses showed a number of common features. There was extensive (>50%) coagulative necrosis of periprosthetic connective tissue and muscle in which the ghost-like outlines of large numbers of infiltrating macrophages were evident; many of these macrophages appear to lie in small (granuloma-like) aggregates in the necrotic areas (Fig. 2). Focal areas of cystic degeneration were noted in the necrotic areas.

Table 1 Clinical, radiological and investigative findings in bilateral pseudotumour patients

	Age	Gender	Pre-operative diagnosis	Interval between surgeries	Type of implant	Timing of onset of symptoms	Symptoms	FBC, inflammatory markers	Immunological tests[a]	Plain X-rays	Ultrasound	MRI
P01	50	Female	OA secondary to dysplasia	34 months	BHR, conserve+	6 weeks post 2nd surgery	Hip pain, swelling	Normal	Normal	Loose femoral component, femoral neck narrowing	Not done	Cystic mass
P02	64	Female	Primary OA	0 months simultaneous	BHRs	60 months post surgery	Hip pain, swelling	Normal	Normal	No loosening/lysis	Cystic mass	Cystic mass, synovial hypertrophy
P03	47	Female	OA secondary to trauma	10 months	BHRs	2 months post 2nd surgery	Hip pain	Mild Eosinophilia	Normal	No loosening/lysis	Cystic mass	Cystic mass, synovial hypertrophy
P04	65	Female	Primary OA	4 months	BHRs	6 months post 2nd surgery	Hip pain, femoral nerve palsy	Raised ESR, CRP	Normal	Acetabular erosion	Solid mass	Solid mass, synovial hypertrophy

All patients developed symptoms after the second surgery and the symptoms developed in the hip which was resurfaced first.
OA Osteoarthritis, *BHR* Birmingham hip resurfacing (Smith & Nephew), *Conserve* + Conserve Plus (Wright Medical)
[a] Immunological tests included Rheumatoid Factor Test, IgG, IgA and IgM levels, anti-nuclear and anti-centromere antibodies.

Table 2 Monoclonal antibodies employed in this study

Antigen	Mouse monoclonal antibodies	Source
CD3	F7.2.38	Dakopatts (UK)
CD4	NCL-L-CD4-368	Novocastra (UK)
CD8	C8/144B	Dakopatts (UK)
CD20	L26	Dakopatts (UK)
CD14	CD14-223	Novocastra (UK)
CD68	KPI	Dakopatts (UK)
DC SIGN	120507	R&D (UK)
HLA-DR	CR3/43	Dakopatts (UK)
Plasma cell	VS38c	Dakopatts (UK)

Surrounding the necrotic areas, there was a very heavy macrophage infiltrate; this took the form of a pseudotuberculoid granulomatous response with aggregates of macrophages and giant cells forming a mantle around the large areas of necrosis (Fig. 2). There were also small discrete granulomas which appeared to represent a viable counterpart of the collections of non-viable macrophages found in necrotic areas of the lesion. There was a diffuse, focally heavy lymphocytic infiltrate and scattered lymphoid aggregates around the necrotic areas. There were also occasional plasma cells and eosinophil polymorphs in two of three cases (Fig. 3). Scattered tiny black particles, presumed aggregates of metallic wear particles, were seen in necrotic connective tissue, but this was not a prominent feature in any of the cases examined.

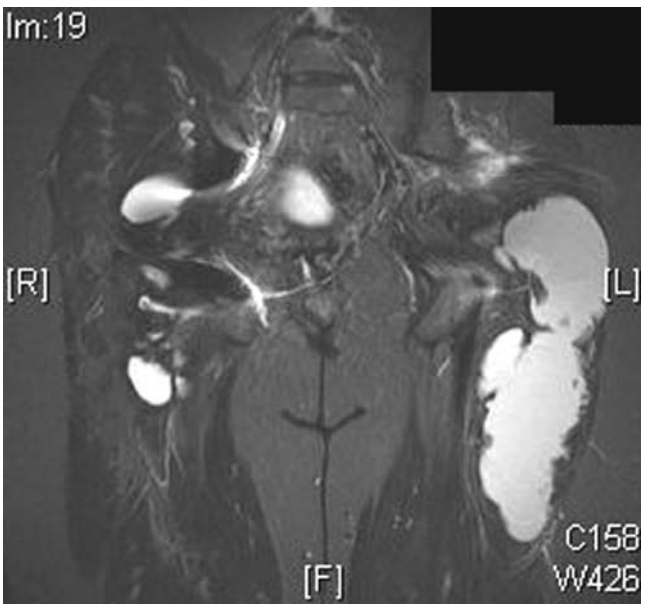

Fig. 1 Coronal T2 STIR-weighted image showing bilateral cystic masses, more extensive on the *left side*. The left-sided mass has a markedly irregular inner wall and extends from the posterior aspect of the hip into the region of the hamstrings, the lateral compartment and the adductors

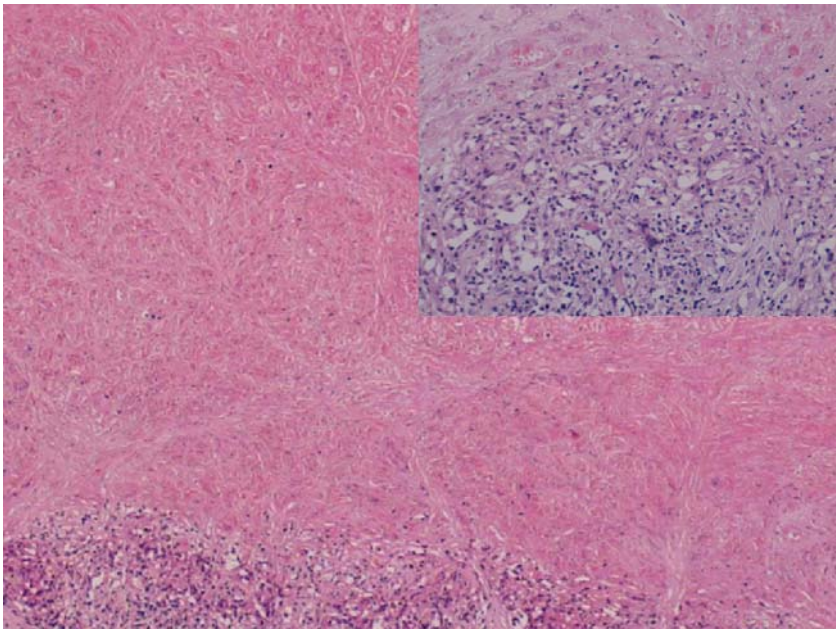

Fig. 2 There is extensive coagulative necrosis which is rimmed by granulomas. The *inset* shows a high power view of the granulomas which contain macrophages and giant cells

No organisms were isolated on microbiological culture of periprosthetic tissues or identified on Ziehl-Neelsen, Grocott, PAS and Giemsa staining. Immunohistochemistry showed prominent HLA-DR expression in both the necrotic and viable (granulomatous) areas of the tumours in which there were numerous CD14+/CD68+ macrophages. Lymphocytes were mainly CD3+/CD4+ T cells (Fig. 4); there were scattered CD20+ B cells, and a few dendritic cells (CD11c+, S100+, DC SIGN+).

Discussion

All four cases in this series presented with an identical history of a large pseudotumoural mass developing after a second bilateral hip resurfacing arthroplasty employing second-generation MoM components. CT, MRI and ultrasound imaging showed that the masses were partly solid and partly cystic. The masses were largely composed of areas of coagulative necrosis in which there were large numbers of macrophages; these areas were surrounded by macrophage and giant cell granulomas as well as T lymphocytes, plasma cells and eosinophil polymorphs. This necrotic granulomatous response and inflammatory infiltrate is typically seen in the context of a delayed hypersensitivity reaction and, taken with the strikingly similar chronological history in all cases of the lesions developing after implantation of a second MoM resurfacing

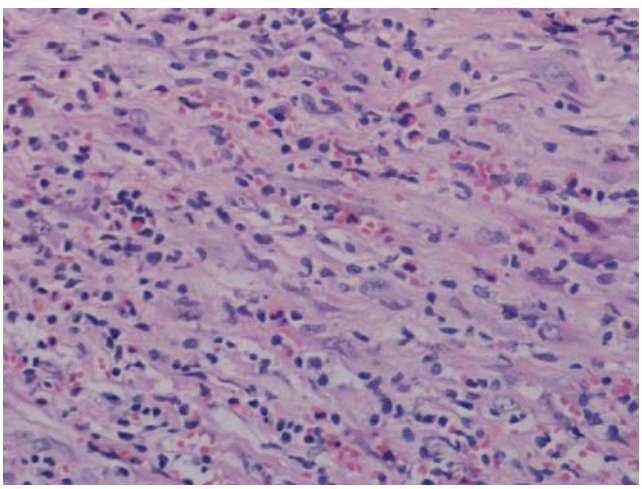

Fig. 3 Eosinophil polymorph infiltrate in inflammatory tissue of the pseudotumour

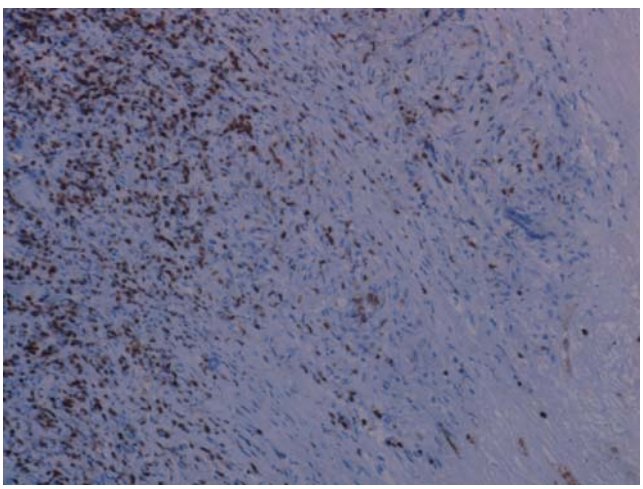

Fig. 4 Immunohistochemical staining around a granuloma adjacent to an area of necrosis of the pseudotumour with monoclonal antibody NCL-L-CD4-368 showing the presence of numerous CD4+ T lymphocytes

arthroplasty, would suggest that a type IV immune response plays a role in their pathogenesis.

A type IV response develops when primed memory T cells, recognise an antigen (often intracellular) which is presented by appropriate HLA-DR-expressing cells such as macrophages; the T cells are then stimulated to undergo blastic transformation, resulting in the release of lymphokines which attract and activate macrophages that may aggregate together to form granulomas [14]. In all the pseudotumours in our series, there were granuloma-like collections of macrophages in areas of coagulative necrosis and well-formed granulomas in the surrounding viable tissue. This pseudotuberculoid macrophage and giant cell reaction and the presence of numerous HLA-DR+/CD14+/CD68+ macrophages in both the viable and necrotic areas of the pseudotumours are consistent with a type IV response. Also typical of a type IV reaction is the fact that all the pseudotumours in our series developed after a second resurfacing arthroplasty, i.e. following previous exposure to MoM implant components. It is upon second exposure to the antigen that the series of events triggered by antigen-sensitised T cells leads to the tissue destruction and inflammation characteristic of a type IV response; it is also in keeping with this response that the pseudotumours were bilateral, developing around both MoM implants.

In addition to lymphocytes and macrophages, scattered plasma cells and eosinophil polymorphs were noted in the pseudotumours. These inflammatory cells have been noted in periprosthetic tissues around failed MoM arthroplasties in previous studies which concluded that this inflammatory infiltrate, particularly the ALVAL component, is associated with a hypersensitivity response to cobalt–chrome particles [5, 9, 10]. Metal wear particle deposition in periprosthetic tissues was not extensive in these studies or in the pseudotumours in our cases; this is not surprising as, although MoM articulations generate huge numbers of cobalt–chromium wear particles, these particles are submicron in size and not visible by light microscopy unless they form tiny aggregates. It has been shown that phagocytosis of these cobalt–chrome particles can induce cytotoxicity and chromosomal damage [10]. Necrosis was a prominent feature of all the pseudotumours in our study. Both necrosis and what some observers have termed “necrobiosis” (on the basis that the connective tissue changes resemble those seen in necrobiosis lipoidica diabeticorum) have previously been noted in periprosthetic tissues around first- and second-generation MoM bearings [6]. It is thus possible that a cytotoxic effect on macrophages which had phagocytosed metal particles may have contributed to the extensive necrosis seen in these pseudotumours.

Skin tests for metal allergy and lymphocyte transformation tests have provided indirect evidence that hypersensitivity to metal alloys may play a role in MoM implant loosening [2, 9, 12]. Morphological and immunophenotypic features of a necrotising granulomatous response, similar to that seen in the MoM-associated pseudotumours, can be seen in the hypersensitivity response to contact metal allergens in cheap jewellery containing nickel and chromate [1, 4]; MoM implants contain only very small amounts of nickel but it should be noted that 13% of patients presenting with contact dermatitis to nickel are sensitised to both nickel and chromium [16, 17]. In this regard, it may be of significance that all of the patients in our series were female and that a recently reported benign psoas mass which formed around a unilateral MoM implant also occurred in a female patient [3]; histologically, this lesion showed tissue necrosis and a heavy lymphocytic infiltrate (but no evidence of a granulomatous response).

The pseudotumours noted in the present series of cases are distinct from those previously reported as granulomatous pseudotumours associated with metal–polymer arthroplasties [7, 8, 15]. These lesions, which are also called aggressive granulomatous lesions or aggressive granulomatosis, have been reported to develop in association with both cemented and cementless hip arthroplasties. They may occur in patients with well-fixed prostheses and may present as soft tissue masses adjacent to the prosthesis. In most cases, these lesions are associated with extensive osteolysis. Histologically, these lesions are distinct from the necrotic granulomatous pseudotumours described in this paper in that they contain a heavy macrophage and giant cell response to particulate debris, particularly ultra-high molecular weight polyethylene particles. Granulomatosis has been reported in both males and females, unlike necrotic granulomatosis pseudotumours, which appear to arise almost exclusively in females [13]. Inflammation in aggressive granulomatosis lesions and in periprosthetic tissues around metal–polymer implants does not contain a prominent lymphocytic infiltrate; scattered T lymphocytes have been noted but these do not express interleukin-2 or transferrin receptors, indicating that these cells are resting T lymphocytes [15]. Extensive tissue necrosis is not generally associated with aggressive granulomatous pseudotumours which are thought to form on the basis of a pronounced foreign body macrophage response to deposited wear particles rather than a hypersensitivity immune response.

The similar chronological history of previous exposure to MoM implant components preceding development of all the pseudotumours in our series, taken with the morphological findings of a granulomatous response and a lymphocytic infiltrate, predominantly T cell in nature, would argue in favour of a cell-mediated immune response playing a role in the formation of these lesions. Clinically, these patients presented with a mass that resembled a neoplasm and caused some diagnostic difficulty. The initial biopsy in some of our cases showed only extensive necrosis which was difficult to

distinguish morphologically with certainty from a necrotic tumour; even in those cases where a pseudotuberculoid granulomatous response could be identified, it was difficult to distinguish this reaction from that seen in other necrotic granulomatous conditions, such as mycobacterial or fungal infections, or Wegener's granulomatosis. Clinicians should be aware that necrotic granulomatous pseudotumours can develop around a MoM resurfacing hip arthroplasty and that these lesions can be bilateral in patients with two MoM implants.

Acknowledgement The authors thank Chris Lowe for typing the manuscript.

Conflict of interest statement We declare that we have no conflict of interest.

References

1. Baldwin L, Hunt JA (2006) Host inflammatory response to NiCr, CoCr, and Ti in a soft tissue implantation model. J Biomed Mater Res 79:574–581
2. Benson MK, Goodwin PG, Brostoff J (1975) Metal sensitivity in patients with joint replacement arthroplasties. Br Med J 4:374–375
3. Boardman DR, Middleton FR, Kavanagh TG (2006) A benign psoas mass following metal-on-metal resurfacing of the hip. J Bone Joint Surg 88B:402–404
4. Casper C, Groth W, Hunzelmann N (2004) Sarcoidal-type allergic contact granuloma: a rare complication of ear piercing. Am J Dermatopathol 26:59–62
5. Davies AP, Willert HG, Campbell PA, Learmonth ID, Case CP (2005) An unusual lymphocytic perivascular infiltration in tissues around contemporary metal-on-metal joint replacements. J Bone Joint Surg 87A:18–27
6. Doorn PF, Mirra JM, Campbell PA, Amstutz HC (1996) Tissue reaction to metal on metal total hip prostheses. Clin Orthop 329 (Suppl):S187–205
7. Eskola A, Santavirta S, Konttinen YT, Hoikka V, Tallroth K, Lindholm TS (1990) Cementless revision of aggressive granulomatous lesions in hip replacements. J Bone Joint Surg B 72B:212–216
8. Griffiths HJ, Burke J, Bonfiglio TA (1987) Granulomatous pseudotumours in total joint replacement. Skeletal Radiol 16:146–52
9. Jacobs JJ, Hallab NJ (2006) Loosening and osteolysis associated with metal-on-metal bearings: a local effect of metal hypersensitivity? J Bone Joint Surg 88A:1171–1172
10. Keegan GM, Learmonth ID, Case CP (2007) Orthopaedic metals and their potential toxicity in the arthroplasty patient. A review of current knowledge and future strategies. J Bone Joint Surg 230B:1307–1308
11. Korovessis P, Petsinis G, Repanti M, Repantis T (2006) Metallosis after contemporary metal-on-metal total hip arthroplasty. Five to nine-year follow-up. J Bone Joint Surg 88A: 1183–1191
12. Nasser S (2007) Orthopedic metal immune hypersensitivity. Orthopedics 8(Suppl):89–91
13. Pandit H, Glyn-Jones S, McLardy-Smith P, Gundle R, Whitwell D, Gibbons CL, Ostlere S, Athanasou N, Gill HS, Murray DW (2008) Pseudotumours associated with metal-on-metal hip resurfacings. J Bone Joint Surg 90B:847–851
14. Roitt I (1991) Essential immunology. Blackwell, Oxford, pp 270–272
15. Santavirta S, Konttinen YT, Bergroth V, Eskola A, Tallroth K, Lindholm TS (1990) Aggressive granulomatous lesions associated with hip arthroplasty. Immunopathological studies. J Bone Joint Surg 72A:252–258
16. Schnuch A, Geier J, Uter W, Frosch PJ, Lehmacher W, Aberer W et al (1997) National rates and regional differences in sensitization to allergens of the standard series. Population-adjusted frequencies of sensitization (PAFS) in 40,000 patients from a multicenter study (IVDK). Contact Dermatitis 37:200–209
17. Schnuch A, Uter W, Geier J, Gefeller O (2002) IDVK study group. Epidemiology of contact allergy: an estimation of morbidity employing the clinical epidemiology and drug-utilization research (CE-DUR) approach. Contact Dermatitis 47:32–39
18. Willert HG, Buchhorn GH, Fayyazi A, Flury R, Windler M, Koster G, Lohmann CH (2005) Metal-on-metal bearings and hypersensitivity in patients with artificial hip joints. A clinical and histomorphological study. J Bone Joint Surg 87A:28–36

Virchows Arch (2008) 453:535–536
DOI 10.1007/s00428-008-0672-z

LETTER TO THE EDITOR

Could the truncated variant of ERBB2 be present in the squamous carcinomas of the cervix?

Carlota Costa · Miguel A. Molina · Teresa Baró · Anabel Aguilar · Pilar De las Heras · Pere Fusté · Gemma Mancebo · Ramón Carreras · Sergi Serrano · Francesc Alameda

Received: 18 June 2008 / Revised: 2 September 2008 / Accepted: 5 September 2008 / Published online: 26 September 2008

Abstract ERBB2, a ligand-less membrane receptor, is frequently overexpressed in a number of human tumors, contributing to uncontrolled cell proliferation. In some cases, gene amplification correlates with protein overexpression and predicts response to trastuzumab. We analyzed the expression of ERBB2 in a group of 40 patients diagnosed with infiltrating squamous cervical carcinomas (ISCC) using a microarray. Immunochemistry was performed using two different antibodies, one against the extramembrane domain and the other one for the intramembrane domain. Ten of the 40 cases included in the study could not be evaluated. Of the 30 remaining biopsies, 13 (42%) showed immunoreactivity only with the antibody against the intramembrane domain. In 5 (16.12%), both intramembrane and extramembrane immunoreactivity was observed, and 12 (40%) were negative for both antibodies. Looking at our results, we propose that, in some ISCC, there is a rupture of the ERBB2 receptor, and this event, with slight genetic amplification, could explain the unfavorable response to trastuzumab observed in some ISCC descript for some authors.

Keywords Cervical lesions · IHC · ERBB2

C. Costa · T. Baró · S. Serrano · F. Alameda
Servei de Patología,
Unitat de Recerca Translacional de Tumors Sòlids—IMAS,
Hospital del Mar, IMAS,
Barcelona, Spain

M. A. Molina
Laboratorio de Oncología, Pangaea Biotech S.A,
USP Instituto Universitario Dexeus,
Barcelona, Spain

A. Aguilar · P. De las Heras · F. Alameda
Centro de Patología, Clinica Corachan,
Barcelona, Spain

P. Fusté · G. Mancebo · R. Carreras
Servei de Ginecologia, Hospital del Mar, IMAS,
Barcelona, Spain

C. Costa (✉)
Laboratori de Citogenètica i Biologia Molecular,
Servei de Patologia, Hospital del Mar,
Pg Marítim, 25–29,
08003 Barcelona, Spain
e-mail: 93710@imas.imim.es

ERBB2, a ligand-less membrane receptor, is frequently overexpressed in a number of human tumors, contributing to uncontrolled cell proliferation. It is encoded by the *ERBB2* genes, located at 17q11–2q12. The ERBB2 status is routinely determined in breast cancer patients, either by immunohistochemistry—with antibodies against the extramembrane domain of the protein—or fluorescence in situ hybridization. Gene amplification, present in 25% of the patients, correlates with protein overexpression and predicts a good response to the therapeutic monoclonal antibody trastuzumab (Herceptin®), which binds to p185ERBB-2 at the cell surface [1].

Although the number of infiltrating squamous cervical carcinomas (ISCC) with ERBB2 amplification is low, three or four copies of the gene have been reported in some patients [2–3]. With respect to protein expression, the percentage of tumors with immunoexpression increases with the grade of the dysplasia with the highest values in the ISCC group [4].

We analyzed the expression of ERBB2 in a group of 40 patients diagnosed with ISCC using a microarray that included two cylinders of 1 mm per case. Immunochemistry was performed using a semiautomated system (TechMate 500 Dako Corporation, Golstroup Denmark) after antigen

retrieval at 110°C for 1 min in an autoclave. The method involved the incubation with an anti-ERBB2 antibody using the dextran peroxidase technique (Dako Envision, Glostrup, Denmark) and an automated system (Ventana, Tucson, AZ, USA). Antibodies against the extramembrane (anti-ERBB2 Dako, Glostrup, Denmark) and the intramembrane domain of ERBB2 (anti-ERBB2 CB11 Zymed Lab, San Francisco, CA, USA) were used. Two independent observers scored each biopsy.

Ten of the 40 cases included in the study could not be evaluated. Of the 30 remaining biopsies, 13 (42%) showed immunoreactivity only when using the antibody against the intramembrane domain. In 5 (16.12%), both intramembrane and extramembrane immunoreactivity was observed, and 12 (40%) were negative for both antibodies.

The ERBB2 receptor undergoes a proteolytic shedding of its ectodomain that can be detected in the serum of advanced breast cancer patients. In addition, this process leaves in the cell membrane an NH_2-terminally truncated fragment, p95ERBB2, which has in vitro kinase activity and is probably constitutively active. This fragment cannot be detected using antibodies against the ERBB2 extramembrane domain, and trastuzumab cannot bind to it. In breast tumors, the presence of p95ERBB2 correlates with a worse prognosis [1] and a poor response to treatment with Herceptin® [5].

Rosty et al. [3] postulated an unfavorable response for cases of SCC to treatment with anti-ERBB2 due to the slight genic amplification. Looking at the results obtained in this study and keeping in mind the writings of other authors, we could propose that the rupture of the receptor, as well as the slight genetic amplification, could explain the unfavorable response to trastuzumab observed in ISCC.

Conflict of interest statement We declare that we have no conflict of interest.

References

1. Saez R, Molina MA, Ramsey EE et al (2006) p95HER-2 predicts worse outcome in patients with HER-2-positive breast cancer. Clin Cancer Res 12:424–431
2. Zhang A, Manér S, Betz R et al (2002) Genetic alterations in cervical carcinomas: frequent low-level amplifications of oncogenes are associated with human papillomavirus infection. Int J Cancer 101:427–433
3. Rosty C, Couturier J, Vincent-Salomon A et al (2004) Overexpression/amplification of HER-2/neu is uncommon in invasive carcinoma of the uterine cervix. Int J Gynecol Pathol 23:13–17
4. Carreras R, Alameda F, Mancebo G et al (2007) Study of Ki-67, cerb-B2 and cyclin D-1 expression in mild dysplasias, severe dysplasias and squamous cell carcinoma of the cervix. Histol Histopathol 22:587–592
5. Scaltriti M, Rojo F, Ocaña A et al (2007) Expression of p95HER2, a truncated form of the HER2 receptor, and response to anti-HER2 therapies in breast cancer. J Natl Cancer Inst 99:628–638

Virchows Arch (2008) 453:537–543
DOI 10.1007/s00428-008-0688-4

ORIGINAL ARTICLE

Proficiency testing of immunohistochemical biomarker assays in breast cancer

Reinhard von Wasielewski · Svenja Hasselmann · Josef Rüschoff · Annette Fisseler-Eckhoff · Hans Kreipe

Received: 30 June 2008 / Revised: 2 September 2008 / Accepted: 7 October 2008 / Published online: 29 October 2008

Abstract Steroid hormone receptor expression and HER2 status have become an integral part of histopathologic characterization of breast cancer and corresponding biomarker assays have gained important prognostic and predictive impact. Because testing inaccuracy could provide a major hazard to modern breast cancer therapy, a laboratory proficiency testing program has been implemented in Germany using tissue microarrays (TMAs). In four consecutive annual trials with 142 laboratories participating on average per trial, estrogen receptor (ER), progesterone receptor (PR), and human epidermal growth factor receptor 2 (Her2) were determined immunohistochemically by participating laboratories followed by central review of all immunostains. Performance strongly depended on the ambiguity of expression of the target molecule in the test samples. In clearly positive (Allred score 7–8; Her2 3+) or negative tissue samples, the majority of participants (86%) achieved concordance rates exceeding 85%. By contrast, low expression of ER or PR (Allred score 3–4) as well as Her2 status 2+ led to considerable lower concordance rates ranging from 41% (Her2 2+) to 75% (PR). Poor reproducibility was predominantly due to inadequate laboratory performance whereas interobserver agreement (weighted kappa statistics) usually was high (>0.81). Laboratories that participated in more than one of the four subsequent trials (n=110) showed a highly significant improvement of performance. In conclusion, a TMA-based proficiency testing of biomarkers in breast cancer has been implemented in Germany over a 5-year period and revealed reliable assessment of unambiguously positive and negative test samples. Low-expressing tumor samples with regard to steroid hormone receptor expression and Her2 status 2+ led to inaccurate evaluations by up to 59% of participants. Regularly participating laboratories showed a significant improvement of performance.

Keywords Steroid receptor · HER2 · Immunohistochemistry · Quality assurance

Reinhard von Wasielewski and Svenja Hasselmann contributed equally to this work.

J. Rüschoff
Institut für Pathologie, Städtisches Klinikum Kassel, Kassel, Germany

A. Fisseler-Eckhoff
Institut für Pathologie, Horst-Schmidt Kliniken, Wiesbaden, Germany

R. v. Wasielewski · S. Hasselmann · H. Kreipe (✉)
Institute of Pathology, Medizinische Hochschule Hannover, Carl Neuberg Strasse 1, 30625 Hannover, Germany
e-mail: Kreipe.Hans@mh-hannover.de

Introduction

Steroid hormone receptor expression is one of the most important biomarkers in breast cancer, which provides the basis for the selection of alternative therapeutic strategies in adjuvant breast cancer treatment [1]. In recent years, the human epidermal growth factor receptor 2 (Her2) has gained a similar impact as prognostic and predictive marker which is meanwhile evaluated on a regular basis and influences therapeutic decisions in the management of breast cancer patients [2, 3]. For several reasons both biomarkers usually are determined by pathologists applying tissue sections and immunohistochemistry (IHC). In particular, differentiation of invasive cancer cells in heterogeneous tissue encompassing normal epithelial cells, stroma, and potentially in situ lesions or necrosis requires microscopic correlation. Immunohistochemical biomarker assays, however, do not represent

a simple extension of traditional histopathologic evaluation because they include quantitative assessments whereas the unquestioned strength of histopathology lies in qualitative analysis. In order to cope with the new challenge of target molecule detection in the age of personalized medicine, pathologists have to prove that quantitative biomarker assays done by them on breast cancer tissue are accurate and reliable.

Testing inaccuracy remains a major issue with both IHC and fluorescence in situ hybridization (FISH) and it has been estimated that approximately 20% of current Her2 testing may be false [4]. There is widespread concern that inaccuracy in detection methods and interpretation may lead to an unacceptably high error rate in determining the true hormone receptor status [5]. Comparison of centrally versus locally assessed estrogen receptor (ER) and progesterone receptor (PR) revealed divergent results in a substantial proportion of patients [6]. Obviously, there is a great need to standardize immunohistochemical biomarker assays to further ensure that similar results are obtained by different institutions. External proficiency testing has been proposed as one potential instrument to enable accurate biomarker determination in a noncentralized approach [7, 8]. Yet the most effective setting for external proficiency testing has not been determined. Open issues refer to selection of material to be distributed, adequate number of challenges (cases), type of challenge (cell lines, cancer tissue), and mode of evaluation.

In this report, the implementation of a nationwide external proficiency testing of ER, PR, and Her2 assessment during five consecutive years from 2002 to 2006 in Germany is described. Unlike previously reported trials [7, 8], tissue microarrays (TMAs) were applied [9, 10] and all immunohistochemical stains done by participants underwent central review in order to enable assessment of interlaboratory and interobserver concordance.

Materials and methods

During the years 2002–2006, four TMAs were generated and distributed to participating laboratories on demand. Tissue cores from routine surgical pathology samples retrieved from the archives of three institutes of pathology in Germany (Hannover, Kassel, Wiesbaden) were used for the construction of TMA. Cases were retrieved from the archives with particular emphasis on low steroid hormone receptor expression (Allred Score 3–4) [11] and equivocal positivity for Her2 (2+). The Allred score combines three grades of staining intensity with five percentage categories (proportion of labeled cells). Thus, a sum results with a maximum value of 8 and a threshold for positivity of ≥3 (e.g., intermediate staining intensity of 0–1% cells leads to 2 points (pts) plus 1 pt=3) [11]. Besides equivocal cases, clearly positive or negative samples were included. Only samples that received identical testing in all three laboratories mentioned above entered the final trial. The methods used by the reference laboratories are described in Table 1. From the 2003 to the 2006 run, all test cases with Her2 status of 2+ and 3+ underwent fluorescence in situ hybridization. Among the 3+ tissue samples, 100% revealed amplification of Her2. Among the 2+ tissue samples, 33–56% were polysome and up to 14% (2004, 2006) displayed amplified copy numbers of the Her2 gene. Between 20 and 24 samples were included in the TMAs which were generated exactly as

Table 1 Immunohistochemical methods applied by the reference laboratories

Reference laboratory	Methods	ER	PR	Her2
1	Retrieval method	Pressure cooker at 125°C, 5 min, Citrat buffer pH 6	Pressure cooker at 125°C, 5 min, Citrat buffer pH 6	Citrat buffer pH 6, water bath 95–99°C, 40 min
	Primary antibody	Clone 1D5 und ER-2-123	Clone PGR1294	Rabbit antihuman Her2 protein
	Detection system	PharmDX, DAKO	PharmDX, DAKO	Hercep-test DAKO
	Automat	DAKO Autostainer Plus	DAKO Autostainer Plus	DAKO Autostainer Plus
2	Retrieval method	Specific heat-based antigen retrieval	Specific heat-based antigen retrieval	Specific heat-based antigen retrieval
	Primary antibody	Clone 6F11	Clone PR312	Clone SP3
	Detection system	XT UltraView DAB	XT UltraView DAB	UltraView Universal DAB
	Automat	Ventana Benchmark XT	Ventana Benchmark XT	Ventana Benchmark XT
3	Retrieval method	Pressure cooker at 125°C, 3 min, Citrat buffer pH 6	Pressure cooker at 125°C, 3 min, Citrat buffer pH 6	Pressure cooker at 125°C, 3 min, Citrat buffer pH 6
	Primary antibody	Clone SP1	Clone PR636	Polyclonal rabbit antibody (NCL-cerbB-2p)
	Detection system	ZytoChem Plus HRP Polymer Kit (mouse/rabbit)	ZytoChem Plus HRP Polymer Kit (mouse/rabbit)	ZytoChem Plus HRP Polymer Kit (mouse/rabbit)
	Automat	Manual	Manual	Manual

described [9]. Pathology departments volunteering to participate in external proficiency testing could order up to three slides which were freshly cut and shipped unstained. Within 2 months, immunohistochemical stainings had to be performed and a protocol of the assessment as well as the stained slides had to be returned to the organizers of the trial. Participants were free to perform only one of the three tests or all of them. Unstained slides could be ordered during a 10-month-long period during which the trial was open for participation.

The composition of the TMAs used as test material for all three biomarkers from 2003 to 2006 is depicted in Table 2.

Evaluation

For ER and PR, the Allred score was recorded by the participants and reviewers. For statistical analysis, this score was further simplified likewise with previous studies into four categories: negative cases (Allred 0, 2) or low- (Allred 3, 4), medium- (Allred 5, 6), and high-expressing cases (Allred 7, 8). All scorings and statistics shown are based on this four-tier classification. Each tissue spot was scored. When the expected staining result was achieved or nearly achieved by the participating laboratory, a score of three points was given. In highly steroid hormone receptor positive cases, participants' staining results corresponding to Allred values 7 or 8 were scored 3 pts; Allred values 5 or 6 were scored 2 pts; Allred values 3 or 4 were scored 1 pt; and a negative result was scored 0 points. The scoring system applied for Her2 discriminated between 0 (no staining or membrane staining in less than 10% of invasive tumor cells), 1+ (faint and partial membrane staining in more than 10% of invasive tumor cells), 2+ (weak to moderate complete membrane staining in more than 10% of invasive tumor cells), and 3+ (strong complete membrane staining in more than 10% of invasive tumor cells) [2]. According to steroid hormone receptor evaluation, participants' staining results were reevaluated and accuracy was graded in a 0–3 point system. In case of a Her2 3+ challenge, 3+ was scored with 3 pts, 2+ with 2 pts, 1+ and 0 with 0 point, respectively. With regard to equivocal Her2 cases (2+), 3+ was scored with 1 pt, 2+ with 3 pts, 1+ and 0 with zero points, respectively. False-positive or -negative results were graded as 0 point with regard to steroid hormone receptors as well as Her2. Lost tissue spots (floaters) or tissue fields with obvious technical problems were excluded from evaluation and did not influence the results. According to this procedure, for each participant and marker tested, the maximum sum of achievable points for a specific slide was determined (e.g., 22 tissue spots, one floater, one spot at the edge wiped off: 20 evaluable spots, maximum point score $3\times20=60=100\%$). Based on this information, the achieved sum of points per slide could be transferred into a percentage score. A result of 80% or more was regarded as successful participation (0–59% poor; 60–69% unsatisfactory; 70–79% moderate; 80–89% good; 90–100% excellent). The results are shown as overall performance per marker tested. Moreover, we subdivided the analysis into the different groups of expected results (low-, medium-, and high-expressing cases) to enable a more profound insight into staining capabilities.

Interobserver agreement was assessed using kappa statistic, which takes into account the agreement expected solely on the basis of chance and can be used if more than two categories are classified. Total agreement is indicated by a value of 1.0, but agreement by chance only results in a 0 value.

Although there is no generally accepted value of kappa in the literature that indicates sufficient (i.e., good) agreement, we applied the following guidelines: kappa$<$0.4 represents poor-to-fair agreement; 0.4–0.6 moderate agreement; 0.6–0.8 substantial agreement; and $>$0.8 almost perfect agreement. To measure the grade of agreement, a weighted kappa statistic was performed using the statistic software package SAS, version 8.0.

A standardized questionnaire with routing questions about protocol procedures as well as the participants' personal opinion about the program, problems, and potential improvements was included.

Results

From about 400 laboratories of pathology in Germany, an average of 142 participated in the four proficiency tests

Table 2 Composition of tissue microarrays (percent of tissue spots in TMA, %)

	ER low	ER medium	ER high	PR low	PR medium	PR high	Her2 0/1+	Her2 2+	Her2 3+
2003	26	33	19	31	19	17	52	7	40
2004	26	26	26	11	21	37	36	36	28
2005	14	29	43	19	33	33	33	33	33
2006	27	23	27	27	23	27	36	32	32

ER- and PR-negative samples are not included and will add to 100%

which took place between 2002 and 2006 (Table 1). A total of 12,411 immunohistochemical ER stains underwent central review. In case of PR and Her2, the number was a little bit smaller. A comparison between central review and evaluation by participants revealed an excellent concordance with very low interobserver variability. Interobserver agreement was calculated for 86 participants. Weighted kappa statistics showed a very good overall concordance between participating pathologist and reviewer for all three markers tested: ER 0.84, PR 0.81, and HER2 0.86. These results did not differ from previous trials and did not vary between the different expectancy groups of low-, medium-, and high-expressing cases (detailed data not shown). Therefore, the interlaboratory differences in staining efficiency were the major cause of discordant results. Consequently, the quality of staining and not the reading emerged as the decisive item to be controlled by external proficiency testing. In order to give participants information on the performance of their immunohistochemical detection methods, all analyses were based on the results of the central review of immunostains.

The unequivocally positive samples were detected with high fidelity by participants. Allred scores 7 and 8 were reproduced by 86% of participating laboratories with regard to ER ad PR. More than 92% of participating laboratories achieved correct results with regard to Her2 3+ cases. By contrast, the equivocal cases of Her2 were stained with considerable variation and only 41% of participants scored correctly. Low-expressing ER and PR samples were correctly identified by 61% and 75%, respectively.

The detailed results of all three markers, subdivided into low-, medium-, and high-expressing cases, are depicted in Figs. 1, 2, and 3. Furthermore, the figures display the results for the runs 2002–2003, 2004, 2005, and 2006 sorted by expressing groups. Whereas during the first two runs the rate of poor performers (<60%) was as high as 40% in the group of low-expressing ER cases, this rate has declined in 2005 and 2006. A similar effect could be observed for PR and HER2 2+ cases. With regard to ER and PR, the number of laboratories showing good and excellent results increased from 2002 to 2006. For HER2, false-positivity rates as high as during the first runs (2002, 2004) were reduced in 2005 and disappeared in 2006. The 0/1+ category and the 3+ category in HER2 were correctly diagnosed by the majority of participating laboratories (Figs. 1, 2, and 3.)

Duplicate or triplicate participation in the four subsequent trials was performed by 110 laboratories. A comparison was made based on the percentage score per marker for all cases (overall performance) and for the difficult cases encompassing low ER- and PR-expressing cases and the HER2 2+ category. With regard to ER (all cases), participants obtained significantly better results in the second trial when compared to what they had achieved

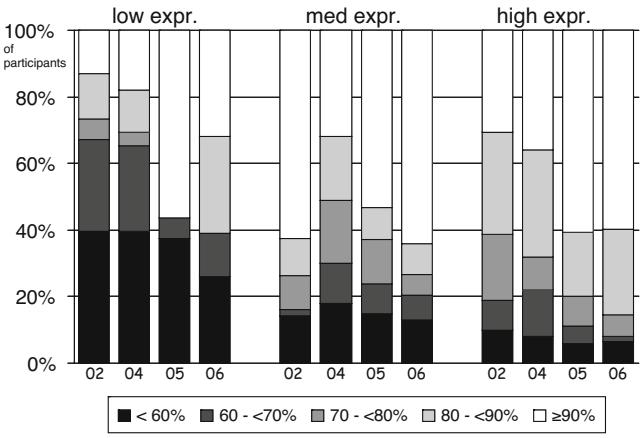

Fig. 1 Results of estrogen receptor staining in four consecutive trials from 2002 to 2006 (*vertical columns*), subdivided according to the level of expression into low, medium, and highly immunopositive cases. The proportion of participants (%) achieving different levels of concordance with expected results is indicated on the *left*. Each *column* encompasses 100% of participants. The *black segments* of the column indicates the proportion of participants with poor concordance (<60%) whereas the *white segment* represents the proportion of participants with good performance (≥90%). Intermediate concordance results (60–<90%) are indicated by different *gray tones* in order to illustrate the difficulty and consequences of setting different thresholds for successful participation. Negative cases had concordance rates of >95% and are not depicted. In all runs from 2002 to 2003, medium- and high-expressing cases had similar results with regards to the good-performance group (>90%, *white segment*) whereas the proportion of participants with poor concordance rates (<60%, *black segments*) were always lowest in the high-expressing group

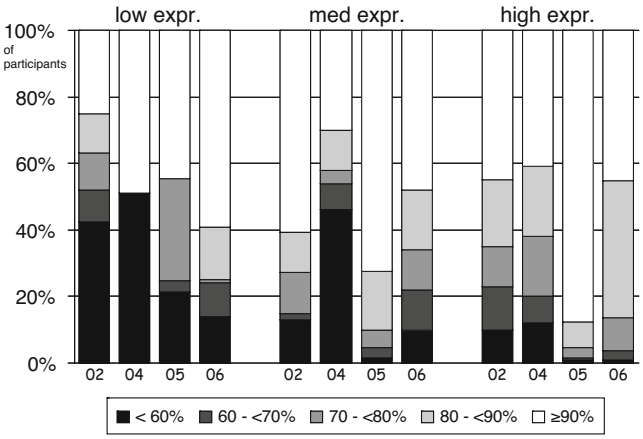

Fig. 2 Results of progesterone receptor staining in four consecutive trials from 2003 to 2006 (*vertical columns*), subdivided according to the level of expression into low, medium, and highly immunopositive cases. The proportion of participants (%) achieving different levels of concordance with expected results is indicated on the *left*. Each *column* encompasses 100% of participants. The *black segments* of the column indicates the proportion of participants with poor concordance (<60%) whereas the *white segment* represents the proportion of participants with good performance (≥90%). Intermediate concordance results (60–<90%) are indicated by different *gray tones* in order to illustrate the difficulty and consequences of setting different thresholds for successful participation. Negative cases had concordance rates of >95% and are not depicted

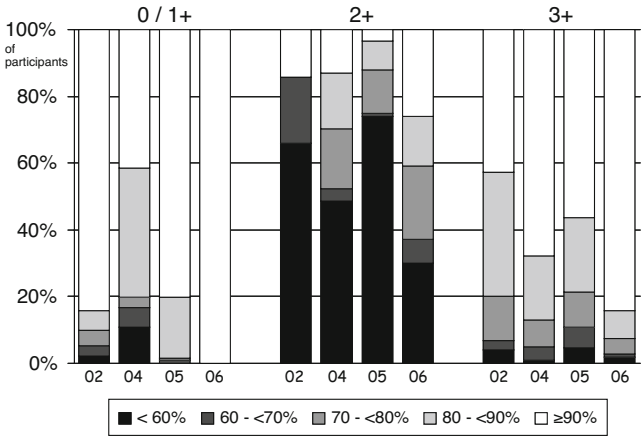

Fig. 3 Results of Her2 staining in four consecutive trials from 2003 to 2006 (*vertical columns*), subdivided according to the level of expression into negative (0, 1+), equivocal (2+), and positive (3+) cases. The proportion of participants (%) achieving different levels of concordance with expected results is indicated on the *left*. Each *column* encompasses 100% of participants. The *black segments* of the column indicates the proportion of participants with poor concordance (<60%) whereas the *white segment* represents the proportion of participants with good performance (≥90%). Intermediate concordance results (60–<90%) are indicated by different *gray tones* in order to illustrate the difficulty and consequences of setting different thresholds for successful participation

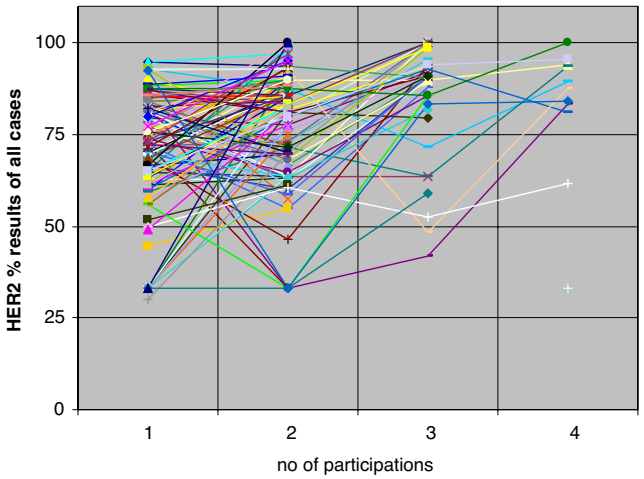

Fig. 4 Percentages of maximum concordance with expected results achieved by individual laboratories in up to four consecutive participations over time. Regardless of the year in which the first participation took place, a duplicate or triplicate participation led to higher concordance scores over time as can be seen from most of the *ascending lines*, each of which represents one single laboratory. Results are shown for HER2 but were similar for ER and PR

before in their first trial (p=0.008; Wilcoxon test). An improvement of performance could also be seen in case of triplicate participation (p<0.001; Friedman test). This improvement could be observed irrespective of which of the four subsequent trials were passed by the laboratories. Hence, the improvement appeared not to be due to different levels of difficulty between the subsequent trials. If low-expressing cases only were included in the analysis, the improvement of the percentage score was 10.8% on average. There was a significant improvement again with regard to duplicate (p=0.008) as well as triplicate participation (p< 0.001). When PR is considered, there was a significant improvement of 7.2% from the first to the second run and to the third run (both p<0.001). With regard to the low-expressing PR cases, the effect was even more pronounced with an improvement of 33.1% (p=0.001 and p=0.003, respectively).

Similarly, the results for HER2 improved when laboratories participated in duplicate or triplicate. When all challenges are considered, a mean improvement of 10.2% was seen in case of duplicate and triplicate participation (p<0.001 and p< 0.001, respectively; Fig. 4). As has been seen with steroid hormone receptors, the improvement of performance with duplicate or triplicate participation became even more obvious when equivocal challenges were taken into consideration. In the 2+ subgroup, there was an increase of 24.9% (p=0.004; one versus two runs) and also when three runs were performed (p<0.001).

Discussion

Breast cancer in recent years has functioned as a pioneer tumor, setting the stage for a new era of diagnostic and therapy in oncology. Steroid hormone receptors and Her2 provided the first examples for targeted therapy and marked the beginning of the age of personalized medicine. There are different modes of determining potential target molecules in cancers. Besides tissue-extract-based quantitative protein and mRNA assays, there are in situ methods which apply IHC or FISH. In most countries, the latter methods are predominantly used to assess target molecules in breast cancer [12]. However, there are a number of caveats and open issues which have to be kept in mind when in situ techniques are applied. First, the demand for quantification has to be met and thresholds for categorization have to be defined [13, 14]. The biological significance and justification of these thresholds is particularly unclear in a gray zone between unequivocal positive and negative cases [1, 4, 15]. Whether this gray zone could be diminished if the corresponding assays were more reliable is a matter of debate [15]. Second, the issue of reproducibility and reliability of these assays emerges. The findings of a number of studies indicate that significant interlaboratory variability for steroid hormone receptor and Her2 testing does occur [6, 15, 16]. Despite these potential hazards, IHC offers a number of decisive advantages like correlation to number of tumor cells and their viability as well as to admixture of normal, noninvasive, and stromal cells. In addition, alternative extract-based methods did not yet prove a higher

degree of reproducibility when applied on a similarly large scale like IHC.

Apart from these considerations, pathologists who apply IHC and clinicians who rely on the results of IHC assays need information on how secure with regard to sensitivity and specificity the method in individual use really is. External proficiency testing is a useful tool to provide this information [4] and national external quality assessment schemes for immunohistochemistry like NEQUAS-ICC have been founded [7, 8]. Whereas the potential benefit of quality assurance trials is unquestioned, there are many open questions with regard to composition of test samples and evaluation. In this report, we have described the German approach and the experiences derived thereof. In order to increase the number of challenges and to diminish the variability of individual tumors or modes of fixation, we have applied TMA with tissues from three different institutions. The usefulness of TMA in interlaboratory trials has been demonstrated before [9, 10, 17]. The compliance of participants with the TMA was very good and reading of the immunostained spots was not a cause of trouble. As has been described previously, the overall concordance was high in unequivocally positive or negative cases [8]. Discordant results with a high percentage of false-negative scorings were encountered in the low steroid hormone receptor positive group and Her2 2+ cases. In each of the four trials, these kinds of borderline cases were enriched in the TMA in order to provide effectively discriminatory challenges [17]. This overrepresentation of difficult cases led to a higher proportion of underperforming laboratories than would have been expected with a more representative composition of challenges in the TMA. Because no generally accepted benchmark criteria are available which could be adapted to the level of difficulty and arbitrary bench marks have to be set, the results are prone to misunderstanding when communicated to nonpathologists, e.g., clinicians. On the other hand, the TMAs enriched for difficult borderline cases will more effectively alert pathologists to potential shortcomings in their immunohistochemistry laboratories. Indeed, it became evident from the analysis of laboratories participating in duplicate or triplicate that the performance significantly improved. These findings demonstrate that, besides testing, external proficiency trials exert a training function and improve overall performance [17]. Furthermore, participants benefited from the information derived from the questionnaires as it became evident which steps of the immunohistochemical staining procedure are particularly crucial. For example, heat pretreatment for antigen retrieval was found to be very heterogeneous with microwaving being overrepresented in the low-performance group. Again, these differences became effectively visible when the difficult challenges were considered. The obvious relevance of antigen retrieval is particularly suited to demonstrate a dilemma which proficiency testing programs in pathology are facing. Whereas standardized material, e.g., cell lines, with known content of the target protein in question would be ideal to evaluate and compare sensitivity of detection methods, diagnostic routine pathology is usually challenged with heterogeneous tissues modified by fixation and embedding. Thus, fixed tissue from resection specimens suffers from the drawback of not being standardized but as test material it covers more and relevant steps of the diagnostic process than would be possible with cell lines.

In conclusion, external proficiency testing as described here fulfills two different functions which have to be considered with regard to selection of challenges and composition of test samples in the TMA as well as with regard to the terms of evaluation. First, it provides information about the current status of laboratory performance. This information should be based on a representative selection of cases resembling everyday practice. Second, it enables training and improvement of laboratory performance. In order to achieve the latter positive effect, the challenges within the TMA have to be enriched for difficult and borderline cases with low steroid hormone receptor expression or Her2 2+ status. Because both aims antagonize each other, TMA for interlaboratory trials should be composed of two sets of cases which should be evaluated and communicated separately. Accordingly, in future trials, there should be a training set and a test set of challenges. Benchmarks to categorize the results on the latter type of challenges need to be developed.

Acknowledgements The authors thank the numerous participants of the trials 2002–2006 for helpful and critical comments given in order to improve quality assurance trials in Germany.

Conflict of interest statement R. von Wasielweski is founder and partial owner of the "Multiblock GmbH" which served as a logistics center in the 2006 trial.

References

1. Goldhirsch A, Glick JH, Gelber RD et al (2005) Meeting highlights: international expert consensus on the primary therapy of early breast cancer 2005. Ann Oncol 16:1569–1583
2. Slamon DJ, Leyland-Jones B, Shak S et al (2001) Use of chemotherapy plus a monoclonal antibody against HER2 for metastatic breast cancer that overexpresses HER2. N Engl J Med 344:783–792
3. Carlson RW, Moench SJ, Hammond ME et al (2006) NCCN HER2 testing in Breast Cancer Task Force. HER2 testing in breast cancer: NCCN Task Force report and recommendations. J Natl Compr Canc Netw Suppl 3:S1–S22
4. Wolff AC, Hammond ME, Schwartz JN et al (2007) American Society of Clinical Oncology; College of America Pathologists. American Society of Clinical Oncology/College of American Pathologists guideline recommendations for human epidermal growth factor receptor 2 testing in breast cancer. J Clin Oncol 25:118–145

5. Ross JS, Symmans WF, Pusztai L et al (2007) Standardizing slide-based assays in breast cancer: hormone receptors, HER2, and sentinel lymph nodes. Clin Cancer Res 2007, 13:2831–2835
6. Viale G, Regan MM, Maiorano E et al (2007) Prognostic and predictive value of centrally reviewed expression of estrogen and progesterone receptors in a randomized trial comparing letrozole and tamoxifen adjuvant therapy for postmenopausal early breast cancer: BIG 1-98. J Clin Oncol 25:3846–3852
7. Rhodes A, Jasani B, Barnes DM et al (2000) Reliability of immunohistochemical demonstration of oestrogen receptors in routine practice: interlaboratory variance in the sensitivity of detection and evaluation of scoring systems. J Clin Pathol 53:125–130
8. Wells CA, Sloane JP, Coleman D et al (2004) Consistency of staining and reporting of oestrogen receptor immunocytochemistry within the European Union—an interlaboratory study. Virchows Arch 445:119–128
9. von Wasielewski R, Mengel M, Wiese B et al (2002) Tissue array technology for testing interlaboratory and interobserver reproducibility of immunohistochemical estrogen receptor analysis in a large multicenter trial. Am J Clin Pathol 118:675–682
10. Hsu FD, Nielsen TO, Alkushi A et al (2002) Tissue microarrays are an effective quality assurance tool for diagnostic immunohistochemistry. Mod Pathol 15:1374–1380
11. Allred DC, Harvey JM, Berardo M et al (1998) Prognostic and predictive factors in breast cancer by immunohistochemical analysis. Mod Pathol 11:155–168
12. Harvey JM, Clark GM, Osborne CK et al (1999) Estrogen receptor status by immunohistochemistry is superior to the ligand-binding assay for predicting response to adjuvant endocrine therapy in breast cancer. J Clin Oncol 17:1474–1481
13. Taylor CR, Levenson RM (2006) Quantification of immunohistochemistry—issues concerning methods, utility and semiquantitative assessment II. Histopathology 49:411–424
14. Swanson PE, Schmidt RA (2005) Beneath the surface of the mud, part II: the dichotomization of continuous biologic variables by maximizing immunohistochemical method sensitivity. Am J Clin Pathol 123:9–12
15. Diaz LK, Sneige N (2005) Estrogen receptor analysis for breast cancer: current issues and keys to increasing testing accuracy. Adv Anat Pathol 12:10–19
16. Layfield LJ, Goldstein N, Perkinson KR et al (2003) Interlaboratory variation in results from immunohistochemical assessment of estrogen receptor status. Breast J 9:257–259
17. Fitzgibbons PL, Murphy DA, Dorfman DM et al (2006) Interlaboratory comparison of immunohistochemical testing for HER2: results of the 2004 and 2005 College of American Pathologists HER2 Immunohistochemistry Tissue Microarray Survey. Arch Pathol Lab Med 130:1440–1445

Virchows Arch (2008) 453:545–555
DOI 10.1007/s00428-008-0687-5

ORIGINAL ARTICLE

Ancillary testing of liquid-based cytology specimens for identification of patients at high risk of cervical cancer

Takuma Fujii · Miyuki Saito · Takashi Iwata · Nobumaru Hirao · Hiroshi Nishio · Akiko Ohno · Katsumi Tsukazaki · Makio Mukai · Kaori Kameyama · Daisuke Aoki

Received: 22 July 2008 / Revised: 10 September 2008 / Accepted: 2 October 2008 / Published online: 21 October 2008

Abstract Integration of human papillomavirus DNAs into the host genome is crucial to the development of cervical cancer. Overexpression of the P16 protein has been reported in cervical intraepithelial neoplasia (CIN) as well as cervical cancer. Such molecular biomarkers have been utilized for ancillary testing of liquid-based cytology specimens; however, their clinical application remains controversial. To detect CIN 2 or more advanced lesions, 153 liquid-based cytology (LBC) specimens were investigated to determine the physical status of the human papillomavirus (HPV) DNA by in situ hybridization (ISH) and to detect overexpression of the P16 protein by immunocytochemistry combined with HPV genotyping by polymerase chain reaction. The combination of ISH, P16 immunocytochemistry, and LBC showed high sensitivity (89.3%) as well as high specificity (92.6%). We confirmed the usefulness of P16 immunocytochemistry combined with ISH and HPV genotyping as ancillary molecular–biological tests of LBC specimens for identifying patients at high risk of cervical cancer.

Keywords In situ hybridization · Integration · P16 · Liquid-based cytology · Human papillomavirus · Cervical cancer screening

T. Fujii (✉) · M. Saito · T. Iwata · N. Hirao · H. Nishio · A. Ohno · K. Tsukazaki · D. Aoki
Department of Obstetrics and Gynecology, Keio University, School of Medicine,
35 Shinanomachi, Shinjuku-ku, Tokyo 160-8582, Japan
e-mail: fujiit@sc.itc.keio.ac.jp

M. Mukai · K. Kameyama
Department of Pathology, Keio University, School of Medicine,
35 Shinanomachi, Shinjuku-ku,
Tokyo 160-8582, Japan

Introduction

Cervical cancer is the second most frequently encountered cancer in women around the world [1]. Human papillomavirus (HPV) DNA is found in more than 90% of cervical cancers [2, 3], and a recent review article described the molecular interactions between the viral and host proteins [4]. Integration of the HPV genome into the host cells is thought to be one of the causes of cancer progression. Integration of the viral DNA into the host genome disrupts some early genes, such as the E1 and E2 open reading frames (ORFs), while others, such as the E6 and E7 ORFs, remain intact. The E6 protein binds to and degrades the tumor suppressor P53 protein via ubiquitin pathways [5]. The E7 protein binds to the tumor suppressor Rb protein. Duensing et al. [6] reported that the E7 protein is capable of causing aneuploidy in stratified squamous cells. E7 protein plays an important role in the onset of dysplastic change, and the level of expression of the E7 protein may depend on the physical status of the HPV genome in the cells. In an in vitro study, Jeon et al. [7] found that the integration of HPV16 results in an increase in the level of E7 transcripts in cultured cells. Thus, it is very important to determine the physical status of the HPV genome in patients of cervical neoplasia to elucidate the mechanisms underlying the development of cervical cancer.

P16 protein is one of the cyclin-dependent kinase inhibitors that prevent phosphorylation of the Rb protein and therefore play an important role in the regulation of the mammalian cell cycle [8–10]. In addition, some studies have demonstrated that the P16 protein is strongly induced and plays an important role in replicative senescence or in premature senescence provoked by the oncogenic *ras* [11–13]. Thus, P16 protein is considered to be very important as a tumor suppressor. In contrast, an inverse relationship has

been reported between the presence of functional Rb protein and overexpression of the P16 protein [14, 15]. High levels of P16 protein expression are associated with dysfunction of the Rb protein caused by gene mutations or its binding to the HPV16 E7 protein [14, 16]. In this scenario, dysfunction of the Rb protein induced by infection with the high-risk HPV E7 protein might result in both abnormal cell cycle progression and P16 protein overexpression [17–23]. Overexpression of the P16 protein has frequently been observed in cervical intraepithelial neoplasia 2 (CIN2) cells and more advanced lesions [19, 24]. Therefore, it is considered that evaluation of the association between the physical status of the HPV genome and overexpression of the P16 protein would be of great interest.

Recently, stored exfoliated cells for liquid-based cytology (LBC) have been reported to be useful for molecular analysis. Examination of exfoliated cells rather than biopsy specimens is more convenient for the screening of patients at high risk of cervical cancer. While a number of independent articles on the usefulness of in situ hybridization (ISH) or P16 immunocytochemistry have been published [25–39], there have been no reports of the usefulness of these techniques applied together to LBC specimens, with the results interpreted in relation to confirmed histological findings. We examined the physical status of the HPV DNA by ISH and the level of expression of the P16 protein by immunocytochemistry in 153 LBC specimens, along with the corresponding biopsy specimens that were available for 106 patients. It is true that not all CIN2 lesions are precursors of cervical cancer: Only some of these lesions progress to cervical cancer, while most regress spontaneously. Follow-up studies over years have shown that CIN 2 lesions progress to cervical cancer in approximately 5% of the patients [40]. In this study, we adopted the recent trend in which CIN2 lesions are considered as the surrogate endpoint in cervical cancer screening and investigated whether such molecular assays might be worthwhile for the identification of patients at high risk of progression to cervical cancer.

Materials and methods

A total of 153 LBC specimens were collected from patients visiting Keio University Hospital, Tokyo, Japan from June 2005 to March 2006. The patients ranged in age from 21 to 80 years, with a median of 37 years. The patient population consisted of a mixture of asymptomatic women and those who were being followed up for previous atypical smears or were under treatment for previously diagnosed as CIN. Written informed consent was obtained from the patients prior to their enrolment of this study. This study was approved by the institutional ethics board (registration number 15-64-4). The 2001 Bethesda System [41] was adopted for cytology, and a total of 153 specimens, consisting of 53 negative for intraepithelial lesions or malignancy (NILM), four with atypical squamous cells of undetermined significance (ASCUS), 29 with low-grade squamous intraepithelial lesions (LSIL), 57 with high-grade squamous intraepithelial lesions (HSIL), and ten with invasive cervical cancer (CA). Colposcopy-guided biopsy was performed in 106 patients on the same day as the collection of the cytology specimens. Among the biopsy specimens, there were 24 with chronic cervicitis, 17 with CIN1, 21 with CIN2, 31 with CIN3, and 13 with squamous cell cancer. LBC specimens were collected using the ThinPrep Cytology Collection System (Hologic Corporation, MA, USA) and processed using ThinPrep 2000 (Hologic Corporation, MA, USA) for Papanicolaou staining, the CINtec™ $P16^{INK4a}$ cytology kit (Dako Norden A/S, Glostrup, Denmark) for P16 immunocytochemistry, and using the GenPoint™, catalyzed signal amplification system (Dako Norden A/S) for ISH.

HPV genotyping

Exfoliated cells were recovered from the residue of PreservCyt media (Cytic Corporation, Boxborough, USA). Approximately 10 ml of PreservCyt media was centrifuged at 3,000 rpm for 30 min. The pellet was washed in phosphate-buffered saline, followed by genomic DNA extraction using proteinase K and phenol–chloroform treatments. The presence of HPV DNA was determined by polymerase chain reaction (PCR) using consensus primer pairs (L1C1; 5′-CGTAAACGTTTTCCCTATTTTTTT-3′, L1C2; 5′-TACCCTAAATACCCTATATTG-3′) designed to amplify an approximately 250-bp segment of the L1 region of HPV [42]. For the internal control, beta-globin primers; KM29(5′-GGTTGGCCAATCTACTCCCAGG-3′) and KM38 (5′-TGGTCTCCTTAAACCTGTCTTG-3′) were employed to amplify 262-bp segment of the human beta-globin gene. As a positive control for PCR, template placental DNA with a PK114/K plasmid containing a variant HPV 16 genome was employed. A 50 μl volume of a mixture containing 20 mM Tris–HCl buffer (pH 8.0), 50 mM KCl, 0.2 mM dNTP mix, 2 mM $MgCl_2$, 0.5 mM each of the L1 and L2 primer, and 0.25 U of Taq polymerase (Takara, Otsu, Japan) was used for each reaction. After an initial period of denaturation at 95°C for 10 min, the amplification was carried out over 43 cycles, each consisting of denaturation at 95°C for 1.5 min, annealing at 48°C for 1.5 min, and extension at 70°C for 2 min. The HPV genotype was determined by L1-PCR restriction fragment length polymorphism analysis. In patients whose genotype could not be determined by this method, the HPV genotyping was determined by the direct sequencing method [43].

P16 immunocytochemistry

ThinPrep slides were stained with antibodies to the P16 protein. Slides were stained on a Dako Autostainer (Dako Norden A/S) using a CINtec ™ $P16^{INK4a}$ cytology kit (Dako Norden A/S) according to the manufacturer's instructions. Briefly, antigen retrieval was performed by heating in a water bath at 95°C for 5 min. After blocking endogenous peroxidase activity, the slides were incubated with the primary antibody (E6H4 clone). A secondary antibody reagent system based on EnVision+ (Dako Norden A/S) was employed. The slides were incubated with DAB (3,3′-diaminobenzidine) substrate–chromogen solution and counterstaining was performed with Mayer's hematoxylin before coverslipping. As a control experiments, cervical cancer cells, HeLa cells in which HPV18 DNA was positive as a positive control, and endometrial cancer cells, SNG-II which were established in our laboratory and showed HPV DNA negative as a negative control, were employed. In practice, P16 immunocytochemistry was then categorized as positive or negative. Cases in which the nuclei of the atypical cells showed positive staining were judged as showing positive, while cases in which only cytoplasm was stained or the number of positive cells was less than ten cells in the slides were judged as showing negative [30, 32].

In situ hybridization

ThinPrep slides were counter-fixed with 10% formalin for 30 min at room temperature. The slides were incubated with 1.25 μg/ml proteinase K solution for 10 min at room temperature, washed with water, and then quenched with 0.3% H_2O_2 in methanol for 20 min at room temperature before being finally washed again with water. Excess liquid was removed by air drying, and one drop of the high-risk HPV probe, consisting of a cocktail directed against the high-risk HPV types 16, 18, 31, 33, 35, 39, 45, 51, 52, 56, 58, 59, and 68 (Dako Norden A/S), was applied. The slides were coverslipped. Denaturation was performed using a hybridizer (Dako Norden A/S) at 90°C for 5 min, and hybridization was allowed to take place overnight at 37°C. Detection was performed using a Dako Autostainer (Dako Norden A/S) and a Dako GenPoint™, catalyzed signal amplification system (Dako Norden A/S) involving tyramide signal amplification. Counterstaining was performed with Mayer's hematoxylin. Comparison of the ISH signal patterns by these assays demonstrated that a punctate pattern, consisting of one or a few discrete signal (s) in the nucleus, indicated HPV integration into the cellular genome. A diffuse nuclear pattern represented multiple copies of episomal HPV and has been shown to be correlated with viral replication [44, 45]. The signal patterns of ISH were thus classified into the punctate (P), diffuse (D), and mixed type (D+P), corresponding to integrated DNA into the genome, episomal DNA, and a combination of both, respectively. HPV 16 positive specimen by PCR from HSIL or CA were selected to be positive control, and HPV negative from NILM were selected to be negative control in each experiment because it could not be the appropriate condition for the positive control by using cultured cells, such as HeLa cells, described in detail in "Discussion".

Combination of assays

The sensitivity, specificity, positive predictive value (PPV), and negative predictive value (NPV) of LBC, P16 immunocytochemistry, ISH, and PCR for detection of the CIN2 or more advanced lesions were investigated with each or the combinations of two or three of these assays: combination-A, high-risk HPV genotyping and P16 immunocytochemistry; combination-B, ISH(D, D+P or P) and P16 immunocytochemistry; combination-C, integration pattern on ISH (P or D+P) and P16 immunocytochemistry; combination-D, ISH (D, D+P or P), P16 immunocytochemistry, and LBC; and combination-E, integration pattern on ISH (P or D+P), P16 immunocytochemistry, and LBC. In the combination assays, a positive test implied that all the selected assays were positive, and a negative test implied that all selected assays were negative. If one of the assays was negative, the result was labeled as equivocal and excluded in the analysis.

Statistical analysis

Fisher's exact test was used to assess the association among the P16 immunocytochemistry, the ISH, HPV genotyping, and the cytological diagnosis.

Results

Examination of LBC

Corresponding to the 153 LBC specimens, colposcopically directed biopsies were obtained from 106 patients. We estimated LBC as the most suitable screening test to detect CIN2 or more advanced lesions. The results on the concomitantly obtained biopsy specimens were regarded as the gold standard for the diagnosis. HSIL or CA was classified as positive LBC. The sensitivity of the cytology was 87.7% (57/65), and the specificity, PPV, and NPV were 85.4% (35/41), 90.5% (57/63), and 81.4% (35/43), respectively (Tables 1 and 4). The representative photos of the ISH and P16 immunocytochemistry were shown in Fig. 1.

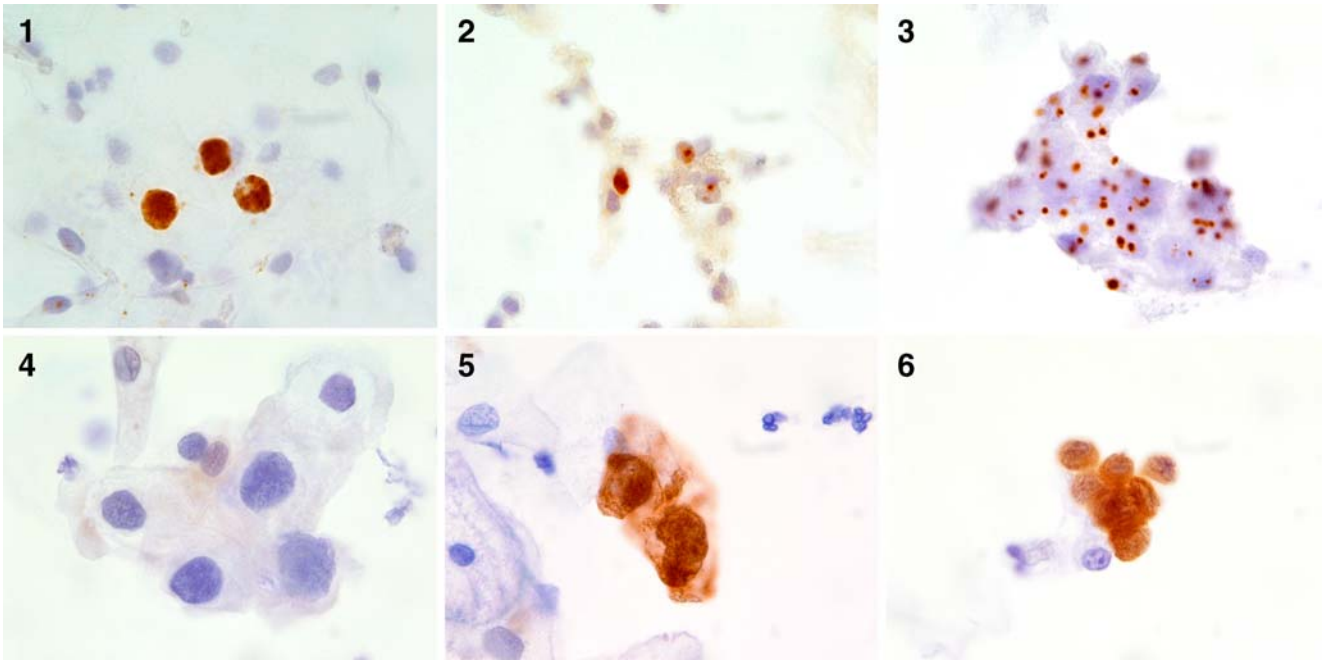

Fig. 1 P16 immunocytochemistry and in situ hybridization with high-risk HPV probes: LBC specimens were analyzed by ISH with a GenPoint catalyzed signal amplification system (*1–3*): *1* D pattern, *2* D+P pattern, *3* P pattern; and a CINtec P16^{ink4a} cytology kit (*4–6*): *4* negative, *5* LSIL, positive, *6* HSIL, positive. Described in detail in "Materials and methods"

HPV genotyping

Eighteen HPV genotypes, 6, 16, 18, 31, 33, 35, 39, 42, 51, 52, 54, 55, 56, 58, 59, 66, 84, 91, and an unknown type (X), were identified. According to the genotyping [46], high-risk HPVs and low-risk HPVs were identified in 71.2% (109/153) and in 5.2% (8/153), respectively. Both high-risk and low-risk HPV genotypes were determined in 41.5%(22/53), 50.0%(2/4), 93.1%(27/29), 98.2% (56/57), and 100%(10/10) of the patients with the cytology results of NILM, ASCUS, LSIL, HSIL, and CA, respectively. The high-risk HPV genotypes were determined in 37.7% (20/53), 50.0% (2/4), 89.7% (26/29), 89.5% (51/57), and 100% (10/10) of the patients with the cytology results of NILM, ASCUS, LSIL, HSIL, and CA, respectively (Fig. 2 and Table 4).

Association among the cytological diagnosis and the physical status of the viral genome

Positive ISH signals were observed in 1.9% (1/53), 0% (0/4), 44.8% (13/29), 50.9% (29/57), and 20.0% (2/10) of patients

Table 1 Association between histological and cytological diagnosis

		Histology						
		N.D.	Cervicitis	CIN1	CIN2	CIN3	SCC	Total
Cytology	NILM	32	13[a]	5[a]	3[b]	0[b]	0[b]	53
	ASCUS	1	2[a]	0[a]	1[b]	0[b]	0[b]	4
	LSIL	10	8[a]	7[a]	4[b]	0[b]	0[b]	29
	HSIL	4	1[c]	5[c]	13[d]	30[d]	4[d]	57
	CA	0	0[c]	0[c]	0[d]	1[d]	9[d]	10
	Total	47	24	17	21	31	13	153

Cytology; terminology according to the 2001 Bethesda System. The calculated sensitivity; D/(C+D), specificity; A/(A+B), PPV; D/(B+D) and NPV; A/(A+C) were shown in Table 4

CA invasive carcinoma, *N.D.* not determined, *SCC* squamous cell carcinoma

[a] Cytology was LSIL or less advanced and histology was CIN1 or less advanced, (A;35)

[b] Cytology was LSIL or less advanced and histology was CIN2 or more advanced condition, (C;8)

[c] Cytology was HSIL or more advanced and histology was CIN1 or less advanced, (B;6)

[d] Cytology was HSIL or more advanced and histology was CIN2 or more advanced, (D;57)

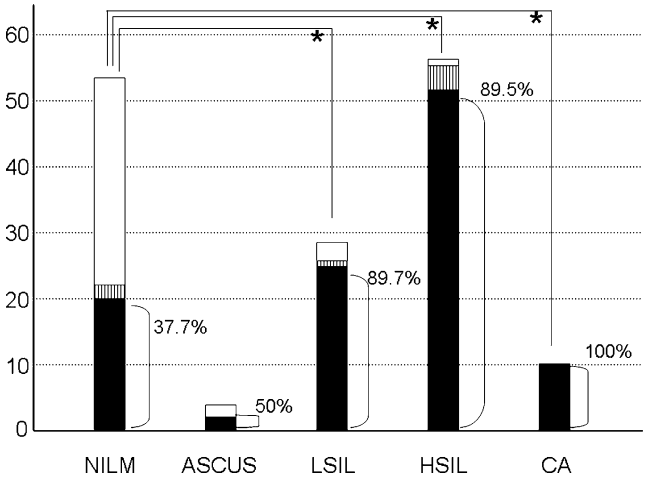

Fig. 2 The rate of HPV genotype group in cytological diagnosis: The HPV genotypes were determined by PCR-RFLP or direct sequencing. HPV genotypes were classified into high-risk or low-risk group based on the classification [46]. The *vertical bar* indicates the number of the patients, and the *horizontal bar* indicates the cytological diagnosis. The *black shaded*, *vertical line* or *white box* indicates the high-risk, low-risk, and negative HPVs, respectively. *$P<0.001$ indicated statistically significant between high-risk HPV-positive (rate indicated) and other (both low-risk and HPV-negative) group

with the cytology results of NILM, ASCUS, LSIL, HSIL, and CA, respectively (Fig. 3). Of the 100 abnormal smears, 44 (44%) were ISH-positive. Of the patients with HSIL and CA lesions, the D pattern was observed in 33.3% (19/57) and 10.0% (1/10), the D+P pattern in 14.0% (8/57) and 0% (0/10), and the P pattern in 3.5% (2/57) and 10.0% (1/10), respectively. Namely, 17.5% (10/57) and 10.0% (1/10) of HSIL and CA showed a P-containing pattern. In patients with HSIL or CA, the D+P pattern was observed in patients with detection of the HPV16, 51, and 58 (Table 2). The P pattern was observed in patients with detection of the only HPV16 and 52. Viral integration into the host genome was observed in some patients with HSIL and CA, and the HPV16, 51, 52, and 58 were determined to be the most high-risk genotypes for integration. In contrast, there were no patients showing either the P or the D+P pattern among the patients with NILM, ASCUS, or LSIL.

Association among P16 immunocytochemistry, in situ hybridization, and the cytological diagnosis

The positive P16 immunocytochemistry was observed in 0% (0/53), 25.0% (1/4), 44.8% (13/29), 93.0% (53/57), and 80.0% (8/10) of patients with NILM, ASCUS, LSIL, HSIL, and CA, respectively, as shown in Fig. 4. We investigated association between P16 immunocytochemistry and ISH. The positive P16 immunocytochemistry was found in 36.1% (39/108), 73.5% (25/34), 100% (8/8), and 100% (3/3) of the patients who showed ISH negativity, the D pattern, the D+P pattern, and the P pattern, respectively. Strikingly, all (11/11) of the patients showing the P or the D+P pattern on ISH showed the positive P16 immunocytochemistry (Fig. 5).

Association among the HPV genotyping, P16 immunocytochemistry, and cytological diagnosis

Among the patients with HSIL and CA, 91.8% (56/61) who were positive for high-risk HPVs showed the positive P16 immunocytochemistry in Fig. 6. In contrast, of the total 48 patients with LSIL or less advanced lesions showing detection of the high-risk HPVs, 29.2% (14/48) showed the positive P16 immunocytochemistry, indicating that the results of P16 immunocytochemistry were better correlated with the type of cellular abnormality than with the HPV genotyping. Thus, P16 immunocytochemistry appears to be a more appropriate method for screening than HPV genotyping.

HPV genotyping or P16 immunocytochemistry compensate for the discrepancies between cytology and histology

We examined whether HPV genotyping or P16 immunocytochemistry compensated for the discrepancies between the results of cytology and histology (Table 3). The HPV genotype was identified in three of the five patients (patients 1–5) with NILM and CIN 1. P16 immunocytochemistry was negative in this group. The HPV genotype was identified in all of the three patients with NILM and CIN2 (patients 6–8). P16 immunocytochemistry was negative in this group. In the only one of CIN2 with the

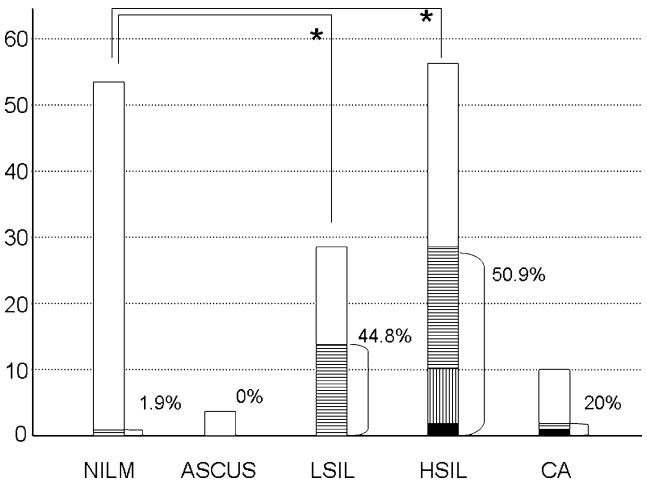

Fig. 3 The rate of positive signals by in situ hybridization: The *vertical bar* indicates the number of the patients, and the *horizontal bar* indicates the cytological diagnosis. Either *D* diffuse, *D+P* diffuse +punctate, or *P* punctate pattern were defined as positive signals. The *black shaded*, *vertical line*, *horizontal line*, or *white box* indicates P, D+P, D, or negative signals, respectively. *Asterisk* indicated statistically significant ($P<0.001$) between positive (rate indicated) and negative signal group

Table 2 Association among the dominant HPV genotypes, cytological diagnosis and results of ISH

HPV	NILM				ASCUS				LSIL				HSIL				CA				Total
Type	–	D	D+P	P	–	D	D+P	P	–	D	D+P	P	–	D	D+P	P	–	D	D+P	P	
16	5	0	0	0	0	0	0	0	2	2	0	0	10	5	3	1	4	1	0	1	34
51	3	0	0	0	0	0	0	0	4	2	0	0	4	3	3	0	1	0	0	0	20
52	2	0	0	0	1	0	0	0	2	4	0	0	1	5	0	1	0	0	0	0	16
56	1	0	0	0	0	0	0	0	4	2	0	0	2	4	0	0	0	0	0	0	13
58	2	1	0	0	1	0	0	0	0	3	0	0	0	2	1	0	0	0	0	0	10

ISH pattern: D; diffuse, D+P; diffuse + punctate, P; punctate signal pattern

cytology result of ASCUS (patient 9), HPV genotyping identified detection of HPV 52 and the patients showed the positive P16 immunocytochemistry. The HPV genotype was identified in six of the eight patients with cervicitis and the cytology result of LSIL (patients 10–17) and in all the four patients with LSIL and CIN2 (patients 18–21), and three of the latter four patients showed positive P16 immunocytochemistry. The HPV genotype was also identified in one patient with HSIL and chronic cervicitis (patient 22), which showed positive P16 immunocytochemistry, and in all five patients with HSIL and CIN1 (patients 23–27); these latter five patients also showed positive P16 immunocytochemistry. There were eight CIN2 patients with the cytology results of NILM, ASCUS, or LSIL. All patients were identified to have detection of high-risk HPV genotypes, and four of the eight (50.0%) patients showed positive P16 immunocytochemistry. Thus, P16 immunocytochemistry and HPV genotyping compensated for under-diagnosis by cytology. Of the six HSIL patients, one had cervicitis and five had CIN1. All patients were found to have detection of high-risk HPV genotypes and four (66.7%) showed positive P16 immunocytochemistry. Among the patients showing discrepancies, seven patients were ISH-positive (D or D+P), of which, six (85.7%) had either CIN2 or HSIL. It was considered that careful and close follow-up of these patients would be necessary. All of the patients showing discrepancy, shown in Table 3, had a past history of CIN, suggesting that HPV genotyping and P16 immunocytochemistry, as well as ISH, were useful as auxiliary diagnostic tools for patients previously diagnosed to have CIN lesions.

Usefulness of combined assays for identifying patients at high risk

LBC, P16 immunocytochemistry, ISH, and PCR were assessed to be useful as screening tests for the detection of CIN2 or more advanced lesions. LBC and P16 immunocytochemistry showed equivalently high sensitivity

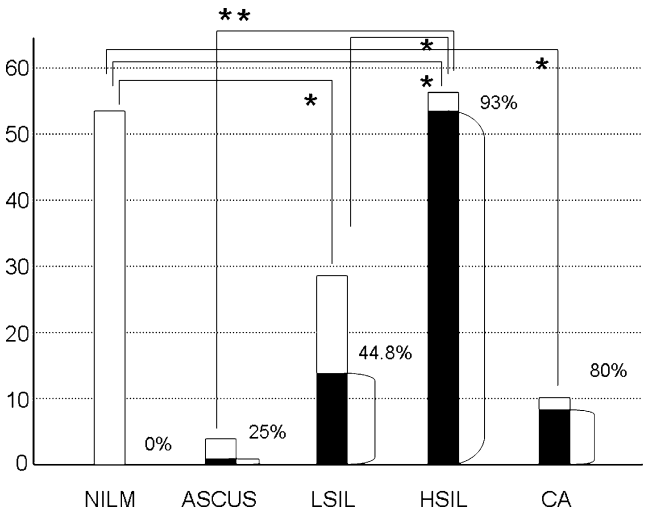

Fig. 4 The rate of positive P16 immunocytochemistry: The *vertical bar* indicates the number of the patients, and the *horizontal bar* indicates the cytological diagnosis. The *black shaded*, *vertical line* or *white box* indicates the positive (rate indicated) or negative P16 immunocytochemistry. *$P<0.001$ and **$P<0.01$ indicated statistically significant

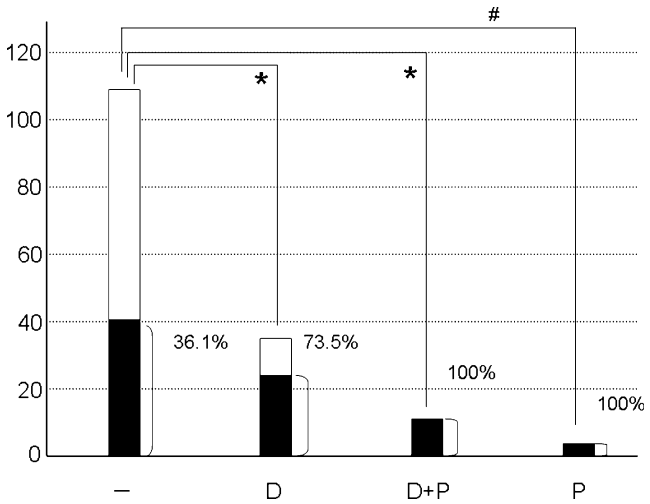

Fig. 5 Association between P16 immunocytochemistry and ISH: The *vertical bar* indicates the number of the patients, and the *horizontal bar* indicates the signal pattern of the P16 immunocytochemistry. The *black shaded*, *vertical line* or *white box* indicates the positive or negative P16 immunocytochemistry. *$P<0.001$ indicated statistically significant. #$P=0.059$ indicated marginally significant possibly due to the small number of the patients

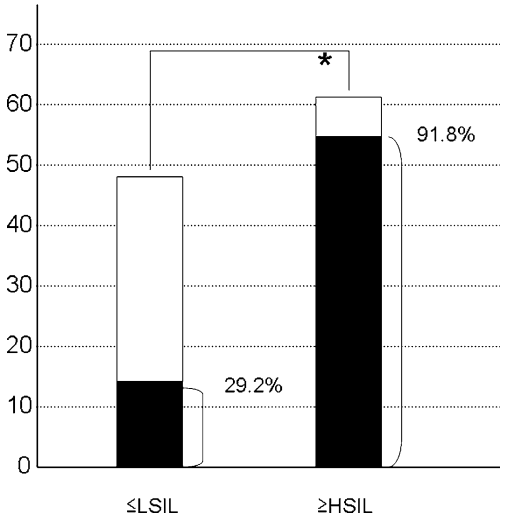

Fig. 6 Correlation between P16 immunocytochemistry and cytology in high-risk HPV genotypes: One hundred and nine patients who had high-risk HPV genotypes were investigated with P16 immunocytochemistry. The *vertical bar* indicates the number of the patients, and the *horizontal bar* indicates ≤LSIL; NILM, ASC-US and LSIL, and ≥HSIL; HSIL and CA, respectively. The *black shaded*, *vertical line* or *white box* indicates positive (rate indicated) or negative P16 immunocytochemistry. The rate of positive P16 immunocytochemistry was higher in ≥HSIL than ≤LSIL. The difference was statistically significant *$P<0.05$

and specificity; therefore, both assays were considered to be equally appropriate as screening tests. In contrast, ISH showed high specificity but low sensitivity. PCR genotyping to identify high-risk genotypes showed high sensitivity but low specificity. Therefore, we sought to determine whether the use of a combination of the assays might compensate for the deficiencies of the individual assays. Combination-A showed the highest sensitivity (100%), but low specificity. Combination-D showed high sensitivity (89.3%) as well as specificity (93.1%). Combinations-A, D, and E showed high NPV (100–88%), indicating that these were excellent combinations for the excluding cervical neoplasia. Double combinations, especially combination-A, showed the highest sensitivity, and the triple combination, combination-D, showed excellent sensitivity, specificity, PPV as well as NPV (Table 4).

Discussion

Use of LBC specimens enabled us to apply a variety of molecular diagnostic tools concomitantly, including P16 immunocytochemistry, ISH, and HPV genotyping. Com-

Table 3 Discrepant patients between cytological and histological diagnosis

Patient no.	ID	Cytology	Histology	HPV genotype	P16	ISH
1	133	NILM	CIN1	–	−	–
2	151	NILM	CIN1	39	−	–
3	92	NILM	CIN1	42	−	–
4	59	NILM	CIN1	51	−	–
5	149	NILM	CIN1	–	−	–
6	150	NILM	CIN2	18	−	–
7	63	NILM	CIN2	51	−	–
8	152	NILM	CIN2	52	−	–
9	121	ASCUS	CIN2	52	+	–
10	21	LSIL	Cervicitis	56	+	–
11	62	LSIL	Cervicitis	−	−	–
12	82	LSIL	Cervicitis	–	−	–
13	95	LSIL	Cervicitis	33	+	–
14	100	LSIL	Cervicitis	51	+	–
15	103	LSIL	Cervicitis	58	+	D
16	113	LSIL	Cervicitis	54	−	–
17	114	LSIL	Cervicitis	56	−	–
18	89	LSIL	CIN2	52	−	D
19	99	LSIL	CIN2	16	+	D
20	131	LSIL	CIN2	51	+	–
21	117	LSIL	CIN2	52	+	D
22	107	HSIL	Cervicitis	51	+	–
23	15	HSIL	CIN1	52	−	D
24	90	HSIL	CIN1	16	−	–
25	119	HSIL	CIN1	31	+	–
26	25	HSIL	CIN1	51	+	D+P
27	112	HSIL	CIN1	51	+	D

Table 4 Estimation of combinations of assays to detect CIN2 or more advanced lesions

	LBC	P16	ISH	all HPV by PCR	HR HPV by PCR	Combo-A	Combo-B	Combo-C	Combo-D	Combo-E
Sensitivity	87.7 (57/65)	89.2 (58/65)	44.6 (29/65)	98.5 (64/65)	90.8 (59/65)	100.0 (52/52)	84.4 (27/32)	58.8 (10/17)	89.3 (25/28)	71.4 (10/14)
Specificity	85.4 (35/41)	78.0 (32/41)	82.9 (34/41)	26.8 (11/41)	34.1 (14/41)	60.9 (14/23)	90.3 (28/31)	97.0 (32/33)	93.1 (27/29)	96.8 (30/31)
PPV	90.5 (57/63)	86.6 (58/67)	80.6 (29/36)	68.1 (64/94)	68.6 (59/86)	85.2 (52/61)	90.0 (27/30)	90.9 (10/11)	92.6 (25/27)	90.9 (10/11)
NPV	81.4 (35/43)	82.1 (32/39)	48.6 (34/70)	91.7 (11/12)	70.0 (14/20)	100.0 (14/14)	84.8 (28/33)	82.1 (32/39)	90.0 (27/30)	88.2 (30/34)

"All HPV by PCR"; HPV genotype was determined by PCR, and "high-risk (HR) HPV by PCR" was selected from all HPV genotypes eliminated HPV 6, 42, 54, 84, 91, and X. A: (combination-A): high-risk HPV genotype and P16 immunocytochemistry; B: ISH (D, D+S or S) and P16 immunocytochemistry; C: integrated pattern of ISH (S or D+S) and P16 immunocytochemistry; D: ISH (D, D+S or S), P16 immunocytochemistry and LBC; E: integrated pattern of ISH (S or D+S), P16 immunocytochemistry and LBC

bined data from all three assays using LBC specimen in relation to the cytological and histological diagnosis have not been reported previously. We investigated the association among overexpression of the P16 protein, the HPV genotyping, and the physical status of the HPV genome in LBC specimens and showed that the combined data from these molecular assays were useful for the identification of patients at high risk for cervical cancer.

The physical status of the HPV DNA is known to be closely related to malignant transformation and has been investigated in tissue specimens by Southern blot hybridization, real-time PCR, and ISH [45, 47–49]. Since specimens from pre-malignant lesions are usually scanty, it is considered that Southern blot hybridization may not be the most suitable for the analysis of the physical status of the HPV genome. We reported a good coincidence between the results of integration of the viral genome assessed by ISH in tissue specimens and those of real-time PCR of exfoliated cells from the cervix despite the starting materials being different [50]. In order to investigate the physical status of the HPV genome by real-time PCR, it is necessary to prepare individual HPV genotype-specific primers and determine the experimental conditions for each high-risk HPV genotype. About 15 high-risk anogenital HPVs have been identified, and it is difficult to set up these conditions for each individual genotype. In regard to the GenPoint ISH system, while there is one report of the use of cultured cells for the sensitivity test, the use of exfoliated cells from the cervix has never been reported. Therefore, we set up ISH conditions for the detection of the high-risk HPV genotypes from the LBC specimens. It was, however, difficult initially to establish these conditions for the LBC specimens. The initial condition of the concentration of the proteinase K according to the protocol for tissue specimens was not appropriate. The concentration of proteinase K for cultured cells has been reported to be 100 μg/ml [25], but under the conditions in our study, it was 1.25 μg/ml. We obtained a more distinct ISH signal, as shown in Fig. 1, by accidental improvement of the concentration of proteinase K, as described in "Materials and methods". We then realized that there would be difference in the optimal conditions between LBC specimens and cultured cells [25].

Positive ISH signals were detected in fewer CA than HSIL lesions. In LBC specimens, cellular clumping and degeneration occurred more commonly in cancer cells than in dysplastic cells, interfering with ISH. Hesselink reported a low detection rate of HPV by ISH in high-grade CIN lesions, as these lesions often show a relatively low viral load [4]. Since there is no gold standard yet in terms of the method, the finding of discrepancies among different protocols has not been resolved. Integration of the HPV DNA was found in some HSIL and CA lesions, but not in any patients with the cytology results of LSIL or NILM,

suggesting that the event of integration may begin at some stage of LSIL. A recent paper described observing the S pattern using their system in almost half of the HSILs and even in some patients of ASCUS or LSIL [51]. The sensitivity of their ISH was similar to that of PCR. A high-sensitive assay occasionally contrasts with a low specificity. Another system of ISH was reported in that it showed a sensitivity of almost half of that of hybrid capture II [52]. Despite the low sensitivity of our ISH, the results of the physical status of the HPV genome as determined by our ISH support those of the P16 immunocytochemistry. The most prevalent genotypes found in our study were HPV16, 51, 52, 56, and 58. It was striking that the P pattern was observed in all the specimens in which HPV16 or 52 was detected. HPV16 was the dominant genotype in our specimens and the most frequently integrated type into the host genome. As integration occurs, expression of the E7 protein is up-regulated [7]; therefore, this integration event is crucial for malignant transformation in the cervical tissues. In contrast, the D pattern was also observed in CA patients with HPV16. We previously reported detection of the episomal form in cervical cancers with HPV16 [50]. In general, HPV16 is believed to be capable of integration into the host genome and to consequently promote cell proliferation. On the other hand, HPV16 in the episomal form is capable of inducing cell proliferation by itself, which is unique among the high-risk HPV genotypes [47, 48].

We investigated the association between the overexpression of P16 and the pattern of integration on ISH. Overexpression of the P16 protein was more frequently observed in patients showing the P pattern rather than those showing the D pattern. Integration of the viral genome into the host genome results in overexpression of the E7 protein. Overexpression of E7 protein, which was not shown, presumably results in overexpression of the P16 protein. This theory supports the notion that overexpression of the P16 protein is a surrogate marker for overexpression of the E7 protein from high-risk HPV genotypes. As shown in Table 2, HPV 16 was detected as the predominant genotype in patients with HSIL, CA, as well as NILM. Overexpression of the P16 protein tended to be recognized more frequently in higher grade rather than in lower grade lesions. While HPV16 is notorious as a high-risk genotype, it must be noted that information about only the HPV16 detection by itself could be rather harmful for the general population. As a surrogate maker of viral activity, determination of overexpression of the P16 protein in combination with HPV genotyping would be useful. The most frequently encountered HPV genotype capable of integration into the host genome was HPV 16. All specimens that were determined by ISH to show integration showed overexpression of the P16 protein. It is known that integration of the HPV genome induces overexpression of the E7 protein and that in turn, E7 protein induces overexpression of the P16 protein. Our study showed a series of dynamic molecular mechanisms from pre-malignant patients. P16 immunocytochemistry combined with ISH may currently be the most reliable for identifying CIN patients who are candidates for a high risk of progression.

In regard to screening tests, appropriate selection of the target population is crucial. This study included selected high-risk patients visiting university hospitals. Most of the patients were detected to have abnormal cytology or histology in the clinics or a previous history of cervical neoplasia. This is the reason why the rate of HPV detection was relatively high, that is, 41.5% in patients of NILM and 50% in patients of ASCUS were identified to have HPV detection. This meant that persistent detection of HPV was common among CIN follow-up patients even in those who were cytology- and histology-negative. Therefore, it would not be appropriate to extrapolate our results to screening of the general population. However, it may be worthwhile discussing our conclusion with reference to screening of the follow-up patients as long as the cost is not a problem. Our data suggested that LBC is the most appropriate tool for cervical cancer screening because of its high sensitivity and specificity. The sensitivity of PCR-based HPV genotyping was too high to make the test useful as a screening test for cervical cancer. ISH showed significantly high specificity; however, the low NPV and sensitivity indicated that it was unsuitable as a screening test. However, the signal pattern was correlated with overexpression of the P16 protein, suggesting that the latter might be a useful indicator of the viral activity. As a screening test, sensitivity as well as specificity of P16 immunocytochemistry was equal to LBC. The advantage of P16 testing is that it is easy to recognize the atypical cells microscopically by their color. Despite the reports of a high rate of false positive results in benign or metaplastic cells [29], it was easy to recognize atypical positive cells under the microscope by their color. From the balance of the results on the sensitivity and specificity, the idea of using combination assays emerged. The double combination assay, combination-A, showed the highest sensitivity and NPV, indicating that it is probably the most suitable for high-risk populations. A triple combination assay showed a high specificity and NPV, suggesting that it would be excellent as an additional screening tool. In relation to the starting material, combinations-B, C, D, and E directly utilize LBC specimens, whereas combination-A requires extraction of DNA from the exfoliated cells for PCR genotyping and is therefore technically more complicated.

To the best of our knowledge, this is the largest study to date in which the molecular markers of cervical neoplasia, namely, P16 immunocytochemistry and ISH, were evaluated in combination with HPV DNA genotyping, and P16 immunocytochemistry was revealed to be a potentially

powerful tool for ancillary molecular testing of LBC specimens.

Acknowledgment This study was supported by a Grant-in-Aid for Scientific Research (C) Japan Society for the Promotion of Science and Research Grants for Life Science and Medicine. We thank Ms. Yuki Kamihara from Dako Japan Inc. and Dr. Katsuaki Dan from Keio University Central Research Laboratory for their technical assistance. We are grateful to Dr. Mattias Durst for the gift of the PK114/K plasmid containing the variant HPV 16 genome.

Disclosure/Conflict of interest I have no conflict of interest to declare in relation to submission of this manuscript.

References

1. Parkin DM, Bray F (2006) Chapter 2: the burden of HPV-related cancers. Vaccine 24(Suppl 3):S11–S25
2. Walboomers JM, Jacobs MV, Manos MM, Bosch FX, Kummer JA, Shah KV, Snijders PJ, Peto J, Meijer CJ, Munoz N (1999) Human papillomavirus is a necessary cause of invasive cervical cancer worldwide. J Pathol 189:12–19
3. zur Hausen H (1991) Viruses in human cancers. Science 254:1167–1173
4. zur Hausen H (2002) Papillomaviruses and cancer: from basic studies to clinical application. Nat Rev Cancer 2:342–350
5. Scheffner M, Nuber U, Huibregtse JM (1995) Protein ubiquitination involving an E1-E2-E3 enzyme ubiquitin thioester cascade. Nature 373:81–83
6. Duensing S, Duensing A, Flores ER, Do A, Lambert PF, Munger K (2001) Centrosome abnormalities and genomic instability by episomal expression of human papillomavirus type 16 in raft cultures of human keratinocytes. J Virol 75:7712–7716
7. Jeon S, Allen-Hoffmann BL, Lambert PF (1995) Integration of human papillomavirus type 16 into the human genome correlates with a selective growth advantage of cells. J Virol 69:2989–2997
8. Serrano M, Hannon GJ, Beach D (1993) A new regulatory motif in cell-cycle control causing specific inhibition of cyclin D/CDK4. Nature 366:704–707
9. Li Y, Nichols MA, Shay JW, Xiong Y (1994) Transcriptional repression of the D-type cyclin-dependent kinase inhibitor p16 by the retinoblastoma susceptibility gene product pRb. Cancer Res 54:6078–6082
10. Bringold F, Serrano M (2000) Tumor suppressors and oncogenes in cellular senescence. Exp Gerontol 35:317–329
11. Hara E, Smith R, Parry D, Tahara H, Stone S, Peters G (1996) Regulation of p16CDKN2 expression and its implications for cell immortalization and senescence. Mol Cell Biol 16:859–867
12. Serrano M, Lin AW, McCurrach ME, Beach D, Lowe SW (1997) Oncogenic ras provokes premature cell senescence associated with accumulation of p53 and p16INK4a. Cell 88:593–602
13. Ohtani N, Zebedee Z, Huot TJ, Stinson JA, Sugimoto M, Ohashi Y, Sharrocks AD, Peters G, Hara E (2001) Opposing effects of Ets and Id proteins on p16INK4a expression during cellular senescence. Nature 409:1067–1070
14. Parry D, Bates S, Mann DJ, Peters G (1995) Lack of cyclin D-Cdk complexes in Rb-negative cells correlates with high levels of p16INK4/MTS1 tumour suppressor gene product. EMBO J 14:503–511
15. Sakaguchi M, Fujii Y, Hirabayashi H, Yoon HE, Komoto Y, Oue T, Kusafuka T, Okada A, Matsuda H (1996) Inversely correlated expression of p16 and Rb protein in non-small cell lung cancers: an immunohistochemical study. Int J Cancer 65:442–445
16. Khleif SN, DeGregori J, Yee CL, Otterson GA, Kaye FJ, Nevins JR, Howley PM (1996) Inhibition of cyclin D-CDK4/CDK6 activity is associated with an E2F-mediated induction of cyclin kinase inhibitor activity. Proc Natl Acad Sci U S A 93:4350–4354
17. Sano T, Oyama T, Kashiwabara K, Fukuda T, Nakajima T (1998) Immunohistochemical overexpression of p16 protein associated with intact retinoblastoma protein expression in cervical cancer and cervical intraepithelial neoplasia. Pathol Int 48:580–585
18. Ishikawa M, Fujii T, Masumoto N, Saito M, Mukai M, Nindl I, Ridder R, Fukuchi T, Kubushiro K, Tsukazaki K, Nozawa S (2003) Correlation of p16INK4A overexpression with human papillomavirus infection in cervical adenocarcinomas. Int J Gynecol Pathol 22:378–385
19. Ishikawa M, Fujii T, Saito M, Nindl I, Ono A, Kubushiro K, Tsukazaki K, Mukai M, Nozawa S (2006) Overexpression of p16 INK4a as an indicator for human papillomavirus oncogenic activity in cervical squamous neoplasia. Int J Gynecol Cancer 16:347–353
20. Masumoto N, Fujii T, Ishikawa M, Saito M, Iwata T, Fukuchi T, Susumu N, Mukai M, Kubushiro K, Tsukazaki K, Nozawa S (2003) P16 overexpression and human papillomavirus infection in small cell carcinoma of the uterine cervix. Hum Pathol 34:778–783
21. Sano T, Hikino T, Xue Q, Saito T, Kashiwabara K, Oyama T, Nakajima T (2000) Immunohistochemical inactivation of p14ARF concomitant with MDM2 overexpression inversely correlates with p53 overexpression in oral squamous cell carcinoma. Pathol Int 50:709–716
22. Sano T, Oyama T, Kashiwabara K, Fukuda T, Nakajima T (1998) Expression status of p16 protein is associated with human papillomavirus oncogenic potential in cervical and genital lesions. Am J of Pathol 153:1741–1748
23. Keating JT, Cviko A, Riethdorf S, Riethdorf L, Quade BJ, Sun D, Duensing S, Sheets EE, Munger K, Crum CP (2001) Ki-67, cyclin E, and p16INK4 are complimentary surrogate biomarkers for human papilloma virus-related cervical neoplasia. Am J Surg Pathol 25:884–891
24. Klaes R, Friedrich T, Spitkovsky D, Ridder R, Rudy W, Petry U, Dallenbach-Hellweg G, Schmidt D, von Knebel Doeberitz M (2001) Overexpression of p16(INK4A) as a specific marker for dysplastic and neoplastic epithelial cells of the cervix uteri. Int J Cancer 92:276–284
25. Lizard G, Demares-Poulet MJ, Roignot P, Gambert P (2001) In situ hybridization detection of single-copy human papillomavirus on isolated cells, using a catalyzed signal amplification system: GenPoint. Diagn Cytopathol 24:112–116
26. Alameda F, Pijuan L, Ferrer L, Marinoso ML, Muset M, Soler I, Gimferrer E, Serrano S (2005) Human papilloma virus detection in liquid cytology, in situ hybridization and polymerase chain reaction. Virchows Arch 446:202–203
27. Guo M, Patel SJ, Chovanec M, Jan YJ, Tarco E, Bevers TB, Anderson K, Sneige N (2007) A human papillomavirus testing system in women with abnormal Pap results: a comparison study with follow-up biopsies. Acta Cytol 51:749–754
28. Bewtra C, Xie Q, Soundararajan S, Gatalica Z, Hatcher L (2005) Genital human papillomavirus testing by in situ hybridization in liquid atypical cytologic materials and follow-up biopsies. Acta Cytol 49:127–131
29. Trunk MJ, Dallenbach-Hellweg G, Ridder R, Petry KU, Ikenberg H, Schneider V, von Knebel Doeberitz M (2004) Morphologic characteristics of p16INK4a-positive cells in cervical cytology samples. Acta Cytol 48:771–782
30. Bose S, Evans H, Lantzy L, Scharre K, Youssef E (2005) p16 (INK4A) is a surrogate biomarker for a subset of human papilloma virus-associated dysplasias of the uterine cervix as determined on the Pap smear. Diagn Cytopathol 32:21–24

31. Yoshida T, Fukuda T, Sano T, Kanuma T, Owada N, Nakajima T (2004) Usefulness of liquid-based cytology specimens for the immunocytochemical study of p16 expression and human papillomavirus testing: a comparative study using simultaneously sampled histology materials. Cancer 102:100–108
32. Saqi A, Pasha TL, McGrath CM, Yu GH, Zhang P, Gupta P (2002) Overexpression of p16INK4A in liquid-based specimens (SurePath) as marker of cervical dysplasia and neoplasia. Diagn Cytopathol 27:365–370
33. Wentzensen N, Bergeron C, Cas F, Eschenbach D, Vinokurova S, von Knebel Doeberitz M (2005) Evaluation of a nuclear score for p16INK4a-stained cervical squamous cells in liquid-based cytology samples. Cancer 105:461–467
34. Sahebali S, Depuydt CE, Boulet GA, Arbyn M, Moeneclaey LM, Vereecken AJ, Van Marck EA, Bogers JJ (2006) Immunocytochemistry in liquid-based cervical cytology: analysis of clinical use following a cross-sectional study. Int J Cancer 118:1254–1260
35. Bibbo M, Klump WJ, DeCecco J, Kovatich AJ (2002) Procedure for immunocytochemical detection of P16INK4A antigen in thin-layer, liquid-based specimens. Acta Cytol 46:25–29
36. Pientong C, Ekalaksananan T, Swadpanich U, Kongyingyoes B, Kritpetcharat O, Yuenyao P, Ruckait N (2003) Immunocytochemical detection of p16INK4a protein in scraped cervical cells. Acta Cytol 47:616–623
37. Monsonego J, Pollini G, Evrard MJ, Sednaoui P, Monfort L, Quinzat D, Dachez R, Syrjanen K (2007) P16(INK4a) immunocytochemistry in liquid-based cytology samples in equivocal Pap smears: added value in management of women with equivocal Pap smear. Acta Cytol 51:755–766
38. Carydis VB, Walker T, Wing A, Colgan TJ (2007) Utility of p16 (ink4a) immunocytochemistry in liquid-based cytology specimens from women treated for high-grade squamous intraepithelial lesions. Acta Cytol 51:517–522
39. Nieh S, Chen SF, Chu TY, Lai HC, Fu E (2004) Expression of p16INK4A in Pap smears containing atypical glandular cells from the uterine cervix. Acta Cytol 48:173–180
40. Ostor AG (1993) Natural history of cervical intraepithelial neoplasia: a critical review. Int J Gynecol Pathol 12:186–192
41. Solomon D, Davey D, Kurman R, Moriarty A, O'Connor D, Prey M, Raab S, Sherman M, Wilbur D, Wright T Jr., Young N (2002) The 2001 Bethesda System: terminology for reporting results of cervical cytology. Jama 287:2114–2119
42. Yoshikawa H, Kawana T, Kitagawa K, Mizuno M, Yoshikura H, Iwamoto A (1991) Detection and typing of multiple genital human papillomaviruses by DNA amplification with consensus primers. Jpn J Cancer Res 82:524–531
43. Masumoto N, Fujii T, Ishikawa M, Mukai M, Saito M, Iwata T, Fukuchi T, Kubushiro K, Tsukazaki K, Nozawa S (2003) Papanicolaou tests and molecular analyses using new fluid-based specimen collection technology in 3000 Japanese women. Br J Cancer 88:1883–1888
44. Hopman AH, Kamps MA, Smedts F, Speel EJ, Herrington CS, Ramaekers FC (2005) HPV in situ hybridization: impact of different protocols on the detection of integrated HPV. Int J Cancer 115:419–428
45. Cooper K, Herrington CS, Stickland JE, Evans MF, McGee JO (1991) Episomal and integrated human papillomavirus in cervical neoplasia shown by non-isotopic in situ hybridisation. J Clin Pathol 44:990–996
46. de Villiers EM, Fauquet C, Broker TR, Bernard HU, zur Hausen H (2004) Classification of papillomaviruses. Virology 324:17–27
47. Matsukura T, Koi S, Sugase M (1989) Both episomal and integrated forms of human papillomavirus type 16 are involved in invasive cervical cancers. Virology 172:63–72
48. Durst M, Kleinheinz A, Hotz M, Gissman L (1985) The physical state of human papillomavirus type 16 DNA in benign and malignant genital tumours. J Gen Virol 66:1515–1522
49. Peitsaro P, Johansson B, Syrjanen S (2002) Integrated human papillomavirus type 16 is frequently found in cervical cancer precursors as demonstrated by a novel quantitative real-time PCR technique. J Clin Microbiol 40:886–891
50. Fujii T, Masumoto N, Saito M, Hirao N, Niimi S, Mukai M, Ono A, Hayashi S, Kubushiro K, Sakai E, Tsukazaki K, Nozawa S (2005) Comparison between in situ hybridization and real-time PCR technique as a means of detecting the integrated form of human papillomavirus 16 in cervical neoplasia. Diagn Mol Pathol 14:103–108
51. Algeciras-Schimnich A, Policht F, Sitailo S, Song M, Morrison L, Sokolova I (2007) Evaluation of quantity and staining pattern of human papillomavirus (HPV)-infected epithelial cells in thin-layer cervical specimens using optimized HPV-CARD assay. Cancer 111:330–338
52. Schiller CL, Nickolov AG, Kaul KL, Hahn EA, Hy JM, Escobar MT, Watkin WG, Sturgis CD (2004) High-risk human papillomavirus detection: a split-sample comparison of hybrid capture and chromogenic in situ hybridization. Am J Clin Pathol 121:537–545

Virchows Arch (2008) 453:557–569
DOI 10.1007/s00428-008-0679-5

ORIGINAL ARTICLE

Estrogen receptor alpha (ERα) phospho-serine-118 is highly expressed in human uterine leiomyomas compared to matched myometrium

Tonia L. Hermon · Alicia B. Moore · Linda Yu · Grace E. Kissling · Frank J. Castora · Darlene Dixon

Received: 25 April 2008 / Revised: 12 September 2008 / Accepted: 16 September 2008 / Published online: 14 October 2008

Abstract It is thought that the growth of uterine leiomyomas may be mediated by the interaction of estrogen receptor alpha (ERα) and growth factor pathways and that phosphorylation of ERα at serine 118 (ERα-phospho-Ser118) is important in this interaction. In this study, immunoblotting and immunohistochemistry were used to investigate the expression of ERα-phospho-Ser118, phosphorylated p44/42 mitogen-activated protein kinase (phospho-p44/42 MAPK), and proliferating cell nuclear antigen (PCNA) in human leiomyoma and myometrial tissues during the proliferative and secretory phases of the menstrual cycle. We found that tumors taken from the proliferative phase expressed significantly higher levels of ERα-phospho-Ser118, phospho-p44/42 MAPK, and PCNA compared to patient-matched myometria and had significantly higher ERα-phospho-Ser118 and PCNA expression compared to secretory phase tumors. Also, enhanced colocalization and association of phospho-p44/42 MAPK and ERα-phospho-Ser118 were observed in proliferative phase tumors by confocal microscopy and immunoprecipitation, respectively. These data suggest that ERα-phospho-Ser118 may be important in leiomyoma growth and is possibly phosphorylated by phospho-p44/42 MAPK.

Keywords Uterine leiomyoma · Estrogen receptor alpha phosphorylated serine 118 · Phosphorylated mitogen-activated protein kinase

T. L. Hermon · A. B. Moore · L. Yu · D. Dixon (✉)
Cellular and Molecular Pathology Branch,
National Institute of Environmental Health Sciences (NIEHS),
National Toxicology Program (NTP),
National Institutes of Health (NIH),
Department of Health and Human Services (DHHS),
P.O. Box 12233, MD C2-09, Research Triangle Park, NC 27709, USA
e-mail: dixon@niehs.nih.gov

G. E. Kissling
Biostatistics Branch,
National Institute of Environmental Health Sciences (NIEHS),
National Toxicology Program (NTP),
National Institutes of Health (NIH),
Department of Health and Human Services (DHHS),
Research Triangle Park, NC 27709, USA

T. L. Hermon · F. J. Castora
Department of Physiological Sciences, Division of Biochemistry,
Eastern Virginia Medical School,
Norfolk, VA 23507, USA

Introduction

Uterine leiomyomas (fibroids; myomas) are one of the most common benign gynecologic tumors in women of reproductive age. These tumors represent a significant public health problem, since they are responsible for approximately 200,000 hysterectomies per year and are the leading cause of hysterectomy in the United States [2, 15, 39]. Fibroids have also been associated with clinical disease with moderate to high frequency in women in Europe [30], Africa [14], and Japan [33].

Uterine leiomyomas tend to grow during the reproductive years, but regress after menopause, suggesting that these tumors are hormonally regulated [10]. The ovarian steroid hormones, estrogen and progesterone, are believed to play an important role in the growth of uterine leiomyomas [10, 28, 31]; however, there is increasing evidence that sex steroids are not the only modulators of leiomyoma growth [28, 35]. Studies have shown that circulating steroid hormone levels are similar in women that have or do not have leiomyomas, indicating that specific local, tissue-regulated factors maybe involved in the pathogenesis of these tumors [5]. The heterogeneity of

leiomyoma growth within a given uterus, despite identical exposure of these tumors to similar circulating sex steroid concentrations, suggests the involvement of local cytokines and/or growth factors [13, 28].

Estrogen exerts its physiological effects by binding to estrogen receptor alpha and beta (ERα and β). In addition to the traditional ERα activation (hormone binding), this receptor can be activated by growth factor signaling pathways via phosphorylation of the ERα at specific serines [11, 25]. In human breast cancer cells, it has been shown that in the presence or absence of estradiol binding, human ERα is predominately phosphorylated on Ser-118 and to a lesser extent on Ser-104 and Ser-106 [4, 7, 25]. Phosphorylation of ERα influences its activity and may lead to ERα-mediated transcription. To our knowledge, there are no studies that have reported the role of phosphorylation of ERα at Ser-118 in human or rodent uterine leiomyomas.

Progesterone has also been shown to be involved in fibroid growth, having both inhibitory and stimulatory effects on growth [8, 9, 26, 40]. Evidence shows that progesterone can induce leiomyoma cell proliferation and up-regulate the growth factor, epidermal growth factor [34]. Progesterone has also been shown to down-regulate insulin-like growth factor-I messenger RNA and protein expression in cultured leiomyoma cells [42]. There is also considerable biological evidence for "crosstalk" between the estrogen and progesterone hormone receptor signaling pathways [23]. In many cases, progestins suppress the stimulatory effects of estrogens in target tissues, although estrogen up-regulates the progesterone receptor [19, 24]. In a study using tissue from women with endometrial hyperplasia, which is also a hormonally regulated disease, ERα protein expression was down-regulated after use of the progestins, levonorgestrel, and medroxyprogesterone [38]. Progesterone has been shown to have a negative effect on ERα expression [16, 24], and ERα expression has been reported to be higher in myometrial and leiomyoma tissue from women in the proliferative versus secretory phase of the menstrual cycle based on immunohistochemisty and western blotting. The mechanisms involved in the "crosstalk" between the progesterone and estrogen hormone receptor pathways and how they interact with growth factor receptor pathways have not been fully elucidated in uterine leiomyomas.

Studies have indicated that hormones and growth factor signaling pathways are mediators of leiomyoma growth [28, 35, 37]. In uterine leiomyoma cell cultures, the mitogen-activated protein kinase (MAPK) pathway interacts with the estrogen system via the ER [1]. Constitutively activated MAPK (phospho-p44/42 MAPK) is highly expressed in leiomyoma and myometrial tissues and is increased in leiomyomas compared to normal myometrial tissues [6]. A study has indicated that MAPK activity increases in leiomyoma cells after treatment with estradiol and that an indirect interaction between the ER and growth factor pathways exists, because uterine leiomyoma cells treated with estradiol have increased secretion of platelet-derived growth factor and activation of the MAPK pathway [1]. In breast cancer cells, phosphorylation of ERα at Ser-118 occurs in response to activation of MAPK (phospho-p44/42) [1, 18, 25]. To date, there are no reports of whether ERα is phosphorylated in fibroids. Furthermore, if present, the molecular mechanism(s) by which phosphorylation occurs remains to be understood.

In this study, we evaluated the expression of ERα-phospho-Ser118, phospho-p44/42 MAPK, and proliferating cell nuclear antigen (PCNA) in uterine leiomyomas and patient-matched myometrial tissue and determined if there was differential expression during the menstrual cycle phases. We also examined colocalization and the interaction of ERα-phospho-Ser118 and phospho-p44/42 MAPK in tumors versus myometrial tissue.

Materials and methods

Patients

Uterine leiomyomas (n=26) and unaffected patient-matched myometrial tissue (n=16) samples were taken from 16 premenopausal women (six for western blot analysis×one tumor each and ten for immunohistochemistry×two tumors each) who underwent hysterectomy for symptomatic fibroids. The women had not taken hormonal medication at least 3 months prior to surgery. Informed consent was obtained, and the Institutional Review Board of the NIEHS NIH approved the study. All uterine leiomyoma and unaffected myometrial samples were confirmed by histological evaluation. The menstrual cycle phases were determined as either proliferative or secretory based on endometrial histology (case 11) or menstrual cycle history (cases 1–10 and 12–16) for each patient (Table 1). All patients had multiple fibroids that were typical in histomorphology and located in the intramural (60%), subserosal (25%), or submucosal (15%) regions of the myometrium. Tumor sizes were classified as <2 cm (n=10) or ≥2 cm (n=10) (Table 1), and the age of the patients ranged from 41 to 47 years, with a mean age of 43.5 years.

Western blotting

Western blotting was performed to detect ERα-phospho-Ser118 expression in the leiomyoma and patient-matched myometrial tissue lysates, which were taken from six women in the proliferative (three) and secretory (three)

Table 1 Tumor size and menstrual cycle phase of premenopausal women with fibroids

Case #	Menstrual cycle phase	Tumor ID	Tumor size (cm)
1	Proliferative	1a	<2
		1b	≥2
2	Proliferative	2a	<2
		2b	≥2
3	Proliferative	3a	<2
		3b	≥2
4	Proliferative	4a	<2
		4b	≥2
5	Proliferative	5a	<2
		5b	≥2
6	Secretory	6a	<2
		6b	≥2
7	Secretory	7a	<2
		7b	≥2
8	Secretory	8a	<2
		8b	≥2
9	Secretory	9a	<2
		9b	≥2
10	Secretory	10a	<2
		10b	≥2
11	Proliferative	11a	≥2
12	Proliferative	12a	≥2
13	Proliferative	13a	≥2
14	Secretory	14a	≥2
15	Secretory	15a	≥2
16	Secretory	16a	≥2

phases of the menstrual cycle. Aliquots of 30 μg of protein were electrophoresed on a 4–12% Bis–Tris Gel (Invitrogen, Carlsbad, CA, USA) under reducing conditions as previously described [37]. The proteins were electrotransferred onto 0.45 μm polyvinylidene fluoride membranes (Immobilon-P, Millipore, Bedford, MA, USA). Blots were incubated with a mouse monoclonal antibody (Cell Signaling Technology, Danvers, MA, USA) against ERα-phospho-Ser118 diluted at 1:500. Antibody binding was detected with horseradish peroxidase-conjugated anti-mouse (Amersham Biosciences, Arlington Heights, IL, USA) diluted at 1:2,000. Antigen-antibody complexes were detected with the ECL western blot detection system (Amersham Biosciences). A densitometer (Fluor Chem™8900, Alpha Innotech, San Landro, CA, USA) was used for quantitation of ERα-phospho-Ser118 band densities.

Immunohistochemistry

ERα-phospho-Ser118, ERα, and phospho-p44/42 MAPK expression

Uterine leiomyoma (20) and myometrial (10) tissue samples were fixed overnight in 10% neutral-buffered formalin. Tissues were then processed through a graded series of alcohols, embedded in paraffin, sectioned at 6 μm, and mounted onto charged glass slides (ProbeOn Plus, Fisher Scientific, Pittsburgh, PA, USA). Tissues were deparaffinized, and endogenous peroxidase activation was blocked using 3% H_2O_2 for 15 min at room temperature. Antigen retrieval was performed by microwaving for 10 min (ERα and ERα-phospho-Ser118 staining) or by incubation for 20 min in a decloaker (phospho-p44/42 MAPK staining). Tissues were blocked using normal horse or goat serum at room temperature for 1 h. The tissues used for ERα and ERα-phospho-Ser118 were additionally blocked using an Avidin/Biotin Blocking Kit (Vector Laboratories, Burlingame, CA, USA). Tissues were incubated with phospho-estrogen receptor α (Ser-118) monoclonal antibody (1:30 dilution), estrogen receptor monoclonal antibody (1:25 dilution; Immunotech Beckman Coulter, Fullerton, CA, USA), or phospho-p44/42 MAPK polyclonal rabbit IgG (1:50 dilution; Cell Signaling Technology) overnight at 4°C. Negative controls consisted of normal mouse or rabbit serum at a concentration the same as the respective primary antibody. The tissues were incubated in the secondary antibody (horse anti-mouse or goat anti-rabbit; Elite Vectastain ABC Kit, Vector Laboratories) for 30 min at room temperature. Immunoreactive complexes were detected by avidin–biotin affinity system (Elite Vectastain ABC Kit, Vector Laboratories) and visualized using 3,3′-diaminobenzidine tetrahydrachloride substrate chromogen system (Dako Cytometry, Carpinteria, CA, USA). Tissues were counterstained with Mayer's hematoxylin (Poly Scientific, Bay Shore, NY, USA), dehydrated, coverslipped, and observed by light microscopy.

A semiquantitative method described by Detre et al. [12], which incorporates the overall percent of positive staining and intensity of immunostaining, was used for assessing ERα-phospho-Ser118, ERα, and phospho-p44/42 MAPK protein expression in leiomyoma and myometrial tissue samples. Slides were evaluated blindly with a light microscope and a ×20 objective. Quickscores were assigned independently by two scorers and then averaged to obtain a mean quickscore. Sections were scanned at ×40 using an Aperio ScanScopeXT model (Aperio Technologies, Vista, CA, USA).

Proliferating cell nuclear antigen (PCNA) labeling

For PCNA staining, the deparaffinization and rehydration were done similarly to the immunohistochemical procedures described above. After inactivation of endogenous peroxidases, antigen retrieval was performed by microwaving the samples for 10 min in dH_20. Samples were blocked using 0.5% milk for 20 min and then a primary antibody, monoclonal mouse anti-PCNA IgM (1:500

dilution; Chemicon, Temecula, CA, USA), was placed on the tissues for 1 h at room temperature. After rinsing, the tissues were incubated with a secondary antibody (Biotin-SP-conjugated AffiniPure Goat anti-mouse IgM, μ chain specific; Jackson Immunoresearch, West Grove, PA, USA) for 30 min at room temperature. Tissues were labeled with supersensitive conjugated streptavidin peroxidase (BioGenex, San Ramon, CA, USA). Immunoreactive complexes were visualized, and tissues were counterstained and coverslipped using the procedures mentioned in the previous section.

The percentage of PCNA labeling in the tissue samples was later determined using a light microscope, ×40 objective and an ocular grid. Approximately eight to 12 high power fields per tissue section were counted to reach a total cell count of 1,000 cells in uterine leiomyoma and myometrial tissues. Nuclei that stained intensely brown were counted as positive. Percent PCNA labeling was determined by the number of cells having positively stained nuclei divided by 1,000 cells (labeled and unlabeled) and multiplied by 100. A mean percent PCNA labeling was determined by averaging the numbers from the independent scorers.

Immunoflourescence

Frozen samples of uterine leiomyoma and patient-matched myometrial tissue were sectioned at 5 μm, thawed for 15 min at room temperature, and fixed in 4% paraformaldehyde at 4°C for 10 min followed by −20°C methanol for 20 min. The sections were then blocked for 1 h in 5% milk, 1% BSA, and 1.5% normal goat serum (Vectastain Kit) in 1× automation buffer. Tissues were incubated in primary antibodies for both ERα-phospho-Ser118 and phospho-p44/42 MAPK together overnight (4°C) at dilutions as stated above in the "Immunohistochemistry" section. The sections were then incubated with Alexa Fluor 488 goat anti-mouse IgG (green fluorescence) and Alexa Fluor 594 goat anti-rabbit IgG (red fluorescence; Molecular Probes, Carlsbad, CA, USA) for 45 min at room temperature in the dark. Tissues were counterstained using 4′, 6-diamidino-2-phenylindole (DAPI; Molecular Probes, Carlsbad, CA, USA) in the dark for 30 min at room temperature. Sections were coverslipped with aqueous anti-fade fluorescent mounting medium (Vector Laboratories). The tissue sections were observed with a laser scanning confocal microscope (LSM 510 UV mounted on Axiovert 100M microscope, Carl Zeiss) and analyzed using LSM Image Examiner v3.2 software.

Immunoprecipitation

To assess the association of ERα-phospho-Ser118 and phospho-p44/42 MAPK in myometrial and leiomyoma tissues, phospho-p44/42 MAPK was immunoprecipitated and immunoblotted for ERα-phospho-Ser118 and phospho-p44/42 MAPK (as a control). Aliquots of 500 μg of leiomyoma and myometrial tissue lysates were cleared by adding 50 μL of Protein A-Sepharose beads (Zymed Laboratories, San Francisco, CA, USA) and incubated for 30 min at 4°C with gentle rotation. The protein lysates were immunoprecipitated with 5 μg of phospho-p44/42 MAPK polyclonal rabbit antibody (Cell Signal Technology) overnight at 4°C with gentle rotation. Protein A-Sepharose beads (50 μL) were added to each tube, the mixtures were incubated overnight at 4°C, and the immune complexes were collected by centrifugation. The beads were washed with RIPA buffer (10 mL of 50 mM Tris HCL pH 7.4 with 150 mM NaCL, 1 mM EGTA, 1 mM NaF, and 1% triton X 100, 250 μL of 10% sodium deoxycholate, 50 μL of 200 mM activated sodium vanadate, 50 μL of 10 mM sodium molybdate, 20 μL of aprotinin and leupeptin, and 20 μL of 2 μg/mL of A-PMSF), and the supernatant was discarded. The sepharose beads were resuspended in 30 μL of Laemmli sample buffer (Bio-Rad Laboratories, Hercules, CA, USA) and then centrifuged. Amounts of 15 μL of the supernatant were used for western blotting as previously described (mouse monoclonal ERα-phospho-Ser118 antibody at 1:500 dilution and rabbit polyclonal phospho-p44/42 MAPK antibody at 1:1000 dilution (Cell Signaling Technology)). Antibody binding was detected with horseradish peroxidase-conjugated anti-mouse and anti-rabbit (Amersham Biosciences) diluted at 1:2000. Antigen-antibody complexes were detected with an ECL western blot detection system (Amersham Biosciences).

Statistics

Statistical comparisons were performed for mean of quick-scores and intensities for western blot bands of uterine leiomyoma and patient-matched myometrial samples. Significant differences were determined using Wilcoxon signed ranks tests ($p \leq 0.05$) and Mann–Whitney tests ($p \leq 0.05$).

Results

ERα-phospho-Ser118 expression by western blot and densitometry

Western blot analysis showed significantly increased expression of ERα-phospho-Ser118 in uterine leiomyomas compared to myometrial samples from the proliferative phase (Fig. 1a and b). The overall mean expression of ERα-phospho-Ser118 was slightly higher in uterine leiomyomas from the secretory phase compared to myometrial samples, although this difference was not significant (Fig. 1a and b).

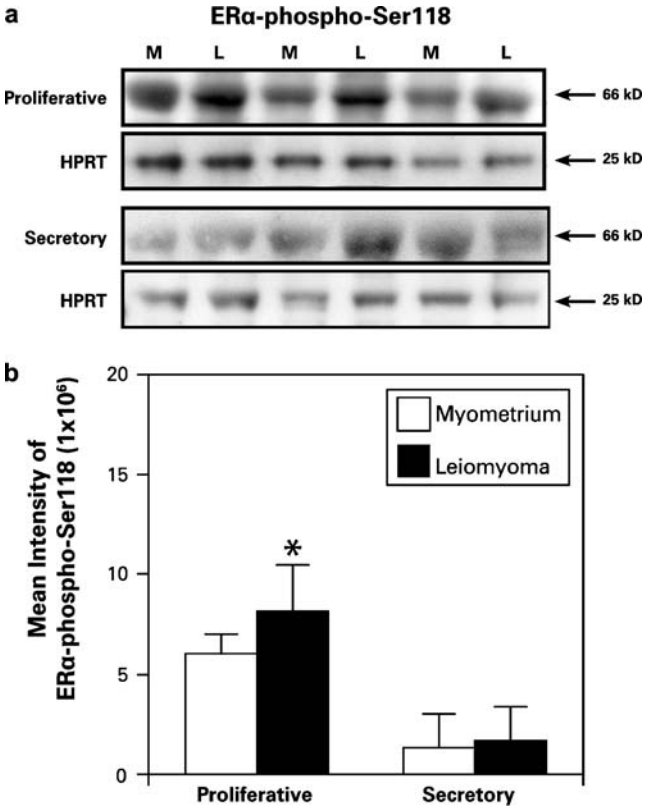

Fig. 1 Immunoblot of ERα-phospho-Ser118 and HPRT (loading control) in uterine leiomyoma (*L*) and patient-matched myometrial (*M*) tissue lysates from women (n=6) in the proliferative or secretory phase of the menstrual cycle. **a** ERα-phospho-Ser118 is expressed in leiomyoma and myometrial tissue. **b** The bar graph represents the mean±SE intensity of western blot bands for ERα-phospho-Ser118 protein. Increased expression of ERα-phospho-Ser118 was observed in the leiomyomas compared to the myometrial tissue samples from the proliferative phase of the menstrual cycle. *$p \leq 0.05$; a significant difference versus myometrial samples (n=3)

Also, ERα-phospho-Ser118 expression was higher in both tumors and myometrial samples from the proliferative phase compared to those from the secretory phase (Fig. 1a and b).

ERα phospho-Ser118 and ERα expression by immunohistochemistry

Proliferative phase

Immunohistochemistry confirmed that leiomyoma samples from the proliferative phase had increased protein expression of ERα-phospho-Ser118 compared to matched myometrial tissue (Fig. 2). ERα-phospho-Ser118 was expressed in the nuclei of myometrial and leiomyoma cells (Fig. 2a and b). Also in this phase, ERα expression was increased in the tumors compared to myometrial tissue and was expressed predominantly in the nuclei of myometrial and leiomyoma cells with minimal staining in the cytoplasm (Fig. 2c and d). Scores of immunostaining intensity showed significant differences in ERα-phospho-Ser118 expression in myometrial versus leiomyoma samples with mean quickscores of 2.4±1.0 and 8.0±1.3, respectively (Fig. 2e). Mean quickscores for ERα immunoexpression in myometrial and leiomyoma samples were 7.7±2.0 and 16.6±0.6, respectively (Fig. 2e).

Secretory phase

Both leiomyoma and myometrial tissues from the secretory phase showed expression of ERα-phospho-Ser118 (Fig. 3); however, ERα-phospho-Ser118 expression was significantly lower in the myometrium (0.1±0.1) compared to leiomyoma (3.6±0.5) tissues (Fig. 3a and b). ERα expression was also significantly lower in myometrial tissue compared to leiomyomas (myometrium=6.4±1.3; leiomyoma=12.7±2.2; Fig. 3e).

When ERα-phospho-Ser118 expression in leiomyomas from the secretory phase was compared to those from the proliferative phase, we found that ERα-phospho-Ser118 was expressed at significantly higher levels in the leiomyomas from the proliferative (8.0±1.3) versus secretory (3.6±0.5) phase (Figs. 2e and 3e). Also, no significant differences in ERα and ERα-phospho-Ser118 immunoexpression were observed between small leiomyomas (<2 cm) and large leiomyomas (≥2 cm) when tumors from both phases were combined or evaluated independently by phase (data not shown).

Expression of phospho-p44/42 MAPK by immunohistochemistry

Due to increased expression of ERα-phospho-Ser118 in leiomyomas, we evaluated phosphorylated p44/42 MAPK (phospho-p44/42 MAPK) expression in leiomyomas and myometrial tissue samples from the same ten patients used for the ERα and ERα-phospho-Ser118 studies (Fig. 4). Overall, phospho-p44/42 MAPK was expressed in the nuclei of myometrial and leiomyoma cells (Fig. 4a and b). In the proliferative phase, phospho-p44/42 MAPK was expressed at significantly higher levels in leiomyomas (9.2±2.4) compared to myometrial (4.8±2.3) tissues (Fig. 4c). No significant difference was observed in the expression of phospho-p44/42 MAPK in myometrial (4.4±1.4) and leiomyoma (4.4±0.9) samples from women in the secretory phase. Although phospho-p44/42 MAPK was higher in leiomyomas from the proliferative phase, when mean expression data were compared between the two phases, there was no statistical difference in expression. Interestingly, a significant difference ($p \leq 0.05$) in phospho-p44/42 MAPK immunoexpression was observed between myometrial samples and small leiomyomas (≤2 cm) from the proliferative phase (4.8±2.3 and 11±3.1, respectively).

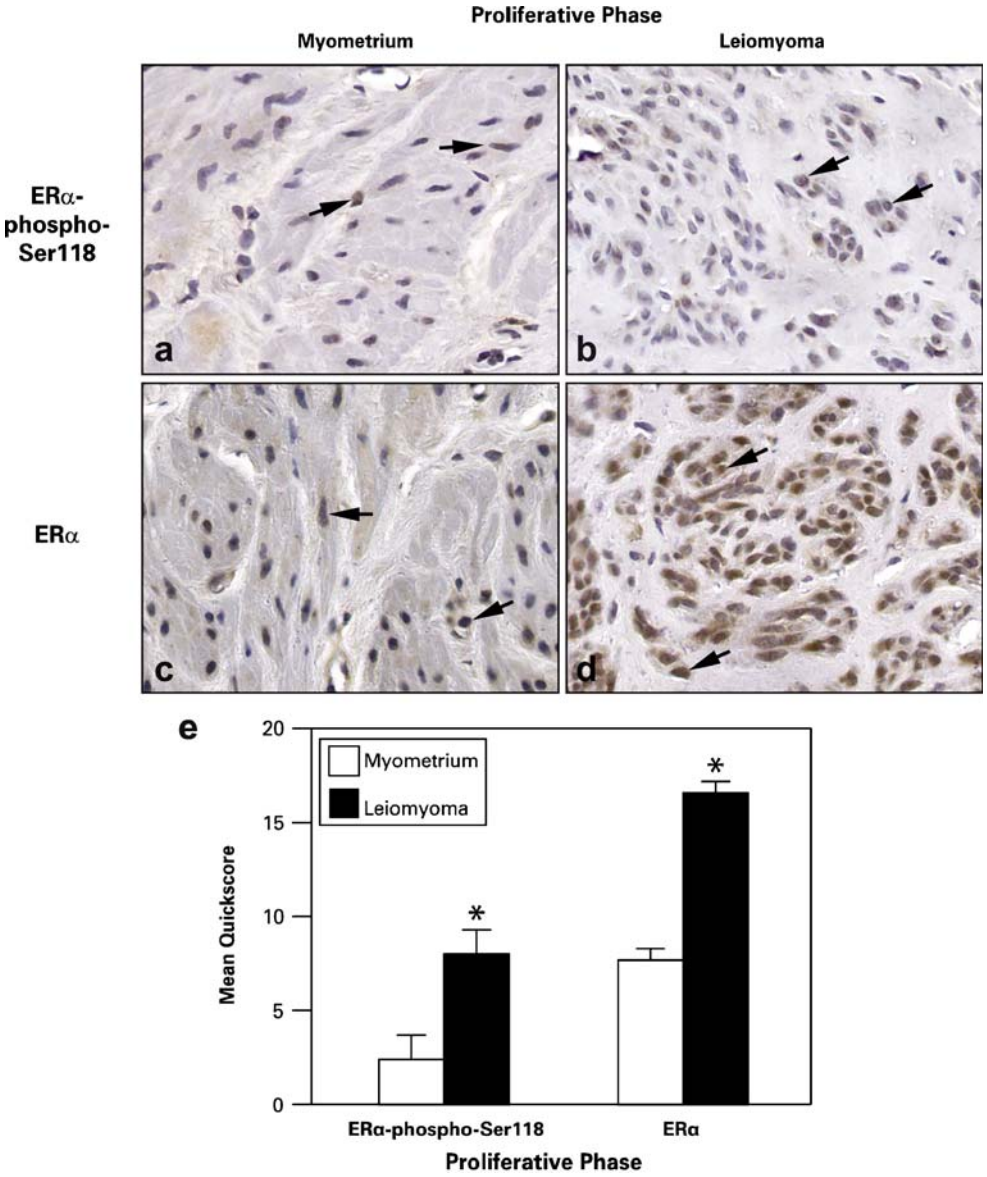

Fig. 2 Representative immunohistochemical staining of ERα-phospho-Ser118 and ERα in patient-matched myometrium and uterine leiomyoma tissue samples from women in the proliferative phase of the menstrual cycle. **a** and **b** ERα-phospho-Ser118 expression in myometrium (**a**) and leiomyoma (**b**) tissue samples. **c** and **d** ERα expression in myometrium (**c**) and leiomyoma (**d**) tissue samples. *Arrows* show positively stained nuclei of cells. **e** The bar graph represents the mean±SE of quickscore values for ERα-phospho-Ser118 and ERα in myometrial tissue and tumors. *$p \leq 0.05$; a significant difference versus myometrial samples ($n=10$ for myometrial samples and $n=20$ for leiomyoma samples; original magnification, ×40)

Colocalization of ERα-phospho-Ser118 and phospho-p44/42 MAPK

To determine if significantly increased levels of ERα-phospho-Ser118 and phospho-p44/42 MAPK observed in the tumors from the proliferative phase were colocalized, we conducted immunoflourescence and confocal microscopy studies to evaluate the localization of ERα-phospho-Ser118 (Fig. 5a and b) and phospho-p44/42 MAPK (Fig. 5c and d) in tumor and myometrial tissues from the proliferative phase. Both ERα-phospho-Ser118 and phospho-p44/42 MAPK were present in the nuclei of myometrial and leiomyoma tissue samples (Fig. 5a,b,c,d). Colocalization was more apparent in the nuclei of leiomyoma cells compared to myometrial cells in tissue samples (Fig. 5e and f).

Immunoprecipitation of ERα-phospho-Ser118 and phospho-p44/42 MAPK

To show the interaction of ER-phospho-Ser118 and phospho-p44/42 MAPK in myometrial and leiomyoma tissues from the proliferative phase, phospho-p44/42 MAPK was immunoprecipitated from myometrial and leiomyoma tissues and then immunoblotted for ER-phospho-Ser118 and phospho-p44/42 MAPK (control; Fig. 6). There was an increased association of ERα-phospho-Ser118 and

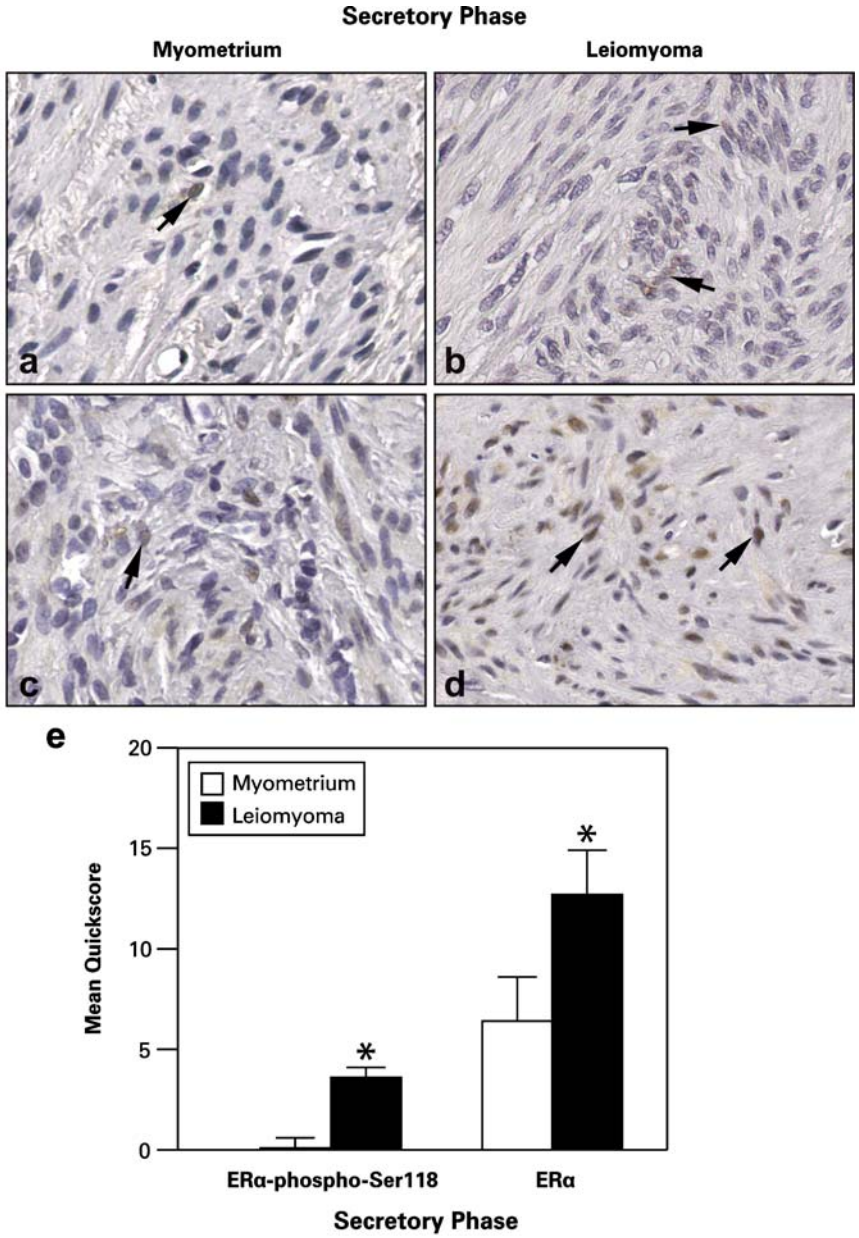

Fig. 3 Representative immunohistochemical staining of ERα-phospho-Ser118 and ERα in patient-matched myometrium and uterine leiomyoma tissue samples from women in the secretory phase of the menstrual cycle. **a** and **b** ERα-phospho-Ser118 expression in myometrium (**a**) and leiomyoma (**b**) tissue. **c** and **d** ERα expression in myometrium (**c**) and leiomyoma (**d**) tissue samples. *Arrows* show positively stained nuclei of cells. **e** The bar graph represents the mean±SE of quickscore values for ERα-phospho-Ser118 and ERα in myometrial tissue and tumors. *$p \leq 0.05$; a significant difference versus myometrial samples ($n=10$ for myometrial samples and $n=20$ for leiomyoma samples; original magnification, ×40)

phospho-p44/42 MAPK in leiomyomas compared to myometrial tissue.

Proliferating cell nuclear antigen (PCNA) labeling

Based on our findings of increased ERα-phospho-Ser118 expression in leiomyomas and the abundant association and colocalization of phospho-p44/42 MAPK and ERα-phospho-Ser118 in tumors during the proliferative phase, we conducted PCNA labeling studies to assess whether there would be differential expression of this cell proliferation marker in tumors versus myometrial samples from the proliferative and secretory phases. PCNA was highly expressed in tumors compared to myometrial tissue in both the proliferative and secretory phases with more expression in the proliferative phase tumors compared to those from the secretory phase (Fig. 7a–d). We found that the mean PCNA labeling indices were significantly higher in tumors versus myometrial tissue in both the proliferative and secretory phases of the menstrual cycle (Fig. 7e). Also, PCNA labeling in tumors from women in the proliferative phase was significantly higher than in tumors from the secretory phase (28.60±3.20 and 18.39±3.20, respectively). No significant differences were observed in the PCNA labeling in small leiomyomas (<2 cm) compared to large (≥2 cm) leiomyomas when combined or evaluated independently by phase, although in both phases, the mean labeling indices were higher in the smaller leiomyomas.

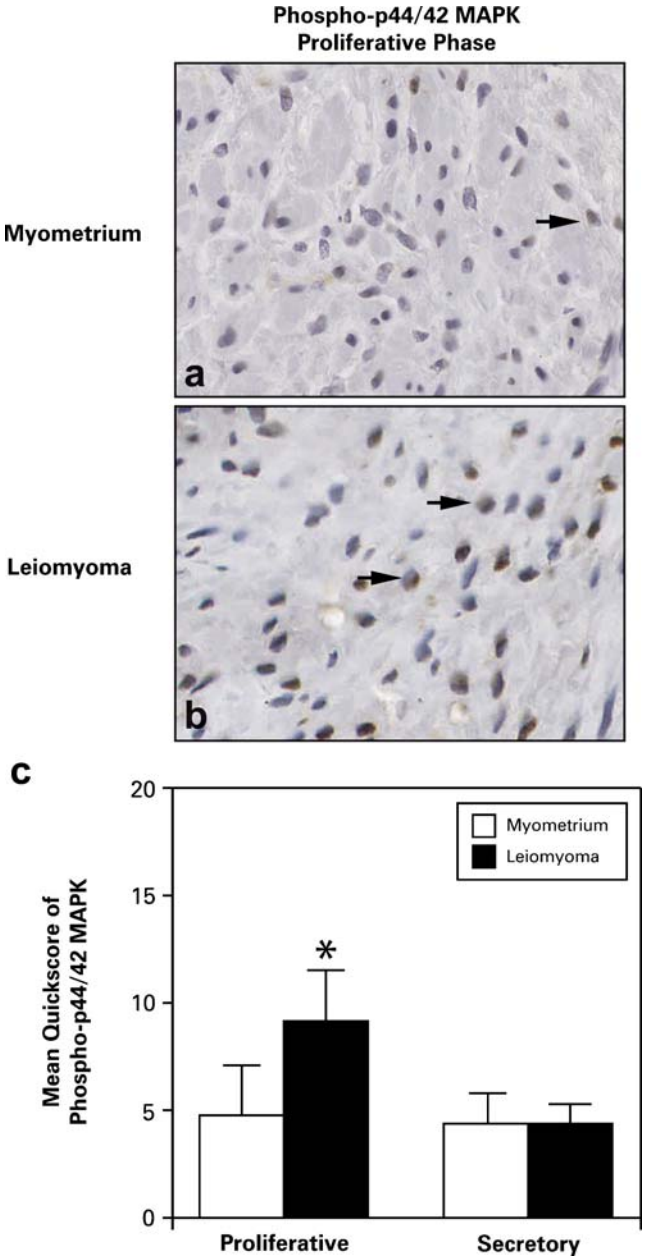

Fig. 4 Representative immunohistochemical staining of phospho-p44/42 MAPK in patient-matched myometrial and uterine leiomyoma tissues from the proliferative phase of the menstrual cycle. **a** and **b** Phospho-p44/42 MAPK expression was expressed in the nuclei (*arrows*) of myometrial (**a**) and tumor (**b**) smooth muscle cells, although it was significantly increased in tumors from the proliferative phase. **c** The bar graph represents the mean±SE of quickscore values for phospho-p44/42 MAPK in myometrial tissue and leiomyomas from the proliferative and secretory phases of the menstrual cycle. *$p \leq 0.05$; a significant difference versus myometrial samples in the proliferative phase ($n=10$ for myometrial samples and $n=20$ for leiomyoma samples; original magnification, ×40)

Discussion

To our knowledge, this is the first study to evaluate ERα-phospho-Ser118 expression in uterine leiomyomas. These data show that ERα is a phosphoprotein that is phosphorylated at serine 118 residues in uterine leiomyomas. Phosphorylation of ERα at serine 118 has been extensively studied in breast cancer cells and is enhanced in response to estradiol binding and through the action of second messenger signaling pathways [25]. Previous in vitro and in vivo studies have demonstrated that ERα is phosphorylated at serine 118 in the presence or absence of estradiol and by growth factor peptides and their receptors through activation of the MAPK (ERK 1/2) pathway, which can lead to transcription [7, 11]. ERα from calf uterus is phosphorylated at serine residues in response to estradiol [11]. Also, phosphorylation of mouse uterine ERα at serine residues is enhanced in response to estrogen [41].

In our study, ERα-phospho-Ser118 immunoexpression was significantly higher in tumors from women in the proliferative phase of the menstrual cycle compared to those in the secretory phase, although expression was present in tumors and significantly higher than the myometrium in samples from both the secretory and proliferative phases. Increased phosphorylation of ERα at serine 118 observed in tumors from the proliferative (estrogen dominant) phase may indicate that phosphorylation may be regulated by higher concentrations of estrogen and lower concentrations of progesterone. There is evidence suggesting that estradiol can increase the expression of ERα-phospho-Ser118 in breast cancer cells [7]. Estrogen has also been shown to increase uterine leiomyoma cell proliferation and progesterone receptor mRNA and protein expression [1, 16, 19], whereas progesterone has been shown to have a dual effect on the growth of uterine leiomyomas by decreasing and increasing the size of some fibroids through regulation of the local growth factor milieu in women treated with the progestin, levonorgestrel [27]. In our study, the phosphorylation of ERα was lower in the secretory phase where progesterone is the dominant hormone. Also, other studies comparing estrogen receptor protein expression in leiomyomas from women in the proliferative and secretory phases have shown that ER was expressed at lower levels during the secretory phase. This supports the concept that progesterone may be decreasing the levels of ERα, thereby making less receptor available for phosphorylation [3, 22, 43].

In this study, we used immunohistochemistry and found nuclear expression of phospho-p44/42 MAPK to be significantly increased in leiomyomas compared to myometrial tissue from the proliferative phase of the cycle. Chegini et al. have demonstrated that phospho-p44/42 MAPK is expressed more in leiomyomas compared to myometrial tissue, but this difference was not significant, and no menstrual phase data were reported in their study. In our study, there was no significant difference in phospho-p44/42 MAPK expression in tumors in the secretory phase compared to patient-matched myometrial samples, and

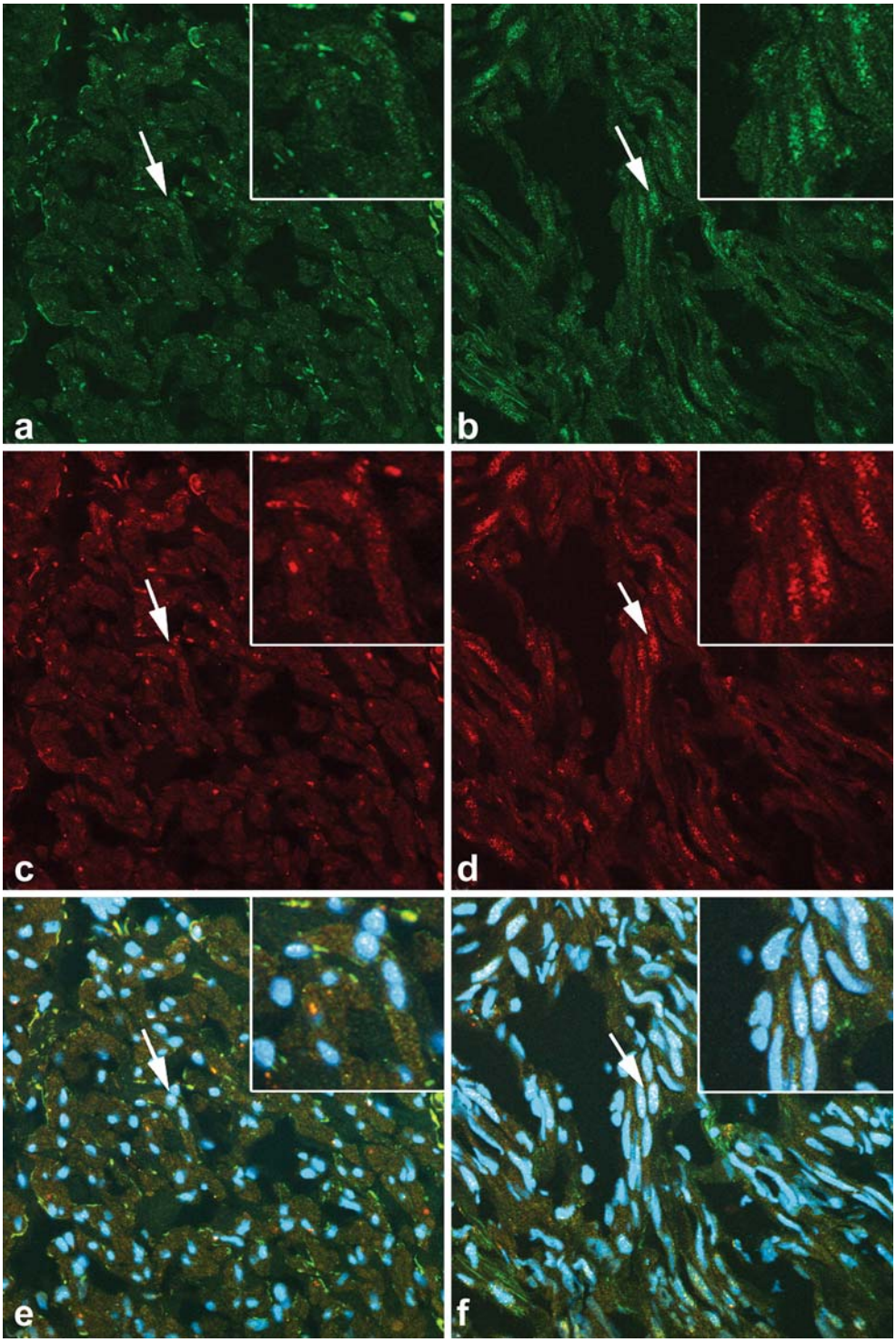

Fig. 5 Colocalization of ERα-phospho-Ser118 and phospho-p44/42 MAPK in myometrium and uterine leiomyoma tissue. *Arrows* show nuclei in the inset (*top right corner*) that are positively stained for ERα-phospho-Ser118 (*green fluorescence*; **a** and **b**), phospho-p44/42 MAPK (*red fluorescence*; **c** and **d**), and both ERα-phospho-Ser118 and phospho-p44/42 MAPK (*white/yellow fluorescence*; **e** and **f**) in myometrial (**a**, **c**, and **e**) and leiomyoma (**b**, **d**, and **f**) tissues. DAPI was used to stain the nuclei (*blue fluorescence*; **e** and **f**; original magnification, ×40/zoom of 1)

when tumors from both phases of the cycle were combined, this resulted in a lack of significance of expression of phospho-p44/42 MAPK in leiomyoma versus myometrial tissue. This is most likely due to significant phospho-p44/42 MAPK expression being phase specific and could be missed if data from the two phases are combined.

In breast cancer cells, phospho-p44/42 MAPK has been found to phosphorylate the ER at serine 118 in response to estrogen [7]. In this study, we found higher expression and colocalization of phospho-p44/42 MAPK and ERα-phospho-Ser118 in leiomyomas from the proliferative phase, which is the phase of the cycle where the estradiol/progesterone ratio is

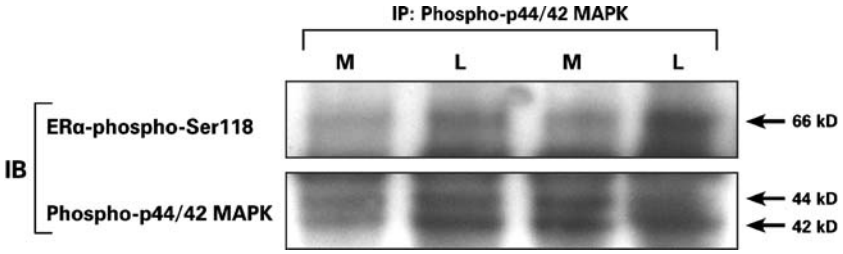

Fig. 6 Immunoprecipitation of ERα-phospho-Ser118 and phospho-p44/42 MAPK in myometrial (*M*) and uterine leiomyoma (*L*) tissue lysates from the proliferative phase. Phospho-p44/42 MAPK was immunoprecipitated (*IP*) from leiomyoma and myometrial tissue and then immunoblotted (*IB*) with the anti-ERα-phospho-Ser118 (66 kDa) and phospho-p44/42 MAPK (44 and 42 kDa; control) antibodies

high. These data imply that in leiomyomas, phospho-p44/42 MAPK may be the kinase that phosphorylates the ER at serine 118, and this phosphorylation may be enhanced during the proliferative phase by higher concentrations of estradiol and lower concentrations of progesterone.

Previously, we found PCNA expression to be significantly higher in leiomyomas than in matched myometrial samples [13]. In this study, PCNA expression was also significantly higher in leiomyomas than in matched myometrial samples. On average, PCNA labeling was

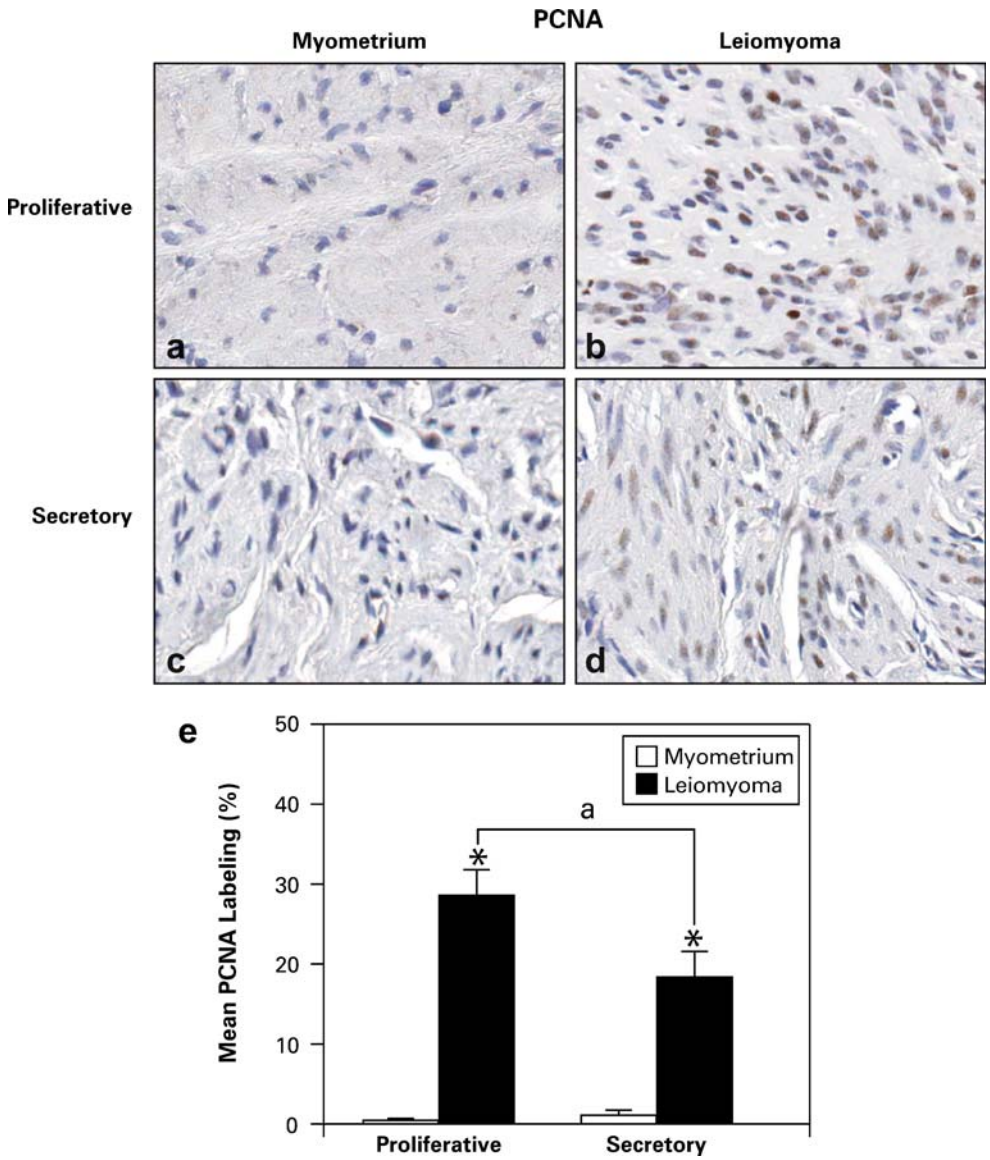

Fig. 7 Representative PCNA immunohistochemical staining in patient-matched myometrium and uterine leiomyoma tissue samples from the proliferative (**a** and **b**) and secretory (**c** and **d**) phases (original magnification, ×40). **e** Bar graph represents the mean±SE of percent of cells labeled with PCNA in myometrial (*white bar*) and leiomyoma (*black bar*) tissues. *$p \leq 0.05$; a significant difference versus myometrial tissue, and "*a*" represents significance ($p \leq 0.05$) between leiomyomas of the proliferative versus secretory phase of the menstrual cycle ($n=10$ for myometrial samples and $n=20$ for leiomyoma samples)

0.77% in the myometrium and 23.50% in leiomyomas. PCNA labeling of cells in tumors from women in the proliferative phase (28.60%) was significantly higher compared to tumors from women of the secretory phase (18.39%). These data show that leiomyomas proliferate at a higher rate than normal myometrium and that proliferation is increased in tumors from the proliferative phase compared to those from the secretory phase of the menstrual cycle. The PCNA labeling indices in this study were higher compared to the values from a previous study, which was most likely due to the increased sensitivity of the primary antibody used in this study compared to our earlier studies. More importantly, however, the overall trend of increased PCNA labeling in leiomyomas versus myometria and increased labeling of proliferative phase tumors versus secretory phase are in agreement with our earlier findings and others, respectively [13, 20]. Also, although PCNA labeling was increased overall in the leiomyomas, there was variation of PCNA expression between tumors from individual women, which supports the importance of hormones in up- or down-regulating local cytokines and growth factors that in turn may control autonomous tumor growth. In this study, it appears that phosphorylation of ER at serine 118 is a predominant feature of the proliferative phase, and this may be an important factor in increased transcription, translation, and proliferation observed in uterine leiomyomas during this phase.

No significant differences in ERα-phospho-Ser118, ERα, and PCNA immunoexpression were observed between small leiomyomas and large leiomyomas when tumors from both phases were combined or evaluated independently by phase, which may be due to the abundant amount of extracellular matrix proteins that is involved in the expansion of fibroids [36]. Many uterine leiomyomas contain an abundant amount of fibrous connective tissue and extracellular matrix proteins (collagen, proteoglycans, and fibronectin) [36]. ERα-phospho-Ser118, ERα, and PCNA are expressed predominantly in the nuclei of smooth muscle tumor cells, which may not be the main contributor to size in larger leiomyomas containing an abundance of extracellular matrix proteins.

In summary, the mechanisms whereby ER and growth factor signaling pathways interact and promote leiomyoma growth are not known and have not been widely studied. In this study, we found that ERα-phospho-Ser118 and phospho-p44/42 MAPK protein expression levels were significantly increased independently and highly coexpressed in leiomyomas from women in the proliferative phase of the menstrual cycle compared to myometrial tissue samples. In addition, leiomyomas from the proliferative phase had significantly increased PCNA labeling compared to patient-matched myometrial tissue samples and tumors from the secretory phase.

Our data suggest that there are interactions between ER and growth factor signaling pathways in uterine leiomyomas. Also, these data show that ERα may be phosphorylated by phospho-p44/42 MAPK at Ser-118 and possibly play an important role in the growth of fibroids. Additionally, the expression of ERα-phospho-Ser118 may be, in part, regulated by high amounts of estrogen and low amounts of progesterone. To provide further evidence that ERα may be phosphorylated by phospho-p44/42 MAPK at Ser-118 in fibroids, immunoprecipitation assays were done and showed an increased association of ERα-phospho-Ser118 and phospho-p44/42 MAPK proteins in leiomyomas compared to myometrial tissue. The pathways involved in phosphorylation of ERα in uterine leiomyomas have not been studied. In Fig. 8, we propose a possible mechanism of interaction between the ERα and growth factor signaling pathways and the regulation of these pathways by estradiol (E_2) and progesterone (P_4), which is highly supported by the data reported in this paper. This schematic shows that activation of ERα via phosphorylation at serine 118 by phospho-p44/42 MAPK is regulated by E_2 (positively) and P_4 (positively or negatively) through the up-

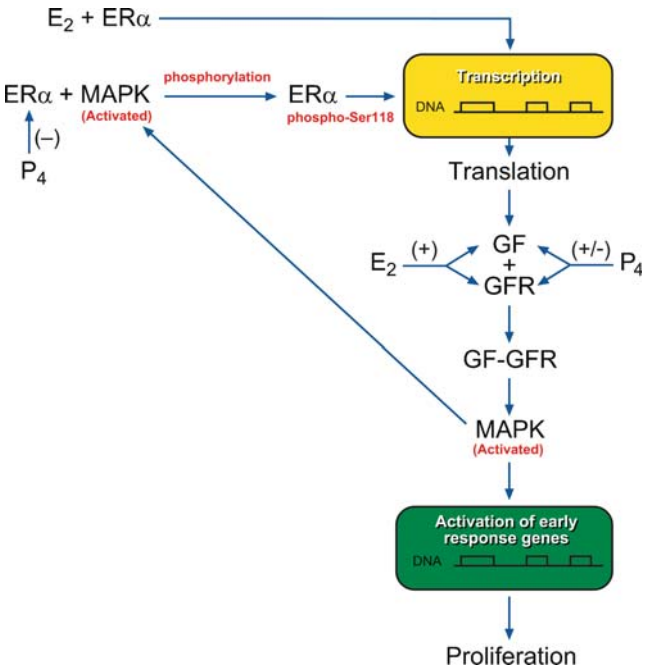

Fig. 8 Proposed pathway for the interaction between ERα and growth factor (*GF*) signaling pathways and regulation by estradiol (E_2) and progesterone (P_4). The ERα is activated by classical E_2 binding and/or by phosphorylation at serine 118 by activated MAPK. Activated ERα then activates gene transcription and translation of a GF. The GF will bind to its receptor (*GFR*), and the activated GFR will in turn activate the MAPK pathway, which can result in proliferation and also possible phosphorylation of ERα at serine 118. E_2 can up-regulate GFs and GFRs with an increase in downstream MAPK activation and possible ERα-phospho-Ser118 phosphorylation, whereas P_4 can decrease or increase ERα, GF, and GFR production, which in turn results in up- or down-regulation of activated MAPK and ERα-phospho-Ser118 expression

or down-regulation of local cytokines, growth factors, and growth factor receptors [17, 21, 29, 32]. Future studies are underway to test this hypothesis.

Acknowledgments The authors would like to thank Norris Flagler, Elizabeth Ney, Paul Cacioppo, and C. Jeffrey Tucker for their technical assistance with imaging. This research was supported, in part, by the Intramural Research Program of the NIH, National Institute of Environmental Health Sciences.

Conflict of interest statement We declare that we have no conflict of interest.

References

1. Barbarisi A, Petillo O, Di Lieto A, Melone MA, Margarucci S, Cannas M, Peluso G (2001) 17-beta estradiol elicits an autocrine leiomyoma cell proliferation: evidence for a stimulation of protein kinase-dependent pathway. J Cell Physiol 186(3):414–424
2. Beinfeld MT, Bosch JL, Isaacson KB, Gazelle GS (2004) Cost-effectiveness of uterine artery embolization and hysterectomy for uterine fibroids. Radiology 230(1):207–213
3. Bourlev V, Pavlovitch S, Stygar D, Volkov N, Lindblom B, Olovsson M (2003) Different proliferative and apoptotic activity in peripheral versus central parts of human uterine leiomyomas. Gynecol Obstet Invest 55(4):199–204
4. Bunone G, Briand PA, Miksicek RJ, Picard D (1996) Activation of the unliganded estrogen receptor by EGF involves the MAP kinase pathway and direct phosphorylation. Embo J 15(9):2174–2183
5. Buttram VC Jr (1986) Uterine leiomyomata—aetiology, symptomatology and management. Prog Clin Biol Res 225:275–296
6. Chegini N, Kornberg L (2003) Gonadotropin releasing hormone analogue therapy alters signal transduction pathways involving mitogen-activated protein and focal adhesion kinases in leiomyoma. J Soc Gynecol Investig 10(1):21–26
7. Chen D, Washbrook E, Sarwar N, Bates GJ, Pace PE, Thirunuvakkarasu V, Taylor J, Epstein RJ, Fuller-Pace FV, Egly JM, Coombes RC, Ali S (2002) Phosphorylation of human estrogen receptor alpha at serine 118 by two distinct signal transduction pathways revealed by phosphorylation-specific antisera. Oncogene 21(32):4921–4931
8. Chwalisz K, DeManno D, Garg R, Larsen L, Mattia-Goldberg C, Stickler T (2004) Therapeutic potential for the selective progesterone receptor modulator asoprisnil in the treatment of leiomyomata. Semin Reprod Med 22(2):113–119
9. Chwalisz K, Perez MC, Demanno D, Winkel C, Schubert G, Elger W (2005) Selective progesterone receptor modulator development and use in the treatment of leiomyomata and endometriosis. Endocr Rev 26(3):423–438
10. Cook JD, Walker CL (2004) Treatment strategies for uterine leiomyoma: the role of hormonal modulation. Semin Reprod Med 22(2):105–111
11. Denton RR, Koszewski NJ, Notides AC (1992) Estrogen receptor phosphorylation. Hormonal dependence and consequence on specific DNA binding. J Biol Chem 267(11):7263–7268
12. Detre S, Saclani Jotti G, Dowsett M (1995) A "quickscore" method for immunohistochemical semiquantitation: validation for oestrogen receptor in breast carcinomas. J Clin Pathol 48(9):876–878
13. Dixon D, Flake GP, Moore AB, He H, Haseman JK, Risinger JI, Lancaster JM, Berchuck A, Barrett JC, Robboy SJ (2002) Cell proliferation and apoptosis in human uterine leiomyomas and myometria. Virchows Arch 441(1):53–62
14. Emembolu JO (1987) Uterine fibromyomata: presentation and management in northern Nigeria. Int J Gynaecol Obstet 25 (5):413–416
15. Farquhar CM, Steiner CA, Sozen I, Arici A (2002) Hysterectomy rates in the United States 1990–1997. Obstet Gynecol 99(2):229–234
16. Hodges LC, Houston KD, Hunter DS, Fuchs-Young R, Zhang Z, Wineker RC, Walker CL (2002) Transdominant suppression of estrogen receptor signaling by progesterone receptor ligands in uterine leiomyoma cells. Mol Cell Endocrinol 196(1–2):11–20
17. Jasonni VM, La Marca A, Santini D (2005) Progestin effects on epidermal growth factor receptor (EGFR) endometrial expression in normal and hyperplastic endometrium. Int J Gynaecol Obstet 89(3):297–298
18. Kato S, Endoh H, Masuhiro Y, Kitamoto T, Uchiyama S, Sasaki H, Masushige S, Gotoh Y, Nishida E, Kawashima H, Metzger D, Chambon P (1995) Activation of the estrogen receptor through phosphorylation by mitogen-activated protein kinase. Science 270 (5241):1491–1494
19. Katzenellenbogen BS (2000) Mechanisms of action and cross-talk between estrogen receptor and progesterone receptor pathways. J Soc Gynecol Investig 7(1 Suppl):S33–S37
20. Kayisli UA, Berkkanoglu M, Kizilay G, Senturk L, Arici A (2007) Expression of proliferative and preapoptotic molecules in human myometrium and leiomyoma throughout the menstrual cycle. Reprod Sci 14(7):678–686
21. Kim MR, Park DW, Lee JH, Choi DS, Hwang KJ, Ryu HS, Min CK (2005) Progesterone-dependent release of transforming growth factor-beta1 from epithelial cells enhances the endometrial decidualization by turning on the Smad signalling in stromal cells. Mol Hum Reprod 11(11):801–808
22. Kovacs KA, Oszter A, Gocze PM, Kornyei JL, Szabo I (2001) Comparative analysis of cyclin D1 and oestrogen receptor (alpha and beta) levels in human leiomyoma and adjacent myometrium. Mol Hum Reprod 7(11):1085–1091
23. Kraus WL, Katzenellenbogen BS (1993) Regulation of progesterone receptor gene expression and growth in the rat uterus: modulation of estrogen actions by progesterone and sex steroid hormone antagonists. Endocrinology 132(6):2371–2379
24. Kraus WL, Weis KE, Katzenellenbogen BS (1995) Inhibitory cross-talk between steroid hormone receptors: differential targeting of estrogen receptor in the repression of its transcriptional activity by agonist- and antagonist-occupied progestin receptors. Mol Cell Biol 15(4):1847–1857
25. Lannigan DA (2003) Estrogen receptor phosphorylation. Steroids 68(1):1–9
26. Marsh EE, Bulun SE (2006) Steroid hormones and leiomyomas. Obstet Gynecol Clin North Am 33(1):59–67
27. Maruo T, Ohara N, Matsuo H, Xu Q, Chen W, Sitruk-Ware R, Johansson ED (2007) Effects of levonorgestrel-releasing IUS and progesterone receptor modulator PRM CDB-2914 on uterine leiomyomas. Contraception 75(6 Suppl):S99–103
28. Maruo T, Ohara N, Wang J, Matsuo H (2004) Sex steroidal regulation of uterine leiomyoma growth and apoptosis. Hum Reprod Update 10(3):207–220
29. Matsuzaki S, Canis M, Pouly JL, Botchorishvili R, Dechelotte PJ, Mage G (2007) Both GnRH agonist and continuous oral progestin treatments reduce the expression of the tyrosine kinase receptor B and mu-opioid receptor in deep infiltrating endometriosis. Hum Reprod 22(1):124–128
30. Parazzini F (2006) Risk factors for clinically diagnosed uterine fibroids in women around menopause. Maturitas 55(2):174–179
31. Rein M (1992) Biology of uterine myomas and myometrium in vitro. In: Barbieri RL (ed) Seminars in reproductive endocrinology. Thieme, New York, pp 310–319
32. Reis FM, Lhullier C, Edelweiss MI, Spritzer PM (2005) In vivo assessment of the regulation of transforming growth factor alpha,

epidermal growth factor (EGF), and EGF receptor in the human endometrium by medroxyprogesterone acetate. J Assist Reprod Genet 22(1):19–24
33. Sato F, Mori M, Nishi M, Kudo R, Miyake H (2002) Familial aggregation of uterine myomas in Japanese women. J Epidemiol 12(3):249–253
34. Shimomura Y, Matsuo H, Samoto T, Maruo T (1998) Up-regulation by progesterone of proliferating cell nuclear antigen and epidermal growth factor expression in human uterine leiomyoma. J Clin Endocrinol Metab 83(6):2192–2198
35. Sozen I, Arici A (2002) Interactions of cytokines, growth factors, and the extracellular matrix in the cellular biology of uterine leiomyomata. Fertil Steril 78(1):1–12
36. Stewart EA, Friedman AJ, Peck K, Nowak RA (1994) Relative overexpression of collagen type I and collagen type III messenger ribonucleic acids by uterine leiomyomas during the proliferative phase of the menstrual cycle. J Clin Endocrinol Metab 79(3):900–906
37. Swartz CD, Afshari CA, Yu L, Hall KE, Dixon D (2005) Estrogen-induced changes in IGF-I, Myb family and MAP kinase pathway genes in human uterine leiomyoma and normal uterine smooth muscle cell lines. Mol Hum Reprod 11(6):441–450
38. Vereide AB, Kaino T, Sager G, Arnes M, Orbo A (2006) Effect of levonorgestrel IUD and oral medroxyprogesterone acetate on glandular and stromal progesterone receptors (PRA and PRB), and estrogen receptors (ER-alpha and ER-beta) in human endometrial hyperplasia. Gynecol Oncol 101(2):214–223
39. Vollenhoven B (1998) Introduction: the epidemiology of uterine leiomyomas. Baillieres Clin Obstet Gynaecol 12(2):169–176
40. Wang J, Ohara N, Wang Z, Chen W, Morikawa A, Sasaki H, DeManno DA, Chwalisz K, Maruo T (2006) A novel selective progesterone receptor modulator asoprisnil (J867) down-regulates the expression of EGF, IGF-I, TGFbeta3 and their receptors in cultured uterine leiomyoma cells. Hum Reprod 21 (7):1869–1877
41. Washburn T, Hocutt A, Brautigan DL, Korach KS (1991) Uterine estrogen receptor in vivo: phosphorylation of nuclear specific forms on serine residues. Mol Endocrinol 5(2):235–242
42. Yamada T, Nakago S, Kurachi O, Wang J, Takekida S, Matsuo H, Maruo T (2004) Progesterone down-regulates insulin-like growth factor-I expression in cultured human uterine leiomyoma cells. Hum Reprod 19(4):815–821
43. Zaslawski R, Surowiak P, Dziegiel P, Pretnik L, Zabel M (2001) Analysis of the expression of estrogen and progesterone receptors, and of PCNA and Ki67 proliferation antigens, in uterine myomata cells in relation to the phase of the menstrual cycle. Med Sci Monit 7(5):908–913

Virchows Arch (2008) 453:571–578
DOI 10.1007/s00428-008-0681-y

ORIGINAL ARTICLE

Caveolin-1 immuno-expression in human gastric cancer: histopathogenetic hypotheses

V. Barresi · G. Giuffre' · E. Vitarelli · P. Todaro · G. Tuccari

Received: 19 June 2008 / Revised: 4 September 2008 / Accepted: 26 September 2008 / Published online: 21 October 2008

Abstract The immunohistochemical expression of caveolin-1 (cav-1) was evaluated in a series of gastric carcinomas (GC) and in the adjacent normal gastric mucosa. Cav-1 immuno-expression was found in most GC (94%) with a significantly higher amount in the Lauren intestinal type in comparison to the diffuse-type carcinomas. Interestingly, gastric intestinal metaplasia as well as the cells at the base and neck of gastric pits within all fundic mucosal fragments showed an evident cav-1 immuno-staining, suggesting a histogenetic derivation of these lesions from the *trans*-differentiation of chief cells or from a cryptic progenitor population at the base of fundic glands, as recently hypothesized by other authors. The absence of significant correlations between cav-1 immuno-expression and the other clinico-pathological parameters, such as the stage of disease or the patients overall survival, indicates that the role of cav-1 in GC is neither stage-specific nor related to prognosis.

Keywords Caveolin-1 · Gastric cancer · Histogenesis · Fundic mucosa · Prognosis

Introduction

Caveolin-1 (cav-1) is a 22-kDa protein which is mainly expressed by fibroblasts, adipocytes, and endothelial and smooth muscle cells [1]. It is involved in transmembrane transport processes [2] and signal transduction mechanisms [3].

An ambivalent role in tumorigenesis has been attributed to cav-1. Indeed, even if it may exert a tumor suppressor activity by inhibiting the signalling products of several proto-oncogenes [4], its tyrosine-14 phosphorylation results in growth stimulation [5], suggesting that cav-1 may also behave as a pro-tumorigenic factor.

When cav-1 expression has been investigated in human neoplasms, cav-1 down-regulation has been found in certain tumors [6, 7], whereas its over-expression has been documented in others [8–10], thus indicating a tissue-dependent behavior of cav-1 in cancerogenesis.

Among the digestive system neoplasms, cav-1 over-expression has been shown in colorectal adenocarcinoma [11] and esophageal squamous cell carcinoma [12, 13], consistently with a pro-tumorigenic action in both malignancies; moreover, an additional role in tumor progression and aggressiveness has been demonstrated in esophageal squamous cell carcinoma [12, 13]. By contrast, recent data seem to indicate that cav-1 acts as a tumor suppressor factor in gastric carcinoma (GC) [14]. Indeed, cav-1 down-regulation has been documented in association with the acquisition of a tumor phenotype in gastric mucosa [14]. Nonetheless, since a high cav-1 expression has been found in cell lines derived from GC distant metastases, it has been proposed that cav-1 is down-regulated during gastric epithelial cell transformation, and then regained in GC cells undergoing detachment from the basal membrane and invasion into the underlying stroma [14].

In view of this, in the present study, cav-1 immunohistochemical expression has been investigated in a series of surgically resected GC and correlated with clinico-pathological parameters, in an attempt to verify its eventual

V. Barresi · G. Giuffre' · E. Vitarelli · P. Todaro · G. Tuccari
Department of Human Pathology, University of Messina, Messina, Italy

V. Barresi (✉)
Department of Human Pathology,
Policlinico Universitario G. Martino,
Pad D, Via Consolare Valeria,
98125 Messina, Italy
e-mail: valeriabarresi@hotmail.com

Table 1 Clinico-pathological characteristics and cav-1 immuno-expression data of 49 analyzed GC

Case	Sex	Age	Site	Type	WHO histotype	Lauren histotype	Grade	pT	pN	pM	Stage	FU (months)	Status	Cav-1 ID score	Cav-1 ASP	Cav-1 IS
1	F	62	Antrum	EGC	Tubular	Intestinal	LG	T1	N1	Mx	1b	126	Alive	6	3	2
2	M	71	Antrum	AGC	SRC	diffuse	/	T3	N1	Mx	2	0	DOD	4	2	2
3	M	68	Body	AGC	Tubular	Intestinal	HG	T2	N2	Mx	3a	46	DOD	6	3	2
4	F	69	Antrum	AGC	Tubular	Intestinal	HG	T2	N0	Mx	1b	144	Alive	2	2	1
5	F	46	Antrum	EGC	Tubular	Intestinal	HG	T1	N0	Mx	1a	168	Alive	1	1	1
6	M	65	Antrum	AGC	Tubular	Intestinal	LG	T2	N0	Mx	1b	122	Alive	9	3	3
7	M	*61*	Antrum	AGC	Tubular	Intestinal	HG	T2	N1	Mx	2	NA	NA	1	1	1
8	M	55	Antrum	AGC	Mucinous	Intestinal	/	T3	N0	Mx	2	12	DOD	6	3	2
9	M	70	Body	AGC	Tubular	Intestinal	LG	T2	N0	Mx	1b	0	DOD	4	2	2
10	M	78	Cardia	AGC	Tubular	Intestinal	LG	T3	N2	M1	4	27	DOD	1	1	1
11	F	78	Antrum	AGC	SRC	Diffuse	/	T2	N1	Mx	2	NA	NA	1	1	1
12	F	66	Cardia	AGC	Tubular	Intestinal	LG	T3	N1	Mx	3a	20	DOD	4	2	2
13	M	64	Body	AGC	SRC	Diffuse	/	T2	N0	Mx	1b	123	Alive	0	0	0
14	M	81	Cardia	AGC	Tubular	Intestinal	LG	T2	N0	Mx	1b	24	DOD	4	2	2
15	M	50	Body	AGC	Mucinous	Intestinal	/	T3	N1	Mx	2	103	Alive	4	2	2
16	F	79	Antrum	EGC	Tubular	Intestinal	LG	T1	N0	Mx	1a	60	Alive	4	2	2
17	M	77	Antrum	AGC	SRC	Diffuse	/	T3	N2	Mx	3b	22	DOD	2	2	1
18	M	66	AB	AGC	Tubular	Intestinal	LG	T2	N1	Mx	2	4	DOD	1	1	1
19	F	67	Antrum	AGC	Tubular	Intestinal	HG	T3	N2	Mx	3b	26	DOD	2	2	1
20	F	55	Body	EGC	Tubular	Intestinal	HG	T1	N1	Mx	1b	60	Alive	1	1	1
21	F	76	Antrum	EGC	Mucinous	Intestinal	/	T1	N1	Mx	1b	58	DOD	6	3	2
22	F	58	Body	AGC	Tubular	Intestinal	LG	T2	N2	Mx	3a	12	DOD	4	2	2
23	F	62	Cardia	AGC	Tubular	Intestinal	LG	T3	N2	M1	4	12	DOD	8	4	2
24	F	50	Body	EGC	SRC	Diffuse	/	T1	N0	Mx	1a	132	Alive	0	0	0
25	F	57	Antrum	AGC	Tubular	Intestinal	LG	T4	N1	Mx	3b	60	Alive	4	2	2
26	M	60	Antrum	AGC	Tubular	Intestinal	LG	T3	N0	Mx	2	34	DOD	4	2	2
27	F	64	Antrum	AGC	SRC	Diffuse	/	T2	N2	Mx	3a	34	DOD	4	2	2
28	F	67	Antrum	AGC	Tubular	Intestinal	HG	T4	N1	Mx	3b	12	DOD	1	1	1
29	M	63	Antrum	AGC	Tubular	Intestinal	LG	T4	N0	Mx	3a	62	DOD	1	1	1
30	F	39	Antrum	EGC	SRC	Diffuse	/	T1	N1	Mx	1b	167	DOD	1	1	1
31	M	60	AB	AGC	Tubular	Intestinal	LG	T3	N0	Mx	2	27	DOD	4	2	2
32	F	77	Antrum	AGC	SRC	Diffuse	/	T2	N0	Mx	1b	91	Alive	0	0	0
33	F	39	Body	AGC	SRC	Diffuse	/	T2	N2	Mx	3a	12	DOD	2	1	2
34	M	67	AB	AGC	SRC	Diffuse	/	T3	N1	Mx	3a	13	DOD	2	1	2
35	F	67	Antrum	AGC	Tubular	Intestinal	LG	T2	N1	Mx	2	121	Alive	4	2	2
36	M	64	Antrum	AGC	Tubular	Intestinal	HG	T3	N1	Mx	2	21	DOD	6	2	3
37	M	79	Antrum	AGC	Tubular	Intestinal	HG	T3	N1	Mx	3a	10	DOD	12	4	3
38	F	77	Cardia	AGC	Tubular	Intestinal	HG	T3	N0	Mx	2	56	Alive	4	2	2
39	M	51	Antrum	EGC	Tubular	Intestinal	LG	T1	N0	Mx	1a	134	Alive	4	2	2
40	M	69	Body	AGC	Tubular	Intestinal	HG	T2	N1	Mx	2	11	DOD	6	3	2
41	M	78	Cardia	AGC	Tubular	Intestinal	HG	T2	N2	Mx	3a	18	DOD	6	3	2

42	M	62	Cardia	AGC	Tubular	Intestinal	LG	T3	N1	Mx	3a	30		DOD	9	3	3
43	M	72	Body	AGC	Tubular	Intestinal	LG	T2	N0	Mx	1b	55		DOD	6	3	2
44	F	45	AB	AGC	Tubular	Intestinal	LG	T3	N1	Mx	3a	144		Alive	2	2	1
45	M	37	Antrum	AGC	SRC	Diffuse	/	T2	N1	Mx	2	30		DOD	2	2	1
46	M	61	Antrum	AGC	SRC	Diffuse	/	T2	N0	Mx	1b	140		Alive	4	2	2
47	M	41	Antrum	AGC	Tubular	Intestinal	LG	T3	N1	Mx	2	144		Alive	12	4	3
48	M	64	Antrum	AGC	Tubular	Intestinal	LG	T3	N1	Mx	3a	30		DOD	4	2	2
49	F	55	Antrum	AGC	SRC	Diffuse	/	T3	N2	Mx	3b	7		DOD	4	2	2

FU follow-up, *ID* intensity distribution, *IS* intensity of staining, *ASP* area of staining positivity, *IM* intestinal metaplasia, *AB* antrum-body, *EGC* early gastric cancer, *AGC* advanced gastric cancer, *LG* low grade, *HG* high grade, *DOD* dead of disease

changes in association with the stage, histotype, presence of lymph node metastases, or overall survival of the patients.

Materials and methods

Forty nine cases of surgically resected GC, obtained from 27 male and 22 female patients (mean age 63 years; age range 37–81 years), were taken from the files of the Department of Human Pathology, University of Messina, Italy. Patients who had received preoperative neo-adjuvant therapy were excluded from the study. Thirty six cases (74%) contained adjacent non-neoplastic and not infiltrated gastric mucosa; specifically, a cardiac or antral mucosa was present in twenty-seven cases, whereas fundic gastric mucosa was found in nine cases. Moreover, in 22/49 (45%) cases, intestinal metaplasia (IM) was evidenced in the normal mucosa adjacent to the tumor.

For each case, the age and gender of the patients, the site as well as the World Health Organization (WHO) [15] and Lauren [16] histotypes of the tumors were considered. Histological grading and tumor staging were based on the criteria of the WHO classification [15] and TNM system. Well and moderately differentiated GC were grouped together for the statistical analyses and considered as low grade tumors in contraposition to high grade GC. In addition, tumors were subdivided into early gastric cancers (EGC) (limited to the mucosa or the submucosa) and advanced gastric cancers (AGC) (infiltration beyond the submucosa) [15], with our cohort comprising eight EGC and 41 AGC.

Follow-up data concerning the patients specific survival to GC were available in 47/49 (96%) cases. Follow-up ranged from 4 to 168 months (mean 58.8 months).

Immunohistochemistry

All specimens, fixed in 10% neutral formalin for 24 h at room temperature, and embedded in paraffin at 55°C, were cut into 4-μm-thick sections for the immunohistochemical procedures. Briefly, the intrinsic endogenous peroxidase activity was blocked with 0.1% H_2O_2 in methanol for 20 min; then, normal sheep serum was applied for 30 min to prevent unspecific adherence of serum proteins. Sections were successively incubated at 4°C overnight with the polyclonal rabbit antibody against Cav-1 (Santa Cruz Biotechnology, Inc., Santa Cruz, CA, USA; working dilution 1:500); a sheep anti-rabbit immunoglobulin antiserum (Behring Institute; w.d. 1:25) was applied and the bound primary antibody was visualized by avidin-biotin-peroxidase detection using the Vectastain Rabbit/Mouse Elite Kit, according to the manufacturer's instructions. To reveal the immuno-staining, the sections were incubated in

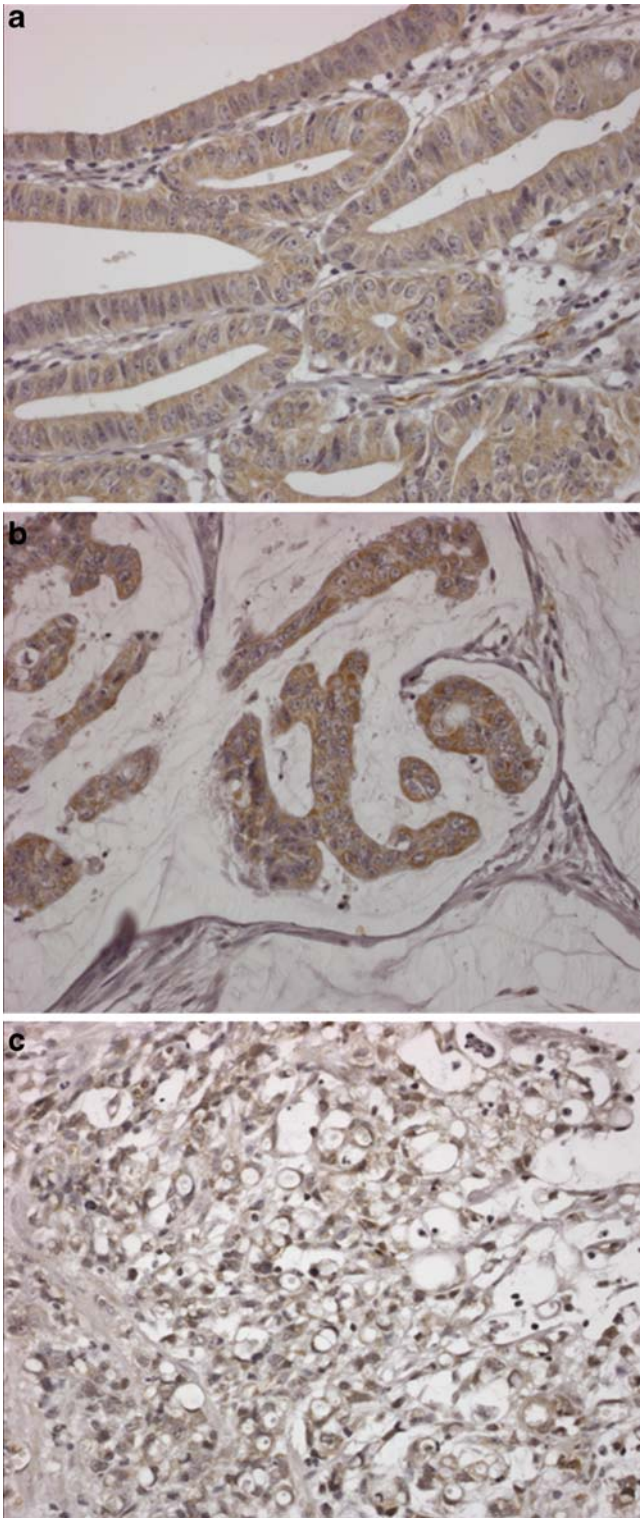

Fig. 1 **a** A positive cav-1 immuno-expression was encountered in intestinal type GC and, specifically, in both **a** tubular (cav-1 stain; original magnification ×200) and **b** mucinous (cav-1 stain; original magnification ×200) histotypes according to the WHO classification. **c** Cav-1 staining was also found in diffuse-type (signet ring carcinoma, according to the WHO classification) GC (cav-1 stain; original magnification ×100)

darkness [17] for 10 min with 3–3′ diaminobenzidine tetra hydrochloride (Sigma Chemical Co., St. Louis, MO, USA), in the amount of 100 mg in 200 ml 0.03% hydrogen peroxide in phosphate-buffered saline. Nuclear counter-staining was performed by Mayer's hemalum. Specificity of the Cav-1 binding was assessed by (1) omitting the primary antiserum and (2) replacing it with normal rabbit serum. Specimens of adipose tissue as well as the endothelium and smooth muscle of the vessels present within the examined tissue were used as positive controls for the immunohistochemical reactions [10, 18].

Immunostained sections were examined by light microscopy using a ×20 and ×40 objective lens and ×10 eyepiece. Two pathologists (V.B. and G.T.) using a double-headed microscope performed the assessment of immunostained sections on a consensus basis. Cav-1 expression was based on the presence of cytoplasmic and/or membranous staining. The intensity of staining (IS) was graded as (0) negative, (1) weak, (2) moderate, and (3) strong; the area of staining positivity (ASP), recorded as percentage of positive cells, was assessed by providing the following values: 0 (<10%), 1 (11–25%), 2 (26–50%), 3 (51–75%), 4 (>75%), according to the procedure described by Joo et al. [8], already applied in our previous papers on cav-1 immuno-expression in human meningiomas [10, 19]. For each case, a cav-1 intensity distribution (ID) score was generated by multiplying the values of IS and ASP. Cases displaying a score 0 were considered as negative.

For the statistical analyses, samples were subdivided into low (cav-1 ID score 0–4) and high (cav-1 ID score 6–12) cav-1 expressing GC on the basis of their ID scores, with the median ID score value (ID score 4) used as the cut-off [10, 19]. Chi-squared and Fisher exact tests were used to analyze the correlations between cav-1 immuno-expression

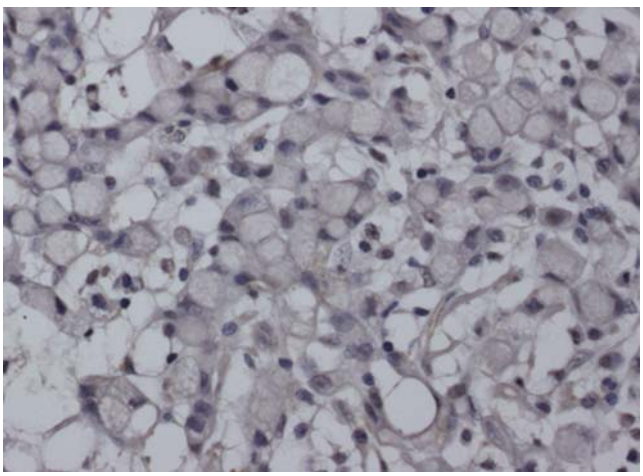

Fig. 2 A diffuse-type GC showing no cav-1 immuno-labelling in the neoplastic cells (cav-1 stain; original magnification ×200)

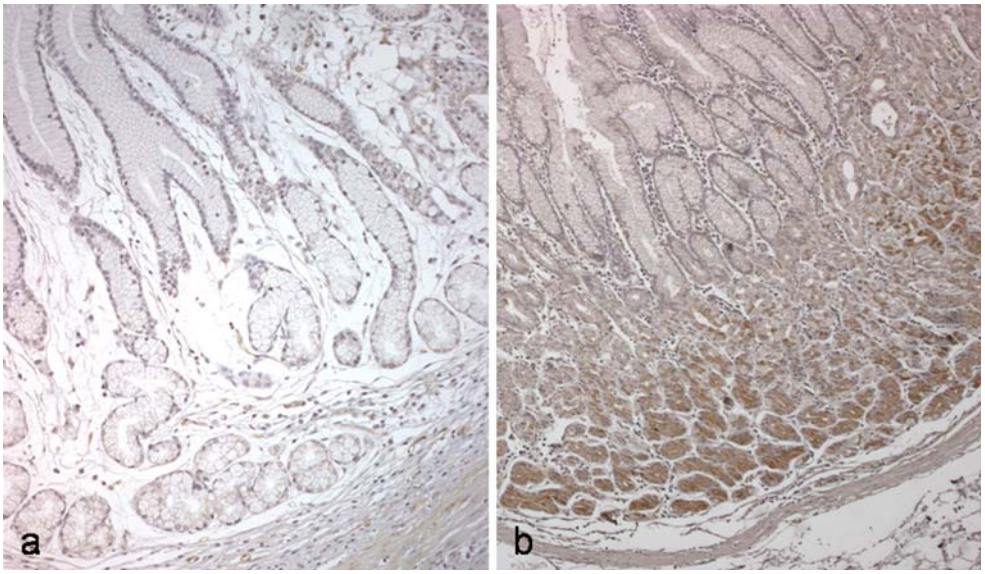

Fig. 3 **a** Normal gastric antral mucosa adjacent to the tumor did not show any staining for cav-1 (cav-1 stain; original magnification ×100). **b** By contrast, a strong cav-1 immuno-reactivity was evident in cells at the base and neck of the fundic pits (cav-1 stain; original magnification ×100)

as reflected by cav-1 ID scores, ASP and IS, and the clinico-pathological parameters.

Overall survival was assessed by the Kaplan–Meier method, with the date of primary surgery as the entry data. The end point was the length of survival to death for GC. The Mantel–Cox log rank test was applied to assess the strength of association between survival time and cav-1 ID scores, ASP, and IS of the tumors. A P value less than 0.05 was considered to be statistically significant.

Results

The clinico-pathological characteristics as well as the cav-1 immuno-expression data relative to the GC of the cohort are illustrated in Table 1.

In all cases, cav-1 immuno-expression was evidenced in the endothelial cells and smooth muscle cells of the vessels within the specimens. A variable cav-1 immuno-expression was found in the neoplastic cells of 46/49 (94%) cases (Fig. 1). More specifically, a low cav-1 immuno-expression (cav-1 ID score 0–4) was encountered in 36/49 (73%) GC, whereas 13/49 (27%) displayed a high cav-1 immuno-expression (cav-1 ID score 6–12). All cav-1 negative (3/3) GC were characterized by a Lauren diffuse histotype and a signet ring WHO one (Fig. 2); by contrast, cav-1 highly expressing GC (cav-1 ID score 6–12) all (13/13) showed an intestinal histotype (tubular or mucinous according to the WHO classification).

As expected, a positive cav-1 immunoreaction was evidenced in the adipose tissue used as a positive control for the immunoassay. On the contrary, negative controls did not show any staining for cav-1.

Normal gastric cardiac and antral mucosa was negative for cav-1 in 27/27 (100%) cases (Fig. 3a). By contrast, in 9/9 (100%) cases, a strong positive cav-1 immunoreaction was uniformly evidenced in the cytoplasm of the cells at the base and neck of the pits within the fundic gastric mucosa (Fig. 3b). A variable (cav-1 ID score 2–8) positive cav-1 immuno-staining was encountered in IM in 17/22 (77%) cases (Fig. 4) (Table 2).

When the correlations between cav-1 immuno-expression in GC and the various clinico-pathological parameters were investigated, GC showing an intestinal histotype were found to display significantly higher cav-1 ID scores (P=0.010816) and ASP (ASP>2) (P=0.021457) in comparison to diffuse GC (Tables 2 and 3). Consistently, significantly higher cav-1 ID scores and ASP (P=0.0187; P=0.0212) were encountered in the WHO tubular and mucinous histotypes in comparison to the signet ring one. By contrast,

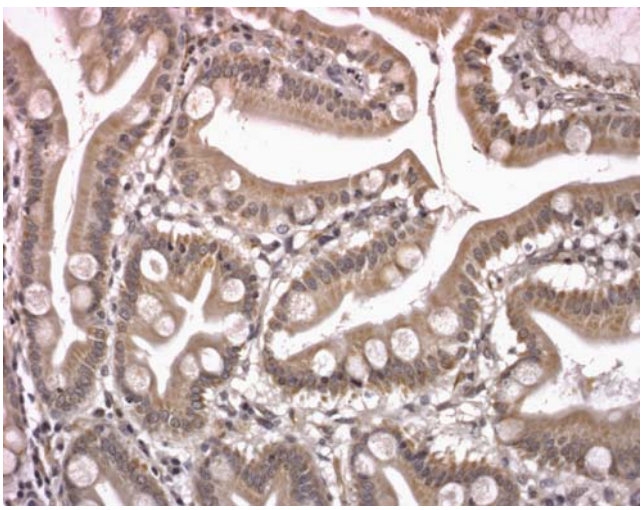

Fig. 4 An IM area nearby GC showed a positive cav-1 immuno-staining in the cytoplasm of metaplastic glands (cav-1 stain; original magnification ×200)

Table 2 Fisher exact test and chi-squared test were used to assess the statistical correlations between cav-1 ID scores and the clinico-pathological characteristics of the 49 analyzed gastric carcinomas

	Cav-1 ID score		*P* value
	0–4	6–12	
Age			
≤50 years	7	1	0.308
>50 years	29	12	
Sex			
Male	17	10	0.062
Female	19	3	
Location			
Cardia	4	3	0.4758
Body	7	3	
Antrum-body	4	0	
Antrum	21	7	
Type			
EGC	6	2	1.00
AGC	30	11	
WHO histotype			
Tubular	22	11	0.0187
Mucinous	1	2	
Signet ring	13	0	
Lauren histotype			
Intestinal	23	13	0.0108
Diffuse	13	0	
Histologic grade			
G1–G2 (LG)	15	6	0.4712
G3 (HG)	7	5	
Pt			
T1	6	2	0.7192
T2	14	5	
T3	13	6	
T4	3	0	
pN			
N0	14	3	0.4979
N1–N2	22	10	
Stage			
1	12	4	0.8749
2	10	4	
3	13	4	
4	1	1	
Survival			
Alive	14	3	0.321
Dead	20	10	

EGC early gastric cancer, *AGC* advanced gastric cancer, *LG* low grade, *HG* high grade

cav-1 IS did not show any significant correlation with the GC histotype (Table 4). No significant associations were evidenced between cav-1 ID scores ASP and IS in GC and the other parameters (age and gender of the patients, the site, histologic grade, and stage of the tumors). In addition, the overall survival of the patients to GC did not differ on the basis of cav-1 ID score, ASP, and IS in their tumors (P=0.2618; P=0.3873; P=0.9885).

Discussion

Since the first report of its involvement in cancerogenesis, cav-1 expression has been investigated in a number of human malignancies [6–9, 10, 12, 13]. An ambivalent, tissue-dependent role has been shown for this protein in tumorigenesis; indeed, the significant down-regulation of

Table 3 Fisher exact test and chi-squared test were used to assess the statistical correlations between cav-1 ASP and the clinico-pathological characteristics of the 49 analyzed gastric carcinomas

	Cav-1 ASP		*P*
	0–2	3–4	
Age			
≤50 years	7	1	0.659
>50 years	30	11	
Sex			
Male	18	9	0.181
Female	19	3	
Location			
Cardia	4	3	0.410
Body	7	3	
Antrum-body	4	0	
Antrum	22	6	
Type			
EGC	6	2	1.00
AGC	31	10	
WHO histotype			
Tubular	23	10	0.021
Mucinous	1	2	
Signet ring	13	0	
Lauren histotype			
Intestinal	24	12	0.021
Diffuse	13	0	
Histologic grade			
G1–G2 (LG)	15	6	0.487
G3 (HG)	8	4	
pT			
T1	6	2	0.790
T2	14	5	
T3	14	5	
T4	3	0	
pN			
N0	14	3	0.502
N1–N2	23	9	
Stage			
1	12	4	0.852
2	11	3	
3	13	4	
4	1	1	
Survival			
Alive	14	3	0.492
Dead	21	9	

ASP area of staining positivity, *EGC* early gastric cancer, *AGC* advanced gastric cancer, *LG* low grade, *HG* high grade

Table 4 Fisher exact test and chi-squared test were used to assess the statistical correlations between cav-1 IS and the clinico-pathological characteristics of the 49 analyzed gastric carcinomas

	Cav-1 IS		*P*
	0–2	3	
Age			
≤50 years	7	1	1.00
>50 years	37	4	
Sex			
Male	22	5	0.056
Female	22	0	
Location			
Cardia	6	1	0.526
Body	10	0	
Antrum-body	4	0	
Antrum	24	4	
Type			
EGC	8	0	0.577
AGC	37	5	
WHO histotype			
Tubular	28	5	0.259
Mucinous	3	0	
Signet ring	13	0	
Lauren histotype			
Intestinal	31	5	0.30
Diffuse	13	0	
Histologic grade			
G1–G2 (LG)	18	3	1.00
G3 (HG)	10	2	
pT			
T1	8	0	0.241
T2	18	1	
T3	15	4	
T4	3	0	
pN			
N0	16	1	0.642
N1–N2	28	4	
Stage			
1	15	1	0.849
2	12	2	
3	15	2	
4	2	0	
Survival			
Alive	15	2	1.00
Dead	27	3	

IS intensity of staining, *EGC* early gastric cancer, *AGC* advanced gastric cancer, *LG* low grade, *HG* high grade

cav-1, reflecting its tumor suppressor action, has been demonstrated in ovarian adenocarcinomas [6] and soft tissue sarcomas [7], whereas cav-1 over-expression, suggestive of a pro-tumorigenic function, has been documented in esophageal squamous cell carcinomas [12] and colorectal adenocarcinomas [11].

In contrast to Burgermeister and colleagues [14] who recently described cav-1 loss in GC, in the present study, we found that cav-1 is frequently expressed in both the diffuse and intestinal types of this malignancy. Differently from these authors, who analyzed frozen samples with a monoclonal antibody [14], we assessed cav-1 immuno-expression on formalin-fixed and paraffin-embedded specimens of GC by using a polyclonal antibody. Specifically, we evidenced a significantly higher cav-1 immuno-expression in the Lauren intestinal type GC in comparison to the diffuse one, and, accordingly, in the mucinous as well as the in the tubular WHO histotypes if compared to the signet ring one. The different expression of cav-1 in relation to the neoplastic histotype is not a novel finding. Indeed, whereas cav-1 loss characterizes the pulmonary adenocarcinoma [20], cav-1 over-expression has been demonstrated in the squamous cell lung carcinoma [20]. As known, diffuse GC can be discriminated from the intestinal form on the basis of its abnormal expression of the cell-to-cell adhesion molecule E-cadherin [21], which is more commonly lost in the former. Since the co-localization and co-immunoprecipitation of cav-1 with E-cadherin has been demonstrated in normal epithelial cells [22], we may speculate that the simultaneous down-regulation of these proteins may occur in diffuse GC cancerogenesis. Such a mechanism may provide a suitable explanation for the lower cav-1 immuno-expression which we observed in the diffuse histotype in comparison to the intestinal type GC; nonetheless, further studies are needed to better elucidate the mechanisms underlying the difference in terms of cav-1 expression between the diffuse and intestinal GC.

When we analyzed the normal gastric mucosa adjacent to the tumors, no cav-1 labelling was observed in the antral or cardiac specimens in all cases, whereas a strong cav-1 positive immunoreaction was evidenced in the cells at the neck and at the base of gastric pits within all fundic mucosal fragments. In addition, a variable cav-1 immuno-expression was found in the majority of IM areas nearby the tumors, in accordance with the findings already reported by Burgermeister et al. [14]. In terms of histogenesis, it is generally accepted that the Lauren's intestinal type GC is preceded by the sequential steps of chronic atrophic gastritis, intestinal metaplasia, and dysplasia [23], whereas the diffuse-type GC seems to arise via hyperplastic or de novo changes, with or without concurrent non metaplastic dysplasia [24]. Nonetheless, both GC types are supposed to originate from gastric progenitor cells, present within the fundic gastric mucosa [25]. Our findings showing cav-1 expression in the cells at the base or neck of fundic gastric glands and its maintenance in GC as well as in IM are in line with a histogenetic origin of the these lesions from the *trans*-differentiation of chief cells or from a cryptic

progenitor population at the bases of fundic glands, as recently suggested by Nozaki et al. [26].

In the present study, we evaluated for the first time the existence of eventual correlations between cav-1 immuno-expression and the clinico-pathological parameters of GC, in an attempt to verify whether cav-1 expression may be considered as related to GC biological aggressiveness, similarly to what already observed in other tumors [7, 9, 10, 12, 13]. In addition, we aimed to test the assumption that cav-1 expression in GC is stage specific, as proposed by other authors [14]. No significant associations were evidenced between cav-1 expression and the age and gender of the patients or the site, histologic grade, and stage of the tumors. Thus, cav-1 amount does not seem to be connected to the biological behavior of GC. Moreover, the absence of significant differences in terms of cav-1 immuno-expression in the various stages of GC seems to confute the hypothesis according to which cav-1 acts as a stage-specific GC tumor modulator, which is down-regulated during gastric cancerogenesis and then regained during GC progression [14]. Finally, we assessed for the first time the prognostic value of cav-1 immuno-expression on the patient's overall survival to GC, and showed, in contrast to what observed in other tumors [8, 10, 12], the lack of a significant association between cav-1 expression and the length of survival to GC. Thus, in conclusion, on the basis of our data, the role of cav-1 in GC does not appear to be stage specific neither related to prognosis.

Conflict of interest statement We declare that we have no conflict of interest.

References

1. Scherer PE, Lewis RY, Volontè D et al (1997) Cell-type and tissue-specific expression of caveolin-2. Caveolins 1 and 2 co-localize and form a stable hetero-oligomeric complex in vivo. J Biol Chem 272:29337–29346
2. Anderson RG, Kamen BA, Tothberg KG et al (1992) Potocytosis: sequestration and transport of small molecules by caveolae. Science 255:410–411
3. Anderson RG (1993) Caveolae: where incoming and outcoming messengers meet. Proc Natl Acad Sci U S A 90:10909–10913
4. Razani B, Engelman JA, Wang XB et al (2001) Caveolin-1 null mice are viable but show evidence of hyperproliferative and vascular abnormalities. J Biol Chem 276:38121–38138
5. Lee H, Volonte D, Galbiati F et al (2000) Constitutive and growth factor-regulated phosphorylation of caveolin-1 occurs at the same site (Tyr-14) in vivo: identification of a c-Src/Cav-1/Grb7 signaling cassette. Mol Endocrinol 14:1750–1775
6. Wiechen K, Diatchenko L, Agoulnik A et al (2001) Caveolin-1 is down-regulated in human ovarian carcinoma and acts as a candidate tumor suppressor gene. Am J Pathol 159:1635–1643
7. Wiechen K, Sers C, Agoulnik A et al (2001) Down-regulation of caveolin1, a candidate tumor suppressor gene, in sarcomas. Am J Pathol 158:833–839
8. Joo HJ, Oh DK, Kim YS et al (2004) Increased expression of caveolin-1 and microvessel density correlates with metastasis and poor prognosis in clear cell renal cell carcinoma. BJU Int 93:291–296
9. Yang G, Timme TL, Frolov A et al (2005) Combined c-myc and caveolins-1 expression in human prostate carcinoma predicts prostate carcinoma progression. Cancer 103:1186–1194
10. Barresi V, Cerasoli S, Paioli G et al (2006) Caveolin-1 in meningiomas: expression and clinico-pathological correlations. Acta Neuropathol 112:617–626
11. Fine SW, Lisanti MP, Galbiati F et al (2001) Elevated expression of caveolin-1 in adenocarcinoma of the colon. Am J Clin Pathol 115:719–724
12. Kato K, Hida Y, Miyamoto M et al (2002) Overexpression of caveolin-1 in esophageal squamous cell carcinoma correlates with lymph node metastasis and pathologic stage. Cancer 94:929–933
13. Ando T, Ishiguro H, Kimura M et al (2007) The overexpression of caveolin-1 and caveolin-2 correlates with a poor prognosis and tumor progression in esophageal squamous cell carcinoma. Oncol Rep 18:601–609
14. Burgermeister E, Xing X, Röcken C et al (2007) Differential expression and function of caveolin-1 in human gastric cancer progression. Cancer Res 67:8519–8526
15. Fenoglio-Preiser C, Carneiro F, Correa P et al (2000) Gastric carcinoma. In: Hamilton SR, Aaltonen LA (eds) Tumours of the digestive system. IARC, Lyon, pp 39–52
16. Lauren T (1965) The two histologic main types of gastric carcinoma. Acta Pathol Microbiol Scand 64:34
17. Weir EE, Pretlow TG, Pitts A (1974) A more sensitive and specific histochemical peroxidase stain for the localization of cellular antigen by the enzyme–antibody conjugate method. J Histochem Cytochem 22:1135–1140
18. Barresi V, Grosso M, Barresi G (2008) Immunohistochemical evidence of caveolin-1 expression in human fetal and neonatal striated muscle and absence in the adult's. Appl Immunohistochem Mol Morphol 16:267–273
19. Barresi V, Cerasoli S, Tuccari G (2008) Correlative evidence that tumor cell-derived caveolin-1 mediates angiogenesis in meningiomas. Neuropathology 28:472–478
20. Kato T, Miyamoto M, Kato K et al (2004) Difference of caveolin-1 expression pattern in human lung neoplastic tissue. Atypical adenomatous hyperplasia, adenocarcinomas and squamous cell carcinoma. Cancer Lett 214:121–128
21. Karayiannakis AJ, Syrigos KN, Chatzigianni E et al (1998) E-cadherin expression as a differentiation marker in gastric cancer. Hepatogastroenterology 45:2437–2442
22. Galbiati F, Volonte D, Brown AM et al (2000) Caveolin-1 expression inhibits Wnt/betacatenin/Lef-1 signaling by recruiting beta-catenin to caveolae membrane domains. J Biol Chem 275:23368–23377
23. Uchino S, Noguchi M, Ochiai A et al (1993) p53 mutation in gastric cancer: a genetic model for carcinogenesis is common to gastric and colorectal cancer. Int J Cancer 54:759–764
24. Correa P (1992) Human gastric carcinogenesis: a multistep and multifactorial process—First American Cancer Society Award Lecture on Cancer Epidemiology and Prevention. Cancer Res 52:6735–6740
25. Syder AJ, Guruge JL, Li Q et al (1999) *Helicobacter pylori* attaches to NeuAc alpha 2,3Gal beta 1,4 glycoconjugates produced in the stomach of transgenic mice lacking parietal cells. Mol Cell 3:263–274
26. Nozaki K, Ogawa M, Williams JA et al (2008) A molecular signature of gastric metaplasia arising in response to acute parietal cell loss. Gastroeneterology 134:511–522

Virchows Arch (2008) 453:579–588
DOI 10.1007/s00428-008-0669-7

ORIGINAL ARTICLE

Immunophenotyping and oncogene amplifications in tumors of the papilla of Vater

Daniel Baumhoer · Inti Zlobec · Luigi Tornillo · Wolfgang Dietmaier · Peter H. Wuensch · Arndt Hartmann · Fausto Sessa · Petra Ruemmele · Luigi M. Terracciano

Received: 27 June 2008 / Revised: 15 August 2008 / Accepted: 28 August 2008 / Published online: 21 October 2008

Abstract Carcinomas of the ampulla of Vater are rare and assumed to generally arise from preexisting adenomas (adenoma–carcinoma sequence). Histologically, distinct subtypes can be distinguished that were shown to differ significantly in terms of clinical outcome. Since pathologists usually receive bioptic tissue samples of ampullary tumors obtained during endoscopy, accurate classification of carcinoma subtypes can sometimes be difficult on morphological criteria alone. We therefore performed immunohistochemistry using a panel of established marker proteins (CK7, CK20, p21, p27, ESA, bax, and ephrin-B2) on 175 carcinoma, 111 adenoma, and 152 normal mucosa specimens of the ampulla of Vater and identified distinct immunoprofiles for every carcinoma subtype. Fluorescence in situ hybridization analyses of therapeutic target genes (c-myc, EGFR1, CCND1, HER2) found CCND1 to represent the most frequently amplified gene in our series (7.5%).

Keywords Ampullary carcinoma · Papilla of Vater · FISH · TMA · Amplification · CCND1

Petra Ruemmele and Luigi M. Terracciano shared senior authorship.

D. Baumhoer (✉) · I. Zlobec · L. Tornillo · L. M. Terracciano
Institute of Pathology, University of Basel,
Schönbeinstrasse 40,
4003 Basel, Switzerland
e-mail: dbaumhoer@mac.com

W. Dietmaier · P. Ruemmele
Institute of Pathology, University of Regensburg,
Regensburg, Germany

P. H. Wuensch
Institute of Pathology, Municipal Hospitals of Nuremberg,
Nuremberg, Germany

A. Hartmann
Institute of Pathology, University of Erlangen,
Erlangen, Germany

F. Sessa
Anatomic Pathology Unit, Department of Human Morphology,
University of Insubria,
Varese, Italy

Introduction

The papilla of Vater is a complex anatomical unit composed of highly specialized mucosa and musculature and represents the orifice of the pancreatic and bile duct within the duodenum. It contains the border between two completely different types of mucosa (intestinal mucosa of the duodenum and pancreatico-biliary duct mucosa) and regulates the flow of bile and pancreatic secretions with its sphincteric muscle (sphincter of Oddi) [1].

Tumors of the ampulla of Vater are rare, with an incidence of approximately 5.7 cases per million population per year, but are still more common than tumors of the rest of the small intestine [2–4]. Among periampullary tumors, they rank second after tumors of the pancreatic head and account for 6–20% of cases [5, 6]. In 30–91% of ampullary carcinomas, residual adenomatous areas are detectable, indicating an adenoma–carcinoma sequence with stepwise accumulation of genetic alterations, similar to that observed in colorectal cancer [7, 8]. Due to the crucial function of the ampulla of Vater, neoplastic lesions early lead to an occlusion of the papillary orifice and therefore result in congestion of bile and pancreatic secretions. Patients generally present with obstructive jaundice, and histologic diagnosis can be achieved after biopsy during endoscopic retrograde cholangiopancreatography [9]. Early detection

but also biologic differences are thought to be responsible for the better prognosis of ampullary tumors following pancreaticoduodenectomy compared to other periampullary tumors [10–12]. Concerning ampullary carcinomas, several surgical series have reported a median survival of 30 to 50 months and 5-year survival rates between 21% and 64% [6, 13–15].

The histopathology of ampullary carcinomas includes a broad spectrum of distinct subtypes, deriving from the different types of mucosa adjoining in the papilla of Vater [3, 5]. According to the classification by the Armed Forces Institute of Pathology (AFIP), an intestinal type (IT), resembling carcinomas of intestinal origin, and a pancreatico-biliary type (PBT), resembling carcinomas of the extrahepatic bile ducts or the pancreas, are the most common subtypes and account for 70–95% of cases [5, 6, 16–21]. Other subtypes include an intestinal-mucinous type (IMT), an invasive papillary type (IPT), a poorly differentiated adenocarcinoma (G3AC), and several rather uncommon entities [18]. Interestingly, the distinct subtypes were shown to differ significantly in cumulative survival, with IT demonstrating a mean survival of 76 months compared to 41 months in PBT (Ruemmele et al., submitted for publication). Since classification of ampullary tumors, particularly in bioptic material, can sometimes be difficult on histological criteria alone, we investigated 175 carcinoma, 111 adenoma, and 152 normal mucosa specimens of the papilla of Vater for their immunohistochemical expression of marker proteins commonly altered during carcinogenesis, including cytokeratins 7 and 20, cell cycle inhibitors p21 and p27, epithelium-specific intercellular adhesion molecule [epithelial specific antigen (ESA)], promoter of apoptosis bax, and regulator of angiogenesis ephrin-B2, and created immunoprofiles of the distinct subtypes. Additionally, fluorescence in situ hybridization (FISH) analyses were performed to determine whether known oncogenes, that can serve as potential target genes for current or future gene-specific therapies (c-myc, EGFR1, CCND1, HER2), participate in genomic rearrangements and could therefore be of clinical significance in ampullary carcinoma.

Materials and methods

Tissue samples and patient characteristics

The files of the Institute of Pathology, University Hospital Basel (Switzerland), the Institute of Pathology, University of Regensburg (Germany), the Institute of Pathology Nuernberg, and the Anatomic Pathology Unit, Department of Human Morphology, University of Insubria, Varese (Italy) were searched for adenomas or carcinomas of the ampulla of Vater over the period from 1985 to 2005. In total, 175 carcinoma, 111 adenoma, and 152 normal mucosa samples were retrieved. Sufficient paraffin-embedded tissue for tissue microarray (TMA) construction was available in all cases. The male-to-female ratio was 3:2; mean age at diagnosis was 63 years (range 15–81 years).

TMA construction

Tissue samples were fixed in buffered 4% formalin, embedded in paraffin, and used to construct a TMA. Briefly, hematoxylin–eosin (H&E)-stained sections were made from each selected primary block (donor blocks) to define representative tissue regions. Tissue cylinders (0.6 mm in diameter) were then punched from the region of the donor block with the use of a custom-made precision instrument (Beecher Instruments, Silver Spring, USA). Tissue cylinders were transferred to a 25×35 mm paraffin block to produce the TMA block used for the study. The resulting TMA block was cut into 3 μm sections that were transferred to glass slides by use of the Paraffin Sectioning Aid System (Instrumedics, Hackensack, USA). Sections from the TMA block were used for immunohistochemistry. The number of punches per patient ranged from one to three for both normal tissue and carcinoma and from one to five for patients with adenomas. One punch was collected per patient on average (median 1.0) for each of the tissue types.

Histology and immunophenotyping

All tissue samples were reviewed by two experienced surgical pathologists (P.R. and L.M.T.) based exclusively on H&E staining. Carcinomas were subclassified according to the criteria published by the AFIP [18]. Tumors essentially indistinguishable from colorectal carcinomas were classified as intestinal types, whereas carcinomas showing a dense desmoplastic stroma surrounding small glands or solid nests of tumor cells were referred to as the pancreaticobiliary subtype. Invasive papillary carcinomas typically formed papillary and micropapillary structures in their invasive component, and poorly differentiated adenocarcinomas lacked histologic features of glandular or other differentiation. Additionally, an intestinal-mucinous subtype, characterized by any mucinous differentiation, was defined. Characteristics of antibodies are listed in Table 1.

Evaluation of immunohistochemistry

Immunoreactivity for each protein marker was scored semi-quantitatively by evaluating the number of positive tumor cells over the total number of tumor cells. Scores were assigned using 5% intervals and ranged from 0% to 100%.

Table 1 Characteristics of antibodies

Antibody	Dilution	Detection	Manufacturer
CK7	1:200	Bond	Dako Cytomation
CK20	1:50	Bond	Dako Cytomation
p21	1:25	Bond	Dako Cytomation
p27	1:200	Bond	Dako Cytomation
ESA	1:200	Bond	Novocastra
bax	1:100	Bond	Neomarkers
ephrin-B2	1:200	ABC	R&D Systems

ESA epithelial specific antigen, *Bond* Bond Vision Biosystems, *ABC* avidin–biotin–peroxidase-complex

The reproducibility of this scoring method between pathologists has previously been demonstrated for TMAs [22, 23]. In order to select the cut-off score for protein marker positivity, receiver operating characteristic curve (ROC) analysis was performed [24]. Using this method, the sensitivity and 1-specificity of the protein marker for the outcome at each protein expression score is plotted, thus generating the ROC curve. The (0,1 criterion) was used to identify the point on the curve maximizing the sensitivity and specificity for the outcome and thereby having the shortest distance to the coordinate (0,1). The protein expression score corresponding to this point was thus selected as the threshold value above which a tumor was considered "positive".

Fluorescence in situ hybridization

Five-micrometer sections of the TMA were made and treated according to the paraffin pretreatment reagent kit protocol before hybridization (Vysis, IL, USA). SpectrumOrange-labelled gene-specific probes were used together with SpectrumGreen-labelled probes for the respective centromere as a reference. The probe combinations were: c-myc/centromere 8 (Vysis), EGFR1/centromere, 7 (Vysis) CCND1/centromere 11 (Vysis), and HER2/centromere 17 (Vysis). Hybridization was performed according to the manufacturer's instructions (Vysis). Tumors were considered amplified if the ratio between oncogene and corresponding centromere was >2.0. Polysomy on the other hand was defined as more than two oncogene and centromere copies per nucleus without an increase in the ratio between oncogene and corresponding centromere.

Statistical analyses

Differences in negative and positive expression between tumor types were evaluated by the chi-square test. The predictive and independent value of the immunohistochemical markers to discriminate between tumor types was carried out by univariate and multiple logistic regression analysis. The odds ratio (OR), 95%CI, and p values were used to determine the effect of each marker on outcome. All analyses were carried out using SAS V9 (The SAS Institute, Cary, NC, USA), and p values <0.05 were considered statistically significant.

Results

Histologic classification of ampullary carcinomas

Classification of 175 ampullary carcinomas investigated in our series identified 85 intestinal types, 42 pancreaticobiliary types, 23 poorly differentiated adenocarcinomas, 16 intestinal-mucinous types, and nine invasive papillary types (Fig. 1).

Grading of adenomas and association to carcinoma subtypes

Histologic grading was evaluable in 76 of 111 (68%) adenomas of our series and disclosed low-grade dysplasia in 57 of 76 (75%) and high-grade dysplasia in 19 of 76 (25%) cases. All adenomas demonstrated tubular or tubulovillous architecture. Seventy-eight of 111 (70%) adenoma samples were derived from patients suffering from coexisting carcinoma. The corresponding subtypes were 49 IT, 13 IMT, 8 PBT, 6 G3AC, and 2 IPT.

Immunophenotyping of ampullary carcinomas, adenomas, and normal mucosa

The immunoprofiles of all investigated carcinoma, adenoma, and normal mucosa samples are shown in Table 2 and Fig. 2, respectively. The most discriminating results were demonstrated for CK7 and bax. Whereas normal, premalignant and malignant tissue samples stained increasingly positive for CK7 (2.6%, 12.8%, and 44.7%), bax revealed an opposite trend (55.6%, 64.3%, and 37.6%). Additionally, p21 and p27 showed significant differences in their expression values between the three groups.

Immunophenotyping of ampullary carcinoma subtypes

Of the eight immunohistochemical marker proteins investigated, CK7 ($p<0.001$), p27 ($p=0.012$), ESA ($p=0.038$), and bax ($p<0.001$) expression demonstrated significant differences among the tumor types (Table 3 and Fig. 3). More than 75% of PBT and 72.2% of G3AC showed no expression of bax, while 92.3% of IMT were negative for CK7. IT stained negative for CK7 in 67.5% of cases and were never positive for CK7, p27, and ESA and negative

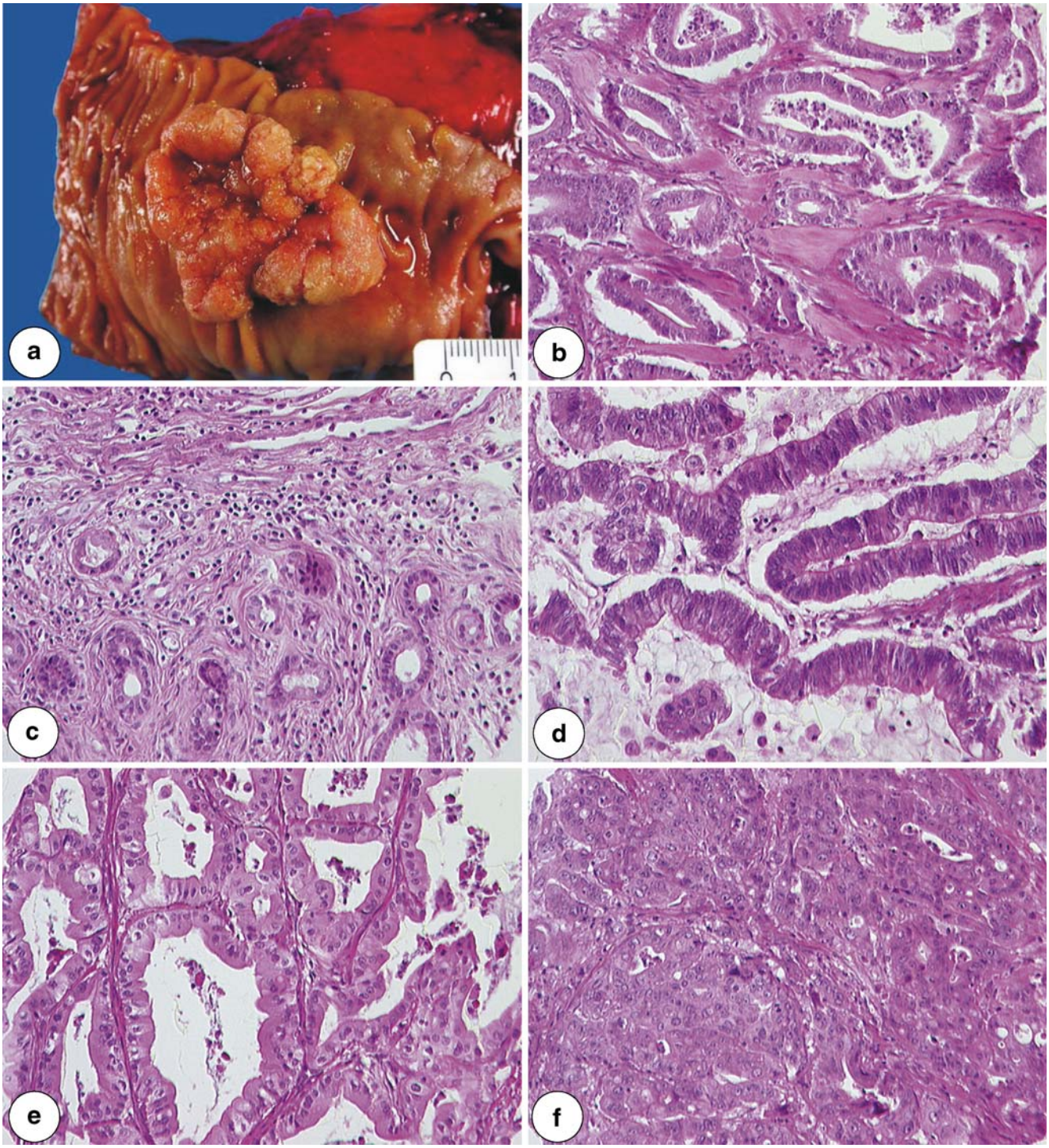

Fig. 1 Gross findings of an ampullary carcinoma showing a sessile exophytic tumor at the ampullary orifice (**a**). Histologic findings of ampullary carcinoma subtypes: IT (**b**), PBT (**c**), IMT (**d**), IPT (**e**), and G3AC (**f**) (H&E ×400)

for bax simultaneously. The association of p27, ESA, bax, and CK7 were evaluated in univariate and multivariable analysis in order to establish immunophenotypes specific for each tumor subtype. Findings are summarized in Fig. 4.

CK7 negativity [p=0.002; OR=0.37 (0.2–0.7)] and positivity of bax [p=0.003; OR=2.76 (0.4–5.4)], p27 [p=0.044; OR=2.0 (1.2–4.2)] and ESA [p=0.012; OR=2.3 (1.2–4.2)] were significantly associated with the IT tumor type. Multivariable analysis demonstrated, however, that

Table 2 Immunoprofiles of normal mucosa, adenoma, and carcinoma tissue samples

Protein	Expression	Cutoff (%)	Histologic type			*p* value
			Normal *N*=152	Adenoma *N*=111	Carcinoma *N*=175	
CK7		80				
	Negative		113 (97.4)	82 (87.2)	89 (55.3)	
						<0.001*
	Positive		3 (2.6)	12 (12.8)	72 (44.7)	
CK20		50				
	Negative		58 (46.4)	52 (53.6)	76 (47.5)	
						0.524
	Positive		67 (53.6)	45 (46.4)	84 (52.5)	
p21		0				
	Negative		90 (74.4)	61 (62.9)	96 (59.6)	
						0.031**
	Positive		31 (25.6)	36 (37.1)	65 (40.4)	
p27		5				
	Negative		39 (32.5)	33 (35.5)	75 (52.8)	
						0.002***
	Positive		81 (67.5)	60 (64.5)	67 (47.2)	
ESA		90				
	Negative		63 (50.4)	51 (52.0)	78 (48.7)	
						0.874
	Positive		62 (49.6)	47 (48.0)	82 (51.3)	
bax		10				
	Negative		51 (44.4)	30 (35.7)	93 (62.4)	
						<0.001****
	Positive		64 (55.6)	54 (64.3)	56 (37.6)	
ephB2		75				
	Negative		76 (65.5)	48 (62.3)	72 (51.4)	
						0.058
	Positive		40 (34.5)	29 (37.7)	68 (48.6)	

*Significant difference between normal and adenoma ($p<0.001$) and normal and carcinoma ($p<0.001$)
**Significant difference between normal and carcinoma ($p=0.01$)
***Significant difference between normal and carcinoma ($p=0.001$) and adenoma and carcinoma ($p=0.009$)
****Significant difference between normal and carcinoma ($p=0.004$) and adenoma and carcinoma ($p<0.001$)

only CK7 ($p<0.001$) and bax ($p<0.001$) were independent predictors of this phenotype and useful in the discrimination of IT from other tumors (sensitivity 0.69, specificity 0.58).

In contrast, CK7 positivity [$p<0.001$; OR=5.03 (2.2–11.3)] and absence of bax [$p<0.001$; OR=0.22 (0.1–0.5)], p27 [$p=0.001$; OR=0.22 (0.1–0.6)], and ESA [$p=0.004$; OR=0.31 (0.1–0.7)] were significantly associated with the PBT tumor type compared to the remaining subtypes. CK7, bax, and p27 were independently predictive ($p<0.001$) of PBT (sensitivity 0.92, specificity 0.48).

The discrimination of IMT tumors could be best performed by assessing CK7. Absence of CK7 [$p=0.023$; OR=0.09 (0.01–0.7)] expression was very strongly predictive of IMT and was the only marker found to discriminate IMT from the remaining tumor types (sensitivity 0.87, specificity 0.65).

None of the immunohistochemical markers were significantly predictive of either G3AC or IPT.

FISH analyses

The results of the FISH analyses are presented in Table 4. The number of evaluable cases varied between different FISH probes due to insufficient hybridization, absence of unequivocal tumor cells in the arrayed tissue, as well as lack of tissue on serial sections of the array. CCND1 showed the highest amplification frequency among the analyzed genes (two of 74 adenomas and ten of 134 carcinomas) in our series, whereas c-myc, EGFR, and HER2 were amplified only infrequently. There were no associations between gene amplifications and distinct histologic subtypes of ampullary carcinomas.

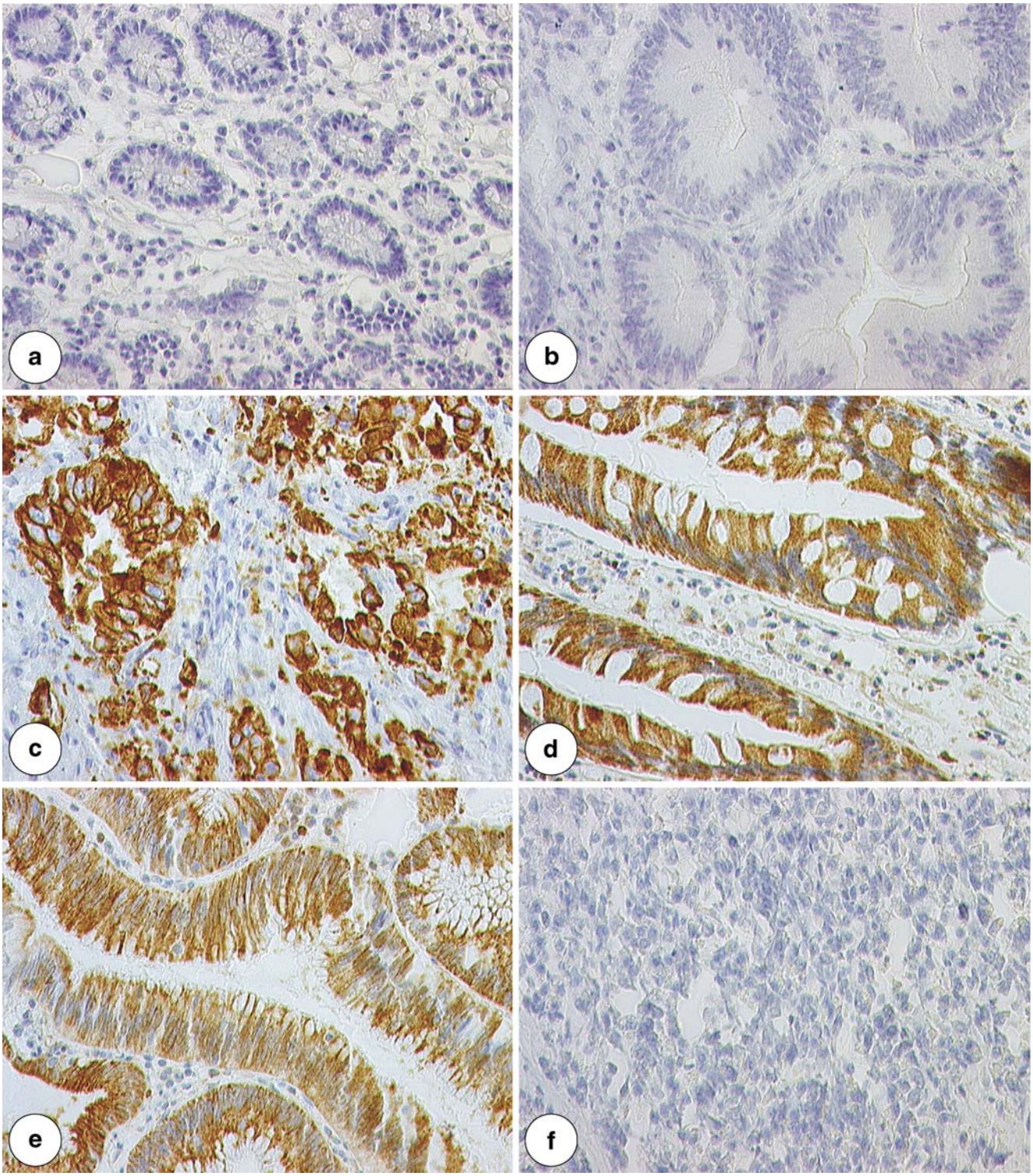

Fig. 2 CK7/bax immunostaining in normal mucosa (**a**, **d**), adenoma (**b**, **e**), and carcinoma (**c**, **f**) (×400)

Discussion

Carcinomas of the small intestine represent only 1% of all gastrointestinal malignant tumors but are most common around the papilla of Vater [25–28]. There is good evidence for an adenoma–carcinoma sequence since ampullary carcinomas demonstrate residual adenomatous areas in up to 84% of cases [29–31]. On the other hand, up to 65% of

Table 3 Immunoprofiles of carcinoma subtypes

Protein	Expression	Cutoff	Histologic type (N=175)					p value
			IT N=85	IMT N=16	PBT N=42	G3AC N=23	IPT N=9	
CK7		80						
	Negative		54 (67.5)	12 (92.3)	10 (26.3)	10 (47.6)	3 (33.3)	
								<0.001
	Positive		26 (32.5)	1 (7.7)	28 (73.7)	11 (52.4)	6 (66.7)	
CK20		50						
	Negative		33 (41.8)	7 (50.0)	19 (51.3)	11 (52.4)	6 (66.7)	
								0.588
	Positive		46 (58.2)	7 (50.0)	18 (48.7)	10 (47.6)	3 (33.3)	
p21		0						
	Negative		41 (52.6)	7 (50.0)	28 (71.7)	14 (66.7)	6 (66.7)	
								0.27
	Positive		37 (47.4)	7 (50.0)	11 (28.3)	7 (33.3)	3 (33.3)	
p27		5						
	Negative		32 (44.4)	5 (45.5)	26 (78.8)	7 (38.9)	5 (62.5)	
								0.012
	Positive		40 (55.6)	6 (54.6)	7 (21.2)	11 (61.1)	3 (37.5)	
ESA		90						
	Negative		31 (38.7)	7 (50.0)	26 (70.3)	10 (50.0)	4 (44.4)	
								0.038
	Positive		49 (61.3)	7 (50.0)	11 (19.7)	10 (50.0)	5 (55.6)	
bax		10						
	Negative		29 (39.2)	3 (25.0)	28 (77.8)	13 (72.2)	4 (44.4)	
								<0.001
	Positive		45 (60.8)	9 (75.0)	8 (22.2)	5 (27.8)	5 (55.6)	
ephB2		75						
	Negative		36 (50.0)	9 (75.0)	15 (46.9)	7 (46.7)	5 (55.6)	
								0.526
	Positive		36 (50.0)	3 (25.0)	17 (53.1)	8 (53.3)	4 (44.4)	

patients suffering from adenoma were shown to have coexisting carcinoma [32]. Ampullary carcinomas are heterogeneous in terms of their histomorphological differentiation, probably due to the distinct epithelial subtypes adjoining in the ampulla of Vater [16–18]. In our series, IT (85 of 175, 49%) and PBT (42 of 175, 24%) were the most common subtypes, followed by G3AC (23 of 175, 13%), IMT (16 of 175, 9%), and IPT (nine of 175, 5%). This is in line with most of the reported series in the literature with only some smaller studies demonstrating PBT to be more common than IT [5, 6, 16–18, 20, 21]. Importantly, the distinct histologic subtypes were shown to exhibit significant differences in clinical outcome, with IT and IMT demonstrating a favorable prognosis [cumulative survival (CS) 97 and 76 months] compared to IPT, PBT, and G3AC (CS 59, 41, and 19 months; Ruemmele et al., submitted for publication). The favorable prognosis of IT compared to PBT has previously been shown in several studies [16, 17, 20]. During staging procedures in patients with ampullary tumors, pathologists generally receive endoscopically obtained biopsies that can be difficult to interpret and to classify on histomorphological criteria alone. Our study therefore aimed to delineate immunohistochemical and genomic profiles of the distinct carcinoma subtypes using FISH analyses and an immunohistochemical panel of common marker proteins.

Carcinoma, adenoma, and normal ampullary mucosa samples demonstrated statistically significant differences in the expression of CK7 and bax. Whereas CK7 expression increased from normal to malignant tissue samples, bax expression decreased in the same manner. The remaining protein markers, particularly p27, also revealed significant differences in their expression values between the three groups but not as unequivocally as CK7 and bax. Concerning the histologic subtypes of ampullary carcinomas, the expression levels of CK7, p27, ESA, and bax demonstrated the most distinctive results. Whereas more than 75% of PBT and 72.2% of G3AC were negative for bax, IMT was negative for CK7 in 92% of cases. Accordingly, multivariable analysis showed lack of CK7

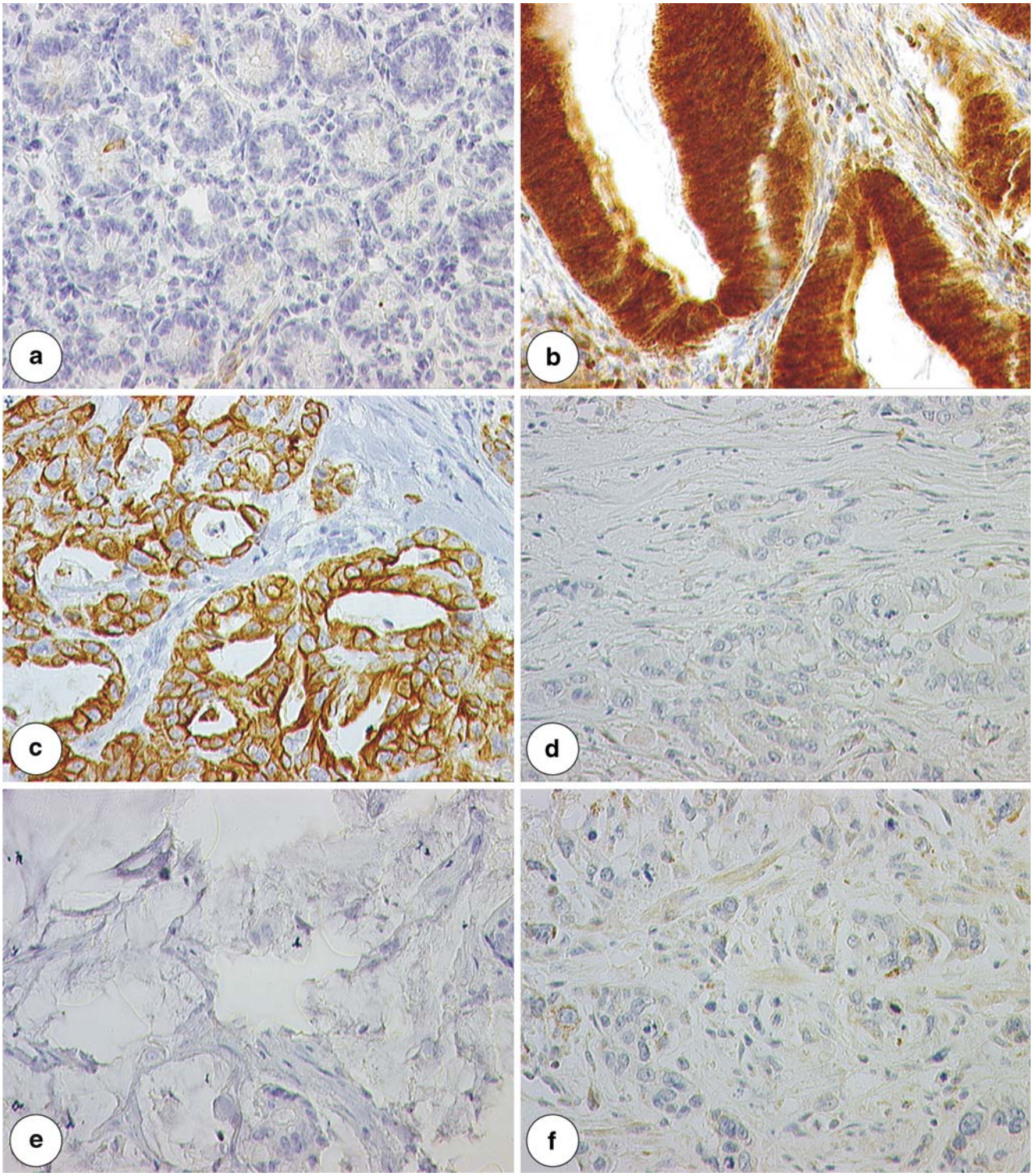

Fig. 3 Immunostaining of CK7 in IT (**a**), bax in IT (**b**), CK7 in PBT (**c**), bax in PBT (**d**), CK7 in IMT (**e**), and bax in G3AC (**f**) (×400)

to be strongly predictive for IMT, whereas CK7 positivity and negativity for bax, p27, and ESA were significantly associated with PBT. Expression of CK7 was rather uncommon in IT (32.5%). Multivariable analysis consistently demonstrated CK7 negativity and positivity for p27, ESA, and bax to be strongly correlated with IT. IPT represented the rarest subtype in our series, and therefore, only limited conclusions can be drawn concerning a

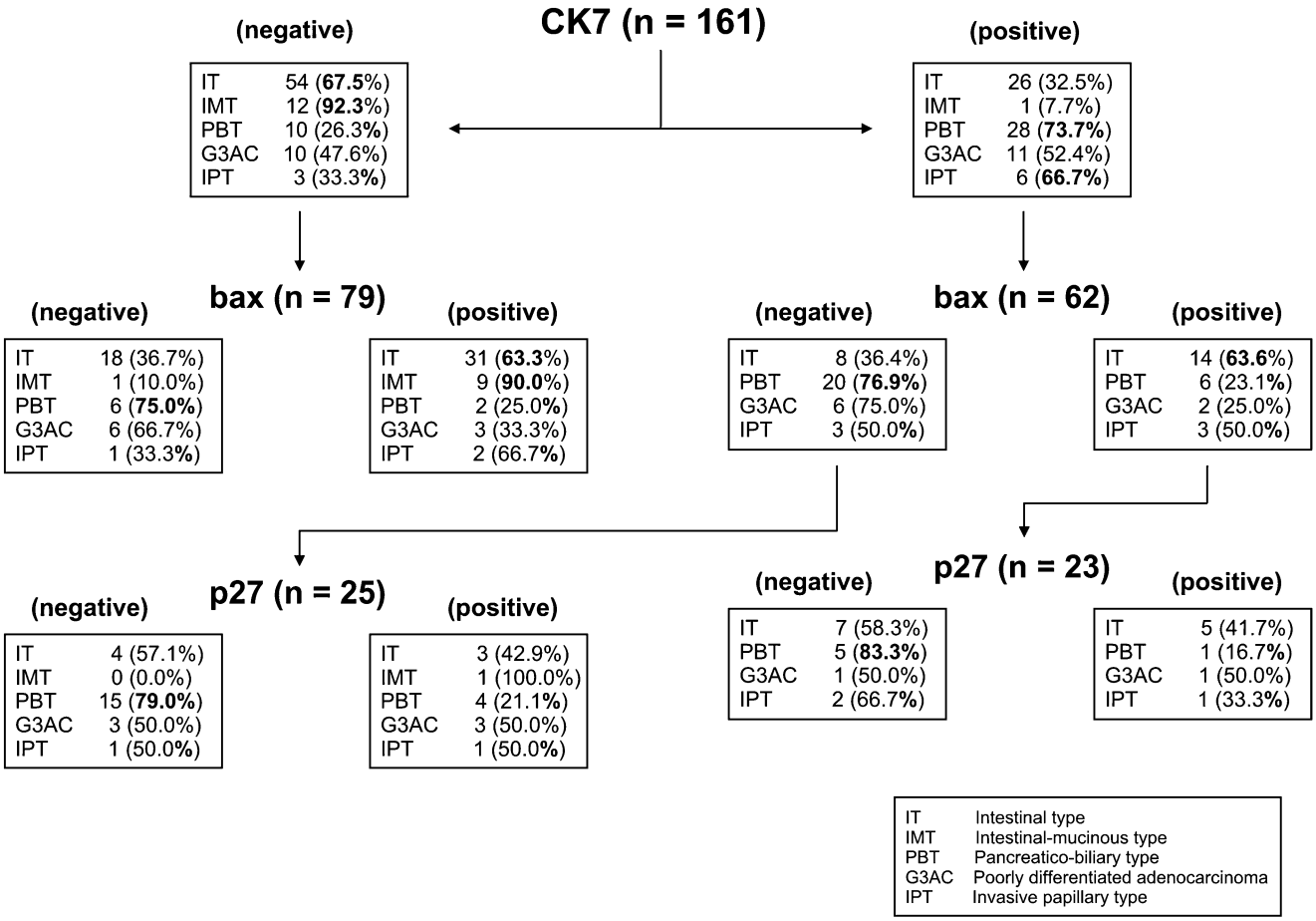

Fig. 4 Flow chart demonstrating immunoprofiles of carcinoma subtypes

representative immunoprofile. Nevertheless, IPT tended to stain positive for CK7 and negative for p27 in most of the investigated cases.

FISH analyses demonstrated amplification of c-myc, EGFR1, CCND1, and HER2 only infrequently with no obvious correlations to carcinoma subtypes. From all investigated oncogenes, CCND1 showed the highest amplification frequency in our series (two of 74 adenomas and ten of 134 carcinomas). The CCND1 gene is coding for a cyclin which is known to be translocated, amplified, and overexpressed in many different tumor types including mantle cell lymphoma, head and neck carcinoma, breast carcinoma, hepatocellular carcinoma, gastrointestinal stromal tumors, and various sarcomas [33–36]. Since CCND1 has been shown to be essential for malignant transformation of epithelial cells, it could play an important role in tumorigenesis in a distinct subset of ampullary carcinomas. C-myc, that we demonstrated only recently to be amplified in up to 14.2% of colorectal carcinomas, showed no amplification in any of the ampullary carcinomas investigated [37]. Whereas EGFR was only amplified in one case, HER2 showed amplification in 6% of adenomas and carcinomas (two IT, two IPT, one G3AC). A small fraction of patients with ampullary carcinomas could therefore be candidates for a targeted therapy with Herceptin.

Taken together, accurate classification of ampullary carcinomas is of crucial importance since the distinct

Table 4 Amplification of oncogenes

Oncogene	Amplification		
	Normal	Adenoma	Carcinoma
c-myc	*N*=26	*N*=36	*N*=70
	0/26	1/36	0/70
EGFR	*N*=83	*N*=79	*N*=137
	0/83	1/79	1/137[a]
CCND1	*N*=88	*N*=74	*N*=134
	0/88	2/74	10/134[b]
HER2	*N*=46	*N*=45	*N*=82
	0/46	3/45	5/82[c]

[a] One IT
[b] Six IT, two PBT, one G3AC, one IPT
[c] Two IT, one G3AC, two IPT

subtypes were shown to differ significantly in clinical outcome. Using an immunohistochemical panel of established marker proteins including CK7, p27, ESA, and bax can improve and facilitate differential diagnosis, especially in small and fragmented biopsy samples. A subset of ampullary tumors, furthermore, shows amplification of CCND1 and HER2 which could represent potential targets for cancer therapy. The large number of tumors included in this study highlights the presence of rare molecular events that can be of potential therapeutic relevance.

Conflict of interest statement We declare that we have no conflict of interest.

References

1. Allescher HD (1989) Papilla of Vater: structure and function. Endoscopy 21(Suppl 1):324–329
2. Neoptolemos JP, Talbot IC, Carr-Locke DL et al (1987) Treatment and outcome in 52 consecutive cases of ampullary carcinoma. Br J Surg 74:957–961
3. Albores-Saavedra J, Scoazec JC, Wittekind C et al (2000) Tumours of the gallbladder and extrahepatic bile ducts. In: Hamilton SR, Aaltonen LA (eds) World Health Organization classification of tumours: pathology and genetics of tumours of the digestive system. IARC, Lyon, pp 203–218
4. Wright NH, Howe JR, Rossini FP et al (2000) Tumours of the small intestine. In: Hamilton SR, Aaltonen LA (eds) World Health Organization classification of tumours: pathology and genetics of tumours of the digestive system. IARC, Lyon, pp 69–92
5. Fischer HP, Zhou H (2004) Pathogenesis of carcinoma of the papilla of Vater. J Hepatobiliary Pancreat Surg 11:301–309
6. Howe JR, Klimstra DS, Moccia RD et al (1998) Factors predictive of survival in ampullary carcinoma. Ann Surg 228:87–94
7. Kaiser A, Jurowich C, Schonekas H et al (2002) The adenoma–carcinoma sequence applies to epithelial tumours of the papilla of Vater. Z Gastroenterol 40:913–920
8. Takashima M, Ueki T, Nagai E et al (2000) Carcinoma of the ampulla of Vater associated with or without adenoma: a clinicopathologic analysis of 198 cases with reference to p53 and Ki-67 immunohistochemical expressions. Mod Pathol 13:1300–1307
9. Todoroki T, Koike N, Morishita Y et al (2003) Patterns and predictors of failure after curative resections of carcinoma of the ampulla of Vater. Ann Surg Oncol 10:1176–1183
10. Bouvet M, Gamagami RA, Gilpin EA et al (2000) Factors influencing survival after resection for periampullary neoplasms. Am J Surg 180:13–17
11. Chang MC, Chang YT, Tien YW et al (2005) Distinct chromosomal aberrations of ampulla of Vater and pancreatic head cancers detected by laser capture microdissection and comparative genomic hybridization. Oncol Rep 14:867–872
12. Yeo CJ, Cameron JL, Sohn TA et al (1997) Six hundred fifty consecutive pancreaticoduodenectomies in the 1990s: pathology, complications, and outcomes. Ann Surg 226:248–257; discussion 57–60
13. Di Giorgio A, Alfieri S, Rotondi F et al (2005) Pancreatoduodenectomy for tumors of Vater's ampulla: report on 94 consecutive patients. World J Surg 29:513–518
14. Sperti C, Pasquali C, Piccoli A et al (1994) Radical resection for ampullary carcinoma: long-term results. Br J Surg 81:668–671
15. Talamini MA, Moesinger RC, Pitt HA et al (1997) Adenocarcinoma of the ampulla of Vater. A 28-year experience. Ann Surg 225:590–599; discussion 9–600
16. Beghelli S, Orlandini S, Moore PS et al (2002) Ampulla of vater cancers: T-stage and histological subtype but not Dpc4 expression predict prognosis. Virchows Arch 441:19–24
17. Westgaard A, Tafjord S, Farstad IN et al (2008) Pancreatobiliary versus intestinal histologic type of differentiation is an independent prognostic factor in resected periampullary adenocarcinoma. BMC Cancer 8:170
18. Albores-Saavedra J, Henson DE, Klimstra DS (2000) Tumors of the gallbladder, extrahepatic bile ducts, and ampulla of Vater. Armed Forces Institute of Pathology, Washington, DC
19. Fischer HP, Zhou H (2003) [Pathogenesis and histomorphology of ampullary carcinomas and their precursor lesions. Review and individual findings]. Pathologe 24:196–203
20. Kimura W, Futakawa N, Yamagata S et al (1994) Different clinicopathologic findings in two histologic types of carcinoma of papilla of Vater. Jpn J Cancer Res 85:161–166
21. Matsubayashi H, Watanabe H, Yamaguchi T et al (1999) Differences in mucus and K-ras mutation in relation to phenotypes of tumors of the papilla of vater. Cancer 86:596–607
22. Zlobec I, Minoo P, Baker K et al (2007) Loss of APAF-1 expression is associated with tumour progression and adverse prognosis in colorectal cancer. Eur J Cancer 43:1101–1107
23. Zlobec I, Vuong T, Hayashi S et al (2007) A simple and reproducible scoring system for EGFR in colorectal cancer: application to prognosis and prediction of response to preoperative brachytherapy. Br J Cancer 96:793–800
24. Zlobec I, Lugli A (2008) Prognostic and predictive factors in colorectal cancer. A critical review. J Clin Pathol 61:561–569
25. Barclay TH, Schapira DV (1983) Malignant tumors of the small intestine. Cancer 51:878–881
26. Santoro E, Sacchi M, Scutari F et al (1997) Primary adenocarcinoma of the duodenum: treatment and survival in 89 patients. Hepatogastroenterology 44:1157–1163
27. Thomas RM, Sobin LH (1995) Gastrointestinal cancer. Cancer 75:154–170
28. Weiss NS, Yang CP (1987) Incidence of histologic types of cancer of the small intestine. J Natl Cancer Inst 78:653–656
29. Kozuka S, Tsubone M, Yamaguchi A et al (1981) Adenomatous residue in cancerous papilla of Vater. Gut 22:1031–1034
30. Perzin KH, Bridge MF (1982) Adenomatous and carcinomatous changes in hamartomatous polyps of the small intestine (Peutz–Jeghers syndrome): report of a case and review of the literature. Cancer 49:971–983
31. Sellner F (1990) Investigations on the significance of the adenoma–carcinoma sequence in the small bowel. Cancer 66:702–715
32. Perzin KH, Bridge MF (1981) Adenomas of the small intestine: a clinicopathologic review of 51 cases and a study of their relationship to carcinoma. Cancer 48:799–819
33. Fritz B, Schubert F, Wrobel G et al (2002) Microarray-based copy number and expression profiling in dedifferentiated and pleomorphic liposarcoma. Cancer Res 62:2993–2998
34. Hall M, Peters G (1996) Genetic alterations of cyclins, cyclin-dependent kinases, and Cdk inhibitors in human cancer. Adv Cancer Res 68:67–108
35. Kim SH, Lewis JJ, Brennan MF et al (1998) Overexpression of cyclin D1 is associated with poor prognosis in extremity soft-tissue sarcomas. Clin Cancer Res 4:2377–2382
36. Tornillo L, Duchini G, Carafa V et al (2005) Patterns of gene amplification in gastrointestinal stromal tumors (GIST). Lab Invest 85:921–931
37. Al-Kuraya K, Novotny H, Bavi P et al (2007) HER2, TOP2A, CCND1, EGFR and C-MYC oncogene amplification in colorectal cancer. J Clin Pathol 60:768–772

Virchows Arch (2008) 453:589–598
DOI 10.1007/s00428-008-0682-x

ORIGINAL ARTICLE

Intraductal papillary neoplasm of the bile duct associated with *Clonorchis sinensis* infection

Kee-Taek Jang · Seung-Mo Hong · Kyu Taek Lee · Jong Gyun Lee · Seoung Ho Choi · Jin Seok Heo · Dong Wook Choi · Dongil Choi · Jae Hoon Lim

Received: 15 April 2008 / Revised: 12 August 2008 / Accepted: 27 September 2008 / Published online: 15 October 2008

Abstract Intraductal papillary neoplasm of bile duct (IPNB) is one of the precursor lesions of cholangiocarcinoma. Although hepatolithiasis has been extensively studied in its association with IPNBs, there had been no comprehensive study of IPNBs with *Clonorchis sinensis* infection. Twelve IPNBs were selected from 20 surgically resected cholangiocarcinomas, positive for *C. sinensis* tests (60%) and compared with eight IPNBs, selected from 51 resected cholangiocarcinomas, negative for *C. sinensis* tests (16%), by histologic and immunohistochemical studies of mucin core proteins and cytokeratin panels. The predominant immuno-phenotype of IPNB cases with Clonorchiasis was pancreatobiliary type (MUC1+/MUC2-/CDX2-; 9/12 cases), while that of IPNB cases with negative for *C. sinensis* was intestinal type (MUC1-/MUC2+/CDX2+; 6/8; $p=0.04$). The prevalence of IPNBs was higher when patients with cholangiocarcinoma had Clonorchiasis. IPNBs with Clonorchiasis tended to have a more pancreatobiliary phenotype, which suggests IPNBs with Clonorchiasis may have a different tumorigenesis pathway from IPNBs with other etiologies.

Keywords *Clonorchis sinensis* · Intraductal papillary neoplasm of bile duct

Drs. Kee-Taek Jang and Seung-Mo Hong contributed equally to this work.

This work was supported by Samsung Medical Center Clinical Research Development Program grant, # CRS-105-43-2.

K.-T. Jang
Department of Pathology, Samsung Medical Center, and Center of Clinical Research, Samsung Biomedical Research Institute, Sungkyunkwan University School of Medicine, Seoul, Korea

S.-M. Hong
Department of Pathology, Johns Hopkins Medical Institutions, Baltimore, MD, USA

K. T. Lee · J. G. Lee
Department of Medicine, Samsung Medical Center, and Center of Clinical Research, Samsung Biomedical Research Institute, Sungkyunkwan University School of Medicine, Seoul, Korea

S. H. Choi · J. S. Heo · D. W. Choi
Department of Surgery, Samsung Medical Center, and Center of Clinical Research, Samsung Biomedical Research Institute, Sungkyunkwan University School of Medicine, Seoul, Korea

D. Choi · J. H. Lim (✉)
Department of Radiology and Center for Imaging Science, Samsung Medical Center, and Center of Clinical Research, Samsung Biomedical Research Institute, Sungkyunkwan University School of Medicine,
#50 Irwon-dong, Gangnam-gu,
Seoul 135-710, South Korea
e-mail: jhlim@skku.edu

Introduction

Papillary forming tumors in the biliary tract are uncommon, but have a better survival than other types of cholangiocarcinoma [2, 11, 29]. Intraductal papillary neoplasms of the bile duct (IPNBs) show the common histopathologic features of papillary proliferations such as dysplastic, tall, columnar, mucin containing biliary epithelia with fibrovascular cores frequently accompanied by overproduction of mucin [4]. These histopathologic characteristics of IPNBs are also commonly observed in intraductal papillary mucinous neoplasms (IPMNs) of the pancreas. However, unlike its histopathologic counter part in the pancreas, which already has a defined nomenclature and histologic

subtype [8], there has not been any consensus on the name and classification for IPNBs. Papillary forming biliary tumors have been called many other names by different groups around the world, including mucin hypersecreting bile duct tumor [16], biliary papillomatosis [20], intraductal mucosal-spreading mucin-producing peripheral cholangiocarcinoma [21], noninvasive, and minimally invasive papillary carcinoma [2], intraductal papillary neoplasia of the liver [4], intraductal papillary neoplasm of the bile duct [1, 34], mucin-producing bile duct tumor [26, 32], and mucin-secreting bile duct adenoma [23]. The current World Health Organization classification of gastrointestinal tract tumors categorized papillary forming biliary tumors into two groups: biliary papillomatosis, as a benign neoplasm, and papillary cholangiocarcinoma, as a malignant counter part [9].

IPNBs share several etiologic factors with infiltrating cholangiocarcinoma for its development, such as hepatolithiasis, infection to liver fluke (*Clonorchis sinensis* and *Opisthorchis viverrini*), primary sclerosing cholangitis, von Meyenberg complexes, and choledochal cysts [4, 19, 32]. IPNBs with hepatolithiasis are often known to have a characterization of intestinal phenotype (MUC2+/CK20+) and are frequently associated with colloid carcinoma [4, 34]. However, there has not been a comprehensive phenotypic study regarding IPNBs association with other risk factors, including Clonorchiasis. Here, we report 12 cases of IPNBs associated with *C. sinensis* infection in conjunction with an immunohistochemical survey of mucin core proteins and cytokeratin panels.

Materials and methods

Study materials and confirmation of *C. sinensis* infection

A schematic flow chart of inclusion and exclusion criteria for this study is summarized in Fig. 1. A total 130 patients with cholangiocarcinoma were screened for *C. sinensis* infection from January, 2001 to December, 2005 at the Departments of Medicine and Pathology, Samsung Medical Center, Sungkyunkwan University, Seoul, Korea. Screening tests for *C. sinensis* included serologic test of enzyme-linked immunosorbent assay (ELISA), skin test for *C. sinensis*, and microscopic detection of eggs for *C. sinensis* in the bile juice or stool. An ELISA with specific serum antibodies for *C. sinensis* was tested as previously described, which is known to have a higher sensitivity (92.5%) and specificity (93.1%). On the other hand, skin test and stool examinations have lower sensitivity and specificity than those of ELISA [6]. Skin test with crude *C. sinensis* antigen was examined as described elsewhere [22]. The microscopic examination of bile juice and stool were used for detection of parasite eggs. The *C. sinensis* infection was considered as positive when more than one positive result was present among the four screening tests, and it was considered as negative when ELISA and one of three other tests (bile cytology, stool or skin tests) were negative.

Immunohistochemistry

Tissue sections on glass slides were deparaffinized with xylene, rehydrated in serially diluted alcohol, and subse-

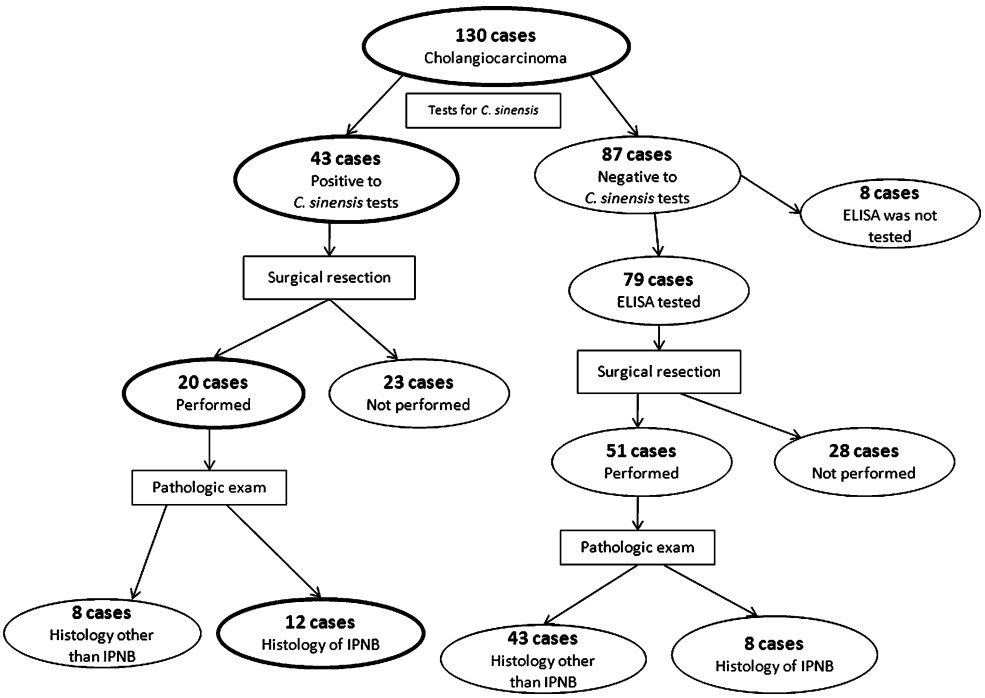

Fig. 1 Flow chart of inclusion and exclusion criteria for selecting intraductal papillary neoplasms of bile duct cases with or without *C. sinensis* infection

quently processed in a microwave for 15 min with pH 9 Tris-ethylene diamine tetraacetic acid (TE) buffer for antigen retrieval. After blocking of endogenous peroxidase with 3% H_2O_2, the sections were immersed in 3% goat serum diluted with phosphate-buffered saline for 60 min. The slides then were incubated with one of the primary antibodies described as follows for 60 min at room temperature: CK7 (clone OV-TL 12/30; 1:100 dilution; Dako Cytomation, Glostrup, Denmark), CK20 (clone Ks20.8; 1:100 dilution; Dako Cytomation), MUC1 (clone: Ma695; 1:100 dilution; Novocastra, New Castle, UK), MUC2 (clone Ccp58, 1:100 dilution; Novocastra), MUC5AC (clone CLH2; 1:100 dilution; Novocastra), and CDX2 (clone: CDX2-88, 1:40 dilution; Novocastra). After rinsing three times with distilled water containing 0.1% Tween 20, the tissue sections were incubated with HRP-conjugated streptavidin for 20 min at room temperature. Slides were then washed, developed for 5 min with liquid 3,3′-diaminobenzidine tetrahydrochloride, counterstained with Meyer's hematoxylin, dehydrated, and mounted with Permount for histologic examination.

Interpretation of mucin core protein and cytokeratin expression

Positive immunostaining patterns of MUC1, MUC2, CDX2, MUC5AC, CK7, and CK20 were identified as follows; MUC1 was expressed mainly in the apical membrane, MUC2 in the cytoplasm, CDX2 in the nuclei, and MUC5AC in the cytoplasm and apical membrane of tumor cells. Expression of MUC1, MUC2, CDX2, MUC5AC, CK7, and CK20 was evaluated semiquantitatively into four scores according to the percentage of positive cells in the individual lesion: negative, 0%; 1+ (focal), 1% to 10%; 2+ (moderate), 11–50%; 3+ (extensive), more than 50%. Two independent pathologists (KTJ and SMH) scored tumors separately. A consensus score was achieved to reduce inter-observer variation in the evaluation of staining patterns. Scores equal to or greater than 1+ were considered positive, which was described elsewhere for previous IPNB study [34]. The immunostaining patterns were separately recorded in both intraductal and invasive components. When no invasive component was present, only the intraductal component was evaluated.

Statistical analysis

Statistical analyses were performed using SPSS version 11 (SPSS Inc., Chicago, IL, USA). Analysis of the prevalence of IPNBs with or without Clonorchiasis was examined by two-sample Z test for proportions. Associations between categorical variables were examined by the Pearson's chi-square and Fisher's exact tests. A p value of less than 0.05 was considered statistically significant.

Results

Prevalence of IPNBs accompanying Clonorchiasis

An ELISA with specific serum antibodies for *C. sinensis* was known to be the most sensitive and specific test for diagnosis of Clonorchiasis (sensitivity 92.5%, specificity 93.1%), while bile cytology has higher specificity but low sensitivity for evaluation of eggs of *C. sinensis*. On the other hand, skin test and stool examinations have lower sensitivity and specificity than those of ELISA [6]. Although bile cytology was negative in patients number 5, 8, and 11, those cases were positive not only by ELISA but also by skin test and stool examinations (Table 2). Therefore, we considered those three cases positive for Clonorchiasis.

The prevalence of IPNBs with *C. sinensis* from patients with cholangiocarcinomas was summarized in Fig. 1 and Table 1. *C. sinensis* infection was detected by four screening tests and was finally confirmed in 43 cases from 130 screened patients with clinical suspicion of cholangiocarcinoma (33%). Surgical resection of biliary tumors was performed in 20 cases of the 43 patients with cholangiocarcinoma with *C. sinensis* infection. Eight cases from 20 resected patients were excluded because histopathologic characteristics of IPNBs were not observed. Therefore 12 IPNB cases (60%) were finally included in this study from 20 surgically resected cholangiocarcinoma cases which were positive for screening tests for *C. sinensis* infection.

Among the remaining 87 cases from the 130 screened patients whose test results were negative, eight cases were excluded because ELISA test was not performed. ELISA tests were performed in 122 cases and negative in 79 patients. Surgical resection was performed in 51 of 79 cholangiocarcinoma cases, which were negative for *C. sinensis* tests. Forty-three patients from the 51 resected cases were excluded because histopathologic characteristics of IPNBs were not observed. Therefore, eight IPNB cases (16%) selected as the control group from 51 resected cholangiocarcinoma cases with negative screening tests for *C. sinensis*. When cholangiocarcinoma patients had a

Table 1 Incidence of IPNB with or without Clonorchiasis in patients of surgically resected cholangiocarcinomas

Histology	Tests for *C. sinensis*	
	Positive	Negative
IPNB	12 (60%)[a]	8 (16%)
Other than IPNB	8	43
Total	20	51

[a] IPNB with Clonorchiasis showed high incidence than IPNB without Clonorchiasis (p=0.001)

Table 2 Clinicopathologic characteristics of IPNB with and without Clonorchiasis

C. sinensis	Case number	Sex	Age	Screening test for *C. sinensis*				Noninvasive component				Invasive component		pT Classification	pN classification
				Stool	Skin	ELISA	Bile	Location	Diagnosis	Histologic grade	Histologic subtype	Histologic subtype	Differentiation		
Positive	1	Male	58	–	ND	ND	+	EBD	Invasive	Carcinoma	Pancreatobiliary	Tubular	Moderate	2	0
Positive	2	Female	67	–	–	–	+	EBD	Noninvasive	Borderline	Intestinal	NA	NA	NA	0
Positive	3	Male	51	–	–	+	+	EBD	Noninvasive	Carcinoma	Pancreatobiliary	NA	NA	is	0
Positive	4	Male	59	–	ND	ND	+	EBD	Invasive	Carcinoma	Pancreatobiliary	Tubular	Poor	3	1
Positive	5	Female	61	+	+	+	–	IHD&EBD	Invasive	Carcinoma	Pancreatobiliary	Tubular	Moderate	2	1
Positive	6	Male	59	–	–	–	+	IHD	Invasive	Carcinoma	Pancreatobiliary	Tubular	Moderate	1	0
Positive	7	Male	70	–	ND	ND	+	IHD	Invasive	Carcinoma	Intestinal	Colloid	Well	1	0
Positive	8	Female	64	–	+	+	–	IHD (Fig. 1a)	Noninvasive	Carcinoma	Pancreatobiliary	NA	NA	is	0
Positive	9	Female	67	+	+	+	+	IHD	Noninvasive	Carcinoma	Intestinal	NA	NA	is	0
Positive	10	Male	68	–	–	–	+	EBD	Invasive	Carcinoma	Pancreatobiliary	Tubular	Moderate	2	0
Positive	11	Male	60	+	+	+	–	EBD (Fig. 1b)	Invasive	Carcinoma	Pancreatobiliary	Tubular	Moderate	2	0
Positive	12	Male	68	+	–	+	+	EBD	Invasive	Carcinoma	Pancreatobiliary	Tubular	Poor	3	1
Negative	13	Male	68	ND	–	–	ND	EBD	Invasive	Carcinoma	Pancreatobiliary	Tubular	Moderate	2	0
Negative	14	Male	71	–	ND	–	–	EBD	Invasive	Carcinoma	Pancreatobiliary	Tubular	Poor	2	0
Negative	15	Male	70	–	–	–	–	IHD	Invasive	Carcinoma	Intestinal	Colloid	Moderate	2	1
Negative	16	Female	56	ND	–	–	–	EBD	Invasive	Carcinoma	Intestinal	Colloid	Poor	2	1
Negative	17	Female	76	–	ND	–	–	EBD	Invasive	Carcinoma	Intestinal	Colloid	Poor	2	0
Negative	18	Female	60	–	–	–	–	EBD	Noninvasive	Carcinoma	Intestinal	NA	NA	is	0
Negative	19	Female	58	–	–	–	–	EBD	Noninvasive	Carcinoma	Intestinal	NA	NA	is	0
Negative	20	Female	62	ND	–	–	–	EBD	Noninvasive	Carcinoma	Intestinal	NA	NA	is	0

CBD common bile duct, *IHD* intrahepatic bile duct, *EHD* extrahepatc bile duct, *ND* not done, *NA* not applicable, *CIS* carcinoma in situ

Clonorchiasis infection, the prevalence of IPNB was significantly higher than that of cholangiocarcinoma cases without accompanying infection to *C. sinensis* (two sample *Z* test, $p=0.001$, Table 1).

Clinicopathologic characteristics of IPNB cases with Clonorchiasis

The clinicopathologic characteristics of the IPNB cases with Clonorchiasis are summarized in Table 2. Eight patients were men and four were women. Their ages ranged from 51 to 70 years (mean, 63 years; SD, 5.6 years). The tumor locations were the extrahepatic bile duct (EBD) in seven cases, intrahepatic duct (IHD) in four cases, and both IHD and EBD in one case. Representative figures of EBD and IHD tumors are depicted in Fig. 2. Four cases were noninvasive IPNBs and eight contained invasive carcinoma components. Of four cases with noninvasive IPNBs, one was borderline neoplasm and three were carcinoma in situ (CIS). When we analyzed the histologic subtypes of IPNBs according to those of IPMNs of the pancreas, the histologic subtypes of noninvasive IPNB components consisted of three intestinal and nine pancreatobiliary types (Figs. 3 and 4). Histologic subtypes of the eight invasive carcinoma components were seven tubular carcinomas and one colloid carcinoma. Differentiation of the invasive component was well differentiated in one, moderately differentiated in five, and poorly differentiated in two cases. T classifications of eight invasive cholangiocarcinoma cases were two T1, three T2, and one T3. Metastasis to lymph nodes was observed in three invasive IPNB cases, and all three were accompanied by tubular carcinoma. Types of surgery included segmental bile duct resection ($n=4$), standard pancreaticoduodenectomy (Whipple's operation, $n=2$), pylorus preserving pancreaticoduodenectomy ($n=1$), right lobectomy ($n=2$), right posterior segmentectomy ($n=1$), hemihepatectomy ($n=1$), and left lateral segmentectomy ($n=1$).

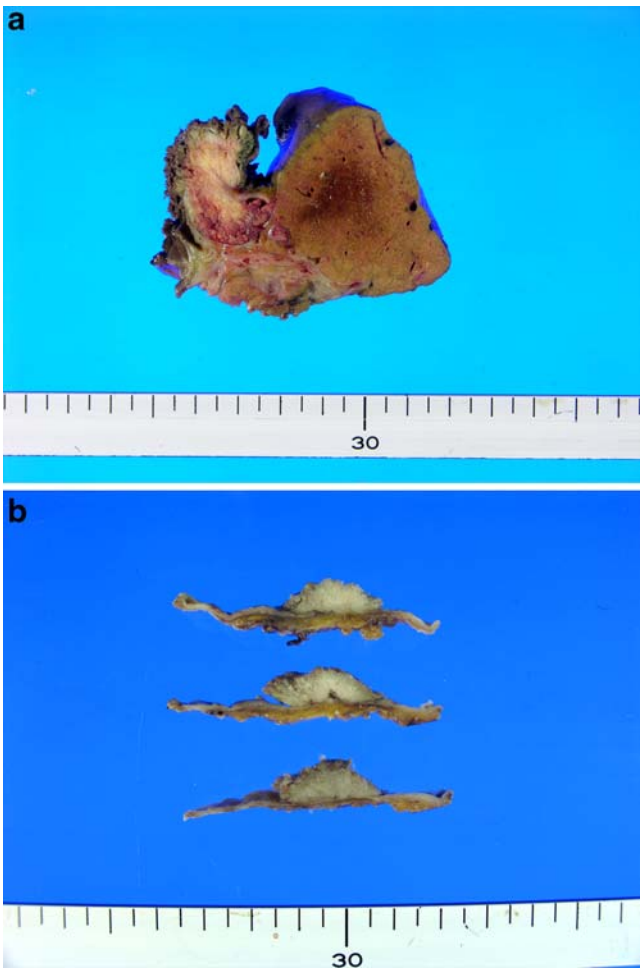

Fig. 2 Intraductal papillary neoplasms of the intrahepatic and extrahepatic bile ducts. **a** A 2.5-cm mass with numerous papillary projections fills entire dilated intrahepatic bile duct (case 8). **b** Serial sections of tumor with papillary projections in extrahepatic bile duct (case 11)

MUC1, MUC2, CDX2, and MUC5AC expression of IPNB cases with Clonorchiasis

Results of immunohistochemical studies for MUC1, MUC2, CDX2, and MUC5AC are summarized in Table 3, and representative figures are presented in Figs. 3 and 4. MUC1 was positive in seven of 12 total cases (58%). Seven of eight invasive IPNBs cases were positive for MUC1 (88%), while one carcinoma and four noninvasive IPNBs were negative, which showed statistically significant difference of MUC1 expression between invasive IPNBs and noninvasive IPNB groups ($p=0.01$). Both MUC2 and CDX2 expressions were observed in two of three cases with intestinal type of noninvasive IPNB component (67%), while both MUC2 and CDX2 were negative in all pancreatobiliary type (0/9 cases, $p=0.04$). MUC5AC was expressed in 11 IPNB cases with diffuse staining pattern (92%).

Combined MUC1 and MUC2 expression of IPNB cases with Clonorchiasis

Combined expression patterns of MUC1 and MUC2 protein between noninvasive and invasive components of IPNBs were evaluated. The predominant MUC1/MUC2 immuno-phenotype of IPNBs with Clonorchiasis was MUC1+/MUC2− (pancreatobiliary type, 7/12, 58%), while MUC1-/MUC2+ (intestinal type, two cases, 17%) and MUC1−/MUC2− (three cases, 25%) were significantly less ($p=0.02$). One of the MUC1−/MUC2+ cases showed

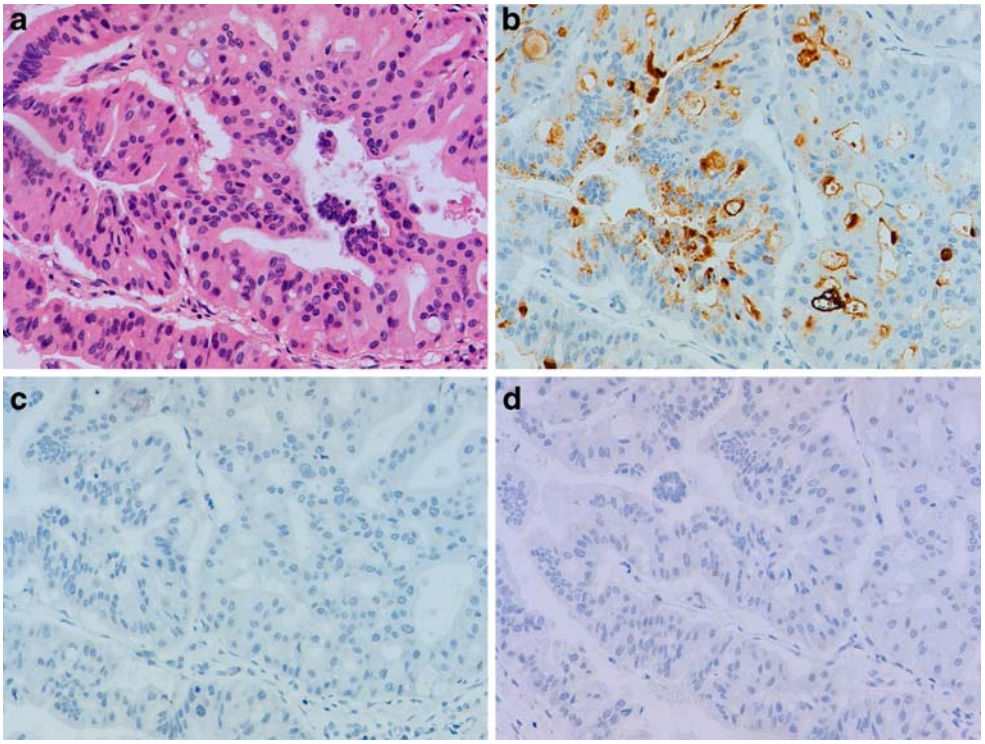

Fig. 3 Pancreatobiliary type intraductal papillary neoplasm of bile duct (case 6). **a** Tumor cells with micropapillary projections display round nuclei. Tumor cells are immuno-labeled for **b** MUC1, however negative to **c** MUC2 and **d** CDX2 (×200 original magnification)

invasive colloid carcinoma as an invasive component (Case 7 in Table 2). All seven cases of MUC1+/MUC2− phenotype were observed solely in invasive carcinoma cases. MUC1−/MUC2+ (two cases) phenotype are noted, one in invasive carcinoma and one in CIS case, while all three MUC1−/MUC2− patterns were observed only in noninvasive carcinoma (one borderline and two CIS cases; $p=0.008$). In the case with invasive carcinoma, the expression pattern of the intraductal component was similar to that of invasive carcinoma component.

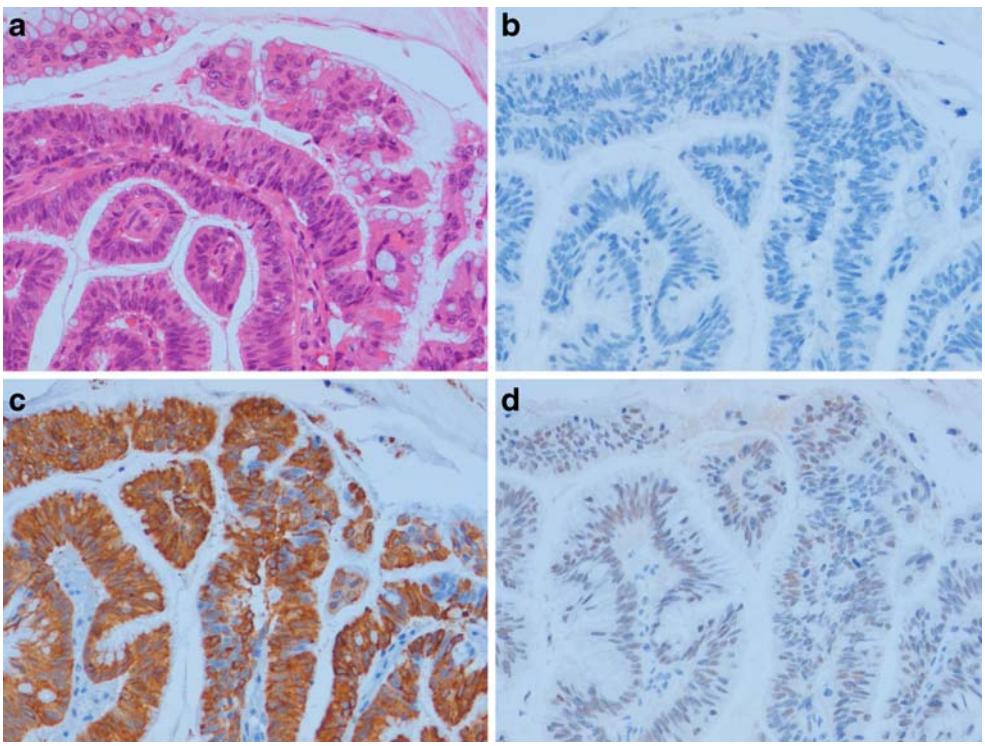

Fig. 4 Intestinal type intraductal papillary neoplasm of bile duct (case 7). **a** Tumor cells with elongated and stratified nuclei contain abundant mucin in their cytoplasm. Tumor cells are **b** MUC1 negative, but **c** MUC2 and **d** CDX2 positive (×200 original magnification)

Table 3 Results of immunohistochemical study of IPNB with Clonorchiasis

C. sinensis	Case number	Histological type	CK7		CK20		MUC1		MUC2		CDX2		MUC5AC	
			Invasive	Noninvasive	Invasive	Noninvasive	Invasive	Noninvasive	Invasive	Noninvasive	Invasive	Noninvasive	Invasive	Non-invasive
Positive	1	Pancreatobiliary	2+	2+	0	0	2+	0	0	0	0	0	2+	3+
Positive	2	Intestinal	NA	1+	NA	2+	NA	0	NA	0	NA	0	NA	0
Positive	3	Pancreatobiliary	NA	2+	NA	0	NA	0	NA	0	NA	0	NA	3+
Positive	4	Pancreatobiliary	1+	2+	0	0	2+	1+	0	0	0	0	2+	2+
Positive	5	Pancreatobiliary	2+	2+	0	0	2+	2+	0	0	0	0	2+	2+
Positive	6	Pancreatobiliary (Fig. 2)	2+	2+	0	0	3+	3+	0	0	0	0	3+	3+
Positive	7	Intestinal (Fig. 3)	0	0	2+	2+	0	0	2+	2+	1+	1+	2+	2+
Positive	8	Pancreatobiliary	NA	2+	NA	0	NA	0	NA	0	NA	0	NA	3+
Positive	9	Intestinal	NA	1+	NA	2+	NA	0	NA	2+	NA	2+	NA	2+
Positive	10	Pancreatobiliary	3+	3+	0	0	2+	2+	0	0	0	0	2+	2+
Positive	11	Pancreatobiliary	3+	3+	1+	1+	2+	2+	0	0	0	0	2+	2+
Positive	12	Pancreatobiliary	2+	2+	1+	1+	2+	2+	0	0	0	0	2+	2+
Negative	1	Pancreatobiliary	2+	2+	0	0	2+	1+	0	0	0	0	2+	2+
Negative	2	Pancreatobiliary	3+	2+	1+	1+	2+	1+	0	0	0	0	2+	2+
Negative	3	Intestinal	1+	1+	2+	2+	1+	0	2+	2+	2+	2+	3+	3+
Negative	4	Intestinal	1+	1+	2+	3+	1+	0	2+	2+	2+	2+	3+	3+
Negative	5	Intestinal	2+	2+	2+	2+	2+	1+	2+	2+	1+	1+	2+	2+
Negative	6	Intestinal	NA	2+	NA	2+	NA	1+	NA	1+	NA	1+	NA	2+
Negative	7	Intestinal	NA	1+	NA	3+	NA	0	NA	1+	NA	1+	NA	3+
Negative	8	Intestinal	NA	1+	NA	3+	NA	0	NA	2+	NA	2+	NA	3+

NA not applicable

CK 7 and CK20 expression of IPNB cases with Clonorchiasis

Results of immunohistochemical studies for CK7 and CK20 are summarized in Table 2. CK7 was observed in 11 of the 12 IPNB cases with Clonorchiasis (92%), and CK20 expression was observed in five cases (42%).

Combined CK7 and CK20 expression of IPNB cases with Clonorchiasis

Combined expression patterns of CK7 and CK20 in noninvasive and invasive components of IPNB cases with Clonorchiasis were evaluated. The predominant CK7/CK20 immuno-phenotype of IPNBs was CK7+/CK20− (seven of 12 cases, 58%). Four cases had CK7+/CK20+ (33%), and one had CK7−/CK20+ pattern (9%). When CK7/CK20 phenotype was compared in invasive carcinoma component, CK7+/CK20− phenotype was observed in five of the seven tubular carcinomas (71%). CK7+/CK20+ was observed in two tubular carcinomas, while CK7−/CK20+ phenotype was observed in only one colloid carcinoma (p=0.02).

Comparison of expression pattern between IPNB cases with and without Clonorchiasis

The predominant histologic subtype of IPNB cases with Clonorchiasis was pancreatobiliary type (nine of 12 cases, 75%), which was validated by immunohistochemical results (MUC1+/MUC2−/CDX2−; nine of 12 cases), while that of IPNB cases negative for *C. sinensis* were intestinal type (six of eight cases, 75%), which showed MUC1−/MUC2+/CDX2+. There was significant difference of histologic subtype between IPNB cases with and without Clonorchiasis (Fisher's exact test, p=0.04). However, when other clinicopathologic factors, such as patients' age, location of tumor, depth of invasion and lymph node metastasis, were compared, there was no difference between IPNB cases with and without Clonorchiasis.

Discussion

Although IPNBs are a minor proportion of the biliary tract neoplasms, recently, they have received much attention due to their association with a better prognosis as compared to invasive cholangiocarcinoma [33]. Many researchers described that IPNBs and IPMNs of the pancreas share many commonalities. First, on gross examination, both IPNBs and IPMNs showed an intraductal growth pattern with papillary proliferation and occasional mucin hypersecretion [33]. Second, they both have the same histologic features, including papillary proliferation with fibrovascular stalks. Third, IPNBs and IPMNs have four distinct histologic subtypes, including gastric, intestinal, pancreatobiliary, and oncocytic types [7, 15, 28, 30]. Finally, both have a better prognosis than their invasive carcinoma counter parts [33]. Because of their distinct histologic characteristics and better prognosis, several researchers proposed that IPNBs should be considered a distinguished disease entity like IPMNs of the pancreas [15, 33]. However, unlike IPMNs of the pancreas which has a defined nomenclature and histologic subtypes [8], a consensus for IPNB naming and histologic classification has yet to be reached. Therefore, in this study, we adopted the currently accepted histologic grading system of IPMNs [13] and observed a significant phenotypical MUC1/MUC2 difference between IPNB cases with and without Clonorchiasis. The IPNB cases accompanying Clonorchiasis showed more pancreatobiliary phenotype (MUC1+/MUC2−) while on the other hand, intestinal phenotype (MUC1−/MUC2+) was predominantly observed in cases without Clonorchiasis infection.

Clonorchiasis, a chronic parasitic infection by *C. sinensis*, is an important etiologic factor in carcinogenesis of the cholangiocarcinoma, in areas of the Far East Asia, including Korea, China, Russia, and Vietnam [5]. Although cholangiocarcinoma associated with Clonorchiasis does not have a great impact on public health of Western people, the recognition about this Clonorchiasis and its complication is important, because the prevalence of this disease is increasing in immigrants or travelers from those endemic areas [24, 25]. Biliary hyperplasia is one of the characteristic histologic pathologic findings of Clonorchiasis [12]. Papillary biliary epithelial hyperplasia was also described as a histologic feature in a case with Clonorchiasis [17]. The exact mechanism of development of cholangiocarcinoma with parasitic infection has not been fully determined; however, chronic exposures to biochemically altered bile by *C. sinensis* or persistent irritations by adult worms have been proposed as a contributor to biliary epithelial proliferation [18].

There are a few previous descriptions regarding IPNB accompanied with Clonorchiasis [19, 29]. In the present study, the prevalence of IPNBs from surgically resected cholangiocarcinoma with Clonorchiasis was 60% (12 of 20 cases). This result was much higher than the prevalence of one previous study (five of 16 cases, 31%) [29]. On the other hand, the prevalence of IPNBs from resected cholangiocarcinoma without Clonorchiasis was only 16% (eight of 51 cases). Therefore, our study supports that IPNBs are more frequent when cholangiocarcinoma is accompanied with the *C. sinensis* infection. Due to this high prevalence of IPNBs from cholangiocarcinomas with Clonorchiasis, a high degree of suspicion about patients carrying Clonorchiasis is warranted, when pathologists examine cases cholangiocarcinomas with IPNBs.

Although one previous study reported that five out of 16 cases of intraductal growth pattern of intrahepatic cholangiocarcinoma had a history of Clonorchiasis infection [29], there was no histopathologic phenotypical information of the mucin proteins regarding IPNB with Clonorchiasis. In the present study, MUC2 and CDX2 expression were rarely identified and frequent MUC1 expression was noted in IPNB with Clonorchiasis when it accompanied invasive tubular adenocarcinoma. The main immuno-phenotype of IPNB with Clonorchiasis was MUC2−/CDX2−/CK7+/CK20− with an enhanced MUC1 expression in this study.

The expression of two well-characterized mucin antigens, MUC1 and MUC2, correlated well with their aggressiveness in the pancreaticobiliary tumors. MUC1 expression was more frequent in invasive conventional carcinoma with poor prognosis, whereas MUC2 expression was higher in the colloid carcinomas with a favorable outcome [3, 10, 31]. IPNB cases are known to mainly present with gastrointestinal phenotype with MUC2, MUC5AC, and CDX2 expression, especially when it is accompanied by intrahepatic bile duct stones [4, 14, 27, 34]. In the present study, we observed that IPNBs with Clonorchiasis had the predominant pancreatobiliary type (75%), while the intestinal type (25%) was much less. In addition, invasive IPNBs with Clonorchiasis cases in this study tended to have more tubular adenocarcinomas (7/8 cases, 88%) than colloid carcinoma (1/8 case, 12%). Regardless of Clonorchiasis status, IPNBs with pancreatobiliary type showed modest tendency to have a higher T classification (either T2 or T3, eight of 11 cases), while intestinal type tumors had a lower T classification (either Tis or T1, five of eight cases, $p=0.09$). These results were also different from the previous studies of IPNBs with hepatolithiasis, which was more frequently related to colloid carcinoma (47%) and had better prognosis [33]. Lee et al. reported that patients with mucin-hypersecreting biliary papillomatosis (IPNB with intestinal phenotype) had a significantly higher prevalence of accompanying symptoms of acute cholangitis, while those with non-mucin producing papillomatosis tended to be asymptomatic [20]. Combining the aforementioned description and the results of the present study, it is possible to assume that IPNB patients with biliary stones may express a more intestinal phenotype, which presents with secretory mucin protein (MUC2) into bile duct, and give rise to early symptoms of cholangitis. Due to these early symptoms, patients with IPNBs may detect their tumors earlier, leading to a better survival of the patients. On the other hand, IPNB patients with Clonorchiasis may not produce and secrete enough mucin into the bile from their papillary epithelia. Therefore, their infiltrating carcinomas may be detected in a later disease stage, because these patients did not present with any other symptoms. However, to test this hypothesis, clinicopathologic examination with a larger number of IPNBs with Clonorchiasis cases is required.

In this study, we observed different mucin and cytokeratin expression patterns in IPNB patients with Clonorchiasis. However, there are several questions still remaining to be answered. First, when Clonorchiasis patients with IPNBs progress to an invasive carcinoma, do they have similar biologic behavior or clinical manifestation to that of Clonorchiasis patients with invasive carcinomas without accompanying IPNBs? Second, do Clonorchiasis IPNB cases have similar genetic or epigenetic changes to those IPNBs associated with hepatolithiasis? Third, do other risk factors of IPNBs, such as Opisthorchiasis, primary sclerosing cholangitis, von Meyenberg complexes, and choledochal cyst, show their own unique mucin and cytokeratin phenotyping? Because IPNB is now a spotlighted-disease entity in carcinogenesis of cholangiocarcinoma, a consensus should be agreed upon for its nomenclature and histologic grading in order to facilitate communications among the researchers.

In summary, the prevalence of IPNBs was higher when patients with cholangiocarcinoma and Clonorchiasis. Therefore, a high degree of suspicion about Clonorchiasis is warranted when pathologists examine cholangiocarcinomas with IPNBs. The pancreatobiliary type was mainly observed in IPNB patients with Clonorchiasis. For more concrete conclusions, further studies with a larger number of IPNB cases with Clonorchiasis are required.

Acknowledgements We thank Ms. Margaret Griffith for editing the manuscript.

Conflicts of interest statement We declare that we have no conflict of interest.

References

1. Abraham SC, Lee JH, Boitnott JK, Argani P, Furth EE, Wu TT (2002) Microsatellite instability in intraductal papillary neoplasms of the biliary tract. Mod Pathol 15:1309–1317
2. Albores-Saavedra J, Murakata L, Krueger JE, Henson DE (2000) Noninvasive and minimally invasive papillary carcinomas of the extrahepatic bile ducts. Cancer 89:508–515
3. Amaya S, Sasaki M, Watanabe Y, Tsui WM, Tsuneyama K, Harada K, Nakanuma Y (2001) Expression of MUC1 and MUC2 and carbohydrate antigen Tn change during malignant transformation of biliary papillomatosis. Histopathology 38:550–560
4. Chen TC, Nakanuma Y, Zen Y, Chen MF, Jan YY, Yeh TS, Chiu CT, Kuo TT, Kamiya J, Oda K, Hamaguchi M, Ohno Y, Hsieh LL, Nimura Y (2001) Intraductal papillary neoplasia of the liver associated with hepatolithiasis. Hepatology 34:651–658
5. Choi BI, Han JK, Hong ST, Lee KH (2004) Clonorchiasis and cholangiocarcinoma: etiologic relationship and imaging diagnosis. Clin Microbiol Rev 17:540–552
6. Choi MH, Park IC, Li S, Hong ST (2003) Excretory-secretory antigen is better than crude antigen for the serodiagnosis of clonorchiasis by ELISA. Korean J Parasitol 41:35–39

7. Fujii T, Harada K, Katayanagi K, Kurumaya H, Nakanuma Y (2005) Intrahepatic cholangiocarcinoma with multicystic, mucinous appearance and oncocytic change. Pathol Int 55:206–209
8. Furukawa T, Kloppel G, Volkan Adsay N, Albores-Saavedra J, Fukushima N, Horii A, Hruban RH, Kato Y, Klimstra DS, Longnecker DS, Luttges J, Offerhaus GJ, Shimizu M, Sunamura M, Suriawinata A, Takaori K, Yonezawa S (2005) Classification of types of intraductal papillary-mucinous neoplasm of the pancreas: a consensus study. Virchows Arch 447:794–799
9. Hamilton SR, Altonen LA (2000) Papillomatosis. In: WHO Classification of Tumours (ed) Pathology and genetics. Tumours of the digestive system. IARC, Lyon, pp 210–214
10. Higashi M, Yonezawa S, Ho JJ, Tanaka S, Irimura T, Kim YS, Sato E (1999) Expression of MUC1 and MUC2 mucin antigens in intrahepatic bile duct tumors: its relationship with a new morphological classification of cholangiocarcinoma. Hepatology 30:1347–1355
11. Hoang MP, Murakata LA, Katabi N, Henson DE, Albores-Saavedra J (2002) Invasive papillary carcinomas of the extrahepatic bile ducts: a clinicopathologic and immunohistochemical study of 13 cases. Mod Pathol 15:1251–1258
12. Hou PC (1955) The pathology of Clonorchis sinensis infestation of the liver. J Pathol Bacteriol 70:53–64
13. Hruban RH, Takaori K, Klimstra DS, Adsay NV, Albores-Saavedra J, Biankin AV, Biankin SA, Compton C, Fukushima N, Furukawa T, Goggins M, Kato Y, Kloppel G, Longnecker DS, Luttges J, Maitra A, Offerhaus GJ, Shimizu M, Yonezawa S (2004) An illustrated consensus on the classification of pancreatic intraepithelial neoplasia and intraductal papillary mucinous neoplasms. Am J Surg Pathol 28:977–987
14. Ishikawa A, Sasaki M, Ohira S, Ohta T, Oda K, Nimura Y, Chen MF, Jan YY, Yeh TS, Nakanuma Y (2004) Aberrant expression of CDX2 is closely related to the intestinal metaplasia and MUC2 expression in intraductal papillary neoplasm of the liver in hepatolithiasis. Lab Invest 84:629–638
15. Ji Y, Fan J, Zhou J, Wang BS, Liu HB, Wu ZW, Tan YS (2008) Intraductal papillary neoplasms of bile duct. A distinct entity like its counterpart in pancreas. Histol Histopathol 23:41–50
16. Kim HJ, Kim MH, Lee SK, Yoo KS, Park ET, Lim BC, Park HJ, Myung SJ, Seo DW, Min YI (2000) Mucin-hypersecreting bile duct tumor characterized by a striking homology with an intraductal papillary mucinous tumor (IPMT) of the pancreas. Endoscopy 32:389–393
17. Kim KH, Kim CD, Lee HS, Lee SJ, Jeen YT, Chun HJ, Song CW, Lee SW, Um SH, Choi JH, Ryu HS, Hyun JH (1999) Biliary papillary hyperplasia with clonorchiasis resembling cholangiocarcinoma. Am J Gastroenterol 94:514–517
18. Kim YI (1984) Liver carcinoma and liver fluke infection. Arzneimittelforschung 34:1121–1126
19. Kim YI, Yu ES, Kim ST (1989) Intraductal variant of peripheral cholangiocarcinoma of the liver with Clonorchis sinensis infection. Cancer 63:1562–1566
20. Lee SS, Kim MH, Lee SK, Jang SJ, Song MH, Kim KP, Kim HJ, Seo DW, Song DE, Yu E, Lee SG, Min YI (2004) Clinicopathologic review of 58 patients with biliary papillomatosis. Cancer 100:783–793
21. Lim JH, Kim YI, Park CK (2000) Intraductal mucosal-spreading mucin-producing peripheral cholangiocarcinoma of the liver. Abdom Imaging 25:89–92
22. Min DY (1984) Remarks on the diagnosis of Clonorchis sinensis infection. Arzneimittelforschung 34:1153–1156
23. Oshikiri T, Kashimura N, Katanuma A, Maguchi H, Shinohara T, Shimizu M, Kondo S, Katoh H (2002) Mucin-secreting bile duct adenoma–clinicopathological resemblance to intraductal papillary mucinous tumor of the pancreas. Dig Surg 19:324–327
24. Papillo JL, Leslie KO, Dean RA (1989) Cytologic diagnosis of liver fluke infestation in a patient with subsequently documented cholangiocarcinoma. Acta Cytol 33:865–869
25. Schwartz DA (1986) Cholangiocarcinoma associated with liver fluke infection: a preventable source of morbidity in Asian immigrants. Am J Gastroenterol 81:76–79
26. Shibahara H, Tamada S, Goto M, Oda K, Nagino M, Nagasaka T, Batra SK, Hollingsworth MA, Imai K, Nimura Y, Yonezawa S (2004) Pathologic features of mucin-producing bile duct tumors: two histopathologic categories as counterparts of pancreatic intraductal papillary-mucinous neoplasms. Am J Surg Pathol 28:327–338
27. Shimonishi T, Zen Y, Chen TC, Chen MF, Jan YY, Yeh TS, Nimura Y, Nakanuma Y (2002) Increasing expression of gastrointestinal phenotypes and p53 along with histologic progression of intraductal papillary neoplasia of the liver. Hum Pathol 33:503–511
28. Spector SA, Bejarano PA, Amortegui JD, Renfrow MR, Livingstone AS (2004) Intraductal oncocytic papillary neoplasm of the extrahepatic biliary tree: first report. Am Surg 70:55–58
29. Suh KS, Roh HR, Koh YT, Lee KU, Park YH, Kim SW (2000) Clinicopathologic features of the intraductal growth type of peripheral cholangiocarcinoma. Hepatology 31:12–17
30. Terada T, Taniguchi M (2004) Intraductal oncocytic papillary neoplasm of the liver. Pathol Int 54:116–123
31. Yamashita K, Yonezawa S, Tanaka S, Shirahama H, Sakoda K, Imai K, Xing PX, McKenzie IF, Hilkens J, Kim YS et al (1993) Immunohistochemical study of mucin carbohydrates and core proteins in hepatolithiasis and cholangiocarcinoma. Int J Cancer 55:82–91
32. Yokomuro S, Arima Y, Mizuguchi Y, Shimizu T, Kawahigashi Y, Kannda T, Arai M, Uchida E, Akimaru K, Tajiri T (2007) Mucin-producing bile duct carcinoma arising from primary sclerosing cholangitis: a case report. J Nippon Med Sch 74:61–64
33. Zen Y, Fujii T, Itatsu K, Nakamura K, Minato H, Kasashima S, Kurumaya H, Katayanagi K, Kawashima A, Masuda S, Niwa H, Mitsui T, Asada Y, Miura S, Ohta T, Nakanuma Y (2006) Biliary papillary tumors share pathological features with intraductal papillary mucinous neoplasm of the pancreas. Hepatology 44:1333–1343
34. Zen Y, Sasaki M, Fujii T, Chen TC, Chen MF, Yeh TS, Jan YY, Huang SF, Nimura Y, Nakanuma Y (2006) Different expression patterns of mucin core proteins and cytokeratins during intrahepatic cholangiocarcinogenesis from biliary intraepithelial neoplasia and intraductal papillary neoplasm of the bile duct–an immunohistochemical study of 110 cases of hepatolithiasis. J Hepatol 44:350–358

Virchows Arch (2008) 453:599–609
DOI 10.1007/s00428-008-0685-7

ORIGINAL ARTICLE

Gene expression profiling in glioblastoma and immunohistochemical evaluation of IGFBP-2 and CDC20

Gianluca Marucci · Luca Morandi · Elisabetta Magrini · Anna Farnedi · Enrico Franceschi · Rossella Miglio · Daniela Calò · Annalisa Pession · Maria P. Foschini · Vincenzo Eusebi

Received: 28 July 2008 / Revised: 29 September 2008 / Accepted: 6 October 2008 / Published online: 25 October 2008

Abstract Thirty-nine glial tumours (28 glioblastomas (GB) and 11 low-grade gliomas) were investigated with DNA microarrays to reveal a possible specific gene expression profile. Unsupervised classification through hierarchical cluster analysis identified two groups of tumours, the first composed of low-grade gliomas and the second mainly composed of GB. Nine genes were identified as most informative: seven were over-expressed in low-grade gliomas and under-expressed in GB; on the contrary, two genes, insulin-like growth factor binding protein 2 (IGFBP-2) and cell division cycle 20 homologue (CDC20), were over-expressed in GB and under-expressed in low-grade tumours. This same genetic profile was confirmed by reverse transcriptase polymerase chain reaction. Immunohistochemistry for IGFBP-2 was positive in 88.8% of the cases of GB and in only one low-grade glioma, whilst CDC20 immunostained 74.1% of the cases of GB and none low-grade glioma. This was confirmed in an additional series of cases studied with immunohistochemistry only. In conclusion, over-expression of mRNA levels of IGFBP-2 and CDC20 is highly related to GB, IGFBP-2 and CDC-20 gene and protein expressions are strongly correlated, and IGFBP-2 and CDC20 immunopositivity can be useful for the identification of GB in small biopsies.

Keywords Glioblastoma · High-grade glioma · Gene expression · IGFBP-2 · CDC20

This work was supported by the MIUR /FISR project 1509 (202).

G. Marucci · L. Morandi · E. Magrini · A. Farnedi · A. Pession · M. P. Foschini · V. Eusebi
Section of Pathology, Bellaria Hospital, University of Bologna, Bologna, Italy

E. Franceschi
Department of Medical Oncology, Bellaria Hospital, Bologna, Italy

R. Miglio · D. Calò
Department of Statistics "Paolo Fortunati", University of Bologna, Bologna, Italy

V. Eusebi (✉)
Sezione di Anatomia Patologica "M. Malpighi", Ospedale Bellaria, Via Altura 3, 40139 Bologna, Italy
e-mail: vincenzo.eusebi@unibo.it

Introduction

Gliomas are the most common primary brain tumours. Amongst high-grade gliomas, glioblastoma (GB) shows the most aggressive clinical course with median overall survival of 10 to 12 months after diagnosis [1]. Despite advances in surgical techniques, post-operative supportive care, radiation and adjuvant systemic therapy, the life expectancy of patients with GB has remained essentially poor over the last several decades. On the other hand, glial tumours with oligodendroglial features, despite anaplastic characteristics, retain sensitivity to chemo and radiation therapy and show better overall survival. Thus, tumour classification [1] is the variable that most affects therapeutic decisions and prognostic estimation.

Unfortunately, inter-observer variability can occur, resulting in limited diagnostic reproducibility. Coons et al. found that complete diagnostic concordance amongst four neuropathologists reviewing gliomas peaked at 69% espe-

cially in grade III lesions [2]. To develop more objective approaches to glioma classification, recent investigations have focused on molecular genetic analyses [3]. The use of DNA microarrays is set to change the development and use of tumour biomarkers. The few brain tumour biomarkers that are currently available include chromosomal loss of 1p and 19q for oligodendrogliomas (OL) [4], neurotrophic thyrosine kinase receptor type 3, N-MYC, C-MYC and v-erb-b2 erythroblastic leukaemia viral oncogene homologue 2 for medulloblastoma [5]. Analysis of the association between any of these single biomarkers and response to therapy requires a large number of patients to achieve sufficient statistical power. A single biomarker usually has limited predictive power especially if many other genes or proteins are important to determine the outcome. DNA microarrays can be used to detect groups of genes that, in aggregate, contain more predictive informations than any individual biomarker. The fact that an eight-gene model can be used to predict survival in medulloblastoma [6], that a six-gene model can be used to predict the outcome in patients with diffuse large-B-cell lymphoma [7] and that 70 genes can predict axillary metastasis in breast carcinoma [8] indicates that chemotherapy-response predictors can be modelled using relatively small panels of genes that can be screened by reverse transcriptase polymerase chain reaction (RT-PCR) or immunohistochemistry. Therefore, a series of 39 gliomas, 11 low grade and 28 high grade, was studied at gene and protein (immunohistochemistry) levels to disclose possible genetic portraits of malignancy.

Materials and methods

We retrieved for this study 100 randomly selected cases of gliomas. All the cases had been received unfixed. A sample of neoplastic tissue had been fresh frozen over liquid nitrogen and stored at −80°C into the frozen tissue bank of the Section of Pathology of the University of Bologna at Bellaria Hospital (Bologna), between 1990 and 2002. The remaining (specular) tissues were formalin fixed and paraffin embedded and stained with haematoxylin eosin for routine histological diagnosis. Informed consent was obtained from the subjects.

Only samples with rRNA 28S/18S ratio >1.5, measured by Bioanalyzer 2100 (Agilent, see below for details) and no evidence of ribosomal degradation, were included. Some cases were excluded as the tissue samples were composed only by necrosis; other cases did not show neoplastic proliferation in the specimen stored; in other cases, tissue was not enough to obtain a frozen section necessary to check the presence of tumour. Therefore, only 39 glial neoplasms were suitable for the study, i.e. 28 GB and 11 low-grade glial tumours, namely four OL, five pilocytic astrocytomas (PA) and two fibrillary astrocytoma (FA), showed good quality RNA.

All the tumours were re-staged and graded according to 2007 WHO [1] criteria at time of gene expression analysis by two pathologists (GM and VE). Any disagreement was discussed at a double head microscope and a consensus was reached.

RNA extraction and labelling

Tissue samples were treated with RNA*later*™ (Qiagen, Hilden, Germany) and homogenised. Total RNA was extracted (RNAeasy Protect mini kit, Qiagen, Hilden, Germany) and analysed by Bioanalyzer 2100 using RNA 6000 Nano kit (Agilent Technologies, Palo Alto, CA, USA).

Agilent Human 1A oligomicroarrays (Agilent Technologies, Palo Alto, CA, USA) were used in this study containing 60-mer DNA probes synthesised in situ in a 22-k format. Of 19,061 spots, 18,086 are non-controls and there are 17,086 unique transcript sequences, matching to 15,989 unique human genes (TIGR Resourcerer 10.0 July 2004 Release; http://www.tigr.org/tigr-scripts/magic/r1.pl).

The labelling of complementary RNA (cRNA), hybridisation to 22K-gene arrays and assessment of expression ratios were all performed as previously described [8]. The cRNA was generated by in vitro transcription with the use of T7 RNA polymerase (low RNA input fluorescent linear amplification kit Agilent cod. 5184–3523) and labelled with Cy3-CTP (Perkin Elmer, Waltham, MA, USA) for the reference RNA or Cy5-CTP (Perkin Elmer, Waltham, MA, USA) for the test RNA. RNA reference pool consisted of a total RNA mixture of four oligodendrogliomas, five pilocytic astrocytomas and two fibrillary astrocytomas enrolled in this study.

Labelled test (0.75 μg) and reference cRNA were fragmented and hybridised at 60°C for 17 h. After hybridisation, the slides were washed and scanned with a confocal laser scanner (Agilent Catalogue, Number G2565BA). Fluorescent intensities on scanned images were quantified by the feature extraction software 7.5, and LogRatio data were available for further statistical analysis.

Microarray data analysis

The scan data were analysed with Agilent Feature Extraction Software, which performs spots localisation (find spot algorithm), outlier pixels rejection based on the interquartile range method (cookie cutter algorithm) and flagging of saturated features (a feature is considered saturated when more than 50% of its pixels had an intensity of above 65,502). Thirty-nine specimens (28 GB and 11 low-grade gliomas) passed routine quality control analysis.

Loess normalisation and between-array scale normalisation [9] were performed using the "LIMMA" package [10] of Bioconductor (www.bioconductor.org). Hierarchical clustering was performed using Ward's method of linkage and Euclidean distance as a metric.

The nearest shrunken centroid classification method was used to identify genes useful to classify and best characterise high- and low-grade gliomas [11]. This method consists in "shrinking" each of the class centroids toward the overall centroid by a given amount, with the aim of reducing the effect of noisy genes. This shrinkage does automatic gene selection. Tenfold balanced cross validation was used to choose the optimal amount of shrinkage and the corresponding optimal subset of genes. The analysis was performed using the PAMR package of Bioconductor. A list of differentially expressed genes was performed through LIMMA package [12], using a t statistic with pooled variance; adjustment for multiple comparisons was made using false discovery rate (0.001).

Overall survival time was defined as the time elapsed between surgery and death from the disease. Gene expression levels were categorised in order to obtain two groups: low and high expression level, the value 0 was chosen as cut-point. Univariate survival analysis was performed for each gene, selected from the shrunken centroid method using the log-rank test, and survival curves were estimated using the Kaplan–Meier method. Cox multivariate regression model was estimated considering all genes and age at diagnosis as covariates. Variables were selected using a backward stepwise selection procedure forcing age at diagnosis to be present in the model. Statistical analyses were performed using STATA (V.9).

Validation by real time RT-PCR

Real time RT-PCR was used to confirm the gene expression microarray results for five selected genes (insulin-like growth factor binding protein 2 (IGFBP-2), cell division cycle 20 homologue (CDC20), lymphocyte antigen 6 complex, locus H (LY6H), NADH dehydrogenase (ubiquinone) Fe-S protein 2 (NDUFS2) and transmembrane 4 super-family 2 (TM4SF2)) in all the cases. Amongst the genes selected by the nearest shrunken centroid method, only these five genes were studied as these were the most discriminating genes between high- and low-grade tumours in view of the paucity of residual RNA material (see the "Results" section).

In brief, an aliquot of 1 μg of the same RNA used for microarray analysis was reverse-transcribed using SuperScript™ First-Strand Synthesis System for RT-PCR (Invitrogen), according to the manufacturer's instructions. PCR was carried out in a 25-μl reaction volume containing 10 pmol of each primers, 1 U of FastStart Taq DNA Polymerase™ (Roche), 1× GC rich solution (Roche), 4 mM $MgCl_2$, 1× Rox (Invitrogen) and 1× GelStar in DMSO (Lonza). Real-time RT-PCR was carried out by the Applied Bio systems SDS-7000 thermal cycle (Applied Bio systems, CA, USA). Cycling parameters consisted of an initial dye normalisation at 50°C for 2 min, a denaturation step at 95°C for 4 min, followed by 40 cycles of denaturation at 95°C for 30 s, primer annealing at 58°C, extension at 72°C for 30 s with data acquisition, followed by melt curve analysis. Primer sequences are listed in Table 1 and were retrieved from the RTPrimerDB database (http://medgen.ugent.be/rtprimerdb/) [13]. Four housekeeping genes were chosen for data normalisation (ACTB, B2M, TBP and HPRT1).

Relative quantification were performed using qBase (http://medgen.ugent.be/qbase/; Vandesompele et al.) [14]. A Wilcoxon two group test has been used to compare the two pools of ΔCt values, using Bonferroni correction for multiple comparisons.

Immunohistochemistry

The immunohistochemical study was performed in 37 cases (27 GB and 10 low-grade tumours) of the series submitted to microarray analysis, as in two cases there was no residual

Table 1 Primer sequences used for RT-qPCR

Gene name	Forward primer	Reverse primer
ACTB	TTGCCGACAGGATGCAGAAGGA	AGGTGGACAGCGAGGCCAGGAT
B2M	ATGAGTATGCCTGCCGTGTGA	GGCATCTTCAAACCTCCATG
TBP	TGCACAGGAGCCAAGAGTGAA	CACATCACAGCTCCCCACCA
HPRT	TGACACTGGCAAAACAATGCCA	GGTCCTTTTCACCAGCAAGCT
IGFBP2	GCCCTCTGGAGCACCTCTACT	CATCTTGCACTGTTTGAGGTTGTAC
CDC20	AGACCTGCCGTTACATTCCTTC	GCCAGTACATTCCCAGAACTCC
LY6H	GTGTGTGCCAGTGTCCGAATC	AGTCACAGGAGGAGGCACACAT
NDUFS2	CAGGCCTATTCTCTAGCTGTGGA	GCCATGATGTGGTTCAACAAAC
TM4SF2	CTGCTGCATGAACGAAACTGAT	CAGCGATGATTCCCATGTTAGT

material available. Furthermore, additional ten cases of grade II gliomas (five FA and five OL) and ten cases of grade III gliomas (six anaplastic astrocytomas, three anaplastic oligodendrogliomas and one anaplastic oligoastrocytomas) were randomly selected in order to enhance the immunohistochemical study.

Cases were immunostained with anti-GFAP (Dako, clone 6F2, dilution 1:1,200), anti-Ki 67 (Novocastra, clone Mib1, dilution 1:200), anti-IGFBP-2 (Cell Signalling Technology, polyclonal antibody, dilution 1:25) and anti-CDC20 antisera (Santa Cruz Biotechnology, clone p55 CDC (E-7), dilution 1:50). Standard avidin–biotin immunoperoxidase procedures were performed on paraffin-embedded sections. For IGFBP-2, semi-quantitative scores were recorded for cytoplasmatic staining, using normal brain as positive control. For CDC20, semi-quantitative scores were recorded for nuclear staining, using endothelial cells as positive control. The absence of primary antibody was used as negative control.

Counting was performed on ten areas in each case (×400 magnification). Negative is <5% of positive cells; + is 5% to 10% of positive cells; ++ is >11 of positive cells. For statistical purposes, tissue samples were considered positive with score + and ++. For Ki 67, a percentage value was attributed to each case evaluating ten fields (×400 magnification).

Statistical analysis of immunohistochemical results

The associations between tumour grade and the immunoistochemical expression of IGFBP-2 and CDC 20 were evaluated using the Fisher exact test. A one-way ANOVA was conducted to compare the mean IGFBP2 and CDC20 gene expression levels amongst the corresponding immunohistochemical groups. Levene's test was used to examine the homogeneity of variance assumption. The association of IGFBP-2 and CDC20 with overall survival was also evaluated in the cases studied for genetic expression. The survival curves were estimated using the standard Kaplan-Meier method and compared with log-rank test.

Results

Gene expression data were obtained from 39 samples (28 GB and 11 low-grade gliomas) and are available on the GEO web site (http://www.ncbi.nlm.nih.gov/geo/) with the accession number GSE9885. Clinical and pathological variables are reported in Table 2.

Hierarchical clustering, based on gene expression data and performed using Ward's method of linkage and Euclidean distance as a metric (Fig. 1), separated two groups showing good concordance with histology: 100% for OL (four of four clustered in group 1), 100% for PA (five of five PA clustered in group 1) and 50% for FA (one of two in group 1). GB clustered mainly in group 2 (25 of 28, 89.3%) together with one FA.

Median overall survival time for group 1 was not reached after a median follow-up of 4 years. Median overall survival time for group 2 was 10 months.

Three GB clustered with group 1 that included most of the low-grade glioma cases. However, survival in these three patients was 2, 11 and 13 months, respectively, consistent with GB.

The nearest shrunken centroid method identified nine genes (IGFBP-2, CDC20, LY6H, NDUFS2, TM4SF2, SNURF, GABARAPL1, AZGP1, BC016828) as the most important genes for distinguishing between low- and high-grade gliomas. Amongst them, seven genes were over-expressed in low-grade gliomas but under-expressed in GB; on the contrary, two genes (IGFBP-2 and CDC20) were over-expressed in GB but under-expressed in low-grade tumours (Fig. 2). All nine genes are included amongst the 50 significantly expressed top-ranked genes (Table 3).

The rate of misclassification on the basis of tenfold balanced cross validation was 0% for low-grade gliomas, 10.7% (three of 28) for GB and 7.7% (three of 39) for all cases. Adequate mRNA quantities of five out of the nine genes, identified with nearest shrunken centroid method, were tested by RT-PCR for validation (see Supplementary informations for details). Four reference genes were used for normalisation as indicated by Vandesompele et al. [14].

We found significant expression differences between the two groups in three out of the five genes: IGFBP2 ($p<0.0005$), CDC20 ($p<0.0005$) and TM4SF2 ($p<0.025$) evaluated with the Wilcoxon test. Immunohistochemical findings of the cases submitted to microarray analysis are reported in Table 2.

IGFBP-2 immunohistochemical staining (including the additional series of cases studied with immunohistochemistry only) was negative in 19 cases of low-grade gliomas (Fig. 3a). It was focally positive in one case (5% of cells) only, namely a pilocytic astrocytoma (one of 10, 10%; 95% confidence interval (CI) 0.3–44.5%) and in one anaplastic astrocytoma out of ten grade III gliomas (about 20% of positive cells). On the contrary, it was positive in 24 out of 27 GB (88.8%; 95% CI 69.7–95.1%; Fisher's exact test, $p=0.00002$).

Immunopositivity evidenced cytoplasmatic localisation and in GB was significantly brisk in areas of pseudopalisading necrosis and it was not related to microvascular proliferation (Fig. 4a,b). For this antibody, the log-rank test was statistically significant for the immunohistochemistry score ($p<0.0001$; Fig. 5).

CDC20 immunopositivity was nuclear and cytoplasmic. Staining was negative in all the 20 cases of low-grade

Table 2 Clinical, pathological and immunohistochemical data

Case n.	Age	Sex	Site	OS (months)	Ki67	Mitoses X 10 HPF	IGFBP2 ICH	CDC20
GB1	68	F	Fr	0.5 OD	10%	2	+	−
GB2	78	F	Fr	5.2	8%	2	+	+
GB3	69	M	Te	4.9	5%	1	+	−
GB4	41	M	Pa	1.5	10%	1	+	−
GB5	43	M	Fr	7.7	18%	3	++	+
GB6	71	F	Pa	14.2	NA	NA	NA	NA
GB7	54	F	Fr	14.5	15%	2	+	+
GB8	31	M	Suprat	32.9	15%	4	++	−
GB9	31	M	Te	18.6	25%	3	++	+
GB10	67	F	Te	1.6	30%	12	++	+
GB12	73	M	Suprat	1.9	10%	2	+	+
GB15	59	F	Te	9.1	30%	5	+	+
GB16	36	F	Te	18.8	15%	3	++	+
GB17	67	F	Fr	5.8	8%	1	+	+
GB18	53	F	Fr	26.3	20%	4	++	++
GB19	60	M	Fr–Te	11.5	30%	7	+	++
GB20	58	M	Fr	13.2	20%	4	+	−
PA21	7	M	Cereb	Alive after 122	2%	0	−	−
PA22	10	F	Cereb	Alive after 184	4%	1	−	−
PA23	39	F	Suprat	Alive after 105	0%	0	−	−
FA24	29	M	Fr	Alive after 175	NA	NA	NA	NA
GB25	63	M	Suprat	18.9	15%	2	++	+
GB26	39	F	Fr	10.1	20%	4	+	++
GB27	54	M	Fr	NA	5%	1	+	+
PA28	26	M	Te	Alive after 180	3%	1	+	−
OL29	32	M	Fr	105	1%	0	−	−
OL30	60	F	Suprat	Alive after 92	3%	0	−	−
OL31	56	M	Fr	Alive after 85	6%	0	−	−
OL32	41	F	Fr	132	5%	0	−	−
PA33	3	F	Cereb	Alive after 195	2%	1	−	−
FA34	34	F	Pa	134	2%	0	−	−
GB35	50	M	Fr	14.2	8%	1	+	++
GB36	69	M	Te	1.0	10%	4	−	+
GB37	67	F	Suprat	19.8	20%	2	+	++
GB38	67	M	Occ	0.4 OD	7%	1	+	−
GB42	57	M	Te	10.2	6%	1	+	−
GB44	54	F	Suprat	11.4	20%	2	+	+
GB46	71	F	Suprat	Alive after 42	6%	1	−	+
GB47	73	M	Occ	36.0	15%	4	−	+

GB glioblastoma, *PA* pilocytic astrocytoma, *FA* fibrillary astrocytoma, *OL* oligodendroglioma, *NA* not available, *OD* dead from other disease, *Fr* frontal lobe, *Te* temporal lobe, *Pa* parietal lobe, *Occ* occipital lobe, *Suprat* supratentorial (not specified), *Cereb* cerebellum, *OS* overall survival, *ICH* immunohistochemistry, − <5% of positive cells, + 5% to 10% of positive cells, ++ >11 of positive cells

gliomas (Fig. 3b) with only occasional stained nuclei in a fibrillary astrocytoma (FA34, lower than 5% of cells). On the contrary, it was found positive in three anaplastic astrocytomas out of ten grade III gliomas and in 20 out of 27 GB (74.1%; 95% CI 57.5–90.6%; Fisher's exact test, $p<0.001$ (Fig. 6a,b). For CDC20, the log-rank test was statistically significant for the immunohistochemistry score ($p<0.0122$).

We found significant expression differences of IGFBP2 and CDC20 genes expression levels amongst the corresponding immunohistochemical groups ($p<0.001$ for both). As evidenced in Tables 4 and 5, immunopositivity for IGFBP2 and CDC20 in GB are strongly associated but not statistically significant with Ki67 label index.

Considering the expression level of microarray data, the log-rank test was statistically significant for all the nine selected genes ($p<0.05$). When these same genes were chosen in a backward stepwise procedure to be inserted as covariates in a Cox regression model, IGFBP-2 was the only independent predictor of overall survival that remains in the multivariate model that includes age at diagnosis.

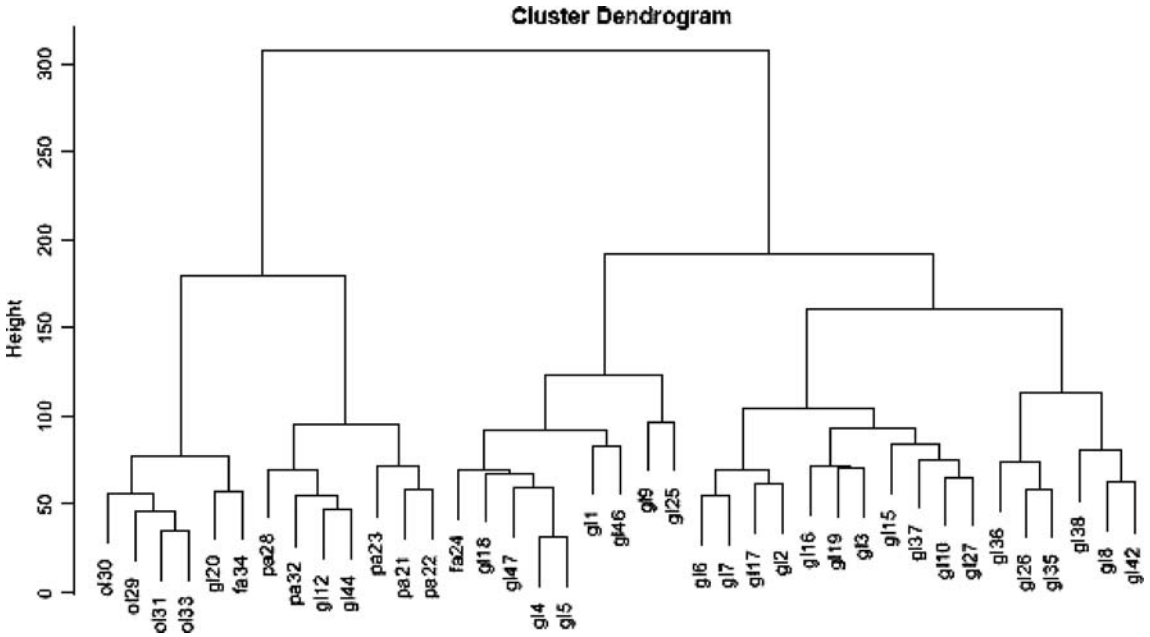

Fig. 1 Cluster dendrogram using Ward's minimum variance method and Euclidean distance. *GL* glioblastoma, *PA* pilocytic astrocytoma, *FA* fibrillary astrocytoma, *OL* oligodendroglioma

Discussion

The present gene expression profiling of human gliomas has identified an event highly related (more than 95%) to GB which consists in over-expression of insulin-like growth factor binding protein 2 and CDC20. These data were also validated by RT-quantitative real time polymerase chain reaction (qPCR) and by immunohistochemistry.

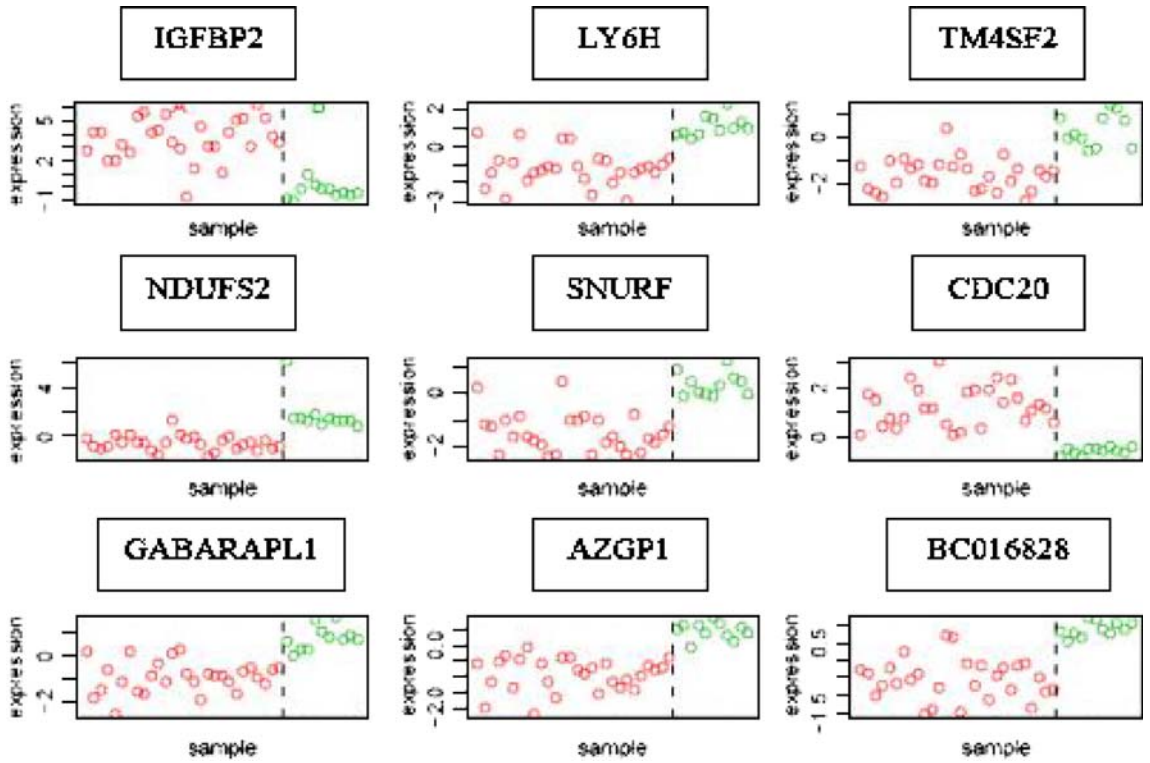

Fig. 2 Gene expression is plotted for the nine genes selected by the nearest shrunken centroid classifier. Plot is stratified by class. The genes are plotted from the strongest to the weakest

Table 3 Top-ranked 50 genes from the linear model fitted by LIMMA

	Probe name	Gene name	logFC	AveExpr	*t*	*p*.value	adj.*p*.value	*B*
1	A_23_P100653	ZBTB4	−1.031	11.444	−9.328	1.53406E-11	2.86251E-06	16.080
2	A_23_P169587	THC1942991	−1.113	7.533	−8.747	8.67318E-11	6.7725E-06	14.448
3	A_23_P71270	AZGP1	−1.388	8.699	−8.590	1.39631E-10	6.7725E-06	13.998
4	A_23_P117599	AHSA1	−1.312	8.259	−8.547	1.59044E-10	6.7725E-06	13.875
5	A_23_P67708	M65214	1.254	9.420	8.504	1.81473E-10	6.7725E-06	13.750
6	A_23_P216325	BC016828	−1.421	8.122	−8.296	3.42001E-10	7.90833E-06	13.150
7	A_23_P207125	NLGN2	−0.746	9.490	−8.295	3.43279E-10	7.90833E-06	13.147
8	A_23_P119943	IGFBP2	3.839	11.245	8.262	3.79834E-10	7.90833E-06	13.051
9	A_23_P60640	NM_017921	−1.030	8.070	−8.255	3.88939E-10	7.90833E-06	13.028
10	A_23_P155695	GAK	−1.002	7.464	−8.227	4.23818E-10	7.90833E-06	12.947
11	A_23_P145297	NFKBIL1	−1.070	7.883	−8.151	5.34856E-10	8.20308E-06	12.726
12	A_23_P114144	NM_014008	−0.788	7.688	−8.145	5.44401E-10	8.20308E-06	12.710
13	A_23_P131899	SDCBP2	−0.950	8.064	−8.130	5.71498E-10	8.20308E-06	12.664
14	A_23_P120182	NDUFA10	−1.055	8.798	−7.945	1.01223E-09	1.2802E-05	12.121
15	A_23_P77066	SNURF	−1.802	7.976	−7.940	1.02912E-09	1.2802E-05	12.106
16	A_23_P114185	TM4SF2	−1.931	8.810	−7.912	1.12048E-09	1.30674E-05	12.025
17	A_23_P156568	KLHDC3	−0.828	8.059	−7.800	1.5892E-09	1.73017E-05	11.693
18	A_23_P3574	NM_030819	−0.893	8.613	−7.785	1.669E-09	1.73017E-05	11.646
19	A_23_P162640	GABARAPL1	−1.708	9.221	−7.761	1.79763E-09	1.74373E-05	11.576
20	A_23_P1307	AKR1C1	−1.404	7.134	−7.748	1.86897E-09	1.74373E-05	11.539
21	A_23_P38497	SLC25A11	−0.739	7.773	−7.721	2.03425E-09	1.80755E-05	11.458
22	A_23_P149195	CDC20	1.803	8.811	7.695	2.20592E-09	1.83837E-05	11.381
23	A_23_P166609	DHX30	−1.086	8.637	−7.676	2.34274E-09	1.83837E-05	11.324
24	A_23_P72807	SHC3	−1.283	7.539	−7.673	2.3645E-09	1.83837E-05	11.315
25	A_23_P39024	NM_032332	−0.677	8.487	−7.602	2.95628E-09	2.13067E-05	11.103
26	A_23_P134914	LY6H	−2.266	8.190	−7.599	2.9859E-09	2.13067E-05	11.093
27	A_23_P79251	EHD3	−1.050	7.326	−7.589	3.08301E-09	2.13067E-05	11.063
28	A_23_P112397	FBXW5	−1.379	8.549	−7.553	3.44924E-09	2.29864E-05	10.956
29	A_23_P76983	C14orf45	0.537	7.522	7.521	3.81187E-09	2.4527E-05	10.861
30	A_23_P210400	KCNQ2	−1.121	8.191	−7.447	4.81339E-09	2.99389E-05	10.639
31	A_23_P98037	NM_020123	−1.095	10.712	−7.434	5.0127E-09	3.01728E-05	10.600
32	A_23_P36647	NM_177441	−0.542	8.388	−7.371	6.12498E-09	3.57158E-05	10.410
33	A_23_P106778	SULT1A2	−0.798	8.062	−7.333	6.90225E-09	3.90285E-05	10.296
34	A_23_P149470	NDUFS2	−2.350	8.418	−7.318	7.23347E-09	3.93263E-05	10.251
35	A_23_P102517	PDE6D	−0.989	8.365	−7.309	7.45277E-09	3.93263E-05	10.223
36	A_23_P256282	BX537520	−0.413	7.375	−7.303	7.58718E-09	3.93263E-05	10.206
37	A_23_P26640	BC033681	−1.269	7.077	−7.291	7.87552E-09	3.97176E-05	10.170
38	A_23_P211247	HRMT1L1	−0.965	8.239	−7.272	8.35588E-09	4.10312E-05	10.114
39	A_23_P158265	AF410455	0.687	10.525	7.257	8.7733E-09	4.19763E-05	10.067
40	A_23_P53211	PLEKHB1	−1.090	7.073	−7.213	1.00731E-08	4.60692E-05	9.936
41	A_23_P259166	NM_024863	−0.872	12.476	−7.212	1.01225E-08	4.60692E-05	9.931
42	A_23_P28233	AF037332	−0.968	7.269	−7.195	1.06802E-08	4.745E-05	9.880
43	A_23_P157545	NKX3–1	0.356	8.371	7.173	1.14421E-08	4.96526E-05	9.814
44	A_23_P144563	GRIA2	−1.047	7.889	−7.137	1.28315E-08	5.44164E-05	9.705
45	A_23_P70045	H2AFY	0.689	11.036	7.117	1.36699E-08	5.66838E-05	9.645
46	A_23_P133232	HARS	−0.773	7.806	−7.090	1.49151E-08	6.05026E-05	9.562
47	A_23_P218412	SPAG7	−1.324	7.836	−7.061	1.63459E-08	6.48958E-05	9.475
48	A_23_P140876	ABCA3	−1.365	9.112	−7.041	1.74216E-08	6.77255E-05	9.414
49	A_23_P91902	SMC4L1	0.752	9.701	7.017	1.8814E-08	7.16457E-05	9.340
50	A_23_P143569	DGCR6L	−1.156	8.578	−7.006	1.95008E-08	7.27758E-05	9.306

logFC log2-fold-change, *AveExpr* average log2-expression across all the arrays and channels, *t* moderated *t* statistic, *p.value* raw *p* value, *adj.p.value p* value adjusted for multiple testing according to Benjamini and Hocberg's method, *B* log odds that the gene is differentially expressed

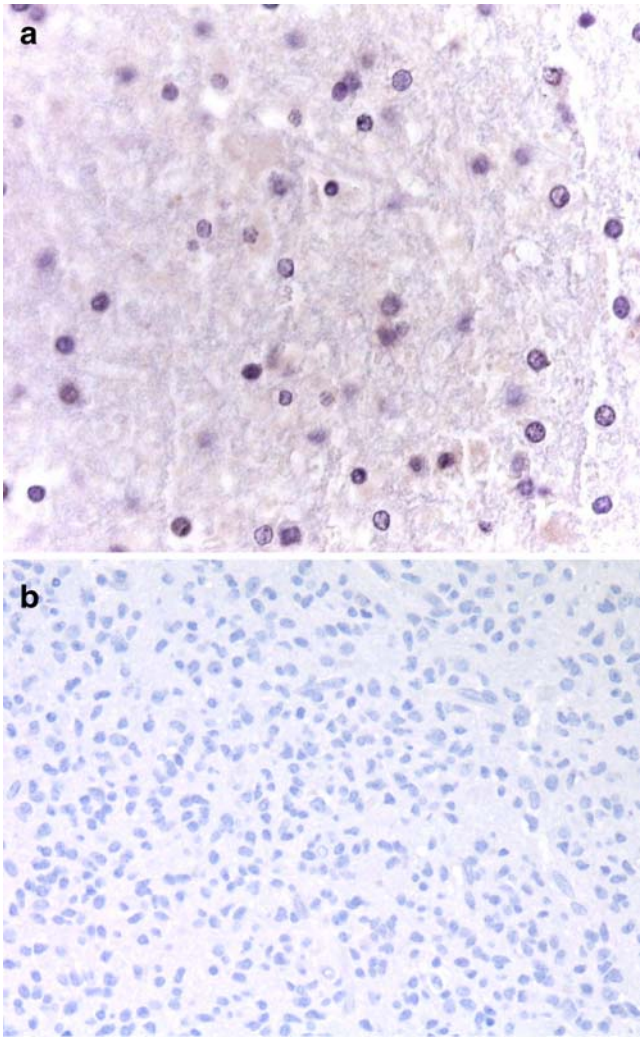

Fig. 3 **a** Oligodendroglioma case 30: no cells are positive for IGFBP-2. **b** Oligodendroglioma case 32: no cells are positive for CDC-20

IGFBP-2, a member of a large protein family, is normally expressed in foetal cells and is low or absent in many adult tissues. It acts not only as carrier of IGFs, prolonging their half-life, but also functions as modulator of IGF availability and activity.

IGFBP-2 is over-expressed in ovarian [15], colorectal [16], prostate [17, 18], hepatocellular carcinomas [19] and in neuroblastoma [20]. It has also been demonstrated that IGFBP-2 over-expression might promote glioma development and progression [21] and enhance GB invasion [22]. A significant positive correlation between the expression of IGFBP-2 and metalloproteinase-2 [23] and the vascular–endothelial growth factor [23] has been observed in GB, indicating that the expression of IGFBP-2 is associated with pathways enhancing invasiveness and angiogenesis.

Similarly to IGFBP-2, CDC20 gene was found to be over-expressed in high-grade gliomas and downregulated in low-grade gliomas ($p<0.0005$; evaluated with the Wilcoxon test), a finding also validated by immunohistochemistry. This gene appears to act as a regulatory protein in the cell cycle. It is required for two microtubule-dependent processes, movements before the anaphase and chromosome separation. CDC20 is an activating regulatory factor for the anaphase promoting complex/cyclosome (APC/C) and for the ubiquitination activity of the APC/C. CDC20 confers a strict destruction-box dependence on APC [24]. Levels of CDC20, as well as its binding to APC, peak in mitosis and decrease drastically in early G1. Upregulation of CDC20 is associated with poor prognosis in ovarian cancer [25], and it is found to be over-expressed in gastric cancer [26], in oral squamous cell carcinoma [27] and in breast cancer [28]. Recently, it has been shown that CDC20 is frequently upregulated in many types of malignancies, including gliomas, and remarkably suppressed by the ectopic introduction of p53 [29]. Therefore, it seems that CDC20 is a good potential therapeutic target for a broad spectrum of human cancer [29].

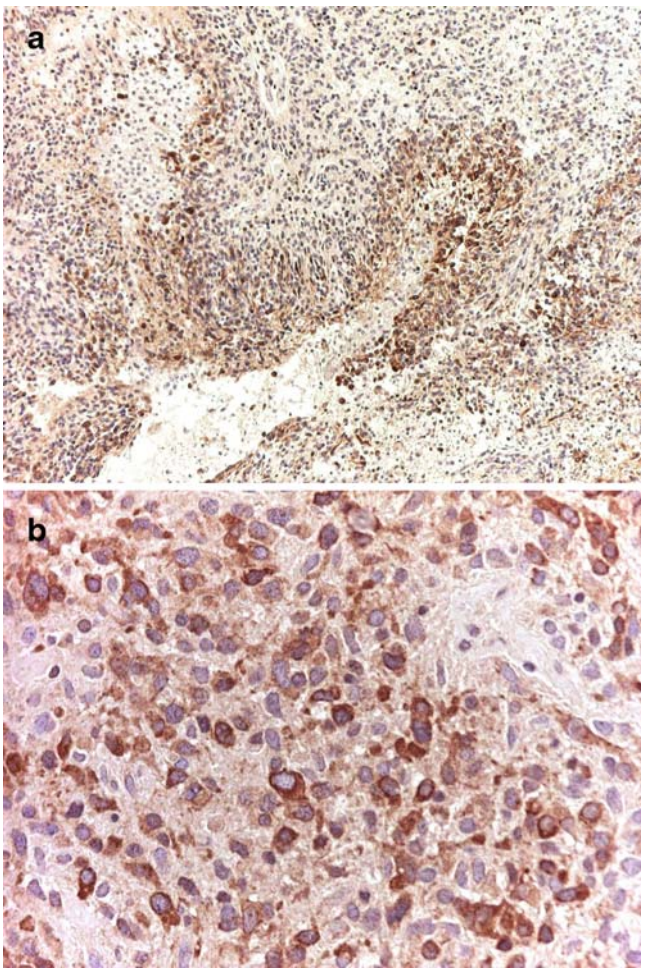

Fig. 4 **a**, **b** Glioblastoma case 5: immunopositivity for IGFBP-2 was mostly seen in the cytoplasm of neoplastic cells in GL, especially in those palisading around foci of necrosis

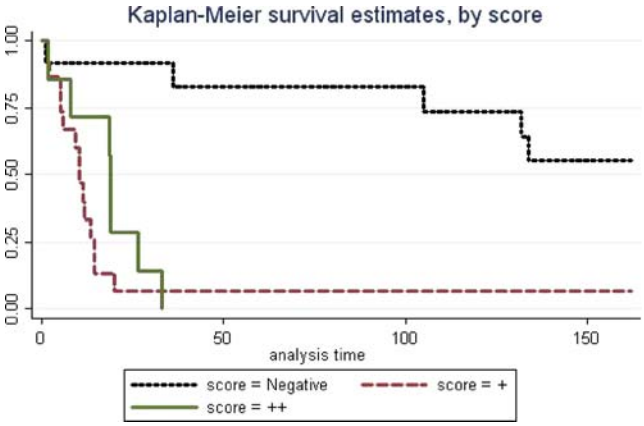

Fig. 5 IGFBP-2 immunohistochemistry related to overall survival

In the present series, when IGFBP-2 and CDC-20 proteins were investigated at immunohistochemical level, we found significant expression differences of IGFBP2 and CDC20 genes expression levels amongst the corresponding

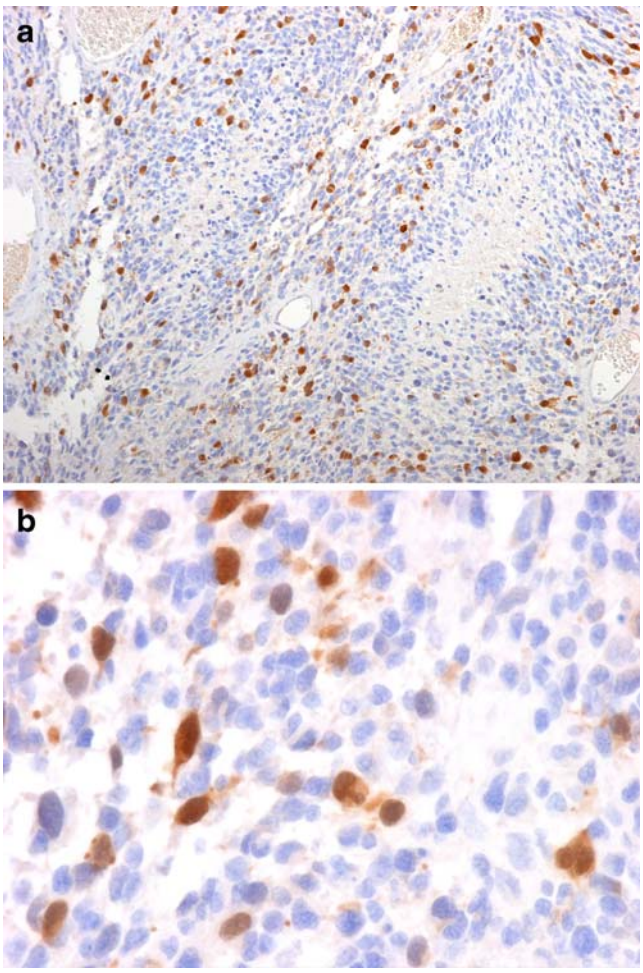

Fig. 6 Glioblastoma case 19: **a** nuclear immunopositivity for CDC20. Neoplastic cells are located around necrotic area. **b** Same case. Positive cells are observed also in areas in which necrosis is absent

Table 4 Immunohistochemical correlation between IGFBP-2 (0 to ++ score) and Ki67 label index

	All GB (27 cases)	GB ++ (7 cases)	GB + (17 cases)	GB 0 (3cases)
Ki67 average	14.9%	19.7%	13.7%	11%

immunohistochemical groups ($p<0.001$ for both). In fact, immunohistochemistry for IGFBP-2 stained 24 out of 27 cases of GB, whilst on the contrary, only one out of 20 cases of low-grade glioma was stained. In addition, CDC-20 was found positive in 20 out of 27 GB, in three out of ten grade III gliomas whilst it was negative in all the 20 cases of low-grade glioma.

Furthermore, as also previously found in gastric carcinoma [30], immunopositivity for IGFBP2 and CDC20 in GB are significantly associated with Ki67 label index (Tables 4 and 5). Elmlinger et al. [31] demonstrated that IGFBP-2 positive macrophage/microglial and glioma cells clustered in the immediate vicinity of areas of necrosis of human gliomas as well as of rat C6 glioblastoma and that IGFBP-2 over-expression in glioma cells correlated positively with the tumour grade of the gliomas.

These data are in keeping with the present findings, as immunopositivity for IGFBP-2 was mostly seen in the cytoplasm of neoplastic cells in GB, especially in those palisading around foci of necrosis. The low percentage of immunopositivity of IGFBP-2 and CDC-20 observed in anaplastic gliomas may be a useful diagnostic criteria to reduce inter-observer variability, especially in small biopsies when the tissue is scanty, where necrotic areas and vascular proliferation are lacking.

TM4SF2 had opposite expression than IGFBP-2and CDC20: it was over-expressed in low-grade gliomas and downregulated in high-grade gliomas. Yokota et al. [32] found same result analysing 11 GB which all under-expressed TM4SF2 gene. This gene is associated with X-linked mental retardation and neuropsychiatric diseases such as Huntington's chorea and fragile X syndrome [33]. The protein encoded by this TM4SF2 is a member of the transmembrane 4 superfamily, also known as tetraspanin. Most of these proteins are cell-surface proteins character-

Table 5 Immunohistochemical correlation between CDC-20 (0 to ++ score) and Ki67 label index

	All GB (27 cases)	GB ++ (5 cases)	GB + (15 cases)	GB 0 (7cases)
Ki67 average	14.9%	19.6%	15.3%	10.4%

ised by the presence of four hydrophobic domains. The proteins mediate signal transduction events that play a role in the regulation of cell development, activation, growth and motility and complex with integrins.

In conclusion, the present study indicates:

1. The over-expression of mRNA levels of IGFBP-2 and CDC20 is highly related to GB. These same genes in combination are not over-expressed in low-grade gliomas, a consistent difference indicating that the simultaneous over-expression of IGFBP-2 and CDC20 genes is a sign of malignancy in glial tumours
2. IGFBP-2 and CDC-20 gene and protein expressions are strongly correlated, a relation statistically significant and probably exclusive of high-grade glial tumours
3. IGFBP-2 was the most important predictor of overall survival in the multivariate Cox model based on microarray data
4. IGFBP-2 and CDC20 immunohistochemical localisation in neoplastic cells of glial tumours can be useful for the identification of GB in small biopsies when the tissue is scanty. Thus, IGFBP-2 and CDC-20 over-expression might be added to current histological diagnostic criteria such as necrotic areas and vascular proliferation

Acknowledgment We wish to thank Dr. M. Guizzardi for the encouragement to enter into the world of gene array. This work was presented as Presidential free paper at the 3rd Intercontinental Congress of Pathology, May 2008, Barcelona

Conflict of interest statement We declare that we have no conflict of interest.

References

1. Louis DN, Ohgaki H, Wiestler OD et al (2007) World Health Organization classification of tumours of the central nervous system. IARC, Lyon
2. Coons SW, Johnson PC, Scheithauer BW et al (1997) Improving diagnostic accuracy and interobserver concordance in the classification and grading of primary gliomas. Cancer 79:1381–1393
3. Nutt CL, Mani DR, Betensky RA et al (2003) Gene expression-based classification of malignant gliomas correlates better with survival than histological classification. Cancer Res 63:1602–1607
4. Reifenberger G, Louis DN (2003) Oligodendroglioma: toward molecular definitions in diagnostic neuro-oncology. J Neuropathol Exp Neurol 62:111–126
5. Gajjar A, Hernan R, Kocak M et al (2004) Clinical, histopathologic and molecular markers of prognosis: toward a new disease risk stratification system for medulloblastoma. J Clin Oncol 22:984–993
6. Pomeroy SL, Tamayo P, Gaasenbeek M et al (2002) Prediction of central nervous system embryonal tumour outcome based on gene expression. Nature 415:436–442
7. Lossos IS, Czerwinski DK, Alizadeh AA et al (2004) Prediction of survival in diffuse large-B-cell lymphoma based on the expression of six genes. N Engl J Med 350:1828–1837
8. van 't Veer LJ, Dai H, van de Vijver MJ et al (2002) Gene expression profiling predicts clinical outcome of breast cancer. Nature 415:530–536
9. Zahrak M, Parmigiani G, Wayne Y (2007) Pre-processing Agilent microarray data. BMC Bioinformatics 8:142
10. Smyth GK, Speed TP (2003) Normalization of cDNA microarry data. Methods 31:265–273
11. Tibshirani R, Hastie T, Narasimhan B et al (2002) Diagnosis of multiple cancer types by shrunken centroids of gene expression. Proc Natl Acad Sci U S A 99:6567–6572
12. Smyth GK (2004) Linear models and empirical Bayes methods for assessing differential expression in microarray experiments. Stat Appl Genet Mol Biol 3:1–10
13. Pattyn F, Speleman F, De Paepe A et al (2003) RTPrimerDB: the real-time PCR primer and probe database. Nucleic Acids Res 31:122–123
14. Vandesompele J, De Preter K, Pattyn F et al (2002) Accurate normalization of real-time quantitative RT-PCR data by geometric averaging of multiple internal control genes. Genome Biol 18:3–4
15. Flyvbjerg A, Mogensen O, Mogensen B et al (1997) Elevated serum insulin-like growth factor-binding protein 2 (IGFBP-2) and decreased IGFBP-3 in epithelial ovarian cancer: correlation with cancer antigen 125 and tumor-associated trypsin inhibitor. J Clin Endocrinol Metab 82:2308–2313
16. el Atiq F, Garrouste F, Remacle-Bonnet M et al (1994) Alterations in serum levels of insulin-like growth factors and insulin-like growth-factor-binding proteins in patients with colorectal cancer. Int J Cancer 57:491–497
17. Ho PJ, Baxter RC (1997) Insulin-like growth factor-binding protein-2 in patients with prostate carcinoma and benign prostatic hyperplasia. Clin Endocrinol 46:333–342
18. Richardsen E, Ukkonen T, Bjørnsen T et al (2003) Overexpression of IGBFB2 is a marker for malignant transformation in prostate epithelium. Virchows Arch 442:329–335
19. Ranke MB, Maier KP, Schweizer R et al (2003) Pilot study of elevated levels of insulin-like growth factor-binding protein-2 as indicators of hepatocellular carcinoma. Horm Res 60:174–180
20. Russo VC, Schütt BS, Andaloro E et al (2005) Insulin-like growth factor binding protein-2 binding to extracellular matrix plays a critical role in neuroblastoma cell proliferation, migration, and invasion. Endocrinology 146:4445–4455
21. Dunlap SM, Celestino J, Wang H et al (2007) Insulin-like growth factor binding protein 2 promotes glioma development and progression. Proc Natl Acad Sci U S A 104:11736–11741
22. Wang H, Wang H, Shen W et al (2003) Insulin-like growth factor binding protein 2 enhances glioblastoma invasion by activating invasion-enhancing genes. Cancer Res 63:4315–4321
23. Godard S, Getz G, Delorenzi M et al (2003) Classification of human astrocytic gliomas on the basis of gene expression: a correlated group of genes with angiogenic activity emerges as a strong predictor of subtypes. Cancer Res 63:6613–6625
24. Fang G, Yu H, Kirschner MW (1998) Direct binding of CDC20 protein family members activates the anaphase-promoting complex in mitosis and G1. Mol Cell 2:163–171
25. Ouellet V, Guyot MC, Le Page C et al (2006) Tissue array analysis of expression microarray candidates identifies markers associated with tumor grade and outcome in serous epithelial ovarian cancer. Int J Cancer 119:599–607

26. Kim JM, Sohn HY, Yoon SY et al (2005) Identification of gastric cancer-related genes using a cDNA microarray containing novel expressed sequence tags expressed in gastric cancer cells. Clin Cancer Res 11:473–482
27. Mondal G, Sengupta S, Panda CK et al (2007) Overexpression of CDC20 leads to impairment of the spindle assembly checkpoint and aneuploidization in oral cancer. Carcinogenesis 28:81–92
28. Yuan B, Xu Y, Woo JH et al (2006) Increased expression of mitotic checkpoint genes in breast cancer cells with chromosomal instability. Clin Cancer Res 12:405–410
29. Kidokoro T, Tanikawa C, Furukawa Y et al (2008) CDC20, a potential cancer therapeutic target, is negatively regulated by p53. Oncogene 27:1562–71
30. Zhang L, Huang W, Chen J et al (2007) Expression of IGFBP2 in gastric carcinoma and relationship with clinicopathologic parameters and cell proliferation. Dig Dis Sci. 52:248–253
31. Elmlinger MW, Deininger MH, Schuett BS et al (2001) In vivo expression of insulin-like growth factor-binding protein-2 in human gliomas increases with the tumor grade. Endocrinology 142:1652–1658
32. Yokota T, Kouno J, Adachi K et al (2006) Identification of histological markers for malignant glioma by genome-wide expression analysis: dynein, alpha-PIX and sorcin. Acta Neuropathol 111:29–38
33. Boda B, Mas C, Muller D (2002) Activity-dependent regulation of genes implicated in X-linked non-specific mental retardation. Neuroscience 114:13–17

Virchows Arch (2008) 453:611–616
DOI 10.1007/s00428-008-0683-9

ORIGINAL ARTICLE

Lymphocyte-depleted classic Hodgkin lymphoma—a neglected entity?

Daniel Benharroch · Amalia Levy · Jacob Gopas · Martin Sacks

Received: 28 July 2008 / Revised: 25 September 2008 / Accepted: 1 October 2008 / Published online: 29 October 2008

Abstract Changes in the definition of lymphocyte-depleted classic Hodgkin lymphoma (LDcHL) have recently led to reclassification of many cases as other pleomorphic lymphomas. We have set out to identify LD cases in our cohort of cHL patients and determine their clinical and biological characteristics properties. We defined the morphologic picture of LDcHL according to selected criteria and determined how its features differ from those of other subtypes of cHL. Twelve of 201 cHL patients (5.9%) were diagnosed as showing LDcHL histology, a higher percentage of LDcHL than in most recent series. The LD cases were most often positive for Epstein–Barr virus and for sialyl-CD15. Defining the cases as either reticular (eight) or as diffuse fibrosis (three) variants was critical to the diagnostic approach. We conclude that LDcHL may be a neglected entity.

Keywords Hodgkin lymphoma · Lymphocyte-depleted · Reticular · Diffuse fibrosis

D. Benharroch · M. Sacks
Department of Pathology, Soroka University Medical Center,
Beer-Sheva, Israel

A. Levy
Department of Epidemiology, Faculty of Health Sciences,
Ben-Gurion University of the Negev,
Beer-Sheva, Israel

J. Gopas
Department of Oncology, Soroka University Medical Center,
Beer-Sheva, Israel

J. Gopas
Department of Microbiology-Immunology,
Faculty of Health Sciences, Ben-Gurion University of the Negev,
Beer-Sheva, Israel

D. Benharroch (✉)
Hematopathology Unit, Department of Pathology,
Soroka University Medical Center,
P.O.Box 151, Beer-Sheva 84101, Israel
e-mail: benaroch@bgu.ac.il

Introduction

In the last three decades, the diagnostic criteria of lymphocyte-depleted classic Hodgkin lymphoma (LDcHL) have been modified to exclude cases of anaplastic large-cell lymphoma (ALCL), of the lymphocyte-depleted variant of nodular sclerosis Hodgkin lymphoma, and of pleomorphic large-cell lymphomas, all of which may show confusing resemblance with this subtype of classic Hodgkin lymphoma (cHL) [1]. In the process of separating genuine cases of LDcHL from the mimicking entities, the diagnostic criteria have paradoxically lost their sharp edge and, more important, the clinical features of LDcHL are no longer well defined [2]. We have set out to evaluate the clinical, morphologic, and immunohistochemical features of LDcHL by selected criteria and to determine the degree to which these features differ from those of nodular sclerosis (NS) and mixed cellularity (MC) cHL.

We believe that the role of apoptosis in classic Hodgkin lymphoma should be further clarified. We therefore decided to study the patients' tissues for some apoptosis-associated factors.

In our cohort of cHL patients, we identified bona fide cases of LDcHL using the criteria defined in the WHO Classification of Tumours [2] but also criteria used recently by other authors [3, 4].

Materials and methods

We reviewed 205 untreated cases of cHL, eight of which had originally been diagnosed as LDcHL. Two hematopathologists (D.B. and M.S.) reviewed the slides. Four of the cases previously diagnosed as LDcHL were reclassified as anaplastic large-cell lymphoma (two cases), indeterminate HL (one case), and LD variant of NScHL (one case).

The morphologic criteria of LDcHL were determined according to the WHO Classification of Tumours of the Haematopoietic and Lymphoid Tissues [2] but modified in part according to the criteria outlined by Kurtin [3] and by Wright et al. [4]. According to these criteria, the reticular variant shows an overwhelming predominance of Hodgkin–Reed–Sternberg (HRS) cells, with few lymphocytes and other inflammatory cells. Interwoven with the cellular component, there is an interlacing pattern of fibrosis which often imparts a sarcomatoid appearance to the tumor. In the diffuse fibrosis variant, fewer HRS cells are surrounded by rare inflammatory cells but mainly by a weakly eosinophilic, periodic acid–Schiff (PAS)-positive background consistent with an immature, non-birefringent collagen. In both types, the HRS cells are pleomorphic, and lacunar cells and birefringent collagen are, by definition, absent. In contrast to the white-to-light green birefringence of the elongated and fragmented fibers found in NScHL, the birefringence in LDcHL is negative or very faint. In a few cases, numerous reactive lymphocytes are found, despite prominent HRS cells and fibrosis [3].

In view of the possible overlap between LDcHL and other lymphomas, the phenotype in LDcHL, more than in other subtypes of cHL, should conform strictly to that of classic HL: CD15+ ; CD30+ ; LCA−; CD20—usually negative, but scarce CD20+ cells may be found, and ALK1 and CD3 are negative [3, 5].

The patient files were reviewed for demographic data, prognostic factors, therapy, and outcome. We also studied LMP1/Epstein–Barr virus (EBV; Dako, Glostrup, Denmark). We used an immunohistochemical method and the ENVISION system of Dakopatts (Glostrup, Denmark). For the terminal uridine deoxynucleotidyl transferase dUTP nick end labeling assay, we used the ApopTag kit of Intergen (Oxford, UK) and calculated the apoptotic index as the percentage of apoptotic HRS cell among the total tumor cell count [6–7].

In addition to the apoptotic index, we studied the expression of the apoptotic-associated factors: caspase 3 (cleaved), Biocare Medical, Walnut Creek, CA, USA; caspase 8 (FLICE), DBS, Pleasanton, CA, USA.

Institutional guidelines regarding human experimental investigations were followed.

For contingency table analysis, the chi-square or Fisher's exact (FE) test was used as appropriate, and the Mann–Whitney U test was used for analysis of descriptive values. All statistical analyses were performed using SPSS version 14 for Windows, and p values of 0.05 or less were considered statistically significant.

Results

In the cohort of 201 of the original 205 cHL patients included, only four LDcHL cases were left. On the basis of the above-mentioned criteria, we identified another eight patients with LDcHL among the 201 cases in the cohort. These were originally diagnosed as MCcHL (five cases), NScHL (one case), diffuse lymphocyte predominant Hodgkin lymphoma (DLPHL) (one case) and indeterminate cHL (one case) (Table 1).

In 11 of the 12 cases, LDcHL was diagnosed in peripheral lymph nodes. In the 12th case, the patient first

Table 1 Histological and immunohistochemical features of LDcHL cases

Case number	Primary diagnosis	Final diagnosis	Variant	Birefringent	CD30	CD15	LCA	CD20
1	NS	LD	Reticular	Faint	+	+	−	−
2	LD	LD	Reticular	Faint	+	+	−	−
3	LD	LD	Reticular	None	+	+	−	−
4	LD	LD	Diffuse fibrosis	None	+	+	−	−
5	MC	LD	Reticular	None	+	+	−	+
6	LD	LD	Reticular	None	+	+	−	−
7	DLPHL	LD	Diffuse fibrosis	None	+	+	−	−
8	MC	LD	Reticular	None	+	−, CLex+[a]	−	−
9	MC	LD	Reticular	None	+	+	−	−
10	MC vs NS	LD	Reticular	None	+	+	−	−
11	MC	LD	Diffuse fibrosis	None	+	+	−	+
12	Indeterminate	LD	Early phase	Faint	+	+	−	+

[a] Clex1, an anti-sialyl-CD15 antibody

sought help at a very late stage of her disease, and the diagnosis was only established at autopsy, with prominent involvement of subdiaphragmatic lymph nodes, liver, and large intestine.

Eight of the 12 cases were diagnosed as reticular variant (Fig. 1) and three as the diffuse fibrosis variant of LDcHL (Fig. 2a,b). In one case, in addition to areas of typical reticular LDcHL, there were extensive, markedly cellular areas composed of numerous small round lymphocytes (Fig. 3a–c). The possibility of a cellular (early) phase of LDcHL has been considered in this case.

In the cases of diffuse fibrosis, the background was PAS-positive, probably indicating an immature type of collagen. Birefringence was faint or absent. All cases showed the classical HL immunophenotype. One case was CD15 (LeuM1)-negative but was positive for the sialyl-CD15, CLex1. In three of the cases, 10–20% of the HRS cells showed CD20 positivity of variable intensity.

The clinical findings in the LDcHL cases are shown in Table 2 and compared with those of NS- and MCcHL. There were relatively more men and more patients with B symptoms and with advanced stages of the tumor in the LDcHL group. However, the differences did not reach statistical significance. The mean age of the LDcHL patients was higher than those with NS- and MCcHL (p=0.119). Details of therapy were available in only six of the 12 LDcHL patients. Most patients were treated with Mustine, Vincristine, Procarbazine, and Prednisolone (MOPP), Doxorubicin, Bleomycin, Vinblastin, and Dacarbazine (ABVD) or both (five of six). Radiotherapy was administered to two of six LDcHL patients. The follow-up was significantly shorter in LDcHL patients (p=0.002; Table 3). Six of the 12 patients with LDcHL had died of HL. This rate differs from that of NS- and MCcHL but not to a significant degree (p=0.08, FE two-tailed). Lymphocyte-depleted cHL was found in two of 20 Bedouin patients (10%) as compared with three of 89 (3.4%) of Jewish town dwellers, the largest Jewish group—NS.

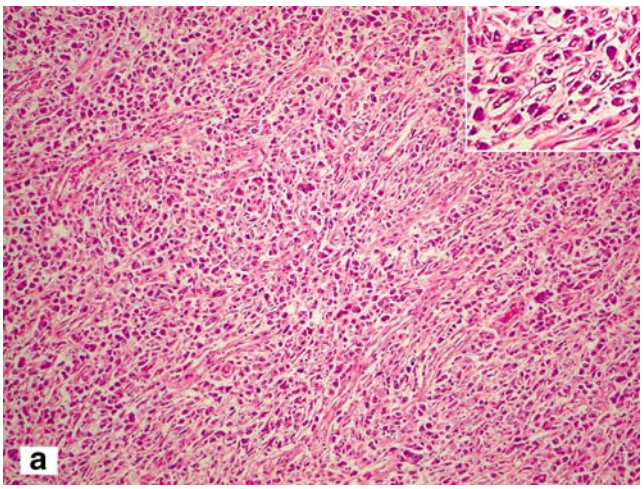

Fig. 1 Lymphocyte-depleted classic Hodgkin lymphoma, reticular variant. Numerous pleomorphic HRS cells are included within a fibrous network. *Inset* Large tumor cells are trapped in the fibrosis (H&E ×260)

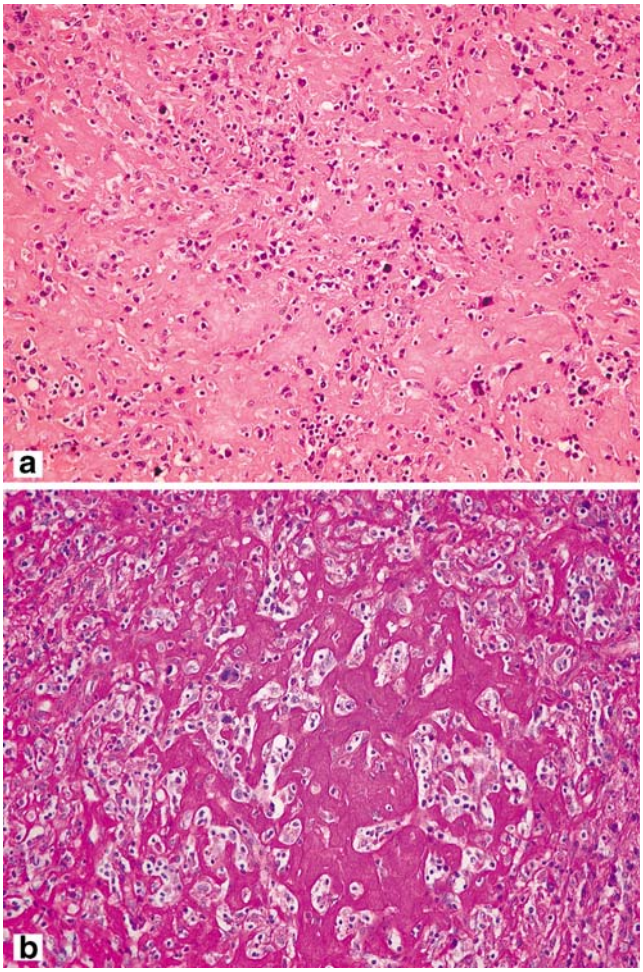

Fig. 2 LDcHL, diffuse fibrosis. **a** Relatively few HRS and inflammatory cells are embedded in predominantly fibrotic background fibrosis (H&E ×260). **b** Another case of diffuse fibrosis type of LDcHL showing a PAS-positive, immature fibrosis background (PAS ×320)

Laboratory data are shown in Table 4. The classical phenotype, including negative ALK1 immunostaining, was found in all the 12 patients; this also included negative ALK1 immunostaining. The sialyl-CD15 (CLex1) was expressed to a significantly higher degree in LDcHL, including the one case with negative LeuM1. CD30 was positive in the tumor cells of all cases of LDcHL, and CD20 was negative in almost all but three of the cases as indicated above. These immunohistochemical findings do not differ significantly from those of NScHL and MCcHL patients. Caspase 8 was expressed in seven of the 12 cases

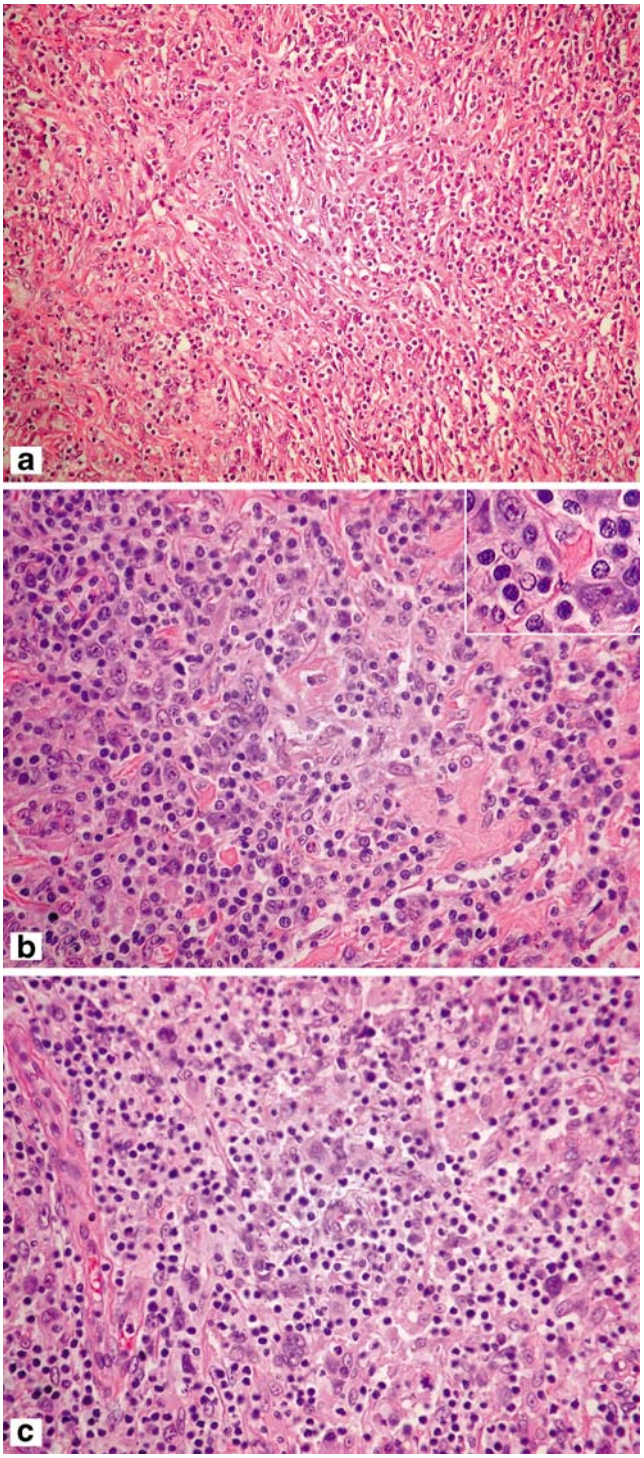

Fig. 3 This case raises the possible diagnosis of cellular or early phase of LDcHL. **a** An area of LDcHL, reticular. HRS cells and small lymphocytes are embedded in a fibrous network (H&E ×210). **b** Area with fibrosis and numerous atypical HRS cells. *Inset* Atypical HRS cells are included in the fibrotic area. (H&E ×320). **c** One of the more cellular areas (H&E ×320)

Table 2 Comparison of clinical features between LD-HL and NS- and MCHL

	Total	LDHL *n* (%)	NSHL, MCHL *n* (%)	*p* value
Gender				
Male	117	7 (6)	110 (94)	NS
Female	84	5 (6)	79 (94)	
Stage				
I-II	85	3 (3.5)	82 (96.5)	NS
III-IV	70	5 (7.1)	65 (92.9)	
B symptoms				
Yes	74	5 (6.8)	69 (93.2)	NS
No	83	3 (3.6)	80 (96.4)	
Bulky				
Yes	40	3 (7.5)	37 (92.5)	NS
No	107	3 (2.8)	104 (97.2)	
Chemotherapy				
MOPP/ABVD	111	5 (4.5)	106 (95.5)	NS
Other	14	1 (7.1)	13 (92.9)	
Radiotherapy				
Yes	53	2 (3.8)	51 (96.2)	NS
No	98	4 (4.1)	94 (95.9)	
Outcome				
NED[a]/AWD[b]	130	6 (4.6)	124 (95.4)	FE 2t=0.08[d]
DOD[c]	46	6 (13)	40 (87)	

[a] No evidence of HL
[b] Alive with HL
[c] Dead of HL.
[d] Fisher exact test, two tailed

of LDcHL (p=0.069, FE two-tailed). The apoptotic index was higher in LDcHL but not to a significant degree. LMP1/EBV was expressed in eight of 12 cases of LDcHL (p=0.009; FE two-tailed). To our knowledge, none of our LDcHL patients was HIV positive.

Discussion

Our histological criteria for the diagnosis of LDcHL were based on the WHO Classification of Tumours of Haematopoietic and Lymphoid Tissues [2] together with the modifications suggested by Kurtin [3] and by Wright et al.

Table 3 Comparison of age and duration in months of the follow-up between LD-HL and NS- and MCHL

	Subtype	Total (n)	Mean rank	*p* value[a]
Age	LD	12	121.96	0.119
	NS and MC	182	95.89	
Follow-up	LD	11	43.50	0.002
	NS and MC	168	93.04	

[a] Mann–Whitney *U* test

Table 4 Comparison of laboratory data—LD-HL versus NS- and MCHL

		LD-HL(%)	NS MCHL(%)	*p* value
EBV/LMP1	Positive	8 (12.9)	54 (87.1)	FE 2t=
	Negative	4 (2.9)	135 (97.1)	0.009[a]
Caspase 8	Positive	7 (12.3)	50 (87.7)	0.069
	Negative	5 (4.6)	104 (95.4)	
Caspase 3	Positive	5 (4.8)	99 (95.2)	NS
	Negative	6 (9.7)	56 (90.3)	
Apoptotic index	<Median	3 (4.3)	69 (95.7)	NS
	≥Median	4 (6.6)	57 (93.4)	
Sialyl-CD15	Positive	3 (18.8)	13 (18.2)	FE 2t=
	Negative	2 (1.4)	139 (98.6)	0.008[a]
CD30	Positive	12 (6.1)	155 (93.9)	NS
	Negative	0	25 (100)	

[a] Fisher's exact test, two tailed

[4]. In the latter publications, both groups of authors emphasize the need to restore the subclassification of LDcHL into reticular and diffuse fibrosis variants. We agree, as this subclassification is essential in order to firmly establish the diagnosis of LDcHL. We also agree with the statement that cases of LDcHL need not be totally depleted of small reactive lymphocytes [3]. The reticular variant shows a striking predominance of pleomorphic HRS cells with few reactive cells. There is often an interlacing type of fibrosis which may mimic a sarcomatoid tumor. In the diffuse fibrosis variant, HRS cells are more scarce, and the histologic picture is dominated by the fibrosis. The PAS-positive immature collagen found in cases of diffuse fibrosis LDcHL is probably a very helpful feature in the identification of this variant. Despite the small number of cases, our finding of LDcHL in as many as 5.9% of cases may be characteristic of HL in our geographic area. The possibility of under-diagnosis of this subtype of cHL in other studies should, however, be considered. A tendency to under-diagnose LDcHL is not unexpected since some authors hold the view that this entity is doomed to disappear [8–9]. This cHL subtype may be a neglected entity, partly due to its resemblance to other pleomorphic lymphomas but also partly to the repeated emphasis on its rarity.

In the process of comparing the features of LDcHL with those of NS- and MCcHL, we have been able to determine several characteristic clinical or laboratory features of patients with LDcHL, at least in our geographic area. They are mainly older patients, with a significantly shorter follow-up (p=0.002), which may be due to their advanced age at diagnosis but may also represent a further aspect of the biology of LDcHL. They also show a somewhat increased mortality from HL which did not, however, differ significantly from that of our patients with NS- and MCcHL. The high disease-specific mortality found in our cohort as a whole may be related with the advanced stage found in 70 of 155 (45.2%) and the B symptoms found in 74 of 157 (47.1%) patients.

The Hodgkin–Reed–Sternberg cells of patients with LDcHL expressed sialyl-CD15 more frequently than patients with NS- and MCcHL. We have previously reported that the expression of sialyl-CD15 was an independent negative prognostic factor in HL [10]. The HRS cells in LDcHL show a higher expression of LMP1/EBV and of caspase 8.

The diagnosis of B-cell lymphoma with features intermediate between diffuse large B-cell lymphoma and classic Hodgkin lymphoma could be raised. This entity shows cohesive pleomorphic tumor cells in patterns resembling primary mediastinal large B-cell lymphoma or nodular sclerosis cHL [11, 12].

The diffusely fibrotic stroma or focal fibrous bands described in gray zone lymphoma were not seen in our cases in which the fibrosis was PAS-positive and/or non-birefringent.

Consideration was not given to the diagnoses of primary mediastinal large B-cell lymphoma (MLBCL) or of NScHL in our 12 cases, none of which was located in the mediastinum. Although one case had been originally diagnosed as NScHL, it did not fulfill the criteria of this type of cHL. None of our cases was diagnosed as ALCL. We would stress that the immunophenotype of our 12 cases included negativity for CD45 and CD20.

Lymphocyte-depleted cHL has not been considered in the differential diagnosis of mediastinal gray zone lymphoma. We also believe that large B-cell lymphoma with Hodgkin features, also termed Hodgkin-like ALCL, can be excluded in our LDcHL cases.

As mentioned above, numerous small reactive lymphocytes may be found in cases of LDcHL [3], and it is noteworthy that one of our cases showed features consistent with the reticular type of LDcHL in some areas, whereas other fields were more cellular and richer in small round lymphocytes. We would tentatively like to suggest that this case may represent a cellular or early phase of LDcHL, similar to the description of a cellular phase of NScHL.

In conclusion, we have described the morphologic, clinical, and immunohistochemical features of an unselected group of 12 LDcHL patients from Southern Israel. Subclassification into reticular and diffuse fibrosis variants seems to be essential for recognition of this entity. We have compared these features with those of cases of NS- and MCcHL. The LDcHL patients are older, and they show a higher mortality but not to a significant degree. On the other hand, their follow-up is significantly limited. They tend to show a higher association with EBV and with a positive staining for sialyl-CD15.

Acknowledgments This study was supported in part by grants from the Weinkselbaum Family Medical Research Fund, the Israel Ministry of Health; Kibbutz Sde-Boker, Israel; the Richard H. Holtzer Memorial Foundation; and the Samuel Goldstein Foundation.

Conflict of interest The authors declare that they have no conflict of interest.

References

1. Kant JA, Hubbard SM, Longo DL et al (1986) The pathologic and clinical hetereogeneity of lymphocyte-depleted Hodgkin's disease. J Clin Oncol 4:284–294
2. Stein H, Delsol G, Pileri S et al (2001) Classical Hodgkin lymphoma. In: Jaffe ES et al (ed) Pathology & genetics—tumours of haematopoietic and lymphoid tissues. IARC Press, Lyon, pp 252–253
3. Kurtin P (2001) Hodgkin diseases. In: Collins RD, Swerdlow SH (eds) Pediatric hematopathology. Churchill-Livingstone, New York, p 219
4. Wright DH, Leong ASY, Addis BJ (2006) Diagnostic lymph node pathology. Hodder Arnold, London, p 128
5. Ponzoni M, Arrigoni G, Doglioni C (2007) New transcription factors in diagnostic hematopathology. Adv Anat Pathol 14:25–35
6. Benharroch D, Prinsloo I, Goldstein J et al (1996) A comparison of distinct modes of tumor cell death in Hodgkin's disease using morphology and in situ DNA fragmentation. Ultrastruct Pathol 20:497–505
7. Benharroch D, Levy A, Prinsloo I et al (1999) Apoptotic index as a prognostic factor in Hodgkin's disease. Leuk Lymphoma 33:351–359
8. Shimabukuro-Vornhagen A, Haverkamp H, Engert A et al (2005) Lymphocyte-rich classical Hodgkin's lymphoma: clinical presentation and treatment outcome in 100 patients treated within German Hodgkin's Study Group trials. J Clin Oncol 23:5739–5745
9. Glaser SL, Dorfman RF, Clarke CA (2001) Expert review of the diagnosis and histologic classification of Hodgkin's disease in a population based cancer registry: interobserver reliability and impact on incidence and survival rates. Cancer 92:218–224
10. Benharroch D, Dima E, Levy A et al (2000) Differential expression of sialyl and non-sialyl-CD15 antigens in Hodgkin-Reed-Sternberg cells: significance in Hodgkin's disease. Leuk Lymphoma 39:185–194
11. Garcia JF, Mollejo M, Fraga M et al (2005) Large B-cell lymphoma with Hodgkin features. Histopathology 47:101–110
12. Traverse-Glehen A, Pittaluga S, Gaulard P et al (2005) Mediastinal gray zone lymphoma—the missing link between classic Hodgkin's lymphoma and mediastinal large B-cell lymphoma. Am J Surg Pathol 29:1411–1421

Virchows Arch (2008) 453:617–625
DOI 10.1007/s00428-008-0684-8

ORIGINAL ARTICLE

Dog as model for down-expression of E-cadherin and β-catenin in tubular epithelial cells in renal fibrosis

Luca Aresu · Maria Pia Rastaldi · Paola Pregel · Federico Valenza · Enrico Radaelli · Eugenio Scanziani · Massimo Castagnaro

Received: 8 April 2008 / Revised: 29 September 2008 / Accepted: 1 October 2008 / Published online: 24 October 2008

Abstract Mechanism of renal fibrosis leading to end stage kidney remains still a challenge of interest in humans. The pathogenesis of chronic kidney disease is characterized by progressive loss of kidney function and fibrosis. The mechanism of epithelial–mesenchymal transition (EMT) has been predominantly studied in in vitro studies, and we previously demonstrated the EMT of tubular epithelial cells in dogs. In this study, we examined and quantified the modifications of cadherin–catenin complex by immunohistochemistry of E-cadherin and β-catenin and the mesenchymal marker vimentin in 25 dogs with three different spontaneous inflammatory renal diseases. Results showed a significant down-expression of levels of E-cadherin and β-catenin directly correlated with the tubular–interstitial damage (TID). In TID grades 2 and 3, E-cadherin expression was significantly reduced ($p<0.001$). β-catenin expression was overall similar to E-cadherin. The mesenchymal-associated protein, vimentin, was de novo identified in tubules within areas of inflammation. In this work, we identified the loss of cadherin or catenin expression as a progressive mechanism in tubulo-interstitial fibrosis, which allows dissociation of structural integrity of renal epithelia and loss of epithelial polarity. The dog might result more significant as model for new therapies.

Keywords Adhesion molecule · Canine · Fibrosis

P. Pregel · F. Valenza
Dipartimento di Patologia Animale,
Facoltà di Medicina Veterinaria, Università degli studi di Torino,
Via L. da Vinci 44,
10095 Grugliasco, TO, Italy

M. P. Rastaldi
Renal Research Laboratory,
Fondazione IRCCS,
Milano, Italy

E. Radaelli · E. Scanziani
Dipartimento di Patologia Animale, Igiene e Sanità Pubblica Veterinaria, Università degli Studi di Milano,
Milano, Italy

L. Aresu (✉) · M. Castagnaro
Dipartimento di Sanità Pubblica, Patologia Comparata e Igiene Veterinaria, Facoltà di Medicina Veterinaria,
Università degli Studi di Padova,
Agripolis, Padova, Italy
e-mail: luca.aresu@unito.it

Introduction

By definition, epithelial–mesenchymal transition (EMT) is a phenotypic conversion of epithelial cells, leading to the loss of epithelial cell–cell-basement membrane contacts, structural–functional polarity, and acquisition of a fibroblastic phenotype [23]. A number of steps appear necessary to complete the process of EMT. Loss of the epithelial phenotype and disruption of adhesion molecules is the first phase of EMT, reported in several types of pathological processes: tumors, embryogenesis, and organ fibrosis [2, 15, 16, 21, 22]. Emerging evidence has established EMT as one of the major mechanism of renal fibrosis in human and other species [14]. In the latest studies, the authors showed that tubulo-interstitial damage (TID) is characterized by loss of differentiated epithelial cells and activation of mesenchymal cells (renal fibroblasts) leading to renal fibrosis [27]. Tubular epithelial cells (TECs) undergo phenotypic change as demonstrated by de novo vimentin expression and loss of cytokeratin during chronic renal disease. While, under normal circumstances, the TECs are attached to each other and to the basement membrane through specialized junctional complexes that include

molecules such as cadherin and catenin, during the injury, epithelial cells lose the polarity and the mechanisms of adhesion [18, 20]. These processes of cellular injury and detachment lead to the release of cytokines, different inflammatory mediators, and the recruitment of leukocytes to the site of injury. These inflammatory processes may both contribute to the injury and play a role in the repair mechanism that follows the injury [6, 7].

Canine renal pathology represents a good model for the examination of changes in the tubulo-interstitial compartment. In renal biopsies, early histomorphological signs of interstitial fibrosis in dogs are associated with an unfavorable prognosis, even if routine clinical parameters still indicate a compensated kidney function. We have recently demonstrated the similarity of the renal canine model to human, showing that the number of TECs undergoing EMT features is associated with the degree of TID [1]. The aim of the current study was to examine in the same distribution of damage the regulation of adherens junction complex (E-cadherin and β-catenin) in TECs. Numerous recent studies have shown that cellular adhesion molecules and their associated proteins may be critical early target in renal fibrosis murine model and in human transplanted kidney [2, 20]. To study the origin of the EMT, we focused our attention on the potential mechanisms of TECs activation in dogs with different types of spontaneous glomerular disease and associated tubulo-interstitial damage. We postulated that E-cadherin and β-catenin are key molecules in tubular EMT, and loss of expression of both markers is relevant in development of kidney fibrosis, through tubular EMT.

Materials and methods

We collected open renal specimens from 25 dogs who were examined and diagnosed with renal disease in the Department of Pathology, University of Turin in 2007. Disease categories were based on histological, immunofluorescent, and ultrastructural examination, and the diagnosis were given using the criteria of the WHO classification of glomerular diseases. The following groups were included in this study: membranous glomerulonephritis (6), membranoproliferative glomerulonephritis (13), and minimal change disease (6). Clinical parameters (plasma creatinine and proteinuria) were obtained at the time of collection (see Table 1).

Histological examination

Renal samples were fixed in 10% neutral buffered formalin, and sections were cut at 3 μm in thickness and routinely stained. On Masson's Trichrome staining, interstitial fibrosis and inflammation were assessed at ×200 magnification and scored as follow: normal tubulo-interstitium (TID grade=0), mild tubular atrophy, and interstitial edema or fibrosis affecting up to 25% of the field of view (TID grade=1); moderate tubulo-interstitial fibrosis affecting 25–50% of a given field (TID grade=2); severe tubulo-interstitial fibrosis >50% of a field (TID grade=3).

Table 1 Summary of clinical results of dogs

TID grade	Plasma creatinine (mg/dl)	UPC[a] value
0	1.1±0.2	<0.2
1	1.8±0.4	0.3±0.04
2	3.8±1.2	0.7±0.14
3	5.3±2.5	0.9±0.24

[a] Urine protein/creatinine ratio

Immunofluorescence

For immunofluorescence, unfixed renal tissue was OCT-embedded, snap-frozen in liquid nitrogen, and stored at −80°C. Fluorescein Isothiocyanate-labeled anti-goat IgA, IgG, IgM, and complement C3 antibodies specific for the dog (Bethyl Laboratories INC., Montgomery, AL, USA) were used. Primary antibodies were omitted as negative controls.

Immunohistochemistry

An immunohistochemical panel was performed to assess the changes to the TECs. The following antibodies were used in this work: antihuman E-cadherin (clone 36, Transduction Laboratories, Lexington, KY, USA), anti-mouse β-catenin (clone 14, Transduction Laboratories) and anti vimentin (Dako, Glostrup, Denmark). For the immunostaining, paraffin kidney sections (4 μm) were dewaxed and rehydrated, and antigen retrieval was performed by microwave exposure for 3 min (three times) in a citrate buffer (pH 6.0) at 600 W. When the temperature of the buffer reached room temperature, the slides were rinsed in phosphate-buffered saline (PBS) and incubated with hydrogen peroxide (H_2O_2) 3% in methanol for 15 min to block endogenous peroxidase activity. After rinsing in PBS, background staining was blocked using PBS added of 10% bovine serum albumin (BSA, Sigma–Aldrich, St. Louis, MO, USA) for 20 min. The sections were then incubated with the primary antibody diluted in PBS 10% BSA for 60 min. Anti E-cadherin and anti β-catenin were diluted 1:70, anti vimentin 1:50 in PBS 10% BSA. After two washings with PBS, the sections were incubated with the secondary antibody provided by a commercial kit (Real EnVision™ peroxidase Detection System, Dako) for 30 min then washed twice in PBS; the reaction was

developed with the DAB solution provided by the kit, washed in tap water, and counterstained with hematoxylin and PAS. Normal mammary gland was also used as positive control of the immune reaction for E-cadherin and β-catenin. We tested normal canine kidney tissue to quantify the expression of E-cadherin and β-catenin in TECs, and we used normal mammary gland for comparison. Expression of both markers in control dogs results to be mostly total in cytoplasm and membrane of TECs.

Double immunohistochemistry

Vimentin and β-catenin double antigen-immunoperoxidase labeling was performed using a commercial kit (Vector Laboratories, Burlingame, CA, USA), according to manufacturer's instructions. Peroxidase activity was demonstrated firstly by DAB + Ni^{2+} (grey to black chromogen reaction) for Vimentin and secondly by 3-amino-9-ethylcarbazole (AEC, red chromogen reaction) for β-catenin.

Quantification of immunohistochemistry and statistical analysis

Immunohistochemical staining was assessed with respect to its localization and its intensity. E-cadherin and β-catenin immunoreactivity was classified as membranous (localized to cell–cell boundaries) or cytoplasmic (uniformly distributed through the cytoplasm, with no recognizable distinction between membrane and cytoplasm). Quantification of E-cadherin and β-catenin expression in each case was graded according to loss in TEC of immune reaction for the two markers. Loss of cytoplasmic staining of adhesion molecules (E-cadherin and β-catenin) was assessed by counting the percentage of stain-negative cells per HPFs. For each case examined, analysis was performed by counting ten fields (×200), focusing on TECs. Expression of cytoplasmic staining for mesenchymal marker (vimentin) was evaluated by counting the percentage of positively stained TEC per HPFs. The staining intensity, based on the area of distribution, was also assigned from 0% to 100%. The semiquantitative evaluation of immunostaining was evaluated by an electronic image analysis system (Adobe Photoshop CS3). Images were digitalized using a video camera connected to a single microscope and to a computer equipped with a frame grabber (Neotech Ltd, Eastleigh Hampshire, UK). In order to detect a possible relationship between the two percentages of the variables (E-cadherin or β-catenin and area), a scatter plot was used, grouping their values according to the nominal variable TID. Furthermore, the product of the percentage of the values for the intensity and the area was used to increase the sensitivity of the data. Data are presented as means ± SD. Analysis of variance (ANOVA) was performed, and the six comparisons among the mean values of the pairs were performed using the Bonferroni Multiple Comparison Test. Statistical analyses were performed with GraphPad-InStat software (GraphPad Software, San Diego, CA, USA).

Results

Tubulo-interstitial damage was a common finding in membranous and membranoproliferative glomerulonephritis (Fig. 1). In minimal change disease, only minimal areas of inflammation and fibrosis were detected (TID grade 1). All three grades of TID were present among the samples examined. For each case, the quantitative analysis data corresponding to the grade of TID are summarized in Table 2.

Renal samples, independent of the diagnosis, showed a variable intensity of positive immunostaining in the TECs for E-cadherin and β-catenin.

Expression of E-cadherin

Uniform, strong membranous, and cytoplasmatic E-cadherin staining was localized in TECs in the controls (87.7±2.0 product, see Fig. 2a). In TID grade 1, E-cadherin immunoreactivity was minimally reduced when compared to normal TECs (62.2±2.5 product). In TID grades 2 (33.7±2.0) and 3 (12.5±4.0, see Fig. 2b and c), E-cadherin expression was significantly reduced. Distribution in TECs, independently of the disease, was heterogeneous or negative compared with that in normal tubular epithelium and was characterized by patterns with variable degrees of membrane and cytoplasmic staining. This expression was preserved in the intact tubules next to the areas of inflammation. Table 1 summarizes the relationship between E-cadherin expression and the TID grade. E-cadherin expression in all cases examined significantly correlated with the histological grade ($p<0.001$).

Expression of β-catenin

Normal TECs showed expression of β-catenin; the signal was recorded not only more intensely at cell junctions, but also diffusely in the cytoplasm (92.5±2.0 product, see Fig. 2d).

The β-catenin expression was similar to E-cadherin in all lesions examined. Expression of β-catenin was reduced in TID grade 1 (58.8±2.2 product, see Fig. 2e) compared to normal TECs ($p<0.001$). Scattered positive TECs in the TID grade 3 showed an exclusively granular cytoplasmic pattern (see Fig. 2f). Tubules next to the inflammation retained the cytoplasmic and membrane localization of catenin. Nuclear staining was also observed in some cells. Data are shown in Table 1.

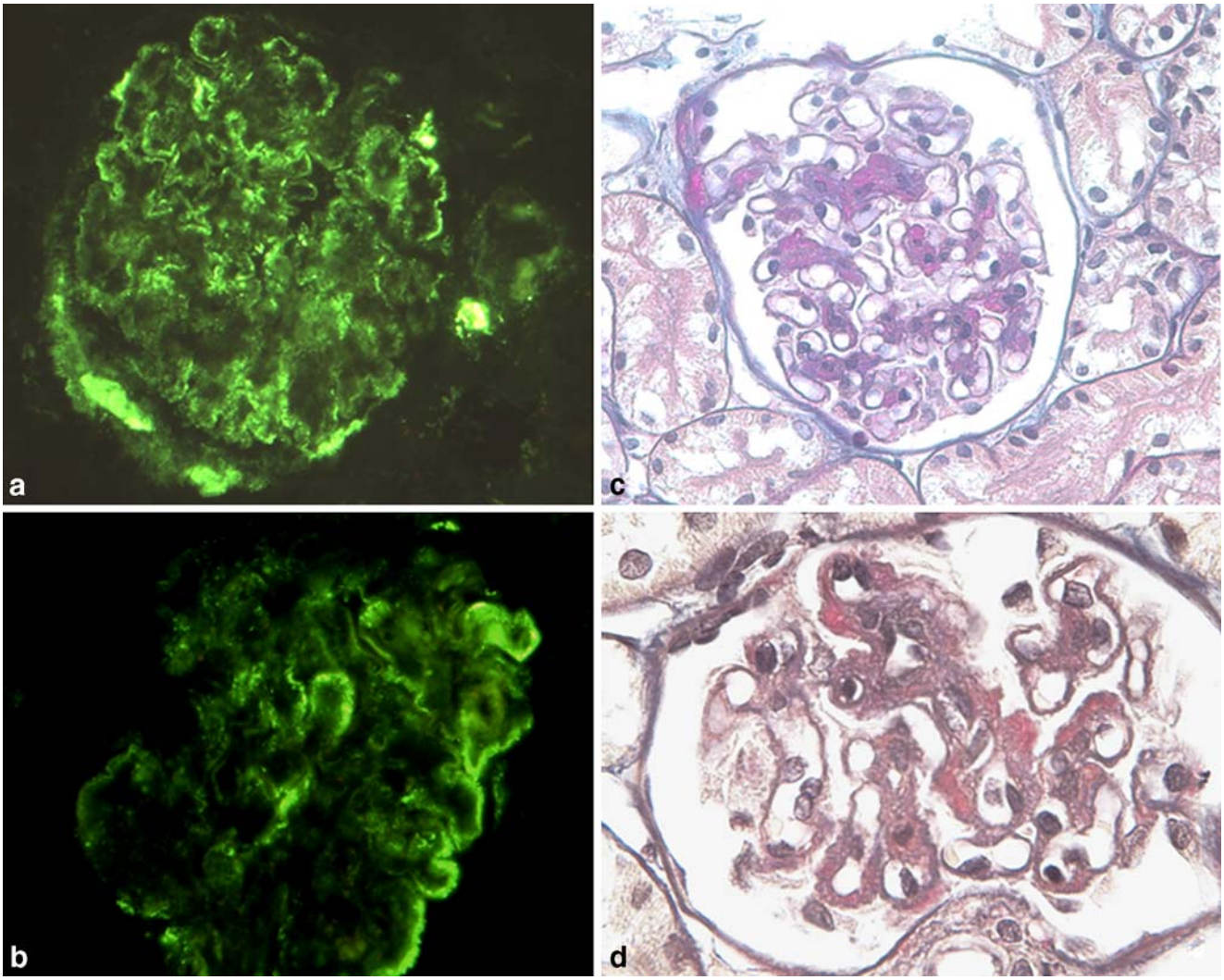

Fig. 1 **a** Granular pattern deposition along the glomerular basement membrane associated with mesangial distribution. (FITC-anti-goat IgG, ×400). **b** Diffuse, intense granular deposits along the glomerular basement membrane. (FITC-anti-goat IgG, ×400). **c** Deposition along the basement membrane and in the mesangium in a membranoproliferative glomerulonephritis (AFOG, ×400). **d** Diffuse thickening of glomerular basement membrane due to intramembranous deposition in a membranous glomerulonephritis (AFOG, ×400)

Expression of vimentin

No tubular expression of vimentin was detected in control dogs (Figs. 3, 4). De novo expression of vimentin marker was identified in tubular epithelial cells in different proportion, statistically correlated with the TID grade ($p<0.01$). More intense vimentin expression was restricted to areas of tubular damage, and concomitant expression of vimentin and β-catenin was recorded in the same tubular cross sections in double immunohistochemistry (see Fig. 5a and b). However, the expression of vimentin marker was demonstrated in TECs of degenerate atrophic tubules within areas of inflammation (48.2±10.3 TECs/field in TID grade 3). Both intact tubules closed to the inflammation showed

Table 2 Summary of immunohistochemical results

TID grade	0 (5 dogs)	1 (11 dogs)	2 (7 dogs)	3 (7 dogs)	*p* Value
E-cadherin	87.7±2.0	62.2±2.5	33.7±2.0	12.5±4.0	<0.0001
β-catenin	92.5±2.0	58.8±2.2	31.5±3.0	12.0±4.4	<0.0001
Vimentin	0.0±0.0	10.2±2.1	26.3±5.2	48.2±10.3	<0.0001

Results are reported as means (obtained from the multiplication of the values for the intensity and the percentage of positive tubular epithelial cells) ± SD

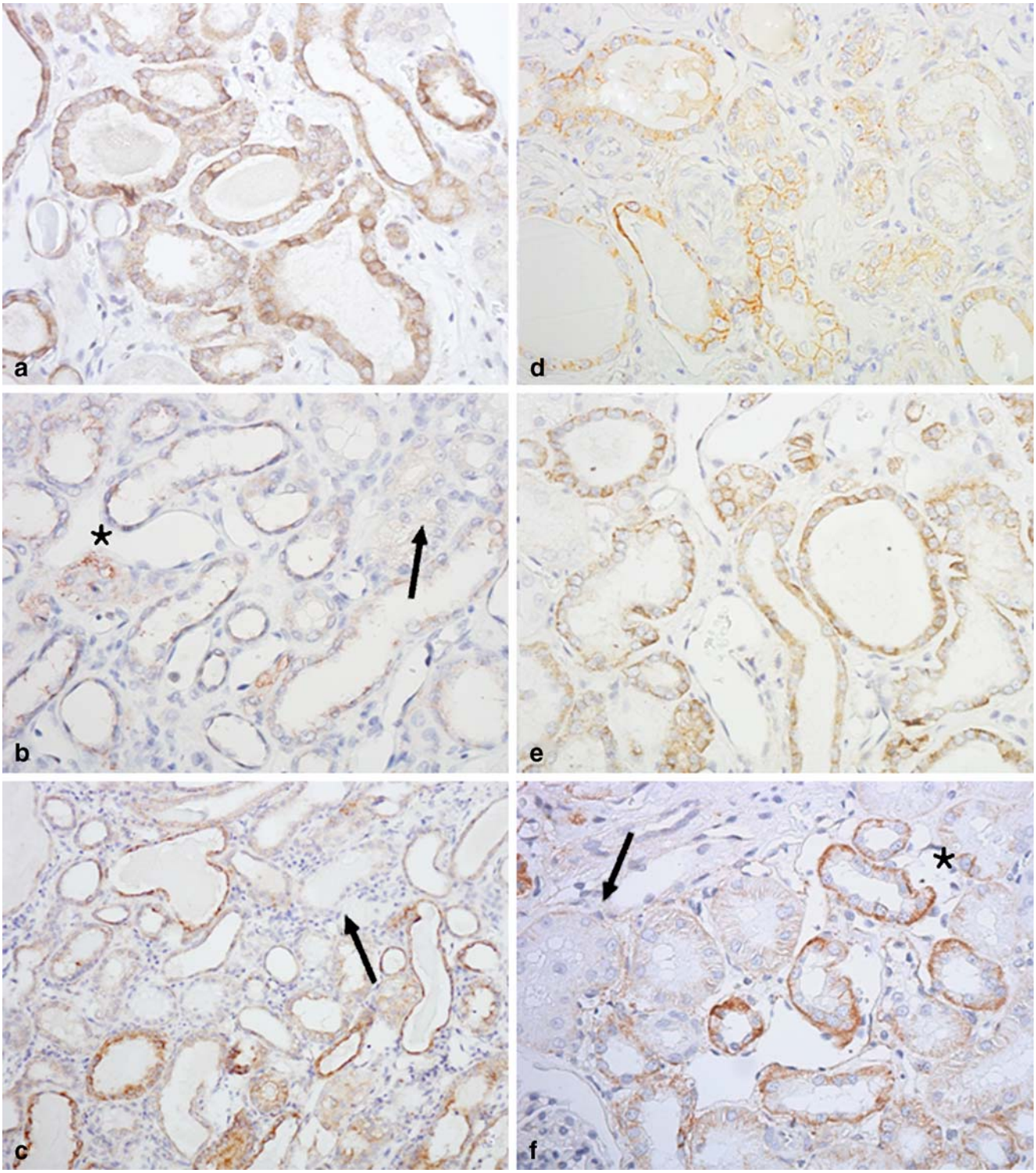

Fig. 2 **a** Normal E-cadherin cytoplasm and membrane expression in control kidney (×200). **b** Progressive lost of cadherin expression in tubular epithelial cells (*arrow*) and tubules with normal expression (*asterisk*) in TID grade 2 (×400). **c** Negative staining of E-cadherin in multifocal tubules (*arrow*) in TID grade 3 (×100). **d** β-catenin intensely stained membrane of epithelial tubular cells in control kidney (×200). **e** Progressive lost of β-catenin expression in scattered epithelial cells in TID grade 1 (×200). **f** Lost of β-catenin expression evident in tubular cross sections (*arrow*) and tubules with normal expression (*asterisk*) in TID grade 3 (×200)

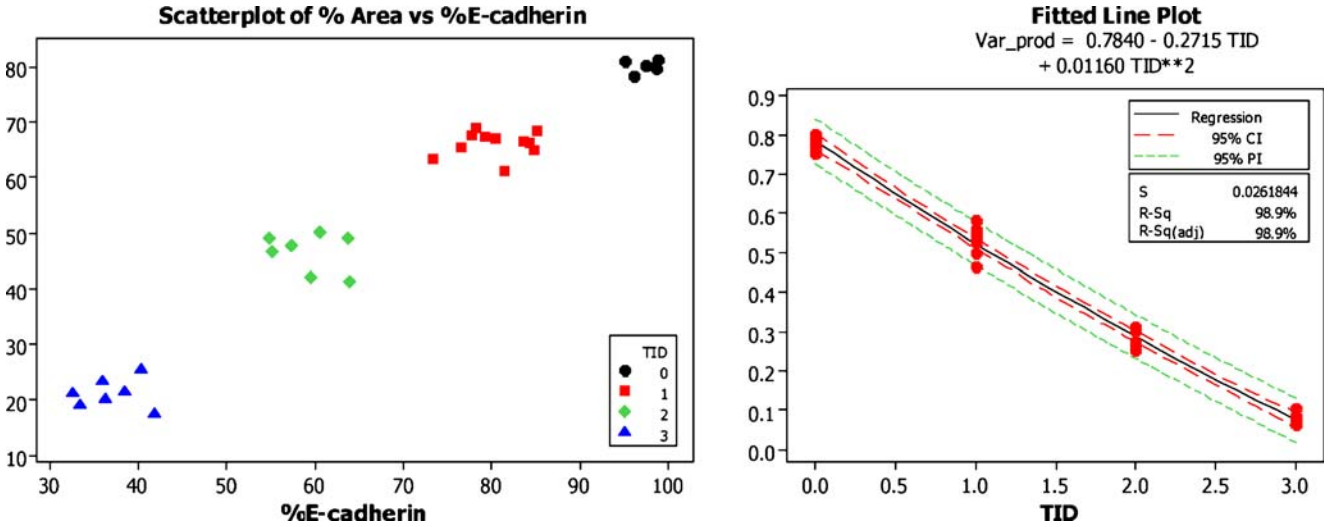

Fig. 3 *Left* scatter plot to detect the relationship between the two variables percentages of E-cadherin and area. *Right* modelization of the composed variable product for E-cadherin with respect to TID

vimentin staining. Quantification of the percentage of tubules expressing vimentin marker is shown in Table 1. Examination of PAS-vimentin immunohistochemistry showed a thickening of tubular basement membrane correlated with tubules vimentin positive; no ruptures were identified (see Fig. 6).

Statistical results

The scatter plot used to detect the relationship between the two variables percentages of E-cadherin or β-catenin, and area showed that the four clusters of TID were homogeneous and evidenced a systematic difference between them (see Figs. 3 and 4). Moreover, the two variables were strongly correlated; so, a new variable, the product of the mentioned ones, was considered for the statistical analysis. ANOVA revealed that all the differences were highly significant ($p<0.001$). Therefore, the six comparisons among the mean values of the pairs were performed using the Bonferroni Multiple Comparison Test, and the differences were again highly significant ($p<0.001$).

The last analysis was the modelization of the composed variable product with respect to TID according to a linear model. Both the line plot and the statistical indices p value and R^2 encourage to predict the variable product of E-cadherin or β-catenin and area according to a more suitable model, a quadratic one (see Figs. 3 and 4).

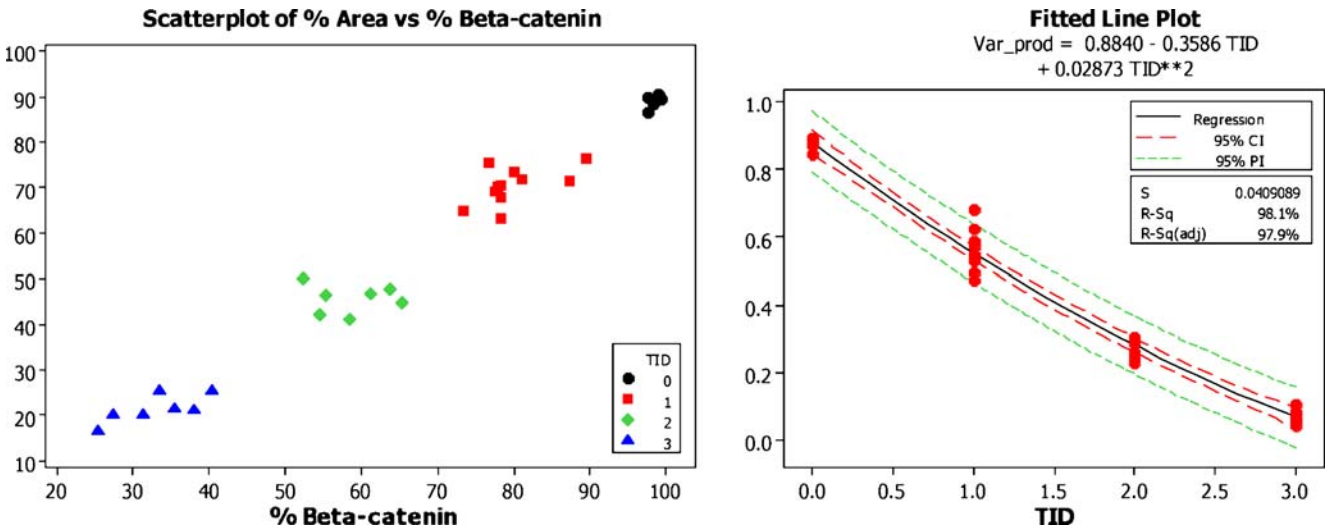

Fig. 4 *Left* scatter plot to detect the relationship between the two variables percentages of β-catenin and Area. *Right* modelization of the composed variable product for β-catenin with respect to TID

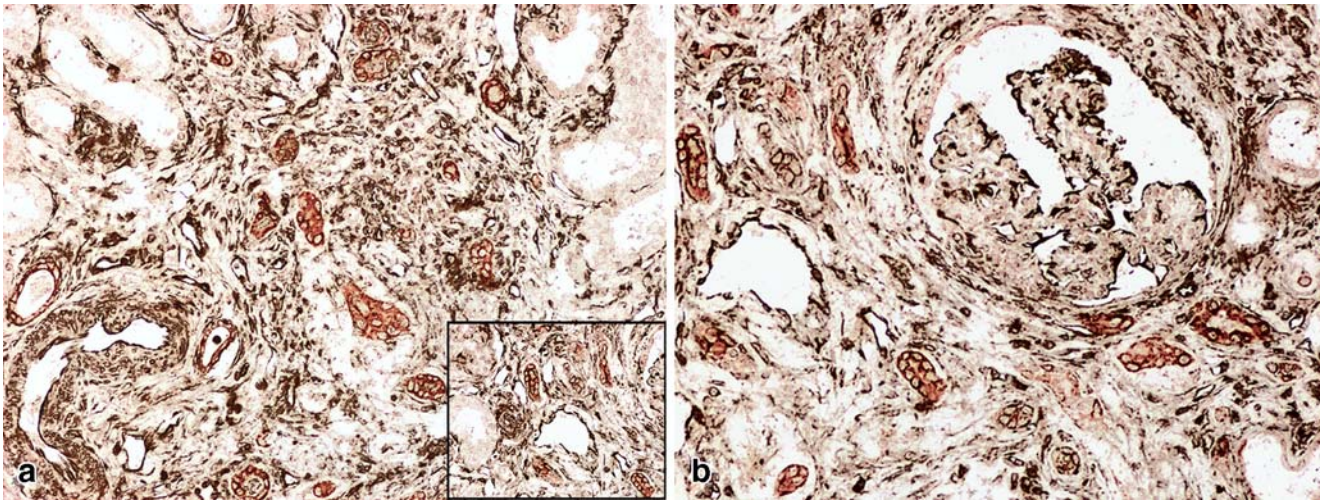

Fig. 5 **a**, **b** Scattered epithelial tubular cells β-catenin positive stained in red and several epithelial tubular cells vimentin positive stained in black in same tubular cross section (*arrow*) in TID grade 2 (double immunohistochemistry, **a** ×400, **b** ×600)

Discussion

In this study, we sought to determine whether the EMT process was related to down-expression of E-cadherin and β-catenin and if this correlated with the different grades of TID in the most common spontaneous canine renal diseases.

The E-cadherin–catenin complex plays a fundamental role in the construction of epithelia. Cadherins comprise a family of calcium-dependent cell–cell adhesion proteins that play important role in embryonic development and maintenance of normal tissue architecture [5, 6, 28]. The cadherin–catenin complex binds to the cytoskeletal components, including actin bundles, and the linkage in this complex is crucial for E-cadherin to function normally [17].

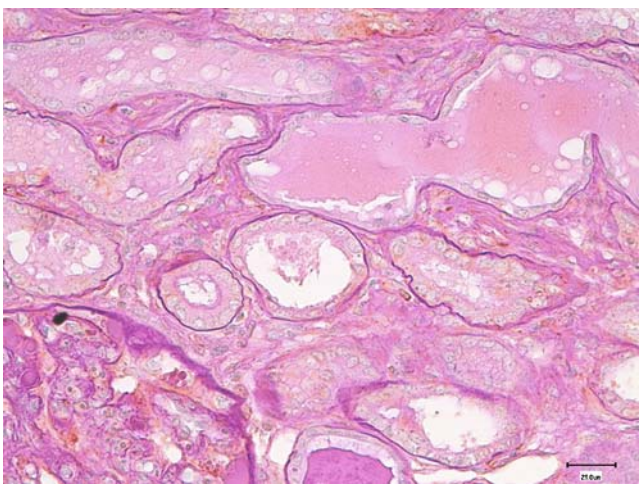

Fig. 6 Down-expression of β-catenin associated with tubular basement membrane thickening, no sign of rupture (Vimentin-PAS counterstained, ×200)

The predominant epithelial isoform, E-cadherin, localizes in the lateral membrane of differentiated epithelia, providing the structural foundation for adherens junctions [18]. In fact, they not only function as static structural components of adherens junctions but they, along with some of their associated molecules, also play critical role in regulating cell-signaling pathways [3, 19, 26]. Likewise, the inflammatory processes may either contribute to the initial injury or occur as a consequence of the cellular injury involving specific changes in the expression and function of cell adhesion molecules that are necessary for the migration, attachment, and activation of leukocytes [26].

Cadherin–catenin complex alterations have been studied in the development of carcinogenesis model and to understand the mechanism of epithelial mesenchymal transition in the fibrotic process [2, 4]. Few papers demonstrate that changes in cadherin expression are fundamentals to the process of EMT and cellular motility [19, 24]. In the human adult kidney, the cadherins are differently expressed in various segments of the nephron. In a study of mouse kidney, Piepenhagen and Nelson [25] showed that E-cadherin is abundantly expressed in most segments of the nephron, including the proximal tubules. Cho and colleagues [8] also reported that E-cadherin is present in the proximal and distal tubules of newborn mice. In the present experiment, normal kidney from control dogs showed cytoplasmatic and membrane expression of both adhesion markers in all segments of the nephron.

The immunohistochemical profiles of E-cadherin and β-catenin observed in this study result not associated with the glomerular lesions; no correlation was found among the different classes of disease. On the contrary, the reduction in cadherin and catenin expression was strictly related to the TID: a statistical significant association ($p<0.01$) was

found that correlated with the different evolution of TID. Data on the expression of β-catenin in renal specimens are similar for E-cadherin with a similar frequency of alterations, and we also identified the presence on nuclear expression of catenin. Different in vitro studies have demonstrated that down-expression of E-cadherin is related with translocation of β-catenin from the membrane leading to the cytoplasm and then into the nucleus. This translocation suggests the loss of epithelial polarity and integrity [9]. β-Catenin has a dual role in the EMT: it enhances cell–cell adhesion when bound to cadherin complexes in adherens junctions and also functions as a transcriptional co-activator upon entry into the nucleus [7, 11, 13]. The results obtained in this experiment evoke an interesting speculation: down-expression of cadherin–catenin system in TECs is a necessary step for transdifferentiation of these cells into cells acquiring mesenchymal features. The entire process requires alterations in morphology, cellular architecture, and adhesion capacity [10, 12, 31]. TECs under normal conditions are tightly connected to each other to form an integrated epithelial sheet through cell adhesion mechanisms fundamental for their functions, and no mesenchymal features are evident in TECs (vimentin expression in control dogs: 0.0±0.0). As disease progresses, epithelial tubular markers largely disappeared, and coexpression of vimentin and epithelial markers in TECs becomes evident (β-catenin expression in TID grade 3: 12.0±4.4). Positivity for mesenchymal antigen and loss of adhesion junction properties were mainly detected in well-preserved tubular structures without signs of tubular basement membrane disruption or possible cell migration into the interstitium, as demonstrated by PAS counterstain.

To investigate this mechanism, we performed double immunohistochemistry for vimentin and β-catenin. This technique permits to identify the colocalization of both markers and define the process as *step by step* due to the progressive modification in the same tubular cross section.

This work confirms that loss of cadherin or catenin expression is an early mechanism in tubulo-interstitial fibrosis, which allows dissociation of structural integrity of renal epithelia and loss of epithelial polarity. To enable migration of single epithelial cells, the strong cell–cell adhesion, a feature of epithelial cells, has to be reduced. Therefore, the reduction of cellular adhesion is associated with epithelial dedifferentiation mechanism. EMT is easily started by a combination of cytokines associated with proteolytic digestion of basement membranes upon which epithelia reside [10, 29, 30]. The canine renal model offers different advantages in the study for the role of adhesion molecules and the EMT mechanism in kidney, such as the development of spontaneous diseases, the slow progression of the disease, and overall, the similarity of inflammatory lesions in the canine kidney to humans.

In summary, we could describe the process of EMT in different events involving: loss of adhesion properties (loss of catenin and cadherin expression) and de novo expression of mesenchymal features (vimentin positive reaction in TECs). This study provides the first evidence that TECs can undergo phenotypic change toward a mesenchymal expression during progressive renal fibrosis in canine glomerulonephritis on the basis of de novo vimentin expression and down-expression of epithelial markers of junction. While down-regulation of cadherins is well described in cultured cells and murine model, it still remains to be shown whether such events occur in spontaneous renal pathology in human [28, 29, 32]. On the base of this experimental study, the dog becomes an important model for further investigations, especially for the expression of TGF-β, a major regulator of EMT and cadherins expression in the TECs.

Conflict of interest statement We declare that we have no conflict of interest.

References

1. Aresu L, Rastaldi MP, Scanziani E, Baily J, Radaelli E, Pregel P, Valenza F (2007) Epithelial-mesenchymal transition (EMT) of renal tubular cells in canine glomerulonephritis. Virchows Arch 451:937–942
2. Blanco D, Vicent S, Elizegi E, Pino I, Fraga MF, Esteller M, Saffiotti U, Lecanda F, Montuenga LM (2004) Altered expression of adhesion molecules and epithelial-mesenchymal transition in silica-induced rat lung carcinogenesis. Lab Invest 84:999–1012
3. Bottinger EP (2007) TGF-beta in renal injury and disease. Semin Nephrol 27:309–320
4. Brunetti B, Sarli G, Preziosi R, Monari I, Benazzi C (2005) E-cadherin and beta-catenin reduction influence invasion but not proliferation and survival in canine malignant mammary tumors. Vet Pathol 42:781–787
5. Bush KT, Tsukamoto T, Nigam SK (2000) Selective degradation of E-cadherin and dissolution of E-cadherin-catenin complexes in epithelial ischemia. Am J Physiol Renal Physiol 278:F847–F852
6. Capaldo CT, Macara IG (2007) Depletion of E-cadherin disrupts establishment but not maintenance of cell junctions in Madin-Darby canine kidney epithelial cells. Mol Biol Cell 18:189–200
7. Chen H, Paradies NE, Fedor-Chaiken M, Brackenbury R (1997) E-cadherin mediates adhesion and suppresses cell motility via distinct mechanisms. J Cell Sci 110:345–356
8. Cho EA, Patterson LT, Brookhiser WT, Mah S, Kintner C, Dressler GR (1998) Differential expression and function of cadherin-6 during renal epithelium development. Development 125:803–812
9. Conacci-Sorrell M, Simcha I, Ben-Yedidia T, Blechman J, Savagner P, Ben-Ze'ev A (2003) Autoregulation of E-cadherin expression by cadherin-cadherin interactions: the roles of beta-catenin signaling, Slug, and MAPK. J Cell Biol 163:847–857
10. Gupta S, Clarkson MR, Duggan J, Brady HR (2000) Connective tissue growth factor: potential role in glomerulosclerosis and tubulointerstitial fibrosis. Kidney Int 58:1389–1399

11. Hayashida Y, Honda K, Idogawa M, Ino Y, Ono M, Tsuchida A, Aoki T, Hirohashi S, Yamada T (2005) E-cadherin regulates the association between beta-catenin and actinin-4. Cancer Res 65:8836–8845
12. Hertig A, Verine J, Mougenot B, Jouanneau C, Ouali N, Sebe P, Glotz D, Ancel PY, Rondeau E, Xu-Dubois YC (2006) Risk factors for early epithelial to mesenchymal transition in renal grafts. Am J Transplant 6:2937–2946
13. Hirohashi S, Kanai Y (2003) E-cadherin mediates adhesion and suppresses cell motility via distinct mechanisms. Cancer Sci 110:345–356
14. Jinde K, Nikolic-Paterson DJ, Huang XR, Sakai H, Kurokawa K, Atkins RC, Lan HY (2001) Tubular phenotypic change in progressive tubulointerstitial fibrosis in human glomerulonephritis. Am J Kidney Dis 38:761–769
15. Kalluri R, Neilson EG (2003) Epithelial-mesenchymal transition and its implications for fibrosis. J Clin Invest 112:1776–1784
16. Kirchner T, Brabletz T (2000) Patterning and nuclear beta-catenin expression in the colonic adenoma-carcinoma sequence. Analogies with embryonic gastrulation. Am J Pathol 157:1113–1121
17. Kitagawa T, Matsumoto K, Nagafuchi A, Tsukita S, Suzuki H (1999) Co-expression of E-cadherin and alpha-catenin molecules in colorectal cancer. Surg Today 29:511–518
18. Kreidberg JA, Symons JM (2000) Integrins in kidney development, function, and disease. Am J Physiol Renal Physiol 279:F233–F242
19. Kwak JM, Min BW, Lee JH, Choi JS, Lee SI, Park SS, Kim J, Um JW, Kim SH, Moon HY (2007) The Prognostic Significance of E-Cadherin and Liver Intestine-Cadherin Expression in Colorectal Cancer. Dis Colon Rectum 50:1873–1880
20. Lee DB, Huang E, Ward HJ (2006) Tight junction biology and kidney dysfunction. Am J Physiol Renal Physiol 290:F20–F34
21. Lee JM, Dedhar S, Kalluri R, Thompson EW (2006) The epithelial-mesenchymal transition: new insights in signalling, development, and disease. J Cell Biol 172:973–981
22. Liu Y (2004) Epithelial to mesenchymal transition in renal fibrogenesis: pathologic significance, molecular mechanism, and therapeutic intervention. J Am Soc Nephrol 15:1–12
23. Masszi A, Fan L, Rosivall L, McCulloch CA, Rotstein OD, Mucsi I, Kapus A (2004) Integrity of cell-cell contacts is a critical regulator of TGF-beta 1-induced epithelial-to-myofibroblast transition: role for beta-catenin. Am J Pathol 165:1955–1967
24. Nakajima S, Doi R, Toyoda E, Tsuji S, Wada M, Koizumi M, Tulachan SS, Ito D, Kami K, Mori T, Kawaguchi Y, Fujimoto K, Hosotani R, Imamura M (2004) N-cadherin expression and epithelial-mesenchymal transition in pancreatic carcinoma. Clin Cancer Res 10:4125–4133
25. Piepenhagen PA, Nelson WJ (1995) Differential expression of cell-cell and cell-substratum adhesion proteins along the kidney nephron. Am J Physiol 269:C1433–C1449
26. Prozialeck WC, Edwards JR (2007) Cell adhesion molecules in chemically-induced renal injury. Pharmacol Ther 114:74–93
27. Rastaldi MP, Ferrario F, Giardino L, Dell'Antonio G, Grillo C, Grillo P, Strutz F, Müller GA, Colasanti G, D'Amico G (2002) Epithelial-mesenchymal transition of tubular epithelial cells in human renal biopsies. Kidney Int 62:137–146
28. Tepass U, Truong K, Godt D, Ikura M, Peifer M (2000) Cadherins in embryonic and neural morphogenesis. Nat Rev Mol Cell Biol 1:91–100
29. Tian YC, Fraser D, Attisano L, Phillips AO (2003) TGF-beta1-mediated alterations of renal proximal tubular epithelial cell phenotype. Am J Physiol Renal Physiol 285:F130–F142
30. van Timmeren MM, van den Heuvel MC, Bailly V, Bakker SJ, van Goor H, Stegeman CA (2007) Tubular kidney injury molecule-1 (KIM-1) in human renal disease. J Pathol 212:209–217
31. Yang J, Liu Y (2001) Dissection of key events in tubular epithelial to myofibroblast transition and its implications in renal interstitial fibrosis. Am J Pathol 159:1465–1475
32. Zeisberg M, Bonner G, Maeshima Y, Colorado P, Müller GA, Strutz F, Kalluri R (2001) Renal fibrosis: collagen composition and assembly regulates epithelial-mesenchymal transdifferentiation. Am J Pathol 159:1313–1321

Virchows Arch (2008) 453:627–635
DOI 10.1007/s00428-008-0689-3

ORIGINAL ARTICLE

Prognostic significance of p16/cdkn2a loss in pleural malignant mesotheliomas

Sanja Dacic · Hannelore Kothmaier · Stephanie Land · Yongli Shuai · Iris Halbwedl · Patrizia Morbini · Bruno Murer · Camilla Comin · Françoise Galateau-Salle · Funda Demirag · Handan Zeren · Richard Attanoos · Alan Gibbs · Philip Cagle · Helmut Popper

Received: 15 August 2008 / Accepted: 9 October 2008 / Published online: 29 October 2008

Abstract Homozygous deletion of p16/CDKN2A is the most common genetic abnormality in malignant mesotheliomas. The aim of this study was to determine prognostic significance of p16/CDKN2A loss in malignant pleural mesotheliomas (MPM) as defined by immunohistochemistry and fluorescence in situ hybridization (FISH). High-density tissue microarrays were constructed from archival formalin-fixed paraffin-embedded samples of 48 MPM. Long survival (LS) was defined as survival greater than 3 years from the time of diagnosis, and short survival was defined as less than 3 years from the time of diagnosis. Both loss of p16 protein expression by immunohistochemistry and homozygous deletion of p16 by FISH were associated with adverse prognosis. Female gender, positive p16 immunoexpression, and lack of p16/CDKN2A deletion significantly predicted the survival for the LS group. Statistical analysis showed a very strong correlation of immunohistochemistry and FISH data. Cases positive for p16 immunoexpression and negative for 9p21 deletion showed the best survival time. Our study is the first to demonstrate decreased frequency of homozygous deletion of 9p21 and loss of p16 immunoreactivity in pleural mesotheliomas from patients

S. Dacic (✉)
Department of Pathology—PUH A610,
University of Pittsburgh Medical Center,
200 Lothrop St.,
Pittsburgh, PA 15213, USA
e-mail: dacics@upmc.edu

H. Kothmaier · I. Halbwedl · H. Popper
Institute of Pathology,
Graz, Austria

S. Land · Y. Shuai
University of Pittsburgh School of Public Health,
Pittsburgh, PA, USA

P. Morbini
Instituto di Anatomia Pathologica,
Pavia, Italy

B. Murer
Ospedale Umberto,
Mestre,
Venice, Italy

C. Comin
Department of Human Pathology and Oncology,
University of Florence,
Florence, Italy

F. Galateau-Salle
CHU Cote de Nacre,
Caen, France

F. Demirag
Ataturk Chest Disease Hospital,
Ankara, Turkey

H. Zeren
Adana University,
Adana, Turkey

R. Attanoos · A. Gibbs
Cardiff and Vale NHS Trust Llandough Hospital,
Cardiff, UK

P. Cagle
The Methodist Hospital,
Houston, TX, USA

with long-term survival of greater than 3 years in contrast to patients with rapidly fatal mesotheliomas. A possible implementation of these tests into preoperative prognostication of MPM and therapeutic decisions should be considered.

Keywords Pleural mesothelioma · p16 · FISH · Immunohistochemistry · Prognosis

Introduction

Malignant pleural mesothelioma (MPM) is an aggressive tumor usually associated with a poor prognosis and median survival period of only 6–12 months [1, 2]. Approximately 2,000 new cases are diagnosed each year in the US and there is an increasing incidence worldwide [3]. More than 80% of cases can be attributed to asbestos exposure, but approximately 20% of cases may be related to other factors such as exposures to simian virus 40, thorotrast, and radiation [4, 5]. The incidence of MPM is expected to rise worldwide in the next 10–20 years as a result of widespread exposure to asbestos in past decades and continuing exposure in developing countries [6].

There is no reliable definitive therapy for MPM, and only a tiny minority of patients is eligible for potentially curative treatments. Response to different treatments is variable but there is a small subset of patients that will have longer survival than typically expected. The major clinical issue is to establish early diagnosis and adequate treatment triage of the patients with MPM. Diagnosis of early disease is difficult and most patients are diagnosed at an advanced stage. The TNM staging system is of limited prognostic value in patients with MPM, and two currently accepted staging systems include the International Mesothelioma Interest Group and Brigham systems [7, 8]. A limitation of both staging systems is that the extent of the disease can be assessed only at thoracotomy, which means that a minority of patients can be adequately staged. Radiologic prediction of stage proposed by these two systems is problematic. Therefore, alternative prognostic scoring systems have been proposed by the European Organization for the Research and Treatment of Cancer and the Cancer and Leukemia Group B [9, 10]. These prognostic scoring systems indicate that the most important predictors of poor prognosis in MPM are nonepithelioid histology, male gender, poor performance status, low hemoglobin, high platelet count, high white blood cell count, and high lactate dehydrogenase level. These prognostic factors are proposed to be very important in selecting appropriate treatment. Nonepithelioid histology of MPM argues against surgery as a treatment option [11, 12]. However, it has been shown that up to 40% of malignant mesotheliomas are inadequately histologically classified on small biopsy specimens [11, 13]. This means that some of the patients will not receive adequate therapy because of inadequate histologic subclassification. This also has an impact on survival, variable response to therapy, and poor outcome. It is clear that the search for other prognostic factors is necessary to improve treatment of patients with MPM.

Molecular studies at DNA and RNA levels, as well as cytogenetic studies, have resulted in identification of potential diagnostic and prognostic markers that may be useful in clinical practice [14–17]. One of the most common genetic alterations in MPM is the homozygous deletion of the 9p21 locus harboring genes CDKN2A, CDKN2B, and MTAP [18–21]. Deletion of p16/CDKN2A deletions has been reported in up to 72% of primary mesotheliomas [22, 23]. Recent studies demonstrated the diagnostic usefulness of this abnormality in separation of benign from malignant mesothelial proliferations in body fluid and biopsy specimens [24, 25]. By gene expression analysis using fluorescence in situ hybridization (FISH) as a validation method, Lopez-Rios et al. [19] demonstrated the prognostic significance of p16 deletion in MPM using 1-year survival as a cutoff for long survival.

From institutions in multiple countries, we have assembled a collection of 26 patients with MPM and very unusually long survivals of three or more years after diagnosis, the largest collection of MPM patients with this exceptional outcome. We hypothesized that the tumors from this unique cohort of patients have molecular markers that should correlate with their unusually good prognosis. The aim of our study was to determine the prognostic significance of the loss of p16 as determined by FISH and immunohistochemistry in epithelioid MPM with long-term survival of three or more years.

Material and methods

Forty-eight cases of epithelioid MPM from either open biopsies or pleurectomies diagnosed between 1987 and 2003 were selected by contributing authors. The tumors were classified according to the World Health Organization Classification of tumors of the lung and pleura [26]. The diagnosis was confirmed immunohistochemically by at least three positive and two negative markers. The study was approved by the University of Pittsburgh Institutional Review Board (IRB # 0612074). The patients were divided into two groups using 36 months as cutoff survival. Twenty-six patients were identified as long survivors (LS; one USA, one UK, one Austria, three France, five Turkey, 15 Italy) and 22 as short survivors (SS; five UK, eight Italy, nine Austria) [27].

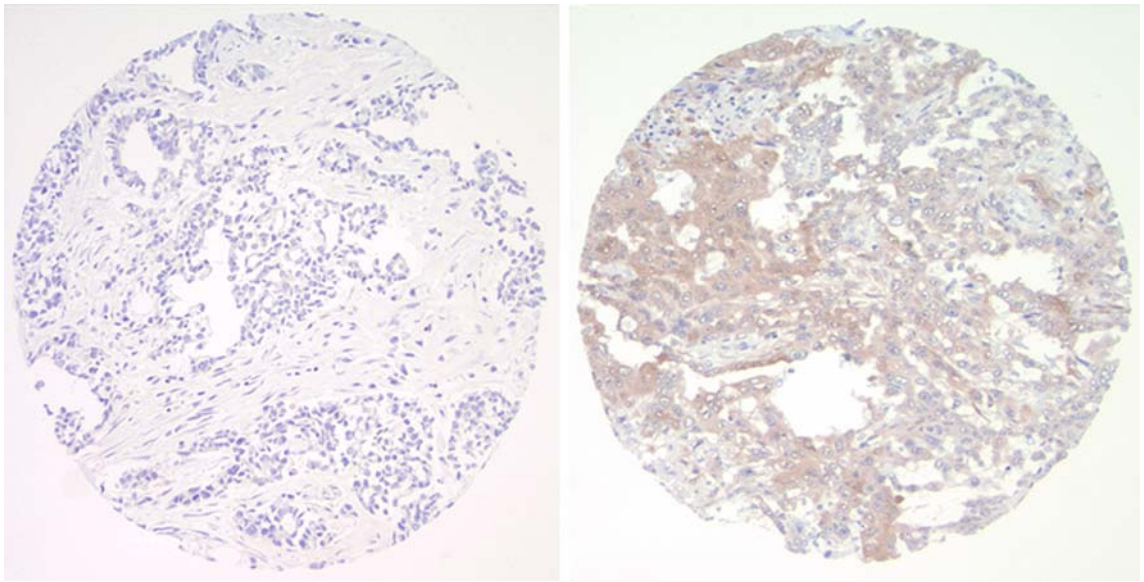

Fig. 1 P16 immunoreactivity was nuclear and cytoplasmic and was scored for intensity and extent. Cases were considered negative if no staining or weak focal staining was present (*left*). Staining was interpreted as positive if weak multifocal–diffuse or strong diffuse staining was observed (*right*)

Tissue microarray constructions

High-density tissue microarrays were constructed from archival formalin-fixed paraffin-embedded samples of 48 cases of epithelioid malignant mesotheliomas collected in USA, UK, Turkey, Italy, France, and Austria. For each sample, five representative areas rich in tumor cells were identified by light microscopic examination and marked on the hematoxylin-and-eosin sections. Five cores measuring 0.6 mm in diameter were taken from the donor paraffin tissue blocks of each case and were arranged in a recipient paraffin tissue array block by using a Manual Tissue Arrayer (MTA-1, Beecher Instruments Inc, Sun Prairie, WI, USA). Each donor block was punched six to ten times for the construction of two recipient blocks, each containing 243 tissue cores. Thirteen cores of morphologically normal-appearing pleura and lung parenchyma were also included [27].

Immunohistochemistry

The immunohistochemical study was performed using anti-p16 mouse monoclonal antibody at a dilution of 1:200 (BD PharMingen, San Diego, CA, USA) according to the standard avidin–biotin–peroxidase complex method. The p16 immunostain for each case was interpreted as previously described [28]. Briefly, nuclear and cytoplasmic p16 immunoreactivity was scored for intensity and extent. Intensity of immunoreactivity was scored as 0—no staining; 1+—weak staining; 2+—strong staining. The extent of immunoreactivity was assessed as focal (<5%) or multifocal–diffuse.

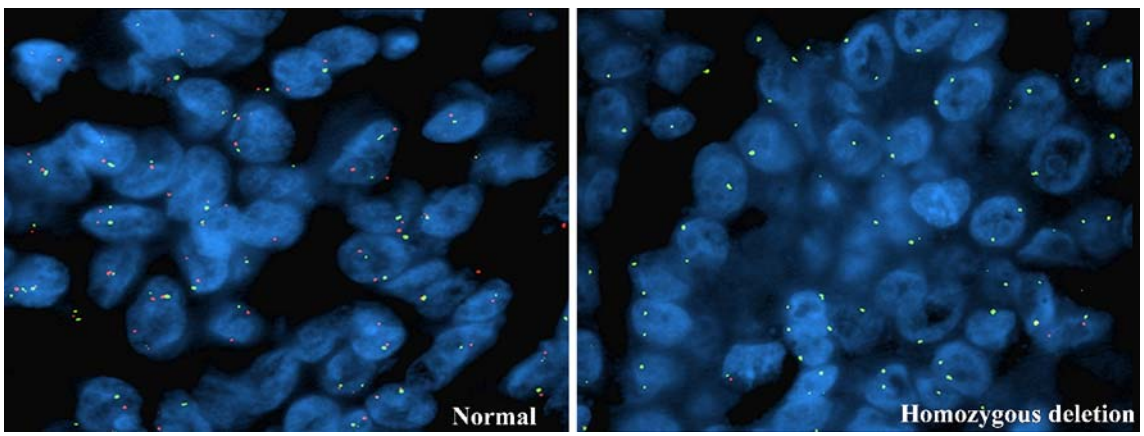

Fig. 2 Homozygous deletion by FISH was defined if both 9p21 signals were lost in at least 20% of nuclei. Normal cells are expected to show two green (chromosome 9 centromeric probe) and two red signals (locus-specific CDKN2A (p16) probe; Vysis, Downers Grove, IL, USA)

Cases were considered negative if 0 or 1+ focal, positive if 1+, multifocal–diffuse if 2+ (Fig. 1). Sections of cervical biopsy previously identified as immunoreactive for p16 protein served as a positive control. Negative controls included omitting the primary antibody and its substitution with normal serum.

Fluorescence in situ hybridization

Dual-color FISH analysis was performed using a Spectrum-Green-labeled chromosome 9 centromeric probe and a Spectrum-Orange-labeled locus-specific CDKN2A (p16) probe (Vysis, Downers Grove, IL, USA), as previously described [24]. In brief, paraffin sections were deparaffinized, dehydrated in ethanol, and air-dried. Sections were digested with protease K (0.5 mg/ml) at 37°C for 28 min. The slides were denatured at 75°C for 5 min in 70% formamide (Chemicon, Billerica, MA, USA) and dehydrated in ethanol. The probes were denatured for 5 min at 75°C prior to hybridization. Slides were hybridized overnight at 37°C and washed in 2XSSC/0.3% Igepal (Sigma, St. Louis, MO USA) at 72°C for 2 min. Nuclei were counterstained with 4',6-diamidino-2-phenylindole (DAPI)–antifade (Vysis, Inc., Downers Grove, IL, USA). Each FISH assay included normal lung tissue sections as a negative control, and sections of malignant mesothelioma previously identified as carrying p16 deletion as a positive control. Analyses were performed using a fluorescence microscope (Nikon Eclipse E600) and Cytovysion Workstation (Applied Imaging, Santa Clara, CA, USA) equipped with filter sets with single- and dual-band excitors for Spectrum Green, Spectrum Orange, and DAPI (UV 360 nm). The histological areas previously identified on the hematoxylin-and-eosin-stained sections were analyzed on the FISH-treated slides. Only individual and well-delineated cells were scored. Overlapping cells were excluded from the analysis. At least 60 cells were scored for each case and control.

Each tumor was assessed by the average and the maximum numbers of copies of p16 gene per cell and the average ratio of p16 gene to chromosome 9 copy numbers (CEP9). Homozygous deletion was defined if both 9p21 signals were lost in at least 20% of nuclei (Fig. 2).

Statistical analysis

The Kaplan–Meier method was used to estimate the survival function. The agreement of immunohistochemistry and FISH was tested by the simple kappa coefficient. Logistic regression was performed to determine whether all available explanatory variables can be used to predict survival status (LS versus SS).

Results

Clinical characteristics

The patients were divided into two groups using the overall median survival for all patients in this study of 36 months. Twenty-six patients were identified as LS and 22 as SS. There

Table 1 Immunoexpression of p16 protein and homozygous deletion of p16 determined by FISH in epithelioid type of malignant pleural mesotheliomas (39 analyzed cases)

Study group	Case #	Gender	Age (years)	Survival (months)	IHC	FISH
LS	1	F	63	47	POS	DEL
	2	F	65	37	NEG	ND
	3	F	63	68	NEG	NA
	4	F	55	37	POS	DEL
	5	M	61	57	POS	ND
	6	M	45	39	NEG	DEL
	7	M	60	44	POS	ND
	8	M	53	39	NEG	DEL
	9	F	56	42	POS	ND
	10	F	71	72	POS	ND
	11	F	56	41	POS	ND
	12	M	64	37	NEG	ND
	13	M	63	76	POS	ND
	14	F	NA	61	POS	ND
	15	F	67	48	NEG	ND
	16	F	30	51	POS	ND
	17	M	72	45	NEG	NA
	18	M	63	55	POS	ND
	19	F	71	36	NEG	DEL
	20	F	41	37	NEG	DEL
SS	1	M	69	8	NEG	DEL
	2	M	64	5	NEG	DEL
	3	M	63	<1	NEG	NA
	4	F	NA	12	NEG	NA
	5	M	78	6	NEG	DEL
	6	M	81	2	POS	DEL
	7	M	67	18	NEG	DEL
	8	M	59	12	POS	DEL
	9	M	54	8	POS	ND
	10	M	47	12	NEG	ND
	11	M	69	12	NEG	DEL
	12	M	62	12	POS	DEL
	13	M	72	3	NEG	DEL
	14	M	73	<1	NEG	DEL
	15	F	63	1	NEG	DEL
	16	M	50	2	NEG	DEL
	17	M	66	18	NEG	DEL
	18	F	41	13	NEG	DEL
	19	M	59	31	NEG	DEL

LS long survival (>3 years), *SS* short survival (<3 years), *IHC* immunohistochemistry, *FISH* fluorescence in situ hybridization, *POS* positive, *NEG* negative, *DEL* deletion, *ND* not deleted, *NA* not applicable

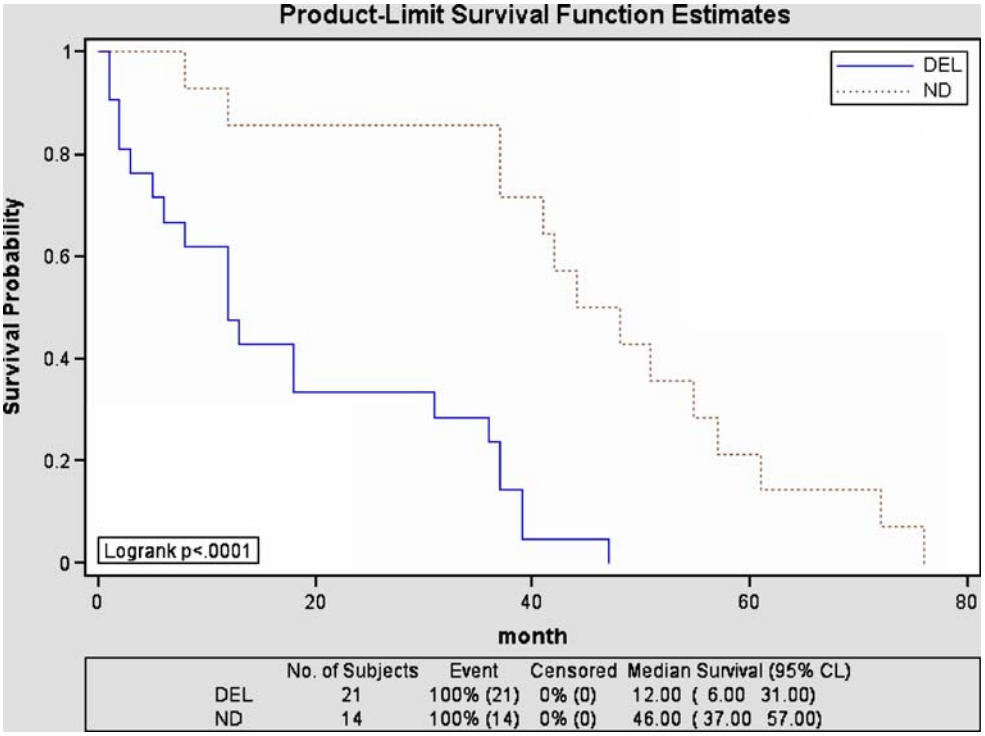

Fig. 3 Survival probability in respect to presence or absence of p16 deletion as determined by FISH in patients with epithelioid MPM

were 11 men and 15 women in LS group and 17 men and five women in SS group. Mean age in LS group was 63.7 years (range 41–78) and 57.4 years (range 30–71) in SS group. Mean survival in LS group was 50.7 months (range 36–116 months) and 9.1 months (range <1–31 months) in SS group.

Fluorescence in situ hybridization

The results of p16 expression assessed by immunohistochemistry and p16 deletion assessed by FISH are shown in Table 1.

Fluorescence in situ hybridization was successful in 35 (18 LS; 17 SS) of 48 cases (73%). Homozygous deletions of p16/CDKN2A was seen in 21 (60%) of cases, more frequently in cases with shorter survival. The estimated median survival time was 46 months for the subjects negative for deletion. For the subjects positive for deletion, the estimated median survival time was 12 months. Subjects negative for deletion as determined by FISH lived significantly longer than those subjects positive for deletion (p value <0.0001 for log-rank test; Fig. 3).

Of 18 cases with LS, homozygous deletion of p16/CDKN2A was identified in six cases (33%), while 12 cases (67%) were negative for deletion (Fig. 4a). Of 17 cases with SS, homozygous deletion of p16/CDKN2A was identified in 15 cases (88%) and two cases (12%) were negative for deletion (Fig. 4a). The difference in frequency of homozygous deletion of gene p16 was statistically significant between the two groups of malignant mesotheliomas (p=0.001). In addition to homozygous loss, two cases in LS group and one case in SS group showed hemizygous loss. Polyploidy of chromosome 9 was observed in three SS cases. Age was not a significant predictor of survival status in respect to presence or absence of deletion determined by FISH. However, gender and FISH results could significantly predict the survival. Subjects negative for deletion were more frequently women in LS group. The estimated odds ratio, female versus male,

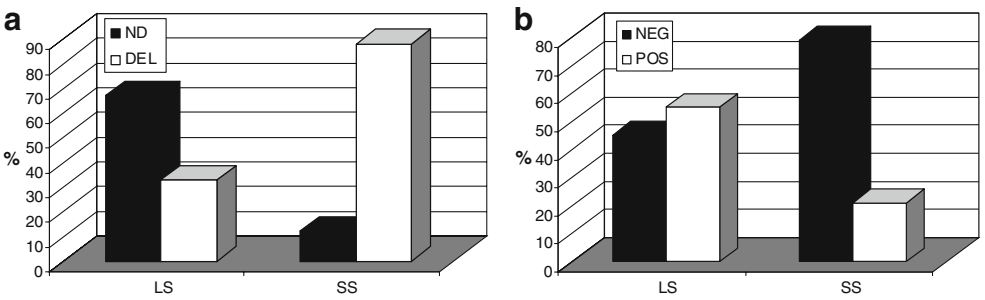

Fig. 4 **a** Frequencies of 9p21 deletion determined by FISH in patients with epithelioid type of MPM with long (*LS*) and short (*SS*) survival. **b** Immunoexpression of p16 protein in patients with epithelioid-type MPM with long (*LS*) and short (*SS*) survival

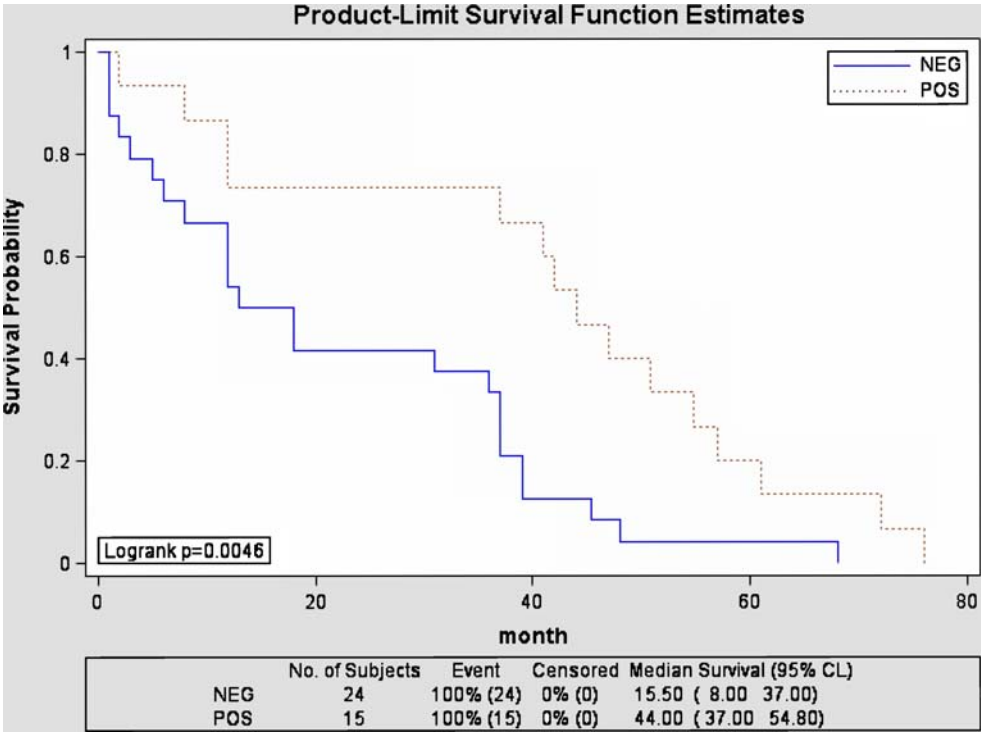

Fig. 5 Survival probability in respect to p16 protein expression determined by immunohistochemistry in patients with epithelioid type of MPM

was 16.014. The estimated odd ratio for negative and positive for deletion was 19.87.

Immunohistochemistry

P16 protein expression by immunohistochemistry was successfully determined in 39 cases. Discrepancies in number of cases analyzed by immunohistochemistry and FISH assay reflect unsuccessful hybridization. Of 20 cases with LS, positive p16 immunoexpression was identified in 11 cases (55%), while nine cases (45%) showed loss of expression (Fig. 4b). Of 19 cases with SS, only four cases (21%) showed positive p16 immunoexpression and 15 cases (79%) were negative (Fig. 4b). The difference in p16 protein expression was statistically significant between the two study groups (p=0.04). Similar to FISH results, age was not a significant predictor of survival status in respect to presence or absence of p16 immunoexpression. Female gender and positive p16 immunoexpression could significantly predict the survival for LS. As for female versus male, the estimated odds ratio was 12.476. For positive versus negative p16 immunoexpression, the estimated odds ratio was 5.495.

The estimated median survival time was 44 months for cases showing positive p16 immunoexpression. For the negative cases, the estimated median survival time was 15.5 months. Subjects with positive p16 immunoexpression lived significantly longer than those subjects with negative results (p value=0.0046 for log-rank test; Fig. 5).

Table 2 summarizes the results of 9p21 homozygous deletion determined by FISH in comparison with p16 expression determined by immunohistochemistry. Statistical analysis showed a very strong correlation of immunohistochemistry and FISH data (kappa coefficient=0.47), with only eight discrepant cases out of 34. Cases with the 9p21 deletion showed loss of p16 protein expression by immunohistochemistry, while cases without a 9p21 deletion maintained intact p16 protein expression (p value=0.003). Five cases were negative for deletion but showed positive p16 expression by immunohistochemistry. There were also three cases that showed loss of p16 immunoexpression, but were negative for deletion. Survival analysis showed that cases with positive p16 protein immunoexpression and negative for deletion of 9p21 as determined by FISH have the best survival time (Fig. 6).

Table 2 Comparison of p16 immunoexpression by IHC and p16 homozygous deletion by FISH

	IHC	
	NEGATIVE	POSITIVE
ND	4	10
DEL	16	5

Kappa coefficient=0.47
ND not deleted by FISH, *DEL* deleted by FISH, *IHC* immunohistochemistry

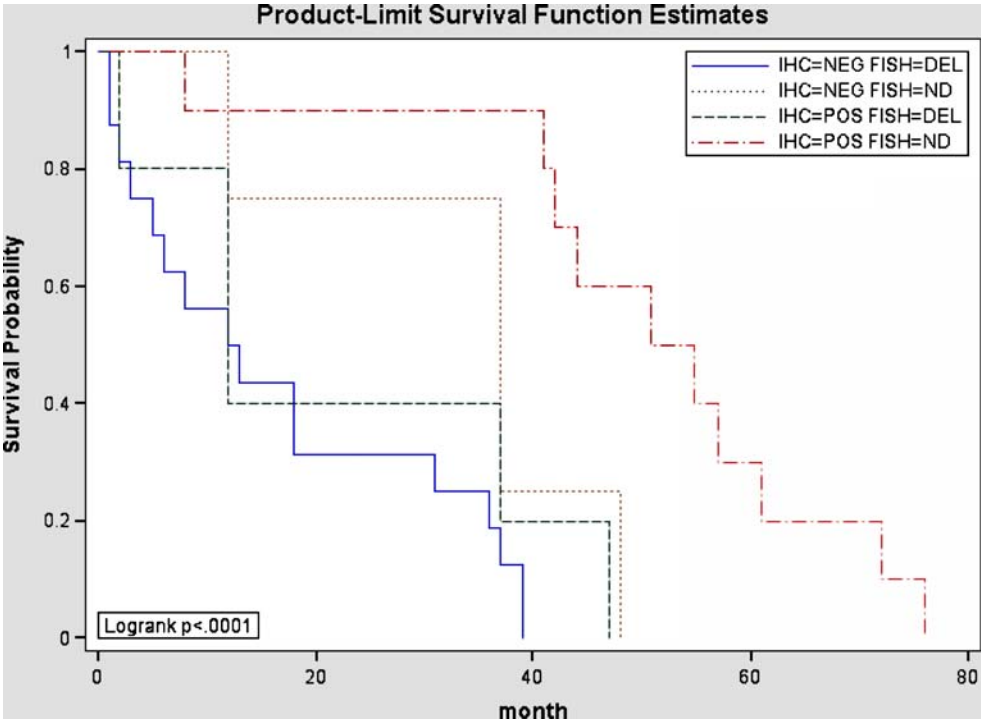

Fig. 6 Survival probability in respect to status of p16 loss determined by FISH and IHC in epithelioid type of MPM

Discussion

Several prognostic factors in pleural mesotheliomas have been reported previously, one of which is histology. Preoperative histologic classification of mesothelioma is very important in treatment decision because in cases of nonepithelioid morphology surgery is not a choice and other therapeutic options are considered. Although epithelioid mesotheliomas are usually surgically treated, there is still variability in survival despite similar treatment. Therefore, it is important to improve prognostic prediction before definitive surgery. For that reason, our study focused on epithelioid mesotheliomas only.

Loss of p16 gene is one of the most frequent genetic alterations in malignant mesotheliomas. Differences in reported frequency of loss of p16 usually reflect different methodology. It is known that loss of p16 may be a result of homozygous deletion, methylation, or point mutation, with homozygous deletion being the most common [14]. Homozygous deletion could be detected either by FISH or polymerase chain reaction (PCR)-based assays. FISH assay has certain advantages of being able to identify homozygous and hemizygous deletions. In contrast to PCR-based assays, contamination with normal cells is not an issue since those could be easily excluded from FISH analysis.

There are several clinical applications for detection of p16 deletion. One is diagnostic, particularly in differentiation between benign and malignant mesothelial proliferations, which is a common diagnostic problem for pathologists [24, 25]. Illei et al. [25] demonstrated that detection of p16/CDKN2A deletion by FISH is a very powerful ancillary test in the body cavity effusion specimens. Our recent study demonstrated that the same diagnostic assay could be used on formalin-fixed paraffin-embedded surgical specimens [24]. This approach has certainly improved the accuracy of diagnosis of malignant mesotheliomas.

Negative prognostic implications of p16/CDKN2A deletion have been reported in a prior study. Illei et al. clearly demonstrated that p16 deletion is associated with shorter survival using 1-year survival as a cutoff for long survival [19]. Similarly, our study confirmed the same observation, but we used 3 years as a cutoff survival demonstrating that the absence of deletion is a predictor of a long survival. These results indicate that FISH analysis of p16 in pleural mesothelioma can be used as an ancillary prognostic test that may guide treatment decisions.

Adverse prognostic significance of p16 loss determined by immunohistochemistry has been reported in peritoneal mesothelioma [28]. However, the results of this approach have not been reported in pleural mesothelioma. To our knowledge, our study is the first demonstration of loss of p16 immunoreactivity as a negative prognostic factor in pleural mesothelioma. Despite the same scoring method, our study demonstrated loss of p16 immunoreactivity in 62% of cases, in contrast to the reported 48% in peritoneal mesotheliomas. This may reflect differences in histologic types analyzed in two studies. Study on peritoneal mesotheliomas focused mainly on biphasic type, while our study was focused on epithelioid type. The second possible explanation would be biologic and genetic differences

between peritoneal and pleural tumors. It is possible that different genetic mechanisms and environmental factors play a role in the development of these two types of mesotheliomas with subsequent impact on different expression of p16. It is known that chromosome 9p represents a chromosomal region that is more prone to DNA damage by asbestos [11]. The level of exposure may be another explanation for lower frequency of detected p16 loss in peritoneal mesotheliomas. This is a speculation since detailed exposure histories are uncertain in our study and were not reported in the study by Borczuk et al. [28]. Hence, it would be interesting to know whether loss of p16 immunoreactivity correlates with the type of asbestos fibers to which patients were exposed.

Another important observation in our study is correlation between the presence of deletion of p16 determined by FISH and loss of p16 immunoreactivity. Our prior study demonstrated the only trend for such correlation that was statistically insignificant [24]. One possible explanation is that this correlation between the two methods depends on the histologic type of mesothelioma. As mentioned earlier, this study included epithelioid mesothelioma only, while the prior study in addition to epithelioid type also included biphasic and sarcomatoid types. The second most likely explanation is a difference in scoring methods. Based on the current study, loss of p16 immunoreactivity has the same prognostic significance as homozygous deletion of p16. Therefore, one may think that, because of availability and cost, p16 immunoreactivity would be a better clinical prognostic test in malignant mesotheliomas. Our survival analysis would argue that probably both tests should be used since the best survival was observed in patients who demonstrated positive p16 immunoreactivity and lack of p16 deletion. Furthermore, about 23% of our cases showed discrepancy between FISH and immunohistochemistry data, indicating that for clinical applications probably both tests should be used. Loss of p16 immunoexpression in the absence of 9p21 deletion that was seen in three cases may be a result of p16 point mutation or methylation. On the other hand, it is somewhat difficult to explain positive p16 immunoexpression in the presence of homozygous deletion as seen in five cases in our study. One possibility would be that we are dealing with FISH artifact and false-positive results. The other explanation would be the size of commercially available FISH probe used in this study. This probe is rather large (190 kb) and also covers p14, p15, and a portion of the MTAP gene which is frequently codeleted with p16 gene. In our study, we did not investigate the status of MTAP gene, but we believe that deletion of this gene is most likely the underlying reason for the above-described discrepancy.

A codeletion of p16 with MTAP, a gene approximately 100 kb telomeric to p16, has potential therapeutic implications [18]. MTAP encodes methylthioadenosine phosphorylase, an enzyme of the salvage pathway that leads to production of adenine for synthesis of adenosine monophosphate. As demonstrated in hematologic malignancies, L-alanosine (inhibitor of de novo purine synthesis) therapy has toxic effect on MTAP-deficient cells [29, 30]. The frequent codeletion of p16 and MTAP suggests that mesotheliomas with p16 deletion may have greater sensitivity to L-alanosine therapy.

In summary, our study is the first to demonstrate decreased frequency of homozygous deletion of 9p21 and loss of p16 immunoreactivity in pleural mesotheliomas from patients with long-term survival of greater than 3 years in contrast to more typical patients with rapidly fatal mesotheliomas. Implementation of these tests into clinical practice may improve preoperative prognostication of malignant mesotheliomas and inclusion of mesothelioma patients into new targeted chemotherapeutic protocols.

Acknowledgments We would like to thank Kathleen Cieply and Carol Sherer in the FISH and aCGH Laboratory and Kimberly Fuhrer in the Developmental Laboratory of the Department of Pathology University of Pittsburgh Medical Center for their excellent technical assistance.

Conflict of interest statement We declare that we have no conflict of interest.

References

1. Neragi-Miandoab S (2006) Multimodality approach in management of malignant pleural mesothelioma. Eur J Cardio Thorac Surg 29:14–19
2. Robinson BWS, Musk AW, Lake RA (2005) Malignant mesothelioma. Lancet 366:397–408
3. Bonomo L, Feragalli B, Sacco R et al (2000) Malignant pleural disease. Eur J Radiol 34:98–118
4. Carbone M, Rizzo P, Grimley PM et al (1997) Simian virus-40 large-T antigen binds p53 in human mesotheliomas. Nat Med 3:908–912
5. Gazdar AF, Carbone M (2003) Molecular pathogenesis of malignant mesothelioma and its relationship to simian virus 40. Clin Lung Cancer 5:177–181
6. Tsiouris A, Walesby RK (2007) Malignant pleural mesothelioma: current concepts in treatment. Nat Clin Pract Oncol 4:344–352
7. Rusch VW (1996) A proposed new international TNM staging system for malignant pleural mesothelioma from the International Mesothelioma Interest Group. Lung Cancer 14:1–12
8. Sugarbaker DJ, Flores RM, Jaklitsch MT et al (1999) Resection margins, extrapleural nodal status, and cell type determine postoperative long-term survival in trimodality therapy of malignant pleural mesothelioma: results in 183 patients. J Thorac Cardiovasc Surg 117:54–63, discussion 63–55
9. Curran D, Sahmoud T, Therasse P et al (1998) Prognostic factors in patients with pleural mesothelioma: the European Organization for Research and Treatment of Cancer experience. J Clin Oncol 16:145–152
10. Herndon JE, Green MR, Chahinian AP et al (1998) Factors predictive of survival among 337 patients with mesothelioma

treated between 1984 and 1994 by the Cancer and Leukemia Group B. Chest 113:723–731
11. Bueno R, Reblando J, Glickman J et al (2004) Pleural biopsy: a reliable method for determining the diagnosis but not subtype in mesothelioma. Ann Thorac Surg 78:1774–1776
12. Steele JPC (2002) Prognostic factors in mesothelioma. Semin Oncol 29:36–40
13. Weder W, Kestenholz P, Taverna C et al (2004) Neoadjuvant chemotherapy followed by extrapleural pneumonectomy in malignant pleural mesothelioma.[see comment]. J Clin Oncol 22:3451–3457
14. Hirao T, Bueno R, Chen C-J et al (2002) Alterations of the p16 (INK4) locus in human malignant mesothelial tumors. Carcinogenesis 23:1127–1130
15. Kumar P, Kratzke RA (2005) Molecular prognostic markers in malignant mesothelioma. Lung Cancer 49 Suppl 1:S53–S60
16. Lee AY, Raz DJ, He B et al (2007) Update on the molecular biology of malignant mesothelioma. Cancer 109:1454–1461
17. Pisick E, Salgia R (2005) Molecular biology of malignant mesothelioma: a review. Hematol Oncol Clin North Am 19:997–1023
18. Illei PB, Rusch VW, Zakowski MF et al (2003) Homozygous deletion of CDKN2A and codeletion of the methylthioadenosine phosphorylase gene in the majority of pleural mesotheliomas. Clin Cancer Res 9:2108–2113
19. Lopez-Rios F, Chuai S, Flores R et al (2006) Global gene expression profiling of pleural mesotheliomas: overexpression of aurora kinases and P16/CDKN2A deletion as prognostic factors and critical evaluation of microarray-based prognostic prediction. Cancer Res 66:2970–2979
20. Musti M, Kettunen E, Dragonieri S et al (2006) Cytogenetic and molecular genetic changes in malignant mesothelioma. Cancer Genet Cytogenet 170:9–15
21. Singhal S, Wiewrodt R, Malden LD et al (2003) Gene expression profiling of malignant mesothelioma. Clin Cancer Res 9:3080–3097
22. Prins JB, Williamson KA, Kamp MM et al (1998) The gene for the cyclin-dependent-kinase-4 inhibitor, CDKN2A, is preferentially deleted in malignant mesothelioma. Int J Cancer 75:649–653
23. Xio S, Li D, Vijg J et al (1995) Codeletion of p15 and p16 in primary malignant mesothelioma. Oncogene 11:511–515
24. Chiosea S, Krasinskas A, Cagle PT et al (2008) Diagnostic importance of 9p21 homozygous deletion in malignant mesotheliomas. Mod Pathol 21:742–747
25. Illei PB, Ladanyi M, Rusch VW et al (2003) The use of CDKN2A deletion as a diagnostic marker for malignant mesothelioma in body cavity effusions. Cancer 99:51–56
26. Churg R, Roggli V, Galateau-Salle F (2004) Tumours of the pleura. In: Travis W, Brambilla E, Muller-Hermelink H, Harris C (eds) World Health Organization classification of tumours, pathology and genetics: tumours of the lung, pleura, thymus and heart. IARC, Lyon, pp 126–136
27. Kothmaier H, Quehenberger F, Halbwedl I et al (2008) EGFR and PDGFR differentially promote growth in malignant epithelioid mesothelioma of short and long term survivors. Thorax 63:345–351
28. Borczuk AC, Taub RN, Hesdorffer M et al (2005) P16 loss and mitotic activity predict poor survival in patients with peritoneal malignant mesothelioma. Clin Cancer Res 11:3303–3308
29. Batova A, Diccianni MB, Omura-Minamisawa M et al (1999) Use of alanosine as a methylthioadenosine phosphorylase-selective therapy for T-cell acute lymphoblastic leukemia in vitro. Cancer Res 59:1492–1497
30. Harasawa H, Yamada Y, Kudoh M et al (2002) Chemotherapy targeting methylthioadenosine phosphorylase (MTAP) deficiency in adult T cell leukemia (ATL). Leukemia 16:1799–1807

Virchows Arch (2008) 453:637
DOI 10.1007/s00428-008-0690-x

ERRATUM

Intraductal acinar cell carcinoma of the pancreas

Aurélie Fabre · Alain Sauvanet · Jean-François Flejou · Jacques Belghiti · Laurent Palazzo · Philippe Ruszniewski · Claude Degott · Benoît Terris

Published online: 29 October 2008

Erratum to: Virchows Arch
DOI: 10.1007/s004280000342

One of the co-authors´ names was spelled wrongly.
The correct spelling is:
Philippe Ruszniewski

The online version of the original article can be found at http://dx.doi.org/10.1007/s004280000342.

A. Fabre · J.-F. Flejou · C. Degott · B. Terris (✉)
Service d'Anatomie Pathologique, Hôpital Beaujon,
110 boulevard du Général Leclerc,
92118 Clichy Cédex, France
e-mail: benoitterris@hotmail.com

A. Sauvanet · J. Belghiti
Service de Chirurgie Digestive, Hôpital Beaujon,
Clichy Cédex, France

L. Palazzo · P. Ruszniewski
Service de Gastroentérologie, Hôpital Beaujon,
Clichy Cédex, France